BNL 719 (C-32) Vol I
Volume I of IV
The Scattering Law

325
10-9-62

MASTER

12

PROCEEDINGS OF THE BROOKHAVEN CONFERENCE ON NEUTRON THERMALIZATION

Volume I, The Scattering Law

April 30 to May 2, 1962

BROOKHAVEN NATIONAL LABORATORY
ASSOCIATED UNIVERSITIES, INC.
under contract with the
UNITED STATES ATOMIC ENERGY COMMISSION

DISCLAIMER

BNL 719 (C-32)
(Physics and Mathematics – TID 4500, 17th Ed.)

PROCEEDINGS OF THE BROOKHAVEN CONFERENCE ON NEUTRON THERMALIZATION

Volume I, The Scattering Law

April 30 to May 2, 1962

BROOKHAVEN NATIONAL LABORATORY
UPTON, NEW YORK

LEGAL NOTICE

PRINTED IN USA
PRICE $15 00 FOR THE FOUR VOLUMES

Available from the
Office of Technical Services
Department of Commerce
Washington 25, D C

June 1962 850 copies

PREFACE

A conference on the subject of neutron thermalization was held at the Brookhaven National Laboratory from April 30 to May 2, 1962, precisely four years after the close of the last thermalization conference, the Gatlinburg conference of April 28-30, 1958. The subject of thermalization, which concerns the approach to thermal equilibrium and the manner of the equilibrium distribution of neutrons in matter, has elicited a great deal of interest in the meantime. While the seventeen papers contributed at Gatlinburg could be assembled into a single, convenient volume, presenting the seventy Brookhaven papers has required four weighty books.

The Brookhaven conference was conducted as a "reporter" conference. The technical papers which were submitted were sorted into six categories, viz., the experimental and theoretical aspects of the "scattering law," of spectra in infinite media, and of transient phenomena. A reporter was chosen for each of the six topics, and was asked to prepare a talk which would contain an appreciation of the technical papers. The reporter talk, followed by a general discussion constituted each session. Thus, the individual papers were not presented, though copies were available to all who attended, and are presented in these proceedings. (While the papers from our Soviet colleagues were received too late for discussion at the conference, translated versions will also be found in these volumes.)

The success of a technical conference is always due to the efforts of many people. We must first thank the reporters and authors for the fine quality of their contributions. Mr. Robert Brown of Brookhaven's Graphic Arts Division was responsible for the prompt publication of the proceedings and for having more than ten thousand copies of the technical papers ready in time for the conference. Mrs. Mariette Kuper and Mr. Edward Bergin and their staffs directed the mechanics of the conference with skill and aplomb, while several members of the Theoretical Reactor Physics Group made important contributions to its planning and execution. In particular, we should thank Drs. Paul Michael and Henry Honeck, and for his kind encouragement throughout, Mr. Jack Chernick, the Group's Director.

NOEL CORNGOLD

VOLUME I

PROGRAM AND TABLE OF CONTENTS

THE SCATTERING LAW

A. Experimental Aspects

EXPERIMENTAL INFORMATION FOR THERMALIZATION PROBLEMS*

Robert M. Brugger

Phillips Petroleum Company, Atomic Energy Division
Idaho Falls, Idaho

*Work done under the auspices of the U. S. Atomic Energy Commission.

For neutron energies much above 1 ev the neutron scattering and thermalizations are well described by billiard ball collisions with atoms of the moderator. Therefore this discussion will only consider neutrons of 1 ev or less. Most reactors are not constructed of single crystal materials or aligned materials. Thus this discussion will be limited to polycrystalline and amorphous solids, liquids, and gases.

What neutron scattering information does the reactor physicist want for his calculations of neutron thermalization?

Within these limits, the cross section $\sigma(E_o,E,\theta,S)$ completely describes the scattering of neutrons from these samples. Here E_o is the energy of the initial neutrons, E is the energy of the neutrons after scattering, θ is the angle of scattering with respect to the direction of the initial neutrons and S denotes the "physical state" of the sample. From $\sigma(E_o,E,\theta,S)$, flux distributions can be calculated or all of the integral values now used in reactor calculations, like the transport cross section and the scattering kernels can be obtained. $\sigma(E_o,E,\theta,S)$ contains the complete information about the neutron scattering.

Over what range would the reactor physicist like these cross sections?

I think it is safe to say the following ranges are adequate:

E_o	from 0 to 1 ev
E	from 0 to 1 ev
θ	from 0 to 180^0
S	all "states" of the sample that are encountered in reactors
Accuracy ±10%	

Further these cross sections are to be for all materials encountered in reactors.

How does the experimenter attempt to measure these cross sections and how successful has he been?

I would like to answer this question by describing some of the methods that are being used to obtain $\sigma(E_o,E,\theta,S)$ and by showing some of the data that has been obtained. To make these measurements, the experimenter must produce a beam of monoenergetic neutrons in the desired range for use as the initial neutrons. After scattering these from a sample, the energies of the scattered neutrons must be measured and the scattering angle must be measured.

The two most successful instruments making these measurements are the phased chopper velocity selectors and the triple axis spectrometers. Figure 1 is a cut-away drawing of the Materials Testing Reactor phased chopper velocity selector.[1] The first chopper chops the beam of neutrons

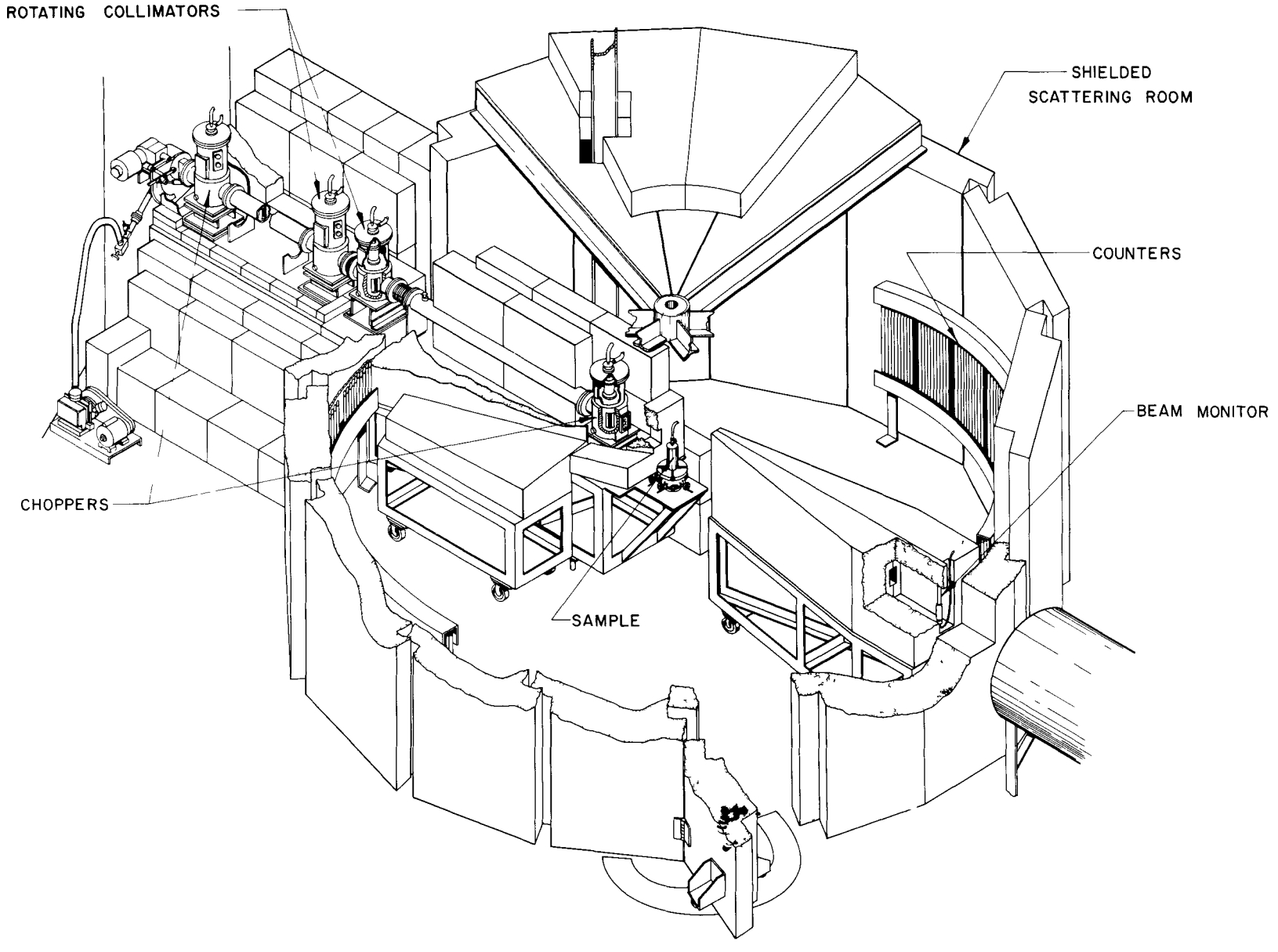
ROTATING COLLIMATORS
SHIELDED
SCATTERING ROOM
COUNTERS
BEAM MONITOR
CHOPPERS
SAMPLE

Figure 1

from the reactor into bursts of polychromatic neutrons. The second chopper which opens at a predetermined time after the first chopper opens passes only bursts of monochromatic neutrons. These monochromatic neutrons are scattered by the sample, and some change energy because of inelastic scattering. The energies of the scattered neutrons are determined by measuring their time-of-flight from the sample to the detectors. The angle of scattering is measured by the detectors placed at different angles around the sample. By changing the phase or open times between the two choppers, E_0 may be varied allowing $\sigma(E_0,E,\theta,S)$ to be completely measured. Similar velocity selectors are in operation at Chalk River and Harwell and another is being constructed at the University of Michigan.

The triple axis spectrometer[2] produces a monoenergetic initial beam by Bragg reflecting one energy neutron from a reactor beam. These monoenergetic neutrons are scattered by a sample located at the second axis of the instrument. The scattered neutrons are energy analyzed at each scattering angle by a second crystal spectrometer located at the third axis. Instruments of this type are in operation at Chalk River, at Hanford, at Los Alamos, and are being built for the Belgium reactors.

Other types of instruments that show promise or have a limited

range are the polycrystalline filter plus chopper time-of-flight arrangement, the rotating crystal time-of-flight spectrometer, the linear electron accelerators with time-of-flight analyzers, and the filter counter method.

To date, the phased chopper velocity selectors have produced the major share of the $\sigma(E_o,E,\theta,S)$ data. As an example of these measurements, I would like to discuss the data presented in the contributed paper by Haywood and Thorson of Chalk River. Figure 2 is an example of their data for scattering at 86.9^0 from a sample of 20^0C H_2O. The initial energy of the neutrons is 0.096 ev. The upper figure shows the counting rate as a function of time channels for both sample and open. The open distribution has structure due mainly to neutrons scattered by air near the sample and neutrons scattered by the empty sample container.

By knowing the incident flux and the counter efficiencies, the data of the upper figure are converted to the cross section differential in both energy and angle as shown in the middle of Figure 2. Here the cross section is displayed as energy change, $\omega = (E-E_o)/K_BT$, instead of as E. The solid line represents the initial energy resolution of the instrument. The lower curve is the same data presented as Scattering Law. This presentation will be discussed later.

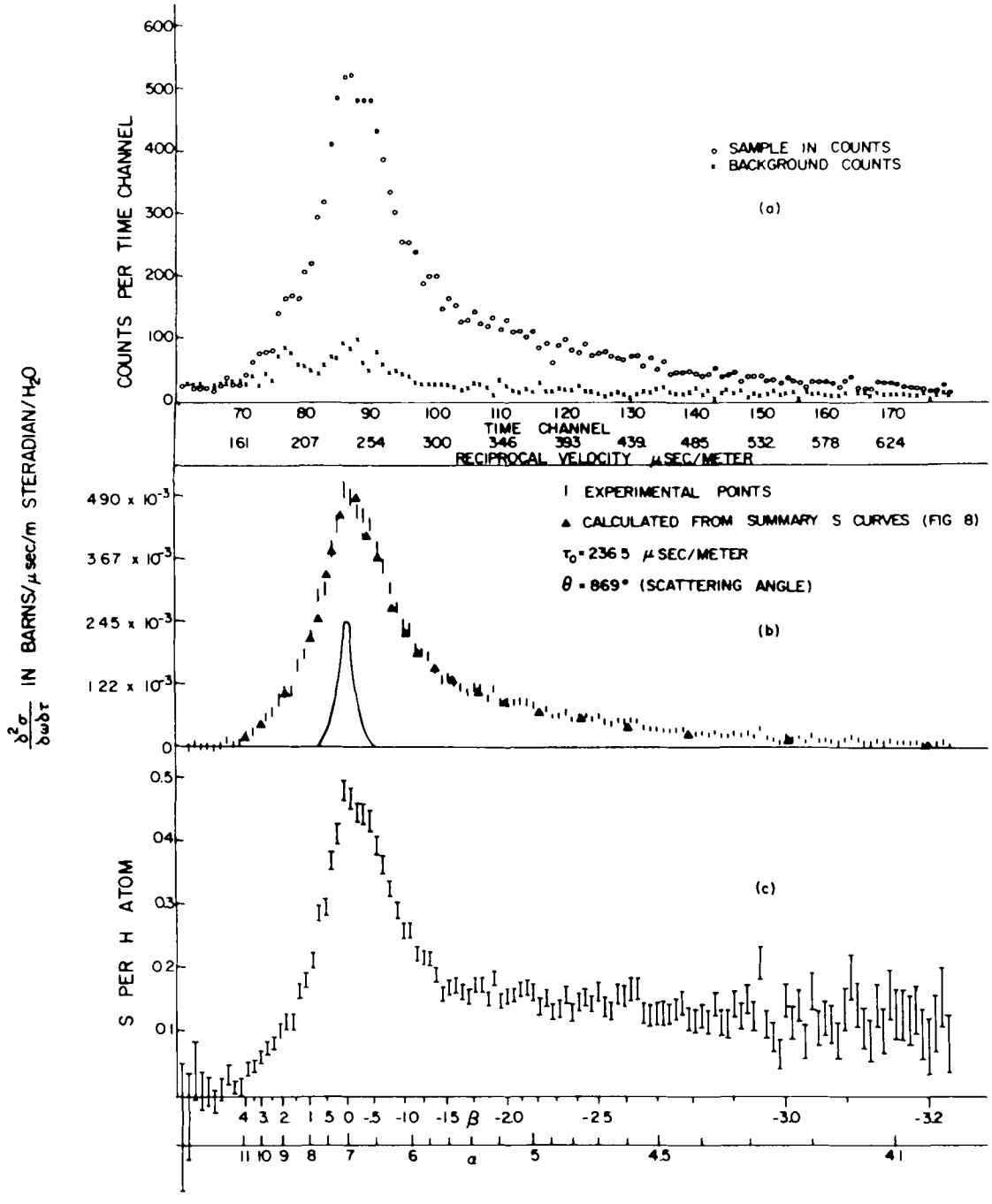
COUNTS PER TIME CHANNEL
600
500
400
300
200
100
0
SAMPLE IN COUNTS
BACKGROUND COUNTS
(a)
70 80 90 100 110 120 130 140 150 160 170
TIME CHANNEL
161 207 254 300 346 393 439 485 532 578 624
RECIPROCAL VELOCITY μSEC/METER
$\frac{\delta^2\sigma}{\delta\omega\delta\tau}$ IN BARNS/μsec/m STERADIAN/H_2O
490 x 10^{-3}
367 x 10^{-3}
245 x 10^{-3}
122 x 10^{-3}
0
EXPERIMENTAL POINTS
CALCULATED FROM SUMMARY S CURVES (FIG 8)
τ_0 = 2365 μSEC/METER
θ = 869° (SCATTERING ANGLE)
(b)
S PER H ATOM
0.5
0.4
0.3
0.2
0.1
(c)
4 3 2 1 5 0 -5 -10 -15 β -20 -25 -30 -32
11 10 9 8 7 6 α 5 4.5 4.1

Figure 2

Now that you have seen an example of the data, consider over what ranges these measurements are being made. The ranges to date are:

E_o	from 0.005 to 0.4 ev
E	somewhat less than E_o
θ	from 12 to 155^0
S	several different "physical states"
Accuracy $\leq$10%	

Having obtained the data, what is the best form of presentation?

The data can be presented as $d^2\sigma/d\Omega d\omega$ as in the middle figure of Figure 2. These are close in appearance to the actual measurements, but there are so many of them for each sample, that one tends to miss the forest for the trees. A presentation suggested by Egelstaff and Schofield[3] introduces the important simplification of extracting detailed balance. This is not appropriate for single crystal samples but it is for all the states to which this discussion has been limited. Egelstaff calls his presentation Scattering Law, $S(\alpha,\beta)$, where:

$$S(\alpha,\beta) = \frac{4\pi}{\sigma_b} K_B T \frac{k_o}{k} e^{+\beta/2} \frac{d^2\sigma}{d\Omega d\omega}$$

and

$$\alpha = \frac{\hbar^2 \kappa^2}{2MK_B T} \qquad \beta = \frac{\hbar\omega}{K_B T}$$

Here σ_b is the bound atom cross section, K_B is the Boltzmann constant, T is the absolute temperature of the sample, $\hbar$ is $1/2\pi$ of Planck's constant, κ is the momentum change, and M is the mass, usually of the principle scatterer. Figure 3 is the data of Haywood and Thorson presented in the Scattering Law. The advantages of this presentation are 1) that it condenses the data; only measurements at a few initial energies and angles are needed to determine all of the curves, and 2) $d^2\sigma/d\Omega d\omega$ can be determined from $S(\alpha,\beta)$ at values other than those that were originally measured. Figure 4 is a set of smoothed curves of the Haywood and Thorson data in $S(\alpha,\beta)$ presentation.

The mass M and the cross section σ_b are somewhat arbitrarily selected in the Scattering Law presentation. Therefore there is a third presentation which keeps the detailed balance simplification but does not introduce M and σ_b. I have called this presentation the reduced partial differential cross section $S(\kappa,\hbar\omega)$ where:

$$S(\kappa,\hbar\omega) = \frac{\sigma_b}{4\pi} \frac{1}{K_B T} S(\alpha,\beta)$$

$$= \frac{k_o}{k} e^{+\hbar\omega/K_B T} \frac{d^2\sigma}{d\Omega d\omega}$$

AECL Ref # A 2770 A

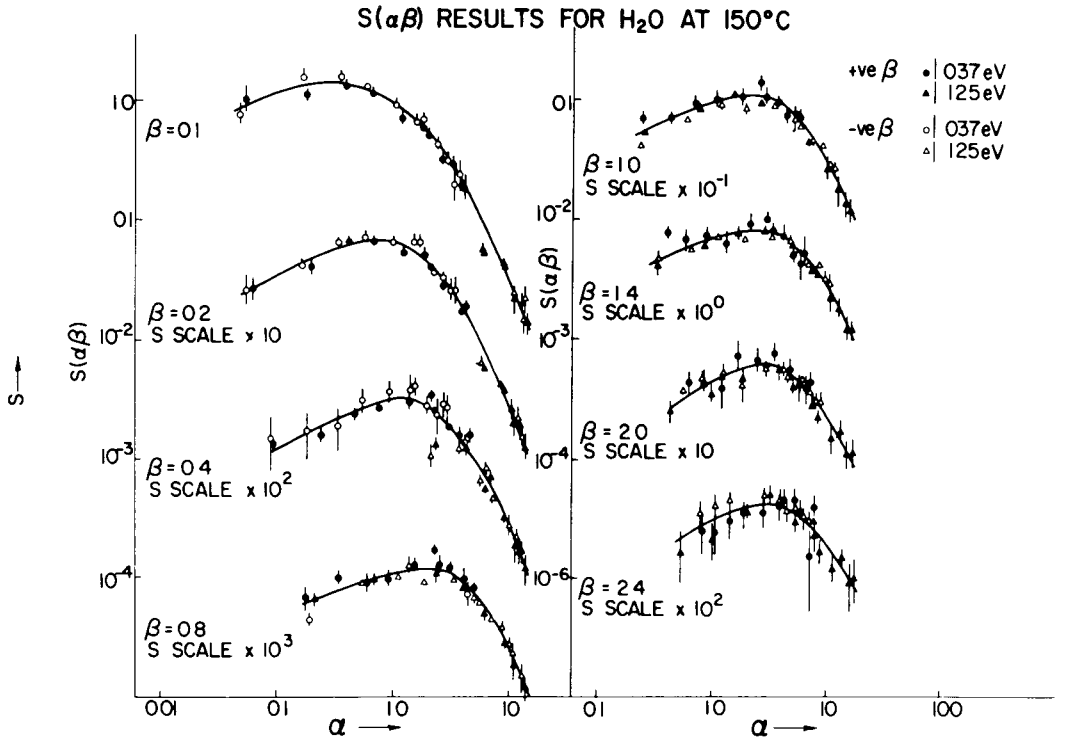

Figure 3

AECL Ref # A 2778 G

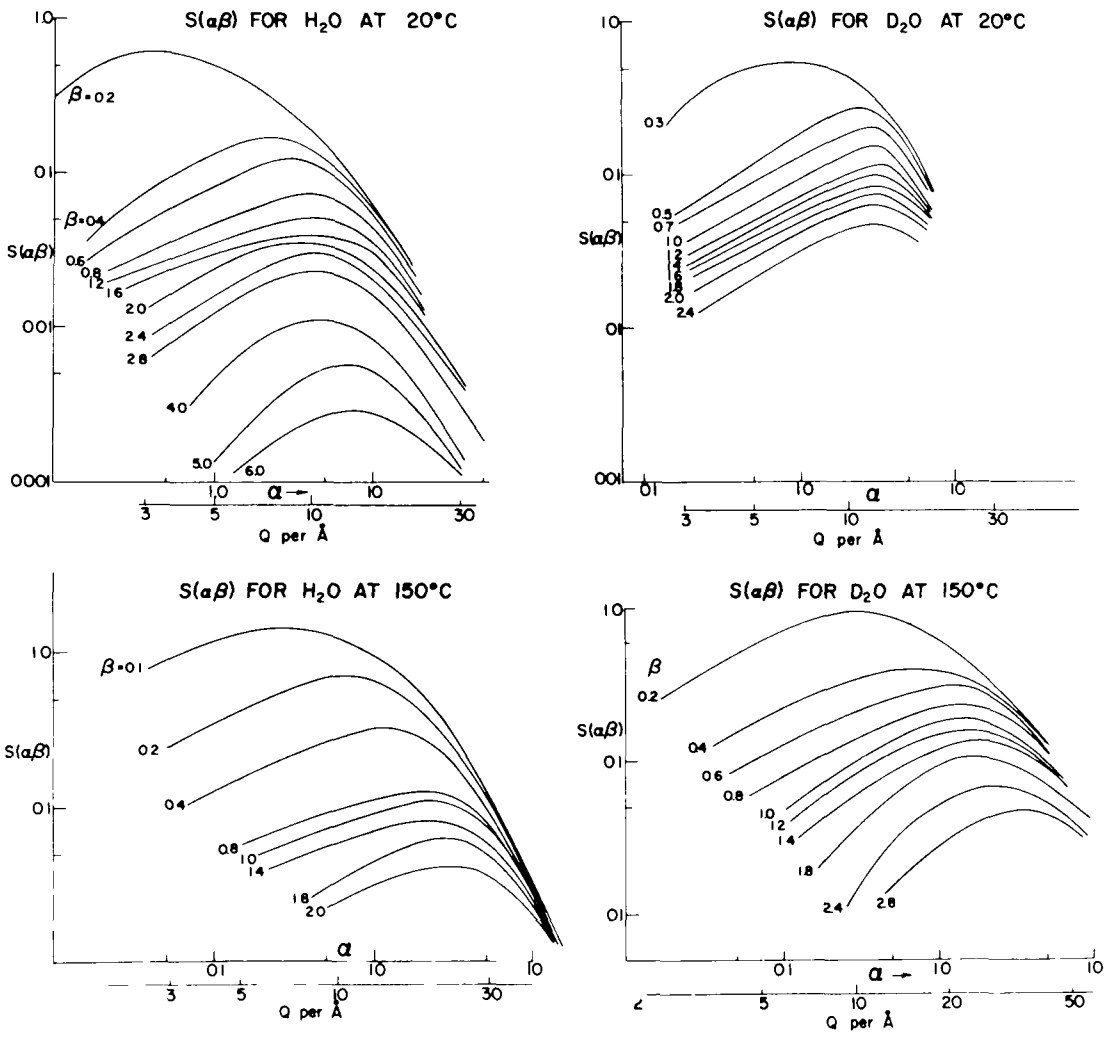

Figure 4

Here $K_B T$ is in units of ev and κ is in reciprocal angstroms. The advantage of $S(\kappa,\hbar\omega)$ over $S(\alpha,\beta)$ is that M and σ_b have not been introduced. Figure 5 is an example of the Santowax data presented as a reduced partial cross section.

In plotting curves, one has the choice of showing $S(\alpha,\beta)$ as a function of α with contours of fixed β or $S(\alpha,\beta)$ as a function of β with contours of fixed α. The first tends to emphasize the coherent and diffraction effects while the last tends to emphasize the energy change effects.

What consistency checks does the experimenter have available to test his data?

By presenting the data as $S(\alpha,\beta)$ or $S(\kappa,\hbar\omega)$ several points of consistency are introduced. First, points for $+\beta$ and $-\beta$ must fall on the same curve. This can be seen in Figure 3. Secondly, data at one β from measurements at different initial energies must fall on the same line. Thirdly, data at one β from different angles must fall on one curve. These are rather stringent internal consistency checks which are not evident when the data is presented as $d^2\sigma/d\Omega d\omega$.

One external consistency check is that the data integrated over energy and angle must equal the total cross section. Likewise the integral

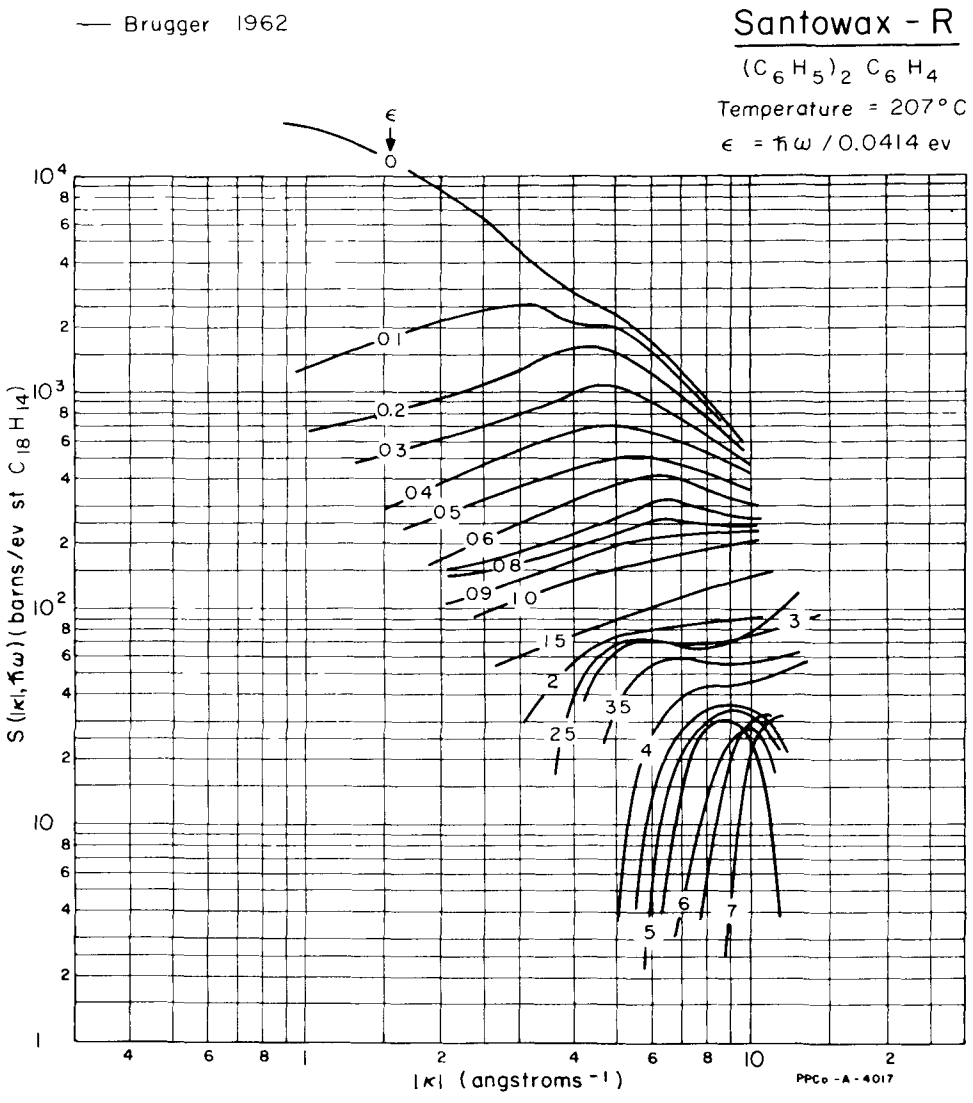
— Brugger 1962
Santowax - R
$(C_6H_5)_2\ C_6H_4$
Temperature = 207°C
$\epsilon = \hbar\omega / 0.0414$ ev
$S(|\kappa|, \hbar\omega)$ (barns/ev st $C_{18}H_{14}$)
$|\kappa|$ (angstroms^{-1})
PPCo-A-4017

Figure 5

over all energies must fit the angular distributions. Thus it is desirable to have separate total cross section and angular distribution measurements. These two checks are necessary but they are not sufficient. This last statement is also true for theories predicting $d^2\sigma/d\Omega d\omega$. Many theories that do not completely explain $d^2\sigma/d\Omega d\omega$ will fit the total cross sections. Springer, in a paper at this meeting, discusses the theoretical fitting of total cross sections and angular distributions.

The third set of consistency checks is the moment conditions. In Scattering Law notation the zero'th moment <1> is

$$<1> = \int_0^\infty \cosh \beta/2 \; S_{inc}(\alpha,\beta)d\beta = 1$$

and the first moment $<\beta>$ is

$$<\beta> = \int_0^\infty \beta \sinh \beta/2 \; S(\alpha,\beta)d\beta = \alpha$$

These hold for all values of α. Since the zero'th moment weighs the values of $S(\alpha,\beta)$ at small β more heavily, this condition is easily satisfied by the data if the total cross section condition is satisfied. The first moment is more difficult since the major contribution to it comes from large β values where the data is poor or nonexistent. To satisfy the first moment condition, all of the "effects" of the sample must be detected. These "effects"

are sometimes small and outside the range of the experiment. All one can say is that $\langle\beta\rangle \leq \alpha$.

How may this data be used by reactor physicists in their calculations?

As has been shown, the data are not as accurate or extensive as the reactor physicists desire. Thus the profitable approach is to fit theoretical curves to the existing data and use these theories to make the extrapolations. This can be attempted in several ways. One way is that suggested by Vineyard and by Rahman[4] where a radius of the intermediate function $\chi(\kappa,t)$ can be obtained by Fourier transformation. Here:

$$\rho(t) = \frac{\hbar^2}{MK_B T\alpha} \ln \int_0^\infty \cos(\omega,t)\, S(\alpha,\beta)d\beta$$

This requires that the intermediate function be Gaussian in α and the self correlation function $G_s(r,t)$ be Gaussian in r. If this condition is satisfied, a single $\rho(t)$ for all values of α can be obtained. By Fourier inversion, $S(\alpha,\beta)$ at all values of α and β could then be generated. This method was tried on the Santowax data and was not successful. The lack of success may be due to the experimental error or it may be that $G_s(r,t)$ is not Gaussian.

A second method is that proposed by Egelstaff and is presented in

the paper by Haywood and Thorson. $S_{inc}(\alpha,\beta)$ is divided by α and extrapolated to $\alpha = 0$. These values of $(S_{inc}(\alpha,\beta)/\alpha)_{\alpha=0}$ are plotted as a function of β giving a function called $P(\beta)$. Once a $P(\beta)$ has been obtained it can be used to regenerate $S_{inc}(\alpha,\beta)$ at other values. Figure 6 shows the $P(\beta)$ functions they obtained for H_2O and D_2O. An assumption of this method is that the intermediate function is Gaussian in α and that the coherent effects can be extracted from $S(\alpha,\beta)$.

McMurry has contributed a paper to this meeting in which the results of different theories are compared and their success analyzed. I am sure these will be discussed at a later session. Along this same line I would like to mention some experiments on methane and the theoretical fitting of the data. Figure 7 shows the methane data obtained at the MTR. Four theoretical fits are attempted. The first three are discussed by McMurry. I would like to call your attention to a theory developed by George Griffing[5] in which a complete quantum mechanical treatment of the roations including coherence was necessary to fit these data at low energy. To me this shows that to accurately fit the data that are becoming available, more detailed theories are necessary. Figure 8 shows the results of Griffing's theory at values outside the range of the data.

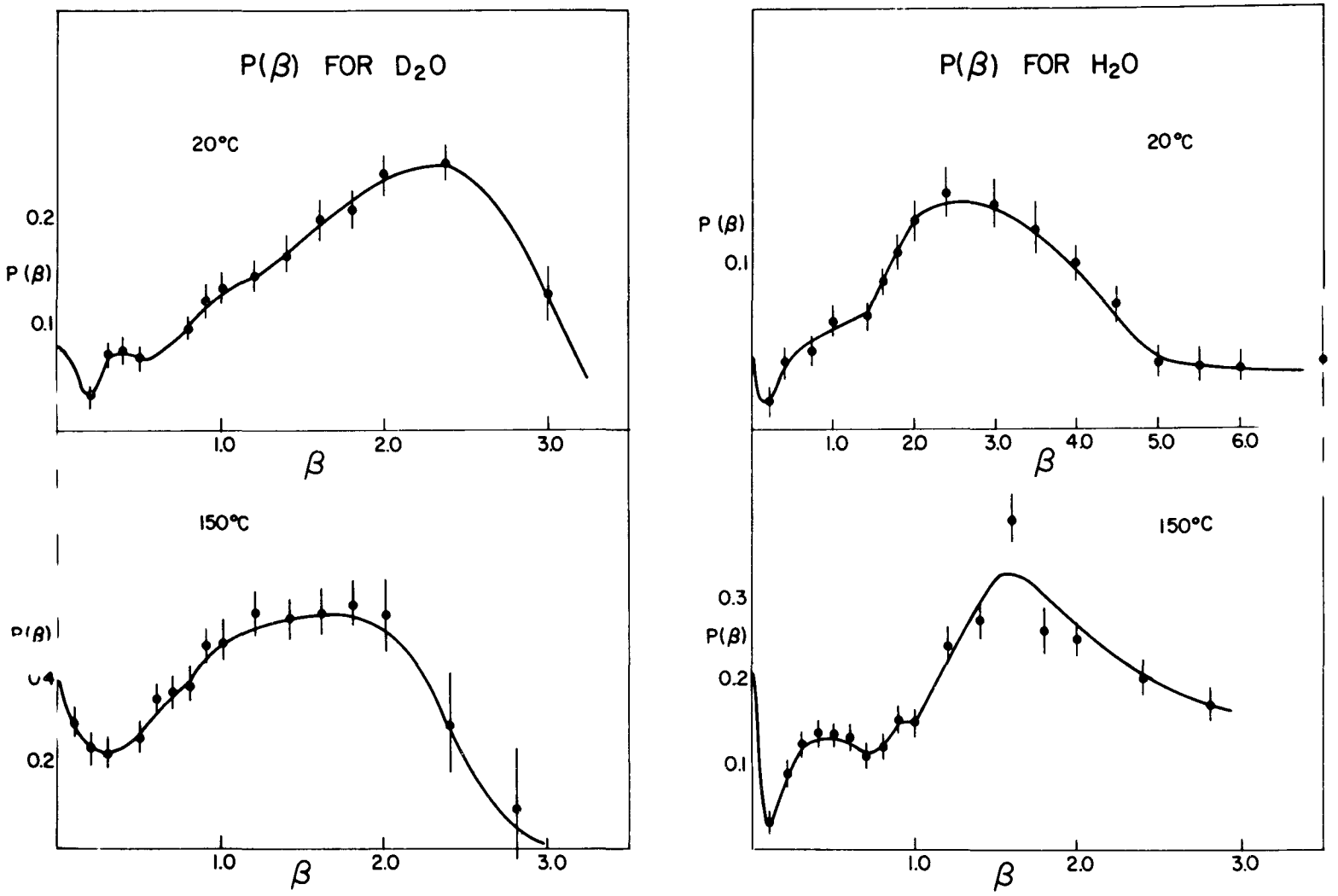
P(β) FOR D2O
20°C
0.2
P(β)
0.1
1.0
2.0
3.0
β
150°C
0.2
1.0
2.0
3.0
β
P(β) FOR H2O
20°C
P(β)
0.1
1.0
2.0
3.0
4.0
5.0
6.0
β
150°C
0.3
P(β)
0.2
0.1
1.0
2.0
3.0
β

Figure 6

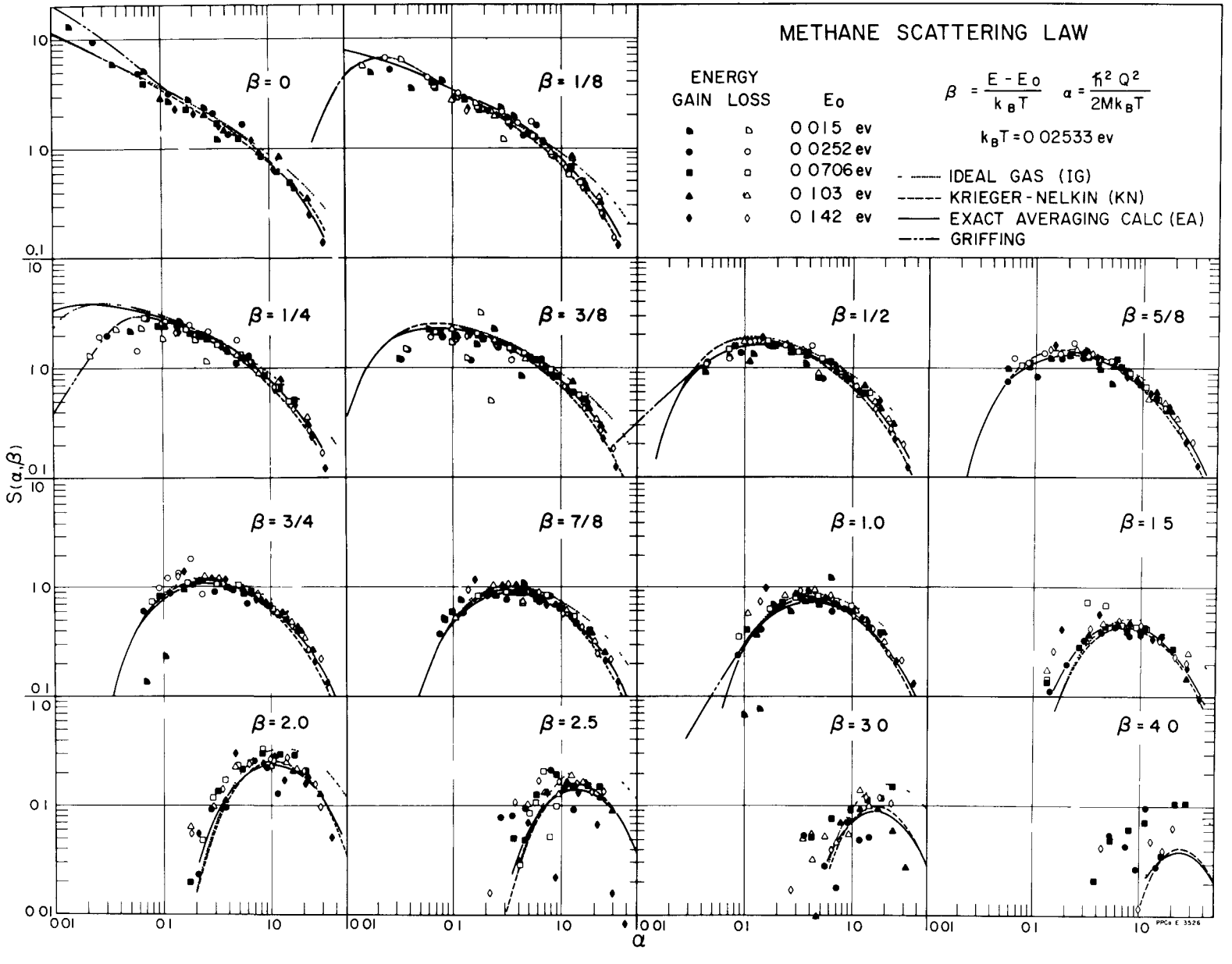
METHANE SCATTERING LAW
ENERGY GAIN LOSS Eo
0 015 ev
0 0252 ev
0 0706 ev
0 103 ev
0 142 ev
$\beta = \frac{E - E_o}{k_B T}$ $\alpha = \frac{\hbar^2 Q^2}{2Mk_B T}$
$k_B T = 0\ 02533$ ev
IDEAL GAS (IG)
KRIEGER-NELKIN (KN)
EXACT AVERAGING CALC (EA)
GRIFFING
β = 0
β = 1/8
β = 1/4
β = 3/8
β = 1/2
β = 5/8
β = 3/4
β = 7/8
β = 1.0
β = 1 5
β = 2.0
β = 2.5
β = 3 0
β = 4 0
S(α,β)
α
PPC-E 3526

Figure 7

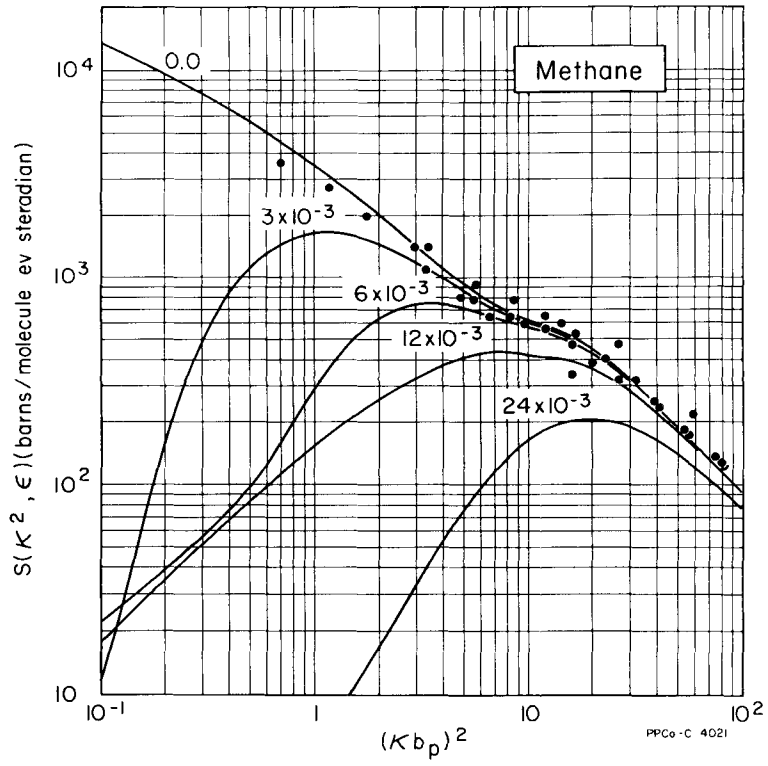
Methane
0.0
3x10-3
6x10-3
12x10-3
24x10-3
10⁴
10³
10²
10
10-1
1
10
10²
S(K², ε)(barns/molecule ev steradian)
(Kbp)²
PPCo-C 4021

Figure 8

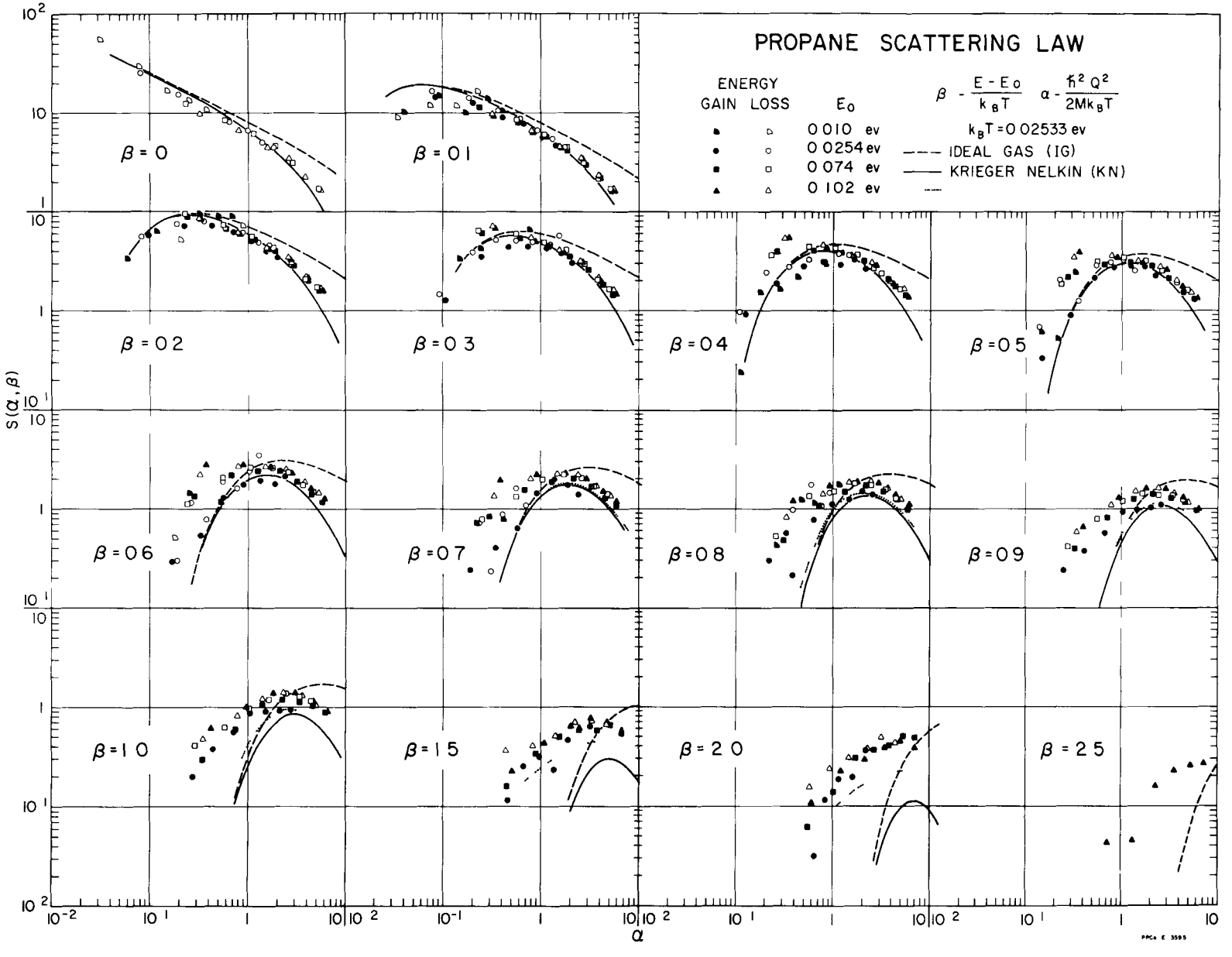
PROPANE SCATTERING LAW
ENERGY
GAIN LOSS
E_0
0 010 ev
0 0254 ev
0 074 ev
0 102 ev
$\beta = \frac{E - E_0}{k_B T}$
$\alpha = \frac{\hbar^2 Q^2}{2Mk_B T}$
$k_B T = 0.02533$ ev
IDEAL GAS (IG)
KRIEGER NELKIN (KN)
$\beta = 0$
$\beta = 01$
$\beta = 02$
$\beta = 03$
$\beta = 04$
$\beta = 05$
$\beta = 06$
$\beta = 07$
$\beta = 08$
$\beta = 09$
$\beta = 10$
$\beta = 15$
$\beta = 20$
$\beta = 25$
$S(\alpha, \beta)$
α

Figure 9

Figure 9 shows data for propane gas, again a relatively simple sample, but more complex than methane. Here a theory, including the quantum effects of vibrations, is necessary to more closely fit the data.

Figure 10 is the data obtained at the MTR for the dispersion relations for beryllium. I show this because, if one had a complete and accurate set of these dispersion relations, and knew the structure factors, one could calculate the Scattering Law for beryllium. Since we did not measure a complete set of these dispersion relations, Figure 11 shows our attempts to theoretically fit the data. If a good fit is achieved, the theory can be used to generate a complete set and calculate the Scattering Law. There are several limited sets of dispersion relations now available for different substances.

What data is available to the reactor physicist for his calculations?

In a paper that I have contributed to this meeting, I have given the reduced partial differential cross sections for eight materials. Besides these I understand that Leonard at Hanford has extensions of the H_2O data, and that Egelstaff has measured uranium and uranium oxide. Brockhouse has presented data as G(r,t) for liquid lead and water. There are also dispersion relations for Ge, Si, Na, Al, graphite and several other materials.

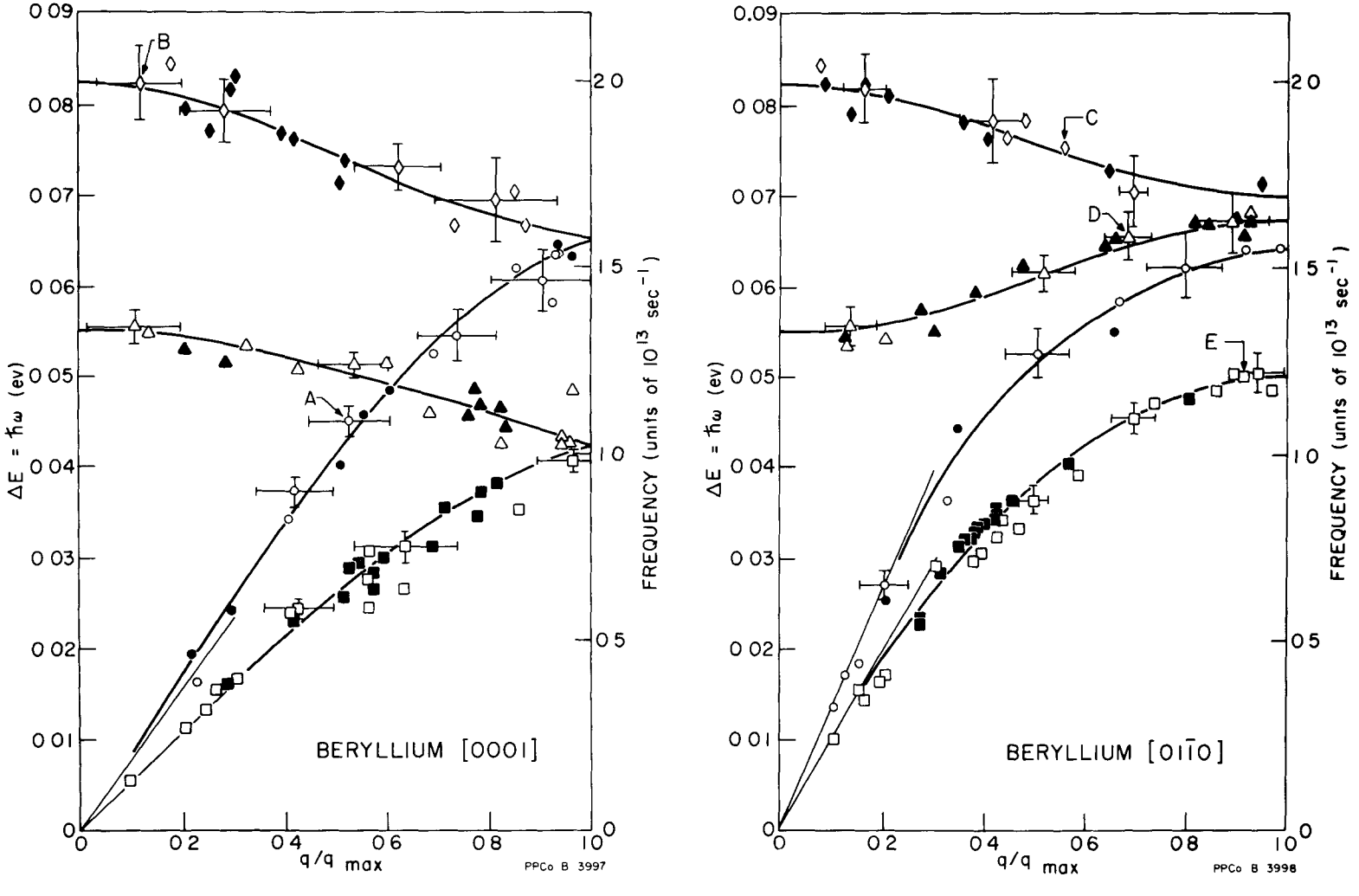
0 09
0 08
0 07
0 06
0 05
0 04
0 03
0 02
0 01
0
ΔE = ħω (ev)
2 0
1 5
1 0
0 5
0
FREQUENCY (units of 10^13 sec^-1)
B
A
BERYLLIUM [0001]
0 2
0 4
0 6
0 8
1 0
q/q max
PPCo B 3997
0.09
C
D
E
BERYLLIUM [01$\bar{1}$0]
PPCo B 3998

Figure 10

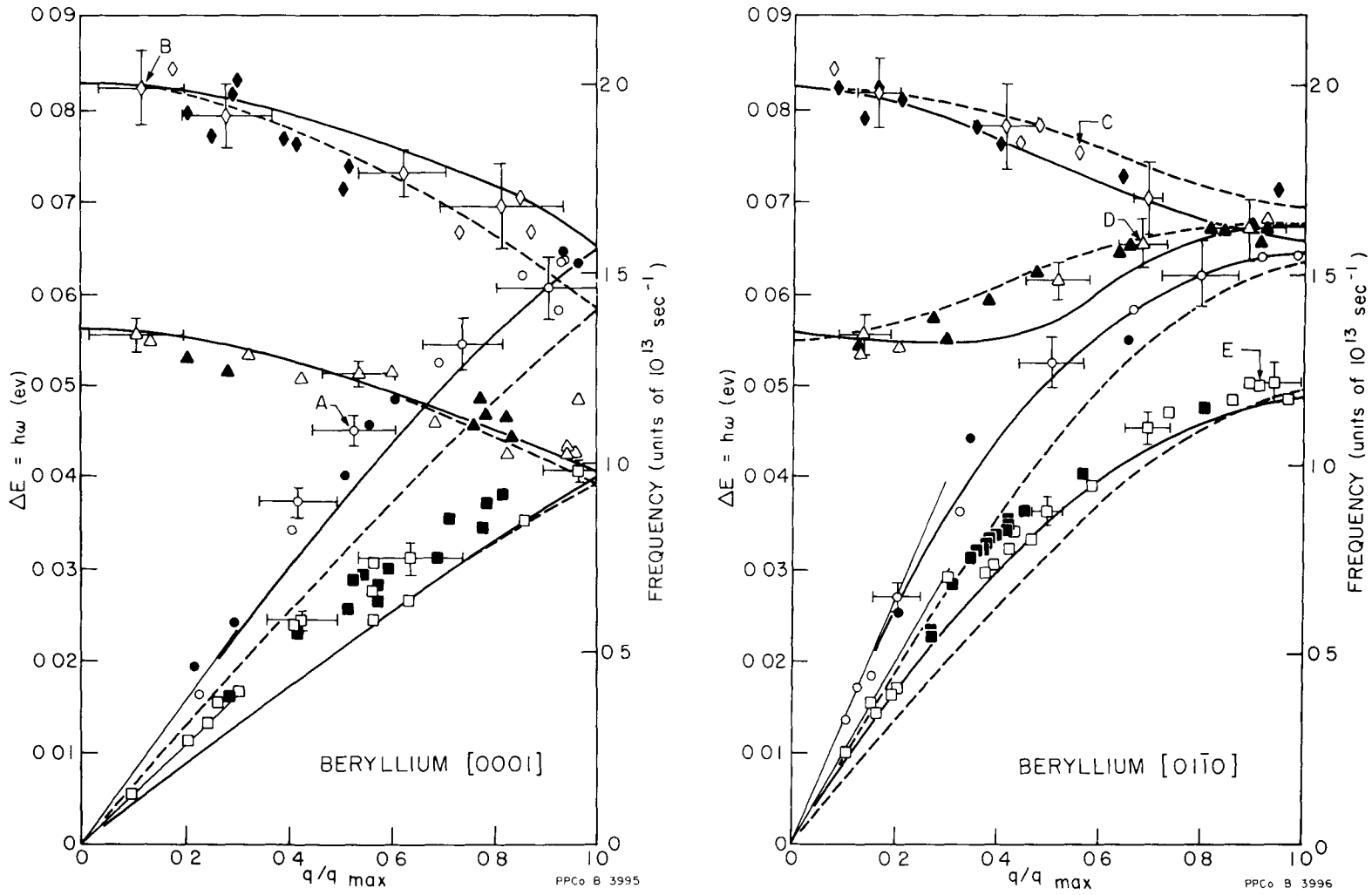
ΔE = hω (ev)
FREQUENCY (units of 10^13 sec^-1)
q/q max
BERYLLIUM [0001]
BERYLLIUM [01$\bar{1}$0]
A
B
C
D
E
PPCo B 3995
PPCo B 3996

Figure 11

REFERENCES

1. R. M. Brugger and J. E. Evans, Nucl. Inst. and Methods 12, 75 (1961).
2. B. N. Brockhouse, IAEA Symposium on "Inelastic Scattering of Slow Neutrons from Solids and Liquids," Vienna (1961), pp. 113.
3. P. A. Egelstaff and P. Schofield, Nucl. Sci. and Eng. 12, 250-260 (1962).
4. G. H. Vineyard, Phys. Rev. 110, 999 (1958); Rahman, Singwi, Sjolander, Phys. Rev. 122, 9 (1961).
5. G. W. Griffing, Phys. Rev. (submitted for publication).
6. Schmunk, Brugger, Randolph, and Strong, Bull. Am. Phys. Soc. 7, 236 (1962).

COMPILATION OF REDUCED SLOW NEUTRON PARTIAL DIFFERENTIAL SCATTERING CROSS SECTIONS

By

Robert M. Brugger
Phillips Petroleum Company

ABSTRACT

In a previous compilation,[1] the slow neutron scattering data were presented in the dimensionless form of the Egelstaff Scattering Law $S(\alpha,\beta)$.[2] This compilation has been criticized because the data are not as easily compared with other sets of data or with theory as would be the case if the data were in the customary units. Also the cross section σ_b used in converting the partial differential cross section to $S(\alpha,\beta)$ and the mass M used in converting the momentum change to α are sometimes arbitrarily selected. In the present compilation, an attempt has been made to present the data in a form which satisfies the wishes of the critics while still preserving the valuable simplifications introduced by Egelstaff[2] and Schofield.[3] In this compilation the magnitude of the scattering effect is presented as the reduced partial differential cross section $S(|\kappa|,\hbar\omega)$ where

$$S(|\kappa|,\hbar\omega) = \frac{k_o}{k} e^{+\frac{\hbar\omega}{2K_B T}} \frac{d^2\sigma}{d\Omega\, dE}$$

and the variables are the magnitude of the momentum transfer $|\vec{\kappa}|$ in reciprocal angstroms and energy change $\hbar\omega$ in ev. The available experimental scattering data are presented as smoothed curves.

COMPILATION OF REDUCED SLOW NEUTRON PARTIAL DIFFERENTIAL SCATTERING CROSS SECTIONS

By

Robert M. Brugger

I. INTRODUCTION

Data covering a wide range of parameters for the inelastic scattering of slow neutrons from elements and compounds are becoming available and it appears that a good form of presentation of these data is as a reduced partial differential cross section. This compilation presents smoothed curves of the available experimental reduced partial differential scattering cross sections. It is hoped that this compilation will be a convenience for reactor physicists when using the information in reactor calculations and for physicists when comparing experimental results to determine the basic physical phenomena.

No attempt is made to evaluate the precision of the measurements; the reader should refer to the original publications and make his own evaluation. In most cases the smooth curves were drawn by the original experimenter. No attempt has been made to re-evaluate the many sets of inelastic scattering data that have not been converted to the reduced cross section by the experimenter and will yield only a few points of the reduced cross section at best.

II. THE REDUCED PARTIAL DIFFERENTIAL CROSS SECTION

The usual experimentally measured values and the ones desired by reactor physicists for reactor calculations are the partial differential cross sections

$$\frac{d^2\sigma}{dE\ d\Omega}(E_o, E, \theta, T, P)$$

where E_o is the incident neutron energy, E is the final neutron energy, θ is the scattering angle in the laboratory system, T is the temperature of the sample and P indicates the physical state of the sample. For gases, liquids or polycrystalline solids it has been shown that this function of five variables can be reduced to a four variable function by applying the condition of detailed balance.[2,3] Thus

$$\frac{d^2\sigma}{dE\ d\Omega} = \frac{k}{k_o} e^{-\frac{\hbar\omega}{2K_B T}} S(|\vec{\kappa}|, \hbar\omega, T, P)$$

where k_o is the wave number before scattering, k is the wave number after scattering, K_B is the Boltzman constant, $|\vec{\kappa}|$ is the magnitude of the momentum transfer where $\hbar|\vec{\kappa}| = \hbar|\vec{k}_o - \vec{k}| = \hbar(k_o^2 + k^2 - 2k_o k\cos\theta)^{1/2} = (2[2E_o + \hbar\omega - 2[E_o(E_o+\hbar\omega)]^{1/2}\cos\theta])^{1/2}$, and $\hbar\omega = \hbar^2(k^2 - k_o^2)/2m$. The neutron mass is m. In this form $\hbar\omega$ is positive for neutron energy gain. $S(\kappa, \hbar\omega)$ is in units of barns per electron volt steradian molecule, while κ is in units of reciprocal angstroms and $\hbar\omega$ is in units of electron volts.

The advantages of using $S(\kappa, \hbar\omega)$ rather than $d^2\sigma/d\Omega\ dE$ are that 1) there is one fewer variable, 2) it guarantees a maxwellian distribution of flux in a large homogeneous medium because of the treatment of detailed balance and 3) $d^2\sigma/dE\ d\Omega$ may be generated at energies and angles other than those actually measured in the determination of $S(\kappa, \hbar\omega)$.

III. PRESENTATION

The reduced partial differential cross section curves are arranged in three sections; 1) inorganic compounds, 2) organic compounds, and 3) theoretical curves. The arrangement of compounds within sections 1 and 2 are as in the "Handbook of Physics and Chemistry". Sets of curves for each compound are in increasing order of temperature.

The reduced partial differential cross sections are presented as a set of smoothed curves for discrete values of $\hbar\omega$ as a function of $|\vec{\kappa}|$. Each curve is indexed by a value of ϵ ; the magnitude in ev of the $\hbar\omega$ steps are obtained from the simple relation between ϵ and $\hbar\omega$ in the title of each graph. The short reference notation corresponds to a complete reference at the end of the paper.

IV. REFERENCES TO TEXT

1. R. M. Brugger, U. S. Atomic Energy Commission Report IDO 16699 (1961).

2. P. A. Egelstaff, AERE-R-3622, 1961 and IAEA Symposium on "Inelastic Scattering of Neutrons in Solids and Liquids", Vienna, 1960, papers IS/P17, IS/P10, IS/P7.

3. P. Schofield, Phys. Rev. Letters $\underline{4}$ 239 (1960).

—— Cocking 1961

Beryllium

Be

Temperature = 20° C

$\epsilon = \hbar\omega / 0\ 0252$ ev

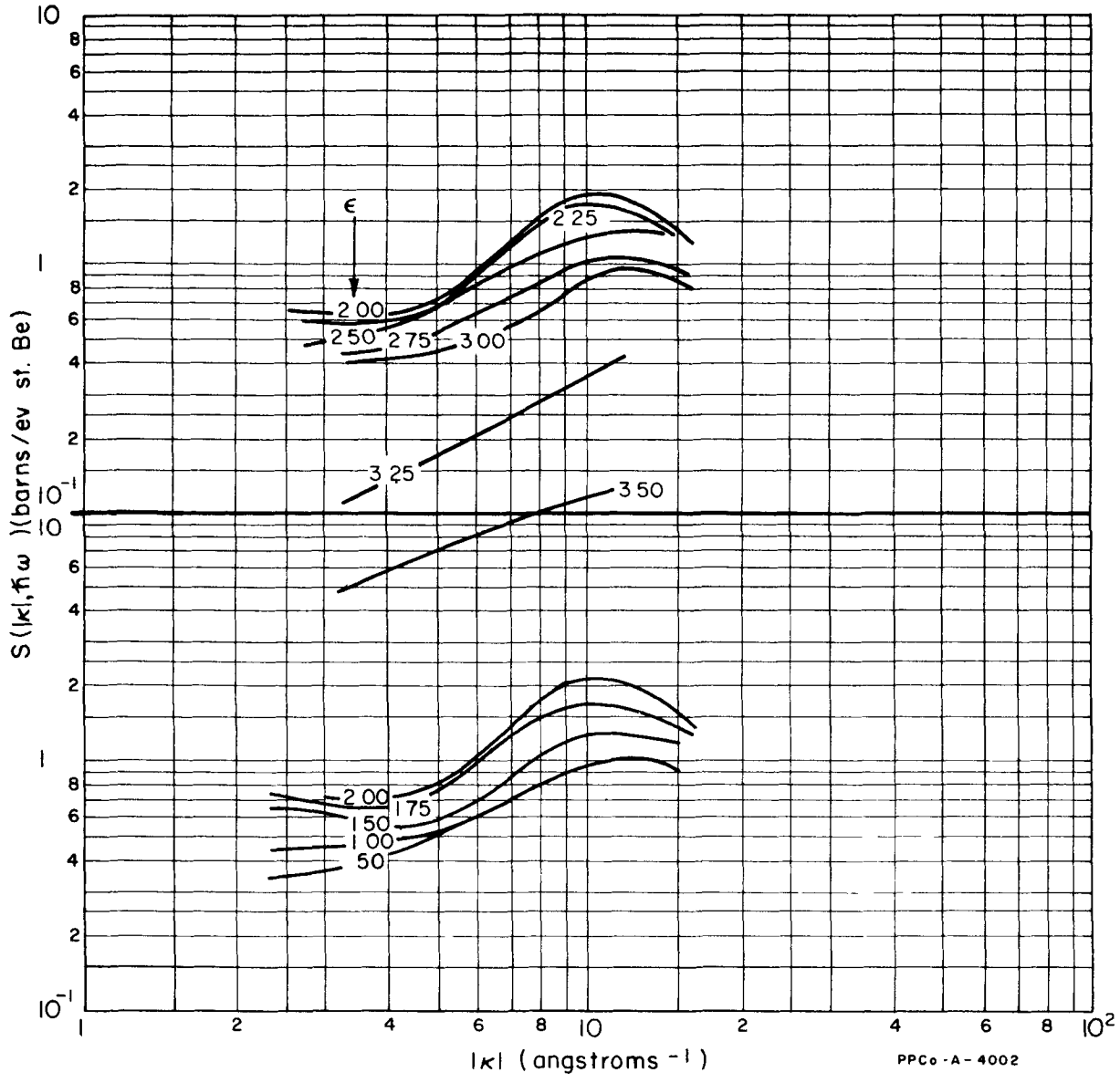

— Cocking-1961

Beryllium Oxide

BeO
Temperature = 20°C
$\epsilon = \hbar\omega / 0.0252$ ev

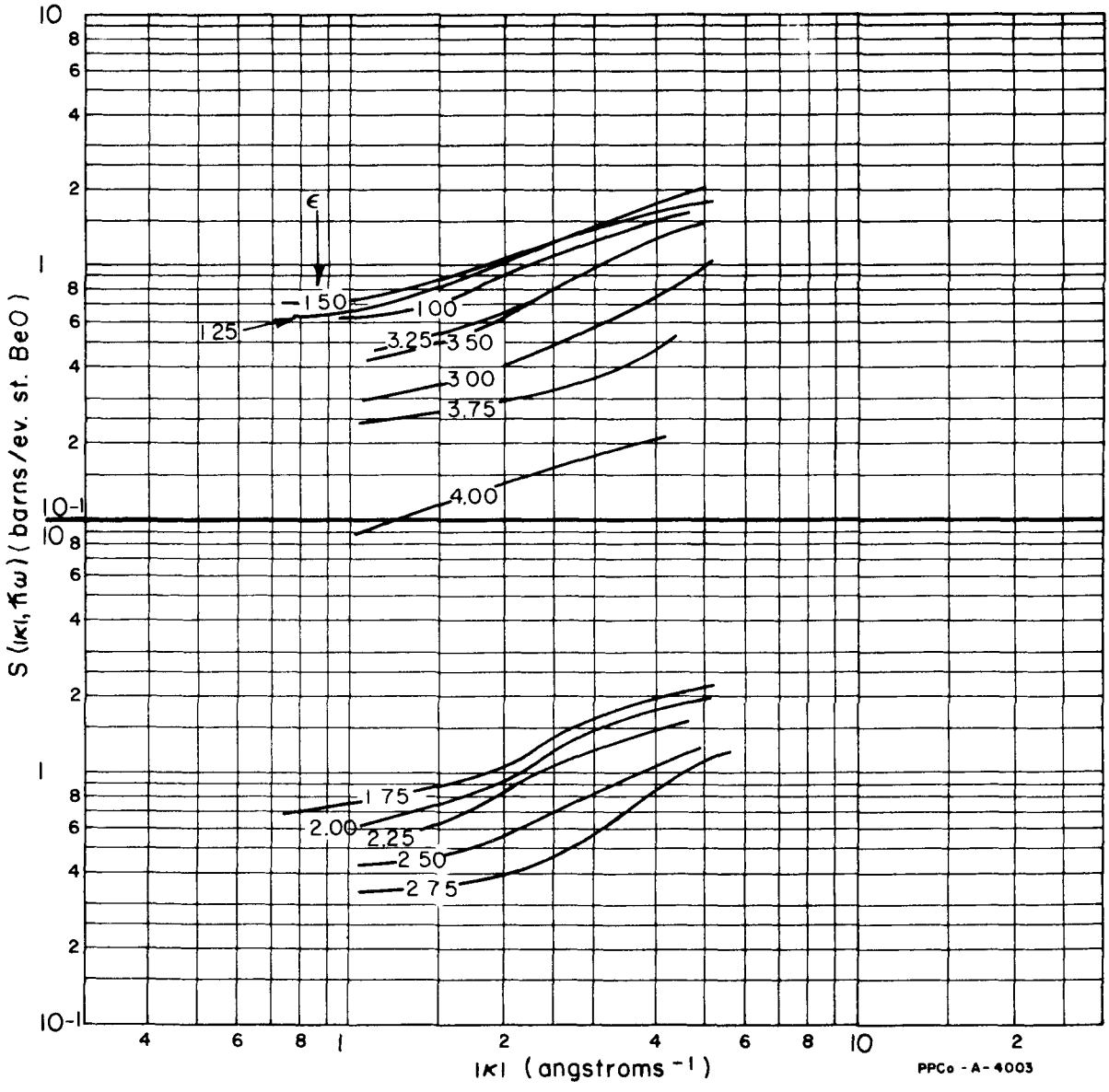

— Egelstaff et al 1960a

Graphite

C

Temperature = 21° C

$\epsilon = \hbar\omega / 0.0253$ ev

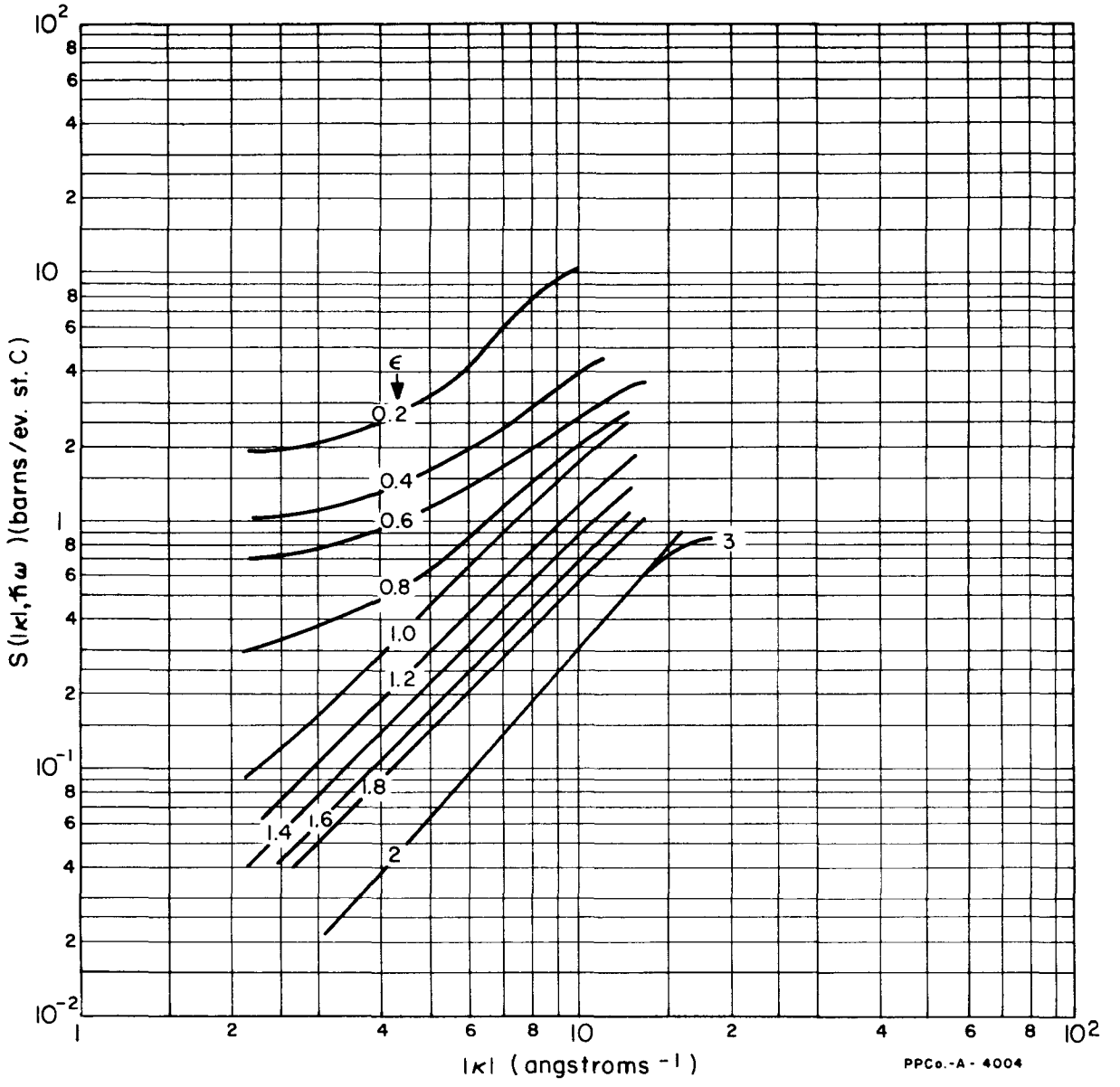

—Egelstaff -1962

Graphite

C

Temperature = 300° - 400° C

$\epsilon = \hbar\omega / 0.0536$ ev

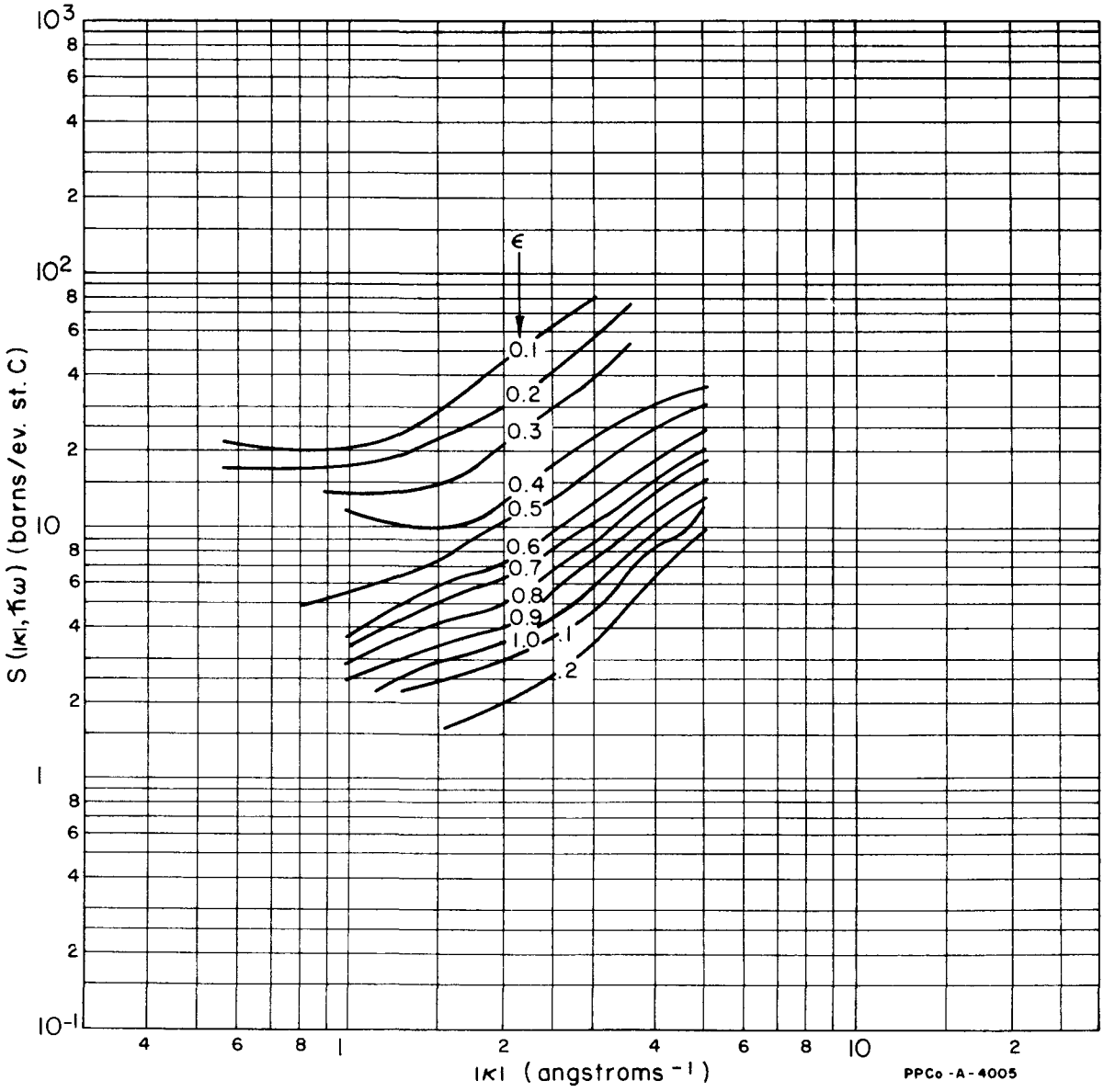

— Egelstaff et al. 1960a

Graphite

C

Temperature = 600°C

$\epsilon = \hbar\omega / 0.0752$ ev

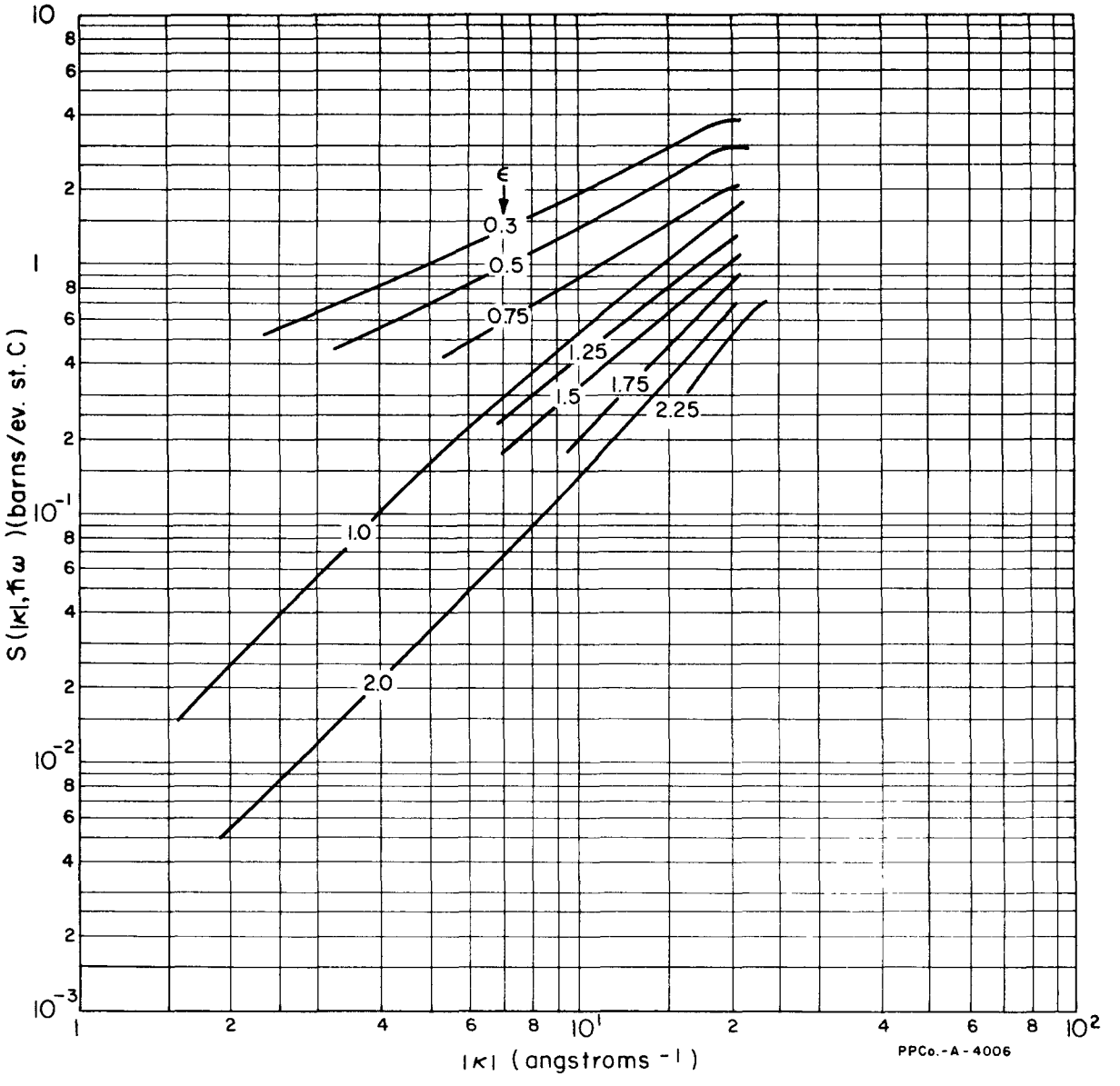

—Egelstaff et al - 1960 b

Water

H_2O

Temperature = 20° C

$\epsilon = \hbar\omega / 0.0252$ ev

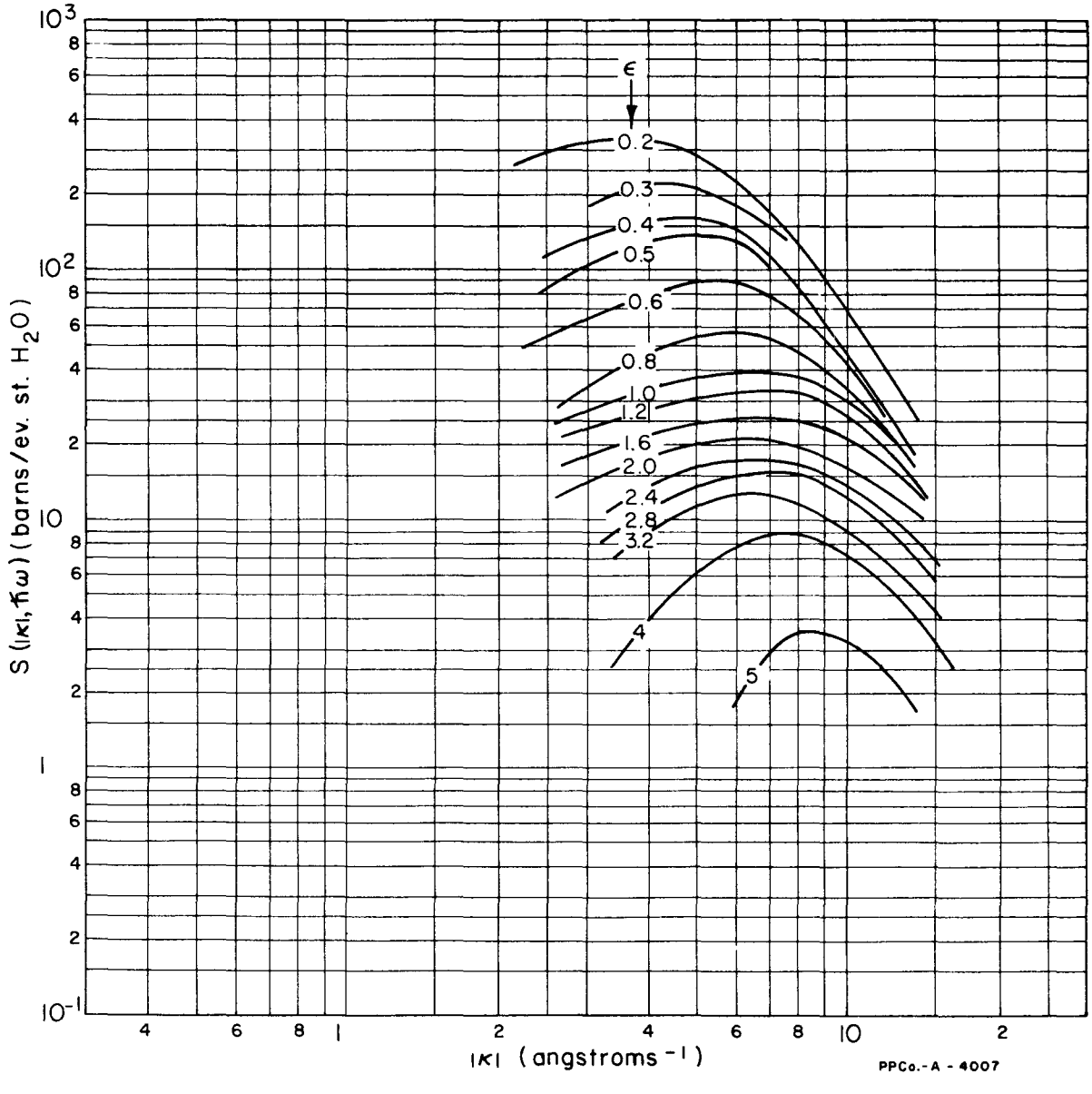

— Cocking - 1961

Water

H_2O

Temperature = 150° C

Pressure = 70 psi

$\epsilon = \hbar\omega / 0.0364$ ev

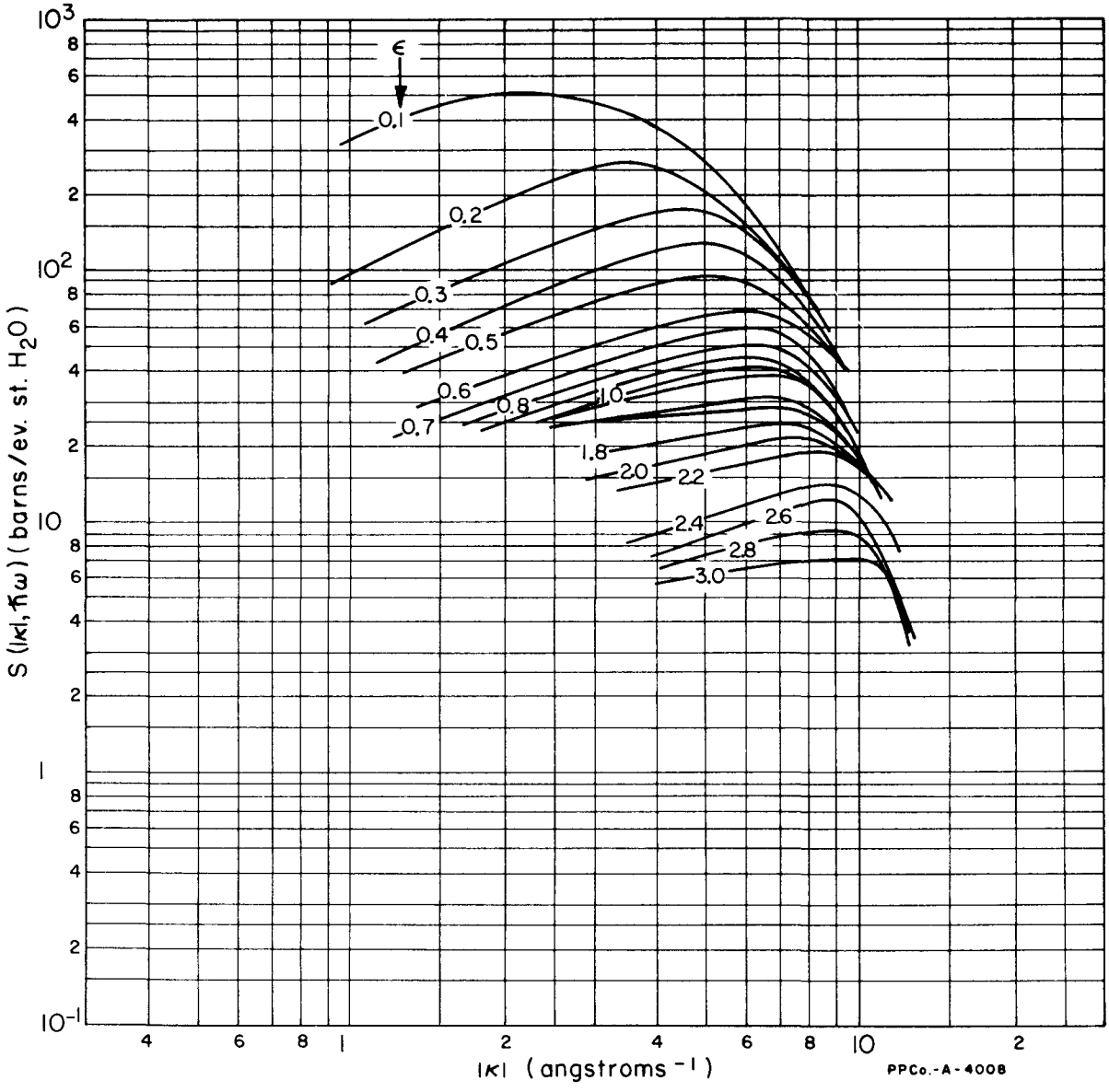

— Egelstaff 1960 b

Heavy Water

D_2O

Temperature = 20° C

$\epsilon = \hbar\omega / 0.0252$ ev

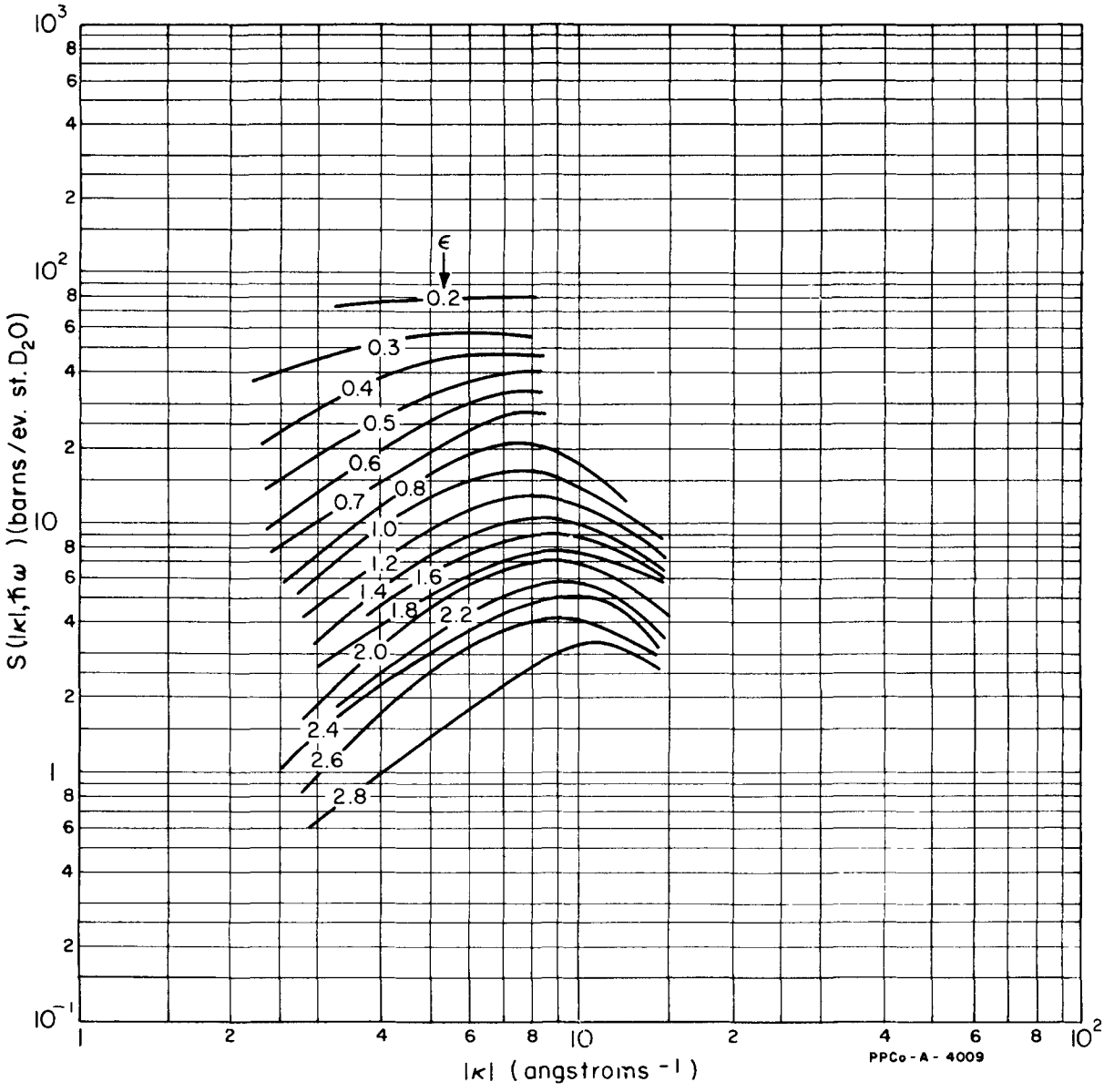

— Cocking 1961

Heavy Water

D_2O

Temperature = 150° C

Pressure = 70 psi

$\epsilon = \hbar\omega / 0\ 0364$ ev

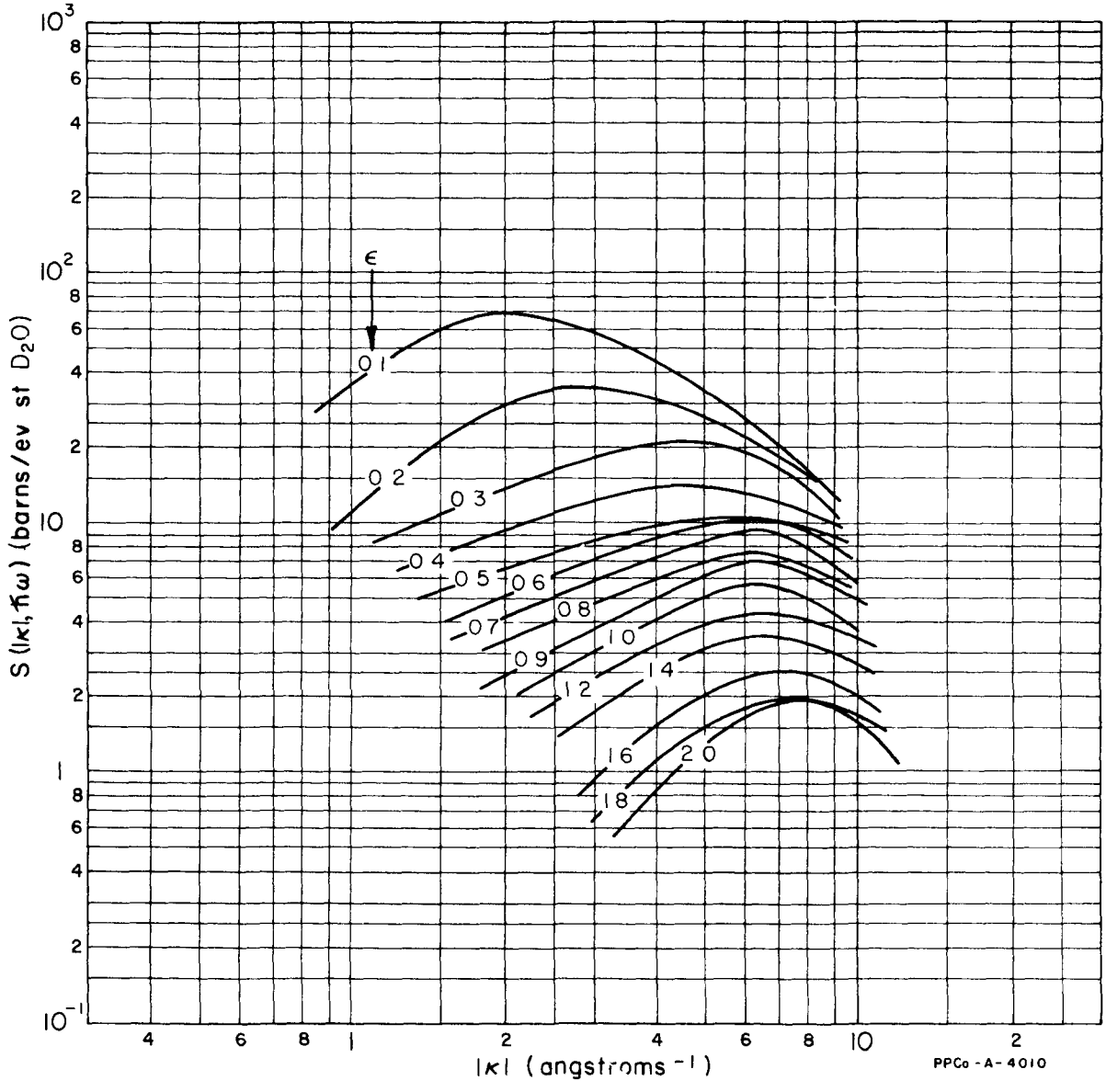

— Randolph et al 1961

Methane

CH_4

Temperature = 21° C

Pressure < 65 psig

$\epsilon = \hbar\omega / 0\ 0253$ ev

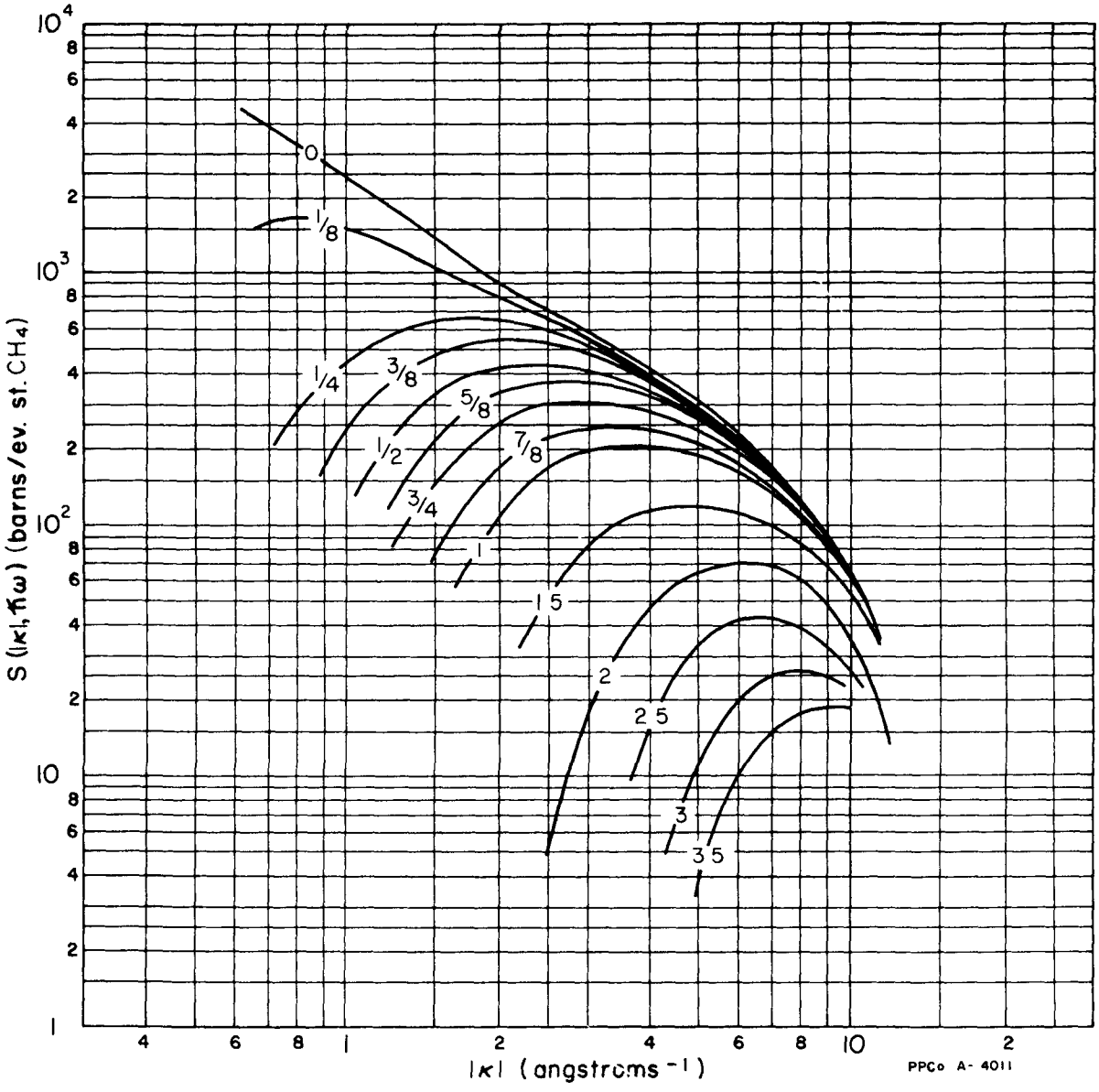

— Strong et al. 1962

Propane

$CH_3\ CH_2\ CH_3$

Temperature = 21°C

Pressure < 50psig

$\epsilon = h\omega / 0.0253$ ev

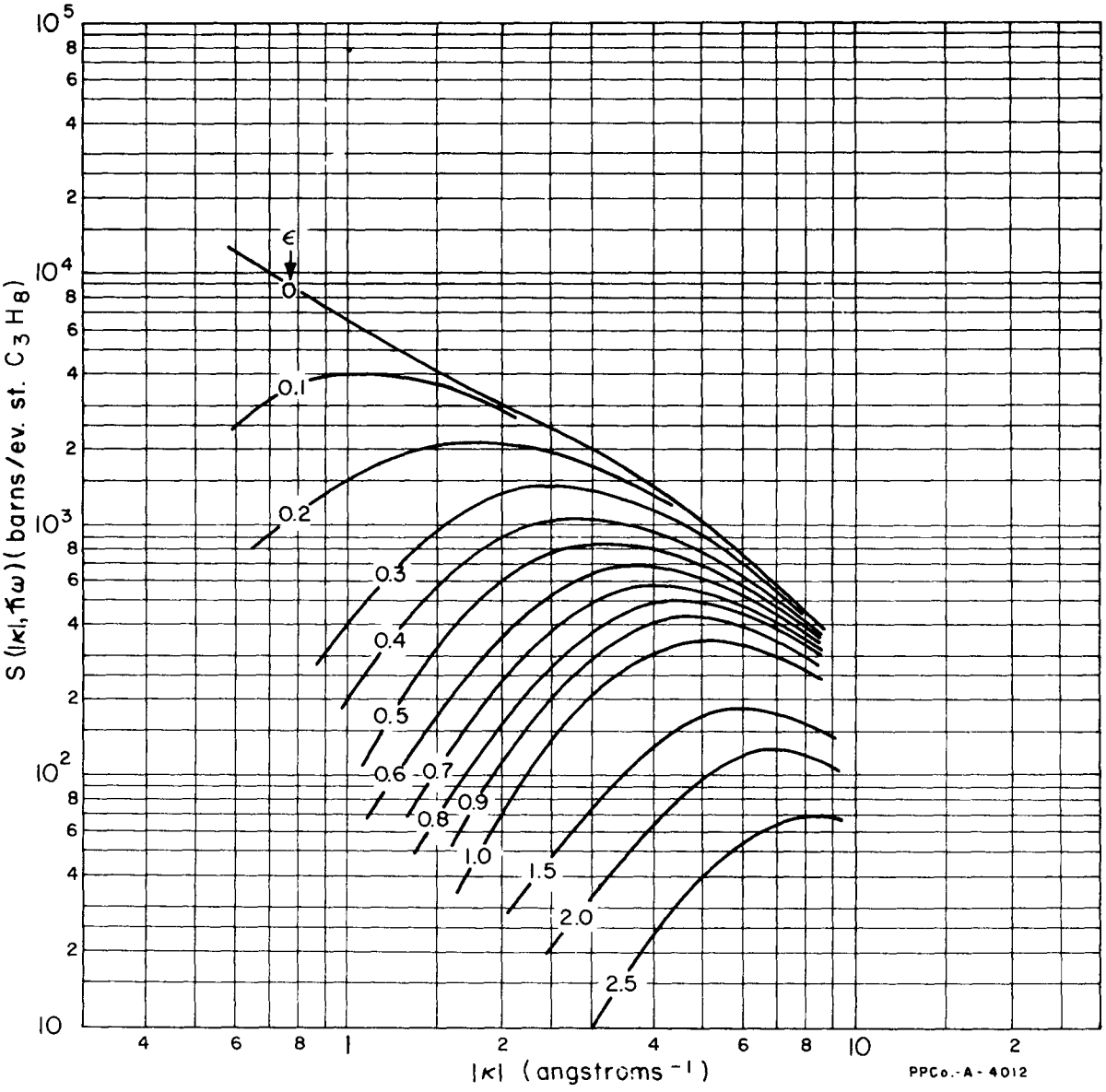

—Brugger-1962

O-Terphenyl

$(C_6H_5)_2C_6H_4$
Temperature = 21° C
$\epsilon = \hbar\omega / 0.0253$ ev

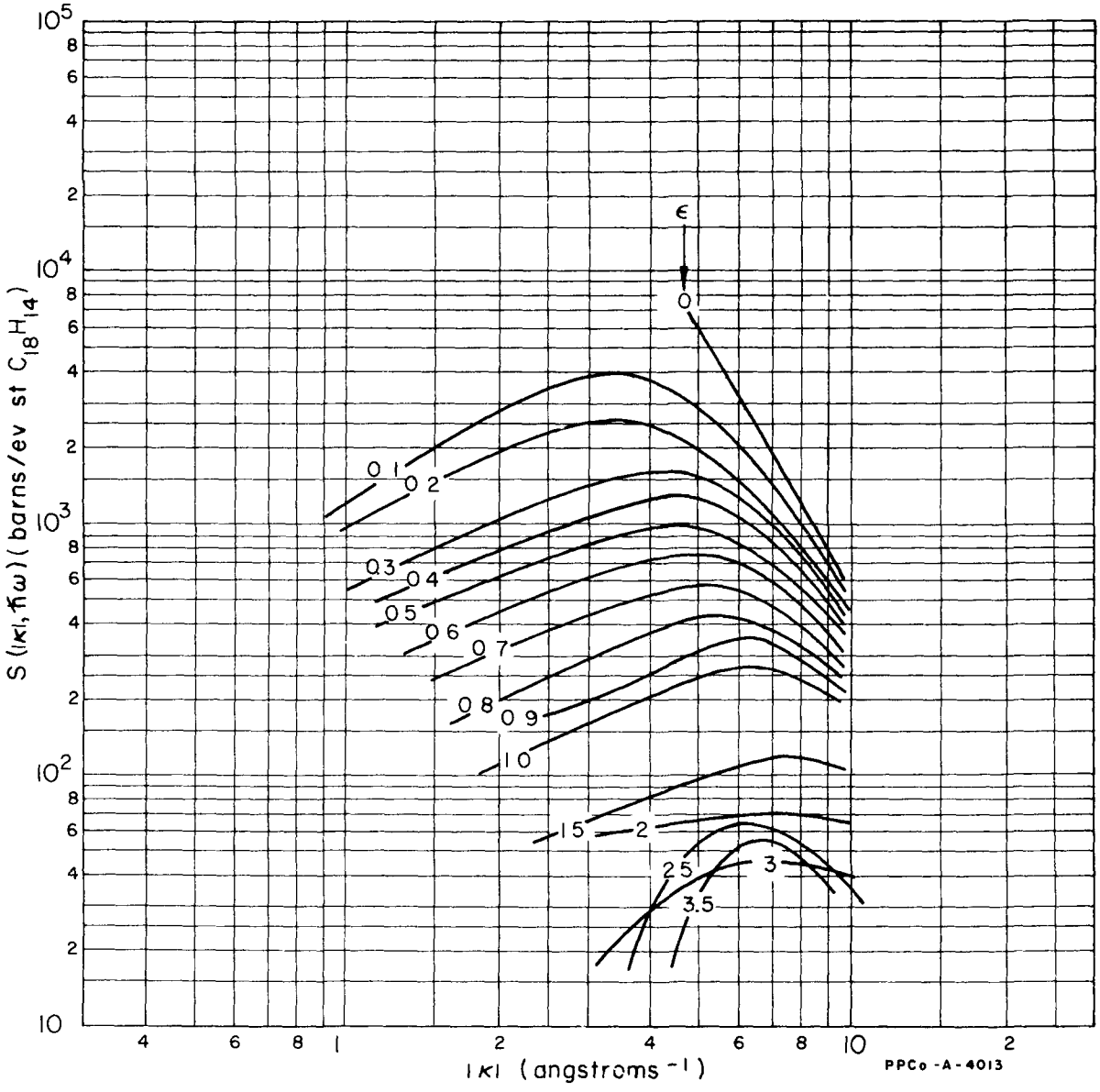

— Brugger-1962

M-Terphenyl

$(C_6H_5)_2C_5H_4$

Temperature = 21°C

$\epsilon = \hbar\omega / 0.0253$ ev

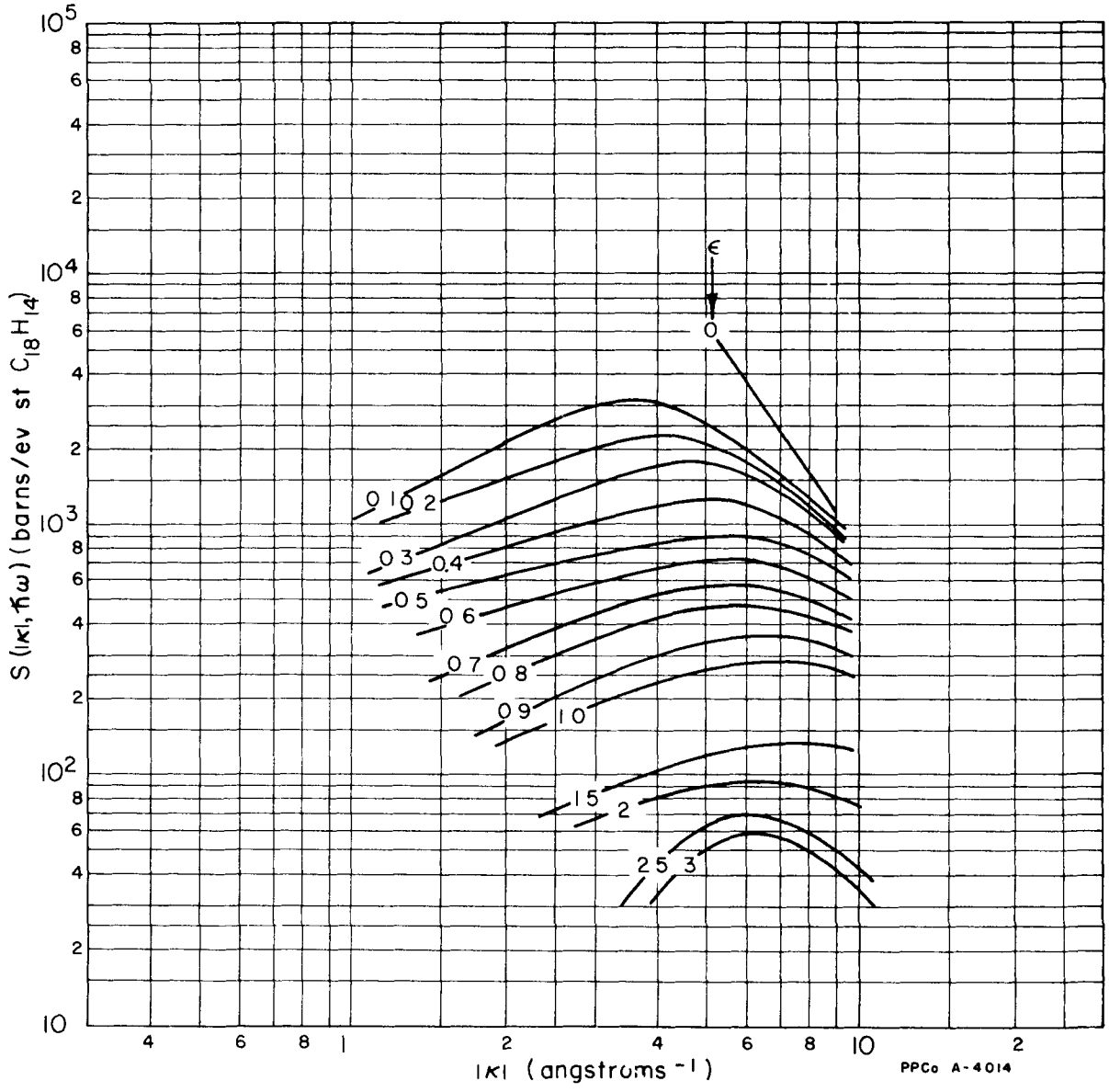

—— Brugger-1962

P-Terphenyl

$(C_6H_5)_2C_6H_5$

Temperature = 21° C

$\epsilon = \hbar\omega / 0.0253$ ev

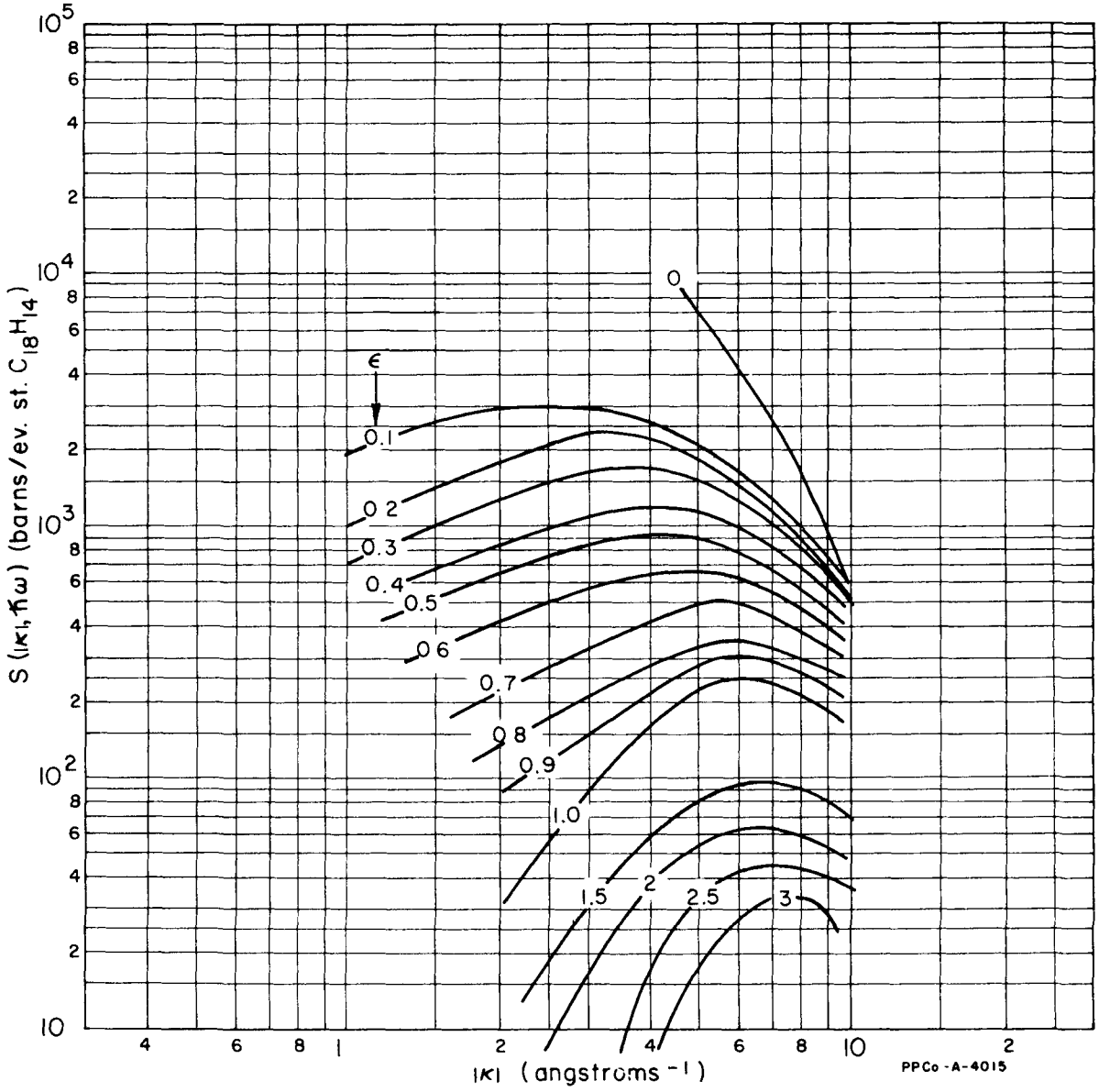

— Brugger 1962

Santowax-R

$(C_6H_5)_2\ C_6H_4$

Temperature = 21° C

$\epsilon = \hbar\omega / 0.0253$ ev

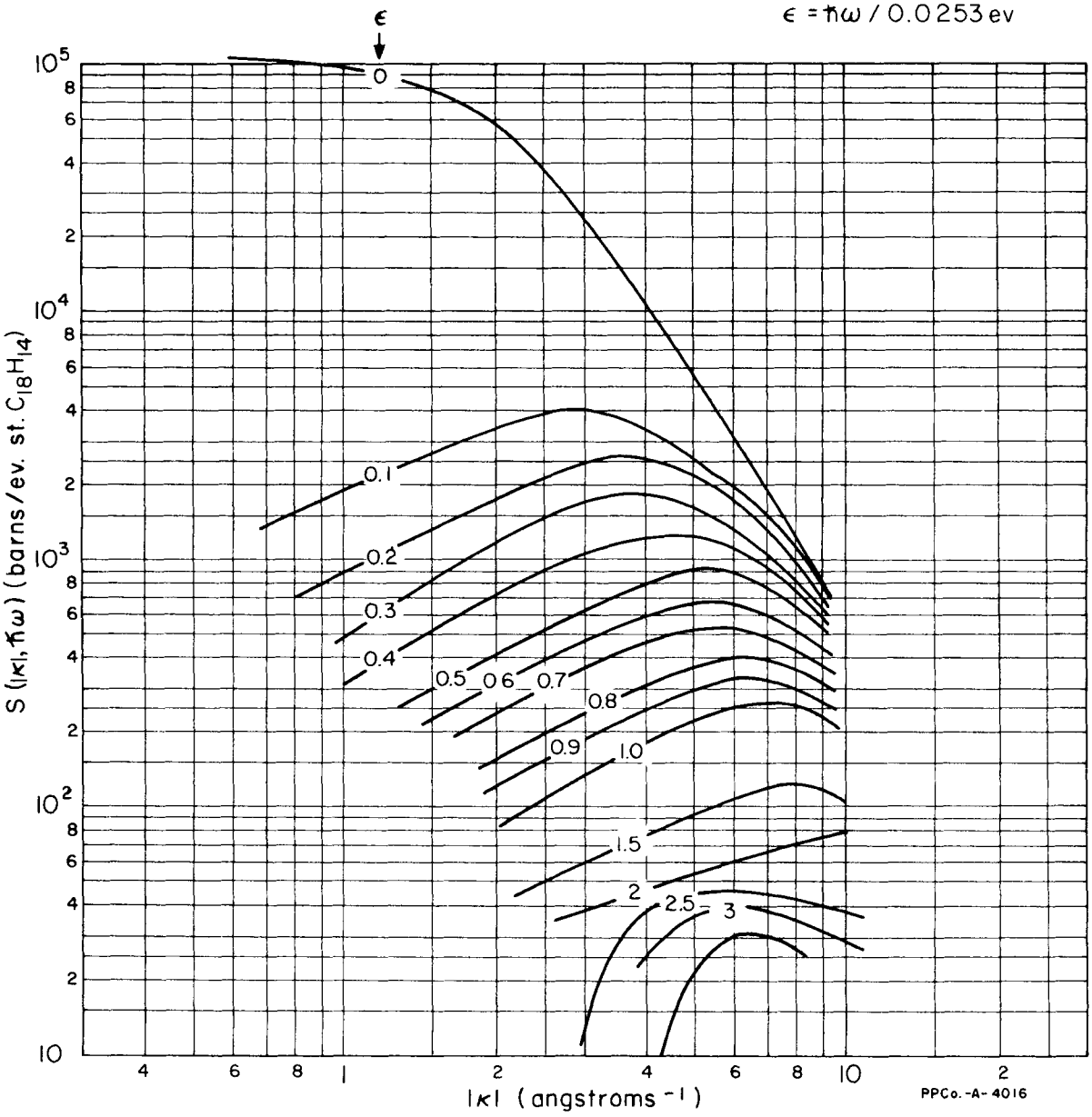

— Brugger 1962

Santowax - R

$(C_6H_5)_2\ C_6H_4$

Temperature = 207° C

$\epsilon = \hbar\omega / 0.0414$ ev

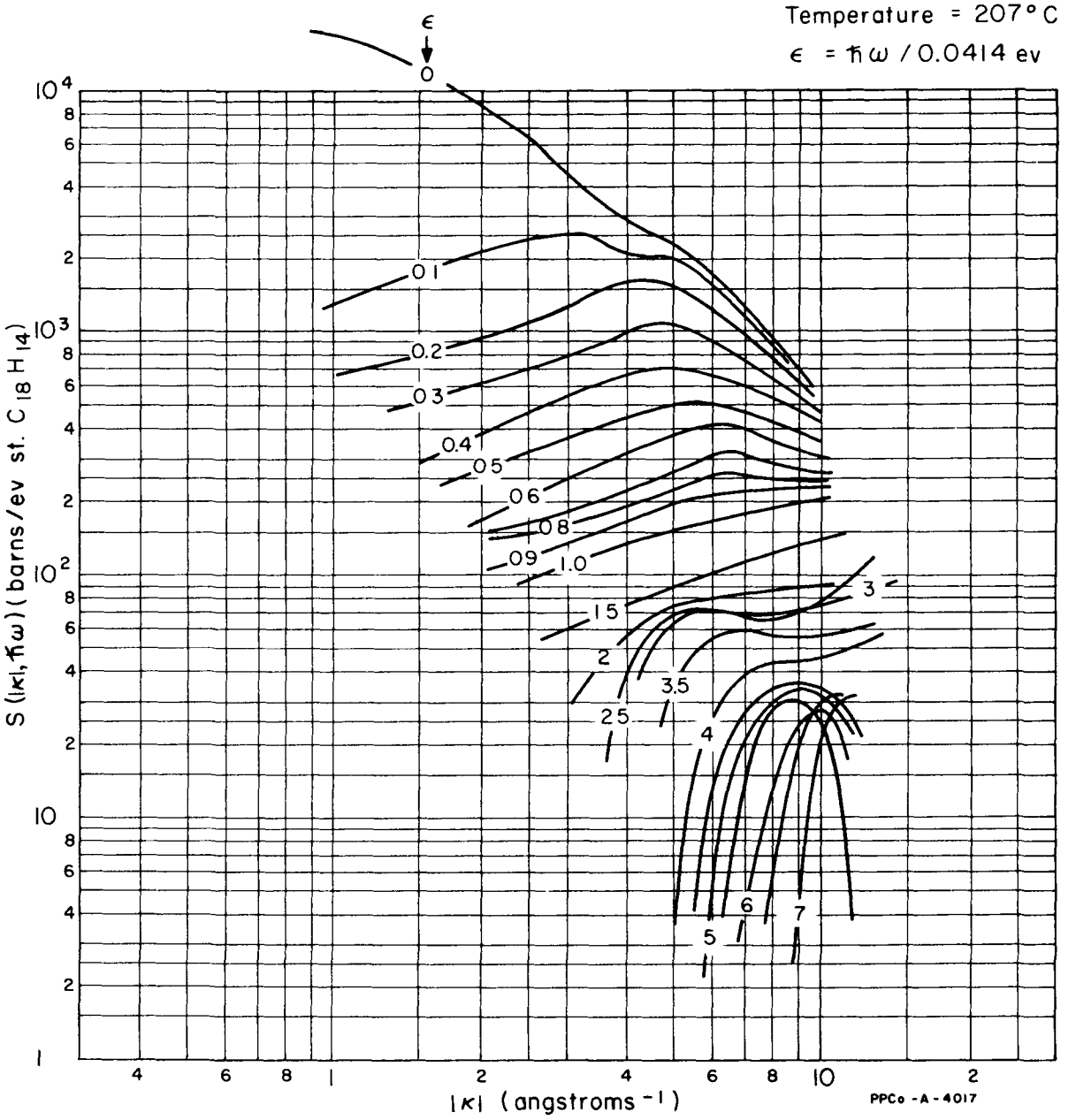

— Brugger 1962

Santowax - R

$(C_6H_5)_2\ C_6H_4$

Temperature = 267°C

$\epsilon = \hbar\omega/0.0467$ ev

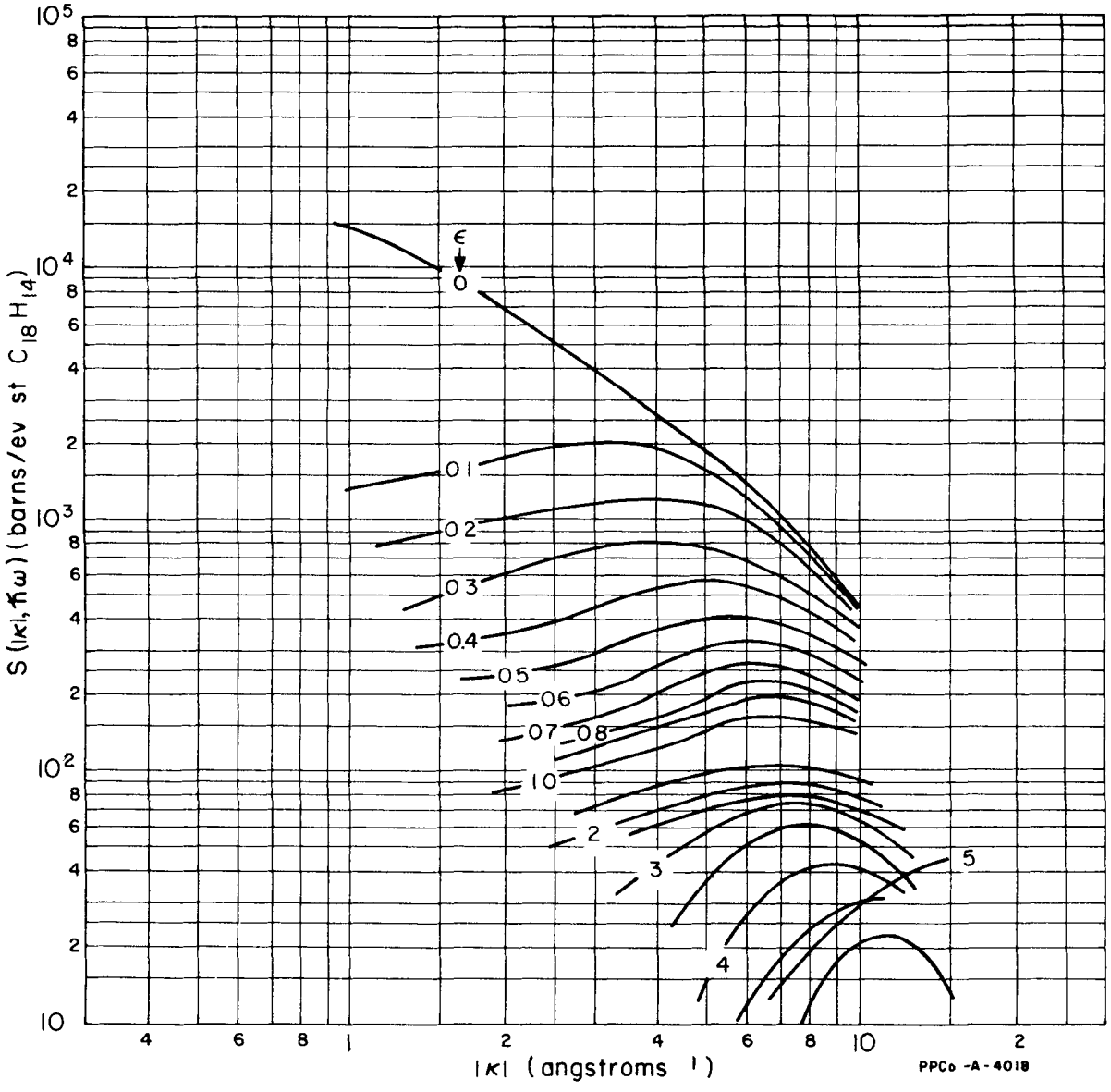

Ideal Gas

$$S(\alpha,\beta) = \left(\frac{1}{\sqrt{4\pi\alpha}}\right) e^{-\frac{1}{4\alpha}(\alpha^2+\beta^2)}$$

$$S(\alpha,\beta) = \frac{4\pi}{\sigma_b} K_B T S(|K|,\hbar\omega)$$

$$\alpha = \frac{\hbar^2 K^2}{2MK_BT} \qquad \beta = \frac{\hbar\omega}{2K_BT}$$

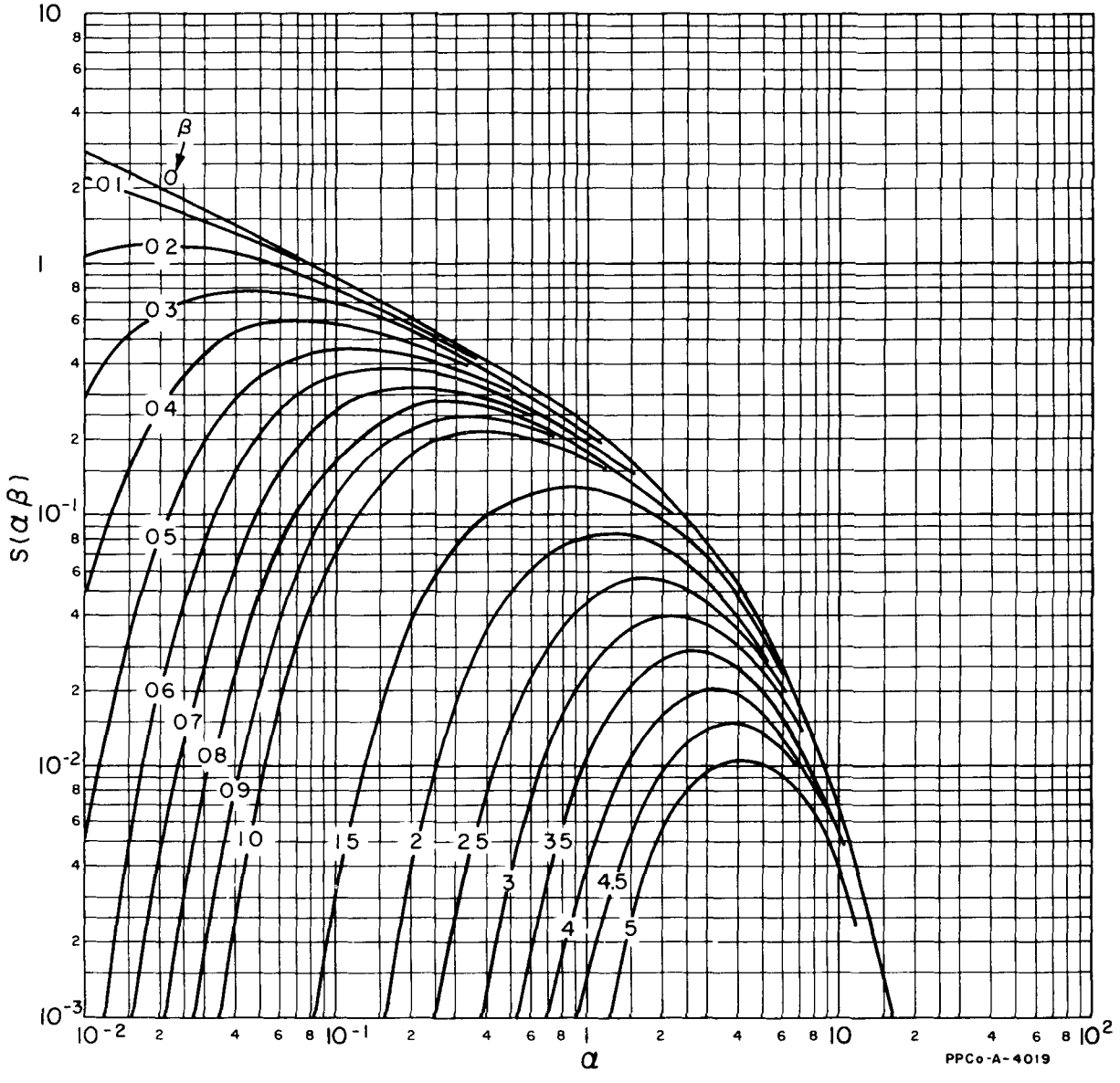

REFERENCES TO REDUCED CROSS SECTION CURVES

Brugger, 1962	R. M. Brugger, Physical Review 126 (to be published) (1962)
Cocking, 1961	S. J. Cocking, European-American Nuclear Data Committee Symposium on Neutron Time-of-Flight Methods, Saclay pp 251 (1961).
Egelstaff, et.al 1960a	P. A. Egelstaff and S. J. Cocking, International Atomic Energy Agency Symposium on Inelastic Scattering of Neutrons in Solids and Liquids, Vienna, paper IS/8.
Egelstaff, et.al 1960b	Egelstaff, Cocking, Royston and Thorson, International Atomic Energy Agency Symposium on Inelastic Scattering of Neutrons in Solids and Liquids, Vienna, paper IS/10 (1960).
Egelstaff 1962	P. A. Egelstaff private communications
Randolph, et.al 1961	Randolph, Brugger, Strong and Schmunk Phys. Rev. 124 460 (1961).
Strong, et.al 1961	Strong, Marshall, Brugger and Randolph Phys. Rev. 125 (1962) (to be published).

The Scattering Law for Light and Heavy Water at 20°C and 150°C

*B.C. Haywood

I.M. Thorson

Atomic Energy of Canada Limited

Chalk River, Ontario

Presented to BNL Conference on Neutron Thermalization

April 30, 1962.

*On attachment from AERE, Harwell

Abstract

The thermal neutron scattering law for both light and heavy water, at 20°C and 150°C have been measured using the phased-rotor neutron velocity selector and time of flight apparatus at the Chalk River NRU reactor. The experimental results are reported and an initial estimate of Egelstaff's $p(\beta)$ function for use in the calculation of a complete scattering law for reactor physics purposes is derived.

I. Introduction

The differential neutron scattering cross section for any material is a function of the detailed arrangement and motions of its constituent atoms[1][2]. Sufficient data have not been available in the past to make adequate estimates of these cross sections for reactor physics purposes, but various crude models for the more important moderating materials have been devised and used with some success. The success of these models can be attributed to the inherent averaging done in most reactor calculations, and the fundamental constraints applied to these averages often make the detailed shape of these cross sections unimportant. The adequacy of the models often breaks down however when the scattering of neutrons of thermal or near thermal energies are important. This is the region of momentum and energy transfer for which it is possible to measure these cross sections.

In this paper recently measured partial differential scattering cross sections are presented for light and heavy water at 20°C and 150°C for energy transfers up to 0.15 eV obtained using the Chalk River phased rotor time-of-flight spectrometer. The range of momentum transfer covered is approximately 2 to 50 per A° and is much wider than that reported for any other experiments[3][4]. For most reactor physics calculations these results must be extrapolated to larger momentum and energy transfer ranges and a smoothed function obtained.

Egelstaff has suggested[5][6] basing a range of models on a generalized frequency distribution $p(\beta)$ and first approximations to this function are derived from the experimental data. Using this $p(\beta)$ elaborate computer programmes are now available[7] to

generate differential cross sections over the entire range of momentum and energy change.

It is convenient to present results in a form which involves only the energy and momentum transferred during the interaction, and a function of these variables has been described by Van Hove[1]. In this formalism the scattering law $S'(\omega\underline{Q})$ is defined for a system made up of one type of atom by the relationship

$$\frac{d^2\sigma}{d\Omega dE} = \frac{\sigma_f\left(\frac{A+1}{A}\right)^2}{4\pi} \frac{E}{E_o} S'(\omega\underline{Q}) \qquad \ldots \quad (1)$$

where σ_f is the free atom cross section for the atoms of atomic weight A,

E_o and E are the initial and final neutron energies,

$\hbar\omega$ and $\hbar\underline{Q}$ are the energy and momentum transfers in the interaction.

The formalism used in this paper is slightly different from that used by Van Hove in that:

(i) the detailed balance factor is removed so that S becomes independent of the sign of the energy transfer,

(ii) the material is assumed to be isotropic and thus S is a function of scalar Q,

(iii) two new temperature normalized variables are defined to replace the energy and momentum transfer

$$\alpha = \frac{\hbar^2 Q^2}{2Mk_BT} = \frac{E_o + E - 2(E_oE)^{1/2}\cos\theta}{Ak_BT} ;$$

$$\beta = \frac{\hbar\omega}{k_BT} \qquad \ldots \quad (2)$$

where M is the mass of the scattering nucleus,

A is the ratio of mass of the scattering nucleus to the mass of the neutron,

k_B is Boltzman's constant,

T is the absolute temperature of the scatterer,

E_o and E are the initial and final neutron energies.

The definition of the differential cross section then becomes

$$k_B T . \frac{d^2\sigma}{d\Omega dE} = \frac{\sigma_b}{4\pi} \frac{E}{E_o} e^{-\beta/2} S(\alpha,\beta) \qquad \ldots \quad (3)$$

In this representation the value of S for the perfect gas is independent of mass and temperature. In this paper the definition of $S(\alpha,\beta)$ as in (3) above is retained even when the system is composed of more than one type of atom; the convention used is that the σ_f and A are those for the type of nuclei in the system having the largest product of σ_f and abundance.

$S(\alpha,\beta)$ is composed of two parts, one the "self" part S_s which describes scattering of the neutron by a single scattering nucleus, and a part S_d which involves the correlation in time and position of a pair of nuclei. The contribution from $S_d(\alpha,\beta)$ is proportional to the coherent cross section and is zero for completely incoherent scattering materials.

The generalised frequency distribution $p(\beta)$ which can be used to derive a cross section model[6] is given by

$$p(\beta) = \lim_{\alpha \to 0} \left(\frac{S_s}{\alpha}\right) \beta^2 \qquad \ldots \quad (4)$$

The shape of this function for the perfect gas, diffusion and Debye models is shown in Fig. 1. The evaluation of this function

depends on the separation of $S_s(\alpha,\beta)$ from the experimental $S(\alpha,\beta)$ over a wide range of β.

For predominantly incoherent scatterers the value of S measured by experiment is nearly equal to S_s and extrapolation of S/α to $\alpha = 0$ is readily performed. Typical extrapolations of this type, S/α results for H_2O are shown in Section III. It has been found advantageous both in theory and practice to plot log (S/α) against α in order to perform these extrapolations. This arises because terms in S as a power series in α of higher order than α produce a function similar to $\log S/\alpha = a\alpha+b$.

Experimental curves of $p(\beta)$ derived from these extrapolations for room temperature and 150°C water are given in Section III. For materials in which coherent scattering occurs $S(\alpha,\beta)$ contains contributions from $S_d(\alpha,\beta)$ which are most significant as $\alpha \rightarrow 0$. At large values of α and β however these contributions tend to zero and it is possible to extrapolate (S/α) to $\alpha = 0$ using data at these values only. Extrapolations for D_2O are given together with the corresponding $p(\beta)$.

II. Experimental Details

The experiments described here were carried out using a neutron beam from the NRU reactor at Chalk River. Neutrons of a specified velocity are selected from the beam by a phased rotor monochromator apparatus. These neutrons are scattered by a thin sample of water and then detected by an array of scintillation counters. The velocity of the scattered neutrons is determined by time-of-flight methods.

Apparatus

The neutron monochromator described by Egelstaff et al[12] consists basically of two curved slot choppers 2.74 metres apart running at high speed in synchronism. The relative phasing of these rotors is continuously adjustable and by choice of rotors of suitable slot curvature it is possible to select neutrons over a wide range of velocities. At an operating rotor speed of 24,000 rpm the neutron bursts have standard deviation of 5.9 μsec in time of arrival at the sample position and of 2.3 μsec/m in reciprocal velocity. A schematic diagram of the apparatus is shown in Fig. 2.

Neutrons are scattered from a plane sample held at 45° to the incident beam and are detected 1.29 m from the sample in two banks of scintillation detectors mounted in the first and third quadrants. Detectors at angles between 10.5° and 90° have scintillators 15.2 cm by 7.6 cm[8] while those between 90° and 160° are 12.1 cm square[9]. Provision is made in the apparatus for 30 detectors but for these experiments between 11 and 22 were used. Pulses from these detectors are fed into the input circuits of a time analyser described by Alexander and Leng[10]. In this analyser a series of 270 time channels each 6 μsec long is started by a pulse derived from rotor 4 drive shaft and the neutron pulses are sorted according to the channel in which they arrive. Data is read out of this time analyser in the form of punched paper tape for processing on the Burroughs "Datatron" at Chalk River or as punched binary cards for use with the IBM 704 at Argonne National Laboratory.

A typical example of the data obtained from one detector in these experiments is shown in Fig. 3a.

Samples

Water samples were made by enclosing a plane slab of water between two flat aluminum foils. Two, as near as possible identical, sample holders, one empty and one filled with water were alternated in the beam every fifteen minutes. Information from the full and empty sample periods was accumulated separately and the results for the empty holder were subtracted from those of the full holder to obtain the net water scattering.

This method of background compensation was satisfactory for the room temperature samples which had foil windows 0.025 cm thick. The 150°C samples however had much thicker windows to contain the 70 psia vapour pressure of the water, and differences of crystal orientation of the microcrystals comprising the windows gave dissimilar intensities of Bragg scattering for the full and empty sample holders. Since this was a source of error for data involving only low values of energy transfer these points were generally discarded during analysis.

The temperature of the samples was measured by means of calibrated thermocouples. Hot samples were heated electrically and maintained at $150^{\circ} \pm 5^{\circ}$C by adjustment of the power input to the heaters using a recorder-controller.

The pulses from three fission chamber monitors in the beam were time-analysed simultaneously with the detector pulses throughout each run. Monitor No. 1 was placed in the short space between rotor No. 4 and the sample, and monitors Nos. 2a and 2b in the beam path behind the sample (see Fig. 2). From the ratios of monitor counts with the full and empty samples in the beam, the net water

sample transmission was determined to $\pm$ 1/2%. The time sorted output of these three monitors was also used to determine the resolution function of the apparatus and the time-of-flight of the incident neutrons. The samples used had a transmission of .88.

Calibration and Data Processing

Efficiencies of the scintillation counters relative to beam monitor M1 are found by auxiliary measurements using a vanadium scattering sample. For this purpose the differential elastic scattering cross section for neutrons with energy less than 0.04 eV is assumed to be given by the Debye-Waller factor. The total (elastic + inelastic) differential scattering cross section for neutrons with energy above 0.03 eV is assumed to be that derived by Placzek[2]. In the overlapping energy region both methods gave the same values for the detector efficiencies within the statistical errors.

The detector efficiencies as a function of neutron energy were determined by a series of vanadium scattering measurements at several different incident neutron energies. The efficiency of the monitor as a function of neutron energy is assumed to follow the fission cross section for U^{235}. These results were interpolated and extrapolated by fitting a curve to the efficiency versus neutron energy plot which was derived assuming an exponential decrease in light transmission with scintillator thickness. A vanadium measurement was made before and after each series of experimental runs at the same incident neutron energy. The detector efficiencies at that neutron energy were thus set relative to monitor No. 1 by using the calculated angular distributions and the transmission

determination for the vanadium sample. This method gives detector efficiencies obtained under identical conditions to those prevailing during the experimental runs, thus allowing for any differences in geometry factors among the detectors.

Sample runs are usually carried out for 4-6 days continuously, and the results from each 24-hour run are combined to give the total number of neutrons scattered into time channel i of detector j by use of the formula

$$N_{ij} = \frac{\sum_r (F_{ij} - \gamma_r E_{ij})}{\epsilon_{ij}} \qquad \ldots \quad (5)$$

where F_{ij} and E_{ij} are the events recorded in time channel i of detector j with the full and empty sample holder in the scattering position respectively,

ϵ_{ij} is the detection efficiency for neutrons arriving in time channel i of detector j derived from the vanadium measurements,

γ_r is the sample/background normalisation factor for run r deduced from the monitor M1 results.

For the water data two independent methods were used to determine the absolute cross section scale. The first depends on knowing the scintillation detector efficiencies relative to the monitor efficiency and so depends on the accuracy of the vanadium measurements. The second method relates the total number of counts observed to the total scattering cross section σ_T for water. This method is independent of any transmission or monitor determinations and depends only on having correct detector efficiencies relative to each other. In this second method the integral

$$\int_0^{2\pi} \sum_{i=0}^{270} N_{ij} \sin\theta_j \frac{2\pi}{\Delta\Omega_j} d\theta = \sigma_T \, nm \qquad \ldots \quad (6)$$

is evaluated by summing the counts in all time channels of the detector j at a scattering angle θ_j which subtends a solid angle $\Delta\Omega_j$ and integrating over all angles numerically. This establishes the product nm, where m is the number of water molecules per cm^2 of beam, and n the number of neutrons falling on the sample corrected for transmission of the sample and this is used in evaluating S_{ij} in equation (9) below.

A correction for the velocity resolution of the apparatus is made to the partial differential scattering cross section in the region of the quasi elastic peak. This correction is calculated by fitting a gaussian plus linear terms to the quasi elastic peakfrom each detector and unfolding from this a gaussian whose variance is calculated from the monitor distributions. The experimental points are then adjusted by the difference between the original and unfolded gaussians.

This method is satisfactory where the correction to be applied is less than 20% but the quality of the gaussian fit is inadequate to remove larger resolution effects. The angular resolution of the detectors is important only at low angles and no correction has been made.

Data is converted to Egelstaff's[17] $S(\alpha,\beta)$ by a computer programme which evaluates the expressions

$$\beta_i = \frac{6.0576 \times 10^7}{T}\left(\frac{1}{t_1^2} - \frac{1}{t_o^2}\right) \qquad \ldots \quad (7)$$

$$\alpha_{ij} = \frac{6.1121 \times 10^7}{MT}\left(\frac{1}{t_1^2} + \frac{1}{t_o^2} - \frac{2\cos\theta_j}{t_o t_i}\right) \quad \ldots \quad (8)$$

$$S_{ij}(\alpha\beta) = 1.1957 \times 10^{-5} \frac{T}{\sigma_b mn} \frac{t_i^4 \, e^{\beta/2}}{\Delta t \; t_o} N_{ij} \quad \ldots \quad (9)$$

where t_o and t_i are the incident reciprocal velocity and the reciprocal velocity in time channel i in μs/m

Δt is the channel width at the detectors in μs/m/time channel

T is the absolute temperature of the sample

M is the mass in a.m.u. of the principal scattering nucleus, i.e., mass of H for H_2O, mass at D for D_2O

σ_b is the bound atom cross section for the principal scattering nucleus

θ_j is the mean scattering angle for neutrons detected in counter j

m is the number of principal scattering nuclei per sq. cm of beam derived from the transmission of the sample

n is the total number of neutrons which passed through the full sample, corrected for sample transmission

(mn may be calculated from equation (6) above)

S is then plotted as a function of time channel for each detector and a best line is drawn in by eye. From these graphs the values of S are read off at fixed β and plotted as a function of α. This procedure is desirable for two reasons. The first is the need to compare directly values of S at a fixed $|\beta|$, say $\beta = \beta_1$, measured under different experimental conditions, viz., energy gain or energy

loss or different incident neutron energy. Since the same $\beta = \beta_1$ value will not, in general, be found at integral time channel points the data must be interpolated to find the S at $\beta = \beta_1$. The other requirement is compression of the data into a reasonable number of graphs or tables compatible with the variation of S as a function of β and the precision to which it is measured.

III. Results

An example of the steps used in processing the information from a single detector is shown in Fig. 3 for H_2O at 20°C. In Fig. 3a are shown the curves of sample-in counts and background for a ~ 24 hour run. In curve Fig. 3b these raw data have been combined with data from three similar runs and converted into partial differential cross sections by correcting for counter efficiency, and normalising the result. The effects of energy resolution of the apparatus are then removed from the elastic scattering regions of this curve. $S(\alpha,\beta)$ is then plotted for each time channel in Fig. 3c. A smooth curve is drawn by eye through the S vs. time channel results and values of S at given values of β are read off and plotted at the appropriate α. Also shown in Fig. 3b are points which have been recalculated from the smoothed $S(\alpha,\beta)$ curves derived from two separate sets of data taken with different incident neutron energies. This demonstrates the accuracy with which the differential cross section can be obtained from the information in its final form and the adequacy of the representation of the scattering surface by a limited number of constant β curves.

The graphs of $S(\alpha,\beta)$ vs. α for water and heavy water at 20°C and 150°C are shown in Figs. 4 - 8. In these curves the errors

indicated on the points are the statistical errors on the S vs. time channel plots only, and include no contribution from other sources. The positive and negative β points are plotted together on the same curves and as can be seen are self-consistent. Since the sets of results given in these graphs were obtained under different experimental conditions the spread on the points gives an indication of their reliability.

The light water results are shown in Figs. 4 and 5. The 20°C results Fig. 4 consists of points from runs with incident neutron energy 0.095 and 0.25 eV. As can be seen, the two sets of points are in good agreement. Values above $\beta = 4$ are not well defined but allow an estimate of $S(\alpha,\beta)$ up to $\beta = 6$ to be made.

The 150°C results Fig. 5 were taken with neutrons of incident energies 0.13 eV and 0.036 eV and results are shown to $\beta = 3$ and $\alpha = 20$.

The heavy water results are shown in Figs. 6 and 7. Since D_2O has a substantial coherent scattering cross section, contributions for S_d are expected especially at low values of α and β. The values of S vs. α at 20°C shown in Fig. 6 are rather limited in range since neutrons of only one energy, 0.15 eV, were used. The results of S vs. α for 150°C shown in Fig. 7 were taken using two incident neutron energies, 0.097 eV and 0.034 eV.

The derivation of $p(\beta)$ from these data is relatively straightforward. An estimate of the values of α below which the S_d part of the scattering law will be important is first made from the angular distribution of the scattered neutrons. Experimental points with α below this value are discarded for the extrapolation procedure. The remaining points are then plotted as log S/α vs. α for each β, the

best line drawn in by eye, and extrapolated to $\alpha = 0$. The values of S/α found at $\alpha = 0$ multiplied by the appropriate β^2 are then plotted as a function of β to give the $p(\beta)$ curve. This curve together with rough estimates of the higher energy contributions to $p(\beta)$ from the atomic vibrational motions in water, is fed into the LEAP programme[7] and values of (S/α) as a function of α and β are obtained. From the slope of these lines improved extrapolations of the experimental data can be made. In Fig. 9 are shown some extrapolations made with the help of the predicted lines. The H_2O results were ignored below $\alpha = 1$ and the D_2O results below $\alpha = 1/2$ on the basis of the published angular distributions[4][14][15]. As can be seen, below these values the experimental points rise sharply.

The experimental values of $p(\beta)$ derived from the extrapolations are shown in Fig. 10. Several features of these curves can be related to the different internal motions of the atoms of the sample.

A portion of the curve due to diffusion can be seen as a small tail which falls from the intercept on the $\beta = 0$ axis. The value of this intercept is calculated from the diffusion coefficient (d in cm^2/sec) for the sample material and is given by

$$p(0) = \frac{2}{\pi} \frac{Md}{\hbar}$$

Peaks can be seen in the region $\beta = 0.2$ to 3.0, which correspond in energy to levels found by infra-red measurements[16] and have been assigned to hindered rotational states of the H_2O molecule. The highest β part of this region will be due to the hindered rotation of a single water molecule while the region at lower values of β are due to the rotation or vibration of several molecules.

It should be noted that in the case of 24°C water these data show that the hindered rotation states extend to $\beta \sim 5$ (0.125 eV). This is in contrast to the conclusions which have been drawn from cold neutron scattering experiments[4] in which a sharp peak is observed at $\beta \simeq 2.3$ (0.06 eV). That peak in the cold neutron data is magnified greatly by the Boltzmann factor and the energy to time-of-flight conversion factor. It seems to be rather difficult to obtain the true shape of this part of the distribution without taking an extensive series of measurements as described here.

One interesting conclusion from these results is that the hindered rotations (β = 2 to 5) of the single H_2O molecules is more important (relative to the other rotational states) at 20°C than at 150°C. Presumably this is because the intramolecular bonds can be broken more easily at the higher temperature and this causes the levels to shift to a lower energy. The area of the rotational part of $p(\beta)$ is in agreement with that predicted by Sachs and Teller[13].

It has been shown by Egelstaff and Schofield[6] how the function $p(\beta)$ may be used to calculate the whole $S(\alpha,\beta)$ surface. Using these methods the present data will yield accurate input information for future neutron spectrum calculations.

Acknowledgements

The authors wish to thank Dr. P.A. Egelstaff for many stimulating discussions on this work and for providing the calculated S/α curves in Fig. 9. The authors would also like to thank Messrs. C. Duffill and R.B. Werden for their help in running the experimental equipment, and Mr. H. Greenspan, Mr. R.J. Royston and Miss Irene Baksys of ANL for help in the processing of the data.

References

(1) Van Hove, Phys. Rev. 95, 249 (1954).

(2) Placzek, Phys. Rev. 86, 377 (1952).

(3) Egelstaff, Cocking, Royston and Thorson, STI/PUB/35*, 309 (1961).

(4) Larsson, Holmroyd and Otnes, STI/PUB/35*, 329 (1961).

(5) Egelstaff, STI/PUB/35*, 25 (1961).

(6) Egelstaff and Schofield, Nuclear Sci. & Eng. 12, 260 (1962).

(7) McLatchie, LEAP programme to be published.

(8) Harris, AERE R 3688 (1961).

(9) Stedman, R.S.I. 31, 1156 (1960), CRRP-931.

(10) Alexander and Leng, CREL-1036, (1961).

(11) McKenzie, Nucleonics Jan. 1951, P. 60.

(12) Egelstaff, Cocking and Alexander, STI/PUB/35*, 165 (1961).

(13) Sachs and Teller, Phys. Rev. 60, 18 (1941).

(14) Brockhouse, Nuovo Cimento 9, 45.

(15) Mikke, STI/PUB/35*, 351 (1961).

(16) Megat, Ann. Phys. 6, 108.

(17) Egelstaff, TNCC(Can)18, 1959, AERE R/3622.

*STI/PUB/35 is the proceedings of the conference on Inelastic Scattering of Neutrons in Solids and Liquids held at Vienna on Oct. 11-14, 1960 sponsored by the I.A.E.A.

Figures

Fig. 1. The $p(\beta)$ function for the Debye, the perfect gas and the diffusion models.

Fig. 2. Schematic diagram of the apparatus giving the principal dimensions.

Fig. 3. Example of the steps used in data processing. (a) shows the counts with full and empty sample in the beam over a 24 hour period. In (b) these counts have been combined with 3 other 24 hour runs and converted to $\frac{d^2\sigma}{d\Omega\, dt}$ and in (c) converted to $S(\alpha,\beta)$. In (b) the solid triangular points are obtained by calculating $\frac{d^2\sigma}{d\Omega dt}$ from the summary graph of $S(\alpha,\beta)$ in Fig. 8.

Fig. 4. $S(\alpha,\beta)$ for light water at 20°C.
Fig. 5. $S(\alpha,\beta)$ for light water at 150°C.
Fig. 6. $S(\alpha,\beta)$ for heavy water at 20°C.
Fig. 7. $S(\alpha,\beta)$ for heavy water at 150°C.

} Errors shown on the points are those due to counting statistics only.

Fig. 8. Summary curves of $S(\alpha,\beta)$ for water. These curves are the best line drawn by eye through the individual points.

Fig. 9. Examples of the extrapolation of S/α to $\alpha = 0$. The dotted lines are derived by LEAP from a tentative $p(\beta)$ and are then used as a guide in making an accurate extrapolation.

Fig. 10. Experimental values of $p(\beta)$ for water.

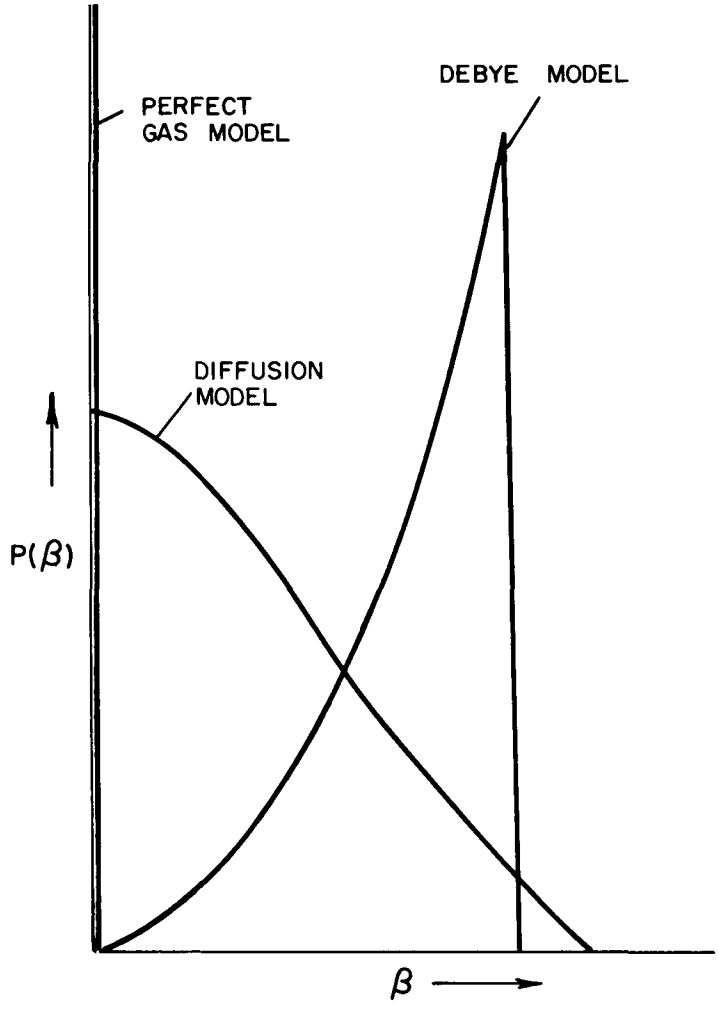

FIG. 1

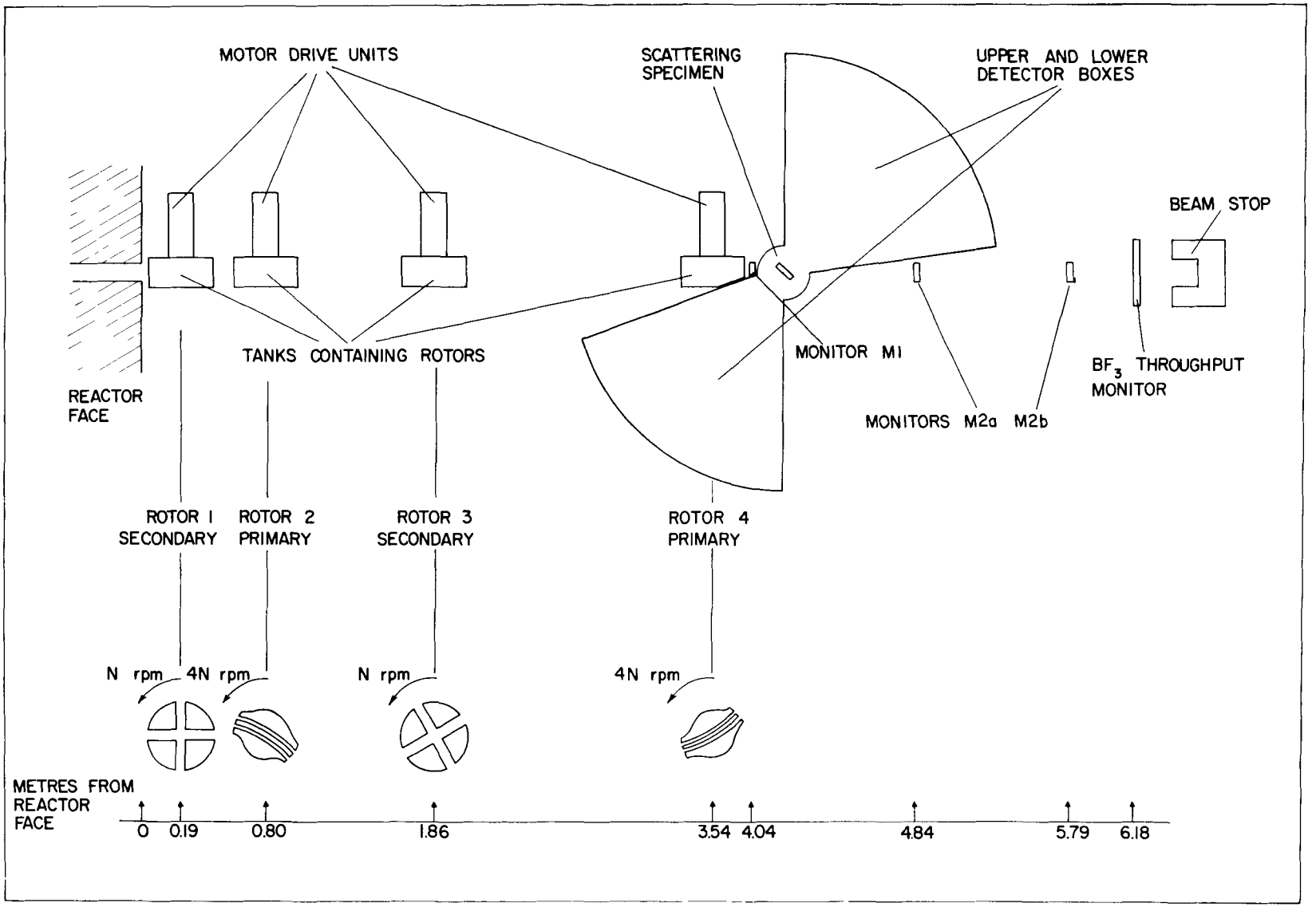
MOTOR DRIVE UNITS
SCATTERING SPECIMEN
UPPER AND LOWER DETECTOR BOXES
BEAM STOP
TANKS CONTAINING ROTORS
MONITOR M1
REACTOR FACE
BF3 THROUGHPUT MONITOR
MONITORS M2a M2b
ROTOR 1 SECONDARY
ROTOR 2 PRIMARY
ROTOR 3 SECONDARY
ROTOR 4 PRIMARY
N rpm
4N rpm
N rpm
4N rpm
METRES FROM REACTOR FACE
0
0.19
0.80
1.86
3.54
4.04
4.84
5.79
6.18

FIG. 2

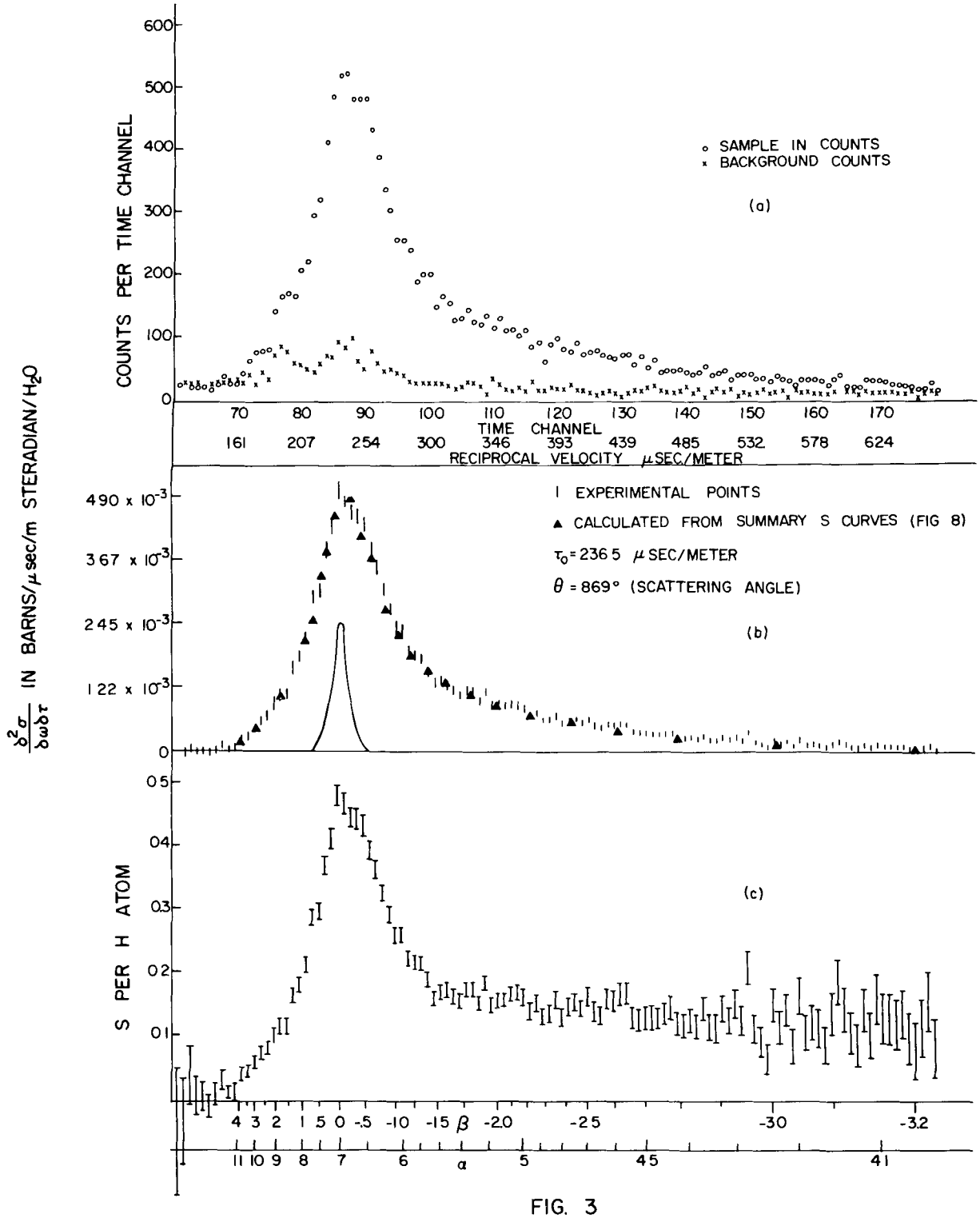
COUNTS PER TIME CHANNEL
600
500
400
300
200
100
0
o SAMPLE IN COUNTS
x BACKGROUND COUNTS
(a)
70 80 90 100 110 120 130 140 150 160 170
TIME CHANNEL
161 207 254 300 346 393 439 485 532 578 624
RECIPROCAL VELOCITY μSEC/METER
$\frac{\delta^2\sigma}{\delta\omega\delta\tau}$ IN BARNS/μsec/m STERADIAN/H_2O
490 x 10^{-3}
367 x 10^{-3}
245 x 10^{-3}
122 x 10^{-3}
0
I EXPERIMENTAL POINTS
▲ CALCULATED FROM SUMMARY S CURVES (FIG 8)
τ_0 = 236 5 μSEC/METER
θ = 869° (SCATTERING ANGLE)
(b)
S PER H ATOM
0.5
0.4
0.3
0.2
0.1
(c)
4 3 2 1 5 0 -.5 -1.0 -1.5 β -2.0 -2.5 -3.0 -3.2
11 10 9 8 7 6 α 5 4.5 4.1

FIG. 3

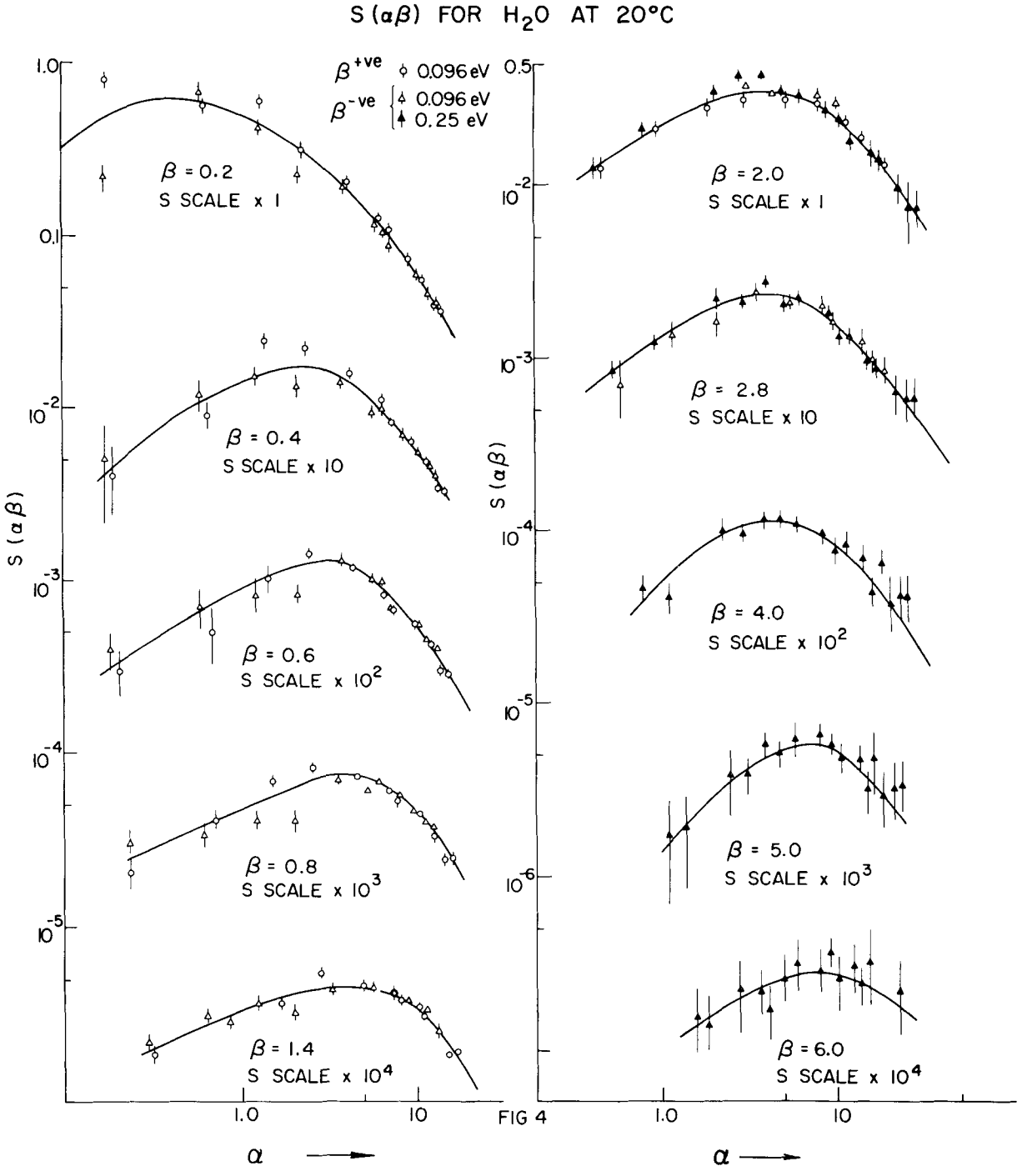
S (αβ) FOR H2O AT 20°C
β+ve 0.096 eV
β-ve 0.096 eV
0.25 eV
β = 0.2
S SCALE x 1
β = 0.4
S SCALE x 10
β = 0.6
S SCALE x 10²
β = 0.8
S SCALE x 10³
β = 1.4
S SCALE x 10⁴
β = 2.0
S SCALE x 1
β = 2.8
S SCALE x 10
β = 4.0
S SCALE x 10²
β = 5.0
S SCALE x 10³
β = 6.0
S SCALE x 10⁴
S (αβ)
α
1.0
10
0.5
0.1
10⁻²
10⁻³
10⁻⁴
10⁻⁵
10⁻⁶

FIG 4

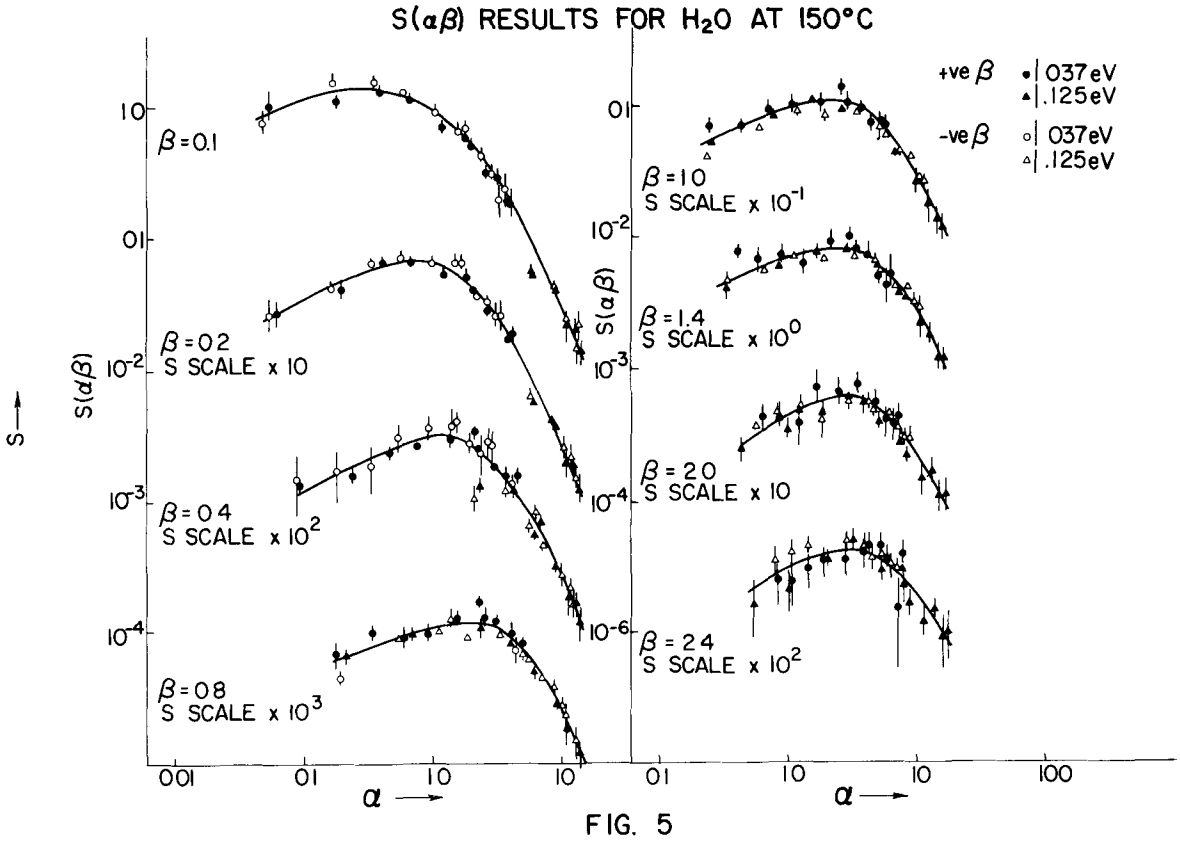
S(αβ) RESULTS FOR H2O AT 150°C
+ve β
037eV
.125eV
-ve β
037eV
.125eV
β=0.1
β=0.2
S SCALE x 10
β=0.4
S SCALE x 10^2
β=0.8
S SCALE x 10^3
β=1.0
S SCALE x 10^-1
β=1.4
S SCALE x 10^0
β=2.0
S SCALE x 10
β=2.4
S SCALE x 10^2
S(αβ)
S
α
α

FIG. 5

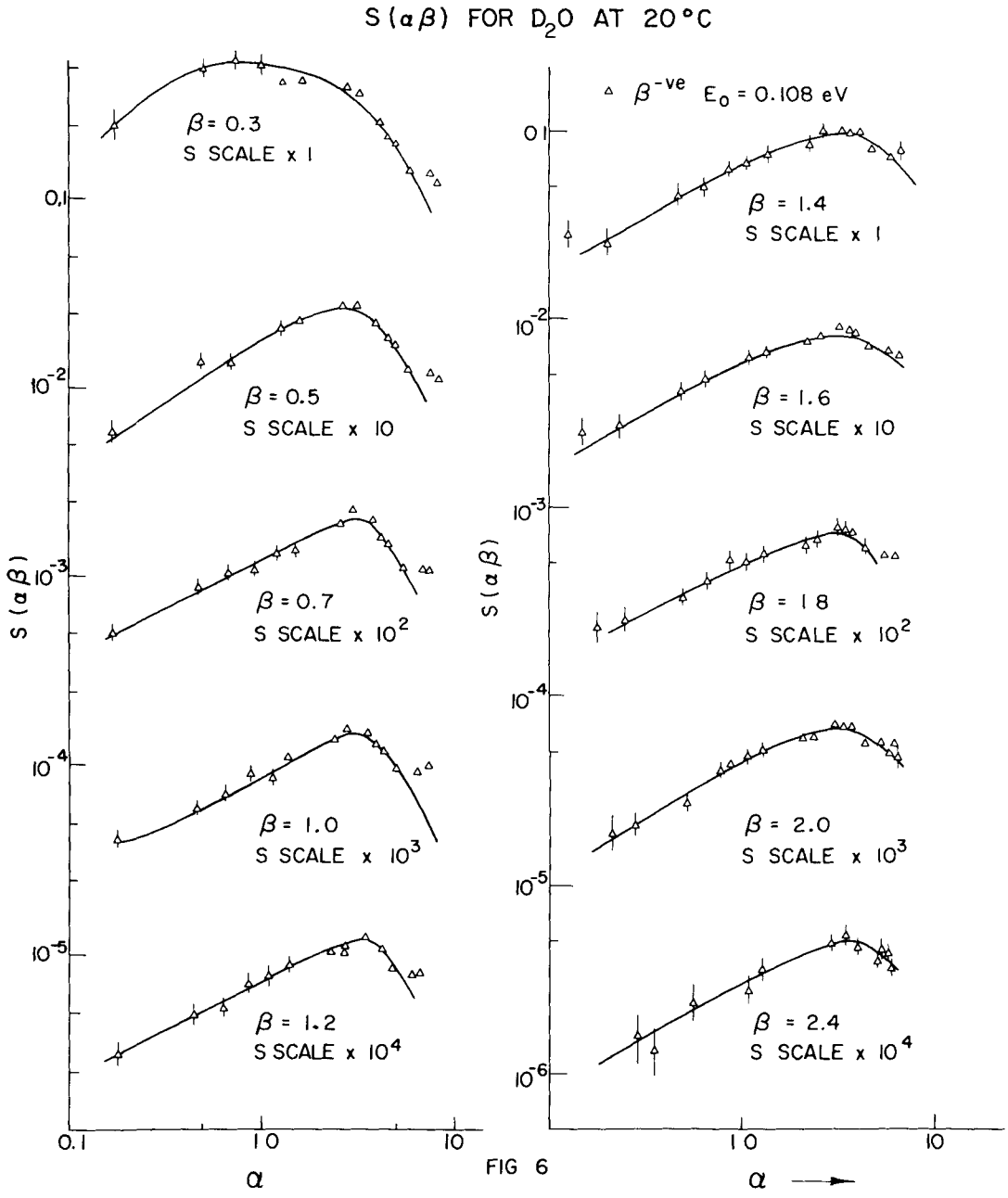
S(αβ) FOR D2O AT 20°C
β = 0.3
S SCALE x 1
β = 0.5
S SCALE x 10
β = 0.7
S SCALE x 10^2
β = 1.0
S SCALE x 10^3
β = 1.2
S SCALE x 10^4
△ β^-ve E0 = 0.108 eV
β = 1.4
S SCALE x 1
β = 1.6
S SCALE x 10
β = 1.8
S SCALE x 10^2
β = 2.0
S SCALE x 10^3
β = 2.4
S SCALE x 10^4
S(αβ)
α
0.1
1.0
10

FIG 6

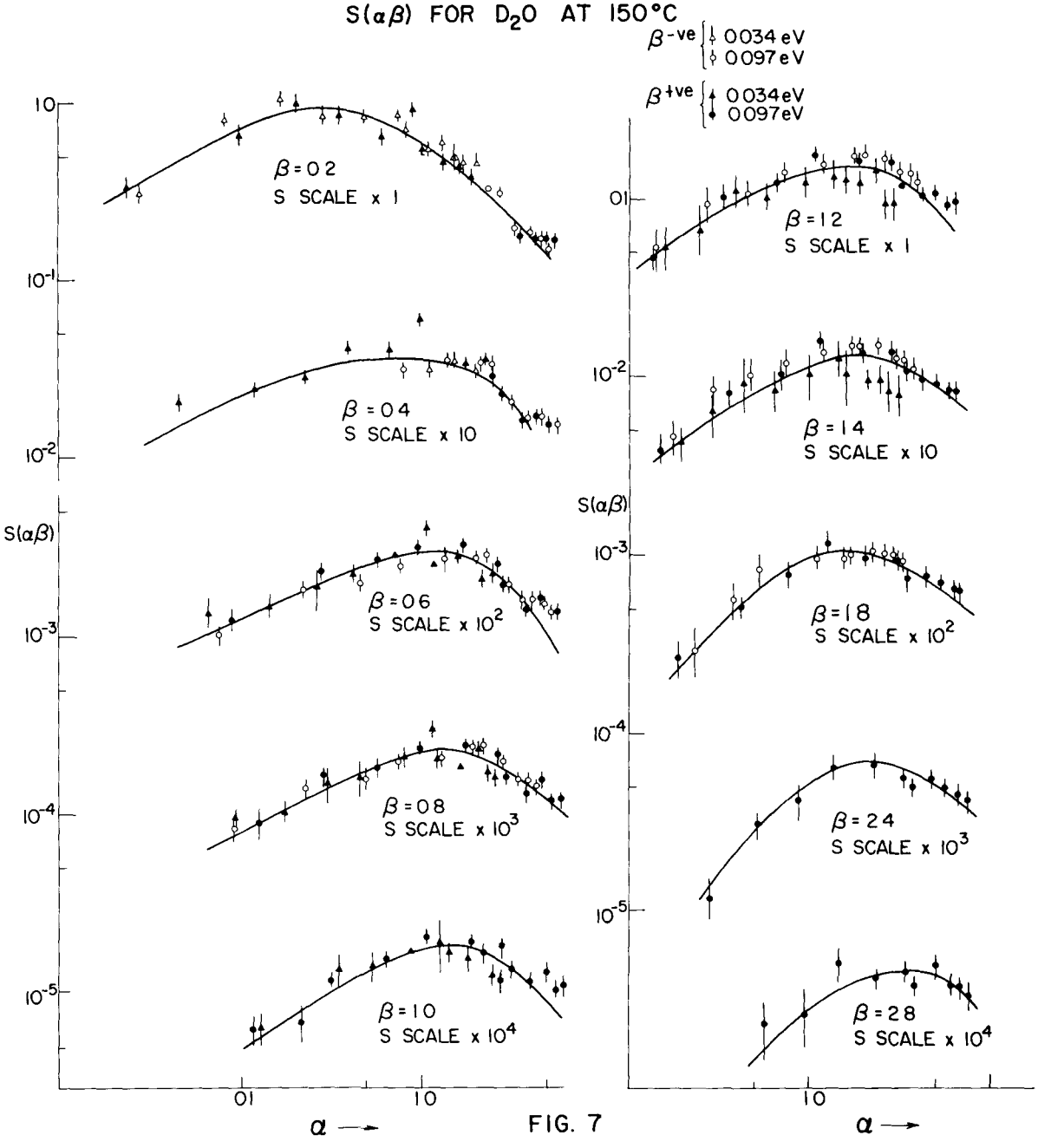
S(αβ) FOR D2O AT 150°C
β -ve 0034 eV
0097 eV
β +ve 0034 eV
0097 eV
β = 0 2
S SCALE x 1
β = 0 4
S SCALE x 10
β = 0 6
S SCALE x 10²
β = 0 8
S SCALE x 10³
β = 1 0
S SCALE x 10⁴
β = 1 2
S SCALE x 1
β = 1 4
S SCALE x 10
β = 1 8
S SCALE x 10²
β = 2 4
S SCALE x 10³
β = 2 8
S SCALE x 10⁴
S(αβ)
α
α

FIG. 7

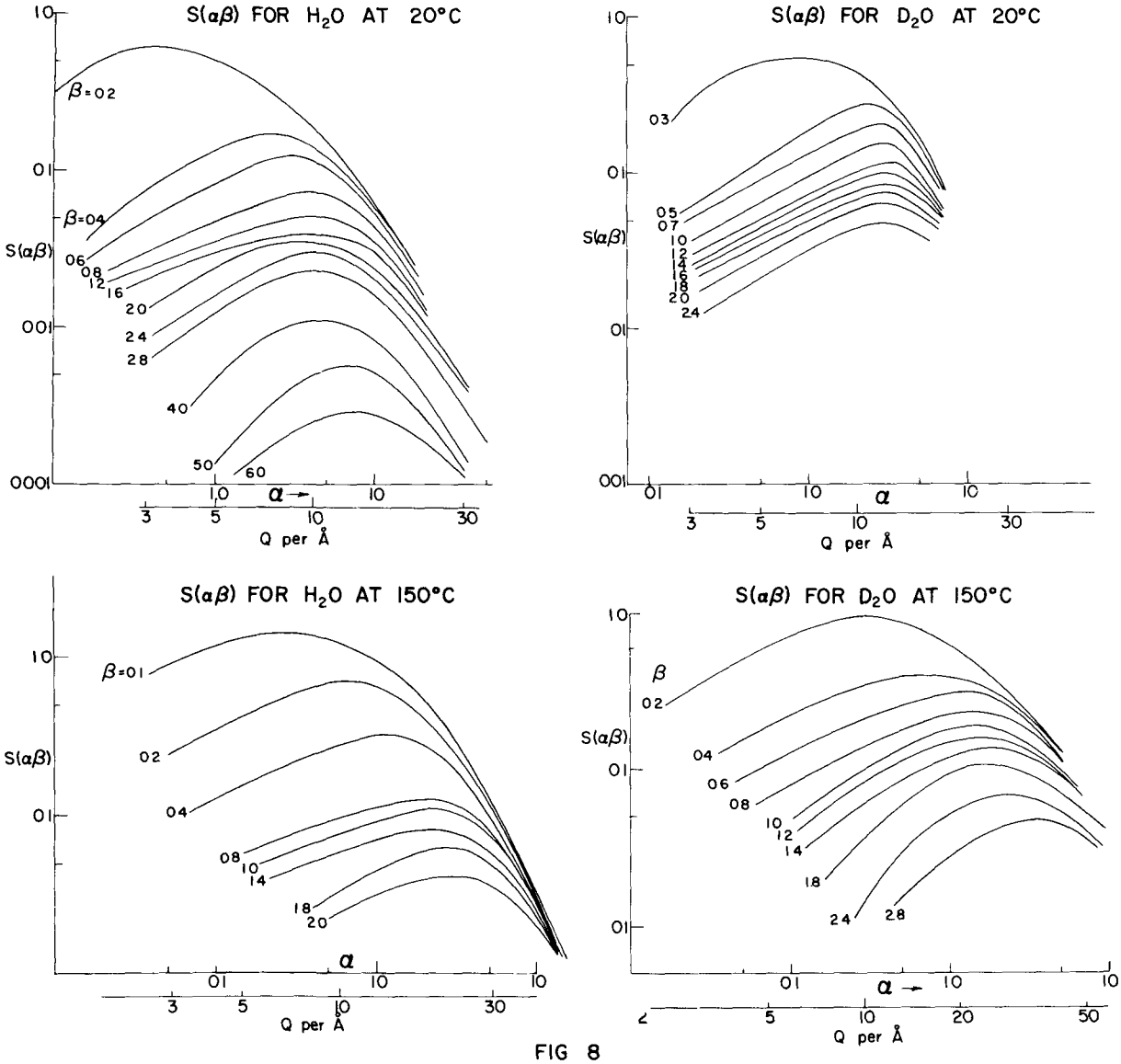
S(αβ) FOR H2O AT 20°C
S(αβ) FOR D2O AT 20°C
S(αβ) FOR H2O AT 150°C
S(αβ) FOR D2O AT 150°C
S(αβ)
α
β
Q per Å

FIG 8

EXTRAPOLATIONS OF $\frac{S}{\alpha}$ TO $\alpha = 0$

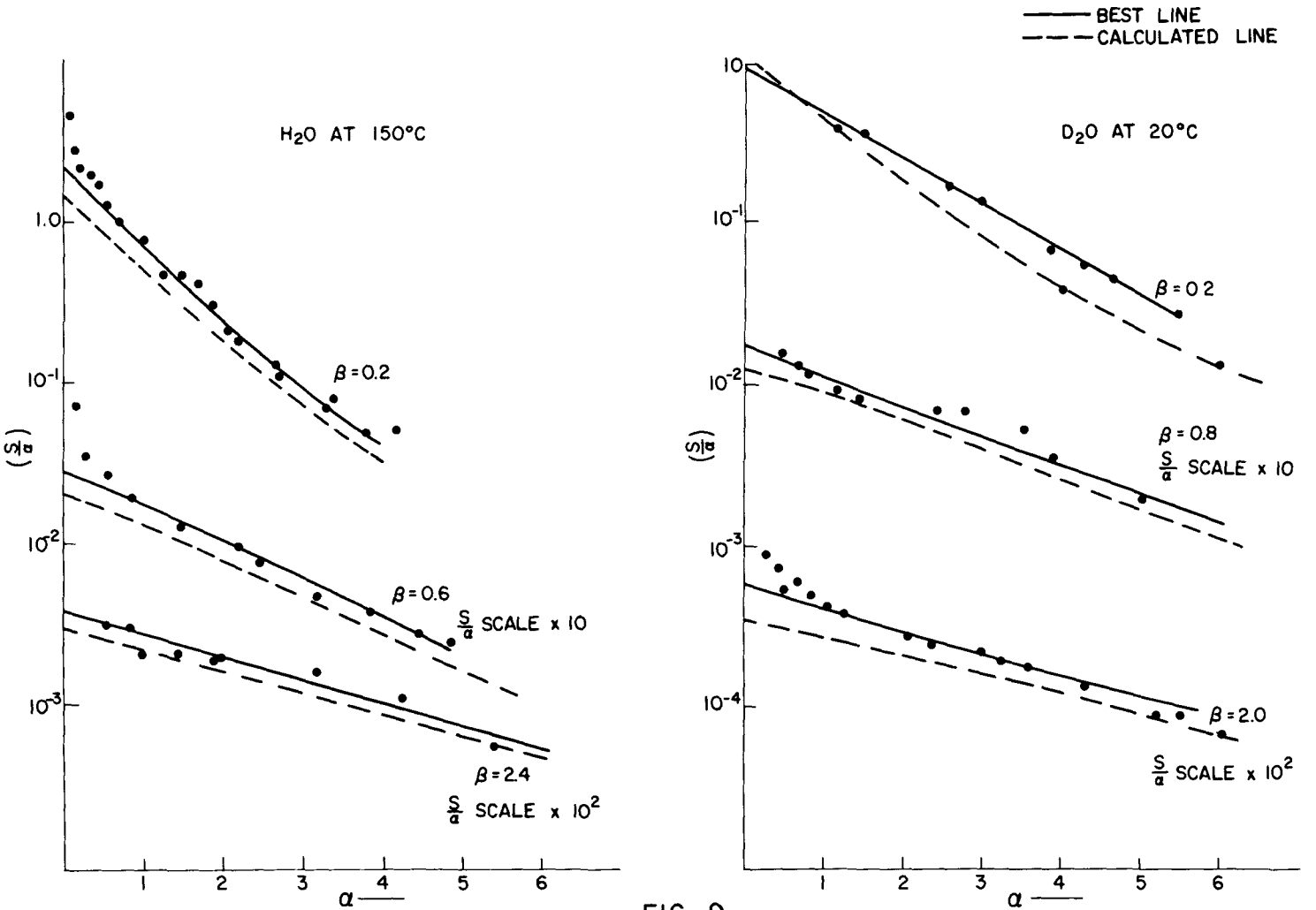

FIG. 9

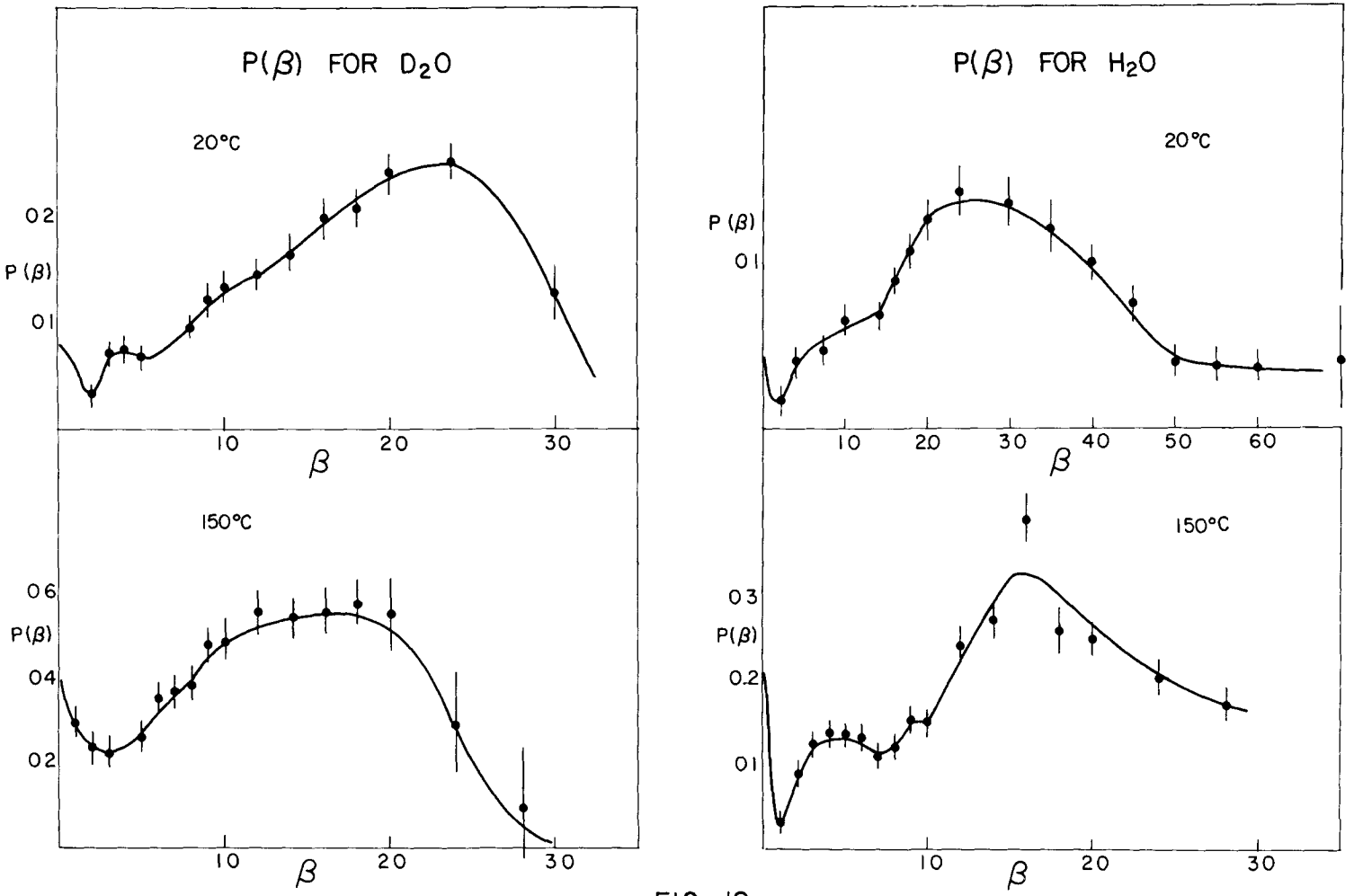
P(β) FOR D2O
20°C
02
P(β)
01
10
20
30
β
150°C
06
P(β)
04
02
10
20
30
β
P(β) FOR H2O
20°C
P(β)
01
10
20
30
40
50
60
β
150°C
03
P(β)
0.2
01
10
20
30
β

FIG. 10

Conference on Neutron Thermalization, Brookhaven, April 30, 1962

Some Remarks on the Experimental Information Necessary to Obtain Scattering Data for Diffusion Problems

by T. Springer+

1. Introduction

The moderation and diffusion properties of a material can be fully characterized by the double differential cross section $d^2\sigma/dE'd\Omega$

For an isotropic medium it can be written as (e.g./1/)

$$d^2\sigma/dE'd\Omega = \sqrt{\frac{E'}{E}}\left[a_i^2 S_i(K,\omega) + a_c^2 S_c(K,\omega)\right] \qquad (1)$$

from which the more "integral" quantities $\sigma(E \to E')$, $d\sigma/d\Omega$, and others can be derived.

$$\hbar K = |\vec{k} - \vec{k}'| = \sqrt{2m}\left(E + E' - 2\sqrt{EE'}\cos\vartheta\right)^{1/2} \qquad (2)$$

is the momentum transfer, ϑ is the scattering angle, $\hbar\omega = E - E'$ is the energy transfer, a_i and a_c are the incoherent and coherent scattering lengths; E and E' are the energies before and after scattering, respectively.

For reactor calculations tabulations of $d^2\sigma/dE'd\Omega$ are needed for a wide range of the relevant parameters: E, E', ϑ, and T. The aim of neutron physics is to find methods by which these values can be made available with a minimum amount of experimental and computational effort and with a high degree of reliability. In section 2 of this paper a method is recommended which fits a simplified function $S(K, \omega)$ directly to those experimental quantities which can be accurately determined by rather simple procedures.

Until now the following procedures have been applied to obtain the function $S(K, \omega)$ for the usual reactor moderators: $S_i(K,\omega)$ is proportional

+ Laboratorium für Technische Physik der Technischen Hochschule München

to the double Fourier transform over space and time of the self correlation function $G_s(r, t)$ which contains the whole information on the scattering system. By assuming that $G_s(r, t)$ approximately is a Gaussian simple relations can be established between the measured data and the width w(t) of this Gaussian. From the experimental knowledge of w(t) the scattering law $S(K, \omega)$ can be computed for a wider range of the parameters K and ω. This method has been proposed and applied in the case of water by Egelstaff /2,3/.

A more indirect concept is the complete quantum mechanical calculation of $S(K, \omega)$ which implies a high amount of mathematical and numerical work. The only informations needed concern the lattice or molecule structure, and the lattice spectrum which is known indirectly in most cases. For beryllium earlier calculations have been performed by the incoherent approximation using a simple Debye spectrum /4,5/. Improvements have been achieved by regarding coherence effects /6,7/, or by using a Born-Karman spectrum (with two characteristic temperatures) in the incoherent approximation /8/. The Debye approach considering coherence effects has been applied to the case of BeO /9/. For graphite the Debye model is insufficient. The Krumhansl-Brooks spectrum (proportional to ω^2 at low and to ω for higher modes /14/) has been used in the incoherent /11/ and later in the coherent approximation /12/. The more realistic spectrum by Baldock /15/ has been also applied /13/. A comparison of the cross section integrated over final energy and solid angle with transmission experiments in the sub-Bragg range shows rather good agreement for beryllium /5,7,6,8,9/ (better than 5 to 10 percent in most cases). One should keep in mind that in some cases a certain compensation of errors can occur, resulting from the different approximations applied. In the case of graphite the comparison with experiments below the Bragg cut-off is rather unsuccessful because of small angle scattering effects /12/

and, at higher energies, because of the influence of preferred microcrystal orientations /16/. In view of the complicated lattice spectrum a more direct experimental approach would be needed to obtain $S(K, \omega)$ at least for graphite.

In molecular moderators both the spectrum, and the amplitudes (or the "effective masses") for the different oscillation modes have to be known. Calculations by Nelkin /17/ in the case of water will be compared with calculations which have been performed recently at Karlsruhe (see section 3).

2. Experimental determination of a Ansatz function $S(K,\omega)$ with several free parameters

The first calculations of $S(K,\omega)$ have been performed approximately by means of a free gas model. For energies below about 10 kT, there is a considerable amount of purely elastic scattering without quantum exchange, especially for graphite and beryllium because of their exceedingly high Debye temperatures. Therefore, the free gas model is a rather crude picture. A reasonable improvement of the scattering law could be achieved by the introduction of an elastic line $\delta(\omega)$ and a semi-empirical inelastic contribution S_0, namely

$$S(K,\omega) = \delta(\omega) F(K) + e^{\hbar\omega/2k_0T} S_0(K,\omega) \qquad (3)$$

where $S_0(K,-\omega) = S_0(K,\omega)$ +).

By this formulation the condition of detailed balance is fulfilled automatically. The intensity of the elastic line, $F(K)$, is proportional to the Debye-Waller factor. For energies above the Bragg cut-off $F(K)$ is further proportional to the intensity distribution of the Bragg reflections in a

---

+) The distinction between coherent and incoherent scattering can be dropped by using only the first term of (1) with a_{tot}^2 instead of a_i^2. k_0 is Boltzmann's constant.

polycrystal. Absolute values of the function F (K) can be measured by selecting neutrons which have been scattered without energy exchange. The experimental curve can be easily normalized by the condition that F(0)= 1. F(K) could be also determined by x-ray reflections if the same momentum is transferred as in the case of neutron scattering.

The inelastic part S_0 can be represented by a reasonable chosen simple function with two free parameters which are allowed to depend on K: they can be determined by means of the sum rule /1,29/

$$\int_{-\infty}^{+\infty} S(K,\omega)\,\omega\,d\omega = \hbar K^2/2M \tag{4}$$

which is valid for both coherent, and incoherent scattering; and by means of a second experimental function. For this function the simple differential cross section should be chosen

$$\int_0^{\infty} (d^2\sigma[K(E,E',\vartheta),\omega]/dE'd\Omega)\,dE' = d\sigma(E,\vartheta)/d\Omega \tag{5}$$

This quantity can be accurately measured by a "black" neutron counter /18/. The normalization of the experiment can be performed by the well-known value of $\sigma_s = \int_{(4\pi)} (d\sigma/d\Omega)\,d\Omega$.

The shortest possible "Ansatz" for S_0 is

$$S_0(K,\omega) = H(K)e^{-\hbar^2\omega^2/\varepsilon^2(K)} \tag{6}$$

where H and ε^2 are even functions of **K**. (5) with (4,6) gives with $F(\vartheta)$ instead of $F(K)$

$$d\sigma/d\Omega = a_{tot}^2\left[F(\vartheta) + \int_0^{\infty} \sqrt{\frac{E'}{E}}\frac{2\hbar^2K^2k_0T}{\sqrt{\pi}M\varepsilon^2(K)}\, e^{-\frac{[\hbar\omega-\varepsilon^2(K)/4k_0T]^2}{\varepsilon^2(K)}}\right] \tag{7}$$

where ε and ω depend on E'. $F(\vartheta) \equiv 0$ and $\varepsilon^2 = 2\hbar^2K^2k_0T/M$ gives the free gas limit. For low energies and temperatures where the single phonon processes are dominating ε tends to approach a constant value

and H becomes approximately proportional to k^{2} +).

Therefore, a reasonable approximation would be

$$\varepsilon^{2} = a(T) + b(T)\,k^{2} \tag{8}$$

Now, (7) can be integrated explicitly and the constants a, and b can be determined by a least square fit.

The method recommended takes into account rather exactly the transport properties of the moderator by using the experimental cross section $d\sigma(\vartheta)/d\Omega$. The moderation properties are included by taking into account the sum rule, the detailed balance condition, and by the introduction of the intensity of elastic scattering directly from experiment. It is reasonable to assume that the description of the inelastic scattering distribution by a simple function (6) with (8) is a rather good description for thermalization problems.

3. The scattering cross section of water

The scattering cross section $d^{2}\sigma/dE'd\Omega$ of water has been calculated by Nelkin /17/ with the following approximations: (a) translational motion is treated like that of an ideal gas, (b) the hindered rotation is treated as a torsional oscillation with a single quantum energy of 0.06 eV, and (c) three molecular vibrations were regarded with quantum energies of 0.205, 0.481 and 0.481 eV. The integral of $d^{2}\sigma/dE'd\Omega$ over dE' and $d\Omega$ gives the total scattering cross section $\sigma_{s}(E)$ in very good agreement with experiment between 0.01 and 0.5 eV/17/. The calculations have been extended to lower energies by Goeßmann /19/ using a Debye model for the translational motion. The results are compared with experimental curves from /20/ in fig. 1. It

+) The single phonon term in the Gaussian approximation of Sjölander /30/ is similar but not identical with (7) in this case. For the incoherent case, (7) with (8) is in accordance with the sum rule of the second moment of $S(K,\omega)$ (cf. [1]).

can be seen, however, that the Debye model with a constant Debye temperature fails completely as soon as the free gas concept begins to fail. The step at the melting point in fig. 1 results partly from the change of the hindered rotation energy and partly from the change of the Debye temperature. The comparatively small difference between the bound and the free molecule case can be understood by the opposite influence of the Doppler effect and the reduced mass factor.

The differential cross section $d\sigma(\vartheta)/d\Omega$ has been calculated by Kiefhaber /21/ by integration of Nelkin's cross section over E'. The results are compared with experiments /18,22/ in fig. 2. There is rather good agreement at 0.04 eV. At 0.08 eV the agreement is less good. The calculated mean cosines of the scattering angle, $\bar{\mu}$, are compared with experiments in fig. 3. All experimental points are below the calculated curve. Similarly the transport mean free path (found by averaging $1/(1-\bar{\mu})$ over a Maxwellian) is $\lambda_{tr} = 0.458$ cm instead of $\lambda_{tr} = 0.427 \pm 0.008$ cm from experiment /23/.

We think that the discrepancy is due to the assumption of one single torsion energy instead of a rather broad band. This will induce some error mainly at higher neutron energies where torsional quanta can be transferred. Even in the case of ice there are two separated torsional lines in the Raman spectrum at 0.065 and at 0.10 eV. The first can be related to the oscillation around the molecule dipole axes and the latter around the two other molecule axes, respectively /25/.

In the case of water there are several coordination types /26/ with different torsion forces. This gives a further broadening of the spectrum. On account of Raman spectra in water at 28°C /27/ a rectangular distribution between 0.04 and 0.09 eV should be used. The higher molecule vibration should be changed from 0.48 eV (vapor) to ≃0.43 eV (water /26/28/).

Calculations with this kind of spectrum are planned.

The neglect of the translational hinderance in the theory will, on the other hand, introduce no appreciable error in the dominant range of the reactor spectrum. This can be clearly seen by comparing experimental angular distributions $d\sigma/d\Omega$ of ice and water at the same energy /22/: The difference in the curves is very small in spite of the large difference between the Debye temperature of ice and the (hypothetical) Debye temperature of water.

In this connection we may mention that neutron scattering spectra are not very useful to obtain the quantum energies of higher vibration modes (especially the molecular vibrations): if the neutron gains energy from these states normally a rather large momentum is transferred to the vibrating molecule. By this recoil a large Doppler broadening $\Gamma_{1/2}$ of an (initially sharp) line is induced with $\Gamma_{1/2} \simeq 4(E_v kT m/M)^{1/2}$ for $\vartheta = \pi/2$ (M/m = molecular mass in units of neutron mass). In Raman scattering experiments, on the other hand, the recoil is smaller by a factor of $(E_L^2/2mc^2E_v)^{1/2} \simeq 1/3000$, ($mc^2$ = rest energy of the neutron, E_v = quantum energy exchanged, e.g. 0.06 eV, $E_L \simeq 4$ eV = quantum energy of Hg-lamp).

The author is very indebted to Prof. H. Maier-Leibnitz and Dr. K. Böckmann for valuable suggestions and discussions. Thanks are further due to Mr. E. Kiefhaber and Dr. W. Häfele for communicating results prior to publication.

References:

/1/ M.S. Nelkin, Symposium on "Inelastic Scattering of Neutrons in Solids and Liquids", Proc. of the I.A.E.A., Wien 1961, p. 3

/2/ P.A. Egelstaff, Proc. of the I.A.E.A., Wien 1961, p. 25, further: P. Schofield, Proc. of the I.A.E.A., Wien 1961, p. 39

/3/ P.A. Egelstaff, S.J. Cocking, R. Royston, and I. Thorson, Proc. of the I.A.E.A., Wien 1961, p. 309

/4/ L.S. Kothari and K.S. Singwi, J. Nucl. Energy 5, 342 (1957)

/5/ M.S. Nelkin, Nucl. Sci. Eng. 2, 199 (1957)

/6/ R.C. Bhandari, J. Nucl. Energy 6, 104 (1957)

/7/ K.S. Singwi and L.S. Kothari, Geneva Conf. 1955, Vol. 2, p. 56

/8/ R. Subramanian, J. Phys. Chem. Solids 19, 173 (1961)

/9/ R.C. Bhandari, L.S. Kothari, and K.S. Singwi, J. Nucl. Energy 7, 45 (1958)

/10/ D.A. Kleinman, Phys. Rev. 81, 326 (1951)

/11/ L.S. Kothari and K.S. Singwi, Phys. Rev. 106, 230 (1957)

/12/ P.G. Kübchandani, L.S. Kothari, K.S. Singwi, Phys. Rev. 110, 70 (1958)

/13/ P. Schofield, and A. Hassitt, Geneva Conf. 1958, Vol. 16, p. 217

/14/ J. Krumhansl and H. Brook, J. Chem. Phys. 21, 1663 (1953)

/15/ G.R. Baldock, Phil. Mag., Ser.8, 1, 789 (1956)

/16/ G.P. Arnold, V.W. Myers, and A.H. Weber, Phys. Rev. 75, 217 (1949)

/17/ M.S. Nelkin, Phys. Rev. 119, 741 (1960)

/18/ Ch. Reinsch and T. Springer, Z. Naturforschung 16a, 112 (1961)

/19/ G. Goeßmann, Nukleonik, in print

/20/ K. Heinloth and T. Springer, Proc. of the I.A.E.A., Wien 1961, p. 323, and Z. Physik 163, 218 (1961)

/21/ E. Kiefhaber, (1961), unpubl. report, Karlsruhe

/22/ Ch. Reinsch, Z. Physik 163, 424 (1961)

/23/ M. Küchle, Nukleonik 2, 131 (1960)

/24/ W.L. Whittemore and A.W. McReynolds, Proc. of the I.A.E.A., Wien 1961, p. 511; K. Mikke, Proc. of the I.A.E.A., Wien 1961, p. 351

/25/ D. F. Hornig, H.F.White, F.P. Reding, Spectro-Chim. Acta (London) 12, 338 (1958)

/26/ P.C. Cross, J. Burnham, and P.A. Leighton, J. Amer. Chem. Soc. 59, 1134 (1937)

/27/ J.H. Hibben, J. Chem. Phys. 5, 166 (1937)

/28/ G.B.B.M. Sutherland, Proc. Roy. Soc. A 141, 535 (1933)

/29/ A. Rhaman, K.S. Singwi, and A. Sjolander, unpubl. ANL-report (1961)

/30/ A. Sjölander, Arkiv Fysik 14, 315 (1958)

LEGEND OF FIGURES

Fig. 1. Total cross section of water and ice in barns per molecule. I and solid curve: experimental (Heinloth et al. /20/). • and thin curve: calculated (Göβmann /19/). Θ =Debye temperature; torsion energy 0.06 eV for water, and 0.074 eV for ice. The liquid range cannot be described by a constant Θ at very low energies. At 2.7×10^{-3} eV, on the other hand, the results are rather insensitive against the translational mostions. $\Theta = 0$ and $\Theta = \infty$ describe the case of completely free, and bound molecules, respectively.

Fig. 2. Angular distribution $d\sigma(\vartheta)/d\Omega$ from neutron scattering in water o = experimental (Reinsch et al. /18,22/). Solid curve: calculated with Nelkin's theory /17/ by Kiefhaber /21/.

Fig. 3. Mean cosine of scattering angle $\overline{\cos\vartheta}$ and transport mean free path λ_{tr}. • = Whittemore et al./24/, o = Reinsch et al. /18,22/, solid curve: Kiefhaber /21/.

Fig. 1

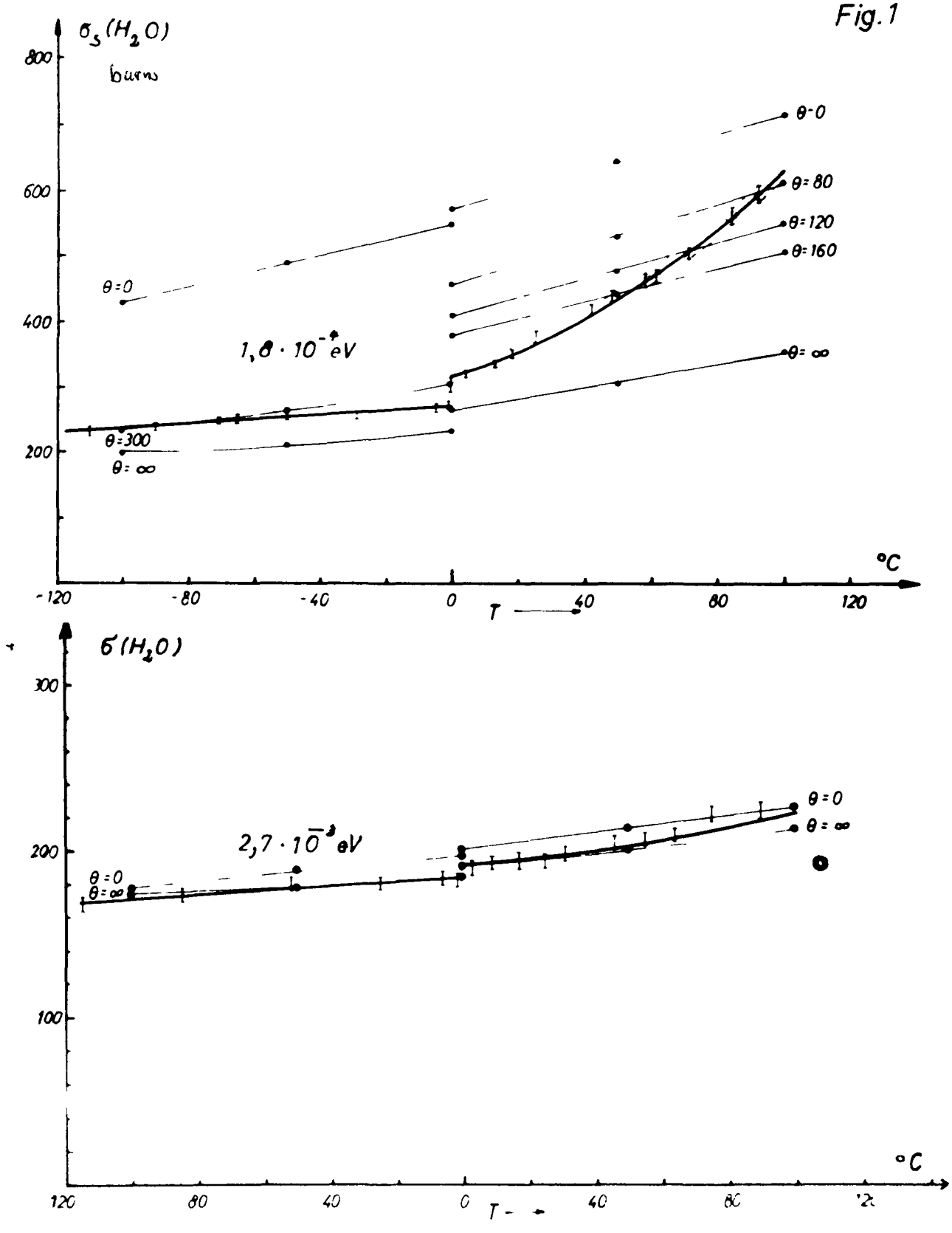
σs (H2O)
barns
800
600
400
200
θ=0
θ=80
θ=120
θ=160
θ=∞
1,8 · 10⁻⁴ eV
θ=300
θ=∞
°C
-120
-80
-40
0
40
80
120
T
σ (H2O)
300
200
100
2,7 · 10⁻³ eV
θ=0
θ=∞
°C
120
80
40
0
40
80
T

Fig.2

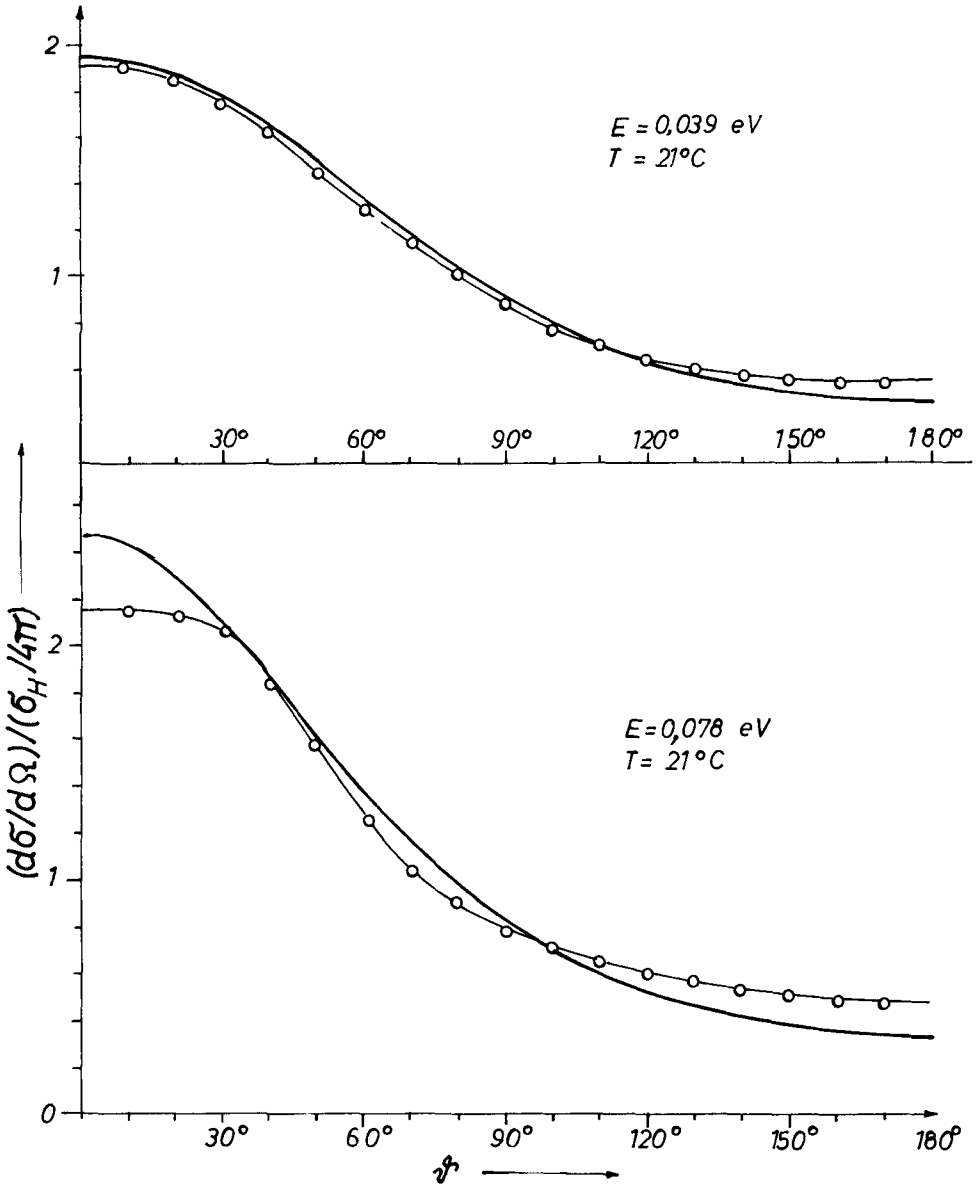

Fig. 3

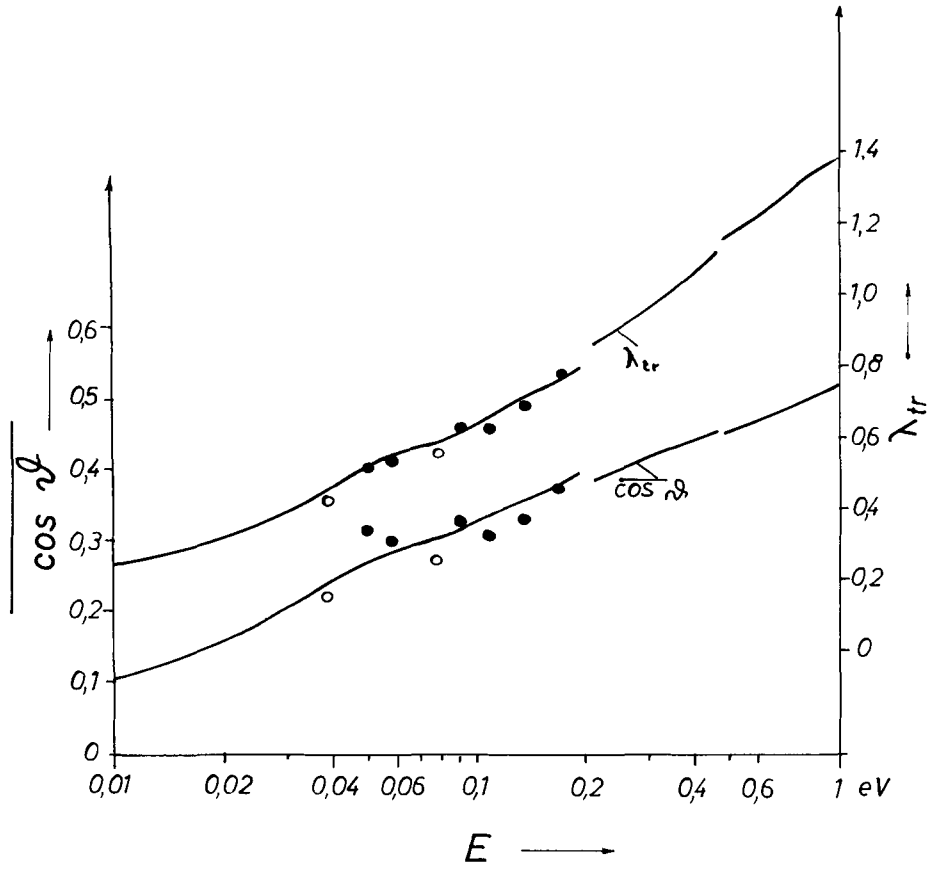
0,6
0,5
0,4
0,3
0,2
0,1
0
cos ϑ
1,4
1,2
1,0
0,8
0,6
0,4
0,2
0
λtr
λtr
cos ϑ
0,01
0,02
0,04
0,06
0,1
0,2
0,4
0,6
1 eV
E

M. G. Zemlyanov, N. A. Chernoplekov

INVESTIGATION OF INELASTIC SCATTERING OF COLD NEUTRONS BY CERTAIN HYDROGEN-CONTAINING SUBSTANCES

ABSTRACT

Using a beryllium filter to separate the spectral line of cold neutrons and the transit time method for an energy analysis, we investigated the spectra of neutrons inelastically scattered by benzene, diphenyl, and non-irradiated and irradiated polyethylene. The measurements were carried out at sample temperatures of 20° C. The data obtained are compared with the results of optical investigations of the spectra of the indicated substances.

1. INTRODUCTION

An investigation of the inelastic scattering of cold neutrons by hydrogen-containing substances such as benzene, diphenyl, and polyethylene is of interest for two reasons.

On the one hand, the polyphenyls and polyethylene are assuming an ever increasing significance as moderator materaisl in reactor building, and the solution of the problem of thermalization of neutrons in these substances calls for a direct investigation of the inelastic interaction processes. On the other hand, a study of inelastic scattering of cold neutrons by substances uncovers new possibilities of obtaining additional information concerning the excitation spectrum, i.e., on the dynamics of the substance, and the extraction of such information is for many hydrogen-containing substances (saturated, unsaturated, and aromatic hydrocarbons) of great practical and theoretical significance. Until recently the dynamics of these substances was investigated principally both by measuring the temperature dependence of their specific heat, and by measuring the infrared absorption spectra and the Raman spectra. However, as is well known, data on the temperature dependence of the specific heat do not make it possible to carry out unambiguous determination of the spectrum of oscillations of a Bose system, while in optical measurements one investigates and interprets, principally the high-energy transitions, corresponding to the intramolecular motions. A study of low-energy transitions, corresponding to intermolecular motions, is difficult to carry out by optical means, this entailing both apparatus difficulties and

factors that are principally physical. Consequently an investigation of the inelastic scattering of neutrons by hydrogen-containing substances is of great interest, particularly in the field of low energies.

Notice must be taken here of the specific features of the information contained in the spectrum of neutrons inelastically scattered by hydrocarbon compounds. Inasmuch as these compounds contain hydrogen and carbon atoms, which differ greatly in mass and in neutron scattering amplitudes, one might think that the information concerning the optical portion of the oscillation spectrum should be more reliable, since the cross section for interaction with hydrogen is larger than that with carbon, and hydrogen participates essentially in the optical oscillations. A factor acting in the opposite direction is that of the level population (the Boltzmann factor), which causes greater excitations to occur, for example, in the acoustic oscillations, and consequently, the cross section for inelastic interaction between neutrons and these levels is higher. In addition, one must note that the use of the experimental results for solving the inverse problem of determining the oscillation spectrum from the spectrum of the inelastically scattered neutrons is impossible for hydrocarbons. It is impossible because we do not know a priori the relationship between the polarization vectors $\bar{e} \propto (\bar{f})$ for

different oscillations, which vectors are contained in the general expression for the inelastic scattering cross section [1]:

$$\frac{d^2\sigma}{d\Omega\, d\varepsilon} \sim e^{-2W} \sum_{\alpha} \int \frac{d^3\bar{f}}{e^{\hbar\omega_\alpha(\bar{f})/kT} - 1} \frac{\left|\bar{x}\cdot\bar{e}_\alpha(\bar{f})\right|^2}{\omega_\alpha(\bar{f})} \delta\left[\varepsilon - \hbar\omega_\alpha(\bar{f})\right]$$

Since the polarization vectors are subject to the single limitation $\sum_{\alpha} \left|\bar{e}_\alpha(\bar{f})\right|^2 = 1$. Consequently, in order to determine the oscillation spectrum by means of a neutron experiment we must make use of model representations for the dynamics of the hydrocarbons. Consequently an analysis of the experimental data on inelastic scattering of cold neutrons by benzene, diphenyl, and irradiated or non-irradiated polyethylene will be limited to a qualitative comparison with the results of optical investigations and with the results of the theoretical work.

2. EXPERIMENTAL PROCEDURE AND DETERMINATION OF ERRORS

The inelastic scattering of cold neutrons by specimens of benzene, diphenyl, irradiated and non-irradiated polyethylene was measured in the I. V. Kurchatov Atomic Energy Institute using a setup mounted on the IRT-1000 reactor [2]. The primary line of the cold neutrons was separated with the aid of a filter made of polycrystalline

beryllium, while the analysis of the scattered neutrons was carried out at an angle of 90° to the incident beam using transit time, with the aid of a mechanical interruptor and a 128-channel time analyzer. Specimens 0.1 cm thick were mounted at 45° to the incident beam, their temperature being 20° C. To guarantee maximum resolution of the neutron spectrometer, $\Delta\varepsilon/\varepsilon = 6 -- 7\%$, the entire investigated energy interval of the scattered neutrons, from 5×10^{-3} to 2×10^{-2} ev, was broken up into five sections, each of which was investigated at suitable speeds of rotation of the mechanical interruptor, time delays in magnetostriction lines, time-analyzer channel widths, etc. After taking into account the distortion introduced by the transmission function of the mechanical interruptor, the data on the individual series of measurements were "joined" to each other on the basis of readings of the monitors. Corrections were then introduced into the results to allow for the deviation of the detector efficiency from the 1/v law and for the attenuation of the scattered neutrons via the air between the interruptor and the detector. No correction for the deformation that the specimen introduces into the spectrum of the incoming and scattered neutrons were made, since this correction is small for hydrocarbons. In fact, the expression for the measured spectrum has, after integration

over the thickness of the specimen, the following form

$$I(\lambda_0, \lambda) =$$

$$= I_0(\lambda_0) \frac{d^2\sigma(\lambda_0,\lambda)}{d\Omega\, d\lambda} \frac{1-\exp\left\{-\sqrt{2}\, N\left[\sigma_t(\lambda_0)+\sigma_a(\lambda)\right] d\right\}}{\sqrt{2}\, N\left[\sigma_t(\lambda_0)+\sigma_a(\lambda)\right]}$$

where $I_0(\lambda_0)$ -- spectral line of cold neutrons,

$d^2\sigma(\lambda_0, \lambda)/d\Omega\, d\lambda$ -- inelastic scattering cross section.

$\sigma_t(\lambda_0)$ -- total cross section for cold neutrons,

$\sigma_a(\lambda)$ -- absorption cross section for scattered neutrons.

d -- thickness of specimen,

N -- density of the nuclei.

Assuming that $I_0(\lambda_0) = \delta(\lambda_0 - \lambda_{av})$ and a specimen thickness of 0.1 cm, we can neglect the correction, since $\sigma_t(\lambda_0) \gg \sigma_a(\lambda)$ and

$$1 \gg \exp\left\{-\sqrt{2}\, N\left[\sigma_t(\lambda_0)+\sigma_a(\lambda)\right] d\right\}$$

3. MEASUREMENT RESULTS AND DISCUSSION

a) Benzene. The benzene molecule is one of the simplest among the polyatomic cyclic molecules, and its

spectrum has been investigated in detail theoretically and experimentally both in the condensed state and in vapor. In connection with the fact that the symmetry group of the benzene molecule is D_{6n} and that the alternative forbiddenness holds for the optical spectra of this molecule (levels that are inactive in the Raman spectrum are active in the infrared absorption spectrum and vice versa), one should not expect the neutronoscopic investigation of the benzene spectrum to yield additional information at energies above the first vibrational level of the benzene molecule ($E \simeq 0.05$ ev). If there are any differences, they should be sought at lower energies.

Fig. 1 shows the spectrum of the neutrons scattered by a specimen of liquid benzol at 20° C, obtained after 180 hours of operation of the apparatus. The intensity is plotted as a function of the wavelength of the scattered neutron, the resolution of the spectrometer during the transit time is indicated by the triangles, while the arrows designate the positions of the lines obtained in the Raman spectra and in the infrared absorption spectra [3, 4, 5]. It must be noted first of all that the maximum at ~ 4 Å ($\lambda_H = 3.952$ Å), corresponding to elastic scattering of the primary cold-neutron line, manifests itself weakly in the spectrum, and is comparable in intensity with the weak maximum in the primary line (Fig. 2), correspond-

ing to the system of planes Be(1, 1, 1). This change in the spectrum is obviously explained by the fact that there exist in liquid benzol, at low energies, a large level density, connected both with the quasi-phonon spectrum and with the rotational states of the molecules, and also with the presence of the strong diffusive motion in liquid benzene at 20° C. Therefore the inelastic scattering cross section of cold neutrons turns out to be comparable with the elastic scattering cross section, and this causes the elastic scattering peak to become smeared.

Further, as can be concluded from a comparison of the results of the optical investigations with the spectrum of inelastically scattered neutrons, it follows that all the levels that appear in the optical spectrum of benzene appeared also in the neutron spectrum. The difference lies only in the fact that the lines with frequencies 63 and 69 cm^{-1} (λ_H = ?.68 and ?.60 Å), corresponding to the rotational oscillation about the planar axis and the sixfold axis, are not resolved, and the line at $\nu = 405$ cm^{-1} (λ_H = 1.23 Å) which usually appears weakly in optical observations, was clearly pronounced in the neutron spectrum. However, along with the maxima of the inelastically scattered neutron,spectrum, which coincide in position with the lines of the optical spectra, certain maximum not observed in optical spectra also appear. This is first of all the

maximum at $\lambda_H = 1.30$ Å($\nu \simeq 360$ cm^{-1}) and the very weak maximum at $\lambda_H = 1.48$ Å($\nu \simeq 262$ cm^{-1}), and also two maxima at $\lambda_H = 2.80$ Å and $\lambda_H = 3$ Å($\nu = 55$ cm^{-1} and $\nu = 44$ cm^{-1}), situated between the levels of the rotational oscillations about the planar axes and sixfold axis.

b) Diphenyl. The experimental spectrum of inelastically scattered neutrons from a specimen of polycrystalline diphenyl is shown in Fig. 3. As in the case of benzene, the results of the optical investigations of the diphenyl spectrum, obtained essentially from the depolarization of Raman scattering [3], are indicated in the figure by arrows. Unlike benzene, the neutron spectrum of diphenyl has a clearly pronounced region of elastic neutron scattering of the first line ($\lambda_H = 3.64$ Å and 4 Å). The slope of the leading front of the main maximum of elastic scattering at $\lambda_H \simeq 4$ Å is determined only by the resolution of the neutron spectrometer, and consequently, at the temperature of the experiment, which was 50° lower than the melting point of diphenyl, the diffuse motion in diphenyl is practically nonexistent. From the ratio of the ordinates of the maxima of the elastic scattering at $\lambda_H = 3.64$ Å and $\lambda_H = 4$ Å, which does not differ strongly from the ratio of the ordinates in the primary line, one can conclude that the level density in solid diphenyl is insignificant in the low energy region near 10^{-3} ev. As in

the case of benzene, the spectrum of the neutrons inelastically scattered by diphenyl contains along with the lines that appear in the optical spectra also lines missing from the optical spectra. These lines are situated in the diphenyl spectrum near $\lambda_H = 2.23$ Å ($\nu \simeq 104$ cm^{-1}) and $\lambda_H = 3.25$ A ($\nu \simeq 34$ cm^{-1}). In Fig. 3 these lines are indicated with arrows marked with a question mark. Although the nature of these maxima has not yet been established, it must be noted that both in the optical and in the neutron spectra of the benzene, maxima appear at these wavelengths.

c) Non-irradiated and irradiated polyethylene. The specimens used were polyethylene low-pressure films with average molecular weight 5×10^4 and 60% degree of crystallinity. One of the polyethylene specimens was irradiated in a reactor with an integral dose of about 500 Mrad, corresponding to the formation of about 10% of joinings between the polymer chains. The experimental results on the measurement of the spectra of inelastically scattered neutrons from the polyethylene specimens are shown in Figs. 4 and 5. For the sake of convenience in comparison, the spectra have been normalized to equal intensity at the elastic-scattering maximum at $\lambda_H = 4$ Å, and the entire investigated wavelength interval of the scattered neutrons is broken up into two parts, the range from 0.7 to 1.2 A (Fig. 4), and the range from 1.2 to 4.5 A (Fig. 5). As

before, the arrows indicate the positions of the lines observed in the optical spectra of polyethylene [6, 7, 8]. From a comparison of the results of the optical investigations with the spectrum of the inelastically scattered neutrons (Fig. 4) we can conclude that the spectrum of the inelastically scattered neutrons duplicates to a considerable degree the optical spectrum, i.e., the infrared absorption lines and the Raman lines correspond within the limits of the resolution, to maxima of the neutron spectrum. The neutron spectrum contains also lines which are classified as very weak in the optical spectrum, and for a series of very closely lying lines of the optical spectrum (λ_H = 0.745 -- 0.780 Å) the neutron spectrum yields an envelope, owing to the insufficient resolution. As can be seen from Fig. 4. in the wavelength interval of the scattered neutrons from 0.7 to 1.2 Å, no noticeable difference is seen between the spectra of the non-irradiated and irradiated polyethylene and between the neutron and the optical spectra. The difference manifests itself at long wavelengths of the scattered neutrons, with $\lambda_H >$ 1.2 Å (Fig. 5). What is striking in this region is the transition from elastic scattering (maxima at λ_H = 4 and 3.64 Å) to inelastic scattering. The ratio of intensities of elastic to inelastic scattering is 3:1. Such a ratio indicates that in both the non-irradiated and irradiated

polyethylene there is a considerable level density in the region of low energies, connected possibily with the rotation of the segments of the polymer chains. This result agrees with results obtained by investigating the nuclear magnetic resonance lines in polyethylene, where it becomes necessary to assume that polyethylene contains a system of low-lying energy levels in order to explain the small width of the experimentally observed lines [9].

The cited references on the investigation of optical spectra of polyethylene contain indications that weak lines have been observed, with frequencies $\nu = 150$ cm^{-1} and $\nu = 200$ cm^{-1} (corresponding to $\lambda_H = 1.94$ and 1.71 Å). As can be seen from Fig. 5, two maxima appear in the neutron spectrum of both non-irradiated and irradiated polyethylene. These can be regarded as coinciding, within the limits of resolution, with the results of the optical investigations. These are the lines at $\lambda_H = 2.04$ Å and $\lambda_H = 1.78$ Å (optical frequencies $\nu \simeq 135$ and $\nu \simeq 184$ cm^{-1}). However, the structure of the neutron spectra is more complicated. In this connection it would be desirable to compare the results of the neutron research on the polyethylene spectrum, in the considered region of wavelengths, with the theoretical work on the dynamics highly-anisotropic chain materials, used to explain the temperature dependence of the specific heat [10, 11]. However, the

polyethylene model that was used as the basis of the theoretical analysis of [10], in which the true structure of the crystalline regions of the polyethylene is approximated by a tetragonal lattice, and in which no account is taken of the presence of the amorphous phase and the solutions of the dynamic matrix are unstable with respect to the choice of the force constants, is far from reality. Consequently, a comparison of the data of the neutron experiment with this theory is not convincing.

The spectrum of inelastically scattered neutrons at $\lambda_H > 1.2$ Å contains along with the lines at $\lambda_H = 2.04$ and $\lambda_H = 1.78$ Å a few other maxima, namely a clearly pronounced maximum at $\lambda_H = 1.51$ Å ($\nu \simeq 264$ cm^{-1}) in both the irradiated and non-irradiated polyethylene, and maxima at $\lambda_H = 2.20$ and 2.94 Å, which manifest themselves more pronouncedly in the spectrum of the non-irradiated polyethylene. The spectrum of the irradiated polyethylene displays also a weak maximum at $\lambda_H = 2.63$ Å ($\nu \simeq 64$ cm^{-1}). The degree to which these maxima are connected with the singularities of the phonon spectrum of the polyethylene cannot be judged from the results of this experiment. As regards the difference in the spectrum of inelastically scattered neutrons from non-irradiated and irradiated polyethylene, we can see from Figs. 4 and 5 that there is no appreciable difference between these spec-

tra. All that is observed are weak discrepancies between the spectra, which manifest themselves only in the long-wave portion of the spectrum and apparently call for a more detailed investigation.

CONCLUSION

By investigating the spectra of neutrons inelastically scattered by samples of benzene, diphenyl, and non-irradiated and irradiated polyethylene at 20° C, it was established that the neutron spectra of these substances have certain singularities that do not appear in their optical spectra. A more exact determination of the energy position of these singularities and a determination of their nature require, on the one hand, an increase in the resolution of the neutron spectrometer with respect to the transit time and a considerable narrowing down of the spectral line of the cold neutrons, and on the other hand measurements of the spectrum of the inelastically scattered neutrons at different temperature above and below the melting temperature and the temperature T_g.

The authors are grateful to M. I. Pevzner for continuous interest in the work and for participating in the discussion of the results.

BIBLIOGRAPHY

1. G. Placzek, L. Van Hove, Phys. Rev. 93, 1027 (1954).

2. M. G. Zemlyanov, N. A. Chernoplekov, PTÉ (Instruments and Measurement Techniques), in press.

3. A. Fruhling, Ann. de Phys. 6, 401 (1951).

4. R. D. Mair, D. F. Morig, J. Chem. Phys. 17, 1236 (1949).

5. V. L. Broude, UFN (Advances in Physical Sciences), LXXIV, 577 (1961).

6. S. Krimm, Y. Chiang, G. Sutherland, J. Chem. Phys. 25, 549 (1956).

7. J. R. Nielsen, A. H. Woolett, J. Chem. Phys. 26, 1391 (1957).

8. M. C. Tobin, M. J. Carrano, J. Chem. Phys. 25, 1044 (1956).

9. U. Slichter, Collection "Fizika polimerov" (Polymer Physics)(Translations), IIL, 1960, p. 171.

10. S. M. Genensky, G. F. Newell, J. Chem. Phys. 26, 486 (1957).

11. H. W. Starkweather, Jr., J. Polymer Sci. 45, 525 (1960).

Figure Captions

Fig. 1. Spectrum of neutrons scattered by liquid benzene.

Fig. 2. Spectral line of neutrons filtered by polycrystalline beryllium.

Fig. 3. Spectrum of neutrons scattered by polycrystalline diphenyl.

Fig. 4. Spectrum of neutrons scattered by irradiated and non-irradiated polyethylene in the wavelength interval from 0.7 to 1.2 Å.

Fig. 5. Spectrum of neutrons scattered by irradiated and non-irradiated polyethylene in the wavelength interval from 1.2 to 4.5 Å.

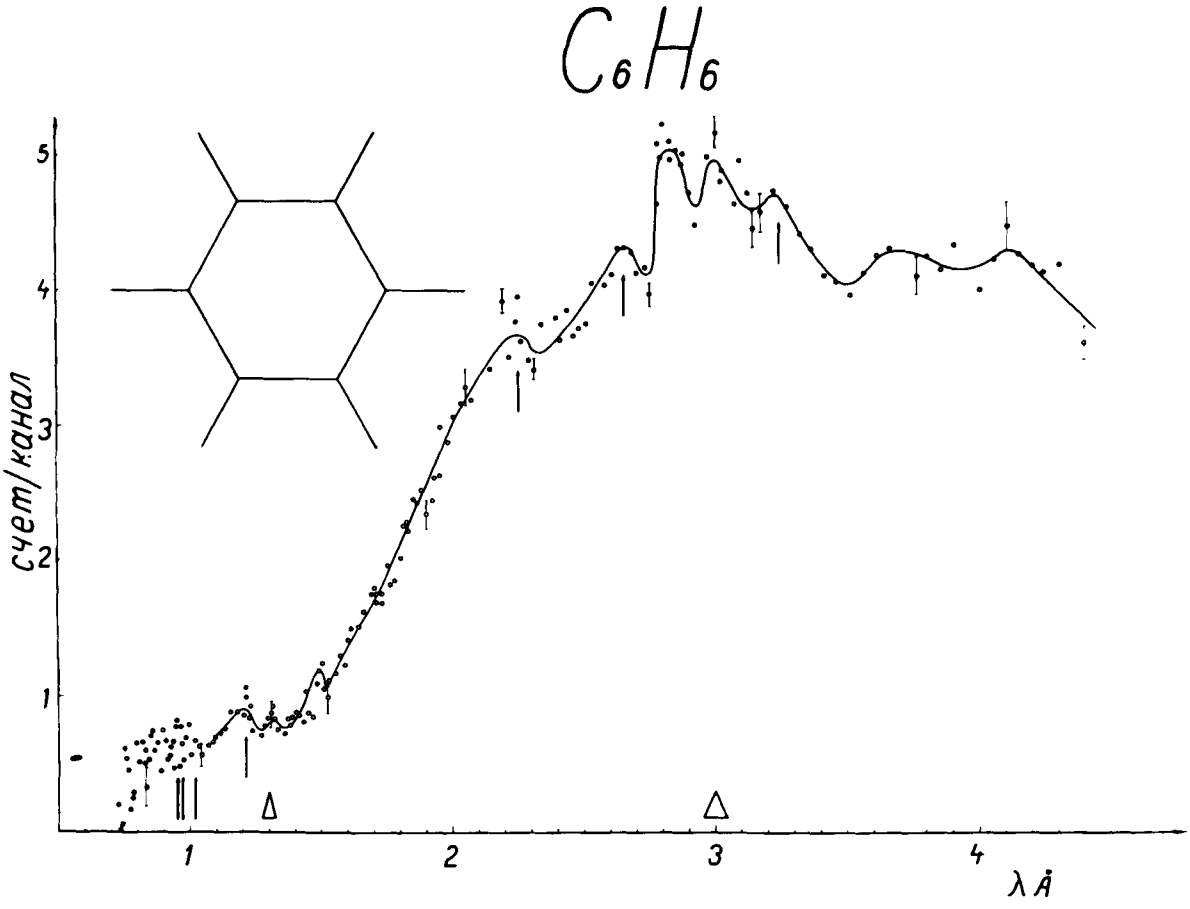

Figure 1

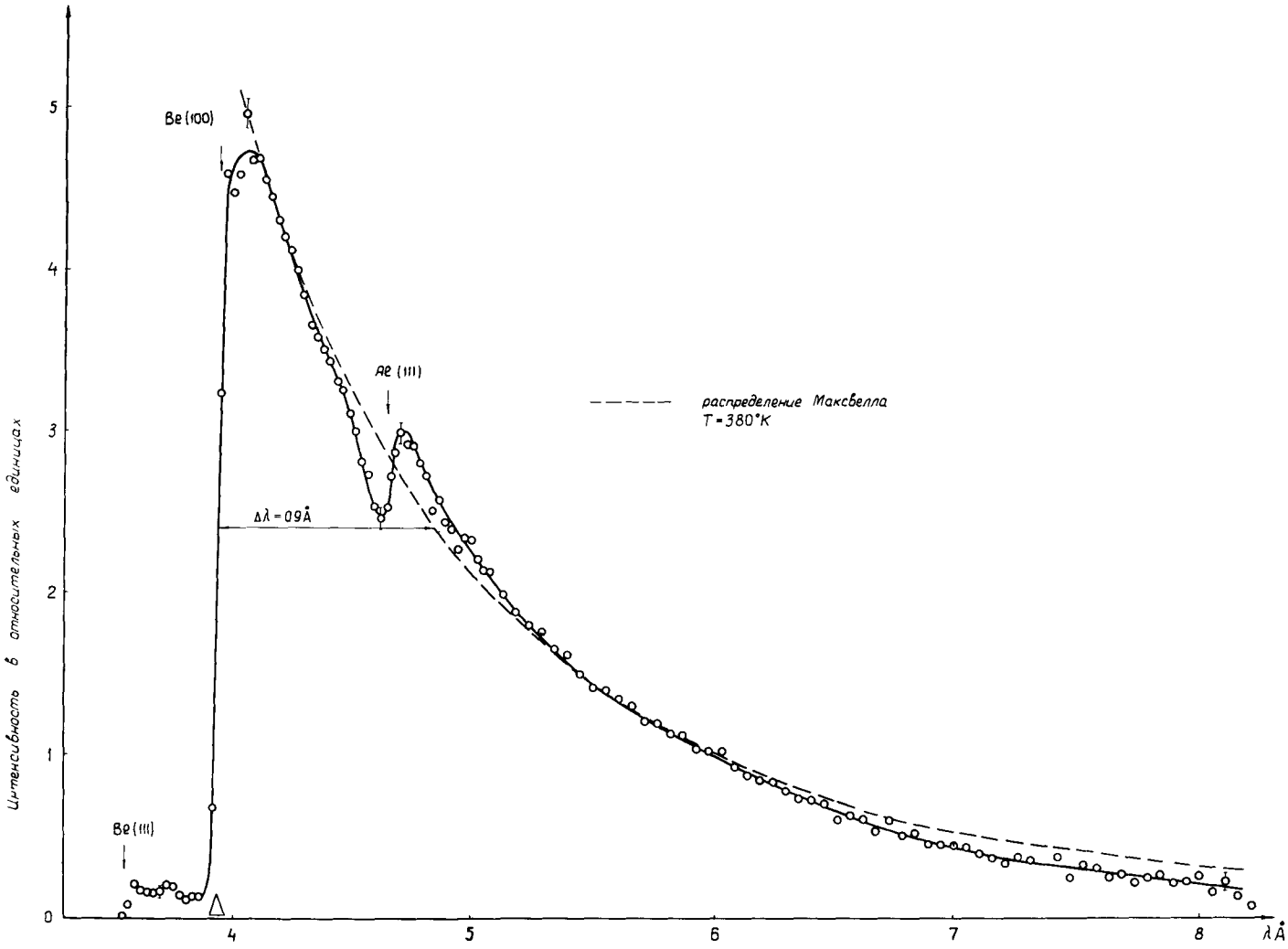
Be(100)
Be(111)
Ae (111)
Δλ = 0.9Å
распределение Максвелла
T = 380°K
Интенсивность в относительных единицах
λÅ
0
1
2
3
4
5
4
5
6
7
8

Figure 2

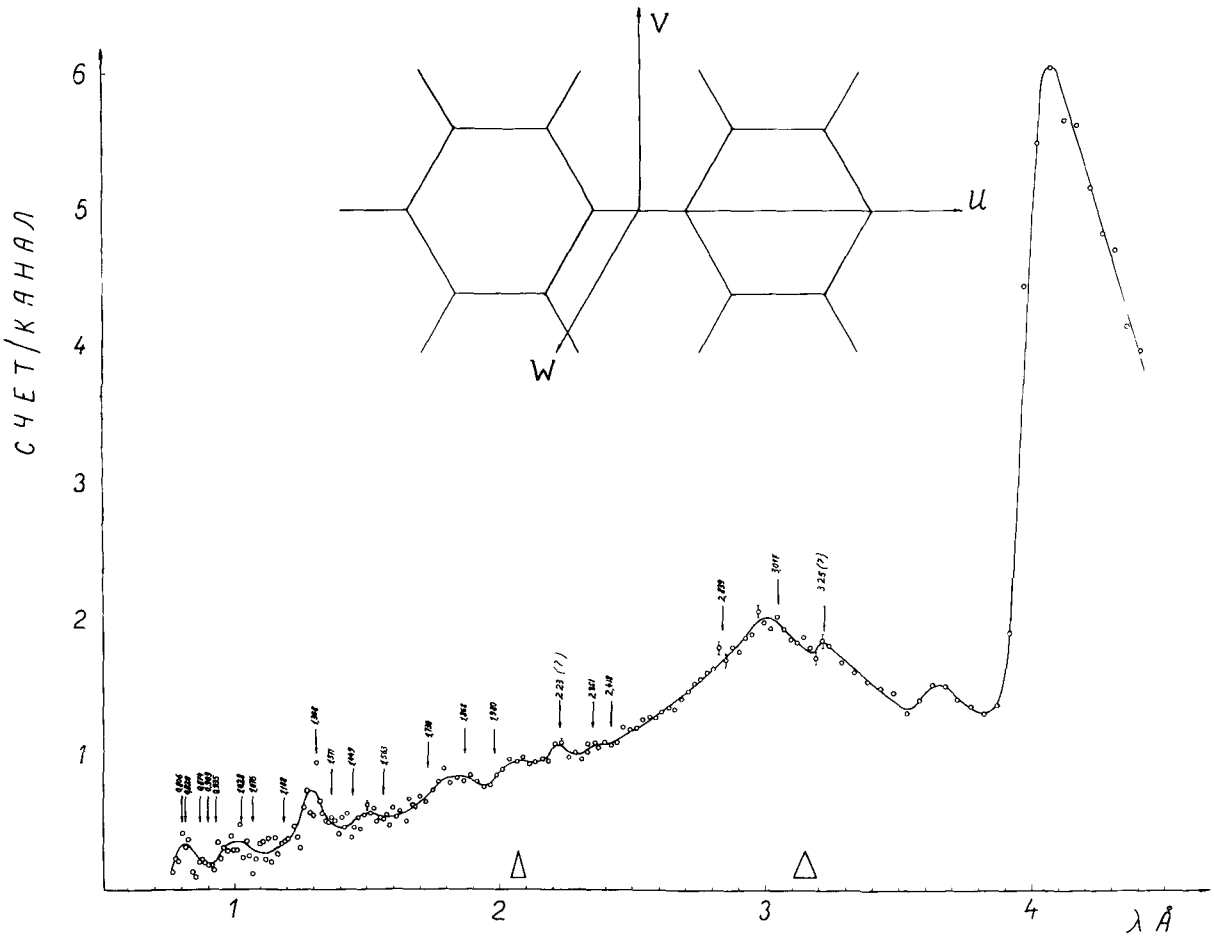

Figure 3

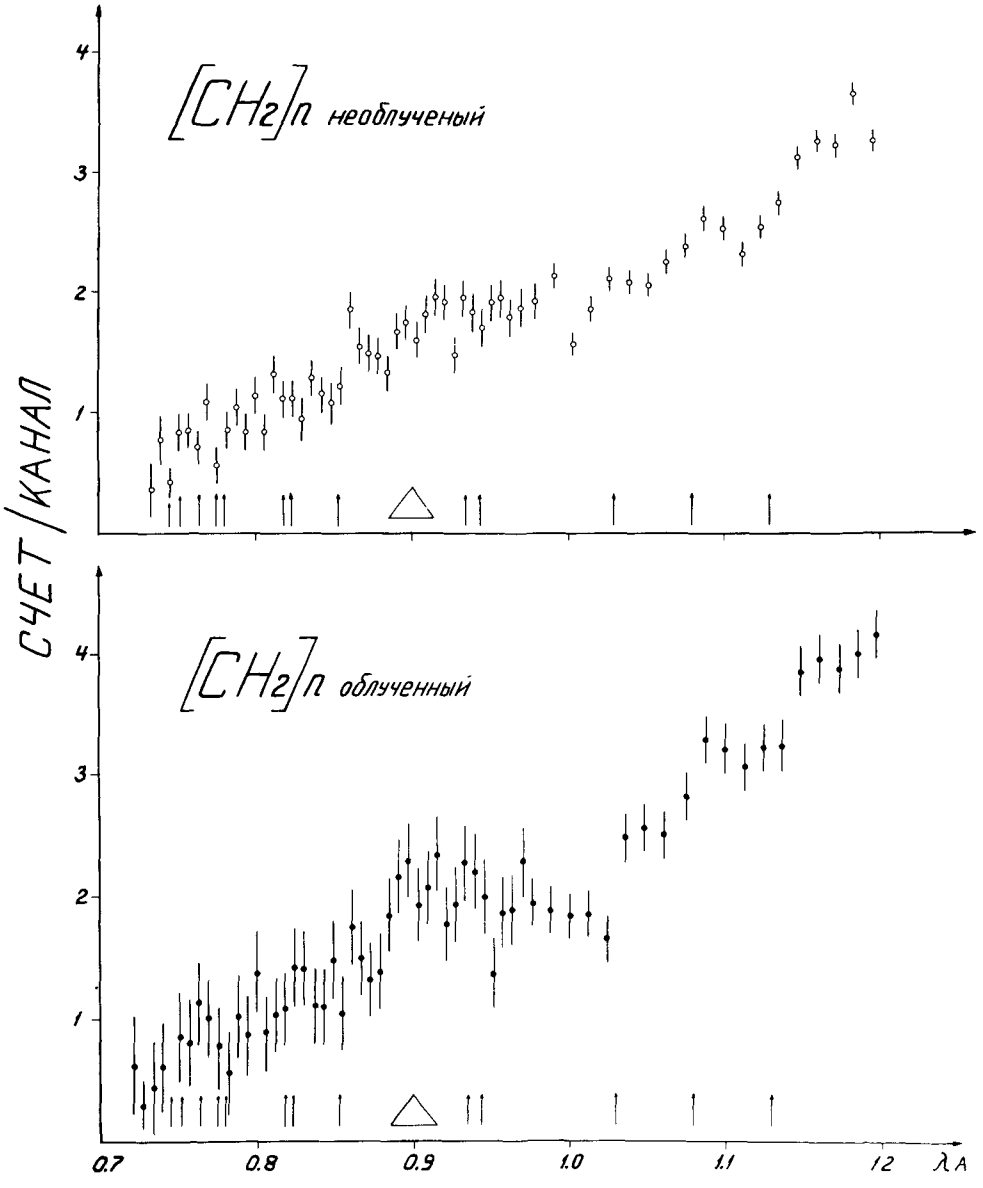
[CH2]n необлученый
[CH2]n облученный
СЧЕТ/КАНАЛ
1
2
3
4
0.7
0.8
0.9
1.0
1.1
1.2
λA

Figure 4

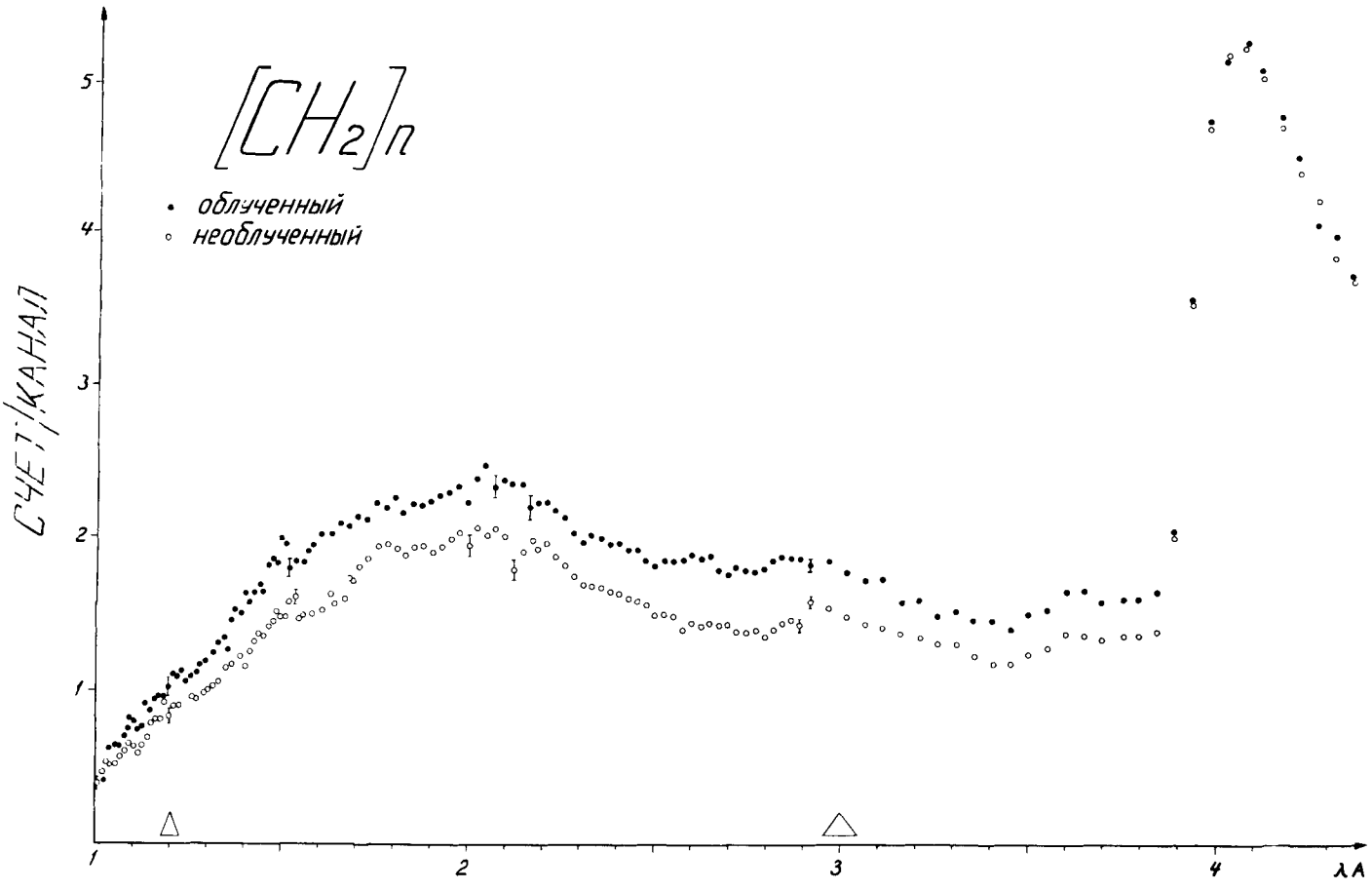

Figure 5

THE SCATTERING LAW

B. Theoretical Aspects

THEORETICAL ASPECTS OF THE SCATTERING LAW

P. Schofield*

Brookhaven National Laboratory
Upton, New York

*Research Collaborator, October 1961 to May 1962. Permanent address: Theoretical Physics Division, Harwell, Didcot, Berks., England.

1. Introduction

This report falls into two parts – a review of methods of calculation of the scattering law, illustrated by the examples given in papers presented to the conference (1-6), followed by a discussion of various integral properties of the scattering law, and their sensitivity to its detailed nature.

In the first part of the paper emphasis is placed on the mathematical nature of the approximation used rather than on detailed physical considerations. This is because the scattering law is subject to various constants (detailed balance, and the Placzek moment theorem) which from the point of view of thermalization theory are of greater significance than for example details of the energy level structure of the scattering system.

A. Scattering Law Calculations

2. General Formulation

In the general discussion, I shall restrict attention to the contribution to the total scattering due to the incoherent scattering from one species of atom, chemically bound in a particular way. For this the scattering cross section for neutrons from initial energy E to final energy E′ through an angle θ is given by

$$\sigma(E \rightarrow E', \theta) = \frac{\sigma_o}{4\pi} (E'/E)^{\frac{1}{2}} \frac{1}{2\pi\hbar} \int_{-\infty}^{\infty} \gamma(\underline{\kappa}, t) e^{i\omega t} \, dt \qquad (1)$$

where σ_o is the bound atom cross section, $\hbar\underline{\kappa}$ the momentum transfer and $\hbar\omega$ the energy transfer between neutron and scattering system. $\gamma(\underline{\kappa}, t)$ defined below is a correlation function for the motion of the type of atom under consideration.

To obtain the macroscopic cross section which appears in the Boltzmann equation for thermal neutrons, we have to take a sum of terms of the form (1) for each possible type of binding of atoms in the system, weighted with the number density of such atoms, followed by a sum over the different atomic species in the system. In addition there may be terms due to interference in the scattering from different atoms.

There are thus two problems involved in constructing a theoretical scattering law. These are a) the physical problem of obtaining $\gamma(\underline{\kappa}, t)$ and b) the mathematical problem of the evaluation of the Fourier transform integral (1). However, whatever physical or mathematical approximations are made, it is essential that certain "rules" should be borne in mind in computing cross sections for the calculation of neutron spectra. These may be summarized under (A) through (D):

(A). $\gamma(\underline{\kappa},t)$ is analytic in t around t = 0 and is such that $\gamma(\underline{\kappa}, t - \frac{i\hbar}{2kT})$ is real for real $\underline{\kappa}$,t, where T is the temperature of the moderator. This is the detailed balance condition.

Rules (B), (C), and (D) relate to the short time behavior of $\gamma(\underline{\kappa},t)$:

(B). $\gamma(\underline{\kappa},0) = 1$ (2)

(C). $\gamma'(\underline{\kappa},0) = i\frac{\hbar\kappa^2}{2M}$ (M the mass of the atom) (3)

(D). $\gamma''(\underline{\kappa},0) = -(\hbar\kappa^2/2M)^2 - \kappa^2\frac{\overline{kT}}{M}$ (4)

where $\overline{kT}$ is two-thirds the mean kinetic energy of the atoms. (Primes denote derivatives with respect to time.)

These rules can also be expressed in terms of the scattering law, $S(\alpha,\beta)$, of the dimensionless variables α and β. $S(\alpha,\beta)$ is defined by

$$e^{-\beta/2} S(\alpha,\beta) = \frac{kT}{\hbar}\frac{1}{2\pi}\int_{-\infty}^{\infty}\gamma(\underline{\kappa},t)\, e^{i\omega t}\, dt \tag{5}$$

where

$$\alpha = \frac{\hbar^2\kappa^2}{2MkT} = \frac{1}{AkT}(E + E' - 2(EE')^{\frac{1}{2}}\cos\theta) \tag{6}$$

$$\beta = \frac{\hbar\omega}{kT} = \frac{1}{kT}(E' - E) \tag{7}$$

Rule (A) then states that $S(\alpha,\beta)$ is an even function of β, while (B), (C), and (D) give respectively

$$(B') \quad 2\int S(\alpha,\beta) \cosh \frac{\beta}{2} d\beta = 1 \tag{8}$$

$$(C') \quad 2\int S(\alpha,\beta)\beta \sinh \frac{\beta}{2} d\beta = \alpha \tag{9}$$

$$(D') \quad 2\int S(\alpha,\beta)\beta^2 \cosh \frac{\beta}{2} d\beta = \alpha^2 + 2\frac{\bar{T}}{T}\alpha \tag{10}$$

These are the moment theorems first obtained by Placzek (8). The significance of these rules in thermalization theory is as follows: if rule A is violated then the Maxwellian distribution of neutrons is no longer a solution of the infinite medium Boltzmann equation in the absence of absorbers. Thus this rule must not be relaxed in calculating cross sections for situations where a thermal spectrum is established. Rules B and C determine the high energy total cross section as the free atom cross section: if rule B is relaxed then in general the cross section will become zero or infinite at high energies. Rules C and D determine the rate of energy transfer between neutron and moderator at high energies, so these rules also should not be relaxed in calculating cross sections above thermal energies.

Although the emphasis here is on the calculation of cross sections for reactor purposes, it is interesting to consider the formal properties of $\gamma(\underline{\kappa},t)$.

In particular in a recent memorandum, R. Aamodt et al. (9) have considered the relation between $\gamma(\underline{\kappa},t)$ and its classical equivalent, and shown that formally

$$S(\alpha,\beta) = S_c(\alpha,\beta)\, e^{-\alpha/4} + O(\hbar^2) \tag{11}$$

where $S_c(\alpha,\beta)$ is computed from the classical $\gamma(\underline{\kappa},t)$. In a paper at this conference Rosenbaum and Zweifel (10) show some numerical results indicating the magnitude of this correction in a number of cases.

3. Scattering by Molecules

In two papers to the conference McMurry et al. (1,2) have compared methods of calculation of the scattering from isolated molecules under the assumption that the Hamiltonian can be separated into non-interacting parts corresponding to translation rotation and vibration. In such a case $\gamma(\underline{\kappa},t)$ separates into a product of two factors γ_T for the translational motion, and γ_{RV} for the rotation and vibation.(10) The vibrational part can be written in the form

$$\gamma_V = \exp\left\{ -\underline{\kappa} \cdot \langle \underline{u}(0)\underline{u}(0)\rangle_T \cdot \underline{\kappa} + \underline{\kappa} \cdot \langle \underline{u}(0)\underline{u}(t)\rangle_T \cdot \underline{\kappa} \right\} \tag{12}$$

where $\underline{u}(t)$ is the displacement of an atom from its equilibrium position with respect to axes fixed in the molecule. γ_{RV} then contains this factor together with the rotational contribution averaged over orientation of the molecule.

Of particular interest in these results is a comparison of the exact average over orientations compared to "Krieger-Nelkin" averaging where the average is performed in the exponent of (12). Figures 1, 9, and 10 of reference 2 show that for the highly symmetric molecule of methane the two agree quite well, while for the linear pseudo-molecule OH, there is a marked disagreement.

Another point of interest is that a classical treatment of the vibrational modes leads to too great an energy loss for scattering of high energy neutrons (Figure 10) as would be expected since rule D is then violated.

A method of calculation which is not given in McMurry's paper is to use the "Gaussian approximation" to calculate the scattering. This has been considered, from the point of view of computation, in a recent paper by Schofield and Egelstaff (12),and has so far been the basis for computations using the experimentally measured $S(\alpha,\beta)$. Here $\gamma(\underline{\kappa},t)$ is specified by a normalized frequency distribution $\rho(\beta)$:

$$S(\alpha,\beta) = \frac{1}{2\pi}\int_{-\infty}^{\infty} I(\alpha,t)e^{i\beta t}\,dt \tag{13}$$

$$I(\alpha,t) = \exp\{-\alpha W(t)\} \tag{14}$$

$$W(t) = \int \frac{\rho(\beta)}{\beta \sinh \beta/2}\,[\cosh \beta/2 - \cos \beta t]\,d\beta \tag{15}$$

[Note that "Krieger-Nelkin" averaging is implicit in this formalism; see, however, Appendix III of reference 12.]

I quote here the form of $\rho(\beta)$ for the rotational motion of an atom in a diatomic molecule. This may be obtained by evaluating the velocity self-correlation function for a particle moving in a sphere without using explicit forms of the rotational wave-functions: (13)

$$\rho_R(\beta) = \frac{2}{3} \frac{\sum_{\ell} \ell^2 (e^{\hbar^2 \ell / IkT} - 1)\, e^{-(\hbar^2/2IkT)\ell(\ell+1)}\, \delta(\beta - \frac{\ell\hbar^2}{IkT})}{\sum_{\ell} (2\ell+1) e^{-(\hbar^2/2IkT)\ell(\ell+1)}} \tag{16}$$

$\rho_R(\beta)$ is normalized to 2/3 since the rotational motion accounts for this fraction of the total degrees of freedom of the atom. In the limit of large moment of inertia (small energy level separation), $\frac{\hbar^2}{IkT} \ll 1$, $\rho_R(\beta)$ may be replaced by a continuous pseudo-classical distribution:

$$\rho_R^c(\beta) = \frac{2}{3} \frac{kT}{\hbar} \frac{1}{2} I^2 \omega^3\, e^{-\frac{1}{2}\frac{I\omega^2}{kT}} \tag{17}$$

where $\omega = \frac{kT}{\hbar}\beta$.

A comparison of this Gaussian approximation with the other methods of calculation would be of great interest, since the rotating system is the only definitely non-Gaussian system for which an exact calculation is possible.

In the paper by Yip and Osborn (3), a model for scattering from a hindered rotator is given, by considering the motion of a dipolar molecule in a strong electric field. An interesting feature of their result is the prediction that to a good first approximation, γ has the form

$$\gamma(\underline{u},t) = f_o(\underline{\kappa}) + f_1(\underline{u})g(\nu,t) \tag{18}$$

where $f_o(\underline{\kappa})$ and $f_1(\underline{\kappa})$ depend only on the structure of the molecule and are independent of the energy of the oscillator, ν, corresponding to the hindered rotation. Thus even in a more realistic model of a liquid where instead of a single frequency there is a distribution of frequencies ν, γ still has the form (18). It should be possible to test experimentally from measurements of $S(\alpha,\beta)$ in an appropriate liquid (ammonia ?) whether this is so in practice.

The papers of Goldman and Federighi (4), and of Boffi et al. (5) treat the scattering from polyethylene and polyphenyls respectively. These calculations are both based on (12) for the vibrational $\gamma(\underline{\kappa},t)$. The $\underline{u}(t)$ for each hydrogen atom are obtained in terms of normal coordinates, and frequencies obtained from infrared data in (4) and for a normal mode analysis of benzene in (5).

The paper by Macdougall (6) describes the computer codes LEAP, which uses the methods of reference (12) to compute $S(\alpha,\beta)$ from a given

$\rho(\beta)$, in the Gaussian approximation, and in particular some calculations of cross section and spectra for graphite using experimental data of Egelstaff (unpublished).

B. The Scattering Law and Neutron Thermalization

4. General Discussion

One of the main difficulties in making a direct assessment of the sensitivity of thermal neutron spectra to the form of $S(\alpha,\beta)$ lies in the rather awkward relation between α and β for given initial and final neutron energy and angle. Although it has long been realized that spectra must be insensitive to fine details in the scattering [as an extreme case of insensitivity, see Table 1 of Macdougall's paper (6)], it is only recently that quantitative estimates have been made of such sensitivity.

In the epithermal range, the expansions of Placzek (8) and of Wick (14) combined with asymptotic solutions of the energy dependent equation for thermal neutrons (15,16) have indicated the importance of certain parameters, such as the mean kinetic energy of the moderating atom, and the curvature of the potential with which they interact. However, the range of validity of such expansions does not reach far into the thermal range.

Recently quite a number of authors have shown, independently, how, within the framework of the Gaussian approximation, various averages over

the scattering law can be evaluated directly in terms of the function W(t) or (equivalently) $\rho(\beta)$ (17-21).

The general results of this work can be derived from a function which I call $F(\lambda,\mu)$. It is defined by

$$\sigma_o F(\lambda,\mu) = \int_0^\infty dE\ E\ e^{-E} \int_0^\infty dE' \sigma(E \to E')\ \exp\{-\lambda E - \mu E'\} \qquad (19)$$

that is, as the double Laplace transform of the symmetrical cross section $Ee^{-E}\sigma(E \to E')$. (The energy is here measured in units of the moderator temperature.)

Within the Gaussian approximation, $F(\lambda,\mu)$ reduces to a single time integral:

$$F(\lambda,\mu) = \frac{1}{8} \int_{-\infty}^{\infty} dt \left\{t^2 + \frac{1}{4}(1+\lambda+\mu)^2 + (1+\lambda+\mu)\frac{1}{A} W(t + \frac{1}{2}(\lambda-\mu))\right\}^{-3/2} \qquad (20)$$

Clearly by taking derivatives with respect to λ and μ and setting $\lambda = \mu = 0$ matrix elements of the scattering kernel between powers of E may be obtained, and hence between orthogonal polynomials: this is discussed with respect to the Laguerre polynomials by Purohit (19) and Takahashi (20). Corngold (17) obtains expressions for arbitrary powers of energy, in terms of integrals over hypergeometric functions.

Purohit and Rajagopal (22) have performed extensive calculations

using various Doppler approximations. Here W(t) is expanded about some point in the complex t-plane by a Taylor series, terms through t^2 being retained. With this approximation it is possible to obtain in fairly simple form the single integral over E′ in (19), and hence evaluate moments of energy transfer between neutrons of incident energy E and the moderator. The difficulty here is that it is impossible to satisfy simultaneously all conditions (A) to (D) (except in the trivial case of the free gas), so that to obtain consistency with these conditions, the expansion should be performed about some point $t + i\tau$, where τ depends on the initial neutron energy.

In reference (21), I have considered the rate of energy exchange between a Maxwellian distribution of neutrons at a temperature T and a moderator of temperature T_M. This has the advantage that while this function of T/T_M contains all the information for the rate of exchange of energy between neutron and moderator, it is much simpler to assess the sensitivity to the form of W(t) in this way.

A brief discussion of this method together with some preliminary results is presented in the next section.

5. Rate of Energy Exchange Between Neutrons and Moderator

As an assessment of the sensitivity of thermalization phenomena to

the form of $\rho(\omega)$,* we consider the function $M^{(1)}(\beta,\omega)$ defined through the following sequence of equations. We consider the rate of exchange of energy between a thermal distribution of neutrons of temperature $T = T_M/\beta$ and a moderator of temperature T_M. This should be a dominant factor in determining the relation between the scattering law and neutron spectra. Let

$$\int_0^\infty dE \int_0^\infty dE'\ \beta^3\, e^{-\beta E}(E - E')\sigma(E \to E') = \sigma_o \frac{4}{A} M_1(\beta) \tag{21}$$

Then it can be shown (21)

$$M_1(\beta) = \int_0^\infty \rho(\omega) M_1^{(1)}(\beta,\omega)d\omega + O(1/A) \tag{22}$$

where

$$M_1^{(1)}(\beta,\omega) = \frac{1}{2 \sinh \frac{\omega}{2}} \sinh\left\{ \frac{1}{2}(1-\beta)\omega\right\} k_2\left(\frac{1}{2}\beta\omega\right) \tag{23}$$

(where $x^{-2}k_2(x) = K_2(x)$, the modified Bessel function).

In thermalization theory we are mainly interested in the range $0 < \beta < 1$, at the ends of the interval. (i) β small

$$M_1^{(1)}(\beta,\omega) \sim 1 - \beta \tfrac{1}{2}\omega \coth \tfrac{1}{2}\omega = 1 - \beta K(\omega) \tag{24}$$

(ii) $\beta \sim 1$

$$M_1^{(1)}(\beta,\omega) \sim (1-\beta) \frac{\omega}{4 \sinh \frac{\omega}{2}} k_2(\tfrac{1}{2}\omega) = (1-\beta)(M/\omega) \tag{25}$$

*Note the change in notation here: I wish to retain β for its conventional use as an inverse temperature.

It turns out that for $\omega < 6$ (that is excitation energies less than 6kT), one can find functions $x(\beta)$ and $y(\beta)$ such that

$$M_1^{(1)}(\beta,\omega) = (1-\beta)\{1 - x(\beta)(K/\omega) - 1) - y(\beta)(1 - M(\omega))\} \quad (26)$$

Hence again for $\omega < 6$, the rate of energy transfer for a moderator of mass A, should be well characterized by the parameters $\overline{K}$ and $\overline{M}$, the average of $K(\omega)$ and $M(\omega)$ over the frequency distribution $\rho(\omega)$.

Some values are illustrated in Figure 1 where $\overline{M}$ is shown against $\overline{K}$ for various models. The lower curve is $K(\omega)$ and $M(\omega)$ for a single frequency while the higher shows $\overline{K}$ vs. $\overline{M}$ for a Debye frequency distribution. The open circles are given by the Yoshimori and Kitano frequency distribution for graphite as used in the calculations of Parks (23), and the full circle represents water at 293°K using the experimental data of Haywood and Thorson (24) for frequencies less than 6kT and the vibrational frequencies used by Nelkin (25) (with weight adjusted to give the correct normalization) for the higher frequencies. (The Nelkin model gives $\overline{K} = 3.37$, $\overline{M} = 0.317$ which is just outside the range of the figure.)

In Table 1, a summary of results for the Parks model of graphite (23) is given. The third column gives calculations of the parameter M_2 defined by

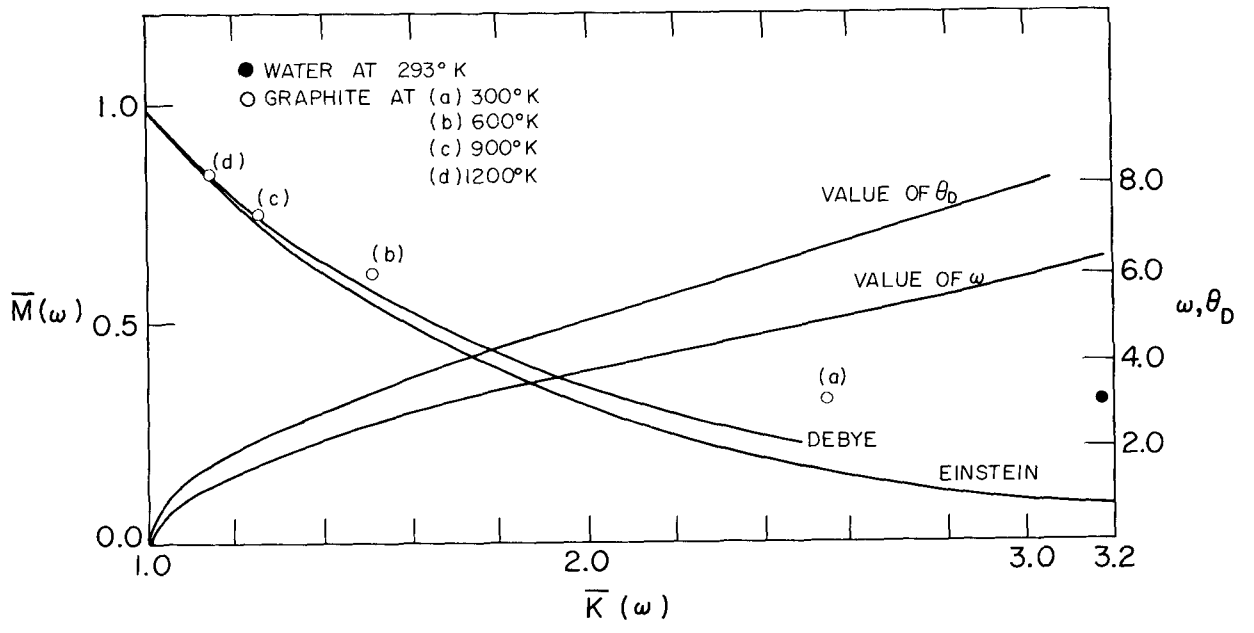

FIGURE 1

Table 1

Graphite (Parks, Yoshimori, and Kitano)

T, °K	$\overline{K}$	$\overline{M}$	M_2, b	$M_2^{(1)}$	$M_2^{(1)}$ (corrected)	θ_D, °K	
						$\overline{K}$	$\overline{M}$
300	2.35	0.314	1.068	1.15*	0.97	1980	1590
600	1.52	0.614	1.863	2.25	1.77	2040	1890
900	1.26	0.700	2.287	2.79	2.16	2120	1980
1200	1.16	0.851	2.467	3.12	2.38	2220	2100

*Krumhansl and Brooks gives 0.80 b. (Kothari)

$$M_2 = \int_0^\infty dE \int_0^\infty dE'\, E e^{-E}(E - E')^2 \sigma(E \rightarrow E') \qquad (27)$$

from the full scattering kernel (26), the fourth column shows the value obtained by the 1/A approximation, while the fifth column shows the result including a Doppler type correction for higher powers of 1/A. Since the latter is less sensitive to $\rho(\omega)$ than are $\overline{K}$ and $\overline{M}$, the good agreement between this corrected value and the exact value, indicates the adequacy of the 1/A approximation in assessing the sensitivity of this parameter to $\rho(\omega)$.

The final two columns of Table 1 give effective Debye temperatures for graphite based on a fit of $\overline{K}$ and $\overline{M}$ respectively. Where these agree, as at the higher temperatures, the analysis indicates that the Debye model should be adequate for calculating thermalization effects in graphite.

The value of 0.80 b for M_2 given in Table 1 is quoted from the paper by Kothari (27), and is based on calculations using the Krumhansl and Brooks frequency distribution.

ACKNOWLEDGEMENT

I wish to thank Dr. N. Corngold for a critical editing of the manuscript of this report.

REFERENCES

1. H. L. McMurry, "Calculation of Differential Scattering Cross Sections for Slow Neutrons," this conference.
2. H. L. McMurry, L. J. Gannon, and W. A. Hestir, "Evaluation of Techniques for Computing Differential Scattering Cross Sections," this conference.
3. S. Yip and R. K. Osborn, "Hindered Rotations in Liquids and Slow Neutron Scattering," this conference.
4. D. T. Goldman and F. D. Federighi, "Calculation of Thermal Neutron Flux Spectra in an Infinite Polyethylene Moderated Medium," this conference.
5. U. C. Boffi, V. G. Molinari, and D. E. Parks, "Slow Neutron Scattering and Thermalization by the Organic Molecules $C_{6n}H_{6n+2}$," this conference.
6. J. D. Macdougall, "Application of Scattering Law Data to the Calculation of Thermal Neutron Spectra," this conference.
7. P. A. Egelstaff, Nuclear Sci. and Eng. 12, 250 (1962).
8. G. Placzek, Phys. Rev. 86, 377 (1952).
9. R. Aamodt, K. M. Case, M. Rosenbaum, and P. F. Zweifel, "The Quasi-Classical Treatment of Neutron Scattering," University of Michigan preprint.
10. M. Rosenbaum and P. F. Zweifel, "Comparison of "Classical" and "Quasi-Classical" Cross Sections for Simple Systems," this conference.
11. A. C. Zemach, R. J. Glauber, Phys. Rev. 101, 118 (1956).
12. P. A. Egelstaff and P. Schofield, Nuclear Sci. and Eng. 12, 260 (1962).
13. P. Schofield, unpublished.

14. G. C. Wick, Phys. Rev. 94, 1228 (1954).

15. N. Corngold, Annals of Phys. 11, 338 (1960).

16. C. S. Shapiro, "On the Asymptotic Thermal Neutron Spectrum in Graphite," this conference.

17. N. Corngold, Brookhaven memorandum (1961).

18. M. V. Kazarnovsky and A. V. Stepanov, "Inelastic Scattering of Neutrons in Solids and Liquids," I.A.E.A. Vienna, p. 87 (1961).

19. S. N. Purohit, "Neutron Thermalization in a Crystalline Medium in Incoherent Approximation," this conference.

20. H. Takahashi, "Space and Time-Dependent Eigenvalue Problem in Neutron Thermalization," this conference.

21. P. Schofield, "The Scattering Law and Neutron Thermalization," to be published.

22. S. N. Purohit and A. K. Rajagopal, "Scattering of Thermal Neutrons in the Doppler Approximation," this conference.

23. S. E. Parks, GA-2438 (1961).

24. B. C. Haywood and I. M. Thorson, "The Scattering Law for Light and Heavy Water at 20°C and 150°C," this conference.

25. M. S. Nelkin, Phys. Rev. 119, 741 (1960).

26. D. E. Parks, private communication.

27. L. S. Kothari, "Thermal Neutron Scattering in Graphite," this conference.

GENERAL ATOMIC

Division of

GENERAL DYNAMICS

John Jay Hopkins Laboratory for Pure and Applied Science

P.O. Box 608, San Diego 12, California

GA-3024

SLOW NEUTRON SCATTERING AND THERMALIZATION BY BENZENE AND OTHER POLYPHENYLS

by

V. C. Boffi,[+] V. C. Molinari,[+] D. E. Parks

This paper is being submitted for presentation at the Conference on Neutron Thermalization to be held April 30 - May 2, 1962, at Brookhaven National Laboratory, Upton, Long Island, New York.

[*] This work was supported by Comitato Nazionale per l'Energia Nucleare, Rome, Italy.

[+] Affiliated with Comitato Nazionale per l'Energia Nucleare, Laboratorio di Fisica Nucleare Applicata, Rome, Italy.

Project No. 1.003 April 25, 1962

INTRODUCTION

In this report we shall discuss the general features of the neutron scattering by heavy organic molecules. Our object is to bring into focus those aspects of the molecular motions which are significant for understanding in detail the thermalization of neutrons in such moderators. In addition, we shall formulate the relation between the scattering and the molecular motions in such a way as to give this relation a form suitable for numerical calculations.

In Section I we shall present the general basis and physical assumptions which are appropriate for a realistic discussion of neutron thermalization by the heavy organic molecules.

In Section II we reduce this general basis to a form which allows one to accomplish a direct evaluation of the neutron energy transfer cross section in terms of the state of the chemical binding of the hydrogen in the hydrocarbons.

In Section III we shall be concerned with those aspects of the molecular motions of the organic compounds which are significant for understanding the scattering of thermal neutrons. In particular, we shall give the normal mode frequencies of benzene, and present our results for the normal mode amplitudes. A calculation of the neutron spectrum in a benzene moderator is given, and the effects of chemical binding are displayed by comparing this spectrum with the ones obtained in the case of moderation by a free proton gas and by H_2O. The spectrum in benzene is significantly harder than spectra in either free hydrogen or H_2O.

I. THE THERMALIZATION OF NEUTRONS BY ORGANIC COMPOUNDS

The point of view which we adopt consists in proceeding as far as possible from first principles. In our initial considerations we make approximations only when they are physically reasonable. As a consequence of the physical approximations, we arrive at an equation for the energy transfer cross sections which we expect to constitute a good basis for making mathematical and numerical approximations which express the cross sections in a form suitable for computation on a high-speed digital computer.

SCATTERING OF NEUTRONS BY ORGANIC COMPOUNDS

The scattering of neutrons by hydrogen is the dominating mechanism for the moderation and thermalization of fast neutrons by the hydrocarbons. A measure of the relative rates at which neutrons are slowed down by carbon and hydrogen atoms can be obtained by comparing the slowing down power $\xi\Sigma_s$, where ξ is the average logarithm energy loss per collision and Σ_s the free atom value of the macroscopic scattering cross section. In the hydrocarbons the numbers of hydrogen and carbon atoms are roughly equal, so that the ratio of the slowing down power in hydrogen to that in carbon is $(\xi\Sigma_s)_H/(\xi\Sigma_s)_C = 29$. Consequently, it is a very good approximation to neglect the effects of scattering by carbon. In any event, the small corrections for the effects of carbon scattering can be accounted for by assuming that the scattering from carbon bound in the hydrocarbons is like that from a free gas of carbon atoms.

Thus, the problem of a detailed understanding of the thermalization of neutrons by organic moderators reduces to that of understanding the scattering of neutrons by the protons bound in them.

We now give the general formulation expressing the relation between the cross section for momentum transfer of slow neutrons and the dynamics of the hydrogen atoms bound in a molecule. Later we shall discuss the relevant hydrogen atom dynamics.

We neglect spin correlation effects, which are not important at temperatures $\geq 300^{\circ}K$. Then because of the approximate cancellation of the neutron scattering amplitudes in the triplet and singlet states of the n-p system, the scattering is nearly completely incoherent. For a molecule consisting of n_H hydrogen atoms, the general expression for the cross section per hydrogen atom for transfer to final momentum $\vec{K}$ of a neutron with initial momentum $\vec{K}_o$ is given by[1] ($\hbar$ = Planck's constant = 1)

$$\frac{d}{d\vec{K}}\sigma(\vec{K}\rightarrow\vec{K}_o) = \frac{\sigma_b}{8\pi^2 K_o n_H}\int_{-\infty}^{\infty} dt\, e^{i\epsilon t}\sum_{k=1}^{n_H} \chi_k(\vec{\varkappa},t), \tag{1}$$

where σ_b is the bound atom n-p cross section, $\epsilon = \frac{K^2-K_o^2}{2}$ is the energy transfer and $\vec{\varkappa} = \vec{K} - \vec{K}_o$ is the momentum transfer. The function $\chi_k(\vec{\varkappa},t)$, which contains the dependence of the scattering on the dynamics of the atoms in the molecule is given by

$$\chi_k(\vec{\varkappa},t) = \left\langle e^{i\vec{\varkappa}\cdot\vec{r}_k(t)}\; e^{-i\vec{\varkappa}\cdot\vec{r}_k(0)}\right\rangle_T, \tag{2}$$

where $\vec{r}_k(t)$, the time dependent position operator of the kth nucleus in the molecule at time t, satisfies the Heisenberg equation of motion

$$i\frac{d}{dt}\vec{r}_k(t) = \vec{r}_k(t)H - H\vec{r}_k(t), \tag{3}$$

in which H is the molecular Hamiltonian. The symbol $\langle\ldots\ldots\rangle_T$ means that an average is to be taken over the equilibrium distribution of initial states of the molecule and over molecular orientations.

From Eq. (2) the relevance of the molecular dynamics for the neutron scattering becomes clear. The precise calculation of the momentum transfer cross section requires a detailed knowledge of the molecular dynamics. In general, it is at best extremely difficult to describe the motion of a hydrogen atom moving in the actual force field of all its neighbors. In particular, effects which are specific to the liquid state, interaction between vibration and rotation, and anharmonic motions of the hydrogen atoms, are extremely difficult to include in theories of neutron scattering.

For our purposes, however, most of the important features are preserved if we ignore interactions between molecules, between vibration and rotation, and use the harmonic approximation for internal molecular vibrations. Under these conditions the dynamical problem is well defined and the methods for determining its solution are well known in principle.

The calculation of the neutron scattering is still a very complex problem, even in terms of our simplified model for the molecular dynamics. This complexity is in the dependence of the scattering on the time dependent nuclear displacements rather than on the dependence of the displacements on time.

However, the large mass and moments of inertia of the organic compounds in which we are interested allow us to make approximations which considerably simplify the problem of calculating $\frac{d\sigma}{d\vec{K}}$. This approximation consists in neglecting the contributions to $\vec{r}_k(t)$ from translations and rotations during the time of interaction between the neutron and the molecule.

This is equivalent to neglecting the contribution to the inelastic scattering which results from excitation of translational and rotational degrees of freedom by the neutron. The approximation will be a good one except for energy transfers which are comparable to or less than T/M or to the rotational level spacing. Here T is the temperature and M is the molecular mass. For

the molecules of interest both of these quantities are very much less than 0.01 ev. On the other hand, except for extremely low neutron energies, the average energy transfer which a neutron experiences in a collision is considerably greater than or comparable to 0.01 ev. Therefore, we may neglect the contributions of translations and rotations to the nuclear displacements for all values of energy transfer which are of importance for thermalization studies. For purposes of neutron thermalization we have established that it is sufficient to view the heavy organic molecules as a system of nuclei vibrating about positions of equilibrium which are fixed in a laboratory system of coordinates. Thus, the problem that we must consider is that of the harmonic vibrations of the atomic constituents of the heavy organic molecules and their interaction with slow neutrons. A more quantitative discussion of the validity of this approximation will be presented in a later section of this paper.

A detailed account of the dynamics of harmonic molecular vibrations has been given by a number of authors.[2] Here we extract only the information which is relevant for us and explain the notation to be used. We consider a molecule composed of N atoms, and denote by $u_k(t)$ the displacement of the kth atom from its equilibrium position at time t. For small vibrations we may separate the displacements into normal modes and write ($\hbar$ = Planck's constant = 1)

$$\vec{u}_k(t) = \sum_{j=1}^{3N-6} \left(\frac{1}{2M_k N\omega_j}\right)^{1/2} i\vec{C}_j^{(k)} \left\{ a_j e^{-i\omega_j t} - a_j^+ e^{i\omega_j t} \right\}. \qquad (4)$$

Here M_k is the mass of the kth particle in the molecule, N is the number of atoms in the molecule, ω_j and $\vec{C}_j^{(k)}$ are the frequency and the amplitude vector, respectively, of the kth particle in the jth normal mode of vibration, a_j and its Hermitian conjugate a_j^+ are the annihilation and creation operators, respectively, associated with the normal mode identified by the index j. The amplitude

vectors $\vec{C}_j^{(k)}$ are real, and to the extent that the translational and rotational inertias of the entire molecule are infinite, they satisfy the orthonormality relations

$$\sum_{j=1}^{3N-6} C_{j,\alpha}^{(k)} C_{j,\beta}^{(k')} = \delta_{kk'} \delta_{\alpha\beta}, \tag{5}$$

where the subscripts α,β identify the rectangular components of $\vec{C}_j^{(k)}$.

By using a well-known theorem due to Bloch,[3] the thermal average indicated in Eq. (2) can be carried out, after the introduction of Eq. (4) into Eq. (2). The result is

$$\chi_k(\vec{\varkappa},t) = \left\langle \exp\left\{ \frac{\varkappa^2}{2M_k} \vec{e}_{\vec{\varkappa}} \left[\Gamma_{kk}(t) - \Gamma_{kk}(0)\right] \vec{e}_{\vec{\varkappa}} \right\} \right\rangle_{\Omega}, \tag{6}$$

where $\vec{e}_{\vec{\varkappa}} = \vec{\varkappa}/\varkappa$ and the symbol $\langle \ldots\ldots\ldots \rangle_{\Omega}$ means that an average over molecular orientations is to be performed. The tensors $\Gamma_{kk}(t)$ are related to the normal modes of vibration by

$$\vec{e}_{\vec{\varkappa}} \Gamma_{kk}(t) \vec{e}_{\vec{\varkappa}} = \sum_{j=1}^{3N-6} g_j(t) \left| \vec{e}_{\vec{\varkappa}} \vec{C}_j^{(k)} \right|^2, \tag{7}$$

where

$$g_j(t) = \frac{(\bar{n}_j + 1)e^{i\omega_j t} + \bar{n}_j e^{-i\omega_j t}}{\omega_j} \tag{8}$$

and (k = Boltzmann's constant = 1)

$$\bar{n}_j = (e^{\omega_j/T} - 1)^{-1} \tag{9}$$

is the background of thermally excited oscillators of frequency ω_j.

Eqs. (1) and (6), together with the definitions (7), (8) and (9), form the working basis for all subsequent discussions of the neutron scattering by the protons bound in the heavy organic moderators.

In principle, the frequencies ω_j and amplitudes $\vec{C}_j^{(k)}$ may be computed provided that the interatomic force constants are known. In practice, however, one does not know the force constants. Even if they are known, the calculation of the $\vec{C}_j^{(k)}$ and ω_j in terms of them would be a problem of considerable practical complexity. In many cases, however, it is possible to determine all of the frequencies and amplitudes by a suitable combination of experimental and theoretical efforts. We shall return to the problem of determining these quantities later in this report.

II. MATHEMATICAL APPROXIMATIONS AND METHODS FOR EVALUATING THE FOURIER TRANSFORM IN EQ. (1)

DEFINITION OF THE PROBLEM

Now we undertake the problem of bringing Eq. (6) into a form which will allow us to give an analytical evaluation of the Fourier transform appearing in Eq. (1).

We first consider the average over molecular orientations indicated in Eq. (6). The approximation which we make consists in setting

$$\chi_k(\vec{\mathscr{K}},t) = \exp\left\langle \frac{\mathscr{K}^2}{2M_k}\ \vec{e}_{\vec{\mathscr{K}}}\left[\Gamma_{kk}(t) - \Gamma_{kk}(0)\right]\vec{e}_{\vec{\mathscr{K}}} \right\rangle_{\Omega}. \tag{10}$$

This amounts to averaging the molecular motions over molecular orientation before computing the cross section instead of averaging the cross section after having computed it for a particular orientation.

Using Eq. (7) and carrying out the average required for use in Eq. (10) gives the result

$$\left\langle \vec{e}_{\vec{\mathscr{K}}} \Gamma_{kk}(t)\, \vec{e}_{\vec{\mathscr{K}}} \right\rangle_{\Omega} = \frac{1}{3} \sum_{j=1}^{3N-6} g_j(t) C_j^{(k)2} . \tag{11}$$

At this point the approximation, Eq. (10), is not necessary but since it will be made in the final analysis, nothing essential is lost in making this approximation now.

For reasons which we indicate below, we introduce the notations

$$\rho_k(\omega) = \frac{1}{3} \sum_{j=1}^{3N-6} \delta(\omega - \omega_j) C_j^{(k)2} \tag{12}$$

and write Eq. (11) in the following form

$$\left\langle \vec{e}_{\vec{\mathscr{K}}} \Gamma_{kk}(t)\, \vec{e}_{\vec{\mathscr{K}}} \right\rangle_{\Omega} = \int_0^{\infty} g(\omega,t) \rho_k(\omega)\, d\omega . \tag{13}$$

Using Eq. (5) we observe that $\rho_k(\omega)$ satisfies the normalization condition

$$\int_0^{\infty} \rho_k(\omega)\, d\omega = 1 . \tag{14}$$

By putting Eq. (13) into Eq. (10), we obtain

$$\chi_k(\vec{\mathscr{K}},t) = \exp\left\{ \frac{\mathscr{K}^2}{2M_k} \int_0^{\infty} \rho_k(\omega) \left[g(\omega,t) - g(\omega,0) \right] d\omega \right\} . \tag{15}$$

Finally, for the case where M_k is independent of k, we make the approximation that

$$\chi(\vec{\mathscr{K}},t) = \frac{1}{n_H} \sum_{k=1}^{n_H} \chi_k(\vec{\mathscr{K}},t) \tag{16}$$

with $X(\vec{\kappa},t)$ obtained from Eq. (15) by replacing $\rho_k(\omega)$ by

$$\rho(\omega) = \frac{1}{n_H} \sum_{k=1}^{n_H} \rho_k(\omega) \ . \tag{17}$$

Now the equation for the scattering of neutrons by organic molecules is formally equivalent to the equation for the incoherent scattering of neutrons by atoms bound in an isotropic cubic crystal having one atom per unit cell.

The advantage of having Eq. (7) cast into the form of Eq. (13) is that in this case there exist extensively developed methods for carrying out the Fourier transform indicated in Eq. (1).[4,5,6] The fact that $\rho_k(\omega)$ is nonvanishing only at discrete points, whereas in a crystal $\rho(\omega)$ consists in general of continuous branches, need not concern us at the moment. In fact, it will be adequate to view $\rho_k(\omega)$ as consisting of continuous branches. We shall consider the implications of the discreteness of $\rho_k(\omega)$ in a later paragraph.

III. THE POLYPHENYLS

THE MOLECULAR DYNAMICS OF THE POLYPHENYLS

We now consider the structure and some aspects of the molecular vibrations of the polyphenyls. We shall also present the body of experimental evidence which is relevant for understanding the scattering of neutrons in the polyphenyls. The simplest of the polyphenyls is benzene, whose structure we indicate schematically in Fig. 1. Following benzene in the order of their structural complexity are diphenyl and the terphenyls, which we indicate schematically in Figs. 2 and 3, respectively. In these figures the large and small circles represent the equilibrium positions of the carbon and hydrogen atoms. The reader should have

no difficulty in visualizing the structures of the higher order polyphenyls. The drawings should be considered to be only schematic and, e.g., should not be interpreted as suggesting that diphenyl and terphenyl are planar molecules. Although benzene is a planar molecule, electron diffraction studies indicate that the two basic hexagonal units of diphenyl are not co-planar in the equilibrium configuration of the molecule. However, questions of this nature will be of little concern to us. Our only objective has been to use a graphical means to focus attention in some of the simplest structural similarities of the different polyphenyls. The recognition of these similarities, together with the experimental and theoretical information that has been made available by extensive studies of the vibration of benzene, provides a basis for at least a qualitative discussion of the vibrations of the polyphenyls. The object of the considerations which immediately follow is to illuminate those aspects of the molecular dynamics which are significant from the viewpoint of the scattering of thermal neutrons.

The normal vibrations of benzene separate into two kinds.[2,7,8] There are sets of normal vibrations for which the amplitude vectors are parallel to the plane of the molecule, and there are other sets for which the amplitude vectors are perpendicular to the plane of the molecule. Altogether there are $3N-6 = 30$ normal modes of vibration. Of these $2N-3 = 21$ are of the parallel type. In the remaining 9 modes, the amplitude vectors are of the perpendicular kind. Because of the high degree of symmetry of the benzene molecule, not all of the 30 modes of vibration have different frequencies. Indeed, symmetry considerations show that 7 of the parallel and 3 of the perpendicular vibration frequencies are doubly degenerate.

In Fig. 4 we indicate the fundamental frequencies of vibration for benzene. The frequencies associated with the planar and perpendicular modes are separately

indicated. We also indicate the degree of degeneracy associated with each frequency. The height of a line in Fig. 4 indicates the average of the squared amplitude of the hydrogen atoms in each normal mode. The evaluation of the amplitude vectors will be discussed in the next paragraph.

For our purposes the significant features of the vibration spectra of benzene are the following:

1. There exist a relatively small numbers of modes of vibrations, all of whose frequencies are very closely spaced around 3080 cm^{-1} (~0.38 ev);
2. The frequencies of these most energetic modes are well separated from the next highest frequency of vibration, which occurs at about 1700 cm^{-1} (~0.20 ev);
3. There are a large number of closely spaced fundamental frequencies extending up to 1700 cm^{-1}. (Taking the degeneracy into account, the average spacing of these frequencies is small and in fact approximately equal to 0.0073 ev. The largest spacing between successive frequencies is 0.025 ev.)

We expect these three general features to be common to all of the polyphenyls. The differences in the vibration spectra of the various polyphenyls should only be reflected in differences of the fine structure in the frequency range below 1700 cm^{-1}.

THE NORMAL MODES OF VIBRATIONS IN BENZENE

Now we shall discuss the problem of obtaining the physical information that we require in order to perform the calculation of the neutron energy transfer cross section by the methods discussed in Section II. From Eq. (4) it is clear that we require the normal modes frequencies and the amplitude vectors.

For molecules which contain many atoms, the determination of the desired quantities presents a problem of great practical complexity. However, the results of extensive theoretical and experimental studies of the vibrations of benzene provide an excellent basis from which to begin our considerations. To do this we recall the general features of the molecular structure of benzene.

The symmetry of benzene is that of the group D_{6h} which consists of the following operations: (2)

$$E,\ 2C_6,\ 2C_3,\ C_2,\ 3C_2',\ 3C_2'',\ i,\ 2S_3,\ 2S_6,\ \sigma_h,\ 3\sigma_d,\ 3\sigma_v.$$

As indicated in Fig. 1, it is assumed that the Cartesian y-axis is coincident with one of the symmetry axes, C_2', and the x-axis with C_2''. The z-axis is instead perpendicular to the plane of the figure, which is the σ_h symmetry plane. Since benzene is a planar molecule, the normal modes of vibrations are motions either in the plane or perpendicular to it.

Thus the structure of the representation formed by the Cartesian coordinates of benzene is: (2)

$$\Gamma_i = 2A_{1g} + A_{2g} + 4E_{2g} + 2B_{1u} + 2B_{2u} + 3E_{1u} \tag{18}$$

for the 21 in-plane modes, and

$$\Gamma_o = 2B_{2g} + E_{1g} + A_{2u} + 2E_{2u} \tag{19}$$

for the 9 out-of-plane modes.

It follows that there are 7 double degenerate in-plane normal modes and 3 double degenerate out-of-plane normal modes.

The symmetry properties have been extensively studied and utilized in the assignment of the fundamental frequencies of vibration, which have been found experimentally from the infrared and Raman techniques. (7,8) In this way the force constants of the harmonic potential function or, in the condensed form, the $\{\vec{F}\}$ matrix for the valence force symmetry coordinates have been evaluated.

The secular equation for benzene is then obtained. In terms of symmetry coordinates, it is factorized and reads as

$$\{\vec{G}\vec{F} - E\lambda\} = 0, \tag{20}$$

where $\{\vec{G}\}$ is a matrix which contains the atomic masses and the internuclear distances and it is related to the kinetic energy of the benzene ring. E is the unit matrix. The roots of the secular equations are

$$\lambda_j = \omega_j^2 , \quad (j = 1, 2, \ldots, 3N-6) \tag{21}$$

where ω_j is the frequency of the jth mode of vibration appearing in Eq. (4).

From the knowledge of the internal symmetry coordinates and of the frequencies, ω_j, we are now able to evaluate the normal mode amplitudes of the benzene molecule. The following procedure is then in order.

The molecular vibrations may be resolved into normal modes by introducing the set of normal coordinates, Q_j, in terms of which the mass-weighted Cartesian displacement coordinates

$$\vec{q}_k(t) = \sqrt{M_k}\ \vec{u}_k \tag{22}$$

read as

$$\vec{q}_k(t) = \sum_{j=1}^{3N-6} \vec{C}_j^{(k)}\ Q_j(t) . \tag{23}$$

In Eq. (22) M_k is the mass of the kth atom and the $\vec{u}_k$'s, as in Eq. (4), are the Cartesian physical displacements. In Eq. (23) $\vec{C}_j^{(k)}$ is the amplitude vector, associated with the jth mode, of the kth atom.

The jth normal coordinate, Q_j, is known to be expressed as a linear combination of the internal symmetry coordinates, S_ℓ, that is

$$Q_j = \sum_{\ell=1}^{3N-6} L_{j\ell}\ S_\ell , \tag{24}$$

where the $L_{j\ell}$'s are the elements of the matrix $\{\vec{L}\}$ which satisfy the set of simultaneous equations

$$\{\vec{L}\} \cdot \{\vec{G}\,\vec{F}\} = \{\vec{\Lambda}\} \cdot \{\vec{L}\}\,, \tag{25}$$

where $\{\vec{\Lambda}\}$ is the diagonal matrix whose elements are the λ_j's given by Eq. (21).

The internal symmetry coordinates are constructed on the basis of the symmetry properties above mentioned and they are related to the internal coordinates, S_i^*, by the linear combination

$$S_\ell = \sum_{i=1}^{3N} U_{\ell i}\, S_i^*\,, \tag{26}$$

where the $U_{\ell i}$ are the elements of the transformation matrix given in References (7,8).

The internal coordinates for the in-plane modes are: (i) the C-H and the C-C bond stretchings; (ii) an appropriate linear combination of the H-C-C bending. The advantage of this combination is that it breaks the set of the H-C-C bending into two sets, each of which is such that no more than one degenerate set occurs in any one species.

For the out-of-plane modes the internal coordinates are: (i) the bendings of a C-H bond out of the plane of the three nearest carbons; (ii) the torsion of the type C-C-C-C.

In turn, the internal coordinates, S_i^*, are related to the physical displacements, $\vec{u}_k(t)$, by the linear combination

$$S_i^* = \sum_{k=1}^{N} \vec{s}_{ik} \cdot \vec{u}_k\,, \tag{27}$$

where the dot, as in Eq. (25), symbolizes a scalar product. The $\vec{s}_{ik}$'s can be deduced by means of the method described in Reference (2).

Finally, one may express Q_j as

$$Q_j(t) = \sum_{k=1}^{N} \vec{C}_j^{(k)} \vec{q}_k(t) \tag{28}$$

by utilizing the orthogonality condition

$$\sum_{k=1}^{N} \sum_{\alpha=1}^{3} C_{k,\alpha}^{(j)} C_{k,\alpha}^{(j')} = \delta_{jj'} , \tag{29}$$

where $C_{k,\alpha}^{(j)}$ is the αth Cartesian component of the amplitude vector, $\vec{C}_k^{(j)}$.

Thus, Eqs. (28) and (29) furnish the sought values of the amplitude vectors. In Tables 1, 2 and 3 we list the values of the x, y and z components, respectively, of the vectors $\vec{C}_j^{(k)}$. Figs. 5, 6 and 7 show instead the normal modes of vibrations associated with fundamental frequencies around 3080 cm^{-1}.

For diphenyl and the higher order polyphenyls, there does not exist a background of abundant experiments and theoretical data. However, as previously discussed, one may expect those features of the molecular vibrations which are most significant for the scattering of neutrons to be insensitive to the differences between the different polyphenyls. The validity of this expectation may, of course, be checked by means of neutron scattering experiments. The possibility of checking the validity of this expectation theoretically is under consideration.

NEUTRON SPECTRA AND TOTAL SCATTERING CROSS SECTION IN BENZENE

The frequencies and amplitude vectors which we have presented in Fig. 4 have been used with Eq. (1) to obtain a scattering kernel for the benzene molecule. The numerical calculations of the benzene kernel were carried out using IBM 7090 code SUMMIT.[9] As the code SUMMIT was designed for calculating

scattering kernel for crystals with a continuous vibration spectrum, it was necessary to artificially broaden the discrete lines of the benzene vibration spectrum.

In turn, the scattering kernel has been used in the calculation of the neutron spectrum in an infinite benzene medium uniformly poisoned with 1/v-material to give a 2200 m/sec. cross section of 6.04 barns per hydrogen atom. Figs. 8, 9 and 10 show the neutron spectrum in benzene at a temperature of 300°K, 600°K and 900°K, respectively. In Fig. 8 we compare the results of our calculation with a similar calculation using a free gas model and with the Nelkin's water model.[10] In the calculation of these spectra, we included the effects of translations and rotations in an approximate manner.

This approximation consists in adding to the benzene vibrations spectrum a Debye spectrum of low frequency vibrations. For this to be a reasonable approximation, the Debye temperature, θ, associated with these vibrations must be less than the temperature of the moderator. We have chosen $\theta = 0.02$ ev. In addition to the Debye temperature, one must know an effective mass to associate with the Debye spectrum. The effective mass, M^*, associated with the acoustical branch is given by

$$M^* = \frac{1}{1 - \frac{1}{n_H} \sum_{j=1}^{3N-6} \sum_{k=1}^{n_H} \left| \vec{C}_j^{(k)} \right|^2} = 15.04 \, . \qquad (30)$$

We evaluated also the total scattering cross section per hydrogen atom bound in benzene in two cases, 1) the effects of translations and rotations were neglected, 2) these effects were taken into account in the approximate manner indicated above. The corresponding results are plotted in Fig. 11. Currently we are attempting a more careful calculation of the cross section for neutron energy less than 0.02 ev.

j= \ k=	1	2	3	4	5	6	7	8	9	10	11	12
1	0	0.128	0.128	0	-0.128	-0.128	0	0.3312	0.3312	0	-0.3312	-0.3312
2	0	0.333	0.333	0	-0.333	-0.333	0	-0.1184	-0.1184	0	0.1184	0.1184
3	0.363	0.1814	-0.1814	-0.363	-0.1814	0.1814	-0.1868	-0.0934	0.0934	0.1868	0.0934	-0.0934
4	0	-0.1286	0.1286	0	-0.1286	0.1286	0	-0.3316	0.3316	0	-0.3316	0.3316
5	0	-0.333	0.333	0	-0.333	0.333	0	0.118	-0.118	0	0.118	-0.118
6	-0.2054	0.1027	0.1027	-0.2054	0.1027	0.1027	-0.3522	0.176	0.176	-0.3522	0.176	0.176
7	-0.3552	0.1776	0.1776	-0.3552	0.1776	0.1776	0.2024	-0.1012	-0.1012	0.2024	-0.1012	-0.1012
8	0	-0.0536	-0.0536	0	0.0536	0.0536	0	-0.3423	-0.3423	0	0.3423	0.3423
9	0	-0.2396	-0.2396	0	0.2396	0.2396	0	0.0686	0.0686	0	-0.0686	-0.0686
10	0	-0.0983	-0.0983	0	0.0983	0.0983	0	0.1116	0.1116	0	-0.1116	-0.1116
11	0	-0.224	-0.224	0	0.224	0.224	0	0.0527	0.0527	0	-0.0527	-0.0527
12	0.111	-0.0181	0.0181	-0.111	0.0181	-0.0181	0.286	0.3072	-0.3072	-0.286	-0.3072	0.3072
13	0.0031	0.4119	-0.4119	-0.0031	-0.4119	0.4119	0.0235	-0.1423	0.1423	-0.0235	0.1423	-0.1423
14	0.155	0.0156	-0.0156	-0.155	-0.0156	0.0156	-0.497	0.3040	-0.3040	0.4968	-0.3040	0.3040
15	0.529	-0.1412	0.1412	-0.529	0.1412	-0.1412	0.066	-0.1571	0.1571	-0.0658	0.1571	-0.1571
16	0	0.1391	-0.1391	0	0.1391	-0.1391	0	-0.2276	0.2276	0	-0.2276	0.2276
17	0	-0.1916	0.1916	0	-0.1916	0.1916	0	-0.2736	0.2736	0	-0.2736	0.2736
18	0	-0.2315	0.2315	0	-0.2315	0.2315	0	0.087	-0.087	0	0.087	-0.087
19	-0.421	-0.1802	-0.1802	-0.421	-0.1802	-0.1802	0.3382	-0.0563	-0.0563	0.3382	-0.0563	-0.0563
20	0.3412	0.0094	0.0094	0.3412	0.0094	0.0094	0.2811	-0.1924	-0.1924	0.2811	-0.1924	-0.1924
21	-0.014	-0.4146	-0.4146	-0.0137	-0.4146	-0.4146	-0.0191	0.1316	0.1316	-0.0191	0.1316	0.1316

Table 1. The x-components of the amplitude vectors $\vec{C}_j^{(k)}$

j= \ k=	1	2	3	4	5	6	7	8	9	10	11	12
1	0.1476	0.074	-0.074	-0.1476	-0.074	0.074	0.3824	0.1912	-0.1912	-0.3824	-0.1912	0.1912
2	0.3843	0.1922	-0.1922	-0.3843	-0.1922	0.1922	-0.137	-0.0684	0.0684	0.137	0.0684	-0.0684
3	0	-0.3143	-0.3143	0	0.3143	0.3143	0	0.162	0.162	0	-0.162	-0.162
4	0.1485	-0.0743	-0.0743	0.1485	-0.0743	-0.0743	0.383	-0.1914	-0.1914	0.383	-0.1914	-0.1914
5	0.3844	-0.1922	-0.1922	0.3844	-0.1922	-0.1922	-0.1362	0.068	0.068	-0.1362	0.068	0.068
6	0	-0.178	0.178	0	-0.178	0.178	0	-0.305	0.305	0	-0.305	0.305
7	0	-0.308	0.308	0	-0.308	0.308	0	0.1753	-0.1753	0	0.1753	-0.1753
8	0.0128	0.080	-0.080	-0.0128	-0.080	0.080	0.505	0.0881	-0.0881	-0.505	-0.0881	0.0881
9	0.5503	-0.135	0.135	-0.5503	0.135	-0.135	-0.1819	0.0631	-0.0631	0.1819	-0.0631	0.0631
10	0.072	0.098	-0.098	-0.072	-0.098	0.098	0.239	0.4326	0.4326	-0.239	0.4326	-0.4326
11	-0.012	0.3995	-0.3995	0.012	-0.3995	0.3995	-0.1875	0.0962	-0.0962	0.1875	-0.0962	0.0962
12	0	0.0536	0.0536	0	-0.0536	-0.0536	0	0.3423	0.3423	0	-0.3423	-0.3423
13	0	0.2396	0.2396	0	-0.2396	-0.2396	0	-0.0686	-0.0686	0	0.0686	0.0686
14	0	0.0983	0.0983	0	-0.0983	-0.0983	0	-0.1116	-0.1116	0	0.1116	0.1116
15	0	0.224	0.224	0	-0.224	-0.224	0	-0.0527	-0.0527	0	0.0527	0.0527
16	-0.01	-0.341	-0.341	-0.01	-0.341	-0.341	-0.1873	0.207	0.207	-0.1873	0.207	0.207
17	-0.1012	0.231	0.231	-0.1012	0.231	0.231	-0.3507	0.1232	0.1232	-0.3507	0.1232	0.1232
18	-0.5484	-0.1474	-0.1474	-0.5484	-0.1474	-0.1474	0.1819	0.0312	0.0312	0.1819	0.0312	0.0312
19	0	0.1391	-0.1391	0	0.1391	-0.1391	0	-0.2276	0.2276	0	-0.2276	0.2276
20	0	-0.1916	0.1916	0	-0.1916	0.1916	0	-0.2736	0.2736	0	-0.2736	0.2736
21	0	-0.2315	0.2315	0	-0.2315	0.2315	0	0.087	-0.087	0	0.087	-0.087

Table 2. The y-components of the amplitude vectors $\vec{C}_j^{(k)}$

k= \ j=	1	2	3	4	5	6	7	8	9
1	0.392	0.176	-0.367	0	0	0.335	-0.476	0	-0.513
2	0.392	-0.176	0.367	0.2904	-0.4124	-0.168	0.238	0.4445	-0.257
3	0.392	0.176	-0.367	-0.2904	0.4124	-0.168	0.238	0.4445	0.257
4	0.392	-0.176	0.367	0	0	0.335	-0.476	0	0.513
5	0.392	0.176	-0.367	0.2904	-0.4124	-0.168	0.238	-0.4445	0.257
6	0.392	-0.176	0.367	-0.2904	0.4124	-0.168	0.238	-0.4445	-0.257
7	-0.114	0.374	0.176	0	0	0.475	0.327	0	0.264
8	-0.114	-0.374	-0.176	0.411	0.2834	-0.2374	-0.164	-0.229	0.132
9	-0.114	0.374	0.176	-0.411	-0.2834	-0.2374	-0.164	-0.229	-0.132
10	-0.114	-0.374	-0.176	0	0	0.475	0.327	0	-0.264
11	-0.114	0.374	0.176	0.411	0.2834	-0.2374	-0.164	0.229	-0.132
12	-0.114	-0.374	-0.176	-0.411	-0.2834	-0.2374	-0.164	0.229	0.132

Table 3. The z-components of the amplitude vectors $\vec{C}_j^{(k)}$

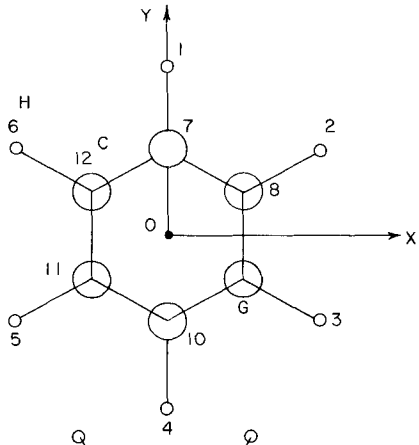

Fig. 1. Benzene

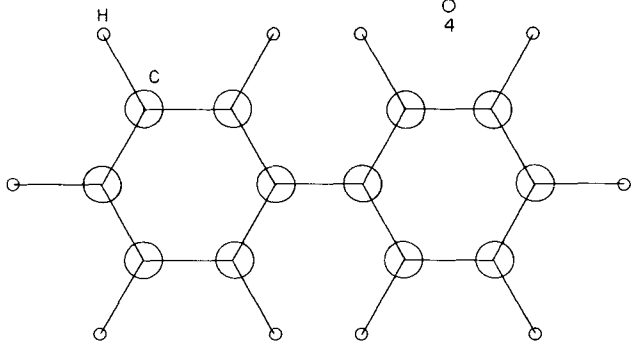

Fig. 2. Diphenyl

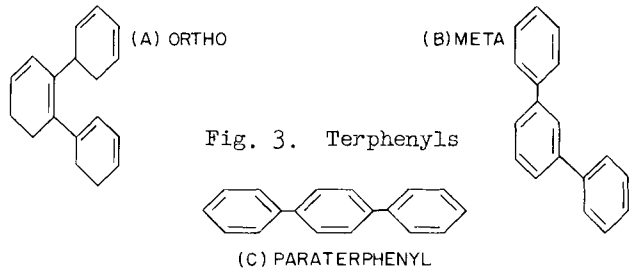

Fig. 3. Terphenyls

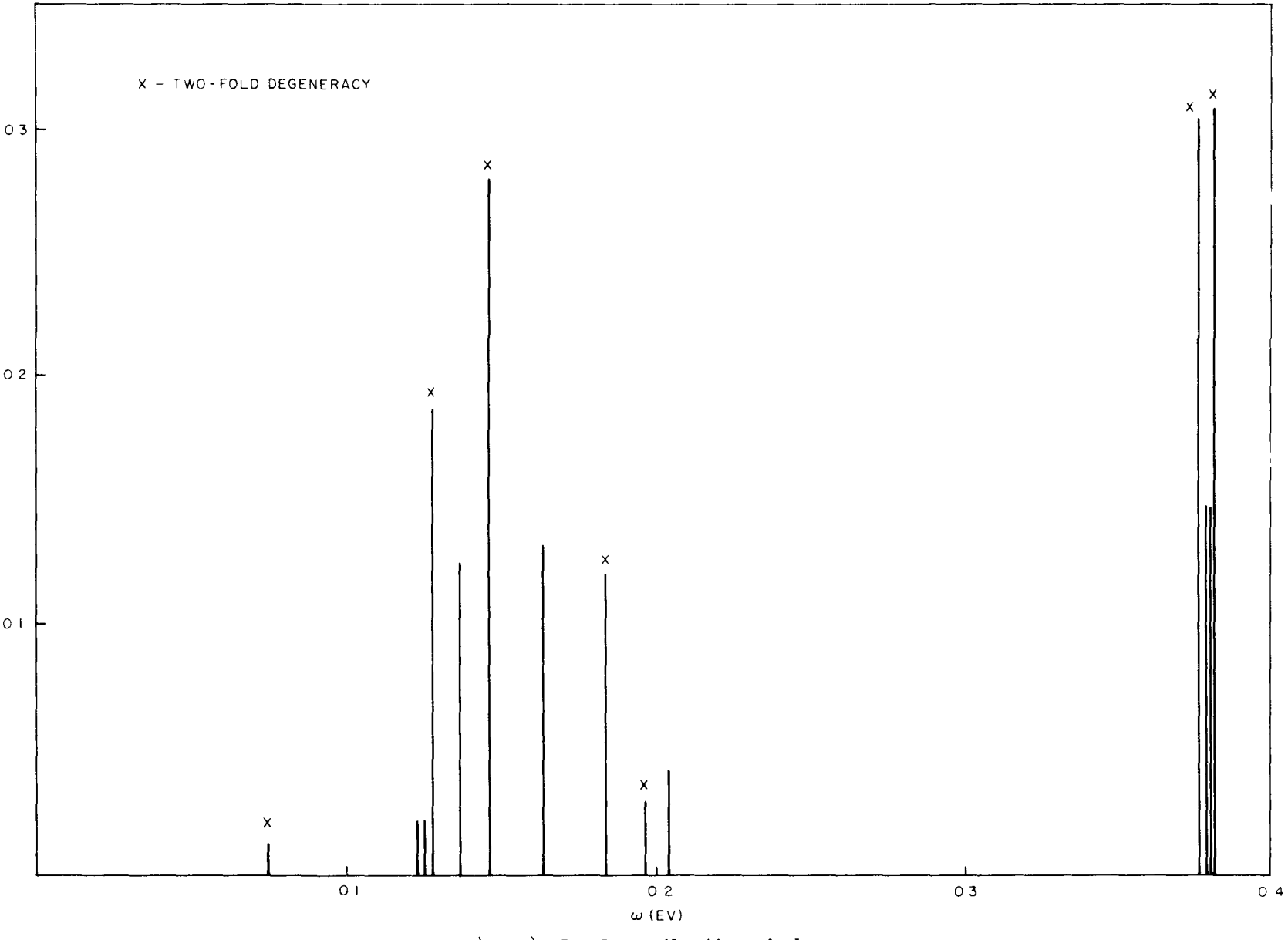

Fig. 4. a) In-plane vibrations in benzene

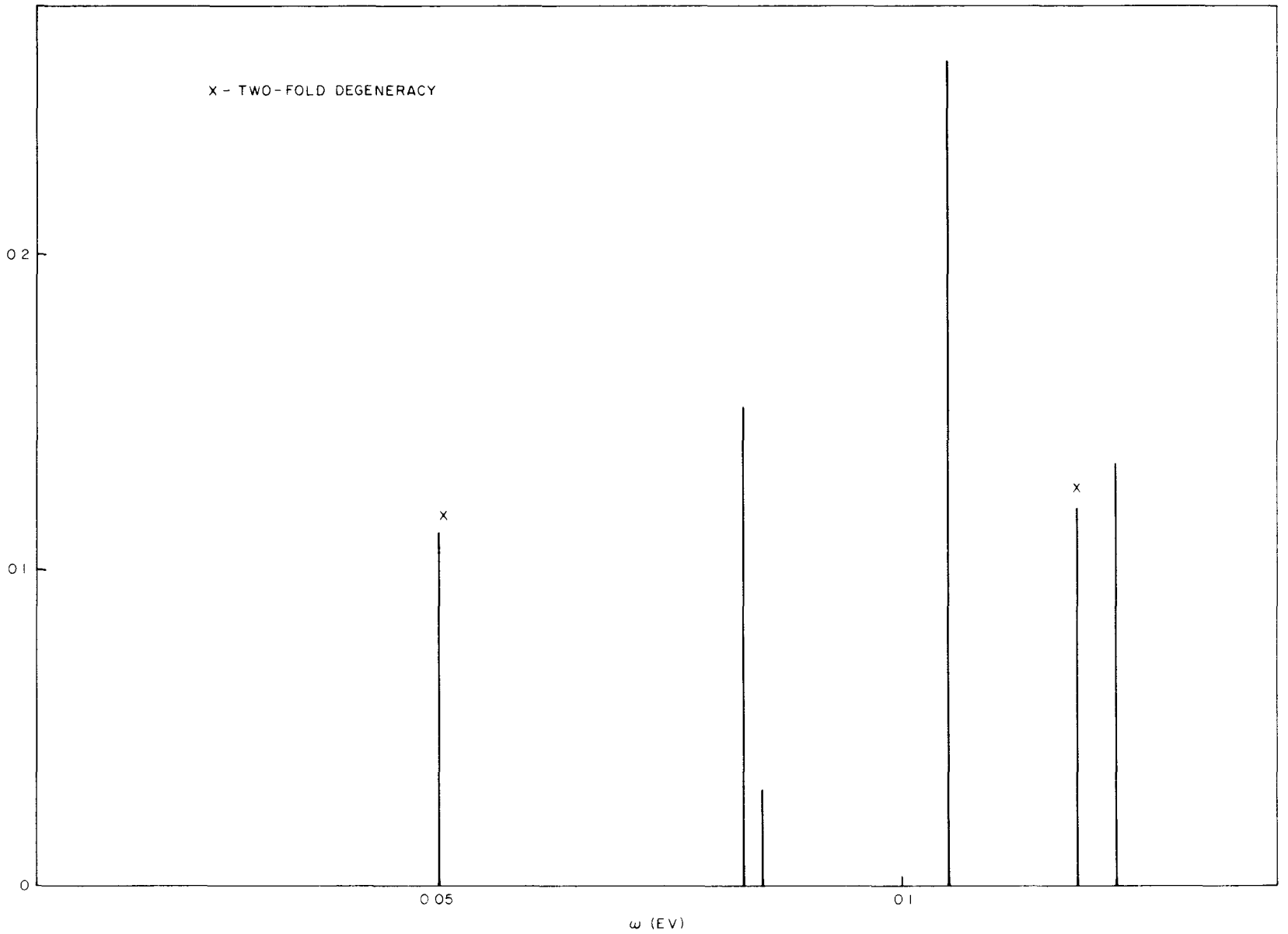

Fig. 4. b) Out-of-plane vibrat' s in benzene

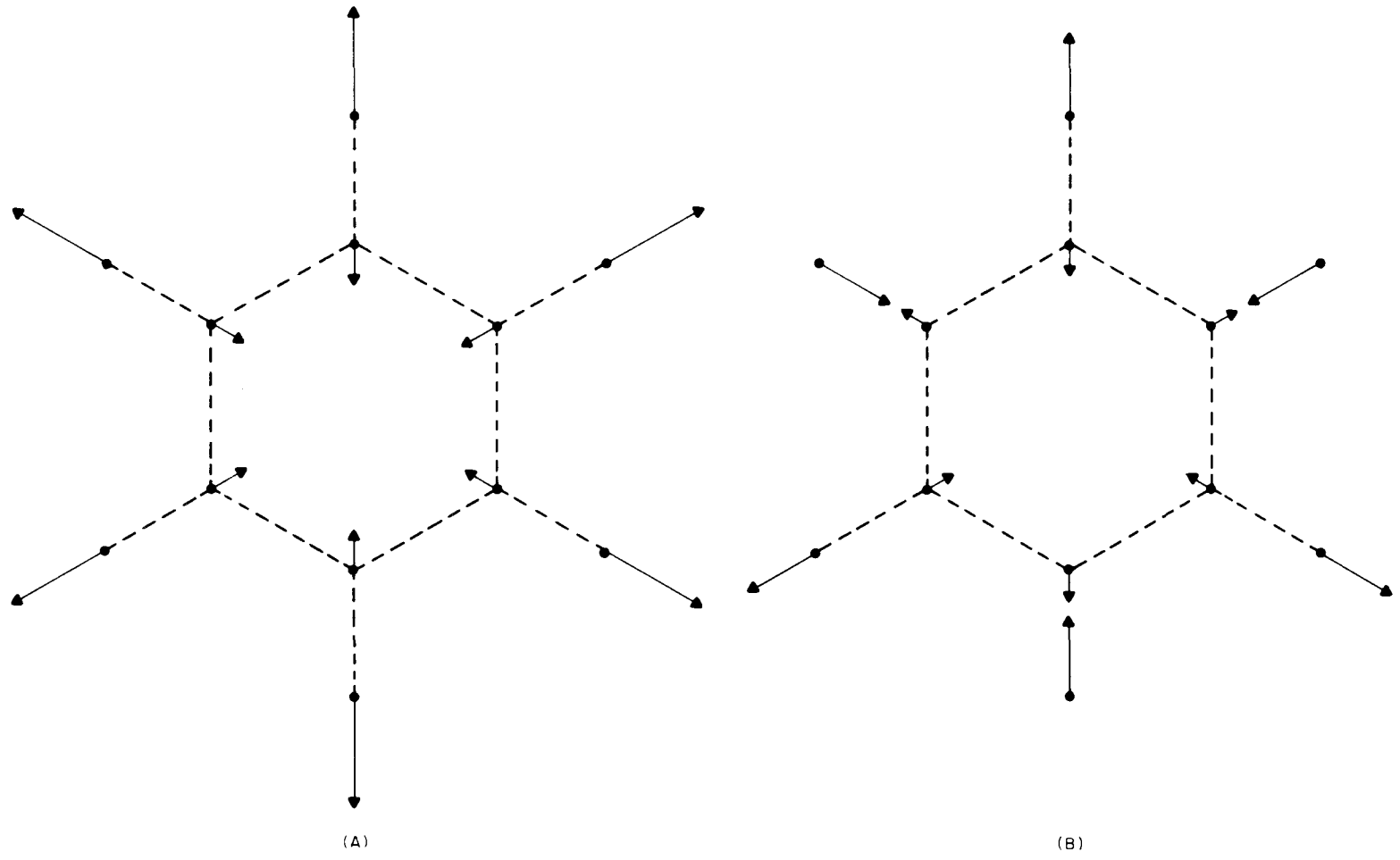

Fig. 5. Normal modes in benzene

a) Species A_{1g} - ω = 3061.6 cm^{-1}

b) Species B_{1u} - ω = 3060 cm^{-1}

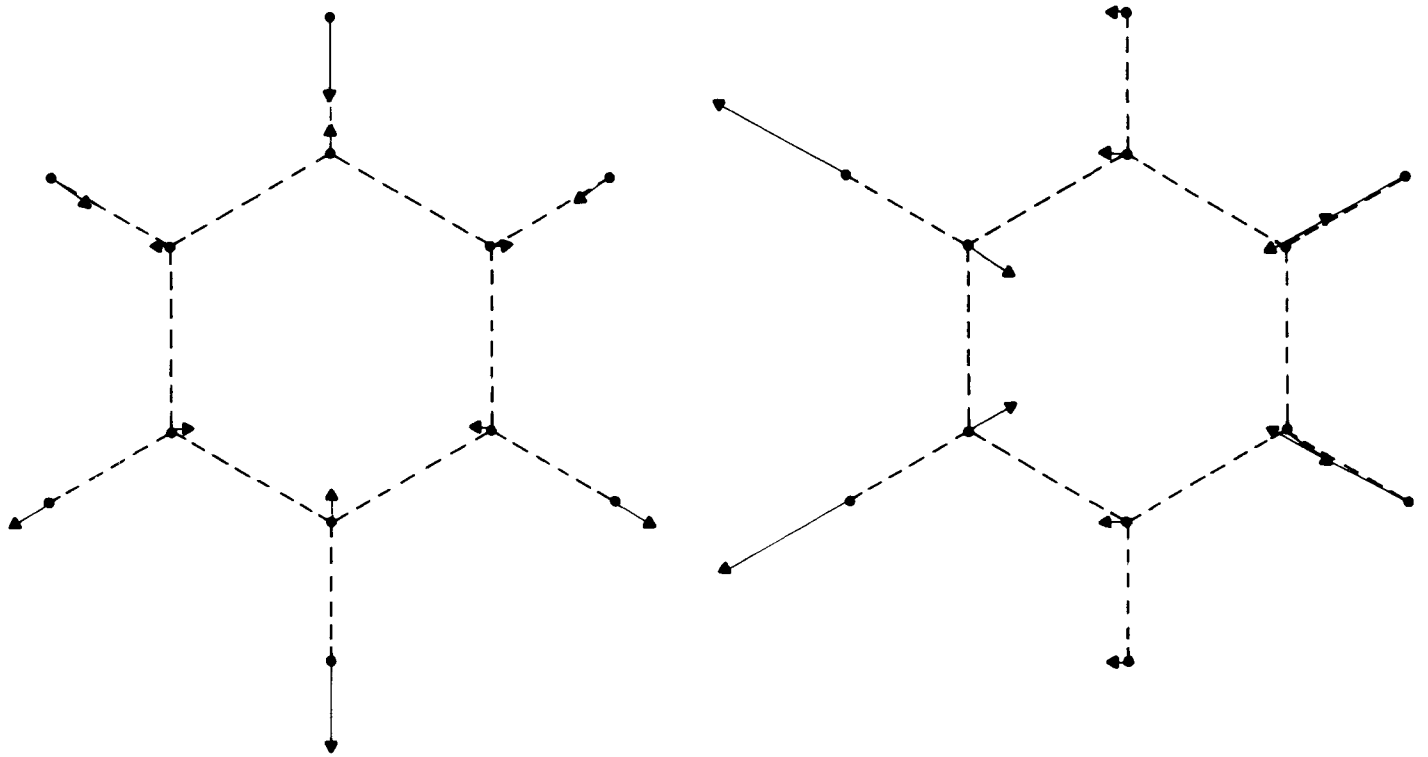

Fig. 6. Normal modes in benzene

Double degenerate mode, species E_{1u} - ω = 3080 cm^{-1}

In b) the arrows representing displacements of 1 and 4 hydrogen and 7 and 10 carbon atoms should be only 1/4 as long as shown here.

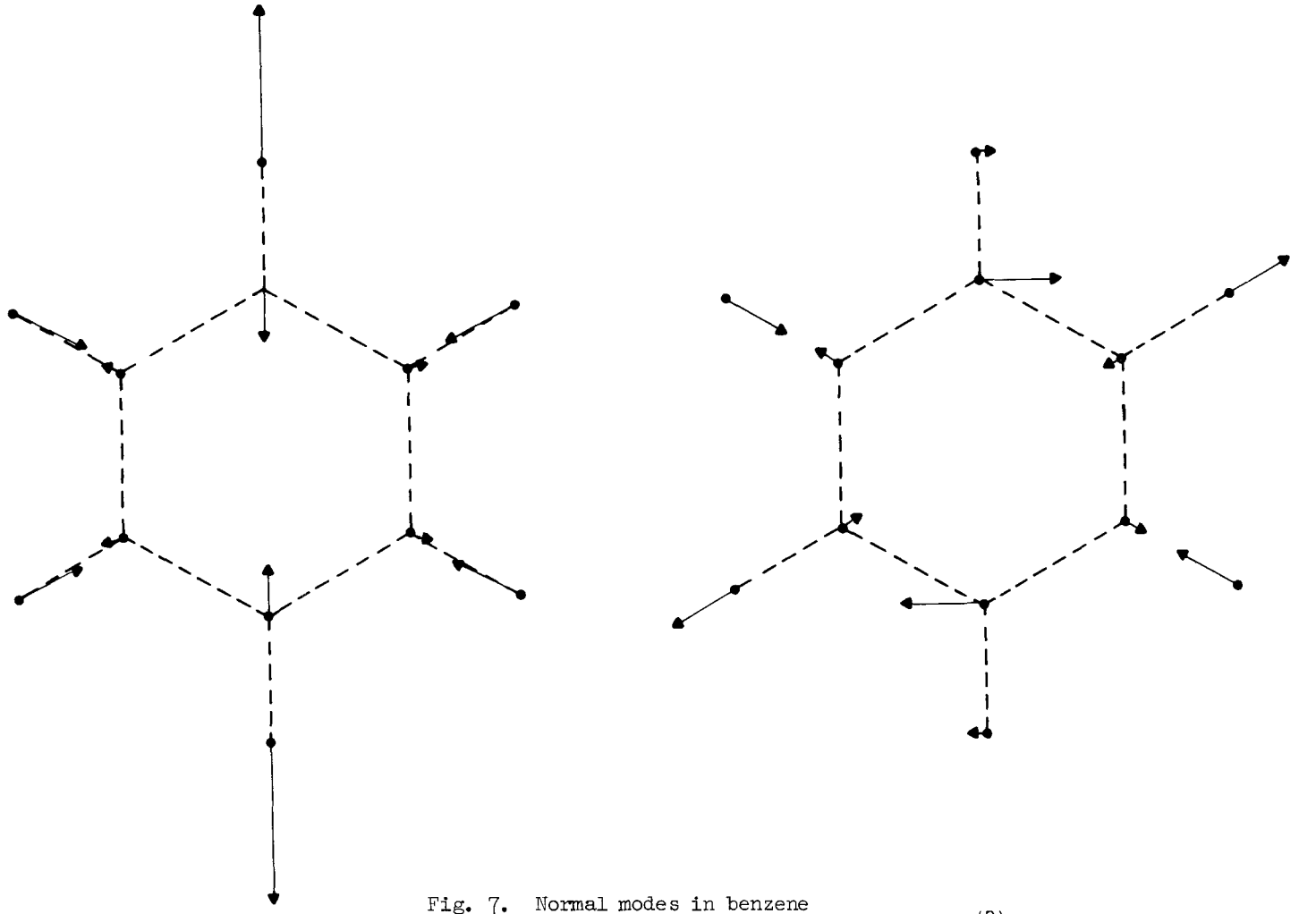

(A) (B)

Fig. 7. Normal modes in benzene

Double degenerate mode, species E_{2g} - ω = 3046.8 cm^{-1}

In b) the arrows representing displacements of 1 and 4 hydrogen and 7 and 10 carbon atoms should be only 1/25 as long as shown here.

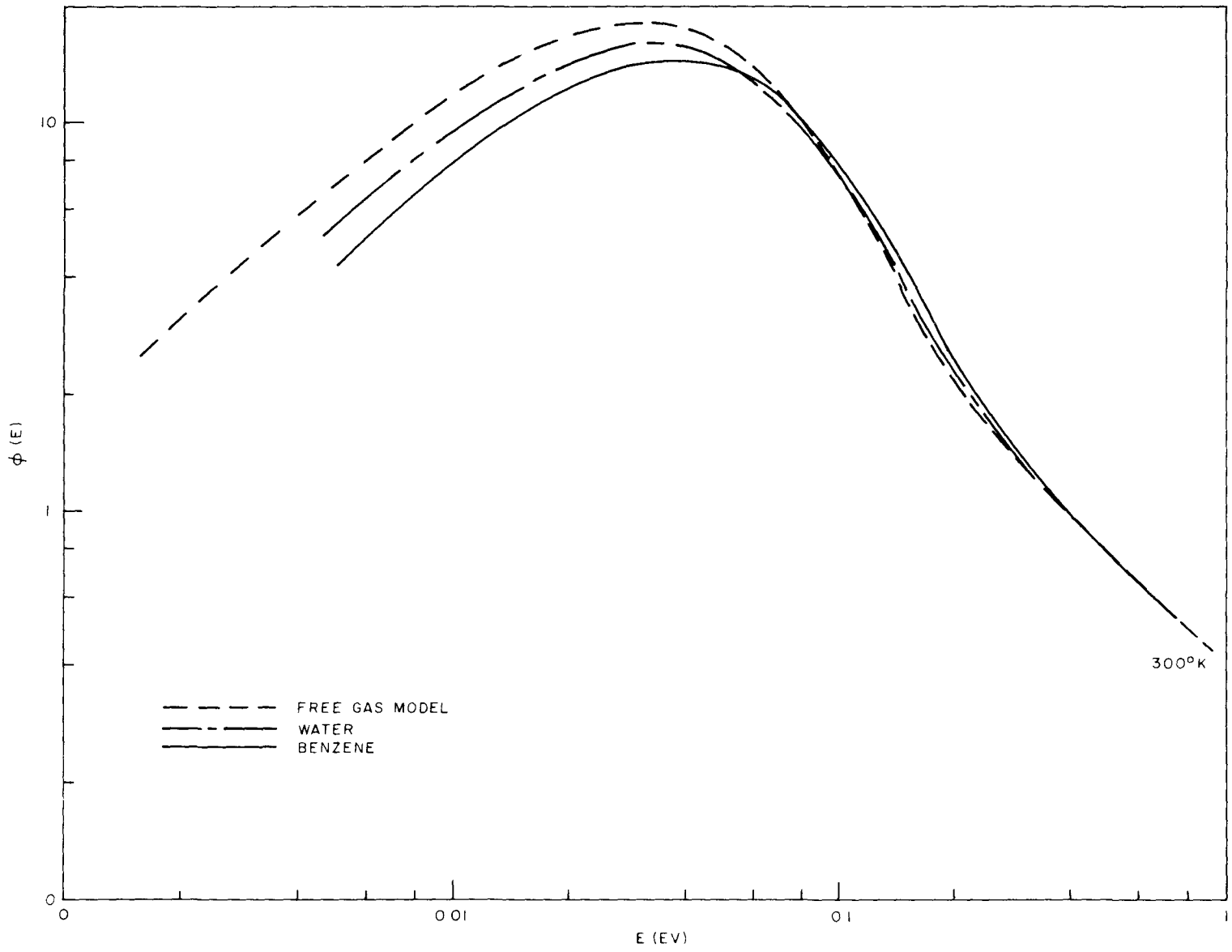

Fig. 8. Neutron spectrum in benzene at 300°K

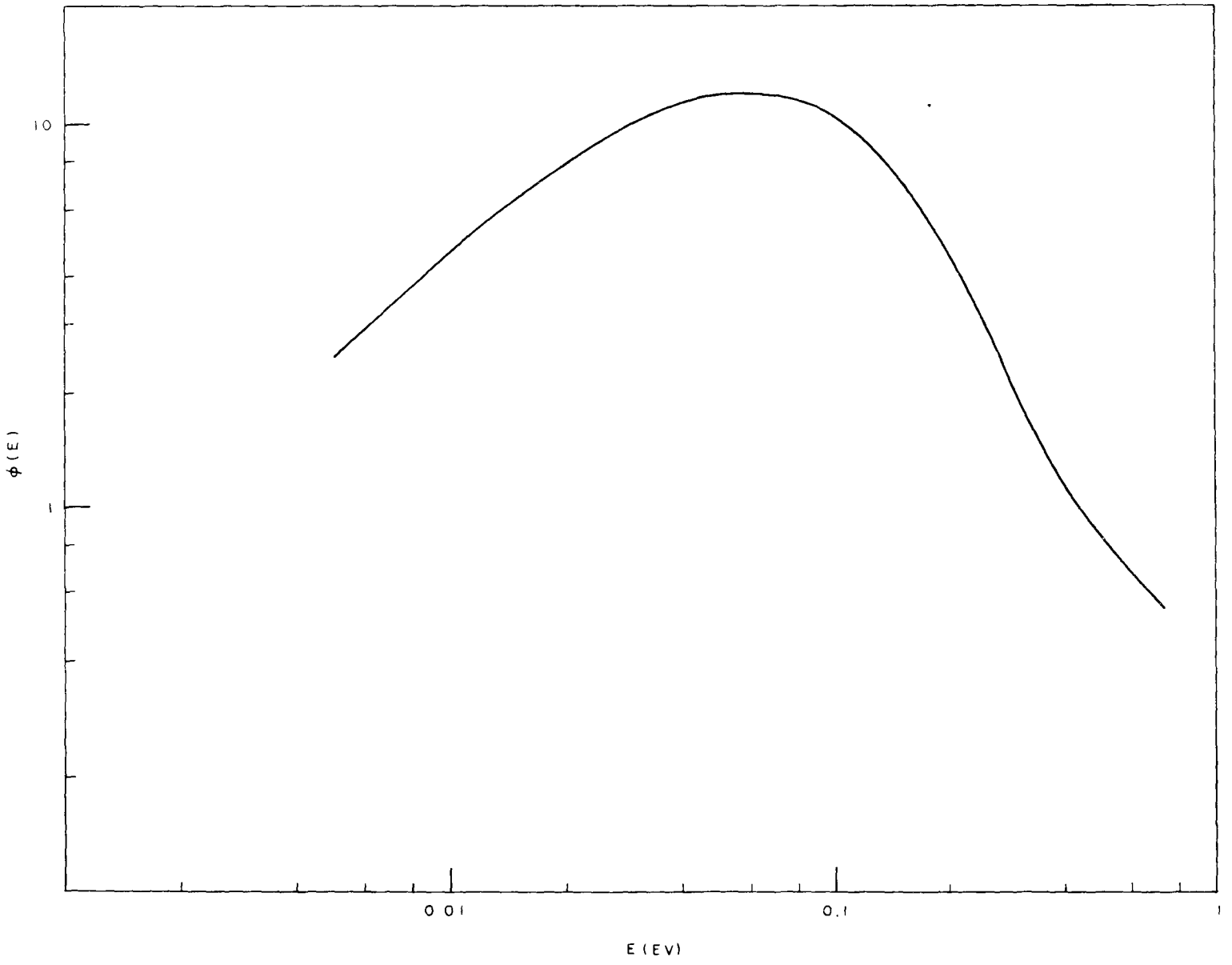

Fig. 9. Neutron spectrum in benzene at 600°K

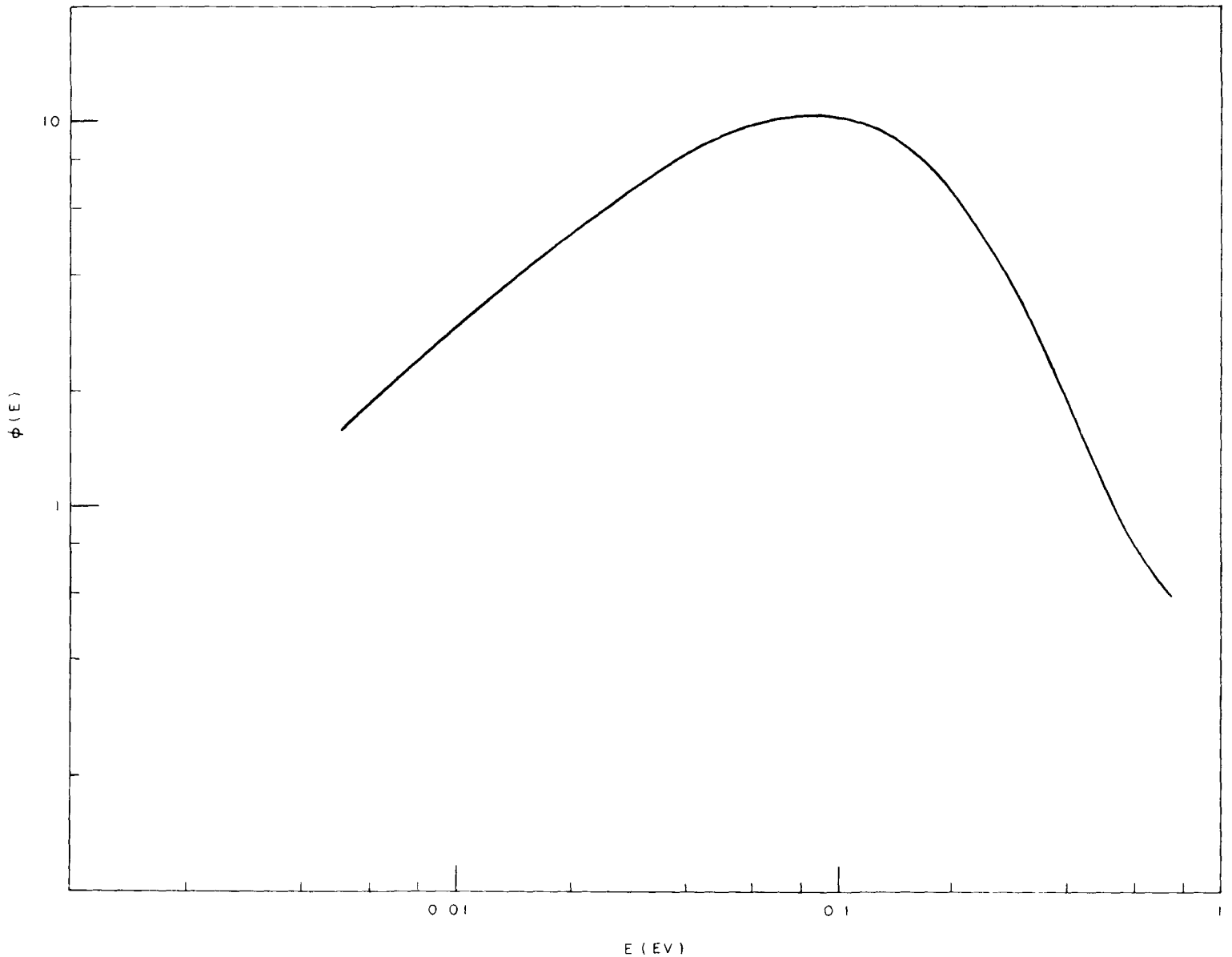

Fig. 10. Neutron spectrum in benzene at 900°K

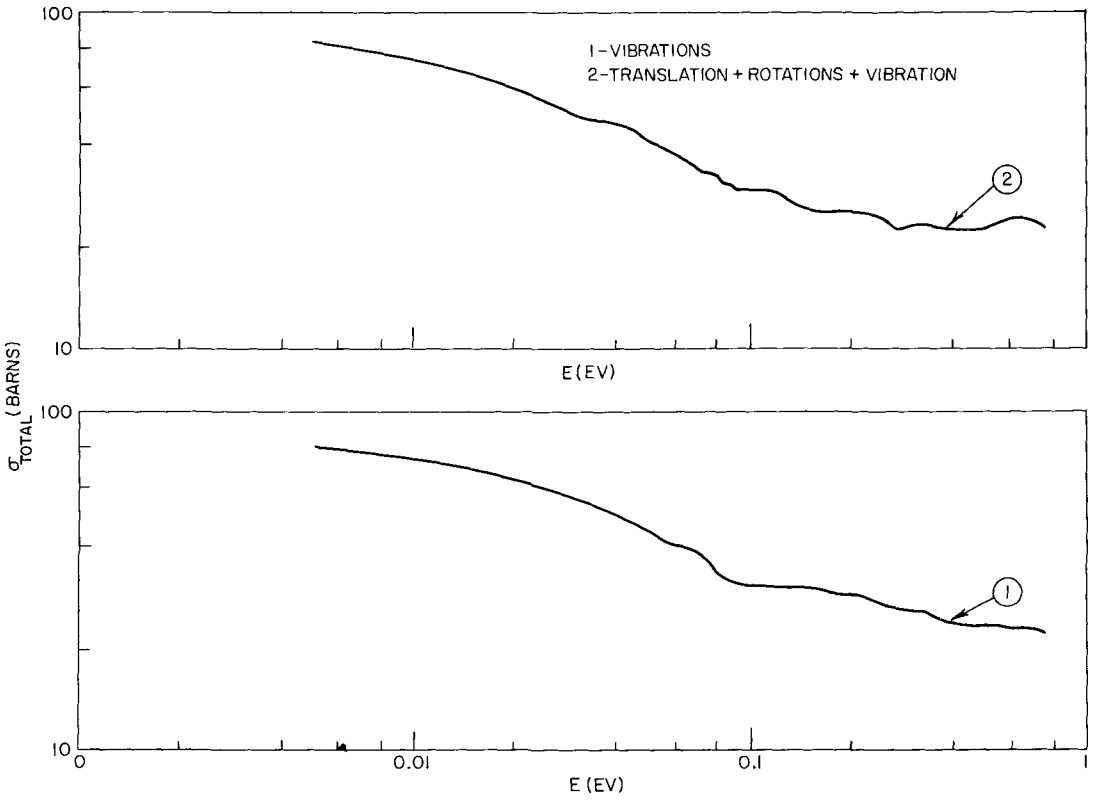

Fig. 11. Total scattering cross section of a proton bound in benzene versus energy

REFERENCES

1. A. C. Zemach and R. J. Glauber, Phys. Rev. 101, 118 (1956).
2. E. B. Wilson, J. C. Decius, P. C. Cross, Molecular Vibrations, McGraw-Hill, New York (1955).
3. F. Bloch, Z. Physik 7, 295 (1932).
4. A. Sjölander, Arkiv Fysik 14, 315 (1958).
5. D. E. Parks, General Atomic Report GA-2438.
6. M. S. Nelkin and D. E. Parks, Phys. Rev. 119, 1060 (1960).
7. F. A. Miller and B. L. Crawford, The Journal of Chem. Phys. 14, 282 (1946).
8. B. L. Crawford and F. A. Miller, The Journal of Chem. Phys. 17, 249 (1949).
9. Joan Bell, General Atomic Report GA-2492.
10. J. R. Beyster, J. L. Wood, W. M. Lopez and R. B. Walton, Nuclear Sci. and Eng. 9, 168 (1961).

Paper to be Presented at the
Conference on Neutron Thermalization
April 30-May 2, 1962
Brookhaven National Laboratory

Calculation Of Thermal Neutron Flux Spectra In an Infinite Polyethylene Moderated Medium With Varying Amounts of Absorption

D. T. Goldman
F. D. Federighi

I. Introduction

The measurement of thermal neutron flux spectra in water moderated configurations is of considerable importance for providing data of interest in reactor analysis and synthesis. A fairly common experimental technique has been to substitute for water moderated media those containing polyethylene which are somewhat more convenient for experimentation. Recently it has been observed that although the thermalization processes are indeed quite similar in water and polyethylene, the details of the experimental information indicate that it is not sufficient to extend the water results directly without modifications to polyethylene moderated media.

It has been found appropriate to calculate the scattering of thermal energy neutrons by polyethylene. The scattering from the polyethylene system is treated as that from a group of harmonically bound oscillators whose normal mode frequencies have been determined by an analysis of spectroscopic data. Thus, it is possible to compare the total scattering cross section with measured results, so as to arrive at some basis for empirically determining the validity of the model.

The differential scattering cross section was used in a program which calculates infinite media spectra. The results of the calculations were compared with experimental data for various amounts of poison material. The agreement between theory and experimental results is sufficiently satisfactory to enable one in the future to use the polyethylene scattering cross section in the analysis of reactor experiments, with reasonable confidence.

II. Scattering Model

The differential cross section for the incoherent scattering of thermal neutrons by a chemical system (except for the ratio of outgoing to incident velocity) is a function of the dynamics of the latter system alone. With this knowledge, Nelkin[1] proposed treating the scattering of slow neutrons by water with a model for the chemical motion associated with the water molecule. Nelkin examined the intermediate scattering function, $\mathcal{X}(\vec{K}, t)$,[2] which is the spatial Fourier transform of the scattering kernel, and treated the Hamiltonian corresponding to the molecular motion as separable into motions corresponding to free translation, a hindered rotation of the water molecule in the presence of its neighbors, and three oscillations of the hydrogen atom inside the molecule. Nelkin then replaced the hindered rotational motion by a torsional oscillation of a single frequency with a torsional mass determined by the mass-tensor approximation for water vapor of Krieger & Nelkin.[3]

The energies of phonon excitation associated with each type of motion are given in Table 1.

Table 1

Phonon Excitation Energy For Water & Polyethylene

Nature of Level	H_2O	$C_n H_{2n}$
rotational	.06 ev	.089 ev
vibrational	.205 ev	.187 ev
vibrational	.474 ev	.354 ev
vibrational	.488 ev	.533 ev

Nelkin further treated the two highest energy levels as a single double degenerate level at .481 ev.

In Nelkin's published calculation, the scattering from only one of the quantum oscillations was treated exactly. For an incoming neutron with sufficiently high energy to excite more than one mode, all but the motion requiring the largest energy transfer are treated in the high energy limit. Since throughout one is concerned with energies considerably above the Debye frequency of the lattice, the translational motion is treated in the high energy limit throughout the calculations. The appropriate Fourier inversion of the intermediate scattering function then results in the following formula for the differential cross section for the scattering of neutrons from a system of translational plus vibrational degrees of freedom:

$$\sigma(E_0, E, \theta) = \frac{\sigma_b}{4\pi}\sqrt{\frac{E}{E_0}}\sqrt{\frac{M}{2\pi\bar{E}k^2}}\, e^{-k^2/2A} \times \sum_{n=-\infty}^{\infty} e^{-\frac{n\omega}{2T}} I_n\left(\frac{k^2}{2B}\right) e^{-\frac{M}{2\bar{E}k^2}\left(E-E_0-n\omega+\frac{k^2}{2m}\right)^2} \quad (1)$$

The parameters appearing in Equation (1) are different depending upon which oscillatory motion is being treated exactly, i.e., depending upon the amount of energy being transferred through the scattering process. These parameters are defined by Nelkin (Reference 1). An examination of equation (1) shows that $e^{-k^2/2A}$ corresponds to the Debye-Waller factor at an effective temperature, $\bar{E}$, where $\bar{E} \geq T$ is introduced to account for the fact that energy is not exchanged in a continuous process to a system of free particles at temperature T. For the case of translation only, $\bar{E} = T$, $n = 0$ and the differential cross section reduces to the formula for the scattering of neutrons by a system of perfect gas particles of mass M. Both to simplify the calculation and to guarantee that the principle of detailed balance is fulfilled, only the down scattering portion of the scattering matrix is calculated

(for each angle) and the upscattering is computed from the detailed balance condition:

$$\frac{d^2\sigma_{f\to i}}{d\Omega\, d\epsilon} = \frac{E_i}{E_f}\,\frac{d^2\sigma_{i\to f}}{d\Omega\, d\epsilon}\, e^{\frac{E_f - E_i}{T}} \quad . \qquad (2)$$

The success of the Nelkin model in predicting the total scattering cross section has appeared in the literature.[1] We have extended the calculations to determine additional quantities both of a fundamental nature such as the "scattering law" of Egelstaff[4] and more integral quantities of interest in reactor computations. These results will be discussed in a subsequent publication. It is sufficient to report that the success of the model indicated that it might be appropriate to extend it to determine the scattering from another chemically bound system which could be represented as a system of harmonic oscillators, specifically polyethylene.

The basic structure of polyethylene is that of a long chain molecule with generic formula representation $C_n H_{2n}$. Whereas it might appear foolhardy to treat solid polyethylene in a manner analogous to liquid water, the fact that polyethylene does not have definite crystalline structure and the success of the model that will be apparent seem to justify this attempt. The frequency spectrum for polyethylene is necessary for the calculation of the scattering cross section. We have used the data of Nielsen and Woolett[5] on the infra-red absorption spectrum of solid polyethylene to infer the energies of the phonon excitation. On the basis of these data, there appear to be reasonably well separated energy levels of polyethylene at energies given in Table 1. The cross section was then calculated according to the following model:

Assume that each of the four levels corresponds to a normal mode of oscillation of the polyethylene molecule. This model is especially simple and involves

the selection of only one arbitrary parameter, chosen so that at high neutron energies, $E \gtrsim 1$ ev, the total cross section would be the same as that for the scattering from free protons (20 barns).

The equation for the scattering cross section is the same as that for the scattering by water, Equation (1). The vibrational mass, m_v is determined by

$$1 = \frac{1}{M} + \frac{1}{m_v}$$

where M is the mass of the polyethylene molecule, 14, so that at high energies the scattering duplicates that form a free proton gas at temperature $\bar{E} = .1365$ ev. The other parameters are determined by the requirements of the model and are given in Table 2. The choice of each set of parameters depends upon the energy transferred in the inelastic collision, as indicated in the Table.

The differential cross section, Equation (1), for the scattering of neutrons by polyethylene was calculated for various scattering angles, θ using the parameters of Table 2. The total cross section was computed from the differential cross section by integrating the result of the numerical evaluation of Equation (1) over angle and final energy. Care must be taken in the numerical integration of the differential cross section to ensure that the integration scheme not introduce spurious results due to the replacing of an analytical continuous integration by a numerical finite size integration mesh. To see where this might arise, we note that for energy transfers less than the lowest phonon excitation of the scattering system, the scattering is similar to that by a free gas. The differential cross section for the scattering of a neutron by a gas of mass M is[2]

$$\sigma(E_0, E, \theta) = a^2 \sqrt{\frac{M}{2\pi T K^2}} \sqrt{\frac{E}{E_0}}\, e^{-\frac{M}{2TK^2}\left(\epsilon + \frac{K^2}{2M}\right)^2} \qquad (3)$$

where $\epsilon = \dfrac{k^2 - k_0^2}{2m}$, the energy transfer

and $\vec{K} = \vec{k} - \vec{k}_0$, the momentum transfer

Table 2

Parameters Entering Into the Equation for the Scattering of Neutrons by Polyethylene

Region I $\quad \Delta E < 0.187$ ev

$m = M = 14$

$E = T = 0.0255$ ev

$$A^{-1} = \alpha_v^{-1} + (4 m_v w_v \tanh w_o/2T)^{-1}$$

$$\alpha_v^{-1} = (4 m_v)^{-1} (w_1^{-1} + w_2^{-1} + w_3^{-1})$$

$A = .195$ ev

$B = 4 m_v w_o/2T$

$= 1.06$ ev

$m_v = 1.08$

$w = w_o = 0.089$

Region II $\quad 0.187 \text{ ev} \leq E < 0.354$ ev

$$\frac{1}{m} = \frac{1}{M} + \frac{1}{4m_v}$$

$M = 3.294$

$$\bar{E} = \frac{4 m_v T + M \bar{E}_o}{M + 4m_v} \qquad \bar{E}_i = \left(\frac{1}{e^{w_i/T} - 1} + 1/2\right) w_i$$

$= 0.0422$ ev

$$A^{-1} = (4 m_v)^{-1} [w_2^{-1} + w_3^{-1} + (4w_1 \tanh w_1/2T)^{-1}]$$

$A = 0.422$ ev

$B = 4m_v w_1 \sinh w_1/2T$

$= 13.89$ ev

$w = w_1 = 0.182$

Region III $0.354 \text{ ev} \leq E < 0.533 \text{ ev}$

$$\frac{1}{m} = \frac{1}{M} + \frac{1}{2} m_v$$

$$m = 1.868$$

$$\bar{E} = \left[\frac{T}{M} + \frac{\bar{E}_o + \bar{E}_1}{4 m_v}\right] m$$

$$= 0.0603 \text{ ev}$$

$$A^{-1} = (4 m_v)^{-1} \left[w_3^{-1} + (w_2 \tanh w_2/2T)^{-1}\right]$$

$$A = 0.916 \text{ ev}$$

$$B = 4 m_v w_2 \sinh w_2/2T = 787.6 \text{ ev}$$

$$w = w_2 = 0.354 \text{ ev}$$

Region IV $0.534 \text{ ev} \leq E \lesssim 1 \text{ ev}$

$$\frac{1}{m} = \frac{1}{M} + \frac{3}{4m_v}$$

$$m = 1.302$$

$$\bar{E} = \frac{T}{M} + \frac{1}{4m_v} (\bar{E}_o + \bar{E}_1 + \bar{E}_2)\, m$$

$$e = 0.0977 \text{ ev}$$

$$A = 4m_v w_3 \tanh w_3/2T$$

$$= 2.296 \text{ ev}$$

$$B = 4m_v w_3 \sinh w_3/2T$$

$$= 3.967 \times 10^4 \text{ ev}$$

$$w_3 = 0.533 \text{ ev}$$

In the limit of zero energy transfer, $\epsilon = 0$ and if we also force our attention on forward scattering $K^2/2M \rightarrow 0$ and Equation (3) becomes

$$\lim_{K^2/2M \to 0} \frac{1}{\sqrt{K^2/2M}} e^{-\frac{1}{4T}(K^2/2M)} = \lim_{K^2/2M \to 0} \frac{1}{\sqrt{K^2/2M}}$$

This square root singularity does not occur for $\epsilon \neq 0$ because for this case the differential cross section aymptotically approaches

$$\lim_{K^2/2M \to 0} \frac{1}{\sqrt{K^2/2M}} e^{-\epsilon^2/4TK^2/2M} = 0$$

This statement emphasizes the fact that for scattering from a scatterer from a finite mass, there cannot be energy change without a change in momentum.

To account numerically for the square-root singularity of the diagonal term, $(K^2/2M)^{-\frac{1}{2}}$ was subtracted from the calculated value of the differential cross section before the numerical integration over angle is undertaken. The analytical value of the integral of this quantity was then added to the result.

It is apparent that the presence of this integrable singularity must be handled properly when computing the total and energy exchange cross section. It is interesting to note, however, that this divergence has no effect on the calculation of infinite medium spectra. The possible source of error arises from the contribution of the term corresponding to forward scattering with no energy loss. This contribution cannot be separated from the unscattered flux and hence no error is introduced in the spectrum determination.

The calculated total cross section for the scattering of neutrons by polyethylene was compared with the experimental data of Bach et. al.[6] The comparison is shown in Figure 1 where we have also included the total cross section for the scattering of neutrons by water to indicate the experimental and theoretical difference between water and polyethylene. The theoretical cross section was then used to calculate flux spectra as described in the next section.

III. Calculation of Flux Spectra

In order to determine the usefulness of the scattering model, it is necessary to compare the results calculated using the various models with available experimental data. Beyster and his co-workers have recently measured infinite media spectra for both homogeneous water and polyethylene moderators with varying amounts of absorption.[7] This presented a reasonable test of the importance of the scattering kernel in the calculation of a quantity of use in reactor analysis.

The neutron balance equation for an infinite medium has a particularly simple form

$$\Sigma_T(E)\,\varphi(E) - \int_0^\infty \Sigma(E'\to E)\,\varphi(E')\,dE' = S(E) \qquad (4)$$

where φ is the flux

$\Sigma(E'\to E)$ is the scattering kernel

$S(E)$ is the slowing down source

and $$\Sigma_T(E) = \int_0^\infty \Sigma(E\to E')\,dE' + \Sigma_a(E)$$

Three different choices of the scattering kernel were employed in the solution of Equation (4). They are:

1) Perfect gas. The differential cross section for the scattering of neutrons by a perfect gas is given in Equation (3). This has the especially simple property that its integral over angle and energy can be performed analytically. In the past for this reason a great deal of calculational endeaver had been performed using this choice for the scattering kernel.

2) Water. Nelkin's model for the scattering of neutrons by water has been described in Section 2. This model was available to Beyster in his analysis of his experiment.

3) Polyethylene. A model for calculating the cross section of the scattering of neutrons by polyethylene has been proposed in Section 2. The scattering function was computed by a machine program and the cross section information necessary for the flux calculation of Equation (4) presented.

The slowing down equation was solved by replacing the integral in (4) by a summation over discrete energy values. Equation (4) then becomes a matrix equation for the values of ϕ at these energy points.

$$\sum_{j=1}^{N} \left\{ \Sigma_T(E_i)\,\delta_{ij} - \Sigma(E_j \to E_i)\,\Delta E_j \right\} \varphi(E_j) = S(E_i) \qquad (5)$$

The flux spectrum is obtained by direct inversion of the scattering and absorption matrix, using the SWAK code.

Infinite medium spectra using the method described above were calculated. Various amounts of poisons were used in the calculations corresponding to the actual absorptions in the infinite medium spectrum measured by Beyster. All spectra are normalized to the same 1/E dependence at high energies. Figure 2 is a graph of the spectrum for a supposedly infinite medium of polyethylene with no added poison absorption. However, as Beyster pointed out, it is not possible experimentally to approach the condition of an infinite medium without any poisoning: inclusion of a DB^2 term, with B^2 arbitrarily determined, would cause the experiment and theory to come into agreement. It is significant to note that even for the very low absorption inherent in the pure moderator, there is a difference in the calculated spectra for the various moderators. This inherent absorption to be sure produces the deviation of the calculated spectrum from a pure Maxwellian for this case.

In Figure 3 the calculated and experimental spectra for two different amounts of poison in water are plotted. These are similar to the curves of Beyster and

indicate the hardening of the spectrum produced by including chemical binding effects in the scattering kernel. A further hardening is seen in Figures 4 and 5 where the calculated and experimental spectra for two different amounts of poison in polyethylene are plotted. The difference in the calculated results are apparent, as is the agreement between experiment and calculations with the appropriate theoretical scattering kernel.

IV. Conclusion

A model has been presented for the calculation of the inelastic scattering of thermal energy neutrons by polyethylene. This model was seen to calculate the total cross section correctly. The scattering matrix predicted by this theory was then used in the calculation of infinite medium spectra. These theoretical results were compared with experimental measurements and the agreement was seen to be extremely good. Thus there is presently available a model for polyethylene which seems able to predict at least some important quantities.

There remains, to be sure, many questions yet to be answered. From the point of view of understanding the dynamical behavior of polyethylene, the details of the scattering calculated with the rather inexact treatment must be compared with as yet unavailable differential cross section measurements. Of interest for reactor applications, the flux spectra in finite media are to be calculated and comparisons with experiments made. Such work has progressed and these results will be presented in a subsequent paper. The behavior of the scattering as a function of temperature is still to be investigated. It is reasonable to expect that a more sophisticated theory be needed to account for a larger body of experimental information.

Of broader significance is the fact that it appears possible for one to utilize a rather simple model to calculate scattering behavior. This approach should

be able to be extended from water and polyethylene to other scatterers with similar chemical properties thus perhaps lending a large amount of experimental data to theoretical analysis.

Acknowledgement

The authors would like to thank Drs. Norman Francis and Mark Nelkin for numerous stimulating and beneficial discussions. Thanks are due to members of the staff of General Atomic for supplying the authors with a version of the scattering kernel machine program. The assistance of Dr. J. Robert Beyster in interpreting the experimental flux measurements is gratefully acknowledged.

References

1. M. Nelkin Phys. Rev. 119, 741 (1960)
2. A.C. Zemach and R.J. Glauber, Phys. Rev. 101, 118, (1956)
3. T.J. Krieger and M.S. Nelkin, Phys. Rev. 106, 290 (1957)
4. P.A. Egelstaff, Nucl. Sci. & Eng. 12, 250 (1962)
5. J.R. Nielsen and A.H. Woolett, J. Chem Phys. 26, 1391 (1957)
6. D.R. Bach, S.I. Bunche, J.R. Roesser, and R.E. Slovacek, private communication.
7. J.R. Beyster et. al., Nucl. Sci. & Eng. 9, 168 (1961)

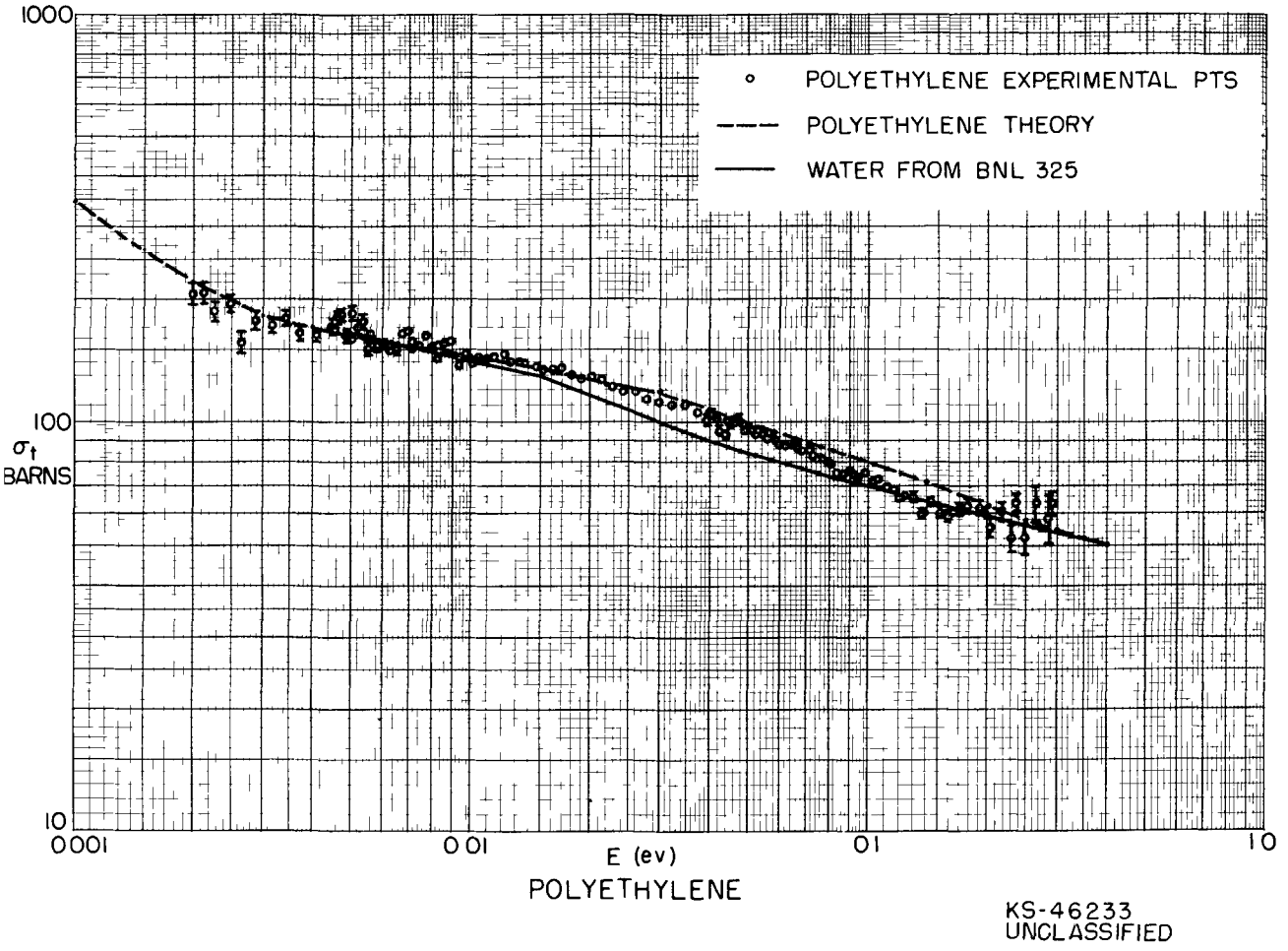

Figure 1 Total Cross Section for the Scattering of Neutrons by Polyethylene

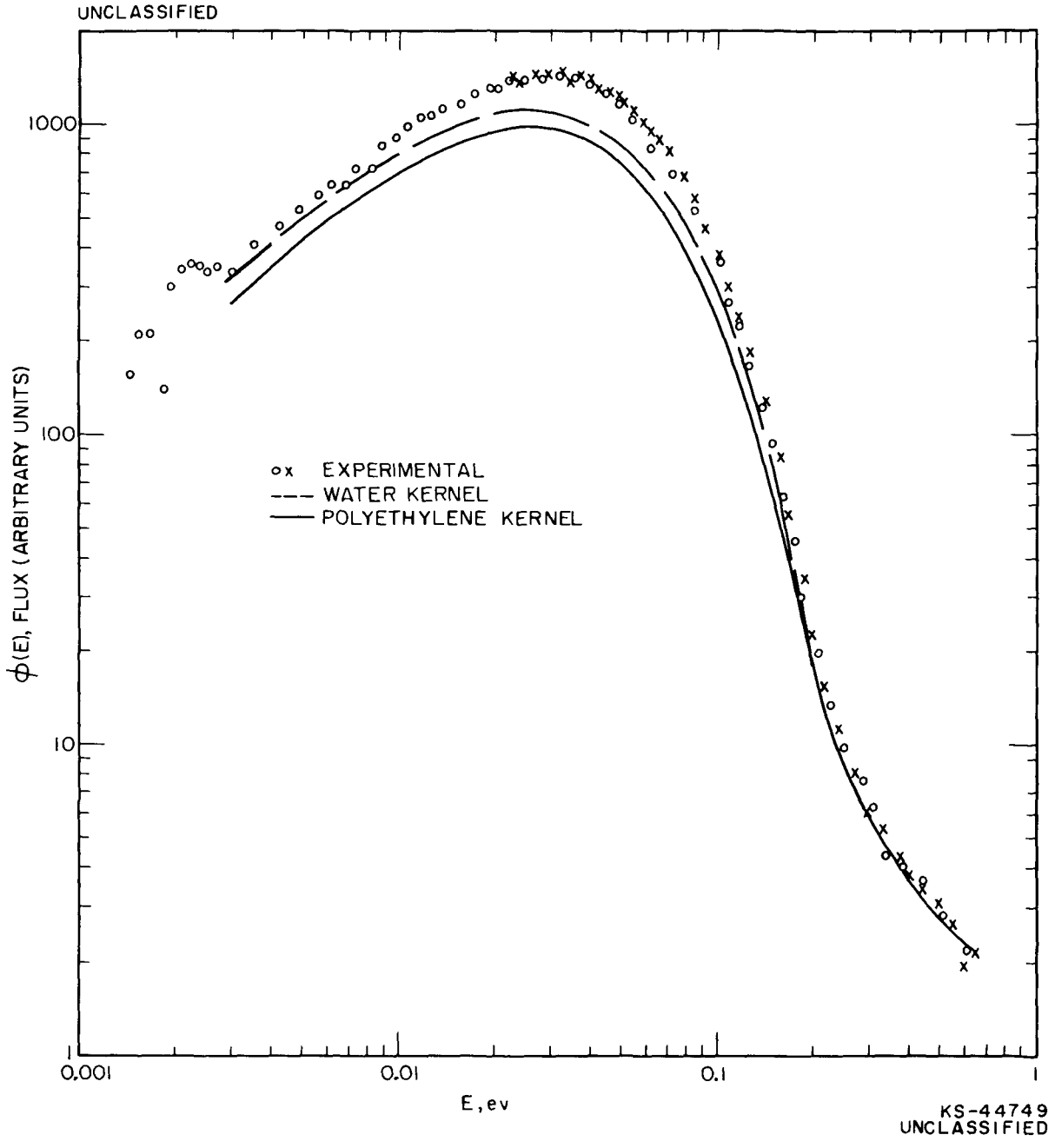

Figure 2 Calculated and Experimental Neutron Spectra in Polyethylene

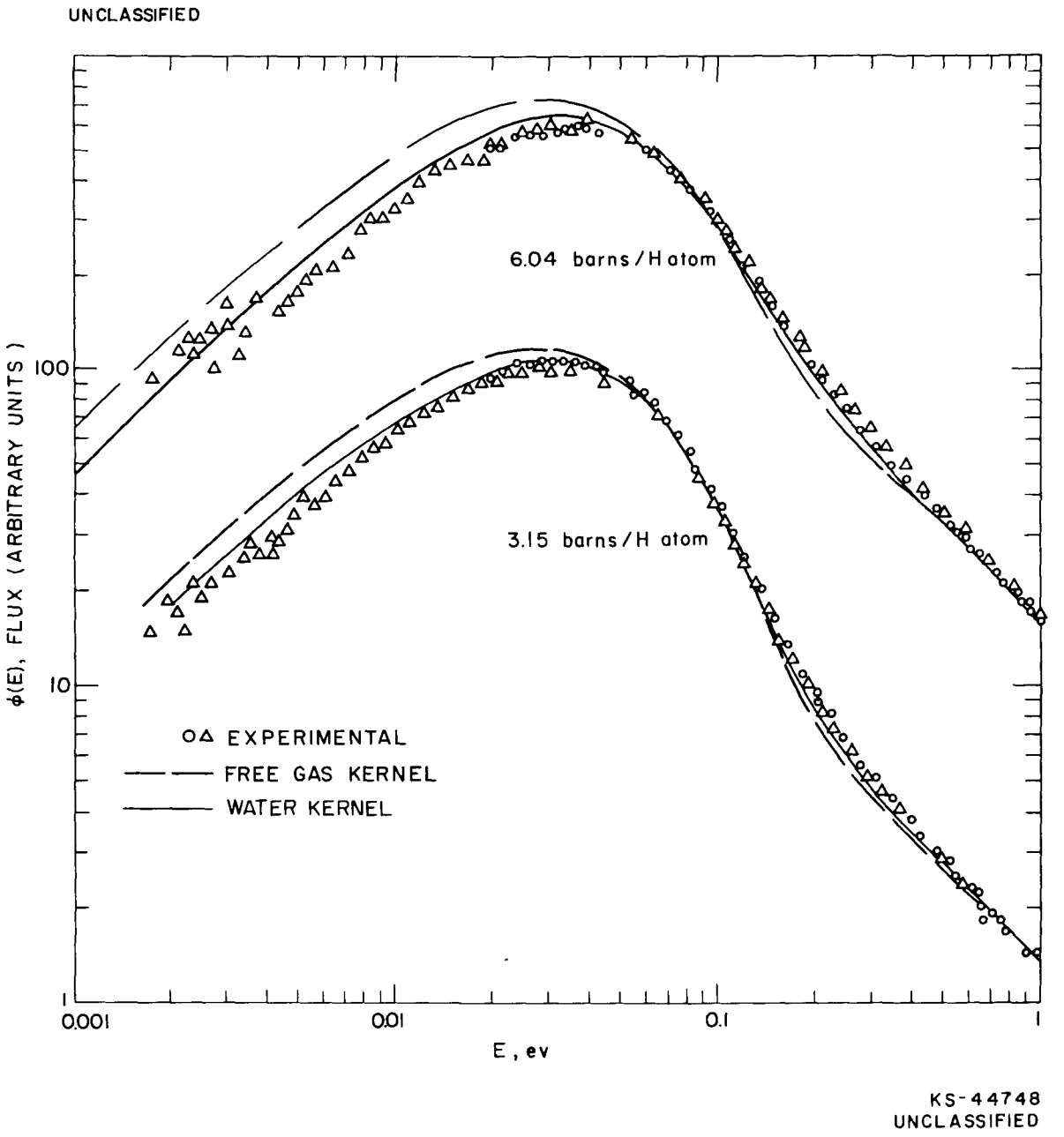

Figure 3 Calculated and Experimental Neutron Spectra in Boric Acid

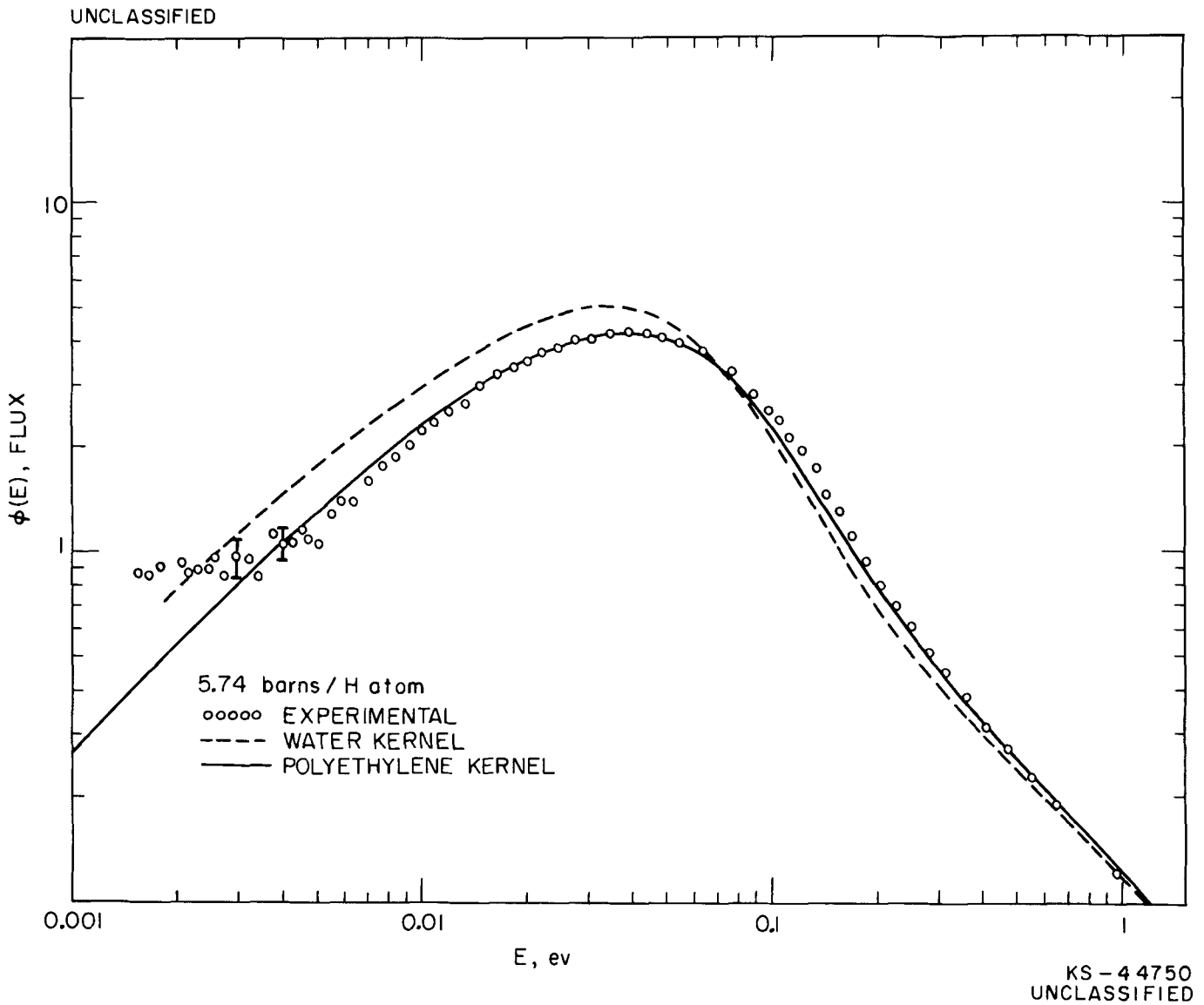

Figure 4 Calculated and Experimental Neutron Spectra in Borated Polyethylene (5.74 barns/H atom)

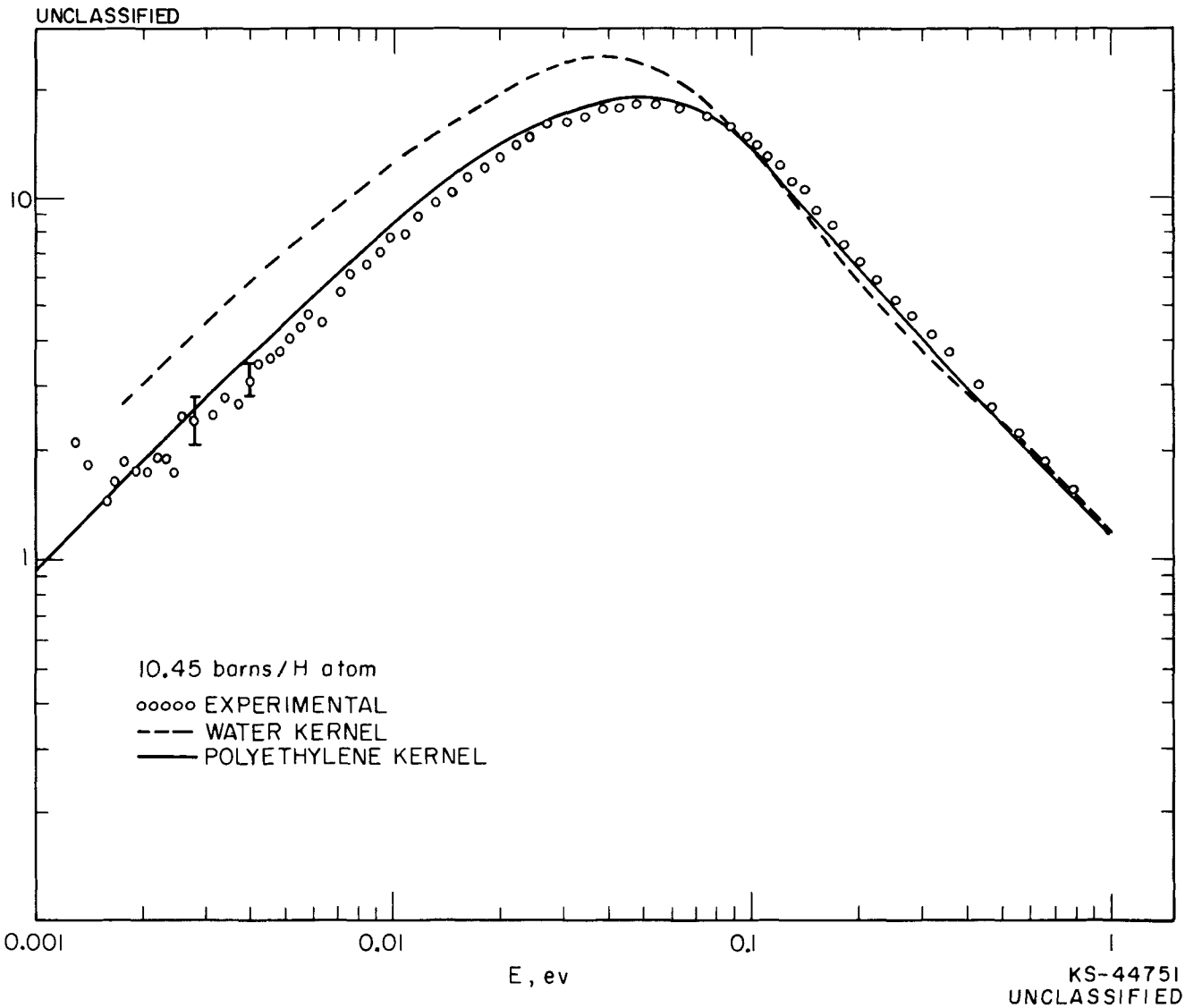

Figure 5 Calculated and Experimental Neutron Spectra in Borated Polyethylene (10.45 barns/H atom)

THERMAL NEUTRON SCATTERING IN GRAPHITE

L.S.Kothari

Physics Department, Delhi University, Delhi 6, India.

The scattering of thermal and cold neutrons from graphite has recently been extensively studied both theoretically[1-4] and experimentally[5]. Using the method suggested by Sjölander[6] and independently by Schofield and Hassitt[3], one can take account of multy-phonon contributions to neutron scattering. However, it is important to note that the approximations used in their method break down for one phonon scattering process and this one must calculate seperately. If one is interested in the slowing down of neutrons near thermal equilibrium in room temperature graphite, then the effect of two and higher phonon processes is small[1]. As such the problem can be worked out by considering just the one-phonon process. The same is also true for the scattering of cold neutrons from graphite.

Assuming the Krumhansl Brooks frequency distribution[7] for lattice vibrations in graphite we have calculated the one-phonon contribution to the scattering cross section for a neutron of initial energy E being scattered into a final energy E', $\sigma(E\rightarrow E')$. Using these values and assuming that the neutron energy distribution remains Maxwellian at some temperature T_θ, which is greater than the temperature of the moderator T, one can calculate the relaxation time τ for the slowing down of neutrons near thermal equilibrium[8],

$$\tau = \frac{3}{2}\left(\frac{\pi m_o}{2 k_B T}\right)^{1/2} \frac{1}{M_2},$$

where m_o is the neutron mass, k_B is the Boltzmann constant, and

$$M_2 = \frac{1}{(k_B T)^4} \int_0^\infty \int_0^\infty \sum(E\rightarrow E')(E-E')^2 E\, e^{-E/k_B T}\, dE\, dE'.$$

$\sum(E\rightarrow E')$ is the macroscopic scattering cross section for neutrons of energy E being scattered into energy E'. For graphite of density 1.60 gm/cm^3 at T=300^{o}K

we get M_2=0.064 cm^{-1}, which gives τ =185 μsec. The experimentally observed value[9] is 185± 45 μsec.

One can also consider this problem in an alternate way[10]. Having calculated $\sigma(E \to E')$ we evaluate mean energy loss per collision for different initial neutron energies E. Again assuming the neutron energy distribution to be Maxwellian one can calculate the rate of decrease of T_o and hence the relaxation time. The average relaxation time in the temperature range 350°K to 300°K is nearly 170 μsec, whereas between 500°K to 400°K it is only 110 μsec.

At a few energies we have calculated the mean energy loss per collision on Baldock model[11] of lattice vibrations. Though the values of $\sigma(E \to E')$ on the two models are quite different, it is found that mean energy loss per collision is the same to within 5 per cent[10].

Another point to note here is that mean energy loss per collision in graphite as one calculates here is much smaller than what a gas model or a Debye model would give. As a matter of fact on a gas model the effective mass number of graphite would be around 50. (To interpret their experiment on rethermalization of neutrons in graphite, Bennett and Heineman[12] require an effective mass of 200m_o for graphite, but this is due to errors in their interpretation.) This large difference between the actual and the effective mass arises because for a layer lattice the number of low frequency modes is much larger than for a three dimensional solid, and hence in the former case scattering is predominantly due to these modes.

We will now discuss the evaluation of the average diffusion constant $\bar{D}_o$ and the diffusion cooling constant C. For this one must know the transport cross section, σ_{tr} as a function of energy. For room temperature graphite this had been calculated and reported earlier[13]. Using those values we get,

$$\bar{D}_o = 2.30 \times 10^5 \text{ cm}^2 \text{ sec}^{-1},$$

$$C = 1.64 \times 10^6 \text{ cm}^4 \text{ sec}^{-1}.$$

These may be compared with the following experimental values (reduced to ρ =1.60 gm/cm^3)

$$\bar{D}_o = \begin{cases} 2.15 \times 10^5 \text{ cm}^2 \text{ sec}^{-1} & [9] \\ 2.07 \pm 0.03 \times 10^5 & [14] \\ 2.08 \times 10^5 & [15] \end{cases}$$

and

$$C = \begin{cases} 1.63 \pm 0.25 \times 10^6 \text{ cm}^4 \text{ sec}^{-1} & [9] \\ 1.37 \pm 0.25 \times 10^6 & [14] \\ 1.27 \times 10^6 & [15] \end{cases}$$

A better method for calculating C would be the one in which for the neutron energy distribution a Maxwellian is not assumed. By successive iterations one can calculate the neutron energy spectrum as well as the decay constant λ in assemblies of different sizes and plotting λ as a function of buckling, determine both $\bar{D}_o$ and C. Such calculations have been done for beryllium[16] and beryllium oxide[17] and are now being performed for graphite.

At the end one can add a few remarks about $\sigma(E \to E')$. Egelstaff[18] has presented his detailed experimental data on graphite in terms of the scattering law $S(\alpha,\beta)$ where $\alpha = \frac{\hbar^2 k^2}{2M k_B T}$ and $\beta = \frac{\hbar\omega}{k_B T}$, $\vec{K}$ being the momentum change of the neutron $\hbar\omega$ the energy change and M the mass of the scatterer atom. Unfortunately this interpretation is valid only in the incoherent approximation, and would hold if the incident neutron energy is reasonably high. For cold neutrons, where the number of $\vec{\tau}$ vectors contributing to the scattering is very small, the scattering cross section, even for a polycrystalline sample will depend not only on α and β but also on E. Thus to be able to compare theory with experiment, it would be valuable if instead of giving $S(\alpha,\beta)$ as function of α and β only, one also indicated the energy of the incident neutrons, particularly if one was working in the cold region.

References

1. L.S.Kothari and K.S.Singwi, Phys. Rev. 106,230(1957).
2. P.G.Khubchandani, L.S.Kothari and K.S.Singwi, Phys. Rev. 110,70 (1958).
3. A.Hassitt and P.Schofield, Proc. II Geneva Conf. 16
4. D.E.Parks, GA 2125 (1961); GA 2438 (1961).
5. P.A.Egelstaff and S.J.Cocking, Vienna Conf. Paper IS/P/8 (1960).
6. A.Sjölander, Arkiv Fysik 14,315 (1958).
7. J.Krumhansl and H.Brooks, J. Chem. Phys. 21,1663 (1953).
8. K.S.Singwi and L.S.Kothari, J.Nuclear Energy 8,59 (1958).
9. K.H.Beckurts, Nuclear Sci. and Eng. 2,516 (1957).
10. L.S.Kothari and P.G.Khubchandani, Nuclear Sci. and Eng. 7,240 (1960).
11. G.R.Baldock, Phil. Mag. 1,789 (1956).
12. R.A.Bennett and R.E.Heineman, Nuclear Sci. and Eng. 8,294 (1960).
13. K.S.Singwi and L.S.Kothari, Proc. II Geneva Conf. 16,325 (1958).
14. A.V.Antonov et al., Proc. I Geneva Conf. 5,3 (1956).
15. E.Starr and G.A.Price, Supp. Nuclear Sci. and Eng. 2, No.2, 125 (1959).
16. S.S.Jha, J. Nuclear Energy, 12A,89 (1960).
17. L.S.Kothari and P.G.Khubchandani, Reactor Sci. and Tech. 15,30 (1961).
18. P.A.Egelstaff, Vienna Conf. Paper IS/P/7 (1960).

APPLICATION OF SCATTERING LAW DATA TO THE CALCULATION OF THERMAL NEUTRON SPECTRA

J. D. Macdougall

The work reported in this paper has been carried out by teams working both at A.E.R.E. Harwell and A.E.E. Winfrith and major contributions have been made by Dr. P. A. Egelstaff, Mr. P. Schofield and Mr. R. McLatchie of Harwell and Dr. J. Askew, Mr. R. Brissenden and Mr. S. Francescon of Winfrith.

Acknowledgement is also due to the scattering law project team at Chalk River under Mr. S. J. Cocking and Dr. B. Haywood, and the time of flight team at Harwell under Dr. M. J. Poole, who made their experimental results available prior to publication.

1. INTRODUCTION

We discuss in this paper the method of using the data from the scattering law experiments at Chalk River in calculations of reactor thermal neutron spectra, and present some comparisons of calculated and measured spectra for a Calder Hall lattice.

In the experiments at Chalk River[1] the differential scattering cross-section $\sigma(E \rightarrow E', \theta)$ for scattering from energy E to energy E' through angle θ is measured; this data may be reduced to a scattering law $S(\alpha, \beta)$ which is a function of two variables only, basically the momentum and energy transfers. The range of the scattering law which is measured does not however include all the energy and momentum transfers required for spectrum calculations, and some method of extrapolating and interpolating the data is required; the extrapolation being particularly difficult. A suitable theoretical method has been developed by Egelstaff and Schofield[2], which involves deducing a generalized frequency spectrum from the experimental results, and then calculating a complete scattering law from this frequency spectrum. The available experimental data and the method of extending this to all required energy and momentum transfers is discussed in Section 2.

In Section 3 the Fortran program LEAP for calculating the scattering law from the generalized frequency spectrum is discussed.

Section 4 discusses the nuclear data required for multigroup spectrum calculations; in particular, methods of group-averaging are discussed and the program PIXSE which produces multigroup cross-sections from the scattering law, primarily for use with the Winfrith DSN programme, is described.

In section 5 is given a brief description of the Winfrith DSN programme. This is a Fortran programme solving the one-dimensional multigroup transport equation in Carlson's discrete S_n approximation, and is at present working in cylindrical geometry. The programme incorporates several improvements on Carlson's DSN code, in particular acceleration of convergence by a group selection technique and a different method of solving the reflected boundary condition.

In Section 6 the results of applying the above techniques to a particular reactor system are given; the thermal neutron spectrum in a

Calder Hall lattice cell is calculated, and a comparison made with some experimental spectra obtained using a neutron chopper[3].

Finally in Section 7 accuracy is discussed. Topics covered are accuracies required in scattering, absorption and fission cross-sections, in group-averaging procedures and in numerical techniques; these topics are considered in relation to both criticality and temperature coefficient determinations.

2. EXPERIMENTAL SCATTERING LAW MEASUREMENTS AND THEORETICAL EXTENSION

The scattering law experiment at Chalk River measures the differential scattering cross-section $\sigma(E \rightarrow E', \theta)$ from energy E to energy E' through angle θ . This cross-section is assumed to be independent of the orientation of the scattering material; this means that crystalline materials are assumed to consist of randomly oriented microcrystals, and this has been found to be a good approximation for the graphite used in the experiments.

The differential scattering cross-section is a function of 3 variables, and thus an enormous quantity of data is required to describe it; however, making only the assumption of the first Born approximation, this data may be reduced to a function S of two variables α and β [4](basically the momentum and energy transfers in the scattering reaction) by the relation

$$\sigma(E \rightarrow E', \theta) = \frac{\sigma_b}{4\pi\, kT} \left(\frac{E'}{E}\right)^{\frac{1}{2}} e^{-\beta/2}\ S(\alpha, \beta) \qquad .....(1)$$

Here

$$\alpha = (E + E' - 2(EE')^{\frac{1}{2}} \cos\theta)/AkT$$

$$\beta = (E' - E)/kT,$$

σ_b, A and T are the bound atom cross-section, atomic mass and temperature of the scatterer; $S(\alpha, \beta)$ which is an even function of β , is called the scattering law. Equation (1) applies to both monatomic and polyatomic scattering law. Equation (1) applies to both monatomic and polyatomic scattering systems; for polyatomic systems care must be taken in the choice of σ_b and A. In this paper we discuss only monatomic systems, the extension of the theory to diatomic systems is considered in Ref. (5); we note here that the generalized frequency spectrum ($p(\beta)$) formalism described below has been used with some success for H_2O, D_2O and BeO where one species of

scattering atom is much more important than the other, but it should be observed that the physical significance of $p(\beta)$ has been largely lost in this application.

The experiment at Chalk River[1] gives scattering law data for energy transfers up to several kT, with a corresponding range of α about $4/A$ times that of β. These data available from the Chalk River experiments are inadequate for reactor thermal spectrum calculations, since if the energy region less than 1 eV only is considered energy transfers up to somewhere between 10 and 40 kT are likely to be important; thus some method of extending the data to higher α and β, and also of interpolating the experimental results is required.

Egelstaff and Schofield[2] have developed a method of extending this scattering law data to the entire α, β plane; we only outline the method here. By means of the relation

$$p(\beta)/\beta^2 = \lim_{\alpha \to 0} S_s(\alpha, \beta)/\alpha \qquad \ldots\ldots(2)$$

a generalized frequency spectrum $p(\beta)$ may be obtained from the experimental scattering law data. In equation 2, $S_s(\alpha, \beta)$ is the 'self' part of the scattering law which results from the motion of individual atoms; the remainder of S, S_d, which results from interference effects, modulates S_s and is important only at low α which are unimportant for reactor calculations (for further details see Ref.(7)). In practise the experimental S/α is extrapolated to $\alpha = 0$, ignoring the fairly clearly distinguishable region near $\alpha = 0$ where interference effect becomes important.

From $p(\beta)$, $S_s(\alpha, \beta)$ may be reconstructed (neglecting anharmonic effects - see Ref. (2)) using the relation

$$S_s(\alpha, \beta) = \frac{1}{2\pi} \int_{-\infty}^{\infty} e^{-\alpha w(t) + i\beta t} \, dt \qquad \ldots\ldots(3a)$$

where

$$w(t) = \int_0^{\infty} (p(\beta)/\beta^2) [\cosh \beta/2 - \cos \beta t] \, d\beta \qquad \ldots\ldots(3b)$$

Direct numerical integration of equations (3) does not appear feasible, and methods used to calculate $S_s(\alpha, \beta)$ from these equations are described in the next section.

The procedure used for obtaining $S_s(\alpha, \beta)$ is to deduce a $p(\beta)$ from relation (2) using the experimental data; because of experimental errors, interference effects, etc., this $p(\beta)$ will not be very accurate. This $p(\beta)$ is then used as the starting point for an iterative scheme in which $S_s(\alpha, \beta)$ is calculated from $p(\beta)$ for the experimental (α, β) region, and from the discrepancies between the experimental and calculated scattering laws corrections to $p(\beta)$ are deduced, giving a more accurate frequency spectrum; this procedure is repeated until satisfactory agreement with the experimental scattering law is obtained.

Satisfactory frequency spectra $p(\beta)$ have to date been obtained for light water at room temperature and 150°C, graphite at room temperature, 380°C and 610°C and for beryllium at room temperature[6]; although work is continuing in order to improve the fit between theory and experiment, including the calculation of interference effects (i.e. $S_d(\alpha, \beta)$). Results for beryllia and heavy water are expected shortly.

3. EVALUATION OF THE SCATTERING LAW

The Fortran programme LEAP has been written by McLatchie to evaluate the self part of the scattering law from the frequency spectrum; the relation between $S_s(\alpha, \beta)$ and $p(\beta)$ being as given by equations (3). In this section we briefly review the methods used in LEAP; in particular the numerical devices and expansions used in evaluating (3). Further details may be found in Ref. (2).

In order to evaluate (3), $p(\beta)$ is split, somewhat arbitrarily, into a 'diffusive' term $p_d(\beta)$ which is finite at the origin, and a 'bounded' term p_b which increases at least as fast as β^2 in the neighbourhood of the origin. The diffusive term only exists where an atom can slowly diffuse away from its initial position (thus this term exists in liquids, but not in crystals). When we have put $p(\beta) = p_b(\beta) + p_d(\beta)$, we may evaluate the scattering law from

$$S(\alpha, \beta) = \int_{-\infty}^{\infty} S_d(\alpha, \beta') \, S_b(\alpha, \beta - \beta') \, d\beta' \qquad \ldots\ldots(4)$$

where S_d and S_b are to be calculated from p_d and p_b using equation (3). By a suitable choice of $w_d(t)$ it is possible to obtain a reasonably simple

form for $S_d(\alpha, \beta)$ and the convolution integral (4) can then be evaluated directly once $S_b(\alpha, \beta)$ has been determined. In LEAP the form

$$w_d(t) = 2d \{ (t^2 + C^2 + \tfrac{1}{4})^{\frac{1}{2}} - C \}$$

is used (this is the simplest possible form satisfying the required restraints); $p_d(\beta)$ and $S_b(\alpha, \beta)$ then appear as simple expressions involving the Bessel function K_1.

The evaluation of $S_b(\alpha, \beta)$ is more troublesome. It has been found that for small α, a 'quasi-phonon' expansion is satisfactory. The expansion used is

$$\left.\begin{aligned} S_b(\alpha, \beta) &= e^{-\alpha\lambda} \sum_{n=0}^{\infty} \frac{1}{n!} (B\alpha)^n T_n(\beta) \\ \text{where } B &= \int_{-\infty}^{\infty} [p(\beta)/\beta^2]\, d\beta \quad , \lambda = 2\int_0^{\infty} [p(\beta)/\beta^2] \cosh\beta/2 \; d\beta \\ T_0(\beta) &= \delta(\beta) \, , \; T_1(\beta) = p(\beta)/B\beta^2 \, , \; T_n(\beta) = \int_{-\infty}^{\infty} T_{b-1}(\beta') \cdot \\ &\qquad T_1(\beta - \beta') d\beta' \end{aligned}\right\} \ldots\ldots(5)$$

In the programme LEAP, the $T_n(\beta)$ may be evaluated by numerical integration (using Simpson's rule) for $1 \leq n \leq 6$. The range of $T_n(\beta)$ is n times the range of $p(\beta)$, and $p(\beta)$ may be specified at up to 2000 equally spaced values of β. (Since $p(\beta)$ is symmetric, only positive β are considered; $p(\beta)$ is assumed zero beyond the greatest β at which it is specified; discontinuities in $p(\beta)$ are allowed.) The $T_n(\beta)$ which are not calculated numerically are evaluated using an Edgeworth series approximation[7]; viz:

$$T_n = (2\pi n E_2)^{\frac{1}{2}} \left[1 + \frac{1}{24\,n} \left(\frac{E_4}{E_2^2} - 3\right) \left\{\left(\frac{\beta^2}{nE_2} - 3\right)^2 - 6\right\}\right] e^{-\beta^2/2nE_2}$$

where $E_i = \frac{1}{B} \int_{-\infty}^{\infty} [p(\beta)/\beta^2]\, \beta^i \cosh \beta/2 \; d\beta \quad (i = 2, 4)$.

For large α this quasiphonon expansion is unsatisfactory (a very large number of terms are required), and a steepest descents method[2], which is an extension of the 'short collision time' approach of Wick[8], is used. This gives rise to an asymptotic expansion in inverse powers of α, in contrast to (5) which is an expansion in ascending powers of α.

The resulting expression is

$$S_s(\alpha,\beta) = (2\pi\,\alpha\, f_2(\tau))^{\frac{1}{2}} \exp\{-(\tau f_1(\tau) - f_0(\tau))\}\,.$$

$$\{1 + (\alpha\, f_2(\tau))^{-1}\, C_1(\tau) + (\alpha\, f_2(\tau))^{-1}\, C_2(\tau) + \ldots.\}$$

where $f_n(\tau) = \int_0^\infty [p(\beta)/\beta^2]\,\beta^n\,[e^{\beta\tau} + (-1)^n e^{-\beta\tau} - 2\,\delta(n)\cosh\beta/2]\,d\beta$, τ is defined by $f_1(\tau) = \beta/\alpha$, and the C_m are simple functions of the f_n/f_2 $(n \geq 3)$.

LEAP calculates $S_s(\alpha,\beta)$ for any set of values of α, where for each α there is an arbitrary set of β. For each value of α, it starts with the highest β requested and evaluates the scattering law using the steepest descents method; it carries on with successive β until it finds that the $S(\alpha,\beta)$ calculated using the steepest descents method does not satisfy an accuracy criterion. For this and for all other smaller β values the quasiphonon expansion is used. The two expansions will agree at the change-over point provided that the Edgeworth approximation is a good one at the lowest convolution at which it is used; the goodness of fit is indicated on the output from the programme. The programme also prints useful quantities such as the Debye/Waller factor constant λ, the mean kinetic energy of the moderator atoms $\bar{K}$ and the related quantities $\bar{B}$, $\bar{C}$.

The time taken to calculate $S(\alpha,\beta)$ is strongly dependent upon the number of points m used to specify the frequency spectrum $p(\beta)$, the number of $T_n(\beta)$ evaluated numerically, and whether the diffusion convolution[4] is required. The evaluation of each $T_n(\beta)$ takes about 3.5 m^2 μmin; and some typical times for runs using an IBM7090 are:-

m = 70, 4 $T_n(\beta)$ evaluated numerically, 10 values each with 35 β values - 2 mins.

a similar run with diffusion - 3 mins.

m = 35, 6 $T_n(\beta)$ evaluated numerically, 24 α values each with 57 βvalues - 9 mins.

a similar run with m = 175 - 20 mins.

m = 350, 6 $T_n(\beta)$ evaluated numerically, 2 α values each with 57 β values - 12 mins.

4. DETERMINATION OF GROUP CROSS-SECTIONS FOR REACTOR CALCULATIONS

The treatment of spatial variation in thermal spectrum calculations in general falls into 3 categories: calculation of spectra in infinite homogeneous media, calculation of spectra using diffusion theory for spatial variation, and calculation of spectra using a transport approximation such as S_n or P_n for spatial variation. The energy dependence may be specified either by a finite difference mesh('point representation') or by a group representation. In the point representation the cross-sections to be used in the equations are clearly just point cross-sections, and there is no difficulty in defining them; however in many cases the group representation is more convenient as in general a smaller energy mesh is required, and in this case care must be taken in defining the group cross-sections.

In this section we discuss the method of averaging necessary to obtain group cross-sections; we confine the discussion to isotropic scattering in the laboratory system, but the arguments are easily extended to anisotropic scattering in the P_n approximation.

Consider first homogeneous calculations; in these the basic equation to be solved is

$$\Sigma_t(E)\,\phi(E) = \int_0^\infty \Sigma(E' \longrightarrow E)\,\phi(E')\,dE' + S(E) \qquad .....(6)$$

and this is represented by the set of G group equations

$$\Sigma_{tg}\,\phi_g = \sum_{g'=1}^{G} \Sigma_{g'g}\,\phi_{g'} + S_g \qquad .....(7)$$

where $\phi_g = \int_g \phi(E)dE$ ($\int_g$ indicates integration over the g^{th} energy group).

By integrating (6) over the g^{th} group we find that

$$\Sigma_{tg} = \int_g \Sigma_t(E)\,\phi(E)\,dE \Big/ \int_g \phi(E)\,dE \qquad .....(8.1)$$

$$\Sigma_{g'g} = \int_{g'} \phi(E') \int_g \Sigma(E' \longrightarrow E)\,dE\,dE' \Big/ \int_{g'} \phi(E')\,dE' \qquad .....(8.2)$$

$$S_g = \int_g S(E)\,dE + \int_{E_m}^\infty \phi(E') \int_g \Sigma(E' \longrightarrow E)\,dE\,dE' \qquad .....(8.3)$$

where E_m is the highest energy considered in the group scheme (for multi-group thermal spectrum calculations E_m is usually of the order of 1 eV). Thus we see that the total and scattering group cross-sections should be weighted with the flux.

In diffusion theory calculations the basic equation differs from (6) only in the addition of a term $D(E)\,\nabla^2\,\phi(E)$ on the left hand side; and the group equations differ from (7) only in the addition of a term $\nabla^2 D_g\,\phi_g$ on the left hand side, where

$$D_g = \int_g D(E)\,\phi\,(E)\,dE \Big/ \int_g \phi(E)\,dE \qquad .....(8.4)$$

We observe that $D(E) = 1/3\ \Sigma_{tr}(E)$; so that although D_g is to be calculated as a flux weighted average, the effective average of Σ_{tr}, the transport cross-section, is the reciprocal of the flux weighted average of the reciprocal.

Let us now consider the transport equation,

$$\underline{\Omega}\ .\ \nabla\phi\ (E,\ \underline{\Omega}) + \Sigma_t(E)\ \phi(E,\ \underline{\Omega}) = \int_0^\infty \Sigma\ (E' \longrightarrow E)\ \phi(E')\ dE' + S(E) \qquad .....(9)$$

In a transport approximation the $\phi(E,\ \underline{\Omega})$ at any energy is represented by a set $\phi_\mu\ (E)$. Examination of equation (9) shows that Σ_t should be averaged by the different $\phi_\mu\ (E)$ spectra for each μ considered. This is impracticable, and Askew and Brissenden have shown that the best definition of Σ_{tg} for a DSN problem when only the scalar flux is available for averaging is

$$\Sigma_{tg} = \int_g \phi(E)dE \Big/ \int_g [\ \phi(E)/\ \Sigma_t(E)\ ]\ \ dE \qquad .....(10.1)$$

and that in this case Σ_{gg} should be defined by

$$\Sigma_{gg} = \Sigma_{tg} + \int_g \left(\int_g \Sigma\ (E \longrightarrow E')\ dE' - \Sigma_t(E)\right)\phi(E)dE \Big/ \int_g \phi(E)dE \qquad .....(10.2)$$

In an extreme case the use of 10.2 instead of 8.2 for a one-group problem (fission and thermal) resulted in a 10% change in reactivity, but the effect in a multigroup problem in the thermal region is normally small.

The FORTRAN programme PIXSE has been written to calculate $\Sigma_{gg'}$ and S_g

as defined by (8.2) and (8.3) from scattering laws calculated by LEAP, or for a monatomic gas scattering law; the function $\emptyset$ is calculated by a subroutine and may thus be chosen arbitrarily. The output is designed for use with the Winfrith DSN, and thus there is a facility which enables Σ_{gg} to be calculated from 10.2. Scattering matrices for Carlson's SNG code can be produced by using PIXSE in conjunction with the program PIXMIX written by H. J. Terry. In addition PIXSE can be used to produce point cross-sections and to calculate quantities such as

$$\int_{-1}^{1} P_n(\mu)\,\sigma(E\rightarrow E',\mu)\,d\mu(\mu = \cos\theta) \quad \text{and} \quad \int_{o}^{E_m} (E' - E)^n\,\sigma(E\rightarrow E')\,dE'.$$

Typically the programme takes 2 or 3 minutes on an IBM7090 to calculate a 40 x 40 group cross-section matrix.

5. THE WINFRITH DSN PROGRAMME

The Winfrith DSN programme conceived by Askew and Brissenden and written by Francescon is a one-dimensional Carlson discrete ordinates programme written in Fortran. At present it is only available in cylindrical geometry. The choice to write the programme in Fortran was made in order that its use would not be restricted to one particular computer. The programme is conceived as an improvement on Carlson's DSN programme for the IBM704; in particular the treatment of reflected boundary conditions and the iteration technique have been radically changed. The facilities in Carlson's DSN for forming mixtures of materials within the programme have been excluded as it is anticipated that the Winfrith DSN will be used with a data-editing programme (see §4). The variable length storage arrays used in Carlson's programme have been retained so that full use is made of machine storage; in addition the cross-section data has been compressed so that only non-zero inter-group scattering cross-sections need be stored. We consider here briefly the methods used for dealing with reflected boundary conditions and in the iteration technique.

In the DSN method, in any energy group, the procedure is to solve the transport equation for each discrete ordinate direction starting from the outside of the system for the inward directions, and from the inside of

the system for the outward directions. For a reflected system, the problem is specifying the inward fluxes to start the calculation; if a naive view is taken and the inward fluxes are taken as, say, the mean of the inward and outward fluxes from the previous iteration, convergence may not be obtained. In the Winfrith DSN, the boundary inward fluxes at the start of the n^{th} iteration, (the vector $\bar{\phi}_n$), are obtained from a relation of the form

$$\phi_n^- = \phi_{n-1}^- + (1 - A)^{-1}(\phi_{n-1}^+ - \phi_{n-1}^-)$$

where ϕ_n^+ is the outward flux at the end of the n^{th} iteration, and A is a (matrix) function of the geometry of the system only. This form is based on the relation

$$\phi^+ = A\phi^- + S$$

between the ingoing and outgoing fluxes; the first term on the right represents the contribution to the outgoing flux from neutrons which pass through the cylinder without collision, the second term the remainder of the outgoing flux. The matrices $(1 - A)^{-1}$ need only to be calculated at the beginning of the computation. The method of treatment of a reflected boundary above is described for specular reflection; the programme will also allow total reflection at the outer boundary which is any combination of white (i.e. isotropic) and specular reflection. This facility is useful for cell calculations in which a very small cell has been cylindricalized.

The iteration technique used in Winfrith DSN in multigroup problems is quite novel. Instead of the usual procedure of solving all groups consecutively a group selection procedure is employed whereby the next group to be solved is chosen as that which has had the greatest proportional change in the source term (i.e. scatterings into the group) since it was last solved. This technique has proved very powerful in many cases, but for certain fixed source problems with no fission it was found only to be equal in power to the scaling method used by Carlson. A combination of scaling and group selection has been found to be very powerful in some of these cases, convergence to an accuracy of about 10^{-6} in about 2000 group passes being obtained in 40-group thermal calculations. The programme has been used with success to solve few group eigenvalue problems for thermal systems (e.g. mixed light and heavy water systems.)

The output from the Winfrith DSN consists essentially of the eigenvalue, and the energy-space flux solution of the problem, together with quantities such as total leakage, total absorption etc. In addition there is a binary dump of useful information which may be edited by the programme RED to give reaction rates of any required substance over any portion of the space energy mesh.

Typical running times using an IBM7090 are:-

Fixed source, 40 group reflected boundary, 25 space points - 15 mins.

Eigenvalue problem, 5 group reflected boundary, 50 space points - 5 mins.

It should be noted that it is believed that there is an inefficiency of a factor of about 1.5 in time due to the use of Fortran rather than machine language.

6. CALDER HALL RESULTS

The thermal neutron spectrum in a Calder Hall lattice cell has been measured at several temperatures using time of flight techniques[3]. These experiments measure the neutron spectrum parallel to the fuel rods at a position midway between two fuel elements. Spectrum calculations have been made (using LEAP, PIXSE and Winfrith DSN) for comparison with experiments for moderator temperatures of 293°K and 594°K; at both temperatures calculations have been made using both the monatomic gas model and a scattering law derived as described above (§2), (in addition a calculation at 293°K has been made assuming graphite to be a Debye crystal with Debye temperature 1172°K).

The frequency spectrum $p(\beta)$ used to represent graphite in these calculations was chosen so that $2\,p(\beta)\sinh(\beta/2)/\beta$ was constant for $300^{\circ}K < \beta kT < 2100^{\circ}K$, and proportional to β for $\beta kT < 300^{\circ}K$ except for a small range of β near $\beta = 0$ where $p(\beta)$ was taken parabolic in order to obtain convergence of the phonon series (see §3).

The $S(\alpha, \beta)$ calculated from LEAP for the 293°K case are shown for several values of β in Figure 2.

Using both the $S(\alpha, \beta)$ calculated from LEAP and the gas law, 40 group cross-sections were calculated using PIXSE; these cross-sections covered the energy range from 0 to 1.5 eV with about 20 groups in the range 0 to 0.2 eV.

These cross-sections and up-scatter and source term data were then used as input for DSN calculations which represented the Calder cell in a cylindrical approximation. (The volume of moderator in the Calder cell is sufficient for cylindricalization to be a good approximation, the cell consists of a Magnox canned natural uranium bar 1.15" in diameter in a 3.75" channel, the channels being set on an 8" square pitch). DSN calculated the energy space distribution of the flux, and the experimentally measured flux is compared with the calculated scalar flux at the outside edge of the cell in Figs 3 - 6. The comparison of the directed experimental flux with the theoretical scalar flux was justified by examination of one of the DSN calculations which showed that the directed flux differed from the mean flux at this point by less than 1% even in the bottom group where the apsorption was highest and the anisotropy would be greatest. The theoretical fluxes in Figs. 3 - 6 are normalised to unit total absorption in the cell. The normalisation of the experimental spectra is rather arbitrary. In the room temperature case it is seen that the agreement of the observed spectrum with the spectrum calculated using the frequency distribution above (EG3A) is much better than the agreement with the gas spectrum particularly below about .2kT. The departure of the EG3A spectrum from 1/E in the 1 eV region is rather peculiar and is thought to be due to numerical error; this point is being investigated. In the 594°K case the difference between the gas and EG6A (calculated using the frequency distribution above) is much less than in the room temperature case (as would be expected), but it is seen that the EG6A spectrum is still closer to the experiment than the gas spectrum.

In Table I is shown the effect of the scattering model on thermal component of reactivity, ηf, on the fission rate ratios in the spectra, and on temperature coefficient. The effect on ηf is very small, one sixth of 1% between the gas and 'best' models for graphite at 293°K, and rather less than half this amount at 594°K. The effect on the 239/235 fission rate ratio is more marked and a comparison with experimental fission chamber

measurements is planned.

The effect on temperature coefficient, a change of 10%, is probably marginally important for control problems.

7. DISCUSSION OF ACCURACY

In this section some remarks are made on the effect of accuracy of data and numerical approximations on the type of calculation described in this paper. We will consider inaccuracies in scattering law data and scattering cross-sections, inaccuracies in absorption and fission cross-section data, inaccuracies in weighting cross-sections and source terms, and the effect of different orders of S_n approximations.

Little work has been done on the accuracy required in scattering data and we must restrict ourselves to general comment. In the well thermalised system described in this paper, it has been shown that the choice of scattering model makes a small difference to quantities of importance in reactor calculations; the differences between the crystal model of graphite and the gas model being of marginal importance in quantities such as reactivity and temperature coefficient. In less well moderated systems the available evidence (see (9)) suggests that the moderator model is more important (giving effects of up to about $\frac{1}{2}$% in reactivity), and the same is likely to be true in mixed Pu/U systems. If the difference between models was 10 times as important as in the system considered here, we would require to know the scattering law to about 1/10 of the difference between the gas and crystal models of graphite, that is an error of some 10 or 20% on $S(\alpha, \beta)$ (see Fig. 2). The calculation of the scattering cross-sections should be such that the accuracy on $\int_0^\infty \sigma(E \longrightarrow E') \cdot (E - E')\, dE'$ (i.e. total scattering cross-section times mean energy transfer) at any energy E is consistent with the permissible errors in $S(\alpha, \beta)$. We stress here that the figure of 10 above is at this stage merely a guess; further we point out that the scattering law requires to be known most accurately in order to calculate the moderator temperature coefficients of small components close to the fuel, such as moderating sleeves, cans and coolant. Work is in progress on this topic.

An investigation of the accuracy required on absorption and fission cross-section data has been made by Griggs and Sumner with particular emphasis

on the energy variation of the fissile isotope cross-sections. We may describe all errors in terms of errors in $\eta(E)$, the number of fission neutrons produced per absorption, and $\sigma_a(E)$ the absorption cross-section. It is quite obvious that an x% error in $\eta(E)$ at all energies gives an x% error in reactivity, but less clear what errors are introduced by variations in $\sigma_a(E)$ and energy dependent variations of η. The result of the investigation above suggested that in order to obtain reactivity correct to $\frac{1}{2}$% for low enrichment reactor systems it is necessary to know the 2200 m/sec cross-sections for the fissile isotopes to $\frac{1}{2}$% at worst, and that the error in $\eta(E)\ \sigma_a(E)$ and $\sigma_a(E)$ should be less than 2% relative to the 2200 m/sec values in the range from about 0.02 to 0.4 eV; for temperature coefficient calculations the accuracy requirement on $\eta(E)\ \sigma_a(E)$ relative to the 2200 m/sec value needs to be 1% in order to obtain temperature coefficients to 0.5 mn/°C. For reactors with a lower moderator to fissile ratio (say approaching 1000:1) the requirements are similar, but extend to rather higher energies.

In early calculations of cell thermal spectra up to 1.5 eV it was assumed in the calculation of the source term for neutrons slowing down past 1.5 eV that above 1.5 eV neutrons were slowed down by stationary moderator atoms and that the spectrum was 1/E. For graphite it was soon observed that this technique gave rise to Placzek wiggles of about 10% of the flux and extending to an energy of about 1 eV; this, while only slightly affecting the reactivity of the system then under consideration, would introduce important errors in a system containing a fair amount of Pu240; it could also introduce significant errors in a water system where the Placzek wiggles would be expected to be smaller but extend over a greater energy range. In Fig. 1 is shown (for graphite at 293°K) the effect of using a slowing down source compared with using the source calculated from PIXSE which uses the correct scattering data above 1.5 eV, but still assumes a 1/E spectrum above 1.5 eV(the use of a 1/E spectrum above 1.5 eV was found to be a sufficient approximation by comparison with an exact calculation up to 3 eV). Also shown in Fig. 1 is the effect of weighting the group scattering cross-sections with a Maxwellian compared with an unweighted average; the group width was about 0.1 eV. The Maxwellian weighting is clearly silly in this 1 eV region as it assumes that the average energy

of the neutrons in a group is practically equal to the lowest energy in the group; in fact the difference in effect between a 1/E weighting and a unit weighting is only about 3% of the difference between a unit weighting and a Maxwellian weighting. In present calculations a Maxwellian weight is used up to energies of a few kT (where T is the physical temperature), and a 1/E weight above this point; this representation is believed to be adequate for 40-group problems such as considered in §6. For few-group problems, care must be taken to use the correct weighting method as discussed in §4, where the extreme case of 10% difference in reactivity was obtained between flux weighting and the weighting described in §4 for a 1-group problem from fission to thermal energies.

Comparison of S_4 and S_8 approximations using Carlson's SNG programme, for a Calder Hall lattice showed a difference of .01% in reactivity and about $\frac{1}{4}$% change in shape of the moderator spectrum in the range up to 1.5 eV. The difference between SNG and Winfrith DSN in S_4 approximation is about $1\frac{3}{4}$% in spectrum shape using Carlson's DSN constant, and about $2\frac{1}{2}$% using improved DSN constants. The effect on ηf has not been ascertained but is expected to be less than 0.1%, which is just acceptable. We thus conclude that S_4 is a satisfactory approximation in the cell calculations considered in this paper; higher S_n approximations will only be required in calculations involving very black rods.

8. CONCLUSIONS

In this paper we have shown how scattering law data may be used in thermal neutron spectrum calculations. The methods and programmes used are satisfactory; but a rather large amount of computer time is required. The graphite scattering law has been found to give quite good agreement with experiment, although there is still room for improvement; work on resolving the remaining discrepancies is continuing. Comparison of experimental spectrum measurements with scattering law calculations for water moderated systems is under way.

TABLE 1

Moderator Model	Temperature	ηf	239/235 Fission ratio	241/235 Fission ratio	Temperature Coefficient mn/°C
Gas	293°K	1.1856	1.567	1.968	- 3.61
Gas	594°K	1.1728	2.273	2.528	
EG3A	293°K	1.1836	1.632	2.014	- 3.29
EG6A	594°K	1.1720	2.309	2.552	
Debye	293°K	1.1844	1.617	2.004	

REFERENCES

1. P. A. Egelstaff, S. J. Cocking and T. K. Alexander — A four rotor thermal neutron analyser. Proc. Symposium on Slow Neutron Scattering, IAEA, Vienna, IS/P/9 (1960)

2. P. A. Egelstaff, P. Schofield — On the evaluation of the thermal neutron scattering law. AERE - R.3803

3. M. S. Coates, D. B. Gayther. — Time of flight measurements of neutron spectra in a graphite uranium lattice at different temperatures. AERE-R.3829.

4. P. A. Egelstaff — The treatment of thermal neutron scattering law data. AERE.-R.3622 (IS/P/7).

5. P. A. Egelstaff — The scattering of thermal neutrons by moderators. American Nuclear Soc. June 1961 meeting.

6. P. A. Egelstaff, C. Heard — Private communication.

7. A. Sjolander — Multiphonon processes in slow neutron scattering by crystals. Arkiv for Fysik 14, 315 (1958)

8. G. E. C. Wick — The scattering of neutrons by systems containing light nuclei. Phys. Rev. 94, 1228 (1954).

9. M. J. Poole and F.H.W.Pitcher — Measurement and analysis of thermal neutron spectra on Zenith. This Conference.

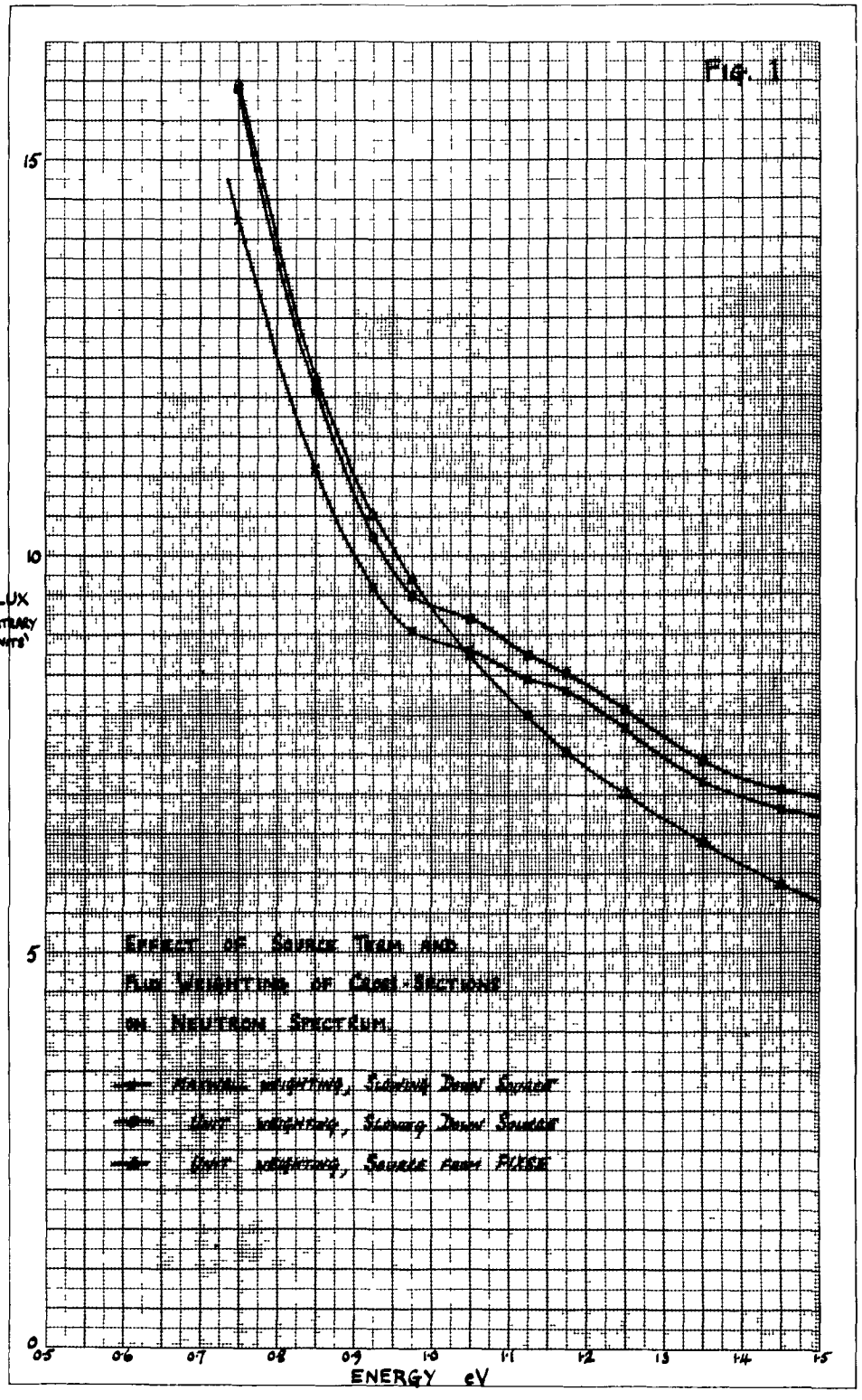
Fig. 1
15
10
5
0
FLUX
(ARBITRARY UNITS)
0·5
0·6
0·7
0·8
0·9
1·0
1·1
1·2
1·3
1·4
1·5
ENERGY eV
EFFECT OF SOURCE TERM AND
FLUX WEIGHTING OF CROSS-SECTIONS
ON NEUTRON SPECTRUM.
Flat weighting, Slowing Down Source
1/E weighting, Slowing Down Source
1/E weighting, Source from FUSE

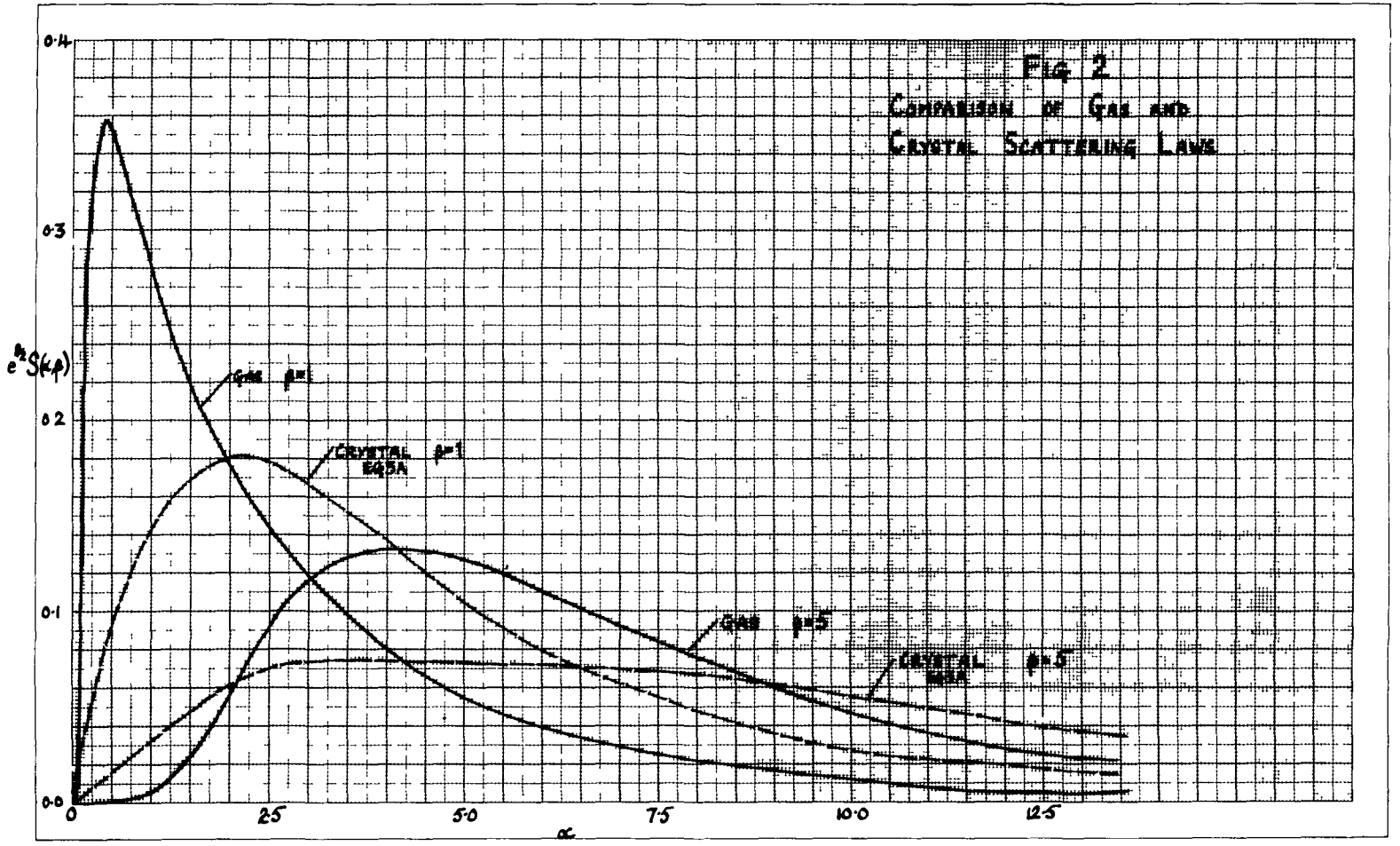
FIG 2
COMPARISON OF GAS AND CRYSTAL SCATTERING LAWS
0·4
0·3
0·2
0·1
0·0
$e^{\frac{1}{2}\alpha}S(k,\rho)$
GAS ρ=1
CRYSTAL ρ=1
E45A
GAS ρ=5
CRYSTAL ρ=5
E45A
0
2·5
5·0
7·5
10·0
12·5
α

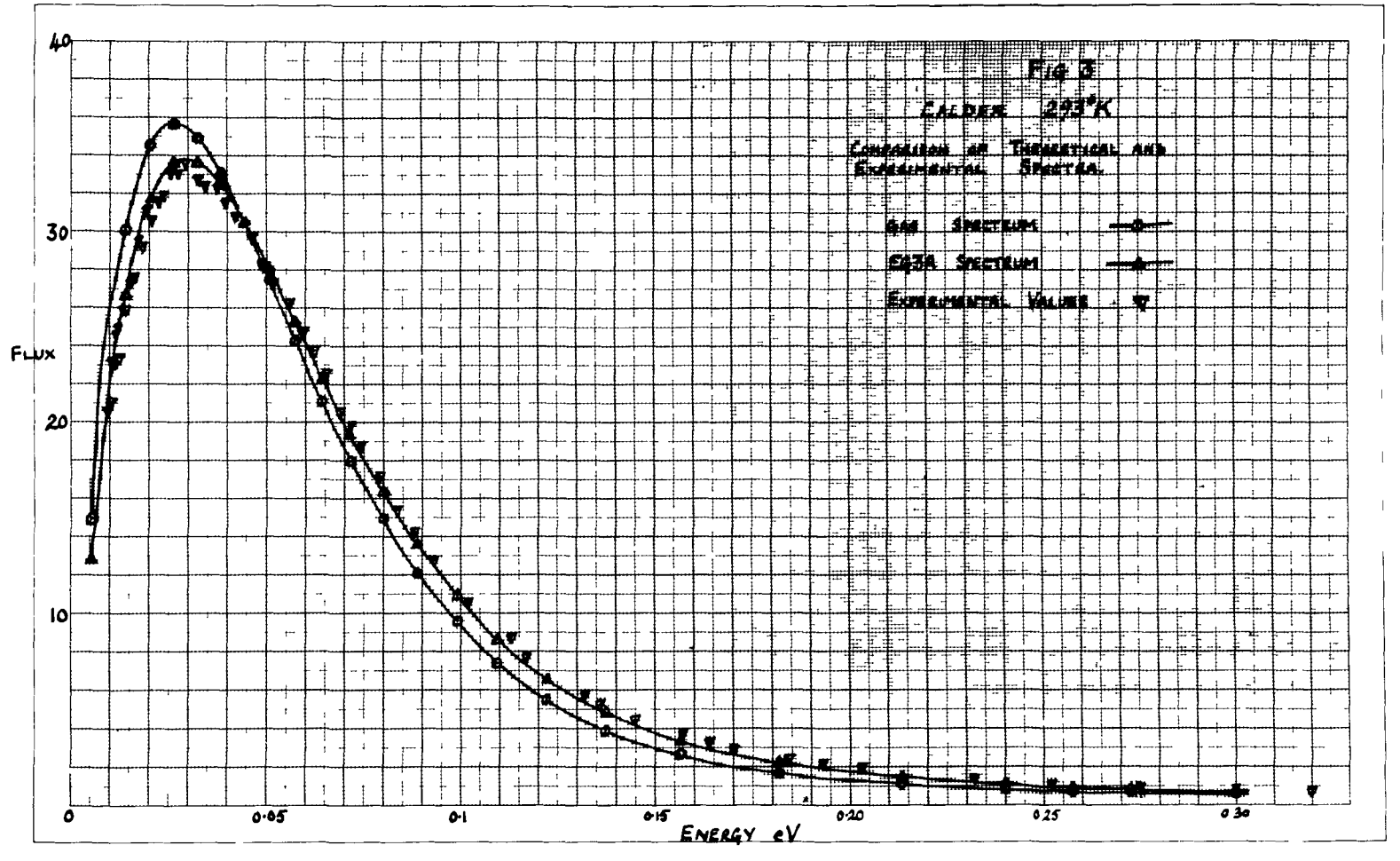
FIG 3
CALDER 293°K
COMPARISON OF THEORETICAL AND EXPERIMENTAL SPECTRA.
GAS SPECTRUM
C6H6 SPECTRUM
EXPERIMENTAL VALUES
FLUX
ENERGY eV
40
30
20
10
0
0·05
0·1
0·15
0·20
0·25
0·30

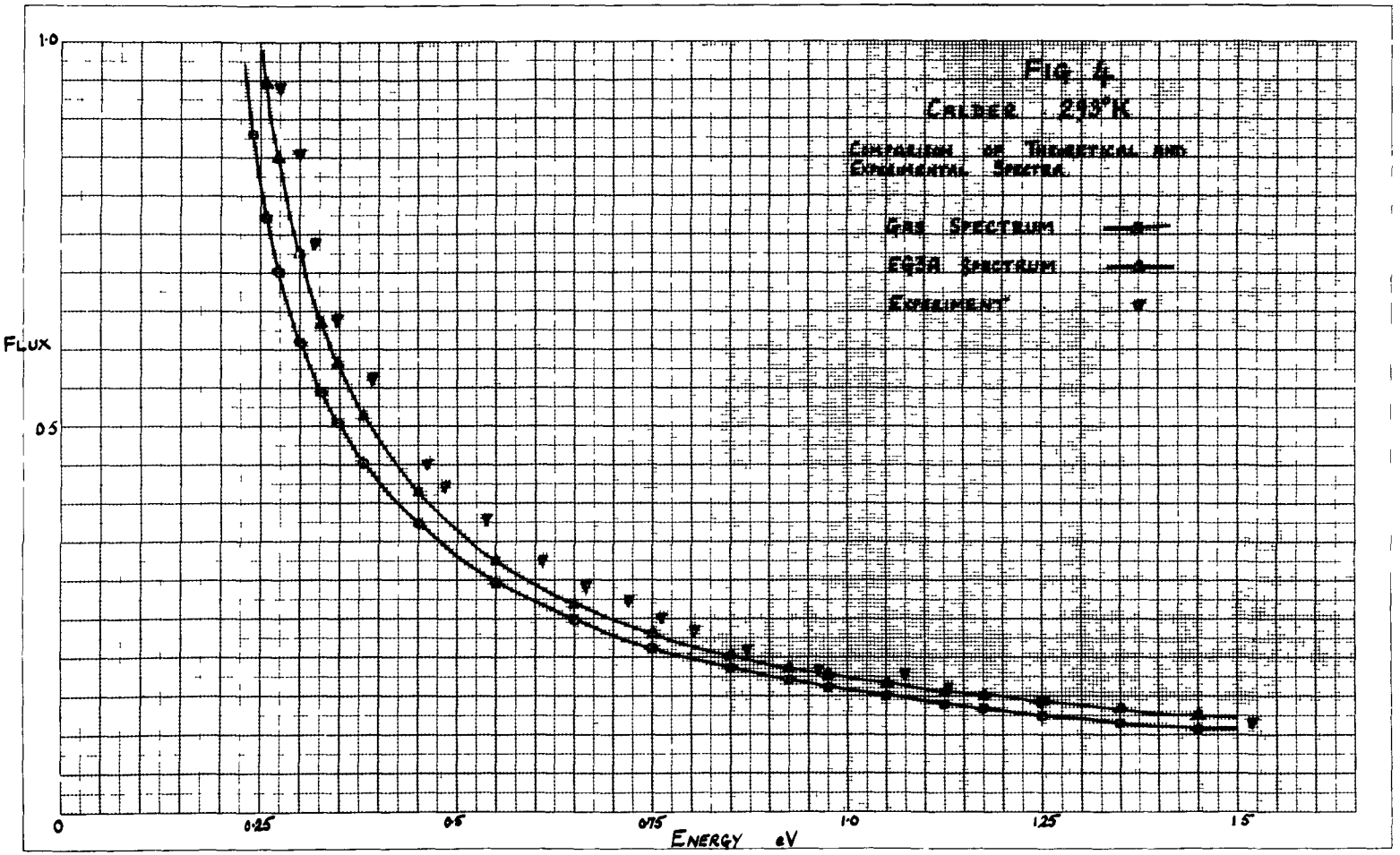
FIG 4.
CALDER 293°K
COMPARISON OF THEORETICAL AND EXPERIMENTAL SPECTRA.
GAS SPECTRUM
EQ2A SPECTRUM
EXPERIMENT
FLUX
1·0
0·5
0
0·25
0·5
0·75
1·0
1·25
1·5
ENERGY eV

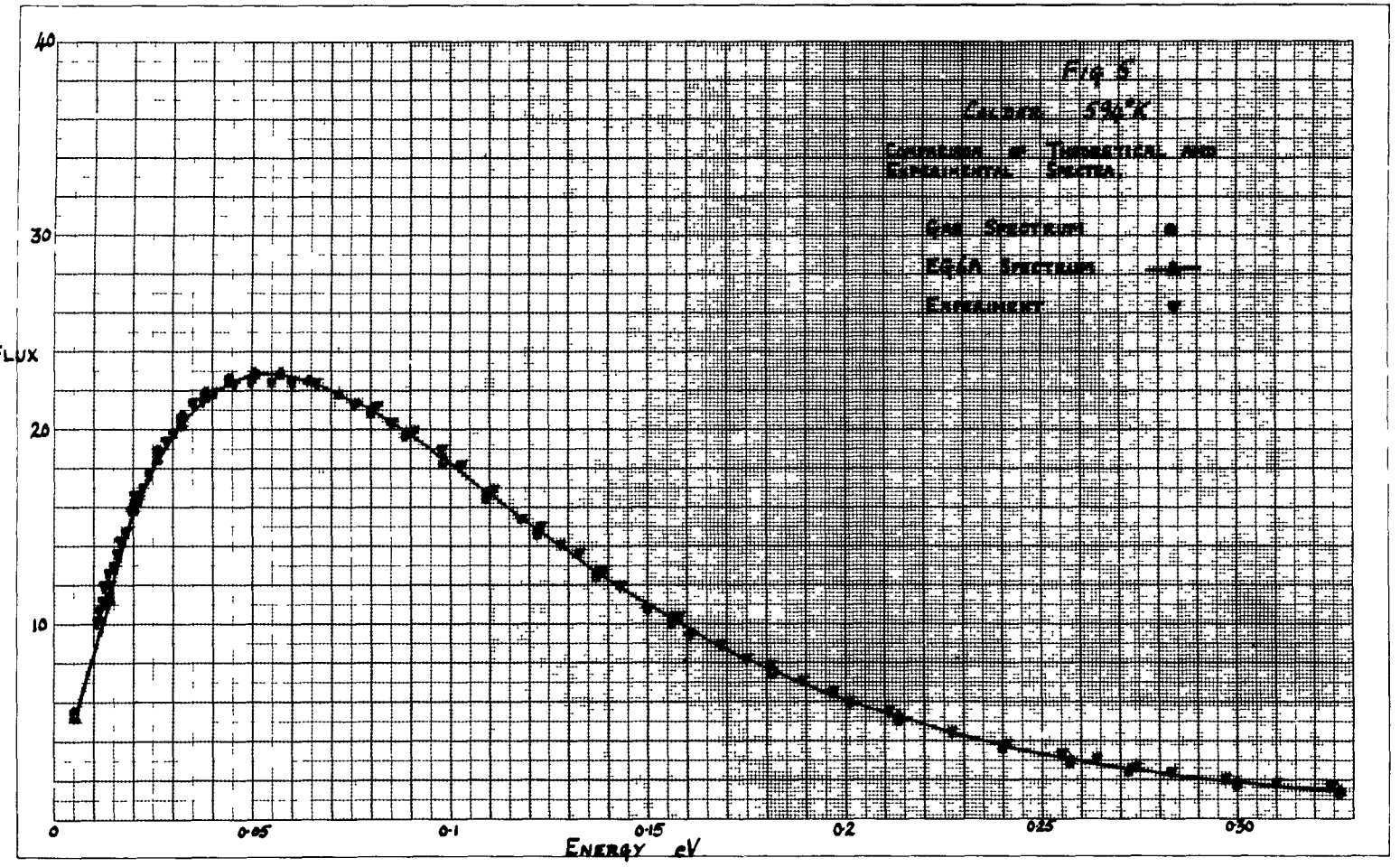
Fig 5
Calcd. 53.6°K
Comparison of Theoretical and Experimental Spectra.
Gas Spectrum
EQ6A Spectrum
Experiment
40
30
20
10
Flux
0
0·05
0·1
0·15
0·2
0·25
0·30
Energy eV

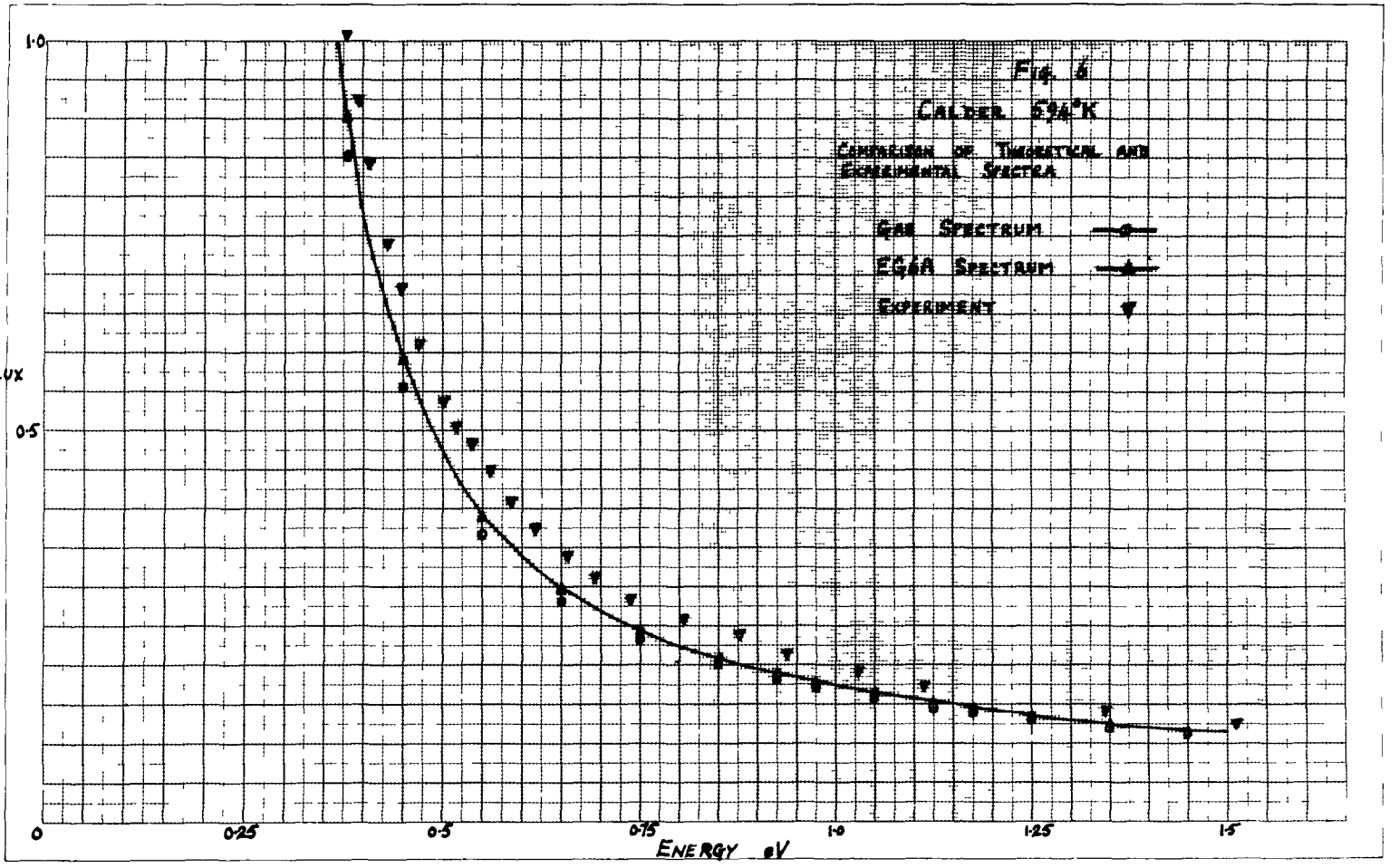
FIG. 6
CALDER 5.94°K
COMPARISON OF THEORETICAL AND EXPERIMENTAL SPECTRA
GAS SPECTRUM
EGAA SPECTRUM
EXPERIMENT
FLUX
1·0
0·5
0
0·25
0·5
0·75
1·0
1·25
1·5
ENERGY eV

CALCULATION OF DIFFERENTIAL SCATTERING CROSS SECTIONS FOR SLOW NEUTRONS*

H. L. McMURRY
Phillips Petroleum Company, Atomic Energy Division, Idaho Falls, Idaho

- -

A B S T R A C T

As an approach to developing methods for calculating differential scattering cross sections of materials for neutrons with energy below 1 ev five approximations to the exact formalism of Zemach and Glauber have been applied to treat the scattering by gases composed of semi-rigid molecules. This paper outlines the theory for the methods which are the following. (1) A quite rigorous method valid when the neutron energy and k_BT are both much less than the characteristic vibrational energies of the molecules. (2) A method which treats vibrations harmonically, rotations classically, and neglects rotation-vibration coupling. Within these limitations the method is valid at all neutron energies. (3) A method like (2) except that averages over orientation are approximated by the Krieger-Nelkin method of introducing average values of functions of the Eulerian angles wherever they appear. (4) A method which treats vibrations with characteristic energies much less than the neutron energy by a short collision time approximation. (5) A method which treats such low energy vibrations classically.

*Work performed under the auspices of the U. S. Atomic Energy Commission.

Method (5) has the feature that when all normal modes are treated classically the equation for the differential scattering cross section reduces to that for scattering by unbound particles. If some, but not all, vibrations are treated classically and averages over orientation are approximated as in method (3) the effective mass for a scattering atom attached to the molecule is intermediate between the mass of the atom and the Sachs-Teller mass which applies when all vibrations are treated exactly by quantum mechanics. Method (5) has the advantage of being easily adapted to treating simple models for liquids and amorphous solids.

These methods are evaluated in the accompanying paper.

INTRODUCTION

Refinements in reactor physics calculations have focused attention on the need for reliable cross section information. For thermal neutrons it is necessary to know, among other things, the differential scattering cross sections with respect to energy and angle of the reactor materials. With such data it becomes possible to attempt detailed calculations of the dependence of thermal neutron flux on neutron energy, position in the reactor and direction of neutron flow. Moreover, less detailed computational techniques can be improved because group constants can be calculated more reliably.

Although studies of inelastic scattering of slow neutrons have emphasized applications to the study of atomic motions in liquids and solids, data more suited to the needs of the reactor physicist are now becoming available[1-2]. They cover scattering of neutrons with energies up to 0.2 ev. However, some time will elapse before all materials of interest have been studied. Moreover, it will never be true that experimental data will cover exactly the materials and physical conditions in every practical problem. In addition to these limitations which apply to data obtainable with present experimental techniques, there is the fact that little work is being done with neutrons above 0.2 ev because of experimental difficulties. For these reasons the development of computational techniques capable of yielding differential scattering cross sections satisfactory for reactor physics calculations is imperative.

The program underway in this laboratory is a study of approximations to the rigorous formalism of Zemach and Glauber (6, hereafter referred to as Z. G.) which takes account of the quantum nature of the scattering system, and the distribution of its energy states due to thermal agitation. The methods described in this paper apply to gases composed of semi-rigid molecules. These are amenable to rather exact treatment and data exist for direct comparison of theory with experiment for neutrons with energy below 0.2 ev(3,4). Computational techniques which give agreement with experiments in this energy range can be used to evaluate approximate methods which are applicable at neutron energies above 0.2 ev. For neutrons in this energy range approximations are developed which make use of the fact that the neutron energy is much higher than k_BT and higher than some or all of the characteristic vibrational energies of the scattering molecules. The insights gained by studying these simple systems should be a guide to finding methods applicable to liquids and solids, at least for scattering of higher energy neutrons.

This paper outlines the theoretical bases for five computational techniques. The accompanying paper evaluates them by comparisons with experimental data from the MTR slow neutron velocity selector, and comparisons of less rigorous with more rigorous methods. The methods discussed are:

(1) A rigorous quantum treatment valid when k_BT and the neutron energy E_o are both much less than any characteristic vibrational energies in the scattering molecule.

(2) A method which treats rotations classically and includes effects due to transfers of vibrational energy to and from the molecule. Vibrations are assumed to be harmonic and vibration-rotation coupling is neglected. Averages over orientation are obtained exactly by numerical integration. Within these limitations the method is valid at all neutron energies.

(3) The same as (2) except that averages over orientation are approximated by replacing functions of the Eulerian angle variables by their average values. This is essentially the Krieger-Nelkin method[7] differing only in that quantities appearing in matrix elements associated with vibrational transitions are also included and averaged in this way.

(4) A short collision time method in which matrix elements associated with vibrations having characteristic energies much lower than the neutron energy are obtained by a Wick type expansion[8] of the operators involved.

(5) A treatment in which vibrations with characteristic energies much lower than E_0 are treated classically. A feature of this method is that when all modes are treated classically the equation for the scattering reduces to that for scattering by unbound atoms. Moreover, when some but not all modes are treated classically the Krieger-Nelkin averaging leads to an effective mass for a scattering atom intermediate between the Sachs-Teller mass which holds when all vibrations are treated quantum mechanically, and the mass of the atom itself which applies when all vibrations are treated classically.

THEORETICAL

A. General Approach

When neutrons are scattered by a moderator or any system of chemically bound atoms impulsive interactions with individual atoms, or atom pairs, are involved. However, the recoiling atoms are part of the larger system and any transfers of energy and momentum from the neutron to the system must be consistent with its quantum nature. Zemach and Glauber(6) have given an exact quantum mechanical formalism for calculating the scattering from any system composed of chemically bound atoms. The quantities calculated are $\sigma_\nu(E_o,\epsilon,\mu)$ and $\sigma_{\nu\nu'}(E_o,\epsilon,\mu)$. The first is the differential scattering cross section for direct scattering by atom ν and the second for scattering by the pair of atoms ν and ν'. The units are conveniently expressed as barns/(atom x ev x steradian). For isotropic systems these differential cross sections depend on the incident neutron energy E_o, its energy change $\epsilon = E - E_o$ and the cosine of the scattering angle μ.

This paper will deal with systems where proton scattering is dominant and the pair scattering $\sigma_{\nu\nu'}$ can be neglected(9). However, σ_ν still depends on how the proton is bound. For example, when neutrons are scattered by the protons in propane gas ($CH_3CH_2CH_3$) the H atoms on the CH_2 group scatter differently from those on the CH_3 groups and, in fact, the protons in the CH_3 groups do not all scatter identically(4).

The measured differential scattering cross section $\sigma(E_o,\epsilon,\mu)$ for an entire system is

$$\sigma(E_o,\epsilon,\mu) = \sum_\nu \frac{N_\nu \sigma_\nu(E_o,\epsilon,\mu)}{N} = \sum_\nu f_\nu \sigma_\nu(E_o,\epsilon,\mu)$$

In this equation N_ν is the number of atoms of type ν (meaning the same species of nuclide in the same environment), N is the total number of atoms in the scattering system and $f_\nu = N_\nu/N$ is the fraction for atoms of type ν.

In semi-rigid molecules the interparticle distances never depart far from equilibrium values. Rotation-vibration coupling can be neglected and for molecules in the gas phase the molecular wave function can be written as a product of factors for the translational, rotational, and vibrational degrees of freedom. Eq. (2.11) of Z. G. can then be put in the form(10)

$$\sigma_\nu(E_o,\epsilon,\mu) = \frac{A_\nu^2 + C_\nu^2}{2\pi E_o}\left(1 + \frac{\epsilon}{E_o}\right)^{\frac{1}{2}} \int_{-\infty}^{\infty} e^{-it\epsilon/E_o} \langle O_C' \rangle_T \langle \bar{O}_{\nu R}' \Pi_T \langle O_{\nu T}' \rangle_T \rangle_T dt \qquad (1)$$

The spin states formed during the interaction between the neutron and atom ν determine the strength of the interaction. Eq. (1) averages over the various spin states by using suitable coherent and incoherent scattering lengths A_ν and C_ν(11). Eq. (1) employs a time in units of $\hbar/E_o$. This makes the time dimensionless and time in seconds is given by $\hbar t/E_o$. The primes on the $O_C'(t)$, $\bar{O}_{\nu R}'(t)$ and $O_{\nu T}'(t)$ are used to distinguish them from other related operators which will be introduced when some of the approximate techniques are developed. The operators are defined as follows:

$$O_C'(t) = e^{itH_C'}\ e^{i\underset{\sim}{\kappa}\cdot\underset{\sim}{r}_C}\ e^{-itH_C'}\ e^{-i\underset{\sim}{\kappa}\cdot\underset{\sim}{r}_C} \qquad (2a)$$

$$O_{\nu T}'(t) = e^{itH_T'}\ e^{i\underset{\sim}{\kappa}\cdot\Delta\underset{\sim}{r}_\nu}\ e^{-itH_T'}\ e^{-i\underset{\sim}{\kappa}\cdot\Delta\underset{\sim}{r}_\nu} \qquad (2b)$$

$$\bar{O}_{\nu R}'(t) = e^{-itH_R'}\ e^{-i\underset{\sim}{\kappa}\cdot\underset{\sim}{r}_\nu^o}\ e^{itH_R'}\ e^{i\underset{\sim}{\kappa}\cdot\underset{\sim}{r}_\nu^o} \qquad (2c)$$

In these equation $H'_C = H_C/E_o$, $H'_R = H_R/E_o$, $H'_\tau = H_\tau/E_o$ where H_C, H_R and H_τ are the Hamiltonian operators for the translational, rotational, and τ normal vibration. The H_R is for a rigid molecule with atoms at their equilibrium positions and H_τ assumes a harmonic potential function. The $\underset{\sim}{r}_C$ is the vector to the center of mass, $\underset{\sim}{r}^o_\nu$ is from the C.M. to the equilibrium position of atom ν and $\Delta\underset{\sim}{r}_\nu$ is from the equilibrium position to the displaced position. For a semi-rigid molecule $|\Delta\underset{\sim}{r}_\nu| \ll r^o_\nu$. The $\hbar\underset{\sim}{\kappa} = \hbar\underset{\sim}{k} - \hbar\underset{\sim}{k}_o$ is the change in momentum of the neutron resulting from the scattering impact. Here $\underset{\sim}{k}_o$ and $\underset{\sim}{k}$ are the wave vectors of the neutron before and after impact, respectively. The π_τ denotes a product over all normal modes.

The thermal expectations in Eq. (1) are defined as follows:

$$\langle O'_C \rangle_T = \sum_j \gamma_{jC} \langle O'_C \rangle_{jC} = e^{-it\alpha/\beta_o} e^{-\alpha t^2/\beta_o^2} \tag{3a}$$

$$\langle O'_{\nu\tau} \rangle_T = \sum_j \gamma_{j\tau} \langle O'_{\nu\tau} \rangle_{j\tau} \tag{3b}$$

$$\langle \bar{O}'_{\nu R} \pi_\tau \langle O'_{\nu\tau} \rangle_T \rangle_T = \sum_{jR} \gamma_{jR} \langle \bar{O}'_{\nu R} \pi_\tau \langle O'_{\nu\tau} \rangle_T \rangle_{jR} \tag{3c}$$

In Eqs. (3a - 3c) the γ_{jC}, γ_{jR} and $\gamma_{j\tau}$ are the probabilities that a scattering impact involves the molecule in a translational wave function ψ_{jC}, a rotational wave function ψ_{jR} and the τ normal vibrational wave function $\psi_{j\tau}$. The expression given for $\langle O'_C \rangle_T$ is given in Eq. (5.1) of Z.G. It involves the neutron mass m, the mass of the molecule M and is conveniently expressed in terms of function ϕ and α defined by

$$\phi = \frac{\epsilon}{E_o} + 2 - 2\left(1 + \frac{\epsilon}{E_o}\right)^{\frac{1}{2}} \mu \tag{4}$$

$$\alpha = \frac{\kappa^2 n^2}{2M} \frac{1}{k_B T} = \frac{m}{M} \beta_o \phi \tag{5}$$

$$\beta_o = E_o/k_B T$$

The use of α and ϕ in place of κ^2 has the advantage that they are dimensionless quantities of moderate magnitude which are closely related to the energy transferred to the motion of the molecular center of mass. Furthermore, the presentation of differential scattering cross sections in terms of functions of α, or quantities proportional to α, is gaining acceptance(2,12).

B. Rigorous Treatment of Rotations

Griffing(13) has used Eq. (1) to calculate the scattering of very low energy neutrons by methane which is a spherical top. When E_o is much less than any of the characteristic vibrational energies the $\langle O'_{\nu_T} \rangle_T$ are nearly unity. Griffing found it satisfactory to use the Krieger-Nelkin expression(7) which inserts average values of functions of the Eulerian angles into the expression for $\langle O'_{\nu T} \rangle_T$. When this is done the expectation in Eq. (3c) may be written in the form

$$\langle \bar{O}'_{\nu R} \Pi_T \langle O'_{\nu_T} \rangle_T \rangle_T = \langle \bar{x}^o_\nu \rangle_T \sum_j \sum_f \gamma_{jR} \, e^{it(E_{jR}-E_{fR})/E_o} \left| \langle \psi_{jR} e^{-i\underline{\kappa}\cdot\underline{r}^o_\nu} \psi_{fR} \rangle \right|^2 \tag{6}$$

Eq. (6) results by introducing the sum over rotational states explicitly analogous to the formulation used in Eq. (2.4) of Z. G.

$$\langle \bar{x}^o_\nu \rangle_T \simeq \Pi_T \exp\left\{ - (E_o \phi m \bar{\delta}_{\nu T}/3E_T) \coth(\beta_T/2) \right\} \tag{7}$$

Eq. (7) is the same as Eq. (20) of Krieger and Nelkin(7) with $\kappa^2 \gamma_{\nu\nu}$ of K.N being the same as the terms in the exponent. The $\bar{\delta}_{\nu T}$ is determined from the transformation between the normal coordinates and the cartesian displacements of the atoms relative to axes fixed in the molecule. Its

derivation for any semi-rigid molecule is outlined in the Appendix. The E_τ is the characteristic energy of the τ vibrational mode, $\beta_\tau = E_\tau/k_B T$ and ϕ is given by Eq. (4).

The matrix elements in Eq. (6) are calculated by expanding $e^{-i\underset{\sim}{\kappa}\cdot\underset{\sim}{r}_\nu^o}$ is a series of Legendre polynomials of cos θ where θ is the angle between $\underset{\sim}{\kappa}$ and $\underset{\sim}{r}_\nu^o$. The coefficients in the series are spherical Bessel's functions of $|\underset{\sim}{\kappa}||\underset{\sim}{r}_\nu^o|$. The cases of greatest interest involve molecules where $\underset{\sim}{r}_\nu^o$ lies on a symmetry axis. Then cos θ is an argument in the rotational wave functions and the integrations over orientation can be obtained in closed form[13]. Then Eq. (6) is a series which, together with Eq. (3a), can be inserted into Eq. (1). The time integration can be carried out yielding

$$\sigma_\nu(E_o,\epsilon,\mu) = (1 + \epsilon/E_o)^{\frac{1}{2}}\, e^{-\beta/2}\, S_\nu(\alpha,\beta) \tag{8}$$

The $S_\nu(\alpha,\beta)$ is the Egelstaff scattering function[12] which is given in this case by

$$S_\nu(\alpha,\beta) = \frac{1}{2k_BT(\pi\alpha)^{\frac{1}{2}}}\frac{A_\nu^2 + C_\nu^2}{}\exp\left\{\frac{-(\beta^2+\alpha^2)}{4\alpha}\right\}\frac{1}{Z}\left\{\sum_j \chi_{jj} + 2\sum_{j>f}\chi_{jf}\right\}\langle \bar{x}_\nu^o\rangle_T \tag{9}$$

$$\chi_{jf} = \cosh\left\{\frac{\beta(\beta_{jR} - \beta_{fR})}{2\alpha}\right\}\exp\left\{\frac{-(\beta_{jR} - \beta_{fR})^2}{4\alpha} - \frac{(\beta_{jR}+\beta_{fR})}{2}\right\}\left|\langle\psi_{jR}e^{-i\underset{\sim}{\kappa}\cdot\underset{\sim}{r}_\nu^o}\psi_{fR}\rangle\right|^2$$

$$Z = \sum_j W_j\, e^{-\beta_{jR}} \tag{10}$$

$$\beta_{jR} = E_{jR}/k_BT \qquad \beta_{jR} = E_{jR}/k_BT$$

The W_j in Eq. (10) is the degeneracy of the states with energy E_{jR}. In linear molecules and spherical top molecules the energy is given by the total angular momentum quantum number J and the degeneracy is 2J+1 for a linear molecule and $(2J+1)^2$ for a spherical molecule. For asymmetric tops the energy depends on the quantum number K associated with the projection of the total angular momentum along the top axis. States with $\pm$ K are degenerate with degeneracy 2(2J+1). When K = 0 the degeneracy is 2J+1. Some writers do not incorporate the $1/k_BT$ into the definition of $S_\nu(\alpha,\beta)$. Its inclusion gives S_ν the same units as σ_ν which has some practical convenience.

C. Classical Treatment of Rotations, Inclusion of Vibrational Excitations.

Molecules with large moments of inertia will have densely spaced rotational levels. When the symmetry is low the splitting of degeneracies will make the levels still more densely distributed. When either or both of these conditions cause a dense distribution of levels a classical treatment of rotations is tenable.

The classical treatment is achieved by commuting the operators $O'_{\nu T}$ and $\bar{O}'_{\nu R}$ in Eqs. (1) and (3c) and calculating the thermal average of the rotational expectations $\langle \bar{O}'_{\nu R} \rangle_T$ by using a classical treatment of the rotational motion. This is done by considering a phase space defined in terms of the classical angular momentum(7,10). When principal axes of inertia are used the result may be expressed in the form(10)

$$\langle \bar{O}'_{\nu R} \rangle_T = \exp\left\{-itm\phi[A'_Z]R'_\nu\, I^{-1}\, R_\nu[A_Z]\right\} \langle O_{\nu R} \rangle_T \tag{11}$$

$$\langle O_{\nu R} \rangle_T = \exp\left\{-t^2 \frac{\phi}{\beta_o} m[A'_Z]R'_\nu\, I^{-1}\, R_\nu[A_Z]\right\} \tag{12}$$

In Eqs. (11, 12) the term $[A_Z']R_\nu' I^{-1} R_\nu [A_Z]$ is a matrix product. Brackets denote column matrices and primes denote transposed matrices. Thus $[A_Z']$ is a row matrix. Its significance is explained below. The I^{-1} is the reciprocal of the moment of inertia tensor which is most conveniently expressed in terms of principal axes of inertia so that I^{-1} is diagonal. The R_ν is in terms of the equilibrium positions x_ν^0, y_ν^0, z_ν^0 of atom ν relative to the axes fixed in the molecule.

$$R_\nu = \begin{bmatrix} 0 & -z_\nu^0 & y_\nu^0 \\ z_\nu^0 & 0 & -x_\nu^0 \\ -y_\nu^0 & x_\nu^0 & 0 \end{bmatrix} \tag{13}$$

In deriving Eqs. (11, 12) the vector product of $\underset{\sim}{\kappa}$ and a vector related to the angular momentum $\underset{\sim}{L}$ is needed. The $\underset{\sim}{L}$ is most conveniently expressed in terms of components along the molecular axes x, y, z, while $\underset{\sim}{\kappa}$ is most easily written in terms of components along space fixed axes X, Y, Z. Hence the vector product of $\underset{\sim}{\kappa}$ with any vector related to $\underset{\sim}{L}$ will depend on molecular orientation. It proves convenient to express such vector products as products of row and column matrices. The general procedure is as follows: let [L] denote a three element column matrix with its elements being L_x, L_y, L_z, the components of $\underset{\sim}{L}$ along the molecular axes x, y, z. Let A denote a 3 x 3 matrix with the top row $[A_X']$, the middle row $[A_Y']$ and bottom row $[A_Z']$ containing the direction cosines of X, Y, Z, respectively, relative to x, y, z. Then the matrix product A[L] gives a three element column matrix with elements L_X, L_Y, L_Z being the components of $\underset{\sim}{L}$ along X, Y, Z. There is no loss in generality if

the Z direction is taken along $\underset{\sim}{\kappa}$. The vector product $\underset{\sim}{\kappa}\cdot\underset{\sim}{L}$ is given then by $\kappa[A'_Z][L]$ where $\kappa = |\underset{\sim}{\kappa}|$. In this way the dependence on orientation in Eqs. (11, 12) appears through the presence of $[A'_Z]$. Specifically

$$[A'_Z] = [-\sin\theta\cos\chi \quad \sin\theta\sin\chi \quad \cos\theta] \tag{14}$$

In Eq. (14) θ and χ are two of the Eulerian angles used in defining the molecular orientation. Eq. (14) is obtained directly from Table I-1 of ref. (14).

In dealing with the operators $O'_{\nu\tau}$ in Eq. (2b and 3b) it is necessary to express the H_τ and $\Delta\underset{\sim}{r}_\nu$ in terms of the normal coordinates. Some useful properties of the transformation between the normal coordinates and the cartesian displacements of the atoms are given in the Appendix. The vector $\Delta\underset{\sim}{r}_\nu$ in terms of components along the space fixed axes X, Y, Z is

$$[\Delta r_\nu] = A\sum\nolimits_\tau [T_{\nu\tau}]Q_\tau \tag{15}$$

In Eq. (15) $[T_{\nu\tau}]$ is a three element column matrix with elements $T_{\nu\tau,x}$, $T_{\nu\tau,y}$, $T_{\nu\tau,z}$ such that $T_{\nu\tau,x}Q_\tau$, $T_{\nu\tau,y}Q_\tau$, $T_{\nu\tau,z}Q_\tau$ give the displacement of atom ν along the x, y, z axes when the τ normal coordinate has the magnitude Q_τ. When the Z axis is taken along $\underset{\sim}{\kappa}$ it is then true that

$$\underset{\sim}{\kappa}\cdot\Delta\underset{\sim}{r}_\nu = \kappa[A'_Z]\sum\nolimits_\tau [T_{\nu\tau}]Q_\tau \tag{16}$$

When the transformation

$$e^{itH'}\, e^{i\underset{\sim}{\kappa}\cdot\underset{\sim}{r}_\nu} e^{-itH'} e^{-i\underset{\sim}{\kappa}\cdot\underset{\sim}{r}_\nu} = e^{itH'} e^{itH'(\underset{\sim}{p}_\nu - \underset{\sim}{\kappa}\hbar)}$$

is specialized to the case where $H' = H'_\tau$ and $\underset{\sim}{r}_\nu = \Delta\underset{\sim}{r}_\nu$ the result is (15)

$$O'_{\nu\tau} = \exp\left\{-it\omega m\delta_{\nu\tau}\right\} O_{\nu\tau} \tag{17}$$

$$O_{\nu\tau} = \exp\left\{itH'_\tau\right\} \exp\left\{-it[H'_\tau - (2m\phi\delta_{\nu\tau}/E_o)^{\frac{1}{2}}p_\tau]\right\} \tag{18}$$

$$\delta_{\nu\tau}(\theta,\chi) = ([A'_Z][T_{\nu\tau}])^2 \tag{19}$$

In Eq. (18) p_τ is the momentum conjugate to the τ normal coordinate. When mass adjusted normal coordinates are used $p_\tau = \dot{Q}_\tau$.

Eq. (3.19) of Z. G. gives the expression for $\langle O'_{\nu\tau}\rangle_T$ which (for $\nu = \nu'$) is

$$\langle O'_{\nu\tau}\rangle_T = \langle \chi^o_\nu\rangle_T \sum_{n_\tau=-\infty}^{\infty} I_{n_\tau}(g_{\nu\tau}) \exp\left\{(n_\tau\beta_\tau/2) - it(n_\tau\beta_\tau/\beta_o)\right\} \tag{20}$$

In Eq. (20)

$$g_{\nu\tau} = \frac{\beta_o}{\beta_\tau \sinh(\beta_\tau/2)} \phi m \delta_{\nu\tau} \tag{21}$$

$\beta_\tau = E_\tau/k_B T$ where E_τ is the characteristic energy of the τ mode.

$$\langle \chi^o_{\nu\tau}\rangle = \exp\left\{-(E_o\phi m\delta_{\nu\tau}/E_\tau)\coth(\beta_\tau/2)\right\} \tag{22}$$

The I_n is the modified Bessel function of order n and $\delta_{\nu\tau}$ is given by Eq (19).

When Eqs. (3a, 11, 20) are used in Eq. (1) the time integration can be carried out yielding

$$\sigma_\nu(E_o,\epsilon,\mu) = \frac{(1 + \epsilon/E_o)^{\frac{1}{2}}}{4\pi} e^{-\beta/2} \int_{\chi=o}^{2\pi} \int_{u=-1}^{1} S_\nu(\alpha,\beta)\,du\,d\chi \tag{23}$$

Integrations are only needed over the Eulerian variables χ and $u = \cos\theta$ since the azimuthal variable φ is not in $[A'_Z]$. The Egelstaff scattering function S_ν includes terms due to vibrational transitions which were not included in Eq. (8). In fact, Eq. (8) uses Eq. (20) with only the terms with n_τ=o and with $\langle \bar{\chi}^o_\nu\rangle$ calculated using a $\bar{\delta}_{\nu\tau}$ obtained by averaging

Eq. (19) over orientation in the Krieger-Nelkin manner[7,15]. Hence, Eq. (23) applies to neutron energies high enough to cause vibrational transitions, and temperatures high enough so that collisions with molecules in thermally excited vibrational states are possible. It assumes no rotation-vibration coupling and neglects anharmonicities in the vibrations. The equation for S_ν is

$$S_\nu(\alpha,\beta) = \frac{A_\nu^2 + C_\nu^2}{2k_B T(\pi\alpha_\nu)^{\frac{1}{2}}} \langle \chi_\nu^o \rangle_T \exp\left\{\frac{-(\beta^2 + \alpha_\nu^2)}{4\alpha_\nu}\right\} \bar{\Psi}_\nu \tag{24}$$

$$\bar{\Psi}_\nu = \prod_\tau I_o(g_{\nu\tau}) + 2\sum_{n_1,n_2\ldots} \prod_\tau I_{n_\tau}(g_{\nu\tau}) \cosh\left\{\frac{\beta(\Sigma_\tau n_\tau \beta_\tau)}{2\alpha_\nu}\right\} \exp\left\{\frac{-(\Sigma_\tau n_\tau \beta_\tau)^2}{4\alpha_\nu}\right\} \tag{25}$$

In the summation term in Eq. (25) each n_τ can take all integral values beginning at 0, but at least one n_τ must be greater than zero. Any factor with $n_\tau = 1$ gives contributions to excitation and de-excitation of one quantum of the τ vibrational mode. If the $n_\tau = 2$ double excitation and de-excitation is involved etc. The $\langle \chi_\nu^o \rangle_T$ is the product of factors given by Eq. (22) for all the normal modes.

$$\alpha_\nu = \beta_o \phi \left\{\frac{m}{M} + m[A_Z'] R_\nu' I^{-1} R_\nu [A_Z]\right\} \tag{26}$$

In many applications some or all of the β_τ are much larger than one. The arguments $g_{\nu\tau}$ are then small and it is possible to approximate using

$$I_{n_\tau}(g_{\nu\tau}) = \frac{1}{n_\tau!}\left(\frac{\beta_o \phi m \delta_{\nu\tau}}{\beta_\tau}\right)^{n_\tau} \exp\left\{-\frac{n_\tau \beta_\tau}{2}\right\} \tag{27}$$

Eq. (24) with the approximation in Eq. (27) has been used to calculate the scattering of CH_4 up to 0.3 ev[16], and in the accompanying paper for evaluating computations made by less rigorous methods.

D. The Equations With Krieger-Nelkin Averaging.

Eqs. (23-27) involve functions of the Eulerian angles through the presence of $[A^{\dagger}_{\tilde{\nu}}]$ in the $g_{\nu\tau}$ and α_ν. In the Krieger-Nelkin method average values of the functions of the Eulerian angles are used(7). This leads to replacing α_ν by $\bar{\alpha}_\nu$ and $g_{\nu\tau}$ by $\bar{g}_{\nu\tau}$ where

$$\bar{\alpha}_\nu = \beta_o \phi \frac{m}{\bar{M}_\nu} \tag{28}$$

$$\frac{1}{\bar{M}_\nu} = \frac{1}{M} + \frac{1}{\bar{M}_{\nu R}} \tag{29}$$

$$\frac{1}{\bar{M}_{\nu R}} = \frac{1}{3}\left[\frac{y_\nu^{o2} + z_\nu^{o2}}{I_x} + \frac{z_\nu^{o2} + x_\nu^{o2}}{I_y} + \frac{x_\nu^{o2} + y_\nu^{o2}}{I_z}\right] \tag{30}$$

$$\bar{g}_{\nu\tau} = \frac{m\phi\bar{\delta}_{\nu\tau}}{3} \frac{\beta_o}{\beta_\tau \sinh(\beta_\tau/2)} \tag{31}$$

$$\bar{\delta}_{\nu\tau} = [T'_{\nu\tau}][T_{\nu\tau}] \tag{32}$$

In Eqs. (28, 29) m_ν is the Sachs-Teller mass for atom ν(7,15,17).

When the approximation in Eq. (27) is valid it is better to use(15)

$$I_{n_\tau}(\bar{g}_{\nu\tau}) \simeq \frac{1}{(2n_\tau + 1)n_\tau!} \left(\frac{\beta_o \phi m \bar{\delta}_{\nu\tau}}{\beta_\tau}\right)^{n_\tau} \exp\left\{-\frac{\tau\beta_\tau}{2}\right\} \tag{33}$$

When Krieger-Nelkin averaging is used Eq. (33) becomes

$$\sigma_\nu(E_o, \epsilon, \mu) = \left(1 + \frac{\epsilon}{E_o}\right)^{\frac{1}{2}} \bar{S}_\nu(\bar{\alpha}, \beta) \tag{34}$$

In Eq. (34) $\bar{S}_\nu$ is calculated from Eq. (24) by inserting average values for $\bar{\alpha}_\nu$, $\bar{\delta}_{\nu\lambda}$ wherever they appear.

E. The Short Collision Time Equation

When the neutron energy $E_o \gg k_B T$ and $E_o \gg E_\tau$ the neutron will pass over an atom before it moves appreciably either because of the thermal motion or of the vibrational motion contributed by the τ mode. In such cases the operator $O_{\nu\tau}$ in Eq. (18) can be represented by an expansion in powers of (it)[8]. In some problems E_o will greatly exceed some of the E_τ but will be near to or less than others. To distinguish these situations the subscript λ is used for those modes with $E_\lambda \ll E_o$ which are treated by the time expansion while τ is reserved for those with $E_\tau \simeq E_o$ or $E_\tau > E_o$ which are treated exactly by Eq. (20).

The time expansion of $O_{\nu\lambda}$ can be obtained by Wick's procedure[8]. It employs the expansion

$$O_{\nu\lambda}(it) = \sum_{n=o}^{\infty} \frac{1}{n!} O_{\nu\lambda}^{(n)} (it)^n$$

In this equation $O_{\nu\lambda}^{(n)}$ denotes the nth derivative of $O_{\nu\lambda}(it)$ with respect to (it) evaluated at t = 0. It is readily shown that[15]

$$\begin{aligned} O_{\nu\lambda}^{(n)} &= [H'_\lambda, O_{\nu\lambda}^{(n-1)}] + O_{\nu\lambda}^{(n-1)} B_{\nu\lambda} \\ B_{\nu\lambda} &= (2m\phi\delta_{\nu\lambda}/E_o)^{\frac{1}{2}} p_\lambda \end{aligned} \tag{35}$$

The thermal average $\langle O_{\nu\lambda} \rangle_T$ is a power series in (it). The necessary expectations can be calculated from the properties of the harmonic oscillator wave functions. The result to the third order is[15]

$$\langle O_{\nu\lambda} \rangle_T \simeq 1 - \frac{t^2}{2} \langle O_{\nu\lambda}^{(2)} \rangle_T - \frac{it^3}{3!} \langle O_{\nu\lambda}^{(3)} \rangle_T \tag{36}$$

$$\langle O_{\nu\lambda}^{(2)} \rangle_T = 2\phi m \delta_{\nu\lambda} \cdot \frac{\beta_\lambda}{\beta_o} \cdot \left(\frac{1}{2} + \frac{1}{e^{\beta_\lambda} - 1}\right) \tag{37}$$

$$\langle o_{\nu\lambda}^{(3)} \rangle_T = - \phi m \delta_{\nu\lambda} \left(\frac{\beta_\lambda}{\beta_o}\right)^2 \tag{38}$$

When Eq. (3a) and (11) are used for the thermal averages of the translational and rotational expectations, Eq. (20) for the τ modes and Eq. (36) for the λ modes the result is

$$\sigma_\nu(E_o,\epsilon,\mu) = \frac{A_\nu^2 + C_\nu^2}{4\pi} \frac{(1 + \epsilon/E_o)^{\frac{1}{2}}}{2k_B T \sqrt{\pi}} \int_{\chi=o}^{2\pi} \int_{u=-1}^{1} \Phi_\nu(\chi,u) du d\chi \tag{39}$$

$$\Phi_\nu(\chi,u) = \langle \chi_{\nu q}^o \rangle_T \frac{1}{\sqrt{\alpha_\nu}} e^{\frac{-\Delta_\nu}{4}} \bar{\psi}_{\nu q} \left\{ 1 - \frac{\beta_o \phi}{2\alpha_\nu} (1 - \frac{\Delta_\nu}{2}) \left[\sum_\lambda \beta_\lambda m \delta_{\nu\lambda} (\tfrac{1}{2} + \frac{1}{e^{\beta_{\lambda-1}}}) \right] \right.$$

$$\left. + \frac{\beta_o \phi}{24\alpha_\nu} \left(\frac{\Delta_\nu}{\alpha_\nu}\right)^{\frac{1}{2}} (3 - \frac{\Delta_\nu}{2}) \left[\sum_\lambda \beta_\lambda^2 m \delta_{\nu\lambda} \right] -- \right\} \tag{40}$$

$$\Delta_\nu = \frac{[\beta + \alpha_\nu + \beta_o \phi m \sum_\lambda \delta_{\nu\lambda}]^2}{\alpha_\nu} \tag{41}$$

In Eq. (40) ϕ is given by Eq. (4), α_ν by Eq. (26), $\delta_{\nu\lambda}$ by Eq. (19). The $\langle \chi_{\nu q}^o \rangle_T$ is calculated from products of factors from Eq. (22) and $\bar{\psi}_{\nu q}$ from Eq. (25). However, only the τ modes are included.

The Krieger-Nelkin equivalent to Eq. (40) is obtained by using average values of functions of the Eulerian angles in Φ_ν. When this is done the numerator in Eq. (41) for Δ_ν involves the sum

$$\bar{\alpha}_\nu + \frac{1}{3} \beta_o \phi \sum_\lambda \bar{\delta}_{\nu\lambda} = \frac{m}{M_{\nu c}} \beta_o \phi \tag{42}$$

$$\frac{1}{M_{\nu c}} = \frac{1}{M_\nu} + \frac{1}{3} \sum_\lambda \bar{\delta}_{\nu\lambda} \tag{43}$$

It is shown in the Appendix that $M_{\nu c}$ defined by Eq. (43) is intermediate between the Sachs-Teller mass M_ν which holds when all modes are treated exactly by Eq. (20), and the mass m_ν of atom ν which holds when all modes are treated by the expansion method in Eq. (36).

E. The Classical Treatment of Vibrations.

When $E_o \gg E_\tau$ it should be permissible to treat the vibrations classically just as is done for the rotational motion when the rotational levels are closely spaced compared to E_o. As before it will be convenient to use the subscript λ for modes with $E_\lambda \ll E_o$ which are treated classically, reserving τ for those with $E_\tau \simeq E_o$ or $E_\tau > E_o$ which are treated exactly.

The classical treatment assumes that the factors in Eq. (18) for $O_{\nu\lambda}$ commute so that

$$O_{\nu\lambda} \simeq \exp\left\{it(2\phi m\delta_{\nu\lambda}/E_o)^{\frac{1}{2}}p_\lambda\right\}$$

The thermal expectation of this operator is found by considering a phase space for the momentum p_λ. The equation for $\langle O_{\nu\lambda}\rangle_T$ in the classical approximation is

$$\langle O_{\nu\lambda}\rangle_T = \left(\frac{1}{2\pi k_B T}\right)^{\frac{1}{2}} \int_{-\infty}^{\infty} \exp\left\{\frac{-p_\lambda^2}{2k_B T}\right\} O_{\nu\lambda} dp_\lambda$$

$$= \exp\left\{-(m\phi\delta_{\nu\lambda}/\beta_o)t^2\right\} \qquad (44)$$

When Eqs. (3a, 11, 20, 44) are used in Eq. (1) and the time integration is carried out the result is

$$\sigma_\nu(E_o,\epsilon,\mu) = \frac{(1+\epsilon/E_o)^{\frac{1}{2}}}{4\pi} e^{-\beta/2} \int_{\chi=o}^{2\pi}\int_{u=-1}^{1} S_{\nu c}(\alpha,\beta)d\chi du \qquad (45)$$

$$S_{\nu c}(\alpha,\beta) = \frac{A_\nu^2 + C_\nu^2}{2k_B T(\pi\alpha_{\nu c})^{\frac{1}{2}}} \langle \chi^o_{\nu q}\rangle_T \exp\left\{-\frac{[\beta^2 + \alpha_{\nu c}^2]}{4\alpha_{\nu c}}\right\} \bar{\Psi}_{\nu q} \qquad (46)$$

$$\alpha_{\nu c} = \beta_o\phi\left\{\frac{m}{M} + m[A'_Z]R'_\nu I^{-1}R_\nu[A_Z] + m\sum\nolimits_\lambda \delta_{\nu\lambda}\right\} \qquad (47)$$

As in Eq. (39, 40) the $\langle \chi^o_{\nu q}\rangle_T$ and $\bar{\Psi}_{\nu q}$ in Eq. (45, 46) are calculated from products of Eq. (22) and from Eq. (25) using only terms for the τ modes.

It is shown in the Appendix that when all modes are treated classically $\alpha_{\nu c}$ reduces to $\beta_o \phi(m/m_\nu)$ where m_ν is the mass of atom ν. The equation is then just that for the scattering by an unbound particle. The equation is

$$\sigma_\nu = (1 + \epsilon/E_o)^{\frac{1}{2}} \; e^{-\beta/2} \; S_\nu(\alpha,\beta) \tag{48}$$

$$S_\nu = \frac{A_\nu^2 + C_\nu^2}{2k_B T(\pi\alpha)^{\frac{1}{2}}} \; e^{\frac{-[\beta^2 + \alpha^2]}{4\alpha}} \tag{49}$$

In Eq. (49) α is given by Eq. (5) with $m = m_\nu$.

When Krieger-Nelkin averages are used Eq. (46) comes out in terms of the $M_{\nu c}$ in Eq. (43). This mass is intermediate between the mass m_ν of the atom, which holds when all modes are treated classically as in Eq. (48) and the Sachs-Teller mass M_ν which applies when all modes are treated exactly.

Although Eq. (44) uses a classical operator it yields a thermally averaged expectation which is not limited by the number of terms taken in a series expansion as in Eq. (36). For that reason Eq. (45) based on the classical treatment may give better results than Eq. (39) based on the time expansion which can only be practical for calculations if a few terms suffice.

When $E_o \gg E_T$ the quantum treatment which uses the harmonic oscillator approximation will be inadequate for calculating the contribution of transitions to high vibrational states. The spacings of the excited states will get closer together and will merge when the excitation exceeds the energy to break the bond. In these situations the equations for scattering by an unbound atom may be preferable to a quantum treatment based on the assumption of harmonic oscillator potential functions.

ACKNOWLEDGEMENTS

The writer has benefited from many discussions with Dr. R. C. Young, Dr. G. W. Griffing and Mr. G. D. Marshall. Dr. R. G. Fluharty, head of the Nuclear Physics Branch, has given much encouragement.

APPENDIX

EFFECTIVE SCATTERING MASS WHEN VIBRATIONS ARE TREATED CLASSICALLY

When some of the normal vibrations are treated classically and averages over orientation are obtained by the Krieger-Nelkin method the effective mass of a scattering atom is intermediate between the Sachs-Teller mass which holds when no vibrations are treated classically, and the mass of the atom itself which holds when all vibrations are treated classically. In the latter case the statement is true in general because the dependence on molecular orientation disappears.

These properties can be shown by using the properties of the orthogonal transformation which relates the normal coordinates to the mass adjusted cartesian displacements. The proof will be given on the assumption that principal axes of inertia are used for the molecule. There is no loss of generality in this.

The normal coordinate transformation may be expressed in the form[14,18]

$$\begin{bmatrix} Q \\ 0 \\ 0 \end{bmatrix} = \begin{bmatrix} \hat{Q} \\ \hat{C}_T \\ \hat{C}_R \end{bmatrix} [q] \qquad \text{(A-1)}$$

If there are N atoms the column matrix [q] has the form

$$[q] = \begin{bmatrix} q_1 \\ q_2 \\ \vdots \\ q_N \end{bmatrix} ; \quad [q_\nu] = \sqrt{m_\nu} \begin{bmatrix} \Delta x_\nu \\ \Delta y_\nu \\ \Delta z_\nu \end{bmatrix} \qquad \text{(A-2)}$$

The column matrix on the left side of Eq. (A-1) contains the 3N-6 normal coordinates as elements, together with two sets of three elements which are zeros. These are indicated by the 0 symbols. The matrix multiplying [q] is orthogonal with dimension 3N. There are 3N-6 rows of 3N elements in $\hat{Q}$ and three rows of 3N elements in $\hat{C}_T$ and $\hat{C}_R$. The normal coordinates Q are defined by the equation

$$[Q] = \hat{Q}[q] \tag{A-3}$$

The equations $[0] = \hat{C}_T[q]$ express the condition that the linear momenta vanish relative to the axes fixed in the molecule. The equations $[0] = \hat{C}_R[q]$ express the condition that the molecular axes x, y, z are oriented so that when the atoms are in their equilibrium positions the angular momenta observed from this coordinate system vanish. The matrices $\hat{C}_T$ and $\hat{C}_R$ may be written(18)

$$\hat{C}_T = [\hat{C}_{1T} - - - \hat{C}_{\nu T} - - - \hat{C}_{NT}]$$

$$\hat{C}_R = [\hat{C}_{1R} - - - \hat{C}_{\nu R} - - - \hat{C}_{NR}]$$

$$\hat{C}_{\nu T} = \left(\frac{m_\nu}{M}\right)^{\frac{1}{2}} \begin{bmatrix} 1 & 0 & 0 \\ 0 & 1 & 0 \\ 0 & 0 & 1 \end{bmatrix} \tag{A-4}$$

$$\hat{C}_{\nu R} = m_\nu^{\frac{1}{2}} \begin{bmatrix} 0 & \frac{-z^o_{\nu_1}}{I_x^{\frac{1}{2}}} & \frac{y^o_{\nu_1}}{I_x^{\frac{1}{2}}} \\ \frac{z^o_{\nu_1}}{I_y^{\frac{1}{2}}} & 0 & \frac{-x^o_{\nu}}{I_y^{\frac{1}{2}}} \\ \frac{-y^o_{\nu_1}}{I_z^{\frac{1}{2}}} & \frac{x^o_{\nu_1}}{I_z^{\frac{1}{2}}} & 0 \end{bmatrix} = m_\nu I^{-\frac{1}{2}} R_\nu \tag{A-5}$$

In Eq. (A-7) R_ν is the matrix in Eq. (13) and $I^{-\frac{1}{2}}$ is such that $I^{-\frac{1}{2}}I^{-\frac{1}{2}} = I^{-1}$ where I^{-1} is the reciprocal of the moment of inertia tensor. Eq. (A-5) assumes the use of principal axes of inertia.

If Eq. (A-3) is expanded the expression for any normal coordinate Q_λ is

$$Q_\lambda = \sum_\nu [\hat{Q}'_{\nu\lambda}][q_\nu]$$

$$[\hat{Q}'_{\nu\lambda}] = [\hat{Q}_{\nu\lambda,x}\ \hat{Q}_{\nu\lambda,y}\ \hat{Q}_{\nu\lambda,z}] \tag{A-6}$$

From Eqs. (A-4, A-5, A-6) it follows that

$$\sum_\lambda([A'_Z][\hat{Q}_{\nu\lambda}])^2 + [A'_Z]\hat{C}'_{\nu T}\hat{C}_{\nu T}[A_Z] + [A'_Z]\hat{C}'_{\nu R}\hat{C}_{\nu R}[A_Z] =$$

$$\sum_\lambda([A'_Z][Q_{\nu\lambda}])^2 + \frac{m_\nu}{M}[A'_Z][A_Z] + m_\nu[A'_Z]R'_\nu I^{-1}R_\nu[A_Z] \tag{A-7}$$

However, from the orthogonality properties of the transformation matrix in Eq. (A-1) it follows that the terms on the left hand side of Eq. (A-7) sum to unity. This can be seen by carrying out the matrix operations. The coefficients of the terms multiplying $A_{Zx}A_{Zy}$, $A_{Zx}A_{Zz}$, $A_{Zy}A_{Zz}$ all vanish because they involve products of different column vectors in the transformation matrix and these are zero because of the orthogonality property. The surviving terms are

$$A_{Zx}^2\left\{\sum_\lambda \hat{Q}_{\nu\lambda,x} + \frac{m_\nu}{M} + m_\nu\left(\frac{z_\nu^{o2}}{I_y} + \frac{y_\nu^{o2}}{I_z}\right)\right\}$$

$$+ A_{Zy}^2\left\{\sum_\lambda \hat{Q}^2_{\nu\lambda,y} + \frac{m_\nu}{M} + m_\nu\left(\frac{x_\nu^{o2}}{I_z} + \frac{z_\nu^{o2}}{I_y}\right)\right\}$$

$$+ A_{Zz}^2\left\{\sum_\lambda \hat{Q}^2_{\nu\lambda,z} + \frac{m_\nu}{M} + m_\nu\left(\frac{y_\nu^{o2}}{I_x} + \frac{x_\nu^{o2}}{I_y}\right)\right\} = A_{Zx}^2 + A_{Zy}^2 + A_{Zz}^2 = 1 \tag{A-8}$$

Each factor in brackets in Eq. (A-8) is a product of a column vector in the transformation matrix in Eq. (A-1) by itself and gives unity because these column vectors are normalized.

The column matrix $[T_{\nu\lambda}]$ which appears in Eq. (15) and other places is related to $[\hat{Q}_{\nu\lambda}]$ by

$$[T_{\nu\lambda}] = \frac{1}{m_\nu^{\frac{1}{2}}} [\hat{Q}_{\nu\lambda}] \tag{A-9}$$

Substituting Eq. (A-9) into Eq. (A-7) and using Eq. (A-8) yields

$$\sum_\lambda ([A_Z'][T_{\nu\lambda}])^2 + \frac{1}{M} + [A_Z']R_\nu' I^{-1} R_\nu [A_Z] = \frac{1}{m_\nu} \tag{A-10}$$

From Eq. (10) it follows that if the sum over λ in Eq. (47) includes all normal modes the result is

$$\alpha_{\nu c} = \frac{m}{m_\nu} \beta_o \phi \tag{A-11}$$

There is then no dependence of $\alpha_{\nu c}$ on the Eulerian angle variables and $S_\nu(\alpha,\beta)$ in Eq. (45) can be integrated to give Eqs. (48, 49).

If some, but not all, modes are treated classically and the Krieger-Nelkin method of averaging is used an effective mass $M_{\nu c}$ intermediate between the Sachs-Teller mass M_ν and the atom mass m_ν is defined by the equation

$$\sum_\lambda \overline{([A_Z'][T_{\nu\lambda}])^2} + \frac{1}{M} + \overline{[A_Z']R_\nu' I^{-1} R_\nu [A_Z]} = \frac{1}{3} \sum \bar{\delta}_{\nu\lambda} + \frac{1}{M_\nu} = \frac{1}{M_{\nu c}} \tag{A-12}$$

In Eq. (A-12) the sum over λ includes only the modes which are treated classically. The mass M_ν in the Sachs-Teller mass for a non-vibrating molecule[17]. When principal axis of inertia are used it is given by Eqs. (29,30). The $\bar{\delta}_{\nu\lambda}$ is defined in Eq. (32) and $[T_{\nu\lambda}]$ by Eq. (A-9).

Eq. (A-1) can be inverted to yield

$$[q] = \hat{Q}'[Q] \tag{A-13}$$

Equation (A-13) shows that the vibrational kinetic energy is given by

$$2T_v = [\dot{q}'][\dot{q}] = [\dot{Q}']\hat{Q}\hat{Q}'[\dot{Q}] = [\dot{Q}'][\dot{Q}] \tag{A-14}$$

Eq. (A-14) shows that the momentum p_λ conjugate to the coordinate Q_λ is $p_\lambda = \dot{Q}_\lambda$.

REFERENCES

(1) The status of current research on the inelastic scattering of slow neutrons is presented very well in the papers presented at the International Atomic Energy Symposium on Inelastic Scattering of Neutrons, Vienna, October 17-21(1960). See especially papers by R. M. Brugger, P. A. Egelstaff and B. N. Brockhouse.

(2) R. M. Brugger, "Compilation of Egelstaff Scattering Law Curves", AEC Report IDO-16999 (1961).

(3) P. D. Randolph, R. M. Brugger, K. A. Strong, and R. E. Schmunk, Phys. Rev. 124,460 (1961).

(4) K. A. Strong, G. D. Marshall, P. D. Randolph, and R. M. Brugger Accepted for publication in Phys. Rev. 125.

(5) R. M. Brugger - accepted for publication in Phys. Rev. 1.

(6) A. C. Zemach and R. J. Glauber, Phys. Rev. 101, 118 (1956).

(7) T. J. Krieger and M. S. Nelkin, Phys. Rev. 106, 290 (1957).

(8) G. C. Wick, Phys. Rev. 94, 1228 (1954). See also M. S. Nelkin General Atomics Report GA-1689 and M. S. Nelkin and D. E. Parks, Phys. Rev. 119, 1060 (1960).

(9) Coherent scattering by protons is weak because of the way the scattering amplitudes in the singlet and triplet states average. See, for example, "Theoretical Nuclear Physics" by J. M. Blatt and V. F. Weisskopf (Wiley, 1952) Chapter II, Section D.

(10) H. L. McMurry, "Scattering of Neutrons by Gaseous Molecules", IDO-16592 (March, 1960). This report gives the theory in considerable detail. There are some errors in the analysis but the final equations are for cases where the treatment is correct.

(11) A. C. Zemach and R. J. Glauber, Phys. Rev. 101, 129 (1956).

(12) P. Egelstaff, TNCC(UK) 62:EANDC(UK)1; Vienna Conf. Paper IS/P/7 (See ref. (1)). P. Egelstaff and C. Heard, AERE report NP/Gen/13. P. Schofield, Phys. Rev. Letters 4, 239 (March, 1960). M. S. Nelkin, General Atomics Report GAMD-1969 (January, 1961).

(13) G. W. Griffing, Phys. Rev. 124, 1489 (1961).

(14) E. B. Wilson,Jr., J. C. Decius, P. C. Cross, "Molecular Vibrations", (McGraw-Hill, 1955).

(15) H. L. McMurry, "Calculation of Differential Scattering Cross Sections In the Short Collision Time Approximation" IDO-16749,

(16) H. L. McMurry, G. W. Griffing, W. A. Hestir and L. J. Gannon, IDO-16692 (1961).

(17) R. G. Sachs and E. Teller, Phys. Rev. 60, 18 (1941).

(18) H. L. McMurry, "Coordinates for Semi-Rigid Molecules" AEC Report IDO-16600 (1960). Also J. Mol. Spect. 6, 439 (1961). Except that Eq. (A-1) is in terms of normal coordinates it is essentially like Eq. (28) of IDO-16600. Another minor difference is that in IDO-16600 the matrix multiplying [q] is indicated as a transposed matrix. The present notation is more consistent with the published work.

EVALUATION OF TECHNIQUES FOR COMPUTING DIFFERENTIAL SCATTERING CROSS SECTIONS*

H. L. McMurry, L. J. Gannon and W. A. Hestir
Phillips Petroleum Company, Atomic Energy Division, Idaho Falls, Idaho

* Work performed under the auspices of the U. S. Atomic Energy Commission.

A B S T R A C T

The methods presented in the accompanying paper for computing partial differential scattering cross sections are evaluated by comparing calculated results with experimental results for methane and propane, and by comparing results on a hypothetical OH molecule of the more approximate methods with the most rigorous ones.

The method which treats rotations quantum mechanically gives good agreement with experiments on methane and can be considered as rigorous. The method which treats rotations classically, vibrations by quantum mechanics and averages over orientation exactly also agrees well with methane experiments, except for scattering at forward angles and low neutron energies where the energy exchanges are comparable to the rotational level spacings. It is used as a standard of comparison for calculations on the OH molecule.

The Krieger-Nelkin method, which averages over orientation by inserting average values of functions of the Eulerian angles wherever they appear, works very well at low neutron energies. Calculations on OH show that when the characteristic vibrational energy is high, but much lower than the incident neutron energy, the K.N. method breaks down.

The short collision time method of treating low energy vibrations is impractical because too many terms in the required series expansion are needed to give good results.

The method which treats low energy vibrations classically is very promising. It gives very good results when the characteristic vibrational energies are low, and is better than the K.N. when the characteristic energy is high, but much lower than the neutron energy.

INTRODUCTION

This paper evaluates the methods presented in the accompanying paper ([1], hereafter referred to as I) for calculating the partial differential scattering cross sections of semi-rigid molecules in the gas phase. Such systems are relatively easy to deal with theoretically and it is hoped that the insights gained from their study will help in devising practical techniques for computing partial differential scattering cross sections of liquids and solids.

Five methods are considered ranging from a quantum treatment, which is strictly valid provided the neutron energy and k_BT are less than any of the characteristic vibrational energies of the molecule, to two methods which treat vibrational contributions approximately and are simple enough to be adaptable to treating liquids and solids.

Several of the methods are evaluated for low neutron energies by comparing calculated values for the partial differential scattering cross section with respect to energy and angle with experimental results for methane and propane obtained using the MTR slow neutron velocity selector[2,3]. Further evaluations, particularly for neutrons with energies beyond the range of present scattering experiments, are made by calculations on methane and a hypothetical OH molecule. Here methods which are shown to be good by comparison with the experiments on methane and propane are used to evaluate the more approximate procedures.

The hypothetical OH molecule is used because it has but one vibrational degree of freedom and this makes it easy to study the effect of changing the characteristic vibrational energy, as well as the incident neutron energy.

METHODS AND PHYSICAL DATA

A. Methods

The most rigorous method was developed by Griffing and treats the translational and rotational motions correctly by quantum mechanics(4). It is applied at temperatures and incident neutron energies low enough so that the effects of zero point vibrations can be dealt with adequately in an approximate way. The method is too cumbersome to apply to scattering by any but highly symmetrical molecules and the results reported here are only for scattering by methane. The method will be denoted by Q.M. for "quantum mechanical".

The second method treats rotations classically but goes beyond the first method by including the contributions due to exchanges of vibrational energy quanta with the neutron. The vibrational contributions are calculated quantum mechanically assuming a harmonic potential function and neglecting rotation-vibration coupling. Averages over molecular orientation are computed exactly by numerical integration and for this reason the method is designated by E.A. for "exact average". The method gives good results for methane and, within the limitations imposed by the classical treatment of rotations, applies rigorously to the case of the hypothetical OH molecule. Hence it is the chief standard of comparison for that case.

The third method is like the second except that averages over orientation are approximated in the manner of Krieger and Nelkin(5) by inserting average values of functions of the Eulerian angles wherever they appear. Hence the method is designated by K.N.. The K.N. averaging

simplifies the equations so that numerical integrations are not required. Hence there are wider possibilities for practical application.

The fourth method treats vibrations with characteristic energies much lower than the incident neutron energy by a short collision time approximation(6) and is denoted by S.C.T.

The fifth method treats these low energy vibrations classically. It is denoted by the letters C.A. which are meant to imply that some or all of the vibrations are treated by a classical approximation.

B. Physical Data

1. Methane

The equation for the partial differential scattering cross section of methane is

$$\sigma_{CH_4} = 4\sigma_H + \sigma_C \tag{1}$$

Eqs. (8-10) of I tell how to calculate σ_H and σ_C in the Q.M. method. The calculations are described in detail by Griffing(4). He used numerical data from the work of Krieger and Nelkin(5). These authors made use of Pope's normal coordinate analysis for methane(7).

The physical data for the K.N. and C.A. calculations may be derived from those needed in the E.A. calculation. The quantities needed appear in Eqs. (23-25) of I. Among them are α_H and α_C for which Eq. (26) of I yields(8)

$$\alpha_H = \beta_o\phi[\frac{1}{16} + \frac{3}{8}(1-u^2)] \tag{2}$$

$$\alpha_C = \beta_o\phi/16 \tag{3}$$

In Eq. (2) u is the cosine of the angle between the momentum change of the neutron $\hbar\underline{\kappa}$ and the vector $\underline{r}_H$ from the molecular center of mass to the scattering proton. The $\beta_o = E_o/k_BT$ where E_o is the incident neutron energy, and ϕ is defined by Eq. (4) of I. The 16 is the mass of methane in atomic units.

The other quantities which are needed to express Eqs. (23-25) of I can be obtained after the quantities δ_{ν_T} defined in Eq. (19) of I are derived from a normal coordinate analysis. Pope's analysis will be used(7). The accepted numbering of the normal modes, together with their degeneracies, characteristic energies and symmetries are shown in Table I.

TABLE I

NORMAL COORDINATE ENERGIES FOR CH_4

Mode	Characteristic Energy (ev)	Symmetry Species	Degeneracy
1	0.361	A_1	1
2, 3	0.188	E	2
4, 5, 6	0.374	F_2	3
7, 8, 9	0.162	F_2	3

The present calculations are for neutron energies no higher than 0.306 ev and take $k_BT = 0.0252$ ev. Under these conditions the only energy transfers to the vibrational modes which contribute significantly to the σ_ν are for single excitations of modes 2, 3, 7, 8, 9. Also, the characteristic vibrational energies are high enough to permit the use of the approximation in Eq. (27) of I. This means that Eq. (25) of I may be approximated by

$$\bar{\Psi}_\nu \simeq 1 + 2\left[\frac{\beta_o}{\beta_2}\,\phi m(\delta_{\nu 2} + \delta_{\nu 3})\exp\left\{-\frac{\beta_2}{2}\right\}\cosh\left\{\frac{\beta\beta_2}{2\alpha_\nu}\right\}\exp\left\{\frac{-\beta_2^2}{4\alpha_\nu}\right\}\right.$$

$$\left. + \frac{\beta_o}{\beta_7}\,\phi m(\delta_{\nu 7} + \delta_{\nu 8} + \delta_{\nu 9})\exp\left\{\frac{-\beta_7}{2}\right\}\cosh\left\{\frac{\beta\beta_7}{2\alpha_\nu}\right\}\exp\left\{\frac{-\beta_7^2}{4\alpha_\nu}\right\}\right] \qquad (4)$$

The use of Pope's normal coordinates leads to(8)

$$\delta_{H2} + \delta_{H3} = 0.2500\ (1-u^2) \qquad (5)$$

$$\delta_{H7} + \delta_{H8} + \delta_{H9} = 0.01875 + 0.5746\ u^2 \qquad (6)$$

$$\delta_{C2} = \delta_{C3} = 0 \qquad (7)$$

$$\delta_{C7} + \delta_{C8} + \delta_{C9} = 0.01341 \qquad (8)$$

Finally, the $\langle \chi_\nu^o \rangle_T$ appearing in Eq. (24) of I are given by(8)

$$\langle \chi_H^o \rangle_T = \exp\left\{-E_o\phi(2.23 + 2.37u^2)\right\} \qquad (9)$$

$$\langle \chi_C^o \rangle_T = \exp\left\{-0.103E_o\phi\right\} \qquad (10)$$

The quantities $\bar{\alpha}_\nu$, $\bar{\delta}_{\nu T}$ which replace α_ν and $\delta_{\nu T}$ in obtaining the K.N. forms of Eqs. (23-25) of I are defined by Eqs. (28) and (32) of I. The $\bar{\alpha}_H$ is obtained readily by replacing u^2 in Eq. (2) by its average value of $\frac{1}{3}$. The α_C and $\bar{\alpha}_C$ are identical. The use of $\bar{\delta}_{\nu T}$ also implies the use of Eq. (33) of I for $I_{nT}(\bar{g}_{\nu T})$. The results for methane are(8)

$$\bar{\alpha}_H = \frac{m}{M_H}\,\beta_o\phi = \frac{1}{3.2}\,\beta_o\phi \qquad (11)$$

$$\bar{\alpha}_C = \frac{m}{M_C}\,\beta_o\phi = \frac{1}{16}\,\beta_o\phi \qquad (12)$$

$$\bar{\delta}_{H2} + \bar{\delta}_{H3} = 0.5000 \qquad (13)$$

$$\bar{\delta}_{H7} + \bar{\delta}_{H8} + \bar{\delta}_{H9} = 0.6303 \qquad (14)$$

$$\bar{\delta}_{C7} + \bar{\delta}_{C8} + \bar{\delta}_{C9} = 0.0402 \tag{15}$$

$$\langle \bar{\chi}^{o}_{H} \rangle_{T} = \exp\left\{-3.02 E_{o} \phi\right\} \tag{16}$$

$$\langle \bar{\chi}^{o}_{C} \rangle_{T} = \langle \chi^{o}_{C} \rangle_{T} \tag{17}$$

The equation for $\bar{\psi}_{\nu}$ is the same as Eq. (4) except that 2/3 replaces the factor 2 and the α_{ν} and $\delta_{\nu T}$ are replaced by the $\bar{\alpha}_{\nu}$ and $\bar{\delta}_{\nu T}$ given in Eqs. (11-15).

The C.A. method was applied only for the case of $E_o = 0.306$ ev. In this application modes 2, 3, 7, 8, 9 with the lowest characteristic energies were treated classically and the others by the K.N. method.
Using the numbers in Eqs. (13-15) in Eqs. (42, 43) of I leads to

$$M_{Hc} = 1.450$$

$$M_{Cc} = 13.16$$

$$\bar{\alpha}_{Hc} = \beta_{o}\phi/1.450$$

$$\bar{\alpha}_{Cc} = \beta_{o}\phi/13.16$$

The $\langle \bar{\chi}^{o}_{\nu q} \rangle_{T}$ quantities called for in Eq. (46) of I are obtained by subtracting out the contributions of modes 2, 3, 7, 8, 9 to the $\langle \bar{\chi}^{o}_{\nu} \rangle_{T}$.
The numbers in Eqs. (13-15) lead to

$$\langle \bar{\chi}^{o}_{Hq} \rangle_{T} = \exp\left\{-0.839 E_{o} \phi\right\} \tag{18}$$

$$\langle \bar{\chi}^{o}_{Cq} \rangle_{T} = \exp\left\{-0.020 E_{o} \phi\right\} \tag{19}$$

In all the calculations the quantities $A_H^2 + C_H^2$ and $A_C^2 + C_C^2$ are the same as used by Krieger and Nelkin[5].

$$A_H^2 + C_H^2 = 6.53 \text{ barns}$$

$$A_C^2 + C_C^2 = 0.41 \text{ barns}$$

2. Propane

Only the K.N. and C.A. methods are used for propane. All of the physical data and most of the computations are from Marshall's work(3,9). The $A_H^2 + C_H^2$ and $A_C^2 + C_C^2$ are the same as for methane. Marshall computed the 27 normal modes using a potential function that gave good agreement for all but two observed frequencies. However, there are no experimental data for some frequencies including the two lowest which involve mainly torsional oscillations of the CH_3 groups about the symmetry axes for these groups. Marshall's work employs values calculated for these energies which arise by using a force constant for the torsional motion derived assuming a potential barrier against rotation about the symmetry axis of a CH_3 group of 3kcal/mol. In writing the K.N. form of Eq. (25) of I Marshall included only the terms associated with transfers of single quanta of vibrational energy to and from the three lowest energy modes. In his work they are denoted by the numbers 9 (0.0455 ev), 14 (0.0387 ev) and 27 (0.0343 ev). The approximation of Eq. (33) of I was used for all modes except these three.

In propane two of the hydrogens on each methyl group are equivalent as far as neutron scattering is concerned, but the third one is so nearly like the others that Marshall treated all methyl hydrogens as equivalent using weighted averages of the $\bar{\alpha}_H$, $\bar{\delta}_{H\tau}$ etc. Then the equation for the partial differential scattering cross section may be expressed as

$$\sigma_{C_3H_8} = 6\sigma_{H1} + 2\sigma_{H2} + 2\sigma_{C1} + \sigma_{C2} \qquad (20)$$

In Eq. (20) subscripts 1 and 2 denote atoms in the methyl and methylene groups, respectively. The molecular dimensions, together with quantities derived from the normal coordinate analysis yield the following quantities

which are needed in the K.N. form of Eq. (23) of I

$$M_{H1} = 12.98;\ M_{H2} = 12.73$$

$$\langle \bar{\chi}^{o}_{H1} \rangle_T = \exp\left\{-9.15\ E_o\phi\right\}$$

$$\langle \bar{\chi}^{o}_{H2} \rangle_T = \exp\left\{-6.78\ E_o\phi\right\}$$

$$M_{C1} = 24.03;\ M_{C2} = 31.8$$

$$\langle \bar{\chi}^{o}_{C1} \rangle_T = \exp\left\{-0.466 E_o\phi\right\}$$

$$\langle \bar{\chi}^{o}_{C2} \rangle_T = \exp\left\{-0.522 E_o\phi\right\}$$

$$\bar{\delta}_{H1,9} = 0.0612;\ \bar{\delta}_{H1,14} = 0.1624;\ \bar{\delta}_{H1,27} = 0.1409$$

$$\bar{\delta}_{H2,9} = 0.00929;\ \bar{\delta}_{H2,14} = 0.00068;\ \bar{\delta}_{H2,27} = 0.0457$$

$$\bar{\delta}_{C1,9} = 0.0202;\ \bar{\delta}_{C1,14} = 0.00105;\ \bar{\delta}_{C1,27} = 0.00142$$

$$\bar{\delta}_{C2,9} = 0.0108;\ \bar{\delta}_{C2,14} = 0.00192;\ \bar{\delta}_{C3,27} = 0.00650$$

When the three low energy modes are treated classically in the C.A. method there results

$$M_{H1,c} = 5.07;\ M_{H2,c} = 10.29$$

$$\langle \bar{\chi}^{o}_{H1,q} \rangle_T = \exp\left\{-4.11\ E_o\phi\right\}$$

$$\langle \bar{\chi}^{o}_{H2,q} \rangle_T = \exp\left\{-5.84\ E_o\phi\right\}$$

$$M_{C1,c} = 20.34;\ M_{C2,c} = 26.84$$

$$\langle \bar{\chi}^{o}_{C1,q} \rangle_T = \exp\left\{-0.225\ E_o\phi\right\}$$

$$\langle \bar{\chi}^{o}_{C2,q} \rangle_T = \exp\left\{-0.306\ E_o\phi\right\}$$

In this approximation the $\bar{\Psi}_{Hq}$ and $\bar{\Psi}_{Cq}$ were put equal to one.

3. The OH Molecule

Only the hydrogen is considered to scatter in this molecule and the equation for the partial differential scattering cross section is

$$\sigma_{OH} = \sigma_H \tag{21}$$

The $A_H^2 + C_H^2$ is as for methane. The α_H, $\bar{\alpha}_H$, $\delta_{H\tau}$ and $\bar{\delta}_{H\tau}$ are given from Eqs. (26, 28, 19, 32) of I, respectively, by

$$\alpha_H = \beta_o\phi \left[1 - \frac{16}{17} u^2\right];$$

$$\bar{\alpha}_H = \frac{1}{1.457} \beta_o\phi; \quad (M_H = 1.457)$$

$$\delta_{H\tau} = \frac{16}{17} u^2 = 0.9412\ u^2$$

$$\bar{\delta}_{H\tau} = 0.9412$$

$$\langle \chi_H^o \rangle_T = \exp\left\{-\frac{E_o\phi}{E_\tau} (0.9412\ u^2) \coth(\beta_\tau/2)\right\}$$

$$\langle \bar{\chi}_H^o \rangle_T = \exp\left\{-0.3134 (E_o\phi/E_\tau) \coth(\beta_\tau/2)\right\}$$

In this simple example the C.A. equation results in

$$\alpha_{Hc} = \bar{\alpha}_{Hc} = \beta_o\phi; \ M_{Hc} = 1$$

$$\langle \chi_{Hq}^o \rangle_T = \langle \bar{\chi}_{Hq}^o \rangle_T = 1$$

Therefore, the equation for the partial differential scattering cross section reduces in the C.A. approximation to that for scattering by hydrogen atoms in a monatomic hydrogen gas.

In the applications several values of E_τ are used so that this quantity enters as a parameter in the equations.

RESULTS AND DISCUSSION

A. Comparison of Theory with Experiment for Methane and Propane

1. Methane

Fig. 1 compares calculated with measured $\sigma(E_o,E,\mu)$ vs. E curves for incident neutrons of 0.015 ev and 0.103 ev scattered at 16.3°. At this low scattering angle the conditions of energy and momentum conservation dictate that the average energy transferred to the molecule in a collision is quite small. The 0.015 ev neutrons have an energy comparable to the spacings of the rotational levels. Hence the quantum nature of the levels is expected to influence the scattering of such neutrons, particularly at forward angles. The results in Fig. 1 bear this out. Only the Q.M. method satisfactorily predicts the profile for the scattering of the 0.015 ev neutrons. The narrowness in the profile is due to the discrete character of the rotational levels which results in an inhibition of energy transfers to the rotational motion. This effect is revealed more dramatically when the partial differential scattering cross section $\sigma(\lambda_o,\lambda,\mu)$ with respect to neutron wavelength λ is presented(4). At 0.103 ev the E.A. and K.N. methods give mush better agreement. This is because the neutron energy is now high enough so that many possibilities exist for transfers of rotational energy and a classical treatment of rotations is more adequate.

There is a sizeable discrepancy in the peak heights at the 16.3° angle. This discrepancy may be due to experimental errors but further work is needed to establish its origin.

Fig. 2 shows the scattering of 0.0252 ev neutrons at the high angle of 59.5°. The Q.M. method gives very close agreement and both the K.N. and E.A. results are also good.

Neutrons of the energies studied here have wavelengths of 0.893, 1.803 and 2.236A° for the 0.103, 0.0252, and 0.015 ev energies, respectively. These wavelengths are comparable to the C-H and H-H distances (r_{CH} = 1.09A°, r_{HH} = 1.79A°) and Griffing(10) finds that scattering by C-H and H-H pairs can be significant. Some of his results are included in Figs. 1, 2. The C-H contribution is often negative and Griffing's calculations show that under some conditions the C-H and H-H contributions nearly cancel. However, there are cases where the C-H scattering dominates and amounts to as much as 15% of the direct scattering.

It can be concluded that at these low energies and temperatures the scattering by a semi-rigid molecule with relatively high characteristic vibrational energies can be calculated satisfactorily by the Q.M. method and, except at forward angles, the K.N. and E.A. methods give good results. However, if precise results are required pair scattering must be considered even for hydrocarbons.

2. Propane

Figs. 3, 4 compare calculated and measured $\sigma(E_o, E, \mu)$ vs E profiles for propane. The results in Fig. 3 for scattering by 0.0254 ev neutrons show very good agreement for the K.N. method and quite good agreement for the C.A. method which treats the three lowest energy vibrations (0.0455, 0.0387 and 0.0343 ev) classically.

For the 0.101 ev neutrons Fig. 4 displays good agreement at 16.3° by both methods, but considerably worse at 84.7°. Even here, however, the C.A. agrees quite well with the more rigorous K.N.

Factors to be considered in seeking the cause of the discrepancy are the contributions from the C-H and H-H pair scattering (not included in any of the propane calculations), the error arising from the K.N. approximation for averaging over orientation, and errors due to using incorrect normal modes and characteristic frequencies for the two lowest frequency vibrations for which lack of experimental data make reliance on computed values necessary.

The contribution of the pair scattering is difficult to assess. Examination of Griffing's calculations(10) for methane shows that there these terms contribute the most in the vicintiy of the peak of the $\sigma(E_o,E,\mu)$ vs E curves and in extreme cases can amount to as much as 15% of the direct scattering contribution. However, the amount is usually less than this and it is often negative because the C-H scattering can make a negative contribution. In propane there are more atom pairs to contribute to the indirect scattering, but the pairs occur with different distances. This means that if conditions are right for a large

scattering at one distance they may be less favorable for another. For example, if the C-H pairs on a methyl group scatter strongly the contribution from the carbon on one methyl and a hydrogen on the other is probably smaller. These facts indicate that the large discrepancy for the 84.7° case in Fig. 4 may be due partly to neglect of pair scattering in the calculation, but that this is probably not the major reason for the difference.

The K.N. averaging inserts average values of $\delta_{\nu T}$ and α_{ν} into Eq. (24) of I and thereby affects all the factors in this equation. Some evaluation of this averaging can be made by comparing the E.A. and K.N. results for methane. Here the K.N. calculations never give results more than a few percent different from the E.A. results near the peaks of the $\sigma(E_o,E,\mu)$ vs E curves. This is true for scattering of 0.306 ev neutrons as shown in Fig. 5 as well as for the scattering of lower energy neutrons already considered.

It is not certain that this situation is repeated in propane. For one thing the exponents of the $\langle x_H^o \rangle_T$ factors are always large in propane because the very low frequency modes have large $\delta_{\nu T}/E_T$ ratios and coth $(\beta_T/2)$ factors (see Eq. (22) of I). However, for 0.306 ev neutrons scattered at 84.7° in methane the exponent in the $\langle x_H^o \rangle_T$ factor is comparable to what it is for 0.1 ev neutrons scattered at this angle in propane. Since in methane the K.N. and E.A. results are fairly close it does not seem that the E.A. treatment of the $\langle x_H^o \rangle_T$ factor in propane would lead to a large change.

In support of this is the fact that when the three lowest frequency vibrations of propane are treated classically the C.A. calculation for the 84.7° scattering of 0.1 ev neutrons is not greatly different from the full K.N. calculation. However, the C.A. calculation uses exponents in the $\langle \bar{\alpha}^{o}_{Hq} \rangle_{T}$ factors, particularly for the methyl hydrogens, which are much smaller than in the K.N. equations. Also, the other factors depend on $\bar{\alpha}_{Hc}$ etc. which have magnitudes rather like those in methane and are much different from those used in the K.N. calculation. This suggests that the C.A. calculations would not change much if exact averages were used rather than the Krieger-Nelkin averages. This implies that if the K.N. calculation for the 84.7° scattering of 0.1 ev neutrons was low because the averaging was a poor approximation the results would be lower than on the C.A. method. However, this is not the case as the values are comparable, a result which lends weight to the conclusion that K.N. averaging is not at fault.

While these arguments are not complete proof that causes other than K.N. averaging are responsible for the discrepancy in Fig. 4, they suggest looking for a more plausible explanation. The use of incorrect normal modes and characteristic energies for the two lowest frequency modes is a good possibility. The frequencies for these vibrations are not known from experiment and they, as well as the associated normal modes, were obtained from calculations which depend most on the value of the force constant for the torsional motion. The assumed value was based on a barrier height inhibiting CH_3 torsional rotations of uncertain validity(9). A higher barrier would result in higher values

of E_T for these modes and lower $\bar{\delta}_{HT}$ values. Both changes would decrease the exponents in the $\langle \bar{x}_H^o \rangle_T$ terms, and that for the methyl hydrogens is particularly sensitive to such a change. Reduction in $\bar{\delta}_{HT}$ would raise the value of M_{Hc} in the C.A. method (see Eq. (43) of I) which would increase the σ values. A complete study would require recalculating the normal modes but a qualitative idea of what would result from an increase in E_T values can be gained by assuming the $\bar{\delta}_{HT}$ remain unchanged. It is found that then increase of 25% in the characteristic energy of each of these modes would alter the $\langle \bar{x}_H^o \rangle_T$ factors so that they alone would cause a 25% increase in the calculated $\sigma(E_o,E,\mu)$ at the peak value for 0.1 ev neutrons scattered at 84.7^o, and only a 5% increase for 0.0254 ev neutrons scattered at this angle. Therefore, it is quite possible that an incorrect choice of barrier height is the main cause of the discrepancy.

It would be useful to study the influence of barrier height on the slow neutron scattering of ethane. This molecule possesses a single low frequency torsional vibration and is simple enough in structure to make more detailed calculations, including interference contributions, feasible. Such a study amounts to exploring the possibility of using slow neutron scattering data to estimate barrier heights.

B. Evaluations from Computations on CH_4 and OH

1. General Remarks

The evaluations based on experimental data focus attention on how well calculated $\sigma(E_o,E,\mu)$ vs E agree with experiment. Available data limit these studies to neutron energies E_o below about 0.15 ev and for molecules whose E_τ values are either all high, or are not all known.

To study the validity of the computational techniques under a wider range of condition the E.A. method is used as a standard against which the other techniques are tested. The exception to this is for some cases where the approximation in Eq. (27) of I is not valid. There reliance has been on the K.N. method because the results on methane (Figs 1,2) show that it is a reasonable standard.

In making these evaluations there always occurs the question as to what constitutes "good" agreement. Thus it is generally true that the $\sigma(E_o,E,\mu)$ vs E profile calculated by the C.A. method is shifted toward lower E from that obtained on the reference method. There will obviously be large differences when an E value is on the slope of one $\sigma(E_o,E,\mu)$ vs E curve and near the peak of the other. Therefore, it is evident that a comparison of $\sigma(E_o,E,\mu)$ vs E profiles is very stringent. Reactor calculations generally use integrals of $\sigma(E_o,E,\mu)$ over ranges of E and μ and techniques which give rather different results for $\sigma(E_o,E,\mu)$ may give close agreement between the integrated quantities. Preliminary calculations of differential scattering cross sections $\sigma(E_o,E) = \int_{-1}^{1} \sigma(E_o,E,\mu)d\mu$ bear this out.

Therefore, in what follows the term "good" and "poor" will be used qualitatively but it is felt that when "good" is used the $\sigma(E_o,E,\mu)$ will suffice for most reactor physics needs.

2. Inadequacy of the S.C.T. Method

Figs. 6,7 compare the K.N., C.A., and S.C.T. calculations on a hypothetical OH molecule with E_o = 0.01 ev, E_T = 0.025 ev, and E_o = 0.20 ev, E_T = 0.10 ev.

It is immediately apparent that S.C.T. calculations based on the three term expansion in Eq. (40) of I has limited value. While the results for E_o = 0.01 ev are fairly close to the K.N. calculation, they are not as good as those given by the simpler C.A. approximation. As E_o is increased the S.C.T. method diverges badly, especially at the forward angles. Calculations at higher E_o than shown in Figs. 6,7 lead to still worse results.

The main difficulty is that more than three terms in the S.C.T. expansion (Eq. (36) of I) are required for many practical cases. A condition for the S.C.T. method to be valid might be that the term $(\sum_\lambda \langle o_{\nu\lambda}^{(3)} \rangle_T) t^3/3!$ arising when Eq. (36) of I is used in Eq. (1) of I should be less than one when the time t is large enough so that the factor $\exp(-\alpha_\nu t^2/\beta_o^2)$ coming from Eqs. (3a) and (11) is small. In the K.N. approximation this leads to a condition

$$\left[\frac{m\sum_\lambda \bar{\delta}_{\nu\lambda}\beta_\lambda^2}{18}\right]^2 \left(\frac{M}{m}\nu\right)^3 \frac{1}{\phi} < \frac{E_o}{k_B T} \qquad (22)$$

For high values of E_o at forward angles ϵ/E_o is small where σ_ν is largest. Then $\phi \sim 2(1-\mu)$ and the criterion in (22) shows that a three term expansion

will be poor at forward angles. It will also be poor when $\beta_\lambda \gg 1$ because the left side of Eq. (22) involves the β_λ to the fourth power.

If enough terms were used in Eqs. (36) and (40) of I, agreement could be obtained with the K.N. or E.A. calculations. However, this is impractical because the higher terms in Eq. (36) become very complicated. Although the C.A. approximation is classical it is not limited by the number of terms in an expansion and turns out to be superior to the S.C.T. method in all cases tried.

3. Evaluation of the C.A. Approximation

The $\sigma(E_o,E,\mu)$ vs E profiles in Figs. 4-10 computed using the C.A. method are always displaced toward lower E from the comparison standard. The heights are usually low at the forward scattering angles and in fair agreement at the larger angles. There is some deviation from this at high E_o where the C.A. peaks are sometimes higher at all angles. Preliminary claculations of $\sigma(E_o,E)$ vs E curves shows that the C.A. method is close to the K.N. in those cases where the latter is expected to be valid.

The C.A. results are especially good when E_T is low (less than 0.1 ev in this work). This is shown in Figs. 6, 7 which give results for the hypothetical OH molecule, and in Fig. 4 for propane.

When E_T is raised the C.A. results are less good, but for a given E_T the result improves as E_o/E_T increases.

The effect of raising E_T can be seen by comparing the good C.A. and K.N. agreement shown in Fig. 4 for 0.1 ev neutrons scattered by propane, and the mediocre agreement shown in Fig. 5 for 0.306 ev neutrons scattered by methane. The vibrations which are treated classically in propane all

have $E_T < 0.05$ ev while those in methane have $E_T = 0.188$ ev (modes 2,3) and 0.162 ev (modes 7,8,9). A further example is shown in Figs. (9-10) where increasing the E_T of the OH molecule from 0.25 ev to 0.50 ev causes a detrimental effect on the C.A. calculation of the scattering of 2.5 ev neutrons.

The effect of raising E_O/E_T when E_T is fixed is shown in Figs. 8,9. The increase in E_O/E_T from 2 to 10 when $E_T = 0.25$ ev is accompanied by an improvement in the C.A. result.

Calculations based on the assumption of harmonic vibrations are of questionable validity when E_O is much over 1 ev. This is because the vibrational eigenstates can no longer be looked on as equally spaced. Rather they begin to converge until they merge into a continuum when the dissociation energy is reached. When E_O is large enough so that vibrational excitations involve more densly distributed upper states the C.A. method, which assumes a continuum at the outset, may be preferable even to the E.A. method, and is certainly to be preferred to the K.N..

4. Deviation of the K.N. Method at High E_O

Fig. 9 shows that even if the assumption of harmonic vibrations were valid the K.N. method is poor when E_O and E_O/E_T are both high. For the more extreme case considered ($E_O = 2.5$ ev, $E_T = 0.25$ ev) it is much worse than the C.A. calculations.

Some calculations have been made for low E_O and E_T low enough so E_O/E_T is quite large. The C.A. and K.N. methods agree well even though many terms in Eq. (25) of I are needed. Since calculations have not been done by the E.A. method it is not certain that the C.A. and K.N. results are applicable in such situations.

DISCUSSION AND CONCLUSION

The results on methane show that the Q.M. method is rigorous when E_o and k_BT are much less than any of the E_T. They also show that the E.A. method is accurate except in special cases where small momentum and energy exchanges take place with a molecule having relatively widely spaced rotational energy levels. These methods are too cumbersome for general application and mainly serve to evaluate more easily used procedures.

Of those studied the S.C.T. approach is impractical because accuracy will require using many terms in the expansion upon which the equation is based, and the coefficient of all but the first few involve complicated algebraic expressions.

The K.N. method is good for small and intermediate values of E_o. Some unreported calculations indicate that it may serve in these cases even when E_o/E_T is quite large. However, more needs to be done on this. When E_T is in the range of the energies associated with H-C-H and H-O-H bending vibrations (about 0.2 ev), or C-H and O-H stretching vibrations (about 0.4 ev) in hydrocarbons and water the K.N. method should apply as long as E_o is less than about 1 ev.

When E_o exceeds 1 ev the C.A. approximation should be preferable to the K.N. partly because the K.N. averaging becomes suspect at these high E_o/E_T, but also because the assumption of harmonic vibrations begins to lose its validity and the C.A. method, which treats vibrational energy states as a continuum, may be closer to reality. If all vibrations are treated by the C.A. method for $E_o > 1$ ev the scattering reduces to that for unbound particles.

Preliminary calculations of $\int_{-1}^{1} \sigma(E_o,E,\mu)d\mu = \sigma(E_o,E)$ for the hypothetical OH molecules show that the C.A. and K.N. results are quite close. For the E_o = 0.01 ev, E_T = 0.025 ev and E_o = 0.2 ev, E_T = 0.1 ev cases they agree to within a few percent over most of the E range. For E_o = 0.50 ev, E_T = 0.25 ev the deviation, while larger, are not very great. For neutron energies above 0.2 ev $\sigma_H(E_o,E)$ approaches σ_{fH}/E_o where σ_{fH} is the free atom cross section for the proton. This is just the result required by a calculation based on scattering by free protons at rest.

In view of these results it appears that the scattering by liquid water for neutrons above a few hundreths of an ev could be calculated by treating the system as a dense gas and using the K.N. method up to 1 ev (possibly less) to calculate the effect of the internal vibrations with high E_T. The dense gas model would result from treating degrees of freedom associated with low energy translational and torsional oscillations of the molecules by the C.A. method which is equivalent to regarding them as unrestricted.

Similarly, it should be possible to calculate the scattering by hydrocarbons of neutrons above about 0.1 ev by treating all interatomic motions and low frequency molecular vibrations on the C.A. method, using the K.N. method to deal with the relatively high energy H-C-H bending and stretching modes.

ACKNOWLEDGEMENTS

Dr. G. W. Griffing supplied his latest Q.M. calculations on methane and Mr. G. D. Marshall provided his K.N. calculations on propane. Dr. R. M. Brugger, Dr. P. D. Randolph and Mr. K. A. Strong made their experimental results on methane and propane available. Miss Mitzi Hutchinson's skillful help in preparing the report has been of great value.

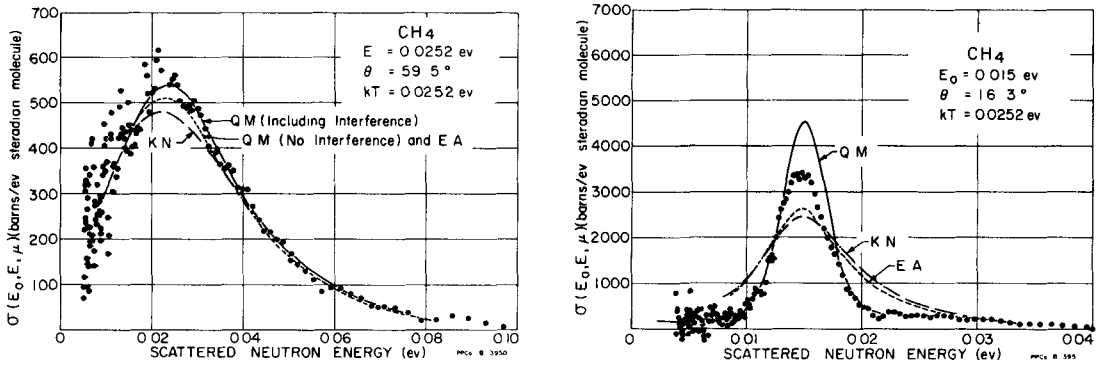

Fig. 1 Partial Differential Scattering Cross Sections of methane for low Neutron Energies

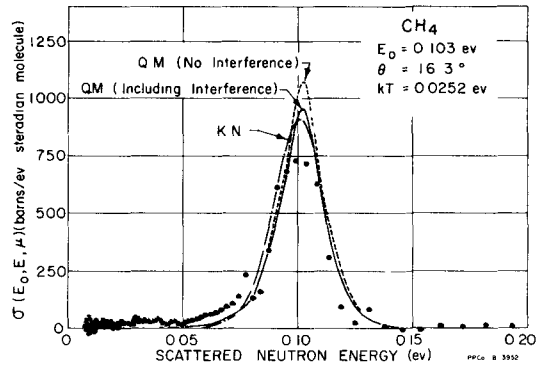

Fig. 2 Partial Differential Scattering Cross Section of Methane for 0.103 ev Neutrons

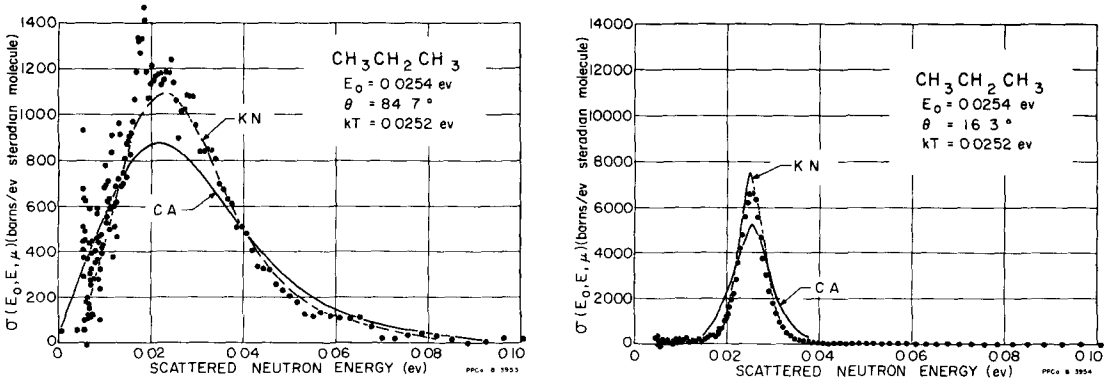

Fig. 3 Partial Differential Scattering Cross Sections of Propane for 0.0252 ev Neutrons

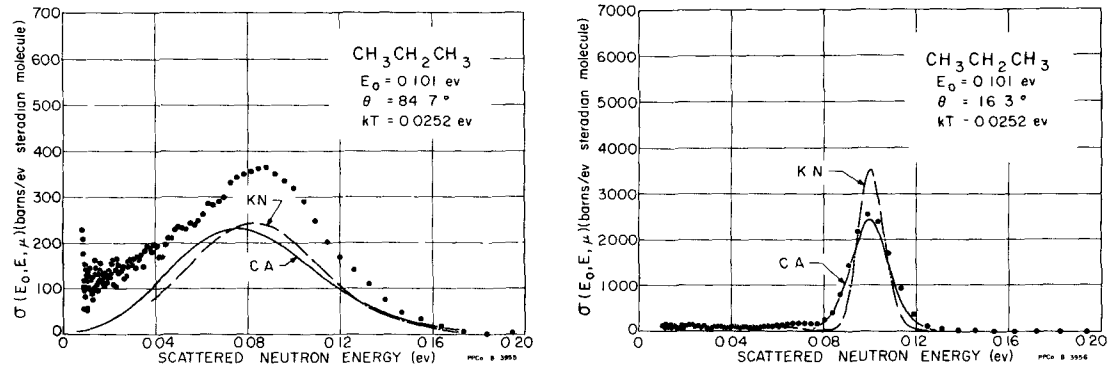

Fig. 4 Partial Differential Scattering Cross Sections of Propane for 0.101 ev Neutrons

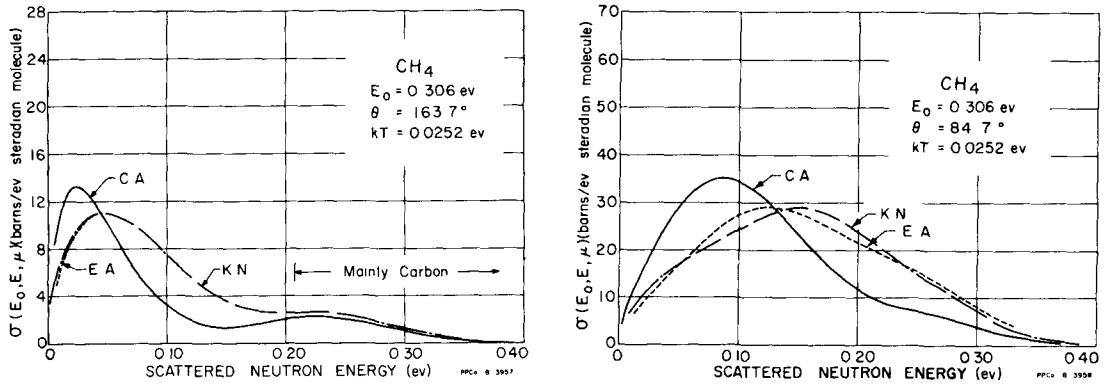

Fig. 5 Comparison of Computational Methods for Partial Differential Scattering Cross Section of Methane for 0.306 ev Neutrons

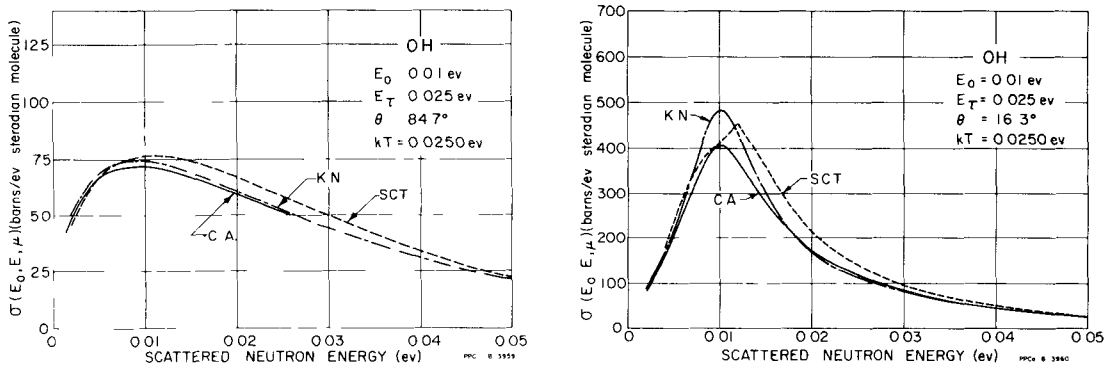

Fig. 6 Calculated Partial Differential Scattering Cross Sections of a Hypothetical OH Molecule for 0.01 ev Neutrons

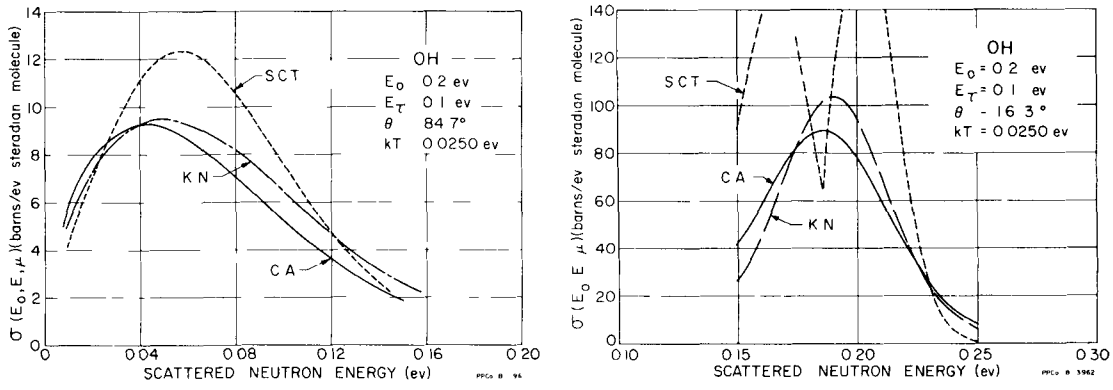

Fig. 7 Calculated Partial Differential Scattering Cross Sections of a Hypothetical OH Molecule for 0.20 ev Neutrons

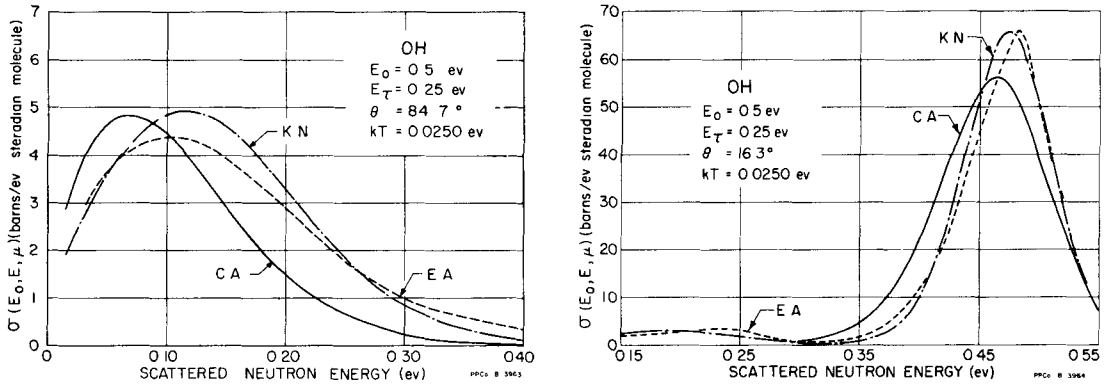

Fig. 8 Calculated Partial Differential Scattering Cross Sections of a Hypothetical OH Molecule for 0.5 ev Neutrons

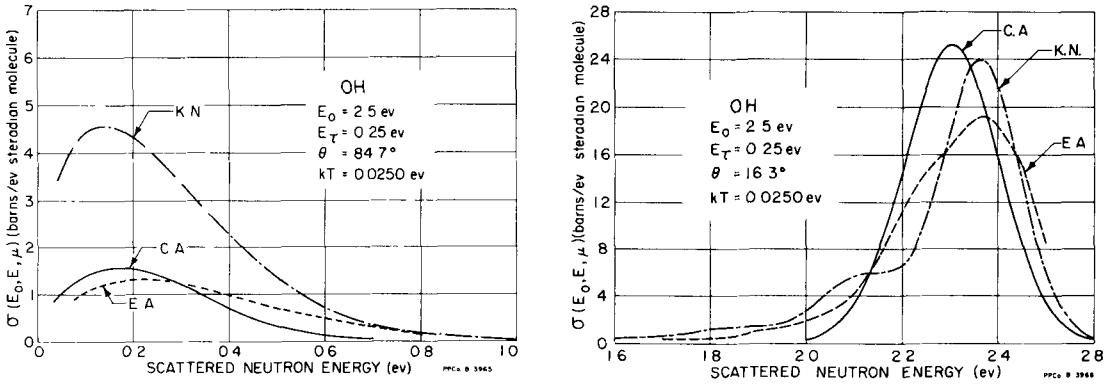

Fig. 9 Calculated Partial Differential Scattering Cross Sections of a Hypothetical OH Molecule for 2.5 ev Neutrons

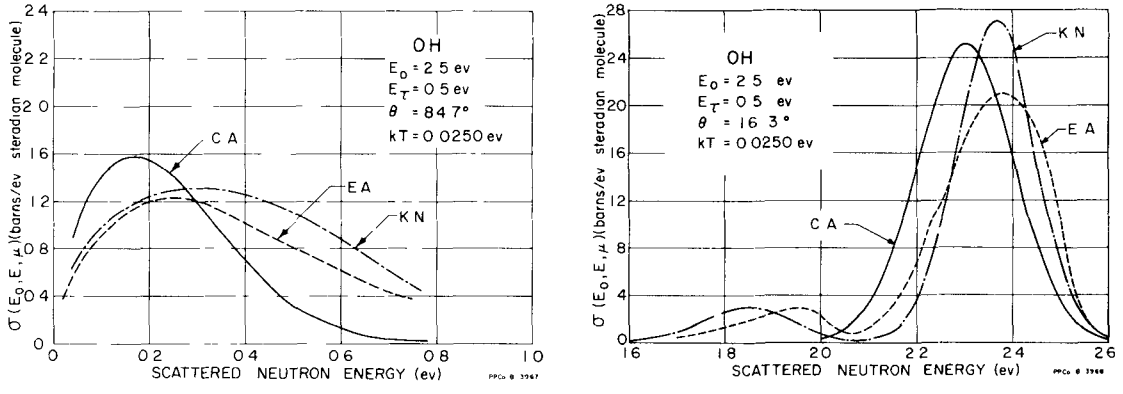

Fig. 10 Calculated Partial Differential Scattering Cross Sections of a Hypothetical OH Molecule for 2.5 ev Neutrons

REFERENCES

1. H. L. McMurry (accompanying report).
2. P. D. Randolph, R. M. Brugger, K. A. Strong and R. E. Schmunk, Phys. Rev. 124, 460 (1961).
3. K. A. Strong, G. D. Marshall, P. D. Randolph and R. M. Brugger, Phys. Rev. 125, (to be published).
4. G. W. Griffing, Phys. Rev. 124, 1489 (1961).
5. T. J. Krieger and M. S. Nelkin, Phys. Rev. 106, 290 (1957).
6. G. C. Wick, Phys. Rev. 94, 1228 (1954).
7. N. K. Pope, Can. Jour. Phys. 30, 597 (1952).
8. H. L. McMurry, G. W. Griffing, W. A. Hestir, and L. J. Gannon, Atomic Energy Commission Report IDO-16692 (1961). (To be issued). The appendix contains all the information required to make calculations on methane.
9. G. D. Marshall and H. L. McMurry, Atomic Energy Commission Report IDO-16759. (To be issued.)
10. G. W. Griffing (to be published).

BROOKHAVEN NATIONAL LABORATORY

CONFERENCE ON NEUTRON THERMALIZATION

APRIL 30 - MAY 2, 1962

NEUTRON THERMALIZATION IN A CRYSTALLINE MEDIUM IN INCOHERENT APPROXIMATION

S. N. PUROHIT

BROOKHAVEN NATIONAL LABORATORY

UPTON, L. I., NEW YORK

Research performed under the auspices of the U.S. Atomic Energy Commission.

1. INTRODUCTION

The numerical study of the Boltzmann equation undertaken by standard multigroup methods is based upon knowledge of the scattering matrix - the differential scattering cross section as a function of energy and angle. Alternatively, the study of the Boltzmann equation using orthogonal polynomials requires determination of the "matrix elements of the scattering operator." By using these matrix elements, a large class of neutron thermalization problems can be reduced to the numerical solution of a set of linear algebraic equations. For the energy variable, the associated Laguerre polynomials are chosen, and for the velocity variable the Hermite polynomials are the logical choice. The matrix elements corresponding to the associated Laguerre polynomials can be obtained from energy transfer moments or their associated integrals. It is the purpose of this study to obtain energy transfer moments and their associated integrals for the crystalline case by using Placzek's mass expansion formalism (1).

In another paper submitted to this conference, Purohit and Rajagopal (2) have discussed formal expressions for obtaining energy transfer moments and their associated integrals in terms of "time integrals" derived from Van Hove's well-known scattering formalism. It is shown that these integral quantities can be

analytically given for the "general Doppler approximation" case. For this approximation, the width function (the mean square displacement of scattering atoms in terms of the collision time between a neutron and an atom) is of the quadratic form. For a scattering medium characterized by vibrational modes, such as crystals, the time integrals can be transformed into integrals involving the frequency distribution of vibrational modes by using mass expansion, or they may be evaluated numerically .

Kothari and Singwi (3) have reviewed thermal neutron scattering in solids by mass and phonon expansions in an excellent article. The usefulness of mass expansion in obtaining the total neutron scattering cross section (coherent and incoherent), demonstrated first by Placzek (1), has been further established by the recent studies of Marshall and Stuart (4) on polycrystalline materials. Nelkin (5) studied the thermal neutron spectrum in a heavy crystal by using the differential scattering cross section obtained by retaining only the first term of the mass expansion. The phonon expansion is also extensively used in studying thermal neutron scattering. The contribution of multiphonon processes, as proposed by Sjölander (6) and also by Schofield and Hasset (7), is obtained by using the central limit theorem. Parks et.al. (8) have undertaken extensive neutron thermalization studies in graphite by using phonon expansion as developed by Parks (8).

We extend the application of Placzek's mass expansion to obtain integral quantities of interest in the study of neutron thermalization. For a heavy crystal, these results are exact and easy to evaluate numerically.

Once energy transfer moments and their associated integrals are determined, the matrix elements of the scattering operator corresponding to any set of polynomials in energy can be constructed. The use of orthogonal polynomials in the study of neutron thermalization problems, especially in a heavy gas, is very well known. A brief summary of such studies is presented below.

Kottwitz (9) studied the problem of neutron flux in two media having a temperature discontinuity at the interface, by using the heavy gas model. Bailly du Bois, Horowitz, and Maurette (10) employed the Hermite polynomials in the study of neutron thermalization in a heavy gas and hydrogen. Kazarnovsky et. al. (11) used the Laguerre polynomials to study many neutron thermalization problems. Häfele and Dresner (12), Michael (13), and Virkkunen (14) have also applied these polynomials to specific problems of a heavy gas, and Singwi (15) used them in the development of a general theory of diffusion cooling in an arbitrary moderator. Purohit (16,17) has given a general formalism for obtaining eigenvalues associated with a decaying pulse of

neutrons in a finite multiplying or nonmultiplying medium and has considered its extension to the spatial decay of neutrons in an infinite medium. The application of the polynomial method to the study of thermal neutron spectrum problem from a slowing-down source has been recently proposed by the author (18).

Schofield (19) has discussed the application of perturbation theory to the study of the thermal neutron spectrum, using the energy polynomials. Nelkin (20) formulated the variational method with the "neutron temperature" as the variational parameter in estimating thermalization parameters. Corngold and Zamick (21) employed the velocity polynomials as the trial function. Takahashi (22) has undertaken studies of time and space dependent neutron thermalization by the supervariational method. Selengut (23) has discussed applications of the general variational method in the study of a large class of neutron thermalization problems.

All these studies emphasize the importance of matrix elements of the scattering operator in studying neutron thermalization problems. In Appendix I we give expressions for the thermalization parameters - the diffusion cooling coefficient, the thermalization time constant, the diffusion length, the rethermalization area, and the "neutron temperature" - in terms of M_2 (second energy transfer moment weighted by the Maxwellian distribution). Nelkin (20) first introduced M_2 in estimating thermalization parameters by the variational method.

We obtain analytical results for energy transfer moments and their associated integrals for a crystalline scatterer in the incoherent approximation. Numerical results for the first two energy transfer moments for a heavy Debye crystal for various values of θ/T_o (ratio of Debye to thermodynamic temperatures) are presented and discussed. The numerical results of the associated integrals for studying neutron thermalization in a heavy Debye crystal $\left(\frac{\theta}{T_o} = 3.33\right)$ using five associated Laguerre polynomials of any order are given in Table I.

We also discuss the variation of M_2 with the frequency distribution of vibrational modes. A comparative study of M_2 as a function of θ/T_o for Debye and Einstein models and the "Detailed Balance Doppler approximation" (2) for a heavy crystal is presented. It indicates that an Einstein temperature $\xi_o \cong 0.75\theta$ and a fictitious Debye temperature $\theta^* \cong 1.5\,\theta$ for the Doppler approximation would give the same value of M_2 as the exact Debye model over a limited range of binding.

2. MATHEMATICAL DEFINITIONS

The differential scattering cross section in the incoherent approximation is given by the following well-known time integral. (See Sjölander (6)).

$$\frac{d^2\Sigma}{d\Omega dE'} = \frac{\sigma_b N}{8\pi^2}\left(\frac{E'}{E}\right)^{\frac{1}{2}} \int_{-\infty}^{+\infty} \exp\left[i(E'-E)t - \frac{K^2}{2M}\gamma(t)\right] dt \qquad (1)$$

where

E', E = final and initial energy of scattered neutrons

M, m = mass of scattering atom and neutron

$\underline{K}$ = gain in momentum of scattered neutrons in units of $\hbar$

σ_b = bound atom scattering cross section

$\gamma(t)$ = width function - the mean square displacement of scattering atoms in terms of collision time between a neutron and an atom

N = number of scattering atoms per c.c.

For a simple cubic Bravais lattice, $\gamma(t)$ is given by

$$\gamma(t) = -\lambda + \int_{-\infty}^{+\infty} \frac{d\xi\, f(\xi)\, e^{-i\xi t}}{\xi\left(e^{\xi/T_o} - 1\right)} \qquad (2)$$

$f(\xi)d\xi$ is the symmetric frequency distribution of phonons. T_o is the thermodynamic temperature measured in Boltzmann constant units. The symbol λ represents the well-known Debye-Waller factor integral.

$$\lambda = \int_0^\infty \frac{d\xi f(\xi)}{\xi} \coth \frac{\xi}{2T_o} d\xi \tag{3}$$

The kth energy transfer moment $A_k(E)$ is obtained by integrating the differential scattering cross section $d^2\Sigma/d\Omega dE'$ over all angles and final energy.

$$A_k(E) = \int_0^\infty \int_\Omega \frac{d^2\Sigma}{d\Omega dE'} (E'-E)^k \, dE' d\Omega \tag{4}$$

We define mathematically the matrix elements of the scattering operator that correspond to the associated Laguerre polynomials of order α, as follows:

$$F_{mn} = \int_0^\infty L_m^\alpha \left(\frac{E}{T_o}\right) \int_0^\infty M(E,T_o)\,\Sigma_s(E \to E')\, L_n^\alpha \left(\frac{E'}{T_o}\right) dE' dE - \int_0^\infty L_m^\alpha \left(\frac{E}{T_o}\right) L_n^\alpha \left(\frac{E}{T_o}\right) \Sigma_s(E)\, M(E,T_o)\, dE \,. \tag{5}$$

where

$L_m^\alpha(\frac{E}{T_o})$; $L_n^\alpha(\frac{E}{T_o})$ = mth and nth associated Laguerre polynomials of order α and argument $(\frac{E}{T_o})$

$M(E,T_o)$ = Maxwellian distribution of neutrons of energy E at thermodynamic temperature T_o

$\Sigma_s(E \to E')$ = partial scattering cross section obtained from eq. (1) by integrating over all angles

The matrix elements F_{mn} are obtained from the Boltzmann equation, when the energy part of the neutron flux is expanded in a complete set of associated Laguerre polynomials of order α and argument (E/T_o). By using the Detailed Balance theorem and the series representation of Laguerre polynomials in powers of E/T_o, F_{mn} is transformed into

$$F_{mn} = \frac{1}{\sqrt{\binom{m+\alpha}{m}\binom{n+\alpha}{n}}} \left[\sum_{q=1}^{m} \left(\frac{1}{q!}\right)\binom{m+\alpha}{m-\alpha} \left\{ \sum_{r=1}^{n} \sum_{k=1}^{r} \left(-\frac{1}{T_o}\right)^{r+q} \left(\frac{1}{r!}\right) \right.\right. \tag{6}$$

$$\left.\left. \binom{n+\alpha}{n-r}\binom{r}{k} M_{k;q+r-k} \right\} \right] \frac{1}{\Gamma(\alpha+1)}$$

The determination of the matrix elements F_{mn} is thus reduced to the evaluation of a series of integrals of the $M_{k,p}$ type. We define $M_{k,p}$ as the associated integral:

$$M_{k,p} = \int_0^\infty E^p \, M(E,T_o) A_k(E) \, dE \tag{7}$$

In Appendix II we give expressions for matrix elements up to $F_{3,3}$ in terms of $M_{k,p}$. Relations between $M_{k,p}$ with odd values of k

obtained using the Detailed Balance theorem are also given.

Purohit and Rajagopal (2) evaluated $A_k(E)$ and $M_{k,p}$ for the general Doppler approximation case. The width function $\gamma(t)$ for this approximation is of the following form:

$$\gamma(t) = ci^2t^2 + bit - a \tag{8}$$

In the next section we treat the crystalline case by using Placzek's mass expansion formalism.

3. THE CRYSTALLINE CASE (PLACZEK'S MASS EXPANSION)

In Placzek's mass expansion (1), the factor $\exp \frac{k^2}{2M} \gamma(t)$ in eq. (1) is expanded in powers of m/M (the ratio of neutron mass to scattering atom mass). This expansion transforms the differential scattering cross section into an infinite series of powers of m/M. The kth energy transfer moment is obtained from eq. (4) by integrating over-all energies and all angles.

$$A_k(E) = \frac{N\sigma_b}{4E} \sum_{n=1}^{\infty} \left(\frac{m}{M}\right)^n \left(\frac{1}{n+1}\right) \left\{ \sum_{\ell=1}^{n} \frac{(-\lambda)^{n-\ell}}{(n-\ell)!\ell!} \right.$$

$$\left. \prod_{i=1}^{\ell} \int_{-\infty}^{+\infty} \frac{z^k f(\xi_i) F(E,z)}{\xi_i (e^{\xi_i/T_o} - 1)} d\xi_i \right\} \tag{9}$$

where $\Gamma(E,z)$ and z are given by

$$F(E,z) = \left(\sqrt{E+z} + \sqrt{E} \right)^{2n+2} - \left(\sqrt{E+z} - \sqrt{E} \right)^{2n+2} \qquad (10)$$

$$z = \sum_{i=1}^{\ell} \xi_i \qquad (11)$$

To obtain the associated integral $M_{k,p}$, we transform the integral representation of $M_{k,p}$ given by eq. (7), by using the differentiation technique

$$M_{k,p} = \frac{1}{T_o^2} \left[\left(\frac{d}{d-\frac{1}{T'}} \right)^{p} \left\{ \int_0^{\infty} A_k(E)\ E \exp - \frac{E}{T'}\, dE' \right\} \right]_{T'=T_o} \qquad (12)$$

The integral in the above expression is evaluated by using the following result for the Laplace transform [Erdelyi (24)]

$$\int_0^{\infty} \exp - \frac{E}{T'} \left\{ \left(\sqrt{E+z} + \sqrt{E} \right)^{2n+2} - \left(\sqrt{E+z} - \sqrt{E} \right)^{2n+2} \right\} dE$$

$$= 2^{n+2}(n+1)T' \left(\frac{z}{2}\right)^{n+1} \exp \left(\frac{z}{2T'}\right) K_{n+1} \left(\frac{z}{2T'}\right) . \qquad (13)$$

The pth differentiation with respect to $\left(\frac{1}{T'}\right)$ is obtained by using the following recurrence relations for the modified Bessel functions of the second kind, $K_n(y)$, according to Watson (25)

$$\frac{K_{n+1}(y)}{y} = \frac{K_{n+2}(y) - K_n(y)}{2(n+1)} \tag{14}$$

$$K_{n-1}(y) + K_{n+1}(y) = -2K'_n(y) \tag{15}$$

The final result for $M_{k,p}$ is as follows

$$M_{k,p} = \frac{N\sigma_b}{2T_o} \left[\sum_{n=1}^{\infty} \left(\frac{m}{M}\right)^n \sum_{\ell=1}^{n} \frac{(-\lambda)^{n-\ell}}{(n-\ell)!\,\ell!} \right.$$

$$\left. \prod_{i=1}^{\ell} \int_{-\infty}^{+\infty} \frac{f(\xi_i) z^{k+n+1} Y_p(\xi, T_o)}{\xi_i (e^{\xi_i/T_o} - 1)} \, d\xi_i \right] \tag{16}$$

$Y_p(z,T_o)$ is given by

$$Y_p(z,T_o) = \left(\frac{z}{2}\right)^p \exp\left(\frac{z}{2T_o}\right) \left[\sum_{s=0}^{p} \sum_{r=0}^{s} \binom{p}{s} \binom{s}{r} (-1)^{p+s} \right.$$

$$\left. \frac{n+1-s+2r}{2^s (n+1)} K_{n+1-s+2r}\left(\frac{z}{2T_o}\right) \right] \tag{17}$$

It is easy to establish that $M_{k,0}$ with odd values of k are zero. This is consistent with the Detailed Balance theorem. $M_{k,p}$ with odd values of k can be transformed into $M_{k,p}$ with even values of k by using the Detailed Balance theorem to minimize

numerical work. See Appendix II.

4. THE HEAVY CRYSTAL

The analytical results given in section 3 for an arbitrary mass reduce to simple expressions involving single integrals, if only the first term of Placzek's mass expansion is retained. This is the heavy crystal case.

4.1 The Energy Transfer Moments.

The kth energy transfer moment is given by

$$A_k(E) = \frac{\sigma_b m N}{M E^{1/2}} \int_{-\infty}^{+\infty} \frac{\xi^{k-1} f(\xi) (2E+\xi) (E+\xi)^{1/2}}{(e^{\xi/T_o} - 1)} d\xi \qquad (18)$$

For the Debye frequency distribution of phonons, where $f(\xi)d\xi = \frac{3\xi^2}{\theta^3} d\xi$, $A_k(E)$ reduces to

$$A_k(E) = \frac{3\sigma_b m N}{M E^{1/2} \theta^3} \int_{\max(-\theta,-E)}^{+\theta} \frac{\xi^{k+1} (2E+\xi) (E+\xi)^{1/2}}{(e^{\xi/T_o} - 1)} d\xi \qquad (19)$$

θ is the Debye temperature in Boltzmann constant units. For neutron energies lower than the Debye temperature, the lower limit of the integral is equal to -E. $A_k(E)$ for such energies is obtained by numerical integration. However, for neutron energies greater than the Debye temperature, $A_k(E)$ is given by

a rapidly convergent series in powers of $\theta/2E$.

$$A_k(E) = \frac{3\sigma_b T_o^{\,k}}{t^k}\frac{m}{M}N\left[2\left(\frac{E}{\theta}\right)\Phi_{k+1} + 2\Phi_{k+2} + \left(\frac{\theta}{4E}\right)\Phi_{k+3} + \sum_{n=3}(-1)^n \frac{1.1.3\ldots(2n-5)(3-n)}{n!}\left(\frac{\theta}{2E}\right)^{n-1}\Phi_{k+n+1}\right] \quad (20)$$

and

$$\Phi_{k+p} = \int_{-1}^{+1} \frac{\xi^{k+p}}{e^{\xi/t}-1}\,d\xi \quad (21)$$

The integrals Φ_{k+p} are essentially Placzek's integrals (26) for the moments of frequency distribution. These integrals are characterized by the binding parameter t equal to T_o/θ. For very large neutron energies compared to the Debye temperature, the first two terms of the above series are sufficient. The asymptotic expression for the first energy transfer moment is given by

$$A_1(E) = \frac{2\sigma_b m\, T_o}{M}\left[\frac{2T_{eff}}{T_o} - \frac{E}{T_o}\right] \quad (22)$$

which reduces to the free particle value for neutron energy greater than $2T_{eff}$. Conventionally, T_{eff} is defined as

$$T_{eff} = \int_0^\infty \xi\, f(\xi)\coth\frac{\xi}{2T_o}\,d\xi \quad (23)$$

In terms of the Φ_3 integral,

$$\frac{T_{eff}}{T_o} = \frac{3}{2t} \Phi_3(t) \tag{24}$$

In the weak binding limit, the first two energy transfer moments are

$$A_1(E) = \frac{2\sigma_b m N}{M} \left[2T_o \left(1 + \frac{\theta^2}{20T_o^2} \right) - E - \frac{3}{40} \frac{\theta^2}{E} \right] \tag{25}$$

$$A_2(E) = \frac{2\sigma_b m N}{M} \left[2ET_o \left(1 + \frac{\theta^2}{20T_o^2} \right) - \frac{3\theta^2}{5} + \frac{3}{20} \frac{\theta^2 T_o}{E} \right] \tag{26}$$

These expressions reduce to the heavy gas moments for the Debye temperature (θ) equal to zero.

In Figs. 1 and 2, we plot the first energy transfer moment as a function of energy for values of T_o/θ equal to ∞, 0.76, 0.3, 0.25 and 0.10. For energies smaller than the Debye temperature, we note that the magnitude of gain in neutron energy decreases with the increase in binding. Over a large range of energy, this gain in neutron energy is constant. At very low energies, the gain in neutron energy for the crystalline case increases rapidly. As shown in Fig. 1, the first moment is zero at neutron energies equal to $2T_o$, $2.1T_o$, $2.79T_o$, $2.95T_o$ and $3.48T_o$ for T_o/θ equal to ∞, 0.76, 0.3, 0.25 and 0.10, respectively. The

values of T_{eff} for the last four cases are equal to $1.0795T_o$, $1.4944T_o$, $1.6817T_o$, and $3.7694T_o$. It should be noted that the deviation between $2T_{eff}$ and the neutron energy for which the first energy transfer moment is zero increases with the increase in binding. For energies greater than the Debye temperature, the first moment decreases linearly and approaches the asymptotic value given by eq. (22) as shown in Fig. 2. However, it is evident that the asymptotic value is reached at a lower energy for the small binding case.

In Fig. 3, we plot the second energy transfer moment. At very low energies, it increases with the decrease in neutron energy. As the neutron energy is increased, the second moment becomes constant over a wide range of energy, and this range increases with the increase in binding. At high neutron energies, the second energy transfer moment increases rapidly and can be given by the first two terms of eq. (20). It should, however, be noted that the second energy transfer moment does not approach the free particle value, which is proportional to $E^2(\frac{m}{M})^2$. According to eq. (20) this term is absent in the heavy mass case.

4.2 The Associated Integral - $M_{k,p}$.

Retaining the first term in eq. (16), we get the following result for $M_{k,p}$

$$M_{k,p} = \frac{N\sigma_b m}{8T_o M} \sum_{s=0}^{p} \sum_{r=0}^{s} \binom{p}{s} \binom{s}{r} \left(-\frac{1}{2}\right)^{p+s} (2-s+2r)$$

$$\int_{-\infty}^{+\infty} \frac{f(\xi)\,\xi^{k+1} K_{2-s+2r}\left(\frac{\xi}{2T_o}\right)}{\sinh \frac{\xi}{2T_o}}\, d\xi \qquad (27)$$

For the heavy gas case, only $M_{1,p}$ and $M_{2,p}$ contribute, since the higher energy transfer moments are zero.

$$M_{1,p} = -2\sigma_b \frac{m}{M} p(p+1)!\, T_o^{p+1} N \qquad (28)$$

$$M_{2,p} = 4\sigma_b \frac{m}{M} (p+2)!\, T_o^{p+2} N \qquad (29)$$

$M_{k,p}$ is equal to zero for k greater than two.

The integrals given in eq. (27) can be analytically evaluated for the Einstein crystal, since the frequency distribution of phonons is just the Dirac delta function $\delta(\xi-\xi_o)$.

In Table I we give numerical values of $M_{k,p}$ for various values of k and p for the heavy Debye crystal with the ratio of the thermodynamic temperature to the Debye temperature equal to 0.3. This corresponds to the beryllium case with the Debye temperature equal to 1000°K and the thermodynamic temperature equal to 300°K. These results are sufficient to construct a 5x5

matrix of F_{mn}, corresponding to five associated Laguerre polynomials of any order.

The well-known thermalization parameter M_2 introduced by Nelkin (20) is the associated integral $M_{2,0}$. We discuss it in detail in the next section.

4.3 The Thermalization Parameter M_2 or $M_{2,0}$.

The expression for $M_{2,0}$ obtained from eq. (26) is as follows

$$M_{2,0} = \frac{N\sigma_b m}{4T_o M} \int_{-\infty}^{+\infty} \frac{f(\xi)\xi^3 K_2(\frac{\xi}{2T_o})}{\text{Sinh } \frac{\xi}{2T_o}} d\xi \quad . \tag{30}$$

In the weak binding limit, by using the following values of $K_n(\frac{\xi}{2T_o})$ and $\text{Sinh } \frac{\xi}{2T_o}$ for small values of $\frac{\xi}{2T_o}$

$$K_n(\frac{\xi}{2T_o}) = \frac{1}{2}(\frac{\xi}{4T_o})^{-n} \Gamma(n) \tag{31}$$

and

$$\text{Sinh } \frac{\xi}{2T_o} = \frac{\xi}{2T_o} \tag{32}$$

we obtain the heavy gas result for $M_{2,0}$ equal to $\frac{8\sigma_b mNT_o^2}{M}$.

Nelkin (20) gave a curve for M_2 versus θ/T_o between zero and six for the Debye model. In Fig. 4 we extend this result to θ/T_o equal to 10. The evaluation of a single integral is sufficient to obtain M_2, without the numerical integration of the double integral as given by Nelkin.

We also plot M_2 in Fig. 4 for the Einstein model and for the Debye model in the Detailed Balanced Doppler approximation (2) according to the following expressions

$$M_{2,0} = \frac{N\sigma_b m}{2T_o M} \frac{\xi_o^3 K_2(\frac{\xi_o}{2T_o})}{\text{Sinh } \frac{\xi_o}{2T_o}} \qquad \text{Einstein} \tag{33}$$

ξ_o = Einstein temperature in Boltzmann constant units

$$M_{2,0} = 12N\sigma_b \frac{m}{M} \frac{T_o^2}{t} \left[\Phi_3(2t) - \Phi_3(t)\right] \qquad \text{Ref. (2)} \tag{34}$$

Comparison of these curves yields the following observations:

(1) The value of M_2 obtained by using the Debye model can be given by an Einstein model by assuming the Einstein temperature ξ_o to be $\cong 0.75\theta$ over a limited range of binding.

(2) Over almost the same range, the Detailed Balance Doppler approximation also gives the same value of M_2 as the exact Debye model, provided an effective Debye temperature $\theta^* \cong 1.5\theta$ is used.

The range over which the above statements hold good is apparent from Fig. 4.

In Fig. 5 we plot $\frac{M_2}{8N\sigma_b T_o^2 \frac{m}{M}}$ versus $(\frac{T_{eff}}{T_o} - 1)$ for the

Einstein and Debye models. In Table II we give $\frac{T_{eff}}{T_o}$ for these models. From these results, it is evident that the variation of M_2 is not strongly dependent upon the detailed knowledge of the frequency distribution of phonons for binding corresponding to $\frac{\theta}{T_o} \lesssim 4.0$.

It is interesting to note that two important moderators, beryllium and beryllium-oxide, are covered in this binding range at room temperature. Beryllium and beryllium-oxide have Debye temperatures of 1000°K and 1200°K, and Einstein temperatures of 740°K and 900°K, respectively. Taking thermodynamic temperatures equal to 300°K, $\frac{M_2}{8\sigma_b T_o^2 \frac{m}{M} N}$ in both models (Einstein and Debye) is equal to 0.585 for beryllium and 0.47 for beryllium-oxide. The fictitious Debye temperatures for beryllium and beryllium-oxide to be used in the Doppler approximation calculations may be taken to be 1500°K and 1800°K, respectively.

The Einstein model and the Doppler approximation can be applied to correct the results obtained from the heavy crystal case due to higher terms in the mass expansion. The value of M_2 decreases by 28% for beryllium, and by 20% for beryllium-oxide when estimated by using the Einstein model and terms up to $(\frac{m}{M})^3$ in Placzek's mass expansion. When the Doppler approximation is used, corrections for beryllium and beryllium-oxide are about 22% and 14% respectively. It should be pointed out that these

corrections are very large and therefore cannot be neglected in the estimation of M_2 for beryllium and even for beryllium-oxide.

5. CONCLUSIONS

We have demonstrated in this paper the usefulness of Placzek's mass expansion in obtaining energy transfer moments, associated integrals, and the matrix elements of the scattering operator corresponding to a set of polynomials of energy variables. For a heavy crystal, these quantities are given by single integrals involving the frequency distribution of vibrational modes, which can be easily evaluated. The importance of the first few energy transfer moments is evident if the integral scattering operator is replaced by a differential operator. The detailed discussion of the first energy transfer moment for a heavy Debye crystal indicates that the gain in neutron energy decreases as the binding increases but takes place over a large range of energy. At high energies, the loss of energy takes place linearly, and the deviation from the free particle value is governed by the effective temperature corresponding to that binding.

A detailed comparative study of M_2 indicates that the variation of M_2 with the frequency distribution of vibrational modes is insensitive over the binding range $\frac{\theta\,(\text{Debye})}{T_o\,(\text{Thermodynamic})} \leq 4$. A correctly chosen binding parameter would give the same value

of M_2. To obtain the same results with the Einstein model as the Debye model, an Einstein temperature $\xi_o \simeq 0.75\theta$ should be chosen. Similarly, the Detailed Balance Doppler approximation gives the same value of M_2 as the exact Debye model, provided an effective Debye temperature $\theta^* \cong 1.5\theta$ is used. These observations should prove useful in evaluating the contribution of higher terms in Placzek's expansion and even in the determination of integral quantities for moderators like beryllium and beryllium-oxide.

REFERENCES

1. G. Placzek, PHYS. REV. 93, 895 (1954) ibid 105, 1240 (1957).
2. S. N. Purohit and A. K. Rajagopal "Scattering of thermal neutrons in the Doppler approximation," to be published in NUCL. SCI. & ENG.
3. L. S. Kotnari and K. S. Singwi, SOLID STATE PHYS. 8, 110 (1959) Academic Press, New York.
4. W. Marshall and R. N. Stuart
   a) Inelastic scattering of neutrons in solids and liquids, IAEA publication in Vienna Conference (1961).
   b) Scattering of neutrons from polycrystalline materials, UCRL-5568, April 8, 1959.
5. M. S. Nelkin, NUCL. SCI.& ENG. 2, 199 (1957).

6. A. Sjölander, ARKIV FOR FYSIK 14, 315 (1958).

7. P. Schofield and Hasset, Proc. 2nd Geneva Conf. Vol. 16, 217 (1958).

8. D. E. Parks, "The calculation of thermal neutron scattering kernels in graphite," GA-2438 (Oct. 1961).

D. E. Parks, J. R. Beyster and N. F. Wikner, "Thermal neutron spectra in graphite," GA-2437 (Sept. 1961).

9. D. A. Kottwitz, BULL. AM. PHYS. SOC. Ser. II, 3, 1 (1958). NUCLEAR SCI. & ENG. 7, 345 (1960).

10. B. Bailly du Bois, J. Horowitz and C. Maurette, "Thermalization of neutrons," Saclay report S.P.M. (525) (Dec. 1958).

11. M. V. Kazarnovsky et. al., Proc. 2nd Geneva Conf. Vol.16, 270 (1958).

12. W. Häfele and L. Dresner, NUCLEAR SCI. & ENG. 7, 304 (1960).

13. P. Michael, NUCLEAR SCI. & ENG. 8, 426 (1960).

14. J. Virkkunen, ANNALES ACADEMICA SCIENTIARUM FENNICE, Helsinki VI, PHYSICS Ser. A, 43 (1960).

15. K. S. Singwi, ARKIV FOR FYSIK 16, 385 (1960).

16. S. N. Purohit, NUCLEAR SCI. & ENG. 9, 157 (1961).

17. S. N. Purohit, "The spatial decay of neutrons in infinite medium," BNL memorandum , Published Sept. 1960.

18. S. N. Purohit, "Application of the polynomial method in the study of thermal neutron spectrum in a heavy crystalline

medium," to be presented at the ANS meeting, Boston, June 1962.

19. P. Schofield, "The calculation of thermal neutron spectra by perturbation theory," AERE R-3400, Harwell (1960).

20. M. S. Nelkin, J. NUCLEAR ENERGY 3, 48 (1958).

21. N. Corngold and L. Zamick, Trans. Am. Nuclear Soc. 3, 504 (1960).

22. H. Takahashi, "Supervariational method for thermalization problem," BNL memorandum (Aug. 14, 1961).

23. D. S. Selengut, "Variational methods in neutron thermalization," Proc. Joint RPI-ANS Symposium of May 1961, Academic Press (1962).

24. A. Erdelyi et. al. "Tables of integral transforms," Bateman Series Vol. 1, McGraw-Hill (1954).

25. G. N. Watson, "A treatise on the theory of Bessel functions," Cambridge Univ. press, London (1945).

26. G. Placzek, PHYS. REV. 86, 377 (1952).

ACKNOWLEDGEMENTS

The author would like to express his appreciation to Jack Chernick and Noel Corngold for their interest in this study. The help given by W. Bornstein in carrying out part of the numerical calculations is also appreciated.

TABLE I

ASSOCIATED INTEGRALS $M_{k,p}$ FOR A HEAVY DEBYE CRYSTAL

$$\frac{T_o}{\theta} = 0.3 \text{ IN UNITS OF } 3\sigma_b \frac{m}{M} \frac{\theta^{k+p+2}}{T_o^{\,2}}$$

p \ k	1	2	3	4	5
0	0	1.247×10^{-2}	0	6.674×10^{-3}	0
1	-6.277×10^{-3}	1.310×10^{-2}	-3.376×10^{-3}	7.238×10^{-3}	-2.211×10^{-3}
2	-1.312×10^{-2}	1.850×10^{-2}	-7.260×10^{-3}	1.057×10^{-2}	-4.915×10^{-3}
3	-2.608×10^{-2}	3.144×10^{-2}	-1.473×10^{-2}	1.841×10^{-2}	-1.014×10^{-2}
4	-5.563×10^{-2}	6.190×10^{-2}	-3.185×10^{-2}	3.688×10^{-2}	-2.200×10^{-2}
5	-1.293×10^{-1}	1.380×10^{-1}	-7.478×10^{-2}	8.309×10^{-2}	-5.228×10^{-2}
6	-3.400×10^{-1}	3.502×10^{-1}	-1.980×10^{-1}	2.129×10^{-1}	-
7	-9.703×10^{-1}	0.790×10^{-1}	-7.023×10^{-1}	-	-
8	- 3.043	3.022	-	-	-
9	-10.398	-	-	-	-

TABLE II

EFFECTIVE TEMPERATURE

Debye Model		Einstein Model	
θ/T	$\frac{T_{eff}}{T_o}$	$\frac{\xi_o}{T_o}$	$\frac{T_{eff}}{T_o}$
0	1.0	0	1.00
0.40	1.00798	0.40	1.013
0.50	1.01246	0.80	1.0528
0.667	1.02211	1.60	1.2048
1.000	1.04946	2.00	1.3130
1.667	1.13453	2.40	1.4394
2.000	1.19113	2.80	1.58129
2.500	1.29165	3.20	1.73598
3.333	1.49441	3.60	1.90113
4.000	1.68174	4.0	2.0746
5.000	1.99259	4.8	2.43983
6.000	2.34027	6.0	3.0149
6.667	2.559	7.0	3.5064
8.000	3.038	8.0	4.003
10.000	3.76935	10.0	5.00

APPENDIX I - THERMALIZATION PARAMETERS (16-18)

By expanding the energy part of the neutron flux in the Boltzmann equation in a set of orthogonal polynomials (associated Laguerre), three specific problems of neutron thermalization can be studied.

1) The decay of a pulse of neutrons in a finite or infinite moderator.
2) The spatial decay of neutrons in an infinite medium.
3) The thermal neutron spectrum in an infinite medium from a slowing down source.

The neutron flux $\Phi(E,r,t)$ as a function of energy (E), space (r) and time (t) variables is expanded as follows:

$$\Phi(E,r,t) = \sum_{p} \psi_p(r) \sum_{i} e^{\lambda_{ip} t} \sum_{n=0} a_{nip} L_n^{1/2}\left(\frac{E}{T_o}\right) M(E,T_o)$$

(Time dependent) (1)

$$\Phi(E,r) = \sum_{i} e^{-\lambda_i r} \sum_{n=0} a_{ni} L_n^{1}\left(\frac{E}{T_o}\right) M(E,T_o)$$

(Space dependent) (2)

$$\Phi(E) = \sum_{n=0} a_n L_n^{1}\left(\frac{E}{T_o}\right) M(E,T_o) \quad \text{(Thermal neutron spectrum)} \quad (3)$$

We give below the expressions for the following thermalization parameters - the diffusion cooling coefficient (c_0), the thermalization time constant (t_{th}), the diffusion length (L_0), the rethermalization area (L_1^2) and the "neutron temperature" T_n. The parameters c_0 and t_{th} occur in the pulsed neutron problem; L_0 and L_1^2 are obtained from the zeroth and first eigenvalues associated with the spatial decay of neutrons. The "neutron temperature" T_n may be considered as a measure of the displacement of thermal neutron spectrum peak due to absorption.

1. Diffusion cooling coefficient (c_0) (16)

$$c_0 = \frac{3\ D_{01}^{\ 2}\sqrt{\pi}}{2\ M_{2,0}} \tag{4}$$

using two polynomials where

$$D_{01} = \int_0^\infty L_0^{\frac{1}{2}} \left(\frac{E}{T_o}\right)\ L_1^{\frac{1}{2}}\left(\frac{E}{T_o}\right)\ D(E)\ M(E,T_o)\,dE\ .$$

2. Thermalization time constant (t_{th}) (16)

$$t_{th} = \frac{3\sqrt{\pi}}{M_{2,0}} \left[\left(1 + \frac{F_{22}}{F_{11}}\right) - \left\{ \left(1 - \frac{F_{22}}{F_{11}}\right)^2 + 4\ \frac{F_{12}^{\ 2}}{F_{11}^{\ 2}} \right\}^{\frac{1}{2}} \right]^{-1} \tag{5}$$

using three polynomials.

See Appendix II. $F_{m,n}$ is corresponding to α equal to $\frac{1}{2}$.

3. Diffusion length (L_0) (17)

For 1/v absorption law and the constant diffusion coefficient, in L_1^1 approximation

$$\frac{1}{L_0^2} = \left(\frac{1}{L^2}\right)_{00} \left[1 - \frac{\Delta\sqrt{\pi}}{16}\,\frac{\xi\Sigma_{s0}}{M_{2,0}}\right] \tag{6}$$

4. Rethermalization area (L_1^2) (17)

$$\frac{1}{L_1^2} = \left(\frac{1}{L^2}\right)_{00} \frac{8}{\Delta\sqrt{\pi}} \left[\frac{M_{2,0}}{4\xi\Sigma_{s0}} + \frac{7\sqrt{\pi}\,\Delta}{64} + \frac{\pi\Delta^2\xi\Sigma_{s0}}{128M_{2,0}}\right] \tag{7}$$

where

$$\Delta = \frac{4\Sigma_{a0}}{\xi\Sigma_{s0}} \quad \text{and} \quad \Sigma_a(E) = \frac{\Sigma_{a0}}{E^{1/2}}\,.$$

5. "Neutron temperature" T_n or ratio a_1/a_0 (18)

In L_1^1 approximation, the ratio of coefficients a_1/a_0 is equal to $-\sqrt{2}\left(\frac{T_n - T_o}{T_o}\right)$, if the neutron flux is given by $M(E,T_n)$ with T_n as the neutron temperature. For 1/v absorption law,

$$\frac{T_n - T_o}{T_o} = \frac{\left[\frac{S_1}{S_0} - \frac{3}{2} \right]}{\left[\frac{S_1}{2S_0} + \frac{3}{4} + \frac{2.257 M_{2,0}}{\Delta\xi \Sigma_{s0}} \right]} = - \frac{a_1}{a_0 \sqrt{2}}$$

S(E) is the slowing down source.

$$\int_0^\infty S(E) \left(\frac{E}{T_o} \right) dE = \frac{S_1}{S_0} \quad .$$

APPENDIX II - MATRIX ELEMENTS AND ASSOCIATED INTEGRALS

1. Associated integrals $M_{k,p}$

By using the Detailed Balance theorem, $M_{k,p}$ with odd values of k are transformed into $M_{k,p}$ with even values of k.

$$M_{k,0} = 0 \tag{1}$$

$$M_{k,1} = - \frac{M_{k+1,0}}{2} \tag{2}$$

$$M_{k,2} = - M_{k+1,1} \tag{3}$$

$$M_{k,3} = - \frac{3}{2} M_{k+1,2} + \frac{1}{4} M_{k+3,0} \tag{4}$$

$$M_{k,4} = - 2 M_{k+1,3} + M_{k+3,1} \tag{5}$$

$$M_{k,5} = \frac{1}{2} \left[- M_{k+5,0} + 5 M_{k+3,2} - 5 M_{k+1,4} \right] \tag{6}$$

2. Matrix elements $F_{m,n}$

$$F_{0n} = F_{n0} = 0 \qquad \text{For all } n \qquad (1)$$

$$F_{1,1} = -\frac{M_{2,0}}{2\sqrt{(\alpha+2)}} \qquad (2)$$

$$F_{2,1} = F_{1,2} = \frac{\sqrt{2}}{\left[\sqrt{(\alpha+2)}\ \sqrt{(\alpha+3)}\right]^{1/2}}\left[-\frac{(\alpha+2)M_{2,0}}{2} + \frac{M_{2,1}}{2}\right] \qquad (3)$$

$$F_{2,2} = \frac{2}{\sqrt{(\alpha+3)}}\left[-\frac{(\alpha+2)^2 M_{2,0}}{2} + (\alpha+2)M_{2,1} - \frac{M_{2,2}}{2} + \frac{M_{4,0}}{8}\right] \qquad (4)$$

$$F_{3,1} = F_{1,3} = \frac{\sqrt{6}}{\left(4\sqrt{(\alpha+2)}\ \sqrt{(\alpha+4)}\right)^{1/2}}\left[\frac{(\alpha+3)(\alpha+2)M_{2,0}}{2} - (\alpha+3)M_{2,1} + \frac{M_{2,2}}{2} - \frac{M_{4,0}}{12}\right] \qquad (5)$$

$$F_{3,2} = F_{2,3} = \frac{\sqrt{12}}{\left(\sqrt{(\alpha+4)}\ \sqrt{(\alpha+3}\right)^{1/2}}\left[-\frac{(\alpha+3)(\alpha+2)^2 M_{2,0}}{4} + \frac{3(\alpha+3)M_{2,1}}{4} - \frac{2(\alpha+3)+(\alpha+2)M_{2,2}}{4} + \frac{M_{2,3}}{4} + \frac{3(\alpha+3)+(\alpha+2)M_{4,0}}{24} - \frac{M_{4,1}}{6}\right] \qquad (6)$$

$$F_{3,3} = \frac{6}{\sqrt{(\alpha+4)}}\left[-\frac{(\alpha+3)^2(\alpha+2)^2 M_{2,0}}{8} + \frac{(\alpha+3)^2(\alpha+2)M_{2,1}}{2}\right] \qquad (7)$$

Eq. (7) continued

$$- \frac{(\alpha+3)(3\alpha+8)M_{2,2}}{4} + \frac{(\alpha+3)M_{2,3}}{2} - \frac{M_{2,4}}{8}$$

$$+ \frac{(\alpha+3)(4\alpha+11)M_{4,0}}{24} - \frac{(\alpha+3)M_{4,1}}{3} + \frac{M_{4,2}}{6}$$

$$- \frac{5\,M_{6,0}}{144} \Big] .$$

Note: $\overline{|\,(\ )}$ represents $\Gamma(\ )$

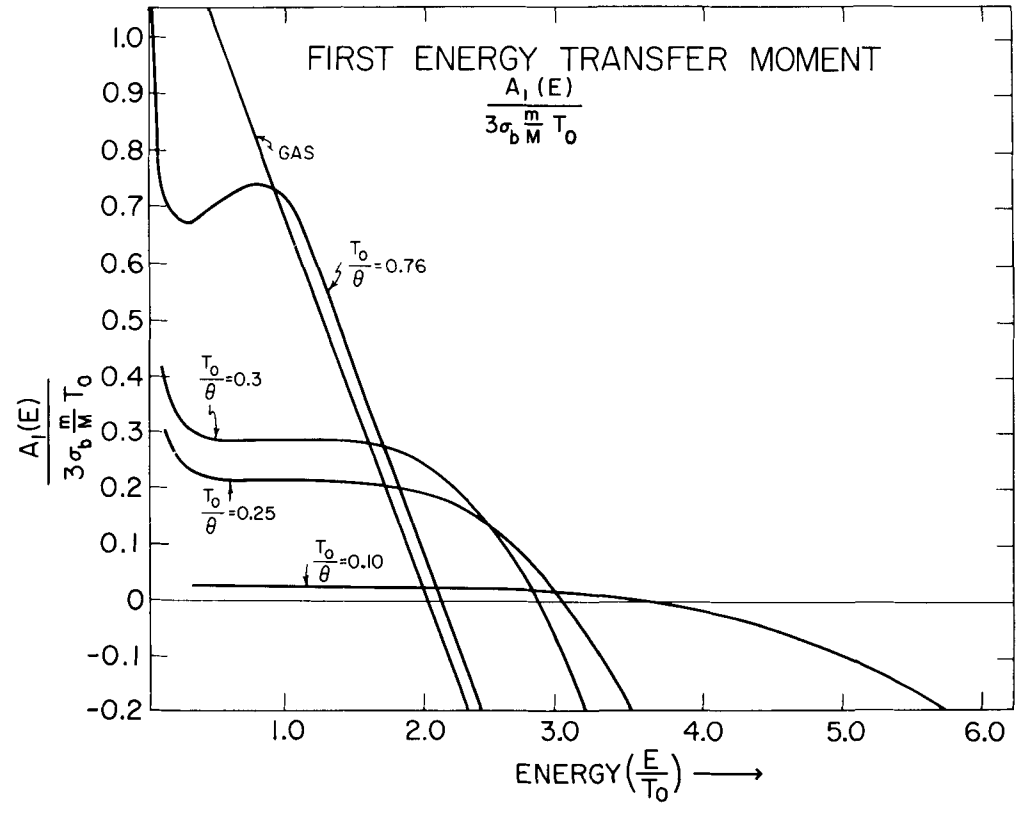
FIRST ENERGY TRANSFER MOMENT
$\frac{A_1(E)}{3\sigma_b \frac{m}{M} T_0}$
GAS
$\frac{T_0}{\theta}$=0.76
$\frac{T_0}{\theta}$=0.3
$\frac{T_0}{\theta}$=0.25
$\frac{T_0}{\theta}$=0.10
1.0
0.9
0.8
0.7
0.6
0.5
0.4
0.3
0.2
0.1
0
-0.1
-0.2
1.0
2.0
3.0
4.0
5.0
6.0
ENERGY$(\frac{E}{T_0})$ ⟶

Fig. 1

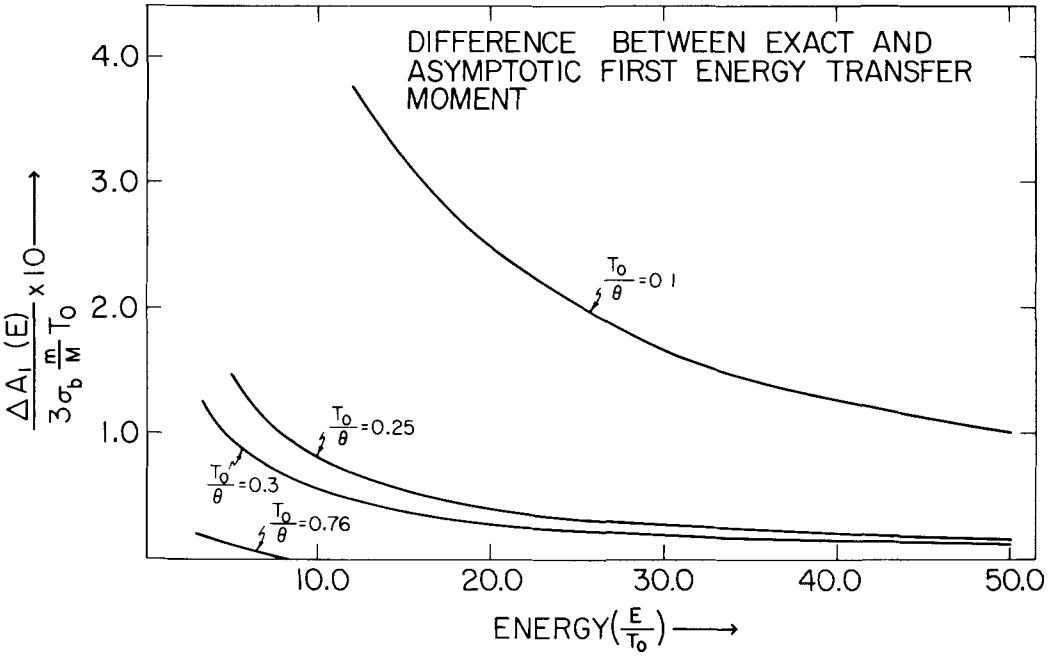
DIFFERENCE BETWEEN EXACT AND ASYMPTOTIC FIRST ENERGY TRANSFER MOMENT
$\frac{\Delta A_1(E)}{3\sigma_b \frac{m}{M} T_0} \times 10$ ⟶
$\frac{T_0}{\theta}$=0.1
$\frac{T_0}{\theta}$=0.25
$\frac{T_0}{\theta}$=0.3
$\frac{T_0}{\theta}$=0.76
4.0
3.0
2.0
1.0
10.0
20.0
30.0
40.0
50.0
ENERGY$(\frac{E}{T_0})$ ⟶

Fig. 2

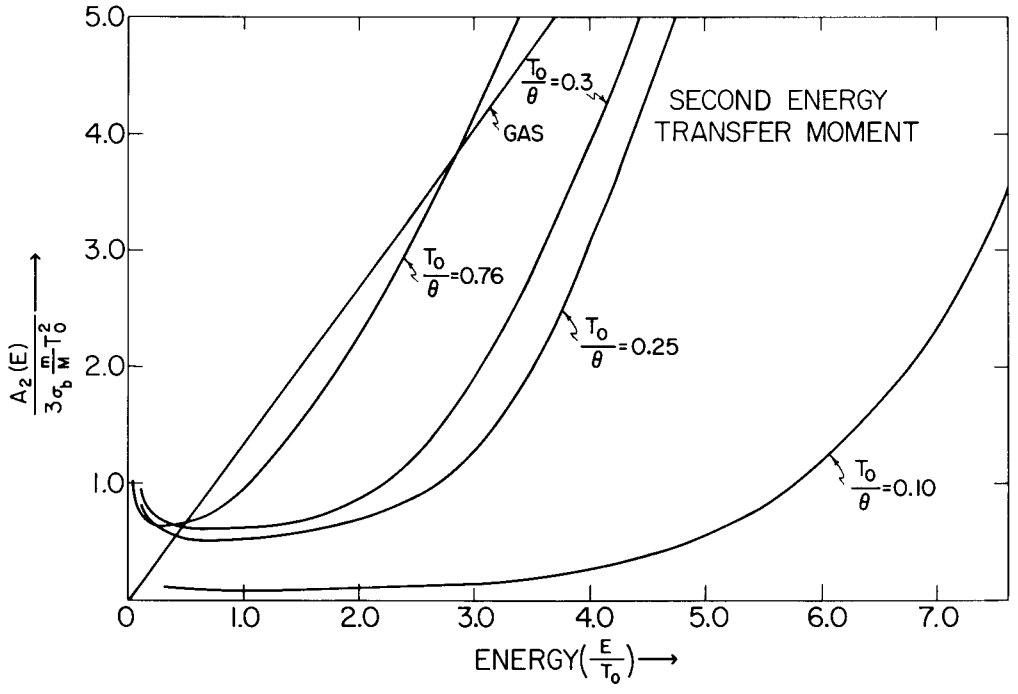
SECOND ENERGY TRANSFER MOMENT
$\frac{T_0}{\theta}$=0.3
GAS
$\frac{T_0}{\theta}$=0.76
$\frac{T_0}{\theta}$=0.25
$\frac{T_0}{\theta}$=0.10
$\frac{A_2(E)}{3\sigma_b \frac{m}{M} T_0^2}$
ENERGY($\frac{E}{T_0}$)

Fig. 3

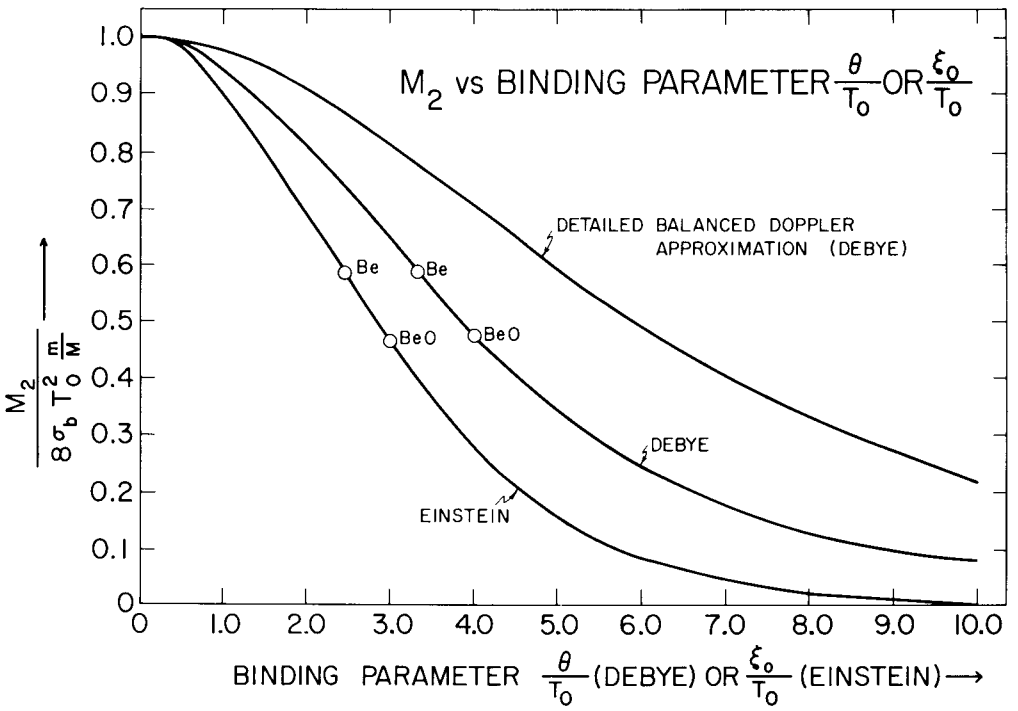
M_2 vs BINDING PARAMETER $\frac{\theta}{T_0}$ OR $\frac{\xi_0}{T_0}$
DETAILED BALANCED DOPPLER APPROXIMATION (DEBYE)
Be
Be
BeO
BeO
DEBYE
EINSTEIN
$\frac{M_2}{8\sigma_b T_0^2 \frac{m}{M}}$
BINDING PARAMETER $\frac{\theta}{T_0}$ (DEBYE) OR $\frac{\xi_0}{T_0}$ (EINSTEIN)

Fig. 4

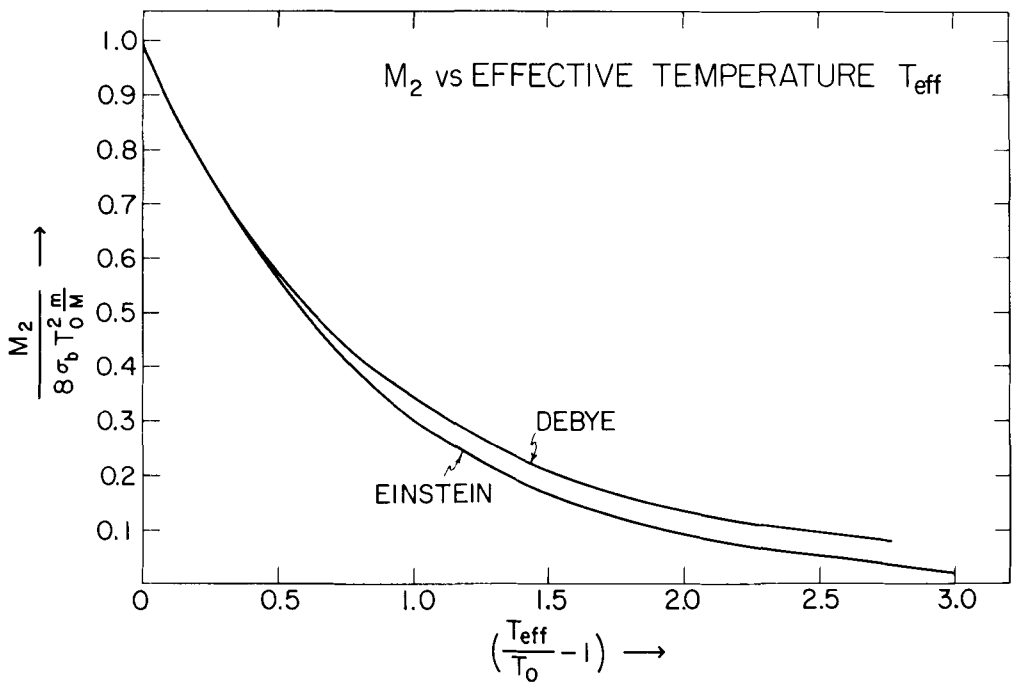
M_2 vs EFFECTIVE TEMPERATURE T_{eff}
DEBYE
EINSTEIN
$\frac{M_2}{8\sigma_b T_0^2 \frac{m}{M}} \longrightarrow$
$\left(\frac{T_{eff}}{T_0} - 1\right) \longrightarrow$
1.0
0.9
0.8
0.7
0.6
0.5
0.4
0.3
0.2
0.1
0
0.5
1.0
1.5
2.0
2.5
3.0

Fig. 5

BROOKHAVEN NATIONAL LABORATORY

Conference on Neutron Thermalization

April 30 - May 2, 1962

Scattering of Thermal Neutrons in the Doppler Approximation*

S. N. Purohit and A. K. Rajagopal**

Brookhaven National Laboratory
Upton, New York

*Research performed under the auspices of the U. S. Atomic Energy Commission.

**Research Assistant, Summer 1961. Present address: Division of Applied Physics and Engineering, Harvard University, Cambridge 38, Massachusetts.

ABSTRACT

A general mathematical formalism for the energy transfer moments and their associated integrals, useful in the study of neutron thermalization, is presented. This formalism has been employed to obtain these quantities for the "general Doppler approximation" case, which represents a large number of approximations that belong to the Doppler class. An exact formula for M_2 (the second energy transfer moment weighted by the Maxwellian distribution) is given in terms of binding parameters for the general Doppler case. A new, useful Doppler approximation, which satisfies the Detailed Balance theorem and is based upon the Debye-Waller factor and the specific heat integral, is also formulated. A comparative study has been undertaken of this and three other previously known Doppler cases (the monatomic gas model, the effective temperature, and the Krieger-Nelkin approximations for rotating molecules) in terms of the validity of the Detailed Balance theorem and the asymptotic scattering behavior. Numerical results based upon the Debye frequency distribution of vibrational modes in the Doppler approximation are presented.

1. INTRODUCTION

We present an analytical study of thermal neutron scattering in the Doppler approximation, which is generalized in this paper. The mean square displacement of scattering atoms in the "general Doppler approximation" is expressed quadratically in terms of the collision time between a neutron and an atom. With the help of Van Hove's scattering formalism (1). the energy transfer moments and their associated integrals useful in the study of neutron thermalization are determined.

A new approximation that belongs to the Doppler class and is useful for studying thermal neutron scattering is formulated. Since the scattering law in this approximation satisfies the Detailed Balance theorem, we term it the "Detailed Balanced Doppler approximation." It is based upon two integral physical parameters – the Debye-Waller factor and the specific heat integral. The former is given by the zero point mean square displacement of scattering atoms and the latter by the second moment of the frequency distribution of vibrational modes in the scattering system. The neutron or x-ray scattering data give the Debye-Waller factor, and the specific heat experiments give the specific heat integral.

Three other cases, well known in the literature, also belong to the Doppler class: the monatomic gas model, the effective temperature or T_{eff}

approximation based upon Lamb's paper (2), and the Krieger-Nelkin approximation (3) for rotating molecules. A comparative study of these four Doppler cases from the standpoint of the Detailed Balance theorem and the asymptotic scattering behavior has been undertaken.

In a previous paper, Purohit (4) has shown the importance of energy transfer moments and their associated integrals in the study of time-dependent neutron thermalization. By using the same formalism, the usefulness of these quantities in space-dependent (5) and thermal neutron spectrum problems can be demonstrated. This formalism is based upon expanding the energy part of the neutron flux in the Boltzmann equation in a complete set of associated Laguerre polynomials of order one. In another paper submitted to this by Purohit (5) expressions for thermalization parameters (the thermalization time constant, the diffusion cooling coefficient, the diffusion length, the rethermalization area and the "neutron temperature") are given in terms of M_2 (the second energy transfer moment weighted by the Maxwellian distribution). Nelkin (6) first pointed out the importance of M_2 in estimating thermalization parameters, using the variational method based upon the neutron temperature concept. Recently, Selengut (7) has stressed its importance in a large class of neutron thermalization problems, using the general variational method. In this paper, we give analytical expressions for M_2 and other associated integrals for the "general Doppler approximation" in terms of binding parameters.

Numerical results for M_2 for various masses and for the incoherent scattering cross section of beryllium in the Doppler approximation are also given.

2. THE GENERAL FORMALISM

The differential scattering cross section in Van Hove's scattering formalism (1) is expressed by the double Fourier transform with respect to space and time of the correlation function. In the absence of interference, this function is given by the self correlation function $G_s(\underline{r},t)$. Classically, $G_s(\underline{r},t)$ defines the probability of finding a particle at position $\underline{r}$ at time t, when at time t equal to zero, the particle was at the origin. If the spatial variation of $G_s(\underline{r},t)$ is assumed to be given by the Gaussian distribution with the width $\gamma(t)$, then the differential scattering cross section can be expressed as follows:

$$\frac{d^2\sigma}{d\Omega dE} = \frac{\sigma_b}{4\pi} \left(\frac{k'}{k_0}\right) \int_{-\infty}^{+\infty} \exp i(E'-E)t + \frac{K^2}{2M}\gamma(t)dt \qquad (1)$$

where

σ_b = bound atom scattering cross section,

k', k_0 = final and initial momentum wave vectors of scattered neutrons in units of $\hbar$,

$K^2 = k'^2 + k_0^2 - 2k' \cdot k_0$,

m,M = mass of neutron and scattering particle respectively,

E',E = final and initial energy of scattered neutrons,

$\gamma(t)$ = width function in terms of collision time t between the neutron and the scattering particle.

The above expression holds rigorously for crystals and gases. For liquids, it is valid only if $G_s(\underline{r},t)$ can be represented by the Gaussian spatial distribution at all collision times. As discussed by Vineyard (8), the Gaussian representation is valid for short and long collision times. At short times, the behavior of atoms can be represented by a gas, and at long times, it can be given by the diffusing type behavior. If the results obtained in this study are applied to liquids, then it must be assumed that the Gaussian representation is valid at intermediate collision times as well.

We introduce two integral quantities, $A_k(E)$, the k^{th} energy transfer moment, and the associated integral $M_{k,p}$. The latter is obtained from the k^{th} energy transfer moment by multiplying with the Maxwellian distribution and E^p and integrating over energy. Mathematically these integrals are expressed in the following manner:

$$A_k(E) = \int_{\Omega} \int_{o}^{\infty} \frac{d^2\sigma}{d\Omega dE} (E' - E)^k \, dE' d\Omega \tag{2}$$

$$M_{k,p} = \frac{1}{T^2} \int_{o}^{\infty} E^{p+1} \exp - \frac{E}{T} A_k(E) dE \, . \tag{3}$$

In the above equation, T is the thermodynamic temperature of the system. The associated integrals $M_{k,p}$ are very useful in the study of

neutron thermalization. The relation between $M_{k,p}$ and $F_{m,n}$ (the matrix elements of the scattering operator) introduced in the study of time and space dependent neutron thermalization is given in reference (5). By putting k equal to two and p equal to zero, $M_{k,p}$ reduces to the thermalization parameter M_2.

The three quantities defined by Eqs. (1), (2), and (3) depend upon the knowledge of the width function $\gamma(t)$. This is determined by the dynamics of atomic motion. For a simple cubic Bravais lattice, $\gamma(t)$ is very well known. See Kothari and Singwi (9) and also Sjölander (10).

$$\gamma(t) = -\int_0^\infty \frac{f(\xi)}{\xi} \coth \frac{\xi}{2T}\, d\xi + \int_0^\infty \left[\coth \frac{\xi}{2T} \cos \xi t + i \sin \xi t\right] \frac{f(\xi)}{\xi}\, d\xi . \tag{4}$$

Alternatively, we can also write

$$\gamma(t) = -\int_0^\infty \frac{f(\xi)}{\xi} \coth \frac{\xi}{2T}\, d\xi + \int_0^\infty f(\xi) \frac{\cos \xi(t-i/2T)}{\xi \sinh \xi/2T}\, d\xi . \tag{5}$$

$f(\xi)d\xi$ is the frequency distribution of vibrational modes. The two above expression for $\gamma(t)$ are identical, if retained intact. However, if $\gamma(t)$ is expressed in powers of t and (t-i/2T) and a finite number of terms are retained, then the two expansions are not equivalent. The expansion of $\gamma(t)$ in powers of (t-i/2T) according to Eq. (5) satisfies the Detailed Balance

theorem, but does not give correct high energy scattering cross section. Conversely, the expansion in t makes $\gamma(t)$ violate the Detailed Balance theorem, but gives the correct asymptotic scattering cross section.

The validity of the Detailed Balance theorem demands that $\gamma(t)$ and $\gamma(-t+i/T)$ be equal. This follows from the well-known property of "imaginary time translational invariance" used extensively in statistical mechanics. The expansion of $\gamma(t)$ in powers of $(t-i/2T)$ does not violate this invariance, but the expansion in t does.

It is also very well known that the asymptotic scattering behavior is governed by the zeroth moment and the first moment theorems for the scattering law, as given by Placzek (11). It is easy to show that the scattering law obtained from the t expansion satisfies these theorems, but the $(t-i/2T)$ expansion does not give correct results.

Several authors discussed various time expansions at the Vienna conference on the inelastic scattering of neutrons in solids and liquids; see Nelkin, Egelstaff, and Schofield (12). Egelstaff proposed the (t^2+it) variable time expansion. The application of this expansion in the determination of neutron scattering law has been investigated by Schofield. Recently, Egelstaff and Schofield (13) have studied the scattering law by using the steepest descent method.

Let us substitute τ for (t-i/2T). The differential scattering cross section in τ-notation is given by

$$\frac{d^2\sigma}{d\Omega dE'} = \frac{\sigma_b}{4\pi}\left(\frac{k'}{k_0}\right)\left[\int_{-\infty}^{+\infty} \exp i(E'-E)\left(\tau+\frac{i}{2T}\right) + \frac{K^2}{2M}\gamma\left(\tau+\frac{i}{2T}\right)d\tau\right] \tag{6}$$

also

$$(E'-E)^k \frac{d^2\sigma}{d\Omega dE'} = \frac{\sigma_b}{4\pi}\left(\frac{k'}{k_0}\right)\frac{1}{i^k}\left[\int_{-\infty}^{+\infty}\left(\frac{d}{d\eta}\right)^k \exp i(E'-E)(\tau+\eta)\right.$$

$$\left. + \frac{K^2}{2M}\gamma\left(\tau+\frac{i}{2T}\right) d\tau\right]_{\eta=i/2T} \tag{7}$$

The differentiation technique to obtain energy transfer moments is widely used in the literature. We integrate Eq. (7) over all angles and final energy. The expression for $A_k(E)$ reduces to the k^{th} differentiation of a single τ-integral. The intermediate steps are omitted here.

$$A_k(E) = \frac{\sigma_b}{4\sqrt{\pi E}\, i^k}\left[\left(\frac{d}{d\eta}\right)^k \int_{-\infty}^{+\infty} \frac{\exp -\dfrac{E(\tau+\eta)^2}{\rho(\tau,\eta)}}{[\rho(\tau,\eta)]^{3/2}}\, d\tau\right]_{\eta=i/2T} \tag{8}$$

Similarly, for $M_{k,p}$ by interchanging the order of τ and E integrations and introducing differentiation technique, we obtain

$$M_{k,p} = \frac{\sigma_b}{8T^2 i^k}\left[\left(\frac{d}{d-\dfrac{1}{T'}}\right)^p \left\{\left(\frac{d}{d\eta}\right)^k \int_{-\infty}^{+\infty} \frac{d\tau}{\left[\dfrac{\rho(\tau,\eta)}{T'} + (\tau+\eta)^2\right]^{3/2}}\right\}_{\eta=i/2T}\right]_{T'=T} \tag{9}$$

$\rho(\tau,\eta)$ appearing in the above equations are given in terms of the width function.

$$\rho(\tau,\eta) = -[i(\tau+\eta) + \frac{m}{M}\gamma(\tau+\frac{i}{2T})] . \tag{10}$$

We define τ-integrals appearing in Eqs. (8) and (9) by functions $F(E,\eta)$ and $G(\eta,T')$ respectively.

$$F(E,\eta) = \frac{\sigma_b}{4\sqrt{\pi E}} \int_{-\infty}^{+\infty} \frac{\exp - \frac{E(\tau+\eta)^2}{\rho(\tau,\eta)}}{[\rho(\tau,\eta)]^{3/2}} d\tau \tag{11}$$

$$G(T',\eta) = \int_{-\infty}^{+\infty} \frac{d\tau}{[\frac{\rho(\tau,\eta)}{T'} + (\tau+\eta)^2]^{3/2}} \tag{12}$$

These functions constitute generating functions for determining $A_k(E)$ and $M_{k,p}$. The technique of generating function was first introduced to us by N. Corngold in connection with the evaluation of $M_{k,o}$ for the gas case. We have extended the use of generating function to $A_k(E)$ and $M_{k,p}$ type integrals.

It has not been found possible to evaluate $F(E,\eta)$ and $G(\eta,T')$ by using the width function as given by Eq. (4) or (5). These integrals can be exactly evaluated for $\gamma(t)$ of the following form:

$$\gamma(t) = ci^2t^2 + bit - a . \tag{13}$$

The representation of $\gamma(t)$ by the above expression is termed the "general Doppler approximation." Four Doppler cases (the monatomic gas model and the T_{eff} (2), Krieger-Nelkin (3), and Detailed Balanced Doppler approximations) can be represented by the above form of the width function. In Table I we give expressions for a, b, and c for four Doppler cases in terms of specific physical parameters. The validity of the Detailed Balance theorem requires bT to be equal to c. This follows from Eq. (13) by using the equality between $\gamma(t)$ and $\gamma(-t+i/T)$. To satisfy Placzek's zeroth moment and first moment theorems for the scattering law obtained from the above expression of $\gamma(t)$, a must be equal to zero and b must be equal to one.

3. THE GENERAL DOPPLER APPROXIMATION

Integrals for $F(E,\eta)$ and $G(E,\eta)$, as given by Eqs. (11) and (12), can be transformed into standard form by making the following substitutions.

$$P(\eta) = \frac{m}{M}\left[a + ib(\eta - \frac{i}{2T}) + c(\eta - \frac{i}{2T})^2\right] \tag{14}$$

$$Q(\eta) = -\left[i(1 + \frac{m}{M}b) + \frac{2m}{M}c(\eta - \frac{i}{2T})\right] \tag{15}$$

$$R(\eta) = \frac{m}{M}c \tag{16}$$

$$x = (\tau + \eta). \tag{17}$$

$F(E,\eta)$ is given by the following integral:

$$F(E,\eta) = \frac{\sigma_b}{4\sqrt{\pi E}} \int_{-\infty}^{+\infty} \frac{\exp - \dfrac{Ex^2}{Rx^2 + Qx + P}}{[Rx^2 + Qx + P]^{3/2}}\, dx \,. \tag{18}$$

This integral has been evaluated in terms of the confluent hypergeometric functions, ${}_1F_1(n,m,x)$, with n and m being positive half integers. These functions are related to error functions. Hurwitz and Zweifel had also evaluated this type of integral, as mentioned by Krieger and Nelkin (3).

$$F(E,\eta) = \frac{\sigma_b \exp - \dfrac{E}{R}}{4\sqrt{\pi ERP^2}} \left[{}_1F_1\left(1; \frac{3}{2}; \frac{E}{R}\right) - \frac{Q^2}{Q^2 - 4PR} \right.$$

$$\left. {}_1F_1\left(1; \frac{3}{2}; \frac{E}{R} \frac{Q^2}{Q^2 - 4PR}\right) \right] . \tag{19}$$

3.1 Energy Transfer Moments

All energy transfer moments can be obtained in principle by the successive differentiation of $F(E,\eta)$ with respect to η and evaluating the resulting expressions for η equal to $i/2T$. We give expressions for the zeroth, first, and second energy transfer moments. The zeroth moment is the total scattering cross section.

$$A_0(E) = \frac{\sigma_b \exp - \frac{EM}{mc}}{(4\pi E \frac{m^3}{M^3} a^2 c)^{1/2}} [{}_1F_1(1; \frac{3}{2}; \frac{EM}{mc}) - x_0 {}_1F_1(1; \frac{3}{2}; \frac{EM}{mc} x_0)] \quad (20)$$

$$A_1(E) = -\frac{b}{a} A_0(E) + \frac{\sigma_b \exp - \frac{EM}{mc}}{(4\pi E \frac{m^3}{M^3} a^2 c)^{1/2}} x_1 {}_1F_1(2; \frac{3}{2}; \frac{EM}{mc} x_0) \quad (21)$$

$$A_2(E) = \frac{2m^2}{M^2} \frac{(b^2+ac)}{a^2} A_0(E) + \frac{\sigma_b \exp - \frac{EM}{mc}}{(4\pi E \frac{m^3}{M^3} a^2 c)^{1/2}}$$

$$[(2x_1 \frac{b}{a} + x_2) {}_1F_1(2; \frac{3}{2}; \frac{x_0 EM}{mc}) - \frac{4}{3} \frac{M}{m} \frac{Ex_1^2}{c} {}_1F_1(3; \frac{5}{2}; \frac{Ex_0 M}{mc})] \quad (22)$$

x_0, x_1, and x_2 are given by

$$x_0 = \frac{(1 + \frac{m}{M} b)^2}{[(1 + \frac{m}{M} b)^2 + 4 \frac{m^2}{M^2} ac]} \quad (23)$$

$$x_1 = \frac{8\,\frac{m^2}{M^2}\,c^2\left(1+\frac{m}{M}\,b\right)\left[\frac{2m}{M}a+\frac{b}{2c}+\frac{mb^2}{2Mc}\right]}{\left[\left(1+\frac{m}{M}\,b\right)^2+\frac{4m^2}{M^2}\,ac\right]^2} \tag{24}$$

$$x_2 = \frac{-8\,\frac{m^2}{M^2}c^2\left[\left(1-\frac{m^2}{M^2}b\right)^2+8ac\,\frac{m^2}{M^2}\left(\frac{m^2}{M^2}b^2+\frac{2m^2}{M^2}ac-1\right)\right]}{\left[\left(1+\frac{m}{M}\,b\right)^2+4\,\frac{m^2}{M^2}ac\right]^2} \tag{25}$$

For a not equal to zero, the energy transfer moments can be given for any Doppler case by using the appropriate a, b, and c. However, for a equal to zero, the monatomic gas case, these moments can be obtained by taking the limit for a equal to zero using "L'Hospital" rule. In the Appendix, we give the first three energy transfer moments for the monatomic gas in terms of error functions. The details of these moments have been treated by Rajagopal (14). The first two of these moments for the gas are well known in the literature. See von Dardel's (15) paper. Takahashi (16) has independently obtained the second energy transfer moment for the gas. He has also obtained the moments for the Krieger-Nelkin case (16).

3.2 The Total Scattering Cross Section

The high energy behavior of the total scattering cross section $A_0(E)$ is obtained by using the following asymptotic expression for ${}_1F_1(n,m,x)$, as given by Slater (17).

$$ {}_1F_1(n,m,x) = \frac{\Gamma(m)}{\Gamma(n)} x^{m-n} \exp x \tag{26} $$

$$ A_0(E) = \frac{\sigma_b M}{4Ema} \left[1 - \left(1 + \frac{4m^2ac}{M^2(1+\frac{m}{M}b)}\right)^{-1/2} \exp -\left(\frac{4Ema}{M\{(1+\frac{m}{M}b)^2 + 4\frac{m^2}{M^2}ac\}}\right)\right] \tag{27} $$

For very large energy, $A_0(E)$ varies as $1/E$. However, for a weakly bound system, where a is small, $A_0(E)$ is given by the constant

$$ A_0(E) = \frac{\sigma_b}{(1+\frac{m}{M})^2} \left[1 + \frac{(b-1)}{(\frac{M}{m}+1)}\right]^{-2} . \tag{28} $$

The correct asymptotic value for $A_0(E)$ is given by the above expression with b equal to unity. From the values of b given in Table I, one notes that the gas and T_{eff} cases give correct high energy limit for $A_0(E)$. On the other hand, the Krieger-Nelkin and the Detailed Balanced Doppler approximations fail to give the correct asymptotic value.

For the Detailed Balanced Doppler approximation using the Debye frequency distribution of vibrational modes, the expression for b is given by

$$b \approx 1 - \frac{\theta^2}{40T^2} + \frac{1}{3840}\frac{\theta^4}{T^4} . \tag{29}$$

θ/T is the ratio between the Debye and thermodynamic temperatures. Thus we note that the corrections to unity are terms of order θ^2/T^2 or higher, which are small for weakly bound systems.

For very low energy, $A_0(E)$ exhibits $1/\sqrt{E}$ behavior, as the confluent hypergeometric function approaches unity. $A_0(E)$ is given by the following expression:

$$A_0(E) = \frac{\text{Constant}}{\sqrt{E}} \tag{30}$$

$$\text{Constant} = \frac{\sigma_b\left(\frac{4mc}{\pi M}\right)^{1/2}}{\left[\left(1 + \frac{m}{M}b\right)^2 + \frac{4m^2}{M^2}ac\right]} \tag{31}$$

For the incoherent scatterer, the total scattering cross section at low energy exhibits $1/\sqrt{E}$ type behavior, as demonstrated by the recent slow neutron scattering experiments of J. J. Rush (18) in bound hydrogenous systems. For the monatomic gas model , the above constant reduces to

$$\frac{\sigma_b(\frac{4m}{M\pi})^{1/2}}{(1+\frac{m}{M})^2}$$

The constant gives the slope of the scattering cross section at low energy. It is a measure of the upward scattering of neutrons or gain in energy transfer. The constant decreases in value with the increase in binding.

3.3 The Associated Integrals $M_{k,p}$

The associated integrals $M_{k,p}$ are given in Eqs. (9) and (12).

$$M_{k,p} = \frac{\sigma_b}{8T^2 i^k}\left[\left(\frac{d}{d-1/T'}\right)^p\left\{\left(\frac{d}{d\eta}\right)^k G(\eta,T')\right\}_{\eta=i/2T}\right]_{T'=T}. \qquad (32)$$

For the determination of $M_{k,p}$, one may consider $G(\eta,T')$ to be the generating function. $G(\eta,T')$ is evaluated by using the transformations given by Eqs. (14), (15), (16), and (17).

$$G(\eta,T) = \frac{8T'^{3/2}(T'+\frac{m}{M}c)^{1/2}}{\left[\frac{4m^2}{M^2}ac+\frac{4m}{M}aT'+(1+\frac{m}{M}b)^2+\frac{4im}{M}(\eta-\frac{i}{2T})(bT'-c)+\frac{4m}{M}cT'(\eta-\frac{i}{2T})^2\right]} \qquad (33)$$

By using the Detailed Balance theorem, it can be shown that $M_{k,p}$ with odd values of k are either zero or can be converted into $M_{k,p}$ with even values of k. This fact is equivalent to the absence of odd powers of $(\eta - \frac{i}{2T})$ in the expression of $G(\eta,T')$. The condition for this is that the coefficient of

$(\eta - \frac{i}{2T})$ is zero. Mathematically, it means

$$bT' - c = 0 \qquad \text{for } T' = T. \tag{34}$$

Eq. (34) furnishes the test for determining the validity of the Detailed Balance theorem. From Table I it is evident that all three cases except the T_{eff} case satisfy the fundamental theorem of the Detailed Balance. We consider only the cases that meet this requirement. $G(\eta,T')$ is then given by the following series:

$$G(\eta,T') = 8T'^{3/2}(T'+\frac{m}{M}c)^{1/2}$$

$$\sum_{n=0}^{\infty} \frac{(-1)^n(\frac{4m}{M}T'c)^n(\eta - \frac{i}{2T})^{2n}}{(\frac{4m^2}{M^2}ac + \frac{4m}{M}aT' + (1+\frac{m}{M}b)^2)^{n+1}} \tag{35}$$

This is equivalent to the Taylor expansion:

$$G(\eta,T') = \sum_{n=0}^{\infty} \frac{(\eta - i/2T)^n}{n!} \left(\frac{d^nG(\eta,T')}{d\eta^n}\right)_{\eta=i/2T} . \tag{36}$$

The associated integral $M_{2k,p}$ using Eqs. (32), (35), and (36) is given by the p^{th} differentiation of the coefficient of the $(\eta - \frac{i}{2T})^{2k}$ term.

$$M_{2k,p} = \frac{\sigma_b 2k!(\frac{4m}{M}c)^k}{T^2} \left[(\frac{d}{d-\frac{1}{T'}})^p \right.$$

$$\left. \frac{T'^{k+3/2}(T'+\frac{m}{M}c)^{1/2}}{(\frac{4m^2}{M^2}ac + (1+\frac{m}{M}b)^2 + \frac{4m}{M}aT')^{k+1}} \right]_{T'=T} \qquad (37)$$

The well known thermalization parameter $M_{2,0}$ is obtained by putting k equal to one and p equal to zero in the above equation.

$$M_{2,0} = \frac{8\sigma_b \frac{m}{M} cT^{1/2}(T+\frac{m}{M}c)^{1/2}}{[\frac{4m^2}{M^2}ac + (1+\frac{m}{M}b)^2 + \frac{4m}{M}aT]^2} \qquad (38)$$

The above expression is the exact formula for M_2, for the general Doppler approximation, which satisfies the Detailed Balance theorem. Using the values of a,b, and c for the gas case, Eq. (38) reduces to the well known formula, first given by von Dardel (15).

$$M_{2,0} = \frac{8\sigma_b T^2 \frac{m}{M}}{(1+\frac{m}{M})^{7/2}} \qquad \text{(gas)} \qquad (39)$$

Since a, b, and c depend upon the binding parameters, therefore, Eq. (38) is useful for studying the effect of binding upon $M_{2,0}$.

4. THE DETAILED BALANCED DOPPLER APPROXIMATION

We discuss a new Doppler approximation in this section. It satisfies the Detailed Balance theorem, which is the basic requirement for an approximation used in the study of neutron thermalization. The width function $\gamma(t)$ is obtained by retaining terms up to τ^2 in the expression of $\gamma(\tau + \frac{1}{2T})$ according to Eq. (5).

$$\gamma(\tau + \frac{1}{2T}) = -\lambda + \alpha i^2 \tau^2 \tag{40}$$

λ and α are characterized by two binding parameters - the Debye Waller factor and the specific heat integral respectively.

$$\lambda = \int_0^\infty \frac{f(\xi)}{\xi} \coth \frac{\xi}{2T} \, d\xi - \int_0^\infty \frac{f(\xi)}{\xi \sinh \xi/2T} \, d\xi \tag{41}$$

$$\alpha = \int_0^\infty \frac{\xi \, f(\xi)}{2 \sinh \xi/2T} \, d\xi \tag{42}$$

After some manipulation, λ and α can be given by the familiar integrals

$$\lambda = 2\int_0^\infty \frac{f(\xi)}{\xi} \coth \frac{\xi}{2T} \, d\xi - \int_0^\infty \frac{f(\xi)}{\xi} \coth \frac{\xi}{4T} \, d\xi \tag{43}$$

$$\alpha = \left[\int_0^\infty \frac{\xi \, f(\xi)}{e^{\xi/2T} - 1} \, d\xi - \int_0^\infty \frac{\xi \, f(\xi)}{e^{\xi/T} - 1} \, d\xi \right] \tag{44}$$

Experimentally, λ can be obtained from the Debye-Waller factor at two different temperatures of sample T and 2T from the x-ray or neutron

in
scattering data. The integrals appearing/the Eq. (43) are related to the zero point mean square displacement of the vibrating atom.

α is obtainable from the specific heat (c_v) integral data. The specific heat integral is given by

$$\int_0^T c_v dT = \int_0^\infty \frac{\xi f(\xi)}{e^{\xi/T} - 1} d\xi \ . \tag{45}$$

The above approximation can be applied to any system provided the frequency distribution of vibrational modes or the parameters λ and α are available from the experiment or otherwise. For known frequency distributions of vibrational modes such as Einstein and Debye λ and α can be theoretically evaluated. For temperatures greater than the frequency of vibrational modes λ and α approach the gas values. In this limit, α and λ reduce to the following simple expressions:

$$\alpha = T \quad \text{and} \quad \lambda = 1/4T \ . \tag{46}$$

All the results given in section 3 for the general Doppler approximation can be obtained for the above case by using the appropriate values of a, b, and c. The expression for the thermalization parameter M_2 reduces to the following form:

$$\frac{M_2}{8\sigma_b T^2} = \frac{(\frac{m}{M})\frac{\alpha}{T}}{(1+\frac{m}{M}\frac{\alpha}{T})^{3/2}(1+\frac{4m}{M}\lambda T)^2} \tag{47}$$

5. NUMERICAL RESULTS (DeBYE MODEL)

In this paper, we consider only the frequency distribution of vibrational modes, as given by the Debye model to obtain numerical results.

$$f(\xi)d\xi = \frac{3\xi^2}{\theta^3}\,d\xi \tag{48}$$

θ is the Debye temperature. For this case α and λ are given by the integrals characterized by parameter t equal to T/θ, the ratio between thermodynamic and Debye temperatures.

$$\lambda = \frac{3}{\theta}[2\phi_1(t) - \phi_1(2t)] \tag{49}$$

$$\alpha = \frac{3\theta}{2}[\phi_3(2t) - \phi_3(t)] \tag{50}$$

$$\phi_n(t) = \int_{-1}^{+1} \frac{\xi^n}{e^{\xi/t}-1}\,d\xi \tag{51}$$

In Table II we give numerical values of λT and α/T for various values of t or T/θ. We also give T_{eff}/T for different values of t. A curve for T_{eff}/T versus t was given by Lamb (2). T_{eff} is defined by

$$\frac{T_{eff}}{T} = \frac{1}{2T} \int_0^\infty \xi f(\xi) \coth \frac{\xi}{2T} d\xi \tag{52}$$

or

$$\frac{T_{eff}}{T} = \frac{3}{2t} \phi_3(t) \qquad \text{(Debye model)} \tag{53}$$

$\phi_n(t)$ integrals were evaluated for θ/T less than 2π using the generating function for the Bernoulli Numbers. For θ/T greater than 2π integrals were evaluated numerically. Since these integrals are connected with Placzek's moments (11) for the Debye model, they are very useful in the study of neutron thermalization. In Table III we give numerical values of the first four integrals. As shown above, the Debye-Waller factor integral and the T_{eff} are given by $\phi_1(t)$ and $\phi_3(t)$ respectively.

We give numerical values of M_2(crystal)/M_2(gas) as a function of T/θ for masses equal to 2, 9, 12, 18, and ∞ in Table IV. We note that M_2 decreases with the increase in mass for a fixed value of θ/T, and for a fixed mass it decreases with the increase in θ/T. Increase in mass as well as θ/T of the moderator are associated with the increase in binding. Thus one can conclude that M_2 decreases with the increase in binding. In Figure 1, we plot M_2(crystal)/M_2(gas) for various masses as a function of T/θ. One notes the existence of a universal curve for various masses.

In Figure 2, we plot $A_0(E)/\sigma_b$ for a moderator of mass 9 a.m.u. and T/θ equal to 0.3 in the incoherent approximation. This corresponds to the beryllium case. Curves A and B represent the gas and the Doppler approximation respectively. Curve C is obtained by adding to the elastic scattering cross section the contribution due to one phonon coherent and two phonons incoherent inelastic scattering, as given by Bhandari (19). The elastic cross section was determined by the following formulae:

$$A_0(E) = \frac{4\sigma_b M}{m\lambda E}\left[1 - \exp - \frac{4mE\lambda}{M}\right] \tag{54}$$

$$\lambda = \int_0^\infty \frac{d\xi}{\xi} f(\xi) \coth \frac{\xi}{2T} d\xi \tag{55}$$

We also plot curve D obtained from Placzek's mass expansion (20) by retaining terms up to $(m/M)^2$. Numerical results for these calculations were taken from Marshall and Stuart's paper (21). In Figure 3, we plot $A_0(E)/\sigma_b$ for the gas and the Doppler approximation for the wide range of energy.

The gas model underestimates the total scattering cross section, except at very low energy and at high energy. At very low energy, it overestimates and at high energy it approaches the constant value. The Detailed Balanced Doppler approximation underestimates the cross section below

47 Mev, and overestimates it above this value. At about 300 Mev the curve for the Doppler case crosses the curve for the gas model. Above this energy The Doppler approximation breaks down as shown in Figure 3. Curves C and D give identical results below 60 Mev. Above this energy, the contribution due to higher phonons causes the mass expansion curve to lie above the phonon expansion curve. It must, however, be pointed out that the Doppler approximation is better than the gas model in the thermal energy region.

6. CONCLUSIONS

We have shown that the thermal neutron scattering problem can be analytically solved by using the general Doppler approximation. A large number of interesting physical cases can be treated with this approximation. We have obtained expressions for the energy transfer moments and their associated integrals including the specific integral M_2 (the second energy transfer moment weighted by the Maxwellian distribution). These quantities are useful in the study of neutron thermalization and in the determination of the thermalization parameters.

It has been demonstrated that, except for the monatomic gas model, it is not possible to achieve correct asymptotic scattering behavior and satisfy the Detailed Balance theorem in a single Doppler approximation. These two types of behavior result from two different kinds of expansion of the

width function $\gamma(t)$ — the mean square displacement of scattering atoms expressed in terms of the collision time t between a neutron and an atom. The expansion of $\gamma(t)$ in powers of t gives the correct asymptotic scattering behavior; however, the Detailed Balance theorem is violated. The converse is true for the expansion of $\gamma(t)$ in powers of $(t - i/2T)$. In the Doppler approximation the effective temperature and the Detailed Balanced Doppler cases respectively represent these two expansions. For neutron thermalization prdblems, since the validity of the Detailed Balance theorem is important, the $(t - i/2T)$ type of expansion is to be preferred. Corngold (22) has used the expansion of $\gamma(t)$ in powers of t to study binding effects on neutron scattering in the joining region between slowing down and thermal energies.

We propose the use of the Detailed Balanced Doppler approximation in the study of neutron thermalization problems, where the validity of Detailed Balance theorem is of importance. This approximation can be employed to investigate thermal neutron scattering in any physical system, given the value of the Debye-Waller factor and the specific heat integral. Experimental values of these integral parameters must be used to ensure internal consistency of the frequency distribution of the vibrational modes.

It is well known that the use of phonon expansion and Placzek's mass expansion techniques in studying thermal neutron scattering in crystals involves tedious numerical calculations to obtain integral quantities of interest in reactor physics. The Doppler approximation, because of its analytical simplicity and the fact that it also takes into account binding, merits serious consideration. Since this approximation gives results for the incoherent scattering, it should also prove useful in investigating the effect of bound hydrogen atoms on thermal neutron scattering. It would be of interest to compare the results obtained with this approximation with those obtained by other methods.

ACKNOWLEDGEMENT

We would like to express our thanks to Noel Corngold for valuable discussions held during the course of this study, especially in formulating the Detailed Balanced Doppler Approximation. Our thanks are also due to Jack Chernick for his interest in this study and for extending to one of the authors, A. K. Rajagopal, summer participant facilities with the Theoretical Reactor Physics Group at the Brookhaven National Laboratory. For carrying out some of the numerical calculations presented in this paper, we extend our thanks to William Bornstein and Joan Weisenbloom.

REFERENCES

1. L. Van Hove, Phys. Rev. 95, 249 (1954).
2. W. E. Lamb, Phys. Rev. 55, 190 (1939).
3. T. J. Krieger and M. S. Nelkin, Phys. Rev. 106, 290 (1957).
4. S. N. Purohit, Nuc. Sci. and Eng. 9, 157 (1961); S. N. Purohit, "The Spatial Decay of Neutrons in an Infinite Medium," Brookhaven National Laboratory Memorandum dated September 22, 1960; S. N. Purohit, "Application of the Polynomial Method in the Study of Thermal Neutron Spectrum in a Heavy Crystalline Medium," to be presented at the A.N.S. meeting, Boston, June 1962.
5. S. N. Purohit, "Neutron Thermalization in a Crystalline Medium in Incoherent Approximation," submitted to the BNL Neutron Thermalization Conference.
6. M. S. Nelkin, J. Nuclear Energy 8, 48 (1958).
7. D. S. Selengut, "Variational Methods in Neutron Thermalization," (unpublished), September 29, 1961.
8. G. H. Vineyard, Phys. Rev. 110, 999 (1958).
9. L. S. Kothari and K. S. Singwi, Solid State Phys. 8, 110 (1959), Academci Press, New York.
10. A. Sjölander, Arkiv för Fysik 14, 315 (1958).
11. G. Placzek, Phys. Rev. 86, 377 (1952).

12. Proc. on Conf. on the "Inelastic Scattering of Neutrons in Solids and Liquids." International Atomic Energy Agency (I.A.E.A.), Vienna (1961).

13. P. A. Egelstaff and P. Schofield, "On the Evaluation of Thermal Neutron Scattering Law." Nuclear Sci. and Eng. 12, 260 (1962).

14. A. K. Rajagopal, "Neutron Thermalization on Doppler Model." Brookhaven National Laboratory Memorandum dated September 1961.

15. G. F. von Dardel, Trans. Roy. Inst. Technol. Stockholm 75, (1954).

16. H. Takahashi, private communication.

17. L. J. Slater, "Confluent Hypergeometric Functions," Cambridge University Press (1960).

18. J. J. Rush, T. I. Taylor, and W. W. Havens, Jr., Phys. Rev. Letters Vol. 5, No. 11, 507 (1960), and J. Chem. Phys. Vol. 35, No. 6, 2265 (1961).

19. R. C. Bhandari, J. Nuclear Energy 6, 104 (1957).

20. G. Placzek, Phys. Rev. 105, 1240 (1957).

21. W. Marshall and R. N. Stuart, "Scattering of Neutrons from Polycrystalline Materials," UCRL-5568, April 8, 1959.

22. N. Corngold. Annals. of Phys. 6, 368 (1959) and Annals. of Phys. 11, 338 (1960).

APPENDIX

Energy Transfer Moments for the Monatomic Gas Model

$$A_0(E) = \frac{\sigma_b}{\mu^2} \frac{\exp -\beta}{\beta^{1/2}\sqrt{\pi}} [1 + Z(\beta + 1/2)] \tag{1}$$

$$A_1(E) = \frac{2\sigma_b E \exp -\beta}{\mu^4 \beta^{5/2} \sqrt{\pi}} [(\frac{5}{2}\beta + \beta^2 - \frac{\mu\beta}{2} - \mu\beta^2) + Z(\frac{3\beta}{4} + 3\beta^2 + \beta^3 + \frac{\mu\beta}{4} - \mu\beta^2 - \mu\beta^3)] \tag{2}$$

$$A_2(E) = \frac{2\sigma_b E^2 \exp -\beta}{\beta^{5/2} \mu^4 \sqrt{\pi}} [(-1 + \frac{14\beta}{3} + \frac{8\beta^2}{3}) + Z(\frac{1}{2} + 6\beta^2 + \frac{8\beta^3}{3})$$

$$-\frac{4}{\mu}\{(1 + \frac{16}{3}\beta + \frac{4}{3}\beta^2) + Z(-\frac{1}{2} + 3\beta + 6\beta^2 + \frac{4\beta^3}{3})\}$$

$$+\frac{4}{\mu^2}\{(\frac{11}{2} + \frac{14}{3}\beta + \frac{2}{3}\beta^2) + Z(\frac{5}{4} + \frac{15}{2}\beta + 5\beta^2 + \frac{2}{3}\beta^3)\}] \tag{3}$$

where

$$Z = \exp \beta \operatorname{erf} \sqrt{\beta}\ \sqrt{\pi/\beta}$$

$$\operatorname{erf} \sqrt{\lambda} = \frac{2}{\pi} \int_0^{\lambda} (\exp -t^2) dt$$

$$\beta = EM/mT$$

$$\mu = (1 + \frac{m}{M}) .$$

TABLE I

Doppler Case Parameters

	Case			
Parameter	Gas	T_{eff}	Detailed Balanced Doppler	Krieger-Nelkin (3)
a	0	0	$(\lambda - \frac{\alpha}{4T^2})$	$-2M\gamma$
b	1	1	α/T	$M/\overline{M_v}$
c	T	T_{eff}	α	$(M/\overline{M_v})T$

where

$$\lambda = \int_0^\infty \frac{f(\xi)}{\xi} \coth \frac{\xi}{2T} - \int_0^\infty \frac{f(\xi)}{\xi \sinh \xi/2T} d\xi$$

$$\alpha = \int_0^\infty \frac{\xi f(\xi)}{2 \sinh \xi/2T} d\xi$$

$$T_{eff} = \int_0^\infty \frac{\xi f(\xi)}{2} \coth \frac{\xi}{2T} d\xi \qquad \text{ref. (2)}$$

$M_v/\overline{M_v}$ = ratio between mass of v^{th} nucleus M_v and the average effective mass $\overline{M_v}$. ref. (3)

γ = Debye-Waller factor integral. ref. (3)

TABLE II

Debye Model Parameters

$t = T/\theta$	$\lambda' T$	α/T	T_{eff}/T
0.10	0.13101	0.21585	3.76935
0.20	0.19540	0.59070	1.99259
0.25	0.21089	0.70050	1.68174
0.30	0.22093	0.77465	1.49441
0.40	0.23240	0.86179	1.29165
0.50	0.23832	0.90771	1.19113
0.60	0.24174	0.93438	1.13453
0.80	0.24526	0.96216	1.07672
1.00	0.24693	0.97551	1.04946
1.50	0.24858	0.98899	1.02211
2.00	0.24924	0.99376	1.01246
2.50	0.24954	0.99602	1.00798
∞	0.25000	1.00000	1.000

T/θ = Ratio between thermodynamic and Debye temperatures.

TABLE III

Placzek's Moment Integrals (Debye Model)

$t = T/\theta$	$\phi_1(t)$	$\phi_3(t)$
0.10	0.53251	0.25129
0.20	0.62835	0.26568
0.25	0.69407	0.28029
0.30	0.76781	0.29888
0.40	0.93103	0.34444
0.50	1.10695	0.39704
0.60	1.29014	0.45381
0.80	1.66839	0.57425
1.00	2.05501	0.69961
1.20	2.44598	1.08740
1.50	3.03687	1.02211
2.00	4.02771	1.34995
2.5	5.02219	1.67997
3.0	6.01850	2.011096
3.5	7.01586	2.34285
4.0	8.01388	2.67499
5.0	10.011107	3.339997

$\phi_2(t) = -0.33334$

$\phi_4(t) = -0.20000$

TABLE IV

Average Second Energy Transfer Moment M_2

(Debye Model)

	M_2(crystal)/M_2(gas)				
$T/\theta = t$	M = 2	M = 9	M = 12	M = 18	M = ∞
0.1	0.48032	0.26919	0.25494	0.24194	0.21585
0.2	0.85646	0.65789	0.64102	0.62092	0.59070
0.25	0.91308	0.75669	0.74323	0.72934	0.70050
0.3	0.94271	0.82043	0.80963	0.79701	0.77465
0.4	0.97000	0.89231	0.88539	0.87744	0.86179
0.5	0.9816	0.92917	0.92398	0.91906	0.90771
0.6	0.98698	0.94998	0.94642	0.94277	0.93438
0.8	0.99326	0.97122	0.96919	0.96704	0.96216
1.0	0.99567	0.98144	0.98028	0.97868	0.97551
1.5	0.99814	0.99174	0.99133	0.99054	0.98899
2.0	0.99890	0.99529	0.99502	0.99475	0.99376
2.5	0.99931	0.99704	0.99688	0.99682	0.99602
∞	1.00000	1.00000	1.00000	1.00000	1.00000
$\frac{M_2}{8\sigma_b T^2}$(gas)	12.09522×10^{-2}	7.6844×10^{-2}	6.2967×10^{-2}	4.59733×10^{-2}	$\frac{m}{M}$

CAPTIONS

Figure 1 M_2(crystal)/M_2(gas) for Various Masses as a Function of Binding Parameter T/θ.

Figure 2 Total Scattering Cross Section $A_0(E)/\sigma_b$ for Beryllium using the Incoherent Approximation.

Figure 3 Comparison of $A_0(E)/\sigma_b$ for Beryllium using the Gas Model and the Detailed Balanced Doppler Approximation.

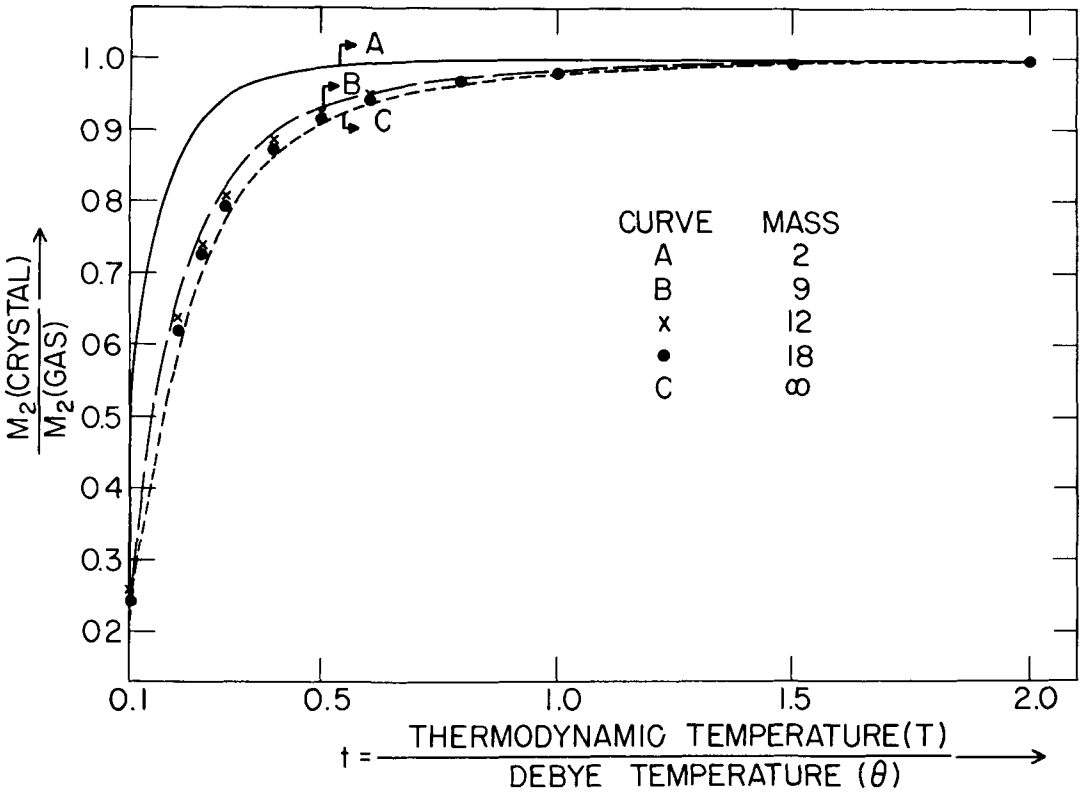
1.0
0.9
0.8
0.7
0.6
0.5
0.4
0.3
0.2
A
B
C
CURVE MASS
A 2
B 9
x 12
• 18
C ∞
$\frac{M_2(CRYSTAL)}{M_2(GAS)}$
0.1
0.5
1.0
1.5
2.0
$t = \frac{THERMODYNAMIC\ TEMPERATURE(T)}{DEBYE\ TEMPERATURE\ (\theta)}$

FIG 1

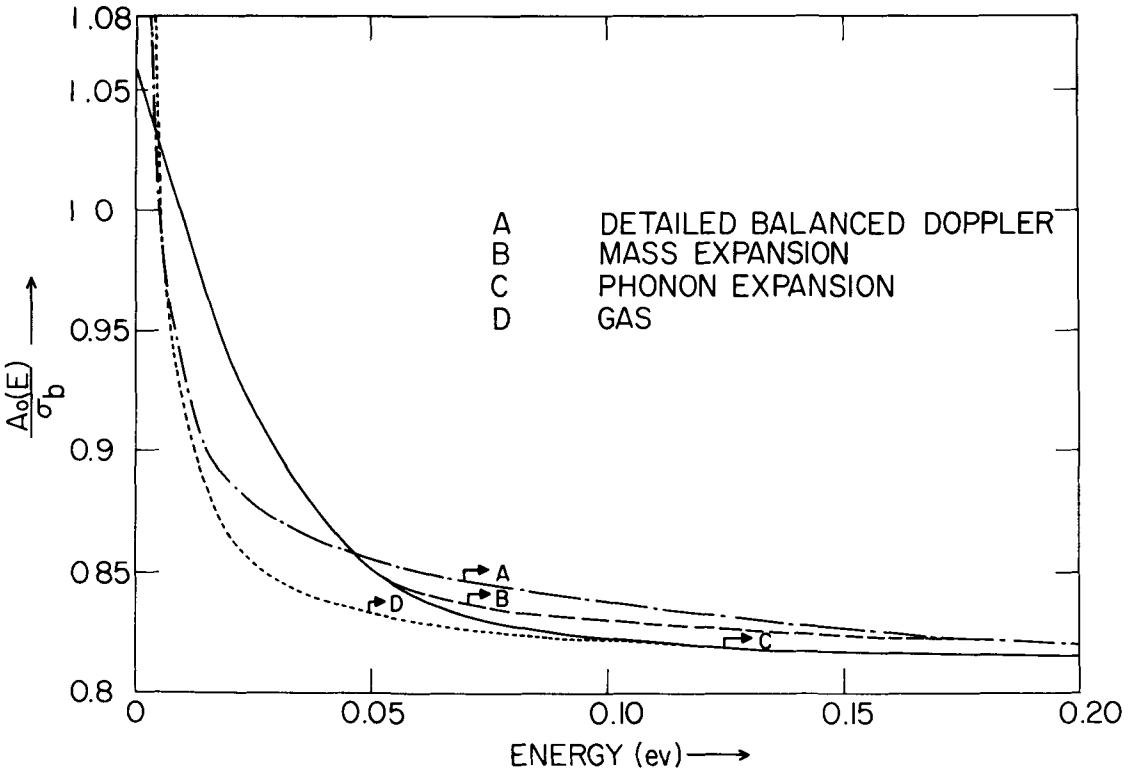
1.08
1.05
1.0
0.95
0.9
0.85
0.8
A DETAILED BALANCED DOPPLER
B MASS EXPANSION
C PHONON EXPANSION
D GAS
A
B
C
D
$\frac{A_0(E)}{\sigma_b}$
0
0.05
0.10
0.15
0.20
ENERGY (ev)

FIG 2

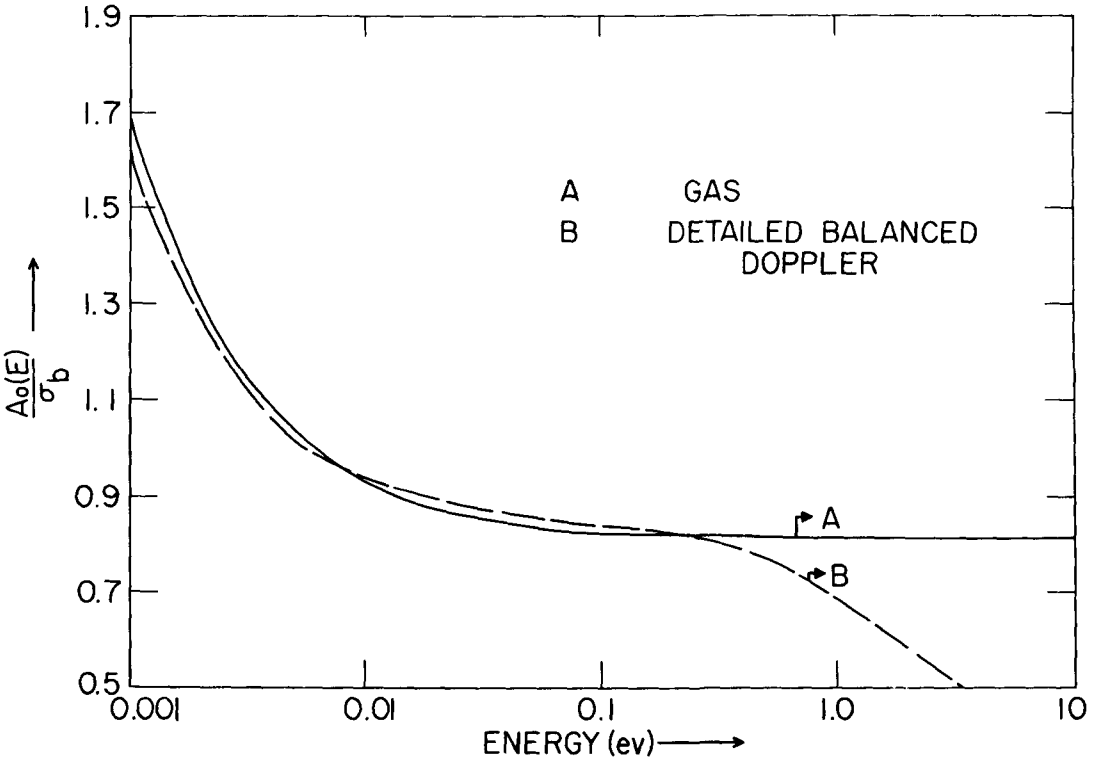
1.9
1.7
1.5
1.3
1.1
0.9
0.7
0.5
$\frac{A_0(E)}{\sigma_b}$
A GAS
B DETAILED BALANCED DOPPLER
A
B
0.001
0.01
0.1
1.0
10
ENERGY (ev)

FIG. 3

COMPARISON OF "CLASSICAL" AND "QUASI-CLASSICAL" CROSS SECTIONS FOR SOME SIMPLE SYSTEMS*

M. Rosenbaum and P. F. Zweifel
Department of Nuclear Engineering
The University of Michigan
Ann Arbor, Michigan

Van Hove[1] and Glauber[2] introduced the concept of a so-called time-dependent pair correlation function $G(r,t)$ which is essentially the Fourier transform of the differential neutron scattering cross section:

$$\frac{d^2\sigma}{dE\,d\Omega} = \frac{a^2}{2\pi\hbar}\frac{k}{k_0}\int d^3r\,dt\,\exp\left[\frac{i}{\hbar}(\mathbf{k}\cdot\mathbf{r}-Et)\right]G(r,t)\,, \tag{1}$$

Here $\mathbf{k}$ and E are the momentum and energy charges in the scattering, $\hbar\mathbf{k}_0$ and $\hbar\mathbf{k}$ are the initial and final neutron moments, and M represents the mass of one of the atoms of the scattering system (which contains N such atoms, assumed identical for simplicity).

Explicitly,

$$G(r,t) = N^{-1}\left\langle \sum_{j,j'=1}^{N}\int d^3r'\,\delta(\mathbf{r}+\mathbf{r}_{j'}(0)-\mathbf{r}')\,\delta(\mathbf{r}'-\mathbf{r}_j(t))\right\rangle \tag{2}$$

where the brackets denote a thermal average, i.e.,

$$\langle X\rangle = \mathrm{Tr}\,\rho X \tag{3}$$

if $\rho = Z^{-1}e^{-\beta H}$ is the density matrix of the system under consideration. Note that in the limit $t\to 0$, $G(r,t)$ becomes the ordinary radial (pair) distribution function $g(r)$ familiar

*Supported by the U. S. Atomic Energy Commission.

in the static approximation in which the energy change in scattering is assumed to be small compared to the incident particle energy ($E << \frac{\hbar^2 k_i^2}{2m}$). However, the interpretation of $G(r,t)$ as the generalization of $g(r)$ to the time dependent case is obscured by the fact that $r_j(t)$ and $r_i(0)$ are non-commuting operators, so that

$$\sum_{i,j=1}^{N} \int d^3r' \delta(r + r_i(0) - r') \delta(r' - r_j(t)) \neq \sum_{i,j=1}^{N} \delta(r - r_j(t) + r_i(0)) \quad ; \quad (4)$$

It is, of course, the thermal average of the righthand side of Equation (4) which is, physically, the probability that if there is a molecule at the origin at time $t=0$ there will be a molecule (the same or another) a distance r away at time t (i.e., the time-dependent pair correlation function).

The question then arises, if $G(r,t)$ is <u>not</u> the time dependent pair correlation function, what is it? It is, of course, a multiple of the Fourier transform of the neutron cross section. If we can then relate it in some physically meaningful way to the motions of the atoms in the scattering system, then a measurement of the neutron cross section will provide a dynamical description of the scattering system. This, of course, is why one does neutron scattering experiments anyway, and was the incentive for the introduction of the function $G(r,t)$ in the first place.

The physical interpretation of the convolution of delta functions in the defining equation for $G(r,t)$ is virtually impossible because this convolution is not an hermitean operator

and thus does not actually represent a measureable quantity. In fact, it is well known that its eigen values are not real[1]. In fact, Schofield[3] has obtained a dispersion relation relating the real and imaginary parts of $G(r,t)$ which is obtained simply by requiring that the cross section obey the principle of detailed balance. Clearly the time dependent pair correlation function (i.e., the thermal average of the righthand side of Equation (4)) cannot obey any such relation since it is an hermitean operator and has real eigen-values.

Nonetheless, it is possible in some sense to attach physical meaning to $G(r,t)$ if we convert it to a function of classical variables. The procedure is described in detail elsewhere[4]. Briefly, one makes use of the fact that one can write thermal averages in either of two equivalent forms

$$Tr\rho A(\underline{r}_1,\underline{r}_2,\cdots\underline{r}_N,\underline{p}_1,\cdots\underline{p}_N)=\int d^3R_1\cdots d^3R_N\, d^3p_1\cdots d^3p_N\, f_W(\underline{R}_1,\cdots\underline{p}_N)\,A_W(R_1,\cdots p_N), \tag{5}$$

Here A is an (operator) function of the operators $(\underline{r}_1,\underline{r}_2,\cdots\underline{r}_N,\underline{p}_1,\cdots\underline{p}_N)$; $f_W(\underline{R}_1,\cdots\underline{p}_N)$ is the Wigner distribution function[5] which depends on the classical variables $\underline{R}_1,\underline{R}_2,\cdots\underline{R}_N,\underline{p}_1,\cdots\underline{p}_N$ and A_W is a function (of classical variables) related to A in a simple manner[6]. Briefly, if $\{\underline{r}_i\},\{\underline{p}_i\}$ are Schrödinger operators, and $f, g, h,$ etc. are arbitrary functions, then simply

$$f_W(\underline{R}_i)=f(\underline{r}_i)$$
$$g_W(\underline{p}_i)=g(\underline{p}_i) \tag{6}$$

However, if $h(\underline{r}_i, \underline{p}_i) = f(\underline{r}_i)\, g(\underline{p}_i)$, then

$$h_w(\underline{R}_i, \underline{P}_i) = f_w(\underline{R}_i) \mathcal{O} g_w(\underline{P}_i). \tag{7}$$

where the operator $\mathcal{O}$ is given by

$$\mathcal{O} = e^{\frac{i\hbar}{2}\sum_i \left(\frac{\overrightarrow{\partial}}{\partial \underline{p}_i} \cdot \frac{\overleftarrow{\partial}}{\partial \underline{R}_i} - \frac{\overrightarrow{\partial}}{\partial \underline{R}_i} \cdot \frac{\overleftarrow{\partial}}{\partial \underline{p}_i} \right)} \tag{8}$$

where the arrows indicate the function to be differentiated. Similarly, if

$$\phi(\underline{r}_i, \underline{p}_i) = \psi(\underline{r}_i)\, \chi(\underline{p}_i)\, f(\underline{r}_i)\, g(\underline{p}_i)$$

$$\phi_w(\underline{R}_i, \underline{P}_i) = \{\psi_w(\underline{R}_i) \mathcal{O} \chi_w(\underline{P}_i)\} \mathcal{O} \{f_w(\underline{R}_i) \mathcal{O} g_w(\underline{P}_i)\} \tag{9}$$

and so forth.

Since $G(\underline{r}, t)$ is defined in terms of Heisenberg operators and this method applies only to Schrödinger operators, it is necessary to reformulate the expression for $G(\underline{r}, t)$ entirely in terms of Schrödinger operators*. This is most conveniently done by using Wick's time expansion[8] of

$$\chi(\underline{p}, t) = \int e^{i\underline{p}\cdot\underline{r}/\hbar} G(\underline{r}, t)\, d^3r$$

and applying these rules term by term. The details are found in Reference (4), where the calculations have been carried out to first order in $\hbar$ **.

---

*Turner[7] attempted to apply these rules to Heisenberg operators, and so his results were not strictly correct.

**However, the procedure, followed by some other authors who let $\hbar \to 0$ but kept $\underline{r} = \underline{p}/\hbar$ and $\omega = E/\hbar$ finite, was not used. Our expansion parameter was essentially $\hbar^n \nabla^m V$, where V is the potential of the scattering system.

Then, making use of the fact that the Wigner distribution function is, to first order in $\hbar$, identical with the classical Maxwell-Boltzmann distribution function, we find

$$\frac{d^2\sigma}{dE\,d\Omega} = \left(\frac{d^2\sigma}{dE\,d\Omega}\right)_V e^{\frac{\beta E}{2}} e^{-\frac{\beta\hbar^2\vec{Q}^2}{8M}} + O(\hbar^2); \qquad (10)$$

where $\left(\frac{d^2\sigma}{dE\,d\Omega}\right)_V$ is simply the Fourier transform of the classical time-dependent pair correlation function. The subscript "V" stands for Vineyard,[9] who used the approximation of calculating the cross section as the Fourier transform of the classical correlation function. Our result, Equation (10), is identical to the result used by Singwi and Sjolander[10] (who speculated that it might be correct because it works exactly for the ideal gas). It differs from a prescription introduced by Schofield[3] only by the factor $e^{-\frac{\beta\hbar^2\vec{Q}^2}{8M}}$ (Schofield's prescription was introduced to force the cross section calculated from the classical correlation function to obey detailed balance).

One important point should not be overlooked. It does <u>not</u> follow that the classical approximation to the cross section for any system can be obtained from the classical correlation function. The limit of the cross section as $\hbar \to 0$ is <u>not</u> the cross section of the limit. This may best be illustrated in the core of the ideal gas, for which the cross section is entirely classical, containing no powers of $\hbar$ at all. Nonetheless, for the gas $G(r,t) = \left[\frac{M\beta}{2\pi t(t-i\hbar\beta)}\right]^{3/2} \exp\left[-\frac{Mr^2\beta}{2t(t-i\hbar\beta)}\right]$

If one takes the limit $\hbar \to 0$ in the expression for $G(r,t)$ one does indeed obtain the classical correlation function. However, the Fourier transform of the latter quantity clearly does <u>not</u> give the correct cross section. Thus, while our prescription is correct to order $\hbar$ the Vineyard prescription is not correct even to order $\hbar^0$.

In Figures I-V, we compare the cross sections for some simple systems at one low and one high incident energy (scattering angle = 90^o) as calculated by the Vineyard prescription (i.e., by taking the Fourier transform of the classical correlation function) with the cross sections obtained from our Equation (10). The differences are seen to be significant, particularly at the higher incident energy. It is perhaps up to the experimentalists to determine if the differences between the two curves are within the realm of experimental observation.

REFERENCES

1. L. Van Hove, Phys. Rev. 95, 249 (1954).
2. R. J. Glauber, Phys. Rev. 98, 1692 (1955).
3. P. Schofield, Phys. Rev. Letters 4, 239 (1960).
4. R. Aamodt, K. M. Case, M. Rosenbaum, P. F. Zweifel, "The Quasi-Classical Treatment of Neutron Scattering", University of Michigan, preprint.
5. J. H. Irving and R. W. Zwanzig, J. Chem. Phys. 19, 1173 (1951).
6. H. J. Groenewald, Physica 12, 405 (1946).
7. R. E. Turner, Physica 27, 260 (1961).
8. G. C. Wick, Phys. Rev. 94, 1228 (1954).
9. G. H. Vineyard, Phys. Rev. 110, 999 (1958)
10. K. S. Singwi, A. Sjolander, Phys. Rev. 120, 1093 (1960).

FIGURE CAPTIONS

Figure 1 - Differential scattering cross section versus outgoing neutron energy for neutrons of incident energy 5×10^{-3} ev scattered at 90° by an ideal gas of mass 18 at $295^{\circ}K$.

Figure 2 - Differential scattering cross section versus outgoing neutron energy for neutrons of incident energy 0.1 ev scattered at 90° by an ideal gas of mass 18 at $295^{\circ}K$.

Figure 3 - Differential scattering cross section versus outgoing neutron energy for neutrons of incident energy 5×10^{-3} ev scattered at 90° by a system of particles of mass 18 diffusing according to the Langevin model at $295^{\circ}K$.

Figure 4 - Differential scattering cross section versus outgoing neutron energy for neutrons of incident energy 0.1 ev scattered at 90° by a system of particles of mass 18 diffusing according to the Langevin model at $295^{\circ}K$.

Figure 5 - Differential scattering cross section versus outgoing neutron energy for neutrons of incident energy 5×10^{-3} scattered at 90° by a Debye model of a solid with $\Theta = 135^{\circ}K$.

Note:- The solid lines correspond to $\left(\frac{\partial^2 \sigma}{\partial E \partial \Omega}\right)_{\nu}$

The dashed lines are obtained from Equation (10).

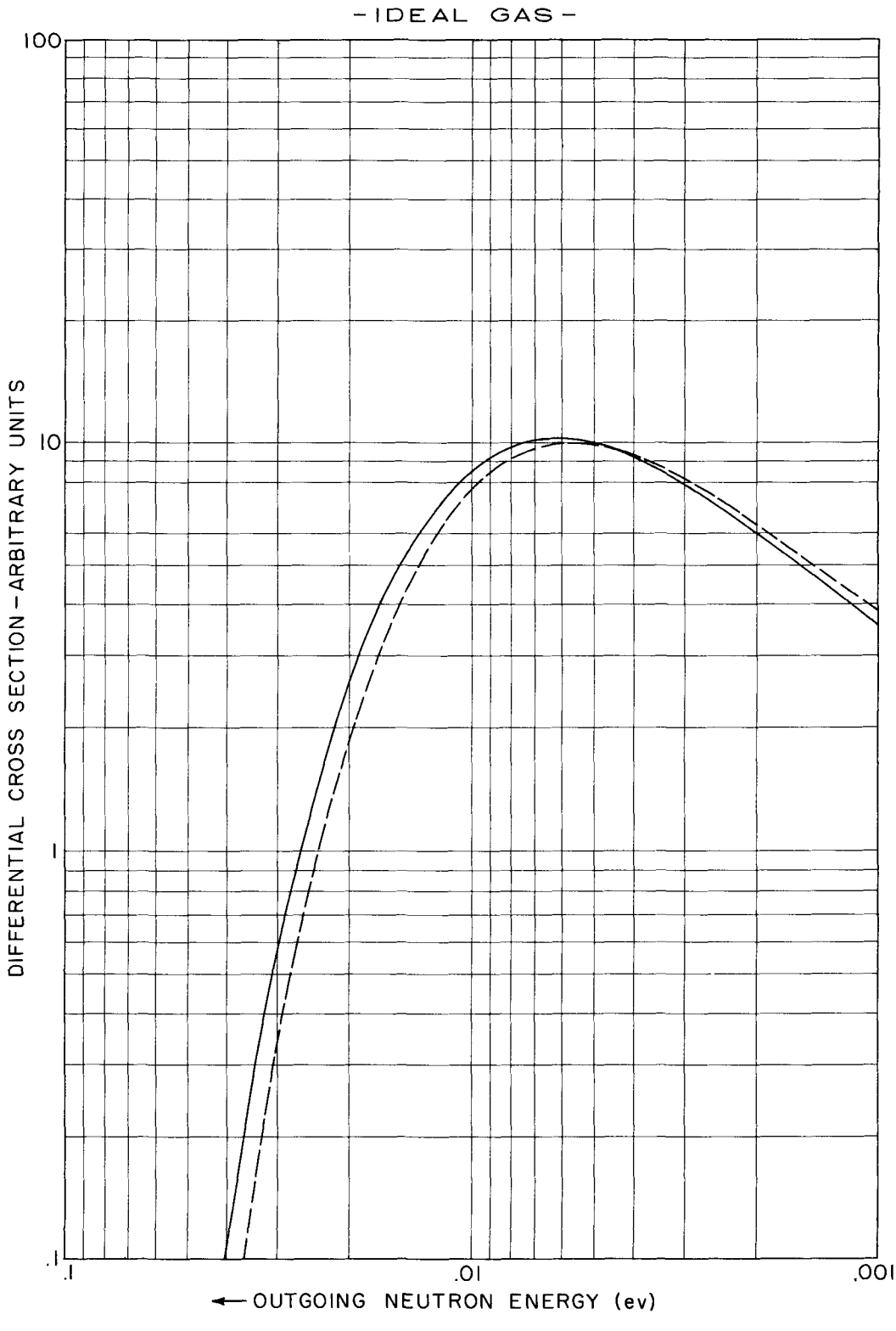
- IDEAL GAS -
100
10
1
.1
DIFFERENTIAL CROSS SECTION - ARBITRARY UNITS
.1
.01
.001
← OUTGOING NEUTRON ENERGY (ev)

FIGURE 1

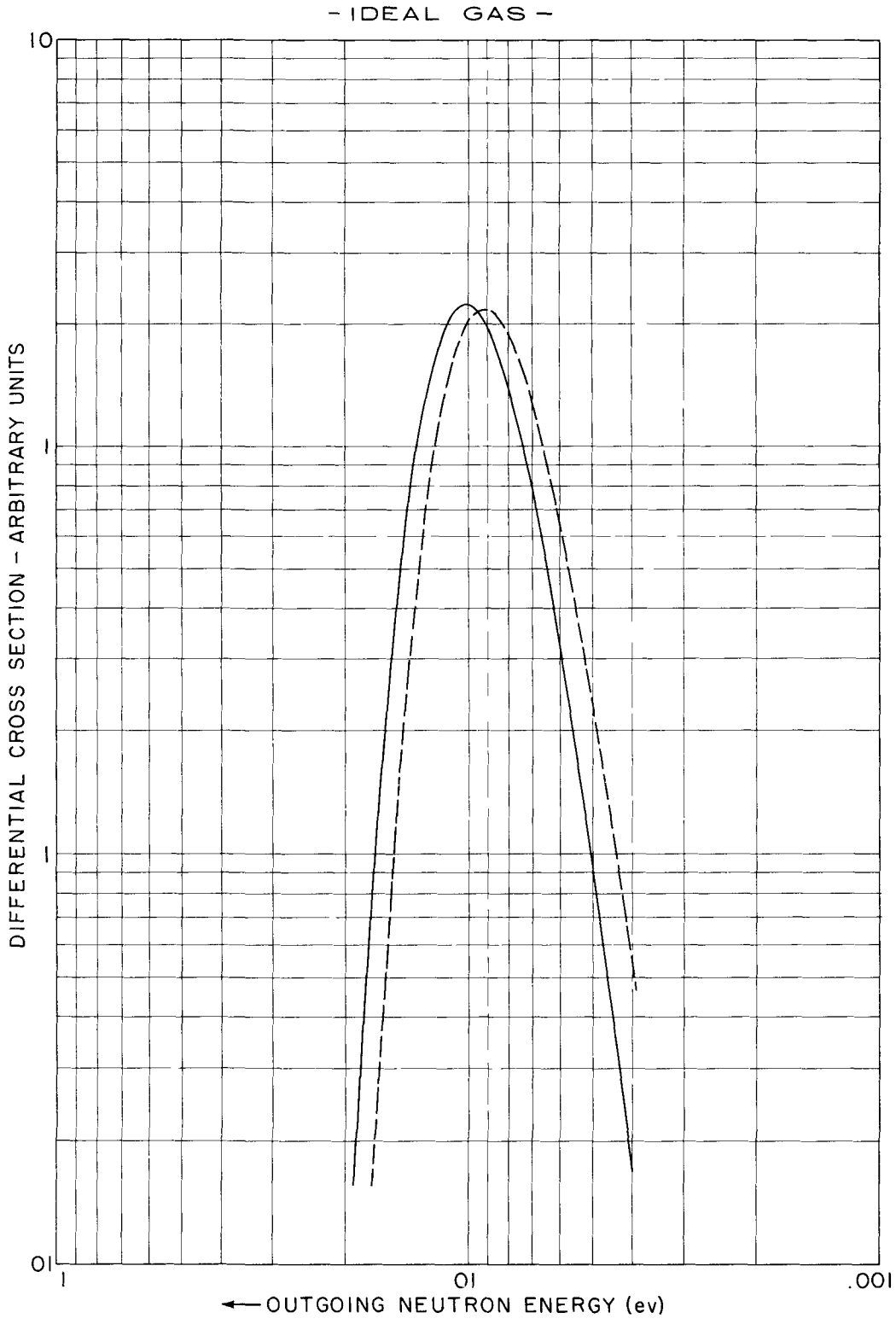
- IDEAL GAS -
10
1
01
DIFFERENTIAL CROSS SECTION - ARBITRARY UNITS
1
01
.001
← OUTGOING NEUTRON ENERGY (ev)

FIGURE 2

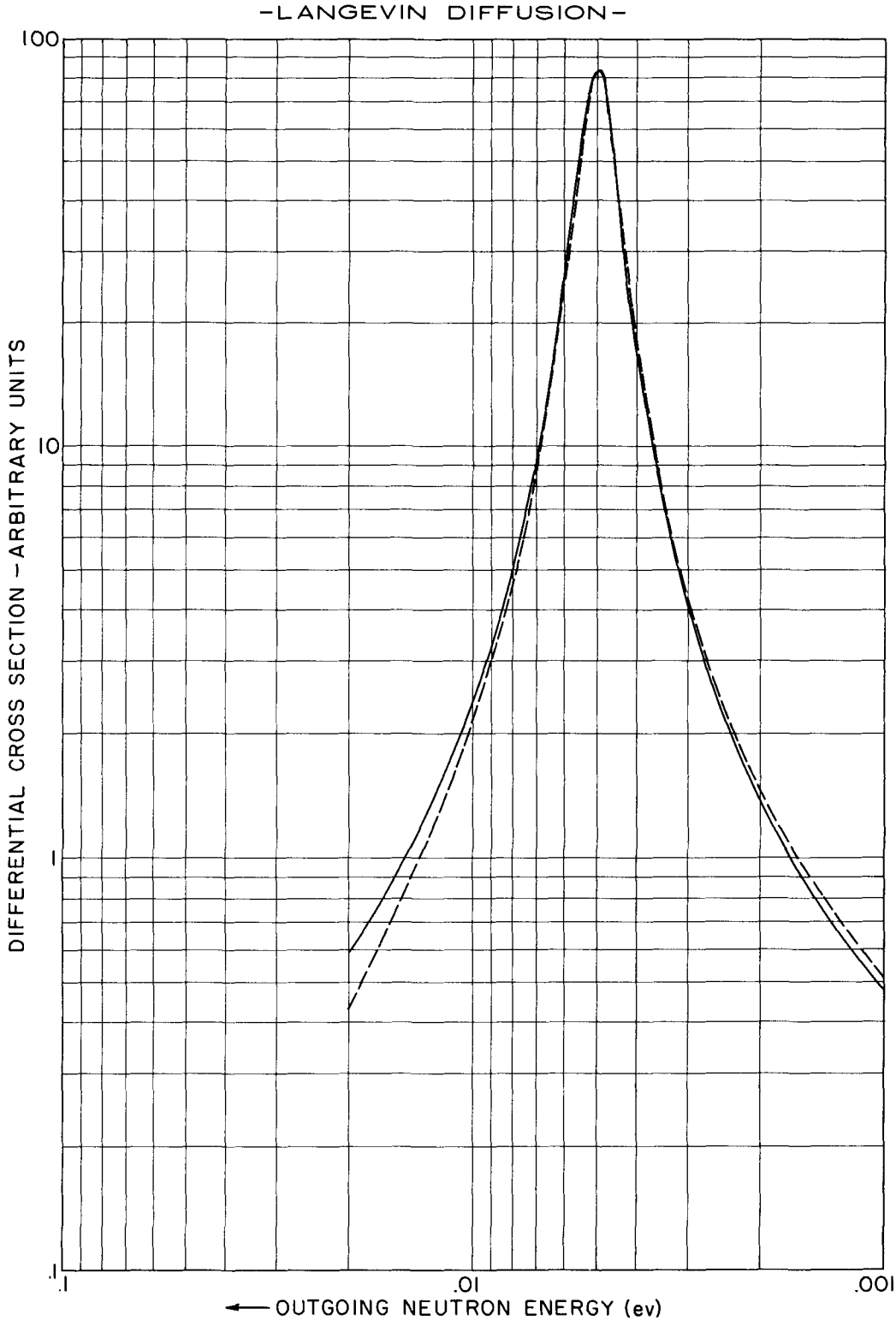
-LANGEVIN DIFFUSION-
100
10
1
.1
DIFFERENTIAL CROSS SECTION - ARBITRARY UNITS
.1
.01
.001
← OUTGOING NEUTRON ENERGY (ev)

FIGURE 3

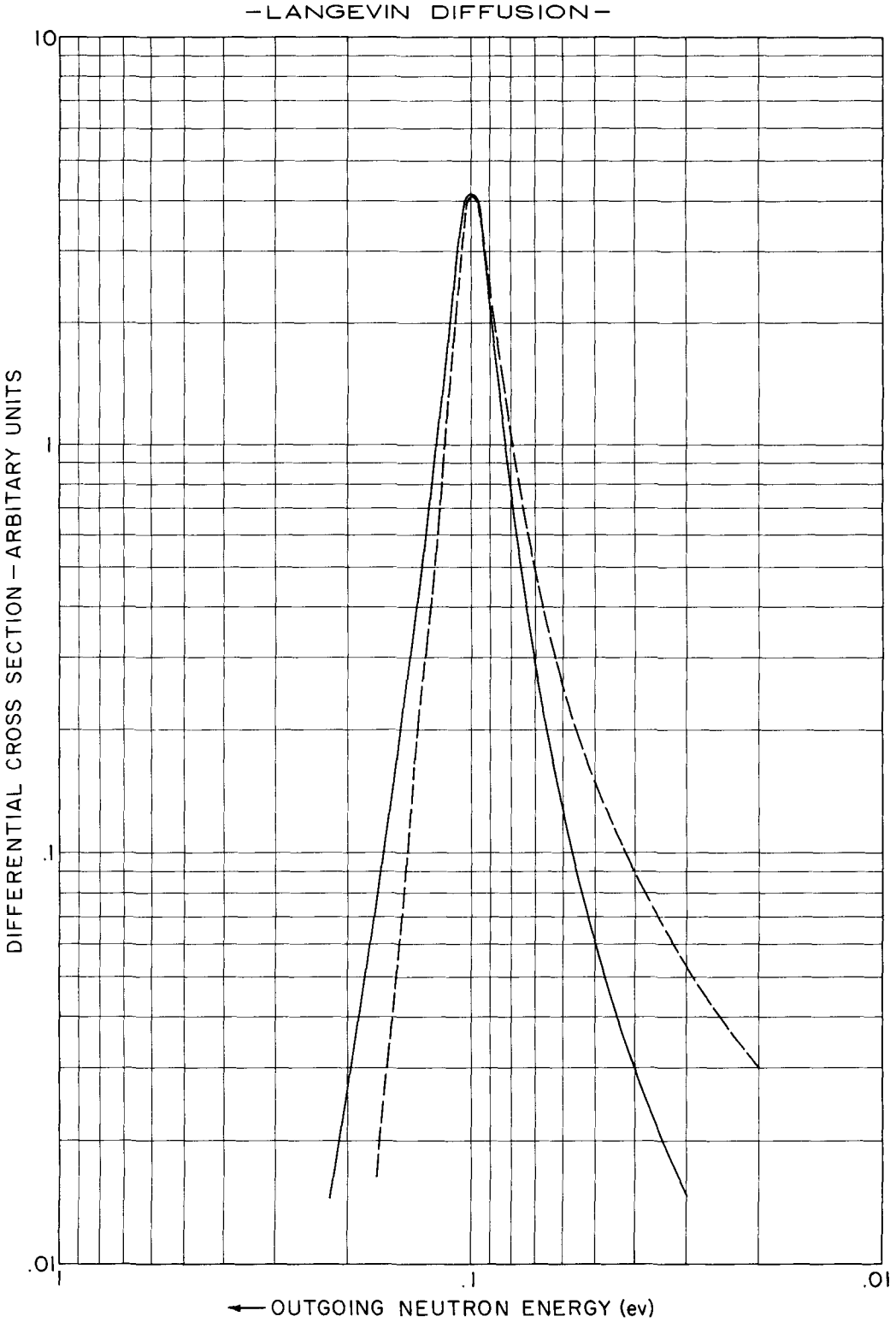
-LANGEVIN DIFFUSION-
10
1
.1
.01
1
.1
.01
DIFFERENTIAL CROSS SECTION - ARBITARY UNITS
← OUTGOING NEUTRON ENERGY (ev)

FIGURE 4

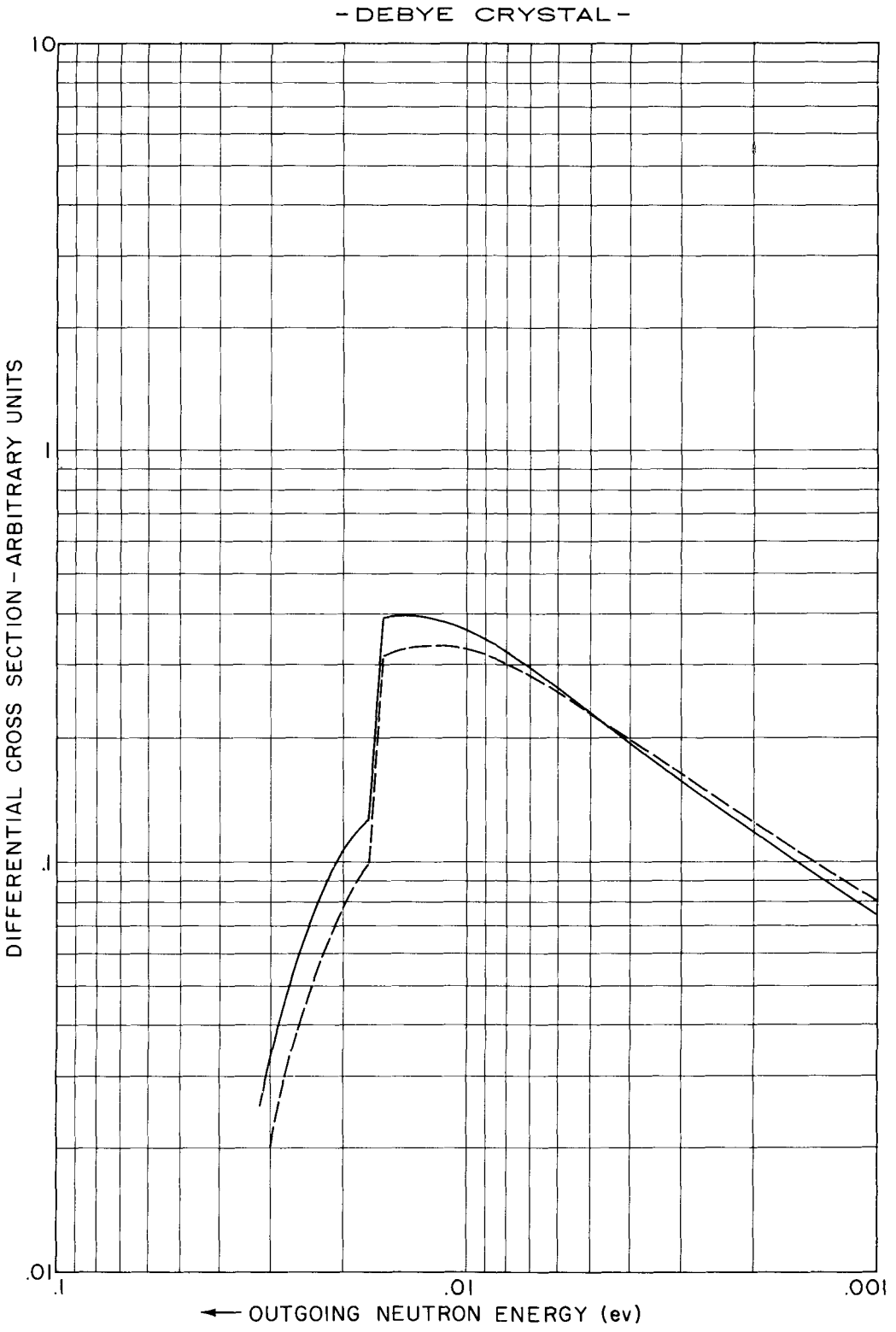
- DEBYE CRYSTAL -
10
1
.1
.01
DIFFERENTIAL CROSS SECTION - ARBITRARY UNITS
.1
.01
.001
← OUTGOING NEUTRON ENERGY (ev)

FIGURE 5

"HINDERED ROTATIONS" IN LIQUIDS AND SLOW-NEUTRON SCATTERING

S. Yip+ and R. K. Osborn
Department of Nuclear Engineering
The University of Michigan

+Phoenix Owens-Corning Predoctoral Fellow.

ABSTRACT

A quasi-crystalline model which describes both free and hindered rotations is proposed for the study of polar molecules in the liquid state. By means of the coupling between molecular dipole moment and a local electric field, which represents orientation-dependent effects of intermolecular interaction, hinderance in the rotational motion of a molecule is produced. Under the condition of strong field oscillator-like solutions are obtained for symmetric and linear molecules.

Differential neutron scattering cross sections are calculated, and effects of hindered and free rotations discussed. When free rotations are ignored, a simple expression suitable for practical applications is given.

INTRODUCTION

In an effort to analyze experiments involving neutron scattering by polar liquids, a simple, quasi-crystalline model of the liquid state is constructed. The fundamental assumption in the model is that for times long compared to neutron-nuclear interaction times, each molecule moves in a potential generated by interactions with its neighbors, which is approximated by a function depending upon the coordinates of that molecule only and is taken as the sum of two parts. One of these is assumed to be a function of the coordinates of the center of mass of the molecule only and, at least for the description of bound (or hindered) translation states, may be approximated by the Hooke's Law potential appropriate to an Einstein-crystal description of the corresponding solid phase. The other part of the potential is a function only of the orientation of the molecular electric dipole moment with respect to a local electric field. This field is presumably produced by the ordered near neighbors of the molecule in question, and its magnitude is expected to be of the same order as that estimated for the corresponding crystal[+]. The orientation of such a field with respect to laboratory axes is taken to be random.

In view of the above assumptions, the energy of the liquid is therefore approximated by the sum of energies of individual

---

[+]This supposition finds support in measurements for water using neutron scattering[1] and Raman spectroscopy[2].

molecules. Furthermore, in the sense of approximations suitable to the present discussion, the energy of any given molecule is also decomposable into parts, i.e., electronic energy, nuclear vibrational energy, energy of center-of-mass motion in the form of the above-mentioned potential, and the energy of orientation arising from the coupling of the molecular dipole moment to the local electric field (energy of hindered rotation). The present discussion is devoted almost exclusively to the influence of the last of these upon neutron scattering.

It should be noted in passing that the proposed model implies no dynamical correlations between molecules. Thus there will be no intermolecular, inelastic interference scattering.

THE MODEL

The dynamical behavior of a molecular rotator, assumed to be rigid, in a potential field is described by the equation

$$\left\{ \frac{1}{2} \sum_{i=1}^{3} \frac{P_i^2}{I_i} + V - E_{SKM} \right\} \Psi_{SKM} = 0 \qquad (1)$$

where P_i is the component of the total angular momentum along the principal axis $\underline{e}_i$ and I_i is the moment of inertia about this axis, Ψ_{SKM} and E_{SKM} are the wave function and energy of the rotator in the state characterized by quantum numbers, S, K and M appropriate to the three degrees of freedom. By taking the molecular dipole moment $\underline{\mu}$ along the body-z axis and the local electric field $\underline{E}$ along the space-z axis, the potential V according to the present description becomes simply $-\lambda \cos\theta$ with $\lambda = \mu E$. Since we assume that quasi-crystalline ordering exists in the liquid and because of relatively close packing of the molecules, E is expected to be sufficiently large so the condition $\lambda \gg \hbar^2/2I_i$ applies[+].

In the presence of a strong field the dipole will tend to be aligned along the direction of $\underline{E}$ so θ, the angle between $\underline{\mu}$ and $\underline{E}$, is restricted to have only small values. This suggests a method of solution in which terms in Equation (1) are

---

[+]A crude estimate of E based upon the known structure of ice shows that indeed the strong-field condition is satisfied. Similar conclusion has been reached by Magat[3].

expanded in a truncated power series in θ about $\theta = 0$. The first-order solution for the symmetric molecule is[+]

$$\Psi_{SKM} = N e^{iM\psi} e^{iK\phi} \chi^{\frac{|K-M|}{2}} e^{-\frac{\chi}{2}} L_S^{|K-M|}(\chi) \qquad (2)$$

$$E_{SKM} = \sqrt{2AB}\,(2S+|K-M|+1) + \frac{BK^2}{3}\left(\frac{I}{I_3} - \frac{2}{3}\right) \qquad (3)$$

$$+ \frac{BM}{3}(K+M) - \lambda$$

where

$$N = \left\{ \frac{(\lambda/2B)^{1/2}\, S!}{2\pi^2 \left[(S+|K-M|)!\right]^3} \right\}^{1/2} \quad ; \quad \chi = \left(\frac{\lambda}{2B}\right)^{1/2} \theta^2$$

$$B = \frac{\hbar^2}{2I} \quad ; \quad S = 0, 1, 2, \ldots \quad ; \quad K, M = 0, \pm 1, \pm 2, \ldots$$

In this notation, I_3 is the moment of inertia about symmetry axis e_3 and $I = I_1 = I_2$, $L_S^{|K-M|}$ is an associated Laguerre polynomial. The above result is valid when $\lambda \gg B$.

The first term in E_{SKM} represents the energy of hindered motions which, although influenced by all three degrees of freedom, is actually determined by only two numbers. We see that by ignoring the small energies of free rotation, terms proportional

---

[+] An approach applicable for any value of λ is to use the free rotator solution to obtain by orthogonal transformation a new basis in which V is diagonal.[4] This method necessarily involves the diagonalization of an infinite tri-diagonal matrix, and results in a continued fraction form of expressions for the energy and transformation matrix elements. Such a solution is not suitable for our purpose since considerable numerical efforts would be involved.

to B, the model describes the dynamical behavior of symmetric molecules as a system with two effective degrees of freedom, in fact, a two-dimensional isotropic oscillator. The energy structure of the rotator will thus appear as a set of complicated levels due to free rotations superimposed upon the equally-spaced hindered-rotation levels.

Evidently not all possible rotator states given by Equation (2) are admissible. The reason for this follows from the restriction to small angles. The expectation value of θ^2 in a given state,

$$\langle \theta^2 \rangle = \left(\frac{2B}{A}\right)^{1/2} (2s + |K-M| + 1) \qquad (4)$$

can be used to provide an estimate of our small-angle approximation, so the model breaks down for large values of s and $|K-M|$ where $\langle \theta^2 \rangle$ is no longer small. Our description also ceases to apply when the energy available for rotation is so large that the molecule effectively rotates without hindrance. This effect corresponds to the limit of weak field and is not derivable from the present results.

Linear molecules can be treated as a special case of the solution just obtained. Since there is no rotation about the molecular-axis the angle ϕ and quantum number K do not exist; consequently the model for linear molecules is the same as that for symmetric molecules with $K=0$ and the factor $(2\pi)^{-1/2}$ removed from normalization constant N. It can be seen that the strong-

field approximation leads to the same description of hindered rotation regardless of the number of degrees of freedom available to the molecule. The difference in dynamical behavior of the two systems therefore lies in free motion. From Equation (3) we observe that the energy of a symmetric molecule can undergo a small change by a change in K and M which still leaves $|K-M|$ the same. Physically this would correspond to altering the rotational frequency about the symmetry axis, and since relative orientation of $\underline{\mu}$ and $\underline{E}$ is not affected the process requires only a small amount of energy. On the other hand, in the case of the linear molecule, this is not possible, and any change in energy affects both hindered and free rotations.

The model has not yet been satisfactorily generalized to the asymmetric molecule. The method of orthogonal transformations, successfully employed by Wang[5] in treating the free asymmetrical top, requires considerable numerical work and is probably not promising. However, as seen earlier, hindered rotations appear to be insensitive to system symmetries, then in the limit of strong field the symmetric model should provide a good approximation since terms introduced by the asymmetry are of the order of free rotation energies.

The hindered rotator model just proposed is suitable for use in calculating differential cross sections. For scattering from a single molecule the expression to be evaluated is of the form[6]

$$\langle \alpha\alpha' \rangle_T = \langle sKM | e^{itH} e^{i\underline{K}\cdot\underline{b}_\alpha} e^{-itH} e^{-i\underline{K}\cdot\underline{b}_{\alpha'}} | sKM \rangle \qquad (5)$$

where $\underline{b}_\alpha$ is equilibrium position of α^{th} nucleus measured with respect to center-of-mass of the molecule and subscript T denotes average over molecular and electric field orientations. The result can be conveniently expressed as a power series in $1/4\xi$, where $\xi = (2B/\lambda)^{1/2}$. For symmetric molecules we obtain

$$\langle \alpha\alpha' \rangle_T = 4\pi \sum_{l,k} j_l(Kb_\alpha) j_l(Kb_{\alpha'}) Y_l^{k*}(\hat{\underline{b}}_\alpha) Y_l^k(\hat{\underline{b}}_{\alpha'}) \qquad (6)$$
$$(*)\left\{ 1 + \frac{(1+e^{-\nu})[l(l+1)-k^2]}{2\xi(1-e^{-2\nu})} \left(e^{-\nu} e^{it\sqrt{2\lambda B}} + e^{-it\sqrt{2\lambda B}} \right) \right\} + \mathcal{O}\left(\frac{1}{16\xi^2}\right)$$

where j_l is a spherical Bessel function, $\hat{\underline{b}}_\alpha$ is the direction of α^{th} nucleus measured in the body system, and $\nu = \sqrt{2\lambda B}/k_B T$. Average over molecular orientations has been computed using all possible states. In cases where this is not consistent with the molecular model, the appropriate partial sum can be performed without difficulty. Corresponding expression for linear molecules is given by the k = 0 terms.

The first term in Equation (6) represents the contribution due to elastic scattering while the two time-dependent terms

correspond to one-quantum inelastic scattering in which neutron energy is increased and decreased respectively by an amount $\sqrt{2\lambda B}$ This rather large energy transfer may be interpreted as the hindered rotation peak, which has been observed in cold-neutron scattering from water[3, 7] and ammonium halides[8]. In fact, the same type of energy transfer can also be obtained by treating the rotator as an ordinary oscillator with frequency equal to $\sqrt{2\lambda B}/\hbar$, and in this respect the nature of approximation in Nelkin's model[9] for treating hindered rotations in water is demonstrated. Aside from this aspect little similarity exists, particularly in the intensity factors and the manner in which molecular constants enter, between Nelkin's calculation and the present treatment, which within the small angle approximation represents a fairly rigorous and formal calculation of scattering by systems with only rotational degrees of freedom.+

The general expression for $\langle \alpha\alpha' \rangle_T$ contains terms corresponding to multiple-quantum transitions. These terms do not appear because they are of order $1/16\xi^2$ and higher. It should be evident that in arriving at Equation (6) we have ignored free rotations, for otherwise energy exchange will involve free-rotation energies and, as in the free rotator calculation, the average over molecular orientation cannot be given in closed form. When free rotations are considered, a broad distribution of energy transfer

---

+The general method of calculation employed here has also been applied to free rotators. Independently Rahman has described a similar approach in his recent paper[10].

centered roughly about each hindered-rotation peak can be expected. It was mentioned earlier that free rotations of a symmetric molecule can be excited independently of the hindered modes; consequently there will appear in the neutron distribution low-energy peaks. Such peaks do not exist for linear molecules.

By taking terms with $\nu = \nu'$ and $\nu \neq \nu'$ we obtain from Equation (6) contributions to the cross section due to direct and "inner" (interference within the same molecule) scatterings. The contribution due to "outer" (interference from different molecules) scattering is given by

$$\begin{aligned} \langle \alpha\alpha' \rangle_T^e &= \langle \varepsilon_{KM} | e^{i\underline{K}\cdot\underline{b}_\alpha} | \varepsilon_{KM} \rangle_T \langle \varepsilon_{KM} | e^{-i\underline{K}\cdot\underline{b}_{\alpha'}} | \varepsilon_{KM} \rangle_T \\ &= j_0(Kb_\alpha) j_0(Kb_{\alpha'}) , \end{aligned} \tag{7}$$

where we have assumed that average over electric field orientation can be performed separately for each molecule, the assumption of no angular correlation previously noted. For this reason the outer scattering is purely elastic which is characteristic of all independent-particle models.

Finally we mention that the mass-ratio expansion discussed by Zemach and Glauber[6] can be applied to the present model. For direct scattering by linear molecules the difference in the free rotator results and that obtained for the hindered rotator first appears in the term proportional to $(m/Mkb)^2$ where M is the "effective" rotational mass, m is neutron mass, and k

is the magnitude of its initial momentum. As we would expect, the distinction between hindered and free rotations vanishes as incident neutron energy becomes large.

REFERENCES

1. D. J. Hughes, H. Palevsky, W. Kley, and E. Tunkelo, Phys. Rev. 119, 872(1960).

2. P. C. Cross, J. Burnham, P. A. Leighton, J. Am. Chem. Soc. 59, 1134(1937).

3. M. Magat, Ann. d. Physique, 6, 109(1936).

4. P. Kusch and V. W. Hughes, Handbuch der Physik XXXVII/1, 1 (1959).

5. S. C. Wang, Phys. Rev. 34, 243(1929).

6. A. C. Zemach and R. J. Glauber, Phys. Rev. 101, 118(1956).

7. B. N. Brockhouse, Nuovo Cimento Suppl. 9, 45(1958).

8. H. Palvesky, V. W. Myers, and V. M. Brajovic, Bull. Am. Phys. Soc. 6, 261(1961).

9. M. Nelkin, Phys. Rev. 119, 741(1960).

10. A. Rahman, J. Nucl. Energy 13, 128(1961).

The Proceedings of the

BROOKHAVEN CONFERENCE ON NEUTRON THERMALIZATION

have been published in four volumes.

Volume I, The Scattering Law

Volume II, Neutron Spectra in Lattices and Infinite Media

Volume III, Experimental Aspects
of Transient and Asymptotic Phenomena

Volume IV, Theoretical Aspects
of Transient and Asymptotic Phenomena

BNL 719 (C-32)
Volume II of IV, Neutron Spectra
in Lattices and Infinite Media

17

325
12-28-62

MASTER

PROCEEDINGS OF THE BROOKHAVEN CONFERENCE ON NEUTRON THERMALIZATION

Volume II, Neutron Spectra in Lattices and Infinite Media

April 30 to May 2, 1962

BROOKHAVEN NATIONAL LABORATORY
ASSOCIATED UNIVERSITIES, INC.
under contract with the
UNITED STATES ATOMIC ENERGY COMMISSION

BNL 719 (C-32)
(Physics - TID 4500, 18th Ed.)

PROCEEDINGS OF THE BROOKHAVEN CONFERENCE ON NEUTRON THERMALIZATION

Volume II, Neutron Spectra in Lattices and Infinite Media

April 30 to May 2, 1962

BROOKHAVEN NATIONAL LABORATORY
UPTON, NEW YORK

LEGAL NOTICE

PRINTED IN USA
PRICE $15 00 FOR THE FOUR VOLUMES

Available from the
Office of Technical Services
Department of Commerce
Washington 25, D C

September 1962 1100 copies

PREFACE

A conference on the subject of neutron thermalization was held at the Brookhaven National Laboratory from April 30 to May 2, 1962, precisely four years after the close of the last thermalization conference, the Gatlinburg conference of April 28-30, 1958. The subject of thermalization, which concerns the approach to thermal equilibrium and the manner of the equilibrium distribution of neutrons in matter, has elicited a great deal of interest in the meantime. While the seventeen papers contributed at Gatlinburg could be assembled into a single, convenient volume, presenting the seventy Brookhaven papers has required four weighty books.

The Brookhaven conference was conducted as a "reporter" conference. The technical papers which were submitted were sorted into six categories, viz., the experimental and theoretical aspects of the "scattering law," of spectra in infinite media, and of transient phenomena. A reporter was chosen for each of the six topics, and was asked to prepare a talk which would contain an appreciation of the technical papers. The reporter talk, followed by a general discussion constituted each session. Thus, the individual papers were not presented, though copies were available to all who attended, and are presented in these proceedings. (While the papers from our Soviet colleagues were received too late for discussion at the conference, translated versions will also be found in these volumes.)

The success of a technical conference is always due to the efforts of many people. We must first thank the reporters and authors for the fine quality of their contributions. Mr. Robert Brown of Brookhaven's Graphic Arts Division was responsible for the prompt publication of the proceedings and for having more than ten thousand copies of the technical papers ready in time for the conference. Mrs. Mariette Kuper and Mr. Edward Bergin and their staffs directed the mechanics of the conference with skill and aplomb, while several members of the Theoretical Reactor Physics Group made important contributions to its planning and execution. In particular, we should thank Drs. Paul Michael and Henry Honeck, and for his kind encouragement throughout, Mr. Jack Chernick, the Group's Director.

NOEL CORNGOLD

VOLUME II

PROGRAM AND TABLE OF CONTENTS

NEUTRON SPECTRA IN LATTICES AND INFINITE MEDIA
Chairman: M.J. POOLE, AERE, Harwell, England

A. Experimental Aspects

B. Theoretical Aspects

NEUTRON SPECTRA IN LATTICES AND INFINITE MEDIA

A. Experimental Aspects

Status of Neutron Spectra Measurements*

J. R. Beyster
General Atomic
John Jay Hopkins Laboratory for Pure and Applied Science
San Diego, California

*GA-3176
Project 48.01
U. S. Atomic Energy Commission
Contract AT(04-3)-167, Project Agreement No. 2

I. Introduction

There have been discussions at this conference of the experimental status of scattering law determinations and discussions of the theoretical procedures used to interpret and extend these measurements. In addition, H. Honeck[1] has discussed the analytical and numerical procedures used to predict reactor neutron spectra and reaction rates using the best scattering laws available for the common moderators. He has pointed out how well much of the experimental data, especially that on reaction rates in actual lattices, can be fit by approximate procedures which preserve only certain important properties of the scattering law. In this paper the status of differential neutron spectra (experiment and theory) will be discussed and existing discrepancies whether of new or old origin pointed out.

Ultimately most spectral investigations are performed for reactor technological reasons. Reliable tested methods for predicting neutron spectra in reactor cores, reflectors, or shields are badly needed and it has been the primary objective of those working in the field to find these methods. Specifically, experimentalists have one of three possible objectives in measuring spectra:

1. to measure or infer information on scattering laws,

2. to perform a check on the adequacy of the physics and transport approximation made in typical problems, and

3. to measure a spectrum for a specific practical application.

The first and third objectives are of rather limited usefulness. In the first case neutron spectra are in general not extremely sensitive to the details of a scattering law so very high precision of measurement of spectra whether they be steady state or time dependent is required – even then ambiguous interpretations are hard to avoid. However, differential spectra if measured precisely, can indicate qualitatively where either better physics information or refinements in theoretical methods is required. For example at present it is clear that at neutron energies above 0.1 ev, for most common moderators, better scattering law information is needed. These methods then are capable of checking the adequacy of various approximations (physical and numerical) for general classes of problems encountered in reactor analysis and are thus of considerable utility.

Next let us review briefly the procedures used for measuring or inferring neutron spectra from measurements and discuss the current status of the experimental results for the common moderators, pointing out where possible the work that needs to be done experimentally and the best approach

to these experiments. It has not been possible here to refer to every paper submitted to this conference which has some bearing on spectra, but general conclusions based on the general run of experiments will be given.

II. Basic Experimental Methods

There are two basic techniques normally for inferring or specifying neutron spectra. These are: 1) direct measurements, and 2) indirect measurements of spectral index – usually done by foil activation procedures.

Having established the motivations for making spectral measurements one is next inclined to ask what precision is needed in the measurements. In general, spectral experiments require relatively high precision since theoreticians desire to make comparisons at experimental tie points they can rely on to be correct. Various workers suggest a need for precision in various parameters as the criteria. Since the product of cross section and flux always occur in reactor analysis, normal cross section precision of about 1% accuracy is often suggested as an acceptable error. This is a very severe requirement and not really realistic. Normally the product of ϕ and σ is integrated over a fairly wide energy interval before use in any reactor analysis code. This certainly decreases, due to the existence for example of conservation effects, the requirement for precision in the relative flux. Relative flux variations of 5 to 10% are usually acceptable before errors in integrated quantities exceed

1 to 2%. Even this is not a truly realistic approach to the matter of precision. What one wants to know well is a quantity like ηf (fission neutrons produced per capture in a typical cell) which contains ratios of reaction rates and is relatively insensitive to spectra. Temperature coefficients of reactivity, on the other hand, place a relatively high precision requirement on temperature determinations of ηf, namely 0.1% accuracy.

Experimentalists measuring neutron spectra should strive to produce experimental data which will not prove to be the limiting factor in comparisons between various theoretical approaches. A fairly safe rule to follow today is that 5 to 10% accuracy in relative spectral shapes should be an experimental objective.

In this paper results and potentialities of the direct spectral measurement technique will mainly be reviewed. However, since an appreciable amount of work is still being done by foil activation procedures, this method will be discussed briefly first.

Integral Methods of Spectral Measurement

This technique consists in general of measuring some index of the neutron spectrum by determining relative reaction rates in bare and cadmium covered absorbers.

Common materials used are: lutetium, europium, plutonium, U^{235}, etc. Good fast to slow indices are provided by Lu^{176} to U^{235} ratios and Pu^{239} to U^{235} ratios. These measurements often have the advantage that they give one very nearly what is needed for reactor analysis, i.e., reaction rates or ratios thereof. However, very often they do not satisfy the exact need and some method must be found to infer the desired answers from the measured quantities. In general, one can proceed two ways: 1) a spectrum can be constructed from the data by the methods of Wescott, Campbell, Freemantle, etc., 2) one can utilize theory to calculate directly measured quantities (the activations for example). In the first method the low energy spectrum is represented by a Maxwellian plus a λ/E tail which joins at some cutoff energy. The parameters describing the spectrum are the Maxwellian temperature T, λ, and the cutoff condition. Usually something like a linear fall off from 4 to 1 KT is postulated for the epithermal spectrum. A comparison of spectra determined in the same assembly by integral and differential measurements is shown in Figure 1. These measurements were reported at the Second Geneva Conference by Poole, Campbell, and Freemantle.[2] It is clear that at least in this specific example one has lost a great deal of precision in doing things this way. From a qualitative point of view this procedure is useful for correlating data from various laboratories since effective temperatures which depend on

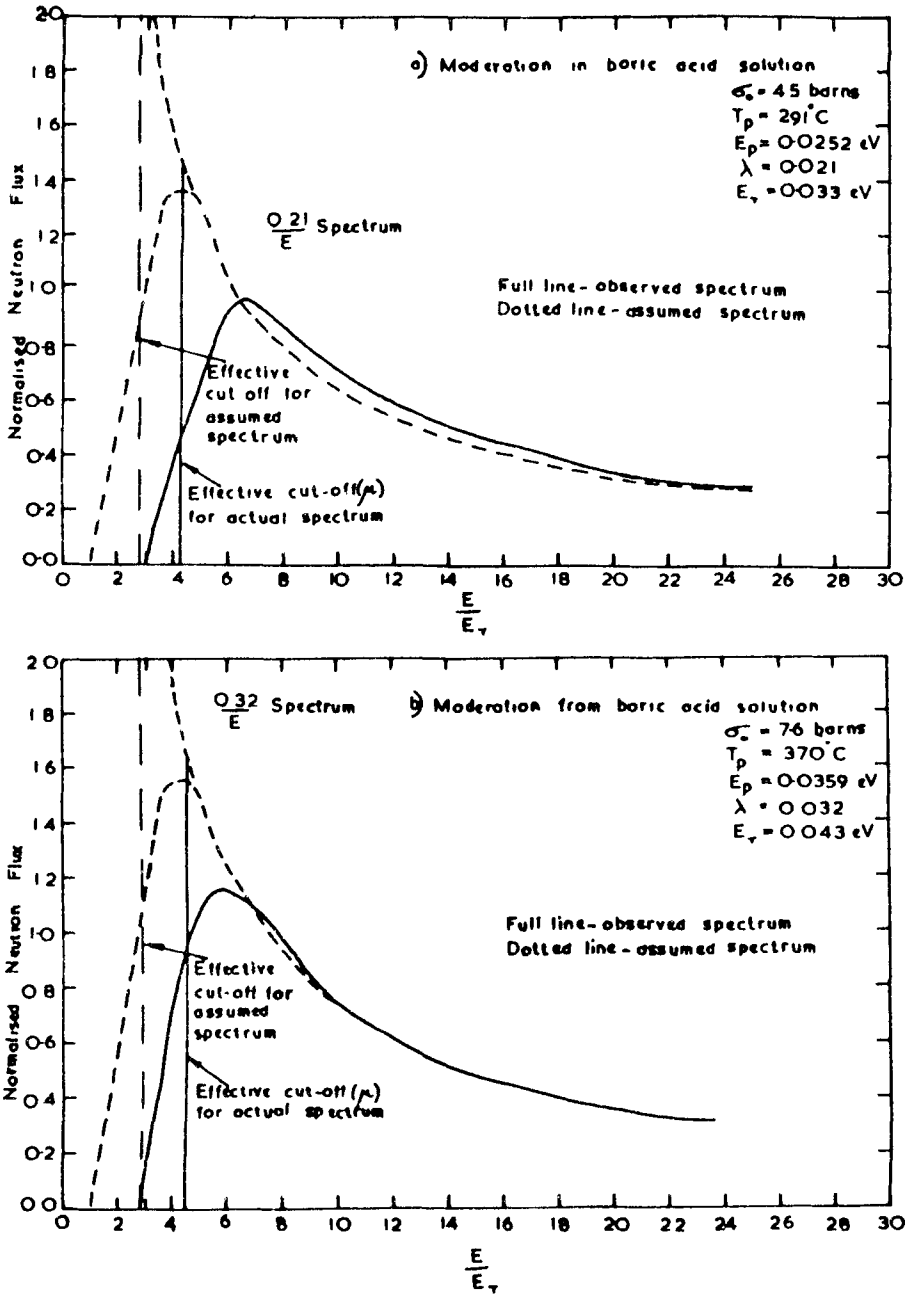

Fig. 1 Observed epithermal spectra (spectra after subtraction of Maxwellian component) for two typical boric acid solutions Energies are plotted in terms of E_τ (=kT for the neutrons) Comparable epithermal spectra according to the prescription used in the integral experiments are also shown, together with the position (λ) for the equivalent sharp cut-off in the $\frac{\lambda'}{E}$ tail

the hardening parameter $\Sigma_a/\xi\Sigma_s = \Delta$ can often be inferred by methods like that of Coveyou,[3] namely $T = T_m (1+.91\Delta)$. Figure 2 shows the spectral work of Reichardt and Burkart[4] reported to this conference together with that for a number of other experiments. A general tendency for the data to behave as one would expect from some simple model of neutron scattering like the heavy gas law is about all that is apparent. Also a general tendency toward disagreement among experimenters on the magnitude of the temperature dependence seems apparent.

The second method of analysis in current use for interpretation of activation data has been discussed by H. Honeck.[1] It would appear that when proper transport codes are used to calculate the measured activation curves in both heavy and light water lattices, relatively good agreement can be obtained with experiment.

In summary, the foil activation technique is rather limited in the detail with which it lends itself to predictions of spectra. Assumptions based on simple energy dependences (i.e., Maxwellian plus λ/E tails) are not in general valid when resonance absorption is prevalent, or when a strongly hardened spectrum is present, whether produced by 1/v absorption or a more complicated energy absorption dependence. It would appear far more profitable to

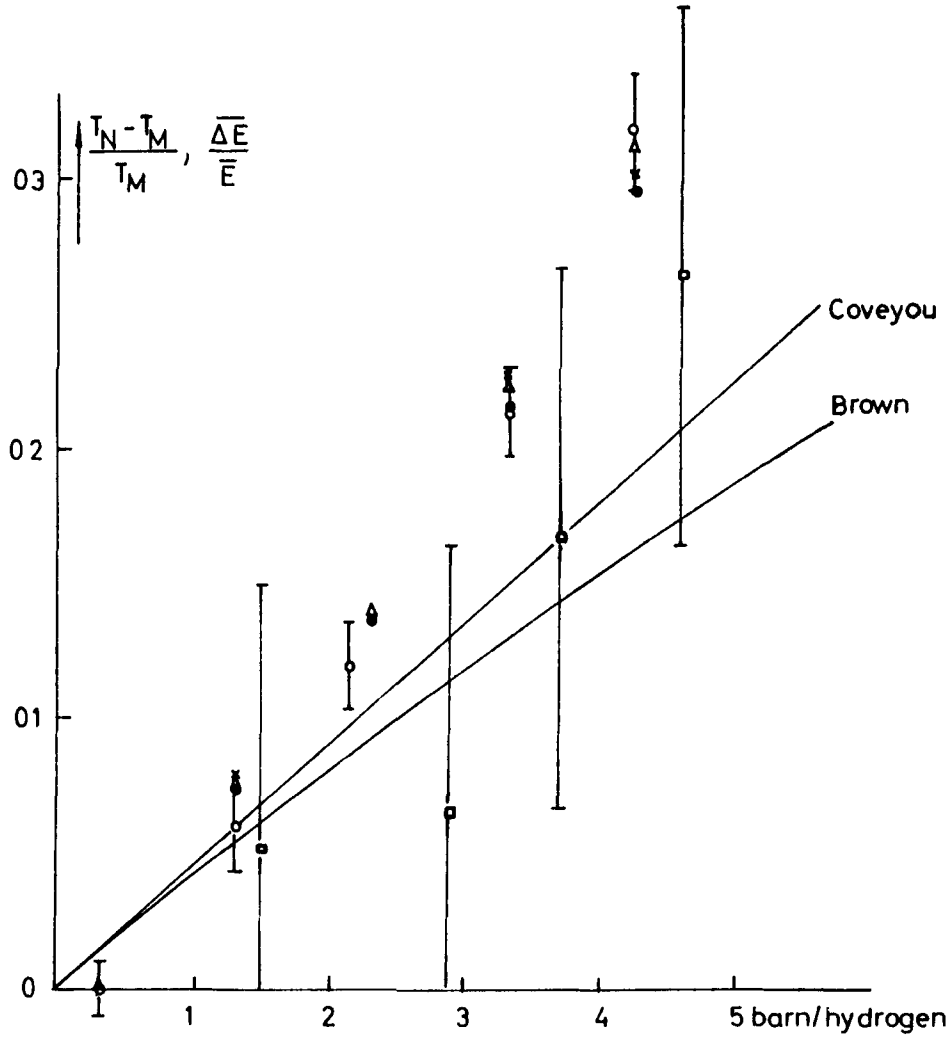

Fig. 2 Plot of $\frac{T_N - T_M}{T_M}$ versus absorption cross section T_N neutron temperature
T_M moderatur temperature

- o values obtained by the spectra measurements (mean of the results from the 15cm and 30cm cube)
- x relative energy shift of the spectra from the surface of 15cm cube
- ▫ results of Poole
- Δ results of the Lutetium foils measurements (case I)
- • results of the Lutetium foils measurements (case II)

compare activation measurements with direct numerical predictions of this quantity rather than attempting to construct equivalent spectra. Precise integral activation measurements can serve a very useful purpose in reactor analysis since spatial resolution is good and cell distortion minimal. These are conditions hard to satisfy in differential spectral determinations because of re-entrant tube perturbations.

Differential Spectrum Determinations

The conditions for a good spectrum experiment are not necessarily easy to specify completely. They depend, to a large extent, on what measurements are desired. Spectra that are subject to measurement can be of the following types:

1. Homogeneous – infinite medium
2. Homogeneous – one-dimensional
3. Homogeneous – two-dimensional
4. Homogeneous – with temperature gradient
5. Heterogeneous – one-dimensional
6. Heterogeneous – two-dimensional
7. Heterogeneous – with temperature gradient
8. Time Dependent Spectra

9. Diffusion Cooled Spectra

10. Diffusion Heated Spectra

Obviously conditions which one tries to eliminate in one class of spectrum measurement are exactly those which one desires to study in another class. In the time permitted here it is not possible to discuss in detail each experimental technique but it is informative to review where the various experimental techniques are useful.

The regions of usefulness of the Poole or chopper technique depend again on what equipment one has available since there is a considerable region of overlap. Accuracy of both methods is influenced by the ability to measure or calculate accurately the energy sensitivity of neutron detection devices. The usefulness of the Poole technique is limited by the time widening of the neutron burst due to assembly characteristics, since no auxiliary attempts to chop the neutron beam are made. The same type of problem arises in the use of a chopper for time-of-flight measurements in that burst width from the chopper will limit experimental resolution. However, somewhat better control is provided than with the Poole technique. Disadvantages of the chopper method are, however, the necessity for making large corrections to the experimental data for the energy dependent chopper transmission.

The existence of time dependent backgrounds and collimator alignments are other critical considerations.

Let us next consider resolution requirements. No discussion of resolution requirements in integral spectra measurements was made since this is not really an adjustable quantity. One takes what one can get, and hopes it is adequate. It can be shown that the uncertainty in the measured neutron flux at any energy is proportional to the second time derivative of the spectrum at that point, according to the relation

$$\phi(t)_{true} = \phi(t)_{obs}\left[1 - \frac{1}{2\phi(t)}\left(\frac{d^2\phi(t)}{dt^2}\right)\int_{-\infty}^{+\infty}\lambda^2 R(\lambda)d\lambda\right]$$

In general, if one wishes less than 1% distortion in the spectrum due to resolution he will find (except in a resonance region) rather poor energy resolution possible in the experiments. Figures 3 and 4 illustrate this point. Figure 3, reported by M. J. Poole, shows requirements for approximately 1% precision of measurement both in the Maxwellian and 1/E energy regions and also the energy resolution being used in various experimental spectral determinations.

In general, the statement can be made that meaningful neutron spectra can be measured for any moderator by either technique up to 10 ev. These

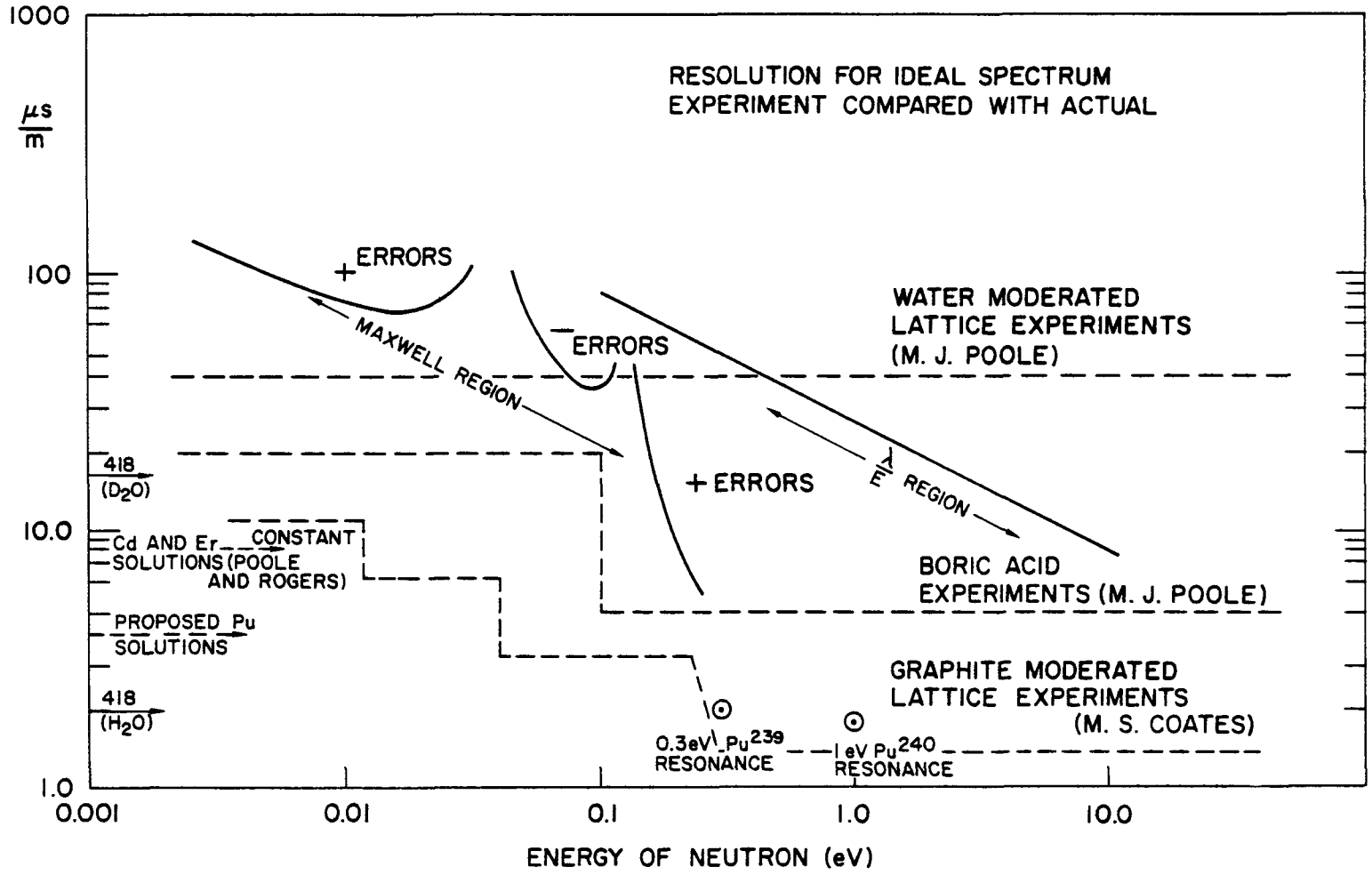

Fig. 3 Resolution for ideal spectra experiment compared with actual

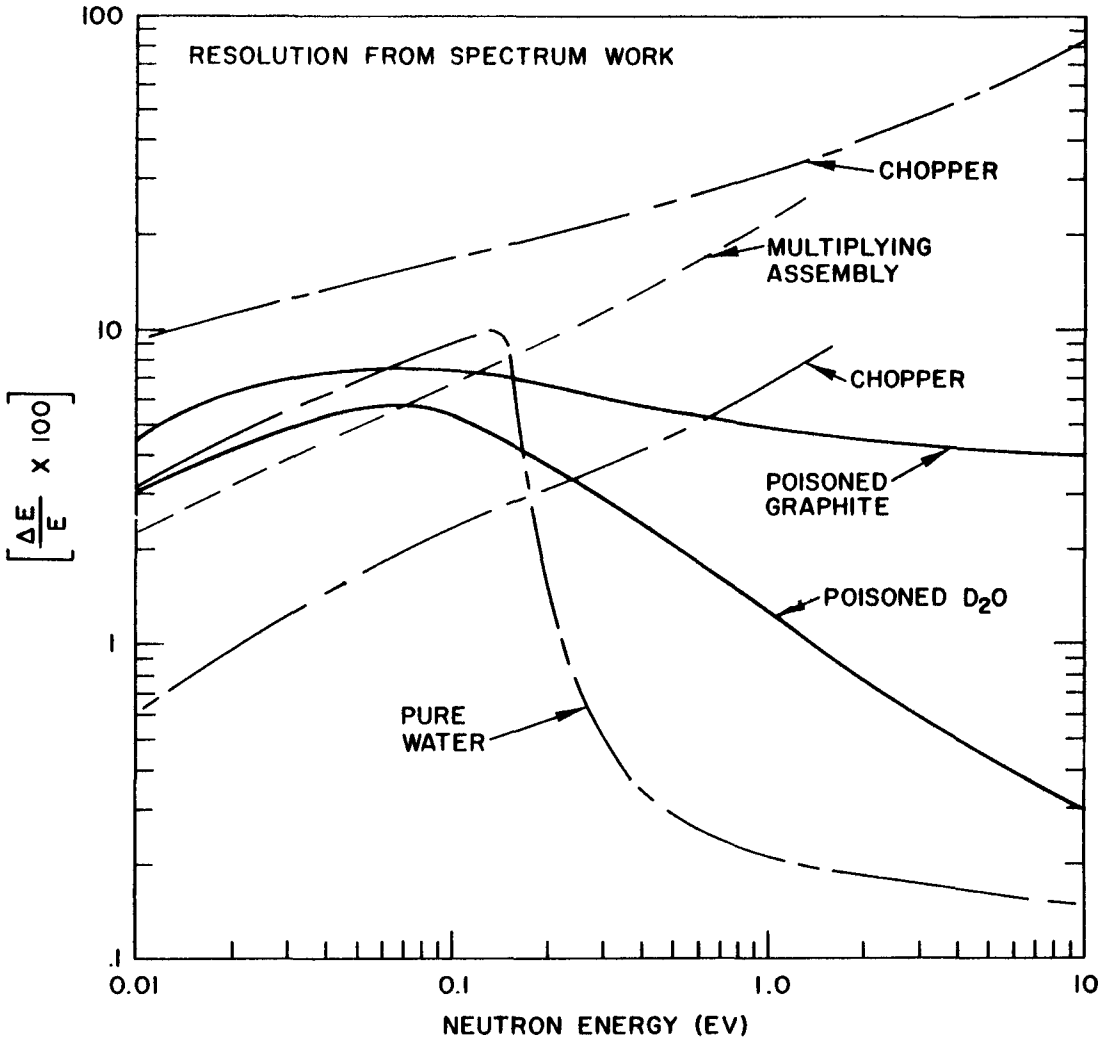

Fig. 4 Resolution from spectra work

measurements are of the precision necessary for rigorously checking theoretical predictions. Above 10 ev the Poole technique has many advantages for non-multiplying systems. For highly multiplying systems the chopper method is in general better. Combinations of the two methods for steady state spectral studies have been devised and can extend the general usefulness of either method.

Figure 4 shows what has been used in some of the work to be reported today. The upper chopper curve is the resolution used in Zenith measurements of graphite spectra. The lower chopper curve is what would seem to be reasonable to obtain with present slow choppers.

The next point worth mentioning is that there are very easy analytical methods of correcting the time spectrum in Poole experiments which should be used. These techniques, due to D. E. Parks,[5] permit one to calculate the first time moment for any neutron energy (mean emission time). There is simply no need to guess this quantity any more. This places pulsed spectra measurements on a completely objective basis even for heavy moderators such as graphite. Calculations of mean emission time for graphite are shown in Figure 5.

Other general considerations in making differential spectral measurements which should be mentioned are the following:

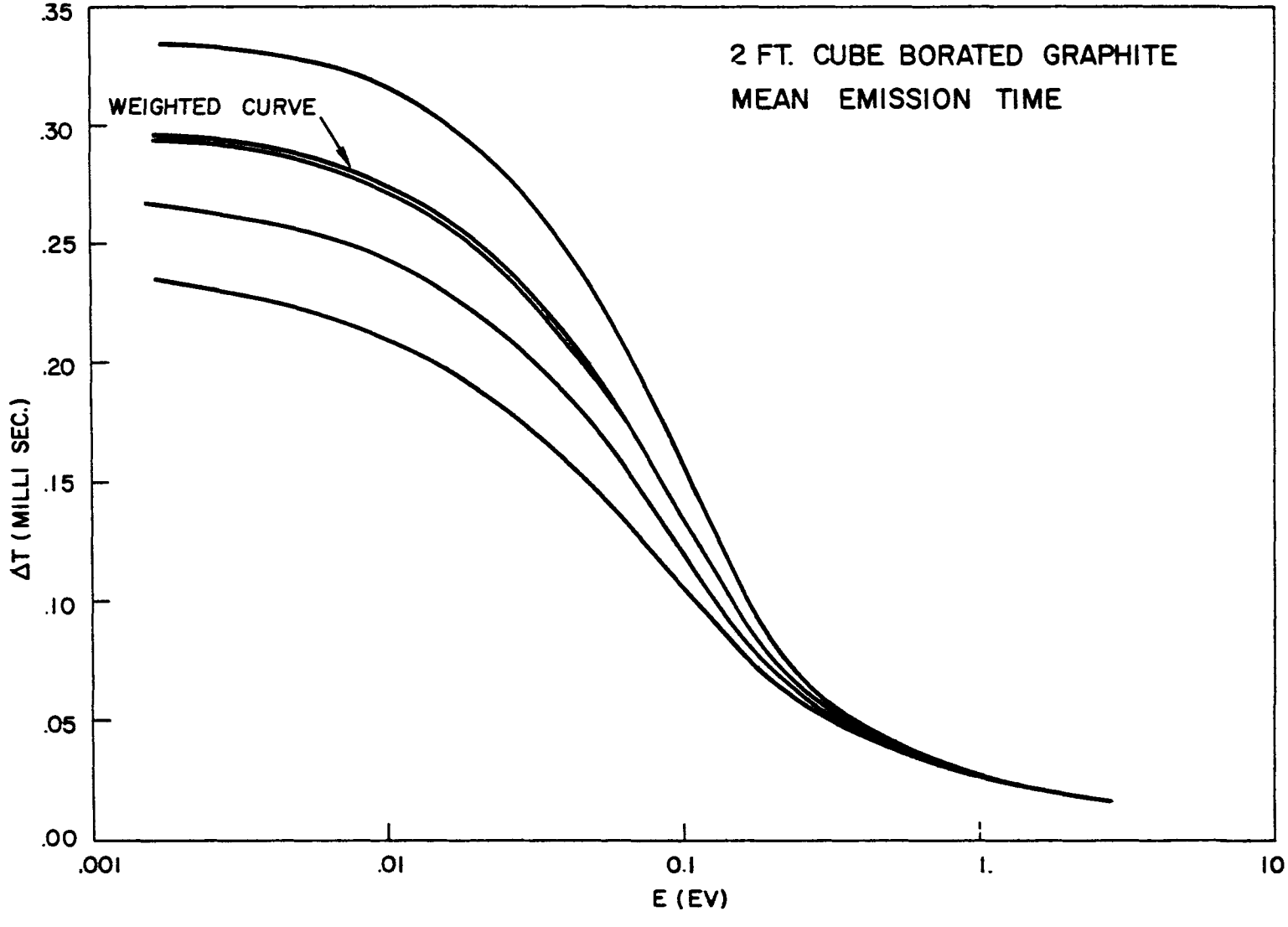

Fig. 5 Calculation of mean emission time for graphite

1. Spectra measurements in arbitrary unpoisoned geometries are hard to understand. This problem is complicated by spatial effects. Simple interpretations of results are not likely.
2. Spectra measurements in the direction of a flux gradient – 0^0 flux leakage spectra are hard to understand. Correction procedures for determining the scalar flux from an angular measurement are not as yet verified.
3. One must watch beam extraction techniques since spectral perturbations are possible. The scatterer techniques should never be used near discontinuities.
4. Lattice studies by direct measurements are very hard to do. Beam extraction can perturb measured quantities severely. In addition, these techniques presently lack sufficient spatial resolution.
5. Energy sensitivity of neutron detectors for these measurements should always be measured relative to a standard rather than calculated.

III. Measurements

Infinite Homogeneous Medium Spectra

Calculations of infinite medium neutron spectra represent one of the

simplest integral applications of scattering law data. What is meant here is that the neutron flux is flat at all energies, no transport of neutrons in or out of a typical volume exists, thus only the competition between thermalization and absorption determines the spectrum. In general, if one desires to check the adequacy of proposed scattering laws for a moderator, in an integral way, this is the place to start. Leakage and transport effects together with self-shielding difficulties should be avoided. This means that homogeneous absorption should be utilized, and measurements where there is either a flux gradient or a large second derivative (B^2) of the flux should be avoided. Once this situation is under control for a moderator then it is proper to proceed to finite medium studies. The ability to solve this problem for a moderator is a very great step forward since it is then not too large a step to the practical problem of predicting reaction rates in fuel and absorbers present in a reactor. Workers in this field have been, M. J. Poole, R. Slovacek, K. Burkart, and W. Reichardt, and the General Atomic group.

The mathematical expressions with which one tries to calculate the measured spectrum or its average properties are:

$$-D\nabla^2\phi(E) + \Sigma_t\phi(E) = \int_0^{E_m} \phi(E')\Sigma(E'\rightarrow E)dE' + S(E) \qquad (1)$$

$$\int_0^{E_o} \phi(E')\Sigma_a(E')dE' = E\phi(E)[\xi\Sigma_s(E) + \gamma\Sigma_a] \qquad (2)$$

The first equation is the neutron balance equation written in diffusion approximation. Leakage plus scattering and absorption losses from a unit cell are set equal to neutron gains from neutron upscattering and downscattering. The second equation is a conservation condition on the spectra which simply states that the total scattering across threshold E_o must equal the total absorption below it. This expression is used to check the validity of a measured spectrum. If it is not satisfied, one does not have infinite medium conditions for the spectrum measurement.

Results from various laboratories in general indicate that spectra can be better predicted with a bound hydrogen scattering kernel, such as that proposed by Nelkin, than with a free hydrogen kernel. The spectra are 15 to 20% different than those predicted by free hydrogen models and in general are harder. Reaction rates calculated using the bound spectra are some 5% different than those using free hydrogen. Figure 6 shows differential experimental results taken at Karlsruhe compared to predictions of the Nelkin water model. A very unusual occurrence is evidenced here, namely the theoretical spectra (dashed curve) is higher than the experimental in the joining energy region around 0.1 ev. This is not in agreement with spectra measured by Poole in England or Beyster et al. at General Atomic. Length of flight path and size of assembly

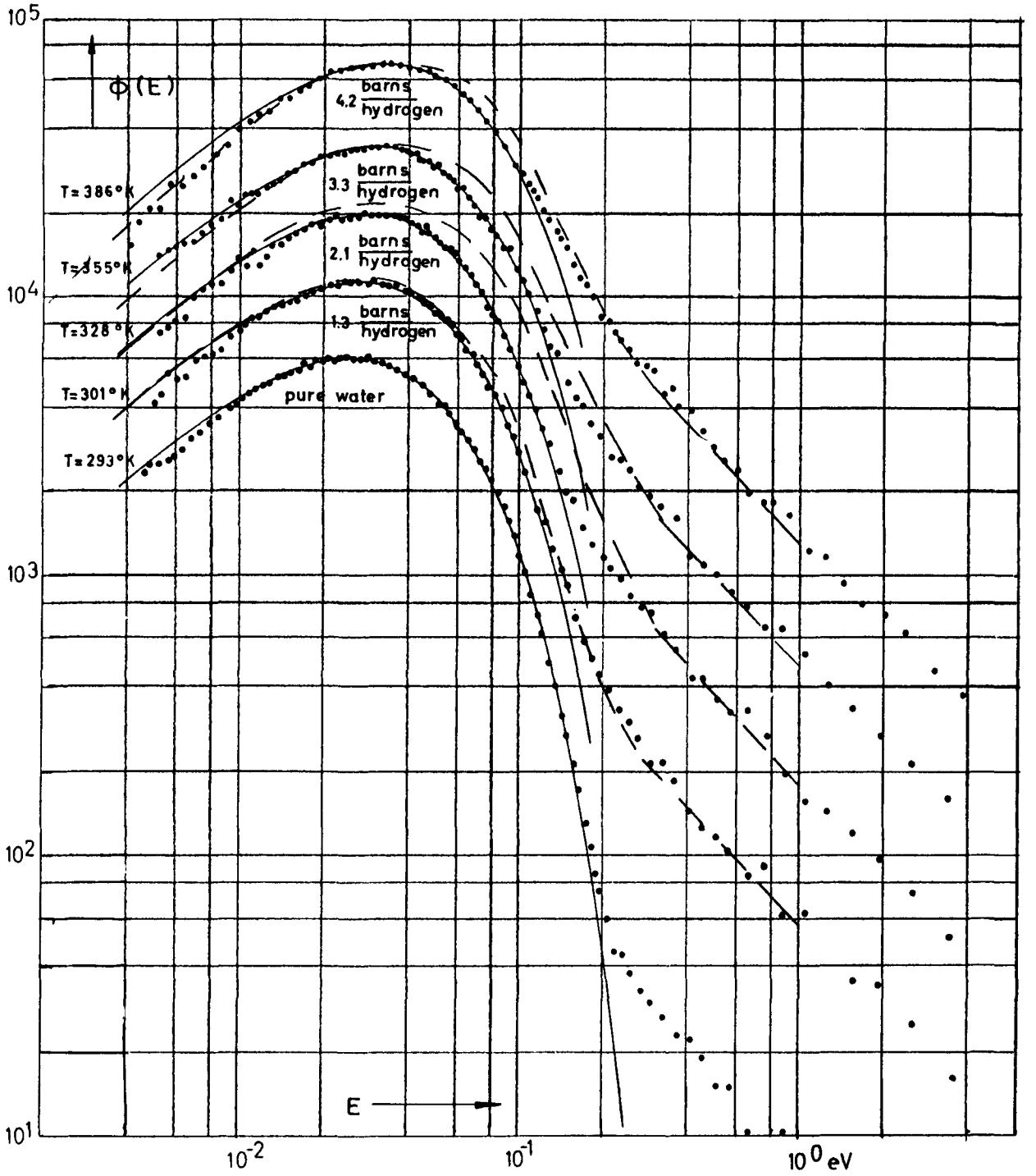

Fig. 6 Neutron spectra in pure water and boron acid solutions,

30 cm cube

——— Maxwellian fit to the thermal part of the spectra

were less in this new experiment than that used in previous work. However, the reason for this disagreement is not at all clear at present and should be ascertained in the near future. The spectra measured for boron and cadmium absorption (taken at General Atomic) are shown in Figure 7. These spectra on cadmium agree with Poole's independent data to within 10% at the same poison concentrations. Both spectra show hardening and agree relatively well with infinite medium spectrum theory using Nelkin's water kernel. Erbium has also been studied under infinite medium conditions at several laboratories and shows good agreement with theory (Figure 8). The study of the effect of the erbium resonance on neutron spectra in water systems is extremely important since the erbium resonance structure is not unlike that of Pu^{239}, often a very important source of reactor absorption after relatively long reactor burnup. It will be observed that the very large erbium resonance perturb the spectrum relatively little in water assemblies since qualitatively there is such a high probability of scattering over the resonances. Gadolinium absorption spectra have also been measured and agree relatively well with analytical predictions. In fact, of the various homogeneous situations studied, only samarium absorption has given really peculiar results. The spectra are too hard and the neutron conservation condition (Figure 9) fails. These are General Atomic measurements. It is a long standing problem. Disagreements

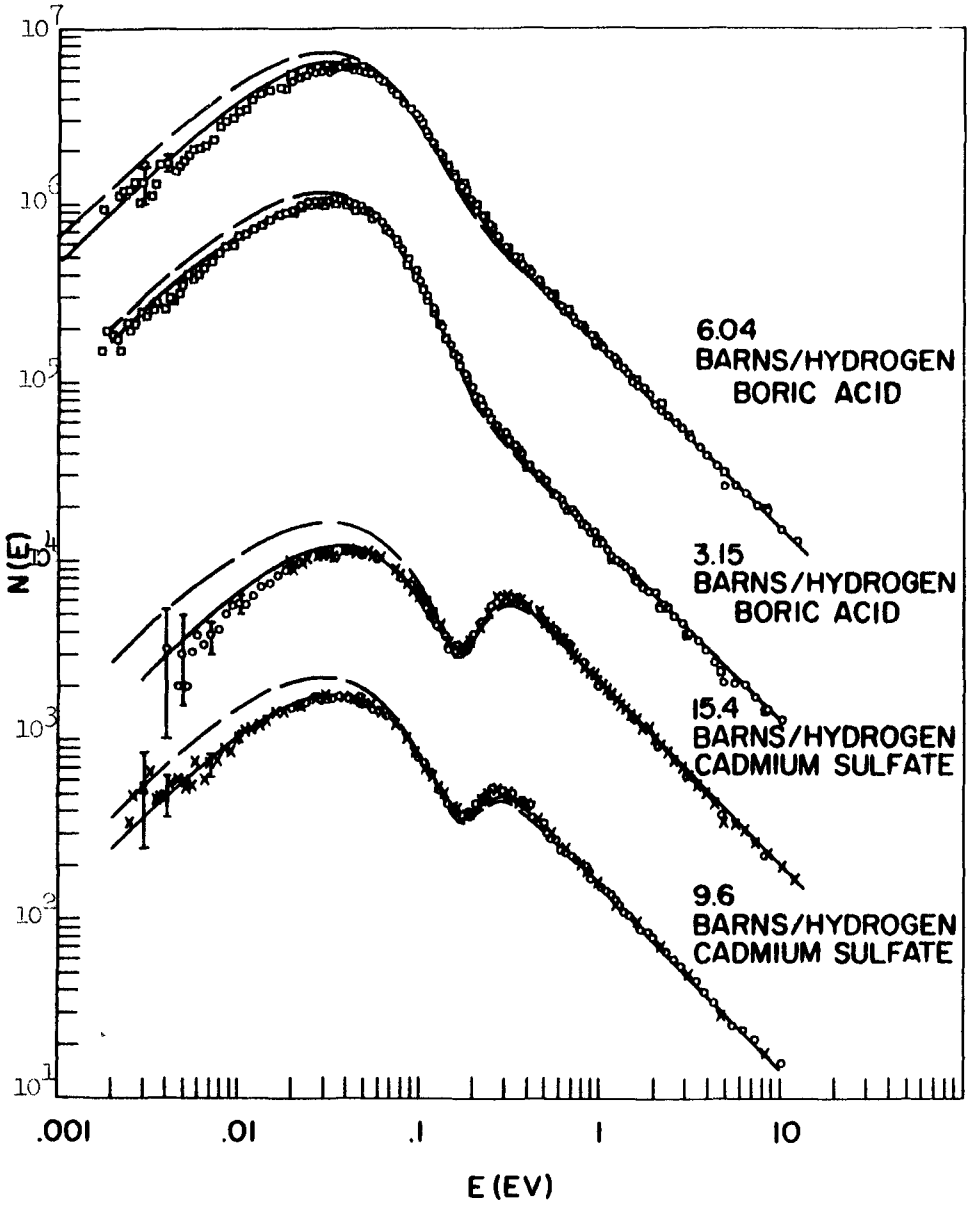

Fig. 7 Neutron spectra measured in cadmium and boric acid

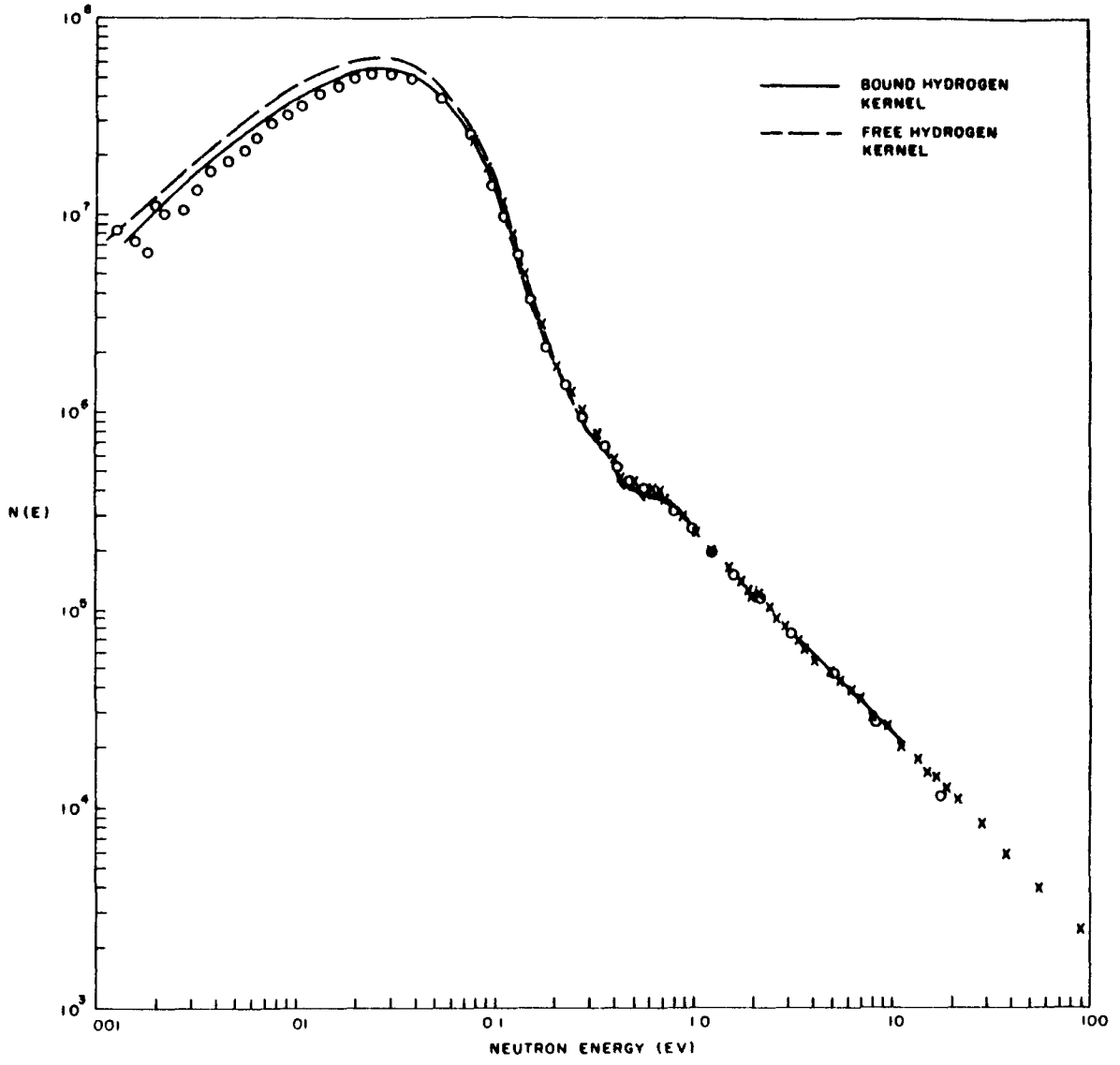

Fig. 8 Neutron spectra in water posioned with erbium

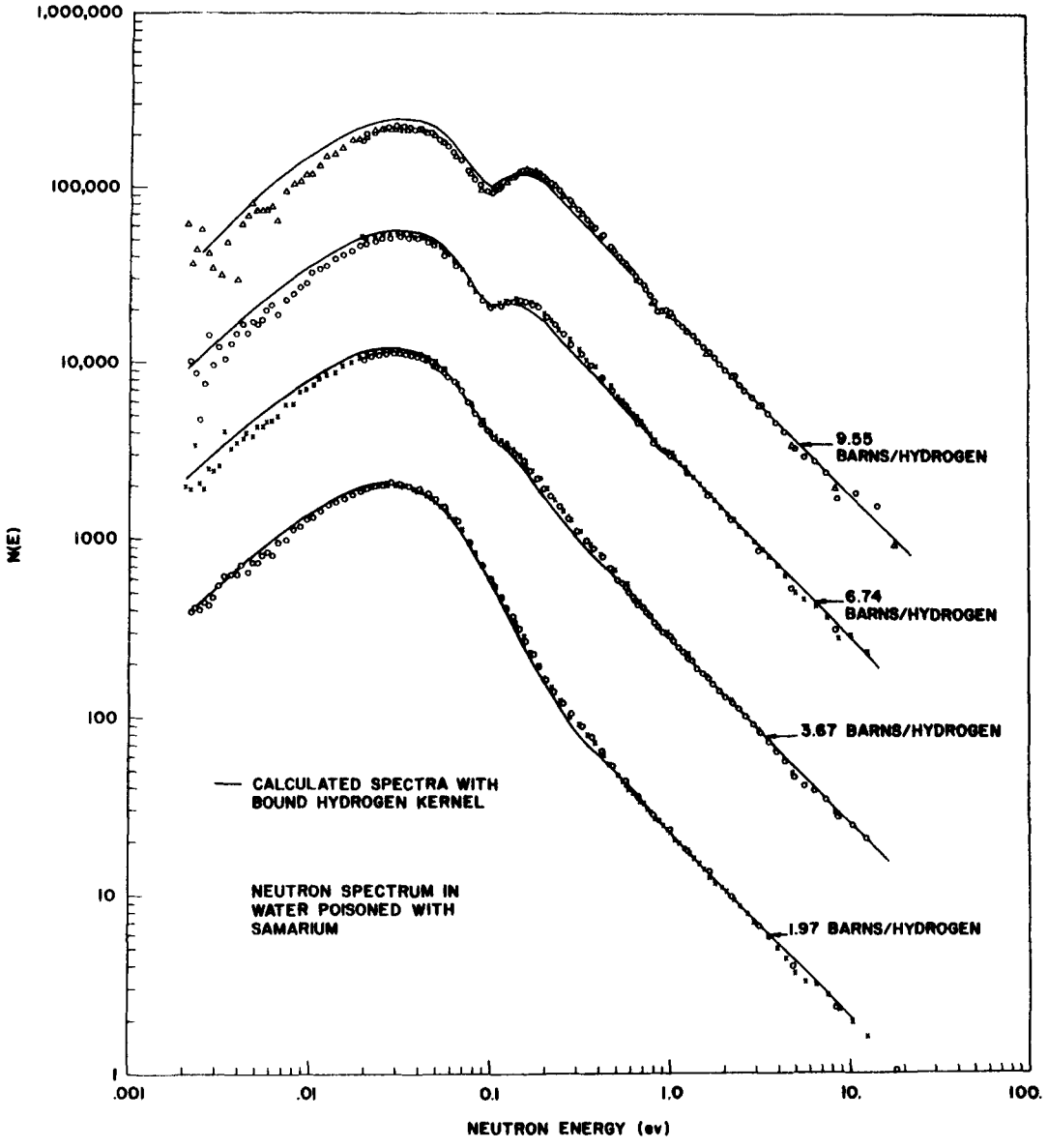

Fig. 9 Neutron spectra in water posioned with samarium

both in relative shape and in the neutron conservation condition of roughly twenty percent are apparent. Since samarium in thermal reactors overrides the effects of all long lived poisons, the importance of resolving this problem is obvious.

A general conclusion which can be drawn from the infinite medium spectrum measurements in water is that even more molecular binding is called for in the model, especially between 0.1 and 0.4 ev neutron energy. Differential measurements to substantiate this conclusion are clearly needed.

For polyethylene, experimental data has been available for some time. D. Goldman[6] at KAPL has recently constructed a scattering law, based on the Nelkin model, and the comparisons between theory and experiment are shown in Figure 10. The agreement is really excellent. The effect of binding on the neutron spectra can be evaluated in an integral sense by calculating the average 1/v cross section for the spectra assuming bound and free polyethylene kernels. These two methods of approach give average cross sections differing by some 16%, a significant number. Polyethylene spectra measured in various matrices at KAPL (Figure 11) using the chopper technique have also been analyzed but the theory tends to differ by some 20% with experiment which gives a harder spectrum. Water spectra on the other hand, measured with the same apparatus are in agreement with those measured elsewhere.

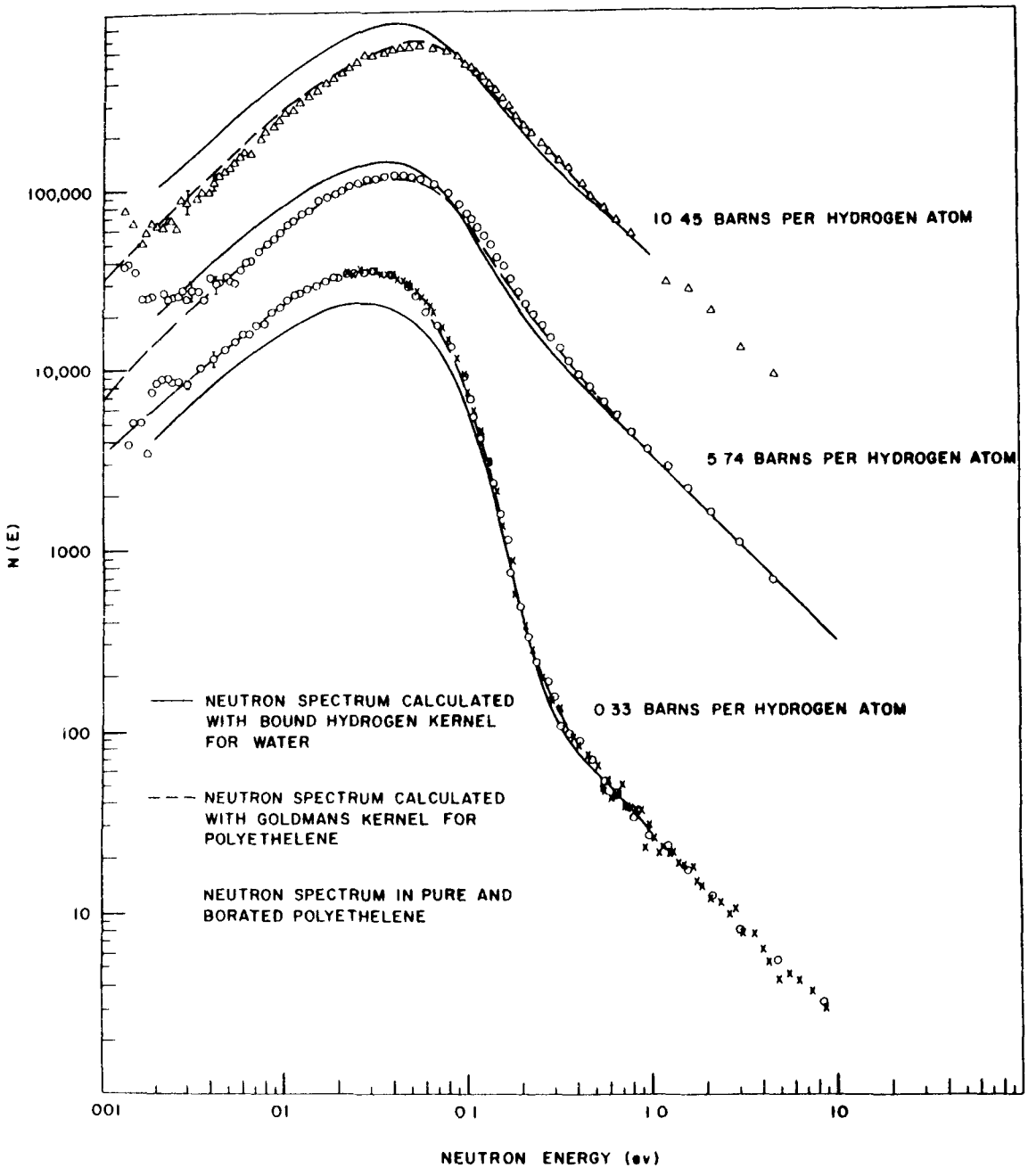

Fig. 10 Neutron spectra in pure and borated polyethylene

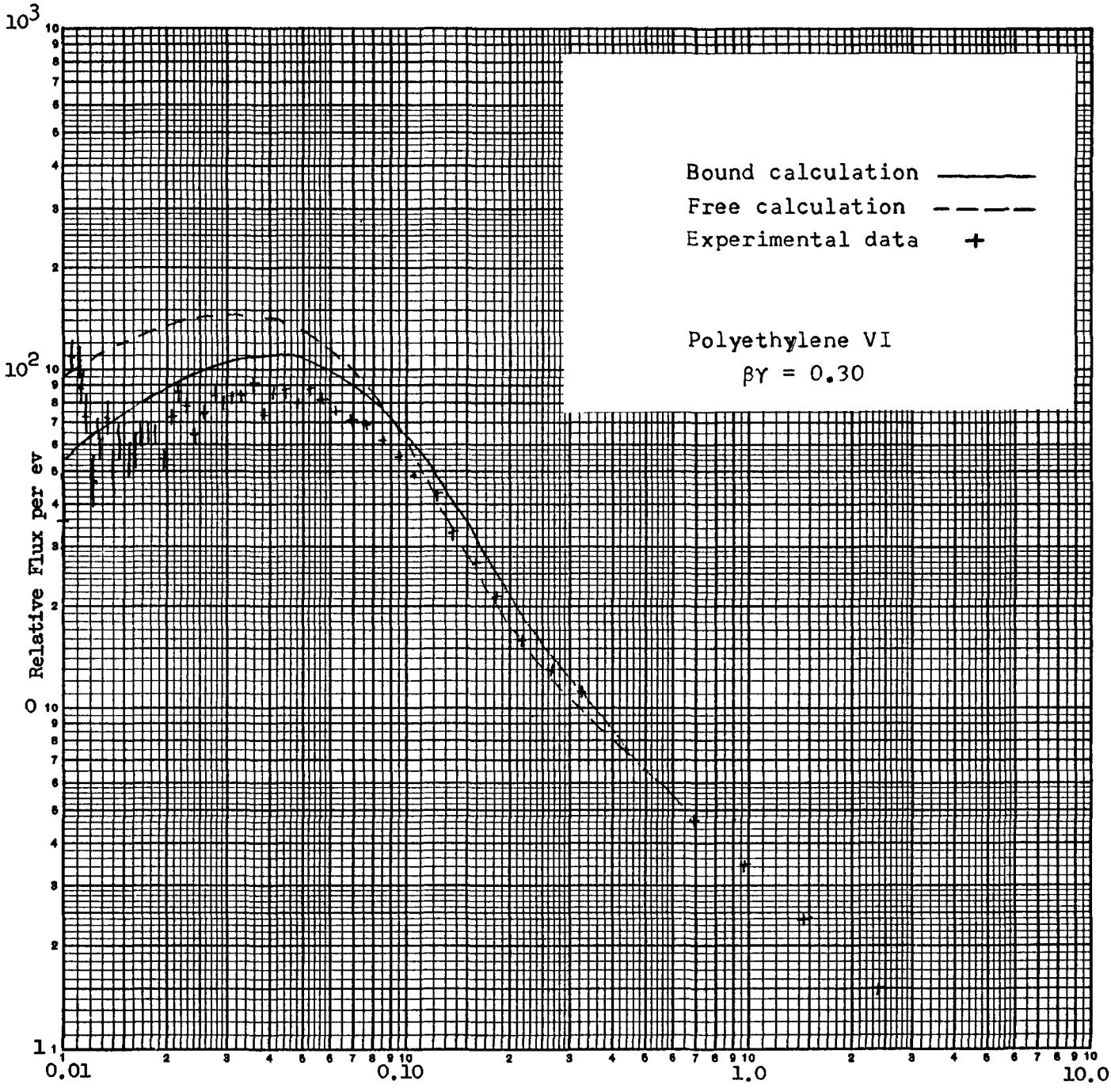

Fig. 11 Neutron spectra in polyethylene

These geometries consisted of thin fuel and moderator (polyethylene) strips so self-shielding corrections are necessary. Here, again, this discrepancy should not be allowed to persist. Either present theoretical techniques are not adequately handling this problem or experimentally there are effects (i.e., leakage or gradient conditions) being overlooked which all workers in the field would like to understand.

Areas where work is needed for this class of experiment is on cleaning up the existing discrepancies enumerated above and proceeding to studies of heated water spectra. The older experimental data indicates that binding effects in water are not important at absolute temperatures of 500^0 to 600^0K. This should be verified since these studies indicated the same conclusion for 300^0K temperatures, which we know now to be incorrect. An experimental apparatus being used to study temperature dependent spectra in water is shown in Figure 12.

IV. Finite Medium Neutron Spectra

The first objective of this type of measurement is to perform studies of spectra under easily understandable one-dimensional geometrical conditions as similar as possible to those normally encountered in the classic Milne problem. This means that one has something like a semi-infinite one-dimensional slab with a vacuum boundary. All spectra to be discussed here have

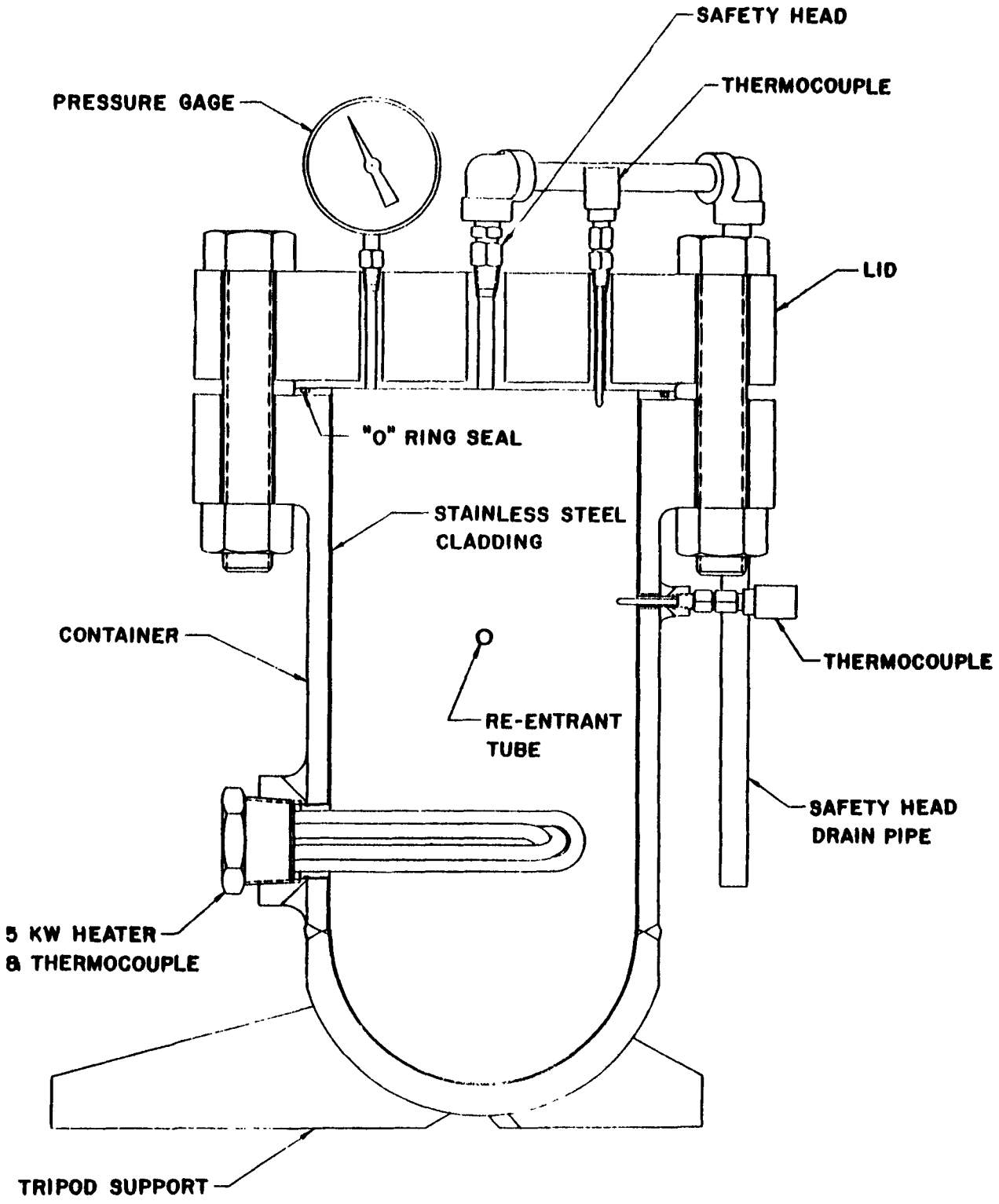

Fig. 12 Pressure vessel for measuring neutron spectra at elevated temperatures

been measured in homogeneous or nearly homogeneous media so that one does not observe flux depression and self-shielding effects.

The next question to consider is why one should measure and analyze angularly dependent spectra in finite medium. Clearly from the reactor design standpoint it is most important to understand scalar flux spectra. One does, however, encounter situations in reactor analysis where a knowledge of the angular flux is extremely important. This occurs in control rod analysis and in general in most change-of-medium problems. In the cylindrical lattice or cell problem one finds marked similarities to the Milne problem when one considers the transition region at the interface between fuel and moderator – namely a strong neutron sink exists in both cases.

In general finite medium spectra constitute a very good check of calculational techniques. For example questions of spatial and energy mesh size, degree of approximation to the scattering kernel and approximate methods of integration are all amenable to careful study. The work to be reported here is mainly that done at General Atomic during the last year.

In these investigations there are a myriad of quantities which could be measured. Limiting this program to the essentials becomes the problem. Geometrically, two possible arrangements are shown in Figure 13. Intermediate angular measurements are also possible. Beam extraction from the

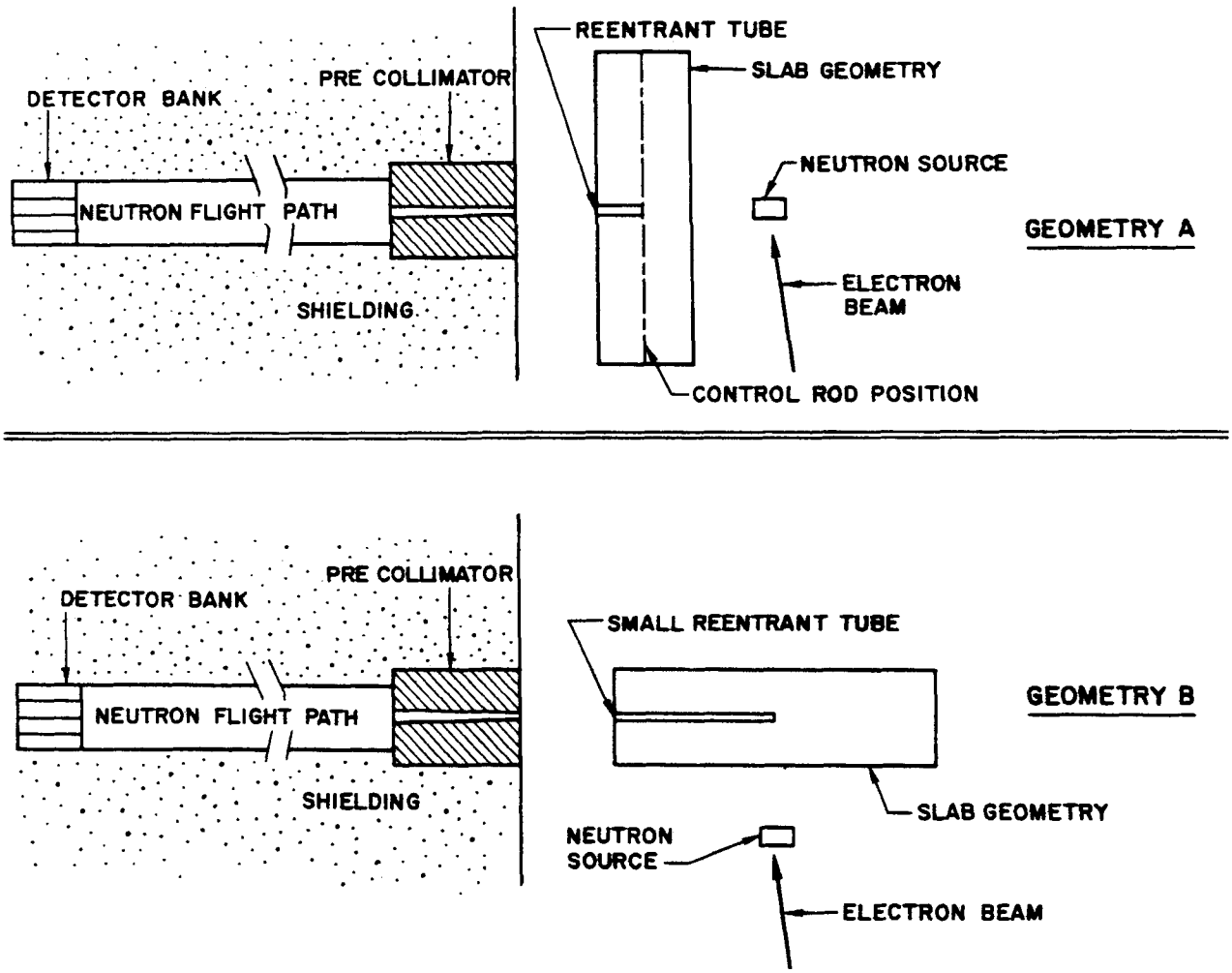

Fig. 13 Typical geometrical arrangements for measuring neutron spectra in finite mediums

assembly can be attained either by standard re-entrant hole methods or by the beam scatterer technique. In the present program most of the emphasis has been placed on measurements at 90 and 0^0 with occasional check points in between. The 90^0 measurements essentially establish the scalar flux whereas the 0^0 measurements specify the spectrum of the angular flux (not current) in this specific direction. The scalar flux is of course defined as the integral over all angles of the angular flux. The slab thickness to be used in the investigation can and should be varied. It is of course essential in these experiments to emphasize the study of situations where strong spatial gradients exist rather than flat flux conditions.

Scalar flux measurements have been made in slabs of pure water, boric acid solutions, and in an effectively homogeneous multiplying assembly. Two typical examples are shown in Figures 14 and 15. The first example is the scalar flux determination in the center of a four-inch slab of pure water. Various calculations of the spectra using the integral transport code THERMOS are given. The top curve is a calculation assuming only a P_0 scattering law whereas the dotted curve has been calculated including many refinements. A diagonal P_1 kernel is used together with the P_0 kernel to describe anisotropic scattering. An anisotropic source specified in diffusion theory approximation and transverse leakage corrections for the geometry are all used. The Nelkin

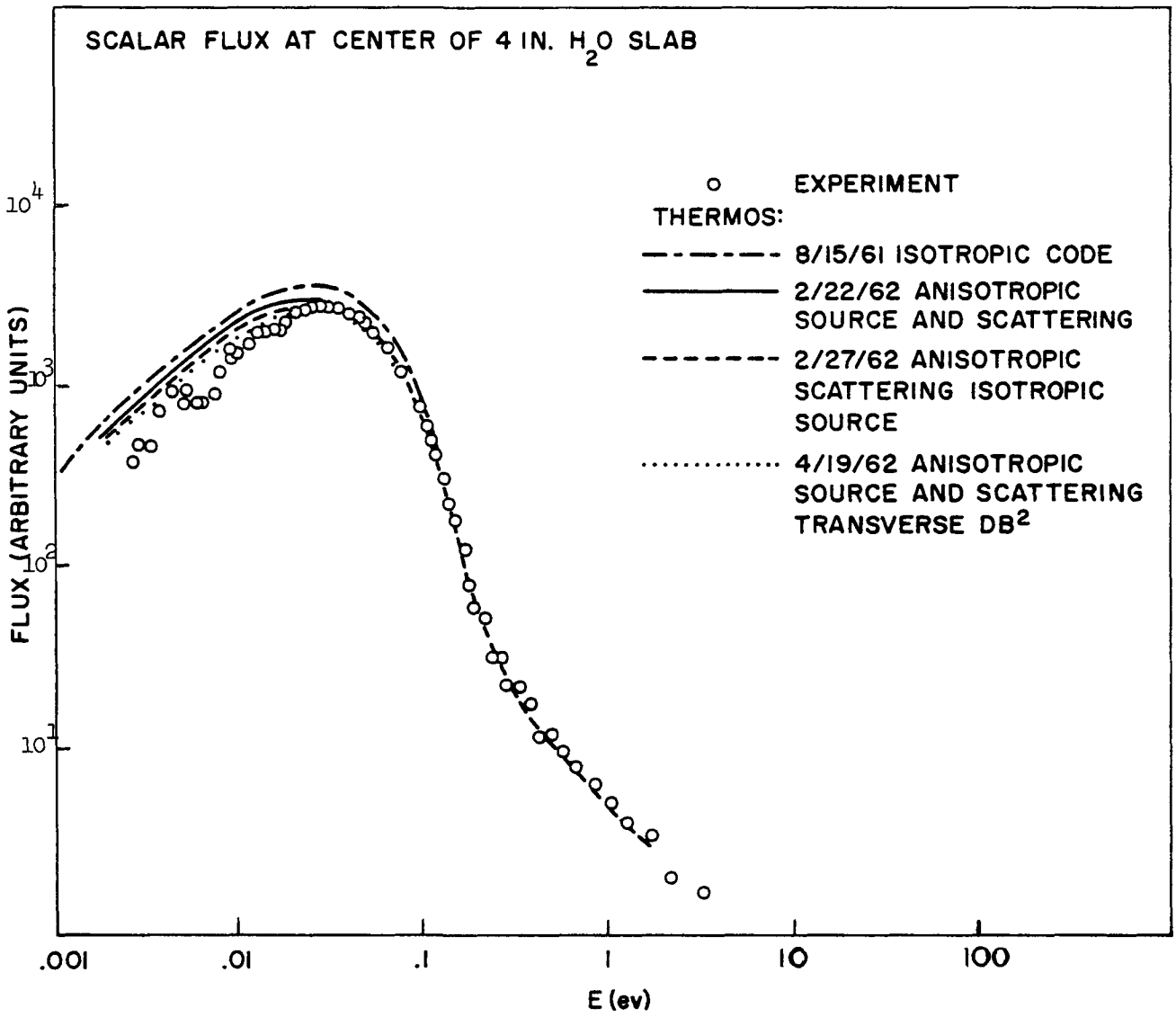

Fig. 14 Scalar neutron spectrum measured in pure water

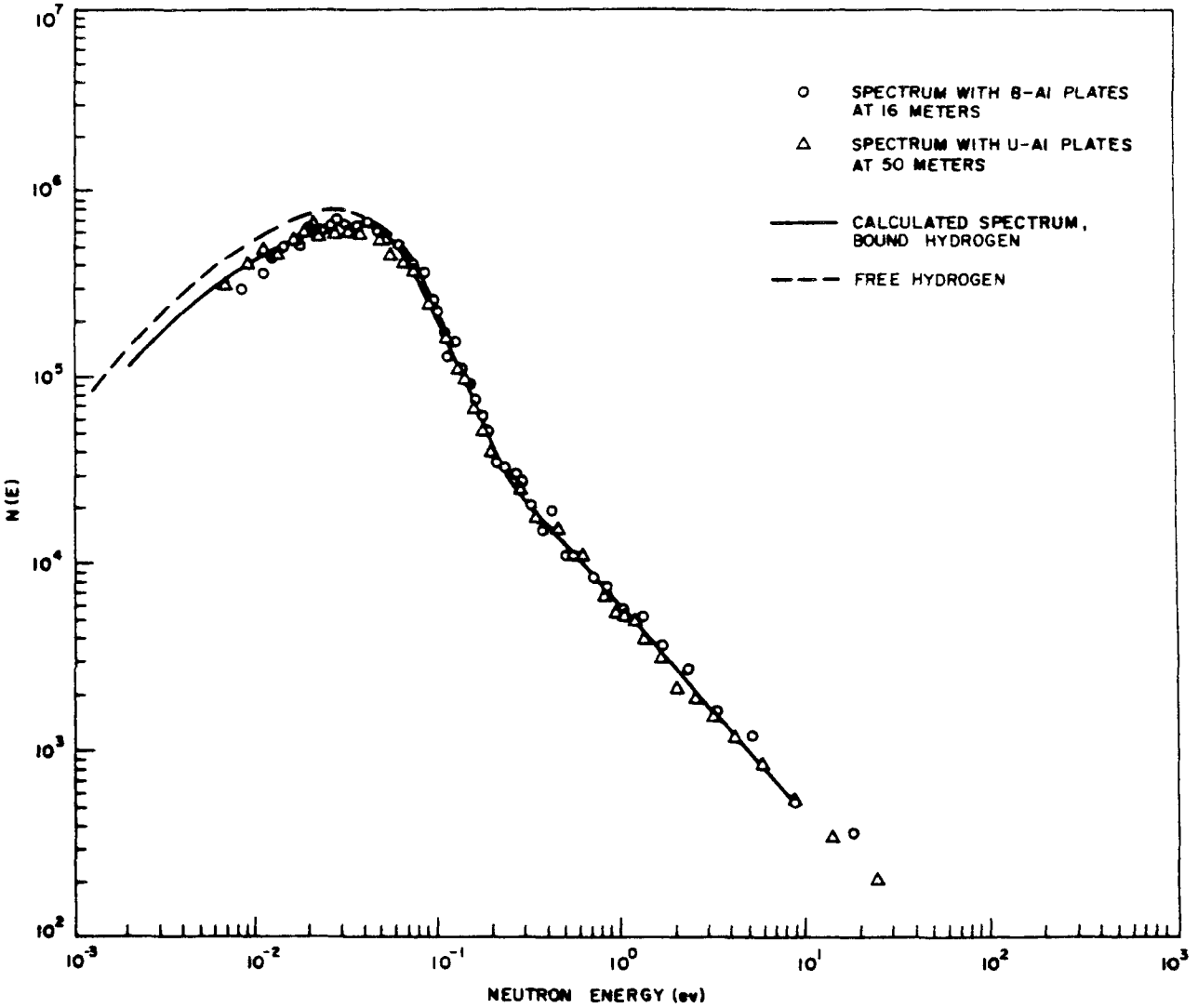

Fig. 15 Scalar neutron spectrum measured in multiplying and non-multiplying media

bound hydrogen scattering model is used. One does not expect theoretical and experimental spectra to agree below 0.01 ev neutron energy because of the method of beam extraction. Above this energy, however, good agreement is attained. Figure 14 illustrates that even for scalar flux determinations the calculated spectrum depends on geometrical and kernel refinements. Figure 15 shows calculated and measured scalar flux spectra in the subcritical assembly. Here, again, good agreement is obtained between theory and experiment.

Difficulties to be encountered in the performance of 0^0 spectrum measurements are indicated by the calculations shown in Figure 16. It is clear that only in the last centimeter from the edge of the slab does one encounter rapid spectral variations. This fact puts a stringent requirement on spatial resolution in any angular flux measurement. The next two figures illustrate some of the current problems with the fitting of the experimental data. In Figure 17 the leakage spectra from a two-inch slab of poisoned water is shown. Residual disagreements after the anisotropy of source and scattering in P_1 approximation have been corrected are about 15%. The source anisotropy is taken into account in both THERMOS and DSN by assuming the diffusion theory angular distribution

$$S(E,X,\mu) = \phi(E)[\frac{Q(x)}{2} - \frac{3}{2}\mu D(E)\frac{dQ}{dx}] .$$

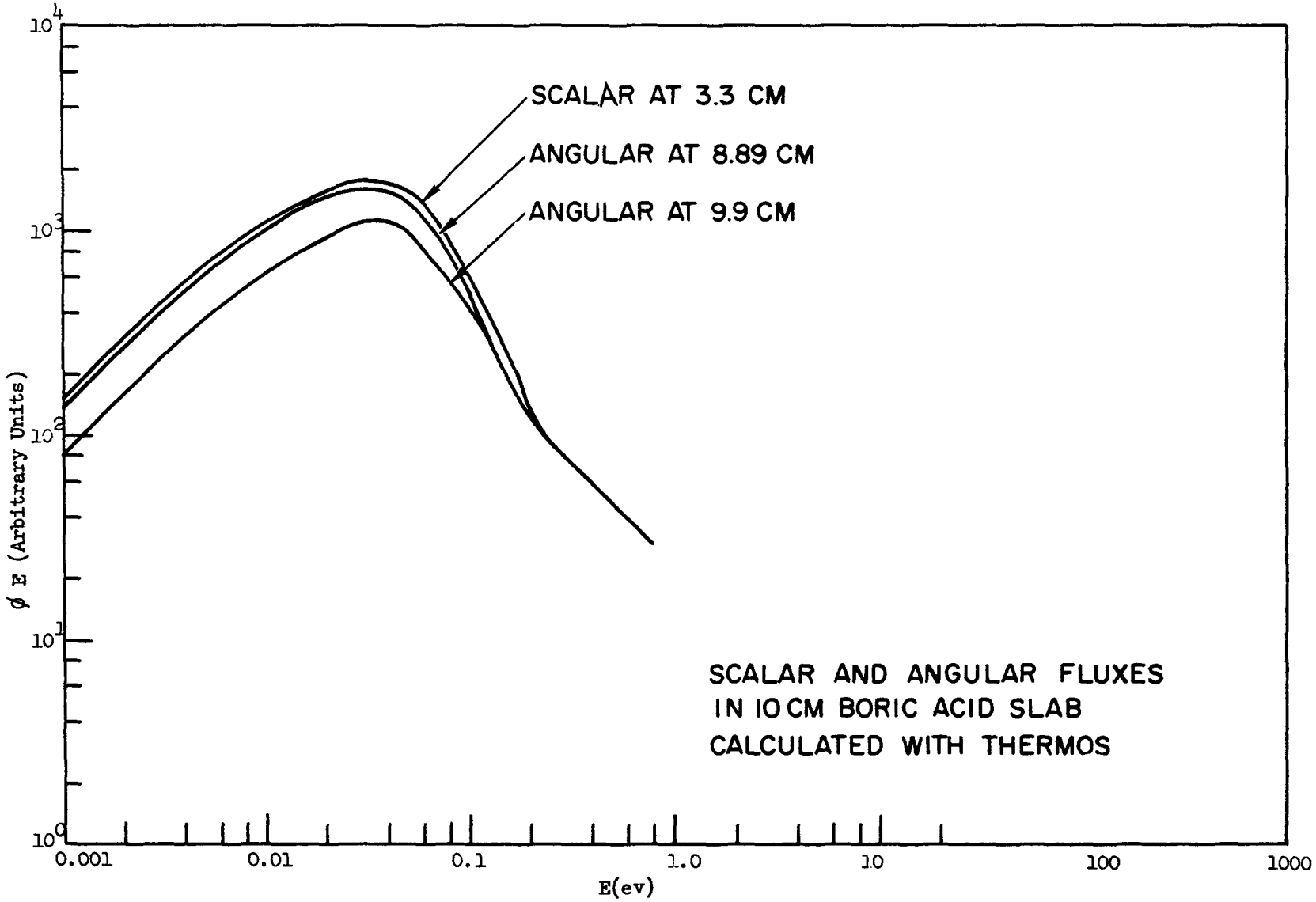

Fig. 16 THERMOS calculations for a 2 inch slab of boric acid

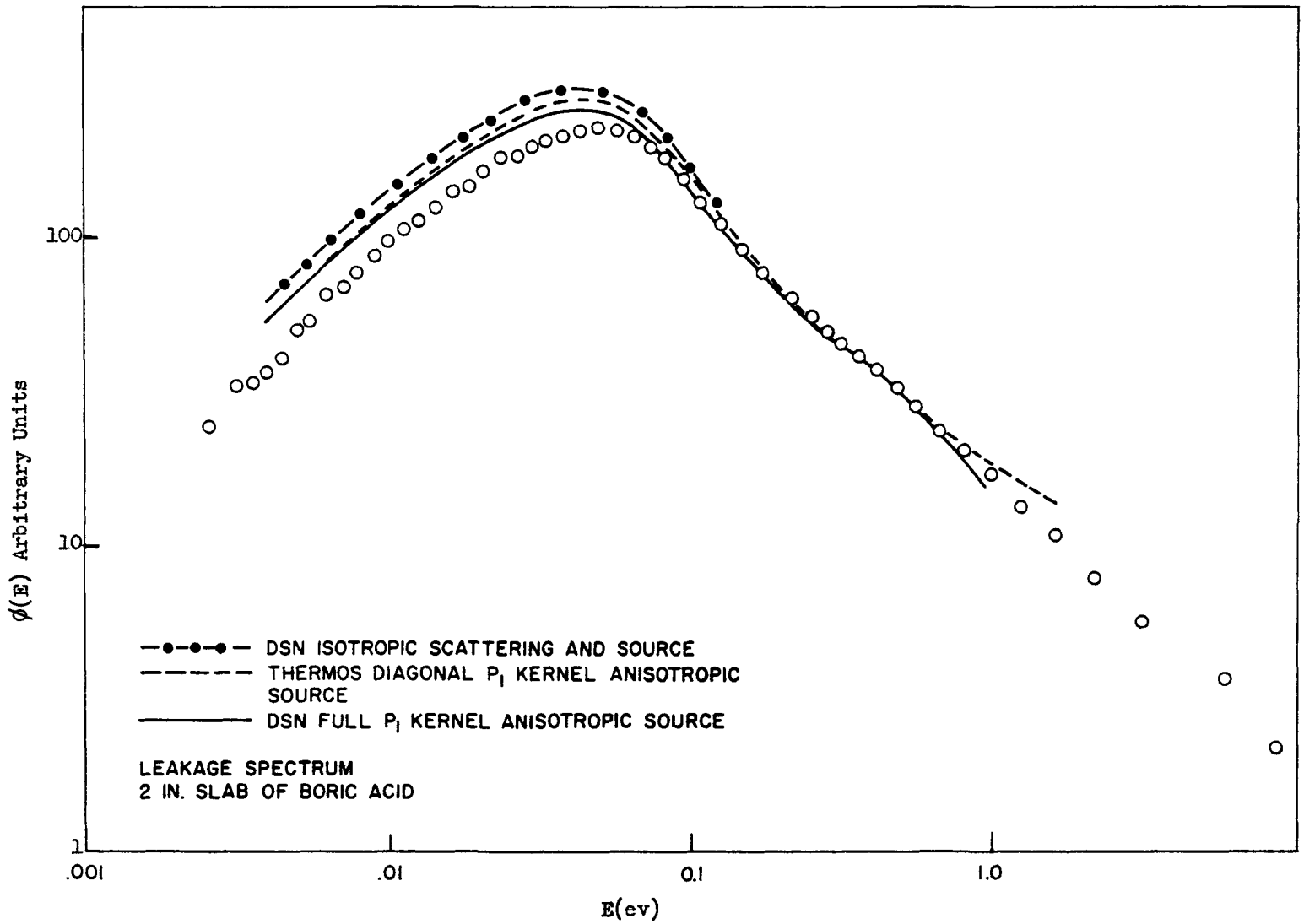

Fig. 17 Leakage neutron spectrum from a 2 inch slab of boric acid

In Figure 18 for pure water the residual disagreements are about 40%. For all of the larger slabs the magnitude of disagreement is around 40%. Both codes DSN and THERMOS appear to give the same result at present. Leakage spectra (0^0 flux) measured in multiplying geometry also disagree by a large amount with theoretical predictions. Thus very little chance exists that a subtle source geometry effect is perturbing the measured spectrum.

The explanation of the large disagreement encountered in the study of angularly dependent spectra is not obvious. More refinements (P_2, P_3, etc.) in the scattering kernel may be necessary. Mesh size used in the calculation may be affecting the predictions. Since this is one of the largest discrepancies existing in the field today a concerted effort to clean it up should be made.

V. Lattice Studies

The understanding of neutron spectra measurements in actual lattices or mock-up lattices is a worthwhile practical objective for people making spectra determinations. The lattice geometries are the most likely to be encountered in reactor design and are thus the problems for which solutions are really desired. The work done for some common moderators will be summarized here. Graphite, D_2O, and water lattices will be considered.

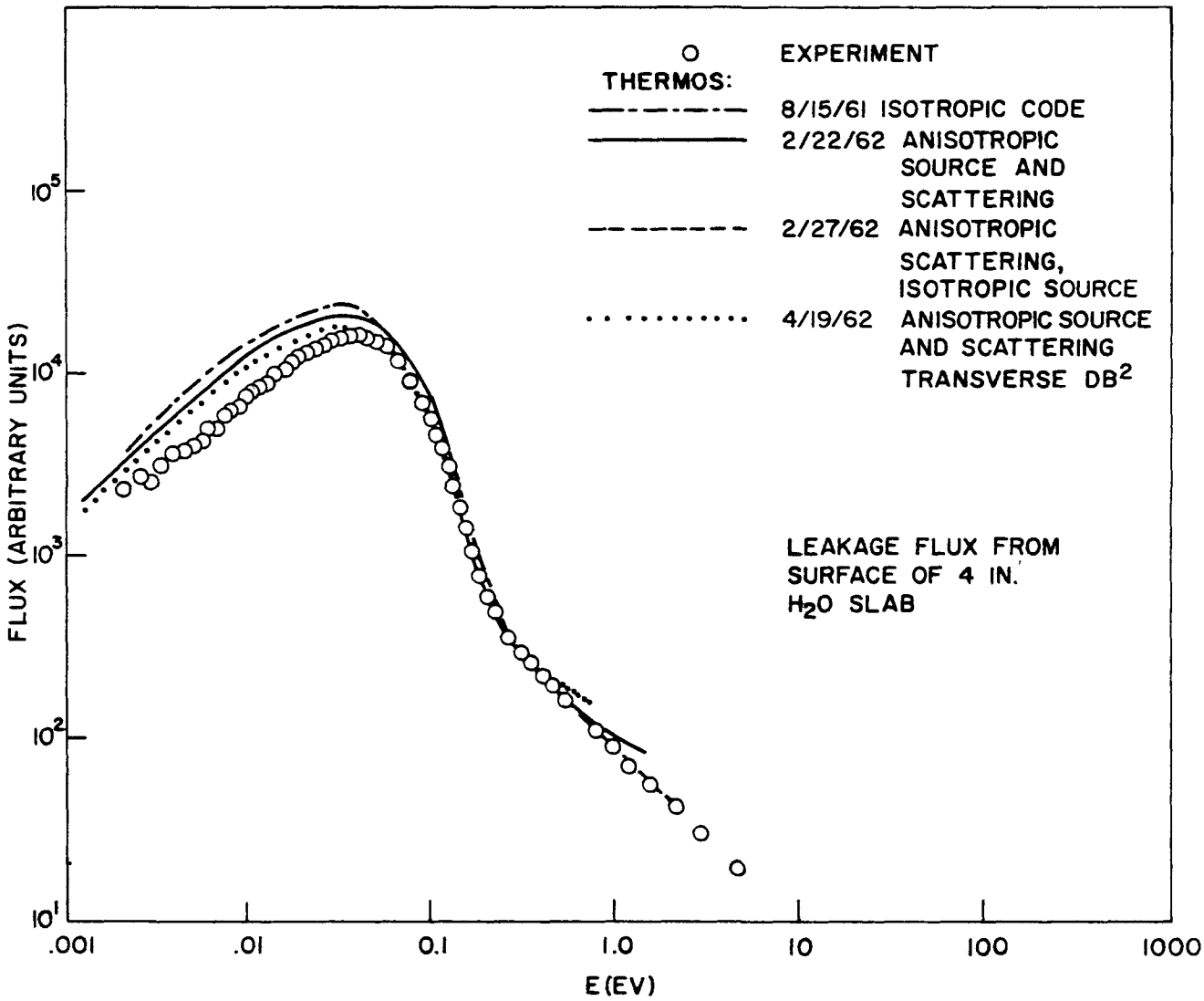

Fig. 18 Leakage flux in pure water from 4 inch slab

Graphite

The work to be discussed here is mainly the new work reported to the thermalization conference on Calder Hall and Zenith experiments.[7] An attempt, however, will be made to indicate the over-all status of experiments on graphite systems. The fuel cell studied in Zenith is shown in Figure 19. Although this is strictly speaking a two-dimensional problem the analysis as handled by essentially a one-dimensional DSN calculation. All graphite was effectively lumped into the graphite regions between the fuel materials by increasing the density by 7.7. Although this experiment appears to be an interpretable one, it is questionable that it is a recommended way to go about verifying the adequacy of a graphite scattering law. The two-dimensional geometry and lumped absorption nature of the cell can possibly make agreements between theory and experiment fortuitous. The experimental conclusions reported are: that with the Egelstaff-Schofield kernel, derived from experimental scattering data, one can predict the measured spectrum in the graphite cell. Using standard homogenization assumptions (self-shielding) rather than transport theory, the spectrum did not agree well with experiment. Further it is apparent in Figure 20 that the measured spectrum is in far better agreement with the E.S. spectrum than with either the spectrum calculated using the free gas or Debye kernels.

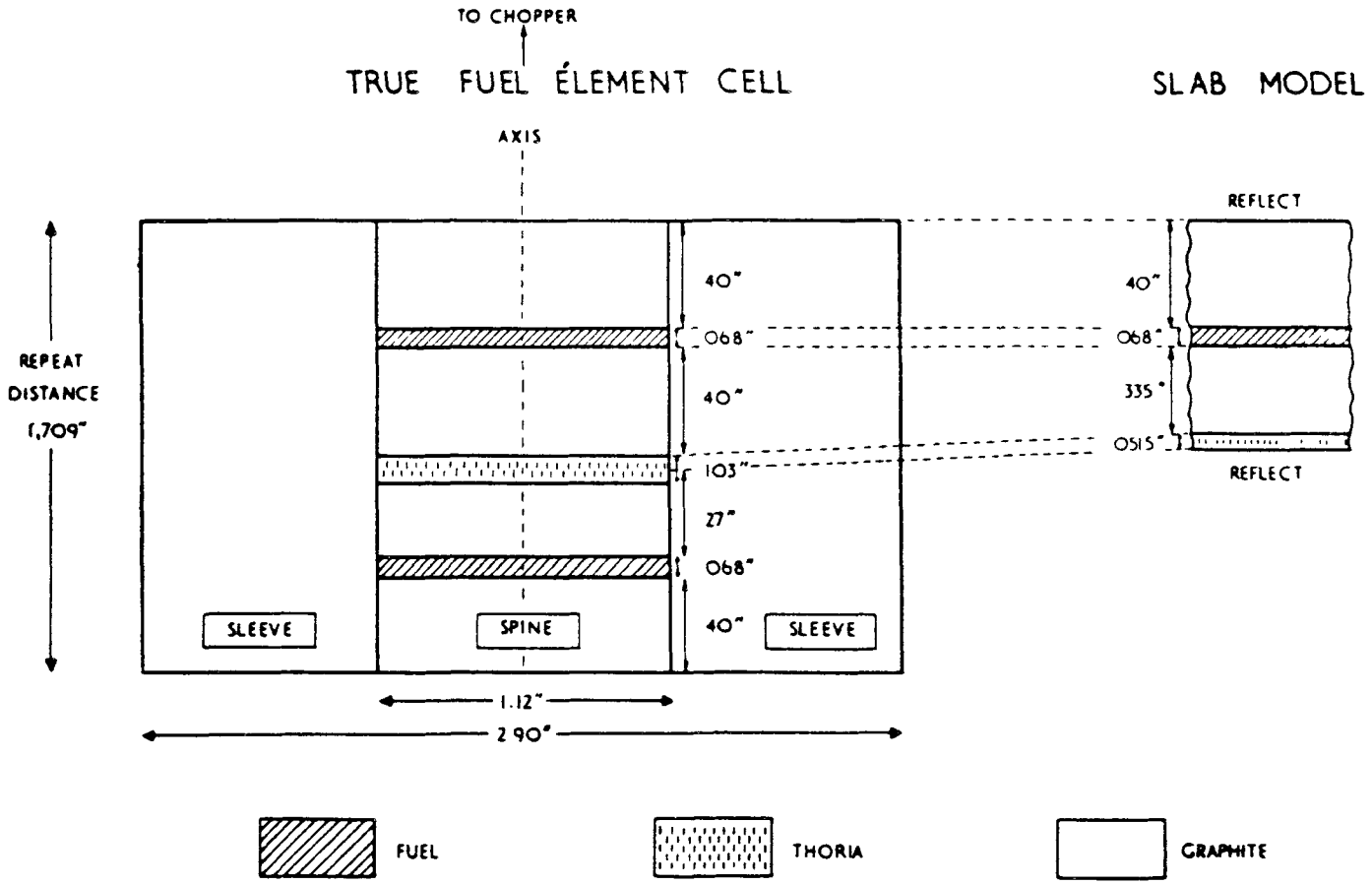

Fig. 19 Geometry used in the Zenith neutron spectrum measurements

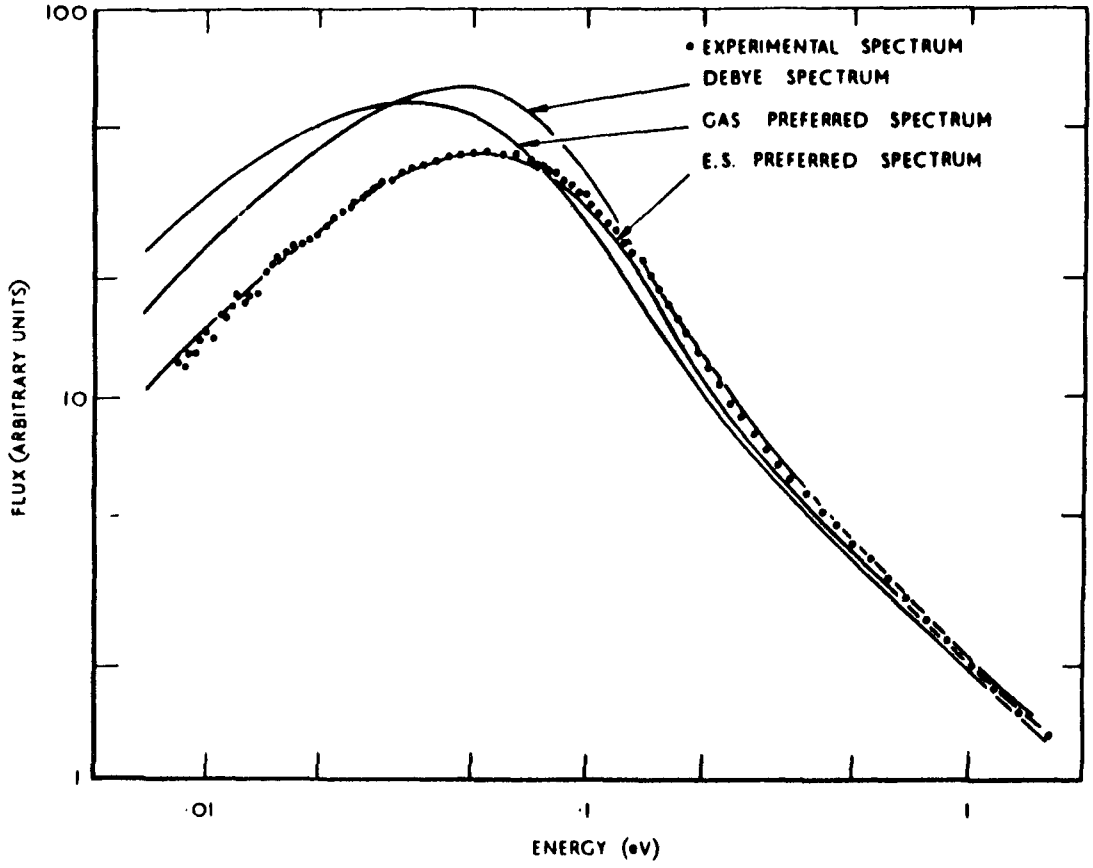

Fig. 20 ROOM – TEMPERATURE ZENITH SPECTRUM

In the paper by J. D. Macdougall[8] on spectra at the Calder Hall cell edge in a graphite natural-uranium lattice, a clear-cut need for the E.S. scattering law or equivalent is indicated. Although not as severe a check on scattering law or calculational methods as the Zenith work, carbon of mass 12 is clearly ruled out. This spectra, however, shown in Figure 21, is calculated to be slightly softer than experiment as in the Zenith case (Figure 20) indicating an underestimate of the high frequency components of the phonon distribution.

Another set of experiments discussed at previous conferences has been done in graphite at General Atomic under homogeneous conditions. Results are shown in Figures 22 and 23. In this case, as in the latter, the calculated spectrum was very sensitive to scattering law. The kernel used in the calculation was devised by Don Parks[9] and is based on the frequency spectrum of Yoshimori and Kitano,[10] derived largely from specific heat data. Thus two different methods of interpretation have been successful in two different experiments. It is thus worthwhile to try to compare the predictions of the two scattering laws for the same case. Figure 24 shows the result calculated for the Zenith lattice. The Parks' kernel was used in calculations of the homogeneous A and B cases for the Zenith lattice. In the A case complete homogenization was used for both kernels and for case B and energy independent

J. D. MACDOUGALL

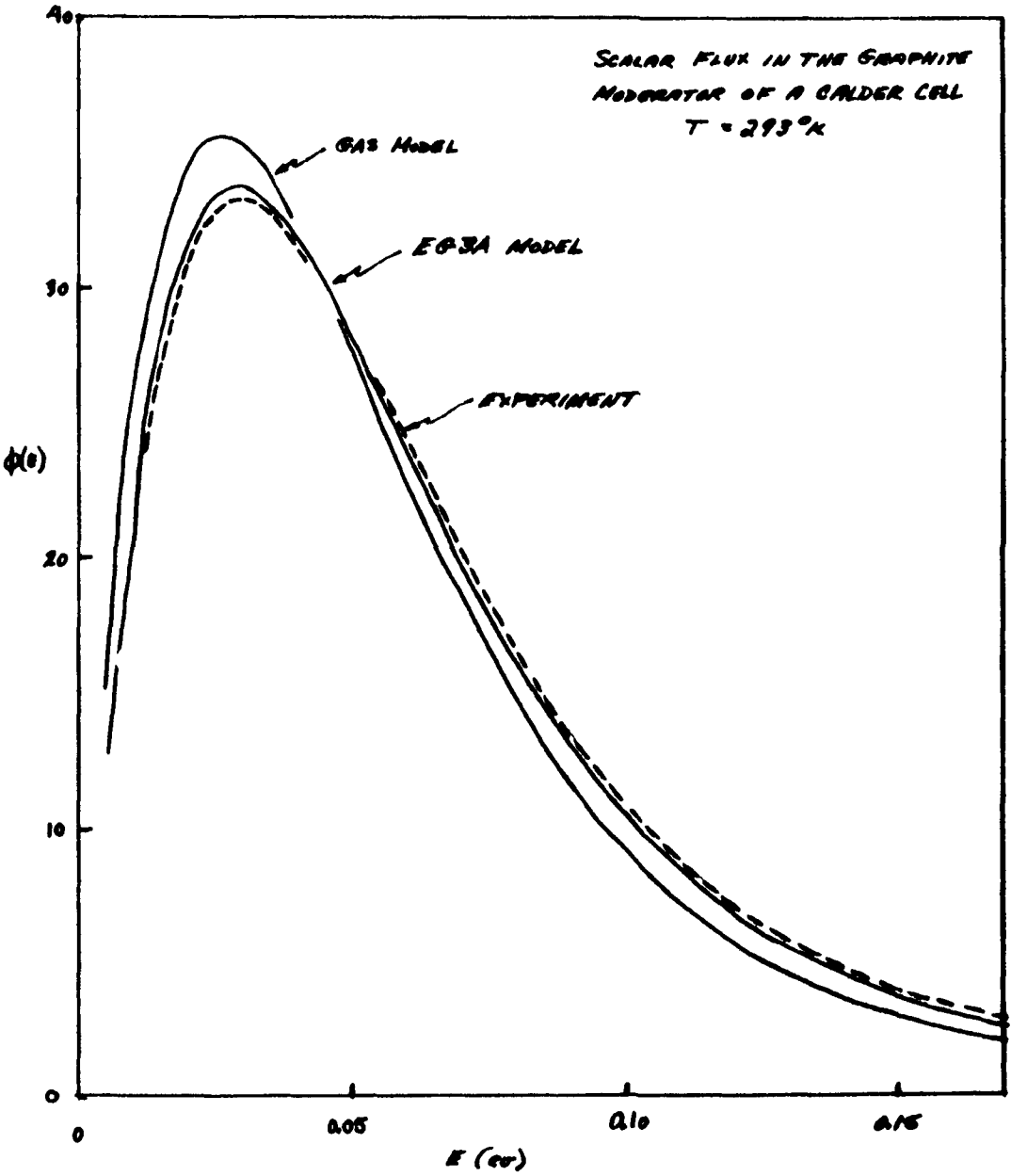

Fig. 21 Neutron spectra in Calder Hall cell

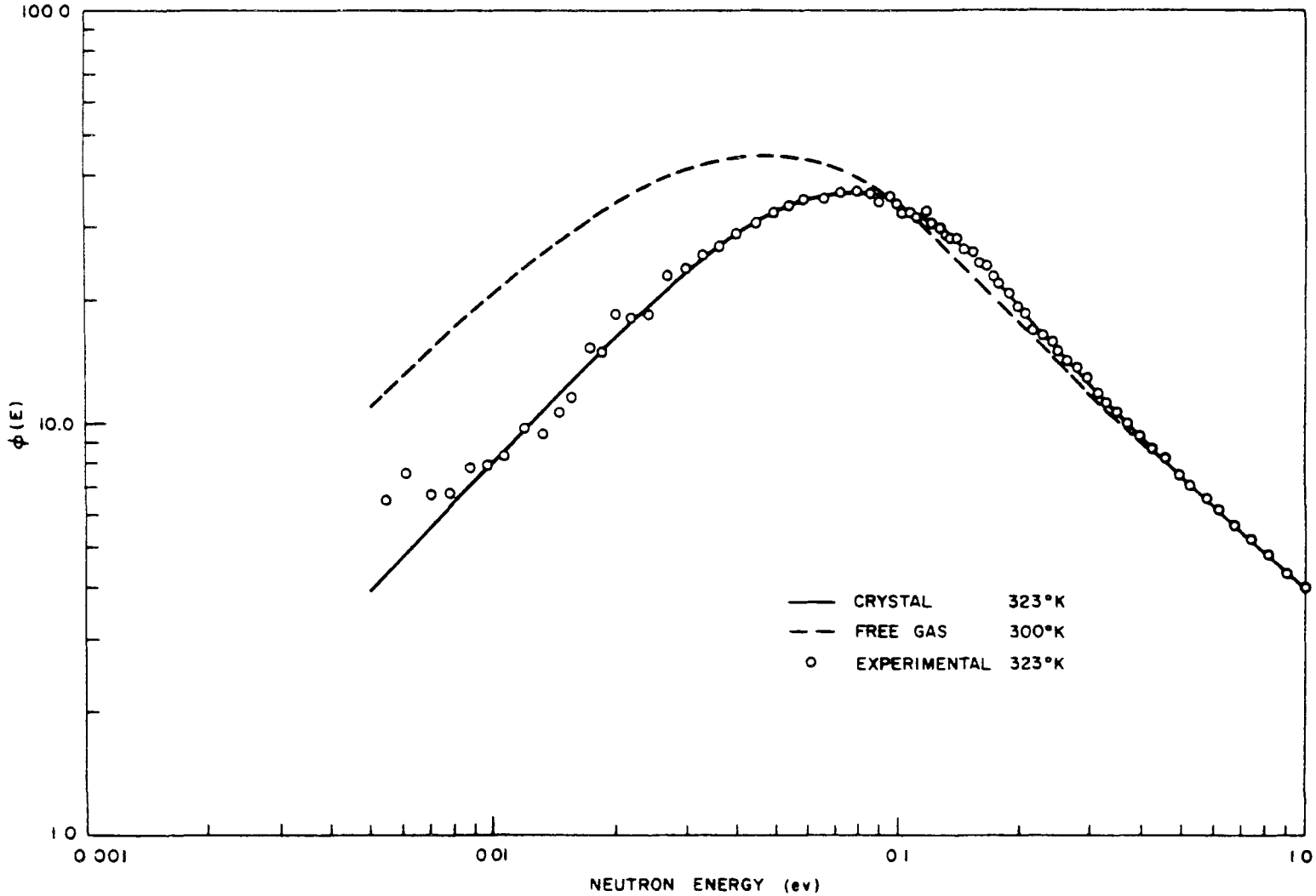

Fig. 22 Neutron spectra in graphite assembly at 323°K

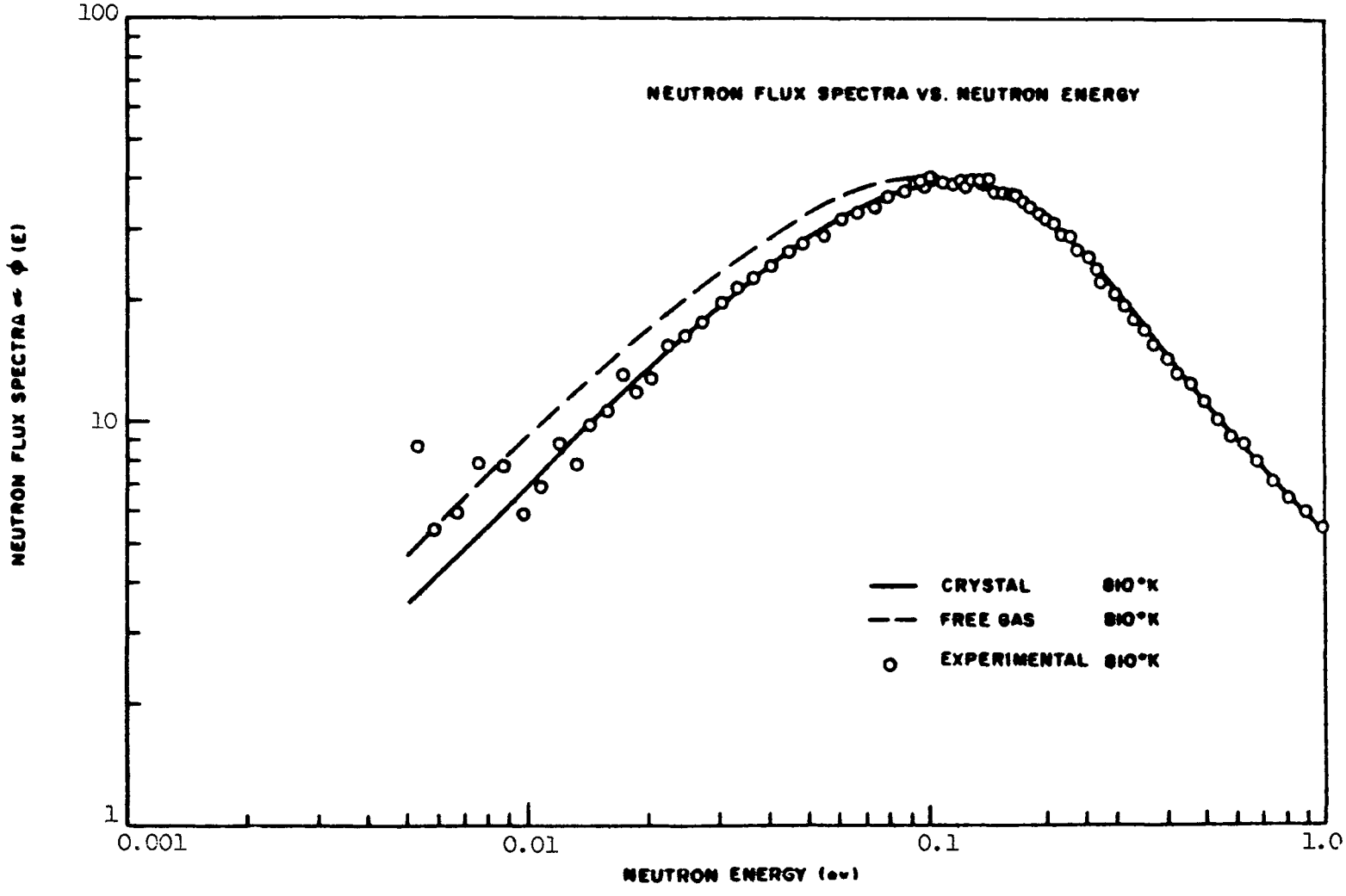

Fig. 23 Neutron spectra in graphite at 810°K

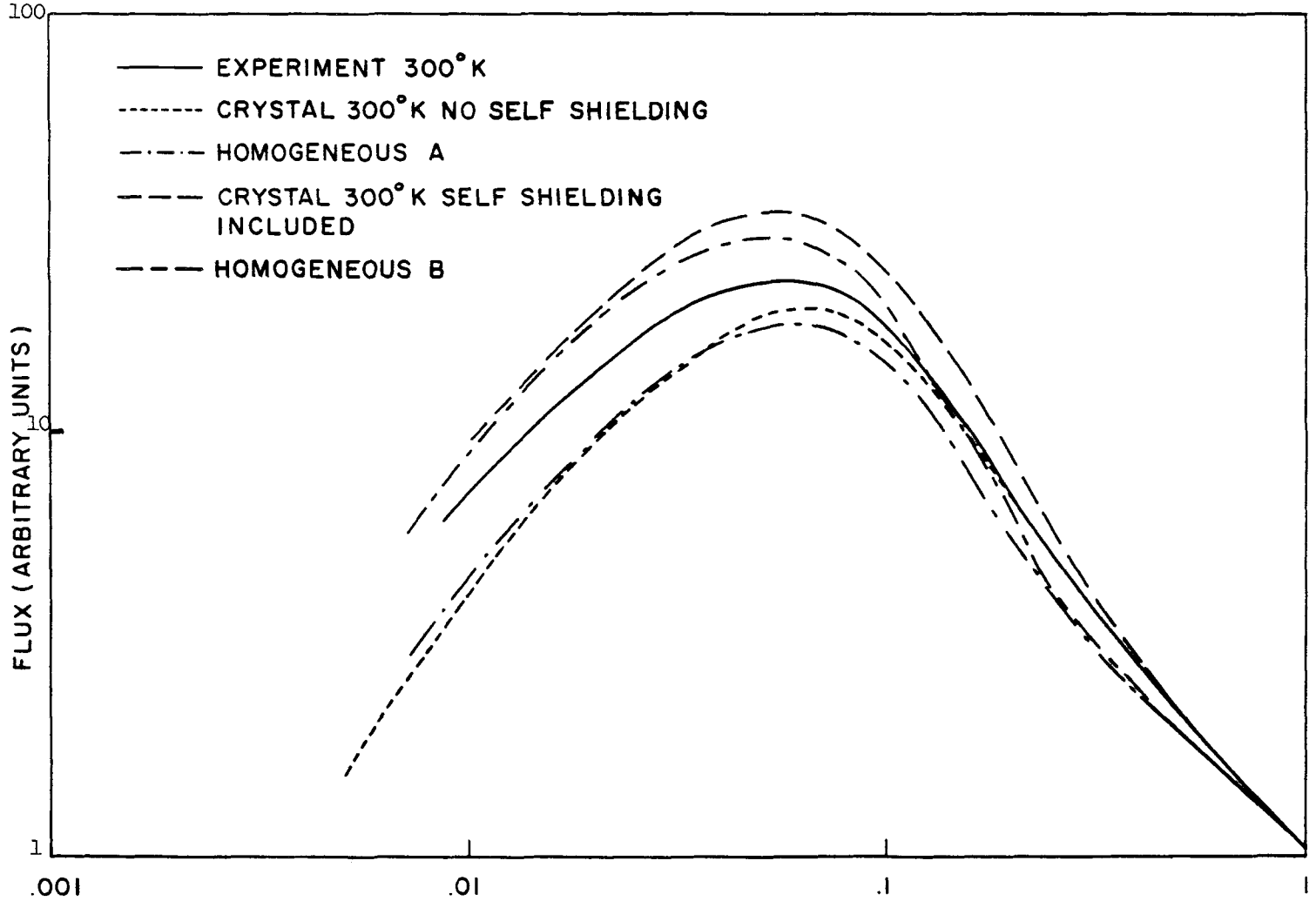

Fig. 24 Neutron spectra calculated for the Zenith lattice

self-shielding factor was introduced. In both comparisons the spectra predicted using the Parks' kernel are harder than the E.S. predictions, indicating the presence of higher frequency components in the phonon spectrum in the former case. Clearly, in addition to further typical experimental investigations it would be desirable to re-analyze the Harwell data using a two-dimensional representation of the cell plus the Parks' kernel and to re-analyze the General Atomic data using the Egelstaff-Schofield's kernel.

The time dependent spectrum studies (at short times) in graphite reported to the conference by E. Barnard[11] do not presently indicate the existence of a spectrum harder than predicted by the Egelstaff-Schofield scattering law. At long times, however, after the introduction of the neutron pulse the spectrum is more diffusion cooled than predicted with the Egelstaff-Schofield kernel indicating as before the need for the higher frequency terms in the phonon distribution.

D_2O Lattices

Here again it is desired to correlate as much as possible spectra measured in homogeneous D_2O systems with that in heterogeneous situations. First, let us consider the available homogeneous data. It was taken at General Atomic in the geometry shown in Figure 25. The resulting spectrum is shown in Figure 26. Clearly, we have a situation where the least physically accurate

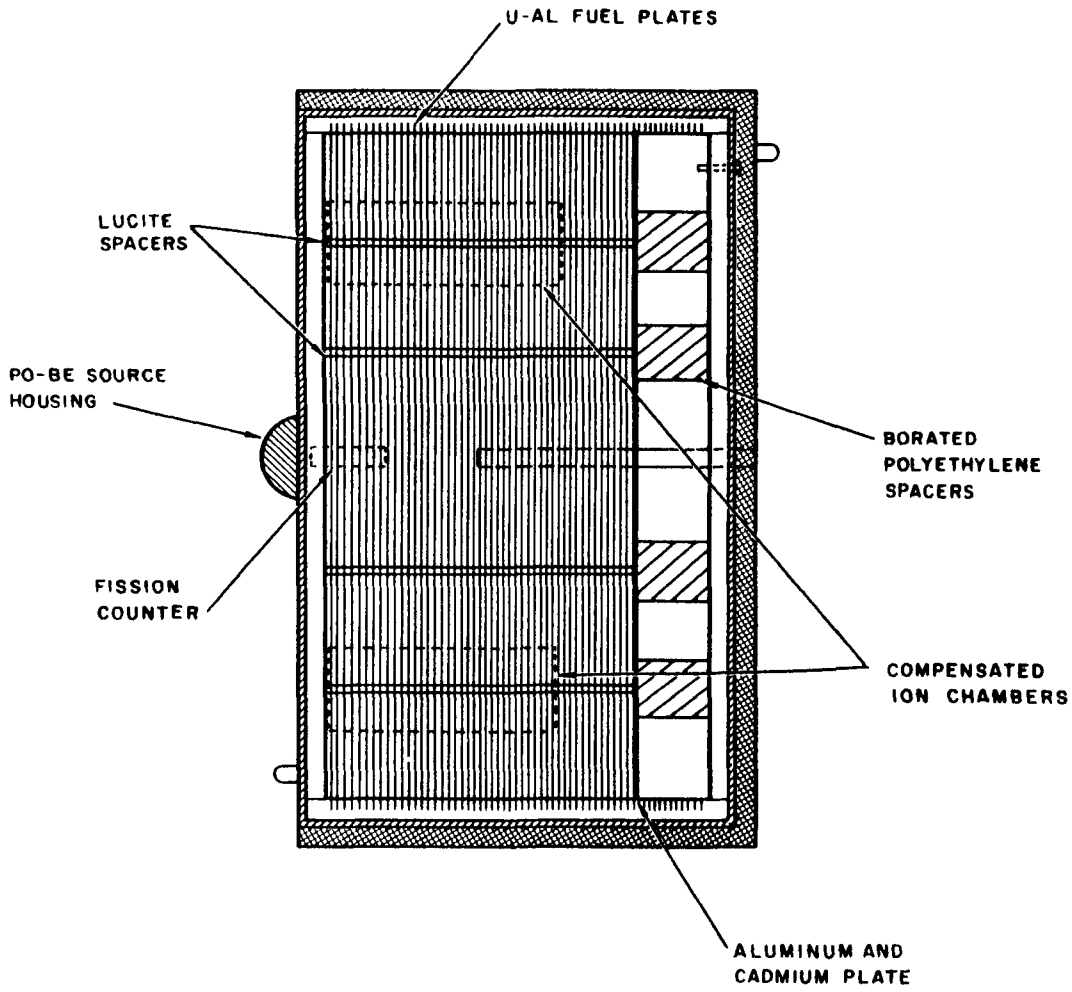

Fig. 25 Geometrical arrangement used for measuring neutron spectra in borated D_2O

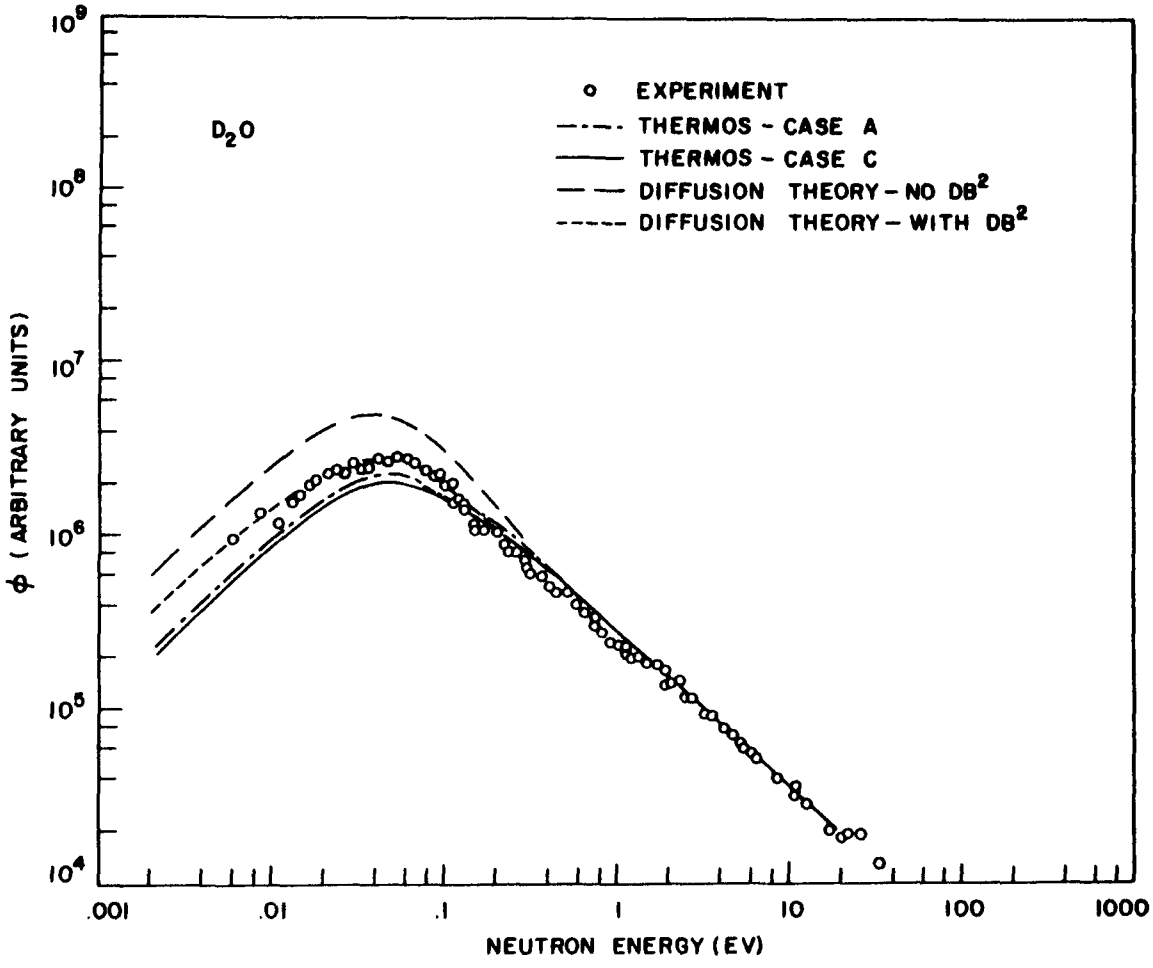

Fig. 26 Scalar neutron spectra measured in borated D_2O

kernel works the best. The Brown and St. John kernel with an effective mass of 3.9 would fall somewhere in between the results presented. All calculations in D_2O were done with the incoherent approximation. Butlers' theoretical work in England indicates this assumption is relatively good.

Considering the integral results now, Brown at Savannah River has made foil measurements in fuel moderator configurations and finds a harder spectrum in fuel than predicted by theory using the Brown and St. John's kernel. The same information is indicated by the M.I.T. work where the Brown and St. John flux shapes agreed reasonably well with experiment but here theory also predicts a softer spectrum in the fuel. The comparison between theory and experiment by D. C. Leslie[12] for the D_2O reactor OCDRE shows the same effect. This effect is opposite to that shown by the differential work, Figure 26. It perhaps is worthwhile reasserting at this time the point that although the integral foil method is somewhat sensitive to scattering law it is more sensitive to transport assumptions concerning the leakage from the moderator and transmission properties of the cell. It thus checks these methods most strongly. The differential spectral measurements are, however, more sensitive to scattering law approximations. Some confusion on how to describe low energy D_2O scattering is thus indicated by the presently available experimental results.

Water Lattices

Workers on heterogeneous water-uranium lattices have included Campbell and Poole at Harwell using pulsed and integral techniques and Mostovoi in Russia who employed a chopper technique. Experimental geometries used in both cases were typical of those employed in non-heterogeneous investigations, i.e., cylindrical rods were spaced in a water tank. In the English work approximately three centimeter rods were spaced on a four centimeter pitch while in the Russian work approximately four centimeter rods were spaced on a six centimeter pitch. Spectra were measured both perpendicular and parallel to the rods' axes both in the rods and in the water channels between rods. Honeck and Takahashi have attempted to calculate the spectrum in both cases and find measured spectra to be considerably harder than the theoretical predictions. In addition, the necessary spectral neutron conservation laws are not obeyed on these spectra. The current situation is shown in Figures 27, 28, and 29. The worst disagreements are encountered when the spectra in the fuel and parallel to it are compared to theory.

The situation for these lattices is not entirely unlike that observed for the finite medium leakage spectra reported in Section III. The affect is in the same direction and the disagreements of the same order. However, the experimental problems are far more severe in the lattice case than in

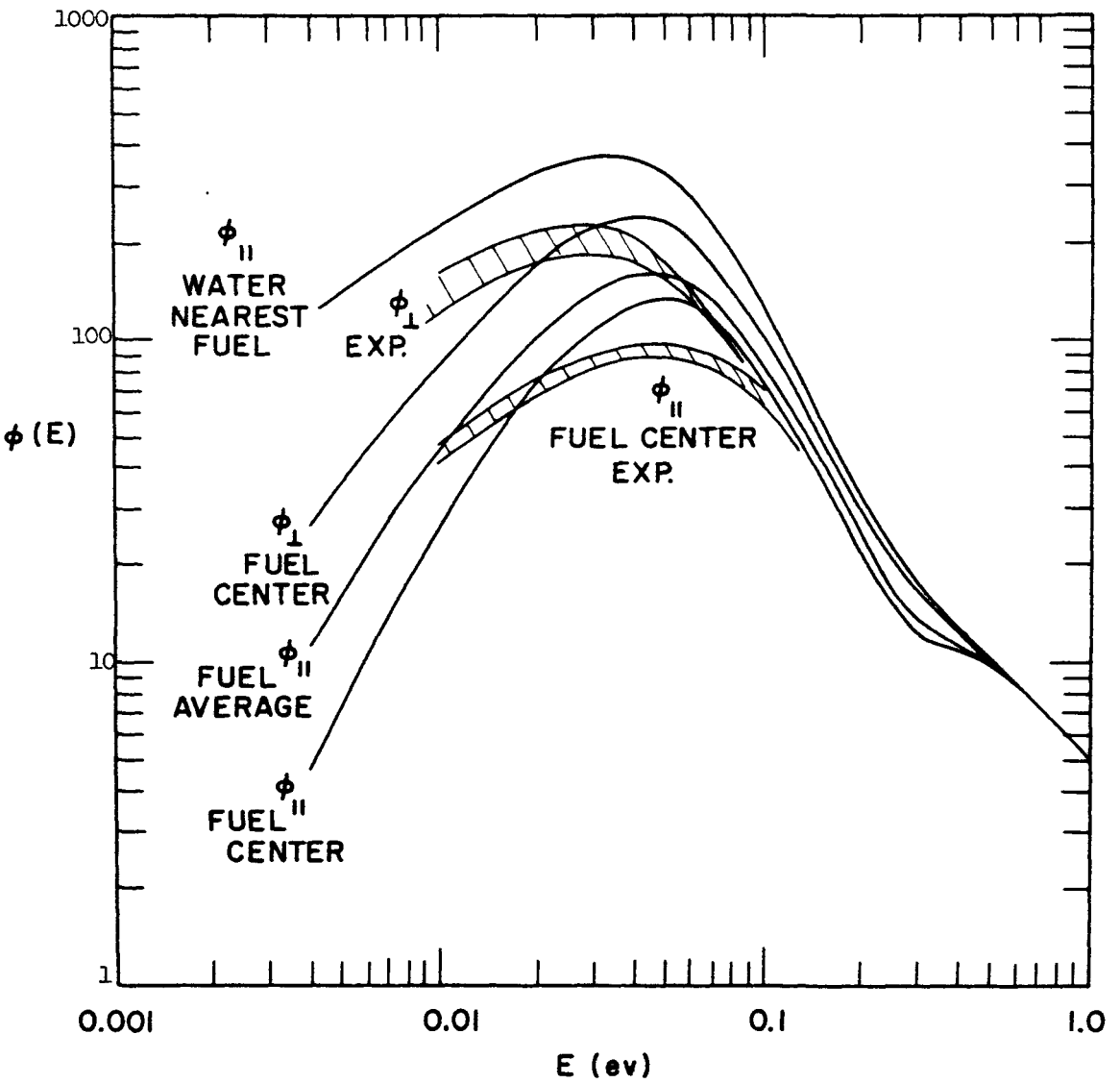

Fig. 27 Neutron spectra in heterogeneous water-uranium lattices

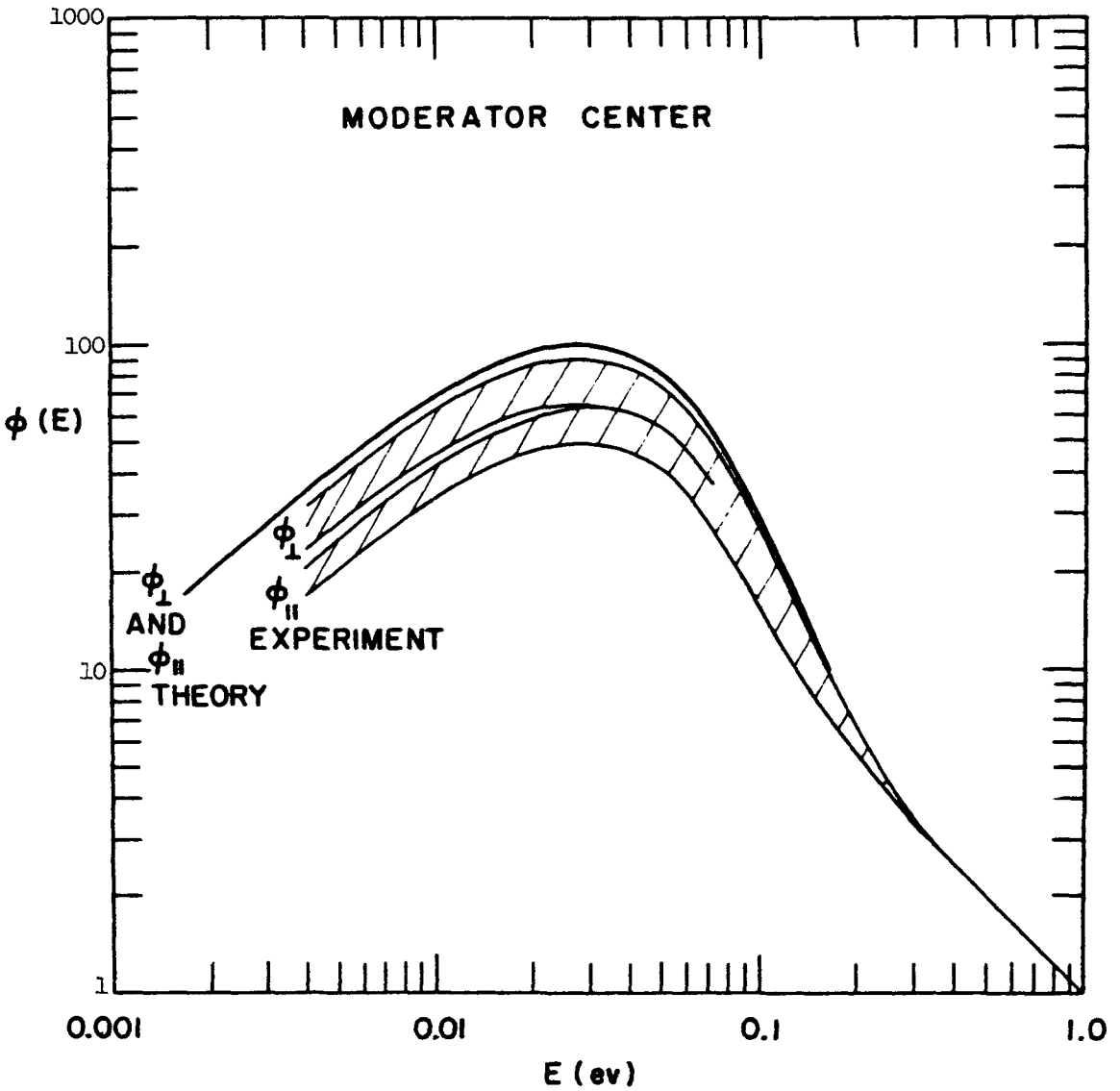

Fig. 28 Neutron spectra in heterogeneous water-uranium lattices

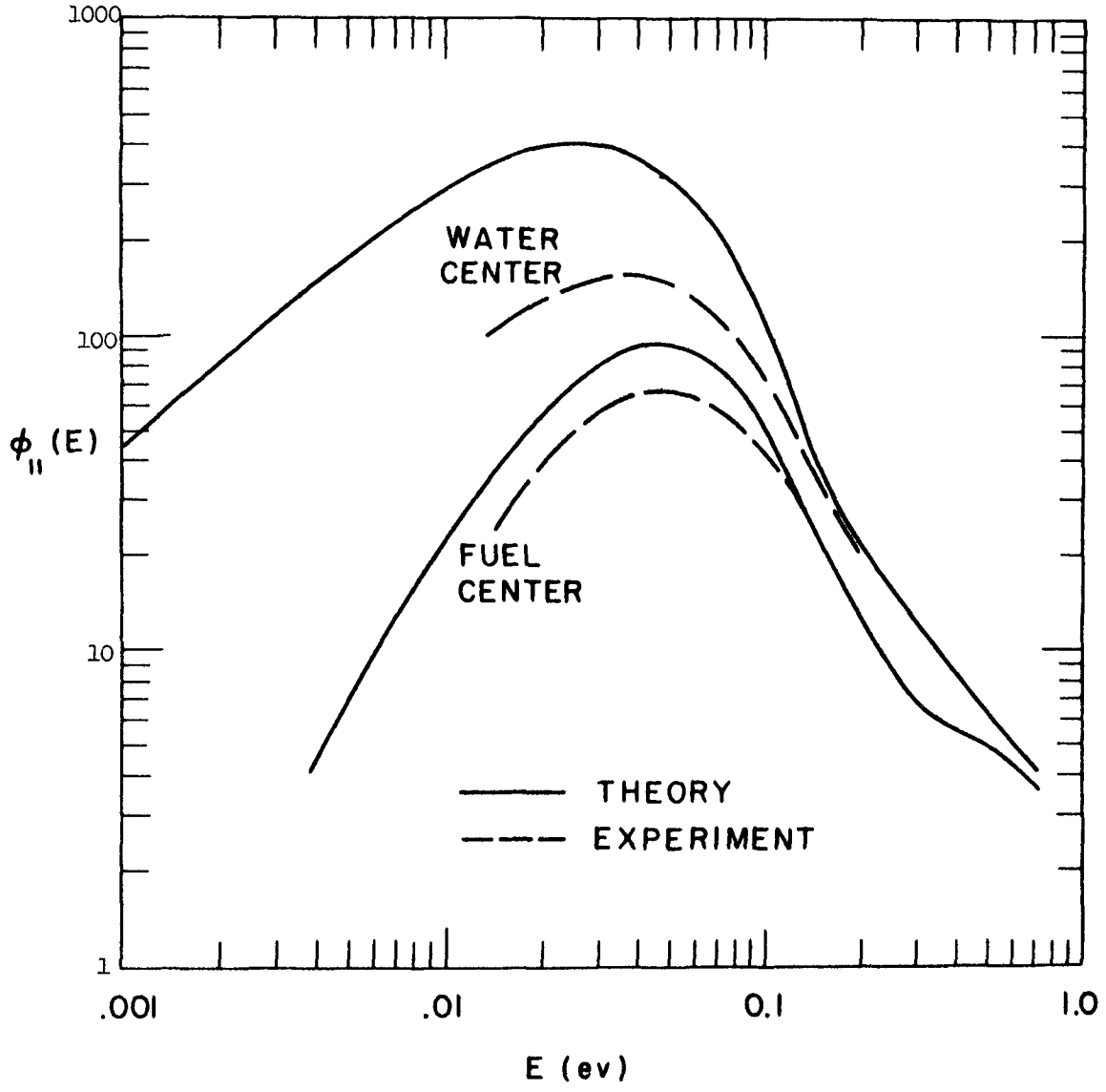

Fig. 29 Neutron spectra in heterogeneous water-uranium lattices

the Milne case. A clear-cut need for further experimental lattice work in clean geometry exists to straighten out the present problems.

At present some suggestions for future experimental work are in order. It is now clear that spatial gradients introduced by source position strongly influence angular spectra. It is thus necessary to guarantee in lattice work that these gradients, and for that matter bucklings, are very small relative to those established by the lattice structure. This can best be assured if the measurements are made in a multiplying system. Flux flattening can be attained for this work with system multiplications of 10 or so. In addition, methods of beam extraction can perturb the measured spectrum strongly when the hole introduced into the lattice is 1/3 or more of the rod or channel size. Thus small re-entrant tubes must be used if good spatial resolution, with no attendant flux perturbation, is desired. It would appear that investigations in which flux averages are measured over many lattice cells would be a less ambitious first course of action. Foil work also has many distinct advantages for this class of experiment. Good spatial resolution with little or no perturbation of measured quantities can be obtained. In addition one often measures the quantity desired directly in a practical reactor problem, namely the activation distribution which can be related to the thermal utilization for the cell. It will be recalled that activation studies reported in the previous paper

by Honeck[1] for water-uranium lattices indicate the existence of relatively good agreement between transport theory predictions and experiment.

References

1. Honeck, Henry C., Reporter Session on Theoretical Neutron Spectra - BNL Conference on Neutron Thermalization, April 30 - May 2 (1962).
2. Poole, C. G., C. G. Campbell, R. G. Freemantle, "Measurements of Reactor Spectra by Time-of-Flight and Integral Methods," paper No. 10 16, p. 233, 2nd United Nations International Conference on Peaceful Uses of Atomic Energy, September 1 - 13 (1958).
3. Coveyou, R. R., R. R. Bate, R. K. Osborn, Journal of Nuclear Energy 2, 153-167 (1956).
4. Reichardt, W. and K. Burkart, "Observations of Hardened Neutron Spectra in Water and Boric Acid Solutions," BNL Conference on Neutron Thermalization, April 30 - May 2 (1962).
5. Parks, D. E., GAMD-2189, "Mean Time of Emission of Neutrons From Pulsed Non-Multiplying Assemblies," October 5, 1961.
6. Goldman, D. T. and F. O. Federighi, "Calculation of Thermal Neutron Spectra in an Infinite Polyethylene Moderated Medium with Varying Amounts of Absorption," BNL Conference on Neutron Thermalization, April 30 - May 2 (1962).
7. Barclay, F. R., et al., "Low Energy Neutron Spectra in the ZENITH Heated Graphite Moderated Reactor," BNL Conference on Neutron Thermalization, April 30 - May 2 (1962).

8. Macdougall, J. D., "Application of Scattering Law Data to the Calculation of Thermal Neutron Spectra," BNL Conference on Neutron Thermalization, April 30 - May 2 (1962).
9. Parks, D. E., "The Calculation of Thermal Neutron Scattering Kernels in Graphite," GA-2438.
10. Yoshimori, A., and Y. Kitano, "Theory of the Lattice Vibration of Graphite," J. Phys. Soc. (Japan), Vol. 11, 1956, p. 352.
11. Barnard, E., et al., "Thermalization of Neutrons in Graphite," BNL Conference on Neutron Thermalization, April 30 - May 2 (1962).
12. Leslie, D. C., "Calculation of Thermal Spectra in Lattice Cells," BNL Conference on Neutron Thermalization, April 30 - May 2 (1962).

Measurements of Spatial and Spectral Distributions of Thermal Neutrons in Heavy Water, Natural Uranium Lattices

P. Brown, I. Kaplan, A. E. Profio,
T. J. Thompson
Masssachusetts Institute of Technology
Cambridge, Massachusetts

March 14, 1962

I. Introduction:

Measurements of the spatial distributions of thermal neutrons in natural uranium, heavy water-moderated lattices have been made with gold, lutetium, and europium in the exponential facility of the M.I.T. Lattice Research Project.[1,2,3] Gold was used as a $\frac{1}{v}$-absorber to measure the relative neutron density; Lu^{176} has a neutron capture resonance at 0.142 ev with the result that the activation depends strongly on the neutron energy spectrum; Eu^{151} has a $(\frac{1}{v})^2$ - thermal neutron absorption cross section and also a strong resonance at 0.46 ev. As in the case of lutetium, but to a lesser degree, europium activities depend on the neutron energy spectrum.

The experimental distributions were compared with those calculated with the THERMOS CODE.[4] THERMOS assumes a cylindrical cell centered on the fuel rod and computes the spatial and spectral thermal neutron distribution for various epithermal cutoffs. The Brown - St. John kernel is used in these calculations. Several integral properties of the cell, such as average velocities and activity distributions for various detectors, are also computed.

II. Experimental Technique:

The M.I.T. Heavy Water Lattice Research facility consists of a well shielded tank containing the lattice and heavy water and fed

from the bottom by a special source arrangement utilizing the M.I.T. Reactor thermal column. Measurements made to date have been in a 4-foot diameter tank containing lattices of 1.010 inch diameter, aluminum clad, natural uranium metal rods on triangular pitches of 4.5-inches, 5.0-inches, and 5.75-inches, respectively. Experiments are presently being performed with 0.250 inch, 1.03% U^{235} metal rods, on spacings of 1.25-inch, 1.5-inch, and 1.75-inch, respectively.

Intracell flux traverses were made in the central cell inside a split fuel rod and on thin aluminum foil holders strapped to the rod and extending out into the moderator both toward the next adjacent rod and to a point midway between the next two adjacent rods, as shown in figure 1. Aluminum was used instead of plastic, because an early experiment showed that plastic holders depressed the flux by as much as 3% whereas the effect of aluminum was only about 0.5%. Foils in the moderator were corrected for this flux depression by aluminum. Foils in the fuel were arranged in a spiral pattern to provide maximum foil spacing and minimum flux perturbation, which was computed to be negligible. Flux traverses were made with bare foils and with foils with 0.023 inch thick cadmium covers. The cadmium covered foils were irradiated at the same time as the bare foils, but at different heights in the tank to avoid thermal flux perturbation by the cadmium. An experimentally measured exponential extrapolation length was used to correct for the differences in height. The Au foils were about 2 mils thick, and were weighed accurately to a fraction of a percent. The Lu and Eu foils were very dilute and only a small fraction of a mean free

path thick. They were fabricated by spraying glyptal suspensions of the oxides on 0.005-inch thick aluminum backing and were calibrated accurately in a uniform flux on a rotating foil wheel. All foils were $\frac{1}{8}$ inch in diameter.

Several measurements were made to determine the effect of macroscopic position on the intracellular flux distribution. Axial and radial macroscopic traverses made with U^{238} foils gave the same shapes as those made with gold,[2,3] indicating that the thermal and epithermal neutron distributions had the same spatial dependence sufficiently far from the source. Similar macroscopic flux shapes were obtained with lutetium foils. Intracellular gold flux traverses made near the edge of the tank showed only small differences from those made at the central cell. It was concluded that, certainly in the central cell, the neutron flux was separable into a macroscopic $J_o\left(\frac{2.405r}{R}\right)$ distribution and a microscopic distribution.

III. Results:

Measured activity distributions were normalized at the cell edge to those calculated by THERMOS. Two sets of measurements with each detector were made at the three lattice spacings; the results were found to be reproducible to within about one percent. The cell edge was chosen as the normalization point because that is where the thermal neutron distribution is closest to a Maxwellian; calculations of effective neutron temperature are then made relative to the temperature at the cell edge. It was found that, in all cases, the shapes of the experimental activity distributions in the moderator were fit very well by THERMOS. Any differences between theory and experiment would thus appear in the

it was possible to extrapolate the cadmium covered europium activity for 0.023 inch thick cadmium to zero thickness of cadmium. The use of the asymptotic activity mentioned above and the extrapolated activity made it possible to correct the europium plots to values of the cutoff energy both below and above the 0.46 ev resonance. The experimental activity at the center of the fuel was higher than that predicted by THERMOS by about 3.7% for an 0.63 ev cutoff and 4.7% for an 0.19 ev cutoff. Typical results are shown in figures 4 and 5. The discrepancies are perhaps due to the simple model used in correcting the activities of the cadmium covered foils. The simplicity of the model seems to be justified, however, by the fact that the activity of the cadmium covered europium foils is less than 10% of the total activity and the model applies a correction to this already relatively small effect.

Spectral hardenings from cell edge to rod center were obtained by assigning at these points a maxwellian temperature, at which the average velocity is equal to that of the computed spectrum over the energy range up to 0.23 ev, the beginning of the $\frac{1}{E}$ tail. The neutron temperature changes from cell edge to cell center were, for the 4.5-inch, 5.0-inch and 5.75-inch lattices, 100.9°C, 97.6°C, 94.2°C, respectively. The temperature changes compare favorably with those computed previously[7] with THERMOS for 1.0-in. natural uranium - heavy water lattices and square pitches of 3.625-in. and 4.5-in.; the temperature changes for these lattices were 100°C and 95°C, respectively. This method of obtaining the changes in neutron temperature seem to be justified by the good agreement between THERMOS and

experiment[a] lutetium, europium, and gold distributions.

IV. Conclusions:

The experimental results show, for the heavy water, natural uranium lattices here treated, that the thermal neutron density can be computed to a high degree of accuracy. In view of the complicated energy dependence of the cross sections of Lu^{176} and Eu^{151}, the results for these detectors agree very well with those computed with THERMOS. It should be pointed out that Lu^{176} is a better detector than Eu^{151}, in that it is much more sensitive to changes in the thermal neutron spectrum, and that it does not require an involved correction for epicadmium activity.

Some of the difference between theory and experiment may be due to approximations in the Brown - St. John kernel. H. C. Honeck, of BNL, has recently developed for THERMOS a method for computing a Nelkin type kernel using parameters for heavy water. The theoretical distributions in the above mentioned lattices will be recomputed with this new kernel.

At present, heavy water lattices of 0.25-inch diameter, uranium rods with a U^{235} concentration of 1.03% are being studied. Possible corrections for the finite size of the system, such as leakage, are being studied. The possible failure of the Wigner-Seitz circular cell approximation at small lattice spacings (e.g. 0.25-in. rods in a 1.25-in. triangular pitch) will also be investigated.

REFERENCES:

1. "MIT Heavy Water Lattice Research Project, Annual Report," AEC-NYO-9658, September 30, 1961.

2. A. Weitzberg, I. Kaplan, T. J. Thompson, "Measurements of Neutron Capture in U^{238} in Lattices of Uranium Rods in Heavy Water," AEC-NYO-9659, January, 1962.

3. P. F. Palmedo, I. Kaplan, T. J. Thompson "Measurements of the Material Bucklings of Lattices of Natural Uranium Rods in D_2O," AEC-NYO-9660, January, 1962.

4. H. C. Honeck, "THERMOS," BNL-5826, September, 1961.

5. J. P. Roberge and V. L. Sailor, "Nuclear Science and Engineering," 7, No. 6, June 1960, p. 502.

6. BNL-325.

7. H. C. Honeck "Nuclear Science and Engineering," 8, No. 3, September 1960, p. 201, figure 4.

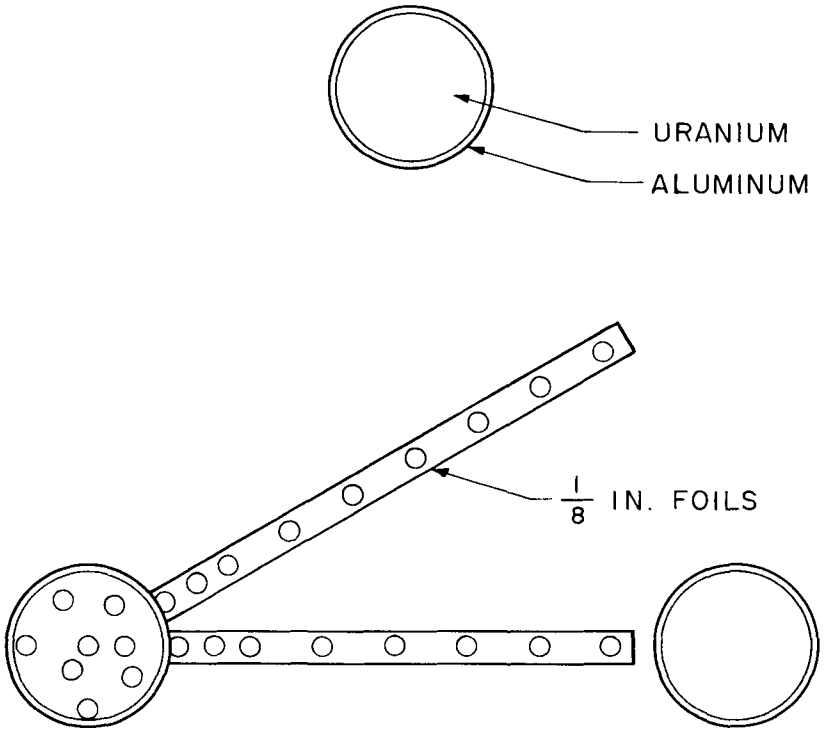

FIG. I FOIL HOLDER ARRANGEMENT

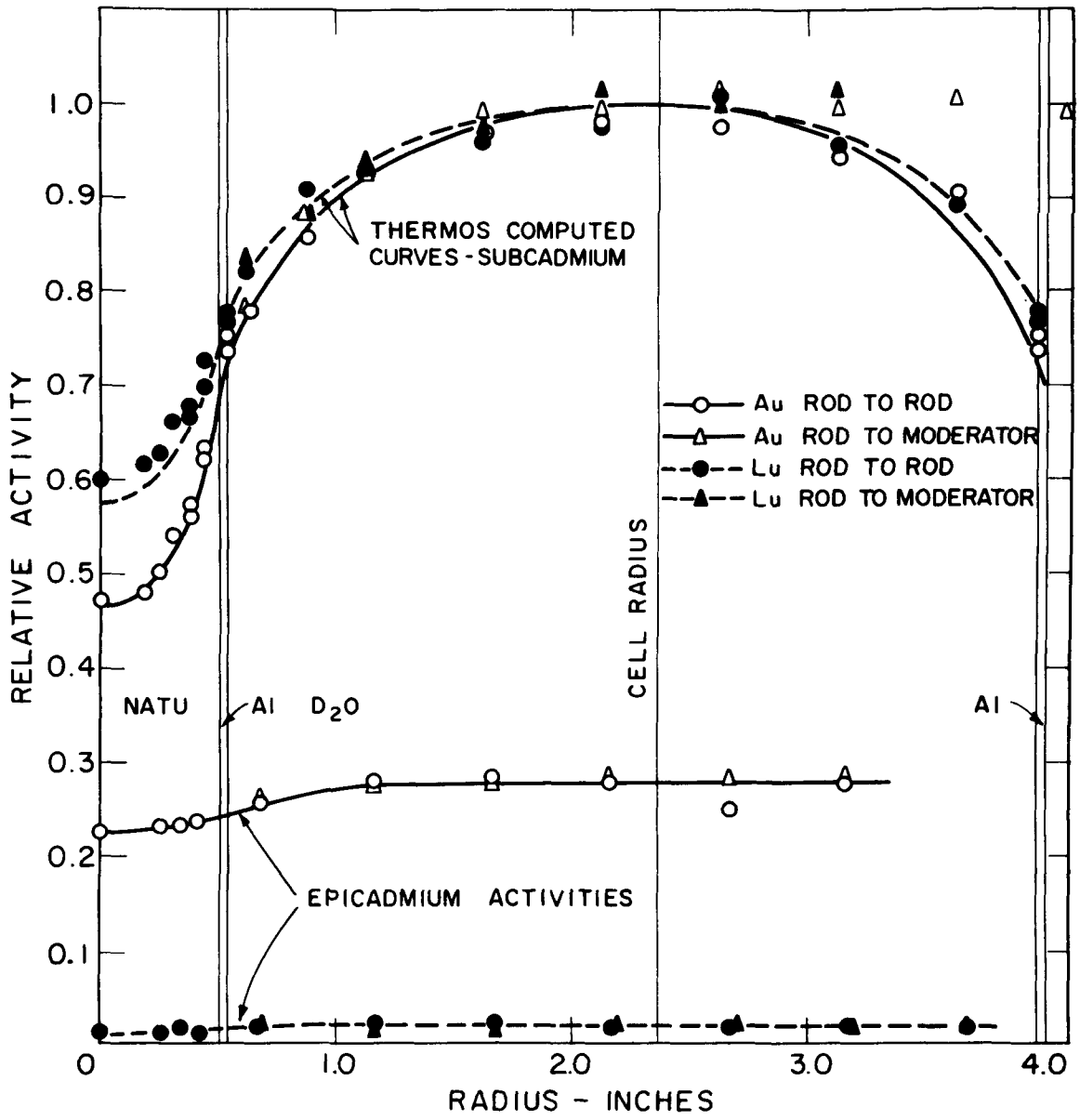

FIG. 2 Au AND Lu DISTRIBUTIONS - 4.5 - IN. LATTICE

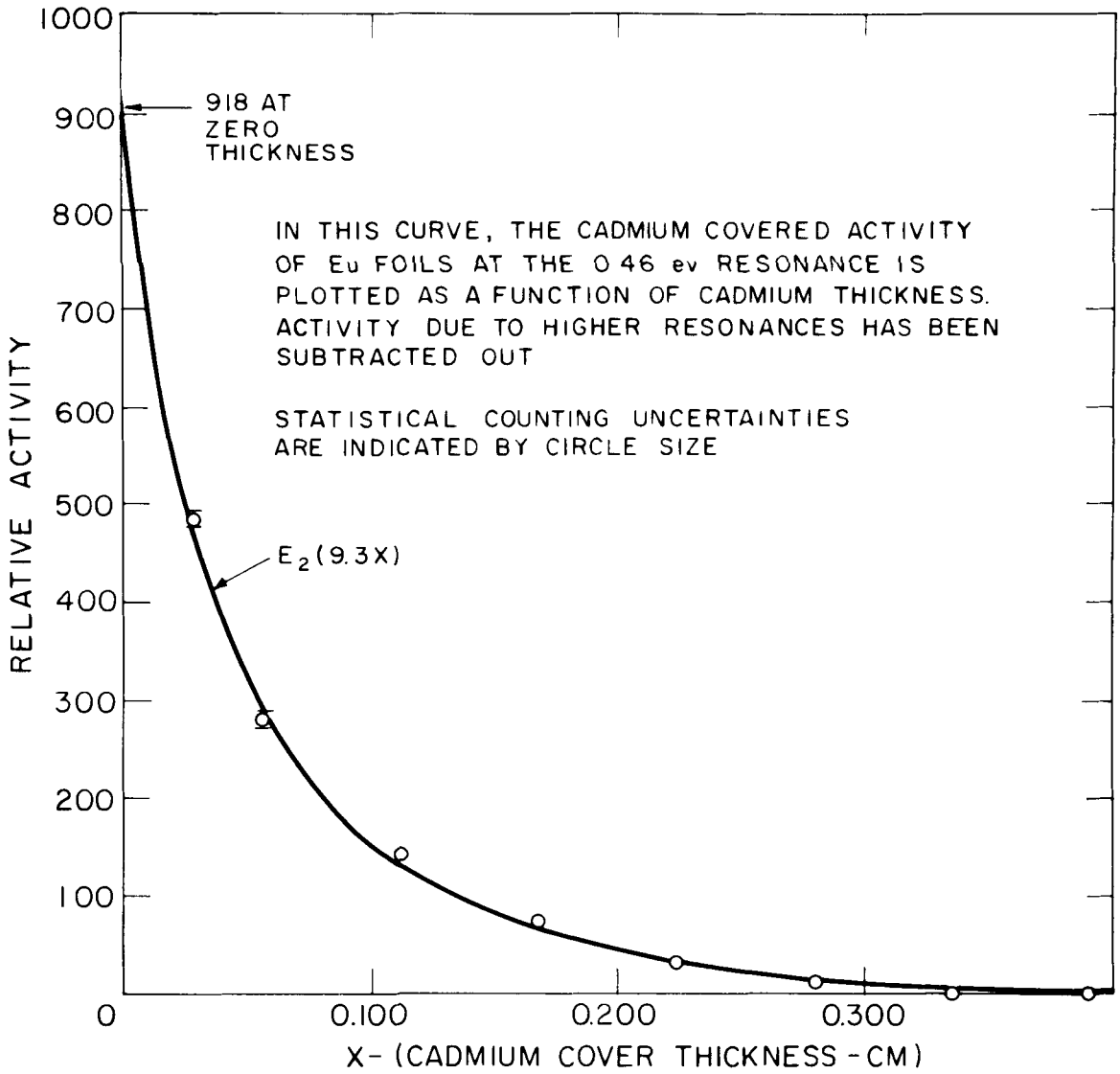

FIG. 3 0.46ev EUROPIUM ACTIVITY AS A FUNCTION OF CADMIUM THICKNESS

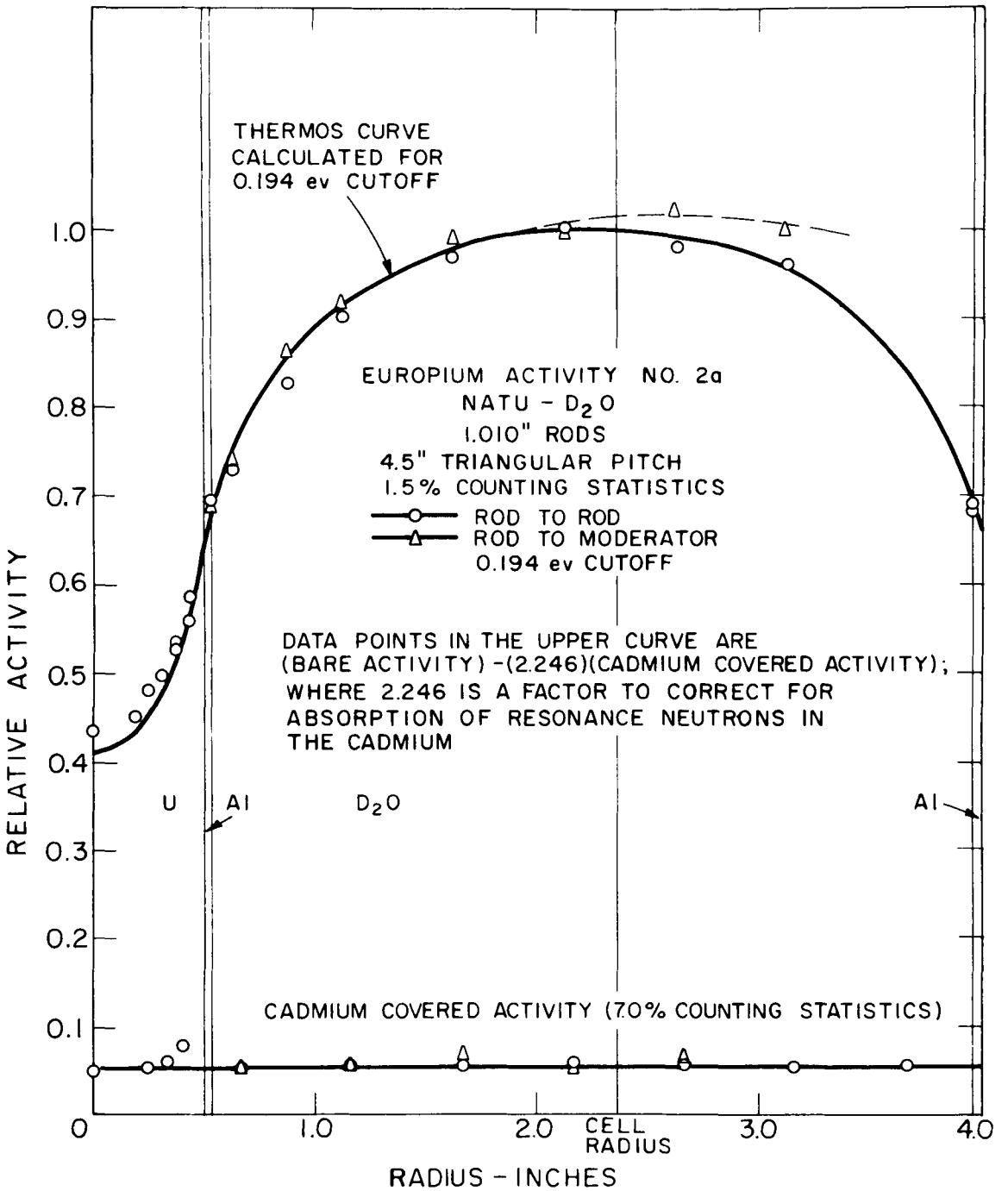
THERMOS CURVE
CALCULATED FOR
0.194 ev CUTOFF
EUROPIUM ACTIVITY NO. 2a
NATU - D_2O
1.010" RODS
4.5" TRIANGULAR PITCH
1.5% COUNTING STATISTICS
ROD TO ROD
ROD TO MODERATOR
0.194 ev CUTOFF
DATA POINTS IN THE UPPER CURVE ARE
(BARE ACTIVITY) -(2.246)(CADMIUM COVERED ACTIVITY);
WHERE 2.246 IS A FACTOR TO CORRECT FOR
ABSORPTION OF RESONANCE NEUTRONS IN
THE CADMIUM
U
Al
D_2O
Al
CADMIUM COVERED ACTIVITY (7.0% COUNTING STATISTICS)
RELATIVE ACTIVITY
0
0.1
0.2
0.3
0.4
0.5
0.6
0.7
0.8
0.9
1.0
1.0
2.0
CELL
RADIUS
3.0
4.0
RADIUS - INCHES

FIG. 4

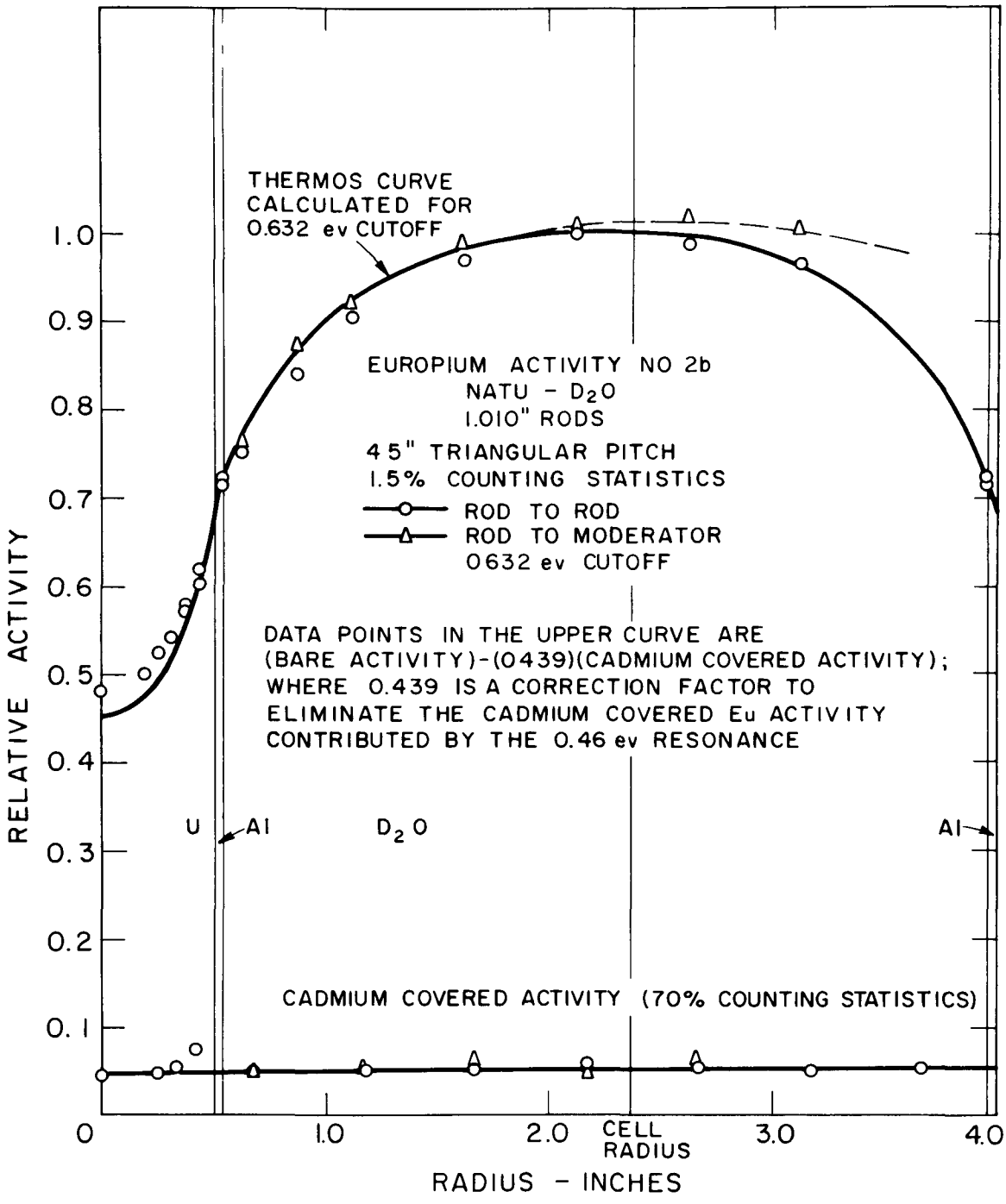
THERMOS CURVE
CALCULATED FOR
0.632 ev CUTOFF
EUROPIUM ACTIVITY NO 2b
NATU - D_2O
1.010" RODS
45" TRIANGULAR PITCH
1.5% COUNTING STATISTICS
ROD TO ROD
ROD TO MODERATOR
0632 ev CUTOFF
DATA POINTS IN THE UPPER CURVE ARE
(BARE ACTIVITY)-(0439)(CADMIUM COVERED ACTIVITY);
WHERE 0.439 IS A CORRECTION FACTOR TO
ELIMINATE THE CADMIUM COVERED Eu ACTIVITY
CONTRIBUTED BY THE 0.46 ev RESONANCE
U
Al
D_2O
Al
CADMIUM COVERED ACTIVITY (70% COUNTING STATISTICS)
RELATIVE ACTIVITY
1.0
0.9
0.8
0.7
0.6
0.5
0.4
0.3
0.2
0.1
0
1.0
2.0
CELL RADIUS
3.0
4.0
RADIUS - INCHES

FIG 5

Observation of Hardened Neutron Spectra in Water and Boric Acid Solutions

by

K. Burkart and W. Reichardt

Institut für Neutronenphysik und Reaktortechnik
des Kernforschungszentrums Karlsruhe

Abstract

Neutron spectra in water and boric acid solutions have been observed by the time-of-flight method and by Lutetium foil techniques. Both methods yield results in good agreement. They show a stronger hardening than those obtained by previous authors. The agreement with the predictions of the Nelkin model is satisfactory.

1. Introduction

In 1958 Westcott [1] suggested that Lu^{176} might be a good indicator of the "temperature" of thermal neutrons because of its large capture resonance at 0,142 eV. Measurements on these lines have been done by G.A. Price [2] and by L.C. Schmid and W.P. Stinson [3]. They compared the activity of Lu^{176} with that of a $\frac{1}{v}$ – detector in heated graphite and showed that the ratio of their activities is a very sensitive measure for the graphite temperature. We have applied this method to determine the hardening of neutron spectra in water poisoned with different amounts of boric acid. When analysing the results using the Westcott convention [4] we found a stronger hardening of the spectra than M.I. Poole [5] had obtained by the time-of-flight method.

The results did not agree, too, with the theoretical predictions of Coveyou's formula [6] and the theory of Brown [7]. We therefore started some differential measurements on neutron spectra in aqueous boric acid solutions by the pulsed source time-of-flight technique [5][8]. The results of the differential and the integral measurements are described in this paper.

2. Experimental Arrangements for the Time-of-Flight Measurements

The experimental set up for the spectrum measurements by the time-of-flight method was essentially the same as that described in ref. 9 . Neutrons were obtained from a pulsed $T(d,n)He^4$ neutron source yielding about 10^8 neutrons per pulse. An evacuated flight path of about 5 m length shielded by 10 cm of B_2O_3 was used. Neutrons were detected by a layer of 8 high pressure BF_3-counters which fed the counting pulses into a TMC 256 channel time analyser. The collimators were made from boron carbide encased in aluminium or from boron carbide mixed with plexiglas. No difference in the measured spectra using these two sorts of collimators could be observed. The neutron beam from the middle of the moderator assemblies was extracted by conical extraction channels. The angular divergence of the cone was slightly greater than that of the neutron beam which was defined by two apertures in the flight tube. No neutrons from the walls could therefore reach the counters. Because of the conical shape the flux distortion caused by the extraction channels is much smaller than when a cylindrical shape is used.

3. Results

As the intensity of our neutron source was not sufficient to do measurements on infinite geometry we have measured the spectra inside 15 cm

and 30 cm cubes. Whereas the leakage from these cubes causes a deviation from the infinite medium spectrum as far as the ratio of thermal to epithermal flux is concerned, it does essentially not affect the shape of the thermal part of the spectrum as the small hardening caused by the leakage loss is compensated to some extend by a "diffusion cooling" effect[9]. This will be shown below by comparing the spectra of the 15 and the 30 cm cubes.

The following corrections had to be applied to the measured data:

1. Subtraction of the background which was determined by closing the collimator with a boron carbide-plexiglas plug.

2. Correction for the energy dependent counter sensitivity which was calculated using the data given by the producer (20th Century Electronics).

3. Correction for the neutron losses in the flight path, i.e. transmission through 80 cm of air, 5 1/2 mm of aluminium, and 0,7 mm of copper.

4. Correction to the flight time due to the delayed emission of the neutrons from the moderator.This effect was neglected in the epithermal region (>0,25 eV). In the thermal region (<0,08 eV) an average delay time equal to the thermal lifetime $\left[(\Sigma_a v)_o + DB^2 \right]^{-1}$ was assumed. The average emission time in the transition range (0,08-0,25 eV) was determined by a transmission measurement through a thin sheet of cadmium (for the case of pure water).

5.Resolution corrections because of the finite time spread of the neutron pulse emerging from the moderator. Resolution corrections were applied to the pure water data only. They amounted up to 8% for the spectrum inside the 30 cm cube but were always smaller than 1% for the boric acid solutions.

Fig.1 and 2 show the spectra obtained from pure water and several boric acid solutions for the 30 cm and the 15 cm cube. In addition to the spectra from inside leakage spectra from the surface of the 15 cm cube were measured. These data are plotted in fig. 3.

4) Analysis of the Results

As can be seen from fig. 1 and 2 the thermal parts of the spectra from inside the moderators can be reasonable well fitted by a Maxwellian distribution. They deviate from the Maxwellian shape only below ~ 0,01 eV. In fig. 4 the data of both vessels are compared by plotting $\phi(E)/E$ versus energy. No significant difference between the spectra of the two cubes can be observed. Furthermore the data follow a straight line thus indicating that a Maxwellian distribution is a good fit, which suggests that the concept of a "neutron temperature" is at least a good approximation. The "neutron temperatures" obtained from the slopes of these straight lines are listed in table I.

The concept of a "neutron temperature" is not applicable to the leakage spectra. Fig.3 shows, however, that the spectra have identical shapes in the thermal range but are shifted towards higher energies with increasing boric acid concentration. The thermal part of the leakage spectrum from pure water is well represented by the asymptotic leakage spectrum from an infinite half-plane calculated by Kiefhaber[10] using the Nelkin scattering kernel of water[11]. In order to fit the leakage spectra from the boric acid solutions, the Kiefhaber spectrum was shifted by an amount $\frac{\Delta E}{E}$ which agrees well with the $\frac{\Delta T}{T}$ values as can be seen from table I.

Table I

Temperatures of the Maxwellian distributions fitted to the measured spectra. The last column shows the relative energy shift of the leakage spectra.

$\sigma_{a\,eff}$ [barns/hydrogen]	Spectrum from inside the cubes				Leakage spectrum
	15 cm cube		30 cm cube		15 cm cube
	T_N[°K]	$\frac{T_N-T_M}{T_M}$	T_N[°K]	$\frac{T_N-T_M}{T_M}$	$\frac{\Delta E}{E}$
0,332	292 ± 4	-	293 ± 3	-	-
1.37	-	-	301 ± 5	0.060 ± 0.017	0.08 ± 0.03
2.13	-	-	328 ± 5	$0,119\pm0.017$	-
3.33	356 ± 5	0.215 ± 0.017	355 ± 5	0.212 ± 0.017	0.23 ± 0.03
4.24	387 ± 6	0.321 ± 0.021	386 ± 6	0.317 ± 0.021	0.30 ± 0.04

T_N = temperature of the fitted Maxwellian

T_M = temperature of the moderator

In the transition region and the epithermal range the accuracy of our data is not sufficient to draw exact conclusions. Therefore no "joining functions" were determined. The ratio of thermal to epithermal flux for pure water in infinite geometry was obtained by plotting $\frac{\phi_{th}}{\phi_{epi}}$ versus the effective thermal absorption cross section and extrapolating to its value of pure water. The extrapolation yields a value of 67 which is in good agreement with Poole's result [5].

Integral Measurements with Lu-Foils.

The integral measurements were performed by comparing the saturation activities of Lu^{176} and Cu^{63} in different boric acid solutions contained in a 30 x 30 x 25 cm plexiglas box. This device was irradiated in the pool of the FRM swimming pool reactor in a distance from the graphite reflector where the cadmium ratio was almost independent of space. The size of the container was sufficient to establish an infinite medium spectrum of thermal neutrons in the boric acid solutions. The slowing down spectra were almost the same inside and outside the box because of the surrounding water.

The Lu-foils contained about $1,5\,^{mg}/cm^2$ of Lutetiumoxide with a purity of 99,9%. They were prepared by a sedimentation technique. The copper foils were punched out of a 8 μ sheet of electrolytic copper and weighed for calibration. The Lu-foils were calibrated relative to a standard by irradiation on a rotating disc in the pool of the FRM.

During irradiations Lu and Cu foils were combined into "sandwiches". The small thickness of the foils allowed to neglect the self shielding and the mutual activation disturbance. Measurements were performed with bare and with cadmium covered sandwiches (Cd-thickness 1 mm). The foil activity was determined using 2π methan flow counters of high stability. The saturation activity ratios as obtained after the usual corrections for counter losses and radioactive decay are listed in table II. The "graphite" values were obtained in the thermal column of the FRF reactor and will be used for normalisation.

Table II

Saturation activity ratios of Lu^{176} and Cu^{63}

$\sigma_{a_{eff}}$ [barns/hydrogen]	$\frac{C^{Cu}}{C^{Cu}_{Cd}}$	$\frac{C^{Lu}}{C^{Cu}}$ [arbitrary units]	$\frac{C^{Lu}-C^{Lu}_{Cd}}{C^{Cu}-C^{Cu}_{Cd}}$ [arbitrary units]
graphite	-	0,45(56±50)	0,45(56±50)
0,332	83,0	0,45(84±60)	0,46(23±70)
1,37	18,26	0,49(19±75)	0,51(32±90)
2,30	10,71	0,51(25±77)	0,5(529±110)
3,33	6,85	0,52(82±80)	0,5(972±120)
4,24	5,60	0,54(29±81)	0,6(350±130)

C = Saturation activity of the bare foils
C_{Cd} = Saturation activity of the cadmium covered foils

6) Analysis of the Lu-Foil Measurements using the Westcott Convention

Following Westcott,[4] we write:

$$\frac{C^{Lu}}{C^{Cu}} = G \cdot \frac{g^{Lu}(T) + rs^{Lu}(T)}{1 + r \cdot s^{Cu}(T)} \qquad (1)$$

Here, g, r, and s have the well-known meaning while the factor G contains the absolute cross sections, the foil thickness, and the counter efficiency. G is only very badly known but can be determined from the graphite measurement: In a thermal column, the neutrons are in thermal equilibrium ($r \approx 0$) and follow a Maxwellian distribution with moderator temperatur T_M. We therefore have

$$\left(\frac{C^{Lu}}{C^{Cu}}\right)_{graphite} = G \cdot g^{Lu}(T_M) \qquad (2)$$

from which G is easily derived. Combining eq (1) and (2) yields

$$\left(\frac{C^{Lu}}{C^{Cu}}\right)^{*} = \frac{g^{Lu}(T) + rs^{Lu}(T)}{1 + rs^{Cu}(T)} \qquad (3)$$

where $\left(\frac{C^{Lu}}{C^{Cu}}\right)^{*}$ is obtained by deviding the measured activity ratios through the experimentally determined G factor. For a given $\left(\frac{C^{Lu}}{C^{Cu}}\right)^{*}$, eq. (3) represents a relation between T and r. A second relation is obtained from the cadmium ratio R_{Cd} of the copper foils[4]:

$$R_{Cd} = \frac{1 + rs^{Cu}(T)}{r(s^{Cu}(T) + 0,437\sqrt{T/T_o})} \qquad (4)$$

Combining (3) and (4), r and T can be determined. For this evaluation, s(T) for copper was computed using an excess resonance integral of 2.82 barns [12] and a 2200 $^{m}/_{sec}$ activation cross section of 4.3 barns. s(T) for Lu was taken from Westcott's table[13].[1] For $g^{Lu}(T)$ the values given in table III were used.

---

[1] Westcott gives s(T) based on two extremely different "joining functions". We found that both of them led to almost identical neutron temperatures. The values in table IV are average values for the two assumptions.

Table III

$g(T)$ for Lu^{176}

T (°C)	Case I g from AECL 1101	Case II g calculated from the resonance parameters of Roberge and Sailor[14] (1st resonance) and Westcott (2nd resonance)
20	1.7011	1.741
40	1.8373	1.886
60	1.9769	2.o35
80	2.1175	2.184
100	2.2576	2.334
120	2.3957	2.482
140	2.5305	2.632

The T and r values thus obtained are listed in table IV.

Table IV

$\sigma_{a_{eff}}$ $\left(\frac{\text{barns}}{\text{hydrogen}}\right)$	Case I			Case II		
	T_N (°K)	$\frac{T_N-T_M}{T_M}$	r	T_N (°K)	$\frac{T_N-T_M}{T_M}$	r
0,332	294,5±2	0,00(48±68)	0,0104	294,5±2	0,00(48±68)	0,0104
1,37	316 ±3	0,0(78±10)	0,0471	315 ±3	0,0(75±10)	0,0471
2.30	334 ±3	0,1(40±10)	0,0800	333 ±3	0,1(35±10)	0,0802
3.33	359 ±4	0,2(25±14)	0,125	356 ±4	0,2(13±14)	0,126
4.24	385 ±5	0,3(15±17)	0,151	380 ±5	0,2(96±17)	0,152

It is seen that the neutron temperatures do not depend sensitively on the Lu resonance parameters used.

7) A Direct Comparision of the Integral and the Time-of-Flight Measurements

It is possible to compare the time-of-flight and the integral measurements without use of the "neutron temperature" concept. Therefore, the saturation activity ratios of Lu^{176} and Cu^{63} were computed from the measured spectra using the Lu^{176} and Cu^{63} activation cross sections. Since the time-of-flight measurements are inaccurate in the epithermal region, the subcadmium activation ratios were compared. The computations were performed using

$$C\text{-}C_{Cd}=\text{const}\int_0^{1eV}\phi_{observed}(E)\sigma_{act}(E)\left[1-E_2(\Sigma_{Cd}(E)d_{Cd})\right]dE \qquad (5)$$

where $E_2(\Sigma_{Cd}(E)d_{Cd})$ describes the absorption of a 1 mm Cd filter. The Cu activation cross section was assumed to follow a 1/v law while the Lu^{176} activation cross section was calculated from the resonance parameters of Westcott (case I as above) and Roberge and Sailor (case II). Normalisation was done via the thermal column measurements where the spectrum was assumed to be a Maxwellian distribution. The results are given in table V.

Table V

Subcadmium Lu^{176}/Cu^{63} activation ratios calculated from the measured spectra

$\sigma_{a_{eff}}$ barns/hydrogen	Case I	Case II
293°K Maxwellian distribution	0,4556	0,4556
0,332	0,4561	0,4596
1,37	0,5023	0,5082
2,13	0,5345	0,5419
3,33	0,5912	0,5999
4,24	0,6389	0,6485

8) Discussion

The measurements by the differential and the integral technique are in good agreement. This is seen by comparing the obtained neutron temperatures (tables I and IV) and the ratios $\frac{Lu-Lu^{Cd}}{Cu-Cu^{Cd}}$ in tables II and V.[2]

The differential neutron spectra (fig. 1 and 2) seem to be in a reasonable agreement with those observed by Beyster et al.[8]. In fig.5 the "neutron temperatures" of tables I and V are compared with the values obtained by Poole[4]. Though the limits of error overlap, our spectra are apparently always harder than Poole's. The figure also shows a remarkable deviation from Coveyou's formula and Brown's theory. The subcadmium $^{Lu}/_{Cu}$ activation ratios are plotted in fig.6 (Lu^{176} parameters from Westcott, case I) and fig.7 (Lu^{176} parameters from Roberge and Sailor, case II) together with a calculation based on the Nelkin model of neutron thermalisation in water.[3] While for higher boron concentrations the activation ratios as predicted by the Nelkin model agree well with those observed, there might be a small discrepancy for low effective cross sections.

Acknowledgements:

Thanks are due to Dr. K.H. Beckurts for his encouragement and for many helpful discussions during the performance of this work.

---

[2] Unfortunately, there is a difference in the boron concentration (2.13 resp. 2.30 $^{b}/_{H}$ in one case)

[3] We are indebted to Dr. I.R. Beyster, San Diego, for providing us with the Nelkin spectra calculated for various boron concentrations.

References:

(1) C.H. Westcott, Report CRRP-787 (1958)

(2) G.A. Price, I. Nuclear Energy, Part A 10, 157 (1959)

(3) L.C. Schmid and W.P. Stinson, Nuclear Science and Engineering 7 477 (1960)

(4) C.H. Westcott, W.H. Walker and T.K. Alexander, Second Geneva Conference, Paper P 202 (1958)

(5) M.I. Poole, I. Nuclear Energy 5, 325 (1957)

(6) R.R. Coveyou, R.R. Bates and R.K.I. Osborne, I. Nuclear Energy 2, 3 (1956)

(7) H.D. Brown, du Pont Report DP-64

(8) I.R. Beyster, I.L. Wood, W.M. Lopez, and R.B. Walton Nuclear Science and Engineering, 9, 168 (1961)

(9) K.H. Beckurts and W. Reichardt, Proceedings of the Symposium on Neutron Time-of-Flight Methods, Saclay, 239 (1961)

(10) E. Kiefhaber, Master Thesis, Karlsruhe 1961

(11) M.S. Nelkin, Report GA-1063 (1960)

(12) E. Johansson, E. Lampa and N.G. Sjöstrand, Arkiv för Fysik 18, 513 (1961)

(13) C.H. Westcott, Report AECL-1101 (1960)

(14) I.P. Roberge and V.L. Sailor, Nuclear Science and Engineering 7, 502 (1960)

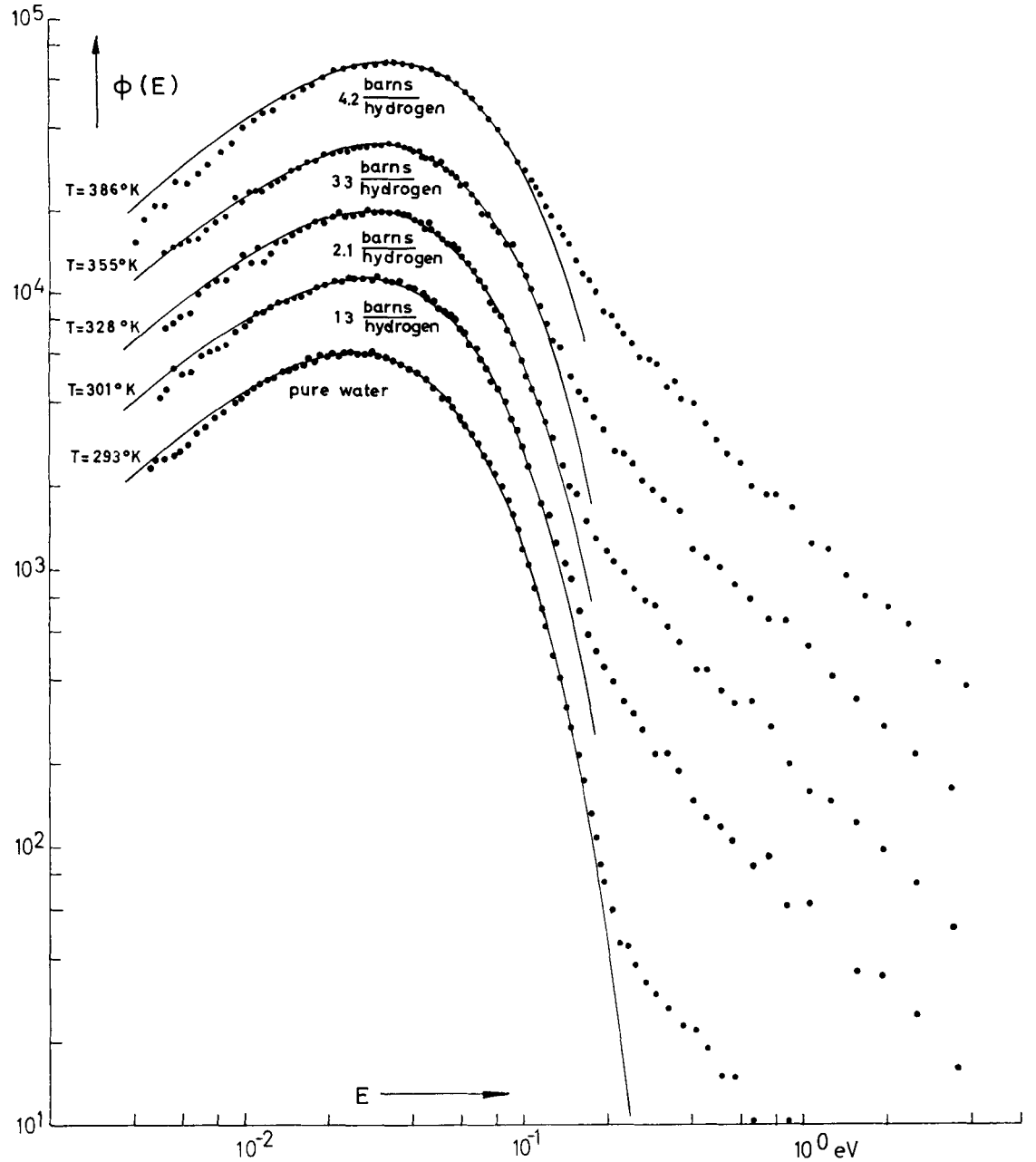

Fig 1 Neutron spectra in pure water and boron acid solutions, 30 cm cube

——— Maxwellian fit to the thermal part of the spectra

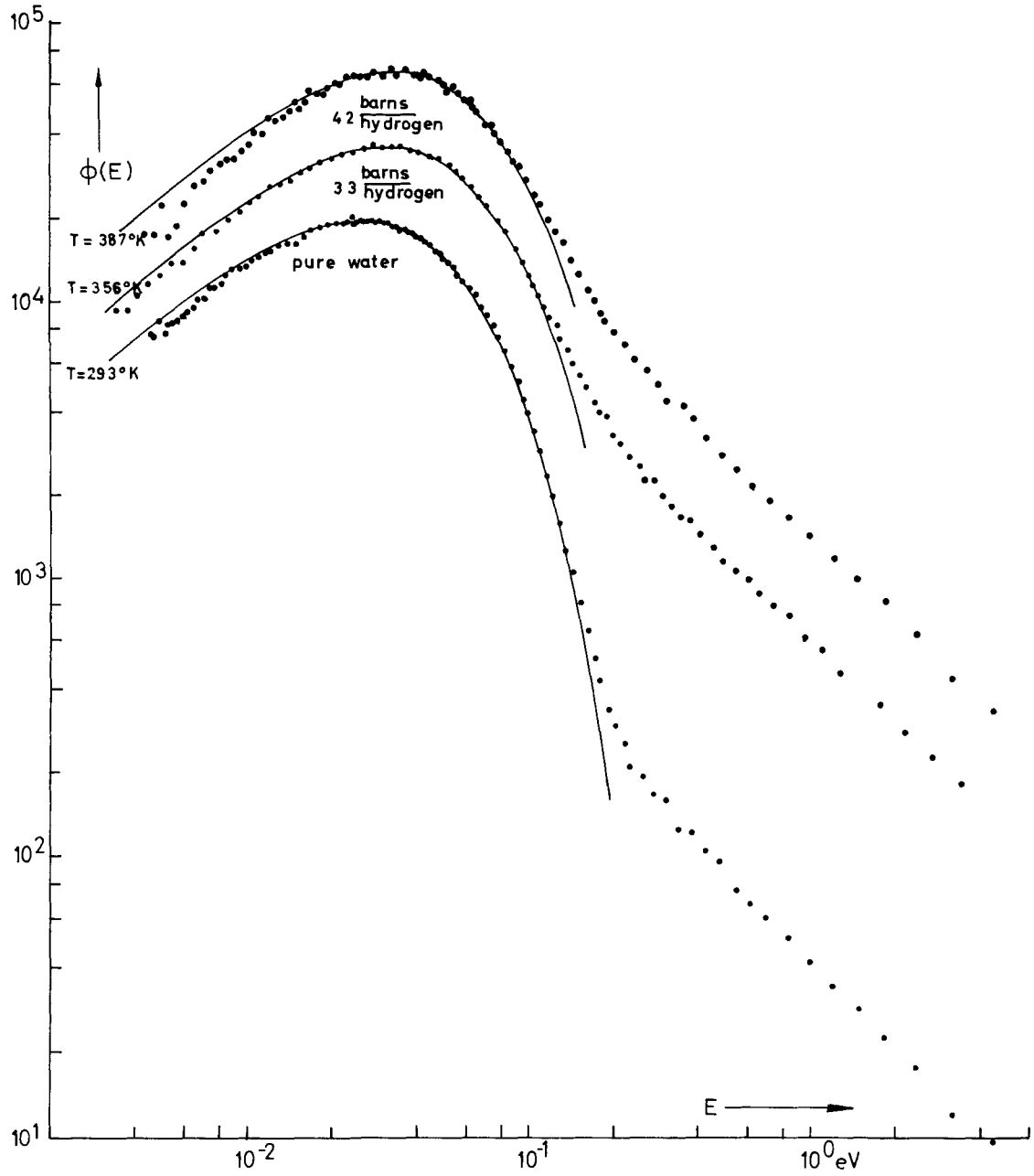

Fig 2 Neutron spectra in pure water and boron acid solutions, 15cm cube

——— Maxwellian fit to the thermal part of the spectra

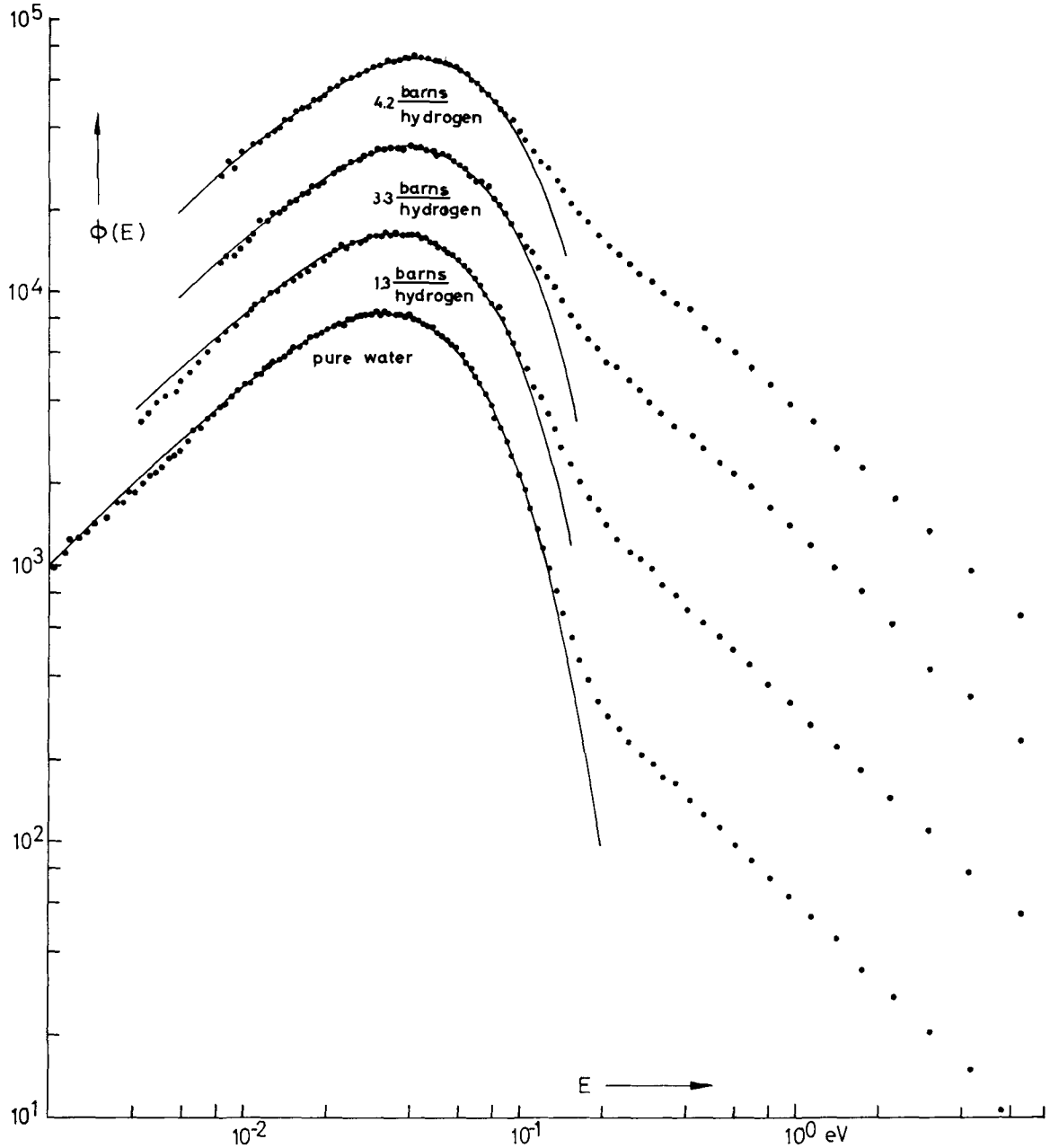

Fig. 3 Leakage spectra from the 15 cm cube of water and boron acid solutions

——— spectrum computed by Kiefhaber using the scattering kernel of Nelkin

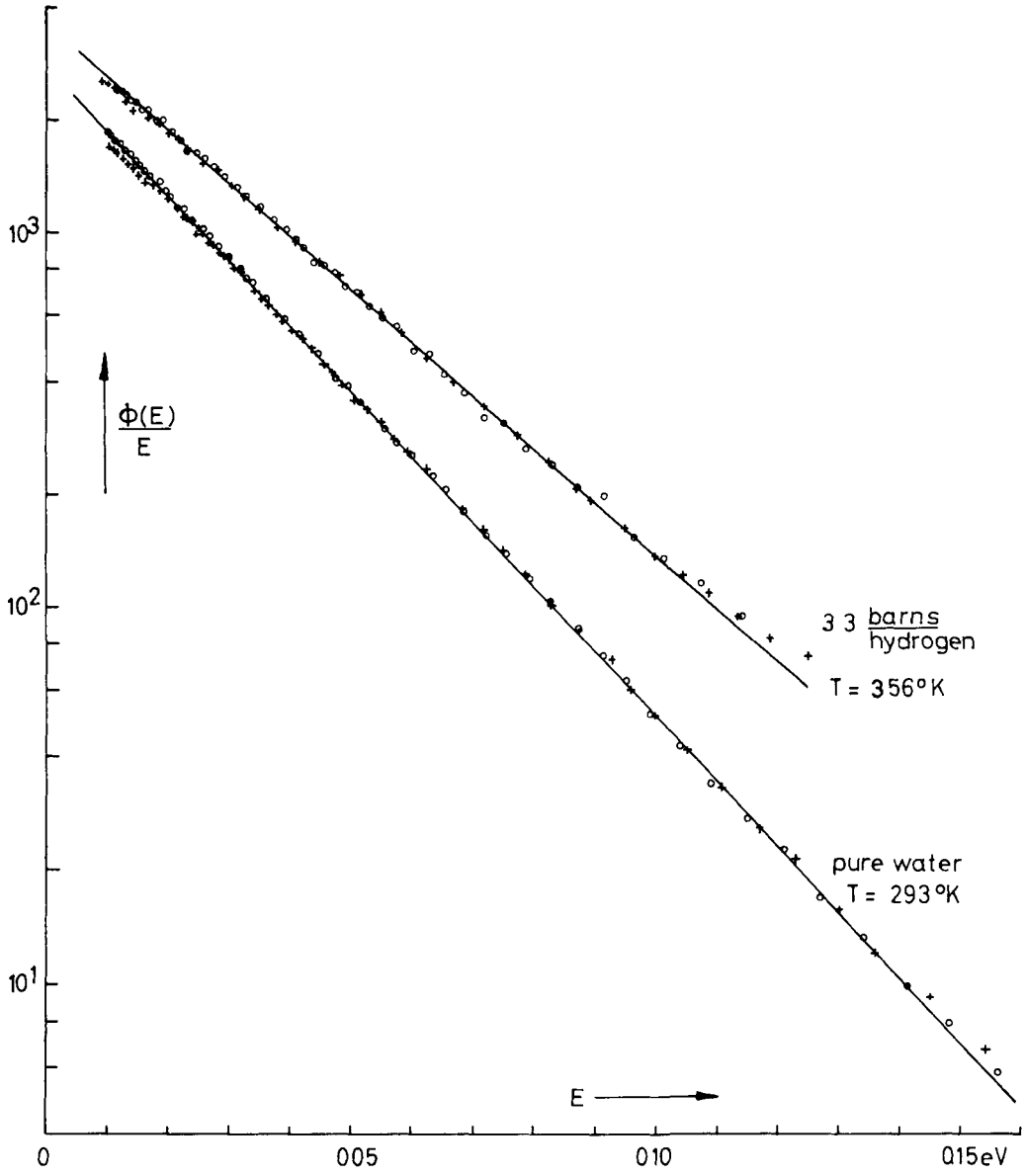

Fig 4 Determination of the neutron temperature

o 30 cm cube

+ 15 cm cube

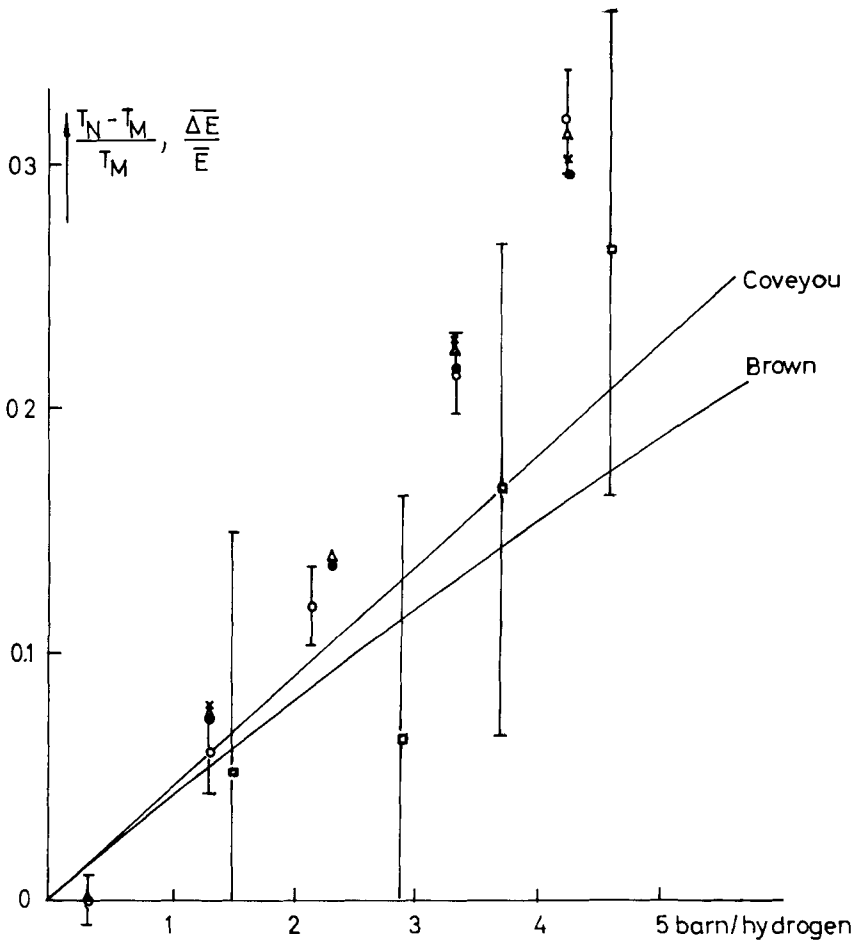

Fig 5 Plot of $\frac{T_N - T_M}{T_M}$ versus absorption cross section T_N neutron temperature
T_M moderatur temperature

o values obtained by the spectra measurements (mean of the results from the 15cm and 30cm cube)

x relative energy shift of the spectra from the surface of 15cm cube

▫ results of Poole

Δ results of the Lutetium foils measurements (case I)

• results of the Lutetium foils measurements (case II)

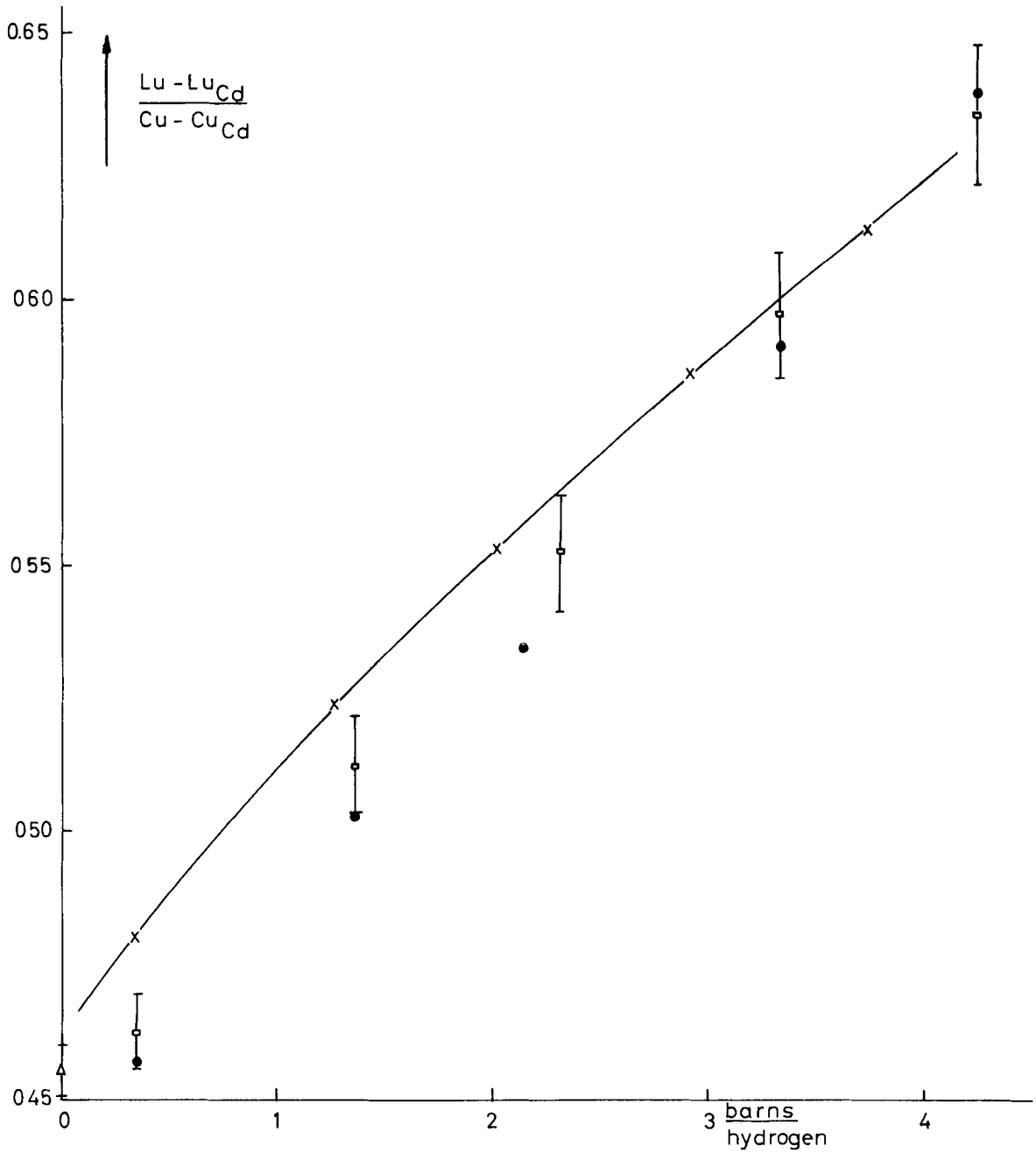

Fig 6 Ratio of the thermal activations of Lu^{176} and Cu^{63} using the Lu^{176} resonance parameters of Westcott

- ▫ results of the activations measurements
- △ graphite value
- ● results obtained from the spectrum measurements
- x results obtained from the Nelkin spectra

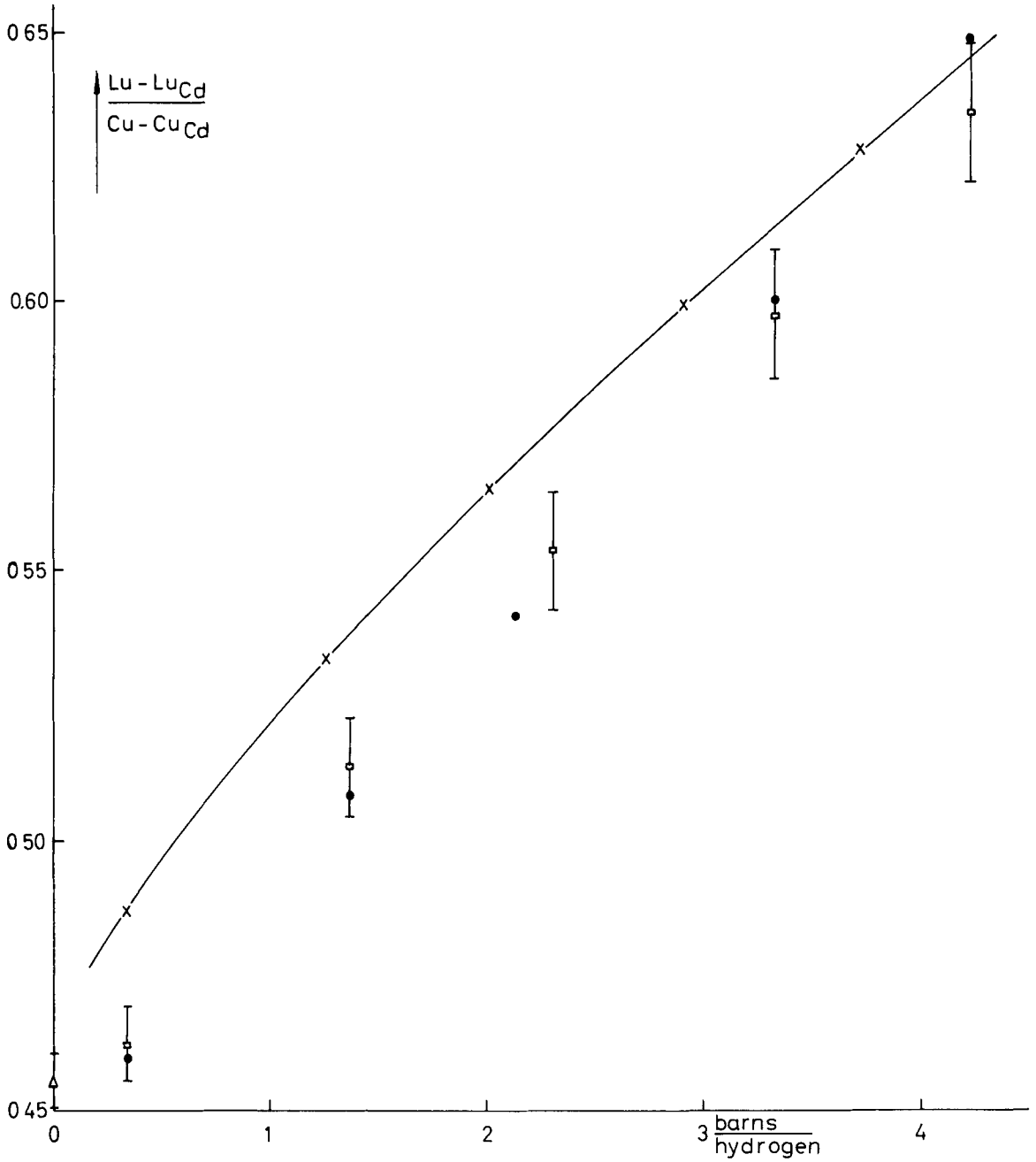

Fig 7 Ratio of the thermal activations of Lu^{176} and Cu^{63} using the the Lu^{176} resonance parameters of Roberge and Sailor

- ▫ results of the activation measurements
- △ graphite value
- ● results obtained from the spectrum measurements
- x results obtained from the Nelkin spectra

INTEGRAL SPECTRUM MEASUREMENTS IN HETEROGENEOUS MEDIA

by

Thomas F. Parkinson
and
Sagid Salah

Department of Nuclear Engineering
University of Florida
Gainesville, Florida

NOTE: Preliminary results of these measurements were reported in the Transactions of the American Nuclear Society, Vol. 4, No. 2, November 1961.

LIST OF FIGURES AND TABLES

INTEGRAL SPECTRUM MEASUREMENTS IN HETEROGENEOUS MEDIA

I. Introduction

In reactor calculations, neutrons are usually considered to be either in a "thermal" group or in one or more higher energy groups and this energy distribution is assumed to be constant throughout a unit cell. In heterogeneous reactors containing regions of high absorption, however, the neutron spectrum can change significantly in different regions of the unit cell with consequent discrepancies between the calculated and the actual neutron economies. Recent improvements in the theoretical method have been developed by Honeck;[1,2] however, very limited experimental data[3] were available for comparison with the calculations. The purpose of our experiments is to provide sufficient data to permit a definitive evaluation of various calculational methods.

Specific information which might be derived from the experiments includes the following: 1) an analytic representation of severely hardened spectra; 2) the form of the joining function for synthesizing a spectrum from a Maxwell-Boltzmann distribution plus a 1/E distribution; 3) properly averaged cross sections for evaluating (ηf), the number of neutrons produced per thermal neutron absorbed in a heterogeneous lattice.

It would be desirable to obtain differential spectrum measurements on heterogeneous lattices; however, experimentally it is much easier to obtain integral data with activation detectors. Accordingly we have used Lu, Au, Mn, and Dy detectors

and we plan also to use Pu. The properties of these materials are shown in Figure 1 and summarized in Table 1.

II. Experimental Techniques

For most of the measurements the activation detectors were fabricated in the form of wires .005 inches to .050 inches in diameter. The Lu was fabricated from a dispersion of Lu_2O_3 (10% by weight) in an Al matrix. This material was drawn into wires .030 inches in diameter and cut into 0.5 inch lengths. The Dy wires were also made from an Al alloy; likewise, Pu detectors will be in the form of wires containing Pu Al alloy.[4]

For activation measurements with strong resonance absorbers, it is desirable to have very thin foils to minimize self shielding. Accordingly, gold goils were prepared in the usual manner by vacuum evaporation. An alternative procedure which proved convenient was to apply a solution containing a gold compound* on an Al foil backing and then baking to obtain a uniform gold film. Foils of 2-4 microns thickness were prepared using this technique. The resonance self shielding correction for this thickness is approximately 15%.

III. Data Reduction and Analysis

Since the activations must be measured to a precision of 0.5% or less, it is necessary to count the detectors several times. To obviate many hand calculations of the decay corrections, a program was written for the IBM 650 computer. After the decay and foil weight corrections were applied, the Lu data were

*Supplied by the Hanovia Chemical and Manufacturing Company, East Newark, New Jersey

analyzed using the method described in Reference 5. The calibration curve for the determination of the effective neutron temperature is shown in Figure 2.

The method described by Westcott[6] has been used to analyze the data where there is an appreciable epithermal component. Using this method the product of the epithermal factor, r, and the ratio $(T/T_o)^{\frac{1}{2}}$ may be obtained as follows:

The effective activation cross section $\tilde{\sigma}$ is

$$\tilde{\sigma} = (g + rs)\ \sigma_{2200} \tag{1}$$

where r is the epithermal index and g and s are functions of the effective neutron temperature, T. For 1/v absorbers, g = 1 and s = 0.

The cadmium ratio for a "thin" foil is

$$R_{Cd} = \frac{g + rs}{r\left\{s + (1/K)(T/T_o)^{\frac{1}{2}}\right\}} \tag{2}$$

where K depends on the Cd thickness, $(K \approx 2)$. Therefore

$$r(T/T_o)^{\frac{1}{2}} = \frac{1}{s\ (T_o/T)^{\frac{1}{2}}\ (R_{Cd} - 1) + R_{Cd}/K} \tag{3}$$

For the Lu detectors,

$$\frac{A^{177}}{A^{176m}} = \frac{(g + rs)_{176}}{(g + rs)_{175}} \tag{3}$$

and

$$g_{176} = \frac{A^{176}}{A^{176m}}\ (1 + rs)_{175} - (rs)_{176} \tag{5}$$

For measurements in the thermal column, r was taken to be zero.

IV. Results of the Measurements

A. Stainless Steel Rod in the UFTR Thermal Column

The results of traverses through a one inch stainless steel rod centered in the UFTR thermal column are given in Table II and are also plotted in Figure 3. As would be expected, the normalized activities of Au-198 and Lu-176m are identical since both have 1/v absorption cross sections. From Figure 2, the change in the effective neutron temperature from the center to the outer edge of the stainless steel rod is 25°C.

B. Uranium Slab in the UFTR

The sensitivity of the method is illustrated by the results summarized in Table III and shown in Figure 4. If one assumes again that the spectra in the interior of the U slab and at the edge of the slab are Maxwellian then the corresponding change in neutron temperature is 16°C.

C. Uranium Rod Clusters

The results of traverses through 3 and 4 rod clusters are summarized in Tables IV and V and shown in Figures 5 and 6. In both cases, the individual U rods were one inch in diameter. For the three rod cluster the assembly was enclosed in a D_2O - filled Al can 2.9 inches in outside diameter. The four rod configuration was housed in a can 3.5 inches in outside diameter. Both of these assemblies were centered in the UFTR thermal column.

D. Traverses through the UFTR Core

Activation measurements were made throughout the UFTR core using Lu and Au detectors for the total flux. In addition cadmium ratio measurements were made with thin Au and In foils

in order to evaluate the epithermal component. A summary of the data is given in Table VI and a plot of cadmium ratios, lutetium activations, and $r(T/T_o)^{\frac{1}{2}}$ is shown in Figure 7.

E. Traverses through the Stanford Pool Reactor Core

Table 7 summarizes the results of Lu and Dy traverses through the SPR core. The data are also plotted in Figure 8. The Lu data illustrate the rapid change in the spectrum above the core-reflector interface.

V. Conclusions and Future Program

The results of the Lu activations indicate the sensitivity of this technique for measuring changes in the effective neutron temperature. Additional activation measurements are planned using Pu detectors. Comparison of the data with the spectra described by Westcott[6] is now in progress. Additional comparisons will be made with spectra calculated using the THERMOS code.[2]

VI. Acknowledgements

The cooperation of J. L. Crandall, E. J. Hennelly and F. E. Kinard of E. I. duPont deNemours and Company, Inc., Savannah River Laboratory, and of T. J. Connolly of Stanford University is gratefully acknowledged.

VII. Bibliography

1. Honeck, H. C., "The Distribution of Thermal Neutrons in Space and Energy in Reactor Lattices," (Part 1), Nuclear Sci. & Eng., 8, 193-202 (1960).

2. Honeck, H. C., THERMOS, A Thermalization Transport Theory Code for Reactor Lattice Calculations, BNL-5826, (1961).

3. Kaplan, I., and Honeck, H. C., "The Distribution of Thermal Neutrons in Space and Energy in Reactor Lattices," (Part II), Nuclear Sci. & Eng., 8, 203-209 (1960).

4. Masselot, M., Nuclear Sci. & Eng., (In Press).

5. Schmid, L. C. and Stinson, W. P., "Calibration of Lu for Measurements of Effective Neutron Temperatures," Nuclear Sci. & Eng. 7, 477 (1960).

6. Westcott, C. H., "Effective Cross Section Values for Well-Moderated Thermal Reactor Spectra," CRRP-960, (1960).

TABLE I

PROPERTIES OF
ACTIVATION DETECTORS

Stable Isotope	Abundance	$T_{\frac{1}{2}}$	Eres (ev)	σ activation (b) 0.25 ev	σ activation (b) Er	E_γ (Mev)
Lu-175	97.4%	2.69h	2.62	35	850	0.089
Lu-176	2.6%	6.74d	0.142	4000	13,600	0.112, 0.206, 0.318
Pu-239	---	≃1 h	0.296	315	5,900	---
Dy-164	28.2%	2.33h	---	2600	1,000	0.095
Au-197	100 %	2.69h	4.9	96	30,000	0.412
Mn-55	100 %	2.57h	337	13.4	2,000	0.822, 1.77, 2.06

TABLE II

Lu AND Au ACTIVATIONS IN
STAINLESS STEEL ROD

Radius, cm	Total Activity Lu-177	Lu-176m	Au-198	Lu-177* / Lu-176m
0.0	1.000	1.000	1.000	---
0.254	1.021	1.057	1.018	---
.381	1.017	1.032	1.029	---
.508	1.022	1.115	1.089	---
.625	1.082	1.117	1.115	---
.762	1.111	1.156	1.162	---
.889	1.178	1.225	1.216	---
1.016	1.193	1.288	1.297	---
1.143	1.284	1.387	1.385	---
0.0	---	---	---	1.000
.200	---	---	---	.997
.400	---	---	---	.987
.600	---	---	---	.973
.800	---	---	---	.948
1.000	---	---	---	.932
1.200	---	---	---	.915

* Ratios obtained from $Io(\mu r)$ fits to experimental data.

TABLE III

Lu ACTIVATION IN U SLAB

Position, cm	Activation	
	Lu-177	Lu-176m
.8255	1.1300	1.1820
.5715	1.1134	1.1431
.15875	1.0126	1.0369
0	1.0000	1.0000
-.15875	1.0092	1.0267
-.5715	1.1187	1.1544
-.8255	1.1360	1.1660

TABLE IV

Lu AND Mn ACTIVATIONS IN 3-ROD CLUSTER

Radial Pos'n., cm	Material	Activation		Cd Ratio		
		Lu-177	Lu-176m	Lu-177	Lu-176m	Mn
0.85	U	1.008	1.003	---	---	---
1.09		1.000	1.000	---	---	---
1.325		1.049	1.027	---	---	---
1.56		1.042	1.032	---	---	---
1.80		1.066	1.053	75.1	1.59	24.6
2.04		1.110	1.078	---	---	---
2.275		1.173	1.136	---	---	---
2.51		1.219	1.185	---	---	---
2.75		1.297	1.282	---	---	---
0.63	D_2O	1.065	1.112	---	---	---
1.27		1.167	1.190	---	---	---
1.90		1.313	1.353	---	---	---
2.54		1.528	1.543	---	---	---

TABLE V

Lu AND Dy ACTIVATION IN 4-ROD CLUSTER

Radius, cm	Material	Activation			Cd Ratios	
		Lu-177	Lu-176m	Dy	Lu-177	Lu-176m
1.35	U	1.021	1.024	1.010	---	---
1.59		1.000	1.000	---	---	---
1.83		---	---	1.000	---	---
2.06		1.053	1.041	---	---	---
2.30		1.102	1.060	1.079	51.8	2.58
2.54		1.142	1.086	1.142	---	---
2.78		1.259	1.183	---	---	---
3.02		---	---	1.333	---	---
3.25		1.402	1.309	1.492	---	---
0.63	D_2O	1.189	1.194	1.277	---	---
1.63		1.219	1.216	---	---	---
2.63		1.492	1.431	2.274	---	---
3.63		1.835	1.677	---	---	---
3.65	U	---	---	---	80.5	2.13

TABLE VI

Lu AND Au ACTIVATIONS IN THE UFTR CORE

Pos'n., cm	Activation			Cd Ratio		$r(T/T_o)^{\frac{1}{2}}$
	Lu-177	Lu-176m	Au	Au	In	
0.0	1.000	1.000	---	2.29 *	2.31*	0.0355(In) 0.0417(Au)
0.0	1.000	1.000	60,467	2.176**	---	0.0457
5.56E	---	---	53,477	---	---	---
14.79E	---	---	52,253	---	---	---
25.85E	---	---	44,006	---	---	---
35.10E	---	---	40,211	---	---	---
5.56W	---	---	55,750	---	---	---
14.79W	---	---	48,096	---	---	---
25.85W	---	---	44,525	---	---	---
35.10W	---	---	41,289	---	---	---
5.56N,S	1.023	1.087	---	---	---	---
13.15N,S	1.017	1.270	---	---	---	---
21.57N,S	0.881	1.307	---	---	---	---

* Vacuum Evaporated Au Foil
** Au Film from Solution

TABLE VII

Lu AND Dy ACTIVATIONS IN SPR CORE

Detector	Position,* cm	Total Activity		
		Lu-177	Lu-176m	Dy-165**
Lu	3.4	1233	28167	---
	28.8	564	8006	---
	41.6	293	2255	---
Dy	4.2	---	---	0.990
	14.2	---	---	0.874
	24.2	---	---	.625
	29.2	---	---	.483
	34.2	---	---	.564
	36.2	---	---	.467
	38.2	---	---	.340
	42.2	---	---	.131
	44.2	---	---	.130
	48.2	---	---	.057
	50.2	---	---	.035
	-0.8	---	---	0.981
	-5.8	---	---	.987
	-15.8	---	---	.817
	-25.8	---	---	.524
	-28.3	---	---	.576
	-33.3	---	---	.655
	-33.8	---	---	.762

* Vertical distance from midplane.
** Normalized to 1 at ℓ .

Fig. 1 Activation Cross Sections

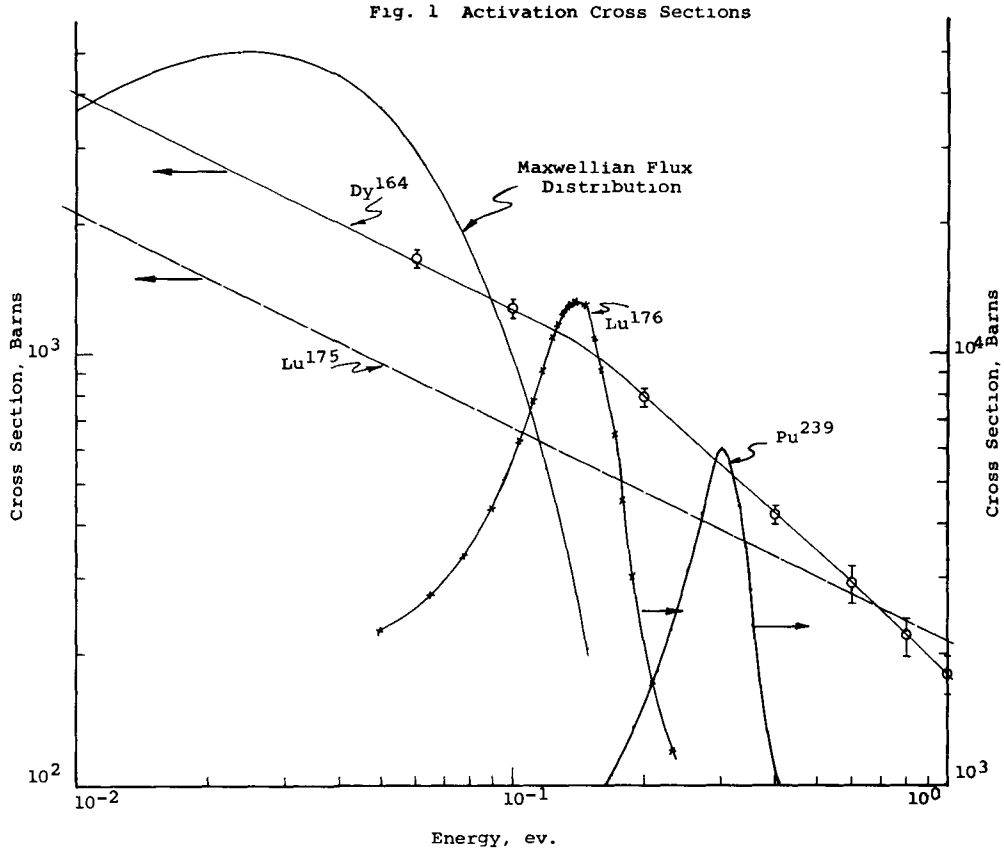

Fig. 2 REF: HW-64866

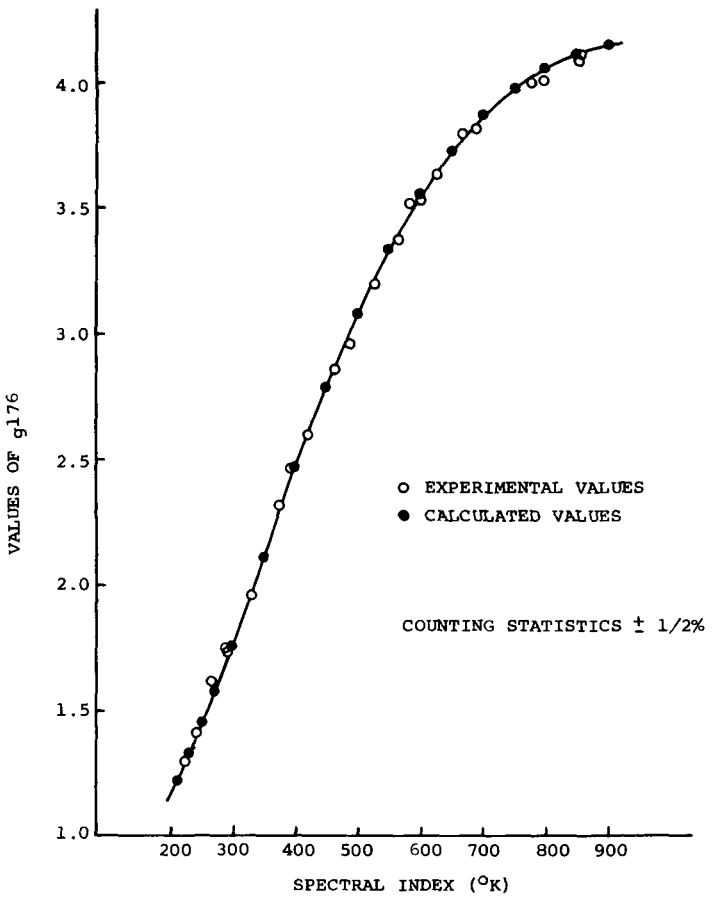

Fig. 3

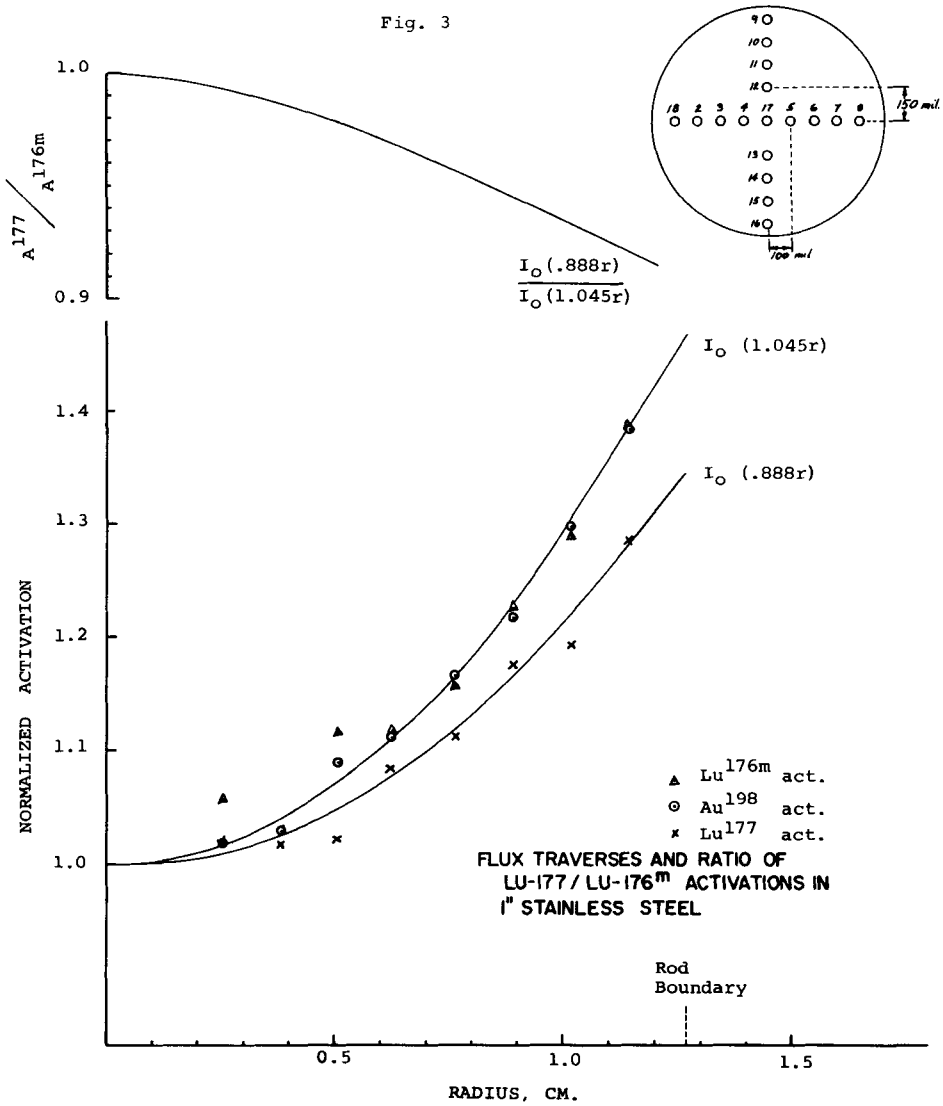
1.0
0.9
A^{177}/A^{176m}
$\frac{I_o(.888r)}{I_o(1.045r)}$
I_o (1.045r)
I_o (.888r)
1.4
1.3
1.2
1.1
1.0
NORMALIZED ACTIVATION
▲ Lu^{176m} act.
⊙ Au^{198} act.
× Lu^{177} act.
FLUX TRAVERSES AND RATIO OF
LU-177 / LU-176^{m} ACTIVATIONS IN
1" STAINLESS STEEL
Rod
Boundary
0.5
1.0
1.5
RADIUS, CM.
150 mil.
100 mil.

Figure 4. Lu Traverse Through U Slab

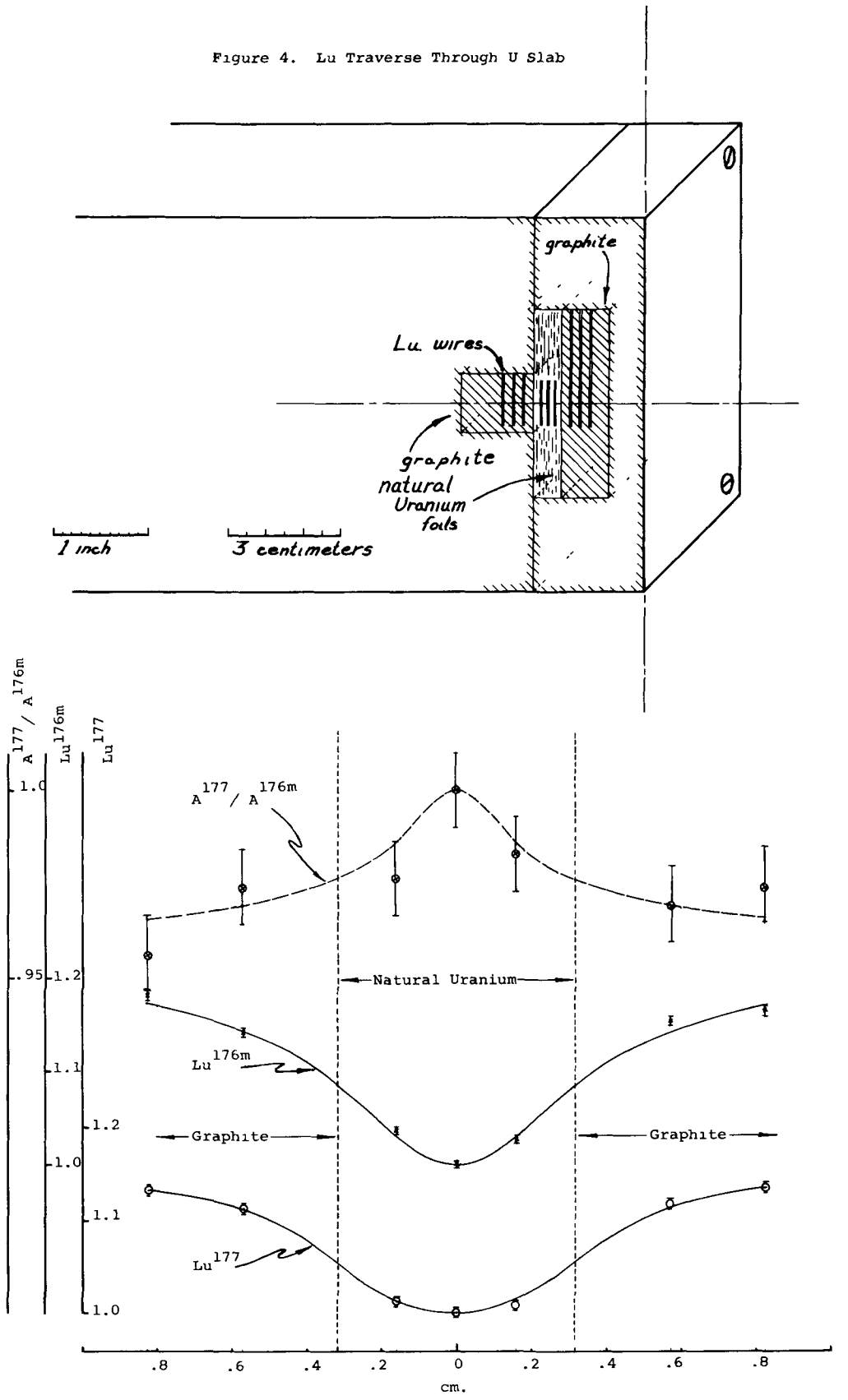

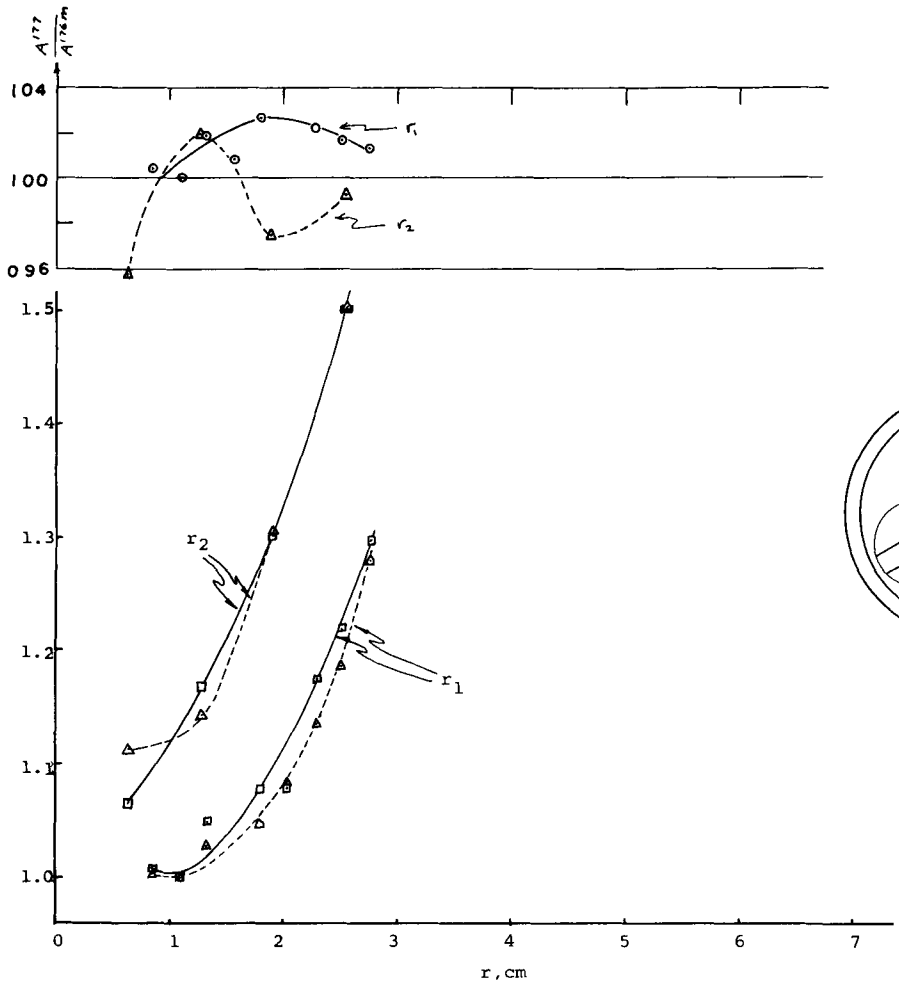

Fig 5

FLUX TRAVERSE
in
U-D_2O ASSEMBLY

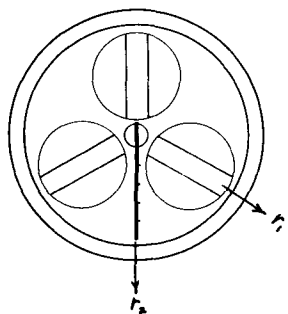

○ Dy 165 Act.
△ Lu 176m Act.
■ Lu 177 Act.

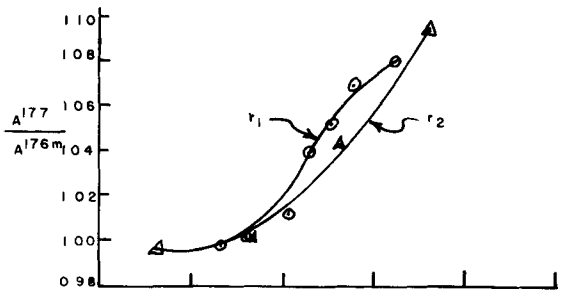

FIGURE 6

FLUX TRAVERSE
IN 4 ROD
U-D_2O ASSEMBLY

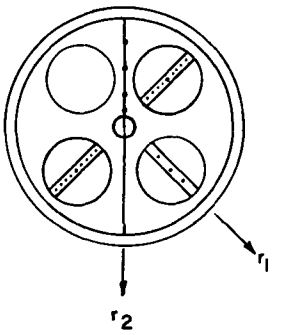

⊙ Lu-177 Act.
△ Lu-176m Act.

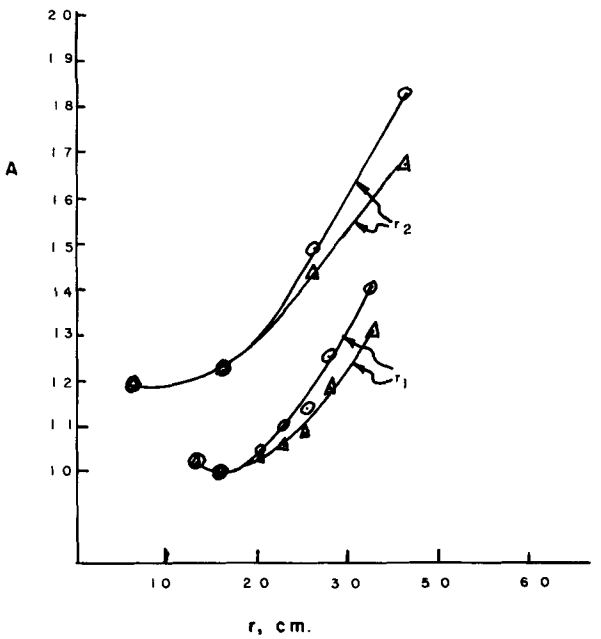

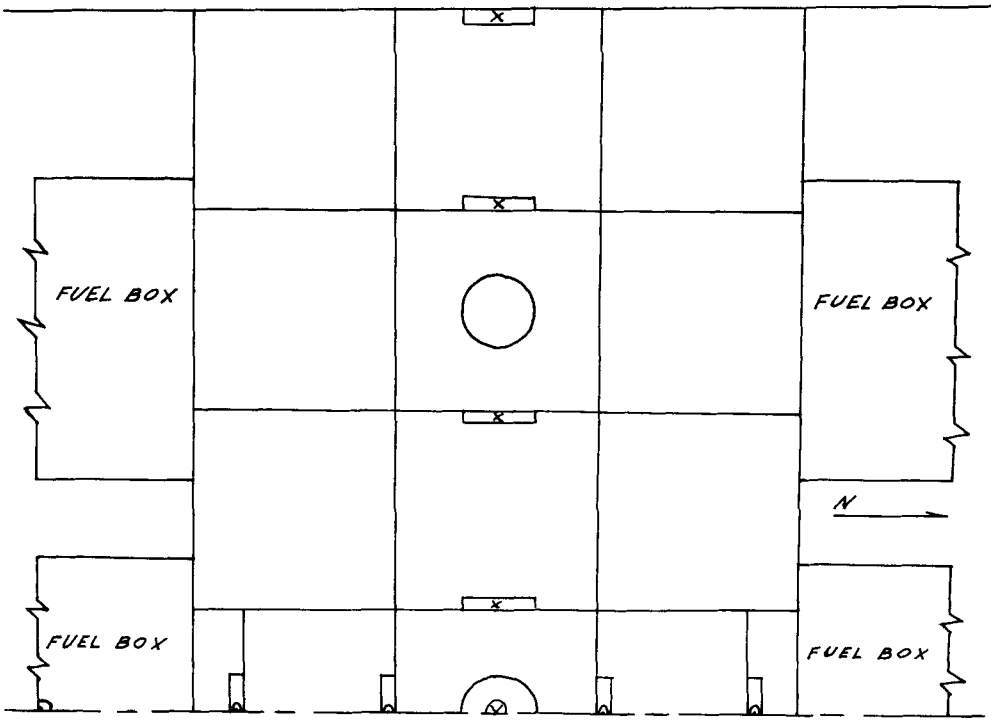

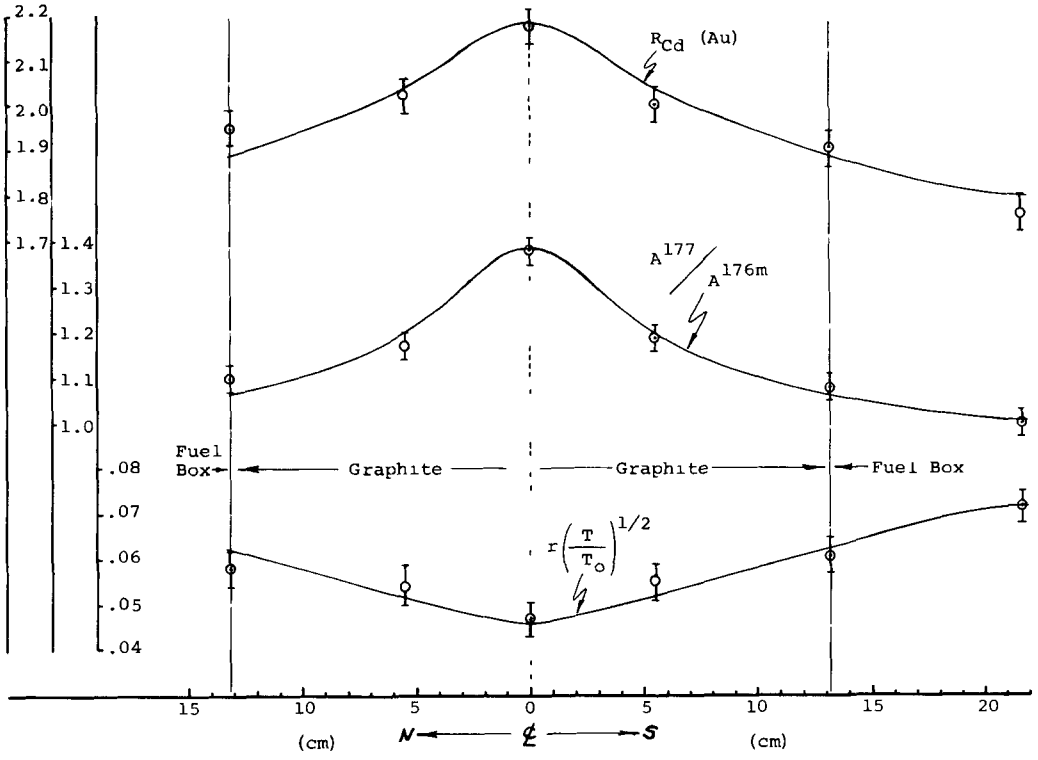

Fig 7. Traverse Through UFTR Core

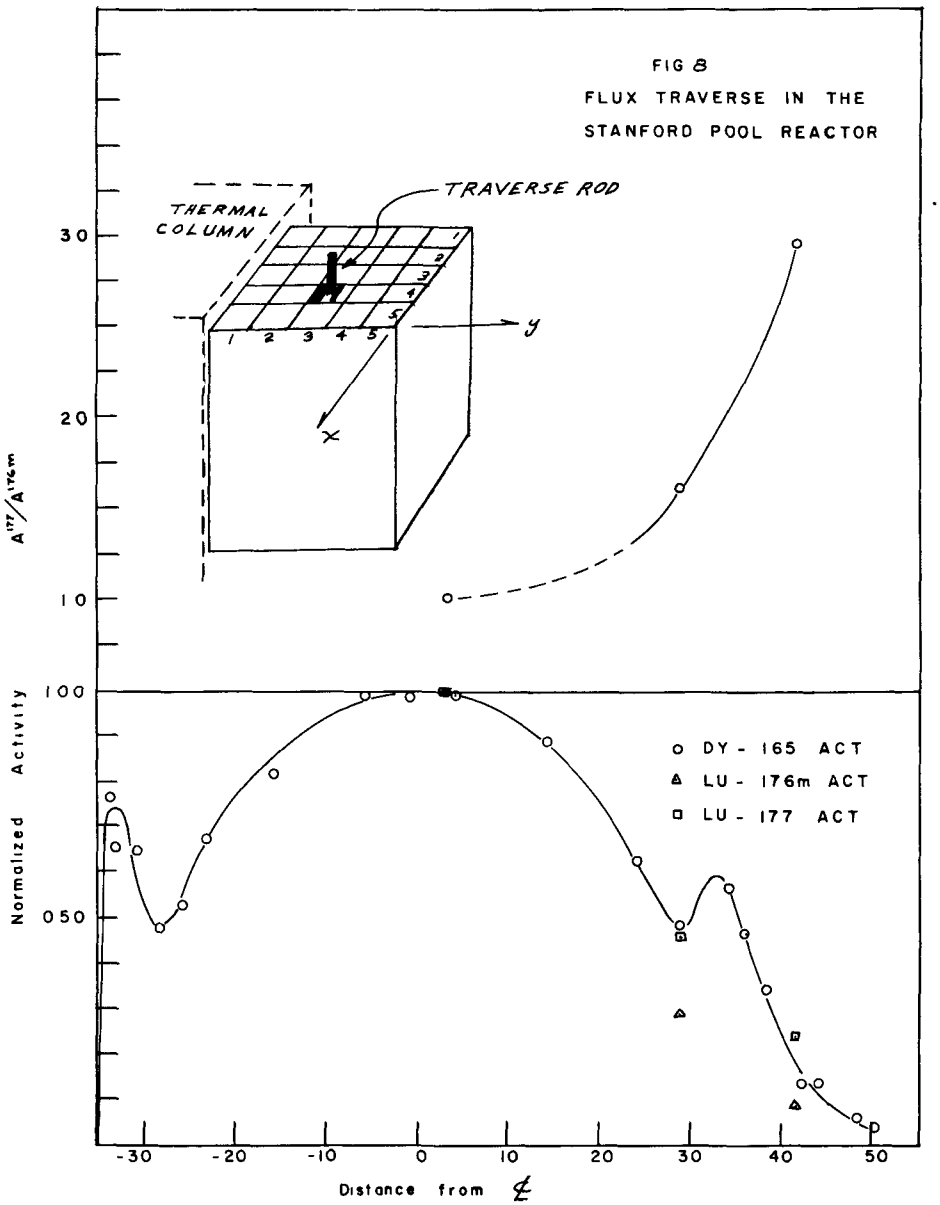
FIG 8
FLUX TRAVERSE IN THE
STANFORD POOL REACTOR
THERMAL COLUMN
TRAVERSE ROD
y
x
1 2 3 4 5
A177/A176m
30
20
10
Normalized Activity
100
050
DY - 165 ACT
LU - 176m ACT
LU - 177 ACT
-30 -20 -10 0 10 20 30 40 50
Distance from ℄

Addendum to paper entitled,

"Integral Spectrum Measurements in Heterogeneous Media,"

by T. F. Parkinson and Sagid Salah

TABLE VIII

Lu and Dy Activation in B_2O_3 Solutions*

B_2O_3 Conc.	Pos'n.,cm**	Activation***			Ratio	
		Lu-177	Lu-176	Dy-165	A^{177}/A^{176m}	A^{177}/A^{165}
H_2O	.6	0.596	0.591	0.640	1.008	---
"	1.6	0.709	0.697	---	1.017	---
"	2.6	0.795	0.781	0.769	1.017	---
"	3.6	0.873	0.871	0.910	1.003	---
"	4.445	1.000	1.000	1.000	1.000	---
5 gm/liter	.6	0.295	0.277	0.274	1.063	1.075
"	1.6	0.347	0.329	0.332	1.055	1.045
"	2.6	0.503	0.476	0.472	1.056	1.065
"	3.6	0.791	0.768	0.759	1.029	1.041
"	4.445	1.000	1.000	1.000	1.000	1.000
10 gm/liter	.6	0.179	0.160	0.155	1.119	1.115
"	1.6	0.223	0.201	0.209	1.106	1.067
"	2.6	0.399	0.373	0.370	1.070	1.078
"	3.6	0.740	0.717	0.706	1.032	1.048
"	4.445	1.000	1.000	1.000	1.000	1.000

* solutions in 3.5 inch Al can
** from center of the can
*** normalized at 4.445 cm

620426

Lu Activations in B_2O_3 Solutions

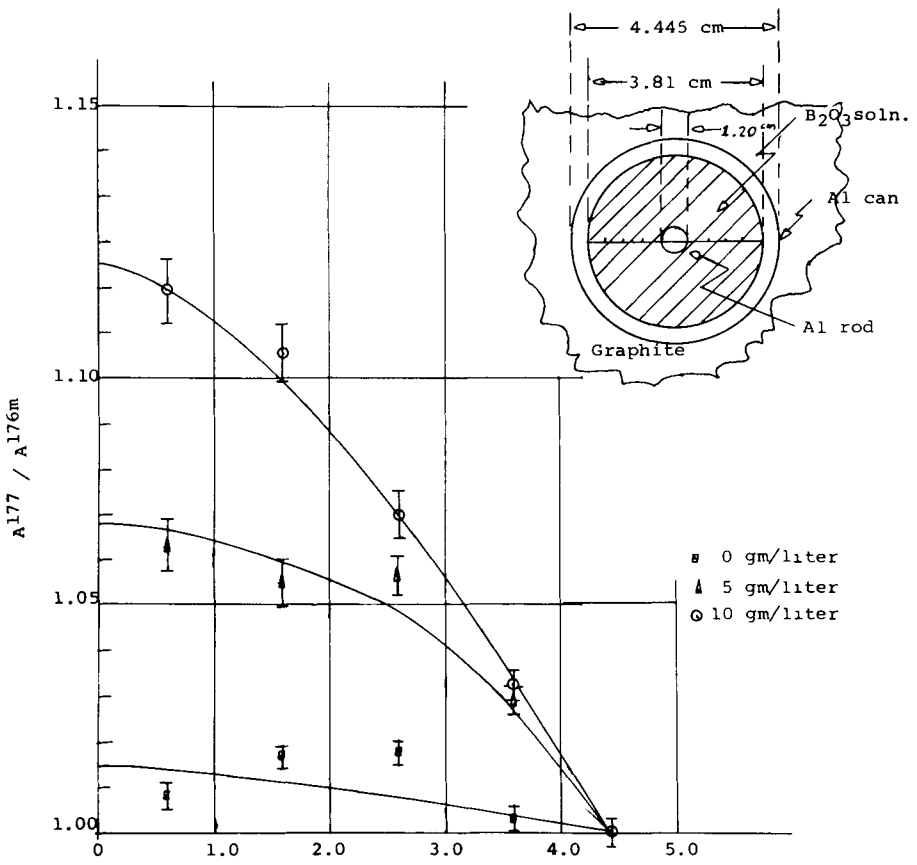

Low Energy Neutron Spectra in the ZENITH Heated Graphite Moderated Reactor

By

F. R. Barclay
M. S. Coates
K. M. Diment
S. A. Durrani*
D. B. Gaythe
H. H. Pitcher
M. J. Poole

Atomic Energy Research Establishment
Harwell, Berks.
England

*General Electric Company Ltd., Erith, Kent.

1. Introduction

The accurate calculations of the neutron energy spectrum plays an important part in the reactor physics design of the DRAGON reactor experiment. As an experimental check on the methods of calculations employed time-of-flight spectra have been measured on the second core loading of ZENITH, which had a composition close to that originally proposed for the initial loading of the DRAGON reactor.

Atomic ratios $C/U^{235} = 2107$

$Th/U^{235} = 4.76$

A comparison of calculated with measured spectra in a given system is a good test of nuclear data, moderater scattering properties and calculating techniques. The main motive for the present calculations was the checking of various scattering models for graphite suggested from the scattering law project[6]. In addition it was expected firstly that the calculations would give useful information on the spacial and angular dependence of the neutron spectrum, thus checking whether the actual spectrum which was measured was a representative cell spectrum and secondly that the validity of space-independent spectrum calculations could be tested.

The general properties of the core are described in Ref[1] and the reactor is shown diagramattically in Fig,1. Spectrum measurements were made in a collimated beam emerging from the top surface of a half length fuel element positioned a) at the centre of the core and b) close to the core side reflector boundary, The measurements covered a range of core and side reflector temperatures between 20°C and 650°C, with a maximum side reflector temeperature of 410°C. The experimental chopper spectra which it is proposed to compare with the calculated ones are those emerging from the centre if the reactor, particularly the spectrum with the reactor at room temperature.

2. The principles of Time of flight Measurements using a Chopper.

The method of obtaining the velocity distribution of neutrons in a directed beam from a reactor using a rotating slit system is much used and is well established (c.f.

Poole et al Ref. 42)

A continuous neutron beam falls onto a spinning rotor, made of material with a high neutron removal cross section, containing a slit system which allows the free passage of neutrons during the interval for which the slits are aligned in the beam. Pulses of neutrons are thus produced of a duration dependent on the dimensions and speed of rotation of the slit system. The neutrons contained in the pulse are allowed to travel along a flight path several metres long before detection. A multi-channel time analyser gives the flight time distribution of these detected neutrons relative to the moment of formation of the neutron pulse at the rotor.

The observed spectrum of counts differs from the true beam spectrum incident on the rotor for four basic reasons.

(i) the presence of background neutrons

(ii) the finite length of the rotor slits in the direction of motion of the neutrons resulting in the transmission factor for neutrons decreasing with decreasing neutron velocity. A detailed discussion of the transmission of straight slit choppers is given by Larsson et al (3) and by Slovacek(4).

(iii) the sensitivity of the detectors used is usually a function of neutron energy.

(iv) counting losses we usually present in the spectrometer, particularly, if it is of the type that can only register one count per neutron burst.

Factors have to be applied to the observed data to allow for these effects.

In using time of flight to measure reactor spectra two limitations must be remembered. Firstly the beam spectrum is proportional to the directed flux $f(\underset{\sim}{r}\ \theta_0)$ where θ_0 denotes the direction of the beam. In a heterogeneous reactor this is not usually the same as the direction averaged flux spectrum at the surface from which the beam emerges. Secondly, in order to extract the neutron beam a hole has to be made into the reactor, and sometimes, as in the experiments in ZENITH, it is necessary

to insert a probe tube into this hole. This can alter the conditions at the source area both by causing changes in the local scattering and absorption, and by allowing neutrons to stream to the source area from the sides of the hole.

3. Design Considerations

ZENITH is a low power reactor, the neutron flux at the positions where the spectrum has been measured being of the order of 10^8 n/cm^2/sec. This low intensity influences the design of the experiment, the basic requirements of which are as follows:

(i) To extract a beam of neutrons from the region where the spectrum is to be measured (the source) with a collimating system which allows only neutron from this region to emerge. The intensity of this beam must be as high as possible, and the presence of the collimator must not perturb the spectrum at the source.

(ii) To design a rotor to measure the energy spectrum of the emergent beam in the energy interval 0.01 eV to 10 eV. The energy resolution of the instrument must not distort the basic shape of the spectrum, but a balance between resolution and intensity has to be struck to enable a complete spectrum to be measured in less than two day's operation and with a statistical accuracy of better than 3% on all points. (These requirements preclude the possibility of studying any detailed structure of the spectrum, which for example might be caused by the low energy resonance of U^{235}).

The rotor was designed to give a basic energy resolution of no worse than, $\frac{\Delta E}{E} = 25\%$, in the energy region (0.01 - 0.5)eV, higher resolution widths being accepted at higher energies. The nominal rotor parameters chosen were x = 4 metres, 2R = 13.34 cm, S = 0.46 cm and d = 0.62 cm. Where x is the flight path length, R the radius of the rotor, S the spacing between the slits and d the slit width. There were seven slits in the rotor. The value of x was chosen to place the detectors above the moveable reactor shielding which helped to reduce extraneous background. Table I illustrates the resolution obtainable at various energies.

It was calculated that with this choice of resolution, the difference between the observed and the true spectrum is less than 1% for all channels. With the parameters listed above it was calculated that the rotor transmitted background should be less than

2% of the true counts for all channels. Ideally with the large energy range which is to be studied, two different rotors should have been used. However it was found that sufficient counting rate was available to study the lower energy regions by merely reducing the speed of the rotor.

Sub-collimators, each with a slit system identical to that of the rotor, were placed on either side of the rotor. These collimators served to reduce broadening of the neutron burst due to the inherent divergence of the incident beam, and also to reduce general background when the rotor was in the closed position.

The experimental arrangement on the reactor is shown in Fig.2 and is described below. Fig.3 shows the fuel element configuration in the neighbourhood of the surface from which the neutron beam emerges. Possible effects of the hetergeneous nature of this region on the measured spectrum are discussed later. To reduce the distance the beam neutrons travel in nitrogen (which fills the free space within the reactor vessel) an argon* filled stainless steel probe tube, 9 ft long and $3\frac{1}{4}$" diameter, penetrated the reactor vessel lid to terminate 2 ft. above the half fuel element. The argon is at atmospheric pressure and is fed from a flexible reservoir which allows the probe tube gas to expand when the reactor is heated. It was not practicable to maintain a vacuum in the probe tube, as the thin window is too much weakened by heat. It was sealed at its lower end by a stainless steel plate 0.019" thick and at its upper end by an Al plate 3/16" thick. (The effects of these end plates, and other plates in the beam, on the measured spectrum are discussed below). The probe tube contained a stainless steel sleeve which held a 3" long collimating boron steel ring which was set in an array of boron steel rings. These additional rings were to prevent unwanted neutrons from being scattered into the beam, and did not define the beam geometry in any way. All the boron steel was above the level of the upper boundary of the reflector. Fig.4 illustrates schematically the collimator geometry.

---

* σ_s (Nitrogen = 10 barns; σ_s (argon) = 1.5 barns.

The seal where the probe tube entered the reactor vessel allowed mechanical adjustment to permit alignment. When measurements were made at the centre of the core the tube was set vertically over the half fuel element. For the core-side reflector measurements a tilt of 0.9' from vertical was introduced to minimise the effects of non uniform expansion of the reactor when heated, since it was calculated that with the core at 650°C the probe tube would tilt by 0.9', to the opposite side of vertical.

The vertically mounted flight tube, shown in Fig.2 was evacuated to ~ 100 microns pressure and was sealed at each end with Al. plates each 3/16" thick, and was lined with ~ 6" thickness of boron loaded paraffin wax to prevent ingress of stray neutrons. The tube was supported on steel girders at its base and adjustment was provided to permit alignment with the probe tube and collimator. At the top of the tube was situated a bank of ten copper walled BF_3 proportional counters arranged, as shown in Fig.2 each counter was 5 cm diameter with an active length of 15 cm, and was filled to a pressure of 70 cm Hg with BF_3 gas enriched to 96% $B^{10}F_3$ content. The counter bank was shielded by blocks of boron loaded paraffin wax 7.3 cm thick. The distance between the centre of the rotor and the centre of the counter* was 4.02 metres.

4. Reduction of Data

The energy spectrum of the neutron flux in the beam from the reactor is given by

$$N(E) = Kt^3 \left[\frac{(t)}{a(T)} - B(t) \right] \left[\tau(t)\, \varepsilon(t) \right]^{-1}$$

where t = time of flight

= counts in corresponding channel of analyser

a(T) = time analyser correction

B(t) = background corrections

$\tau(t)$ = cut off function

$\varepsilon(t)$ = counter efficiency

and K is a constant.

*It may be shown that this is the effective starting point of the neutron flight path (c.f. Larsson et al (loc cit)).

The t^3 factor in this expression arises in the conversion from a time to an energy variable.

The energy corresponding to time of flight t is given by:

$$E = \frac{1}{t^2} (8.448 \times 10^4) \text{ ev where t is in microseconds.}$$

The most significant factors will now be considered.

The background correction to the channel counts has two components; one which is independent of reactor power and which is a constant for each channel, and one due to the variable transmission of neutrons through the body of the rotor, which varies from channel to channel. The power independent part was obtained by proportion from a determination of the total number of counts in a given time with the reactor shut down. The variation of this count rate with time was negligible. The channel dependent component was largely due to fast neutrons transmitted through the material of the rotor. The presence of the slits causes the effective thickness of rotor metal in the neutron beam to change during the cycle between neutron pulses, the maximum amount of metal being presented when the slits are perpendicular to the beam direction: viz. midway through the cycle; the effective thickness varies symmetrically with respect to this position. The majority of these background neutrons have an energy above ~ 20 keV due to the drop in the removal cross section of K-Monel at this energy. The transmission of the rotor with the slits perpendicular to the neutron beam direction varies from ~ 8.10^{-4} for low energy neutrons to ~$1.8\ 10^{-2}$ for neutrons above 20 keV. Since neutrons of energy 20 keV and above have virtually zero time-of-flight, the background in a given channel is determined basically by the position of the rotor at the instant the neutrons are recorded. Hence the background variation over the cycle may be obtained by counting the number of neutrons transmitted with the rotor stationary, as a function of rotor orientation. Such measurements were made and compared with measurements made with the rotor operating at 2400 r.p.m. using 100 μsec channels. Under the latter conditions the beam spectrum was

such that there were virtually no spectrum neutrons present to be recorded in the last 60 channels, which thus gave background counts over a known portion of the cycle. Agreement between the two experiments was good except that details of fine structure in the background variation (caused by the presence of the sub-collimators) differed slightly. the variation could be well approximated however by the linear form shown in Fig.5, which neglects fine structure. The uncertainty in background correction due to this approximation has a negligible effect on the accuracy of the data.

The reactor dependent background for a spectrum was obtained using the variation shown in Fig.5 normalised to a count, corrected for reactor independent background, made with the rotor slits stationary and perpendicular to the beam direction. Reactor power was monitored continuously during both background and spectrum determinations to allow accurate correlation. The reactor independent background was then added to give the total correction.

For measurements made with the rotor operating at 4800 r.p.m. there were insignificant spectrum neutrons in the last 20 channels, which thus recorded background only, and a criterion for acceptance of a measured spectrum was that these counts should be consistent with the calculated total channel background.

Rotor Slit Transmission Factor (Cut Off Function)

A rotating parallel slit does not transmit neutrons of different velocity with equal probability. The form of the transmission, or "cut off" function for a parallel incident neutron beam has been given by Stone and Slovacek (loc.cit.) and Mostovoi et al (loc. cit) as:-

$$\tau(\beta) = 1 - \frac{8}{3}\beta^2 \quad (0 \leq \beta \leq \frac{1}{4}) \qquad (1)$$

$$\tau(\beta) = 8(\frac{1}{3}\beta^2 - \rho + \frac{2}{3}\beta\frac{1}{2}) \quad (\frac{1}{4} \leq \beta \leq 1) \qquad (2)$$

where $\tau(\beta)$ is the transmission relative to neutrons of infinite velocity of neutron characterized by β where:

$$\beta = \frac{v_o}{v}$$

where v = neutron velocity

and $v_o = \frac{R^2\omega}{S}$ the velocity of the slowest neutron transmitted by a slit of width S and length 2R in the direction of the neutron beam, rotating about its centre with an angular velocity ω.

Since the cut off function depends only on $\frac{v_o}{v}$ an experimental determination may be made by comparing the relative intensities of neutrons having equal time-of-flight observed with different speeds of slit rotation. Such data were obtained with the rotor operating at speeds of 2400, 4800, and 9600 r.p.m.

In the first analysis t_o was calculated using the average slit parameters, vix. S = 0.46 cm and $\bar{R}$ = 6.35 cm (R is not constant since the slits are chords of a cylinder), and the experimental cut off function proved markedly different from the theoretical value. Good agreement could be obtained however using a value of t_o lower by 13%. The explanation of this apparent discrepancy is discussed below.

It was discovered, after the experiments had been completed on the reactor, that the rotor-sub-collimator assembly was not in correct alignment with the neutron beam. Although the rotor slits were aligned parallel to the sub-collimator slits prior to attaching the assembly to the base of the flight tube, as indicated in § 4.4, a machining error in the location system caused the plane defined by the walls of the rotor and sub-collimator slits to be set $\frac{1}{2}^o$ out of line with the axis of the neutron beam.

To obtain the effective values of t_o for the actual slit system two factors have to be considered, (the first of which is not basically due to misalignment.)

(i) Each slit of the rotor-sub-collimator assembly accepts neutrons coming from a different region of the upper surface of the half fuel element and these differ in area (even when the assembly is in correct alignment). This results in a weighting factor for each slit which enters into the evaluation of t_o through its dependence on R. Thus a weighted average value of R, determined from the geometry of the system, must be employed, and not the arithmetic average.

(ii) The misalignment results in some slits of the rotor-sub-collimator assembly accepting a neutron beam which is narrower than the physical slit width. The S value used to calculate t_o is thus reduced.

The experimental cut-off function is plotted in Fig.6 together with a theoretical curve calculated by D.J. Reed and taking into account the two factors above. Agreement is good and this curve is used to reduce the data.

The counter bank was calibrated against a bank of BF_3 counters having a $1/v$ response. The measurements were made on Beam Hole 2 of the reactor LIDO at Harwell, using a beam geometry similar to that for the ZENITH experiments. Fig.7 shows the measured counter sensitivity.

It is interesting to note that a calculation of the counter sensitivity, treating the counter bank as alternate layers of Cu and BF_3 of appropriate average thickness yields excellent agreement with the experiment. The copper was treated as a neutron absorber only; neutron scattering effects were ignored.

5. Preliminary Experiments

A number of experiments were carried out (on the central hole K10 only) to obtain information on the perturbation effects on the reactor flux distribution and spectrum produced by the absence of the upper half of the fuel element and the presence of the probe tube, the definition of the time-of-flight neutron beam, and the detailed spectral variation over the upper surface of the half fuel element used in the time-of-flight experiments.

Detailed scans were made along a vertical direction of the hole K10 and in a horizontal direction across the centre of the reactor:-

(i) with the full fuel element in position viz. the reactor operating under normal conditions.

(ii) with the half fuel element used in the time-of-flight experiments in position, but the probe tube absent.

(iii) with both the half fuel element and the probe tube in position.

(For convenience the probe tube used in the time-of-flight experiments was not used to make these measurements. It was considered necessary to simulate only that part of the probe tube in the reactor core, leaving the hole in the reflector void. This was done with a mild steel tube, 2 ft. long.)

Flux scans were made using U^{235} fission chambers and the spectrum of the flux characterised with gold manganese foils. The results of the flux measurements are shown in Fig. 8 and the foil measurements are presented in Table 2.

The only significant perturbation is shown in the flux measurements in the vertical direction made with the probe tube simulator present. The spectral character of this perturbed flux distribution was the same, within the errors of measurements, as that in the unperturbed state. No significant perturbations appeared in the measurements made in the horizontal direction.

The perturbed flux has a gradient in the direction of the time-of-flight neutron beam. In the diffusion theory approximation this causes the measured beam spectrum $I(E)$ to differ from the isotropic flux spectrum $\phi(E)$ at the source area of the beam (cf. Poole et al (loc.cit.)) by an amount given by:

$$\phi(E) = I(E)\left[1 - \frac{\lambda(E)}{\phi(E)} \frac{d\phi(E)}{dz}_{z=o}\right]$$

where $\lambda(E)$ = neutron transport mean free path in the region, and the z axis is in the beam direction with the origin at the source area.

Assuming the λ value for graphite (2.5 cm) the value of

$$\lambda/\phi(E) \quad \frac{d\phi(E)}{dz}$$

is only 0.007. Correction for the observed flux gradient is not therefore significant and in any case the heterogeneous nature of the reactor core will cause a more complicated relation to exist between the directed flux and the direction averaged flux.

In order to investigate the variation of spectrum across the fuel element fine

structure measurements were made using foils irradiated on the top surface of the half fuel element. Two experiments were made. The first used a copper foil 7.3 cm in diameter, which was cut after irradiation into seven concentric annuli, and reactivity on each annulus was measured separately. For the second gold-manganese foils were irradiated distributed along a diameter.

The results of these experiments are shown in Fig.9 and table 3. No significant structure was apparent.

It must be emphasised however that this result applies to the spectrum at the surface. The time-of-flight experiment measures the directed flux spectrum perpendicular to the surface, which could be significantly different because of the heterogeneous nature of the fuel element.

Two experiments were also made to check the collimation of the beam by the boron steel ring in the probe tube (The experimental probe tube was in position for these measurements).

(i) The sharpness of the beam definition was determined by irradiating a strip of indium foil $5\frac{3}{4}$" x 1" placed in the beam at the top of the probe tube. The foil was then cut into 23 sections each $\frac{1}{4}$" wide and analysed. The results indicate that the beam had the cross section expected.

(ii) The neutrons emerging from the top surface of the half fuel element were absorbed by a B_4C plug, 1" thick, placed virtually in surface contact, and a measurement made with a 1" diameter BF_3 counter lying axially along the beam direction at approximately the position occupied by the rotor during the time-of-flight experiments. When the measurement was repeated with the plug removed the count rate increased by a factor of 200. The number of neutrons entering the beam which were not emitted from the surface of the half fuel element, was, therefore, negligible.

The accuracy of the experimental spectra depends on the statistical error in a

channel count, the channel background correction, the precision to which the channel dependent conversion factors are known, the energy calibration of the spectrometer resolution. These are discussed below.

(i) Statistical Error

This is negligible at the high energy end of the spectrum and increases to approximately 2% at 0.02 eV. Below this energy the error rapidly becomes larger.

(ii) Background Correction

The channel background count, which is known to an accuracy of 1-2%, becomes an appreciable fraction of the spectrum count at low energies. Typical values are: (a) in K10, room temperature: 20% at 0.02 eV, 50% at 0.01 eV. (b) in T17, room temperature: 8% at 0.02 eV, 28% at 0.01 eV.

(iii) Analyser Dead Time Factor

The effect of the dead time can be obtained exactly and is such that the maximum change to a channel count is < 25%.

(iv) Rotor Slit Transmission

The cut off function is known to 1-2% over the range used for converting the data. At 4800 r.p.m. the effect is to change the count of 0.02 eV neutrons by about 20%. At 9600 r.p.m. the corresponding neutron energy is 0.1 eV.

(v) Counter Sensitivity

For energies above 0.02 eV this is known to an accuracy of ~ 1%.

(vi) Energy Calibration

A spectrum was measured with a 0.004" thick cadmium filter in the neutron beam and a marked depression was observed at 0.17 eV which corresponds to the peak of the cadmium resonance.

(vii) Resolution

Calculations indicate that a spectrum is distorted < 1% by the effects of spectrometer resolution.

TABLE I

Energy (eV)	Normal Rotor Speed (spin)	Burst Width (usec)	Gate Width (usec)	E/E %
002	5,000	68	200	20
0.05	"	"	100	15
0.1	"	"	50	17
0.5	10,000	34	50	24
1.0	"	"	2550	34
5.0	"	"	25	60
10.0	"	"	25	80

TABLE 2

The values of r' ($= r\sqrt{\frac{T}{T_o}}$) tabulated below were obtained under the following conditions:

(a) Detectors in an intersititial hole adjacent to a normal fuel element in the central hole.

(b) Detectors in same position as for (a) but half element in place of full element.

(c) As for (b) but with pseudo-collimator present.

The distances are measured up (+) and down (-) from the mid-plane of the reactor. r is the Westcott hardening parameter

Distance above core mid-height	Full Element	Half Element	Half element + Pseudo-Collimator
114.3 cms.	0.017 ± .002	0.025 ± .003	0.033 ± .003
101.6	0.023 ± .003	0.028 ± .003	0.040 ± .003
88.9	0.043 ± .003	0.045 ± .003	0.064 ± .0035
76.2	0.063 ± .0035	0.061 ± .0035	0.087 ± .004
63.5	0.006 ± .005	0.116 ± .005	0.137 ± .005
50.8	0.208 ± .007	0.182 ± .007	0.194 ± .007
38.1	0.249 ± .008	0.241 ± .008	0.244 ± .008
25.4	0.264 ± .009	0.261 ± .009	0.257 ± .009
12.7	0.295 ± .009	0.255 ± .009	0.276 ± .009
0	0.264 ± .009	0.260 ± .009	0.275 ± .009
-12. 7		0.260 ± .009	0.257 ± .009
- 25.4		0.268 ± .009	

TABLE 3

Integral spectrum measurements along a diameter on the top of the half element.

Distance from centre of element	r'
-3.3 cms	0.262 ± 0.009
0	0.260 ± 0.009
+3.3 cms	0.264 ± 0.009

6. Results of Measurements.

The spectra obtained from core centre and core edge positions for different temperatures of core and reflector are shown in Figs. 10 and 11, while Figs 12, 13 show comparisons between spectra for the two positions under corresponding conditions of temperature. Detailed comparisons of the cold spectra with theoretically calculated spectra are given in section 7. while section 8. compares reaction rates for various detectors with calculated values.

7. CALCULATION OF THE THERMAL SPECTRUM IN THE COLD SYSTEM

It was believed that the spectrum shape in the centre of the reactor did not vary so much from one fuel element to the next that a single cell calculation for one fuel element with reflective boundary conditions would be incorrect, and, with no two-dimensional neutron transport thermalisation code readily available, a suitable one-dimensional representation of the fuel element was sought. Figure 15 shows a cell of a fuel element, which has cylindrical symmetry about the indicated axis, and the slab model for which calculations were done. The relative proportions of materials, the fuel and thoria density, and the axial dimensions so far as possible, were unchanged, and the sleeve graphite was incorporated with the spine graphite by raising the physical density of the latter by a factor 7.72.

The DOP (discrete ordinates program) code was used for the calculation. This is an improved version for slab geometry, written by M. F. James of A.E.E. Winfrith, of the Carlson SNG program; it represents the forward- and backward-directed angular fluxes by separate polynomials which are evaluated at particular angles, six in number in the present calculation. The energy range from 0 to 1.5 eV was divided into 35 unequal groups, 0(.005) .05(.01) .1(.02) .2(.05) .4(.1) 1.5 eV, and group average absorption cross-sections calculated for 1/v and U235 absorbers (the only ones present, since thorium was treated as a 1/v absorber). The group-to-group scattering cross-sections for all substances present except graphite were calculated on the gas model, which gives to first order the thermalising effect of these relatively uninfluential moderators. Three sets of room-temperature graphite scattering cross-sections were used, derived respectively from

(i) the monatomic gas model, the simplest and basic model.

(ii) the incoherent Debye crystal model with Debye temperature 1172°K, representing the effects of a simple type of crystal binding.

(iii) a model by P. Egelstaff and P. Schofield using the Chalk River scattering law measurements, the best available model for room temperature graphite (for convenience referred to as E.S. graphite hereafter).

For each of these types of graphite the flux as a function of energy, position and direction was calculated throughout the cell. It was not expected that the experimental spectrum, being the neutrons emerging in a particular direction from part of the fuel element, would equal the direction-averaged spectrum at any particular point in the calculated cell; but it was hoped that the observed spectrum would be fairly represented by the flux travelling directly away from the fuel at a point in the raised-density graphite at about the same number of scattering mean-free-paths from the fuel as lay between the fuel and the source point in the experiment. This directed flux, which will be called the preferred spectrum, is compared with the experimental spectrum in Figure 16. It can be seen that the spectrum based on E.S. graphite is in fairly good agreement with the experiments, and that the Debye crystal model, though better than the gas, is not as good. The importance of comparing the experiment with the calculated directed flux in the appropriate direction and position is shown by Figure 17, which shows for E.S. graphite the outward flux at the surface of the fuel, the outward flux at a point in the graphite twice as far from the fuel as the preferred point, and the inward flux at the preferred point.

Further evidence is given by Figure 18, which shows (among other things) the mean cell spectrum in the E.S. graphite calculation. It is clear that a simple comparison of the experimental spectrum and the mean calculated spectrum

is not in the present situation a guide to the accuracy of a bulk moderator scattering law.

Previous thermal spectrum calculations of this reactor system have all had the space-dependence taken out by homogenisation, and the agreement with experimental spectra has not generally been good. These calculations have been intended to give the mean spectrum in the reactor, but since this differs from spectrum experimentally examined, this lack of agreement is not proof that a faulty theoretical moderator model has been used. To test the accuracy of the homogeneous calculation, the calculated spectrum should be compared with an experimentally determined mean spectrum.

In the absence of an experimental spectrum which can properly be regarded as the mean reactor spectrum, certain methods of homogenisation have been tested by comparing the mean spectrum obtained in the heterogeneous calculation with space-independent spectra obtained using the same nuclear data and scattering models. Three different methods of homogenisation were tried:

(A) Intimately mixing the materials of the cell in the proportions in which they are present in the cell.

(B) Intimately mixing the materials of the cell in proportions based on those in (A) but weighted by the ratio of the total thermal neutron densities in the materials, i.e. using energy-independent disadvantage factors.

(C) As (B) but using energy-dependent disadvantage factors corresponding to the ratios at each energy of the neutron densities in the materials. It may easily be shown that if this is done perfectly the spectrum obtained is the mean spectrum in the space-dependent case, but in practice the disadvantage factors are usually not accurately known. A commonly used theoretical formula for the disadvantage factor of a material is

$$d_i(E) \equiv \frac{\bar{\phi}_m(E)}{\bar{\phi}_i(E)} = 1 + c_i \Sigma_i^a(E)$$

where $\bar{\phi}_m(E)$ is the average neutron flux at energy E in the bulk moderator, supposed only weakly absorbing,

$\bar{\phi}_i(E)$ is the average neutron flux at energy E in material i, a strongly absorbing material such as the fuel,

$\Sigma_i^a(E)$ is the macroscopic absorption cross-section of material i, and c_i is an adjustible parameter.

(This formula has the right properties: $\bar{\phi}_i = \bar{\phi}_m$ if $\Sigma_i^a = 0$, d_i an increasing function of Σ_i^a, and $\Sigma_i^a \bar{\phi}_i \to$ constant as $\Sigma_i^a \to \infty$.)

In the calculations with these methods of homogenisation, the disadvantage factors in method (B) and the parameter c_{fuel} in method (C) were fitted from the space-dependent calculation, and so are based on a posteriori information of a type not normally available when homogeneous calculations are attempted. In a sense, therefore, these disadvantage factors are unfairly good.

Figure 18 shows these three homogeneous spectra, together with the mean spectrum from the space-dependent calculation and the experimental spectrum (which, as has been remarked, has no particular relevance in this case). The spectrum calculated with method (A) is, as expected, too much depressed by absorption at low energies. The spectrum calculated with method (C) is intended to be the mean bulk moderator spectrum in the heterogeneous system, which is greater than the mean cell spectrum in that system at those energies at which there is flux-depression in the fuel; the difference is as great as 6% at .01 eV. Making this allowance, the spectra calculated with methods (B) and (C) are in fairly good agreement with the mean heterogeneous spectrum, and method (C) gives the best agreement.

8. REACTION RATE RATIOS

A valuable, because realistic, measure of the importance of spectrum differences is the reaction rate ratio of different isotopes in the spectra. For this reason the reaction rates of a 1/v absorber of cross-section 1 barn at 2200 m/sec. and of Lu176, and the fission rates of U235 and Pu239 detectors, have been calculated for the spectra below 1.5 eV, and the resulting ratios are shown in Table 3. In conjunction with figures 16 and 18 they show the sort of spectrum differences which give rise to substantial changes in reaction rate ratios; also the great sensitivity of Lu176 to spectrum shape is shown. The lower half of the table compares the homogeneous spectra with the corresponding heterogeneous spectrum; it shows that of the methods of homogenisation (A) is much inferior to the other two, which are roughly equally good. Considering the extra labour involved, method (C) shows a disappointing lack of improvement over (B), and the reason for this is being investigated.

In addition it has been possible to check the heterogeneous E.S. graphite spectrum calculation by comparing reaction rate ratios deduced from it with experimental measurements of the ratios obtained with foils and fission chambers placed in the reactor. The experimental ratios are standardised by comparison with the ratio obtained in a very well-thermalised spectrum, and the quoted values are of the type

$$\frac{\text{reaction rate of isotope 1 in reactor spectrum}}{\text{" " " " 2 " " "}} \Big/ \frac{\text{Reaction rate of isotope 1 in a very well-thermalised spectrum}}{\text{" " " " 2 " " " " " "}}$$

To each calculated theoretical thermal reaction rate is added a contribution for epithermal reaction, and the reaction rate in a room-temperature Maxwellian

spectrum is used for that in a very well-thermalised spectrum. The results are as follows:-

Ratio	Experiment	Theory
Pu239 fission/U235 fission	1.66 ± .04	1.67
Lu176/Mn55	1.54 ± .03	1.51

Finally, the disadvantage factors $\frac{\text{Mean neutron density in bulk moderator}}{\text{" " " " fuel (or thoria)}}$ are found experimentally from the reaction rate ratios of Cu foils (corrected for non-1/v behaviour) and compare with calculated values as follows.

Material	Disadvantage Factor	
	Experiment	Theory
Fuel	1.55 ± .06	1.53
Thoria	1.11 ± .04	1.12

These figures suggest that the slab representation of the fuel element is satisfactory.

9. CONCLUSIONS

(1) In the reactor system considered

(a) cell spectra depend as much on position and direction, even within the bulk moderator, as on the particular moderating properties of graphite;

(b) the spectrum on which chopper measurements are made differs considerably from the direction-averaged spectrum in the bulk moderator;

(c) a comparison of the experimental spectrum with a calculated spectrum must allow for the non-typical character of the emerging beam if it is to be a good test of graphite moderating properties;

(d) a direct comparison of experimental integral reaction rate ratios in the core with those calculated from the emerging experimental spectrum is not very meaningful.

(2) In the system considered, homogeneous calculations with suitable simple disadvantage factors can approximate a heterogeneous calculation sufficiently closely to give thermal reaction rate ratios of important isotopes within 1%.

(3) The model of room-temperature graphite due to Egelstaff and Schofield with the data used is sufficiently close to reality for normal spectrum calculations.

Theoretical work continues to explore the effects of fuel element geometry and disadvantage factors, and compare calculated reaction rate ratios with experimental measurements. Spectrum calculations for the hot core have begun, and it is hoped that before long satisfactory scattering laws for graphite at all temperatures between 0 and 600°C will be determined.

TABLE 4

Thermal Reaction Rate Ratios

Spectrum	U235 fission 1/v	Pu239 fission 1/v	Pu239 fission U235 fission	Lu176 1/v
Experimental	516.0	1411	2.74	6610
Gas preferred	530.8	1222	2.30	5290
Debye preferred	524.3	1277	2.44	5970
E.S. preferred	516.2	1379	2.67	6460
E.S. mean	523.8	1309	2.50	6180
E.S. homogeneous (ϕ^A)	510.6	1473	2.89	6760
E.S. homogeneous (ϕ^B)	521.3	1318	2.53	6370
E.S. homogeneous (ϕ^C)				
bulk moderator	526.1	1270	2.41	5990
mean	525.4	1275	2.43	6020

10. Acknowledgements

The authors wish to acknowledge their indebtedness to Dr. I. R. Cameron, Mr. G. B. Dean, Mr. J. D. MacDougall and Mr. J. G. Tyror for valuable assistance with the experiments and calculations.

11. References.

1. R.M. Absalem et.al. "An Interim report on the second loading of ZENITH,AEEW-R55
2. M.J. Poole et;al. "Prog.Nuc.Energy" Series I Vol.II P.91
3. K.E. Larsson et.al. "Arkiv für Fysik" 16 199 (1960)
4. R. S. Stone and R.E. Slovacek KAPL 1499 (1956)
5. V.I. Mostovoi et;al. A/Conf/8/P640

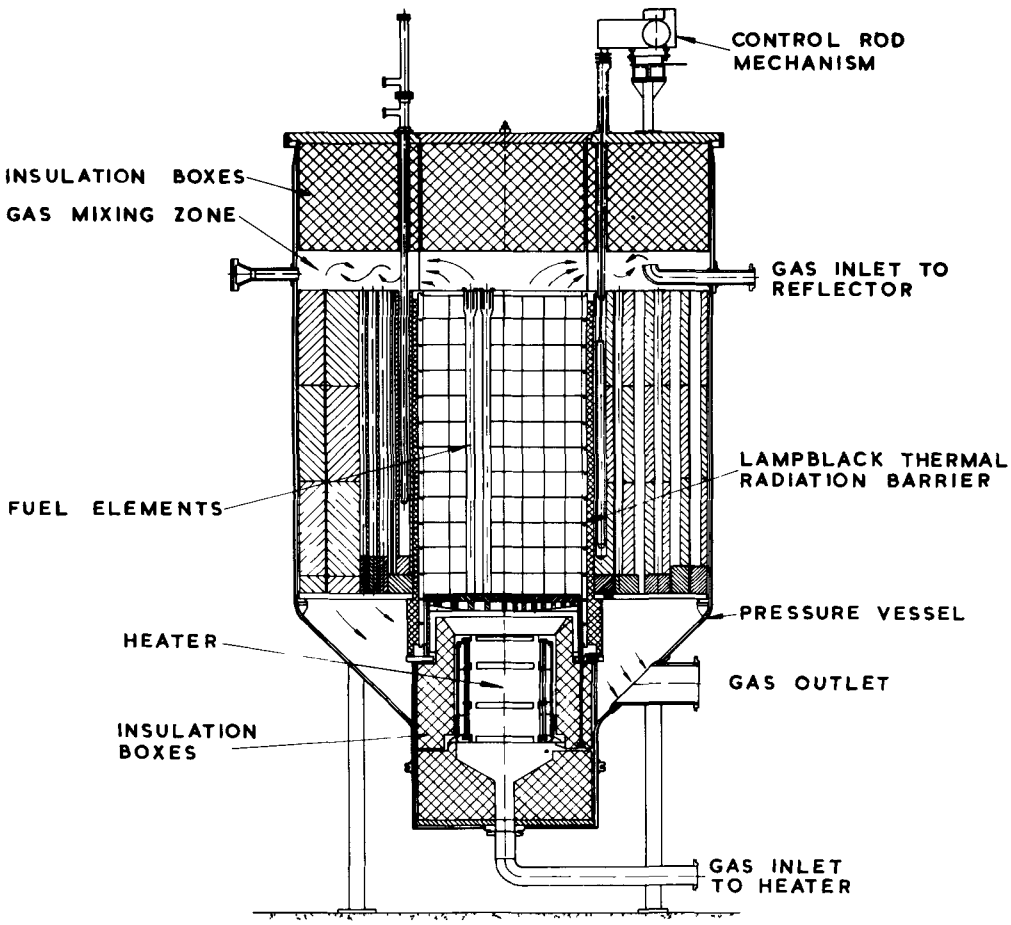

FIG. I. SECTION THROUGH REACTOR VESSEL.

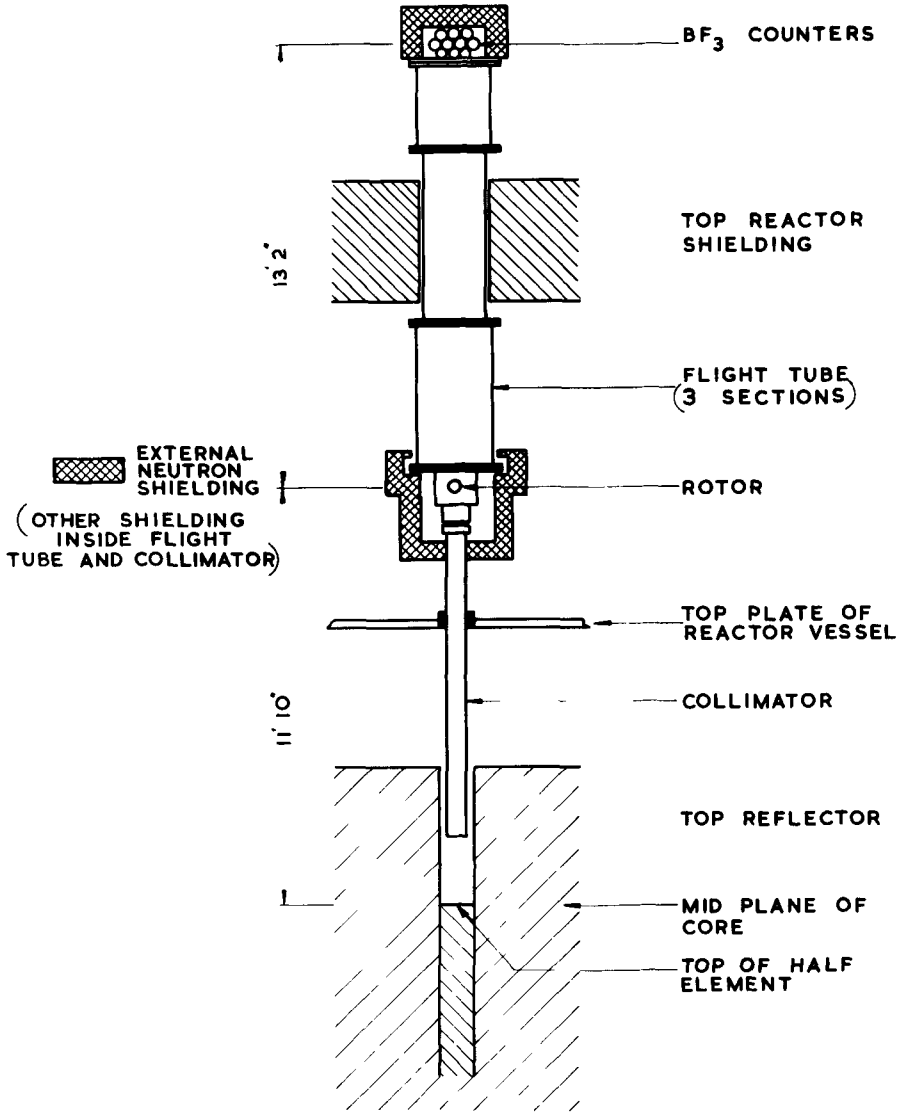

FIG. 2. GENERAL ASSEMBLY.

APPROXIMATELY TO SCALE VERTICALLY
NOT TO SCALE HORIZONTALLY

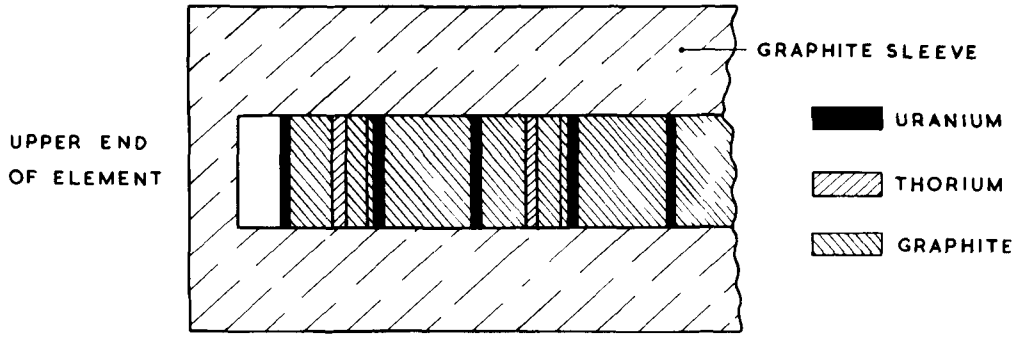

FIG 3 DETAILS OF FUEL PATTERN IN HALF ELEMENT

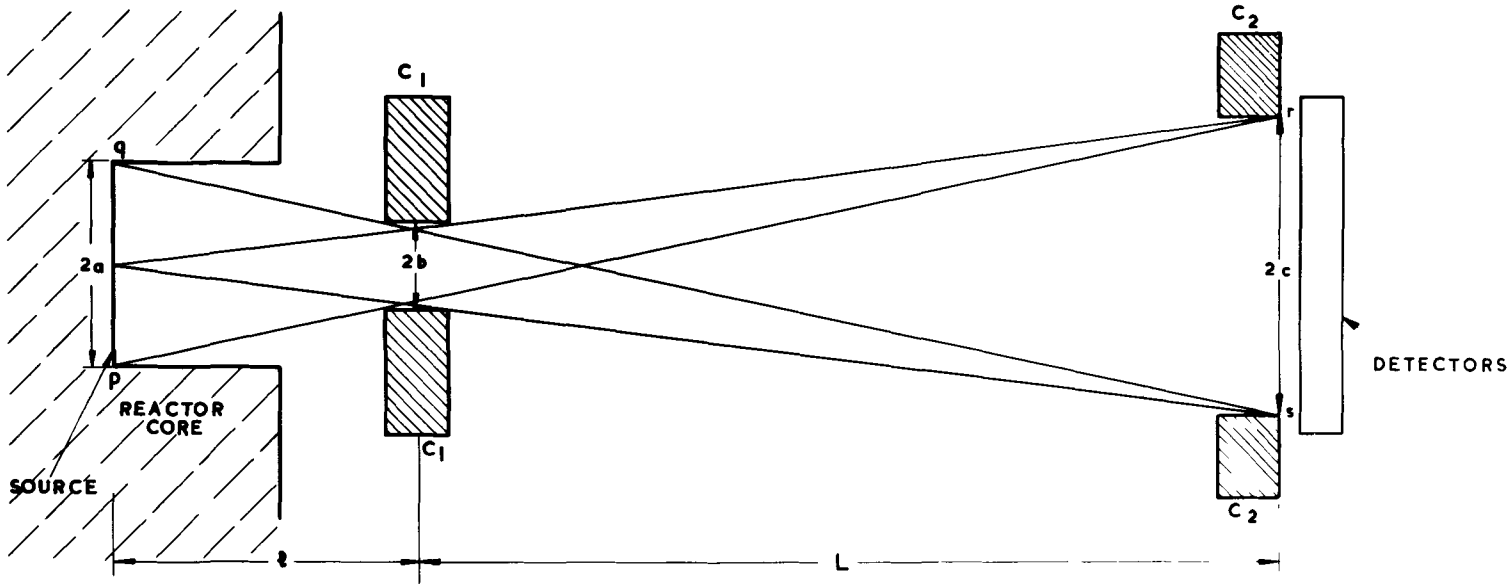

FIG. 4. COLLIMATOR PARAMETERS.
NOT TO SCALE

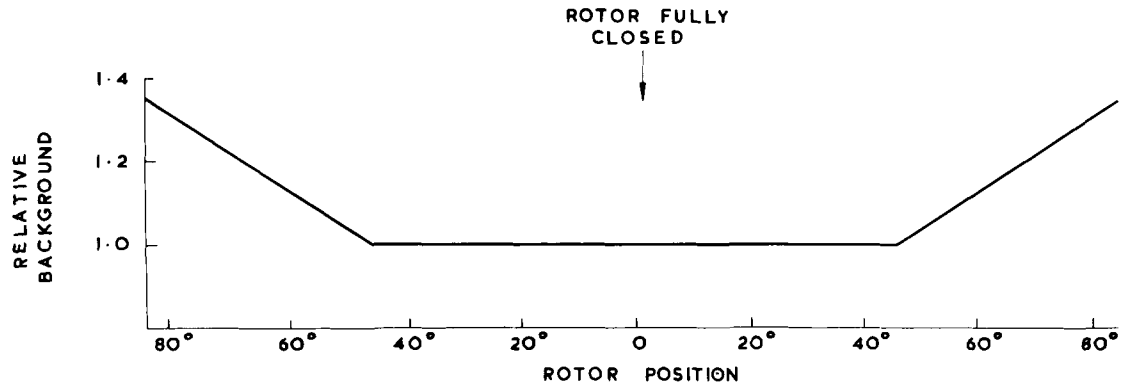

FIG. 5. VARIATION OF BACKGROUND WITH ROTOR POSITION.

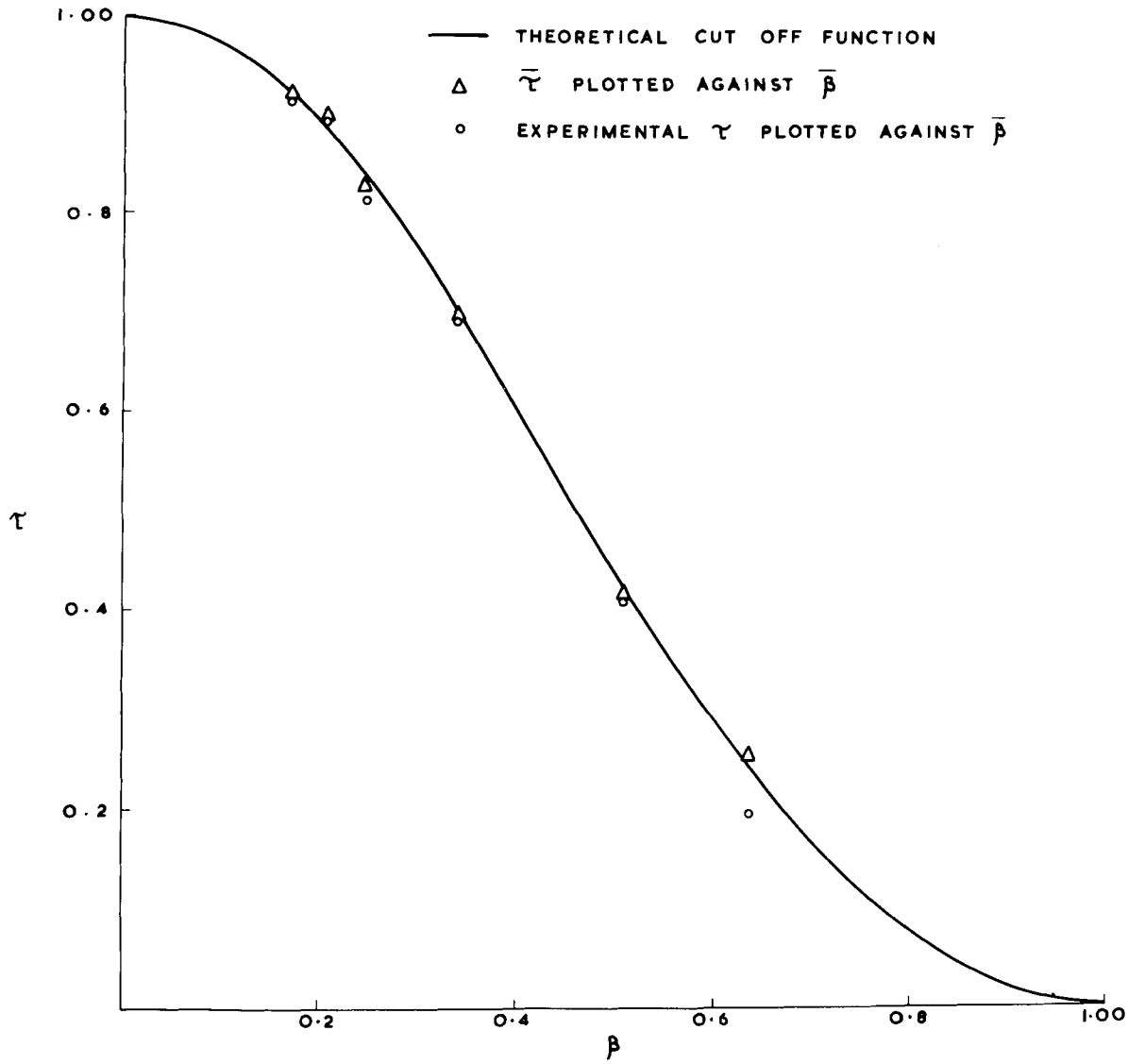

FIG. 6. CUT OFF FUNCTION FOR CHOPPER.

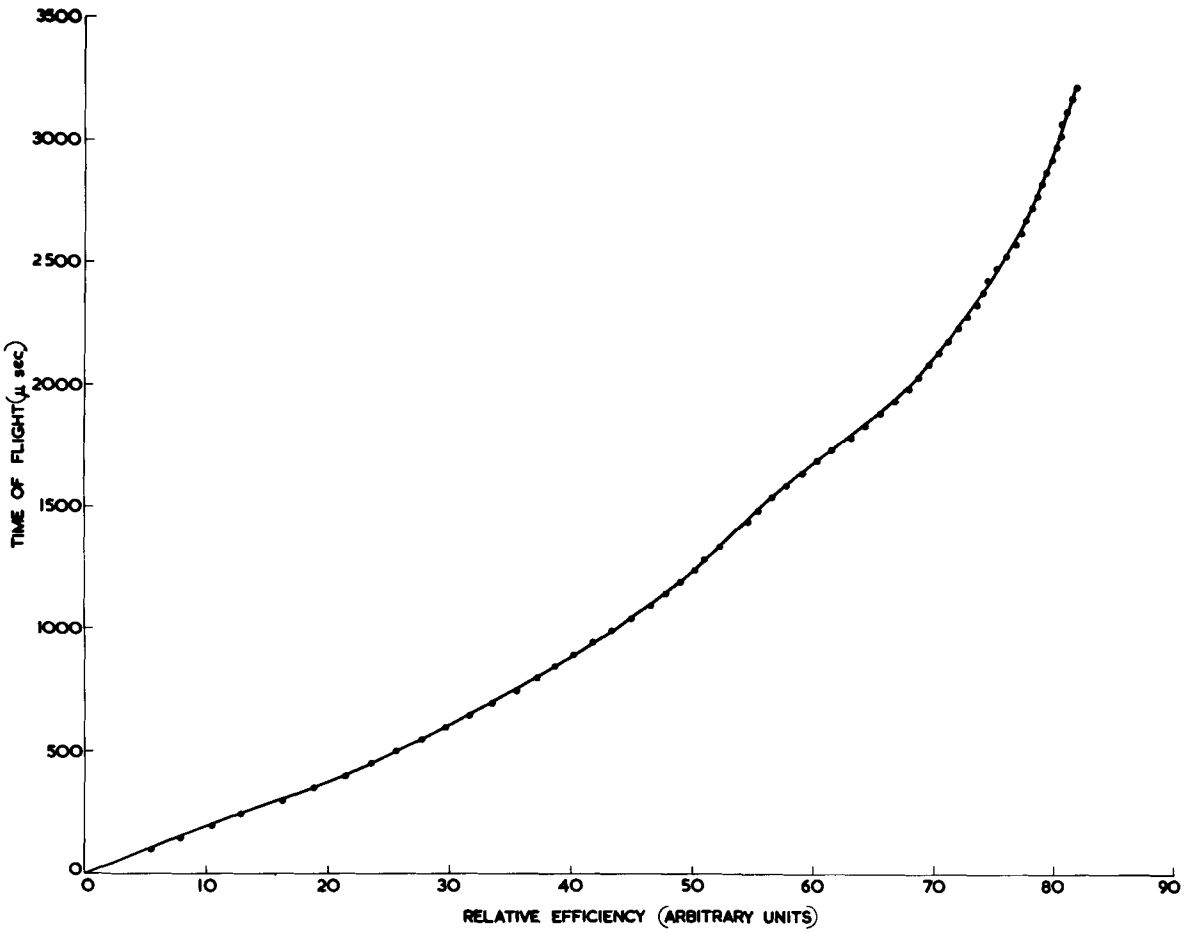

FIG. 7. EFFICIENCY OF BF_3 COUNTERS.

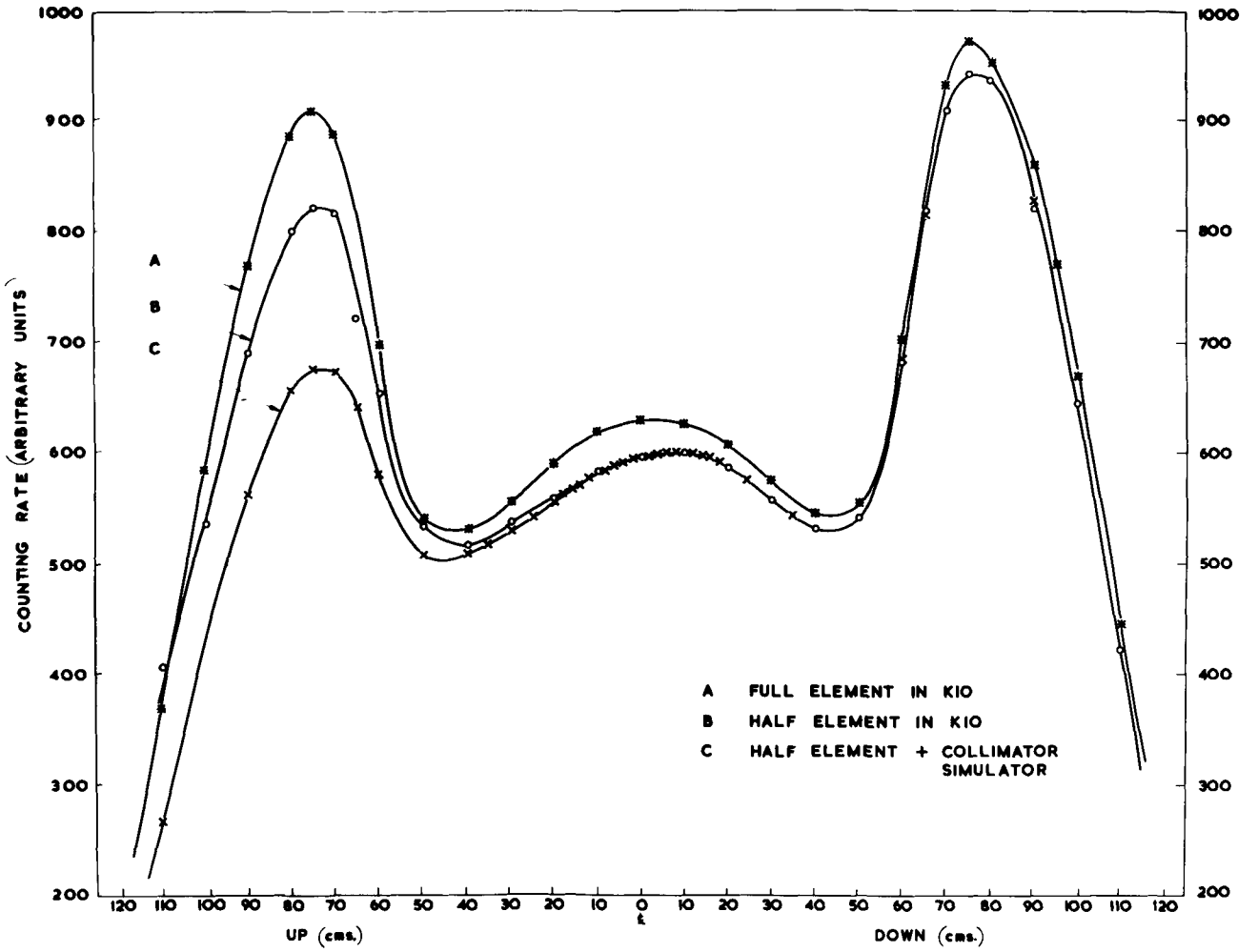

FIG. 8. REACTION RATE MEASUREMENTS IN KIO.

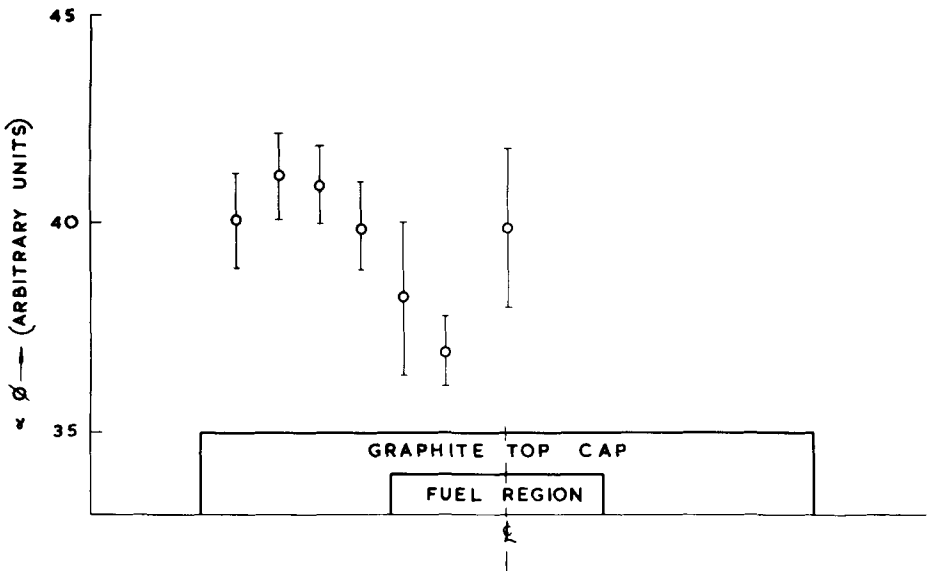

FIG. 9. FLUX DISTRIBUTION ACROSS TOP OF HALF ELEMENT.

FIG. 10.

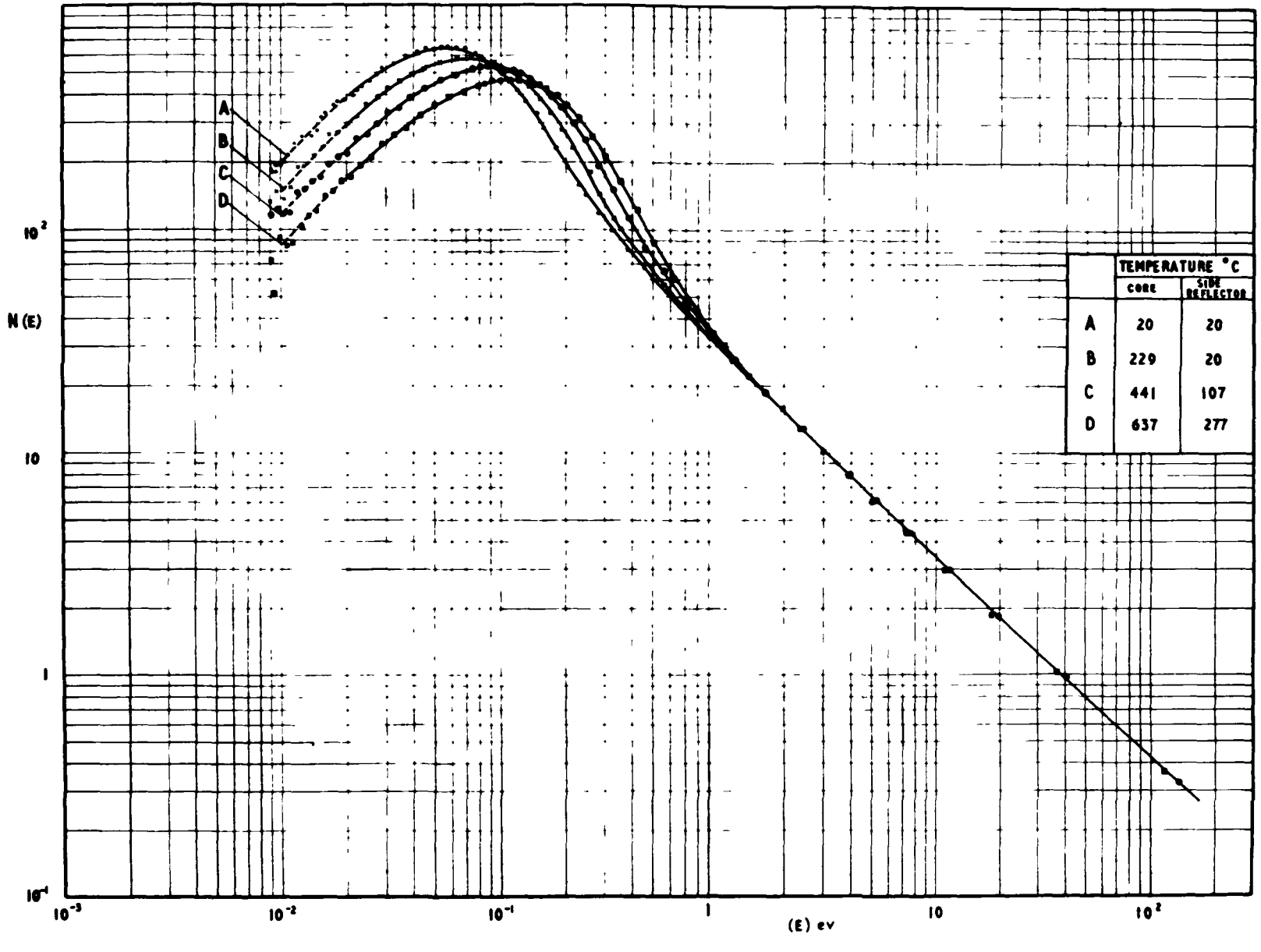
A
B
C
D
N(E)
10^2
10
1
10^{-1}
10^{-3}
10^{-2}
10^{-1}
1
10
10^2
(E) ev
TEMPERATURE °C
CORE
SIDE REFLECTOR
A 20 20
B 229 20
C 441 107
D 637 277

FIG. 11.

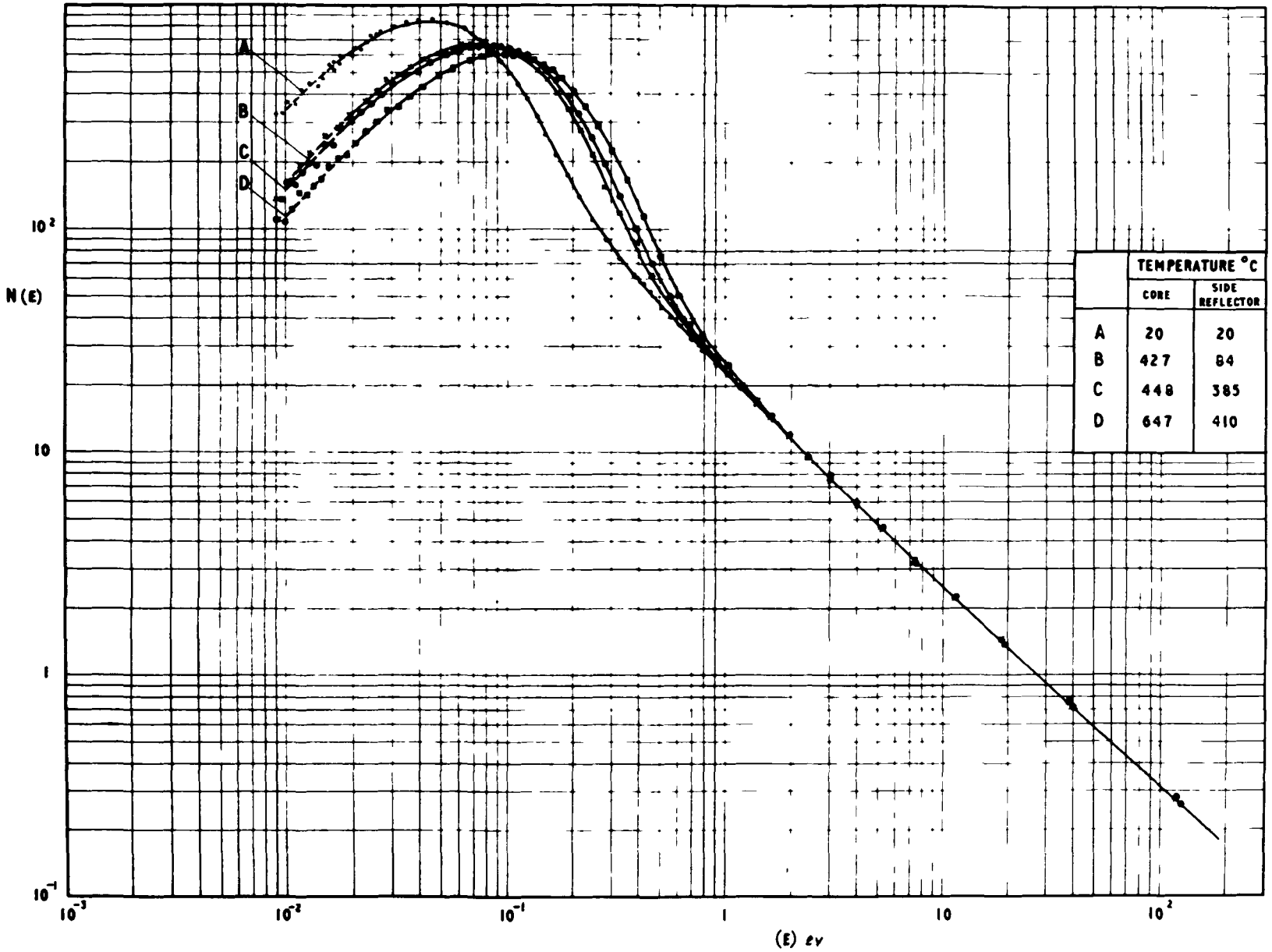
A
B
C
D
N(E)
10^2
10
1
10^{-1}
10^{-3}
10^{-2}
10^{-1}
1
10
10^2
(E) ev
TEMPERATURE °C
CORE
SIDE REFLECTOR
A 20 20
B 427 84
C 448 385
D 647 410

FIG. 12.

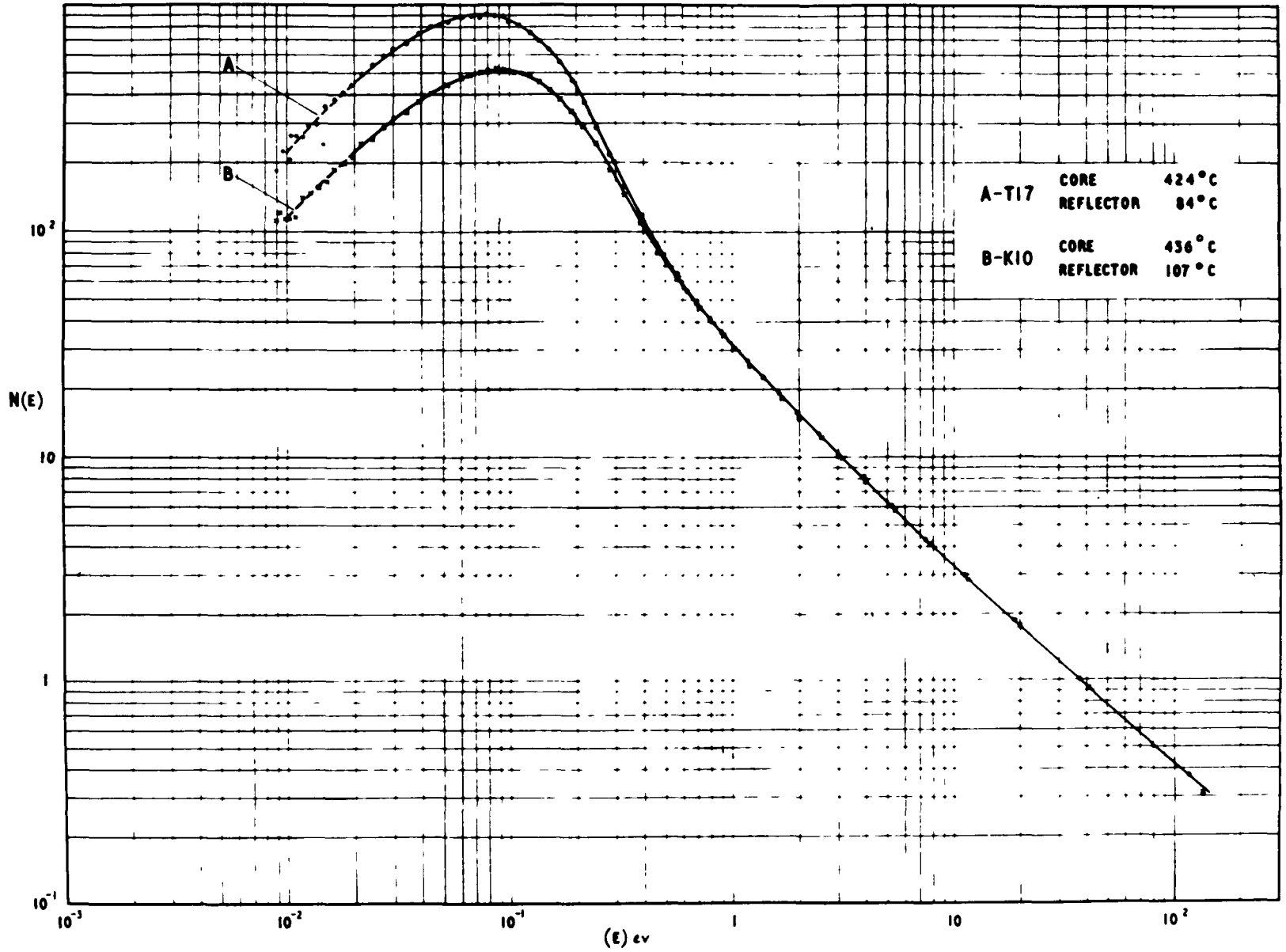
A
B
A-T17
CORE 424°C
REFLECTOR 84°C
B-K10
CORE 436°C
REFLECTOR 107°C
N(E)
10²
10
1
10⁻¹
10⁻³
10⁻²
10⁻¹
1
10
10²
(E) ev

FIG 13

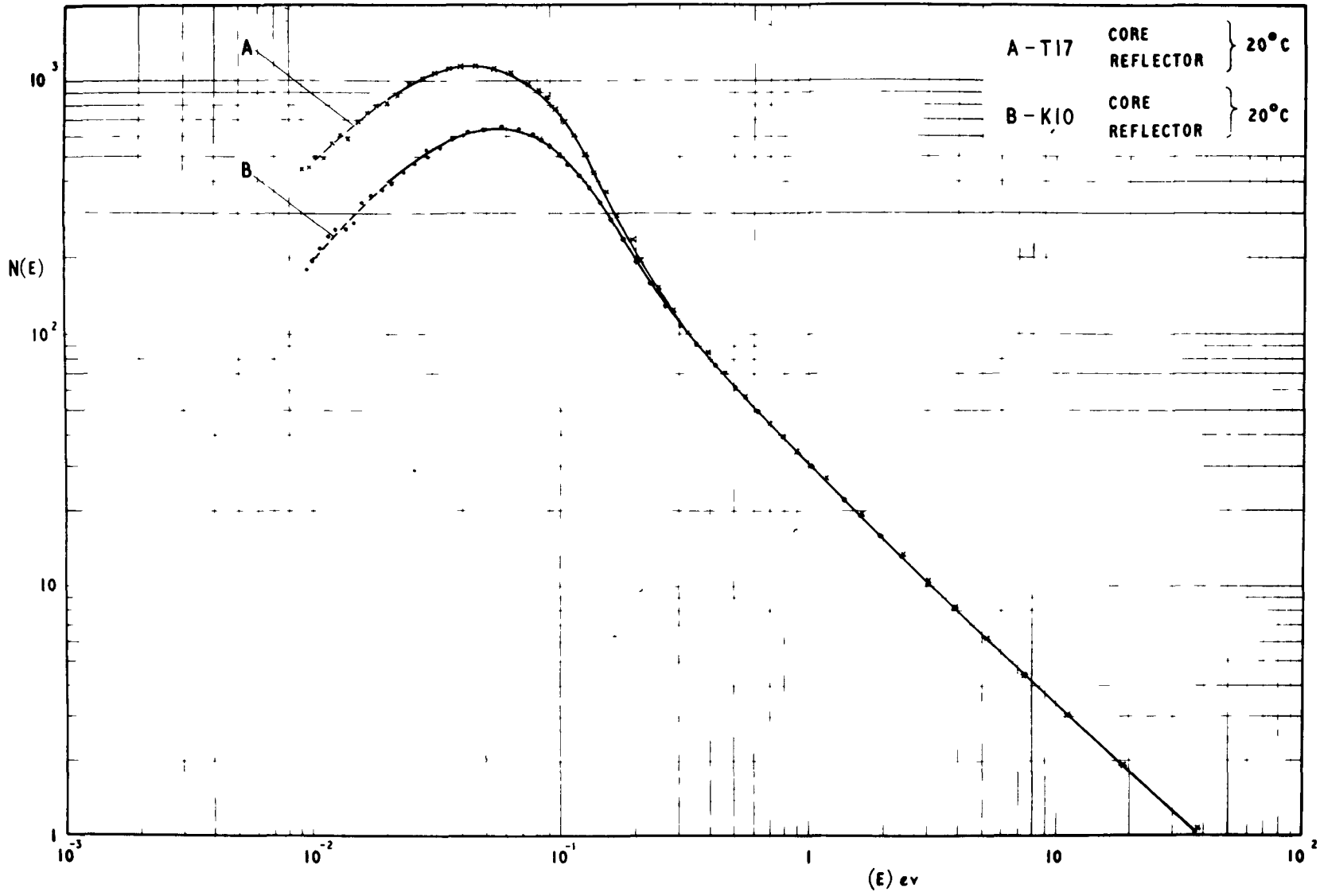
A - T17
CORE
REFLECTOR
20°C
B - K10
CORE
REFLECTOR
20°C
A
B
N(E)
10³
10²
10
1
10⁻³
10⁻²
10⁻¹
1
10
10²
(E) ev

FIG. 14.

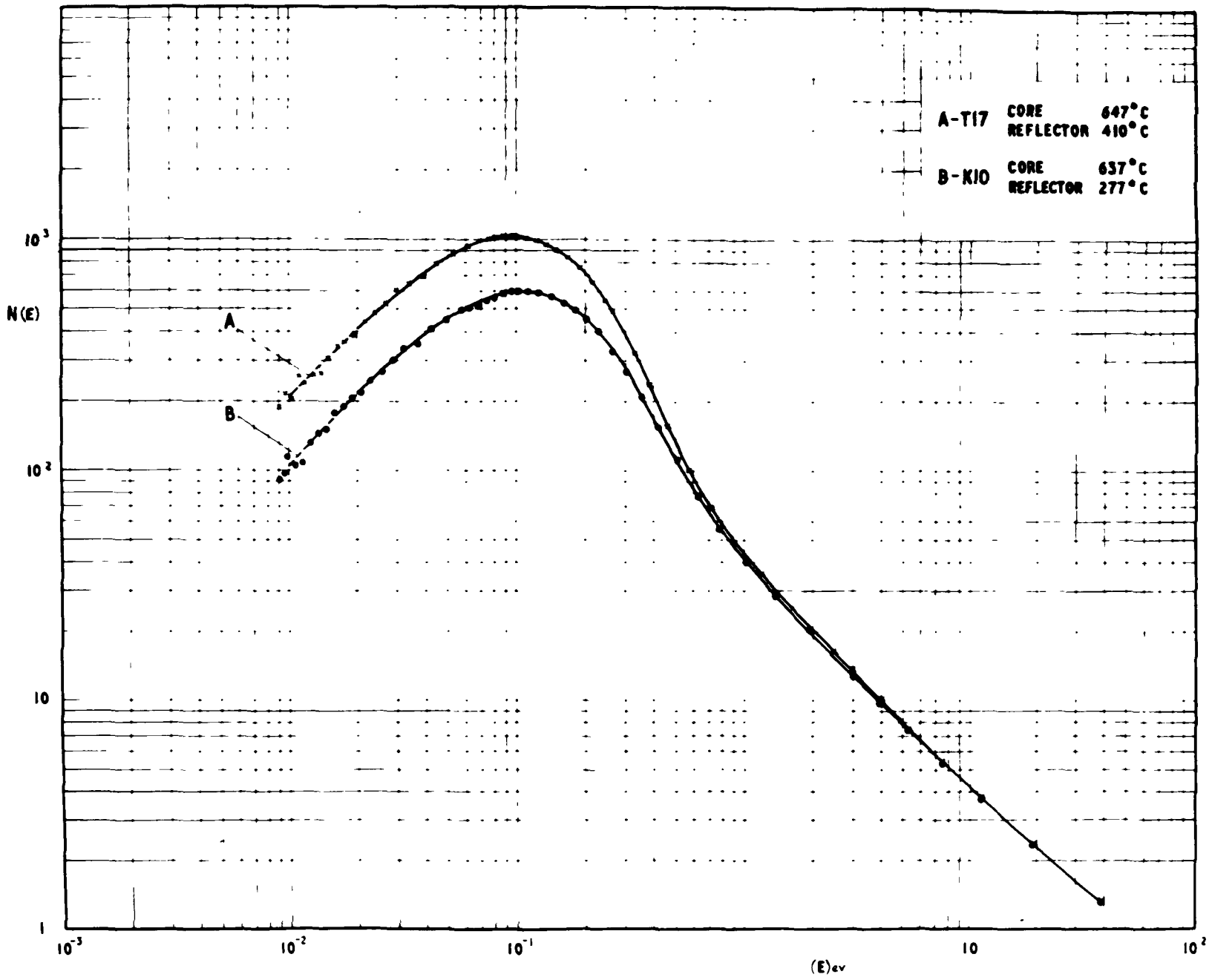
A-T17 CORE 647°C
REFLECTOR 410°C
B-K10 CORE 637°C
REFLECTOR 277°C
N(E)
A
B
10³
10²
10
1
10⁻³
10⁻²
10⁻¹
10
10²
(E)ev

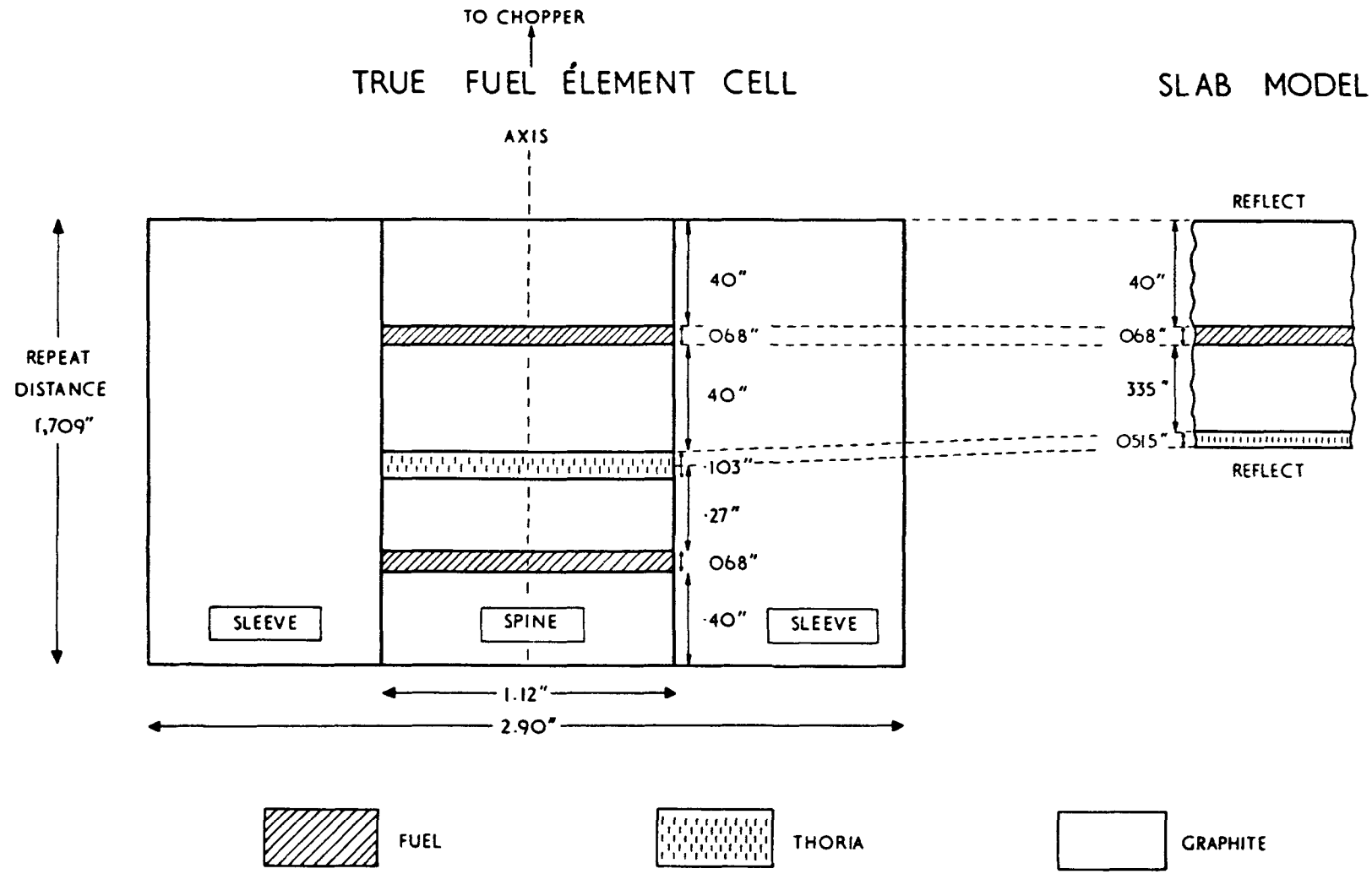
TO CHOPPER
TRUE FUEL ÉLEMENT CELL
SLAB MODEL
AXIS
REFLECT
REPEAT
DISTANCE
1,709"
40"
068"
40"
·103"
·27"
068"
·40"
SLEEVE
SPINE
SLEEVE
1.12"
2.90"
40"
068"
335"
0515"
REFLECT
FUEL
THORIA
GRAPHITE

FIG. 15.

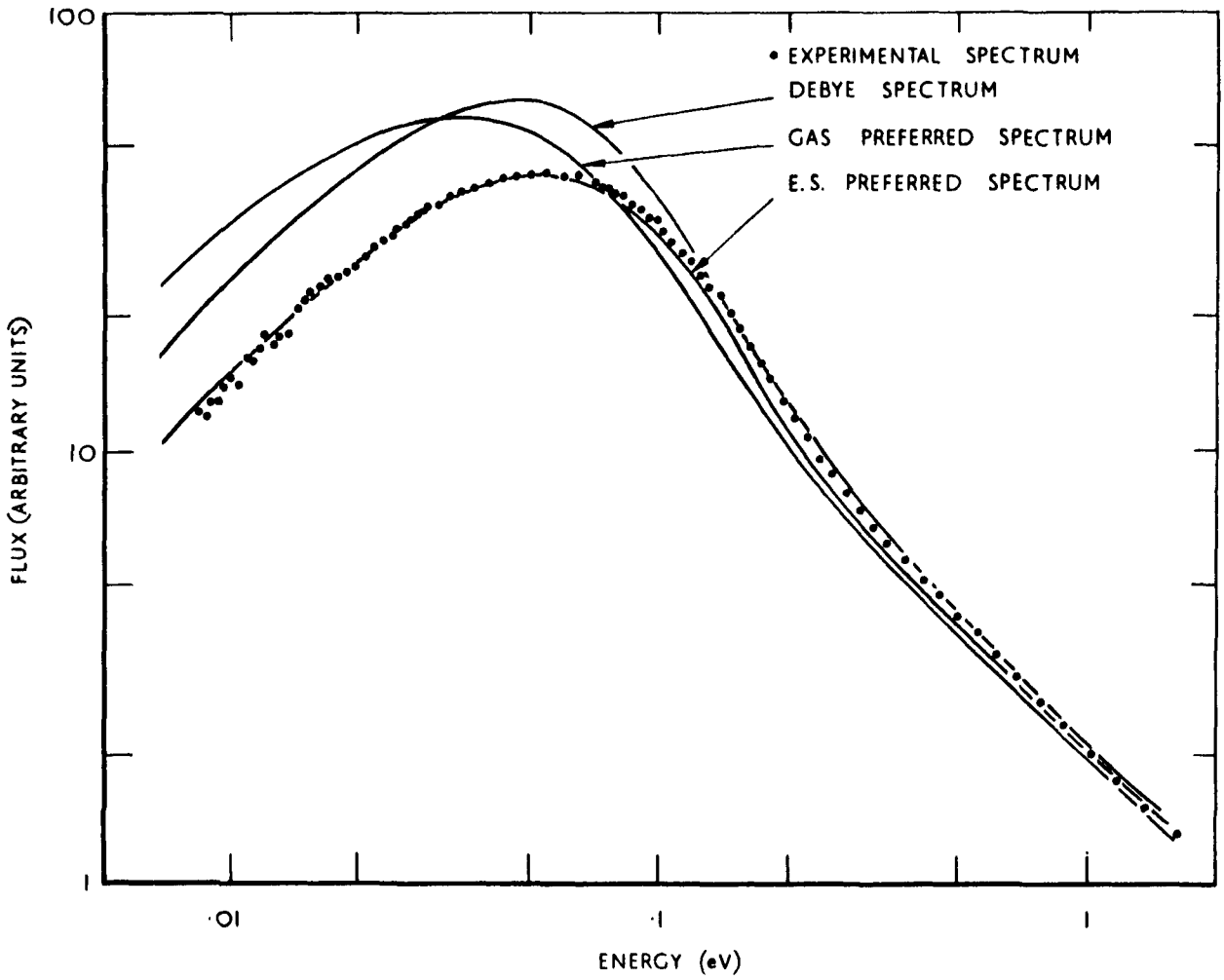

FIG.16. ROOM–TEMPERATURE ZENITH SPECTRUM

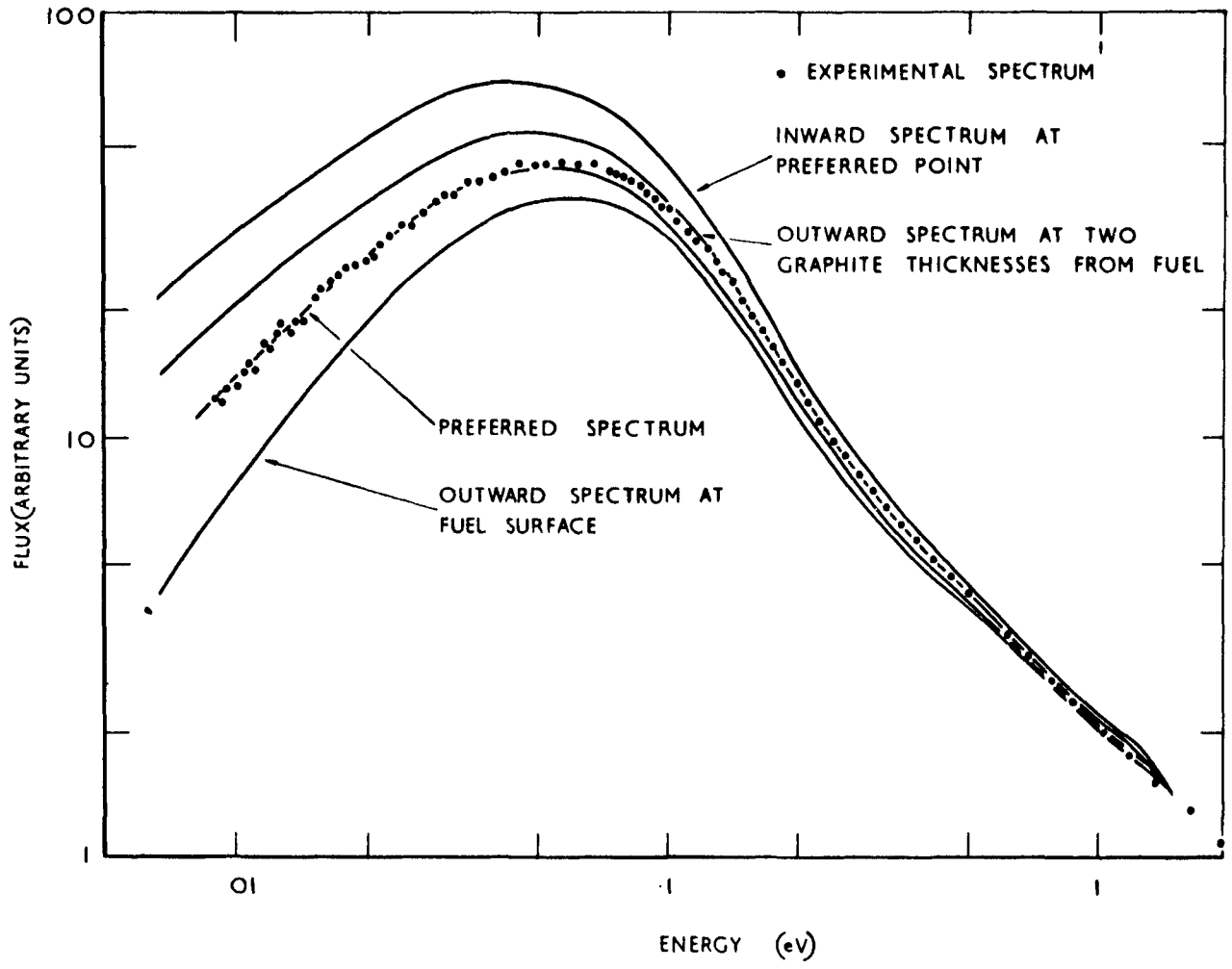

FIG. 17. ROOM – TEMPERATURE ZENITH SPECTRUM

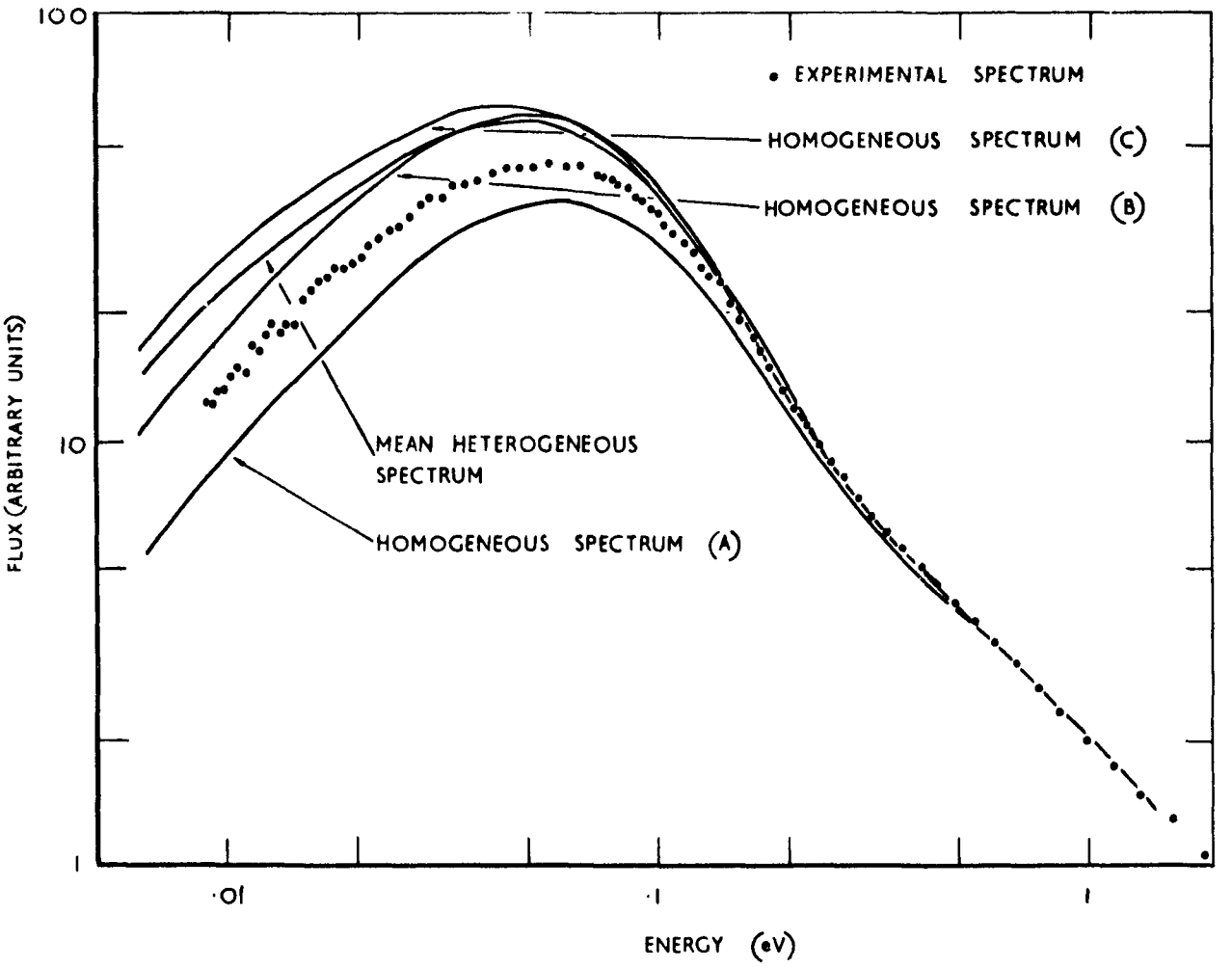

FIG. 18. ROOM—TEMPERATURE ZENITH SPECTRUM

Conference on Neutron Thermalization, Brookhaven, April 30th, 1962

INTEGRAL NEUTRON SPECTRA MEASUREMENTS NEAR A CADMIUM DISK

by P. Korpiun, K. Renz, and T. Springer[+)]

Integral measurements of neutron spectra in moderating substances by foil activations have been performed in several cases using combinations of isotopes with a different energy dependency of their activation cross sections, $\sigma_a(E)$, e.g. for the isotope pairs Lu/Mn, Lu^{175}/Lu^{176}, Eu^{151}/Cu^{63}, and Pu^{239}/U^{235} /1,2,3,12/. The activation measurements give the ratios of the mean cross sections

$$\overline{\sigma_a} = \int_0^\infty \sigma_a(E)\,\phi(E)\,dE \Big/ \int_0^\infty \phi\,dE \qquad (1)$$

where $\phi(E)$ is the neutron spectrum. Theoretically predicted spectra can be examined by averaging over the known cross section curves and by comparing the results with the experimental mean values.

This integral procedure naturally furnishes much less information than a differential time of flight experiment. For hydrogen moderators, however, it is the more reliable method, because in this case the spectrum can change very rapidly over space: The characteristic length λ_T responsible for the temperature relaxation in water near a temperature discontinuity given by

$$\frac{1}{\lambda_T^2} = \frac{9\gamma}{4\bar{v}\lambda_{tr}} + \frac{3\Sigma_a}{\lambda_{tr}}$$

/4, 5/ is only $\simeq 0.7$ cm /6/. The transport mean free path responsible for the spectral relaxation near an absorbing plane /6/ is $\lambda_{tr} = 0.43$ cm (γ = neutron heat transfer coefficient, $\bar{v}$ = mean neutron velocity. In graphite, on the other hand, these quantities are $\lambda_T \simeq 8$ cm and $\lambda_{tr} = 2.6$ cm, respectively.) Under these circumstances a channel of reasonable diameter

---

[+)] Laboratorium fur Technische Physik der Technischen Hochschule München

for neutron extraction parallel to the plane of the temperature discontinuity or absorber would remove too much moderating substance. If the channel is perpendicular to that plane it would more or less average over the range where the spectrum changes. Further, near an absorbing plane the intensity extracted would not be exactly proportional to the neutron flux because of the strong local flux gradient. Thin foils, on the other hand, do neither disturb the flux nor the spectrum. Further they can be used for experiments in very small volumes.

Eu/Cu and Eu/Lu foil pairs have been used by us to measure the changes in the neutron spectrum near a cadmium disk. In order to obtain good spatial reproducibility, the foils were mounted on polystyrene disks. The whole set of foils was put inside a hole in a polystyrene cylinder as shown in fig. 1. Thus the measurement was practically performed in an infinite polystyrene medium*. The cadmium disk was large compared to λ_{tr}, but for technical reasons it was not made large compared with the diffusion length L. Thus the flux change near the disk was a little different from that to be expected for a very large absorbing disk. It is thought that the influence of this fact on the relaxation of the spectrum is small.

The rare earth foils were made of paper soaked with solutions of Eu or Lu salts. The absorption probability in the foils was less than 10^{-3}. Thus the activation is proportional to σ_a; the flux and spectrum perturbation can be neglected. The foils were exposed in the water reflector of the FRM reactor.

*) At the beginning of the experiments, the use of polystyrene instead of water was not thought to cause complications in the theoretical interpretation of the results. Our opinion was that a gas kernel would be used in every case. The transport scattering cross section, λ_{tr}, per H atom was determined from the space dependency of the thermal flux near the cadmium disk by fitting the flux with the theoretical curve /11/. The resulting value, σ_{tr} = 34 barns, is very close to the value for H_2O.

By rotating the polystyrene cylinder perpendicular to its axis the change of the moderation density was kept small over the spatial range investigated. To avoid absolute calibration of the activation measurements double ratios for every foil pair were determined, namely $(A_1/A_2)/(A_1(\infty)/A_2(\infty))$, where 1 and 2 labels the two foil materials used. $A(\infty)$ is the activation with the cadmium plate removed. The latter gives a normalization of the activation by the undisturbed spectrum. This can be considered to be a Maxwellian with the actual moderator temperature. The results of the activation ratios as a function of the distance from the absorbing disk, z, are shown in fig. 2a and b.

Attempts were made to substract the resonance contribution from the measured total activation cross sections and to transform the remaining thermal activation into an effective neutron temperature by assuming a Maxwellian spectrum with temperature T_n, which is different for different detector pairs. Near the cadmium disk the resonance correction is very high because of the large thermal flux depression (see Cu(th) in fig. 3). Furthermore, the resonance correction shows large errors in the case of Lu and Eu (see below) . Thus the error which is introduced by the resonance correction is rather high.

The resonance correction factor that must be applied to the total activation A_{tot}, is

$$k = 1 - F(T_n)/K(z) \qquad (2)$$

where K(z) is the space dependent cadmium ratio which has to be measured. Characteristic flux curves from the activations A_{cd} and A_{tot} of different cadmium-covered and bare detectors are shown in fig. 3 as a function of z. There is a considerable depression of the epicadmium flux as measured by Eu

because its main resonances are situated near the cadmium cut-off. The smallest resonance flux depression was found by gold activation because the main absorption comes from the 4.9 eV resonance. (The slight slope also in the case of gold comes from the non-uniform distribution of the source neutron density.)

Further is $F = \int_{E_g}^{\infty} \sigma_a(E)\,dE/E \,/\, \int_0^{\infty} \alpha(E)\,\sigma_a(E)\,dE/E$, where $\alpha(E)$ is the cadmium transmission for isotropic neutron incidence. The main uncertainties result from uncertainties of the resonance data, especially in the case of europium where the fraction of the 9.3 h activation cross section to the total absorption cross section has different values for different resonances /8/. Further, the applicability of (2) is complicated by an energy dependent depression of the resonance flux, induced by the cadmium disk and by the filter itself because the cut-off is situated just in the surrounding of the main resonances of Eu and Lu. Uncertainties in $\alpha(E)$ result from the influence of the flux anisotropy on the filter transmission, and in F from the lower limit E_g (namely, E_g depends on $T_n(z)$ which introduces a considerable space dependency of F).

The calculation of the effective neutron temperature from the thermal activation A_{th} was performed for Lu by the functions given by Schmid and Stinson /2/ and for Eu by combining the data from Westcott $\left[g_{Eu}(T) \right]$ /9/ and Pattenden $\left[g_{Eu^{153}}(T) \right]$ [10]. The effective neutron temperatures as functions of distance z are shown in fig. 4)+). A strong flux hardening near the cadmium disk is observed. The difference between the results for the

+) As can be shown, a very good approximation for the cross section ratio $\sigma_{th}(Eu)/\sigma_{th}(Cu)$ is the function const. $\mathrm{erf}(0{,}0129\,eV/kT)^{1/2}$ This was found by approximating the curve $\log \sigma_{Eu}(E)$ by two straight lines with an intercept at 0.0129 ev.

effective temperatures from both methods are not large except at $z \cong 0$, where the distortion of the Maxwellian will be largest. The flux hardening at the surface is considerably larger than predicted by the theory in /6/ when the data γ and D of water were used. The discrepancy may be introduced by the inapplicability of the water data, and by the Maxwellian hypothesis used in the theory /6/.

One should not lay too much emphasis on these effective neutron temperature curves because of their uncertainties described above. Rather, one should calculate the total mean cross sections $\overline{\sigma}_a$ according to (1) from computed spectra by using the $\sigma_a(E)$ - curves which are rather well known, at least in a relative ordinate scale. Thus a simple experimental examination of the theory can be achieved if different foil combinations are used. On the other hand, the effective temperature concept is useful for reactor physics in many cases where only the mean cross sections must be known, too.

The experiments will be continued in water with a considerably larger cadmium disk.

Our thanks are due to Professor Maier-Leibnitz for valuable discussions.

References:

/1/ Price, G.A., J. Nucl. Eng. A 10, 157 (1959)

/2/ Schmid, L.C., and W. P. Stinson, HW-62727 (1959), and Nucl. Sci. Eng. 7, 477 (1960), see further Absalom R. et al., AEEW-R50, 1960

/3/ Springer, T., H. Walter, Report from the Symposium at Risø, June 1960 and Ber. d. Reaktorstudiengruppe (1959), Technische Hochschule München

/4/ Kottwitz, D.A., HW56919 (1958), further; HW-51983 (1957) and HW-53492 (1957)

/5/ Selengut, D.S., HW-56919 (1958)

/6/ Springer, T., Nukleonik 2, 144 (1960)

/7/ Renz, K., Dipl. - Arb.(1962) and Korpiun, P., Dipl.-Arb.(1961), Laboratorium für Techn. Physik der Technischen Hochschule München

/8/ Wood, R.E., Phys. Rev. 95, 453 (1954), Hayden, R.J., J. H. Reynolds, M.G. Inghram, Phys. Rev. 75, 1500 (1949), see further; Sailor, V.L., H.H. Landon, and H.L. Foote, Phys. Rev. 93, 1292 (1954)

/9/ Westcott, C.H., AECL-670 (1958)

/10/ Pattenden, N.J., Genfer Konf. 1958, Vol. 16, 44

/11/ LaCaine, J., Canad. J. Res., A 28, 242 (1950)

/12/ Stinson, W.P., L.C. Schmid, and R.E. Heineman, Nucl. Sci. Eng. 7, 435 (1960)

Legends of Figures

Fig. 1. Polystyrene cylinder with foil pairs, placed in the water reflector of the FRM, about 30 cm distant from core.

Fig. 2a and b. Activation ratios for Cu/Eu and Lu/Eu foil pairs as a function of distance z from the cadmium disk. Experimental points, from several independent measurements. Activation ratios are normalized at the activation ratio measured with the cadmium disk removed, $A(\infty)$.

Fig. 3. Space dependency of thermal activation measured with Cu foils = Cu(th), and epithermal activation measured by cadmium covered Eu, Lu, and Au foils (labeled by Au, Lu, and Eu) normalized at the values for $z = \infty$. The activations are representative for the fluxes in different energy ranges.

Fig. 4. Effective neutron temperature as measured by Cu/Eu and Lu/Eu foils pairs. Shaded region represents estimated range of systematic errors, mainly resulting from resonance correction (in the case of Lu/Eu; for Cu/Eu, the error range is of similar magnitude.)

λ_{tr} = transport mean free path, estimated from space dependency of thermal flux in fig. 3.

● = Cu/Eu - method, o = Lu/Eu - method (mean values from several measurements).

Values normalized at $z = \infty$ where $T_n = T_{(moderator)}$

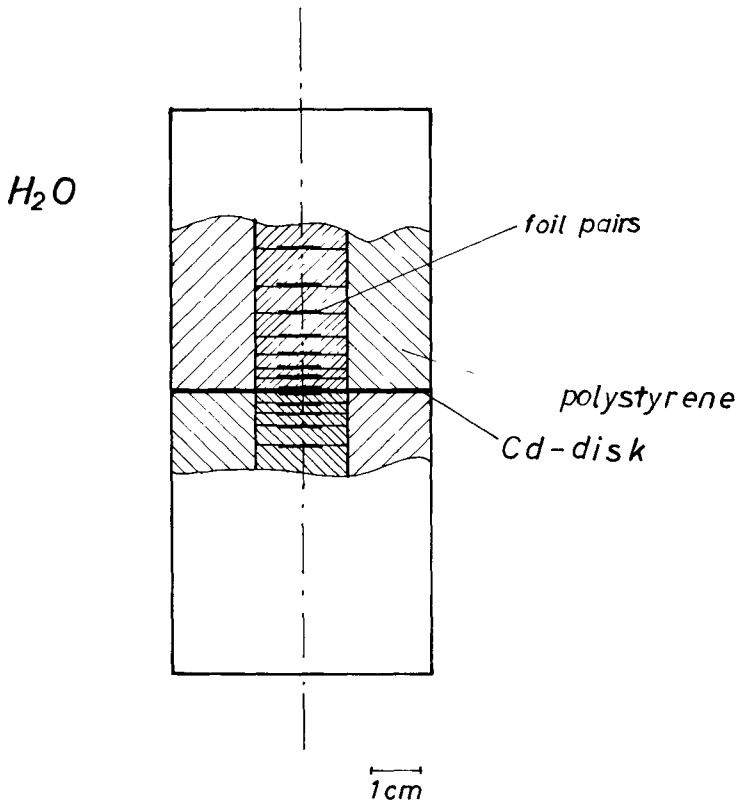

Fig.1

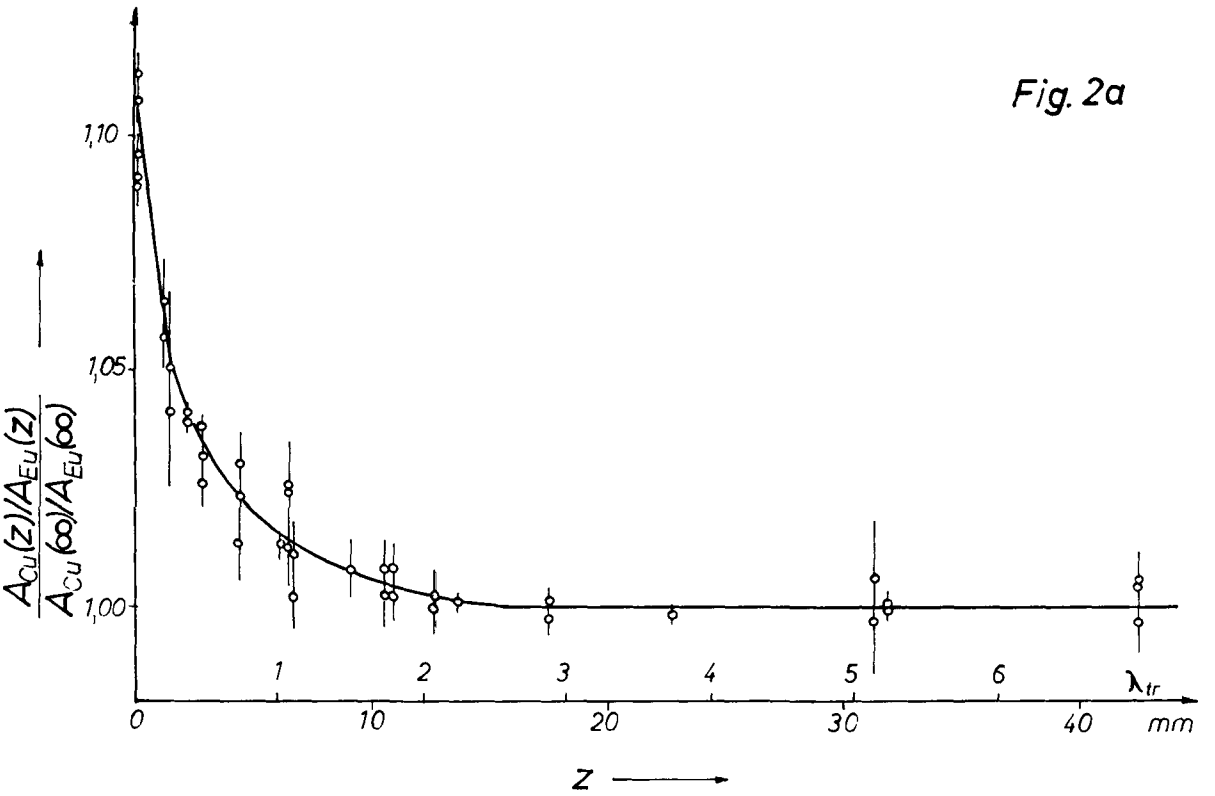
1,10
1,05
1,00
$\frac{A_{Cu}(z)/A_{Eu}(z)}{A_{Cu}(\infty)/A_{Eu}(\infty)}$
1
2
3
4
5
6
λ_{tr}
0
10
20
30
40
mm
z

Fig. 2a

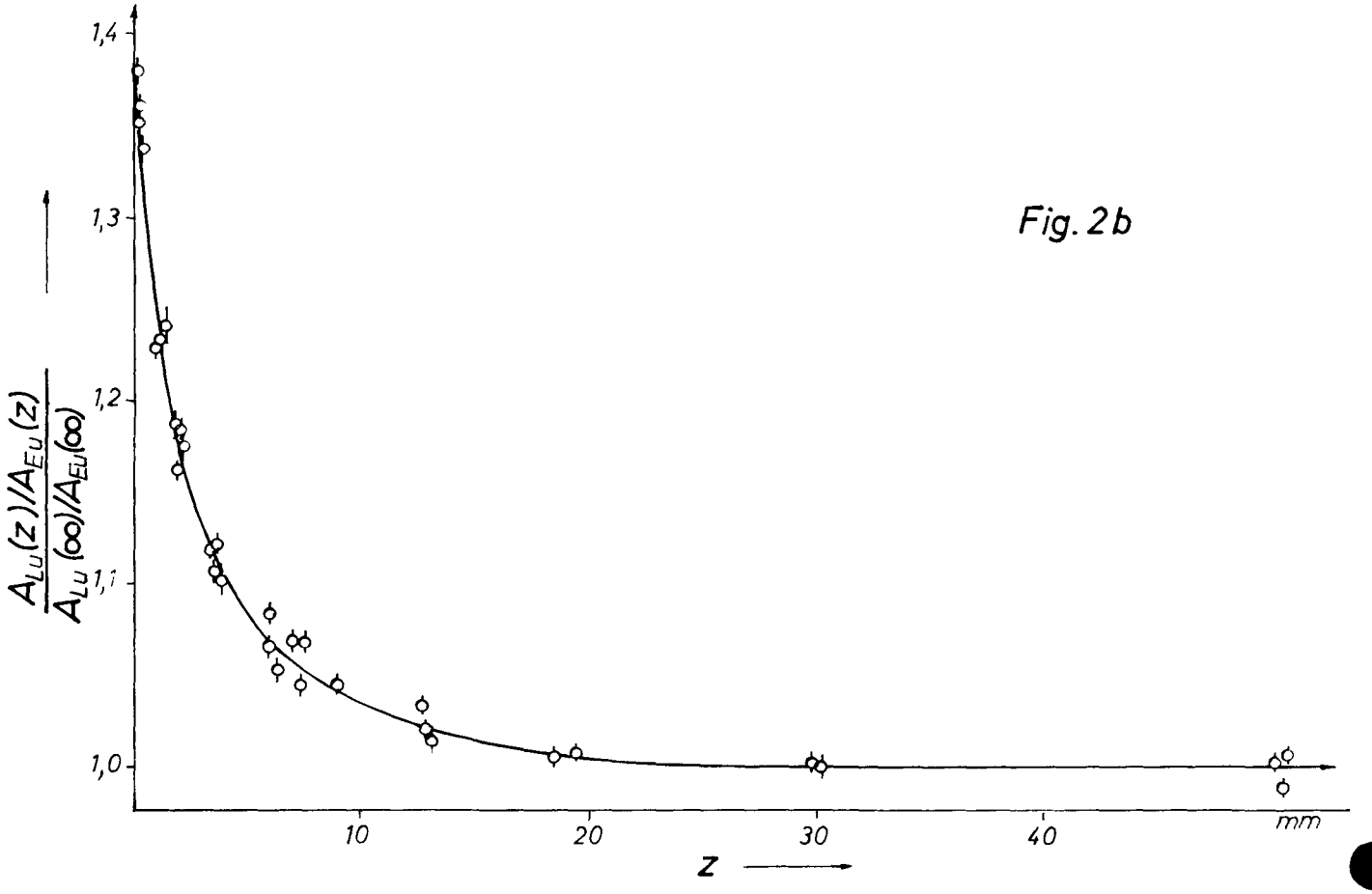
1,4
1,3
1,2
1,1
1,0
$\frac{A_{Lu}(z)/A_{Eu}(z)}{A_{Lu}(\infty)/A_{Eu}(\infty)}$
10
20
30
40
mm
z

Fig. 2b

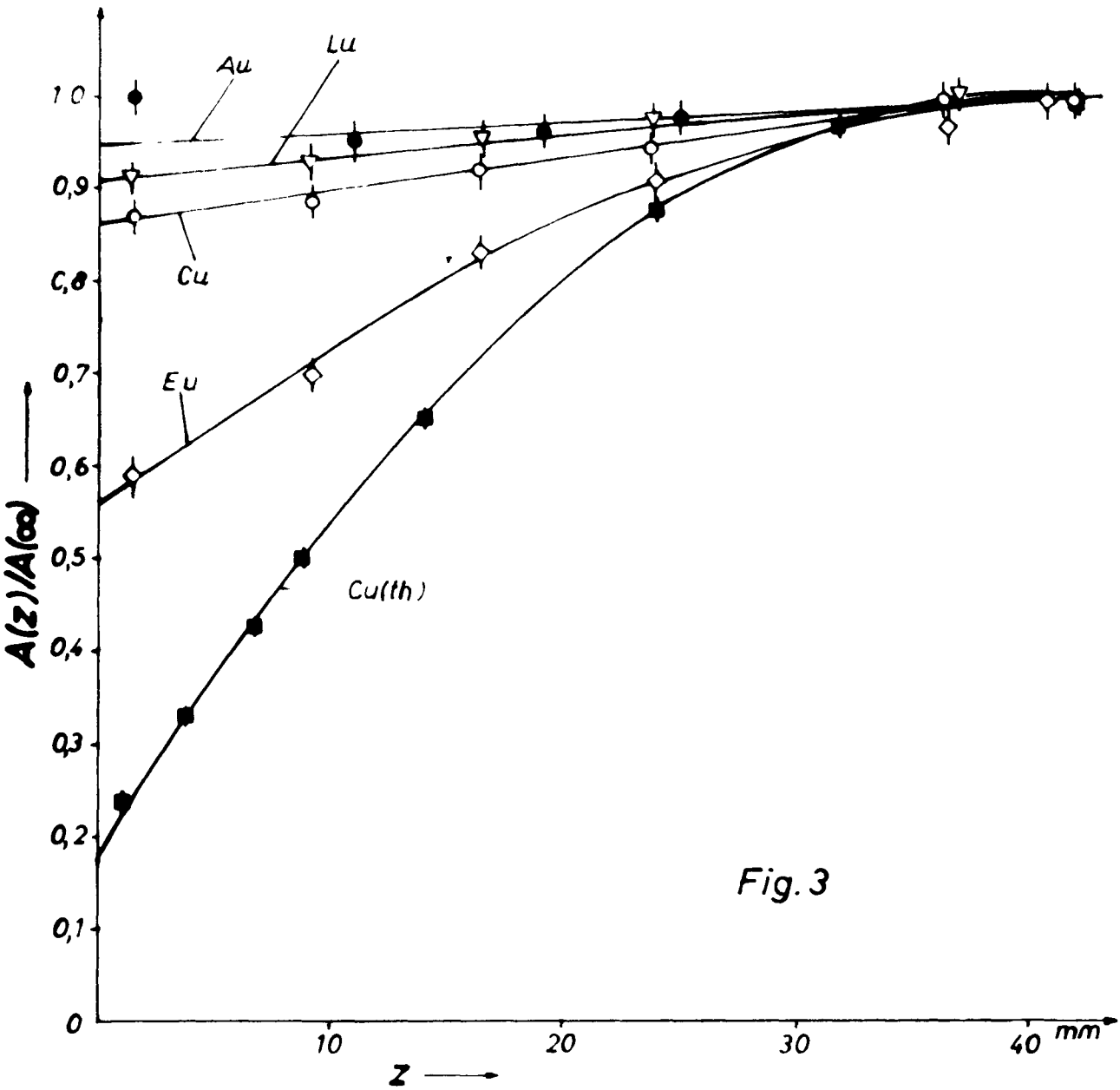

Fig. 3

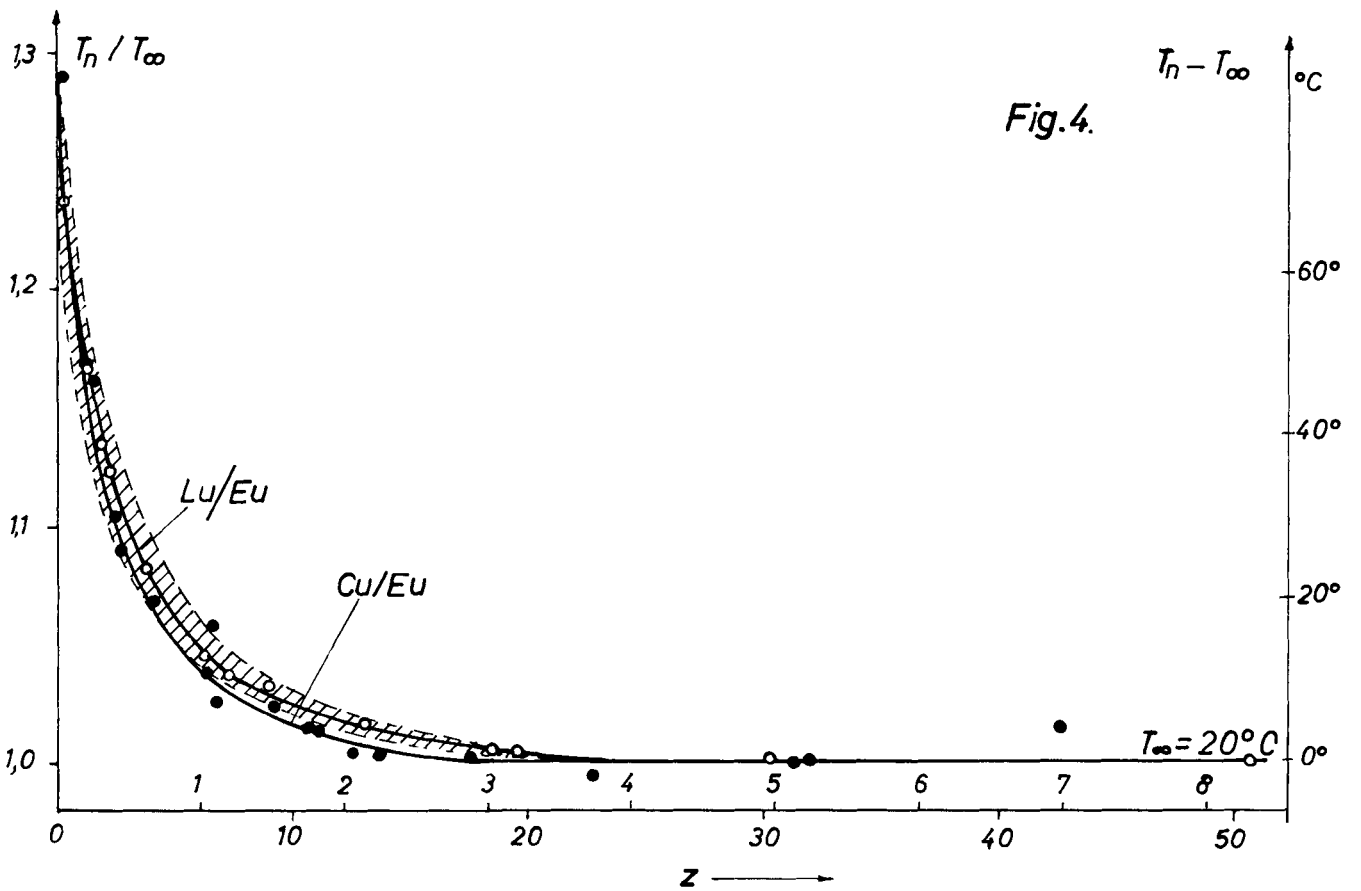
1,3
T_n / T_∞
1,2
1,1
1,0
Lu/Eu
Cu/Eu
$T_n - T_\infty$
°C
60°
40°
20°
0°
$T_\infty = 20°C$
1
2
3
4
5
6
7
8
0
10
20
30
40
50
z

Fig.4.

V. I. Mostovoĭ, V. S. Dikarev, M. B. Egiazarov
and Yu. S. Saltykov

MEASUREMENT OF NEUTRON SPECTRA IN URANIUM-WATER AND URANIUM-MONO ISOPROPYL DIPHENYL LATTICES

INTRODUCTION

Heterogeneous systems containing uranium with ordinary water have found extensive use for power and research reactors. In this connection, more attention is being paid in recent years to the many unique features of the physics of these systems.

The features of physics of heterogeneous reactors using uranium and ordinary water are brought about essentially by the nature of the slowing down and thermalization of the neutrons in these reactors.

As is well known, owing to the large absorption in such systems, the neutrons do not enter into thermal equilibrium with the atoms of the moderator.

Their average energy is much higher than the average thermal energy of the moderator atoms. The neutron spectra

in the fuel and in the moderator are appreciably different.

Heterogeneous systems with organic moderators, offer certain advantages for use in power installations, since they have acceptable thermodynamic properties and have a sufficient resistance to radiation. One can expect that from the point of view of the physics of neutron thermalization such systems are similar to uranium-water systems.

Owing to the lack of complete data on inelastic scattering of neutrons by water molecules, the calculations of the neutron spectra in uranium-water systems have been based until recently on various model representations concerning the character of energy exchange between the neutron and the water molecule [1, 2, 3]. Such calculations need experimental verifications so as to determine their accuracy and practical usefulness.

In many of the researches done on neutron spectra in heterogeneous uranium-water systems [4, 5, 6], valuable information was obtained in the neutron spectrum in the fuel and in the moderator. This information was useful also for a critical estimate of the theoretical calculations. However, these experiments did not answer the question of the character of variation of the neutron spectrum in the uranium and in the moderators themselves, within the limits of the elementary cell, a factor of importance for further improvement of the theoretical calculations.

The present investigation was made in order to obtain a detailed picture of the space-energy distribution of the neutrons and in order to establish the main laws governing their thermalization in heterogeneous uranium-water and uranium-mono isopropyl diphenyl systems.

MEASUREMENT PROCEDURE

The procedure employed for the measurement was already described in previously published papers [6, 7].

A subcritical assembly was made up of blocks of natural uranium 3.5 cm in diameter and 40 cm long, located in the sites of a triangular lattice with spacing 5.5 cm. The subcritical assembly was mounted in a cylindrical tank 50 cm in diameter and 50 cm high, which depending on the type of the measurements was filled either with ordinary water or with mono isopropyl diphenyl ($C_{15}H_{16}$). The lateral surface of the assembly was surrounded by a reflector, made up of a special tank filled with moderator. All the basic measurements were made in the presence of the reflector and only in the control experiments was the reflector removed.

The composition of the elementary cell of the lattice is characterized by the following volume concentration of materials: uranium -- 36.7%, water (or $C_{15}H_{16}$) -- 58.6%, and aluminum -- 9.7%.

The external neutron source was a broad neutron beam from the VVR-2 (water-moderated water-cooled power reactor). The entire arrangement with the assembly were mounted in the well of a thermal column and reactor shielding, located on a moving platform. In some measurements a thermal neutron converter, consisting of an assembly of uranium rods, was placed between the active zone of the reactor and the investigated system. The assembly with the reflector were isolated from the thermal column with cadmium and boron carbide.

The heat released in the lattice during operation was carried away by means of a forced-cooling system.

The space-energy distribution of the neutrons was investigated by measuring the spectrum of the neutrons leaving from different points of the cell. For this purpose seven microbeams were brought out of the central part of the assembly, and the neutron spectrum was measured in these beams by the transit-time method. Four beams left the uranium blocks and three the moderator. To bring out the beams, holes 0.8 cm and 20 cm deep were drilled in the uranium blocks. The neutron beams from the moderator were brought out with the aid of thin-wall aluminum tubes 0.8 cm in diameter with bottoms that reached the center of the assembly. The temperature of the medium at the point where the spectrum was measured was monitored by means of thermocouples

mounted on the bottom of each of the cavities.

To reduce the local perturbations due to the cavities in the uranium and the moderator, the cavities were distributed over three neighboring cells. In this case the centers of their bottoms were arranged along the line of the bisector to the lattice triangle (Fig. 1). In this connection, the coordinates of the point where the spectrum was measured was determined by the distance r measured from the center of the block along the direction of the bisector of the lattice triangle. Special experiments have demonstrated that the system of cavities employed to bring out the beams did not disturb the energy distribution of the neutrons in the cell.

A collimator with holes exactly duplicating the placements of the cavities was placed in the shield of the reactor. The collimator consisted of an assembly of materials that absorb neutrons and gamma rays (boron, paraffin, iron). The collimating holes, covered with cadmium on the outside, were made divergent in such a way that the only neutrons striking the detector were those traveling from the bottom of the cavity. In the measurements, all the holes of the collimator, with the exception of one, were covered with special protective plugs.

The interruptor used for the mechanical selector consisted of an assembly of nickel plates and aluminum

grids 10 cm long, which comprised plane-parallel slots for the neutrons, with width 0.1 cm. To reduce the background, the body of the rotor was made of steel and plastic, and in addition the diameter of the rotor (15 cm) was greater than the length of the interrupting plates.

The neutron detector was an end-window proportional counter 10 cm long, filled with enriched BF_3 to a pressure 600 mm Hg.. The counter was located 398 cm from the mechanical interruptor in a shielding tank, filled with an aqueous solution of boric acid.

The detector with the shielding and the selector were located on special "coordinate" devices, which made it possible to remotely set them at any of the beams.

To register the neutrons by their transit time, a 160-channel time analyzer was used, in which 128 channels registered the effect and 32 channels registered simultaneously the background. The neutron transit time was measured as a function of their energy range with a resolution of 12 μsec/m, 25 μsec/m, and 50 μsec/m. The resolution in the spatial coordinates was determined by the dimension of the cavity (0.8 cm) with which the beam was brought out.

The neutron density was calculated from the measured counting rates in the time-analyzer channels from the known ratio, which includes the transmission function of

the mechanical selector, the energy dependence of the counter sensitivity, the energy dependence of the total cross section of the air and the structural materials along the path of the beam, and a correction for the neutron flux gradient [6, 7]. No corrections were made for the resolution in the measurement of the transit time, since calculations show that these corrections are smaller than the statistical measurement errors.

MEASUREMENT RESULTS

1. Uranium-water lattice.

The results of the measurement show that the neutron spectra in the water and in the block have the following characteristic features.

The neutron spectrum in the water of a uranium-water lattice can be approximated in the thermal-energy region by a Maxwellian distribution with a neutron-gas temperature greater than the temperature of the water. This rise in the neutron-gas temperature above the water temperature amounted to 45°. It increases with increasing ratio of the uranium volume to the water volume, i.e., with decreasing lattice spacing [6]. Compared with the corresponding Maxwellian spectrum, the spectrum measured in the water is noticeably broader.

The neutron density at energies greater than 0.3 ev

follows the $1/v^2$ distribution.

A typical neutron spectrum, representing the results of measurements in water at 50° C for point 7 (r = 3.17 cm) is shown in Fig. 2. In this figure the ordinates represent the neutron density multiplied by the square of the velocity, while the horizontal axis is marked in the reciprocal of the velocity. Here and below we give the spectrum in relative units, not normalized to the integral neutron flux at the measurement point.

The neutron spectrum in the block is much harder in the thermal region than the spectrum in the water. It does not fit a Maxwellian distribution and consequently the concept of the neutron-gas temperature in the block does not have any special meaning. The neutron density in the region of the slowing-down spectrum experiences sharp dips at the resonances of U-238, U-235, and on the average is steeper than the $1/v^2$ distribution. Fig. 3 shows by way of illustration the spectrum of the neutrons measured at the point 1 (r = 0) of the block The water temperature corresponding to these measurements is 323° K.

The described features of the spectra were manifest also in the previously investigated lattice with spacing 5.0 cm [6].

The results of the present measurements show in addition that the energy distribution of the neutrons, both

both in the uranium and in the water, depends little on the coordinates of the measurement point. Only on the boundary between the block and the water does the energy distribution experience an appreciable change.

This can be seen from Figs. 4 and 5, which show the spectrum of the neutrons measured at the point 4 (r = 2.34 cm) near the block, and the spectrum measured at the point 6 (r = 1.30 cm) of the uranium block near its surface, respectively. Additional information concerning the measurement conditions are indicated in the figures. Neutron spectra that differ little from those given here were obtained also at other points of the uranium block and in the water.

Table 1 lists the integral characteristics of the measured spectra, which make it possible to obtain more definite quantitative information concerning the variation of the neutron spectrum over the cell. The average values listed in the table were obtained from the neutron density in the energy interval 0.25 -- 0.005 ev.

An illustrative idea of the variation of the neutron spectrum over the lattice cell is given by Fig. 6. This figure shows curves of the neutron "temperatures," calculated from the experimental values of v_m, $\overline{v}$, and $\overline{v^2}$ using the relations given by the Maxwellian distribution, and also the distribution of the temperature of the medium over the cell, measured with thermocouples. It is seen

from the figure that the neutron spectrum varies little both in the block and in the water. An appreciable change in the neutron spectrum occurs, as was already mentioned, only on the boundary between the block and the water. It must be noted that the curves of Fig. 6 in the vicinity of the uranium-water boundary are distorted because of the effect of resolution over the spatial coordinate. One must therefore expect the character of the variation of the neutron spectrum on the boundary block and in the water to be actually sharper.

The discrepancy between the curves of Fig.6 illustrates the non-Maxwellian character of the neutron spectrum. This pertains in particular to the spectrum of the neutrons in the block, which differs greatly from the Maxwellian distribution.

The main factor determining the spectrum of the thermal neutrons in the block is the absorption of the neutrons incident on the water. The following empirical relationships shows the transformation occurring in the spectrum as a result of absorption on going from the moderator to the block:

$$(v^2 n)_u = (v n)_m \cdot e^{-\Sigma_c(v) \cdot 2R}$$

Here $\Sigma_c(v)$ -- macroscopic capture cross section in uranium,

R -- radius of the block,

u and m -- indices pertaining to the uranium and the moderator, respectively.

The points on Fig. 7 show the spectrum measured at the center of the block (point 1), while the continuous line shows the spectrum calculated from the above relationship. We used in the calculations the spectrum in water, measured at the point 4 (r = 2.34). We see that in the thermal energy region the neutron spectrum calculated in this fashion, in the block, agrees well with the measured spectrum. In the region of the slowing-down spectrum, neutron scattering in uranium manifests itself noticeably along with absorption.

II. Uranium-mono isopropyl diphenyl lattice.

The characteristic features of the space-energy distribution of the neutrons in a uranium-mono isopropyl diphenyl cell are the same as in the uranium-water lattice. A comparison of the neutron spectra measured in both lattices shows that the differences observed between them are due to the relative increase in absorption, as compared with the moderator in the lattice with the mono isopropyl diphenyl. This is the consequence of the fact that the hydrogen-atom concentration in the organic moderator is

lower than in the water. A lattice with mono isopropyl dephenyl is equivalent with respect to slowing down and moderation to a water lattice with a smaller spacing.

Fig. 8 shows the neutron spectrum in the water and in mono isopropyl diphenyl, measured at point 7 of the lattice.

The temperature of the moderator was in both cases 340° K. The spectra measured at the center of the block (point 1) for the same moderator temperature are shown in Fig. 9.

As can be seen from the figures, the neutron spectrum in the uranium-mono isopropyl dephenyl lattice is harder than in the uranium-water one. The average neutron velocities for these spectra, calculated in the region 0.25 -- 0.005 ev, are equal to 3.31×10^5 cm/sec for the mono isopropyl diphenyl and 3.0×10^5 cm/sec for water.

In uranium the values are 3.62×10^5 and 3.16×10^5 cm/sec for the lattice with mono isopropyl diphenyl and water, respectively. The observed hardening of the spectrum is connected with the increase in absorption relative to moderation, $\Delta = \Sigma_c(kT)/\xi\Sigma_s(1-\theta)$ (here $\Sigma_c(kT)$ and Σ_s are the macroscopic cross sections of the moderator), owing to the increase in the coefficient of thermal utilization θ in the lattice with the mono isopropyl diphenyl [8]. For the same reason, the density of the

thermal neutrons is less in the mono isopropyl dephenyl as compared with the density of the moderated neutrons.

From a comparison and an anslysis of the results obtained, we can conclude that the difference in the chemical bond does not appreciably manifest itself on the form of the spectra in the lattice with water and with mono isopropyl dephenyl. The space-energy distribution of the neutrons in uranium-water and uranium-mono isopropyl diphenyl cells with equal ratios of hydrogen to uranium nuclei should be the same.

As already mentioned, the neutron spectrum in the heterogeneous uranium-water lattices was calculated by many authors on the basis of the Wigner-Wilkins and Wilkins models. Recently L. de Sobrino and M. Clark [3] calculated the space-energy distribution of neutrons on the basis of the Wilkins equation with account of the 1/v leakage. Their calculations are in good agreement with the results for a uranium-water lattice with spacing 5.0 cm, which we have obtained previously.

The space-energy distribution of the neutrons for the uranium-water lattice investigated in the present work was obtained by G. I. Marchuk et al. [9]. The neutron spectra were calculated with the aid of the scattering function proposed by van Hove. The dispersion of the autocorrelation function was obtained on the basis of the inter-

polation formulas of V. F. Turchin. The calculations were made in the P_3 approximation using 15-group representation of the balance equations.

Figs. 2 and 3 show the results of these calculations (continuous curves). We see that the calculations duplicate quite well the experimentally obtained spectrum in the thermal energy region. A poorer agreement is observed between the calculated spectrum and that measured in the block.

Table I

Points of measurement	I	3	5	6	4	2	7
Distance from center of rods, cm	0	0,50	0,88	I,30	2,34	2,70	3,I7
Temperature of medium at point of measurement, °K	336	338	338	337	328	32I	323
Most probable velocity $U_m \left[\frac{см}{сек} \cdot I0^5\right]$ *	3,90	3,86	3,78	3,83	3,57	3,47	3,48
$\overline{U} \left[\frac{см}{сек} \cdot I0^5\right]$	3,47	3,48	3,4I	3,36	3,02	2,94	2,95
$\overline{\frac{I}{U}} \left[\frac{сек}{см} \cdot I0^{-5}\right]$	0,330	0,33I	0,338	0,345	0,391	0,402	0,402
$\overline{U^2} \left[\frac{см2}{сек^2} \cdot I0^{I0}\right]$	I3,6	I3,7	I3,I	I2,9	I0,6	I0,I	I0,2
$T_1 = \frac{m U_m^2}{4K}$ [°K]	462	452	434	445	386	365	367
$T_2 = \frac{\pi}{4} \cdot \frac{m(\overline{U})^2}{2K}$ [°K]	575	575	553	539	434	4I3	4I4
$T_3 = \frac{2}{3} \cdot \frac{m\overline{U^2}}{2K}$ [°K]	550	554	53I	520	428	4I0	4II

* The most probable velocity corresponding to the experimentally measured distribution $v^2 \cdot n(v)$.

BIBLIOGRAPHY

1. M. S. Nelkin and E. R. Cohen, Recent Work on Neutron Thermalization. A/Conf./15/P/1839, 1958.

2. R. Greebler, W. Harker, J. Harriman, Nuclear Sci. and Eng. 6, 128 (1959).

3. L. de Sobrino and M. Clark, Nuclear Sci. and Eng. 10, 377 (1961).

4. C. G. Campbell, R. G. Freemantle, M. J. Poole, Measurements of Reactor by Spectra Time-of-Flight and Integral Methods, A/Conf./15/P/10, 1958.

5. R. S. Stone and R. E. Slovacek, Nuclear Sci. and Eng. 6, 466 (1959).

6. V. I. Mostovoĭ, V. S. Dikarev, M. B. Egiazarov, Yu. S. Saltykov. Measurement of the Neutron Spectrum in Uranium-Water Lattices. A/Conf./15/P/2152, 1958.

7. V. S. Dikarev, M. B. Egiazarov, V. I. Mostovoĭ, Yu. S. Saltykov. Procedure for the Measurement of Neutron Spectra in Moderating and Breeding Systems. Paper at Dresden Conference, 1960.

8. V. I. Mostovoĭ, V. S. Dikarev, Yu. S. Saltykov. Study of Neutron Spectra in Systems with Hydrogen-Contain-

ing Moderator. Paper delivered to Colloquium on Nuclear Physics, Balaton-Eszed , Hungary, 1960.

9. G. I. Marchuk, V. F. Turchin, V. V. Smelov, G. A. Ilyasova. Methods of Calculating the Spectrum of Slow Neutrons. Paper delivered to the conference in Brookhaven, USA, 1962.

FIGURE CAPTIONS

Figure 1. Experimental arrangement.

Figure 2. Neutron spectrum in water in a uranium water lattice with spacing of 5.5 cm. Water temperature, 323°K (beam # 7).

Figure 3. Neutron spectrum in rod in a uranium water lattice with spacing of 5.5 cm. Rod temperature at point of measurement 336°K. Water temperature 323°K (beam # 1).

Figure 4. Neutron spectrum in water in a uranium water lattice with spacing of 5.5 cm. Temperature at point of measurement 328°K (beam # 4).

Figure 5. Neutron spectrum in rod in uranium water lattice with spacing of 5.5 cm. Temperature at point of measurement 337°K. Temperature in moderator at point # 7 is 323°K (beam # 6).

Figure 6. Variation of neutron spectrum over lattice cell.

Figure 7. Neutron spectrum in rod in a uranium water lattice with spacing of 5.5 cm. Rod temperature at point of measurement is 336°K. Temperature of water at point # 7 is 323°K (beam # 1).

Figure 8. Neutron spectrum in moderator in a lattice with spacing 5.5 cm. Temperature at point of measurement is 343°K (beam # 7).

Figure 9. Neutron spectrum in rod in a lattice with spacing 5.5 cm. Temperature at point of measurement 358°K. Temperature of moderator at point # 7 343°K (beam # 1).

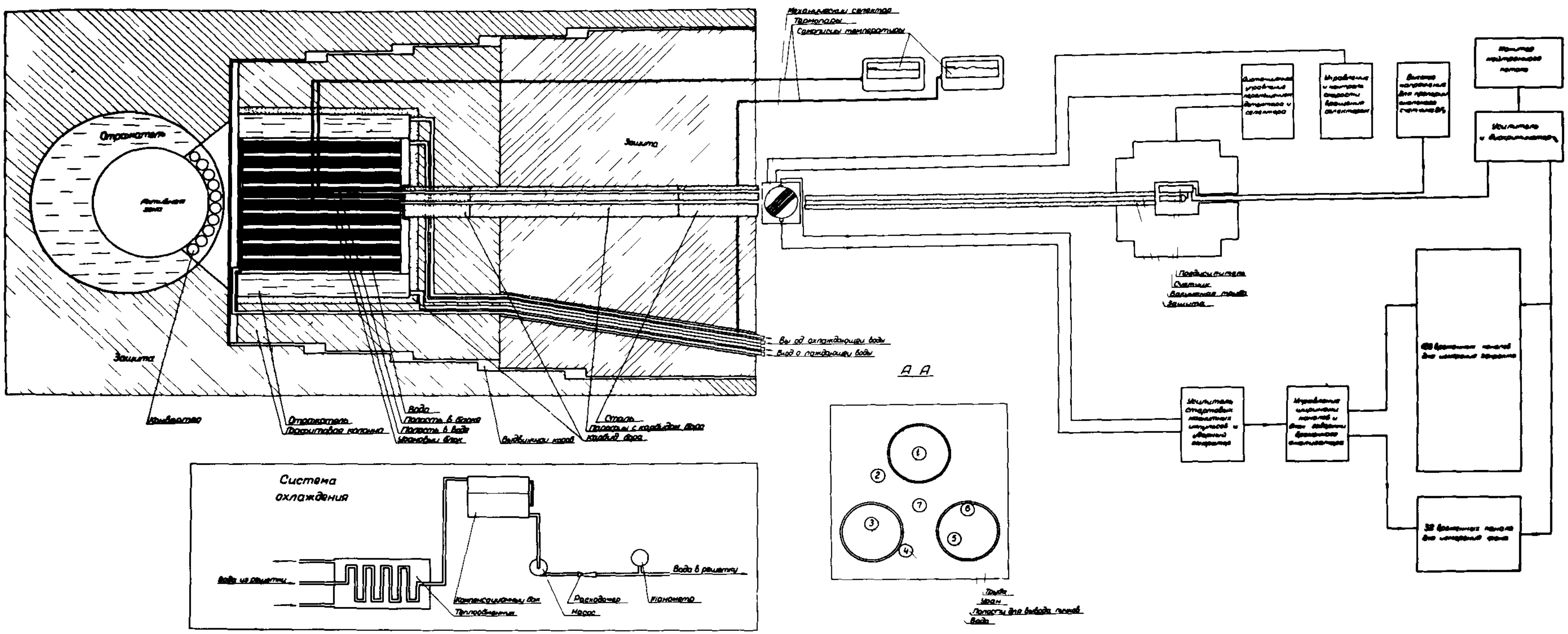
Отражатель
Защита
Механический селектор
Термопары
Самописцы температуры
Вода
Полость в блоке
Полость в воде
Урановый блок
Графитовая колонна
Выдвижной короб
Сталь
Карбид бора
Вход охлаждающей воды
А А
Предусилитель
Счетчик
Вакуумная труба
Система
охлаждения
Вода из решетки
Вода в решетку
Компенсационный бак
Теплообменник
Расходомер
Насос
Манометр
Труба
Уран
Вода
1
2
3
4
5
6
7

Рис. 1

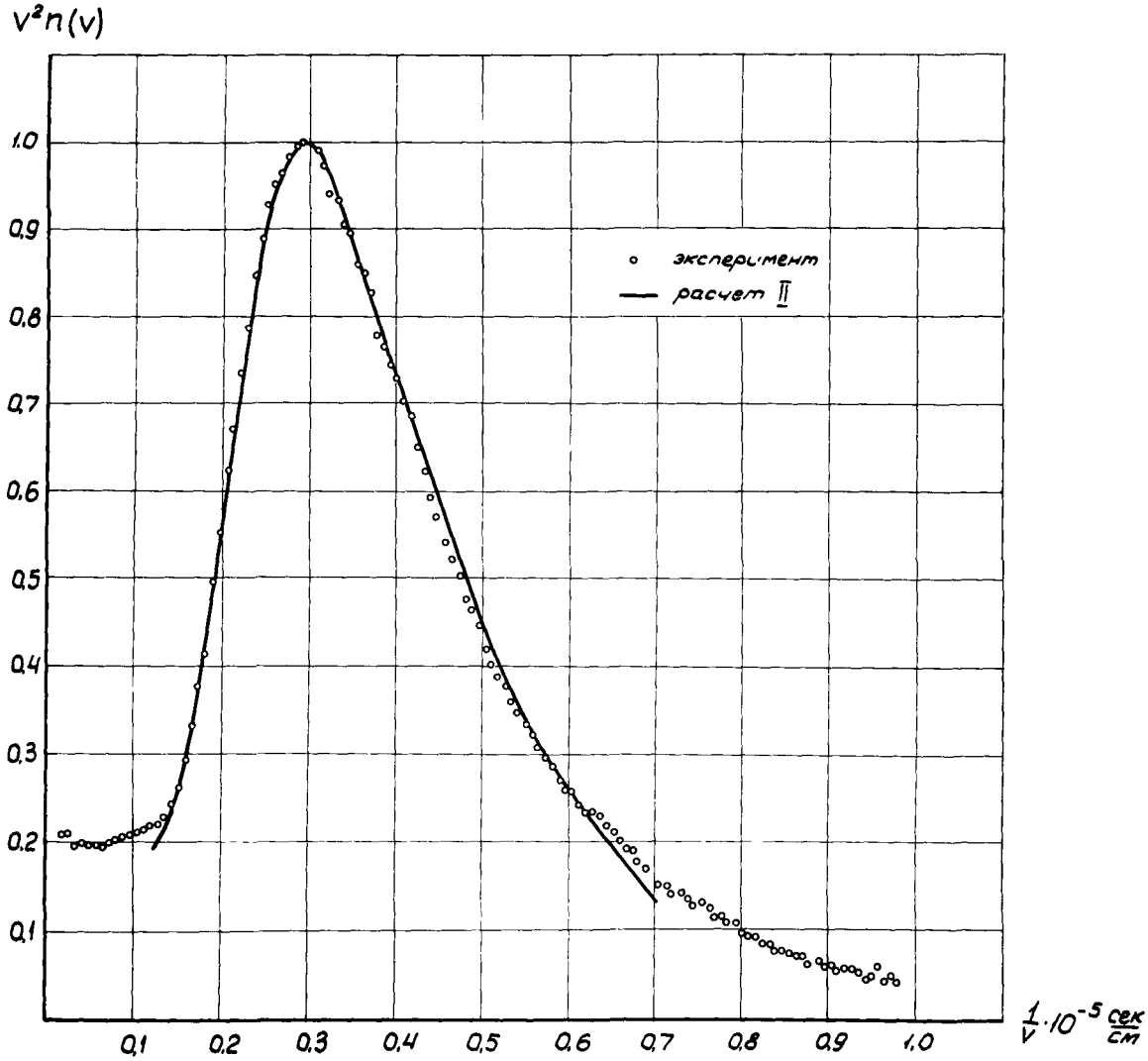

Пучок 7

Спектр нейтронов в воде в уран-водной решетке с шагом 5,5 см. Температура воды 323°К.

Рис. 2

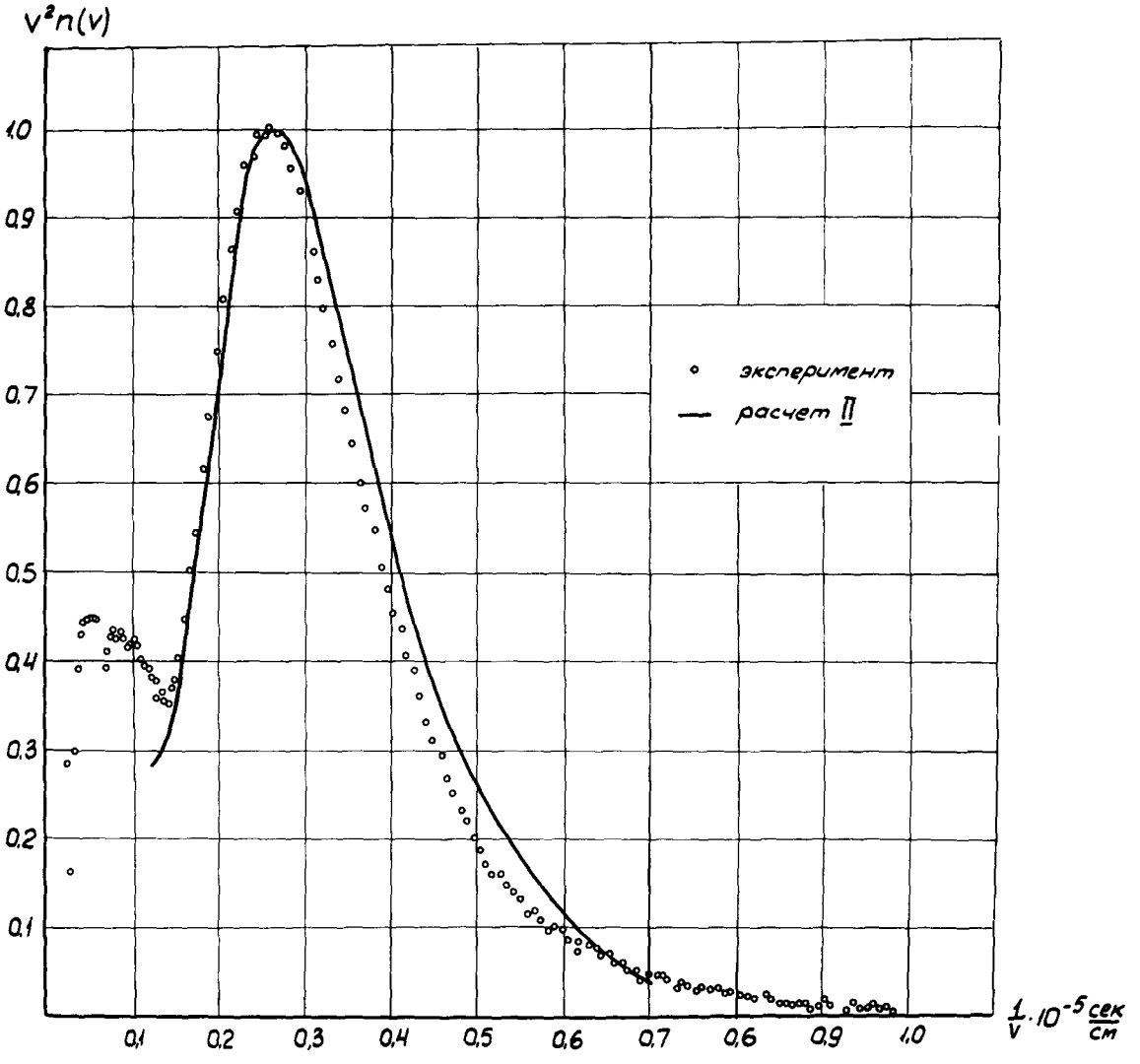

Пучок 1

Спектр нейтронов в блоке в уран-водной решетке с шагом 5,5см.
Температура блока в точке измерения 336°К.
Температура воды в точке №7 323°К.

Рис. 3

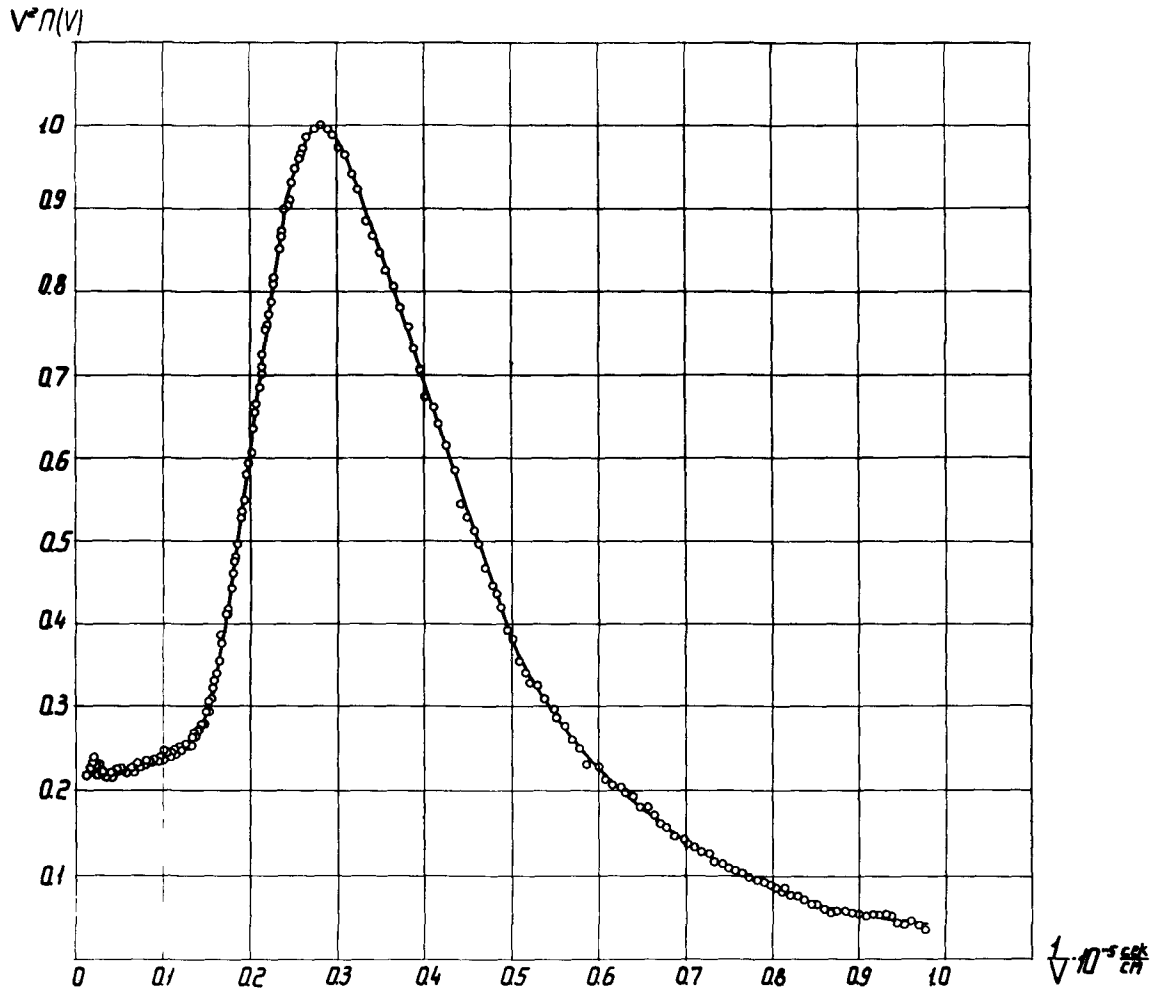

Пучок 4

Спектр нейтронов в воде в уран-водной решетке с шагом 5,5 см.
Температура среды в точке измерения 328°К.
Рис 4.

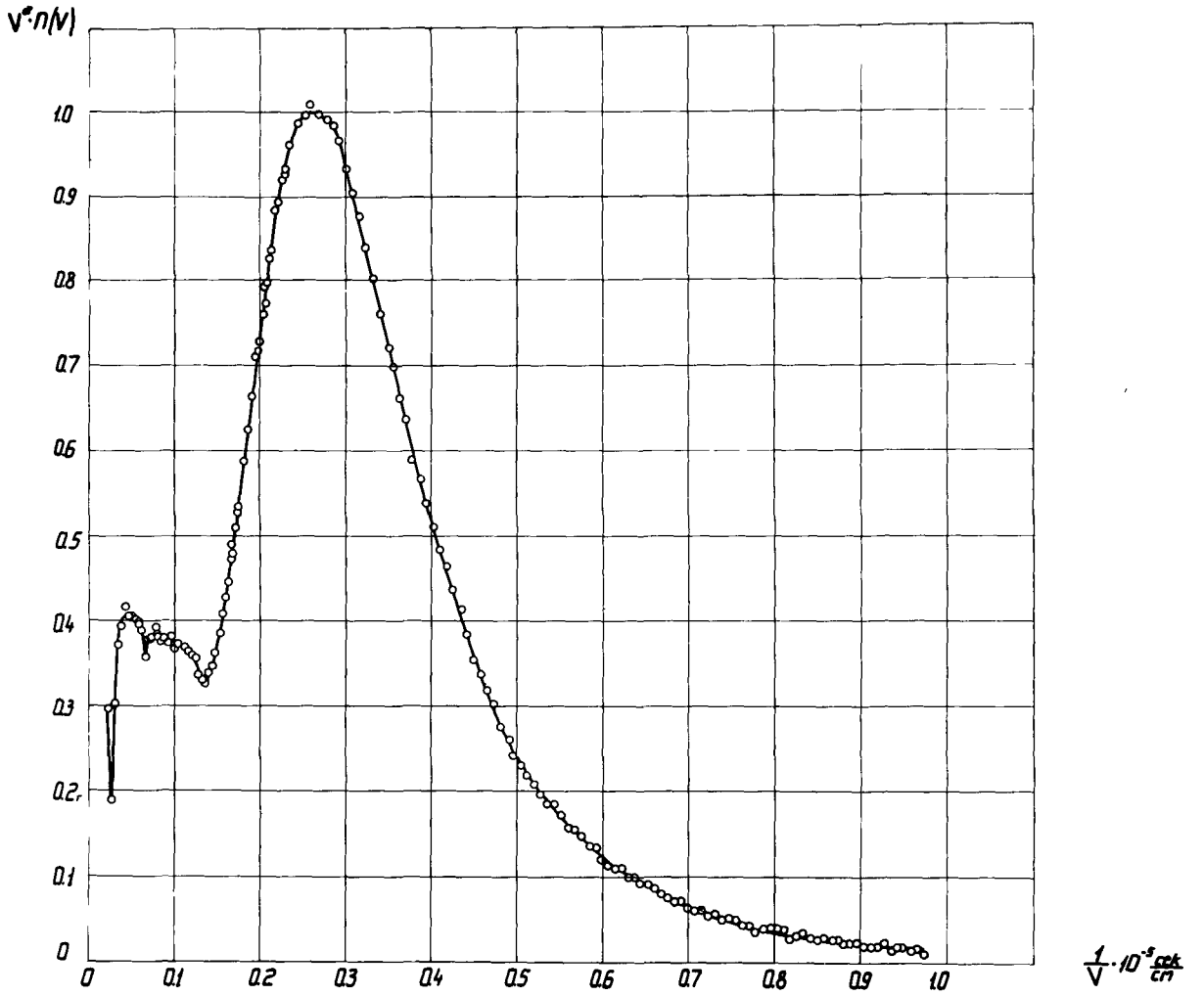

Пучок 6

Спектр нейтронов в блоке в уран-водной решетке с шагом 5,5 см.

Температура среды в точке измерения 337°К

Температура замедлителя в точке №7 323°К

Рис 5

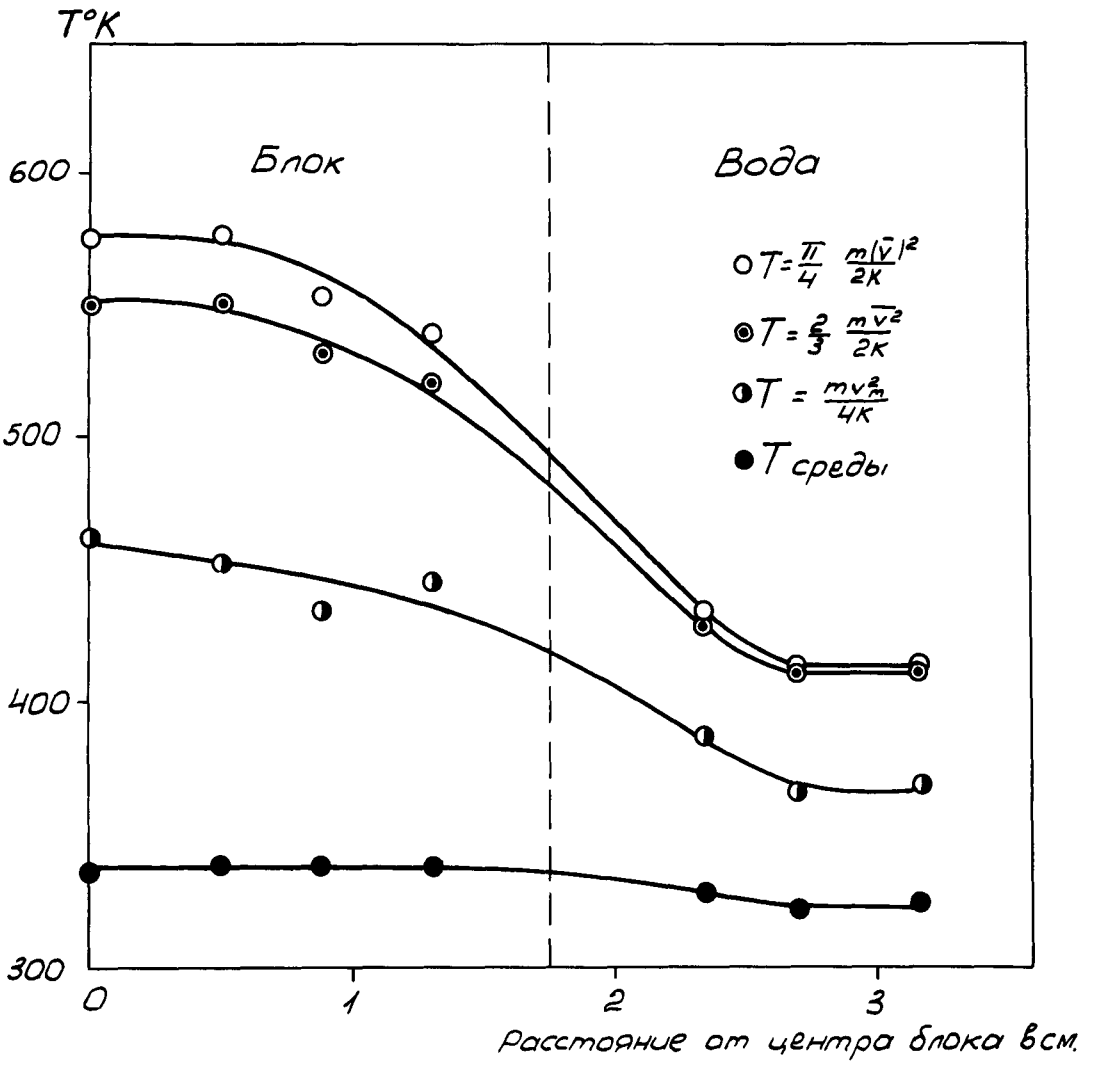
T°K
600
500
400
300
Блок
Вода
$T=\frac{\pi}{4}\frac{m|\bar{v}|^2}{2K}$
$T=\frac{2}{3}\frac{m\bar{v}^2}{2K}$
$T=\frac{mv_m^2}{4K}$
T среды
0
1
2
3
Расстояние от центра блока в см.

Рис. 6

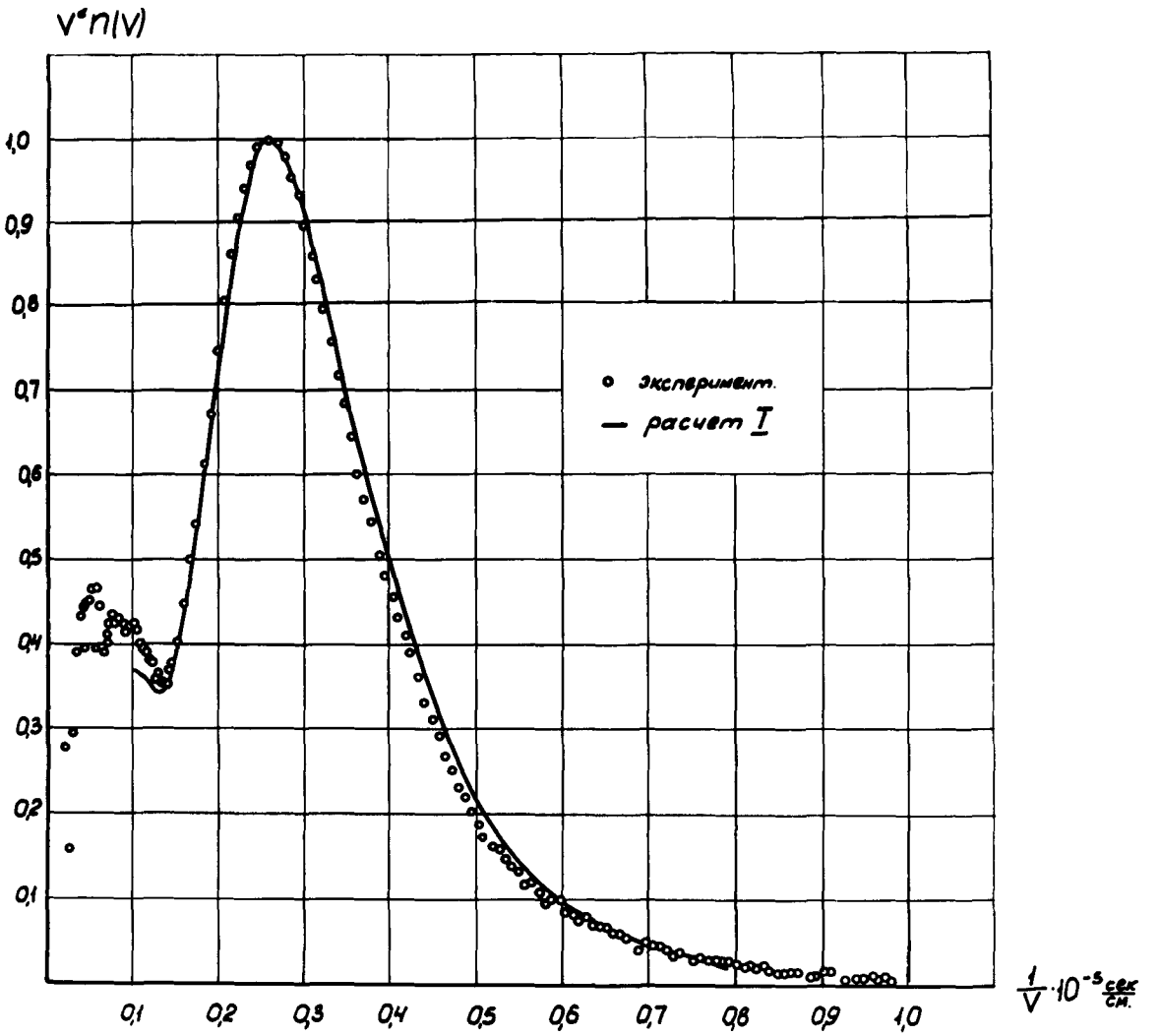

Пучок 1

Спектр нейтронов в блоке в уран-водной решетке с шагом 5,5 см

Температура блока в точке измерения - 336° К

Температура воды в точке № 7 - 323° К

Рис. 7

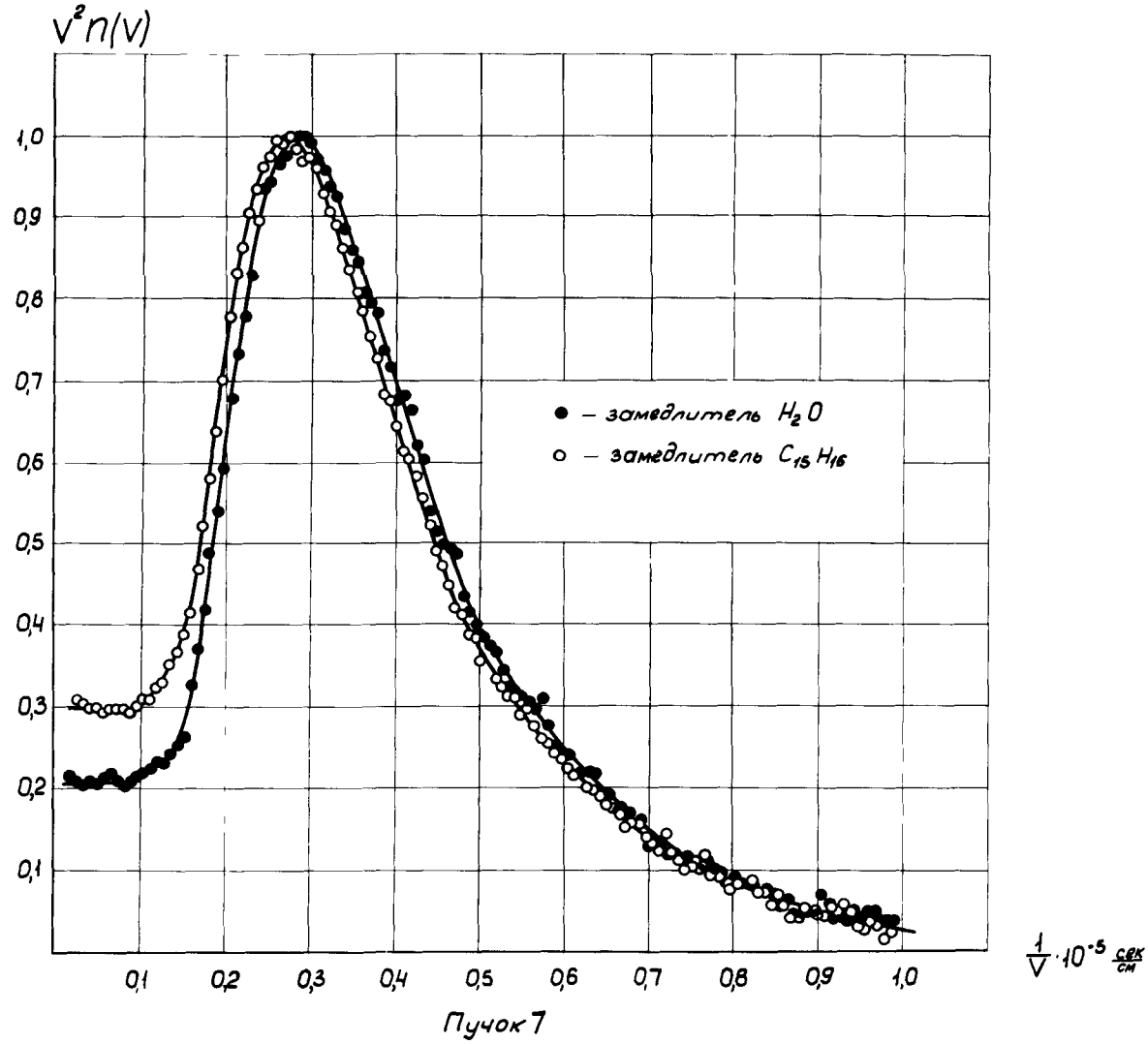

Пучок 7

Спектр нейтронов в замедлителе в решетке с шагом 5,5 см.
Температура среды в точке измерения 343°К.

Рис. 8

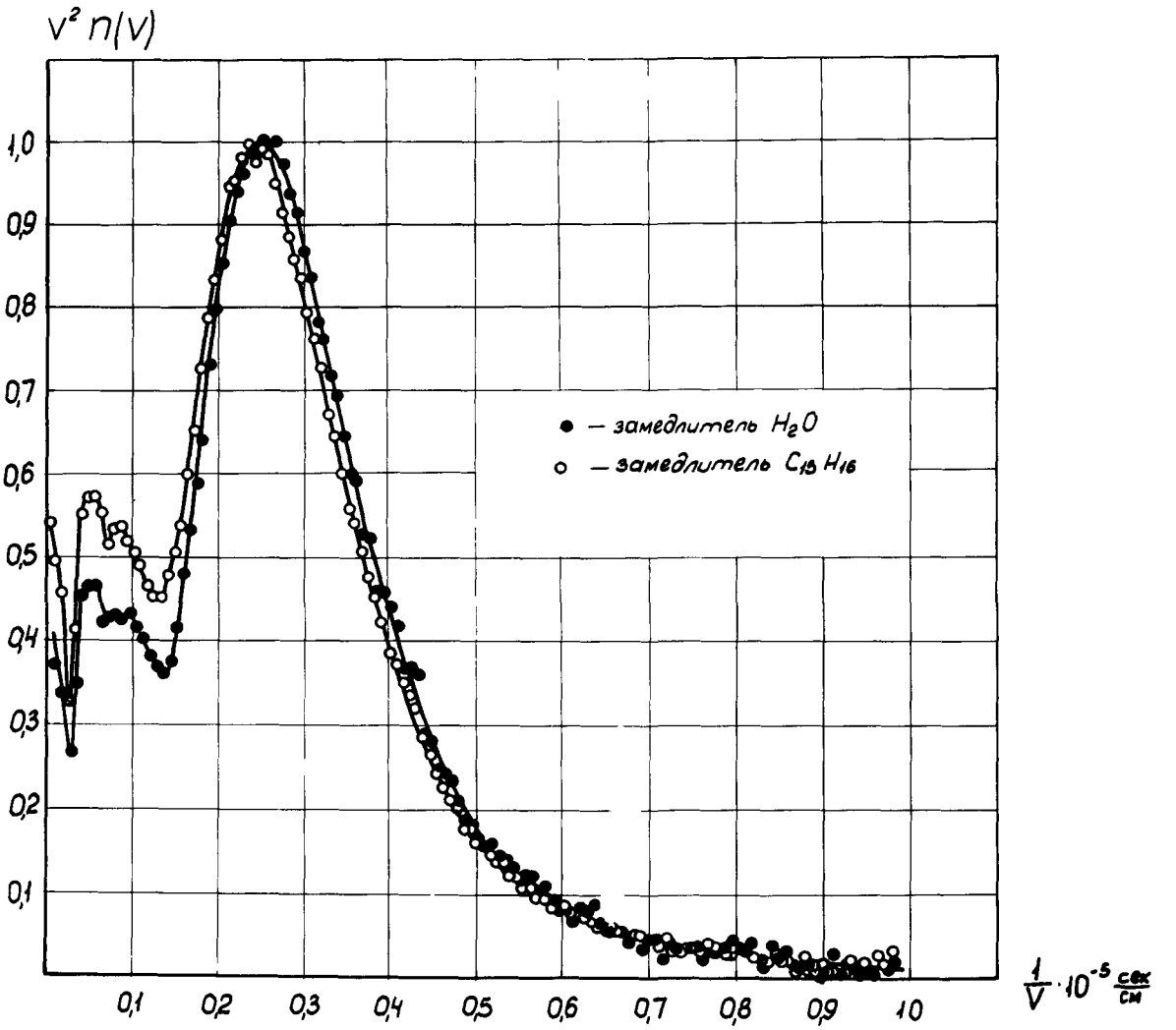

Пучок 1

Спектр нейтронов в блоке в решетке с шагом 5,5 см.
Температура среды в точке измерения 358 °K
Температура замедлителя в точке №7 343 °K

Рис. 9

NEUTRON SPECTRA IN LATTICES AND INFINITE MEDIA

B. Theoretical Aspects

Thermal Neutron Spectra in Heterogeneous Assemblies*

Henry C. Honeck
Brookhaven National Laboratory

*This work was performed under the auspices of the United States Atomic Energy Commission.

Introduction

We will briefly discuss in this review the techniques used to compute thermal neutron spectra in heterogeneous media. Equations will not be derived nor, in most cases, will they even be stated. Rather, we will try to describe in words the approximations that lead to each method and give an over-all picture of the methods that are actually used and their relationship to one another. We will frequently use figures from the contributed papers to illustrate a point; the details of the calculation or experiment represented in the figure can be found in the original papers.

Theoretical Techniques for Computing Spectra

The time independent transport equation describes the steady state behavior of neutrons in a medium in terms of the flux as a function of position $\underline{r}$, direction $\underline{\Omega}$, and energy E. This equation is too complex to be solved exactly and it is necessary to make simplifying approximations to obtain tractable equations. These approximations are made in the:

1) description of the angular variation of the flux,

2) energy transfer kernel and cross sections,

3) description of the angular variation of the scattering process,

4) description of the geometry, and

5) numerical methods used.

It is generally necessary to make approximations in many of these items and the errors introduced are frequently of opposite sign and tend to cancel; the theory then gives apparently accurate results. This cancellation of errors should be kept in mind when one is comparing theory and experiment. Indeed it is often more appropriate to ask the question "Why does this approximate theory give good results?" than to ask "Why does this theory not correctly predict the experimental results?"

Various approximate methods for describing the angular variation of the flux are shown schematically in Figure 1. Computer codes which use these methods are given in parentheses at the bottom of each box. We start with the transport equation written either as a differential equation or, equivalently, as an integral equation. The P_n [used by Gelbard (1)], double P_n, and discrete ordinate equations are obtained from the differential form by representing the angular variation of the flux by an n^{th} order polynomial. The S_n equations used by Leslie (2) and Macdougall (3) are obtained by representing the angular variation of the flux by n linear segments. Both S_n and P_n methods lead to coupled first order differential equations in the spatial variables. Computer storage requirements vary linearly with the size of the region under investigation and the number of angular intervals or polynomials.

A second approach starts from the integral transport equation, many

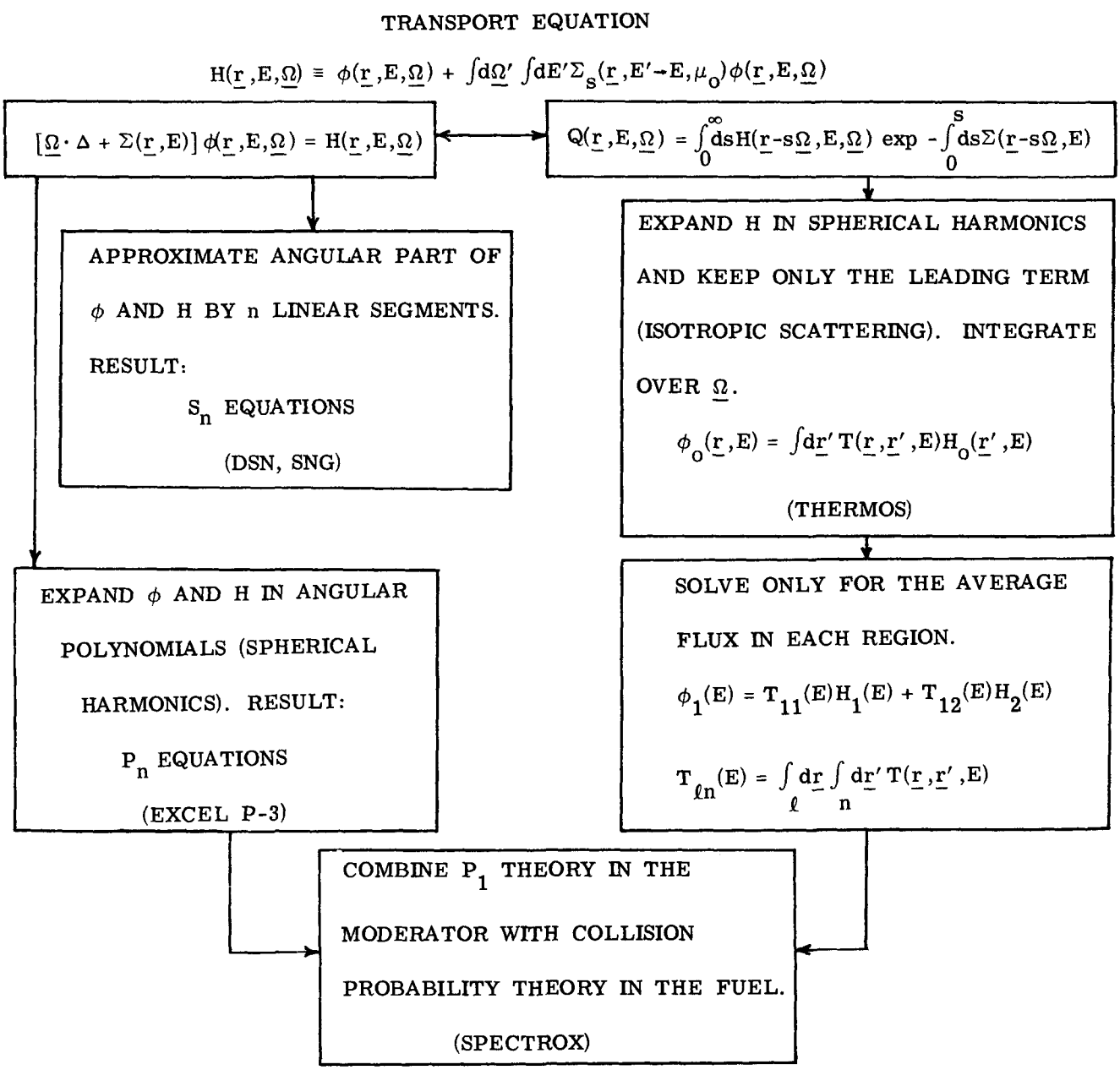
TRANSPORT EQUATION
$H(\underline{r},E,\underline{\Omega}) \equiv \phi(\underline{r},E,\underline{\Omega}) + \int d\underline{\Omega}' \int dE' \Sigma_s(\underline{r},E' \to E,\mu_o)\phi(\underline{r},E,\underline{\Omega})$
$[\underline{\Omega}\cdot\Delta + \Sigma(\underline{r},E)]\,\phi(\underline{r},E,\underline{\Omega}) = H(\underline{r},E,\underline{\Omega})$
$Q(\underline{r},E,\underline{\Omega}) = \int_0^\infty ds H(\underline{r}-s\underline{\Omega},E,\underline{\Omega}) \exp -\int_0^s ds\Sigma(\underline{r}-s\underline{\Omega},E)$
APPROXIMATE ANGULAR PART OF ϕ AND H BY n LINEAR SEGMENTS. RESULT:
S_n EQUATIONS
(DSN, SNG)
EXPAND H IN SPHERICAL HARMONICS AND KEEP ONLY THE LEADING TERM (ISOTROPIC SCATTERING). INTEGRATE OVER $\underline{\Omega}$.
$\phi_o(\underline{r},E) = \int d\underline{r}'\, T(\underline{r},\underline{r}',E) H_o(\underline{r}',E)$
(THERMOS)
EXPAND ϕ AND H IN ANGULAR POLYNOMIALS (SPHERICAL HARMONICS). RESULT:
P_n EQUATIONS
(EXCEL P-3)
SOLVE ONLY FOR THE AVERAGE FLUX IN EACH REGION.
$\phi_1(E) = T_{11}(E)H_1(E) + T_{12}(E)H_2(E)$
$T_{\ell n}(E) = \int_\ell d\underline{r} \int_n d\underline{r}'\, T(\underline{r},\underline{r}',E)$
COMBINE P_1 THEORY IN THE MODERATOR WITH COLLISION PROBABILITY THEORY IN THE FUEL.
(SPECTROX)

Figure 1.

forms of which are discussed by Dalton (4). In this approach the scattering process is assumed to be nearly isotropic and the angular variation of the flux is treated (within numerical approximations) exactly. This method, with isotropic scattering, is used by P. Brown et al. (5) and H. Brown et al. (6), and Honeck (22). Computer storage requirements vary as the square of the size of the spatial region investigated and the number of angular moments used to represent the scattering kernel. If we further restrict ourselves to computing only the average flux in each of two regions, as in a lattice, we obtain the first flight collision probability method used with great success for computing fast fission and resonance escape probabilities in lattices.

If the medium is weakly absorbing, is large in extent, and has a smooth variation of properties, the low order P_n and S_n methods are most applicable. If the medium is highly absorbing, is small in extent, has sharp material discontinuities, and has nearly isotropic scattering, the integral transport theory is most applicable. If one must be able to handle all situations, a high order S_n ($\sim S_8$) method appears to give the most accuracy for the least work. From these arguments it is reasonable to combine P_1 theory in a large graphite or D_2O moderator of a cell with collision probabilities for the fuel regions as reported by Leslie (2). Vaughan (7) and Häfele (8) use diffusion theory and the heavy gas scattering model in the moderator of a cell with

an arbitrary boundary condition [i.e., $\frac{1}{\phi}\frac{d\phi}{dx} = \alpha(E)$] at the fuel surface. Vaughan obtains an analytical expression for ηf when $\alpha(E) = 1$; other forms for $\alpha(E)$ are then treated as perturbations from $\alpha(E) = 1$. Häfele treats the fuel rod as a line absorber and uses Meetz's method (23). The advantage of this approach is that the variation of the spectrum across a finite reactor can be conveniently computed.

Various methods for treating the scattering operator are shown schematically in Figure 2. The numbers following the names of the computer codes are the number of energy groups used. Three techniques have been used to represent the scattering operator; multigroup, factorization of the kernel, and representation by a second order differential equation. If the full scattering kernel is used, the flux can be expanded in orthogonal functions; expansion in delta functions (or step type functions) leads to the multigroup equations. One can also expand in functions which, though not orthogonal, represent much of the known behavior of the flux [Ott et al. (20) and Calame et al. (24)]. Each of the above methods leads to a set of coupled linear equations which are to be solved numerically.

A second method is to represent the scattering operator as a second order differential equation. Klahr (9) suggests a straightforward expansion of the flux in a Taylor series and truncation beyond the second order term.

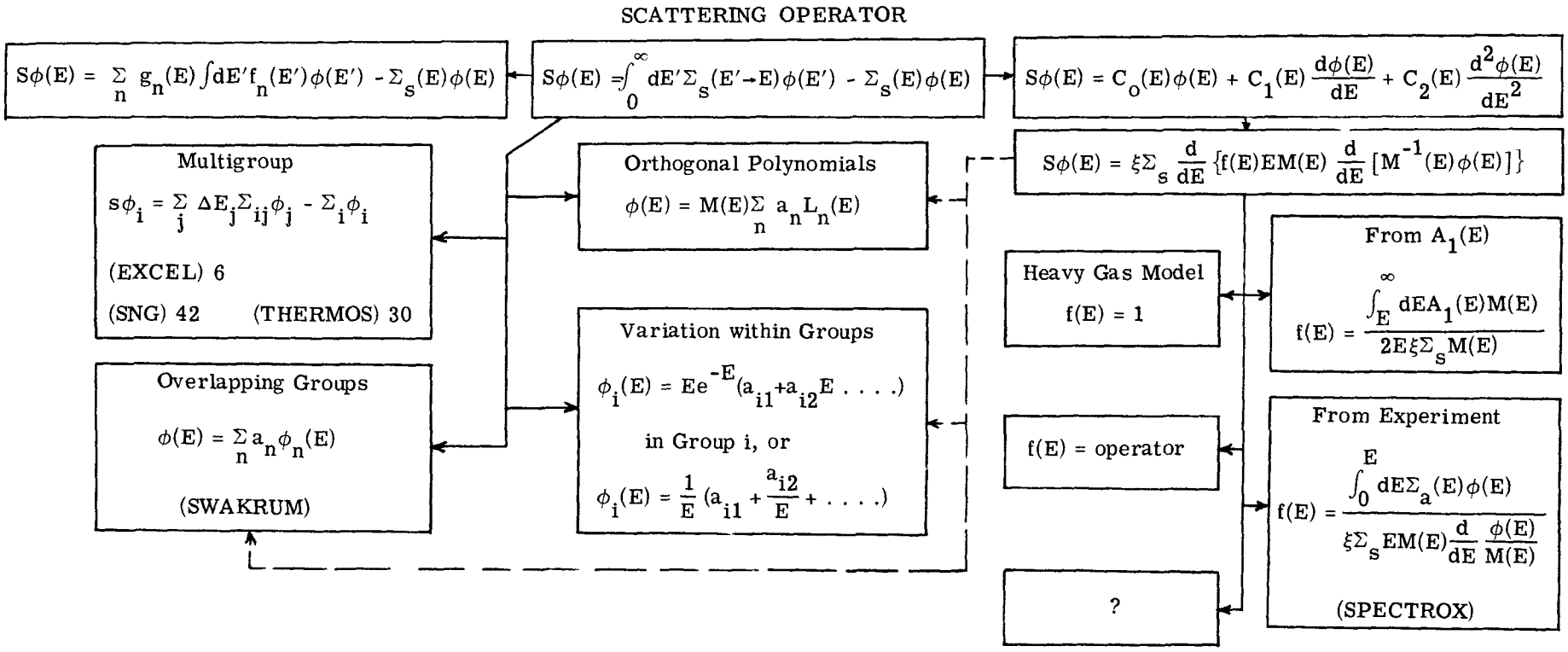
SCATTERING OPERATOR
$S\phi(E) = \sum_n g_n(E)\int dE' f_n(E')\phi(E') - \Sigma_s(E)\phi(E)$
$S\phi(E) = \int_0^\infty dE'\Sigma_s(E'\to E)\phi(E') - \Sigma_s(E)\phi(E)$
$S\phi(E) = C_o(E)\phi(E) + C_1(E)\frac{d\phi(E)}{dE} + C_2(E)\frac{d^2\phi(E)}{dE^2}$
$S\phi(E) = \xi\Sigma_s \frac{d}{dE}\{f(E)EM(E)\frac{d}{dE}[M^{-1}(E)\phi(E)]\}$
Multigroup
$s\phi_i = \sum_j \Delta E_j \Sigma_{ij}\phi_j - \Sigma_i\phi_i$
(EXCEL) 6
(SNG) 42 (THERMOS) 30
Orthogonal Polynomials
$\phi(E) = M(E)\sum_n a_n L_n(E)$
Overlapping Groups
$\phi(E) = \sum_n a_n\phi_n(E)$
(SWAKRUM)
Variation within Groups
$\phi_i(E) = Ee^{-E}(a_{i1}+a_{i2}E \ldots .)$
in Group i, or
$\phi_i(E) = \frac{1}{E}(a_{i1} + \frac{a_{i2}}{E} + \ldots .)$
Heavy Gas Model
$f(E) = 1$
From $A_1(E)$
$f(E) = \frac{\int_E^\infty dEA_1(E)M(E)}{2E\xi\Sigma_s M(E)}$
$f(E) =$ operator
From Experiment
$f(E) = \frac{\int_0^E dE\Sigma_a(E)\phi(E)}{\xi\Sigma_s EM(E)\frac{d}{dE}\frac{\phi(E)}{M(E)}}$
(SPECTROX)
?

Figure 2.

The resulting equation, however, does not satisfy detailed balance and will be inaccurate for systems near equilibrium; since it contains only limited information about the scattering process, it will also be inaccurate for highly absorbing systems. The most general second order differential equation which satisfies detailed balance and neutron conservation contains one arbitrary function f(E), often called the Horowitz function. Setting f(E) = 1 leads to the usual heavy gas equation used by Häfele (8), Vaughan (7), and Takahashi (10); Leslie (2) determines f(E) from a measured spectrum; Corngold (11) bases the choice of f(E) on the first energy transfer moment $A_1(E)$; Schaefer (12) uses a combination of $A_1(E)$ at low energies and Corngold's asymptotic expansion for the flux at high energies to deduce f(E); and finally Cadilhac et al. (13) treat f(E) as an operator and obtain a second order differential equation for the slowing down density which contains two arbitrary functions. Schaefer's choice of f(E) for graphite is shown in Figure 3.

An example of the use of the heavy gas equation, free gas equation and expansion in orthogonal polynomials is given by Takahashi (10) for the case of an infinite non-absorbing homogeneous medium of two materials with different temperatures. The heavy gas equation predicts a Maxwellian distribution at an average temperature T_{eff} while the free gas equation predicts a softer non-Maxwellian spectrum (Figure 4).

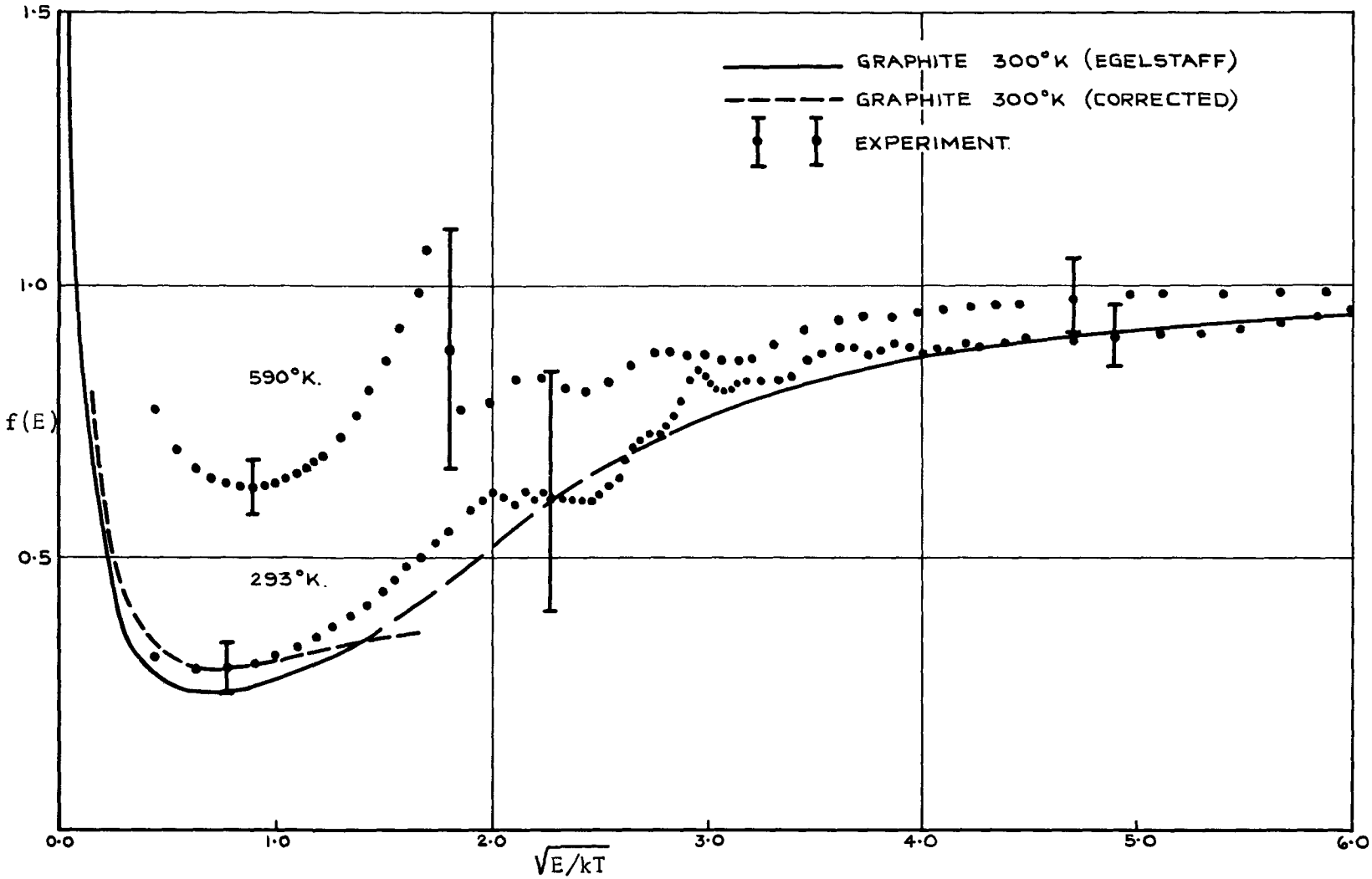

Figure 3. f(E) for graphite. (from reference 12)

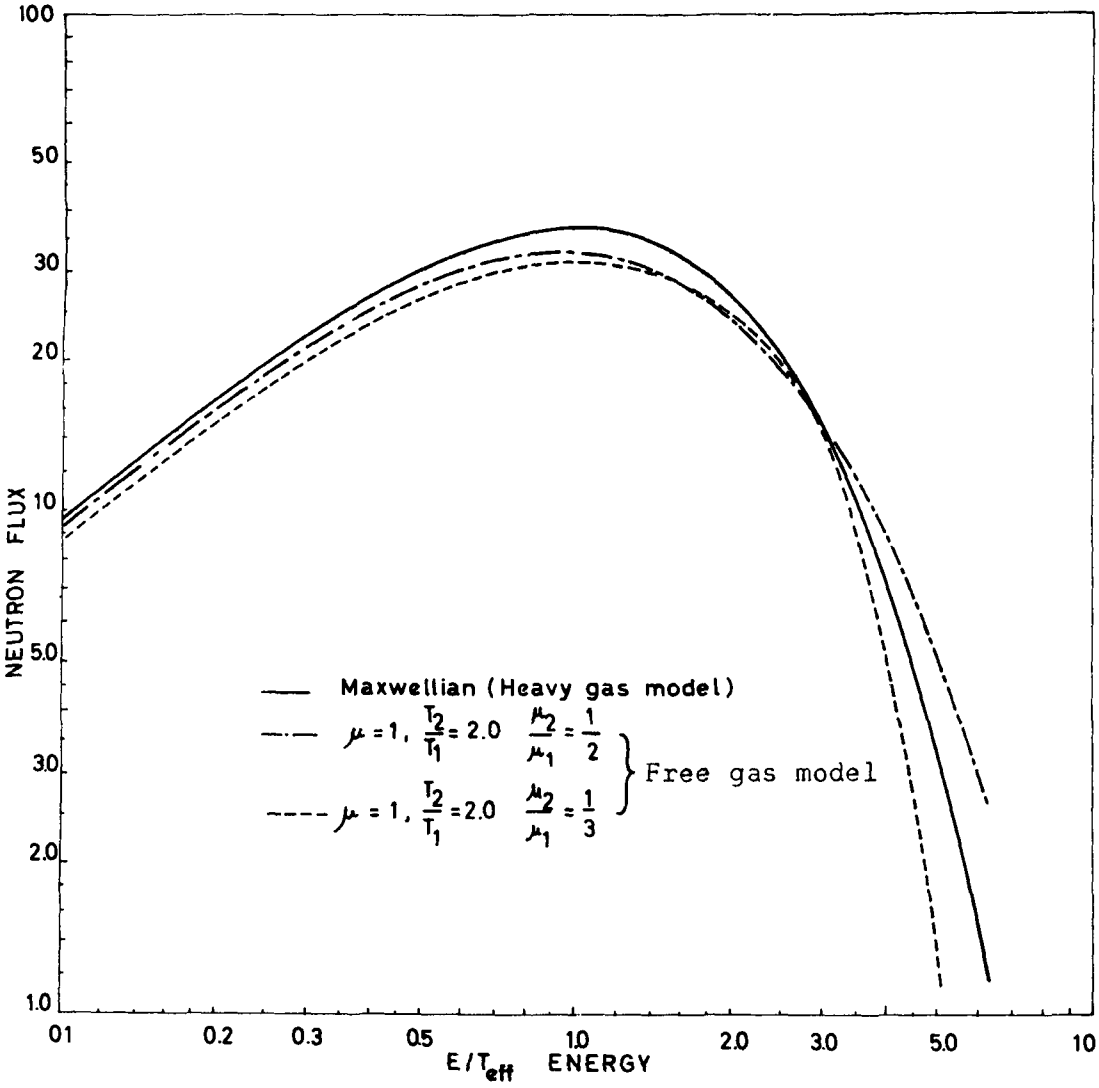

Figure 4. Neutron spectrum in a medium with two temperatures. (from reference 10)

A third method, in which the scattering kernel is approximated by a sum of degenerate scattering kernels (25, 26), is relatively new and unexplored but shows great promise.

The choice of a method for representing the scattering operator depends strongly on the application. The information contained in f(E) is adequate for describing the gross distortions of the spectrum from Maxwellian but certainly cannot provide detailed information about the flux in the vicinity of a resonance absorber. The method of Cadilhac may alleviate this difficulty. The representation of the flux by orthogonal polynomials in energy or velocity is useful only if the flux has an exponential behavior at high energies. The multigroup methods using almost the full information contained in the scattering kernel appear to be the best over-all methods.

The multigroup method implies a high energy cutoff for the thermal group, above which the flux is known. It is necessary to compute the slowing down source, $Q(\underline{r},E)$, given in Figure 5. It is customary to assume that Q can be approximated by a function of $\underline{r}$ (i.e., an indium foil activation distribution) times a function of E obtained by using a 1/E flux and a free gas scattering law. Macdougall (3) shows in Figure 6 that even with a cutoff at 1.5 ev the use of the free gas law can lead to a 10 to 20% error in the flux between 1.0 and 1.5 ev, the region of the Pu^{240} resonance. Both Häfele (8)

EPITHERMAL NEUTRON DENSITY, $N(v) \sim \phi(E)$,

AND THE SLOWING DOWN SOURCE

$$Q(E) = \int_{E_c}^{\infty} dE' \Sigma_s(E' \to E) \phi(E')$$

$E_s >> E$	$E_s << E$
Kelber and Min: $N(v) = \frac{1}{v^2}(v/v+\Gamma)^{\frac{2}{\xi}+1}$	Kostin: $N(v) = v^2 e^{-v^2}\left[1 + \frac{a_1}{v} + \frac{a_2}{v^2} + \ldots\right]$
	$a_1 = \Gamma/\mu$; $\frac{a_2}{a_1} = \frac{\Gamma}{\frac{2}{1-\lambda^2}\ln\frac{1}{\lambda} - 1}$
	$a_3 = \frac{\Gamma}{\mu}\frac{\lambda}{2\lambda+4}\left[\frac{T_{eff}}{T} + 2\Gamma a_2\right]$
Corngold: $N(v) = \frac{1}{v^2}\left[1 + \frac{c_1}{v} + \frac{c_2}{v^2} \ldots\right]$	
$c_1 = c_1(\Delta, M)$	$\Gamma = \frac{v\Sigma_a(v)}{\Sigma_s}$; $\mu = \frac{1}{M}$
$c_2 = c_2(\Delta, M, \frac{T_{eff}}{T})$	$\lambda = \frac{1-\mu}{1+\mu} = \frac{M-1}{M+1}$

Figure 5.

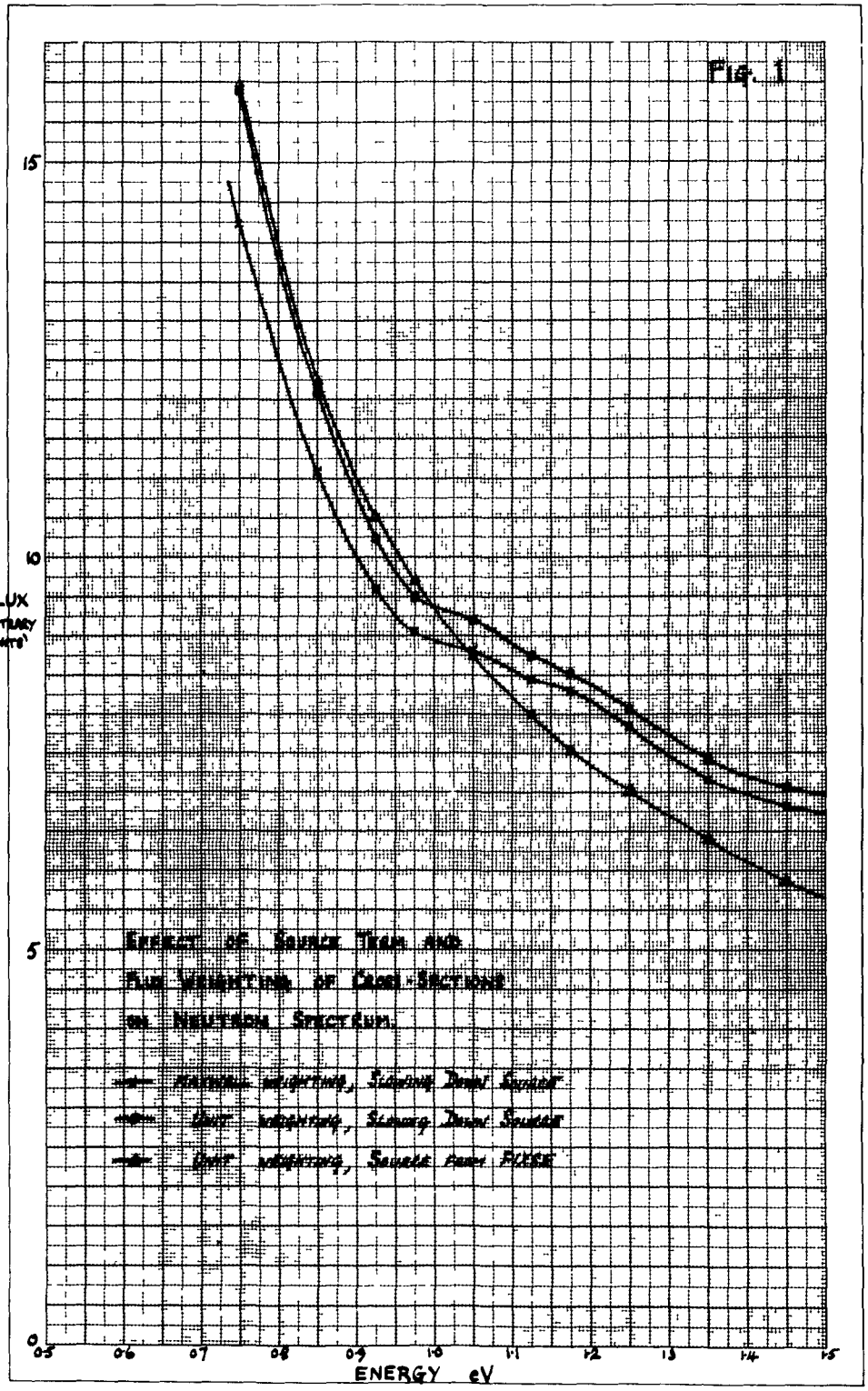

Figure 6. Joining region of a graphite spectrum. (from reference 3)

(Figure 7), and H. Brown (6) show that the epithermal flux is not spatially uniform in large D_2O and graphite cells. The asymptotic high energy behavior of the flux has been investigated by Corngold (21) and Kelber (14) for the case of a very high energy source, and by Kostin (15) for a very low energy source (Figure 5). An illustration of these methods and of the non-1/E behavior of the flux is given by Shapiro (16) in Figure 8 where he uses the Corngold expansion (with a Maxwellian subtracted off) to compute the epithermal bump in the flux in a graphite cell. Pearce (17) notes that this bump has a radial dependence and disappears in the fuel rod; the concept of a Maxwellian distribution in the fuel rod and the subsequent definition of a bump is, however, somewhat artificial. The point to these statements is that accurate methods are available for computing the slowing down source and that the use of approximations (such as spatially flat sources, 1/E flux, and free gas scattering) can cause significant errors.

The angular variation of the scattering process can be directly included in the P_n and S_n methods, but is difficult to include in the integral transport theory methods. It is only recently that scattering models for graphite and heavy water have been developed that are sophisticated enough to predict the anisotropic scattering. Some calculations with anisotropic scattering for water have been done by Gelbard (1) and Honeck (22). It

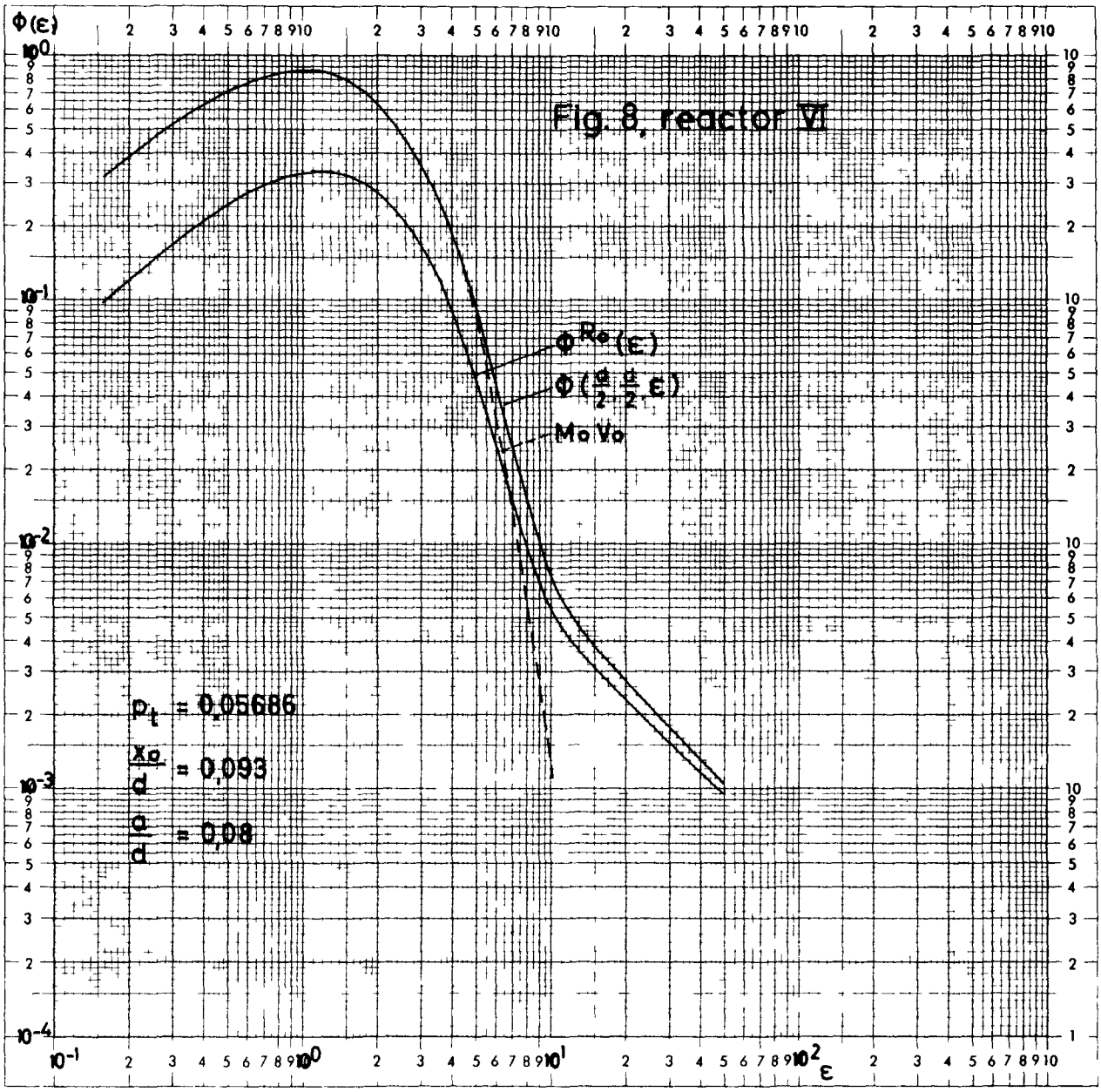

Figure 7. Spectrum in a D_2O lattice. (from reference 8)

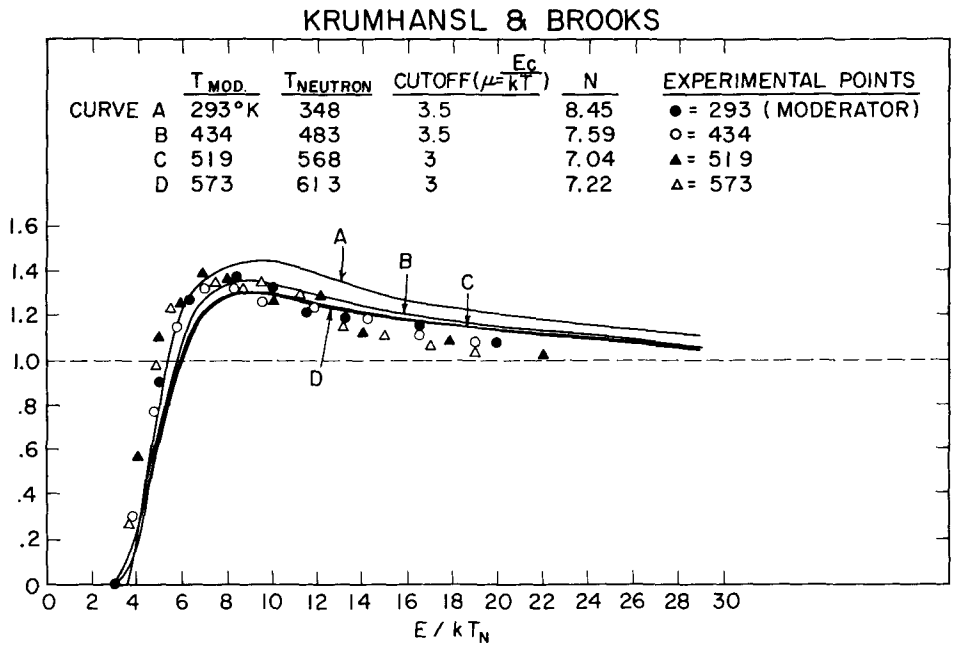

Figure 8. Joining region (with a Maxwellian subtracted) of graphite spectra at various temperatures. (from reference 16)

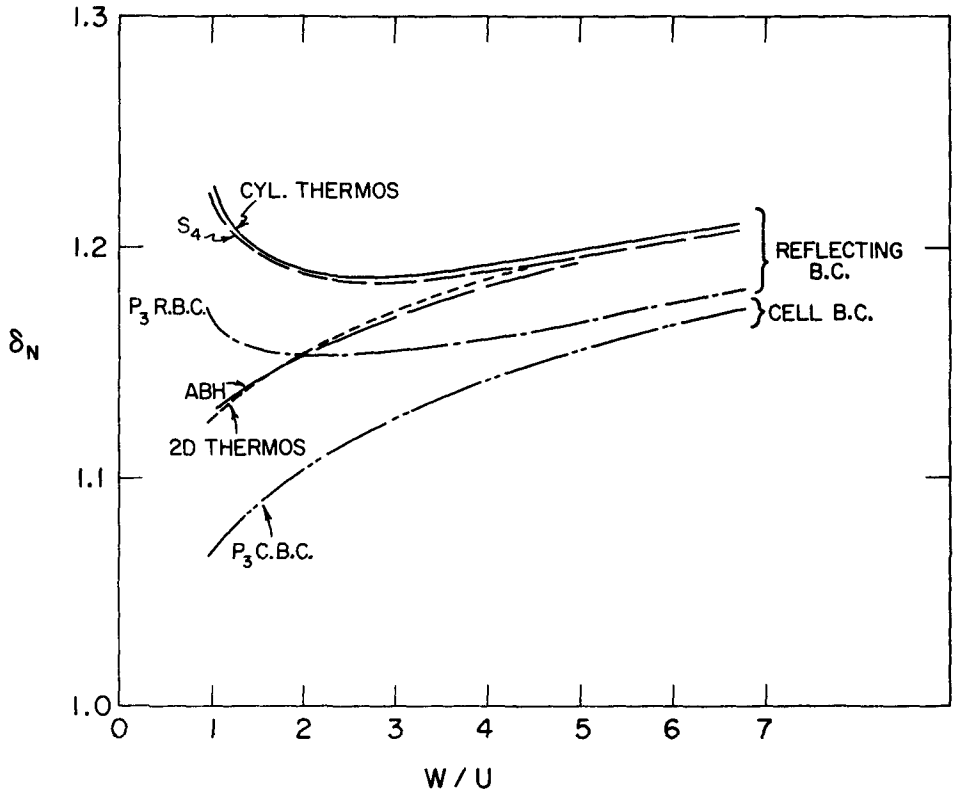

Figure 9. Neutron density disadvantage factors for the 0.250" diameter, 1.00% enriched uranium metal rod lattices. (from reference 22)

appears that, for water, only P_1 scattering need be included and that this can be accurately treated by a Selengut-Goertzel approximation or by defining an effective isotropic scattering kernel (transport correction). More work needs to be done to determine good anisotropic scattering corrections for cell calculations and leakage calculations.

No reactors and few experiments can be described by one dimensional slab geometry. Most reactors consist of fuel rods in a rectangular or square array with moderator in between the rods. To avoid lengthy two dimensional cell calculations one replaces the actual cell with an equivalent cylindrical cell (Wigner-Seitz cell). The circular outer boundary reflects neutrons back into the cell. Honeck (22) has found that this assumption is poor when the moderator thickness is less than about one mean free path (Figure 9). The THERMOS calculations shown in Figure 9 were multigroup calculations. The other calculations are one group calculations with spectrum averaged cross sections. The moderator in most graphite and D_2O cells is many mean free paths thick and the cylindrical cell approximation should be accurate.

Finally, we should remark about numerical accuracy. Experimental results always contain an estimate of uncertainty, yet theorists state their results to many significant figures without any indication of how accurately

the calculation was done (the author is no exception). In many instances, the discrepancy between theory and experiment is only a few percent and certainly the numerical inaccuracy should be investigated and eliminated before attempts are made to improve the physics in the theory or the experimental procedures.

Some Experimental Foil Activation Results

In this section we will describe and briefly comment on the results of foil activation experiments presented at this conference. Foil activations accurately measure the spatial distribution of the flux and, if various types of foils are used, spectral moments of the flux. Kelber and Min (14) compare spectra computed from the Wilkins (heavy gas) equation and the Wigner-Wilkins (gas) equation (Figure 10) and show that Yb^{168} activations would be 14% different for the two spectra while Lu^{176}, Pu^{239}, and U^{235} activations would be only a few percent different. They conclude that Yb^{168} activation is sensitive to details of the scattering kernel while Lu, Pu, and U are insensitive to the fine details of the kernel.

Korpium, Renz, and Springer (18) have measured the Lu/Eu activation ratio as a function of distance from a cadmium disk in water (Figure 11). This ratio, normalized to unity far from the plate, is a direct measure of the change in spectrum near a black (vacuum) boundary. Parkinson and

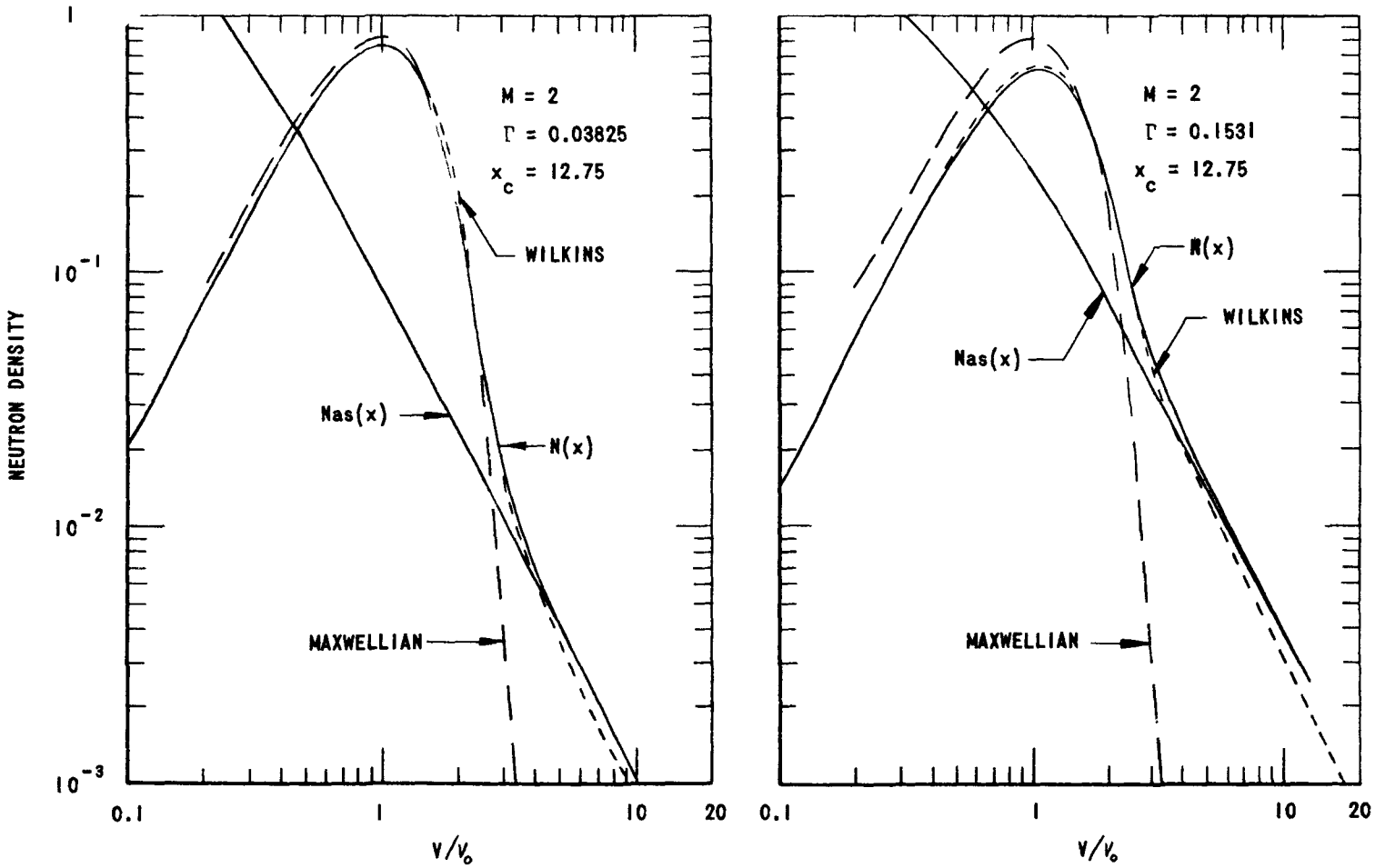

Figure 10. Comparison of spectra computed from the free gas model and heavy gas model. (from reference 14)

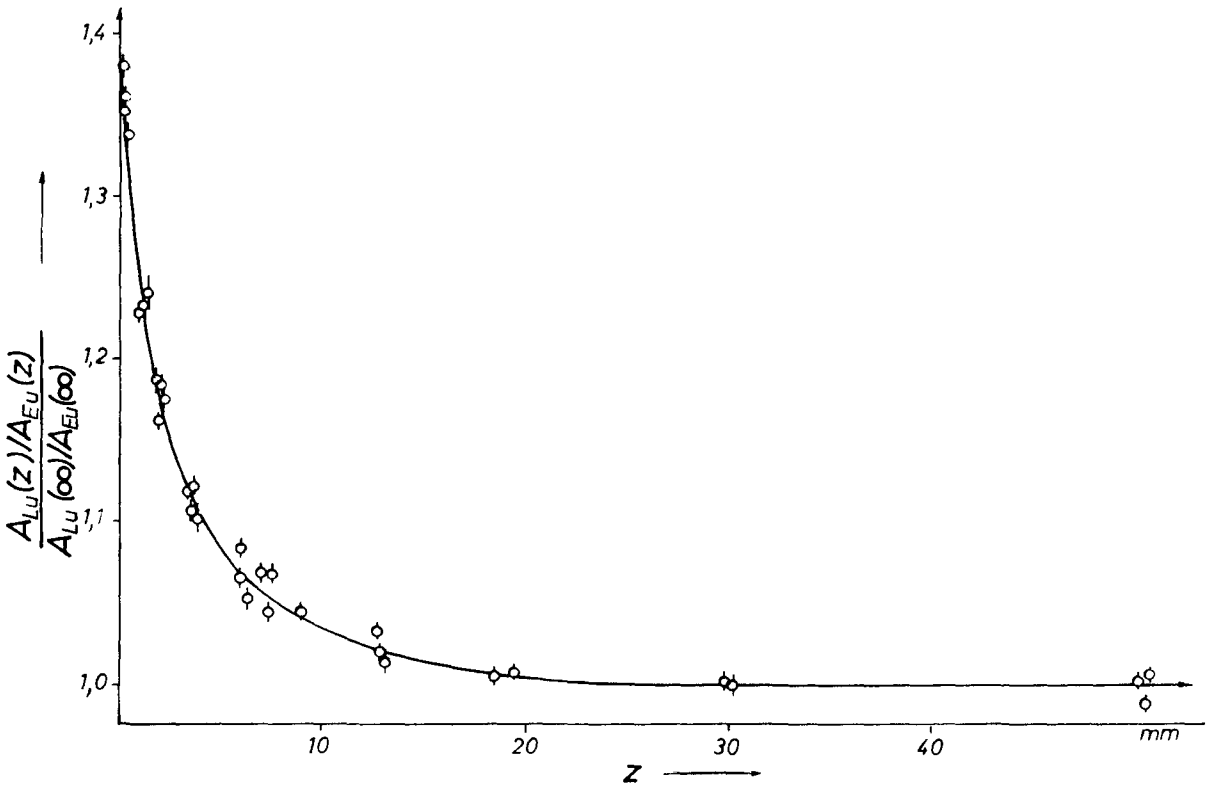

Figure 11. Foil activation ratio as a function of distance from a cadmium disk. (from reference 18)

Salah (19) have measured Lu^{177}/Lu^{176} activation ratios in a one-inch steel rod (Figure 12), 3 and 4-rod clusters in D_2O, and in a reactor core. In both of the above experiments the source of neutrons was a thermal column so that the spectra are distorted Maxwellians. No theoretical comparisons have been made for these cases.

Leslie (2) has computed 1/v and Lu^{176} foil distributions in a CANDU lattice (D_2O moderator, natural uranium and H_2O in the fuel) using an S_4 code with free gas scattering kernels (Figure 13). The 1/v foil activity is in good agreement with experiment but the computed Lu activity is too small (spectrum too soft) in the fuel. This underestimate of the hardening in the fuel is probably due to the use of a free hydrogen kernel for the water in the fuel. Brown, Kaplan, Profio, and Thompson (5) (Figure 14) have measured 1/v and Lu foil activations in a natural uranium, D_2O cell and computed the activations with the THERMOS code using the Brown and St. John scattering kernel. They also find good agreement for 1/v activation but the theory underestimates the Lu activation in the fuel. Brown and Hennelly (6) (Figure 15) measured the 1/v and Pu^{239} foil activation in a large uranium rod in D_2O and computed activations with the THERMOS code using the Brown and St. John scattering kernel. They find good agreement with theory for both foils in the fuel rod but that the theory overestimates the flux in the

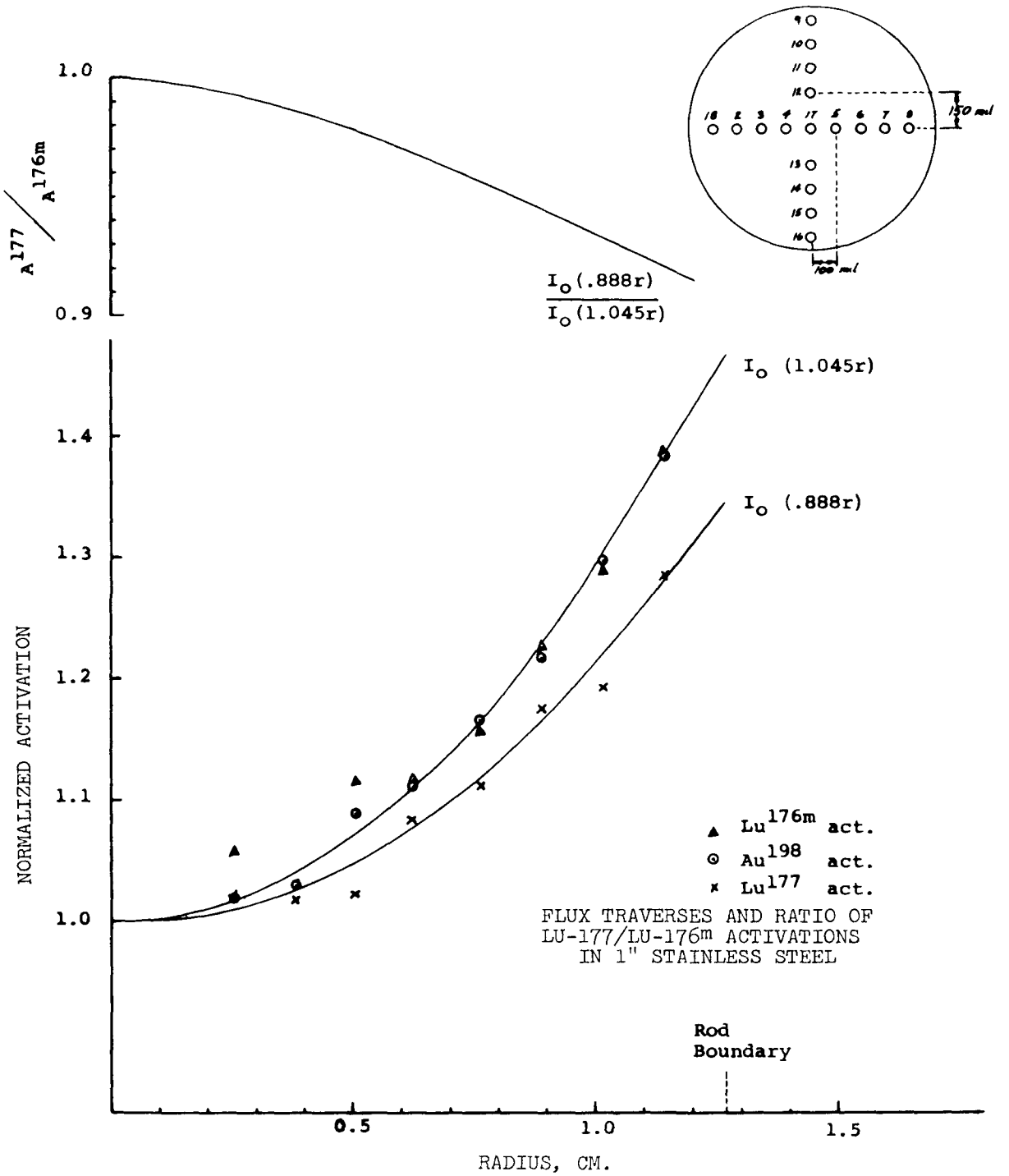

Figure 12. (from reference 19)

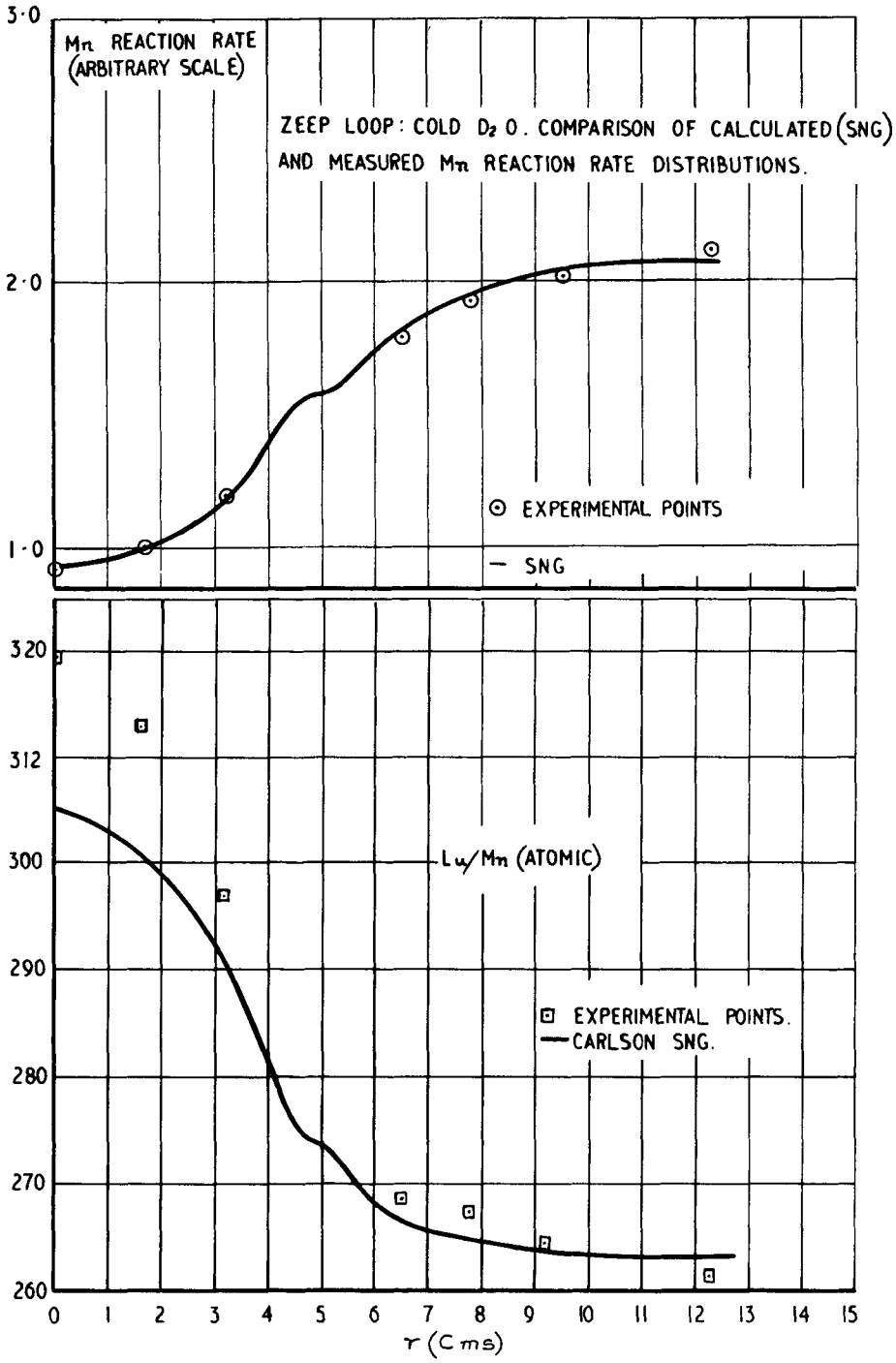

Figure 13. Activation measurements in a D_2O cell. (from reference 2)

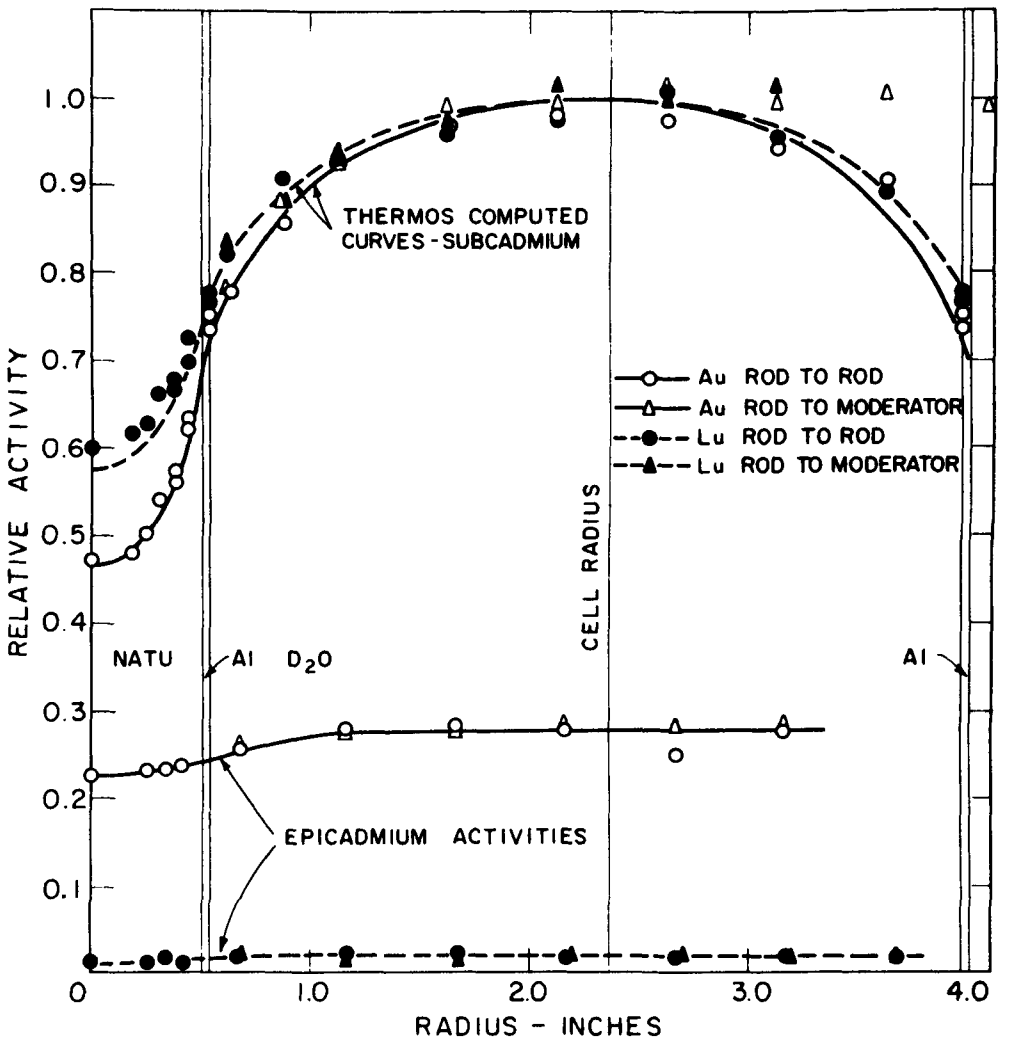

Figure 14. Au and Lu activation distributions in a 4.5-in. pitch D_2O lattice. (from reference 5)

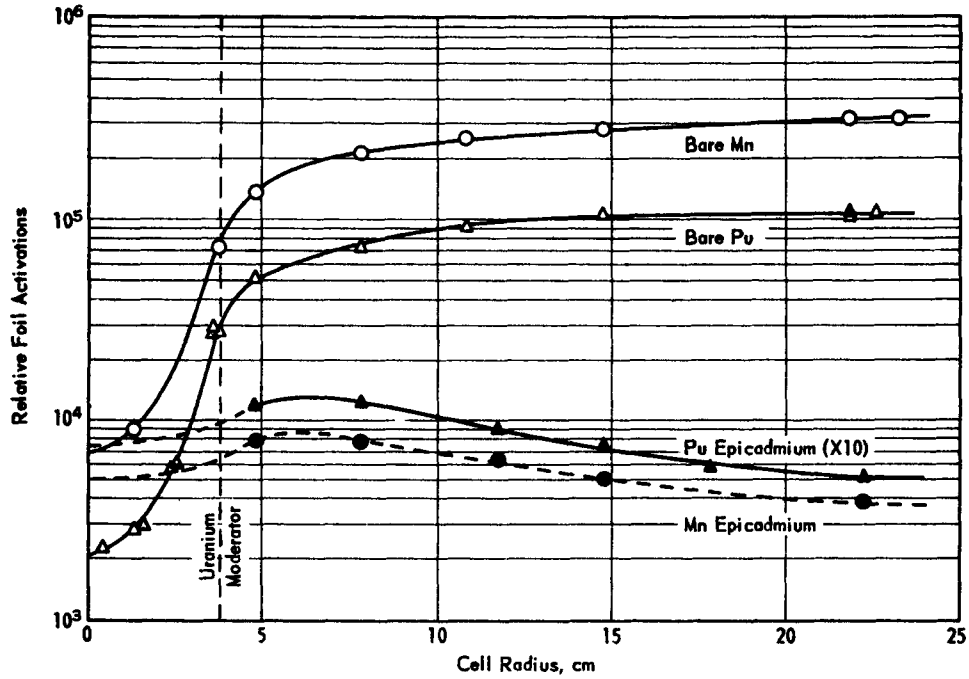

RELATIVE ACTIVATIONS OF BARE AND CADMIUM-COVERED Mn AND Pu FOILS IN A UNIT CELL

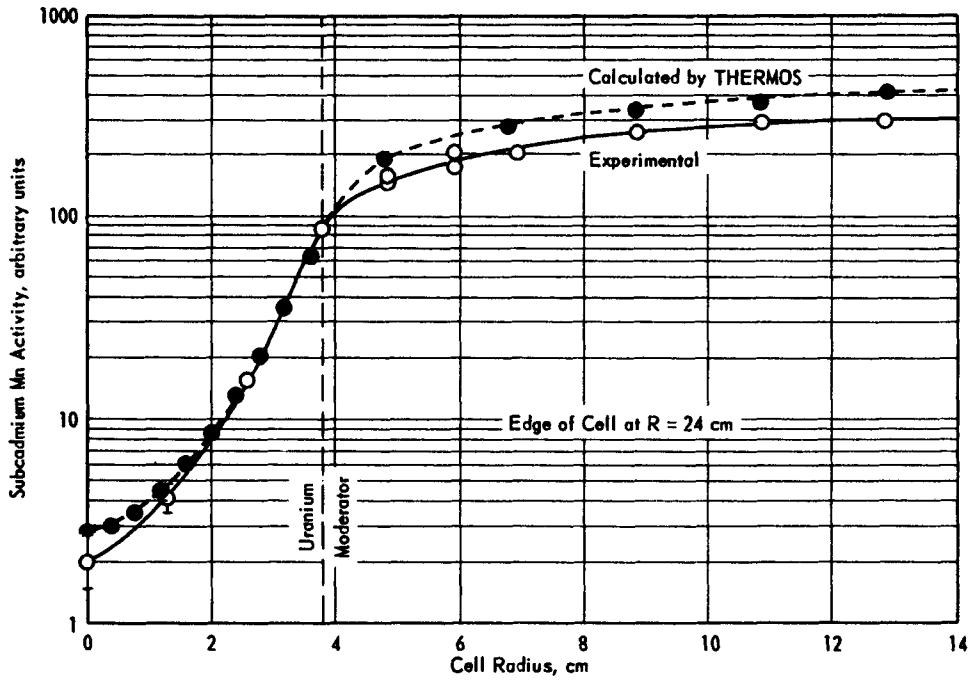

COMPARISON BETWEEN EXPERIMENTAL AND CALCULATED Mn SUBCADMIUM FOIL ACTIVATIONS IN A UNIT CELL

Figure 15. Foil activation distributions in a D_2O cell. (from reference 6)

moderator by about 20%. A large part of this discrepancy is due to the use of a spatially flat slowing down source which in fact varies by a factor of two from the moderator center to the fuel rod surface. The only consistant observation from these three experiments is that the computed spectra in the fuel are too soft indicating that both the mass 2 and Brown and St. John kernels yield too soft a spectrum for D_2O.

A comparison of various scattering models for water has been made by Honeck (22). The disadvantage factors and average neutron speeds in the moderator of a slab lattice as a function of the light water/uranium volume ratio are shown in Figure 16. The disadvantage factors for models which predict the same cross section variation with energy (such as Nelkin and Brown and St. John) have the same slopes but are displaced due to differences in moderating ability. The point here is that since the disadvantage factor is a spatial moment, the scattering cross section involved in the transport of neutrons is more important than the moderating ability of the kernel. Cylindrical THERMOS and two dimensional (2D) THERMOS calculations using the Nelkin kernel are compared in Figure 17 with experimental disadvantage factors for water lattices. The systematic 6% discrepancy is at present not understood although recent measurements indicate that the experimental data presented here may be as much as 4% too

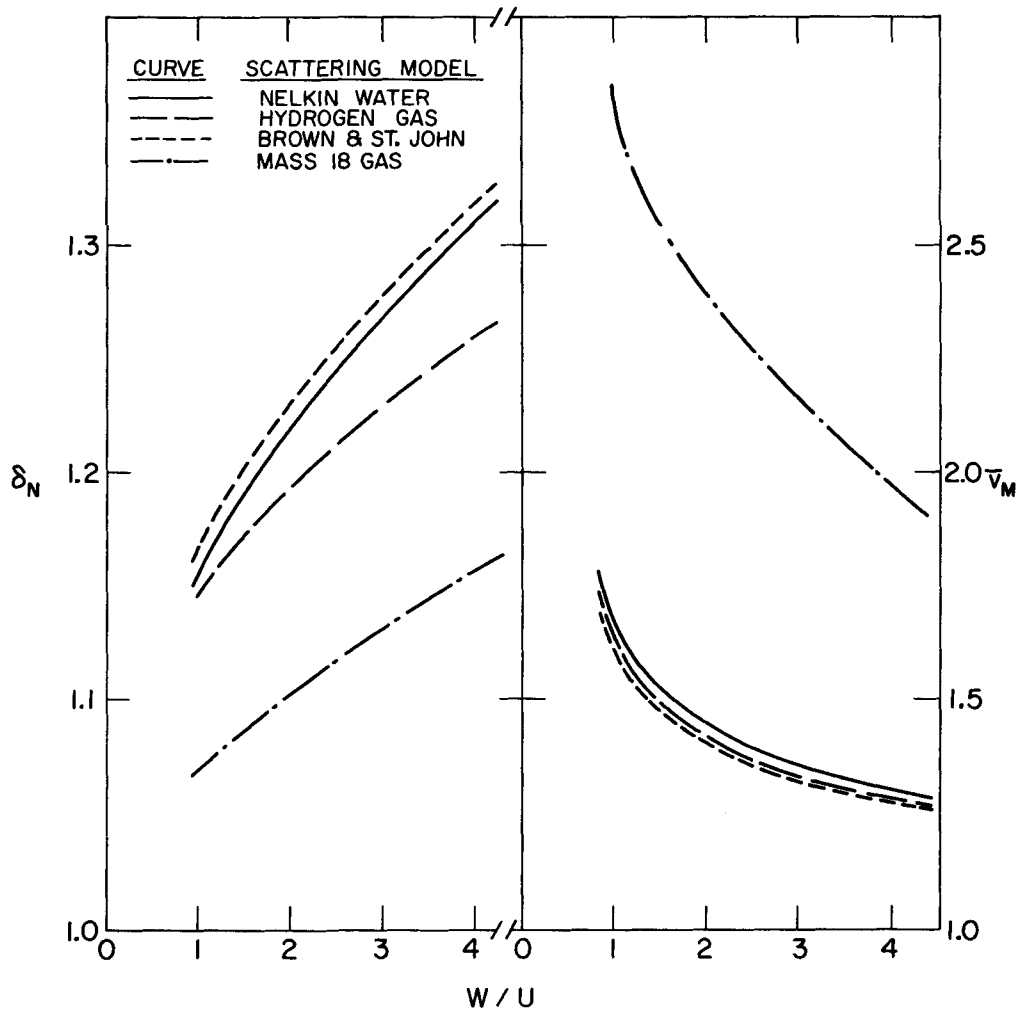

Figure 16. Cell disadvantage factor and average neutron speed in the moderator for the slab lattices using various scattering kernels for water. (from reference 22)

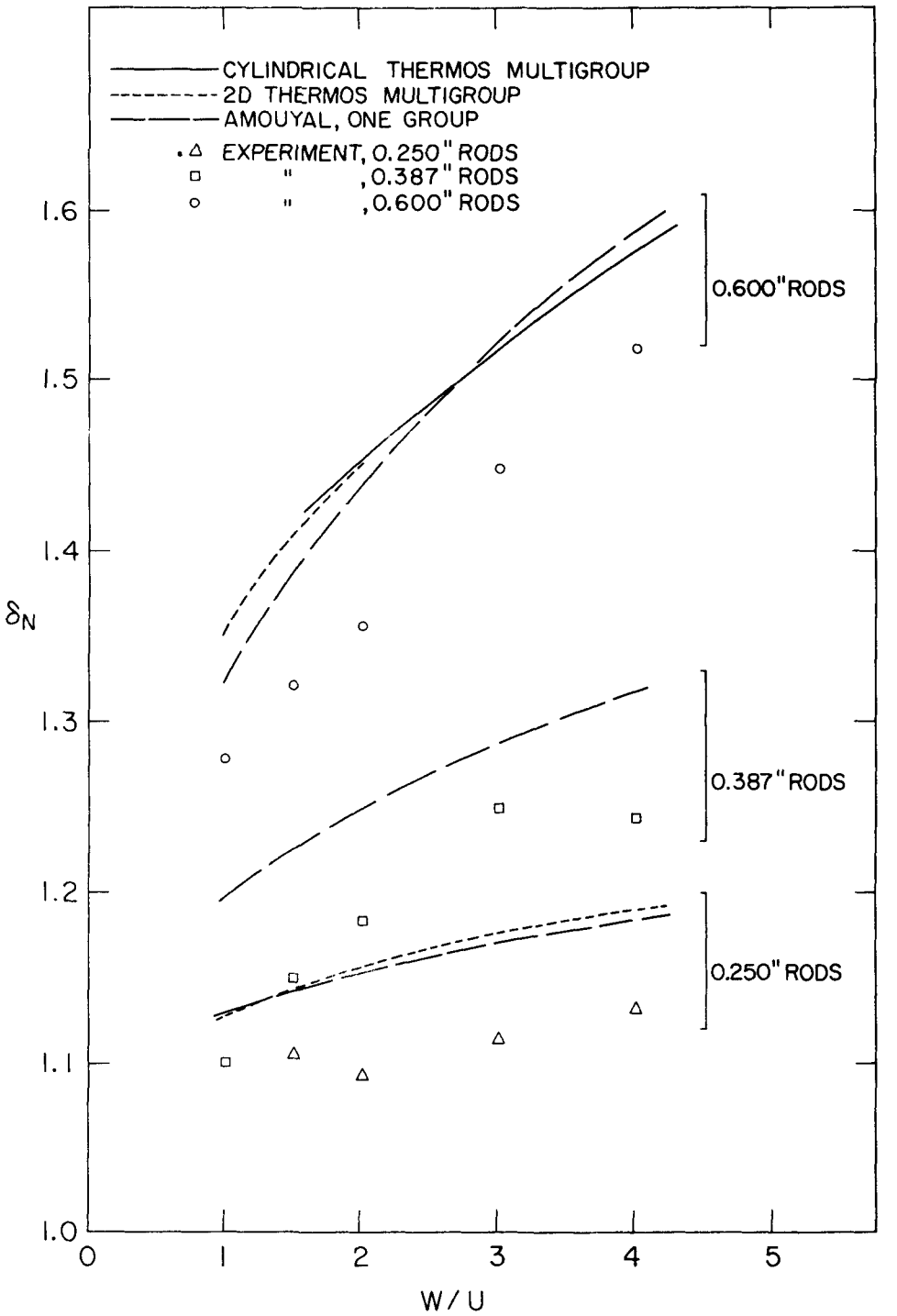

Figure 17. Neutron density disadvantage factors for the 1% enriched uranium metal rod lattices. (from reference 22)

low. Calculations by Gelbard (1) (Figure 18) also indicate this discrepancy. An attempt to correlate the average neutron speed in the moderator (with a cutoff energy of 0.78 ev) with a parameter related to the average absorption cross section is shown in Figure 19 for a series of 60 water lattices. The correlation is quite good indicating that the spectrum in the moderator is insensitive to the geometrical description of the lattice and that it is possible to give simple prescriptions for computing spectrum averaged cross sections. The cross sections used here were nearly 1/v and these statements will probably not be true where resonance absorbers are used.

Summary

The methods for computing thermal neutron spectra have developed along two different lines. In the first approach large high speed computers are used to solve the transport equation with the best scattering kernel available in an attempt to gain a full understanding of the theory and confidence in the ability to compute spectra in any assembly. A second approach recognizes the fact that not all of this physical information and mathematical rigor is required in the practical design of reactors. Not everyone can afford the large investment in computing time required to do these sophisticated calculations. Thus the second approach is in the use of simpler methods such as diffusion theory (perhaps combined with collision probabilities) and second

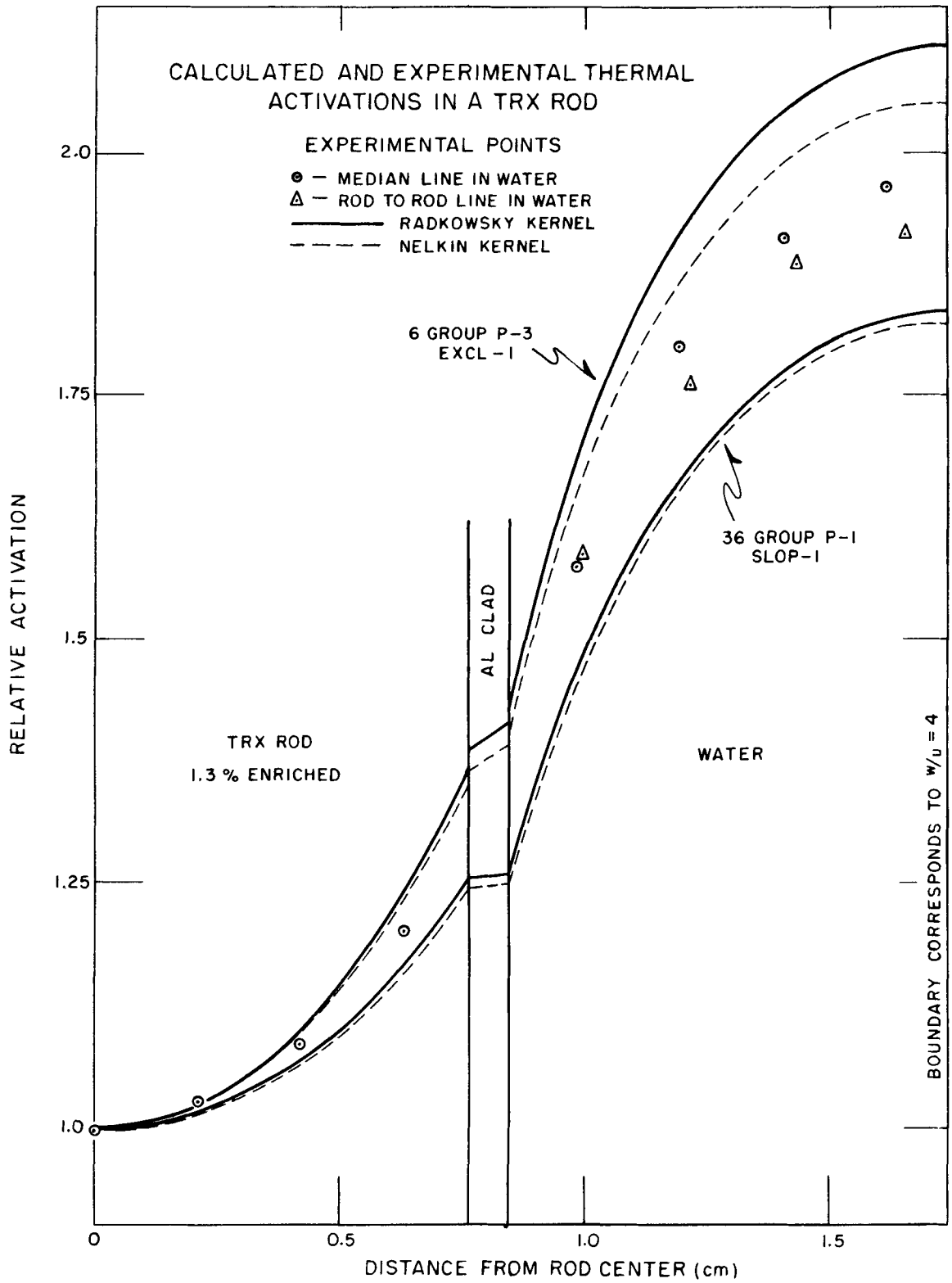

Figure 18. (from reference 1)

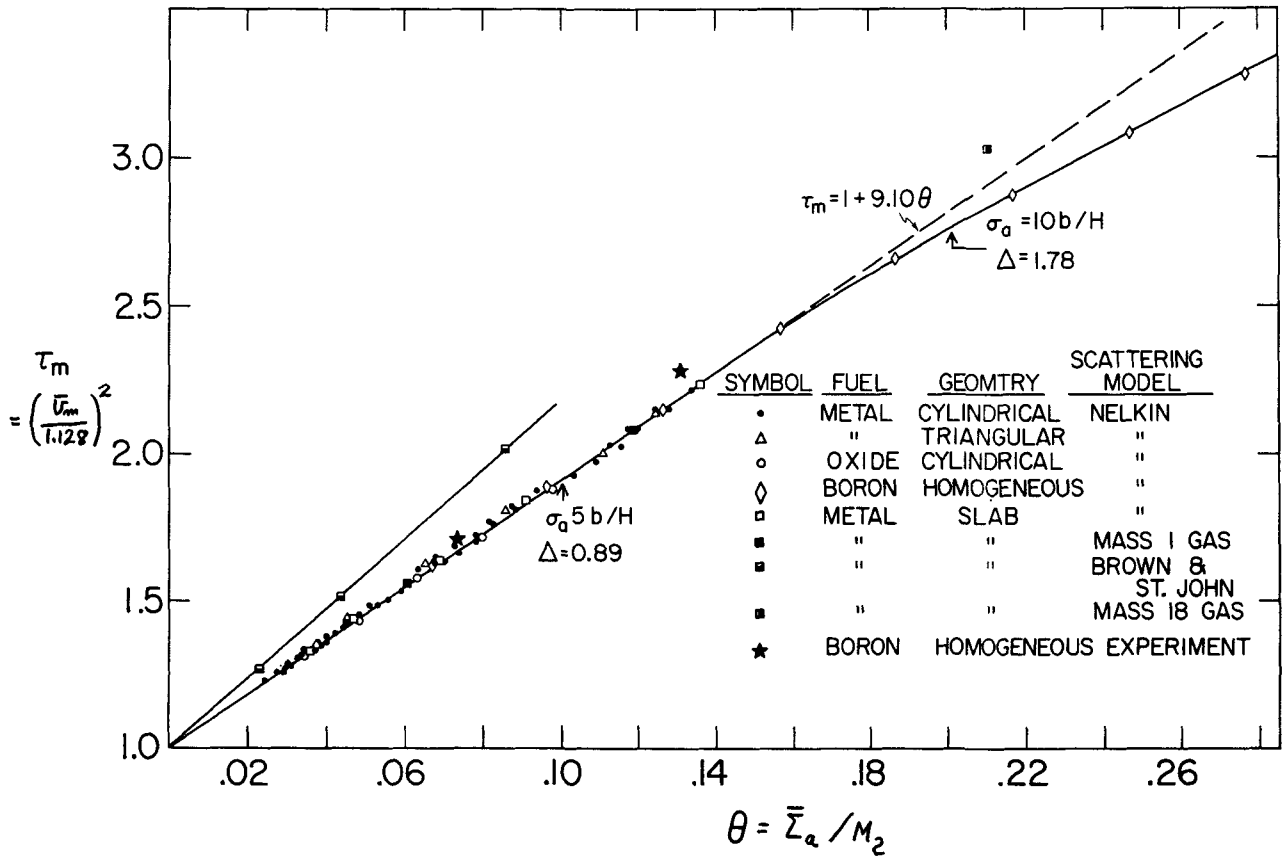

Figure 19. Moderator neutron spectrum hardness parameter τ_m for all lattices. The parameter θ is computed from hardened cross sections and the computed disadvantage factor. (from reference 22)

order differential equations for the scattering operator. Both approaches are necessary.

Our ability to compute intracell activation distributions with our best theories appears to be very good (better than say 5%) for graphite and heavy water cells. The experimental uncertainties for water lattices make it difficult to assign an accuracy here. Our ability to compute ηf is then much better than the precision of the cross sections. Few calculations of temperature coefficients have been made but it is clear that they are at least an order of magnitude more sensitive to the scattering kernel than is ηf, so that there is still a need to refine techniques.

Acknowledgement

The author is indebted to Dr. Paul Michael for his critical review and editing of the manuscript.

References

Papers submitted to this conference:

1. E. Gelbard, J. Davis, and E. Schmidt, "A Comparison of the Properties of the Nelkin and Radkowsky Thermal Neutron Scattering Kernels for Water."
2. D. C. Leslie, "Calculation of Thermal Spectra in Lattice Cells."
3. J. Macdougall, "Application of Scattering Law Data to the Calculation of Thermal Neutron Spectra."
4. G. R. Dalton, "Integral and Numerical Treatments of the Neutron Transport Problem."
5. P. Brown, I. Kaplan, A. Profio, and T. Thompson, "Measurement of Spatial and Spectral Distributions of Thermal Neutrons in Heavy Water, Natural Uranium Lattices."
6. H. Brown and E. Hennelly, "Neutron Thermalization Studies at Savannah River."
7. E. Vaughan, "Simple Expansions for Thermal Neutron Flux and Importance in a Cylindrical Cell."
8. W. Häfele, "Neutron Spectra in Heterogeneous Assemblies, A Summary of the Work of the Karlsruhe Group."
9. C. Klahr, "Use of the SPM Equation for Neutron Thermalization Calculations."
10. H. Takahashi, "Thermal Neutron Spectrum in a Medium with Two Different Temperatures."
11. N. Corngold, "The Phase Integral Method in Neutron Thermalization."

12. G. Schaefer and K. Allsopp, "Chemical Binding Effects in the Generalized Heavy Free Gas Approximation."
13. M. Cadilhac, J. Horowitz, J. Soulé, and O. Tretiakoff, "Some Mathematical and Physical Remarks on Neutron Thermalization in Finite Homogeneous Systems."
14. C. Kelber and K. Min, "Propagation of Approximation Errors in Spectra: The Gas Model."
15. M. Kostin, "Up Scattering Thermalization of Neutrons."
16. C. Shapiro, "On the Asymptotic Neutron Spectrum in Graphite."
17. R. Pearce and J. Kennedy, "Radial Dependence of the Bump Where the Maxwellian Meets the 1/E-Tail."
18. P. Korpium, K. Renz, and T. Springer, "Integral Neutron Spectra Measurements Near a Cadmium Disk."
19. T. Parkinson and S. Salah, "Integral Spectrum Measurements in Heterogeneous Media."

Other References:

20. K. Ott, K. Meetz, and S. Sanatani, Nukleonik 3, 155 (1961).
21. N. Corngold, Ann. Phys. 6, 368 (1959); 11, 338 (1960).
22. H. Honeck, "The Calculation of Thermal Utilization and Disadvantage Factors in Uranium Water Lattices," paper submitted to the IAEA Conference on Light Water Lattices in Vienna, June 1962.
23. K. Meetz, Second Geneva Conference, 1958, P/968.
24. G. Calame, F. Federighi, and P. Ombrellaro, NSE 10, 31 (1961).
25. N. Corngold, P. Michael, and W. Wollman, NSE (to be published) and this conference.
26. J. Koppel, this conference.

CONFERENCE ON NEUTRON THERMALIZATION

Brookhaven April 29 - May 2, 1962

SOME MATHEMATICAL AND PHYSICAL REMARKS ON NEUTRON THERMALIZATION IN INFINITE HOMOGENEOUS SYSTEMS

(M. Cadilhac, J. Horowitz, J.L. Soulé, O. Tretiakoff)

Centre d'Etudes Nucleaires de Saclay
Gif-sur- Yvette (S. et O.)
France

S U M M A R Y

1) The general mathematical properties of the thermalization operator are discussed in order to exhibit its important properties for the behavior of the neutron spectrum at high and low energies.

2) A new model is presented. For the calculation of any spectrum in infinite homogeneous systems this model leads to a second order differential equation. Hydrogen and heavy gas are included in this general model.

3) The adjustment of model parameters on experimental data is discussed.

I - INTRODUCTION

This report deals mainly with the problem of neutron thermalization in an infinite homogeneous medium.

It is well known that in a not too undermoderated system very different scattering laws lead to rather similar flux shapes. Let us consider for instance the two extreme cases $A = 1$ and $A = \infty$ of the gas model with a $\frac{1}{v}$ absorption :

$\Sigma_a(y) = \frac{\Sigma_a(1)}{\sqrt{y}}$. If we assume $\frac{\Sigma_a(1)}{\xi \Sigma_\infty} \ll 1$ the flux $\varphi(y)$ is expressed by

$$\varphi(y) \simeq \frac{2}{\sqrt{\pi}} \frac{Q}{\Sigma_a(1)} \varphi_0(y) + \frac{1}{\xi \Sigma_\infty} \varphi_1(y)$$

where

$$\int_0^\infty \varphi_1(y) \frac{dy}{\sqrt{y}} = 0$$

Fig. 1 shows the functions $\varphi_1(y)$ and their asymptotic expansions limited to the two first terms.

Nevertheless these differences in shape, though small, are of importance in reactor calculations. But it seems desirable to describe mathematically the thermalization process in a manner exhibiting the factors which determine the flux shape more directly than the scattering law. Similarly since the neutron flux is not sensitive to all the details of the scattering law it should be possible to approximate it by a simple model depending on a few adjustable functions.

The fact that the thermalization operator acting on the maxwellian flux $\varphi_0(y)$ gives zero suggests to use the function

$C(y) = \frac{d}{dy} \frac{\varphi(y)}{\varphi_0(y)}$ rather than the flux $\varphi(y)$ itself.

$C(y)$ is related to the slowing down density $q(y)$ by the linear operator L

$$q = L\{C\}$$

The kernel $L(y, y')$ is given by

$$L(y, y') = \int_0^{y_<} \int_{y_>}^{\infty} \varphi_0(z') \Sigma(z' \to z)\, dz\, dz'$$

where $y_<$ and $y_>$ are respectively the smaller and larger of the energies y and y'.

This relation shows that :

$$L(y, y') > 0$$

L is a positive definite hermitian operator, as a consequence of the detailed balance condition.

In the next section we consider the operator $\ell(a, b)$ deduced from $L(y, y')$ by a double Laplace transformation.

In section III we introduce a simple model in approximating $J = L^{-1}$ by a second order differential operator.

II - THE KERNEL $\ell(a,\bar{b})$

$\ell(a,\bar{b})$ is defined by

$$\ell(a,\bar{b}) = \int_0^\infty \int_0^\infty L(y,y')\, e^{-ay-by'}\, dy\, dy' \tag{II,1}$$

Its expression is particularly simple in the case of the gas model :

$$\ell(a,\bar{b}) = \frac{\Sigma_\infty \beta \sqrt{1+\frac{a+\bar{b}+1}{A}}}{(a+\bar{b}+1)^2 (a+\bar{b}+1+\beta a\bar{b})} \qquad \beta = \frac{4A}{(A+1)^2} \tag{II,2}$$

and takes the form

$$\ell(a,\bar{b}) = \frac{\Sigma_\infty \sqrt{2+a+\bar{b}}}{(a+\bar{b}+1)^2 (a+1)(b+1)} \qquad \text{if} \quad A=1$$

$$\ell(a,\bar{b}) = \frac{2\,\Sigma_\infty \xi}{(a+b+1)^3} \qquad \text{if} \quad A=\infty$$

More generally in the case of the heavy gas model with a variable cross section $\Sigma(\infty) = f(y)\,\Sigma_\infty$

$$\ell(a,\bar{b}) = \Sigma_\infty \xi \int_0^\infty f(y)\, y^2\, e^{-y(a+\bar{b}+1)}\, dy$$

$$= \frac{2\,\Sigma_\infty \xi\, I(a+\bar{b}+1)}{(a+b+1)^3}$$

where $I(t) = \frac{1}{2}\int_0^\infty f\left(\frac{z}{t}\right) z^2\, e^{-z}\, dt \quad ; \quad y(0) = 1$

Putting $$g(a,\bar{b}) = \int_0^\infty \int_0^\infty e^{-ay-by'}\, \varphi_0(y')\, \Sigma(y' \to y)\, dy\, dy' \,,$$

$$h(a,\bar{b}) = g(a,\bar{b}) - g(a+\bar{b},0)$$

is the double Laplace transform of the thermalization operator H and

$$\ell(a,\bar{b}) = -\frac{h(a,b)}{ab}$$

In the case of the gas model

$$g(a,b) = \frac{\Sigma_\infty \sqrt{1+\frac{a+b+1}{A}}}{(a+b+1)(a+b+1+\beta a b)}$$

For a scattering law $S(\alpha,\beta)$

$$g(a,b) = \frac{\pi}{2}\frac{1}{a+b+1}\int_0^\infty d\alpha \int_0^\infty d\beta\, e^{-\frac{a+b+1}{4}\left(\alpha+\frac{\beta^2}{\alpha}\right)} S(\alpha,\beta)\, ch\left[(a-b)\frac{\beta}{2}\right]$$

$$\ell(a,b) = -\frac{\pi}{a+b+1}\int_0^\infty d\alpha \int_0^\infty d\beta\, e^{-\frac{a+b+1}{4}\left(\alpha+\frac{\beta^2}{\alpha}\right)} S(\alpha,\beta)\, sh\frac{a\beta}{2}\, sh\frac{b\beta}{2}$$

In the (a,b) plane the domain ($\mathcal{D}$) of interest is limited by the line of singularities (Γ) as shown in fig. 2. In ($\mathcal{D}$) $\ell(a,b)$ is regular and has the properties mentioned above for $L(y,y')$. (Γ) is determined by the scattering cross section at high energy ; thus (Γ) and the dominating singularity on (Γ) are the same for a gas and crystal model.

In practice, it is not necessary to know $\ell(a,b)$ very accurately in the whole domain ($\mathcal{D}$) and even the exact form of (Γ) is of little importance.

For problems involving only thermal energies, it is the behaviour of $\ell(a,b)$ near the origin which is of importance. Note that

$$g(0,0) = \int_0^\infty \varphi_0(y)\,\Sigma(y)\,dy$$

$$\ell(0,0) = \frac{1}{2}\int_0^\infty \int_0^\infty (y'-y)^2\,\varphi_0(y)\,\Sigma(y\to y')\,dy\,dy'$$

On the other hand, the high energy part of the neutron flux

depends only on the behaviour of $\ell(a,\bar{b})$ near the singular point $a = 0$, $b = -1$.

To illustrate this, we consider the case of a $\frac{1}{v}$ absorption with a source of intensity Q at an infinitly high energy.

Putting

$$C(y) = \int_{-1}^{\infty} e^{-by}\, \psi(\bar{b})\, d\bar{b} \tag{II,3}$$

the flux may be written as a sum of two terms

$$\varphi(y) = y e^{-y} \cdot \int_{-1}^{\infty} \frac{(b+1)^{3/2} - e^{-by}}{\bar{b}}\, \psi(\bar{b})\, d\bar{b} + \frac{2Q}{\Sigma_a(1)\sqrt{\pi}}\, y\, e^{-y}$$

The total number of neutrons corresponding to the first term is zero.

$\psi(\bar{b})$ is given by the equation

$$\int_{-1}^{\infty} \ell(a,\bar{b})\, \psi(\bar{b})\, d\bar{b} + \int_{-1}^{\infty} m(a,\bar{b})\, \psi(\bar{b})\, d\bar{b} = \frac{Q}{a(1+a)^{3/2}} \qquad a > 0 \tag{II,4}$$

where

$$m(a,\bar{b}) = \Sigma_a(1)\, \frac{\sqrt{\pi}}{2}\, \frac{1}{a\bar{b}} \left\{ \frac{1}{(a+\bar{b}+1)^{3/2}} - \frac{1}{(1+a)^{3/2}(1+b)^{3/2}} \right\}$$

The asymptotic expansion of the flux corresponds to the expansion of $\psi(b)$ in powers of $1+\bar{b}$ which follows from the condition that

$$a \int_{-1}^{\infty} \left[\ell(a,b) + m(a,\bar{b}) \right] \psi(\bar{b})\, d\bar{b}$$

is a regular function of a in the vicinity of $a = 0$.

In fact, the expansion of $\psi(b)$ in powers of $1+b$ converges for $|1+b| < 1$.

A forthcoming Saclay report describes an analytical and a numerical method for solving the equation (II,4). A division of the interval $(-1, \infty)$ into two parts $(-1, 0)$ and $(0, \infty)$ appears in a natural way, the former giving the "fast part" of the flux, the latter the "thermal part". A characteristic shape for $\psi(b)$ is shown below, in the case of small absorption.

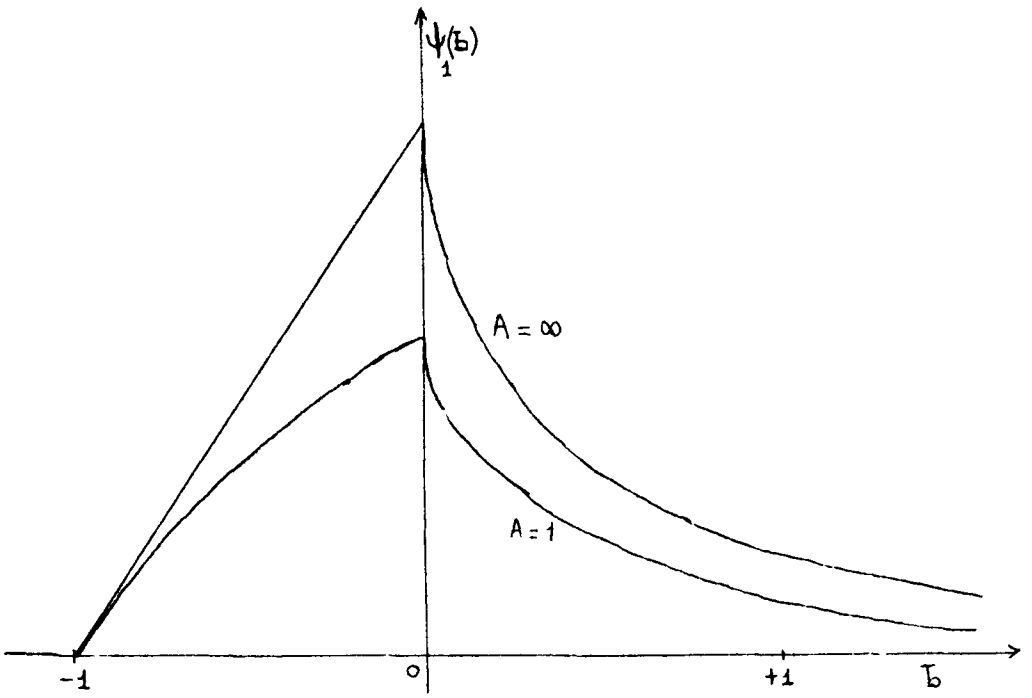

The aim of the " $\rho(a,b)$ method" is to fit theoretical models and experimental data with a small number of parameters. Work on this subject is in progress.

We would like to mention shortly the method using a representation of the thermalization operator or of L in terms of Laguerre or similar functions. Such a representation may be useful for purely thermal problems such as the diffusion cooling or for calculations of spectra if the "fast part" of the flux is dealt with separately.

We can define a set of functions C_i such that

$$\int C_i L C_j \, dy = S_{ij}$$

Putting $L C_i = q_i$ one has

$$\int q_i J q_j \, dy = S_{ij}$$

In many cases, the calculations are simple if the C_i are polynomials ; these are obtained from the derivatives of $\ell(a, b)$ at the origin. This choice may not be the best from the point of view of convergence.

III - The "differential model"

A fundamental problem of the thermalization theory is the determination of the operator $J = L^{-1}$.
In the case of the heavy gas model one has simply

$$J = \frac{e^y}{\xi \Sigma_\infty y^2} \frac{1}{f(y)} \qquad \text{where} \qquad f(y) = \frac{\Sigma(y)}{\Sigma_\infty}$$

This model which has been used at Saclay and by Dr. Leslie at Winfrith has the disadvantage that slowing down takes place in infinitly small steps. On the other hand if f (y) is chosen to give the right flux at very low absorption no degree of freedom is left for other adjustments, if necessary, for instance in order to provide the exact value of the diffusion cooling constant or the flux shape at a stronger capture.

The gas model gives for A = 1

$$J = (1 - D) \frac{e^y}{y\Sigma(y)} (1 + D)$$

where $D = \frac{d}{dy}$ and $y\Sigma(y) = \frac{\Sigma_\infty}{\sqrt{\pi}} \left[(y + \tfrac{1}{2}) \int_0^y \frac{e^{-z} dz}{\sqrt{z}} + \sqrt{y}\, e^{-y} \right]$

Considering these two expressions for J, Cadilhac proposed to approximate generally J by a hermitian second order differential operator :

(III,1) $$J = j(y) - D\, k(y)\, D$$

Thus

(III,2) $$C(y) = J\, q(y) = j(y)\, q(y) - \frac{d}{dy} \left[k(y) \frac{d}{dy} q(y) \right]$$

(III,1) implies (if $k \neq 0$) that $L(y, y')$ has the form

(III,3) $$L(y, y') = u(y_<) \cdot v(y_>)$$

and $$\varphi_0(y)\, \Sigma(y \to y') = -\frac{d}{dy} v(y) \cdot \frac{d}{dy'} u(y') \qquad y' < y$$

$u(y)$ and $v(y)$ are the solutions of $\bar{J} q = 0$ respectively regular for $y = 0$ and $y = \infty$. The operator J may therefore be written as

$$J = -\frac{1}{u} D k u^2 D \frac{1}{u}$$

and one has the relations

$$v(y) = u(y) \int_y^\infty \frac{dz}{k(z)\, u^2(z)}$$

$$J(y) = \frac{1}{u} \frac{1}{dy} \left[\frac{u'(y)}{\Sigma(y) \varphi_0(y)} \right] \qquad k(y) = \frac{1}{\Sigma(y) \varphi_0(y)} \quad (III,4)$$

In general, the differential form for J being only an approximation, the best fit for $\bar{J}$ does not necessarily satisfy (III,4).

High energy behaviour of j and k

At high energy where binding and temperature effects are negligible, the flux is given by the approximate relation :

(III,5) $$\Sigma_\infty \varphi(y) = \frac{q}{\xi y} - \frac{Dq}{\mu}$$

which leads to : $$\varphi(y) \simeq \frac{q(\infty)}{\xi \Sigma_\infty y}$$

To determine the constant μ, we use the condition that in the case of a $\frac{1}{v}$ absorption, the coefficient of the next term in the expansion of $\varphi(y)$, i-e the $\frac{1}{y^{3/2}}$ term, is exact.

This gives

$$\frac{1}{\mu} = \frac{1}{\nu} - \frac{2}{\xi} \qquad \text{with} \qquad \nu = \frac{3A-1}{3A(A+1)}$$

In practice, one may use the approximation :

$$\mu = \frac{3A}{2A+1}$$

The behaviour of j and k at high energies results from the fact that (III,2) reduces to (III,5). We find therefore :

$$j(y) \sim \frac{e^y}{\xi \Sigma_\infty y^2} \qquad k(y) \sim \frac{e^y}{\mu \Sigma_\infty y} \qquad y \to \infty$$

If the moderator is not monoatomic, ξ and ν are to be weighted by the cross-sections of the various elements.

The relation (III,2) shows that the asymptotic expansion of $j(y)$

$$j(y) \sim \frac{e^y}{\xi \Sigma_\infty y^2} \left(1 - \frac{\gamma_1}{y} - \frac{\gamma_2}{y^2} \right)$$

is identical with the expansion of $C(y)$ if the capture is confined to the thermal region, the source of unit intensity being at an infinitely high energy. Since the asymptotic expansion of the flux, even limited to the first two terms, gives a good approximation down to energies $y \simeq 10$ (as shown in fig. 1) it is essential to take for γ_1 the exact value. For a gas :

$$\gamma_1 = \frac{1}{A}$$

As already mentioned, the best fit for k does not necessarily satisfy (III,4), but by writing

(III,6) $$k(y) = \frac{1}{\Sigma^*(y)\, \varphi_0(y)}$$

$\Sigma^*(y)$ will be a slowly varying function of energy with

$$\Sigma^*(\infty) = \mu \Sigma(\infty)$$

Dr Leslie* has adjusted the function $f(y) = \frac{\Sigma(y)}{\Sigma_\infty}$ appearing in the heavy gas model in order to fit the measurements of the spectra in well moderated graphite lattices.

In the "differential model",

$\frac{1}{\xi \Sigma_\infty y \varphi_0 j}$ has a shape similar to $f(y)$.

Calculation of the spectra with the "differential model"

Let us consider the case of a source of intensity Q at an infinitly high energy and an arbitrary absorption law $\Sigma_a(y)$.

To the equations written previously

$$C(y) = \frac{d}{dy} \frac{\varphi(y)}{\varphi_0(y)}$$

$$C(y) = J(y)\, q(y) - \frac{d}{dy}\left[k(y) \frac{d}{dy} q(y) \right] \qquad \text{(III,2)}$$

we add the relation

$$\frac{dq}{dy} = \Sigma_a(y)\, \varphi(y) \qquad \text{(III,6)}$$

which expresses the neutron balance.

Putting

$$k_a(y) = \frac{1}{\Sigma_a(y) \varphi_0(y)} \qquad k_1(y) = k(y) + k_a(y)$$

we obtain

$$J(y)\, q(y) - \frac{d}{dy}\left[k_1(y) \frac{d}{dy} q(y) \right] = 0 \qquad \text{(III,7)}$$

---

* "Calculation of thermal spectra in lattice cells", paper presented at this conference.

with the conditions $q(0) = 0 \qquad q(\infty) = Q$

We wish to emphasize that the calculation of the flux is mathematically as simple here as for the heavy gas model.

In fact, if we take a heavy gas model with $f(y) = \xi \Sigma_\infty y \varphi_0 j$ and an absorption cross section $\overline{\Sigma_a} = \dfrac{\Sigma_a \Sigma^*}{\Sigma_a + \Sigma^*}$

we obtain a flux $\overline{\varphi}(y)$ related to $\varphi(y)$ by

$$\varphi = \frac{\Sigma^*}{\Sigma_a + \Sigma^*} \overline{\varphi}$$

The problem can be solved by an iteration process.

Putting $\overline{\varphi}(y) = \sum_{n=0}^{\infty} \overline{\varphi_n}(y)$ with $\overline{\varphi_0} = y e^{-y}$

$$q(y) = \sum_{n=0}^{\infty} q_n(y)$$

we have

$$q_n(y) = \int_0^y \overline{\Sigma_a}(z)\, \overline{\varphi_n}(z)\, dz$$

$$\overline{\varphi_{n+1}}(y) = \overline{\varphi_0}(y) \int_0^y j(z)\, q_n(z)\, dz$$

When the iteration is stopped, the functions φ and q should be multiplied by a constant such that $q(\infty) = Q$

If the capture is small we obtain

$$\varphi(y) \simeq \frac{Q}{\int_0^\infty \Sigma_a(u)\, \varphi_0(y)\, dy} \left[\varphi_0 + \varphi_1 \right]$$

when $\dfrac{\varphi_1}{\varphi_0} = \int_0^y j(z)\, \varphi_0(z)\, dz - \dfrac{\Sigma_a(y)}{\Sigma^*(y)}$

and $q_0(y) = \int_0^y \Sigma_a(z)\, \varphi_0(z)\, dz$

The adjustment of the functions $j(y)$ and $k(y)$

We want to adjust the "differential model" i-e the functions $j(y)$ and $k(y)$, in order to provide a good approximation to a theoretical model or to fit experimental data.

Since the model depends on two arbitrary functions, one needs for the adjustment two fluxes corresponding to two different absorption laws. Taking a $\frac{1}{v}$ law and values of $\frac{\Sigma_{a(1)}}{\xi \Sigma_\infty}$ respectively equal to 0.1 and 0.2, we have calculated the functions $j(y)$ and $k(y)$ to give exactly the same fluxes as the gas model, for $A = 2$; 4 and 12. The functions, for $A = 1$; 2 and 12 are shown in fig. 3 and 4. An important point to be checked is that with this adjustment the "differential model" approximation gives also the right spectrum with other absorption laws. Therefore, we made the calculations for $\frac{\Sigma_{a(1)}}{\xi \Sigma_\infty} = 0.5$ and 1 ($\frac{1}{v}$ absorption law) and for a capture having a strong resonance (Pu 239). The results were very satisfactory. This proves that the "differential model" provides an excellent approximation for thermal reactor calculations.

IV - CONCLUSION

The study of various theoretical scattering laws and of the available experimental data using the "differential model" and eventually the " $\ell(a,b)$ formalism" is now in progress at Saclay. Applications to heterogeneous reactor problems are included in this work. This will improve the analysis of the rapidly increasing amount of integral data provided by reactor lattice measurements. A few test calculations have been made, using scattering laws data for graphite, kindly communicated to us by Dr Egelstaff, Schofield and Leslie, in order to point out the effect of experimental and theoretical uncertainties.

For instance, we have calculated the second term δ_1 of the asymptotic expansion of the flux for weak absorption

$$\varphi(y) \sim \frac{1}{y}\left(1 + \frac{\delta_1}{y} + \cdots\cdots\right)$$

using the $f(y)$ function given by Dr Leslie and the Egelstaff's $p(\beta)$. One has :

$$\delta_1 = 2 + \lim_{y\to\infty} y\,(1 - f[y]) = \left(2 - \frac{1}{A}\right)\frac{T^*}{T}$$

and

$$\frac{T^*}{T} = \frac{\int_0^\infty p(\beta)\, ch\,\frac{\beta}{2}\, d\beta}{2\int_0^\infty p(\beta)\, sh\,\frac{\beta}{2}\,\frac{d\beta}{\beta}}$$

At room temperature, we obtained respectively :

$$\frac{T^*}{T} = 2.43 \quad \text{from} \quad p(\beta)$$

$$\frac{T^*}{T} = 1.88 \quad \text{from} \quad f(y)$$

$P(\beta)$ has the following shape :

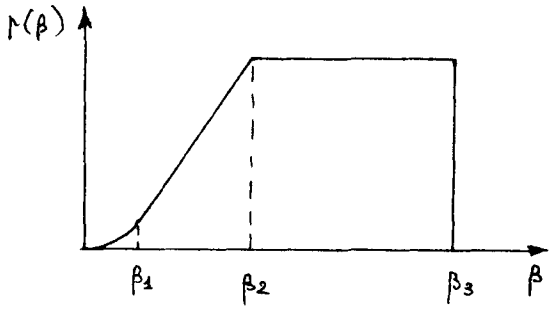

Only the part of the curve corresponding to $\beta \lesssim 2$ is determined experimentally. In order to see how sensitive the asymptotic behaviour of the flux is to the choice of the cut-off β_3 , we have calculated $\frac{T^*}{T}$ as a function of β_3

β_3 (in kT units)	5	6	7
T^*/T	1.76	2.07	2.43

On the other hand, for a given β_3 , T^*/T is almost insensitive to the shape of the left part of the curve.

The knowledge of the neutron flux in a well moderated system does not give enough information on the properties of the thermalization operator in the thermal region. In particular, it does not permit to deduce accurately the diffusion cooling constant or the neutron flux when the absorption is strong or departs considerably from a $1/v$ law in the thermal region. As a test, we have calculated the quantity $\ell(o,o)$ for graphite, using :

- Leslie's $f(y)$ at room temperature :

$$\ell(o,o) = \xi \Sigma_\infty \int_o^\infty f(y)\, y^2 e^{-y}\, dy = 0.166\, \Sigma_\infty$$

- Egelstaff's $S(\alpha,\beta)$:

$$\ell(o,o) = 0.143\, \Sigma_\infty \quad \text{at } 300^\circ \text{ K}$$

$$\left.\begin{matrix} 0.258\, \Sigma_\infty \\ 0.261\, \Sigma_\infty \end{matrix}\right\} \quad \text{at } 900^\circ \text{ K}$$

(The two values at 900° K correspond to two extreme shapes of $S(\alpha,\beta)$ taking into account experimental errors)

- the gas model (A = 12)

$$\ell(0,0) = 4\,\Sigma_\infty\, A^{1/2}(A+1)^{-3/2} = 0.296\ \Sigma_\infty$$

It is necessary to emphasize that the value of $\ell(0,0)$ deduced from $\beta(y)$ is very sensitive to the shape of $f(y)$ in the thermal region, whereas the flux in a well moderated system is rather insensitive.

The uncertainties on the diffusion cooling constant are of the same order as those on $\ell(0,0)$.

If transport corrections are small or satisfactorily taken into account, good measurements of the diffusion cooling constant provide an important check of the thermalization models.

To illustrate this point, we give the expression of $\mathcal{C}$ in the case of the "differential model" :

$$\mathcal{C} = \frac{2}{D_0\sqrt{\pi}} \int_0^\infty dy \left\{ j(y) \left[\int_0^y \left(D(\zeta) - \frac{\lambda}{\sqrt{\zeta}} \right) \varphi_0(\zeta)\, d\zeta \right]^2 + \left[D(y) - \frac{\lambda}{\sqrt{y}} \int^2 \frac{\varphi_0(y)}{\Sigma^*(y)} \right\}$$

with $$D_0 = \frac{2}{\sqrt{\pi}} \int_0^\infty D(y)\, \varphi_0(y)\, dy$$

For simplicity, we assume that $D(y)$ is constant :

$D(y) = \frac{\sqrt{\pi}}{2} D_0$. We compare the value $\mathcal{C}_0$ obtained with the generalized heavy gas model :

$$j(y) = \frac{e^\gamma}{\xi \Sigma_\infty\, y^2 f(y)} \qquad k(y) = 0$$

and the value $\mathcal{C}$ given by a "differential model" ($k(y) \neq 0$) leading to the same flux for a weak $1/v$ capture. One finds :

(IV,1)
$$\mathcal{C} - \mathcal{C}_0 = D \int_0^\infty \frac{\varphi_0(y)}{\Sigma^*(y)}\, Z^2(y)\, dy$$

where

$$z(y) = 1 - \frac{1-(y+1)e^{-y}}{\sqrt{y}\int_0^y e^{-z}\sqrt{z}\,dz}$$

is given in fig. 5.

This shows that a precise determination of $\mathcal{C}$ provides a good discrimination between different models. It is seen in (IV,1) that $\mathcal{C} - \mathcal{C}_0$ is very sensitive to the behaviour of $k(y)$ in the thermal region.

Unfortunately, the experimental situation does not seem satisfactory for the time being.

We hope that the "differential model" or the "$\ell(a,b)$ formalism" with two arbitrary functions will provide a good approximation for the thermalization operators (apart from very special cases, for instance when kT is near to the Bragg cut-off). This will simplify very much the spectra calculations and permit an easy comparison between the thermalization properties of various moderators at different temperatures.

NOTATIONS

y neutron energy in kT units

$\vec{x}$ neutron velocity : $x^2 = y$

$\Sigma(y \to y')\, dy'$ differential scattering cross section

$\Sigma(y) = \int \Sigma(y \to y')\, dy' \qquad \Sigma_\infty = \Sigma(\infty)$

$\Sigma(\vec{x} \to \vec{x}')\, d^3\vec{x}'$ differential scattering cross section

The scattering law $S(\alpha, \beta)$ with $\alpha = (\vec{x}' - \vec{x})^2 \qquad \beta = x'^2 - x^2$

is defined by $\alpha \Sigma(\vec{x} \to \vec{x}') = e^{-\beta/2}\, S(\alpha, \beta)$

$\varphi(y)$ neutron flux

$\varphi_0(y) = y e^{-y}$ maxwellian flux

$$c(y) = \frac{d}{dy} \frac{\varphi(y)}{\varphi_0(y)}$$

$q(y)$ is the slowing down density i-e the difference between the number of neutrons per unit time wich jump from an energy above y to an energy below y , and the number of those which do the reverse

$Q = q(\infty)$

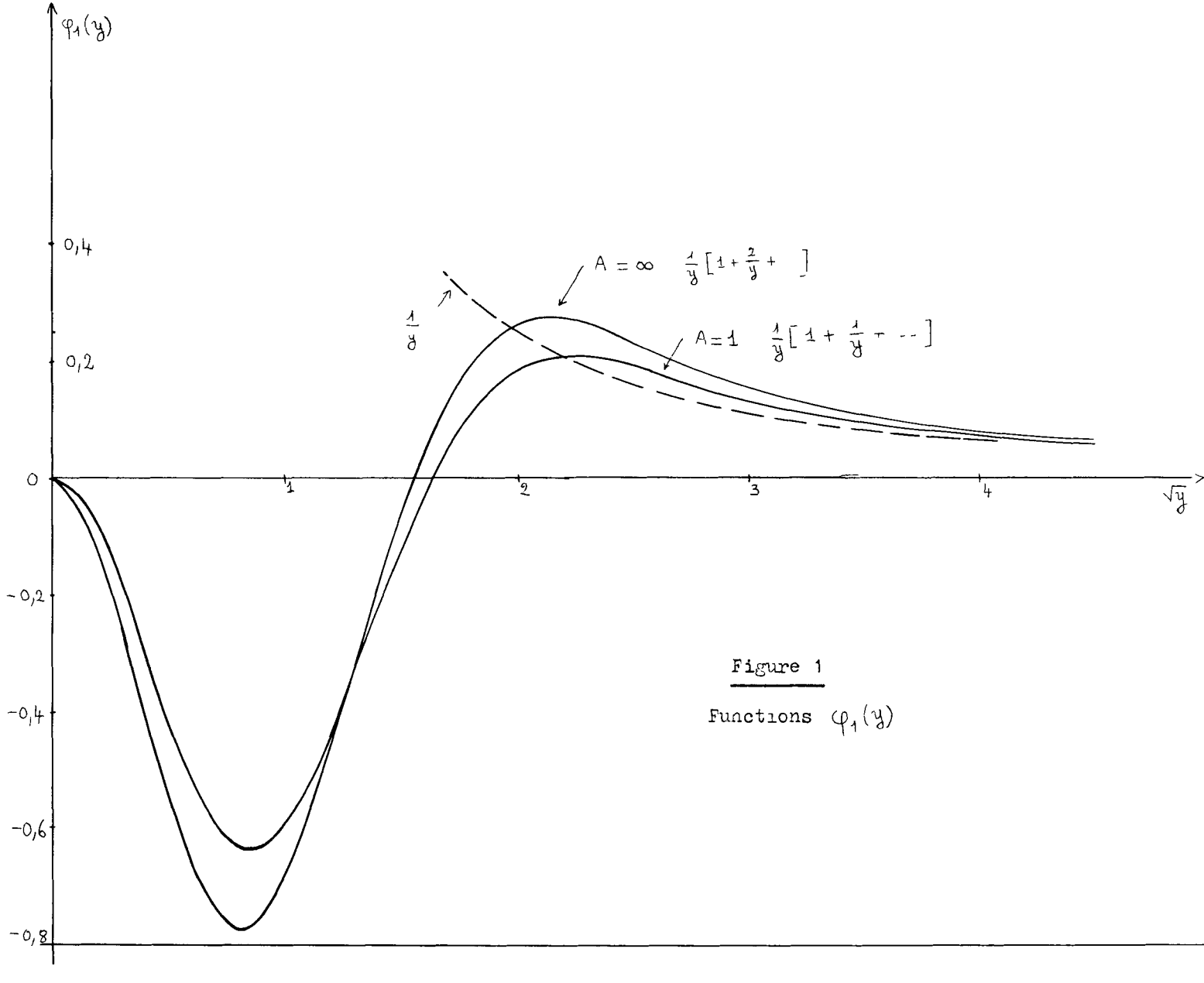

Figure 1

Functions $\varphi_1(y)$

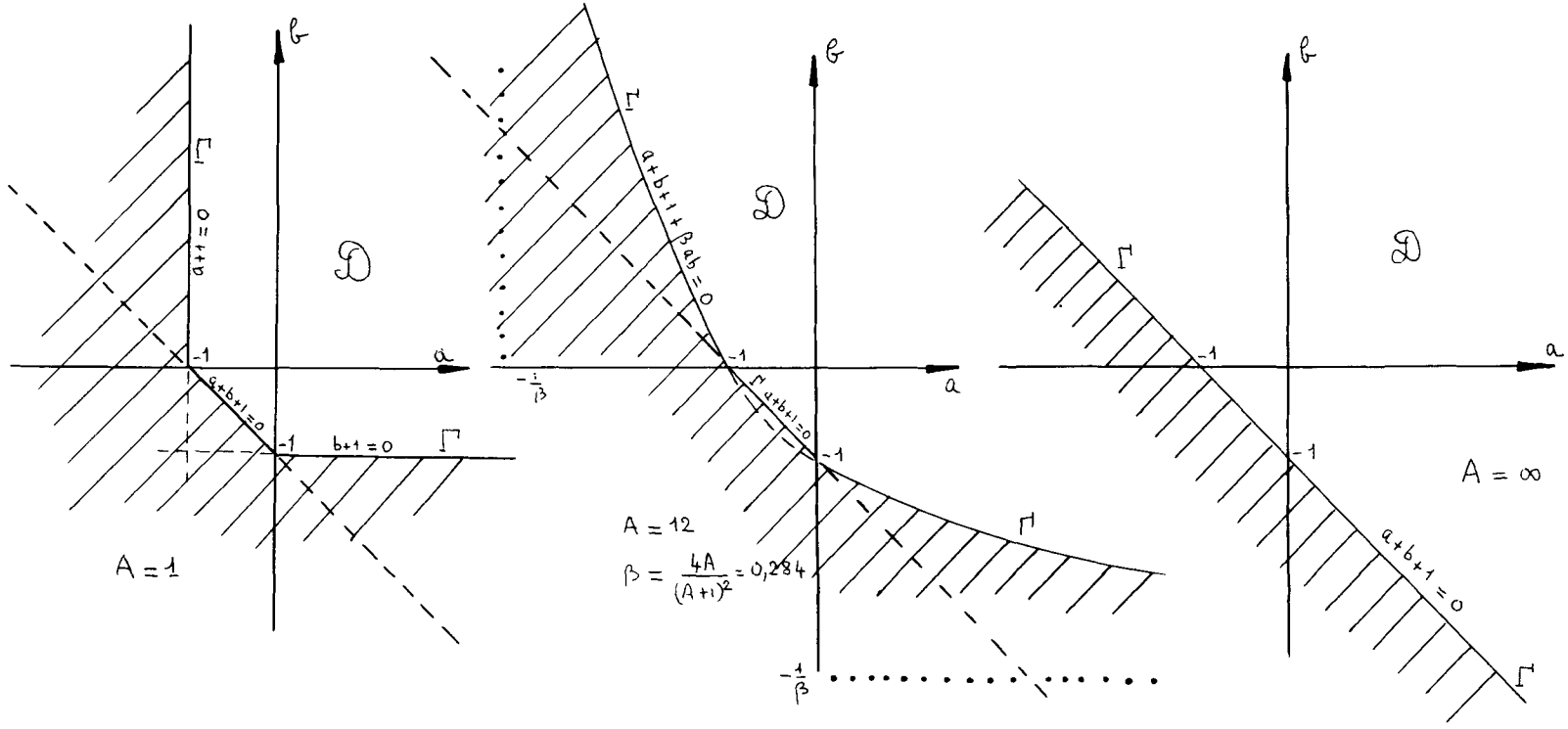

Figure 2 $\mathcal{D}$ and Γ for $A = 1$, $A = 12$ and $A = \infty$

In the case of the "differential model" discussed in section III, $\mathcal{D}$ and Γ are the same as for $A = 1$ (if $k(y) \neq 0$)

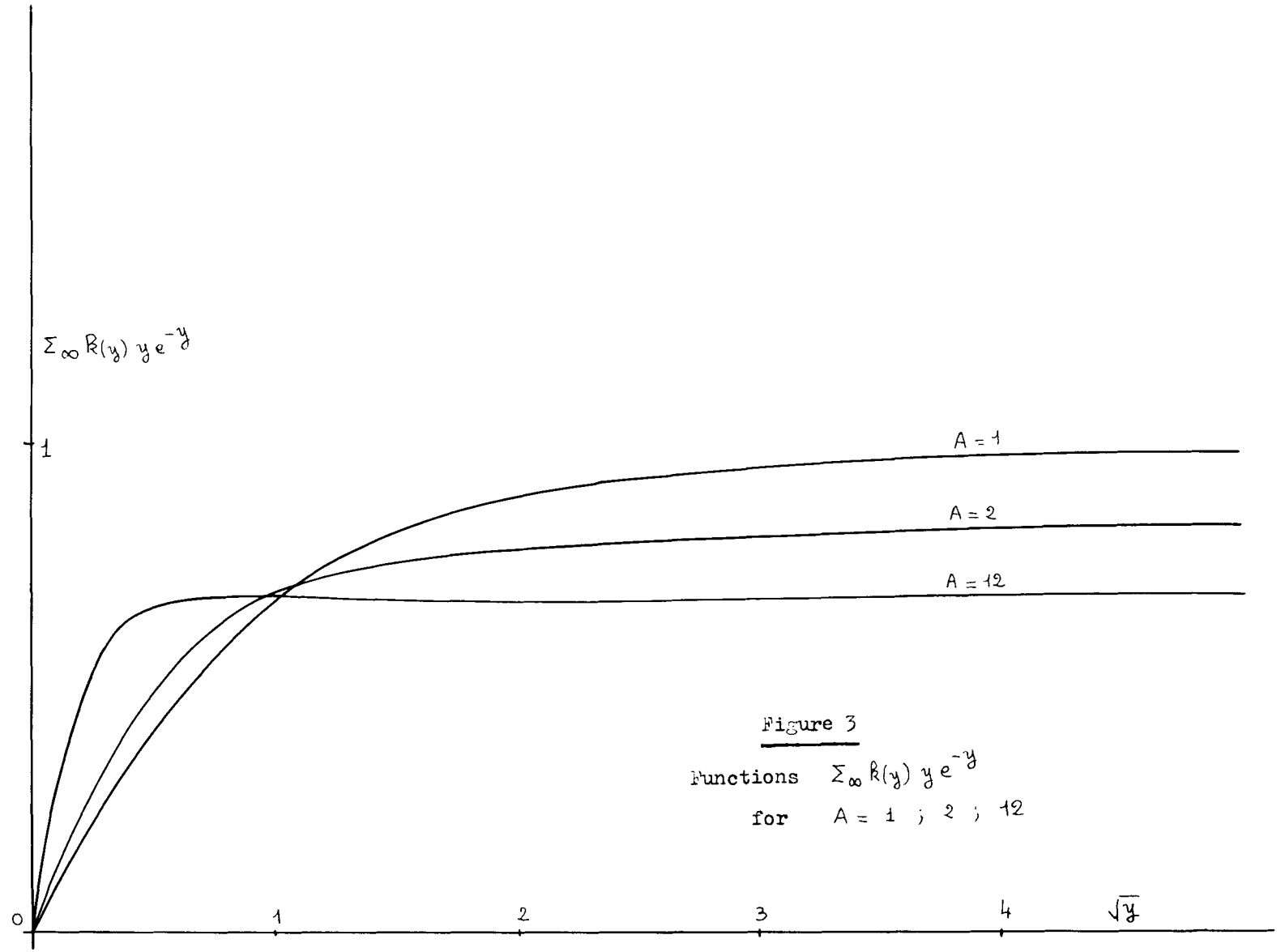

Figure 3

Functions $\Sigma_\infty R(y)\, y\, e^{-y}$

for A = 1 ; 2 ; 12

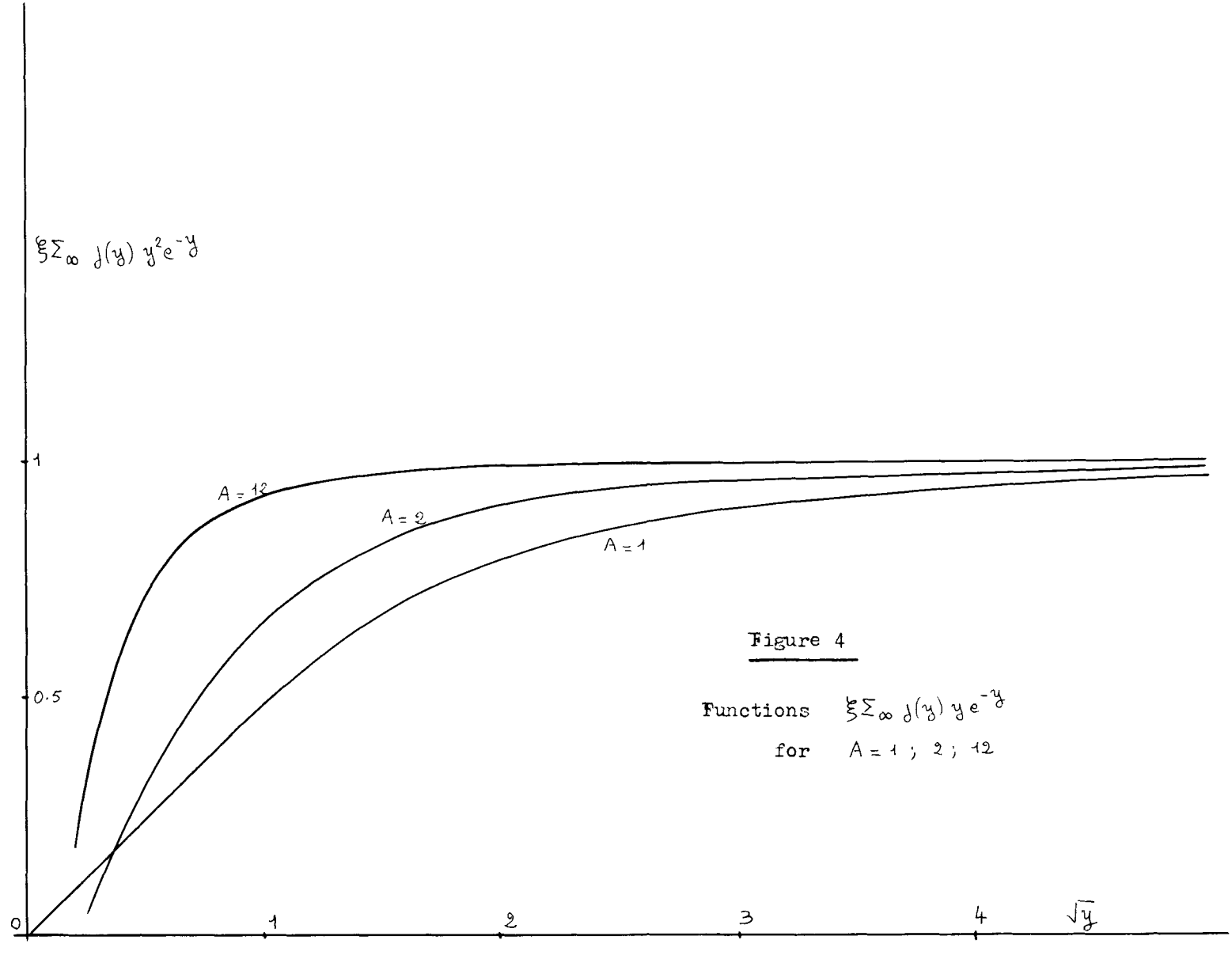

Figure 4

Functions $\xi\Sigma_\infty\, d(y)\, y\, e^{-y}$

for $A = 1\ ;\ 2\ ;\ 12$

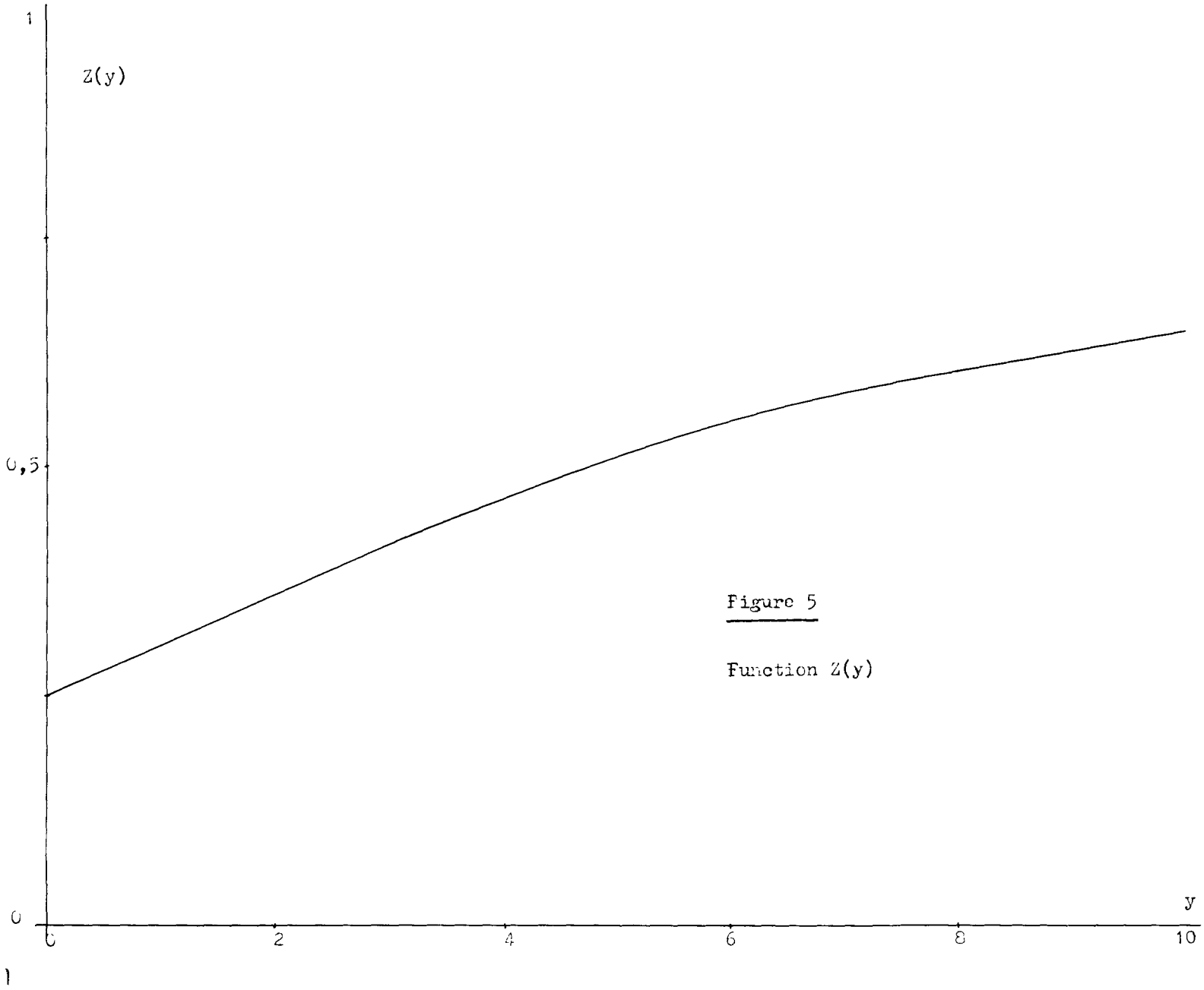

Figure 5

Function Z(y)

INTEGRAL AND NUMERICAL TREATMENTS OF THE NEUTRON TRANSPORT PROBLEM

by

G. Ronald Dalton
Department of Nuclear Engineering
University of Florida
Gainesville, Florida

Since the energy dependent neutron transport equation can be considered as a series of coupled one speed equations with an arbitrary source, the one speed equation is of some interest. The one speed space and angular dependent transport equation for steady state may be written symbolically as:

$$\left[L + T(\underline{r}) - S(\underline{r}, \underline{\Omega})\right] \Phi(\underline{r}, \underline{\Omega}) = q(\underline{r}, \underline{\Omega}) \quad (1)$$

where L is the leakage operator $\underline{\Omega} \cdot \nabla$, $T(\underline{r})$ is the space dependent total cross section $\Sigma_T(\underline{r})$, $S(\underline{r}, \underline{\Omega})$ is the scattering integral operator

$$\int_{\underline{\omega}} \Sigma_s(\underline{r}) f(\underline{\omega} \rightarrow \underline{\Omega}) \left[\Phi(\underline{r}, \underline{\omega})\right] d\underline{\omega}$$

then $q(\underline{r}, \underline{\Omega})$ is the source term due to scattering from other groups and $\Phi(\underline{r}, \underline{\Omega})$ is the neutron path length per cm^3 per sec per unit solid angle. The argument $\underline{r}$ in the $T(\underline{r})$ and $S(\underline{r}, \underline{\Omega})$ is meant to represent a stepwise continuous function associated with several regions of constant composition. Next there must be boundary conditions for the equation. For a unit cell with a perfectly reflecting surface $\Gamma(\underline{r}) = 0$ and surface unit normal $\hat{n}(\underline{r})$ then at the surface

$$\Phi(\underline{r}, \underline{\Omega}) = \Phi(\underline{r}, \underline{\Omega}'')$$

where $\underline{r}$ is on Γ and $\underline{\Omega}'' \times \hat{n} = -\underline{\Omega} \times \hat{n}$.

These same boundary conditions will apply to all differential equations in this paper, even those defining the Green's functions, unless otherwise stated.

Next one imagines the same unit cell with slightly changed nuclear properties in some region(s) of the cell. Using primes to denote the changed situation the transport equation becomes:

$$\left[L + T'(\underline{r}) - S'(\underline{r}, \underline{\Omega})\right]\Phi'(\underline{r}, \underline{\Omega}) = q'(\underline{r}, \underline{\Omega}) \quad (2)$$

Next define the difference flux as

$$\Psi(\underline{r}, \underline{\Omega}) \equiv \Phi(\underline{r}, \underline{\Omega}) - \Phi'(\underline{r}, \underline{\Omega}) \quad (3)$$

Subtracting the two transport equations gives

$$L\Psi(\underline{r}, \underline{\Omega}) + T(\underline{r})\Phi(\underline{r}, \underline{\Omega}) - T'(\underline{r})\Phi'(\underline{r}, \underline{\Omega})$$

$$-S(\underline{r},\underline{\Omega})\underline{\Phi}(\underline{r},\underline{\Omega})+S'(\underline{r},\underline{\Omega})\underline{\Phi}'(\underline{r},\underline{\Omega}) \tag{4}$$
$$=q(\underline{r},\underline{\Omega})-q'(\underline{r},\underline{\Omega})$$

In Eq. (4) the unperturbed flux $\underline{\Phi}(\underline{r},\underline{\Omega})$ in the unit cell is assumed to be known and one is interested only in the changes in flux (i.e. $\bar{\Psi}(\underline{r},\underline{\Omega})$) which occur when the disturbances in materials are introduced in the cell. The sources $q(\underline{r},\underline{\Omega})$ and $q'(\underline{r},\underline{\Omega})$ are assumed known for the one speed case; however, the sources will be calculated for the multi-speed case based on the scattered source from other speeds.

Next add $\Sigma_r^i \bar{\Psi}(\underline{r},\underline{\Omega})$ to both sides of Eq. (4) and use Eq. (3).

$$(L+\Sigma_r^i)\bar{\Psi}(\underline{r},\underline{\Omega})=\Sigma_r^i\bar{\Psi}(\underline{r},\underline{\Omega}) \tag{5}$$
$$-\bar{T}(\underline{r})\underline{\Phi}(\underline{r},\underline{\Omega})+\bar{T}'(\underline{r})\left(\underline{\Phi}(\underline{r},\underline{\Omega})-\bar{\Psi}(\underline{r},\underline{\Omega})\right)$$

$$+ S(\underline{r},\underline{\Omega})\Phi(\underline{r},\underline{\Omega}) - S'(\underline{r},\underline{\Omega})\left(\Phi(\underline{r},\underline{\Omega}) - \Psi(\underline{r},\underline{\Omega})\right)$$

(5)

$$+ q(\underline{r},\underline{\Omega}) - q'(\underline{r},\underline{\Omega})$$

Or

$$(L + \Sigma_T^i)\Psi(\underline{r},\underline{\Omega}) = \Sigma_T^i \Psi(\underline{r},\underline{\Omega})$$

$$\left(T'(\underline{r}) - T(\underline{r})\right)\Phi(\underline{r},\underline{\Omega}) - T'(\underline{r})\Psi(\underline{r},\underline{\Omega})$$

(6)

$$\left(S(\underline{r},\underline{\Omega}) - S'(\underline{r},\underline{\Omega})\right)\Phi(\underline{r},\underline{\Omega})$$

$$+ S'(\underline{r},\underline{\Omega})\Psi(\underline{r},\underline{\Omega}) + q(\underline{r},\underline{\Omega}) - q'(\underline{r},\underline{\Omega})$$

The constant Σ_T^i which is independent of position will be taken equal to the Σ_T for the material which occupies the largest volume in the cell (typically the moderator).

A Green's function for the operator $(L + \Sigma_T^i)$ and the above mentioned outer boundary conditions for a unit cell with perfectly boundaries is defined as the solution of

$$(L + \Sigma_T^i) g(\underline{r}, \underline{\Omega}; \underline{r}', \underline{\Omega}') = \delta(\underline{r} - \underline{r}') \, \delta(\underline{\Omega} - \underline{\Omega}') \qquad (7)$$

in the unit cell. The function $g(\underline{r}, \underline{\Omega}; \underline{r}', \underline{\Omega}')$ is then the first flight or uncollided flux (cm of path length per cm^3 per sec per unit solid angle) in the cell at point $\underline{r}$ in direction $\underline{\Omega}$ due to a unit source emitting one neutron per second at point $\underline{r}'$ in direction $\underline{\Omega}'$. Note that reflection at the cell surface does not constitute a collision.

Using this Green's function to convert Eq. (6) to an integral equation gives

$$\Psi(\underline{r}, \underline{\Omega}) = \int_{\substack{\underline{r}' \text{ in } P \\ \underline{\Omega}'}} g(\underline{r}, \underline{\Omega}; \underline{r}', \underline{\Omega}') \times \left(T'(\underline{r}') - T(\underline{r}') \right) \Phi(\underline{r}', \underline{\Omega}') \, d\underline{r}' \, d\underline{\Omega}'$$

$$+\int_{\substack{r' \text{ in } Q \\ \Omega'}} g(r,\Omega;r',\Omega')\left[\Sigma_T^i - T'(r')\right] \times \bar{\psi}(r';\Omega')\,dr'\,d\Omega'$$

$$+\int_{\substack{r' \text{ in } Q \\ \Omega'}} g(r,\Omega;r',\Omega')\left[S(r';\Omega') - S'(r';\Omega')\right] \times \bar{\phi}(r';\Omega')\,dr'\,d\Omega' \qquad (8)$$

$$+\int_{r',\Omega'} g(r,\Omega;r',\Omega')\,S'(r';\Omega')\,\bar{\psi}(r';\Omega')\,dr'\,d\Omega'$$

$$+\int_{r',\Omega'} g(r,\Omega;r',\Omega')\left[q(r';\Omega') - q'(r';\Omega')\right] \times dr'\,d\Omega'$$

Here the region P is that portion of the cell where $T(r)$ differs from $T'(r)$ and Q is that region where $T(r)$ differs from Σ_T^i. Unless otherwise noted integrals over r extend over the entire cell.

Let us next examine a more conventional use of a first flight Green's function associated with Eq. (4).[1]

Rewriting Eq. (4) gives

$$L\bar{\Psi}(\underline{r},\underline{\Omega}) + T'(\underline{r})\bar{\Psi}(\underline{r},\underline{\Omega}) =$$

$$\left[T'(\underline{r}) - T(\underline{r})\right]\bar{\Phi}(\underline{r},\underline{\Omega}) + S(\underline{r},\underline{\Omega})\bar{\Phi}(\underline{r},\underline{\Omega}) \tag{9}$$

$$- S'(\underline{r},\underline{\Omega})\left[\bar{\Phi}(\underline{r},\underline{\Omega}) - \bar{\Psi}(\underline{r},\underline{\Omega})\right] + q(\underline{r},\underline{\Omega}) - q'(\underline{r},\underline{\Omega})$$

The Green's function corresponding to the operator on the left of Eq. (9) is called $h(\underline{r},\underline{\Omega},\underline{r}',\underline{\Omega}')$ and is defined as the solution to the equation:

$$\underline{\Omega}\cdot\nabla h(\underline{r},\underline{\Omega};\underline{r}',\underline{\Omega}') + T(\underline{r})h(\underline{r},\underline{\Omega};\underline{r}',\underline{\Omega}') \tag{10}$$
$$= \delta(\underline{r}-\underline{r}')\delta(\underline{\Omega}-\underline{\Omega}')$$

The sole difference between the $g(\underline{r},\underline{\Omega};\underline{r}',\underline{\Omega}')$ and $h(\underline{r},\underline{\Omega};\underline{r}',\underline{\Omega}')$ is that g is the flux in a single medium unit cell with Σ_T^i whereas h is the flux in a cell with the perturbed total cross section $T'(\underline{r})$ which is a stepwise function of position. The source and observation coordinates and the unit cell boundary conditions are the same for g and h.

Using the Green's function $h(\underline{r},\underline{\Omega};\underline{r},\underline{\Omega})$

Eq. (9) becomes:

$$\bar{\Psi}(\underline{r},\underline{\Omega}) = \int_{\substack{\underline{r}' \text{ in } P \\ \underline{\Omega}'}} h(\underline{r},\underline{\Omega};\underline{r}',\underline{\Omega}') \cdot$$

$$\left[T'(\underline{r}') - T(\underline{r}')\right] \bar{\Phi}(\underline{r}',\underline{\Omega}') d\underline{r}' d\underline{\Omega}' \qquad (11)$$

$$+ \int_{\substack{\underline{r}' \text{ in } P \\ \underline{\Omega}'}} h(\underline{r},\underline{\Omega};\underline{r}',\underline{\Omega}')\left[S(\underline{r}',\underline{\Omega}' - S'(\underline{r}',\underline{\Omega}')\right]$$

$$\times \bar{\Phi}(\underline{r}',\underline{\Omega}') d\underline{r}'\underline{\Omega}'$$

$$+ \int_{\underline{r}',\underline{\Omega}'} h(\underline{r},\underline{\Omega},\underline{r}',\underline{\Omega}') S(\underline{r}',\underline{\Omega}') \bar{\Psi}(\underline{r}',\underline{\Omega}') d\underline{r}' d\underline{\Omega}'$$

$$+ \int_{\underline{r}',\underline{\Omega}'} h(\underline{r},\underline{\Omega};\underline{r}',\underline{\Omega}')\left[q(\underline{r}',\underline{\Omega}') - q'(\underline{r}',\underline{\Omega}')\right]$$

$$d\underline{r}' d\underline{\Omega}'$$

The above mentioned heterogenities associated with h make it a more difficult function to calculate numerically. Further the integral equation which results from the use of g (Eq. (8)) is no more difficult to integrate numerically than Eq. (11) associated with the h function.

Thus it seems that using the Green's function g associated with a ficticious homogeneous cell has the distinct advantage of being considerably easier to calculate than the Green's function h for the real heterogeneous cell. Once the Green's function has been calculated the difficulty of numerical solution of the resultant integral equation is essentially independent of the Green's function used.

There is yet another integral form of Eq. (4) which is of interest. Rewrite Eq. (4) as:

$$\left[L + T(\underline{r}) - S(\underline{r},\underline{\Omega})\right]\Psi(\underline{r},\underline{\Omega}) =$$

$$\left[T(\underline{r}) - T'(\underline{r})\right]\Psi(\underline{r},\underline{\Omega}) +$$

$$\left[T'(\underline{r}) - T(\underline{r})\right]\Phi(\underline{r},\underline{\Omega}) + \qquad (12)$$

$$\left[S(\underline{r},\underline{\Omega}) - S'(\underline{r},\underline{\Omega})\right]\Psi(\underline{r},\underline{\Omega}) +$$

$$g(\underline{r},\underline{\Omega}) - g'(\underline{r},\underline{\Omega})$$

In this case the Green's function $G(\underline{r}, \underline{\Omega}; \underline{r}', \underline{\Omega}')$ is defined as the solution to the equation:

$$L\, G(\underline{r}, \underline{\Omega}, \underline{r}', \underline{\Omega}') + T(\underline{r}) G(\underline{r}, \underline{\Omega}; \underline{r}', \underline{\Omega}') -$$

$$S(\underline{r}, \underline{\Omega}) G(\underline{r}, \underline{\Omega}; \underline{r}', \underline{\Omega}') = \delta(\underline{r} - \underline{r}') \delta(\underline{\Omega} - \underline{\Omega}') \quad (13)$$

The function $G(\underline{r}, \underline{\Omega}; \underline{r}', \underline{\Omega}')$, sometimes called the transport kernel, is the neutron flux (path length per unit volume per sec per unit solid angle) at $\underline{r}$ and $\underline{\Omega}$ due to a unit source of one neutron per second introduced at $\underline{r}'$ and $\underline{\Omega}'$ in the cell with heterogeneous properties $T(\underline{r})$ and $S(\underline{r}, \underline{\Omega})$. For the special case of a unit cell which is many mean free path in least dimension and homogeneous the function of $G(\underline{r}, \underline{\Omega}; \underline{r}', \underline{\Omega}')$ is known analytically and numerically.[2,3] However, the general $G(\underline{r}, \underline{\Omega}; \underline{r}', \underline{\Omega}')$ can be determined in a systematic fashion for a heterogeneous finite cell if enough effort is expended.

For this case the integral form of Eq. (12) is:

$$\Psi(\underline{r}, \underline{\Omega}) = \int_{\underline{r}' \text{ in } P} \int_{\underline{\Omega}'} G(\underline{r}, \underline{\Omega}; \underline{r}', \underline{\Omega}') \cdot$$

$$\left\{ \left[T(\underline{r}') - \bar{T}(\underline{r}') \right] \Psi(\underline{r}', \underline{\Omega}') + \right.$$

$$\left[\bar{T}'(\underline{r}') - \bar{T}(\underline{r}')\right]\bar{\Phi}(\underline{r};\underline{\Omega}') + \tag{14}$$

$$\left[S(\underline{r};\underline{\Omega}') - S'(\underline{r};\underline{\Omega}')\right]\bar{\Psi}(\underline{r};\underline{\Omega}') +$$

$$\left[q(\underline{r};\underline{\Omega}') - q'(\underline{r};\underline{\Omega}')\right]\Big\} d\underline{r}'d\underline{\Omega}'$$

As before region P is that region or regions in which the properties (T, S or q) have changed between the unprimed and the primed condition. The fact that all of the integrals of Eq. (15) are only over the perturbed region offers a particular advantage in the case of a cell with infinitely remote outer boundaries (e.g. a detector located in an infinite medium) in that the differential Eq. (12) which is infinite in extent in $\underline{r}$ space is reduced to an integral Eq. (14) which is valid for all $\underline{r}$ but need be integrated only over a finite $\underline{r}$ in P. For the case of a small unit cell the integral Eq. (12) still has the advantage that its integrals extend only over the perturbed regions of the cell but is valid everywhere in the cell.

We are now in a position to observe one of the unique advantages of integral equations. For a given order of expansion in spherical harmonics integral

Eqs. (8), (11), and (14) are inherently more accurate than the differential Eq. (4). In order to see this, one expands the $\underline{\Omega}$ angular dependence of $\Phi(\underline{r},\underline{\Omega})$, $\Phi'(\underline{r},\underline{\Omega})$, $\Psi(\underline{r},\underline{\Omega})$, $q(\underline{r},\underline{\Omega})$ and $q'(\underline{r},\underline{\Omega})$ in an infinite series of spherical harmonics $Y_n^m(\underline{\Omega})$. That is, for a general function

$$\omega(x,y\cdots\underline{\Omega}) = \sum_{\substack{n=0\\m=-n}}^{\substack{m=n\\n=\infty}} Y_n^m(\underline{\Omega})\,\omega_n^m(x,y\cdots) \qquad (14)$$

next expand the functions $g(\underline{r},\underline{\Omega};\underline{r}';\underline{\Omega}')$, $h(\underline{r},\underline{\Omega};\underline{r}',\underline{\Omega}')$ and $G(\underline{r},\underline{\Omega};\underline{r}',\underline{\Omega}')$ in an infinite series of the complex conjugate spherical harmonics

$$z(x,y\cdots\underline{\Omega}') = \sum_{\substack{n=0\\m=-n}}^{\substack{m=n\\n=\infty}} Y_n^{m*}(\underline{\Omega}')\,z(x,y\cdots). \qquad (15)$$

Insertion of the expansions for Φ, q, Φ', q' and Ψ in the differential Eq. (4) and use of the recursion relation for the associated Legendre polynomials of the 1st kind gives the usual infinite series of coupled equations in the unknown coefficients $\Psi_n^m(\underline{r})$ similar in form to the equations for the spherical harmonic coefficients developed in Ch. of Ref. (4). In the N^{th}

order approximation of the differential equation one terminates the summation for $\Psi(\underline{r}, \underline{\Omega})$ after N + 1 terms and assumes that

$$\bar{\Psi}_N^i(\underline{r}) >> \bar{\Psi}_j^k(\underline{r}) \quad \text{for } j > N \tag{16}$$

Next insert the expansions for $\Phi, q, \Phi', \bar{\Psi}$ and q into Eq. (8). Carry out the $\underline{\Omega}'$ integration noting that

$$\int_{\underline{\Omega}} Y_a^b(\underline{\Omega}) Y_n^{*m}(\underline{\Omega}) d\underline{\Omega} = \delta(a-n)\delta(b-m) \tag{17}$$

Typical of the terms which now remain is the term resulting from the second term on the right of Eq. (8):

$$\int_{\underline{r}' \text{ in } P} \left[\Sigma_T^i - T'(\underline{r}')\right] \sum_{n,m} \bar{\Psi}_n^m(\underline{r}') \cdot q_n^m(\underline{r}, \underline{\Omega}; \underline{r}') d\underline{r}' \tag{18}$$

If one now terminates the expansion at N terms one implies that

$$\bar{\Psi}_N^i(\underline{r}') q_N^i(\underline{r}, \underline{\Omega}; \underline{r}') >> \bar{\Psi}_j^k(\underline{r}') q_j^k(\underline{r}, \underline{\Omega}; \underline{r}') \quad \text{for } j > N \tag{19}$$

Insertion of the expansions into Eq. (11) and termination

at N terms implies that:

$$\Psi_N^i(\underline{r}')\, h_N^i(\underline{r},\underline{\Omega};\underline{r}') >> \Psi_j^k(\underline{r}')\, h_j^k(\underline{r},\underline{\Omega},\underline{r}') \quad \text{for } j>N \tag{20}$$

Finally insertion of the expansions into Eq. (14) and termination at N terms implies that

$$\Psi_N^i(\underline{r}')\, G_N^i(\underline{r},\underline{\Omega};\underline{r}') >> \Psi_j^k(\underline{r}')\, G_j^k(\underline{r},\underline{\Omega};\underline{r}') \quad \text{for } j>N \tag{21}$$

Note that the expansion in spherical harmonics of $\delta(\underline{\Omega}-\underline{\Omega}')$ is

$$\delta(\underline{\Omega}-\underline{\Omega}') = \sum_{\substack{n=0 \\ m=-n}}^{\substack{n=\infty \\ m=n}} Y_n^{*m}(\underline{\Omega}')\, Y_n^m(\underline{\Omega}) \tag{22}$$

For a given direction $\underline{\Omega}'$ the magnitude of the coefficients $Y_n^{m*}(\underline{\Omega}')$ is

$$\left| Y_n^{*m}(\underline{\Omega}') \right| \sim \left(\frac{2n+1}{4\pi} \cdot \frac{(n-|m|)!}{(n+|m|)!} \right)^{1/2} \tag{23}$$

and these coefficients tend to diverge as $n^{1/2}$. Then the function whose expansion is $\sum_{n,m} 1 \cdot Y_n^m(\underline{\Omega})$ is highly nonisotropic but not quite as nonisotropic as a delta function.

Now h is the uncollided (with nuclei) flux due to a source at $\underline{r}'$ and $\underline{\Omega}'$ in a cell with reflecting boundaries and a medium characterized by $T(\underline{r})$. The function g is similar but for a medium characterized by Σ_T'. Now if either the h or g are for an infinite or very large cell they become

$$h \text{ or } g = \delta(\underline{\Omega} - \underline{\Omega}')\,\delta(\underline{\Omega} - [\hat{\underline{r} - \underline{r}'}]) \cdot \frac{e^{-\int_{\ell=0}^{1} \Sigma_T(\underline{r}' + [\underline{r} - \underline{r}']\ell)\,d\ell}}{|\underline{r} - \underline{r}'|^2} \qquad (23)$$

If we place a reflecting boundary around the source the dependence of h and g on $\underline{\Omega}$ will be more isotropic than given by Eq. (23). In fact, the g with its low Σ_T', long mean free path and many reflections should be considerably more isotropic than the corresponding h which will have regions of high Σ_a due to fuel lumps or other absorbers.

If, then, due to the reflecting boundaries the h and the g are reasonably isotropic, then the coefficients

$g_n^m(\underline{r}, \underline{\Omega}; \underline{r}')$ and $h_n^m(\underline{r}, \underline{\Omega}; \underline{r}')$ will form a decreasing series for increasing n. The coefficients of the expansion of the G can be written[3] as:

$$G_n^m(\underline{r}, \underline{\Omega}; \underline{r}') = G_n(|\underline{r} - \underline{r}'|) Y_n^m(\underline{\Omega}) \tag{24}$$

for an infinite one speed homogeneous cell. These coefficients have been evaluated and it can be seen that G_1 is very small compared to G_0 and higher order terms decrease rapidly as n increases.

Based on the increasing isotropy from h to g to G one can conclude that for a fixed N^{th} order spherical harmonic expansion

$$1\bar{\Psi}_N^m > h_N^m \bar{\Psi}_N^m > g_N^m \bar{\Psi}_N^m > G_N^m \bar{\Psi}_N^m \tag{25}$$

and the solution defined by Eqs. (13) and (14) is more accurate than that defined by Eqs. (7) and (8) which is better than that of Eqs. (10) and (11) which is finally better than the conventional P_N or Y_N approximation to the differential Eq. (4) for the finite cell.

There is, however, one important exception to this set of conclusions. For the special case of an isotropic initial flux $\bar{\phi}$, isotropic scatter S and isotropic sources g then Eqs. (10) and (11) can be

integrated over all $\underline{\Omega}$ and all $\underline{\Omega}'$ to give:

$$L\,h(\underline{r},\underline{r}') + T(\underline{r})\,h(\underline{r},\underline{r}') = \delta(\underline{r}-\underline{r}') \qquad (26)$$

and

$$\psi(\underline{r}) = \int_{\underline{r}' \text{ on } \Gamma} h(\underline{r};\underline{r}')\left[A'(\underline{r}') - A(\underline{r}')\right]\phi(\underline{r}')\,d\underline{r}'$$

$$+ \int_{\underline{r}'} h(\underline{r};\underline{r}')\,S(\underline{r}')\,\psi(\underline{r}')\,d\underline{r}' \qquad (27)$$

$$+ \int h(\underline{r};\underline{r}')\left[q(\underline{r}') - q'(\underline{r}')\right]d\underline{r}'$$

where

$$\psi(\underline{r}) \equiv \int_{\underline{\Omega}} \psi(\underline{r},\underline{\Omega})\,d\underline{\Omega} = \sqrt{4\pi}\,\Psi_0^0(\underline{r})$$

$$\phi(\underline{r}) \equiv \int_{\underline{\Omega}} \Phi(\underline{r},\underline{\Omega})\,d\underline{\Omega} = \sqrt{4\pi}\,\Phi_0^0(\underline{r}) \qquad (28)$$

$$A(\underline{r}) = \Sigma_T(\underline{r})$$

$$A'(\underline{r}) = \Sigma_T'(\underline{r})$$

$$q(\underline{r}) \equiv \int_{\underline{\Omega}} q(\underline{r},\underline{\Omega})\, d\underline{\Omega} = \sqrt{4\pi}\, q_0^0(\underline{r})$$

$$q'(\underline{r}) \equiv \int_{\underline{\Omega}} q'(\underline{r},\underline{\Omega})\, d\underline{\Omega} = \sqrt{4\pi}\, q_0'^0(\underline{r})$$

and $h(\underline{r},\underline{r}')$ is defined as the solution of Eq. (27). However, it can be noted that

$$h(\underline{r},\underline{r}') = \int_{\underline{\Omega},\underline{\Omega}'} h(\underline{r},\underline{\Omega};\underline{r}',\underline{\Omega}')\, d\underline{\Omega}\, d\underline{\Omega}' \qquad (29)$$

So Eq. (28) is the integral equation for root four pi times the zeroth harmonic coefficient (i.e. the neutron scalar flux disturbance). This Eq. (27) for the disturbed flux $\psi(\underline{r})$ is not coupled to any of the other harmonics and so no assumptions nor approximations (by cutting off the sum at N) need be made. Equation (28) is exact.

By way of demonstration of the value and accuracy of the integral equation method consider the calculation of the flux depression caused by a highly absorbing foil placed in a thermal neutron flux in a diffusing medium. It is well known[5] that diffusion theory (i.e. the Y_1^i differential equations) is not adequate to treat this problem and in the typical case P_3 or P_5 calculations have been found to be necessary. Using the

method of Eqs. (26) and (27) which is exact, Ritche's[1] has obtained very accurate solutions to this problem. Using only the Y_o^o terms (i.e. a zeroth order spherical harmonic approximation) the integral Eq. (14) has been evaluated numerically using computers[3,6] and by hand[7]. A comparison[8] with Ritchie's results shows that there is essentially no difference between the two methods over a wide range of parameters.

Thus one is led to the conclusion, incongruous though it sounds, that the zeroth spherical harmonic form of an integral form of the neutron transport equation gives results which can be obtained only with much higher order spherical harmonic approximations to the differential form of the same transport equation.

In view of these advantages of integral forms of the transport equation a number of forms of this problem are being developed. The analytic work has been completed to extend the integral equation using the transport kernel (Eqs. (13) and (14)) to the multi-speed case.[9] Monte Carlo techniques are being applied to the numerical calculation of the Green's function k for a series of specific finite geometries. The energy dependent version of integral method of Eqs. (8) and (9) is being developed.

REFERENCES

1. R. H. Ritchie and H. B. Eldridge, Nuclear Sci. & Eng., 8, 300-311, (1960).

2. K. Case, F. deHoffman & G. Placzek, Introduction to the Theory of Neutron Diffusion, Vol. I, U. S. Government Printing Office, Washington D. C., 1953.

3. G. R. Dalton and R. K. Osborn, Nuclear Sci. & Eng., 9, 198-210, (1960).

4. R. V. Meghreblian and D. K. Holmes, "Reactor Analysis", McGraw-Hill, New York, 1960.

5. C. W. Tittle, Nucleonics 8, 5(1951).

6. G. R. Dalton, Computer Code Abstract Number 33, "Detector", Nuclear Sci. & Eng., 12, 2, (1962).

7. G. R. Dalton, Interaction of Adjacent Neutron Detectors, In Press, Nuclear Sci. & Eng.

8. G. R. Dalton & R. H. Ritchie, Re: "Thermal Neutron Flux Depression by Absorbing Foils" and "Flux Perturbations by Thermal Neutron Detectors," Nuclear Sci. & Eng., 11, 4, (1961).

9. D. E. Emon, "The Effects of Neutron Absorbers on Energy Dependent Neutron Flux," Thesis, University of Florida, (1961).

Neutron Spectra in Heterogeneous Assemblies,

a Summary of the Work of the Karlsruhe Group

by

Wolf Häfele

Institut für Neutronenphysik und Reaktortechnik

des Kernforschungszentrums Karlsruhe

Table of Contents

Neutron Spectra in Heterogeneous Assemblies, a Summary of the Work of the Karlsruhe Group *

by

Wolf Häfele

Institut für Neutronenphysik und Reaktortechnik

des Kernforschungszentrums Karlsruhe

1. Introduction

The investigation of neutron spectra in nuclear reactors and assemblies is of considerable interest. The real precise prediction of the neutron balance in a thermal reactor depends on the knowledge of the neutron spectra particularly at lower energies. Strongly dependent is especially the long time behaviour of a thermal reactor where U^{238} is largely converted into Pu^{239} with its important fission resonance at 0.3 eV. The spectra are mostly used to produce properly averaged cross section data for a more simple multigroup calculation. But the interaction of slow neutrons with the scattering atoms of, say, hydrogen is also of interest for pure physical reasons. Therefore the theory of neutron

* Submitted to the Conference on Neutron Thermalization, Brookhaven National Laboratory, April 30 - May 2, 1962

thermalization is a link between reactor theory and pure physics.

There are two main influences on neutron spectra. The first is the mechanism of the single process, where a neutron is scattered by a moderating atom. The second is the superposed net diffusion process which transports the slow neutrons to the absorbing materials like fuel rods etc. The second process, of course, is of interest only, if the reactor is a heterogeneous one. But this is true for almost all existing reactors. The investigation of the first influence suggests the picture of an infinite homogeneous assembly where no net diffusion process takes place and the interest is focussed on the single scattering process. The investigation of the influence of the heterogeneity suggests a picture where the single scattering process is as simple as possible but typical and the heterogeneity is idealized into the δ function type sink and source model, which allows for a simple mathematical description.

The investigation of the influence of the single scattering process on neutron spectra has found a widespread interest during the last years because of the more physical background. The Karlsruhe group, however, has also emphasized the study of the influence of heterogeneity on neutron spectra. This paper summarizes the work on this second aspect.

2. The heterogeneous reactor model

H. Hurwitz jr., M.S. Nelkin and G.J. Habetler derive in their early paper [1] the equations for space dependent neutron spectra . They start from the Boltzmann equation, use the spherical harmonics method and arrive finally at an equation of the diffusion type.

The equation is the following one:

$$(1) \qquad (\Sigma_a - D\Delta)\ \phi(\vec{r},E) = L(\phi(\vec{r},E))$$

$$(2) \qquad L(\phi(\vec{r},E)) = \int dE'\ \Sigma_o(E' \rightarrow E)\ \phi(\vec{r},E') - \Sigma_S(E) \cdot \phi(\vec{r},E) = -\frac{\partial q}{\partial E}$$

$$(3) \qquad \Sigma_S(E) = \int \Sigma_o(E \rightarrow E')\ dE'$$

$$(4) \qquad D = \frac{1}{3\ \Sigma_S}$$

Σ_a is the absorption cross section, in principle space and energy dependent

q is the slowing down density defined by (2)

Δ is the Laplace Operator

$\vec{r}$ is the spatial vector

E is the energy of the neutron

$\Sigma_o(E' \rightarrow E)$ is the energy transport cross section which gives in case of a scattering process the neutron from E' to E.

The other quantities are defined in the equations (2) - (4).

We deal now with (1) and explain the Meetz model of heterogeneity [2]. In the simplest case we have a one dimensional model, $\vec{r}$ is to be replaced by the simple coordinate x. We consider a finite reactor configuration of thickness 2ℓ with

$$N_o = 2N+1 \tag{5}$$

that is, with an odd number of fuel elements of thickness 2a and spacing d (Fig. 1).

We further require that there shall be moderator to such an extent that the reactor consists of N_o Wigner Seitz cells only, that is

$$2\ell = N_o d \tag{6}$$

If we describe the fuel plates by δ functions, this model leads to the following equation:

$$D \frac{\partial^2 \phi}{\partial x^2} + L(\phi) + f_- = 0 \ , \tag{7}$$

where

$$f_- = -\,2a\,\Sigma_a(\varepsilon) \sum_{k=-N}^{+N} \delta(x-kd)\,\phi(kd,\varepsilon)\ . \tag{8}$$

We use here and in the following the normalized energy

$$\varepsilon = \frac{E}{kT} \tag{9}$$

where k is the Boltzmann constant and T the temperature of the moderator.

$\Sigma_a(\varepsilon)$ is now an effective cross section adapted to the absorption strength in the real, finite plates. In the case of no self shielding $\Sigma_a(E)$ is simply the absorption cross section of the fuel: In case of such a self shielding the value and energy dependence of $\Sigma_a(\varepsilon)$ must be taken from a transport calculation inside the fuel. In the simple but artificial case of the validity of an diffusion equation

$$\frac{d^2\phi}{dx^2} - K^2\,\phi = 0$$

we have

$$\Sigma_a(\varepsilon) = (\Sigma_a)_{fuel} \cdot \frac{\sinh K\,a}{K\,a}$$

The boundary conditions which determine together with (7) the problem are the following:

$$\phi(\pm \ell, \varepsilon) = 0 \tag{10}$$

$$q(x,0) = 0 \tag{11}$$

$$q(x,\varepsilon_f) = \nu \cdot 2a \cdot \sum_{k=-N}^{+N} \delta(x-kd) \cdot \int_0^{\varepsilon_f} \phi(kd,\tilde{\varepsilon})\ \Sigma_f(\tilde{\varepsilon})\ d\tilde{\varepsilon} \tag{12}$$

In (12) we assume that all fission neutrons appear at a discrete energy ε_f. Σ_f is the fission cross section, ν the number of neutrons per fission.

We now introduce two abbreviations:

$$\frac{D}{\xi \Sigma_S} = x_o^2 \tag{13}$$

$$\frac{2a\ \Sigma_a(\varepsilon)}{d\ \xi \Sigma_S} = p(\varepsilon) \tag{14}$$

ξ is the logarithmic energy decrement for scattering down processes at high energy that is: a constant value.

We now make the following ansatz:

$$\phi = \sqrt{\ell} \cdot \sum_{p=o}^{\infty} \varphi_p(\varepsilon)\ v_p(x) \tag{15}$$

v_p are the orthonormalized eigenfunctions of the Δ operator and the boundary conditions (9):

$$v_p = \frac{1}{\sqrt{\ell'}} \cos \alpha_p x \tag{16}$$

$$\alpha_p = \frac{\pi}{2\ell} (2p + 1) \tag{17}$$

Inserting this into (7) leads to the following equation

$$- x_o^2 \alpha_q^2 \varphi_q + \frac{L(\varphi_q)}{\xi \Sigma_S} - p(\varepsilon) \sum_p \varphi_p(\varepsilon) \, d\left[v_p, v_q\right] = 0 \tag{18}$$

$d\left[v_p, v_q\right]$ is Meetz's matrix for heterogeneous plate type assemblies

$$d\left[v_p, v_q\right] = \sum_{k=-N}^{+N} d \cdot v_p(kd) \, v_q(kd) \tag{19}$$

This matrix has a "one" in the diagonal terms:

$$\begin{aligned} 1 + p + q &= N_o n \qquad && n = 1,2,3 \\ p - q &= N_o m \qquad && m = 0, \pm 1, \pm 2, \pm 3 \end{aligned} \tag{20}$$

All other terms are zero. (20) implies the fact, that the system (18)

splits into N+1 different sets of equations, where only the quantities

$$\varphi_{N_o m + s} \quad , \qquad \varphi_{N_o m - s - 1}$$

appear.

We obey the fact that

$$\alpha^2_{N_o m - s - 1} = \alpha^2_{N_o m + s}$$

and rearrange the indices:

$$(21) \qquad \varphi_{N_o m - s - 1} \longrightarrow \varphi_{-(N_o m + s)}$$

(21) implies that now m goes from $-\infty$ to $+\infty$ and covers then all index constellations in question.

Therefore we have

$$(22) \quad -x_o^2 \alpha^2_{N_o r + s} \varphi_{N_o r + s} + \frac{1}{\xi \Sigma_S} L(\varphi_{N_o r + s}) - p(\varepsilon) \sum_{m=-\infty}^{+\infty} \varphi_{N_o m + s} = 0$$

$$r = -\infty \ldots. +\infty$$

$$s = 0,1,2 \ldots. N$$

The boundary condition (12) obeys the same symmetry. The exitation strength of the q mode shall be C_q. We have

$$C_q = \int_{-\ell}^{+\ell} q(x, \epsilon_F)\ v_q\ dx = \sqrt{\ell}\,\frac{2a\,\nu}{d} \sum_p d\left[v_p\ v_q\right]\chi_p$$

(23)

$$\chi_p = \int_0^{\epsilon_F} \varphi_p(\tilde{\epsilon})\ \Sigma_f(\tilde{\epsilon})\ d\tilde{\epsilon}$$

We have the same matrix $d\left[v_p, v_q\right]$ and the same conclusions, therefore it obeys the same frequency selection

(24) $$q = N_o r + s$$

That means

(25) $$C_s = \sqrt{\ell}\,\frac{2a\,\nu}{d} \sum_{m=-\infty}^{+\infty} \chi_{N_o m + s} \qquad \text{for all values of } r$$

By means of this boundary condition our problem becomes an eigenvalue problem with ν as eigenvalue. Therefore only one of the N + 1 sets of equations can have a non trivial solution. From (16) one concludes that the term $\cos \alpha_o x$ must be among the components. Therefore only the set s = 0 is here of interest because the reactor is regular and undisturbed (see [2]).

The frequency selection (24) has an immediate consequence for our ansatz (15).

It happens that

$$\cos \alpha_{N_o m}\, kd = \cos \alpha_o\, kd$$

and

$$\cos \alpha_{N_o m}\, (kd + \tfrac{d}{2}) = \cos \alpha_o (kd + \tfrac{d}{2}) \cdot (-1)^m$$

Applying this result to (15) it follows that at the fuel plates (x=kd) and in the middle of the moderator volume ($x=kd + \frac{d}{2}$) the spectra are the same for all the different Wigner Seits cells. This is the analog to the fact that in the homogeneous case the problem is separable that means, the spectrum there is space independent. L. Dresner [3] has shown that this result is generally true, the only assumptions to be made are the following :

The fuel arrangement in the reactor must be periodical and the outer boundary must be such that the image method can be applied. This immediately shows that this method fails in the case of a cylindrical core boundary, it can be true there only approximately.

3. A principal classification of neutron spectra

The classification in question is a principal one. But it can be demonstrated in the easiest way, if the heavy gas model is choosen for the scattering of the neutron by the moderator. There we have [1]

$$\left.\begin{aligned} (26) \qquad L(\phi) &= \xi \Sigma_S \left(\varepsilon \frac{\partial^2 \phi}{\partial \varepsilon^2} + \varepsilon \frac{\partial \phi}{\partial \varepsilon} + \phi\right) + O\left(\left(\frac{m}{M}\right)^2\right) \\ (27) \qquad q(\phi) &= -\xi \Sigma_S \left(\varepsilon \frac{\partial \phi}{\partial \varepsilon} + (\varepsilon - 1)\,\phi\right) + O\left(\left(\frac{m}{M}\right)^2\right) \end{aligned}\right\} \text{ if } \varepsilon \gg \frac{m}{M}$$

m is the neutron mass and M the mass of the moderator atom. In order to be consistent we must put:

$$\xi = 2\,\frac{m}{M}$$

$$\Sigma_S = \Sigma_S^{\,o} = \text{constant}$$

(26) inserted into (7) gives an elliptical differential equation. This is true in principle for all energies. One can recognize the character of the possible solutions of (7) if one asks for the solutions of $L(\phi) = 0$ (for example in the sense of a perturbation ansatz).

We have two solutions. First:

(28) $$\phi = \phi_1 = \epsilon e^{-\epsilon}$$

(28) is a Maxwell distribution and refers in it's character entirely to the elliptic character of the equation (7), (26). The general implication is that we have a spectrum which refers to an equilibrium or near equilibrium state. Spectra of this type obey the following rule:

(29) $$q(\epsilon) \sim O(e^{-\epsilon}) \quad \text{for large values of } \epsilon$$

Spectra of this type shall be called type A spectra.

Besides of (28) there is another solution for which we can give the asymptotic expansion

(30) $$\phi = \phi_2 = \frac{1}{\epsilon} \sum_{n=1}^{N} n! \left(\frac{1}{\epsilon}\right)^{n-1} + O(e^{-\epsilon}) \quad N = 1,2,3\ldots$$

For values sufficiently large ϕ_2 approximates the solution of the equation

(31) $$\overline{L}(\phi) = \xi \Sigma_s \left(\epsilon \frac{\partial \phi}{\partial \epsilon} + \phi\right) = 0$$

But the equation (7), (31) is of a completely different character. It is

of parabolic nature and describes slowing down processes (Ausgleichsprobleme).

Spectra of this type shall be called type B spectra.

The reactor spectra are of the mixed type in the region of interest and this is the reason why the mathematical treatment is so difficult: Mathematical tools are developed for either the type B or the type A solution, in the first for example the Laplace transformation, in the second for example the expansion into eigenfunctions of $L(\phi) = 0$ with $q(\epsilon) = 0$ for large values of ϵ, because these eigenfunctions belong to the type B.

Reactor spectra for low energies are close to type A, for high energies close to type B and the change tankes place gradually and has no turning point which is physically meaningful.

4. Slowing down spectra in a plate type reactor (type B)

In the following we will concentrate on the heavy gas model which leads to (26) and (27) although the procedure presented here is not restricted to that model.

This chapter refers to a first paper of the author [4]. The details can be seen there.

It is assumed there that only the slowing down case is of interest, where L given by (26) can be replaced by $\overline{L}$ (31). In that case our problem is as follows:

$$(32) \qquad -x_o^2 \alpha_{N_o r}^2 \varphi_{N_o r} + \varepsilon \frac{\partial \phi}{\partial \varepsilon} + \phi - p(\varepsilon) \sum_{m=-\infty}^{+\infty} \varphi_{N_o m} = 0$$

and according to (25)

$$\varphi_{N_o r}(\varepsilon_F) = \sqrt{\ell} \cdot \frac{2a\nu}{d \cdot \xi \Sigma_S} \sum_{m=-\infty}^{+\infty} \chi_{N_o m}$$

but this means

$$(33) \qquad \varphi_{N_o r}(\varepsilon_F) = S_o = \text{constant} \neq f(r)$$

In addition we assume a simple absorption law

$$p(\varepsilon) = p_o \cdot \frac{1}{\sqrt{\varepsilon/\varepsilon_F}} \tag{34}$$

In order to obtain the solution we make the following ansatz, where ß is a constant still to be determined.

$$\varphi_{N_o r}(\varepsilon) = \sum_{\nu=o}^{\infty} \frac{f_{N_o r}^{\nu}}{\varepsilon^{1 - ß + \frac{\nu}{2}}} \tag{35}$$

(35) leads to the equation

$$(\alpha_{N_o r}^2 x_o^2 - ß + \tfrac{\nu}{2}) f_{N_o r}^{\nu} = - p_o \sum_{m=-\infty}^{+\infty} f_{N_o m}^{\nu-1} \tag{36}$$

From here we conclude, that ß has to be one of the values $\alpha_{N_o r}^2 x_o^2$ in order to let $f_{N_o r}^{o} \neq 0$. For very high energies that is for the fission energy ε_F the term $f_{N_o r}^{o}$ in (35) alone survives and represents the mode for which (33) is to be applied. So the absorption $p(\varepsilon)$ at lower energies intermingles the modes, a pure mode at $\varepsilon = \varepsilon_F$ splits into all other modes. The second conclusion is that in (36) the term on the right is independent of r. But this means that the way in which $f_{N_o r}^{\nu}$ depends on r is given in (36). Using the abbreviation

$$F^{\nu} = \sum_{m=-\infty}^{+\infty} f_{N_o m}^{\nu} \tag{37}$$

we obtain

$$(38) \qquad {}^{v}f_{N_o r} = \frac{-\,p_o\,{}^{v-1}F}{\alpha_{N_o r}^{2}\,x_o^{2} - \beta + \frac{v}{2}}$$

Summation over r gives the final formula for obtaining the ${}^{v}F$ and from this by means of (38) the ${}^{v}f_{N_o r}$.

$$(39) \qquad {}^{v}F = -\,p_o \cdot \sum_{r} \frac{1}{\alpha_{N_o r}^{2}\,x_o^{2} - \beta + \frac{v}{2}} \cdot {}^{v-1}F$$

The Fourier series (15) becomes a real result only in the case where all the summation can be performed. Using (35) in (15) leads to the more general series (40), which can be summed up by means of the residue calculus [2] :

$$(40) \qquad \sum_{m=-\infty}^{+\infty} \frac{\cos \alpha_{N_o m}\, x}{\alpha_{N_o m}^{2}\,x_o^{2} + s} = h(s) \cdot F(x,s)$$

$$(40a) \qquad h(s) = \frac{d}{2x_o\sqrt{s}} \frac{\sinh \frac{d}{x_o}\sqrt{s}}{\left(\cosh \frac{d}{x_o}\sqrt{s} - \cos \frac{\pi}{N_o}\right)}$$

$$(40b) \qquad F(x,s) = \frac{\sinh \frac{x'}{x_o}\sqrt{s}\,\cos \frac{k+1}{N_o}\pi - \sinh \frac{x'-d}{x_o}\sqrt{s}\,\cos \frac{k}{N_o}\pi}{\sinh \frac{d}{x_o}\sqrt{s}}$$

$$x = x' + kd$$

$$k = 0, \pm 1, \pm 2, \ldots, \pm N$$

$$0 \leq x' \leq d$$

From here on the calculation is straight forward and leads to the following result:

$$\phi(\varepsilon) = \frac{S_o}{\varepsilon} \sum_{m=-\infty}^{+\infty} \left(\frac{\varepsilon}{\varepsilon_F}\right)^{\alpha_{N_o m}^2 \, x_o^2} A_m$$

$$(41) \qquad A_m = \sum_{\nu=o}^{\infty} (-1)^{\nu} \left(\frac{\varepsilon}{\varepsilon_F}\right)^{-\frac{\nu}{2}} p_o^{\nu} \cdot B_{\nu}^{(m)} \cdot F(x, -\alpha_{N_o m}^2 \, x_o^2 + \frac{\nu}{2})$$

$$B_{\nu}^{(m)} = \prod_{\sigma=1}^{\nu} h(-\alpha_{N_o m}^2 \, x_o^2 + \frac{\sigma}{2})$$

(41) is convergent for all values of $\varepsilon < \varepsilon_F$ and is the solution of our slowing down problem. It has two significant features:

For sufficiently large values of ε only the first term of the series A_m is to be taken into account and a simple series remains which describes the smoothing out process of the δ functions acting as sources of $\varepsilon = \varepsilon_F$. The smoothing out process is of the Θ function type. On the other hand:

for sufficiently small values of ε only the term A_o is significant in the main series. We have again a simple series which describes the flux peaks between the fuel elements in its energy and space dependence. There is a region in between where only one term in both series is significant:

$$(42) \qquad \phi \sim \frac{S_o}{\varepsilon^{1 - \alpha_o^2 \, x_o^2}} \cdot \cos \alpha_o x$$

The smoothing out process of the source δ function produced the ground mode $\cos \alpha_o x$ and the absorption of the fuel plates is not yet significant. For reasonable absorption strengths of the fuel plates this pure ground mode takes over somewhere in the neighborhood of $\frac{\varepsilon_F}{\varepsilon} \sim 100$, that means $\varepsilon \approx 20$ keV if heavy water is used.

The main conclusion we draw from this is the following:
It is possible (at least for heavy water and graphite) to separate the smoothing out process of the heterogeneous fission neutron distribution from the formation of flux peaks in the moderator at low energies.
Details of this calculation can be seen in paper [4].

5. Equilibrium spectra in a plate type reactor (type A)

As indicated in chapter 4. we will use the heavy gas model.

The physical conditions for spectra of the equilibrium type are given in experiments which use pulsed neutrons. Sometime after the shot which injects the neutrons into a non multiplying assembly there are no more fast neutrons to be slowed down and the existing neutrons, although decaying in time, have a sort of equilibrium with the moderator. This type of experiment is investigated in a second paper of the author together with L. Dresner [5].

In the analysis of the pulsed neutron experiments we have to add a term in (7) which cares for the time dependence.

We have:

$$(43) \qquad D \frac{\partial^2 \phi}{\partial x^2} + L(\phi) - \Sigma_a^{mod} \cdot \phi + f_- = \frac{1}{v} \frac{\partial \phi}{\partial t}$$

v is the neutron velocity and Σ_a^{mod} allows for an absorption in the moderator. Please note that we have not yet taken into account an absorption in the moderator up to now.

We make the following ansatz:

$$(44) \qquad \phi = e^{-\lambda t} \sqrt{e} \sum_{p=o}^{\infty} \varphi_p(\varepsilon) \, v_p(x)$$

with the same notation as in (15). Some time after the pulse the frequency selection (24) must hold and we obtain the following equations for the $\varphi_p(\epsilon)$ with $p = N_o r$

(45)

$$- x_o^2 \alpha_{N_o r}^2 \varphi_{N_o r} + \epsilon \frac{\partial^2 \varphi_{N_o r}}{\partial \epsilon^2} + \epsilon \frac{\partial \varphi_{N_o r}}{\partial \epsilon} + \varphi_{N_o r} + \epsilon^{-\frac{1}{2}} (\alpha \varphi_{N_o r} - p_t \sum_{m=-\infty}^{+\infty} \varphi_{N_o m}) = 0$$

(46) $$\alpha = \frac{\lambda - \Sigma_a^{MoD} v}{\int \Sigma_S \cdot (\frac{2T}{m})^{\frac{1}{2}}}$$

(46a) $$p_t = \frac{2a \, \Sigma_a(\epsilon=1)}{d \int \Sigma_S} \cdot \frac{1}{\sqrt{\epsilon}}$$

Additionally we have:

(47)
$$\phi(\pm \ell) = 0$$
$$q(x,0) = 0$$
$$q(x,\epsilon) = 0 \quad \text{for large values of } \epsilon .$$

We now make use of the fact that we look for spectra of the type A. We expand the $\varphi_{N_o r}(\epsilon)$ into eigenfunctions of the heavy gas operator

$\frac{1}{\xi\Sigma_S}$ L. These eigenfunctions are as follows:

(48) $$\frac{1}{\xi\Sigma_S} L(\omega_p) = - \sigma_p \omega_p$$

$$q(\omega_p) = 0 \qquad \text{for } \varepsilon = 0 \text{ and } \varepsilon = \infty$$

For the case of the heavy gas model we have

(49) $$\omega_p = \varepsilon e^{-\varepsilon} L_p^{(1)}(\varepsilon)$$

(50) $$\sigma_p = p \qquad ; \qquad p = 0,1,2,3...$$

$L_p^{(1)}(\varepsilon)$ are the Laguerre polynomials of order one, which we use in the normalized form

(51) $$L_p^{(1)}(\varepsilon) = \sqrt{p+1} \sum_{\mu=o}^{p} (-1)^{\mu} \frac{p!}{\mu!(\mu+1)\,!\,(p-\mu)\,!} \varepsilon^{\mu}$$

The operator is not self adjoint. The adjoints of (49) are:

(52) $$\omega_k^{+} = L_k^{(1)}(\varepsilon)$$

We now consider the following expansion:

(53) $$\varphi_{N_o r} = \sum_{p=o}^{\infty} a_{r,p}\, \omega_p(\epsilon)$$

Inserting (53) into (45) leads to a cumbersome but straight forward calculation, where the matrix elements V_{pq} are to be considered.

(54)

$$V_{pq} = \int_o^{\infty} \omega_p(\epsilon)\epsilon^{-\frac{1}{2}}\, \omega_q^{+}(\epsilon)\, d\epsilon = \frac{1}{\pi\sqrt{(p+1)(q+1)}} \sum_{\ell=o}^{p} \frac{\Gamma(p-\ell+\frac{1}{2})\,\Gamma(q-\ell+\frac{1}{2})\cdot\Gamma(\ell+\frac{3}{2})}{(p-\ell)!\,(q-\ell)!\,\ell!}$$

It should be emphasized that the formalism outlined in [5] does not use in principle a special model for the thermalization. However, if the heavy gas model is used all expressions can be given explicitly as in (54).

The problem (45) - (47) is a homogeneous one and constitutes an eigenvalue problem for α. Because of the two dimensions in question (x,ϵ) α has a two dimensional set of possible values, one degree of freedom refers to the space dependence the other to the energy dependence. Note that only in case of type A spectra the eigenvalue of the problem is double indexed. For type B spectra the condition (12) establishes a source which makes the problem not homogeneous in the ϵ direction, we have only a one dimensional set for the v's there.

The calculation following the insertion of (53) in (43) is cumbersome although straight forward. Under certain conditions it is enough to

consider in (53) only two terms p=0 and p=1. If, for example, the structure of the diffusion cooling effect in heterogeneous non multiplying assemblies is the point of interest, it is enough to have these two terms, because they can indicate a spectrum cooling or heating. The result of this investigation of the diffusion cooling effect is given in [5]. But the several expansions are not driven to the latest stage there. If one does so, the result is as simple as follows:

$$(55) \qquad \lambda = (\Sigma_a^{MoD}\, v) + \alpha_o^2\, D\, \bar{v} - \alpha_o^4\, D^2\, \frac{\bar{v}}{\bar{\xi}\Sigma_S} \cdot \frac{1}{8} + \frac{2a}{d}\, \Sigma_a v - \left[\frac{2a}{d}\, (\Sigma_a v)\right]^2 \frac{1}{\bar{\xi}\Sigma_S\, \bar{v}} \left(\frac{1}{8}\, k\, \left(\frac{d}{x_o}\right) + \frac{1}{12}\, \frac{d^2}{x_o^2}\right) + O\left(\left(\alpha_o^2\, \frac{D}{\Sigma_S}\right)^{\mu} \cdot \left(\frac{2a}{d}\, \Sigma_a v\right)^{\nu}\right); \quad \mu + \nu \geq 3$$

We used the following abbreviations:

$$(56) \qquad k\left(\frac{d}{x_o}\right) = \frac{\frac{x_o}{d}\, \sinh \frac{d}{x_o}}{\frac{2x_o^2}{d^2}\, \left(\cosh \frac{d}{x_o} - 1\right)} - 1 = \frac{d^2}{12\, x_o^2} + \ldots\ldots$$

$\bar{v}$ is the Maxwellian average velocity of a neutron gas at temperature T;

(57) $$\bar{v} = \left(\frac{8T}{\pi m}\right)^{\frac{1}{2}}$$

It is also assumed, that not only $\alpha_o^2 x_o^2$ but also $\alpha_o^2 d^2 \ll 1$.

From the investigation of the diffusion cooling effect in homogeneous assemblies, which is presented in [5], one can argue that at least in the term $\alpha_o^4 \frac{1}{8}$ has to be replaced by $\frac{1}{6}$ if not only the first two terms in (53) but all of them are taken into account.

The discussion of (55) is interesting:
There are three first order terms. The first is the contribution to the decay constant coming from the homogeneous absorption of the moderator, the second is the leakage term $\alpha_o^2 D \bar{v}$ and the third comes from the homogenized heterogeneous absorption in the plates $\frac{2a}{d} \Sigma_a v$. In the second order to which the formalism is given here there are two diffusion cooling effects. The first is the well known leakage effect $\alpha_o^4 D^2$ due to the diffusion of the neutrons, the second refers to the diffusion process into the lumped absorbers. This second diffusion cooling effect disappears if $\frac{d}{x_o} \to 0$ because this implies that for a neutron the assembly is no longer heterogeneous.

It should be mentioned that the energy dependent Milne problem was

investigated for type A spectra by E. Kiefhaber [6] in his master's thesis. Instead of the heavy gas operator the Nelkin kernel was used in (2) and (43). The mathematical procedure was again the expansion into eigenfunctions of the operator L as in (53). But the eigenfunctions are here no longer simply the Laguerre functions. It is necessary to express the eigenfunctions in itself as an expansion into Laguerre functions. The experimental group of K. Beckurts did a lot of measurements using pulsed neutrons in light water and it was very useful and successful to have this comparison.

6. Reactor spectra in the thermal range, type A and type B

As pointed out in chapter 3. the neutron spectrum in an actual thermal reactor is not purely a type A or type B spectrum and this establishes the mathematical difficulty. In the case of a plate type reactor a solution of the spectrum problem was given by the author of this paper [7]. But it was necessary to restrict the application of the method outlined there to small absorption strengths of the plates, because it was not possible to perform the summation of all Fourier series. However, it was possible to give the asymptotic expansion of the problem in question, which goes parallel to the procedure given in chapter 4. of this paper and there it was possible to perform all the Fourier summations. It is an asymptotic solution only because of the essential singularity at ∞ of the heavy gas operator (26). From here on the way to handle the problem was rather obivous:
Suppose that $\overline{\phi}$ is a function with the following features

$$\overline{\phi}(\varepsilon) = \phi_{as}(\varepsilon) \qquad \varepsilon \geq \varepsilon_o$$

$$\overline{\phi}(\varepsilon) = P(\varepsilon) \qquad \varepsilon \leq \varepsilon_o$$

$\phi_{as}(\varepsilon)$ is the asymptotic expansion valid for large values of ε and $P(\varepsilon)$ is an arbitray but smooth function which fullfills the boundary condition at $\varepsilon = 0$ and fits smoothly into ϕ_{as} at $\varepsilon = \varepsilon_o$. Then the function

$$\phi_{Diff}(\varepsilon) = \phi(\varepsilon) - \overline{\phi}(\varepsilon)$$

where $\phi(\epsilon)$ is the solution of the problem, is clearly a function which represents a spectrum of type A. But this means that we can apply for $\phi_{Diff}(\epsilon)$ an expansion into eigenfunctions of the operator L as given in (53). As long as there is no absorption in the moderator, strong enough to influence the neutron spectra there, all Fourier summations can be performed. And this is true even for the two dimensional case.

H. Kunze used this procedure in his masters thesis [8].
The method shall be described here a little bit in more detail. We look into the most simple case of a homogeneous infinite medium. Here we have:

$$\frac{d^2\phi}{d\epsilon^2} + \epsilon \frac{d\phi}{d\epsilon} + \phi - p_t \cdot \epsilon^{\frac{1}{2}} \phi = 0 \tag{58}$$

In the homogeneous case we have to put 2a=d, (14) therefore tends to the following:

$$p_t = \frac{\Sigma_a(\epsilon=1)}{\int \Sigma_S} \tag{59}$$

We have the following boundary conditions:

$$q(0) = 0 \tag{60}$$

$$q(\epsilon) = \text{constant at high energies}$$

In the first step we look into the asymptotic expansion

$$\phi_{as}^{(1)}(\epsilon) = \sum_{\nu=0}^{N} \frac{g_\nu}{\epsilon^{1+\frac{\nu}{2}}} \tag{61}$$

Inserting (61) into (58) we obtain

$$g_{\nu+2} = \frac{2}{\nu+2}\left((1+\tfrac{\nu}{2})(2+\tfrac{\nu}{2})\, g_\nu - p_t\, g_{\nu+1}\right) \tag{62}$$

that is

$$g_1 = -2\, p_t\, g_o \quad ; \quad g_2 = 2\,(1+p_t^{\,2})g_o \,, \quad \ldots\ldots$$

Besides of (61) there is a second asymptotic expansion:

$$\phi_{as}^{(2)}(\epsilon) = \epsilon\, e^{-\epsilon} \sum_{\nu=0}^{N} \frac{g_\nu}{\epsilon^{\frac{\nu}{2}}} \tag{63}$$

$\phi_{as}^{(1)}$ and $\phi_{as}^{(2)}$ are the asymptotic expansion of $\phi^{(1)}$ and $\phi^{(2)}$, functions which have logarithmic singularities at $\epsilon = 0$. We look into the linear combination which cancels the logarithmic terms at $\epsilon = 0$

$$\phi(\epsilon) = \phi^{(1)}(\epsilon) + \lambda\, \phi^{(2)}(\epsilon) \tag{64}$$

Because of the contribution $\phi^{(1)}(\varepsilon)$ ϕ does not belong to the Hilbert space of the eigenfunctions of L, (49).

It is possible to expand the wanted, regular function $\phi(\varepsilon)$ at $\varepsilon = 0$ into a power series of $\varepsilon^{\frac{1}{2}}$.

$$\phi = \sum_{\nu=0}^{\infty} a_\nu \varepsilon^{1+\frac{\nu}{2}} \tag{65}$$

We now consider an auxiliary function $\overline{\phi}(\varepsilon)$ of the following properties:

$$\begin{aligned} \overline{\phi}^N(\varepsilon) &= \phi_{as}^{(1)}(\varepsilon) \quad \text{for} \quad \varepsilon \geq \varepsilon_o \\ \overline{\phi}^N(\varepsilon) &= a\varepsilon + b\varepsilon^{\frac{3}{2}} + c\varepsilon^2 + d\varepsilon^{\frac{5}{2}} \quad \text{for} \quad \varepsilon \leq \varepsilon_o \end{aligned} \tag{66}$$

The notation $\overline{\phi}^N$ indicates that the asymptotic expansion (61) shall be taken up to $\nu=N$. The form of $\overline{\phi}^N$ for $\varepsilon \leq \varepsilon_o$ is suggested by (65). a, b, c and d are determined by the conditions, that $\overline{\phi}^N$ and its first three derivatives at $\varepsilon = \varepsilon_o$ shall be continuous.

We now define a quantity

$$S = -\left[\varepsilon \frac{d^2 \overline{\phi}^N(\varepsilon)}{d\varepsilon^2} + \varepsilon \frac{d \overline{\phi}^N(\varepsilon)}{d\varepsilon} + \overline{\phi}^N(\varepsilon) - p_t \cdot \varepsilon^{-\frac{1}{2}} \overline{\phi}^N(\varepsilon)\right], \quad \varepsilon \leq \varepsilon_o \tag{67}$$

For values $\varepsilon \geq \varepsilon_o$ S has the order $O\left(\frac{1}{\varepsilon^{1+\frac{N+1}{2}}}\right)$.

As an approximation to this we define, that

$$S = 0 \qquad \epsilon \geq \epsilon_o \tag{68}$$

We put now:

$$\phi_{Diff} = \phi - \overline{\phi}^N \tag{69}$$

Then we obtain

$$\epsilon \frac{d^2 \phi_{Diff}}{d\epsilon^2} + \epsilon \frac{d \phi_{Diff}}{d\epsilon} + \phi_{Diff} - p_t \cdot \epsilon^{-\frac{1}{2}} \phi_{Diff} = S(\epsilon) \tag{70}$$

The function ϕ_{Diff} now lies in the Hilbert space of the eigenfunctions of the operator L. We therefore put

$$\phi_{Diff} = \sum_{p=o}^{\infty} a_p \, \omega_p(\epsilon) \tag{71}$$

ω_p is given in (49). Using (71) in (70) we obtain

$$- p \cdot a_p - p_t \sum_{q=o}^{\infty} V_{pq} \, a_q = C_p \tag{72}$$

$$C_p = \int_o^{\infty} \omega_p^+ \, S(\epsilon) \, d\epsilon \tag{73}$$

This equation set determines the a_p and we find in the order p_o the result:

$$\phi(\epsilon) = \overline{\phi}^{N}(\epsilon) + \sum_{p=o}^{p_o} a_p \, \omega_p(\epsilon) \tag{74}$$

This method has been applied to the example $p_t = 0.25$.

We have chosen $\epsilon_o = 16$, N=10 and p_o=5.

Fig. 2 shows the result of this calculation here. There is complete agreement with the solution of Hurwitz, Nelkin and Hebetler [1]. The figure shows $\epsilon\phi(\epsilon)$ in its dependence on $\sqrt{\epsilon}$. Furthermore $\epsilon\,\overline{\phi}^{10}(\epsilon)$ has been drawn, too. $\overline{\phi}^{N}(\epsilon)$ represents qualitativly the neutrons which are slowed down, where as $\sum a_p \, \omega_p$ represents qualitativly the neutrons being in a sort of equilibrium with the moderator.

The significance of this method outlined here is, that it allows to handle the problem of two dimensional heterogeneous spectra. For this case we use the following model:

A reactor of rectangular shape is considerd, for reasons of simplicity it shall be quadratic ,that means, the reactor has now N_o^2 rods of diameter 2a and consists of an integer number of Wigner Seits cells. The absorption in the moderator is again neglected.

In the chapter 4. we saw that it is possible in most of the cases to separate the smooth out process of the fission neutrons into the ground mode from the formation of the flux peaks between the fuel rods at lower energies. We therefore concentrate our attention on the thermal and epithermal part

of the spectrum and do not care for the slowing down part at higher energies. This is possible because we ask for the shape of the spectra only and we do not ask for a proper criticality condition.

Therefore we have the following problem:

(75)

$$x_o^2\left(\frac{\partial^2\phi}{\partial x^2}+\frac{\partial^2\phi}{\partial y^2}\right)+\frac{1}{\bar{\Sigma}_S}L(\phi)-p_t\cdot\epsilon^{-\frac{1}{2}\sum_{k=-N}^{+N}\sum_{\ell=-N}^{+N}d^2\delta(x-kd)\delta(y-\ell d)\cdot\phi^R(kd,\ell d\epsilon)}=0$$

There we have redefined p_t in the following way:

(76)
$$p_t=\frac{\Sigma_a(\epsilon=1)\cdot\pi a^2}{\bar{\Sigma}_S\, d^2}$$

Σ_a is again an effective cross section as described in chapter 2.

Additionally we have

(77)
$$\phi(\pm\ell,y,\epsilon)=0\ ;\qquad \phi(x,\pm\ell,\epsilon)=0$$

(78)
$$q(x,y,0)=0$$

(79)
$$q(x,y,\epsilon)=\text{const}\cdot\cos\alpha_o x\cdot\cos\alpha_o y \text{ for large values of}\epsilon$$

In (75) $\phi^R(kd,\ell d,\epsilon)$ is not the flux at x=kd, y=kd which would be the analog to the one dimensional case. This analog does not work because there is a logarithmic singularity of the flux at x=kd, y=kd. Therefore ϕ^R is the flux average over the surface of the rod approximated by the following expression:

(80)

$$\phi^R(kd,\ell d,\epsilon) = \frac{\phi(kd,\ell d+a,\epsilon) + \phi(kd,\ell d-a,\epsilon) + \phi(kd+a,\ell d,\epsilon) + \phi(kd-a,\ell d,\epsilon)}{4}$$

We now make again a Fourier ansatz. For the same symmetry reasons as in chapter 2. we have a frequency selection. Making use of it we have

$$(81)\quad \phi(x,y,\epsilon) = \sum_{m=-\infty}^{+\infty} \sum_{r=-\infty}^{+\infty} \varphi_{N_o r,\, N_o m}(\epsilon) \cdot \cos \alpha_{N_o r}\, x \cdot \cos \alpha_{N_o m}\, y$$

Inserting (81) in (75) and using (80) we obtain the following:

(82)

$$\epsilon \cdot \frac{d^2 \varphi_{N_o r,N_o s}}{d\epsilon^2} + \epsilon \frac{d \varphi_{N_o r,N_o s}}{d\epsilon} + (1 - (\alpha_{N_o r}^2 + \alpha_{N_o s}^2)\, x_o^2)\, \varphi_{N_o r,N_o s} -$$

$$- p_t \cdot \epsilon^{-\frac{1}{2}} \sum_{m,t=-\infty}^{+\infty} \varphi_{N_o m,N_o t} \cdot \cos^{R_o}(\alpha_{N_o m}\, x) \cdot \cos^{R_o}(\alpha_{N_o t}\, y) = 0$$

The index R_o of the cos in the sum means that the average is to be taken at the central fuel element [2]. The reduction of taking the average at the central fuel element only is a consequence of the special symmetry of the reactor considered here.

We now apply the same calculus to (82) as in the homogeneous case and obtain the result in the following form:

(83)

$$\phi(x,y,\varepsilon) = \sum_{r,s=-\infty}^{+\infty} \left\{ \bar{\varphi}^{N}_{N_o r, N_o s}(\varepsilon) + \sum_{p=o}^{p_o} a_{N_o r, N_o s, p} \cdot \omega_p(\varepsilon) \right\} \cos \alpha_{N_o r}\, x \cdot \cos \alpha_{N_o s}\, y$$

$$\bar{\varphi} = \varphi_{as} \quad , \qquad \varepsilon > \varepsilon_o$$

$$\bar{\varphi} = \text{Polyn.} \, , \quad 0 < \varepsilon < \varepsilon_o$$

All the coefficients of the above Fourier series can be written as linear combinations of terms of the form

(84)
$$\frac{1}{\gamma + (\alpha^2_{N_o r} + \alpha^2_{N_o s})\, x_o^2}$$

Thus evaluating (83) in order to obtain the final result a Fourier series of the type

(85)
$$\sum_{r,s=-\infty}^{+\infty} \frac{\cos \alpha_{N_o r}\, x \cdot \cos \alpha_{N_o s}\, y}{\gamma + (\alpha^2_{N_o r} + \alpha^2_{N_o s})\, x_o^2}$$

has to be evaluated.

But more than that: to establish the asymptotic solution analogous to (61) and (35) and the equation system for the $a_{N_o r, N_o s, p}$ analogous to (72) made it already necessary to evaluate series of the type (85). This was done by K. Meetz [2]. One summation can be carried out by means of the calculus of residues, see (40). The remaining single series converges rather rapidly inside the moderator, but its convergence is very poor at the boundary of the fuel rods, because of the logarithmic singularities of the flux in the lattice points of the reactor. But using a known Fourier series with the same logarithmic singularities and looking for the difference between (85) and these known series one can improve the convergence considerably and therefore it is possible to evaluate (85). For details see either [2] or [8].

The method explained here has been applied to twelve types of reactors in the limit $N_o = \infty$. Besides the neutron spectra themselves the values of the η factor and the thermal utilization have been calculated. In determining the latter quantity a $\frac{1}{v}$ - absorption law in the moderator has been assumed. The mean values of the absorption and fission cross sections of the fuel elements were taken in the energy interval $0 \leq \varepsilon \leq 16$; in the moderator the spatial average of the absorption cross section has been calculated, too, by means of the spectrum determined neglecting the neutron absorption in the moderator.

The parameter of the twelve reactors considered here are given in table 1.

Table 1

Reactor	Moderator	d [cm]	a [cm]	p %	ϱ [g/cm^3]	p_t	x_o/d	p_t^M
I	D_2O (40°C)	10	1,6	0,7115	18,4	0,1046	0,186	$3,33 \cdot 10^{-4}$
II	"	16,8	"	"	"	0,03705	0,1108	"
III	"	20	"	"	"	0,02614	0,093	"
IV	"	10	"	2	"	0,2274	0,186	"
V	"	16,8	"	"	"	0,08058	0,1108	"
VI	"	20	"	"	"	0,05686	0,093	"
VII	Graphite	10	1,2	0,7115	"	0,1791	0,3925	$4,34 \cdot 10^{-4}$
VIII	" (300°C)	20	"	"	"	0,04479	0,1962	"
IX	"	30	"	"	"	0,01991	0,1309	"
X	"	10	"	2	10	0,212	0,3925	"
XI	"	20	"	"	"	0,05299	0,1962	"
XII	"	30	"	"	"	0,02356	0,1309	"

a,d,p_t $\frac{x_o}{d}$ have the meaning defined in the text above, $p_t^M = \frac{\Sigma_a^M(\epsilon=1)}{2\mu\ \Sigma_S^o}$ is the absorption parameter of the moderator, ϱ is the density of the fuel. In the calculation of the f-factor the fuel was assumed to consist of p% U^{235} and (100-p)% U^{238}.

The values p=0,7115; ϱ=18,4 g/cm^3 correspond to those of natural uranium; p=2 and ϱ=10 g/cm^3 are the data of uranium oxide enriched up to 2% U^{235}. The macroscopic absorption cross section of natural uranium at the moderator temperature of 40°C was assumed to be $\Sigma_a(\epsilon=1) = 0,3467\ cm^{-1}$. At a fuel

enrichment of 2,0 we have $\Sigma_a(\epsilon=1) = 0{,}7541\ cm^{-1}$ for metallic uranium at 40°C moderator temperature and $\Sigma_a(\epsilon=1) = 0{,}3034\ cm^{-1}$ for enriched uranium oxide at 300°C moderator temperature. As absorption cross section in heavy water has been used

$$\Sigma_a^M(\epsilon=1) = 7{,}736 \cdot 10^{-5}\ cm^{-1} \text{ at } 40^\circ C \text{ and graphite of } 300^\circ C$$
$$\Sigma_a^M(\epsilon=1) = 2{,}58 \cdot 10^{-4}\ cm^{-1}.$$

Finally the Sachs-Teller-mass has been used for heavy water.

Figures 3 - 14 show the neutron spectra in the reactor I - XII. The neutron flux ϕ is plotted versus the energy ϵ in double logarithmic scale. There is drawn the flux $\phi^{Ro}(\epsilon)$ at the boundary of the fuel rods and the spectrum $\phi(\frac{d}{2}, \frac{d}{2}, \epsilon)$ in the middle of the moderator, respectively.

For comparison a Maxwellian distribution has been fitted to the spectrum in the moderator at low energies. In the low energy range all the spectra have Maxwellian character, the maximum being usually shifted. One recognizes clearly the change from the Maxwellian part of the spectrum to the characteristic $\frac{1}{\epsilon}$ slowing down spectrum. A decrease of the lattice parameter d results in a simultaneous, almost equal increase of the neutron temperature in fuel and moderator. The neutron temperature is here defined as the

temperature of a Maxwellian distribution fitted to the given spectrum in its maximum. An increase of the absorption cross section of the fuel at unchanged geometry to the contrary has as consequence a displacement of the maximum of the spectrum in the fuel, but almost none in the moderator.

Figures 3 - 14 show that the spectra in fuel and moderator are far from being identical in the epithermal region. In an infinite reactor ($N_o=\infty$) they tend to meet asymptotically, of course. But this becomes true only at very high energies. H.C. Honeck [9] made in the numerical treatment of the problem in the Wigner Seitz cell the assumption, that the spectra in moderator and fuel are identical above $\mathcal{E} = 9$. This assumption was necessary because of the limited machine capacity. It seems to us to become dubious at least for strong absorption. According to our experience a small inaccuracy in the calculation of the high energy part of the spectrum results in serious deviations from the rigorous solution in the thermal energy range.

Table 2

Reactor	f	$f^{1\ gr}_{ws}$	$\bar{\sigma}^5_f$ [barn]	$\bar{\sigma}^5_a$	$\bar{\sigma}^8_a$	η
I	0,99648	0,99606	415,96	491,09	2,037	1,30965
II	0,98750	0,98655	446,82	526,56	2,171	1,31500
III	0,98125	0,97996	452,11	532,65	2,194	1,31585
IV	0,99807	0,99764	373,24	441,24	1,853	1,70659
V	0,99217	0,99117	422,12	497,82	2,067	1,71586
VI	0,98786	0,98649	430,90	507,89	2,105	1,71731
VII	0,97453	0,97215	271,48	322,74	1,427	1,27012
VIII	0,89185	0,88192	311,89	370,06	1,606	1,28157
IX	0,77493	0,75494	320,73	380,41	1,645	1,28373
X	0,97801	0,97554	263,40	313,27	1,392	1,68171
XI	0,90395	0,89361	307,96	365,49	1,589	1,69160
XII	0,79586	0,77458	317,20	377,20	1,634	1,69351

Maxwellian dist. at moderator-temperature

Reactor	$\bar{\sigma}^5_f$	$\bar{\sigma}^5_a$	$\bar{\sigma}^8_a$	η
I	481,44	566,94	2,316	1,32037
II	"	"	"	"
III	"	"	"	"
IV	"	"	"	1,72304
V	"	"	"	"
VI	"	"	"	"
VII	341,01	403,86	1,730	1,29026
VIII	"	"	"	"
IX	"	"	"	"
X	"	"	"	1,69962
XI	"	"	"	"
XII	"	"	"	"

Maxwellian dist. with displaced temperature

Reactor	T^U_n [°C]	$\bar{\sigma}^5_f$	$\bar{\sigma}^5_a$	$\bar{\sigma}^8_a$	η
I	74	453,78	534,45	2,203	1,31578
II	65	460,74	542,62	2,231	1,31700
III	56	468,11	551,26	2,261	1,31823
IV	134	414,12	488,16	2,040	1,71469
V	109	429,69	506,29	2,104	1,71703
VI	105	433,59	510,85	2,120	1,71757
VII	443	301,10	358,68	1,556	1,27680
VIII	372	319,22	379,16	1,636	1,28306
IX	357	323,21	383,67	1,653	1,28440
X	472	294,68	351,42	1,527	1,68371
XI	386	315,32	374,74	1,619	1,69121
XII	346	326,56	387,47	1,668	1,69502

Table 2 gives the values of the thermal utilization f calculated for our twelve reactors I - XII. For comparison these quantities have been determined in a one group diffusion calculation for the corresponding Wigner Seitz cells.

An estimate of the improvement in accuracy to be expected from a rigorous consideration of the energy dependence of the neutron density can be obtained from a comparison of the f-factor values in table 2. The difference between these quantities, determined by our method and the one group approximation, respectively, is negligeably small for D_2O-moderated reactors with natural uranium fuel elements (this is true only for a $\frac{1}{v}$ - absorption law). But this is not the case in reactors with enriched fuel elements, especially in graphite moderated reactors. In any case the accuracy of the monoenergetic, transporttheoretical calculation can be improved essentially, if the absorption cross sections used are averaged over the neutron spectra determined in the diffusion approximation.

In table 2 the values of the ηfactor determined by means of the neutron spectra shown in figures 3 - 14 and those calculated from Maxwellian distribution at moderator temperature and the temperature T_n^U of the neutrons at the boundary of the fuel rods are also given for comparison. Finally the mean values of the fission and absorption cross section of U^{238} are given as obtained from the three types of spectra just specified. As expected the mean values of these cross sections, obtained from Maxwellian distributions,

are too large, because these functions decrease so rapidly, that the epithermal cross section values have no influence on the mean value. This has consequence, that the η factors determined with Maxwellian distributions are too large.

7. The representation of reactor spectra (type A and type B) by simple sets of functions

The method outlined in chapter 6. made use of the concept of an auxiliary function $\overline{\phi}^N$ which represents the reactor spectra at high energies. In the case of chapter 6. a special energy ϵ_o was chosen where the asymptotic solution and a polynomial expression (66) were tied together. This has the taste of being artificial and reminds of the concept of a "cut off" although it has nothing to do with it.

There are several possibilities to improve this procedure. One possibility is the following:

Suppose that in (74) one wants to consider an approximation of the degree p_o. Then for $\overline{\phi}^N$ the following unique representation is possible

$$\overline{\phi}^N \rightarrow \overline{\phi}^{p_o} = \epsilon^{\alpha_o^2} x_o^{2-1} \left[\sum_{v=o}^{p_o+1} a_v \epsilon^{-\frac{v}{2}} \right] e^{-\frac{\gamma}{\epsilon}} \tag{86}$$

γ is chosen arbitrarily and it comes out that for example $\gamma=3$ is, for heavy gas model spectra, a reasonable choice in a sense to be described below. The a_v are now chosen in such a way, that for large values of ϵ the asymptotic representation up to the p_o+1 degree is fitted. For small values of ϵ the function ϕ_{p_o} tends strongly toward zero. If one applies analog to (67) the full differential operator to it, the source term S has the

following order:

$$S(\varepsilon) = O\left(\frac{1}{\varepsilon^{-\alpha+1+\frac{p_o+2}{2}}}\right)^{-\frac{\gamma}{\varepsilon}} \tag{87}$$

Because of (87) the first p_o+1 moments C_p are convergent:

$$C_p = \int_o^\infty S(\varepsilon) \cdot \omega_p^+(\varepsilon)\, d\varepsilon = \text{finite for } p \leq p_o \tag{88}$$

Now $\gamma=3$ makes the first p_o+1 values C_p not too large, the source term S is still behaving smoothly. Recent investigations have shown, that $p_o=1$, that is two terms $\omega_p(\varepsilon)$ in (74), is already a good way to represent reactor spectra with an error of about 5% provided that not highly enriched fuels are used. Now, two terms in (74) and three terms in (86) give the chance to do all calculations fully analytically, so that there is a way to make the whole question of reactor spectra an easy thing again. But it should be emphasized that there are also other ways to keep the function $\overline{\phi}^N$ simple and unique.

8. Iterated Multigroup Method

A completely different approach to the problem in question has been given by K. Meetz, K. Ott and S. Sanatani [10]. It does not claim, however, to be a systematic method, because it is partially based on intuitive arguments.

Let us recall that we have, roughly speaking, two categories of problems concerned with either the spatial distribution or the energy spectrum of neutrons in a heterogeneous assembly. In an analysis of the spatial distribution in the moderator one might well use diffusion theory, if the scattering mean free path is small compared with the fuel rod distance d. Introduction of point singularities instead of the boundary conditions at the fuel surface makes the solution of the diffusion problem in a regular lattice an easy task. This has been outlined in detail in Sect. II for a one-dimensional reactor model. The knowledge of the flux on the fuel rod surface is also sufficient for a good estimation of fuel reaction rates, if the absorption length of the fuel is large compared with the rod diameter. Hence, it is reasonable to keep the singularity method for the spatial distribution in any approach to the spectral problem.

There a similarly simple and satisfactory entry does not seem to exist. The use of eigenfunctions of the monatomic gas scattering kernel has its difficulties, as we have seen in the previous section. It may, therefore,

be worthwhile to try a multigroup method. It was felt, however, by the authors of [10] that one should improve the quality of such a method by incorporating an iteration procedure.

Let us briefly outline the way this has been done in [10] for the case of an infinite homogeneous medium. The basic idea is to use the n flux mean values $\overline{\phi}_i$, obtained from the solution of the multigroup equations for a n group theory, for an improvement of the flux distribution that has been used in calculating the group constants. To do this in a systematic way, one may choose a set of spectral functions $\phi_i(a_1^{(i)} \ldots a_{n_i}^{(i)}, \varepsilon)$, which describe the flux in the i-th interval and depend on arbitrary constants $a_1 \ldots a_{n_i}$ besides the energy ε: (ε=E/KT'). The choice of the ϕ_i is determined by physical arg u ments. For groups in the slowing down region one may use the asymptotic expansion

$$\phi(\varepsilon) = \frac{a_1}{\varepsilon} + \frac{a_2}{\varepsilon^{3/2}} + \frac{a_3}{\varepsilon^2} + \ldots\ldots \quad , \tag{89}$$

while in the thermal region the shape is Maxwellian:

$$\phi(\varepsilon) = \varepsilon e^{-\varepsilon}(a'_1 + a'_2\varepsilon + a'_3\varepsilon^2 + \ldots) \tag{90}$$

In the epithermal region a combination of (89) and (90) may be taken as the best description. Now the constants $a^{(i)}_{\cdot\cdot}$ are objects of the iteration: In zero order one starts with a convenient set of constants ${}^{0}a^{(i)}_{\cdot\cdot}$ for the calculation of zero order group constants. The resulting first order mean values $\bar{\phi}_i^{(1)}$ are then required from the functions $\phi_i(..{}^{1}a^{(i)}_{\cdot\cdot}..,\varepsilon)$ in combination with a sufficient number of continuity conditions at the group boundaries. First order constants ${}^{1}a^{(i)}_{\cdot\cdot}$ are obtained by solving the corresponding linear equations and first order group constants from the functions $\phi_i(...{}^{1}a^{(i)}_{\cdot\cdot}..;\varepsilon)$ etc.

The results of this procedure have been compared with the numerical solution of Hurwitz, Nelkin and Habetler [1] for the heavy gas model in heavy water. The agreement is quite good for both values of the absorption parameter $4\,p_t = \Delta = 4\,\Sigma_a / \Sigma\Sigma_S (\Delta = 0{,}1; \Delta = 1)$. However, there is a characteristic difference, namely a minimum in $\varepsilon\phi(\varepsilon)$ in the epithermal region just above the Maxwell peak. This is probably due to the different scattering kernels used: heavy gas approximation in [1] and Wigner-Wilkins kernel in [10]. It may be mentioned that Corngold's correction of the heavy gas model [11] points in the same direction.

There is no difficulty to combine the multigroup method with the singularity approach for the spatial distribution. As an example, the one dimensional model described in Sect. II has been studied in [10]. As has been mentioned

in Sect. II the flux spectra on the fuel boundaries and in the center between the fuel plates are independent of the cell position. It is reasonable to take the spectra at these positions as representative for the neutron spectrum in a heterogeneous assembly. This has the further advantage that the corresponding multigroup constants are likewise independent of the cell position. Spectra calculated this way are in very good agreement with those obtained by Kunze [8] in his more systematic but more tedious approach.

Due to its extreme simplicity and the satisfactory results the iterated multigroup method promises to be useful for practical calculations, although it is certainly unsatisfactory from a more systematic point of view.

9. Final remark

This summary presents the work of the theoretical group of Karlsruhe on the subject of neutron spectra. The goal was to investigate how strong the influence of the heterogeneity is and to predict the thermal and epithermal part of reactor spectra in order to obtain by this properly weighted thermal neutron cross sections.

One successful first application of these spectra was the calculation of the critical experiment of the Karlsruhe reactor FR 2. It came out that 54 fuel elements were predicted and criticality was reached with 52 elements.

It should be mentioned that it is felt that these procedure are not restricted to either the heavy gas model or the diffusion theory. These simple models were chosen only to develope in the most simple cases the general methods.

References

[1] H. Hurwitz jr. M.S. Nelkin and G.J. Habetler: Nuclear Science and Engineering 1, 280-312, 1956

[2] K. Meetz: Second Geneva Conference, 1958, P/968, see also: Zeitschrift für Naturforschung 12a, 9, 1957 and 12, 11, 1957

[3] L. Dresner: Nukleonik (Springer Verlag), 2, 45-47, 1960

[4] W. Häfele: Nukleonik (Springer Verlag), 1, 197-208, 1959

[5] W. Häfele and L. Dresner: Nuclear Science and Engineering 7, 5, April 1960

[6] E. Kiefhaber, Master thesis 1961, not yet published

[7] W. Häfele: Nukleonik (Springer Verlag), 2, 240-246, 1960

[8] H. Kunze: Internal Karlsruhe Report Nr. 23/61, also submitted to Nuclear Science and Engineering for publicatior

[9] H.C. Honeck: Nuclear Science and Engineering 8, Sept. 1960

[10] K. Ott, K. Meetz and S. Sanatani: Nukleonik (Springer Verlag, 3, 155-163, 1961

[11] N. Corngold: ORNL-2739. Proc. of the Neutron Thermalisation Conf. Gatlinburg 1958

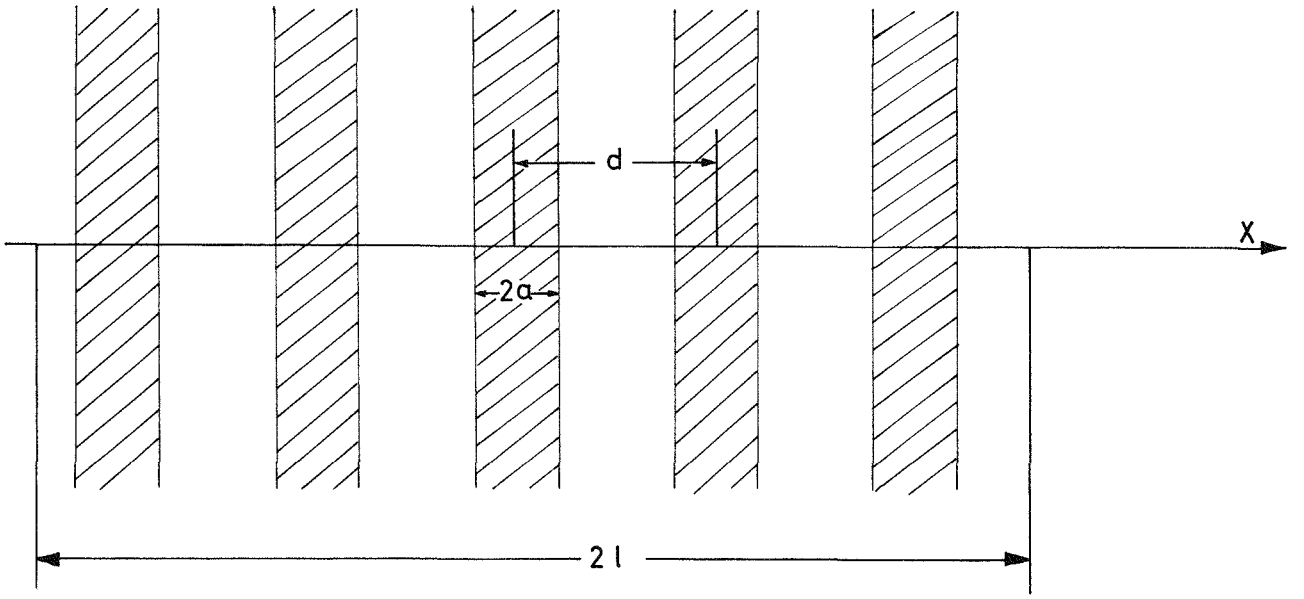

Fig. 1

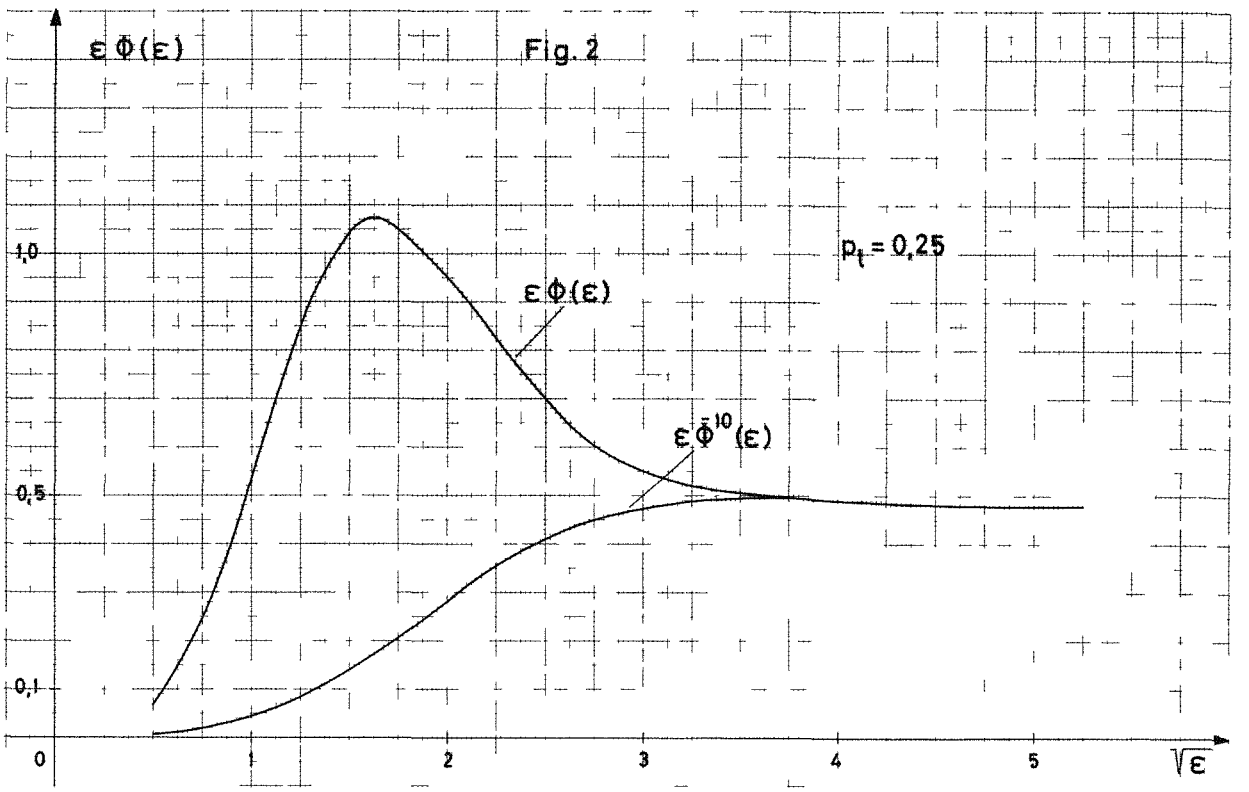

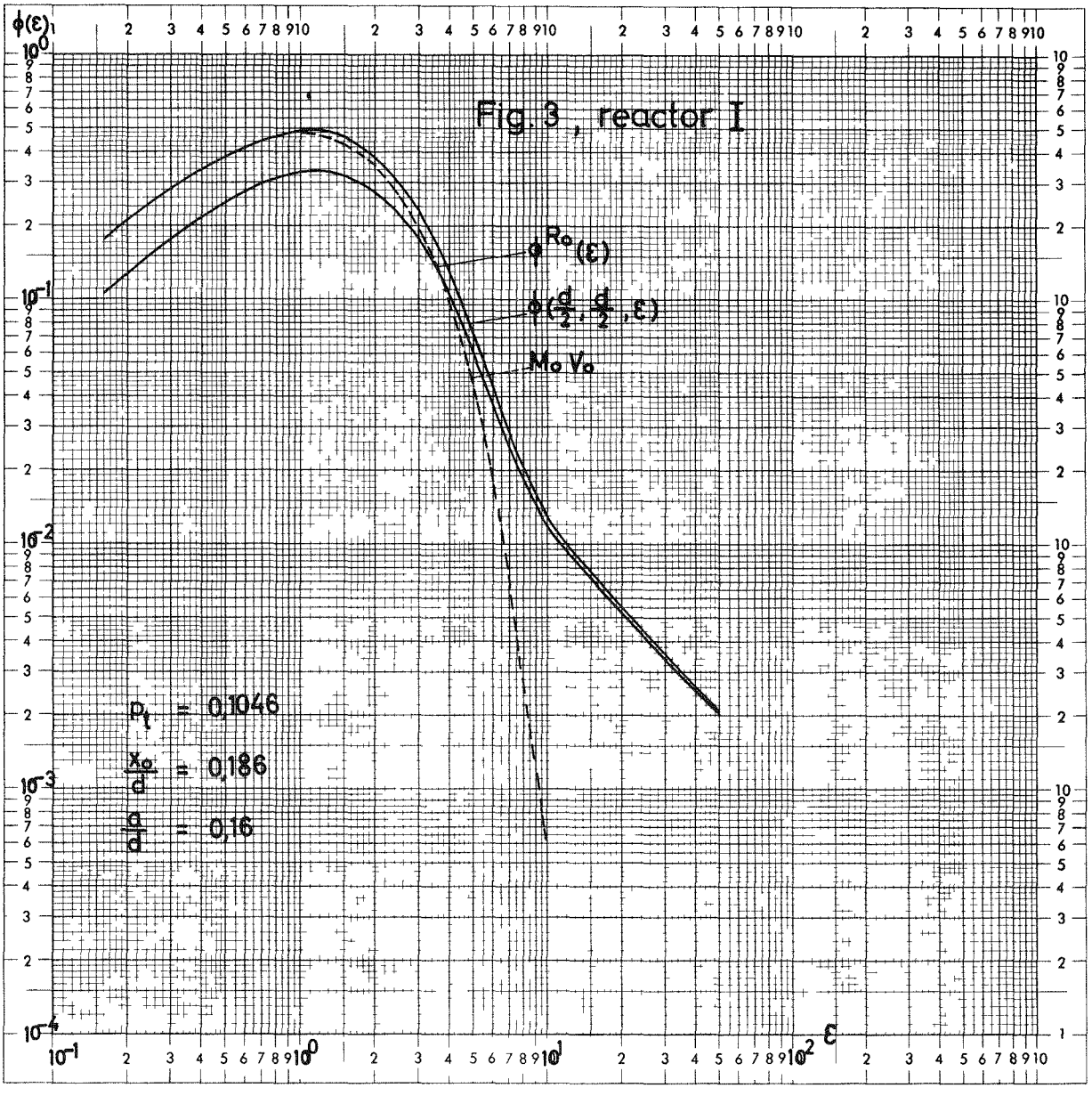
Fig. 3 , reactor I
$\phi(\varepsilon)$
$\phi^{R_o}(\varepsilon)$
$\phi(\frac{d}{2}, \frac{d}{2}, \varepsilon)$
$M_o V_o$
$p_t = 0{,}1046$
$\frac{x_o}{d} = 0{,}186$
$\frac{a}{d} = 0{,}16$
ε

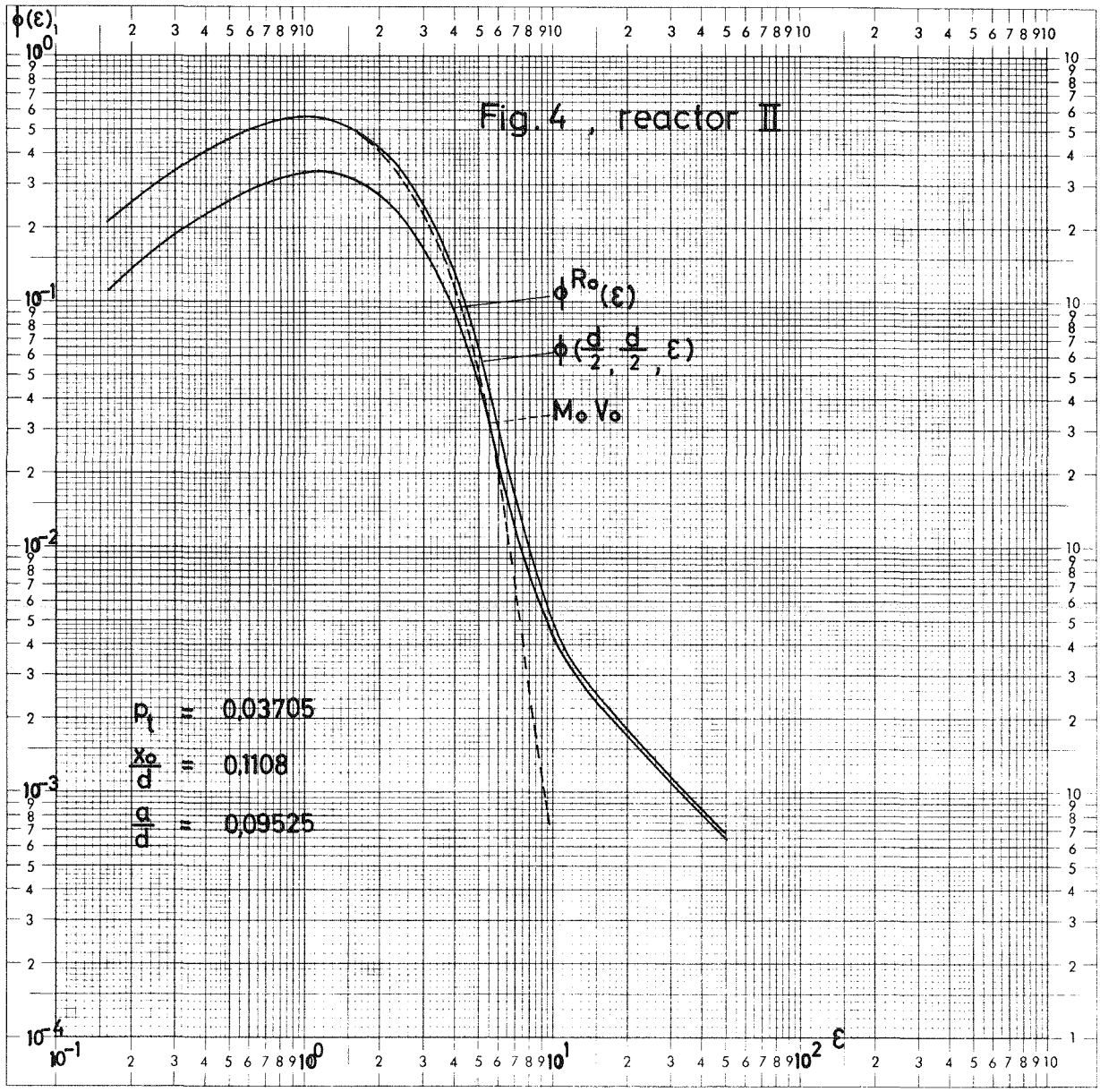
Fig. 4 , reactor II
$\phi(\varepsilon)_1$
$\phi^{R_o}(\varepsilon)$
$\phi(\frac{d}{2}, \frac{d}{2}, \varepsilon)$
$M_o V_o$
$p_t = 0{,}03705$
$\frac{x_o}{d} = 0{,}1108$
$\frac{a}{d} = 0{,}09525$
ε

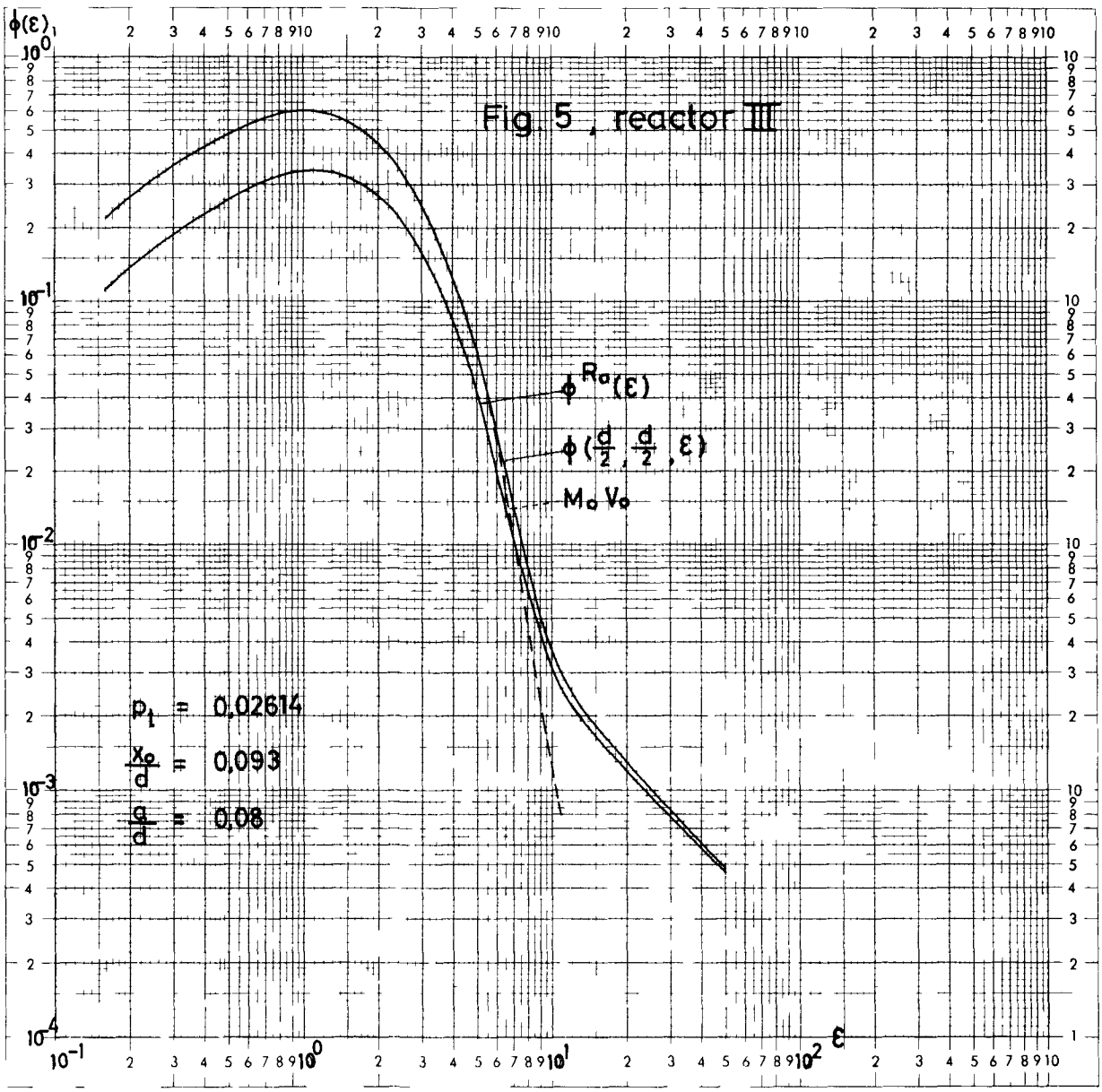
Fig. 5 , reactor III
$\phi(\varepsilon)_1$
$\phi^{R_o}(\varepsilon)$
$\phi(\frac{d}{2}, \frac{d}{2}, \varepsilon)$
$M_o V_o$
p_t = 0,02614
$\frac{x_o}{d}$ = 0,093
$\frac{a}{d}$ = 0,08
ε

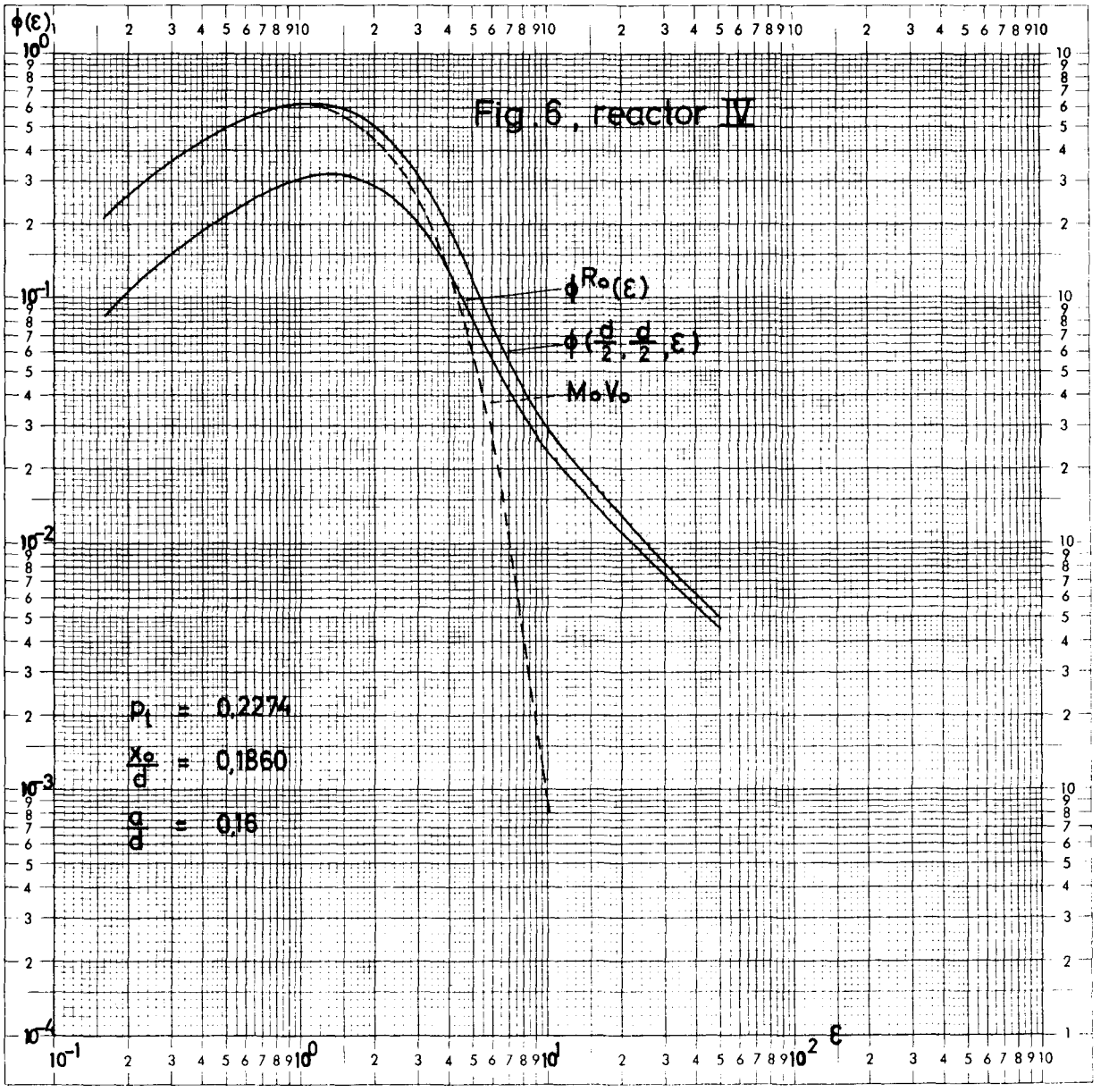
Fig. 6, reactor IV
$\phi(\varepsilon)$
$\phi^{R_0}(\varepsilon)$
$\phi(\frac{d}{2},\frac{d}{2},\varepsilon)$
$M_0 V_0$
$p_1 = 0,2274$
$\frac{x_0}{d} = 0,1860$
$\frac{a}{d} = 0,16$
ε

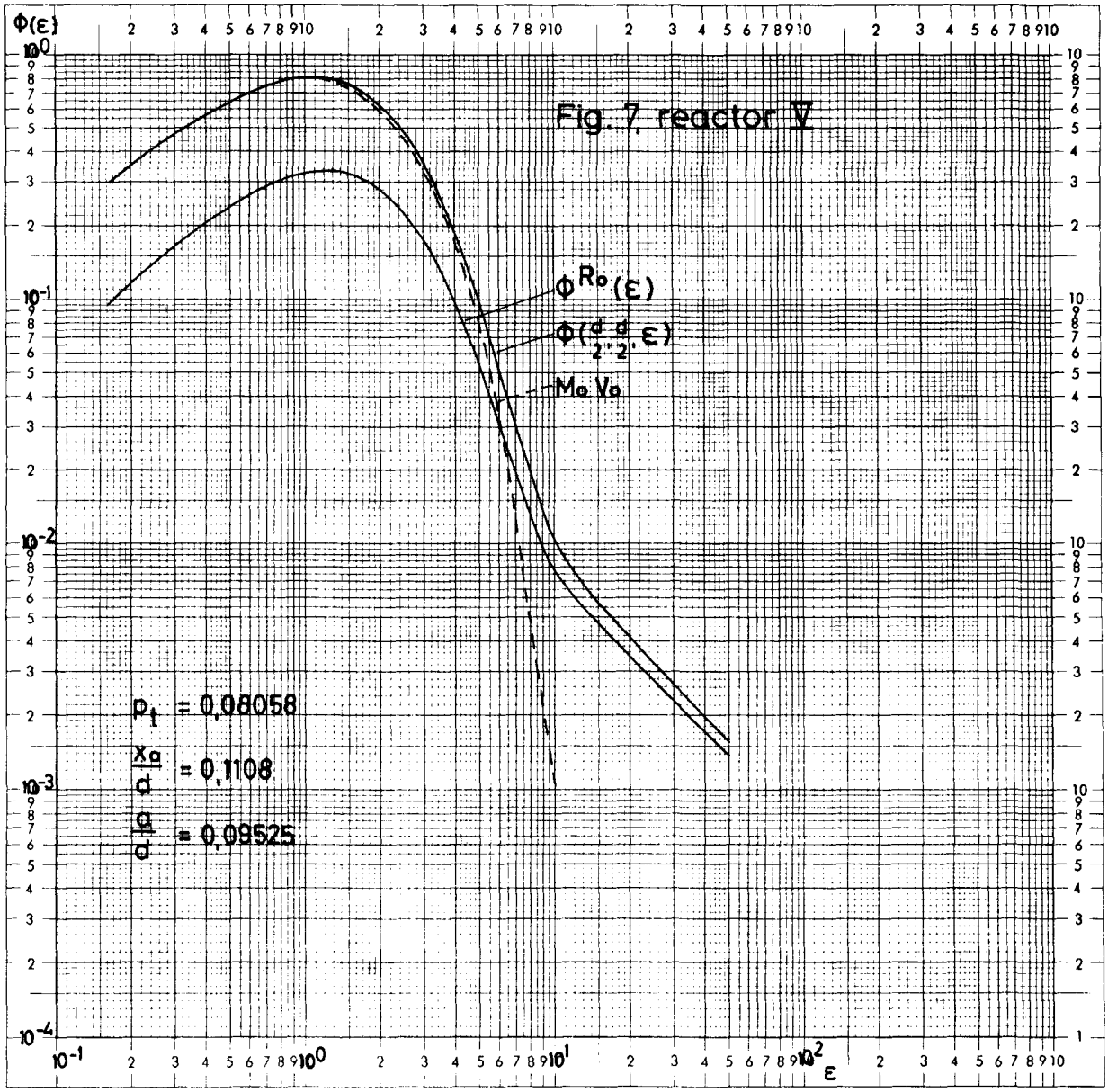
Φ(ε)
Fig. 7, reactor V
$\Phi^{R_0}(\varepsilon)$
$\Phi(\frac{d}{2}\cdot\frac{d}{2}\cdot\varepsilon)$
$M_0 V_0$
$p_f = 0{,}08058$
$\frac{x_a}{d} = 0{,}1108$
$\frac{a}{d} = 0{,}09525$
ε

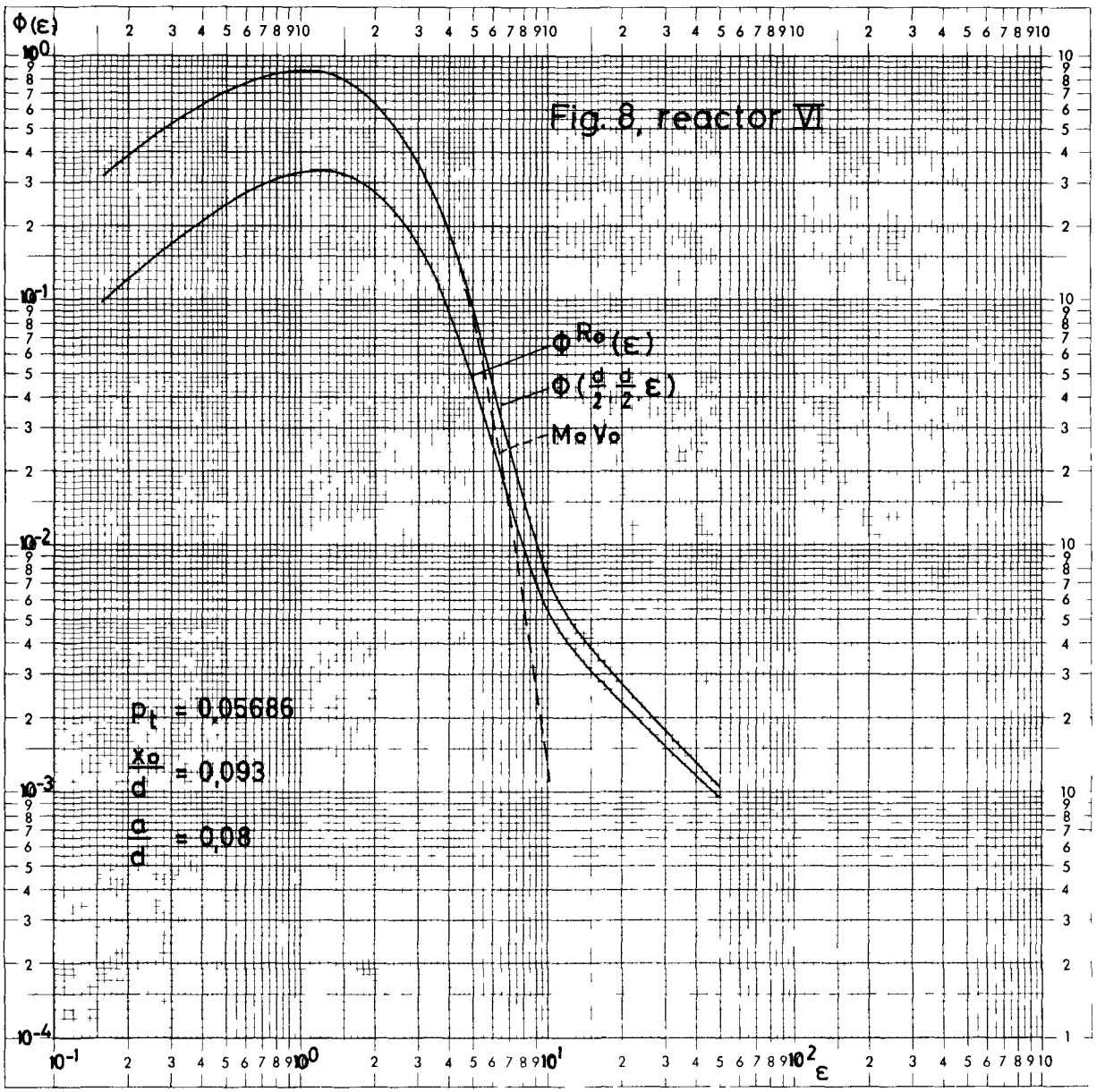
Φ(ε)
Fig. 8, reactor VI
Φ^Ro(ε)
Φ(d/2 a/2 ε)
Mo Vo
p_t = 0,05686
Xo/d = 0,093
a/d = 0,08
ε

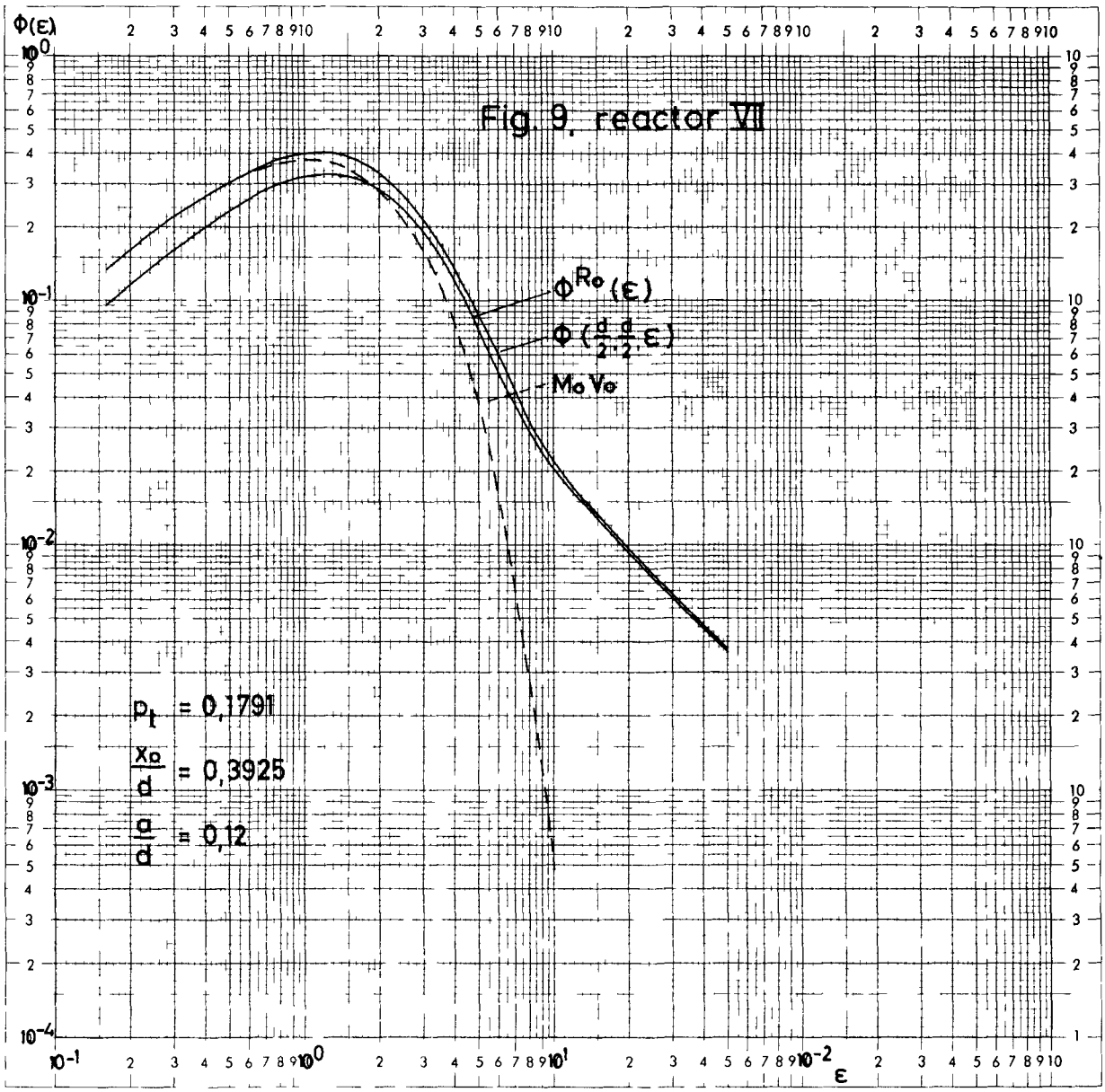
Φ(ε)
Fig. 9. reactor VII
$\Phi^{R_0}(\varepsilon)$
$\Phi\left(\frac{d}{2},\frac{d}{2},\varepsilon\right)$
$M_0 V_0$
$p_t = 0,1791$
$\frac{x_0}{d} = 0,3925$
$\frac{a}{d} = 0,12$
ε

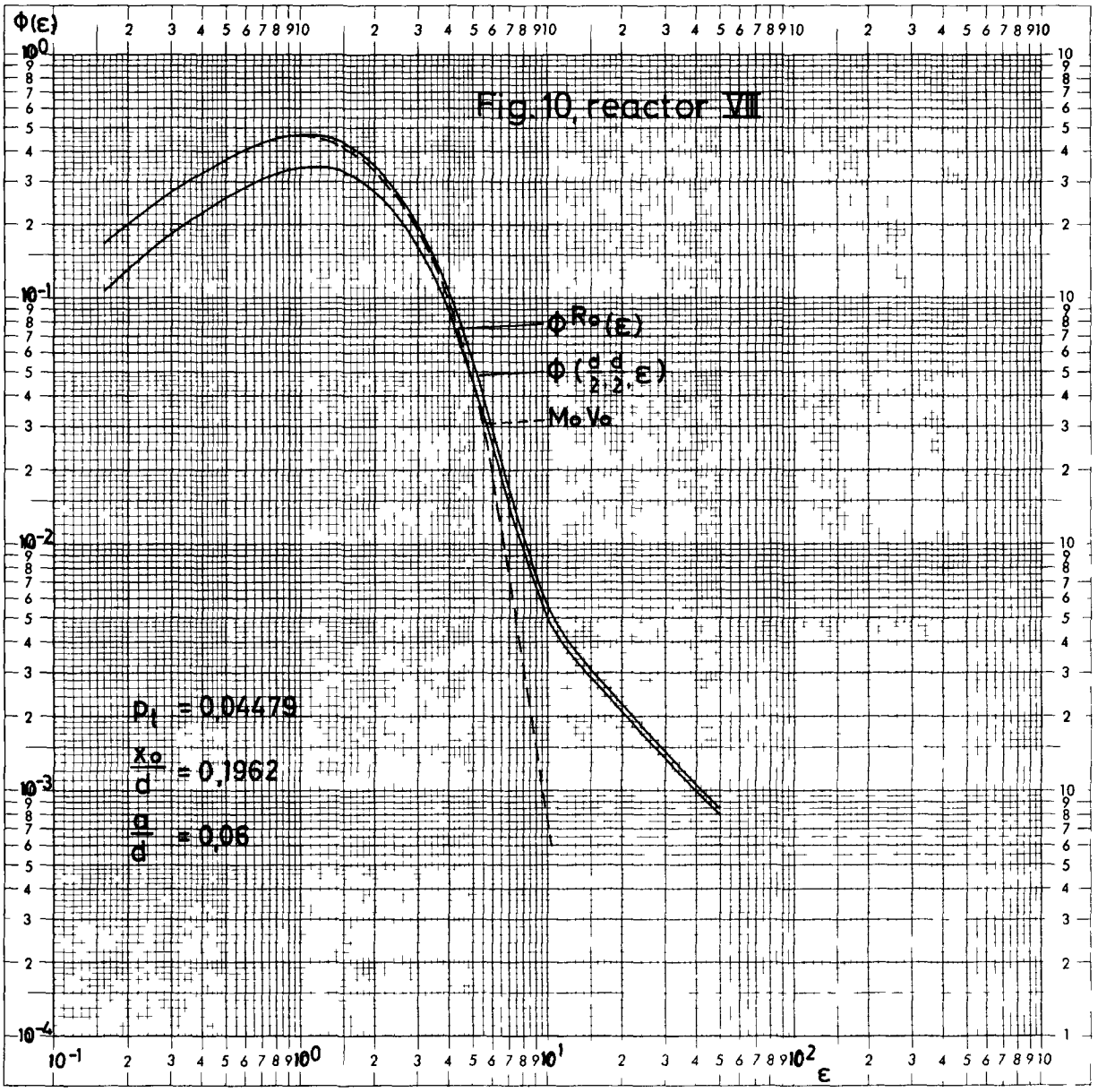
Φ(ε)
Fig.10, reactor VII
$\Phi^{R_0}(\varepsilon)$
$\Phi(\frac{d}{2},\frac{d}{2},\varepsilon)$
$M_0 V_0$
$p_f = 0,04479$
$\frac{x_0}{d} = 0,1962$
$\frac{a}{d} = 0,06$
ε

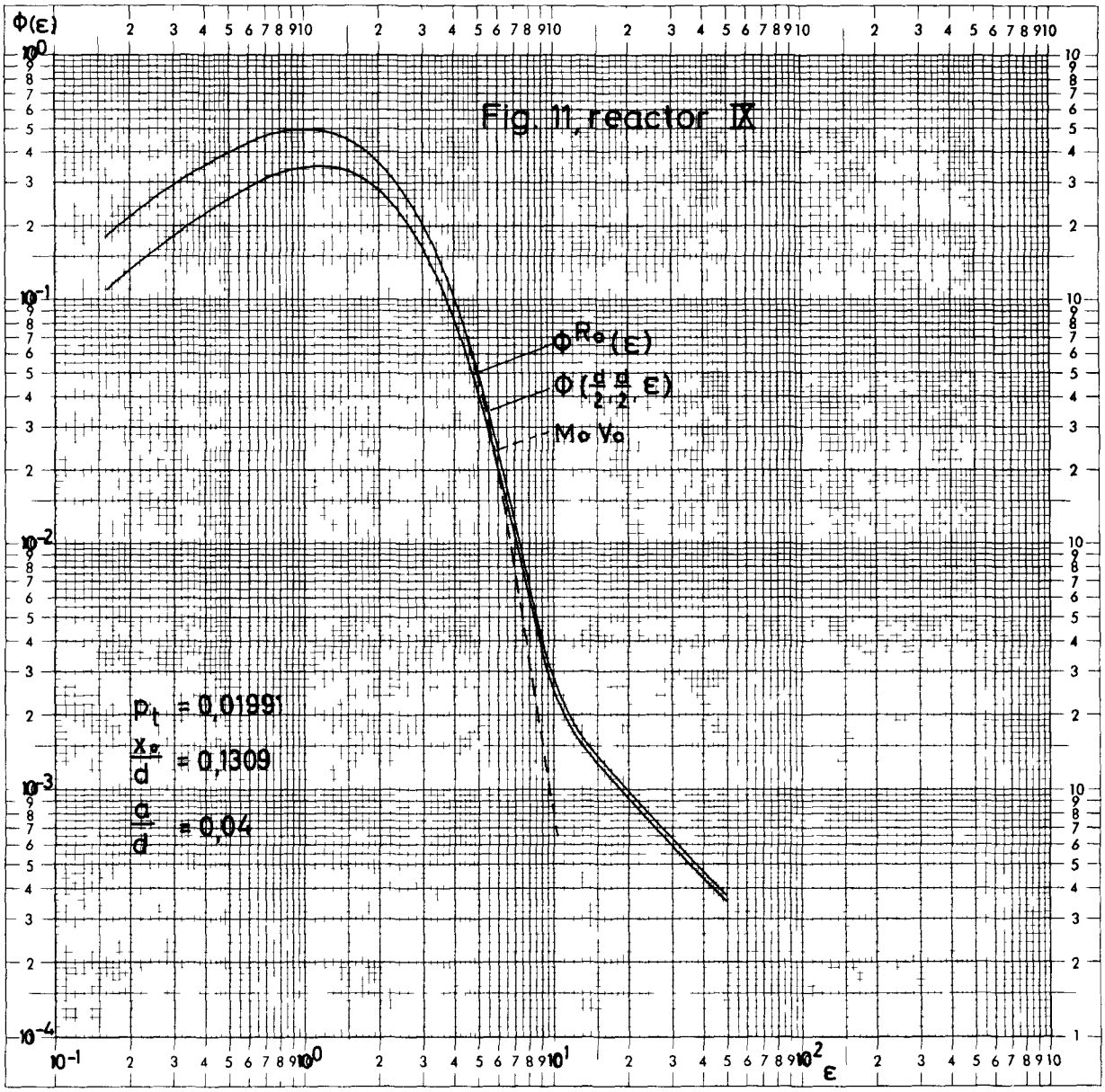
Φ(ε)
Fig. 11, reactor IX
$\Phi^{Ro}(\varepsilon)$
$\Phi(\frac{g}{2},\frac{g}{2},\varepsilon)$
Mo Vo
$p_t = 0,0199$
$\frac{x_o}{d} = 0,1309$
$\frac{a}{d} = 0,04$
ε

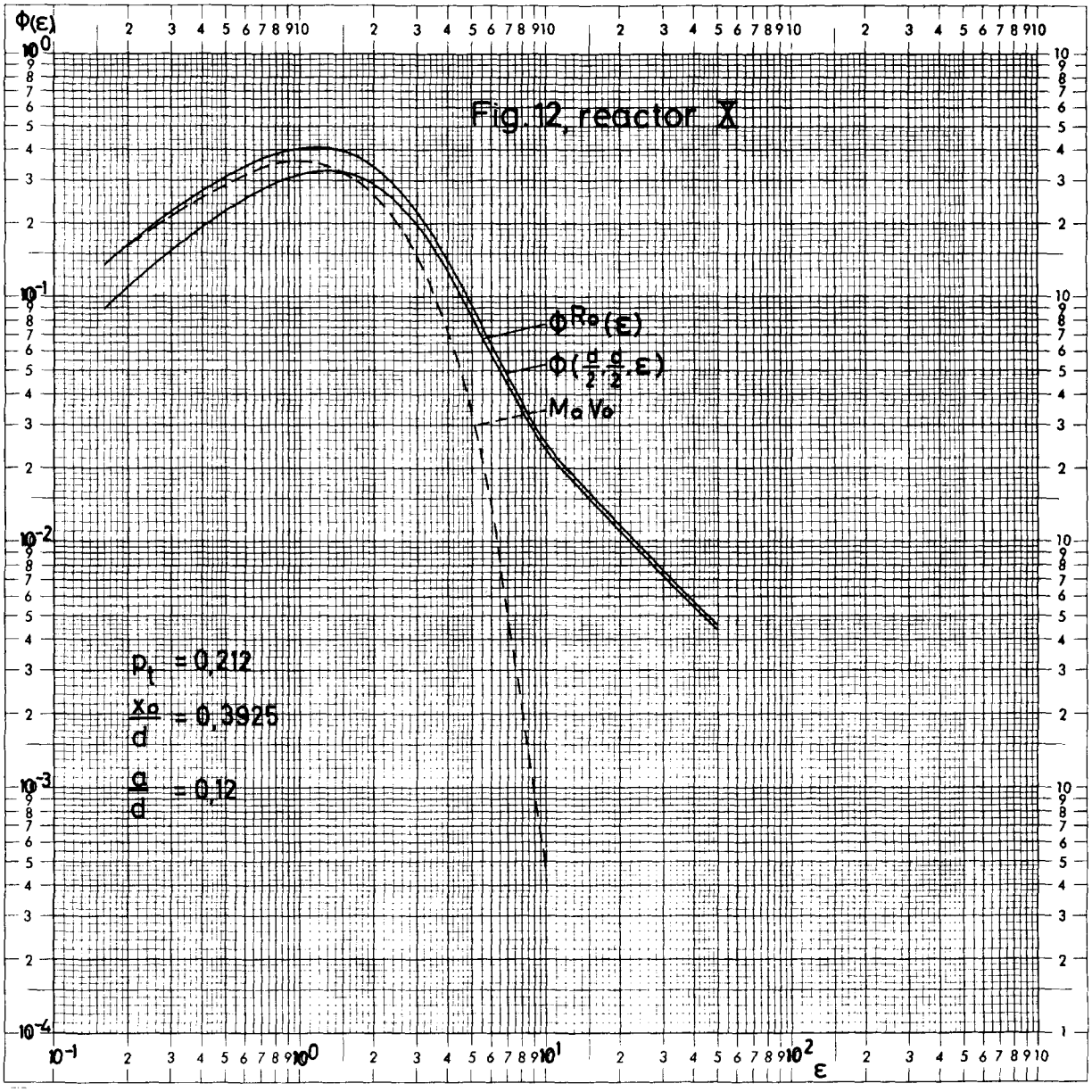
Fig.12, reactor X
Φ(ε)
ε
Φ Ro (ε)
Φ (d/2, a/2, ε)
Mo Vo
pt = 0,212
xo/d = 0,3925
a/d = 0,12

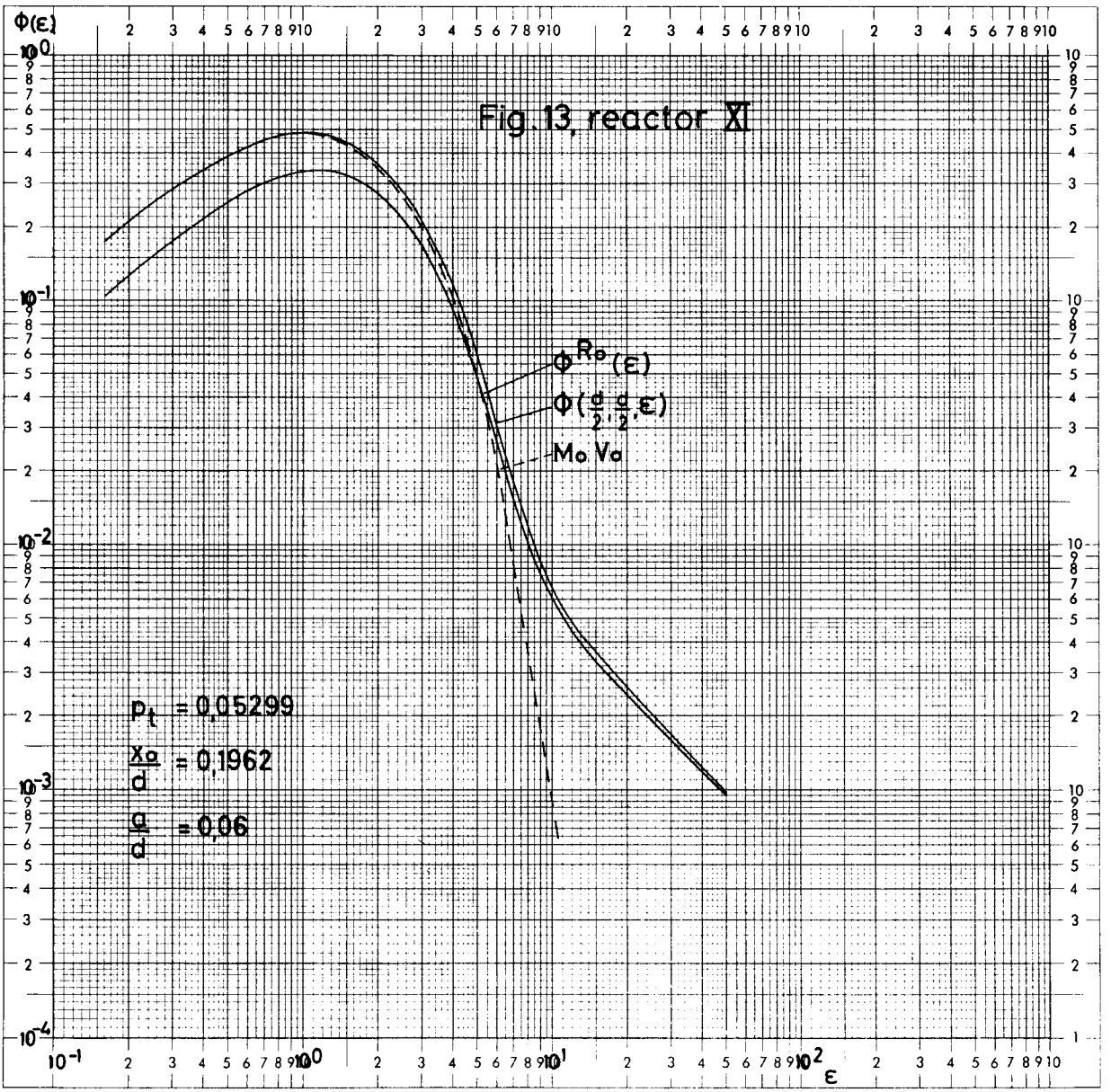
Fig. 13, reactor XI
Φ(ε)
ε
$\Phi^{R_o}(\varepsilon)$
$\Phi(\frac{a}{2},\frac{a}{2},\varepsilon)$
$M_o V_a$
$p_t = 0,05299$
$\frac{x_a}{d} = 0,1962$
$\frac{a}{d} = 0,06$

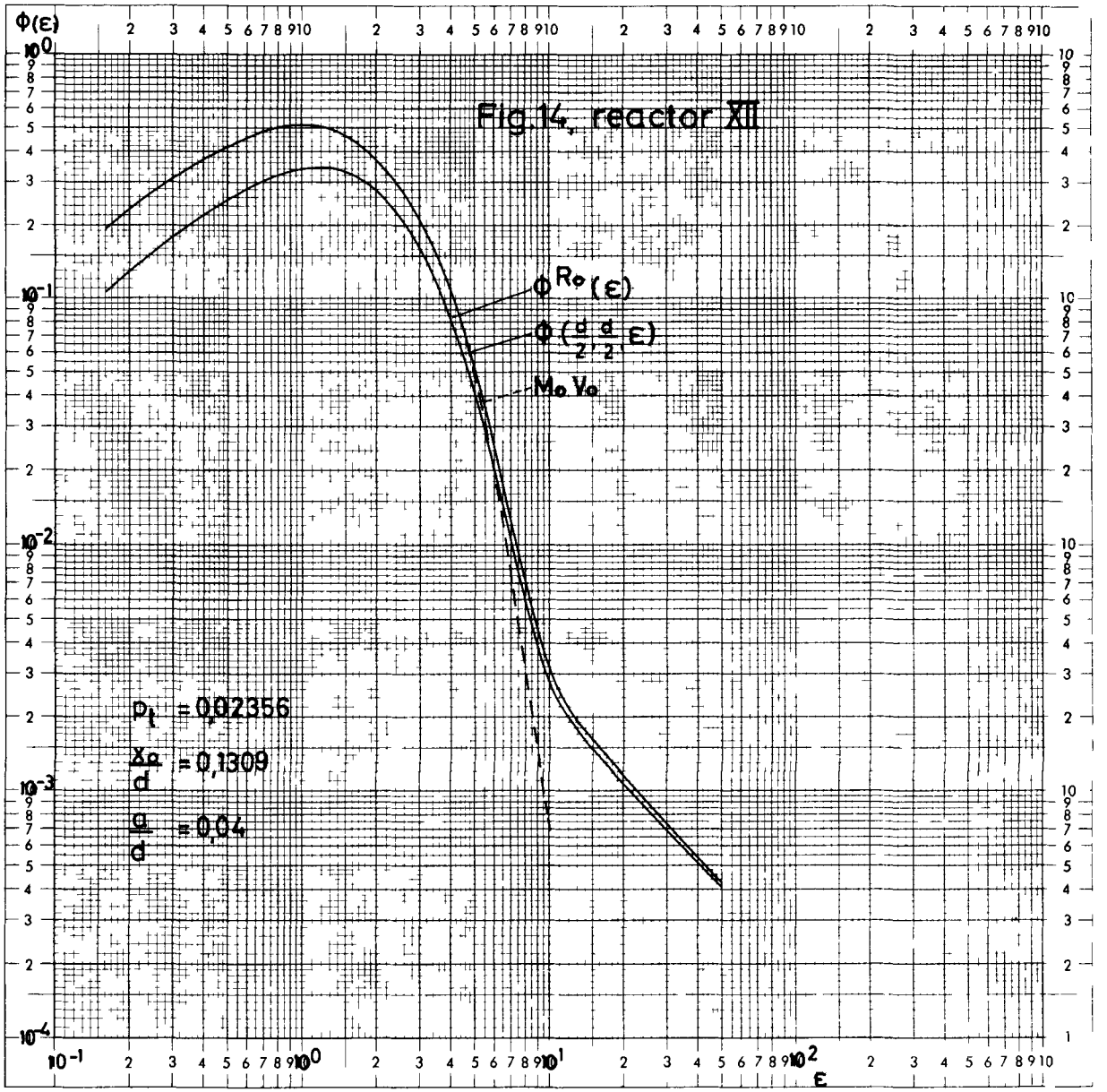
Φ(ε)
Fig.14, reactor XII
Φ Ro (ε)
Φ (d/2, d/2, ε)
Mo Vo
p_t = 0,02356
Δρ/d = 0,1309
q/d = 0,04
ε

PROPAGATION OF APPROXIMATION ERRORS IN SPECTRA: THE GAS MODEL*†

by

C. N. Kelber and K. S. Min

ARGONNE NATIONAL LABORATORY

Argonne, Illinois

A paper to be presented at the Conference on Neutron Thermalization, Brookhaven National Laboratory, April 30 - May 2, 1962.

*Work performed under the auspices of the U.S.A.E.C.

†Part of this work was presented in the doctoral dissertation submitted by K. S. Min to the faculty of the University of Minnesota, August, 1961.

I. INTRODUCTION AND SUMMARY.

There have been a number of estimates of the type of error induced by errors in the scattering kernel of the slowing down equation. In the nature of the problem these estimates have to be qualitative or highly specific. We have chosen to investigate an approximation error which corresponds in many ways to the type of approximation error which can occur with experimental data. This error is that involved in approximating the Wigner-Wilkins integral equation[1] (for a gas of mass M) by Wilkins' differential equation.[2] In addition, we have compared some of solutions of the integral equation with solutions of Corngold's[3] higher approximation equations.

In making the comparison, it quickly became obvious that there are few uniform differences that can be displayed. In general, the integral equation solution is slightly harder than the solution of Wilkin's equation.

The discrepancy in the solutions appears gratifyingly small, however, so what seem at first glance to be crude approximations, turn out to be surprisingly good. To check on this, reaction rates in a number of detectors were estimated for the various solutions. Here it was found that, in operational terms, it is possible to discriminate between the solutions. At the same time it is possible to find useful detectors which are insensitive to the fine structure of the spectrum. Thus we propose that the latter types of detectors be used to correlate experiments, while the former detectors be used to identify spectral structure in a single experiment.

In Part II of this paper we outline the problems posed and the modes of solution, together with the resulting spectra. Part III is a summary and discussion of the data on detector response. Finally, in part IV we present some speculations about the influence of the assumed source on the propagation of error.

II. PROBLEMS CONSIDERED AND THEIR MODE OF SOLUTION.

The conventional slowing down equation is:

$$\left[v\Sigma_s (v) + v\Sigma_a (v) \right] n(v) = \int_o^\infty dv^1 \, v^1 \Sigma (v^1 \rightarrow v) \, n (v^1) + S(v). \quad (1)$$

As usual we consider only the case $v\Sigma_a (v) = \Gamma\Sigma_f$ where Γ is a constant and Σ_f is the free atom scattering cross section. The velocity v is given by the dimensionless variable $v = \sqrt{E/kT}$. Since we are concerned with the low energy behavior, we need not worry about the influence of the details of the fission process on the high energy spectrum. Thus the source term can be considered to be zero except at an indefinitely high energy, and dropped from the r.h.s. of equation (1).

The scattering kernel rate per free atom scattering cross section is $P (v_o \rightarrow v)$:

$$P (v_o \rightarrow v) = \theta \frac{2.v}{v_o} \left\{ \exp (v_o^2 - v^2) \left[\Theta (\theta v_o - \xi v) \pm \Theta (\theta v_o + \xi v) \right] + \Theta (\theta v - \xi v_o) \mp \Theta (\theta v + \xi v_o) \right\} v_o \leq v. \quad (2)$$

$\theta = (M + 1) / 2\sqrt{M}$, M = scattering mass (in neutron masses).

$\xi = (M - 1) / 2\sqrt{M}$.

$\Theta (x) = \text{erf} (x) = (2/\sqrt{\pi}) \int_o^x (\exp - y^2) dy$.

The total scattering rate per free atom scattering cross section, V(v), is:

$$V(v) = (v + (1/2 Mv)) \; \Theta (\sqrt{M} \, v) + (\exp - Mv^2) \, (1/\sqrt{M\pi}).$$

Now we assert that N(v) is identical with its asymptotic form Nas (v) above some high but otherwise arbitrary velocity, v_c. Form the slowing down density (per free atom scattering cross section) at some (high) velocity v:

$$\frac{\xi}{2}\, v\ (v + \Gamma)\ \mathrm{Nas}\ (v) = \int_0^v N\ (x^1)\ dx^1\ .$$

Differentiate with respect to v and obtain, for $v \geq v_c$,

$$N^1_{as}\ (v) + \left(\frac{1 + \frac{2}{\xi}}{v + \Gamma} + \frac{1 - \frac{2}{\xi}}{v} \right) N_{as}\ (v) = 0. \tag{3}$$

Our asymptotic solution is then:

$$\mathrm{Nas}\ (v) = (C/v^2) \left(\frac{v}{v + \Gamma} \right)^{\frac{2}{\xi} + 1} \tag{4}$$

Expanding in powers of 1/v we find

$$\mathrm{Nas}\ (v) \sim \frac{C}{v^2} \left[1 - \frac{\Delta}{2}\ \left(1 + \frac{5}{3M} \right)\ \frac{1}{v}\ + \ldots \right] \tag{5a}$$

$\Delta = 2M\Gamma$

Corngold's (3) accurate asymptotic representation is:

$$\mathrm{Nas}\ (v) \sim \frac{C}{v^2} \left[1 - \frac{\Delta}{2}\ \left(1 + \frac{4}{3M} \right)\ \frac{1}{v}\ + \ldots \right] \tag{5b}$$

The close agreement between the two forms 5a and 5b gives us confidence in the use of the closed form (Eq. 4) for the asymptotic density.

Equation (1) is now replaced by:

$$\left(V(v) + \Gamma \right) N(v) = \int_0^{v_c} dv_o \, P(v_o \longrightarrow v) \, N(v_o)$$

$$+ \int_{v_c}^{\infty} dv_o \, P(v_o \longrightarrow v) \, N_{as}(v) \ldots \qquad (6)$$

In equation 6, the kernel $P(v_o \longrightarrow v)$ is given its asymptotic form in the last term:

$$v > v_c, \quad P(v_o \longrightarrow v) = \theta^2 \frac{v}{v_o} 2 \quad \text{if } v_c < v < v_o$$

$$= 0 \text{ otherwise.}$$

Moreover, we introduce the maximum fractional velocity loss $\alpha = (M-1)/(M+1)$.

The equation for N then becomes:

$$\left(V(v) + \Gamma \right) N(v) = \int_0^{v_c} dv_o \, P(v_o \longrightarrow v) \, N(v_o) + 2\theta^2 v \int_{v_c}^{v/\alpha} \frac{C \, v_o^{\frac{2}{\xi} - 2}}{\left(\frac{2}{\xi} + 1\right) (v_o + \Gamma)} dv_o \quad v \longrightarrow \alpha v_c$$

$$= \int_0^{v_c} dv_o \, P(v_o \longrightarrow v) \, N(v), \quad v < \alpha v_c \ldots \qquad (7)$$

If the interval (o, v_c) is divided into intervals (v_j, v_{j+1}), and the integrals approximated by the trapezoidal rule, then

$$N(v_i) = \frac{1}{V(v_i) + \Gamma} \left(\sum_{j=1}^{M} P(v_i \longrightarrow v_i) \, N(v_j) \, H_j + 2\theta^2 \, v_i \, f(v_i) \right) \ldots . \quad (8)$$

Here, $f(v_i) = 0$, if $v_i < \alpha v_c$

$$= \int_{v_c}^{v_i/\alpha} \frac{dv_o \; C \; v_o^{\frac{2}{\xi} - 2}}{(\frac{2}{\xi} + 1)}, \quad \text{if } v_i > \alpha v_c;$$

$$(v_o + \Gamma)$$

$$H_j = |v_{j+1} - v_j|$$

The constant C is evaluated by noting that at T = 0 (stationery scatterers) Nas (v) is the correct solution over the whole range. Then for neutrons to be conserved,

$\Gamma \int_o^\infty$ Nas (v) dv = S where S is the total volumetric source. This fixes S in terms of the normalization of Nas. We then set $\int_o^\infty$ Nas (v) dv = 1, and find $C = 2\Gamma/\xi$. Whence, $S = \Gamma$. Thus, at any temperature T, to conserve neutrons (1/v absorption), $\int_o^\infty N(v)\, dv = \int_o^\infty$ Nas (v) dv = 1. But for $v > v_c$, N = Nas; so that:

$$\int_o^{v_c} N(v)\, dv = \int_o^{v_c} \text{Nas}(v)\, dv = \left(\frac{v_c}{v_c + \Gamma} \right)^{2/\xi} \quad \cdots \qquad (9)$$

Equations 8 and 9 are solved by an iteration process.

Solutions of the integral equation and of Wilkins differential equation are compared in Figures 1-8. The maxwellian and asymptotic components are also plotted. As might be expected the differences are truly small. Nevertheless, the differences are consistent so that an error is being propagated in a systematic way. To verify this Corngold's (3) higher approximation to the Wilkin's equation was solved, using forward differencing. The equation is:

$$vN_1'' + \left[2v^2 - 1 - \frac{1}{M}\left(\frac{2}{v^2} + \frac{2\Delta}{3}\,\frac{1}{v}\right)\right] N_1' + \left[4v - \Delta + \frac{1}{M}\left(\frac{4}{v^3} + \frac{2\Delta}{v^2} + \frac{\Delta^2}{3} - 4\right)\frac{1}{v} - \frac{\Delta 4}{3}\right] N_1 = 0 \quad \ldots \quad (10)$$

We use the boundary conditions: $N_1(0) = N_1'(0) = 0$

$(\Delta = 2M\Gamma)$

By using the boundary conditions and forward differencing, the numerical troubles caused by the singularity were avoided; but this may lead to some inaccuracy near the origin. Over the range where validity is expected ($v > 1$) the solution of Corngold's equation falls in between the integral equation solution and the differential equation solution. This reinforces the view that the observed error is that induced by the mathematical approximations made in going from the integral equation to the Wilkins equation.

The approximation of the integral equation by differential equations of increasing order is reminiscient of Weirstrass' functional approximation theory. The analytic difficulties in formulating such a theory are formidable however, and we have contented ourselves with noting that the problem exists.

Examining figures 1-8 we note that the discrepancy in the solutions is most noticeable in the region .1 to 1 ev. Yb^{168} has a resonance at .6 ev which is distinct from other known 1/v resonances; moreover the Yb^{169} half-life of 32 days is easily separated from the Yb^{175} half-life of 4.5 days or the Yb^{177} half-life of 2 hours.

Thus, we conclude that Yb^{168} activation is a good candidate to examine spectra where we expect them to be most sensitive to the details of the scattering process.

III. DETECTOR RESPONSES

In line with the observations just made we have calculated the expected activation rates of Yb^{168} with and without cadmium cover, the Lu^{176} activation rate, and the U^{235} and Pu^{239} fission rates. The Lu^{176} rate has been included because it is frequently used as a spectral index. The cadmium thickness has been taken as 0.0254 cm (0.010"); the transmission of the cadmium filter for an isotropic flux has been used in computing the activation rather than a sharp cutoff. Since the cadmium transmission varies sharply in the neighborhood of the Yb^{168} resonance, the cadmium ratio will be dependent on the cadmium thickness. In these calculations we have ignored any local flux depressions arising from the foils.

In Table I we list the activation rates calculated in the various spectra. By Wigner-Wilkins (W.W.) we mean the spectrum yielded by the integral equation. Wilkins (W), then, refers to the spectrum from the Wilkins differential equation. Similarly, by Corngold (C) we mean the solution of equation 10. The latter must be taken with some reservations. Firstly, the solutions of equation 10 have only a limited validity at low velocities; and we suspect that our method of solving equation 10 may not have correctly included the effects of the singularities at the origin. The computed solutions of equation 10 dip below both the other two solutions for $v < 1$; if equation 10 yields a higher approximation than the Wilkins equation it should be intermediate to the two solutions, as it is above $v = 1$.

As can be seen from Table I, the greatest deviation between the various spectra is in the Yb^{168} cadmium ratio. The discrepancies are of the order of 4 to 10%, which are readily observed.

The U^{235}: Pu^{239} fission ratio also shows deviations of the order of 3 to 6 percent. The U^{235} fission rate by itself is remarkably constant. So is the Lu^{176} activation. Thus the Lu^{176}/U^{235} (fission) ratio is a spectral indicator which is insensitive to the fine details of the scattering kernel. Unfortunately, the activities are incommensurable, so that the individual activities must be referred to a calibrating standard such as the activities in a thermal column. Indeed, if absolute counting methods could be relied on the epi-cadmium Yb^{168} rate is highly sensitive to fine details.

If we assume that the discrepancy between the Wigner-Wilkins and the Wilkins spectra propagates in a characteristic way, then insensitive detectors are suitable for correlating experiments since they tend to correspond to lumped theoretical parameters. On the same basis, prediction of the Yb^{168} cadmium ratio is a sensitive test of the accuracy of an assumed scattering kernel.

IV. SOME GENERAL COMMENTS ON THE PROPAGATION OF ERROR

The Wigner-Wilkins equation can be symmetrized using the principle of detailed balancing; hence it is one of a large class of integral equations with well known properties. The general form is:

$$f(x) = \phi(x) - \lambda \int K(x,y)\, \phi(y)\, dy \ldots \qquad (11)$$

$K(x,y)$ is real and symmetric. As usual when the eigenfunctions

$$\psi_i \quad (x) = \lambda_i \int K(x,y)\, \psi_i \quad (y)\, dy \text{ are}$$

introduced the solution takes the form

$$\phi(x) = \sum_{i=1}^{\infty} \frac{\lambda i}{\lambda_i - \lambda} \psi_i(x) f_i \quad \ldots \tag{12}$$

$$\left(f_i = \int \psi_i \quad (y)\, f(y)\, dy \right)$$

In this representation, $K(x,y) = \sum_{i=1}^{\infty} \frac{\psi_i \_\_(x)\, \psi i \_\_(y)}{\lambda_i}$;

truncating the sum at i = N yields an approximation K_N to K which yields in turn a uniform approximation to ϕ, ϕN. (The series in equation 12 also terminates at N.)

Now take the eigenfunctions characteristic of the Wilkins differential equation for zero absorption:

$$\psi_i(E) = \exp(-E/2) \cdot L^1{}_i(E)/i\,!\,, \quad \lambda_i = i$$

Since the approximation is uniform we can estimate the error by computing $\phi_N(0)$: $\phi_N(0) = \sum_{i=1}^{N} \frac{i}{i-\lambda} f_i \quad \ldots$ (13)

Now, let $f = \delta(E - E_o)$, $E_o \rightarrow 0$.

Then $f_f = \frac{(-)^i Eo^i (i+1)}{i!} \exp(-Eo/2) \ldots$ (14)

Then the error $\phi - \phi_N$ is less than the last term in ϕ_N:

$$\left| \phi - \phi_N \right| < \frac{N}{N-\lambda} E_o^N \frac{(N+1)}{N!} \exp(-Eo/2) \ldots \tag{15}$$

Setting $\frac{N}{N-\lambda} \doteq 1$, we can estimate $\left| \theta - \theta_N \right|$ by $\epsilon = \frac{Eo^N (N+1)}{N!} \exp(-Eo/2)$ ...(16)

Now ϵ is not monotone with N; indeed N must be larger than Eo before ϵ can begin to decrease with N. Hence the source energy and thus the source shape may well play a role in determining the size of errors propagated by truncating

the kernel. Since ϵ is only an upper bound we cannot say this definitely, but the suspicion is strong that this is so in general.

CNK:dm

References

1. E. P. Wigner and J. E. Wilkins, Jr., U.S.A.E.C. Report, AECD 2275 (1944).
2. J. E. Wilkins, Jr., U.S.A.E.C. Report, CP-2481 (1944).
3. N. Corngold, Annals of Physics 6, 368 (1959).

TABLE I

ACTIVATION RATES

	Yb^{168} Activation (Unit $Nx10^{-24}$)			Lu^{176} Activation	Pu^{239} and U^{235} Fission		
Mass 2, Γ 0.15310	Bare	0.01" Cd-Shielded	Cd Ratio	Bare (Unit N x 10^{-24})	U^{235} (Unit $N_{25}x10^{-24}$)	Pu^{239} (Unit $N_{49}x10^{-24}$)	Ratio (Unit $\frac{N_{25}}{N_{49}}$)
Wigner-Wilkins	10971	5071	2.1636	4538	8249	16021	0.5149
Wilkins	9431	3957	2.3838	4441	8348	15343	0.5441
Ratio $(\frac{W.W-W.}{W.W.})$	0.1404	0.2196	(-).1018	0.0213	(-)0.0120	0.0423	(-)0.0567
Mass 9, Γ 0.03829							
Wigner-Wilkins	11389	5319	2.1413	4693	8273	16376	0.5052
Wilkins	10142	4431	2.2889	4556	8339	16054	0.5194
Ratio $(\frac{W.W-W.}{W.W})$	0.1095	0.1667	(-)0.0689	0.0292	(-)0.0078	0.0197	(-)0.0281
Mass 12, Γ 0.03829							
Wigner-Wilkins	13508	6868	1.9670	4912	8057	17508	0.4602
Wilkins	11922	5746	2.0747	4748	8108	16629	0.4876
Corngold	12242	5981	2.0471	4751	8082	16737	0.4829
Ratio $\left(\frac{W.W-W.}{W.W.}\right)$	0.1174	0.1633	(-)0.0548	0.0334	(-)0.0063	0.0502	(-)0.0556
Ratio $\left(\frac{W.W.-C}{W.W.}\right)$	0.0937	0.1291	(-)0.0407	0.0328	(-)0.0031	0.0440	(-)0.0493

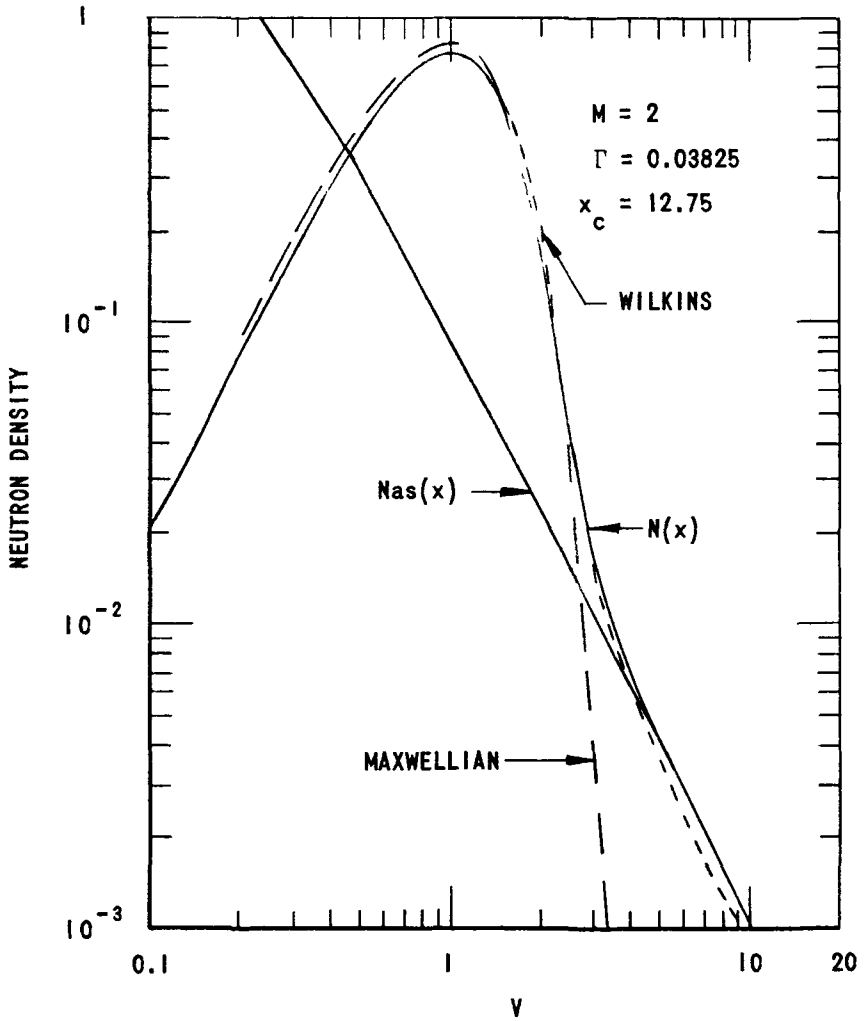
NEUTRON DENSITY
1
10^{-1}
10^{-2}
10^{-3}
0.1
1
10
20
V
M = 2
Γ = 0.03825
x_c = 12.75
WILKINS
Nas(x)
N(x)
MAXWELLIAN

FIG. 1

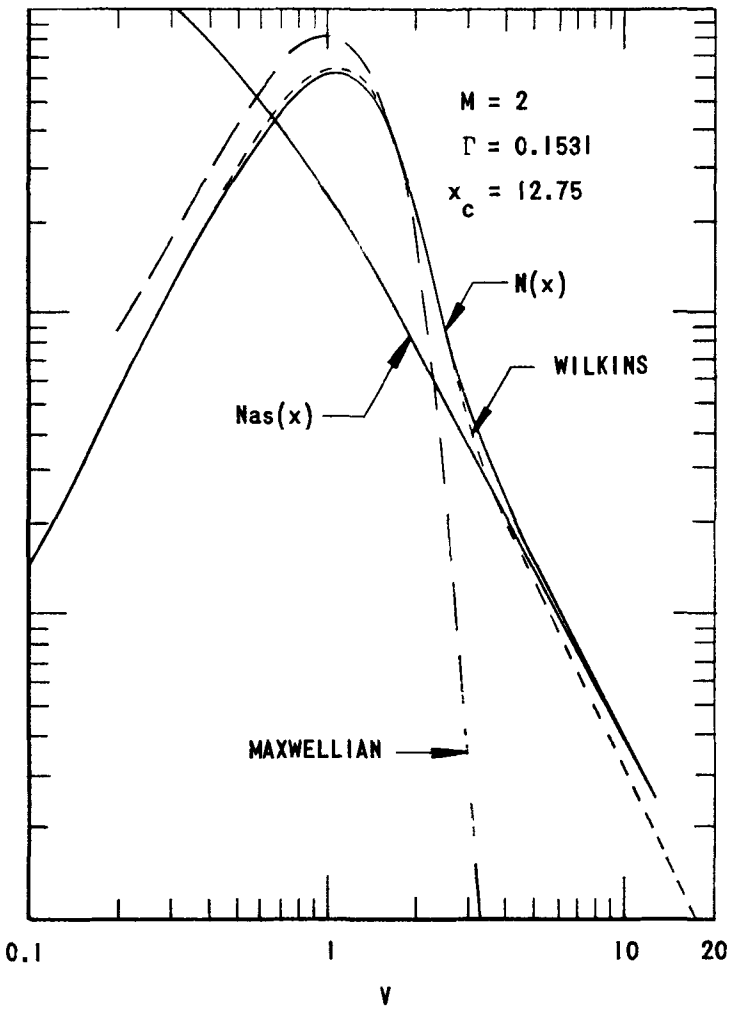
0.1
1
10
20
V
M = 2
Γ = 0.1531
x_c = 12.75
N(x)
WILKINS
Nas(x)
MAXWELLIAN

FIG. 2

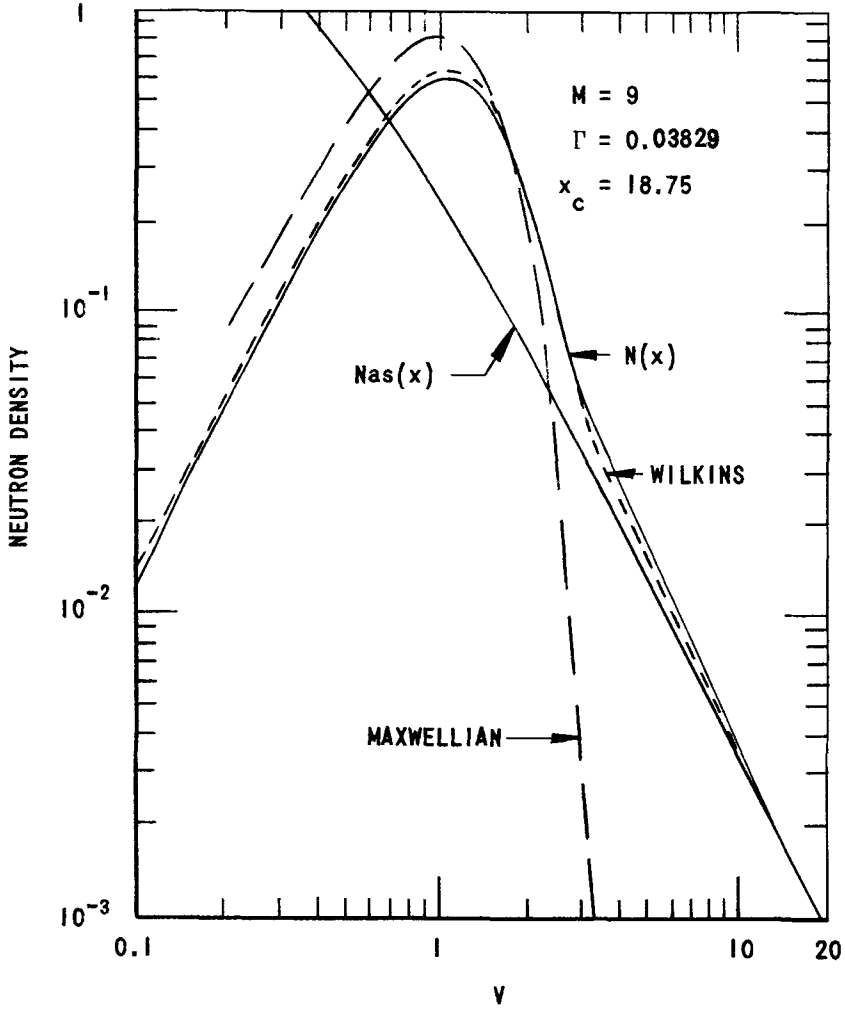
M = 9
Γ = 0.03829
x_c = 18.75
Nas(x)
N(x)
WILKINS
MAXWELLIAN
NEUTRON DENSITY
1
10^{-1}
10^{-2}
10^{-3}
0.1
1
10
20
V

FIG. 3

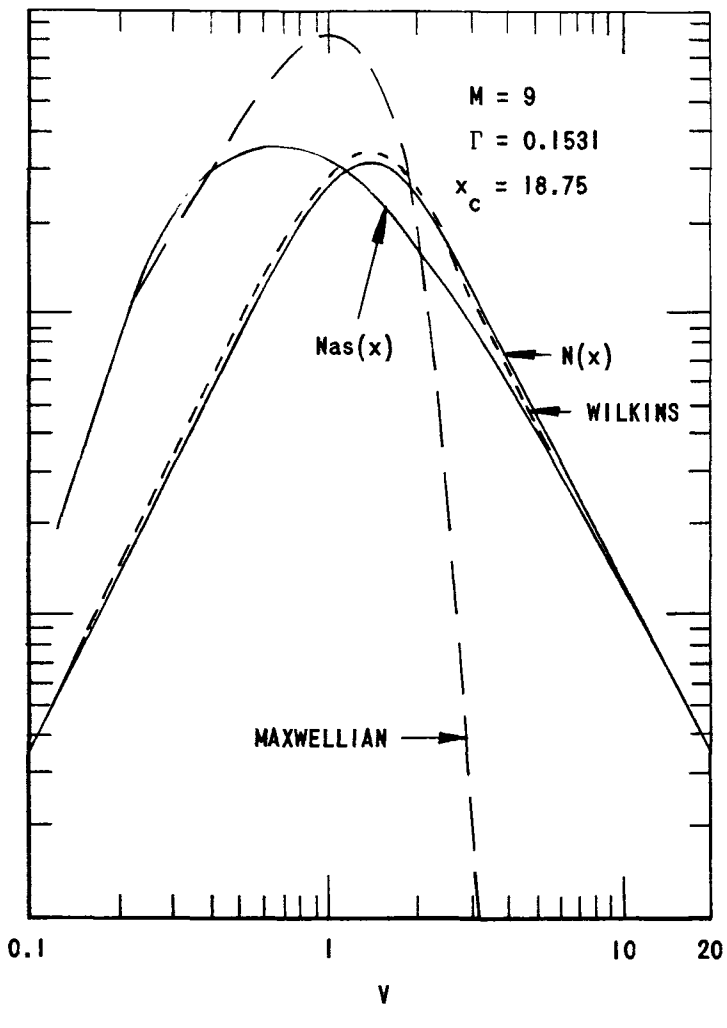
M = 9
Γ = 0.1531
x_c = 18.75
Nas(x)
N(x)
WILKINS
MAXWELLIAN
0.1
1
10
20
V

FIG. 4

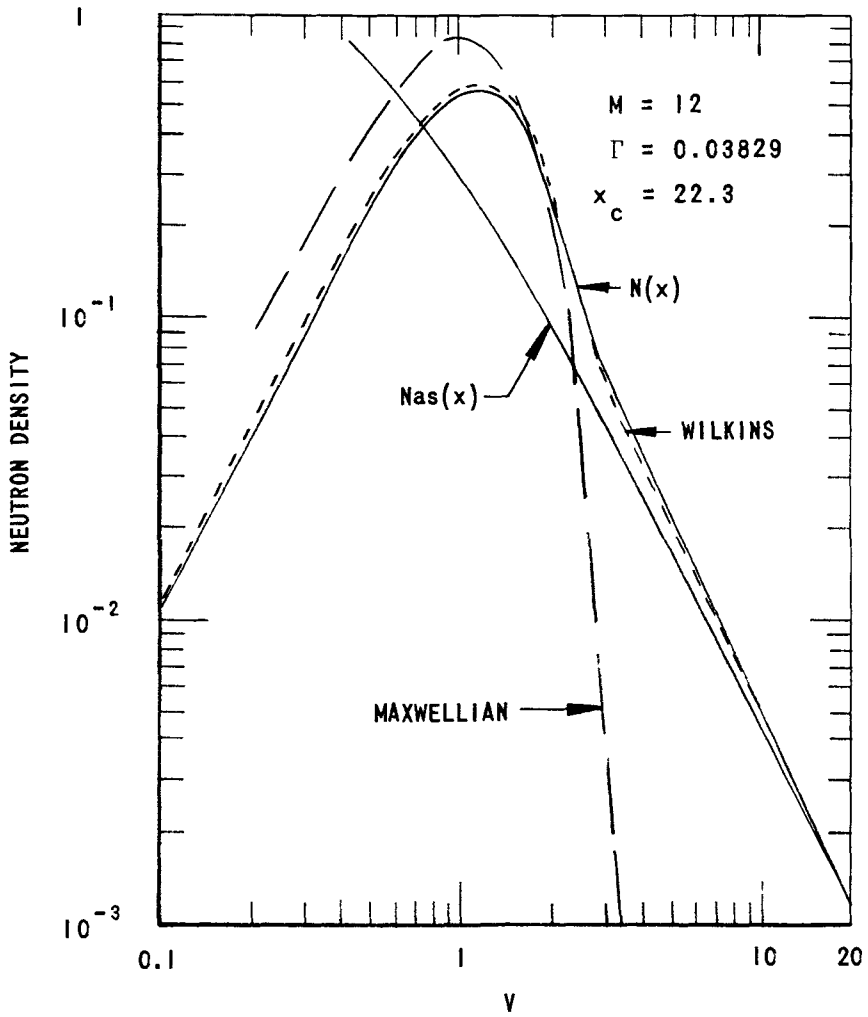
M = 12
Γ = 0.03829
x_c = 22.3
N(x)
Nas(x)
WILKINS
MAXWELLIAN
NEUTRON DENSITY
1
10^{-1}
10^{-2}
10^{-3}
0.1
1
10
20
V

FIG. 5

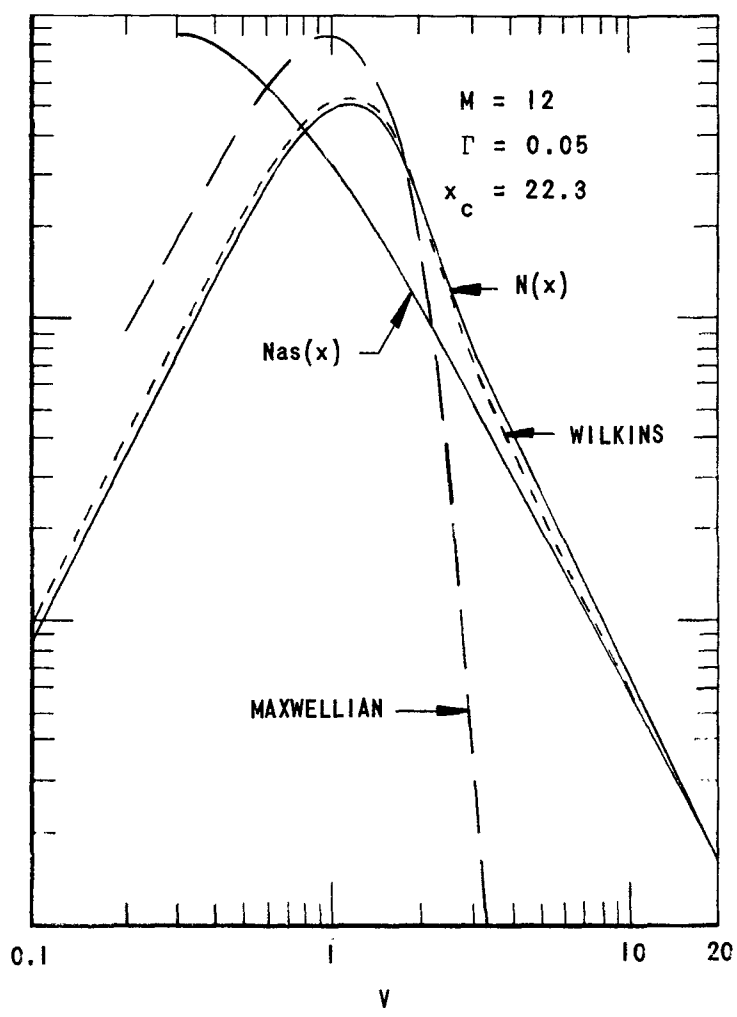
M = 12
Γ = 0.05
x_c = 22.3
N(x)
Nas(x)
WILKINS
MAXWELLIAN
0.1
1
10
20
V

FIG. 6

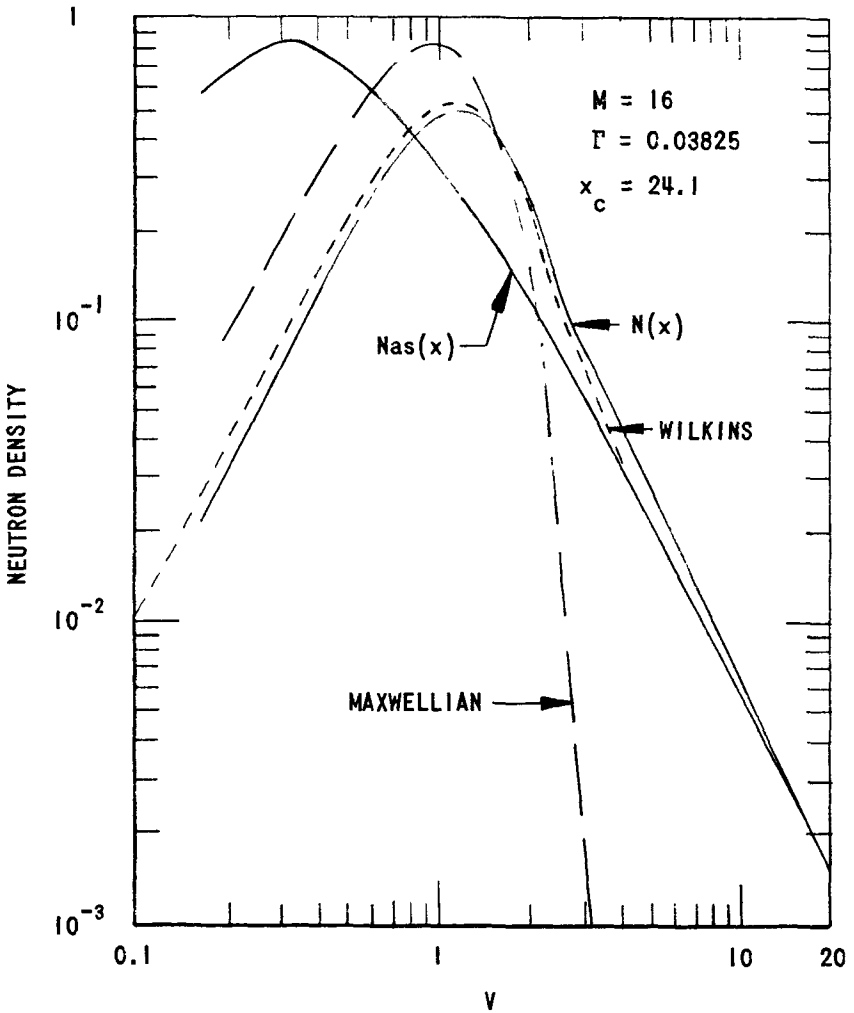
M = 16
Γ = 0.03825
x_c = 24.1
Nas(x)
N(x)
WILKINS
MAXWELLIAN
NEUTRON DENSITY
1
10^{-1}
10^{-2}
10^{-3}
0.1
1
10
20
V

FIG. 7

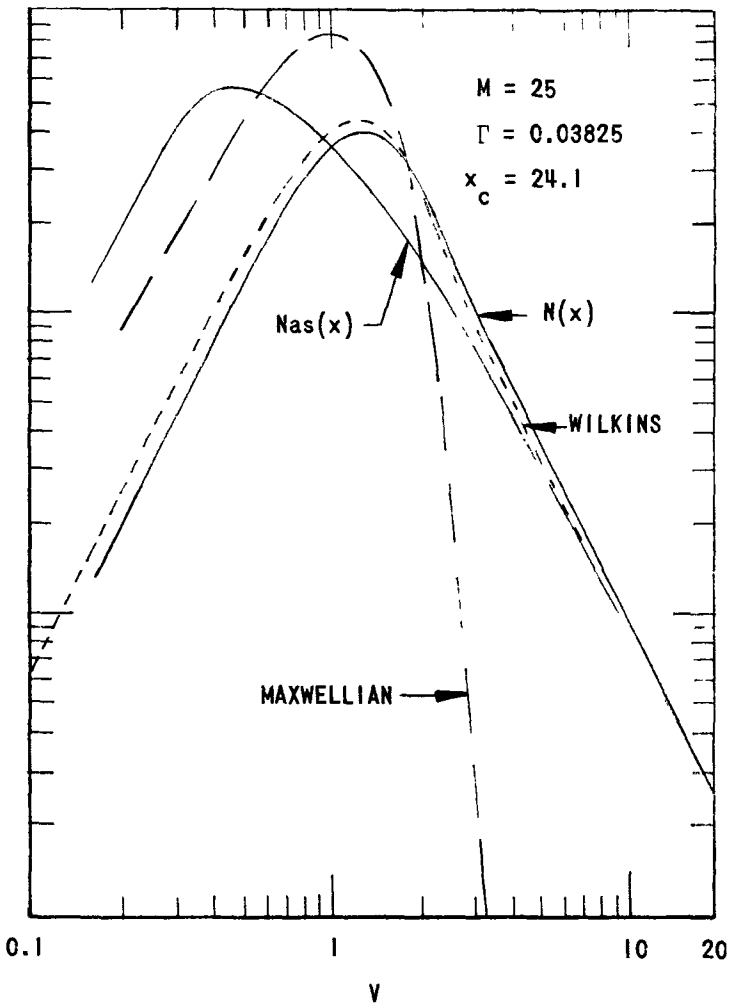
M = 25
Γ = 0.03825
x_c = 24.1
Nas(x)
N(x)
WILKINS
MAXWELLIAN
0.1
1
10
20
V

FIG. 8

Use of the SPM Equation for Neutron Thermalization Calculations

Carl N. Klahr
Fundamental Methods Associates
31 Union Square West
New York 3, N. Y.

The purpose of this paper is to point out the applicability of a rather general method for calculating neutron distributions in space, energy and time to neutron thermalization problems, in particular to multi-region or multi-temperature geometries. The method is the SPM equation,[1,2,3] which has been used for neutron attenuation calculations in shields, and for the spatial and time dependence of the slowing down distribution.

The SPM equation is a second order partial differential equation in neutron space and energy variables which is elliptic in character. In addition to boundary conditions in space it is necessary to impose a source condition at the higher energy limit of the desired energy range, and another boundary condition at the low energy end. For neutron thermalization calculations the low energy boundary condition would be imposed at energies low enough to be without physical interest. The feasibility of numerical solutions of this type of equation has been demonstrated[2] and digital computer codes have been written for it.

The time independent form of this equation can be written as follows, in slab geometry with spatial coordinate x and

neutron energy E :

$$\sigma(x,E)\,\phi(x,E) = \sum_{m=0}^{\infty}\sum_{n=0}^{\infty} \frac{(-1)^{m+n}}{m!\,\sigma^{n}(E)} \frac{\partial^{m+n}}{\partial E^{m}\,\partial x^{n}} C_{mn}(x,E)\,\sigma_s(x,E)\,\phi(x,E)$$

where σ is the total cross section, σ_s the scattering cross section, ϕ is the flux per unit energy and C_{mn} is a spatial and energy moment of the neutron collision probability which can be calculated from the energy transfer cross section. This equation can be shown to be equivalent to the Boltzmann equation.[2] It has been used only in truncated form with derivatives higher than the second arbitrarily dropped. One can advance arguments that the solution to the second order equation represents an asymptotic approximation to the general equation.

Brockhouse has reported[4] that the neutron scattering properties of a liquid depend on the change of neutron momentum in scattering and on the change in neutron energy ϵ . This is equivalent to writing a neutron cross section $\sigma_s(E, V, \epsilon)$ where E is the initial neutron energy and V is the cosine of the angle of deflection in the lab system. We introduce two other kinematic variables, μ , the initial cosine of the neutron velocity with the x axis and w, the change in azimuthal angle of the neutron velocity vector in the collision.

One can now express $C_{mn}(x, E)$ as follows:

$$C_{mn}(x,E) = \int_{-1}^{1} M(\mu|x,E)\,d\mu \int_{-E}^{\infty} d\epsilon \int_{-1}^{1} dV \frac{\sigma_s(E,V,\epsilon)}{\sigma_s(E)} \epsilon^{m} \int_{0}^{2\pi} \left[\mu V + \sqrt{1-\mu^2}\sqrt{1-V^2}\cos w\right]^{n} dw$$

$M(\mu|x,E)$ is the angular distribution of the flux at x, E, which must be regarded as known. Negative values of ϵ correspond to downscattering, positive values to upscattering. $\sigma_s(E)$ can be obtained by integrating $\sigma_s(E, V, \epsilon)$ over V and ϵ .

The coefficients $C_{mn}(x, E)$ can be obtained numerically from measured values of $\sigma_s(E, V, \epsilon)$ and the SPM equation can then be solved as an elliptic equation on a digital computer. In general $\sigma_s(E, V, \epsilon)$ will depend on the moderator material and temperature, so it should be considered x dependent. C_{mn} will therefore vary from region to region. It will also vary with energy. At high energies it will use stationary free atom cross sections. At epithermal energies (gaseous moderator model) the C_{mn} coefficients should have Wigner-Wilkins character. At thermal energies experimental values of $\sigma_s(E, V, \epsilon)$ would be used. The same general equation describes each energy range and a continuous transition from range to range would be obtained, with no arbitrary joining of solutions required. No more than five C_{mn} coefficients will be required and fewer may be sufficient.

A number of investigators have obtained analytic solutions for a somewhat similar second order partial differential equation in both space and energy variables in the special case of a heavy gas moderator. Such an equation was first derived by Hurwitz[5] et al for a heavy gas moderator. Kottwitz[6] and Michael[7] have each obtained analytic solutions using this model for different

geometries. The SPM equation is somewhat more complete in that it contains correlation terms (mixed energy-space derivatives) between the transport and thermalization processes. It can also be applied directly to measured energy transfer cross sections in liquids or solids, and is not restricted to the heavy gas moderator. The same differential equation would apply to the thermal, epithermal, and high energy ranges with different cross section values in each range. Numerical methods are available[2] for solving the SPM equation to obtain the spatial variation of neutron spectra in a medium of varying composition or temperature, using experimental cross section input data.

References

1. Klahr, C. Trans. Am. Nuc. Soc. vol 4 no. 1 June 1961 Paper 17-3

2. Klahr, C., and Zell, H.J. "The SPM Equation for Calculating Spatial Variation of Neutron Spectra", WADD Technical Report 60-312

3. Klahr, C. "Calculation of Neutron Distributions by the Methods of Stochastic Processes" Nuc. Sci. and Eng. 3 (1958) pp. 269-285

4. Brockhouse "Gatlinburg Conference on Neutron Thermalization Proceedings", April 1958 ORNL 2739

5. Hurwitz, H., Nelkin, M., Habetler, G. "Neutron Thermalization I Heavy Gaseous Moderators", Nuc. Sci. and Eng 1 (1956) pp 280-312

6. Kottwitz, D. "Thermal Neutron Spectrum in a Medium with a Temperature Discontinuity", Nuc. Sci. and Eng. 7 (1960) pp 345-354

7. Michael, P., "Thermal Neutron Flux Distributions in Space and Energy", Nuc. Sci. and Eng., 8 (1960) pp 426-431

UP SCATTERING THERMALIZATION OF NEUTRONS

M. D. KOSTIN

Division of Engineering and Applied Physics
Harvard University, Cambridge 38, Massachusetts

ABSTRACT

The Wigner-Wilkins integral equation describing the interaction of neutrons with a thermalizing medium whose atoms are in motion with a Maxwellian velocity distribution is used to investigate the neutron spectrum generated by a neutron source in the thermal or sub-thermal region. For very high energy neutrons ($E \gg kT$) this equation is reduced to a simplier one, the up scattering equation, which resembles the well known $T = 0$ slowing down equation. The transformation from the slowing down equation to the up scattering equation by means of the principle of detailed balance is shown. The very high energy up scattering equation is used to obtain the leading term in the series solution for the neutron density in the high energy region when the source is in the thermal region. A new form of the Wigner-Wilkins integral equation is presented from which some addition terms in the series are easily obtained. The extension of this work to include binding effects by performing a double expansion in delta function derivatives using Wick's expansion is briefly discussed. A method for obtaining approximate slowing down thermalization solutions applicable to the high energy region and most of the thermal region for the weak absorption case is also outlined.

I. INTRODUCTION

Since the time that Wigner and Wilkins[1] formulated the neutron thermalization problem many advances have been made in understanding and describing the neutron distribution produced by a very high energy source and influenced by absorption and the thermal activity of the moderator. Some aspects of the related problems that arise when the neutron source is confined to the thermal or sub-thermal region are examined here.

In Sections II and III we return to the original Wigner-Wilkins integral equation. By considering its behavior in the very high energy region when the neutron source is in the thermal region we obtain an equation similar to the one governing the neutron distribution in a stationary moderator fed by a very high energy neutron source. Neutrons up scattered into the very high energy region experience absorption effects described by this equation. In Sec. IV we investigate the relation between the up scattering and slowing down equations to the principle of detailed balance. Using a modified form of the Wigner-Wilkins integral equation, we obtain in Sec. V a series solution to the up scattering problem which, in Sec. VI, we relate to Wick's expansion of the energy change cross section. In the last section we consider briefly the differential equation forms of the thermalization problem, their up scattering and slowing down facets, and related approximate solutions.

II. TRANSPORT EQUATION

We begin by considering the space and time independent linearized Boltzmann transport equation

$$(v\,\Sigma_s(v) + v\,\Sigma_a(v))\bar{N}(v) = \int_o^\infty dv'\bar{N}(v')v'\Sigma_s(v'\to v) + \bar{S}(v) \quad (2.1)$$

where $\bar{N}(v)dv$ is the number of neutrons per cm^3 with velocity between v and v + dv, $\bar{S}(v)dv$ is the number of neutrons per cm^3 emitted with velocity between v and v + dv by neutron sources, $dv\ v'\Sigma_s(v'\to v)$ is the scattering rate per neutron from velocity v' into a velocity interval dv at v ,

$$v\,\Sigma_s(v) = v\int_o^\infty \Sigma_s(v\to v')dv' \quad (2.2)$$

and $v\Sigma_a(v)$ are the scattering and absorption rates per neutron at v. For a medium whose scattering nuclei are stationary the scattering rate becomes $v\,\Sigma_t(v)$, where $\Sigma_t(v)$ is the macroscopic cross section for the scattering of neutrons by nuclei at rest in the laboratory coordinate system. We will make the usual assumption that Σ_t is independent of the velocity of the neutron.

It is convenient to introduce the normalized neutron velocity variable $x = v/v_p$, where $v_p = (2T/m)^{\frac{1}{2}}$ is the most probable neutron velocity (strictly speaking, speed) in the Maxwellian neutron distribution

$$\bar{M}(v) = (m/2T)^{3/2}v^2\ \exp(-mv^2/2T) \quad (2.3)$$

where Boltzmann's constant is incorporated into the temperature T. The dependent variable $\bar{N}(v)$, is now replaced by N(x), the

number of neutrons per cm^3, per normalized velocity interval, which is related to $\bar{N}(v)$ by the equation

$$N(x)dx = \bar{N}(v)dv \tag{2.4}$$

A similar relation, $S(x)dx = \bar{S}(v)dv$, holds for the source term.

For a medium whose scattering nuclei are in motion with a Maxwellian velocity distribution (Maxwellian moderator) the transport equation (2.1) becomes the well known Wigner-Wilkins integral equation

$$(V + \Gamma)N(x) = \int_0^\infty P(x,y)N(y)dy + S(x)/v_p\Sigma_f \tag{2.5}$$

where $$\Gamma = v\Sigma_a/v_p\Sigma_f = x\Sigma_a/\Sigma_f \tag{2.6}$$

is the ratio of the absorption rate per neutron traveling at velocity v to the scattering rate per neutron traveling at velocity v_p in a stationary moderator,

$$V = v\Sigma_s(v)/v_p\Sigma_f = (x + 1/2Ax)\ \mathrm{erf}(x\sqrt{A}) + (1/\sqrt{\pi A})\ \exp(-x^2A) \tag{2.7}$$

is the ratio of the scattering rate per neutron traveling at velocity v in a Maxwellian moderator to the scattering rate per neutron traveling at velocity v_p in a stationary moderator, and

$$v'\Sigma_s(v'\to v)dv/v_p\Sigma_f = dxP(x,y)$$
$$dx2\theta^2(x/y)\Big\{(\mathrm{erf}(\theta y-\sqrt{x}) \pm \mathrm{erf}(\theta y+\sqrt{x}))\ \exp(y^2-x^2)$$
$$+\mathrm{erf}(\theta x-\sqrt{y}) \mp \mathrm{erf}(\theta x+\sqrt{y})\Big\} \tag{2.8}$$

The upper sign in (2.8) refers to $y < x$ and the lower sign to $y > x$, where $y = v'/v_p$. In (2.7) and (2.8) we have

used the symbols $A = 1/\mu = M/m$, the scattering nucleus mass M divided by the neutron mass m,

$$\theta = (A+1)/2\sqrt{A} \qquad J = (A-1)/2\sqrt{A} \qquad (2.9)$$

and the error function

$$\mathrm{erf}(z) = \frac{2}{\sqrt{\pi}}\int_0^z \exp(-u^2)du \qquad (2.10)$$

Now, by considering the behavior of (2.5) when $x \ggg 1$, we will bring out explicitly some of its essential features.

III. VERY HIGH ENERGY REGION

Several striking parallels can be established between the slowing down and up scattering thermalization problems in the very high energy(VHE) limit. In this region the Wigner-Wilkins integral equation approaches the form

$$\left[1 + \frac{\Sigma_a(x)}{\Sigma_f}\right] N(x) = \frac{2}{1-\lambda^2}\left[\int_x^{x/\lambda} \frac{N(y)}{y}\, dy + e^{-x^2}\int_{\lambda x}^{x} e^{+y^2} \frac{N(y)}{y}\, dy\right] \tag{3.1}$$

plus other terms which we will later consider in more detail. The symbol

$$\lambda = \frac{1-\mu}{1+\mu} = \frac{A-1}{A+1} = \frac{\mathcal{J}}{\theta} \tag{3.2}$$

and is also equal to the minimum value of the neutron velocity after a collision with a scattering nucleus at rest divided by the neutron velocity before the collision. If the neutron source is at infinity, $N(x)$ behaves like some inverse power of x, the second term on the right hand side of (3.1) is small as compared to the first one, and we have the well known stationary moderator equation

$$\left[1 + \frac{\Sigma_a(x)}{\Sigma_f}\right] N(x) = \frac{2}{1-\lambda^2} \int_x^{x/\lambda} \frac{N(y)}{y}\, dy \tag{3.3}$$

If the neutron source is in the thermal region, $N(x)$ in the VHE region exhibits Maxwellian like behavior, the second term on the right hand side of (3.1) dominates the first one, and we obtain the VHE up scattering equation

$$\left[1 + \frac{\Sigma_a(x)}{\Sigma_f}\right] \times \omega(x) = \frac{2}{1-\lambda^2} \int_{\lambda x}^{x} \omega(y)\, dy \tag{3.4}$$

where $$N(x) = x^2 e^{-x^2} \frac{\omega(x)}{x} \tag{3.5}$$

The terms on the left of (3.4) are related to the removal of neutrons by scattering and absorption, and the integral on the right expresses the up scattering of neutrons from lower energies. Because the neutron density decreases in an exponential fashion, down scattering contributions are of secondary importance and do not enter into (3.4).

Both (3.3) and (3.4), due to their relatively simple form and close correspondence with the more complicated thermalization equations, are especially useful for guiding our work on thermalization effects. The behavior of N(x) in the slowing down and up scattering problems in the VHE region can easily be obtained from these equations. For the case of a 1/v absorption cross section, $\Gamma = x\Sigma_a(x)/\Sigma_s$ is constant, and the well known leading terms in the asymptotic series solution of (3.3) are

$$N(x) = \frac{1}{x^2} - \left[\frac{\Gamma}{\mu}\,\frac{3}{1+2\lambda}\right]\frac{1}{x^3} + \cdots \qquad (3.6)$$

The coefficient of the $1/x^3$ term, negative in sign, indicates the depletive effects of absorption which the neutrons experience as they slow down.

The VHE up scatt ring equation (3.4) which resembles (3.3) has a similar solution for 1/v absorption.

$$N(x) = x^2 e^{-x^2}\left[1 + \frac{\Gamma}{\mu}\,\frac{1}{x} + \cdots\right] \qquad (3.7)$$

The coefficient of the 1/x term, now positive, reflects the consumptive effects of absorption. At very high neutron velocities when $x \gg \Gamma/\mu$, the influence of 1/v absorption

becomes unimportant and the Maxwellian distribution is restored.

For the case of a constant absorption cross section, the slowing down equation admits the solution [2]

$$N(x) = \frac{1}{x^p} \tag{3.8}$$

where p is given implicitly by

$$p = \frac{2}{1+\Sigma_a/\Sigma_s} \frac{1-\lambda^p}{1-\lambda^2} \tag{3.9}$$

If $\Sigma_a = 0$, then $p=2$ satisfies (3.9), and we recover the $N(x) = 1/x^2$ solution. When we turn on the absorption, p decreases, $p < 2$, and once again we see how absorption attenuates the neutron density. The corresponding solution to the up scattering equation (3.4) in the presence of a constant absorption cross section is

$$N(x) = x^p e^{-x^2} \tag{3.10}$$

where p is also given by (3.9).

IV. PRINCIPLE OF DETAILED BALANCE

The slowing down and up scattering facets of the thermalization problem are closely related through the priniciple of detailed balance

$$\bar{M}(v)\, v\, \Sigma_s(v \to v') = \bar{M}(v')\, v'\, \Sigma_s(v' \to v) \qquad (4.1)$$

Letting $\bar{N}(v) = \bar{M}(v)\, \psi(v)$ where $\psi(v)$ represents the multiplicative correction to the Maxwellian neutron distribution $\bar{M}(v)$, omitting the source term for convenience, and using the principle of detailed balance (4.1), we obtain

$$\left[v\Sigma_s(v) + v\Sigma_a(v) \right] \psi(v) = v \int_0^\infty \Sigma_s(v \to v')\, \psi(v')\, dv' \qquad (4.2)$$

from the transport equation (2.1). The main difference between expression (2.1) for $\bar{N}(v)$ and expression (4.2) for $\psi(v)$ is the interchange of v and v' in the scattering rate kernal. While (2.1) is the fundamental equation for describing the slowing down distribution, (4.2) is the corresponding fundamental equation in the upscattering problem.

A quick and simple derivation of (3.4) comes from the above application of the principle of detailed balance. It is well known that in the VHE limit, $\Sigma_s(v' \to v)$ approaches the step kernal

$$\Sigma_s(v' \to v) = \frac{2}{1-\lambda^2}\, \Sigma_t\, \frac{v}{v'} \left[H(v'-v) - H(v' - v/\lambda) \right] \qquad (4.3)$$

which gives us the familiar VHE slowing down equation

$$\left[v\Sigma_t + v\Sigma_a(v) \right] \bar{N}(v) = \frac{2}{1-\lambda^2}\, \Sigma_t \int_v^{v/\lambda} \frac{v}{v'}\, \bar{N}(v')\, dv' \qquad (4.4)$$

where $H(z) = 1$ for $z > 0$, and $H(z) = 0$ for $z < 0$.

Interchanging v and v' in (4.3), and substituting the result into (4.2), we immediately get the corresponding VHE up scattering equation

$$\left[v\Sigma_t + v\Sigma_a(v) \right] \psi(v) = \frac{2}{1-\lambda^2} \Sigma_t \int_{\lambda v}^{v} \frac{v'}{v} \psi(v')\, dv' \qquad (4.5)$$

V. SERIES SOLUTION

In Section III we investigated the upscattering form of the transport equation in the VHE region and extracted the leading term in the series for $N(x)$. Guided by these results, we are now ready to push ahead and find additional terms.

We start with the Wigner-Wilkins integral equation (2.5), invoke the principle of detailed balancing (4.1), and obtain

$$\left[V + \Gamma\right]\omega(x) = \theta^2\left[P_1 + P_2\right] \tag{5.1}$$

where

$$P_2 = \int_0^\infty e^{x^2-y^2}\,\mathrm{erf}(\theta x - \beta y)\,\omega(y)\,dy - \int_0^x e^{x^2-y^2}\,\mathrm{erf}(\theta x + \beta y)\,\omega(y)\,dy + \int_x^\infty e^{x^2-y^2}\,\mathrm{erf}(\theta x + \beta y)\,\omega(y)\,dy \tag{5.2}$$

$$P_1 = \int_0^\infty \mathrm{erf}(\theta y - \beta x)\,\omega(y)\,dy + \int_0^x \mathrm{erf}(\theta y + \beta x)\,\omega(y)\,dy - \int_x^\infty \mathrm{erf}(\theta y + \beta x)\,\omega(y)\,dy \tag{5.3}$$

$$N(x) = M(x)\,\frac{\omega(x)}{x} = x^2 e^{-x^2}\,\frac{\omega(x)}{x}$$

This equation will be transformed into a form which resembles the VHE up scattering equation

$$\left[\chi + \Gamma\right]\omega(x) = 2\theta^2\left[\rho(x) - \rho(\lambda x)\right] \tag{5.4}$$

where $\rho(x) = \int \omega(x)\,dx$ (5.5)

is the indefinite integral of $\omega(x)$. We differentiate (5.1) by

$$-\frac{1}{2x}\,e^{x^2}\frac{d}{dx}e^{-x^2} = 1 - \frac{1}{2x}\,\frac{d}{dx}$$

and get

$$\left[1 - \frac{1}{2x}\,\frac{d}{dx}\right]\left[V+\Gamma\right]\omega(x) = 2\theta^2\left[P_1 + \frac{\lambda-1}{2x}\left[\mathcal{U}(\omega) - \mathcal{A}(\omega) + \mathcal{B}(\omega)\right]\right] \tag{5.6}$$

where $$\mathcal{U}(\omega) = \frac{\theta}{\sqrt{\pi}} \int_0^{\infty} e^{-(\theta y - \beta x)^2} \omega(y)\, dy \tag{5.7}$$

$$\mathcal{A}(\omega) = \frac{\theta}{\sqrt{\pi}} \int_0^{x} e^{-(\theta y + \beta x)^2} \omega(y)\, dy \tag{5.8}$$

$$\mathcal{B}(\omega) = \frac{\theta}{\sqrt{\pi}} \int_x^{\infty} e^{-(\theta y + \beta x)^2} \omega(y)\, dy \tag{5.9}$$

thus eliminating $\mathcal{P}_2$, and integrate $\mathcal{P}_1$ by parts

$$\mathcal{P}_1 = 2\left[\rho(x)\ \mathrm{erf}(x\sqrt{A}) - \mathcal{U}(\rho) - \mathcal{A}(\rho) + \mathcal{B}(\rho)\right] \tag{5.10}$$

Equation (5.6), together with (5.10), is a restatement of the Wigner-Wilkins integral equation from which the high energy behavior of the neutron density in the presence of absorption is easily determined. For $\beta x >> 1$, the contributions from $\mathcal{A}$ and $\mathcal{B}$ are very small as compared to the other members of (5.6) and (5.10) and will be neglected, $\mathrm{erf}(x\sqrt{A}) = 1$ plus negligible terms, and we have

$$\left[1 - \frac{1}{2x}\frac{d}{dx}\right]\left[V + \Gamma\right]\omega(x) = 2\theta^2\left[\rho(x) - \mathcal{U}(\rho) + \frac{\lambda - 1}{2x}\,\mathcal{U}(\omega)\right] \tag{5.11}$$

where here V reduces to

$$V = x + 1/2Ax \tag{5.12}$$

Since the kernal $\exp\left[-(\theta y - \beta x)^2\right]$ in $\mathcal{U}$ becomes very narrow about $y = \beta x/\theta = \lambda x$ for the condition $\beta x >> 1$, $\mathcal{U}$ has the expansion

$$\mathcal{U}(\rho) = \rho(\lambda x) + \frac{1}{4\theta^2}\rho''(\lambda x) + \frac{1}{32\theta^4}\rho''''(\lambda x) + \cdots \tag{5.13}$$

In the VHE region where $x >>> 1$, (5.11) simplifies to (5.4), as expected.

The principal terms in the series solution for N(x) in the high energy region for the upscattering thermalization problem with 1/v absorption are found by substituting

$$N(x) = x^2 e^{-x^2} \frac{\omega(x)}{x} = x^2 e^{-x^2} \left[a_0 + \frac{a_1}{x} + \frac{a_2}{x^2} + \cdots \right] \qquad (5.14)$$

in (5.11), using (5.13), and equating corresponding coefficients of powers of x. We get

$$\begin{aligned} a_0 &= 1 \qquad \text{(arbitrary normalization)} \\ a_1 &= \frac{\Gamma}{\mu} \\ a_2 &= \frac{\Gamma}{\frac{2}{1-\lambda}\ln\frac{1}{\lambda} - 1}\, a_1 \\ a_3 &= \frac{\Gamma}{\mu}\,\frac{\lambda}{2(2+\lambda)}\left[1 + 2a_2\right] \end{aligned} \qquad (5.15)$$

To check these results, we go to the heavy gas model limit[3,4] $\mu \to 0$, $\Gamma/\mu \longrightarrow \Delta/2$. Here, (5.15) becomes

$$\begin{aligned} a_0 &= 1 \\ a_1 &= \Delta/2 \\ a_2 &= \Delta^2/8 \\ a_3 &= \Delta^3/48 \quad + \quad \Delta/12 \end{aligned} \qquad (5.16)$$

which agrees with the results obtained directly from Wilkins' heavy gas equation

$$x N''(x) + (2x^2 - 1) N'(x) + (4x - \Delta) N(x) = 0 \qquad (5.17)$$

by de Sobrino and Clark[5].

VI. WICK'S EXPANSION

In our treatment of neutrons interacting with a Maxwellian moderator, we transformed (5.1) into an expression where the scattering term depended on the behavior of ρ at normalized velocity x and at λx, one collision interval below x. A similar expression which also includes chemical binding effects can be obtained from the energy change cross section

$$\Sigma_s(E\to E_o) = \frac{(1+\mu)^2\Sigma_f}{4\pi\hbar}(E_o/E)^{\frac{1}{2}}\int_{-\infty}^{+\infty}dt\int_0^{\pi}\exp(it(E_o-E)/\hbar) \cdot\chi(\kappa^2,t)\sin\theta\, d\theta \qquad (6.1)$$

with Wick's expansion[6]

$$\chi(\kappa^2,t) = \exp(it\hbar R)\sum_{n=0}^{\infty}(it)^n s_n(\kappa^2)/n! \qquad (6.2)$$

Here $\hbar^2\kappa^2 = 2m(E_o + E - 2(EE_o)^{\frac{1}{2}}\cos\theta)$ is the square of the momentum transferred in the collision, θ is the angle between the initial and final neutron momenta and $R = \kappa^2/2M = \mu(E_o + E - 2(EE_o)^{\frac{1}{2}}\cos\theta)/\hbar^2$ is the free atom recoil. The leading moments s_n in Nelkin's notation are[7]

$$\begin{aligned} &s_0 = 1, \qquad s_1 = 0, \qquad s_2 = R\,4\langle K\rangle/3 \\ &s_3 = R\,\langle\nabla^2 V\rangle\hbar/3M \\ &s_4 = R^2\,16\langle K^2\rangle/5 + R\,2\langle(\vec{\nabla}V)^2\rangle/3M \end{aligned} \qquad (6.3)$$

where K and V are the kinetic and potential energies of the scattering atom, and the average $\langle\cdots\rangle$ is over the initial states and orientations of the scattering system.

By performing the integration over θ, and using the integral representation of the derivatives of the delta function,

$$\delta^n(x) = d^n\delta(x)/dx^n = (1/2\pi)\int_{-\infty}^{+\infty} dt(it)^n \exp(ixt) \tag{6.4}$$

we obtain the desired form of the velocity change cross section

$$\Sigma_s(x \to y) = 2yT\,\Sigma_s(E \to E_o) \tag{6.5}$$

$$= \frac{\Sigma_t}{1-\lambda^2}\frac{2y}{x^2}\sum_{n=0}^{\infty}\sum_{l=0}^{[n/2]}\sum_{m=0}^{l} r_l^n \frac{l!}{n!}(-)^{l-m}\frac{\mu^m}{m!}$$

$$\cdot\left\{(y+x)^{2m}\delta^{n+m-l-1}[(y-\lambda x)(1+\mu)(y+x)] - (y-x)^{2m}\delta^{n+m-l-1}[(y-x)(1+\mu)(y+\lambda x)]\right\}$$

where the factor $2yT = dE_o/dy$ is a result of the change of the independent variable from energy to normalized velocity; $x^2 = E/T$ and $y^2 = E_o/T$. The symbol $[n/2]$ is equal to the largest integer $\leq n/2$, e.g., $[5/2] = 2$. The dimensionless coefficients

$$r_o^0 = 1, \qquad r_o^1 = 0 \qquad r_1^2 = 4\langle K\rangle/3T$$

$$r_1^3 = \langle \nabla^2 V\rangle \hbar/3MT^2 \qquad r_2^4 = 16\langle K^2\rangle/5T^2 \tag{6.6}$$

originate from the moments given by (6.3), and are closely related to Corngold's γ_l^n.[8]

The arguements of the first series of derivatives of delta functions in (6.5) are zero at $y = \lambda x$ and those of the second are zero at $y = x$. When we use (6.5) with the up scattering transport equation

$$(\Sigma_s(x) + \Sigma_a(x))\psi(x) = \int_0^\infty \Sigma_s(x \to y)\, \psi(y)\, dy \qquad (6.7)$$

$$N(x) = x^2 \exp(-x^2)\, \psi(x)$$

we see that these terms give rise to a series of derivatives of ψ evaluated at x and λx. Thus, we have made contact with (5.11) and (5.13).

We now obtain the leading terms in the series solution for N(x) with 1/v absorption and the velocity change cross section (6.5). On substituting (5.14) into (6.7) and again equating corresponding coefficients of powers of x, we find that the first three coefficients, a_0, a_1, a_2, are identical to those given for a Maxwellian moderator in (5.15); the fourth one depends explicitly on the mean kinetic energy of the scatterer

$$a_3 = (\Gamma/\mu)(\lambda/(2\lambda+4))((2\langle K\rangle/3T) + 2a_2) \qquad (6.8)$$

For a Maxwellian moderator, $\langle K\rangle = 3T/2$ and we recover the coefficient a_3 given in (5.15).

In a subsequent paper we will treat binding phenomena in more detail and extend the treatment to cover space and time dependent problems.

VII. UP SCATTERING AND SLOWING DOWN SOLUTIONS

In Section IV we established a connection between the slowing down and up scattering thermalization cases through the principle of detailed balance. Another connection can be obtained in the limiting situation of $\mu \to 1$, for which Wigner and Wilkins have shown that the integral equation (2.5) can be transformed into the differential form

$$(d/dx)(1/P)(d/dx)(V(x,1) + \Gamma)\,\psi(x) + (4/\sqrt{\pi} - W(V(x,1) + \Gamma))\,\psi(x) = 0 \qquad (7.1)$$

where $N(x) = \psi(x)(M(x))^{\frac{1}{2}} = \psi(x)x\exp(-x^2/2)$ (7.2)

$$P = \exp(-x^2) + x\sqrt{\pi}\,\mathrm{erf}(x) \qquad (7.3)$$

$$W = x^2/P - P^{-2}\exp(-x^2) \qquad (7.4)$$

and $V(x,\mu) = (x + \mu/2x)\,\mathrm{erf}(x/\sqrt{\mu}) + (\mu/\pi)^{\frac{1}{2}}\exp(-x^2/\mu)$ (7.5)

is the dimensionless ratio of scattering rates mentioned in Section II. This second order linear ordinary differential equation posesses two linearly independent solutions. In the absence of absorption (i.e., $\Gamma = 0$) and neutron sources, one solution is the Maxwellian

$$N_1(x) = M(x) = x^2\exp(-x^2)$$
$$\psi_1(x) = x\exp(-x^2/2) \qquad (7.6)$$

This can be easily verified by substituting it into (7.1).

We construct the other solution by rewriting (7.1) in the standard form

$$\psi''(x) + p(x)\,\psi'(x) + q(x)\,\psi(x) = 0 \tag{7.7}$$

where $p(x) = 2V'/V - P'/P$ (7.8)

$$q(x) = V''/V - V'P'/VP + 4P/\pi V - WP \tag{7.9}$$

and employing the relation

$$\psi_2(x) = \psi_1(x)\int^x \psi_1(y)^{-2} \exp(-\int p\,dy)\,dy \tag{7.10}$$

Simple integration gives us

$$\exp(-\int p\,dy) = P(y)/V(y,1)^2 \tag{7.11}$$

so that the second solution independent of N_1 is

$$\begin{aligned} N_2(x) &= \psi_2(x)\, x \exp(-x^2/2) \\ &= x^2 \exp(-x^2) \int^x (P(y)/V(y,1)^2 y^2) \exp(y^2)\,dy \end{aligned} \tag{7.12}$$

By noting that

$$P/(Vx)^2 = -\tfrac{1}{2}\pi\,(d/dx)(1/Vx) \tag{7.13}$$

we can write $N_2(x)$ in the alternative form

$$\begin{aligned} N_2(x) = \text{constant}(&2x^2 \exp(-x^2) \int^x \exp(y^2)\,dy/V(y,1) \\ &- x/V(x,1)) \end{aligned} \tag{7.14}$$

For $x \gg 1$, we integrate (7.12) or (7.14) by parts and obtain an asymptotic series in powers of $1/x^2$.

$$N_2(x) = (\text{constant}/x^2)(1 + 1/x^2 + 15/4x^4 + 29/2x^6 + \cdots) \tag{7.15}$$

This is the well known asymptotic series for the neutron density produced by neutrons slowing down from the very high energy region in a unit mass moderator with neglegible absorption in the high energy region.

The neutron density (7.14) was derived under the condition that $\mu = 1$. However, let us replace V(y,1), the scattering rate ratio for $\mu = 1$, in (7.14) by $V(y,\mu)$ given in (7.5).

$$N_2(x) = \text{constant}(2x^2 \exp(-x^2) \int^x \exp(y^2)\, dy/V(y,\mu) - x/V(x,\mu)) \qquad (7.16)$$

For $x \gg 1$ we integrate (7.16) by parts and obtain the asymptotic series.

$$N_2(x) = (\text{constant}/x^2)(1 + b_2/x^2 + b_4/x^4 + b_6/x^6 + \cdots) \qquad (7.17)$$

where the coefficients

$$\begin{aligned} b_2 &= 2 - \mu \\ b_4 &= 3b_2 + 3\mu^2/4 \\ b_6 &= 4b_4 - \mu^3/2 \end{aligned} \qquad (7.18)$$

compare favorably with the exact results given by Corngold.[8]

Asymptotic Series Coefficients

		b_2	b_4	b_6
Deuterium	$\mu = 1/2$			
Approximate		1.50000	4.69	18.7
Exact		1.50000	4.71	18.8
Beryllium	$\mu = 1/9$			
Approximate		1.88889	5.675	22.70
Exact		1.88889	5.680	22.72
Carbon	$\mu = 1/12$			
Approximate		1.91667	5.755	23.02
Exact		1.91667	5.759	23.04

In the heavy moderator limit ($\mu \to 0$), $V(x,0) = x$ and (7.16) reduces to a form which is equivalent to the exact second solution for the heavy moderator

$$N_2(x) = \text{constant } (x^2 \exp(-x^2)\ \mathrm{Ei}(x^2) - 1) \tag{7.19}$$

given by Cohen.[9] Here, $\mathrm{Ei}(x^2)$ is the exponential integral

$$\mathrm{Ei}(x^2) = \int_{-\infty}^{x^2} \exp(z)\ dz/z \tag{7.20}$$

An appoximate solution for the neutron density generated by a very high energy neutron source and removed by weak absorption can be obtained from a superposition of the two zero absorption solutions discussed previously. For example, we assume that an approximate solution to the heavy gaseous moderator slowing down thermalization problem with 1/v absorption can be expressed in the form

$$N(x) = c_1\ x^2 \exp(-x^2) + c_2\ (x^2 \exp(-x^2)\ \mathrm{Ei}(x^2) - 1) \tag{7.21}$$

The coefficient c_2 is determined by the source condition which states that $N(x) \to 2S/\xi\ v_p \Sigma_f x^2$ for $x \ggg 1$, where S is the number of neutrons per cm^3 per sec. emitted at very high energy. In this limit, (7.21) has the asymptotic expansion

$$N(x) \simeq c_2/x^2 \tag{7.22}$$

so that $c_2 = 2S/\xi\ v_p \Sigma_f$ (7.23)

The remaining coefficient c_1 is found from the neutron conservation condition

$$\int_0^\infty v\Sigma_a N(x)\ dx = S \tag{7.24}$$

which for a 1/v absorption cross section becomes

$$\int_0^\infty N(x)\,dx = (4/\Delta)\; S/\xi\; v_p\, \Sigma_f \qquad (7.25)$$

where $\Delta 4 = \Sigma_a(v_p)/\xi\Sigma_f$ is the familiar absorption parameter. On substituting (7.21) into (7.25), we find that

$$c_1 = (16/\Delta\sqrt{\pi})\; S/\xi\; v_p\, \Sigma_f \qquad (7.26)$$

The methods used to derive this simple approximate solution valid for $\Delta << 1$ can be extended to treat more complicated thermalization problems.

ACKNOWLEDGMENT

I wish to thank Professor Harvey Brooks for valuable discussions and suggestions.

REFERENCES

1. E. P. Wigner and J. E. Wilkins, Jr., AECD-2275, (1944).
2. A. M. Weinberg and E. P. Wigner, "The Physical Theory of Neutron Chain Reactors," Univ. of Chicago Press, Chicago, 1958.
3. J. E. Wilkins, Jr., CP-2481, (1944).
4. H. Hurwitz, Jr., M. S. Nelkin, and G. J. Habetler, Nuclear Sci. and Eng. 1, 280 (1956).
5. L. G. de Sobrino and M. Clark, Jr., Nuclear Sci. and Eng. 10, 388 (1961).
6. G. C. Wick, Phys. Rev. 94, 1228 (1954).
7. M. S. Nelkin, GA-1689, (1960).
8. N. Corngold, Annals of Physics 6, 368 (1959).
   N. Corngold, Annals of Physics 11, 338 (1960).
9. E. R. Cohen, Nuclear Sci. and Eng. 2, 227 (1957).

CALCULATION OF THERMAL SPECTRA IN LATTICE CELLS

by

D. C. LESLIE

U.K.A.E.A.,
Atomic Energy Establishment
Winfrith, Dorchester, England

- A B S T R A C T -

The methods normally used in reactor physics calculations either ignore altogether the spatial dependence of the thermal spectrum in a lattice cell or grossly over-simplify it. This approach is not satisfactory for interpreting experiments and it is dubious for design work on reactors containing two moderators at widely differing temperatures such, for example, as the heavy water moderated organic cooled OCDRE.

The most obvious method of studying the spatial variation of thermal spectrum is to use a multi-group transport code with no restrictions on the energy transfer matrix. The Carlson SNG programme is suitable for this work and the first part of the paper describes how it has been used, together with some results which have been obtained. This method is laborious and expensive in machine time and a simple method known as SPECTROX has been developed in parallel with this work. The SPECTROX method is based on a collision probability treatment of the flux in the fuel and it leads to a pair of simultaneous energy-dependent equations which determine the mean flux in the fuel and in the moderator. The second part of the paper describes the theory of this method, the computer programmes that have been written to exploit it and some results that have been obtained with it. It appears to give adequate accuracy for the thermal spectrum in normal systems.

1. Introduction

In addition to its theoretical interest, the spatial distribution of the thermal neutron spectrum in a heterogeneous lattice cell is of considerable practical importance. It influences the buildup of plutonium isotopes and it also affects the power peaking factor in reactors, such as OCDRE (organic-cooled, D_2O moderated), which have two moderators at very different temperatures. This problem tends to be ignored or grossly oversimplified in most practical schemes for reactor physics calculations. This paper represents an attempt to solve the problem using only basic methods and basic cross-sections.

The calculations reported in this paper are all purely thermal, and therefore cover the energy range between 0 and some cutoff energy E_c above which thermalisation effects are negligible. In the WAPD 4-group scheme, E_c is taken as 0.625 e.V. The same value of E_c has been used in much of the work at Winfrith; this makes it possible to combine the thermal calculation with a MUFT computation of fast effects. However, this value does seem rather low if there is much Pu-240 in the system. According to the heavy atom (Wilkins) model of thermalisation, the asymptotic spectrum in a weakly absorbing system is of the form

$$\frac{1}{E}\left[1 + \frac{2kT}{E} + O\left\{\left(\frac{kT}{E}\right)^2, \left(\frac{\Sigma_a}{\Sigma_s}\right)\right\}\right]$$

If kT = 0.07 e.V., which is a typical value for an H_2O reactor, the thermalisation correction at 1 e.V. is about 15%. A calculation which neglects thermalisation effects will therefore underestimate absorption in the 1.05 e.V. resonance of Pu-240 by about the same amount (15%). This matter is discussed further in the following sections.

2. Calculations using Carlson-type programmes

The obvious tool for a frontal attack on this problem is a multigroup transport code: the use of diffusion theory is undesirable, since lattice cells contain thin regions such as air gaps and pressure tubes. Carlson's codes are very suitable for this work, since they can accommodate large numbers of space points and energy groups, and have no restrictions on the group transfer matrix. We in the U.K.A.E.A. began by using the SNG code, and we have so far seen no reason to switch to Carlson's DSN. We normally use the S_4 approximation though we have done a few S_8 calculations to convince ourselves that S_4 is giving adequate accuracy: we find that S_2 is not sufficient.

The principal drawback of the SNG code is that it is one-dimensional (the cylindrical version is naturally used in this work). Thus in order to use it one must cylindricalise the whole lattice cell. The errors involved in cylindricalising the outer boundary will be insignificant, since the bulk moderator

will be several mean free paths across and neutrons arriving at the fuel channel will not "remember" the precise shape of the outer boundary. In a magnox (Calder Hall) type of cell, no further cylindricalisation is required. In lattice cells of CANDU or OCDRE type, the fuel pins and the coolant must be smeared into a paste ring by ring. Hyperfine structure in the pins is allowed for by applying hyperfine weighting factors to the raw number densities, these factors being calculated by the RIPPLE collision-probability routine (1). If the number densities in the various rings of paste are not very different, these rings may be further smeared into a uniform rod. In gas-cooled cells of the AGR (EGCR) variety we find it convenient to use an equivalent uniform rod whose radius, deduced by collision probability considerations, varies with energy. However, more conventional smearing is also quite successful. Monte Carlo tests have convinced us that the errors involved in using either of these methods of cylindricalisation is small.

Also, in its present form, the SNG code does not allow the scattering to be other than isotropic in the laboratory system. The effect of this restriction is not known, but it is unlikely to be large.

The method of using the SNG programme (and its successor, the Winfrith DSN code) is discussed by Macdougall (2) in another paper submitted to this Symposium, and need not be described here. A standard set of 42 groups has been devised for these calculations. This set extends up to 4 e.V., and groups are concentrated near the 0.3 e.V. resonances of Pu-239 and Pu-241 and round the 1.05 e.V. resonance of Pu-240. There is a group cut at 0.625 e.V., so that effective thermal cross-sections which are compatible with the WAPD 4-group scheme can be produced. A typical S_4 calculation with 30 radial points will take about $2\frac{1}{4}$ hrs. of 704 time, of which 30 minutes is printing time.

In our calculations on liquid-moderated reactors, we have so far only used the free gas model of thermalisation. (However, Egelstaff has recently supplied us with Scattering Laws for H_2O at room temperature and 150°C, and these are now being introduced into our work. Work by Macdougall (2) has shown that the change from the free gas model of thermalisation to a more realistic model does not produce a large change in reaction rates). All gases are given their actual masses (1 for H, 2 for D and so on). Devices such as that of Brown and St. John (3) lead to serious difficulties in matching the tail of the thermal spectrum to the epithermal sources, since they make ξ for H and D too small.

A very extensive series of reaction rate measurements in a CANDU-type lattice has recently been reported by Bigham, Chidley and Turner (4). The measurements in which the coolant channel was filled with cold (23°C) D_2O have been selected for analysis by the Carlson method. Figure 1 compares the measured and calculated distribution of the reaction rate of a bare manganese foil, while Figures 2 and 3 give similar comparisons for the variation across the lattice cell of the fission ratio of Pu-239 to U-235, and of the Lu/Mn reaction rate ratio. The agreement on fine structure and on the fission ratio is extremely good. The analysis of the Lu/Mn ratio is not quite so satisfactory, the maximum discrepancy being 4.6% at the centre of the fuel cluster: the mean discrepancy in the fuel is 2.8%. However it must be remembered that the Lu cross-section is not nearly as well known as those for the fissile isotopes; the data used in these calculations may well be several per cent in error. Such an error would be

particularly important in the fuel, where the spectrum is markedly non-Maxwellian. Also, errors in the model of theramlisation will probably have more effect on the Lu/Mn ratio than on the Pu/U ratio.

The agreement may thus be considered satisfactory, and similar results are obtained with other experiments of high accuracy. Thus there is every reason to suppose that the SNG method does represent faithfully the spatial variation of thermal spectra in lattice cells. However the method is fearfully expensive in machine time and quite laborious to use, in spite of the effort which has been put into mechanising it. There is a clear need for an alternative procedure which gives comparable results with much less computation. The SPECTROX method, which is described in the remainder of this paper, has been developed to meet this need.

3. The SPECTROX method: the SPECTROX 1 approximation

The SNG method consumes so much machine time because it treats simultaneously three different dimensions, namely, space, energy, and the direction of motion of the neutrons. The calculation can only be speeded up by eliminating at least one, and preferably two, of these dimensions. The conventional method of doing this is to use one or two thermal groups in which the spectra and cross-sections are specified in advance, and to compute only the distribution of the thermal group or groups across the cell. Regarded as a piece of fundamental theory, this method has been a failure. It is necessary to "adjust" the cross-sections in order to force agreement with the experiments, and there is no unique prescription for this adjustment.

The SPECTROX method is the opposite of this few-group procedure. The space-dependence is eliminated and attention is concentrated on the mean fluxes in fuel and moderator: the thermalisation equations determining the energy dependence of these fluxes are solved as accurately as possible. The ultimate basis of the method is the observation that the flux shape in the moderator is almost unaffected by the moderation there. In a 1-group diffusion problem, the flux shape in the moderator is given by

$$\phi(r) = \phi(a) + a\frac{\partial\phi}{\partial r}(a)\left\{\frac{b^2}{b^2-a^2}\ln\frac{r}{a} - \frac{r^2-a^2}{2(b^2-a^2)}\right\}$$

where a, b are the inner and outer radii of the moderator. It is found that this equation is very nearly valid even in an energy-dependent problem in which energy transfers (moderation) in the moderator are taken into account. Explicitly

$$\phi(r,E) = \phi(a,E) + a\frac{\partial\phi}{\partial r}(a,E)\left\{\frac{b^2}{b^2-a^2}\ln\frac{r}{a} - \frac{r^2-a^2}{2(b^2-a^2)}\right\} \qquad (3.1)$$

In physical terms, equation (3.1) states that the flux rise in the moderator at any energy is proportional to the current leaving the moderator at that energy, the constant of proportionality being taken from 1-group diffusion theory. This equation was formulated independently by Dr. G. W. Schaefer of the English Electric Company Limited, by M. O. Tretiakoff of C. E. A., Saclay, and by myself. Schaefer (5) was the first to show its surprising accuracy by comparison with detailed computations. Tretiakoff (6) has provided a theoretical explanation by showing that (3.1) is the first term in an expansion of the flux in the moderator in a series of "buckling eigenfunctions," and that subsequent terms are small.

Figure 4 shows a comparison between equation (3.1) and an SNG computation in the moderator of the CANDU lattice cell (cold D_2O coolant) in the group lying between 0.0250 e.V. and 0.0300 e.V. The agreement is not perfect, but it is extremely good. This is particularly striking, since (3.1) is a diffusion theory assumption, while the SNG code produces a more exact solution of the transport equation. It seems likely that (3.1) will be adequate in most practical cases, though it may fail if the moderator is very thin.

The equation of neutron balance in the moderator is

$$L_m(\chi_m) = \Sigma'_{am}(E)\chi_m(E) + \frac{1}{V_m} J(E) \qquad (3.2)$$

where $\chi_m(E) = \frac{1}{V_m}\int_a^b 2\pi r \phi(r,E)\,dr$ is the mean flux in the moderator at energy E (V_m being the moderator volume).

Σ'_{am} is the moderator macroscopic absorption cross-section.

$J(E)$ is the net current out of the moderator at energy E.

and $L_m(\chi_m) = \int_0^\infty \{\Sigma'_{sm}(E'\to E)\chi_m(E') - \Sigma'_{sm}(E\to E')\chi_m(E)\}\,dE'$

is the moderator thermalisation operator.

It also follows from (3.1) that

$$\phi(a,E) = \chi_m(E) - \frac{h(y)}{2\pi D_m} J(E) \qquad (3.3)$$

where $D_m(E)$ is the moderator diffusion coefficient

and $h(y) = \frac{y^4 \ln y}{(y^2-1)^2} - \frac{3y^2-1}{4(y^2-1)}$; $y = \frac{b}{a}$

(In order to keep this paper reasonably short, most of the mathematical detail has been omitted. The final published version will contain full deductions of (3.3) and other salient equations).

In the fuel region we use the method of successive collision probabilities. If the fuel is uniform and non-thermalising (so that a neutron can neither gain nor lose energy at a collision within the fuel), the mean flux in the fuel χ_f and the current entering the fuel J_{fuel} are related by

$$\Sigma'_{tf} V_f \chi_f = \left[1 + cP_1 + c^2 P_1 P_2 + c^3 P_1 P_2 P_3 + \ldots\right] . P_o J_{fuel} \qquad (3.4)$$

where Σ'_{tf} is the macroscopic total cross-section in the fuel

V_f is the volume of the fuel region

$c = \Sigma'_{sf} / \Sigma'_{tf}$ Σ'_{sf} being the macroscopic scattering cross-section in the fuel

P_o is the non-escape probability for a neutron entering the fuel from outside, $P_o P_1$ is the probability that such a neutron will make at least two collisions before escaping, and so on. If the fuel has thermalising properties, equation (3.4) must be generalised to

$$\Sigma'_{tf} V_f \chi_f = \left[1 + (P_1 Y) + (P_2 Y)(P_1 Y) + \ldots\right] . P_o J_{fuel} \qquad (3.5)$$

where

$$Y = \frac{\Sigma'_{sf} + L_f}{\Sigma'_{tf}}$$

The definition of the fuel thermalisation operator L_f is similar to that of the moderator thermalisation operator L_m.

If the fuel region is uniform (as is assumed in the SPECTROX 1 approximation), the successive collision probabilities, P_0, P_1, P_2, ... depend only on the single variable Σ'_{tg}. Stuart and Woodruff (7) have tabulated the probabilities up to P_5 for $\Sigma'_{tg} \leq 2$. (As explained below, there is no need to extend these tables to larger rod sizes). These tables are, in effect, a solution of the spatial part of the transport equation. Thus these tables remove the need for such a solution within the programme: the assumption (3.1) plays a similar role in the moderator. (g is the radius of the fuel rod).

Equation (3.5) is not usable as it stands, since it is of infinite order in the operator Y. However, figure 6 of Stuart and Woodruff's paper shows that for smallish fuel regions ($\Sigma'_{tg} \leq 1$) the assumption

$$P_1 = P_2 = P_3 = \ldots \qquad (3.6)$$

is quite accurate. This assumption is fundamental to the SPECTROX 1 procedure. We therefore expect this procedure to work for small fuel regions but not for large ones, and this expectation is confirmed by the results presented in the

next section. Combining (3.5) and (3.6), we find

$$P_0 J_{fuel} = (1 - P_1 Y) \Sigma'_{tf} V_f \chi_f \qquad (3.7)$$

Since we have had to assume that the fuel and moderator regions are uniform, we cannot treat pressure (and calandria) tubes in the SPECTROX 1 approximation. However an air gap between the fuel and the moderator is allowed $(g < a)$ and the current flows through it are treated by the method of Newmarch (8). Newmarch's arguments show that

$$J_{fuel} = 2\pi a \left[\frac{1}{4} x \phi(a,E) + \frac{1}{2} n(x) . D_m \frac{\partial \phi}{\partial r}(a,E) \right] \qquad (3.8)$$

where $x = g/a$

and $$n(x) = \frac{2}{\pi} \left(\sin^{-1} x + x \sqrt{1-x^2} \right)$$

Combining (3.8) with (3.3), we find

$$J_{fuel} = \frac{1}{2} \pi g . \chi_m(E) + X . J(E) \qquad (3.9)$$

where $$X = \frac{1}{2} n(x) - \frac{g}{4 D_m} h(y)$$

is a parameter which summarises the geometry of the lattice cell. We also note that the neutron balance equation in the fuel gives

$$J(E) = (1 - Y) \Sigma'_{tf} V_f \chi_f \qquad (3.10)$$

It may be shown that for a uniform circular rod the requirement of neutron conservation implies

$$P_0 (1 + P_1 + P_1 P_2 + P_1 P_2 P_3 + \ldots) = 2 \Sigma'_t g \qquad (3.11)$$

Substituting from the assumption (3.6) into this last equation, we find

$$P_0 = 2 \Sigma'_t g (1 - P_1) \qquad (3.12)$$

This equation is not, of course, exact but it is as accurate as (3.6). If (3.6) is to be used (as it is in the SPECTROX 1 procedure) then it is important to ensure that (3.12) is satisfied. If this is not done, neutrons will not be conserved and seriously wrong results may be obtained. Combining equations (3.8), (3.9), (3.10) and (3.11), we arrive at the basic equations of the SPECTROX 1 approximation

$$L_f(\chi_f) = \Sigma'_{af} \chi_f - \frac{P_0}{2g (P_1 - P_0 X)} (\chi_m - \chi_f) \qquad (3.13)$$

$$L_m(\chi_m) = \Sigma'_{am}\chi_m + \frac{V_f}{V_m}\frac{P_o}{2g(P_1 - P_o x)}(\chi_m - \chi_f) \qquad (3.14)$$

The second term on the right hand sides of these equations represents the current of neutrons out of the moderator into the fuel. In the SPECTROX 1 approximation the current at any energy is proportional to $(\chi_m - \chi_f)$, an interesting and rather unexpected result. Analytical examination of these equations suggests that this current term is equivalent to a 1/v absorber at high energies, and to an absorber of constant cross-section at low energies.

4. The SPECTROX 1 programme: results

R. W. Taylor [lately of the (British) General Electric Company Limited] has written a programme for the Ferranti Mercury computer to solve the SPECTROX 1 equations. Experience has shown that it is desirable to use about 40 energy groups (as in the Carlson calculations). Since the capacity of the Mercury fast store is only 1024 words, it would be difficult to accommodate this calculation if L_m and L_f were represented as integral operators (that is, as 40 x 40 matrices). They are therefore represented as second-order differential operators. de Sobrino and Clark (9) have shown that the Wilkins operator represents the thermalising properties of H_2O quite well (it is certainly better than the Wigner-Wilkins or free hydrogen model). Unfortunately, this operator is not so satisfactory for graphite. Horowitz (10) has suggested that this difficulty could be overcome to some extent by using instead of the Wilkins operator the more general form

$$L(\chi) = \xi\Sigma'_s \cdot \frac{d}{dE}\left[f(E)\left\{EkT\frac{d\chi}{dE} + (E - kT)\chi\right\}\right] \qquad (4.1)$$

This "Horowitz" operator is the most general second-order differential operator which satisfies all the necessary conservation conditions: the Wilkins operator is obtained by putting $f(E) = 1$. Griggs (11) has deduced the form of f for graphite at room temperature by analysing the experiments of Coates and Gaylher (12); his result is shown in figure 5. The use of the form (4.1) is justified as a programming convenience which has given good results in practice, but it must be emphasised that the SPECTROX method is not tied to this form. Indeed, a FORTRAN programme with unrestricted thermalisation operators is now projected.

Using the form (4.1), the SPECTROX equations (3.13) and (3.14) reduce to a pair of simultaneous differential equations, and these are integrated by simultaneous forward elimination and backward substitution. The SPECTROX 1 programme takes as input a stated geometry and fuel composition. P_o is calculated from a formula due to Neumann (which is valid for all values of Σ_{tg}) and P_1 is then computed from (3.12). When χ_m and χ_f have been calculated, the reaction rates of a variety of isotopes can be computed in these spectra from the programme's built-in library of basic cross-sections compiled from the recommendations of Story and Sjöstrand (13).

An extensive series of fine structure measurements has been made in graphite lattice cells under the BICEP (British Industrial Collaborative Experimental Programme), and Griggs and Choules (14) have analysed these measurements using the SPECTROX method. These authors will be reporting their work in detail at

a later date: we are quoting a few of their results to establish the validity of the method. The Table below lists results for single bare natural uranium metal rods:

TABLE I

Lattice Pitch (in)	Channel Diam (in)	Fuel Diam (in)	Experimental GCRS	SPECTROX GCRS
7	4.5	1.0	1.566 ± .033	1.553
8	4.5	1.0	1.572 ± .055	1.602
$7\sqrt{2}$	4.5	1.64	2.053 error not quoted	2.077
$8\sqrt{2}$	4.5	1.64	2.371 ± .094	2.334

The experimental quantity GCRS is the ratio of the mean reaction rate of a Cd-covered Mn foil in the moderator to the mean reaction rate of the same foil in the fuel. In the SPECTROX calculation, the Cd-covered Mn is represented as a $\frac{1}{v}$ - absorber below E_c = 0.5 e.V., with zero cross-section above $E = E_c$ (it has been shown that the calculated GCRS is insensitive to E_c, changing by about 1% when E_c is increased to 0.75 e.V.). It will be seen that the agreement is extremely satisfactory, the difference between SPECTROX and the experimental value being less than the quoted error in the latter in all cases.

Griggs and Choules have also compared SPECTROX with fine structure experiments on 44 different AGR lattice cells, in which the fuel element is in the form of an air-cooled oxide cluster. The agreement is again very good. The discrepancy between SPECTROX and the experimental value is less than the standard deviation of the latter (σ) in 28 cases, lies between σ and 2σ in 14 cases, and exceeds 2σ in only 2 cases: these proportions are very similar to those which would be found if the discrepancy were all due to a Gaussian distribution of experimental errors. It is particularly gratifying that SPECTROX, which uses only basic data, fits the experiments at least as well as methods which rely on correlation (that is, adjustment of the basic data to force agreement with the experiments).

SPECTROX 1 has also been tested against the fission chamber measurements reported by Campbell, Freemantle and Poole (15). Measurements were made at the centres of single uranium metal rods of differing enrichments (these rods being bored out to accommodate the fission chambers), and also at various positions in the moderator. The interpretation of the measurements in the moderator is rather difficult because only one fuel rod was bored out and the lattice is not therefore homogeneous: this problem is still being studied. It is easier to calculate the spectrum at the centre of the fuel, since the geometry is uniform. It would not, however, be correct to treat the bored-out experimental rod as if it were uniform. Griggs (11) has therefore used an extended version of SPECTROX 1 which incorporates a collision probability routine and can treat non-uniform fuel regions. (This version, known as MINX, was written under the direction of J. G. Tyror).

TABLE II

Reference no. of experiment	Experimental σ_{f9}/σ_{f5}	MINX σ_{f9}/σ_{f5}	% difference
36	1.841	1.834	- 0.4%
37	1.915	1.909	- 0.3%
44	1.769	1.840	+ 4.0%
45	1.885	1.880	- 0.3%
46	2.417	2.483	+ 2.7%
47	2.063	2.104	+ 2.0%
48	2.456	2.497	+ 1.7%

The quantity quoted is the sub-cadmium atomic fission ratio of Pu-239 to U-235; in the MINX computations, the Cd cut-off has been taken as 0.5 e.V., and it has been shown that the fission ratio is not sensitive to the precise value. Since the quoted error on the experiments is ± 2%, the agreement is satisfactory. However, there is a tendency, which seems to be just significant, for the MINX values to be higher than the experimental ones.

The SPECTROX 1 procedure has also been applied to the calculation of burnup and of moderator temperature coefficients with equally encouraging results. It may be concluded that this is an accurate and convenient method for analysing thermal phenomena in magnox and AGR lattice cells.

5. The extension to large fuel clusters

The assumption (3.6), which underlies the SPECTROX 1 procedure is only valid if $\Sigma'_{t9} \leq 1$. The Table below shows that the procedure does indeed cease to work if this condition is violated.

TABLE III

Type of lattice	Σ'_{t9}	Σ'_{af9}	Exptl. or SNG GCRS	SPECTROX 1 GCRS	Epithermal cutoff
13 rod AGR	0.72	- -	1.279 ± .022	1.289	0.5 e.V.
37 rod AGR	0.85	- -	1.678 ± .014	1.690	0.5 e.V.
Cold D_2O core of ZEEP	1.89	0.329	1.77	1.568	∞
OCGR	1.52	0.546	1.762	1.496	0.625 e.V.

All cross-sections are evaluated at the peak of the thermal spectrum in the fuel. The OCGR (Organic-Cooled Graphite Reactor) is a purely conceptual design, selected to give a large value of Σ'_{tg} . The fuel cluster consists of 91 rods of uranium carbide 0.35" in diameter and enriched to 1.8 Co: the canning is SAP and the coolant is terphenyl at 400°C. The overall diameter of the fuel cluster, which is contained in a SAP tube, is 5.93". A 0.5" gas gap separates this tube from the graphite bulk moderator, and the lattice pitch is 12".

For the ZEEP core, the SPECTROX 1 calculation is not strictly comparable with experiment since the pressure and calandria tubes are perforce omitted from this calculation. These are believed to contribute 0.1 to 0.15 to GCRS. Subtracting this amount from the experimental value still leaves a discrepancy of over 5% in fine structure. SPECTROX 1 underestimates the fine structure in the OCGR by 15%, but this core has an exceptionally large fuel cluster. (The coolant containment tube does not increase the fine structure appreciably).

Table III also shows that Σ'_{afg} is quite small, even in the OCGR. This suggests a different type of approximation for simplifying equation (3.5). We assume that

$$Y - 1 = \frac{L_f - \Sigma'_{af}}{\Sigma'_{tf}}$$

is small, and that terms of order $(Y-1)^2$ may be neglected. To this order, there are no commutation difficulties. With this assumption and a little rearrangement, equation (3.5) simplifies to

$$J_{fuel} = \left[\left(\frac{1}{2\Sigma'_{tg}} + H\right) - HY\right] \Sigma'_t V_f \chi_f \qquad (5.1)$$

where $$H = \frac{P_0(P_1 + 2P_1P_2 + 3P_1P_2P_3 + \ldots)}{(2\Sigma'_{tg})^2} \qquad (5.2)$$

H is a function of Σ'_{tg} only. $H(0) = 2/3$, and it may be shown from diffusion theory that

$$H \to \frac{1}{2} + \frac{3}{16}\Sigma'_{tg} \qquad (5.3)$$

for Σ'_{tg} large. Values for $\Sigma'_{tg} \leq 2$ can be computed from the Stuart and Woodruff tables, while values for $\Sigma'_{tg} > 2$ can be inferred from (5.3): there is no need to compute P_0, P_1, P_2, ... for $\Sigma'_{tg} > 2$. Equation (5.1) is a replacement for, and generalisation of, equation (3.7). It embodies the SPECTROX 3 method for calculating χ_f and χ_m . The remainder of the analysis for this method is taken over unchanged from section 3.

The SPECTROX 1 programme has been adopted to solve the SPECTROX 3 equations. This is done by substituting for the table of P_0 (the probability that an entrant neutron will make a collision) a table of

$$P_0^*(\Sigma'_{tg}) = \frac{2\Sigma'_{tg}}{1 + 2\Sigma'_{tg}.H(\Sigma'_{tg})} \qquad (5.4)$$

P_0^* is not a collision probability, and in fact it tends to zero as Σ_{tg} becomes large.

The Table below compares total reaction rates averaged across the fuel and the moderator in the cold D_2O core of ZEEP.

TABLE IV

Quantity	SPECTROX 1	SPECTROX 3	SNG	Experiment
GCRS	1.568	1.639	1.769	1.77
Lu/Mn (fuel)	286	287	291	299
Pu/U (fuel)	1.534	1.535	1.550	1.56
Lu/Mn (mod.)	265	264	265	265
Pu/U (fuel)	n.a.	1.480	1.482	1.50

It has already been stated that the SPECTROX programmes make no allowance for the pressure and calandria tubes, and that these are believed to contribute between 0.1 and 0.15 to GCRS. Thus SPECTROX 3 would seem to give good agreement on fine structure with experiment and with SNG. The change in method from SPECTROX 1 to SPECTROX 3 hardly affects the mean spectra in the fuel and in the moderator, and the SPECTROX values for the spectrum indices (Lu/Mn and Pu/U ratios) are in good agreement with the SNG values. It has been noted that the SNG value for the Lu/Mn ratio in the fuel is slightly different from the experimental value. Obviously SPECTROX cannot be expected to do better in this respect than SNG, since SPECTROX is solving approximately the equation which Carlson solves exactly.

Table IV does not establish definitely that SPECTROX 3 is superior to SPECTROX 1 for large fuel clusters: this is because, in the cold D_2O core of ZEEP, the fuel cluster is not really large. The OCGR fuel cluster is really large ($\Sigma_{tg} = 6.5$) and the Table below does demonstrate conclusively the superiority of SPECTROX 3 (in this case there are no experiments, and the reaction rates are cut off at 0.625 e.V.).

TABLE V

Quantity	SPECTROX 1	SPECTROX 3	SNG
GCRS	1.496	1.740	1.762
Lu/Mn (fuel)	595	597	590
Pu/U (fuel)	2.838	2.854	2.732
Lu/Mn (mod.)	520	519	517
Pu/U (mod.)	2.303	2.221	2.212

The OCGR cluster has been "designed" to ensure that the coolant-containing tube does not contribute appreciably to the fine structure. It will be seen that

SPECTROX 3 is now giving a very good value for the fine structure (1.2% low) while the SPECTROX value is poor (15.1% low). The comparison of spectrum indices is complicated by the fact that SPECTROX and SNG are using different moderation models (heavy gas and free gas respectively). These models are similar in the graphite moderator, and it will be seen that in the moderator the SPECTROX 3 spectrum indices are nearer to the SNG values, though the discrepancies are all small. In the moderator, the model of hydrogen moderation used by SNG is considerably softer than that employed by the SPECTROX programmes: this is confirmed by the values of the spectrum indices listed in Table V.

It may be concluded that, unlike SPECTROX 1, SPECTROX 3 will give good results even for large clusters. Its main defects are that it deals only with uniform clusters, that it cannot allow for pressure and calandria tubes, and that it gives only the mean flux in fuel and moderator and not the spatial distribution. These defects are all overcome by the MINX extension of the SPECTROX method. This extension, which is mentioned in section 4, was devised by J. G. Tyror and worked out in detail by C. F. Griggs. The basic assumption of MINX is that the fine structure in the fuel cluster (including pressure and calandria tubes, if these are incorporated) is unaffected by thermalisation: this is the precise analogue of the assumption (3.1) which is made in the moderator. The MINX programme incorporates the SPECTROX programme and a collision probability routine. This routine is used to compute the fine structure (in the absence of thermalisation) at a number of different energies. From this fine structure an equation similar to (3.7) can be derived, whence quantities analogous to P_0 and P_1 can be calculated. These are substituted into the SPECTROX equations (3.13) and (3.14).

The MINX programme was primarily intended for the study of small non-uniform clusters, but the idea of generalising P_0 is also used in SPECTROX 3. This suggests that the two methods must be basically similar. The writer has been able to show that SPECTROX 3 is actually the limiting form of MINX when the fuel cluster is uniform and the absorption weak, and that the MINX approximation is valid as long as

$$kq = q\sqrt{3\Sigma_{af}\Sigma_t'} < 3$$

Thus MINX should be just adequate even for the very largest clusters: its use for large fuel clusters is now being investigated.

6. Acknowledgments

I am most grateful for the work of Mr. C. F. Griggs and Mr. M. J. Terry, both of A. E. E., Winfrith. Mr. Griggs has shouldered the heavy burden of proving that SPECTROX 1 is a valid method for small fuel regions, while Mr. Terry has carried out most of the Carlson calculations. I have had interesting and helpful discussions with Mr. J. G. Tyror of A. E. E., Winfrith, Dr. G. W. Schaefer of the English Electric Co., Limited, and with Dr. J. Horowitz and M. O. Tretiakoff of C. E. A., Saclay: I am also indebted to Dr. Horowitz for permission to describe his thermalisation operator.

Lastly I am indebted to the British Industrial Consortia (English Electric /British Babcock and Wilcox/Taylor Woodrow, The Nuclear Power Group Limited, and the United Power Company Limited) for permission to use results from the BICEP programme in advance of publication.

- REFERENCES -

1.	D. A. NEWMARCH	AERE R/R 2425
2.	J. D. MACDOUGALL	Application of Scattering Law Data to the calculation of thermal neutron spectra. Paper submitted to the BNL Symposium on neutron thermalisation.
3.	H. BROWN and D. ST. JOHN	DP - 33
4.	C. B. BIGHAM, B. G. CHIDLEY and R. B. TURNER	CRRP - 985 - B
5.	G. W. SCHAEFER	Private communication
6.	J. HOROWITZ and O. TRETIAKOFF	EANDC (E) 14
7.	G. W. STUART and R. W. WOODRUFF	Nuc. Sci. and Eng. 3, 339 (1958)
8.	D. A. NEWMARCH	J. Nuc. Energy 2 52 (1955)
9.	L. de SOBRINO and M. CLARK, Jr.	Nuc. Sci. and Eng. 10 377 (1961)
10.	J. HOROWITZ	Private communication
11.	C. F. GRIGGS	To be published
12.	M. S. COATES and D. B. GAYTHER	AERE - R.3829
13.	N. G. SJOSTRAND J. S. STORY	Nuclear Data for reactor design. To be published.
14.	A. J. CHOULES and C. F. GRIGGS	To be published.
15.	C. G. CAMPBELL, R. G. FREEMANTLE and M. J. POOLE	Second Geneva Conference. A/CONF.15/P/10.

ZEEP LOOP: COLD D_2O. COMPARISON OF CALCULATED (SNG) AND MEASURED Mn REACTION RATE DISTRIBUTIONS

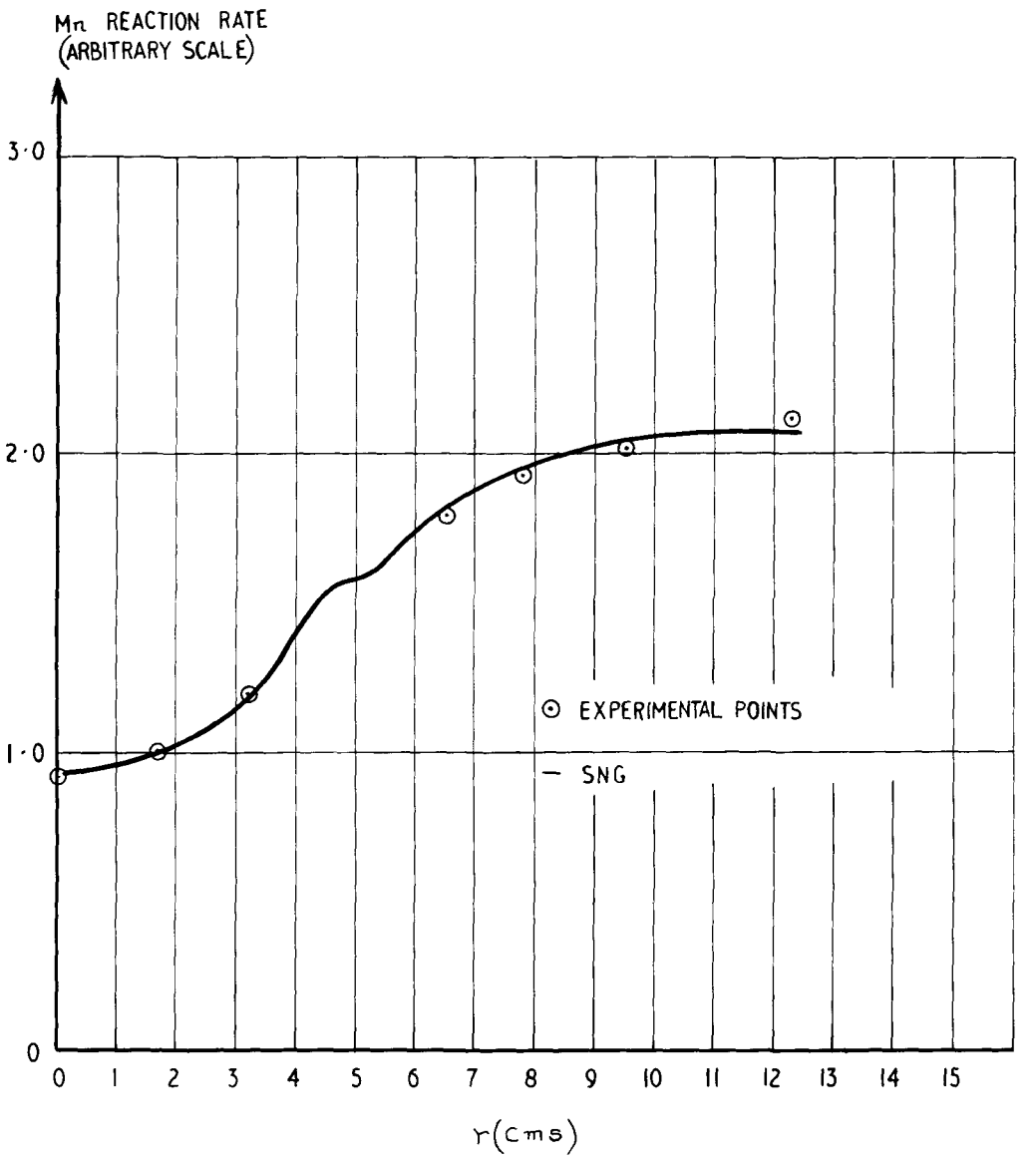

FIGURE 1.

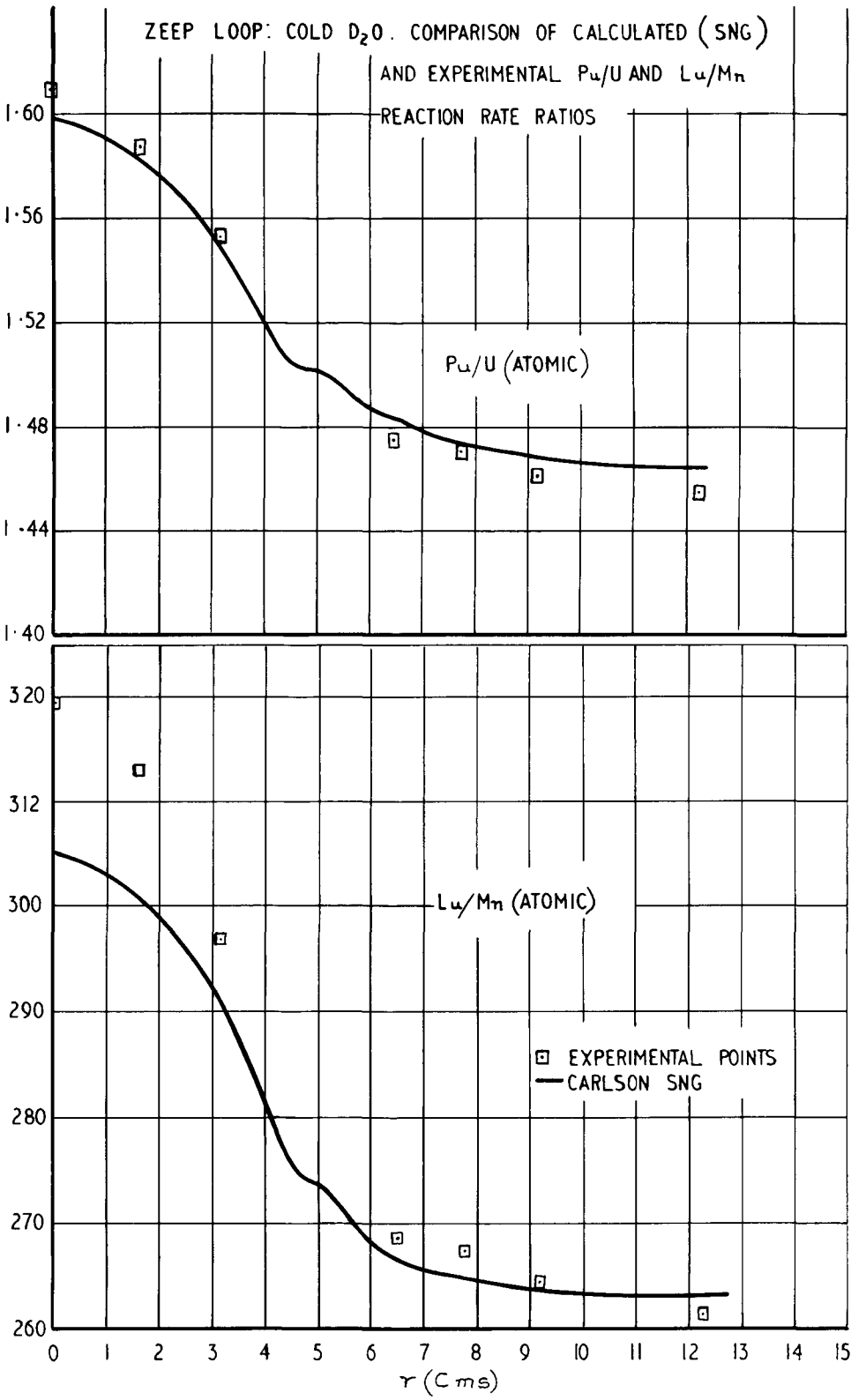
ZEEP LOOP: COLD D_2O. COMPARISON OF CALCULATED (SNG)
AND EXPERIMENTAL Pu/U AND Lu/Mn
REACTION RATE RATIOS
1·60
1·56
1·52
1·48
1·44
1·40
Pu/U (ATOMIC)
320
312
300
290
280
270
260
Lu/Mn (ATOMIC)
EXPERIMENTAL POINTS
CARLSON SNG
0 1 2 3 4 5 6 7 8 9 10 11 12 13 14 15
r (C ms)

FIGURES 2 & 3

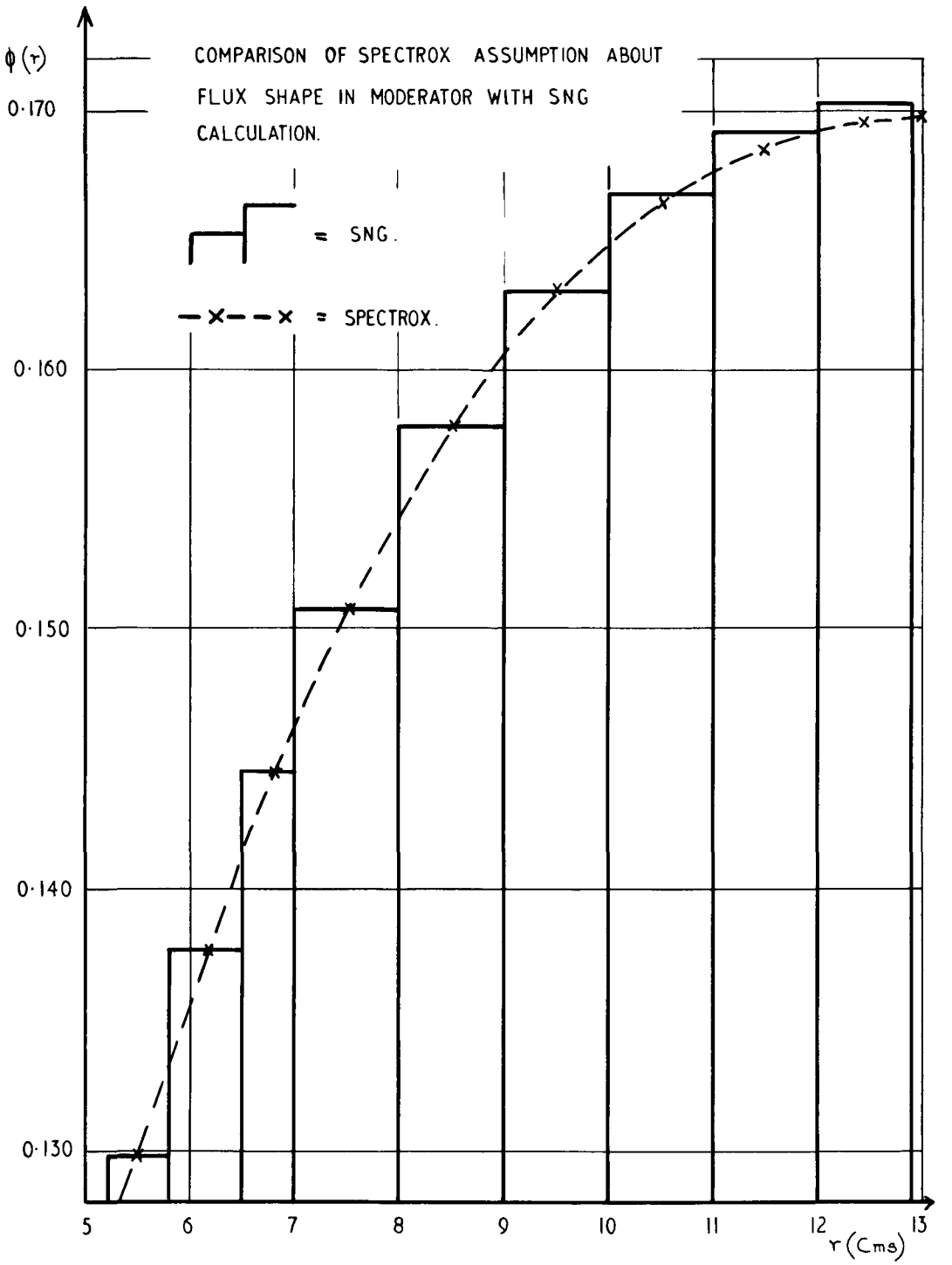
COMPARISON OF SPECTROX ASSUMPTION ABOUT FLUX SHAPE IN MODERATOR WITH SNG CALCULATION.
= SNG.
= SPECTROX.
φ(r)
0·170
0·160
0·150
0·140
0·130
5
6
7
8
9
10
11
12
13
r (Cms)

FIGURE 4.

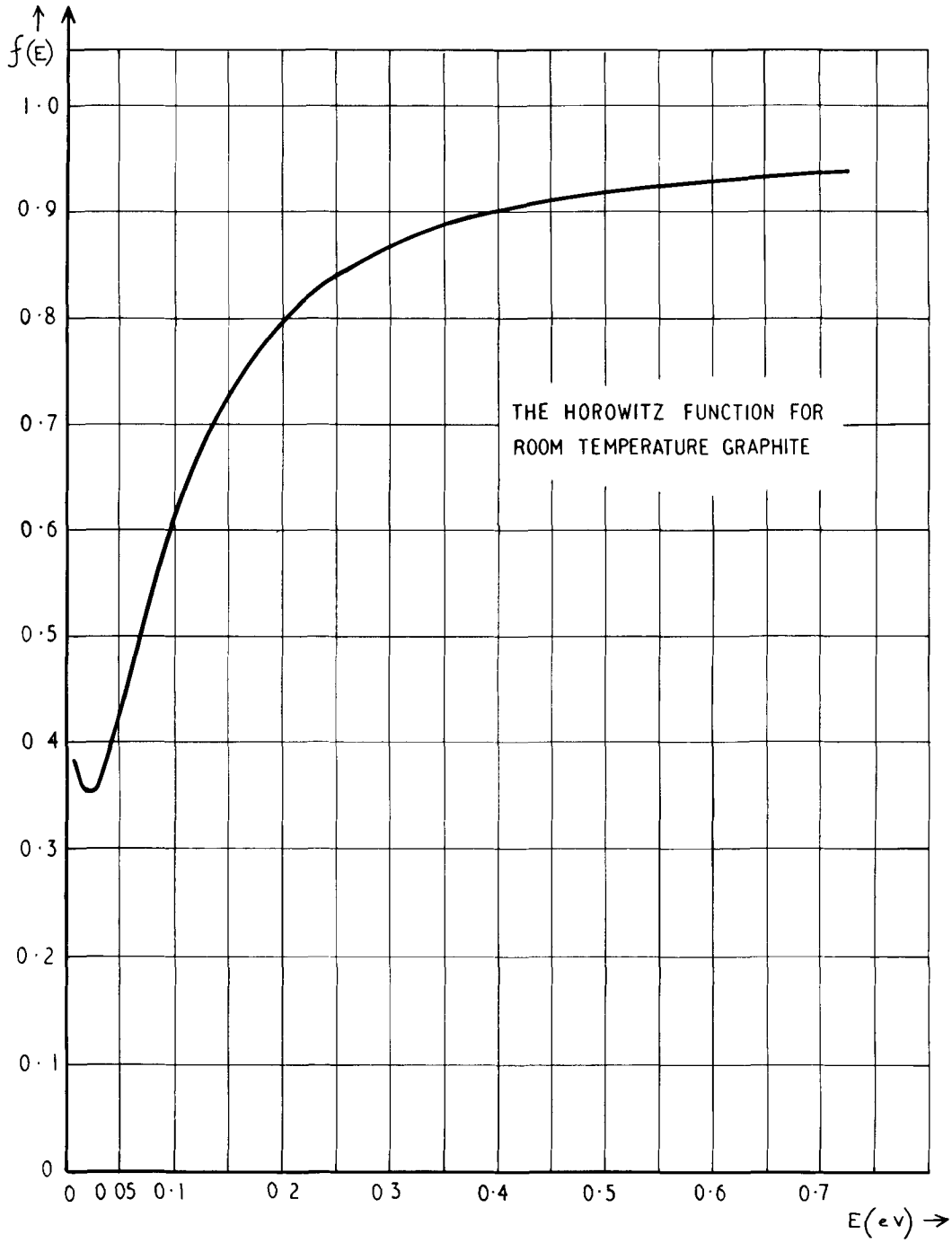
f(E)
1·0
0·9
0·8
0·7
0·6
0·5
0 4
0·3
0·2
0·1
0
0 0 05 0·1 0 2 0 3 0·4 0·5 0·6 0·7
E(ev) →
THE HOROWITZ FUNCTION FOR
ROOM TEMPERATURE GRAPHITE

FIGURE 5

Paper to be submitted to the Brookhaven Conference on Neutron Thermalization, April 30, 1962

Radial Dependence of the Bump Where the Maxwellian Meets the 1/E-Tail

by R.M. Pearce and J.M. Kennedy

In 1957 Galanin[1] predicted theoretically that when the maxwellian component is subtracted from the spectrum in a homogeneous reactor, that as well as the 1/E-slowing down spectrum remaining there is a bump superimposed at an energy of approximately 6 to 8 kT. The bump reached 20 to 30% of the 1/E-tail in heavy gas theory, and 12 to 15% for a mass one moderator. The presence of the bump was later found experimentally by Johansson et al[2] at the cell boundary of a D_2O-moderated reactor, and by Poole[3] in the moderator of a graphite-moderated reactor. There has been no report in the literature of the bump inside the fuel. This paper predicts that the bump, as defined by subtracting the best fitting maxwellian, does not exist inside the fuel.

The present work on the bump occurred in the course of calculating the thermal spectrum in a lattice cell of CANDU, the Canadian power reactor under construction at Douglas Point. CANDU is D_2O cooled and moderated and is fueled by zirconium-clad 19 element natural uranium oxide. In the calculations, the fuel, cladding, coolant and pressure tube were homogenized into a single central region and a twenty-energy-group diffusion code with twenty-one space points was used as described in more detail in reference (4). The transfer cross sections between groups were calculated for a free gas and were spectrum-weighted because of the relatively large

energy widths. The weighting was maxwellian below 5 kT and 1/E above 5 kT.

At the cell boundary of CANDU the low energy spectrum calculated by the code was found to be closely maxwellian with the result that the maxwellian functions to be subtraced at ~ 8 kT, and therefore the bump, were well defined. Fig. 1 shows $E(\phi - \phi_{max})$ versus energy, where ϕ_{max} is the best fitting maxwellian and the energy E for a group with limits E_1 and E_2 was taken to be the effective energy $(E_2-E_1)/\log E_2/E_1$ to account for 1/E-variation in the finite group width. The bump shown for free gases of mass 2 and 3.6 in Fig. 1 are approximately 20 - 25% of the slowing down spectrum. There may be some uncertainty in the magnitude of the bump because of the rather large group widths.

The bump was also calculated at the centre of the oxide cluster and at the cluster surface in a similar manner by subtracting the maxwellian which fitted most closely at that position. (At these positions the bump is not as uniquely defined as it was in the moderator because the low energy spectrum is not exactly maxwellian.) The results shown in Fig. 1 show that the bump is smaller at the cluster surface, and almost zero inside the fuel cluster.

The explanation of this radial dependence of the bump is as follows. The bump is caused by a loss of moderating power due to the thermal motion of the moderator atoms, and in order to properly display the excess neutrons as a bump the subtracted maxwellian should therefore be at the moderator temperature. It is known experimentally and theoretically[4] that the neutron temperature

at the cell boundary is only slightly above the moderator temperature with the result that the bump is properly displayed, but in the fuel the neutron temperature is considerably higher because of absorption and the bump is largely removed in the subtraction process.

Compilations of effective cross sections conventionally divide the contributions into a maxwellian plus a slowing down term. These calculations suggest that no single convention will suffice for all points in the cell, because of the radial change of the bump and therefore of the slowing-down term.

References:

1. A.D. Galanin, Supp. 2 and 3, Soviet Journal of Atomic Energy (1957); Consultants Bureau Inc. Trans. (1958).
2. E. Johansson, E. Lampa, and N.G. Sjöstrand, Arkiv für Physik 18, 513 (1960).
3. M.J. Poole, Symposium on Neutron Time-of-Flight Methods, Saclay, July (1961).
4. J.M. Kennedy and R.M. Pearce AECL-1414.

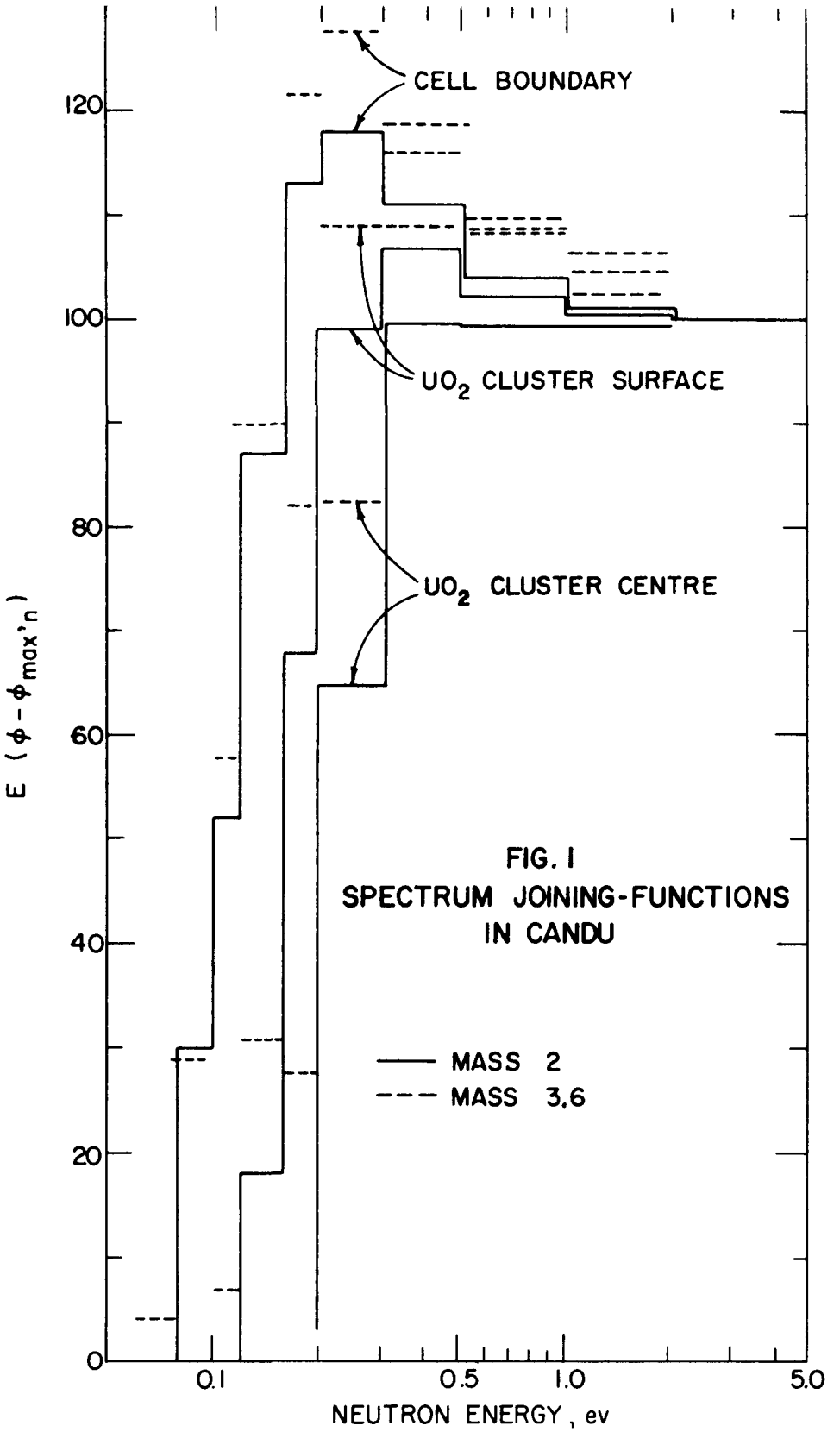

FIG. I
SPECTRUM JOINING-FUNCTIONS
IN CANDU

CHEMICAL BINDING EFFECTS IN THE GENERALIZED HEAVY FREE GAS APPROXIMATION

by

G. W. SCHAEFER, K. ALLSOPP

Theoretical Physics Group
Atomic Power Division
English Electric Co. Ltd.,
Whetstone, Leicestershire, England.

A B S T R A C T

It is shown that the integral Boltzmann scattering operator may be replaced by a second order differential operator of the heavy free gas (Wilkins) form, by letting $\xi\Sigma_s$ be an arbitrary function of energy. This variable is determined by the moderating properties of a medium, but it also depends on the solution of each particular problem. However, it is shown that for a wide class of reactor problems the variable is insensitive to the problem. In these cases it may be obtained simply from the neutron "scattering law" at high and low energies. For heavy moderators this is true to a good approximation at all energies.

Some properties of this generalized equation are discussed. Criteria are derived for deciding which problems may be solved by this theory. Then the sensitivity of slowing down spectra, of thermal reactivity ηf and its temperature coefficients, and of eigenvalues to the "scattering law" is studied and illustrated. Theoretical values of $\xi\Sigma_s(E)$, calculated from various scattering models of graphite and water, are compared with experimentally deduced values.

Submitted to Brookhaven Thermalization Conference - April, 1962.

Introduction

In many problems of interest to the reactor physicist the neutron thermalization process is governed by the Boltzmann integral operator L, defined by

$$L(E)\,\phi(E) = \int_0^\infty \Sigma_s(E' \to E)\,\phi(E')\,dE' - \Sigma_s(E)\,\phi(E), \tag{1}$$

using conventional symbols. Such problems include the calculation of the neutron spectrum in an infinite medium, the solution of the Boltzmann equation in the diffusion approximation, and the solution of the integral Boltzmann equation in the isotropic scattering approximation (soluble by the method of first collision probabilities). It would be most desirable to be able to replace L by a low order differential operator, having the properties of L and making due allowance for the chemical binding of the scattering nuclei. It is the purpose of this paper to show that this may be done, to determine the range of usefulness of the resulting second order operator, to show its limitations and accuracy, and to use the new operator to study the sensitivity of various reactor calculations to the neutron "scattering law".

Several authors have investigated differential representations of L, but none have been successful in finding an operator which allows for chemical binding and is valid (or sufficiently accurate) at all neutron energies. On the one hand there are two second order differential equations valid over a wide range of energy, but only for free gases. These are the Wigner Wilkins equation for hydrogen gas, and the heavy free gas (H.F.G.) Wilkins equation, valid for small μ, the ratio of neutron mass to the atomic mass of the gas. On the other hand, there

are those differential operators which include atomic binding, are good approximations for high neutron energies $E >> kT$, but which fail badly in the "Maxwellian" region $E \lesssim kT$. These include Corngold's[1] modification to the H.F.G. theory, in which the moderator temperature is replaced by an effective temperature which makes allowance for atomic binding effects; the third order equation of Corngold[1] and the fourth order equation of Sobrino and Clark[2], derived by adding terms of order μ^2 to the H.F.G. theory; and the accurate first order equation of Parks[3] for light or heavy "bound" moderators.

In Sections 1 and 2 it is shown that a second order operator can be chosen "ad hoc", which obeys detailed balance, conserves neutrons, and includes chemical binding. It has the form of the H.F.G. equation, but the moderating power $P = \xi\Sigma_s$ is now energy dependent. This generalization was first suggested by Horowitz[4], but was never developed as far as the authors are aware. Any solution of the Boltzmann equation in the diffusion approximation can be written as a solution of this generalized heavy free gas (G.H.F.G.) equation by suitable choice of $P(E)$. The new operator will be useful only when $P(E)$ is a function of the moderator scattering law, and is otherwise independent of the problem in hand, that is, independent of absorption and leakage. It will turn out that to a good approximation this is the case in those problems in which the flux deviates only slightly from a "Maxwellian". This condition is consistent with the diffusion approximation (and the H.F.G. theory), in which absorption and leakage are assumed small relative to scattering.

In Section 3 the high energy values of $P(E)$ are determined analytically in terms of the scattering law. At low energies, $E \lesssim 3kT$,

the first energy transfer moment of the scattering kernel, $M_1(E)$, determines P(E), as is shown in Section 4. For intermediate energies it is not possible to find P(E) analytically. However, Section 5 contains an approximate method, in terms of $M_1(E)$. Several models of graphite, beryllium, and water are used for illustration. These three sections give criteria for determining whether a problem is suitable for solution by the differential representation. For the heavier moderators, such as graphite and beryllium, P(E) may be found with sufficient accuracy from $M_1(E)$ at all energies, and it is for these moderators that the G.H.F.G. theory is best suited. The theory may be used for water systems, but only in a very limited range of problems.

Section 6 gives the generalized equation in integral form, suitable for interative methods of solution.

In Section 7 the sensitivity of infinite medium spectra to the scattering law (and hence to P(E)) is investigated. It is shown that these spectra are insensitive to P(E) at intermediate energies. Egelstaff[5] has recommended a "sensitivity function" for these spectra. The generalized theory throws considerably light on this function. A Debye model of graphite is used in illustration. For those spectra for which an effective neutron temperature T_n applies, a simple new relation is given between T_n amd $M_1(kT)$.

In Section 8 the experimental time-of-flight measurements of Coates and Gaythe[6] on graphite assemblies, and of Beyster et al.[7] on water systems, are used to determine P(E) for these moderators. The results are compared with various theoretical models.

In numerical applications, the use of the G.H.F.G. equation eliminates

much of the labour involved in solving the integral equation. Solutions may be obtained on small computers, even for space-energy calculations involving as many as a thousand mesh points. For several years the authors have been using a machine code for the spectrum in a (cylindricalized) lattice cell, which combined the differential energy operator with diffusion theory in the main moderator and collision probability methods in the fuel region. The resulting coupled finite difference equations are of "band" form, and may be solved readily by triangularization and back substitution. Leslie (this conference) has used a simplified model of this method in the Spectrox codes. In Sections 9 and 10 a few numerical results are presented to illustrate the sensitivity of a lattice cell thermal reactivity ηf and its temperature coefficients to the scattering law and to the inaccuracies in the experimental fission cross sections.

Section 11 deals with the determination of eigenvalues and eigenfunctions on the G.H.F.G. theory, and the limitations of this theory for this type of problem.

1. The Generalized Heavy Free Gas Operator

The Boltzmann equation in the P_1 approximation is

$$\left[\frac{1}{v}\frac{\partial}{\partial t} - \nabla \cdot D(x,r)\nabla + \Sigma_a(x,r)\right]\phi(x,r,t) = L(x,r)\,\phi(x,r,t) + S(x,r,t) \quad , \qquad (2)$$

or, symbolically,

$$A\,\phi = L\,\phi + S = \frac{\partial q}{\partial x} + S \, . \qquad (3)$$

L is defined in (1). Energy is measured in dimensionless units $x = \frac{E}{kT}$. $q(x, r, t)$ is the number of neutrons per unit volume at position r

slowing down past x per second at time t. The other symbols have their usual definition. In the following, position and time co-ordinates will be omitted when not essential.

It will be useful to review some of the properties of this equation. If q is written as $Q\phi$, it follows from (1) and (2) that the integral operator Q is defined by

$$Q(x)\phi(x) = \int_0^x dy \int_x^\infty dz \left[\Sigma_s(z \to y)\phi(z) - \Sigma_s(y \to z)\phi(y) \right] . \qquad (4)$$

The scattering kernel $\Sigma_s(x \to y)$ obeys the detailed balance relation

$$\Sigma_s(x \to y) M(x) = \Sigma_s(y \to x) M(y) , \qquad (5)$$

with M(x) the Maxwellian distribution xe^{-x}. It follows that LM and QM are identically zero, and that the flux ϕ becomes proportional to M as A and S vanish. Equation (2) conserves neutrons, since by definition

$$q(x) = \int_0^x \left[A(y)\phi(y) - S(y) \right] dy . \qquad (6)$$

Also, when neutrons slow down from a constant source at infinite energy in a infinite non-absorbing medium, then $x\phi(x)$ becomes constant for large x, and q(x) tends to $\Sigma_f x\phi(x)$. Σ_f is the free atom macroscopic scattering cross section.

It is desired to replace L and Q by low order differential operators L_A and Q_A respectively. From the above summary it is clear that the new operators will obey detailed balance and conserve neutrons if Q_A is chosen such that $Q_A M$ vanishes identically, and $Q_A\phi$ tends to Σ_f when $x\phi(x)$ tends to unity for large x in the slowing down problem.

Q_A will be chosen "ad hoc" as the lowest order differential operator satisfying these two conditions. It is easy to verify that

$$Q_A \equiv P(x)\left[x\frac{\partial}{\partial x} + x - 1\right] \quad , \tag{7}$$

with P(x) arbitrary except for the condition

$$P(x) \xrightarrow[x\to\infty]{} \xi\Sigma_f \quad . \tag{8}$$

Q_A is a generalized H.F.G. operator, and P(x) is an effective moderating power. Substituting (7) into (3) gives the Generalized Heavy Free Gas equation:

$$A\phi - S = \frac{\partial}{\partial x} P(x)\left[x\frac{\partial}{\partial x} + x - 1\right]\phi \quad . \tag{9}$$

The H.F.G. equation is the special case for which $P(x) = \xi\Sigma_f$ (the value used in this paper in place of the usual $2\mu\Sigma_p$).

2. Determination of P(x)

Any solution of the transport equation (2), found theoretically or experimentally (time-of-flight techniques), is also a solution of the G.H.F.G. equation (9) by a suitable choice of P(x). This is possible because P possesses an infinity of degrees of freedom. Let $\bar{\phi}$ be a solution of (2). Then the corresponding P is

$$\bar{P}(x,\underline{r},t) = \frac{\bar{q}(x,\underline{r},t)}{\left[x\frac{\partial}{\partial x} + x - 1\right]\bar{\phi}(x,\underline{r},t)} \quad , \tag{10}$$

with $\bar{q}$ given by (6). Clearly, each $\bar{P}$ is a function of A and S, as well as the moderating properties of the medium. Thus the G.H.F.G. theory will be useful only for the class of problems for which P is independent

of A and S to a good approximation.

Problems involving only heavy free gases, in which the absorption (A) to scattering ratio is of order μ, are contained in the class[8]. In the following three sections, P(x) will be determined analytically, as far as possible, in terms of the scattering law, A, and S. Criteria will emerge for deciding which problems are members of the class. At high energies the asymptotic solution of Corngold[9] will be used to calculate P(x). At low energies, P(x) will be determined from the "moments expansion"[8] of (2). Section 5 discusses the joining of the high and low values.

3. P(x) at High Energies ($x \gtrsim 10$)

An analytical solution of the transport equation for neutrons slowing down in an infinite absorbing medium has been given for $x \gtrsim 10$ by two authors. Corngold[9] has treated the special case of $\frac{1}{v}$ absorption, and has found an asymptotic expansion in powers of $x^{-\frac{1}{2}}$. Parks[3] derived a very accurate first order differential equation for the flux at high energies, with general (small) absorption. P may be determined from either of these theories. The former will be used, since it contains the chemical binding exactly, and is easier to handle. Although it applies only to a particular type of absorption, this should not be serious when considering the sensitivity of P to absorption.

Let $\sigma_a(x) = \sigma_{ao} x^{-\frac{1}{2}}$, and $\Delta = 2\sigma_{ao}/\mu\sigma_f$. Then Corngold's solution is

$$x\,\phi_\Delta(x) = 1 - a_{1\Delta}\frac{\Delta}{2}\frac{1}{x^{1/2}} + \left[a_{2\Delta}\left(\frac{\Delta}{2}\right)^2 + (2-\mu)\frac{\bar{T}}{T}\right]\frac{1}{x} - \left[a_{3\Delta}\left(\frac{\Delta}{2}\right)^3 + b_{1\Delta}\frac{\Delta}{2}\frac{\bar{T}}{T}\right]\frac{1}{x^{3/2}}$$

$$+\left[a_{4\Delta}\left(\frac{\Delta}{2}\right)^4 + b_{2\Delta}\left(\frac{\Delta}{2}\right)^2\frac{\bar{T}}{T} + d\left(\frac{\bar{T}}{T}\right)^2 + e\left(\frac{K^2}{T^2}\right)_{av} - f\frac{B_{av}}{T^2}\right]\frac{1}{x^2} + o\left(\frac{1}{x^{5/2}}\right). \qquad (11)$$

The coefficients a...f are rational functions of μ, given explicitly in Appendix A. Chemical binding effects enter through the quantities $\bar{T}$, $(K^2)_{av}$, B_{av}. These are simple averages over the phonon frequency spectrum of the moderator. Their properties, and numerical values for several models of graphite, beryllium, and water, are given in Appendix B. For a free gas $\bar{T} = T$, $(K^2)_{av} = \frac{15}{4} T^2$, and $B_{av} = 0$. For $x \gtrsim 10$, the dominant chemical binding effects are given by the $(2 - \mu) \frac{\bar{T}}{T}$ term.

The effective moderating power, $P_\Delta(x)$, corresponding to the above solution can be found readily by expanding $P_\Delta(x)$ in powers of $x^{-\frac{1}{2}}$, and identifying the asymptotic solution of (9) with (11). Define $p(x)$ by $P(x) = \xi \Sigma_f p(x)$. Then

$$
\begin{aligned}
p_\Delta(x) = 1 &+ \alpha_{1\Delta} \frac{\Delta}{2} \frac{1}{x^{1/2}} + \left[\alpha_{2\Delta} \left(\frac{\Delta}{2}\right)^2 - (2-\mu)\left(\frac{\bar{T}}{T} - 1\right) + \mu\right] \frac{1}{x} \\
&+ \left[\alpha_{3\Delta} \left(\frac{\Delta}{2}\right)^3 + \beta_{1\Delta} \frac{\Delta}{2} \left(\frac{\bar{T}}{T} - 1\right) + (\beta_{1\Delta} + \gamma_{1\Delta}) \frac{\Delta}{2}\right] \frac{1}{x^{3/2}} \\
&+ \left[\alpha_{4\Delta} \left(\frac{\Delta}{2}\right)^4 + \beta_{2\Delta} \left(\frac{\Delta}{2}\right)^2 \left(\frac{\bar{T}}{T} - 1\right) + (\beta_{2\Delta} + \alpha_{2\Delta}) \left(\frac{\Delta}{2}\right)^2 + \left(6 - 3\mu + \mu^2 - d - \frac{15}{4} e\right)\right. \\
&\quad \left. + f \frac{B_{av}}{T^2} - e\left\{\left(\frac{K^2}{T^2}\right)_{av} - \frac{15}{4}\right\} + \left(4 - 4\mu + \mu^2 - d\right)\left(\frac{\bar{T}}{T} - 1\right)^2 + \mu\left(\frac{\bar{T}}{T} - 1\right)\right] \frac{1}{x^2} + o\left(\frac{1}{x^{5/2}}\right).
\end{aligned}
$$

(12)

The α, β, γ are functions of μ. Their dependence on the coefficients of (11) is given in Appendix A. In writing (12), the terms which vanish for a free gas have been separated. Several important features of $P_\Delta(x)$ should be noted.

In the heavy free gas limit all coefficients vanish, leaving $p_\Delta(x) = 1$ as expected. Thus the terms of (12) represent corrections to the H.F.G. theory. These are of three types: (a) for free gases

of finite μ, (b) for absorption, (c) for chemical binding. In all cases considered the dominant corrections are given by the $x^{-\frac{1}{2}}$ and x^{-1} terms, and these only will be discussed. Explicitly,

$$\alpha_{1\Delta} = \frac{1+\mu}{1-\frac{1}{3}\mu} - \frac{2\mu}{\xi} \sim \mu \ ,$$

while $\alpha_{2\Delta}$ is negligible for all μ.

(a) For a non-absorbing free gas, the change in p from unity is μ/x. At x = 10, this is small for graphite (~1%), and is a maximum for hydrogen (10%). Since a decrease in P is similar to increased atomic binding, the H.F.G. theory effectively adds some binding relative to the exact free gas theory, and increases the flux at high energies. This has been observed by Sobrino and Clark[2]. It accounts in part for the greater success in calculating spectra in water by the Wilkins theory rather then the Wigner Wilkins theory at these energies[10]. These effects are shown in Figures 1 and 2 for graphite and water (hydrogen).

(b) For an absorbing free gas there is an additional term, $\alpha_{1\Delta} \frac{\Delta}{2} \frac{1}{x^{\frac{1}{2}}} = \alpha_{1\Delta} \frac{\sigma_a(x)}{\mu\sigma_f} \sim \frac{\sigma_a(x)}{\sigma_f}$. This term gives a direct estimate of the sensitivity of p_Δ to absorption. It will be taken that p_Δ is independent of absorption when this term is less than a few per cent for $x \gtrsim 10$. Alternatively, the criterion is, $\Delta < 2$ (graphite) and $\Delta < 0.2$ (hydrogen). This condition is not too stingent, since it allows most problems of practical interest to be solved by the G.H.F.G. theory. The class of acceptable problems is much wider for the heavier moderators. The above criterion probably applies to general absorption (including equivalent leakage). In the derivation of the H.F.G. theory by Horowitz et al.[8], it was assumed that $\sigma_a \sim \mu \sigma_f$, which is equivalent to the above. The

same condition is implied in the use of the diffusion approximation. As in (a), this term effectively adds binding when the H.F.G. theory is used. Figures 1 and 2 illustrate the effect of this term.

(c) The leading chemical binding term decreases the effective moderating power in the proportion that the mean kinetic energy of the moderator nuclei exceeds the mean kinetic energy of a free gas of the same atoms at the same temperature.

The complete expansion (12) is shown graphically in Figures 1 and 2, with and without absorption, using for graphite at room temperature a phonon spectrum derived by Egelstaff (see Section 4(ii)), and for water the Nelkin model[11].

In summary, when the above criterion is satisfied, $p(x)$ is given at high energies by $p_o(x)$, the value of (12) when $\Delta = 0$. p_o is a function only of the moderating properties of the medium.

It should be noted that $P_o(x)$ is not related to the asymptotic expansion of $\xi\Sigma_s(x)$. The latter is[1]

$$\xi\Sigma_s(x) = \xi\Sigma_f\left[1 + C_1(\mu)\frac{\overline{T}}{T}\frac{1}{x} + o\left(\frac{1}{x^2}\right)\right],$$

with

$$C_1(\mu) = \frac{1}{\xi}\left[1 + \frac{1+2\mu-\mu^2}{2\mu}\ln\left(\frac{1-\mu}{1+\mu}\right)\right].$$

Not only does this differ in form from $P_o(x)$, but also in numerical value ($C_1 \to -1$ in the H.F.G. limit, rather than zero).

4. P(x) at Low Energies ($x \lesssim 3$)

Two methods for determining $P(x)$ will be discussed. These are

based on (a) a solution of the Boltzmann equation (2) by a power series expansion about the origin, (b) the reduction of L to a differential operator by a "moments expansion"[8,12].

It is in general useful to remove a Maxwellian distribution from the flux at these energies, and to work with the more slowly varying flux Ψ defined by $\phi(x) = M(x)\Psi(x)$. Using (5), the operator L becomes

$$L\,\phi(x) = M(x)\left[\int_0^\infty \Sigma_s(x\to y)\,\Psi(y)\,dy \;-\; \Sigma_s(x)\,\Psi(x)\right] . \qquad (13)$$

(a) Origin Expansion

This method of solution is an analogue at low energies of Corngold's asymptotic method at high energies. It is not useful in practice, but a brief summary is instructive.

The solution of (2) is sought in the form

$$\Psi(x) = \Psi_0\left[1 + \Psi_1 x^{1/2} + \Psi_2 x + \dots\right] . \qquad (14)$$

This is possible when A(x) may be expanded as

$$A(x) = \frac{1}{x^{1/2}}\left[A_0 + A_1 x^{1/2} + \dots\right] .$$

The expansion coefficients may be functions of $\underline{r}$ and t. Substituting (14) into (13) gives rise to energy weighted moments of the form

$$\bar{M}_n(x,T) = \int_0^\infty \Sigma_s(x\to y,T)\,y^{n/2}\,dy \quad ,$$

which have expansions of the form (see Appendix C)

$$\bar{M}_n(x,T) = \frac{1}{x^{1/2}}\left[\bar{M}_{n0}(T) + \bar{M}_{n2}(T)\,x + \dots\right] . \qquad (15)$$

Using the above expansions in (2), the Ψ_i may be determined as the solution of an infinite set of coupled linear equations. Ψ_1 is given exactly as

$$\Psi_1 = \frac{A_1}{A_0 + \overline{M}_{00}} \quad .$$

It appears that the values of the higher Ψ_i converge slowly with the order of truncation of the set of equations, thus requiring many $\overline{M}_{mn}$, which are very laborious to calculate. When found, the solution (14) will not show clearly its relation to the scattering law. Finally, (15) is essentially an expansion in x/μ (this is true exactly for a free gas), and thus will be useful only for very small energies, especially for the heavier moderators. For these reasons, method (a) was abandoned.

(b) Moments Expansion

L may be expressed as a differential operator by expanding $\Psi(y)$ in (13) in a Taylor series about x. This gives rise to the "moments expansion" [8,12],

$$L(M\Psi) = M(x) \sum_{n=1}^{\infty} \frac{1}{n!} M_n(x,T)\, \Psi^{(n)}(x) \quad , \tag{16}$$

where

$$M_n(x,T) = \int_0^{\infty} \Sigma_s(x \to y, T)\,(y-x)^n\, dy \quad . \tag{17}$$

These energy transfer moments have power series expansions similar to (15).

It can be proved that the series (16) gives rise to the same origin expansion as in (a) whenever $A_i = 0$, i odd. When even values

of i occur, (16) should be replaced by a Taylor expansion in $V = x^{\frac{1}{2}}$, and (17) by velocity transfer moments. However, (16) is a proper expansion for values of x away from the origin, whatever the A_i, and the possible error made near the origin will have little consequence on the flux at important energies. Therefore (16) will be used in all cases.

The convergence of the series in (16), of great importance in the present context, has been little discussed[12]. For a free gas with small μ, M_1 and M_2 are of order μ, while higher moments are of order μ^2. Thus (16) converges over a wide energy range for a heavy free gas. But in general the $(n!)^{-1} M_n(x,T)$ are all comparable in magnitude for $x \lesssim 3$, and are proportional to x^n for large x. The convergence then depends on the $\Psi^{(n)}$, which have to be assessed in each particular problem. For example, for fluxes having a "1/E tail", the $\Psi^{(n)}$ are all equal in the "tail", so that (16) fails at these energies, independently of the magnitude of the "tail". If the flux may be fitted accurately at thermal energies by a Maxwellian distribution with effective temperature T_n, then

$$\Psi^{(n)}(x) = \left(\frac{T_n - T}{T_n}\right)^n \Psi(x) \ , \qquad (18)$$

and the requirement for rapid convergence is that $T_n - T \ll T_n$. In general, one may expect the $\Psi^{(n)}$ to converge at thermal energies when the flux deviates little from a Maxwellian at moderator temperature, that is, when leakage and absorption are small in slowing down problems or when an eigenfunction expansion converges rapidly.

P(x) may be computed from (16), but a more direct method is to

apply the "moments expansion" to q, equation (4), giving

$$q(x) = \sum_{n=1}^{\infty} \frac{1}{n!} F_n(x,T) \Psi^{(n)}(x) \quad , \tag{19}$$

with

$$F_n(x,T) = \int_0^x dy \int_x^{\infty} dz \, \Sigma_s(z \to y, T) M(z) \left[(z-x)^n - (y-x)^n \right] \quad .$$

The F_n are connected by the recurrence relation $F_0(x) = 0$,

$$F_n(x,T) = \int_0^x dy \left[-n F_{n-1}(y,T) + M(y) M_n(y,T) \right] \quad .$$

For large x, $F_n(x,T) \propto (-x)^{n+1} e^{-x}$. Equating (19) to $Q_A \emptyset$ gives immediately

$$P(x) = P_1(x,T) + \sum_{n=2}^{\infty} P_n(x,T) \, \Psi^{(n)}(x) \Big/ \Psi^{(1)}(x) \quad , \tag{20}$$

where

$$P_n(x,T) = \frac{1}{n!} x^{-2} e^{x} F_n(x,T) \quad .$$

Thus P(x) is independent of the problem whenever the summation in (20) is negligible. It is unfortunate that this criterion for the applicability of the G.H.F.G. theory depends on the particular problem. All that can be said in general is that the convergence of (20) is similar to that of (16), since the $P_n(x,T)$ have properties similar to the $(n!)^{-1} M_n(x,T)$. (For a heavy free gas, $P_1 = \xi \Sigma_f$, $P_2 = 0$, and the higher P_n are proportional to μ^2). Thus one may expect the criterion to be satisfied for $x \lesssim 3$ whenever A(x) is small relative to Σ_s. In general, the criterion is more restrictive than that at high energies. However, the examples in later sections will show that many problems of practical

interest may be solved sufficiently accurately by using only the first term of (20).

For this class of problems and $x \lesssim 3$,

$$P(x) = P_1(x,T) = x^{-2} e^{x} \int_0^x y\, e^{-y}\, M_1(y,T)\, dy \quad . \tag{21}$$

The scattering law enters the problem only through the first moment. For a free gas both M_1 and P_1 are analytic functions (Appendix C). The evaluation of M_1 for a bound system is very laborious. The "incoherent gaussian" approximation[13] for the calculation of $\Sigma_s(x \to y)$ is generally accurate enough for this purpose. Then $M_1(x)$ and $P_1(x)$ are given by a single integration over a rational function of $w(t)$, the width function, which is related to the phonon spectrum $\rho(\beta)$ by[13]

$$w(t) = \int_0^\infty \frac{\rho(\beta)\left[\cosh\frac{\beta}{2} - \cos\beta t\right]}{\beta \sinh\frac{\beta}{2}}\, d\beta \quad . \tag{22}$$

(See Appendix C.) Thus there is a direct connection between $\rho(\beta)$ and $P_1(x)$. Because of the double integration, details of $\rho(\beta)$ are less unimportant, and an approximate form of the phonon spectrum suffices.

Figures 1 and 2 illustrate $p_1(x)$ for graphite and water, using for each a free gas and a bound model. The first moments for the latter were calculated[14,15] by a combination of the "phonon expansion" and "short collision time" methods, rather than via the width function (22). Several important features should be noted.

(i) For a free gas $p_1(x)$ differs from unity, reflecting the approximations of the H.F.G. theory. Hurwitz et al.[8] showed that this theory is incorrect for $x \lesssim \mu$, with errors of order μ^2 (or μ in the present context) for other x. This is clear in Figures 1 and 2. In fact, for small x,

$p_1(x) \propto (x/\mu)^{-\frac{1}{2}}$. Equation (C,5) shows that $p_1(x)$ becomes unity as μ vanishes, for all x. Relative to a free gas, the H.F.G. theory gives more binding at very low x and less at higher x. Generally the effect is to harden the thermal neutron spectrum, as observed by Sobrino and Clark for hydrogen[10].

(ii) The effect of chemical binding is simply to reduce the magnitude of the effective moderating power. This is illustrated in Figure 3, which shows the "p_1 ratio", the ratio of the bound p_1 to the free p_1, for graphite, using several Debye models (Θ/T = 1.1, 2.7, 4.0)[16] and the Egelstaff model (at 300°K). The latter is dicussed by Macdougall (this conference). Assuming graphite to be isotropic, Egelstaff fitted the data from the Chalk River scattering law experiment approximately by the use of a phonon spectrum $\rho(\beta)$ proportional to β for $0 < \beta < 0.0253$ ev, and constant for $0.0253 < \beta < 0.1771$ ev = 2050°K.

Figure 3 shows that the effects of chemical binding on the neutron spectrum should be negligible when the moderator physical temperature $T > \Theta$, even though the free gas spectrum $\rho(\beta) = \delta(\beta)$ differs greatly from the bound $\rho(\beta)$. In the presence of strong binding, $T << \Theta$, the form of $\rho(\beta)$ may be more important. For example, it is seen that for T = 300°K the Egelstaff model and Debye model ($\Theta = 4T = 1200$°K) give nearly the same p_1 ratio at thermal energies, but differ at higher energies (the Egelstaff values being less because of the relatively harder phonon spectrum). However, the main difference between the models is in the temperature dependence of $p_1(x)$ (Section 8 (i)).

The influence of absorption on p(x) is shown in Figure 1 (short dashes), where the p_2 term of (20) has been added. This term was

evaluated for a Debye ($\Theta = 4T$) model, $\Psi^{(2)}/\Psi^{(1)}$ being taken from the 293°K Calder Hall spectrum measured by Coates et al.[6]. The effective Δ in this case is approximately 0.75, and the correction is about 12%. Thus P(x) is more sensitive to absorption at low energies than at high.

5. P(x) at Intermediate Energies

In considering the joining of p_1 and p_0 it is of interest to examine the high energy expansion of p_1, derived from the asymptotic form of $M_1(x)$ in Appendix C.

$$p_1(x) = \frac{2\mu}{(1+\mu)^2 \xi}\left\{ 1 + \left[2 - (2-\mu)\frac{\bar{T}}{T}\right]\frac{1}{x} + \left[2-(2-\mu)\frac{\bar{T}}{T} + \frac{1}{8}(1+\mu)(1+\tfrac{1}{3}\mu)\frac{B_{av}}{\bar{T}^2} - \frac{4}{15}\mu\left(1+\tfrac{1}{4}\mu\right)\left(\frac{K^2}{T^2}\right)_{av}\right]\frac{1}{x^2} + O\left(\frac{1}{x^3}\right)\right\}. \quad (23)$$

Its limiting value varies from 0.50 for hydrogen to 0.90 for graphite and unity for a heavy moderator. The first two terms within brackets are identical to the leading terms of $p_0(x)$. The third term differs in form but little in value (less than 0.015 at $x = 10$ for all models considered). Thus, for a heavy moderator, $p_1(x)$ is a good approximation for p(x) at high and low energies, and may be used as a generalization of the H.F.G. theory to include chemical binding at all energies.

For many practical moderators this is too approximate. However, no analytical method for determining P(x) at intermediate energies has been found. Fortunately, these are the very energies for which the flux in slowing down problems is insensitive to P(x) (Section 7 (i)), although this is not true for many eigenvalue problems (Section 11).

If p(x) can be determined for a free gas, then the p_1 ratio, which is correct at high and low energies, may be used for interpolating

approximately between p_1 and p_0 for bound moderators. Using (10), $p(x)$ for a free gas may be calculated from the numerical solution of the infinite medium Boltzmann equation for small $\frac{1}{v}$ absorption, for example. No results are yet available. It is expected that the calculated $p(x)$ will be insensitive to small absorption, as are p_1 and p_0. A rough estimate of $p(x)$ for graphite and hydrogen is shown in Figures 1 and 2 (long dashes). Using these values and the p_1 ratio, the $p(x)$ curves for the Egelstaff and Nelkin models were interpolated and are shown in the same Figures.

The criteria used at high and low energies for determining which problems may be solved by the G.H.F.G. theory, now completely specified, may be used also as a guide at intermediate energies.

6. The Integral Equation

The G.H.F.G. equation (9) may be rewritten as the integral equation

$$\phi(x) = M(x)\left[1 + \int_0^x \frac{e^z \; q(z)}{z^2 \; P(z)} \, dz \right], \qquad (24)$$

with q given by (6). This form is well suited for iterative methods of solution, and for qualitative discussions of the sensitivity of neutron spectra to $P(x)$. It is a generalization to include chemical binding of the H.F.G. integral equation derived by Hurwitz et al.[8].

7. Sensitivity of Infinite Medium Spectra to Scattering Law

(i) Sensitivity Function

Egelstaff[5] has discussed the use of "sensitivity functions" to display the sensitivity of neutron spectra to the scattering law. For a weakly absorbing infinite medium he has recommended a function first

proposed by Horowitz and Tretiakoff[17]. The spectrum is written as a Maxwellian plus perturbation.

$$\phi(x) = M(x) + 2r E(x) . \tag{25}$$

E(x) is a function tending to $\frac{1}{x}$ for large x, and r measures the strength of the "tail". Egelstaff determines E(x) by requiring that the total neutron density should be accounted for by the Maxwellian. In general, this means that for the same number of neutrons slowing down, but different scattering laws, r assumes different values. The authors believe that E(x) would be a more genuine sensitivity function if the Maxwellian accounted instead for the total absorption, giving equal r values for all laws. For $\frac{1}{v}$ absorbers the prescriptions are identical.

For weak absorption, the relationship between E(x) and P(x), or the scattering law, may be derived readily by solving the integral equation (24) by interation. The first interate is sufficient, and is obtained by setting ϕ equal to M in q on the R.H.S. Hurwitz et al.* have discussed this solution in the special case $P(x) = 2\mu\Sigma_f$ (H.F.G.) and $\sigma_a(x) = \sigma_{ao} x^{-\frac{1}{2}}$. Using their notation, and the same cross section for the purpose of illustration, the flux may be written

$$\phi(x) = M(x) + A \frac{\Delta}{4} \frac{H(x)}{x} , \tag{26}$$

where

$$H(x) = x^2 e^{-x} \int_0^x dz \, \frac{2\mu\Sigma_f e^z}{P(z)\, z^2} \int_0^z dt \, t^{1/2} e^{-t} . \tag{27}$$

A is inserted to conserve neutrons, and has the value

$$A = \left(1 - \frac{W\Delta}{2\pi^{1/2}}\right)^{-1},$$

where

$$W = \int_0^\infty x^{-3/2} H(x)\, dx \quad .$$

This is a valid renormalization only for small ΔW. The sensitivity function for the solution (26) is easily found to be

$$2\pi E(x) = \frac{\Delta}{4}\left[\frac{H(x)}{x} - \frac{2W}{\pi^{1/2}} M(x)\right] . \qquad (28)$$

An inspection of (27) shows that $H(x)$ is sensitive to $P(x)$, and hence $M_1(x)$, at low x; becomes insensitive to $P(x)$ at intermediate energies $4 \lesssim x \lesssim 8$; and is sensitive to $P(x)$ at high energies because of the e^x factor. W is most sensitive to $P(x)$ for low x. $E(x)$ is determined by W at small x, and by $H(x)$ at intermediate and high x. One may conclude that the most important aspects of the scattering law for slowing down spectra in media of weak absorption (or leakage) are $\bar{T}$ and the low x values of $M_1(x)$.

As an example, a comparison is made between the H.F.G. theory and a Debye theory, taking $P(x)/2\mu\Sigma_t$ as unity, and as the p_1 ratio for a Debye solid of mass 12 and $\Theta = 4T$ (see Figure 3), respectively. The latter is an approximate model for graphite at room temperature. Figure 4 shows $H(x)$ in each case, the H.F.G. result being taken from reference 8. Δ was chosen as 0.1. The two values of W are 2.83 and 7.63. The large differences in H are reflected also in $2\pi E(x)$, plotted in Figure 5, which demonstrates the importance of chemical binding to spectra in graphite. Each model gives the same flux at $x \sim 2$, a result observed also by

Clendenin[18] for spectra in free gases over a wide range of atomic mass. The present results are in great contrast to the two examples of $E(x)$ shown by Egelstaff[3].

(ii) Absorption Heating

In many problems the flux may be fitted to a good approximation at thermal energies by a displaced Maxwellian of effective temperature T_n. A simple relationship may be found between T_n, absorption, and scattering law.

Using (16) and (18)

$$\frac{\Sigma_a(kT)}{M_1(kT)} = \sum_{n=1}^{\infty} \frac{M_n(kT)}{n!\, M_1(kT)} \left(\frac{T_n - T}{T_n}\right)^n .$$

For small absorption one finds

$$T_n \simeq T\left(1 + \frac{\Sigma_a(kT)}{M_1(kT)}\right) . \qquad (29)$$

As noted earlier, the coefficients in the above series are of order unity. If they were exactly unity, the series may be summed, and (29) is obtained exactly. Thus (29) is also valid for stronger absorption. This useful approximation has been confirmed for many calculated spectra fitted in the range $\frac{1}{4} \lesssim x \lesssim 3$. It is clear that the shift in effective temperature is sensitive to chemical binding, being for example two and a half times as large for a Debye model ($\Theta = 4T$) as for a free gas model for graphite at room temperature.

For a H.F.G. (29) gives

$$T_n \simeq T\left(1 + 0.50\, \frac{\Sigma_a(kT)}{\mu \Sigma_s}\right) .$$

Cohen[12], using an approximate analytical method, found a coefficient of 0.60, while Coveyou et al.[19], using Monte Carlo techniques, found a value 1.1 over a wide range of μ. (An inspection of their results for the heavier gases only, Table I of reference 12, shows the coefficient is closer to 0.8. This result is probably too high as the flux was fitted over the range $0 \leq x \leq 3.6$, which is too long in view of the strong absorption used.)

8. Experimental Determination of P(x)

Using a time-of-flight technique, Coates and Gaylher[6] have measured the neutron spectrum in a graphite moderated (Calder Hall) lattice, and Beyster et al.[7] the spectrum in a homogeneous "poisoned" water assembly. Their results will be used in (10) to find an experimental P(x), which is then compared with theory.

(i) Graphite

The spectrum was measured at the boundary of the lattice pitch. This flux was converted into a mean moderator flux $\bar{\phi}(x)$ by multiplying it by the ratio of mean to boundary flux derived numerically from a multi-group heterogeneous calculation for the same cell using the machine code mentioned in the Introduction. (This ratio is insensitive to scattering model.) $\bar{q}$ was found from (6) using $\Sigma_{ae}(x) + D_g B_m^2$ for A(x). Here the effective absorption is

$$\Sigma_{ae}(x) = \Sigma_{ago}\, x^{-1/2} + \Sigma_{af}(x)\, \frac{V_f\, \bar{\phi}_f(x)}{V_g\, \bar{\phi}(x)} \quad ,$$

which is rigorous when diffusion theory is used in the moderator. Σ_{ago} is the 2200 m./sec. absorption cross-section for graphite, V is volume, f stands for fuel. The fuel absorption was taken fron BNL 325. DB_m^2

has the value 0.0002 cm^{-1}. An approximate value of $\bar{\phi}_f/\bar{\phi}$ was found from the machine calculation mentioned above. It was found that the calculated $\bar{q}$ at 5 ev was within 1% of the number of neutrons slowing down at 5 ev in the measured spectrum, both at 293°K and 594°K. This shows that the problem has been reduced satisfactorily to an infinite medium problem.

The experimentally determined values of p(x) at 293°K and 594°K are illustrated in Figure 6. Estimated errors are indicated. Very little value can be attached to the results at intermediate energies because of the insensitivity of the flux at these energies to p(x) (Section 7 (i)), resulting in a large cancellation in the denominator of (10), which magnifies the experimental errors. The theoretical (Egelstaff) curve at 300°K is also shown, reproduced from Figure 1.

At high energies $20 < x < 200$ it was found by a least squares fit to the experimental data that

$$\frac{\bar{T}}{T} = \begin{matrix} 2.07, & 293^{\circ}K \\ 1.24, & 594^{\circ}K \end{matrix} ,$$

with a standard deviation of $\pm$ 0.5. The Egelstaff phonon spectrum gives 2.06 and 1.29 respectively, in good agreement. If a Debye model were used, the corresponding effective temperature would be $\Theta = 5.18T = 1518^{\circ}K$ and $\Theta = 2.24T = 1330^{\circ}K$. The Krumhansl Brooks model gives[3] 2.36 and 1.43, thus predicting too much binding.

At thermal energies the Egelstaff model again gives good agreement at room temperature, particularly when absorption corrections are made to p(x). A Debye model would fit the experimental results with $\Theta = 4T = 1172^{\circ}K$ for room temperature, and $\Theta = 2.2T = 1307^{\circ}K$ for the higher temperature. The Krumhansl Brooks model predicts nearly twice too much binding (not illustrated).

It is clear that a single Debye temperature will not fit all the experimental results.

The two converted experimental spectra $\bar{\phi}$ may be fitted accurately by displaced Maxwellian fluxes, with $\frac{T_n}{T}$ = 1.191 at 293°K and 1.079 at 594°K. These values may be compared with the formula (29). For a free gas of mass 12, the corresponding values are 1.080 and 1.064, while the Egelstaff model gives 1.203 and 1.081 respectively. The latter is again in good agreement.

Macdougall (this conference) has calculated these two spectra using the Egelstaff model and finds a good fit with experiment, in confirmation of the above analysis.

(ii) Water

The experimental spectrum[7], with 3.15 barns of $\frac{1}{v}$ absorber per hydrogen atom, was used to calculate p(x). The result is shown in Figure 2. Again the sensitivity of p(x) to the experimental errors at intermediate energies is apparent. Nelkin's theory is in agreement, within experimental error, for x > 1. At smaller x it is evident that $M_1(x)$ is overestimated by the Nelkin theory. Since the experimental $\Psi(x)$ was linear for 0.1 < x < 1, this discrepancy cannot be accounted for by absorption corrections to the theoretical $p_1(x)$. Rather, it is probably due to the neglect of molecular translational impedance in the model. Using the linearity of $\Psi(x)$, $M_1(x)$ may be deduced directly from the experimental results. It is found that for x < 1,

$$M_1(x) = 9.3\ x^{-1/2}\left(1 + 0.34\ x + \dots\right).$$

Nelkin gives[14]

$$M_1(x) = 11.4\, x^{-1/2} \left(1 + 14.5\, x + \ldots\right),$$

for $x < 0.1$, while for free hydrogen,

$$M_1(x) = 22.9\, x^{-1/2} \left(1 - \tfrac{1}{3} x + \cdots\right),$$

for $x < 0.5$.

It is clear from Figure 2 why the H.F.G. model gives a better description of water spectra than the free gas model. At both high and low energies it effectively accounts for some binding. The research of Sobrino and Clark[10] confirms this conclusion.

9. Lattice Calculations - ηf

A quantity of importance in reactor calculations is ηf, the number of fission neutrons produced at thermal energies per neutron slowing down in a reactor lattice cell past some reference energy. It is of interest to know the sensitivity of ηf to the moderator scattering law.

To illustrate this, the neutron spectrum in a graphite moderated (Calder Hall) lattice cell was computed using the G.H.F.G. theory, diffusion theory in the moderator, and a "blackness" boundary condition on the fuel surface. Three models of graphite were used; the H.F.G. of mass 12, and the experimental P(x) for 293°K and 505°K (characteristic operating moderator temperature). The latter P(x) was derived by interpolation from the (smoothed) experimental curves. Irradiations of 0 and 400 MWD/Te were considered. The threshold energy was 0.9 ev. Sixty-four energy mesh points were used.

The standard fuel absorption cross-sections were taken from BNL 325 (Second Edition, July, 1958). To test the sensitivity of ηf to experimental inaccuracies in the fission cross-sections, three sets of these were used: (α), as computed from the measured α-ratios (of capture to fission) given in BNL 325, Supplement No. 1 to Second Edition, January 1960, and the standard capture cross-section; (β), the same, but α-ratios taken from the 1958 edition; (γ), as read directly from the fission cross-section curves of the 1958 edition.

The results are shown in Table 1 below. They may be compared

TABLE 1

Model	MWD/Te	T °K	ηf α	ηf β	ηf γ	Temperature Coefficient mn/°C α	Temperature Coefficient mn/°C β	Temperature Coefficient mn/°C γ
Gas	0	293	-	-	1.2222	-	-	-5.12
	0	505	1.2359	1.2210	1.2106	-3.63	-3.13	-2.65
	400	505	1.2570	1.2439	1.2394	+2.01	+2.57	+3.00
P(x) Experimental	0	293	-	-	1.2211	-	-	-5.64
	0	505	-	-	1.2098	-	-	-2.49
	400	505	-	-	1.2314	-	+3.24	+3.91

directly with the calculations of Macdougall (this conference) on the same system, but using the Winfrith DSN code. In absolute value the ηf differ by a few per cent, reflecting the absence of the canning material in the present calculations. In passing from a gas to a bound model at zero irradiation, ηf drops by 0.09% at 293°K and by 0.06% at 505°K, in good agreement with Macdougall. This change is negligible for reactor calculations. However, at the higher irradiation, the drop is 0.65%, which is important to this type of reactor. The

explanation is that the α-ratio of U^{235} has nearly a zero energy gradient, but that for Pu^{239} a steep positive gradient. Thus, hardening of the spectrum due to the influence of chemical binding is important when Pu is present, but not in virgin fuel.

The Table shows that uncertainties in cross-sections may affect ηf by about $\pm 1\%$, which is as large as the binding effects.

10. Temperature Coefficients of ηf

The above cases were recalculated with the moderator temperature raised by 100 C^{o}. $\frac{1}{\eta f}\frac{d\eta f}{dT}$ was estimated from the difference in ηf (and strictly refers to a temperature 50 C^{o} above the temperature shown in the Table). The results are given in Table 1, in units of $mn/^{o}C$ ($10^{-5}/^{o}C$). At zero irradiation the coefficients agree very well with Macdougall's (when calculated over the same temperature range), and the difference in the coefficient due to binding is also comparable. It is seen that chemical binding can change the coefficient by up to 1 $mn/^{o}C$, which is not serious for reactor control. The uncertainties in the coefficient due to possible inaccuracies in the cross-section data are about the same size. As with ηf, the latest data gives the most optimistic estimate.

Temperature coefficients associated with the minor moderators in the lattice, such as the fuel and canning material, are very sensitive to the scattering law of these materials, especially if they are closely associated with the fuel. It has been found in many calculations that these temperature coefficients are roughly proportional to the average value of $P(x)$ in the thermal region.

11. Eigenfunctions

The G.H.F.G. operator L_A has been determined in terms of the scattering law in previous Sections. The eigenfunctions ϕ_n and eigenvalues $\lambda_n \xi \Sigma_f$ of this operator are defined by the equation

$$\frac{d}{dx} p(x) \left(x \frac{d}{dx} + x - 1 \right) \phi_n(x) = -\lambda_n \phi_n(x) . \qquad (30)$$

It is of interest to know whether these will be good approximations to the eigenfunctions and eigenvalues of L.

For a H.F.G. ($p = 1$) the ϕ_n are the generalized Laguerre functions $M(x) L_n^{(1)}(x)$ and $\lambda_n = n$. The solution of (30) may be expanded over the complete set $M(x) L_n^{(1)}(x)$.

$$\phi_n(x) = \sum_{m=1}^{\infty} a_m^n \; L_m^{(1)}(x) \, M(x) . \qquad (31)$$

$\phi_0 = M(x)$. The $L_m^{(1)}(x)$ are polynomials of degree m in x. Referring to equation (20) it is clear that the solutions of (30) will be good approximations only when the a_m^n for $m \geq 2$ are negligible. Thus second and higher eigenfunctions of L are likely to be given inaccurately by (30). In fact, (30) will be useful only for those first eigenfunctions which have a predominant $L_1^{(1)}$ component. Now, for free hydrogen, $|a_2^1|$ is about one-half of a_1^1. Therefore (30) must be restricted to heavy moderators. Also, chemical binding must be "weak", since it increases $|a_2^1|$. In practice it has been found that ϕ_1 and λ_1 may be obtained with sufficient accuracy from (30) for the heavier practical moderators, such as beryllium and graphite. For other eigenvalue problems the G.H.F.G. theory has not been found useful.

A few remarks should be made about the sensitivity of λ_1 to the

scattering law. In general the λ_n are solutions of the determinantal equation

$$\left| b_{mn} - \lambda \delta_{mn} \right| = 0 \quad , \tag{32}$$

obtained from (31) and (30). Here

$$b_{mn} = \frac{1}{(n+1)(\overline{n+1}!)^2} \int_0^\infty x^2 e^{-x} \left[\frac{d}{dx} L_m^{(1)}(x) \right] p(x) \left[\frac{d}{dx} L_n^{(1)}(x) \right] dx \quad . \tag{33}$$

Restricting attention to the heavier moderators, it is sufficient to truncate (32) to

$$\begin{vmatrix} b_{11} - \lambda & b_{12} \\ b_{21} & b_{22} - \lambda \end{vmatrix} = 0 \tag{34}$$

For these moderators b_{12} is generally small so that λ_1 has the approximate value

$$\lambda_1 \simeq b_{11} + \frac{6\, b_{21}^2}{b_{11} - b_{22}} \quad . \tag{35}$$

It can easily be shown that b_{11} is one quarter of the Maxwellian averaged second moment. b_{21} and b_{22} are more complicated averages over $M_2(x)$ and $M_4(x)$.

Table 2 gives values of λ_1 calculated from (34) and (35) for several models of graphite and beryllium. The b_{ij} were derived from (33), using the appropriate $p(x)$ curves from Figures 1 and 6 for graphite, and similar curves for beryllium. b_{11} is also tabulated. It is seen that b_{11} generally overestimates λ_1 by only a few per cent. λ_1 is very sensitive to the scattering law.

The G.H.F.G. has been quite successful in solving problems

TABLE 2

Model	b_{11}	λ_1 Exact (34)	λ_1 Approximate (35)
Be, free gas	0.961	0.960	0.960
Be, Debye ($\theta = 2.7T$)	0.689	0.657	0.656
Graphite, free gas	0.969	0.969	0.969
Graphite, Experimental (293°K)	0.491	0.452	0.450
Graphite, Experimental 594°K)	0.747	0.740	0.740

involving non-absorbing differentially heated media (Kottwitz type of problem). λ_1 is then the rethermalization cross section. This work will be reported elsewhere.

Acknowledgments

The authors are grateful to H. Pitcher, J. MacdougalI, H. Honeck, and M. S. Coates for communicating their results; and to D. Butler for supplying the information in Appendix C. They have had helpful discussions with D. C. Leslie of the A.E.A., Winfrith, in the early stages of this study. The English Electric Company have generously provided facilities and encouragement.

Appendix A

The coefficients in equation (11) are the following functions of μ, derived from equations (2) and (3) of reference 1.

$$a_{1\Delta}(\mu) = \frac{1+\mu}{1-\frac{1}{3}\mu}$$

$$a_{2\Delta}(\mu) = \frac{1}{2}\,\frac{(1+\mu)^3}{1-\frac{1}{3}\mu}$$

$$a_{3\Delta}(\mu) = \frac{1}{6}\,\frac{(1+\mu)^6}{(1-\frac{1}{3}\mu)(1+\frac{1}{3}\mu+\frac{1}{3}\mu^2-\frac{1}{15}\mu^3)}$$

$$b_{1\Delta}(\mu) = \frac{19}{6}\,\frac{(1+\frac{2}{3}\mu-\frac{10}{57}\mu^2-\frac{7}{57}\mu^4+\frac{2}{57}\mu^5)}{(1-\frac{1}{3}\mu)(1+\frac{1}{3}\mu+\frac{1}{3}\mu^2-\frac{1}{15}\mu^3)}$$

$$a_{4\Delta}(\mu) = \frac{1}{24}\,\frac{(1+\mu)^{10}}{(1-\frac{1}{3}\mu)(1+\frac{1}{3}\mu+\frac{1}{3}\mu^2-\frac{1}{15}\mu^3)(1+\frac{2}{3}\mu+\mu^2)}$$

$$b_{2\Delta}(\mu) = \frac{1}{24}\,\frac{(1+\mu)^3(55+\frac{23}{3}\mu+\frac{136}{3}\mu^2-\frac{266}{15}\mu^3+\frac{121}{15}\mu^4(1-\mu)+\frac{22}{15}\mu^6}{(1-\frac{1}{3}\mu)(1+\frac{1}{3}\mu+\frac{1}{3}\mu^2-\frac{1}{15}\mu^3)(1+\frac{2}{3}\mu+\mu^2)}$$

$$d(\mu) = 6\,\frac{(1-\frac{1}{2}\mu)(1-\mu+\mu^2-\frac{1}{3}\mu^3)}{(1+\frac{2}{3}\mu+\mu^2)}$$

$$e(\mu) = \frac{8}{3}\,\frac{\mu(1-\frac{3}{8}\mu+\frac{3}{20}\mu^2+\frac{1}{40}\mu^3)}{(1+\frac{2}{3}\mu+\mu^2)}$$

$$f(\mu) = \frac{5}{8}\,\frac{(1+\mu)(1-\frac{1}{3}\mu+\frac{1}{3}\mu^2+\frac{1}{15}\mu^3)}{(1+\frac{2}{3}\mu+\mu^2)}$$

The α, β, and γ of equation (12) are derived from the above functions by the following relations:

$$\alpha_{1\Delta} = a_{1\Delta} - \frac{2\mu}{\xi} \qquad (1)$$

$$\alpha_{2\Delta} = a_{1\Delta}\left[\, a_{1\Delta} - \frac{\mu}{\xi} - \frac{a_{2\Delta}}{a_{1\Delta}} \,\right] \qquad (2)$$

$$\alpha_{3\Delta} = \alpha_{2\Delta}\, a_{1\Delta} - \alpha_{1\Delta}\, a_{2\Delta} + a_{3\Delta} - \frac{2}{3}\, a_{2\Delta}\, \frac{\mu}{\xi} \qquad (3)$$

$$\beta_{1\Delta} = -(2-\mu)\left(a_{1\Delta} + \alpha_{1\Delta} + \frac{2}{3}\frac{\mu}{\xi}\right) + b_{1\Delta} \qquad (4)$$

$$\gamma_{1\Delta} = 2(a_{1\Delta} + \alpha_{1\Delta}) - \frac{5}{2} a_{1\Delta} \qquad (5)$$

$$\alpha_{4\Delta} = \alpha_{3\Delta} a_{1\Delta} - \alpha_{2\Delta} a_{2\Delta} - a_{4\Delta} + a_{3\Delta}\left(\alpha_{1\Delta} + \frac{1}{2}\frac{\mu}{\xi}\right) \qquad (6)$$

$$\beta_{2\Delta} = \beta_{1\Delta} a_{1\Delta} + (2-\mu)(a_{2\Delta} - \alpha_{2\Delta}) - b_{2\Delta} + b_{1\Delta}\left(\alpha_{1\Delta} + \frac{1}{2}\frac{\mu}{\xi}\right) \qquad (7)$$

Appendix B

The quantities $\bar{T}$, B_{av}, $(K^2)_{av}$ introduced in equation (11) are related to the phonon frequency spectrum $\rho(x)$ of an isotropic "solid" by[1]

$$\bar{T} = \frac{T}{2}\int_0^\infty \rho(x)\, x \coth\left(\frac{x}{2}\right) dx \quad , \qquad (1)$$

$$B_{av} = T^2 \int_0^\infty x^2 \rho(x)\, dx \quad , \qquad (2)$$

$$(K^2)_{av} = \frac{15}{4}\left(\bar{T}\right)^2 \quad . \qquad (3)$$

Examples of these quantities for some moderators of interest in this paper are given in Table 3 below.

TABLE 3

Model	$\frac{\bar{T}}{T}$	$\frac{B_{av}}{T^2}$	$\left(\frac{K^2}{T^2}\right)_{av}$
Graphite (Egelstaff, 300°K)	2.063	4.394	15.96
Water (Nelkin, 293°K)	4.345	126.09	53.63
Debye (Θ = 1.1T)	1.065	0.726	4.253
Debye (Θ = 2.7T)	1.33	4.374	6.633
Debye (Θ = 4.0T)	1.68	9.60	10.58

Appendix C

D. Butler [20] has shown how to calculate $M_1(x)$ directly from the width function $w(t)$, equation (22). The basic equations are given in reference 13, hereafter called I. The differential cross section I (2.1) is substituted into (17) for $M_1(x)$. For $S(\alpha,\beta)$ we use the "gaussian" approximation I (3.2). The angular integration is performed readily, followed by a laborious but straightforward energy integration. This leaves a single time integration, and gives finally the desired result,

$$M_1(x) = \frac{(1+\mu)^2 \Sigma_f}{4(\pi x)^{1/2}} \int_{-\infty}^{\infty} dt \left\{ \frac{\frac{3}{2} - 2x\left(\frac{1}{2}-it\right)}{W(t)^{5/2}} + \frac{x\left(\frac{1}{2}-it\right)^2}{W(t)^{7/2}} \right\} \exp\left[\frac{-x\left(t^2+it-\frac{1}{4}\right)}{W(t)} \right], \quad (1)$$

where

$$W(t) = \mu w(t) + \frac{1}{2} - it \quad .$$

For a free gas $w(t) = t^2 + \frac{1}{4}$. With this simplification it is possible to integrate (1) by contour integration to give

$$M_1(x) = \frac{\mu \Sigma_f}{4(1+\mu)^2(\pi\beta)^{1/2}} \left[R(\beta)\, e^{-\beta} + S(\beta) \left(\frac{\pi}{\beta}\right)^{1/2} erf\left(\beta^{1/2}\right) \right], \quad (2)$$

where $\beta = \frac{x}{\mu}$, and

$$R(\beta) = 4\left[4 - \mu(1 + 2\beta)\right],$$

$$S(\beta) = 2\left[4 + 8\beta + \mu(1 - 4\beta - 4\beta^2)\right].$$

The asymptotic expansion of $M_1(x)$ is [1]

$$M_1(x) = \frac{2\mu\Sigma_f x}{(1+\mu)^2} \left[1 - (2-\mu)\frac{\bar{T}}{T}\frac{1}{x} + \left\{ \frac{(1+\mu)(3+\mu)}{24}\frac{B_{av}}{T^2} - \frac{\mu(4+\mu)}{15}\left(\frac{K^2}{T^2}\right)_{av} \right\} \frac{1}{x^2} + \cdots \right]. \quad (3)$$

$P_1(x)$ is related to $M_1(x)$ by (21). Using the form (0,1) for M_1, the integration in (21) may be done, giving

$$x^2 e^{-x} P_1(x) = \frac{(1+\mu)^2 \Sigma_f}{4(\pi)^{1/2}} \int_{-\infty}^{\infty} dt \left[\frac{3(\pi)^{1/2} i t}{2\left(\mu w(t) + \frac{1}{4}\right)} \operatorname{erf}\left(\sqrt{\alpha x}\right) \right.$$

$$\left. - x^{1/2} \left(\frac{3 i t}{W(t)^{1/2} \left(\mu w(t) + \frac{1}{4}\right)} - \frac{x}{\alpha} \right) \exp(-\alpha x) \right], \quad (4)$$

with

$$\alpha = 1 - \frac{\left(\frac{1}{2} - i t\right)^2}{W(t)} \quad .$$

This simplifies greatly for a free gas, becoming

$$P_1(x) = \frac{\mu \Sigma_f}{2(1+\mu)^2} \left[\left(t + 2t^3\right) \frac{2}{\pi^{1/2}} e^{-t} + \left(4t^4 + 4t^2 - 1\right) \operatorname{erf}(t) \right] \frac{1}{t^4} \quad , \quad (5)$$

with $t = \left(\frac{x}{\mu}\right)^{\frac{1}{2}}$.

References

1. N. Corngold, Annals of Physics 11, 338 (1960).
2. L. de Sobrino, M. Clark, Nuc. Sci. and Eng. 10, 384 (1961).
3. D. E. Parks, Nuc. Sci. and Eng. 9, 430 (1961).
4. J. Horowitz, private communication via D. C. Leslie.
5. P. A. Egelstaff, Nuc. Sci. and Eng. 12, 250 (1962).
6. M. S. Coates, D. B. Gayther, Report A.E.R.E. - R 3829 (1961)
7. J. R. Beyster, J. L. Wood, W. M. Lopez, R. B. Walton, Nuc. Sci. and Eng. 9, 168 (1961).
8. H. Hurwitz, M. S. Nelkin, G. J. Hebetler, Nuc. Sci. and Eng. 1, 280 (1956).
9. N. Corngold, Annals of Physics 6, 368 (1959).
10. L. de Sobrino, M. Clark, Nuc. Sci. and Eng. 10, 377 (1961).
11. M. S. Nelkin, Phys. Rev. 119, 741 (1960).
12. E. R. Cohen, Proc. 1st Intern. Conf. Peaceful Uses Atom. Eng., Geneva, 5, 405 (1955).
13. P. A. Egelstaff, P. Schofield, Nuc. Sci. and Eng. 12, 260 (1962).
14. H. Honeck, private communication of $M_1(x)$ for Nelkin model of water.
15. J. D. Macdougall, private co munication of $M_1(x)$ for Egelstaff model of graphite at 300°K.
16. H. Pitcher, private communication of $M_1(x)$ for the Debye model of graphite.
17. J. Horowitz, O. Tretiakoff, Report EANDC(E) 14 (1960).
18. W. Clendenin, J. Nuc. Energy, A13, 25 (1960).
19. R. Coveyou, R. Bate, R. Osborn, J. Nuc. Energy 2, 153 (1956).
20. D. Butler, private communication.

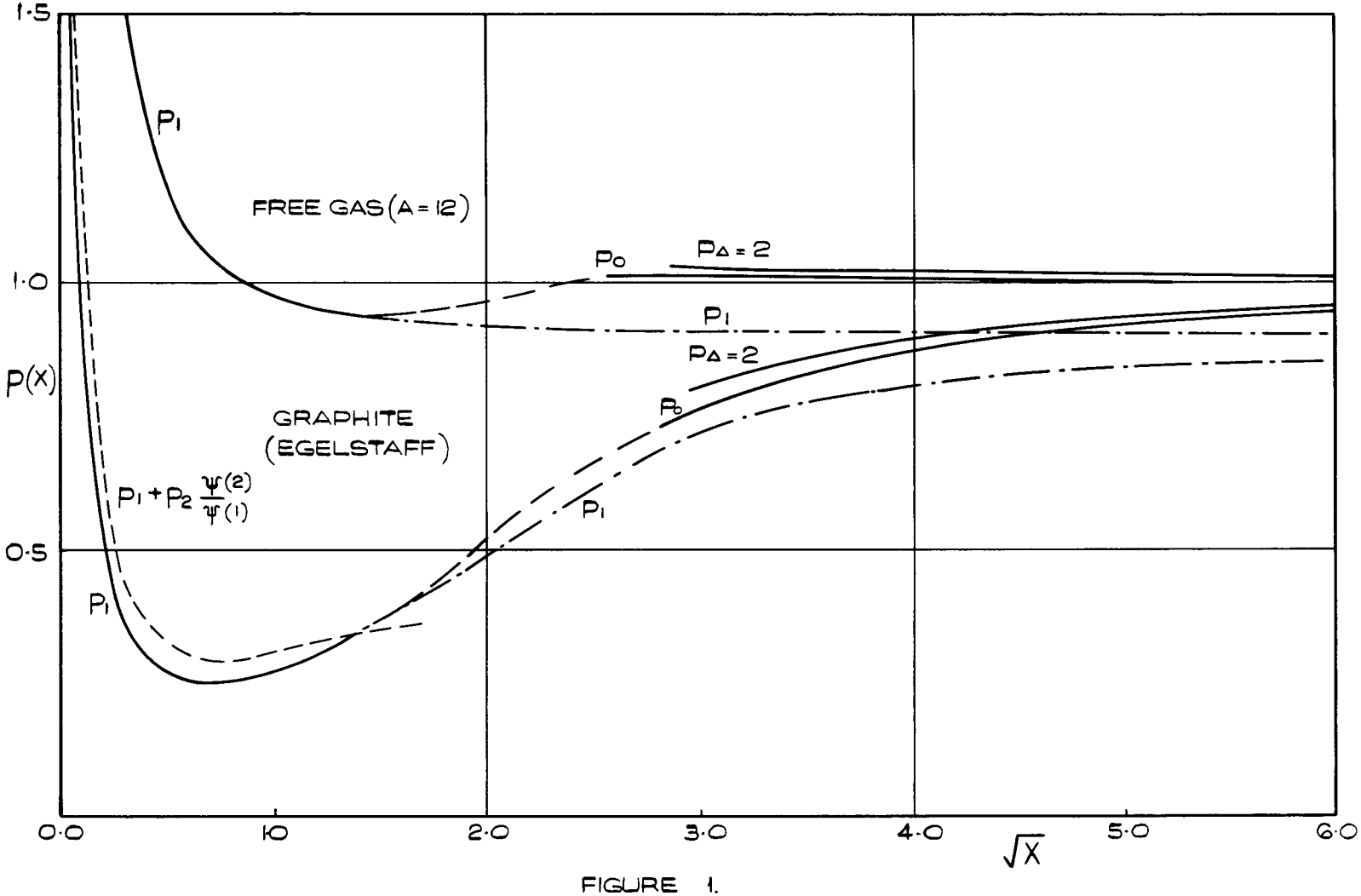
1·5
1·0
0·5
P(X)
P1
FREE GAS (A = 12)
P0
PΔ = 2
P1
PΔ = 2
P0
GRAPHITE
(EGELSTAFF)
P1 + P2 Ψ(2)/Ψ(1)
P1
P1
0·0
1·0
2·0
3·0
4·0
5·0
6·0
√X

FIGURE 1.

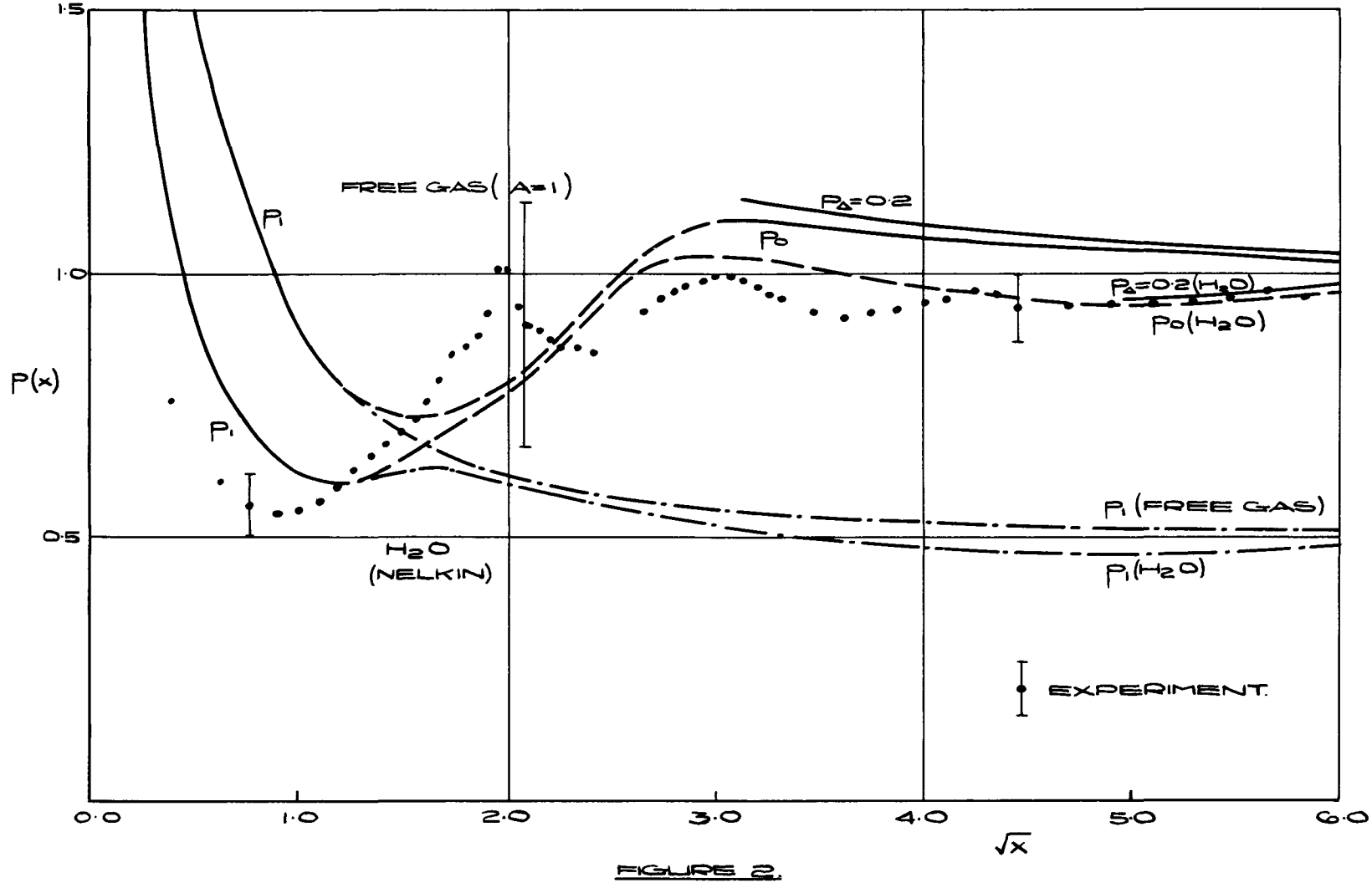
1·5
1·0
0·5
P(x)
FREE GAS (A=1)
P₁
P₀
P₂=0·2
P₂=0·2(H₂O)
P₀(H₂O)
P₁
P₁ (FREE GAS)
H₂O
(NELKIN)
P₁(H₂O)
EXPERIMENT
0·0
1·0
2·0
3·0
4·0
5·0
6·0
√x

FIGURE 2.

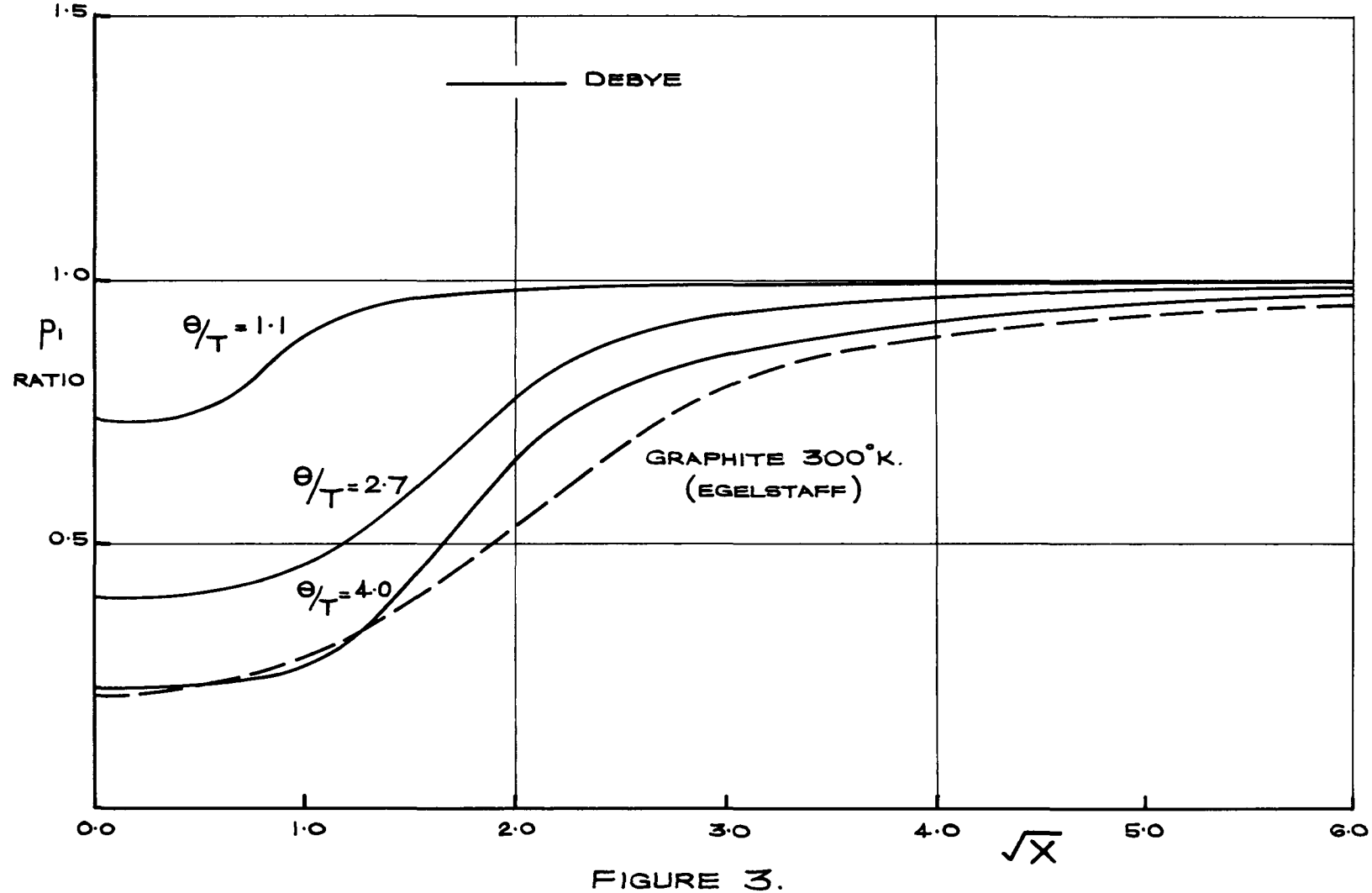
1·5
1·0
0·5
P1
RATIO
DEBYE
θ/T = 1·1
θ/T = 2·7
θ/T = 4·0
GRAPHITE 300°K.
(EGELSTAFF)
0·0
1·0
2·0
3·0
4·0
5·0
6·0
√X

FIGURE 3.

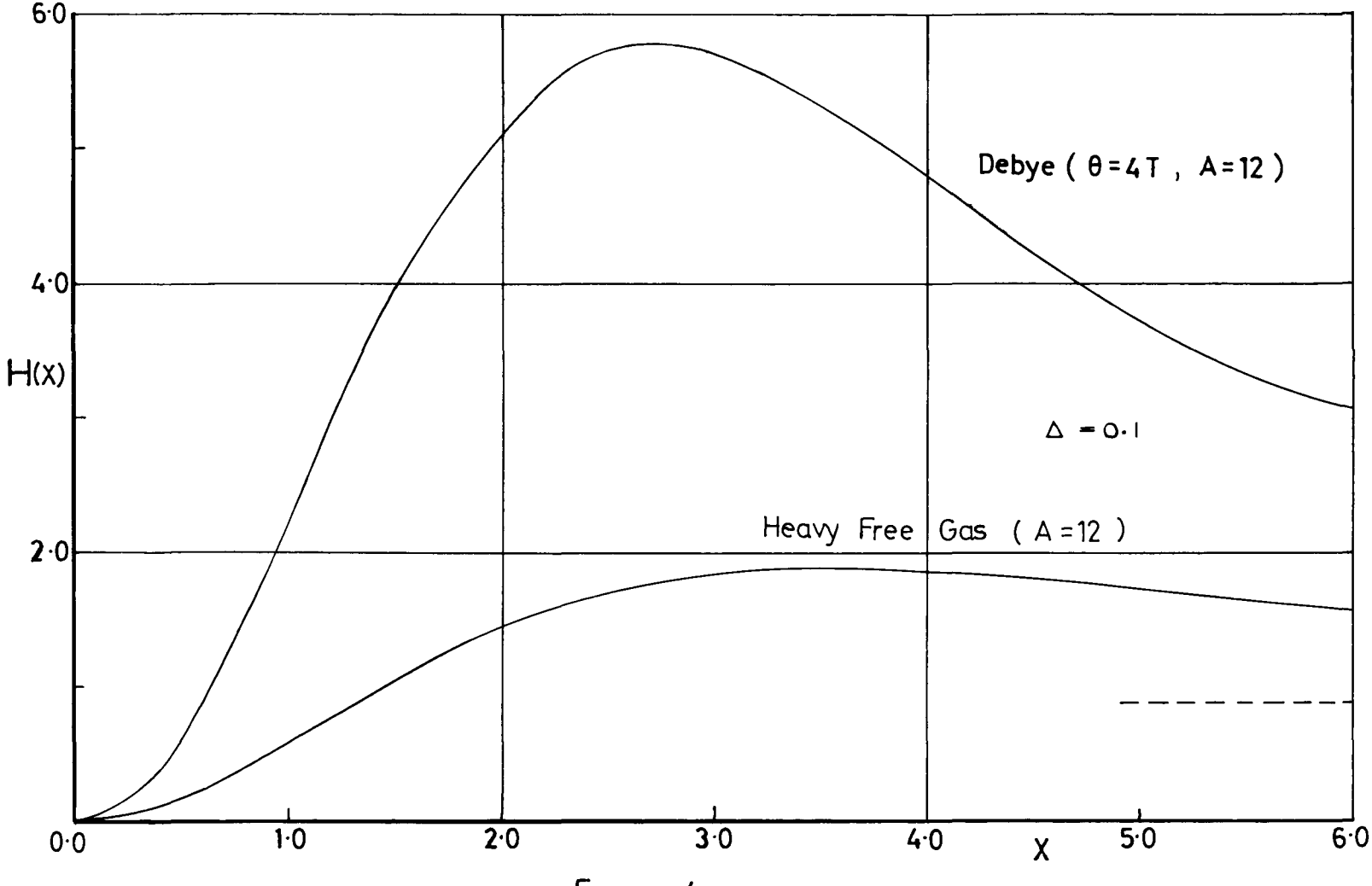
6·0
4·0
2·0
H(X)
0·0
1·0
2·0
3·0
4·0
X
5·0
6·0
Debye (θ = 4 T , A = 12)
Δ = 0·1
Heavy Free Gas (A = 12)

Figure 4

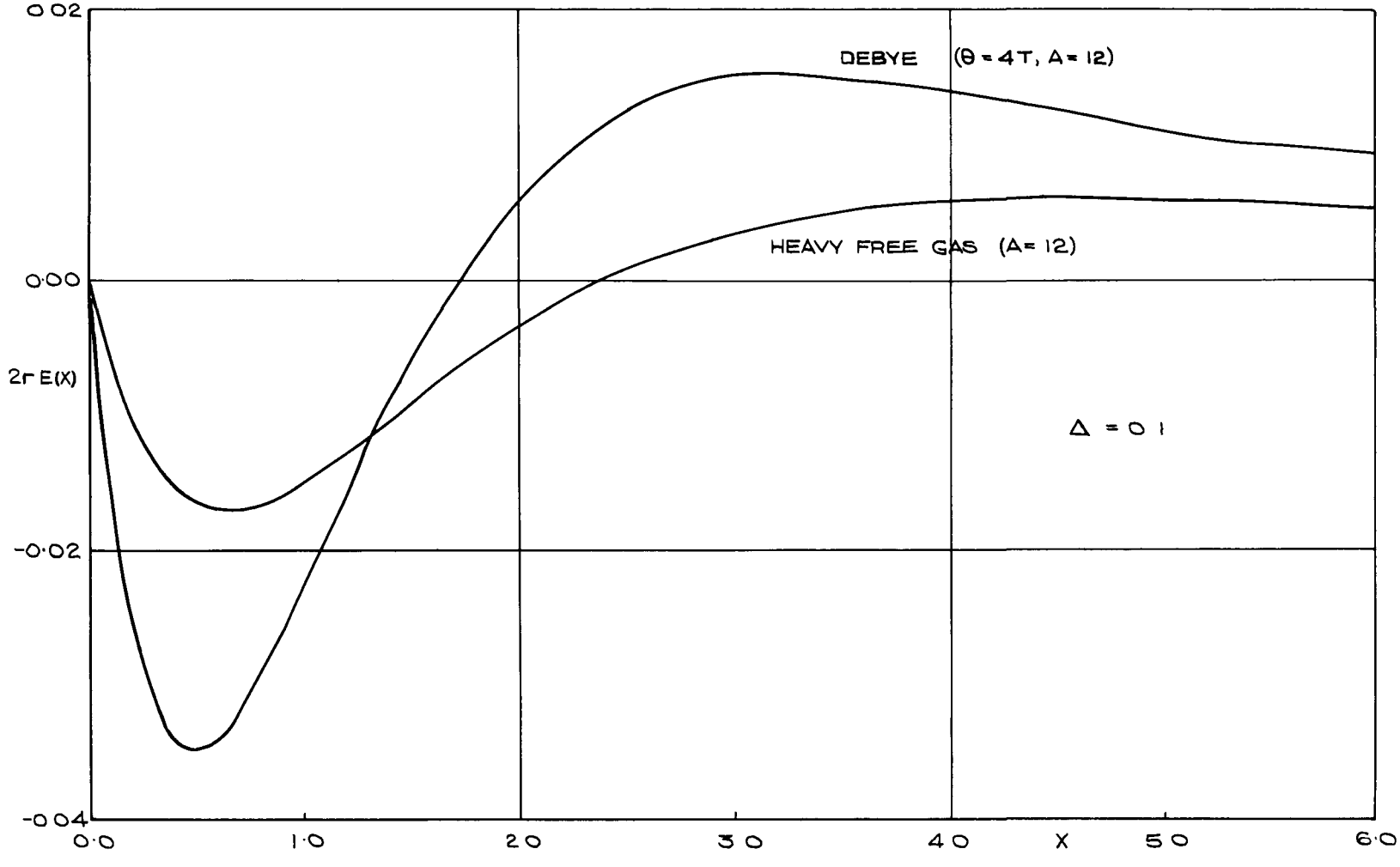
0 02
0·00
-0·02
-0 04
2r E(X)
DEBYE (θ = 4T, A = 12)
HEAVY FREE GAS (A = 12)
Δ = 0 1
0·0
1·0
2 0
3 0
4 0
X
5 0
6·0

FIGURE 5

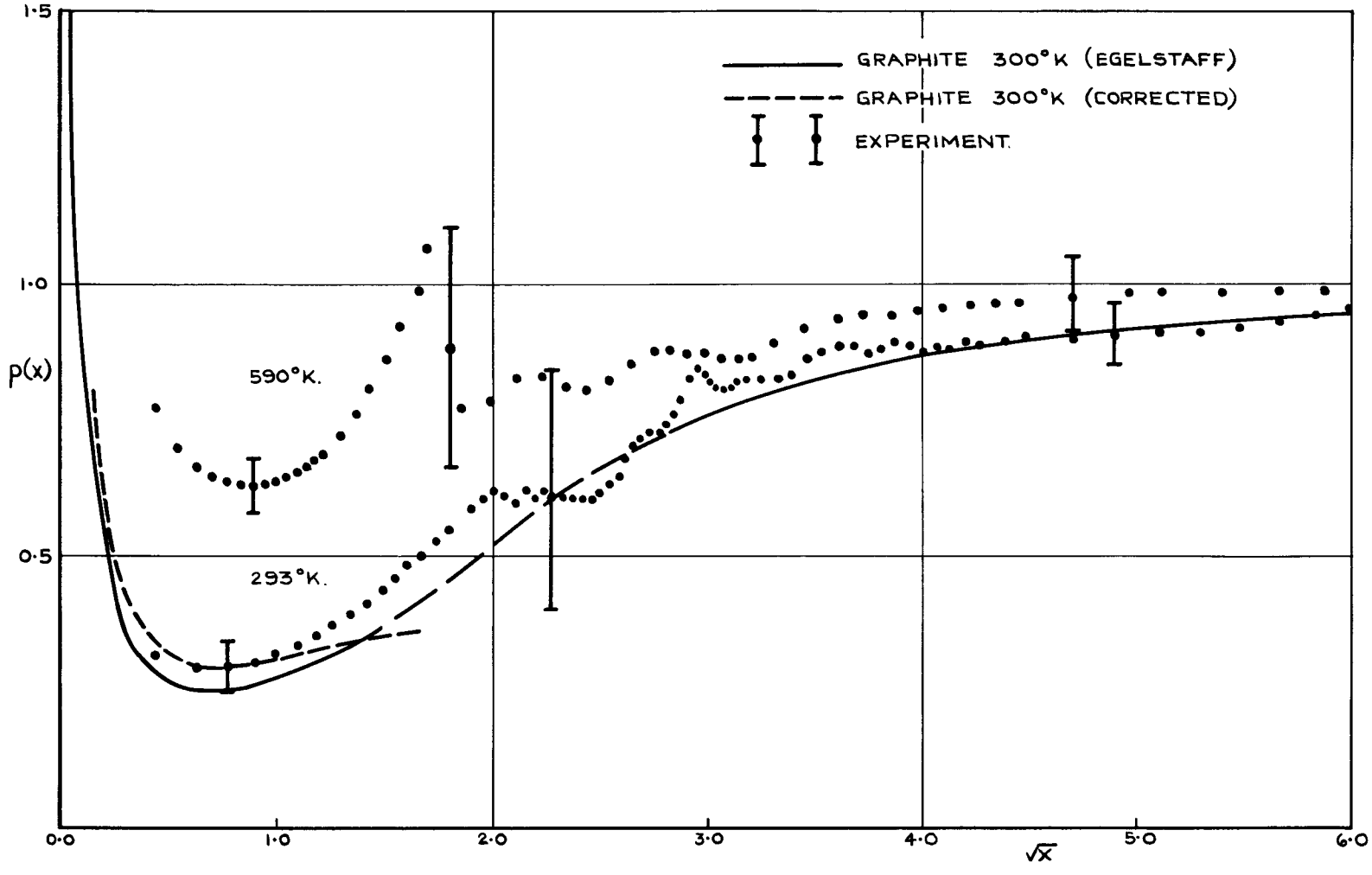
GRAPHITE 300°K (EGELSTAFF)
GRAPHITE 300°K (CORRECTED)
EXPERIMENT.
590°K.
293°K.
p(x)
1·5
1·0
0·5
0·0
1·0
2·0
3·0
4·0
5·0
6·0
√x

FIGURE 6.

BROOKHAVEN NATIONAL LABORATORY

CONFERENCE ON NEUTRON THERMALIZATION

APRIL 30 - MAY 2, 1962

ON THE ASYMPTOTIC THERMAL NEUTRON SPECTRUM IN GRAPHITE

CHARLES S. SHAPIRO[†]*

BROOKHAVEN NATIONAL LABORATORY

UPTON, L. I., NEW YORK

[†]Graduate Student from Syracuse University.

*International Business Machines Corporation Pre-doctoral Fellow.

The asymptotic thermal neutron spectrum in a graphite moderated lattice at four different moderator temperatures, has been measured at Harwell by Poole et. al. (1). This paper contains the results of a comparison of the measured data, with a calculation utilizing Corngold's asymptotic expansion for an infinite homogeneous medium (2,3).

The flux was calculated (using seven terms in the expansion) with three different models for the phonon frequency distribution in graphite. These include the Debye, Krumhansl-Brooks, and the free gas models. The Debye model utilized a Debye temperature of $\frac{1}{3}\theta_1 + \frac{2}{3}\theta_2 = 2000^{\circ}K$. The Krumhansl-Brooks model is given essentially by $p_i(\omega) = \frac{2\omega}{\theta_i^2}$ $i = 1,2$ where $i = 1$ corresponds to the longitudinal vibrations and $i = 2$ to the transverse vibrations. Here, $\theta_1 = 1000^{\circ}K$. and $\theta_2 = 2500^{\circ}K$. (4).

In comparing the infinite medium calculations with an experiment performed with a finite lattice, consideration must be given to the effects of absorption and leakage. An effective macroscopic absorption coefficient was defined as

$$\Sigma_{a\ eff.} = \frac{\int \Sigma_0 \Phi_0 dV_0 + \int \Sigma_1 \Phi_1 dV_1}{\int \Phi_0 dV_0 + \int \Phi_1 dV_1} = \frac{\Sigma_0 + \Sigma_1 \frac{\bar{\Phi}_1}{\bar{\Phi}_0} \frac{V_1}{V_0}}{1 + \frac{\bar{\Phi}_1}{\bar{\Phi}_0} \frac{V_1}{V_0}}$$

where subscripts 0 refers to the fuel region, 1 to the moderator region, and $\bar{\Phi}_1/\bar{\Phi}_0$ is the disadvantage factor. Using monoenergetic diffusion theory to calculate the disadvantage factor, the absorption parameter $\Delta \left(= \frac{2\Sigma_a(T)}{\mu\Sigma_s}\right)$ was calculated to be .18 for a moderator temperature $T_m = 293^oK.$, a $\frac{1}{v}$ dependence in Δ was assumed for the other temperatures. Leakage was also estimated using monoenergetic diffusion theory. Here, the ratio of leakage to absorption is given by $\frac{DB^2}{\Sigma_{a\ eff.}}$ which was determined to be .667. Since the $\Sigma_{a\ eff.}$ is small, the leakage affects the asymptotic flux only slightly and can be neglected. Leakage will also cause a deviation in the flux from $\frac{1}{E}$ in the high energy region (see Corngold and Zamick (5)). To a first order of approximation, the deviation from $\frac{1}{E}$ is given by $\frac{1}{E\left(1+\frac{DB^2}{\xi\Sigma_s}\right)}$. In this case $\frac{DB^2}{\xi\Sigma_s} \approx .025$, which is also small enough to be neglected in the calculation.

The values of the $\gamma_\rho^{p+\rho'}$ (which are the parameters in the calculation that contain detailed information about the scattering process and vary with model and temperature) are presented in Table I for the Debye and gas models. These parameters are defined in (3) $\left(\gamma_1^2\right.$ for example is $\frac{1}{T}\int d\omega p(\omega)\omega \coth\right.$ $\left(\frac{\omega}{2kT}\right)$ and is simply related to the average kinetic energy of

the oscillators). For the anisotropic Krumhansl-Brooks model, the values of $T_{eff.}$, $\langle K^2 \rangle_{av.}$ (the mean of the square of the kinetic energy, and $B_{av.}\left(= \frac{\langle \nabla^2 V \rangle}{6}\right.$, where V is the potential energy of the nucleus in the inter-atomic force field of all its neighbors) are presented in Table II.

Because some of the $E_\ell^{p+\ell}$ have never appeared explicitly in print, these are presented for convenience in Appendix A.

The results are displayed in the graphs, which are drawn up in the same manner as the data is presented in (1). There, a best fit Maxwellian, and a cutoff energy between the Maxwellian and the joining region are determined. The Maxwellian is subtracted from the measured flux, leaving what is essentially the joining region. The theoretical curves are obtained by using the same cutoff energies and Maxwellian temperatures as Poole. The Maxwellian was normalized so that its magnitude equaled that of the calculated flux at the cutoff energy. The values of N (the normalization factor in $M(E) = N \frac{E}{T_n^2} e^{-E/T_n}$) are listed on the graphs.

The results seem to be in good agreement with experiment, and Poole's observation that the asymptotic region is relatively insensitive to temperature when the curves are

displayed in the above manner, seems to be justified by the theory. Use of the Krumhansl-Brooks model (which is obtained through the use of specific heat data) gives slightly better agreement than the Debye model (which does not agree with the specific heat data). An appropriate choice of the Debye temperature would yield the experimental value for the specific heat integral.

From the slope of the data points, it would appear that the 1/E region had not been reached in determining the normalization. If this is true, a change in the normalization would improve the agreement with the two crystal models, and increase the difference between the free gas model and the data.

REFERENCES

1. Progress Report to the U. K. Nuclear Reactor Data Committee, N.R.D.C. 135 (May 9, 1961).
2. N. Corngold, ANNALS OF PHYSICS 6, 363 (1959).
3. N. Corngold, ANNALS OF PHYSICS 11, 333 (1960).
4. J. Krumhansl and H. Brooks, J. CHEMICAL PHYSICS 21, 1663 (1953).
5. N. Corngold and L. Zamick, NUCLEAR SCI. & ENG. 9, 367 (1961).

TABLE I - DEBYE MODEL

$\gamma_\ell^{p+\ell}$	T = 293°K.	T = 434°K.	T = 519°K.	T = 573°K.
$\gamma_1^{\,2}$	5.20	3.73	3.26	3.09
$\gamma_1^{\,3}$	2.78×10^{1}	1.27×10^{1}	8.91	7.32
$\gamma_1^{\,4}$	1.59×10^{2}	5.16×10^{1}	3.11×10^{1}	2.31×10^{1}
$\gamma_2^{\,4}$	8.11×10^{1}	4.17×10^{1}	3.19×10^{1}	2.36×10^{1}
$\gamma_2^{\,5}$	1.45×10^{3}	4.76×10^{2}	2.92×10^{2}	2.17×10^{2}
$\gamma_3^{\,6}$	2.11×10^{3}	7.30×10^{2}	5.27×10^{2}	4.42×10^{2}

For gas case $\gamma_p^{2p} = \dfrac{(2p)!}{(p)!}$, all others = 0

TABLE II - KRUMHANSL-BROOKS MODEL

	T = 293°K.	T = 434°K.	T = 519°K.	T = 573°K.
T_{eff}/T	2.42	1.77	1.55	1.49
$\langle K^2\rangle_{av.}$	1.94×10^{6}	2.27×10^{6}	2.43×10^{6}	2.75×10^{6}
$B_{av.}$	2.25×10^{6}	2.25×10^{6}	2.25×10^{6}	2.25×10^{6}

Here $T_{eff.} = \frac{1}{3} T_1 + \frac{2}{3} T_2$

$$T_i = \frac{1}{2} \int_0^{\theta_i} \omega p_i(\omega) \coth\left(\frac{\omega}{2T}\right) d\omega$$

$$B_{av.} = \frac{1}{3} \int_0^{\theta_1} \omega^2 p_1(\omega)\, d\omega + \frac{2}{3} \int_0^{\theta_2} \omega^2 p_2(\omega)\, d\omega$$

$$\langle K^2\rangle_{av.} = \frac{3}{4} T_1^{\,2} + T_1 T_2 + 2T_2^{\,2}$$

Appendix A

$$\mu = \frac{\text{neutron mass}}{\text{moderator mass}} \qquad \alpha = \frac{(1-\mu)^2}{(1+\mu)^2}$$

$$E_\ell^{p+\ell}(s) = \frac{(1+\mu)^2}{2}\,\frac{(1-\mu)^{2s-p-\ell}}{\mu^{\ell+1}}\left[\frac{\partial^{\,p+\ell}}{\partial\, y^{p+\ell}}\int_{-\mu}^{\mu}\frac{dx\left[(\sqrt{y}+x)^2-(1-\mu)\,(y-\mu)\right]^{\ell}}{(\sqrt{y}+x)^{2\,(s-p)+1}}\right]_{y=1}$$

$$E_o^o = \frac{1-\alpha^s}{(1-\alpha)s} \qquad E_o^1 = \frac{1}{(1-\alpha)}\left(\alpha^{s-\frac{1}{2}}-1\right) \qquad E_o^2 = \frac{1}{2(1-\alpha)}\left[(1-\mu)+(2s-3)-(2s-3)\,\alpha^{s-1}-(1+\mu)\,\alpha^{s-1}\right]$$

$$E_o^3 = \frac{1}{4(1-\alpha)}\left\{\left[3(1+\mu)^2+3(2s-5)\,(1+\mu)+(2s-5)\,(2s-4)\right]\alpha^{s-\frac{3}{2}}+3(1-\mu)^2+3(2s-5)\,(1-\mu)+(2s-5)\,(2s-4)\right\}$$

$$E_1^2 = \frac{1}{2\mu(1-\alpha)}\left[1-\alpha^{s-\frac{1}{2}}\right]-\frac{(2s-1)}{4\mu}\alpha^{s-1} \qquad E_1^3 = \frac{1}{2\mu(1-\alpha)}\left\{(2s-2)\,\alpha^{s-\frac{3}{2}}-(2s-2)\right\}+\frac{(2s-3)\,(2s-2)}{4\mu}\alpha^{s-\frac{3}{2}}$$

$$E_1^4 = \frac{1}{4(1-\alpha)}\left\{6(1-\mu)+\frac{3(2s-5)}{\mu}+\frac{(2s-5)\,(2s-4)}{\mu}-\left(\frac{6(2s-5)\,(2s-4)}{(1-\mu)}+\frac{3(1+\mu)^2}{\mu}+\frac{3(2s-5)\,(1+\mu)}{\mu}+\frac{(2s-5)\,(2s-4)}{\mu}\right)\alpha^{s-\frac{3}{2}}-\left(6(1+\mu)+9(2s-5)\right)\alpha^{s-2}\right\}$$
$$-\frac{(2s-5)\,(2s-4)\,(2s-3)}{8\mu}\alpha^{s-2}+\frac{3(1-\mu)^2}{4\mu(1-\alpha)}$$

$$E_2^4 = \frac{1}{\mu^2}\left\{\frac{1}{(1-\alpha)}\left[1-\alpha^{s-\frac{3}{2}}+(2s-3)-(2s-3)\,\alpha^{s-1}\right]-\frac{1}{2}\left[(2s-3)\,(1-\mu)\,\alpha^{s-2}+(2s-3)\,(2s-2)\,\alpha^{s-\frac{3}{2}}-\frac{(2s-3)\,(2s-2)\,(2s-1)\mu}{(1+\mu)^2}\alpha^{s-2}\right]\right\}$$

$$E_2^5 = \frac{1}{2(1-\alpha)}\left[3\alpha^{s-\frac{5}{2}}+\frac{6}{\mu}(1+\mu)\,\alpha^{s-2}+\frac{9}{\mu}(2s-5)\,\alpha^{s-2}+\frac{3(1+\mu)^2}{\mu^2}\alpha^{s-\frac{3}{2}}+\frac{3(2s-5)\,(1+\mu)}{\mu^2}\alpha^{s-\frac{3}{2}}+\frac{(2s-5)\,(2s-4)}{\mu^2}\alpha^{s-\frac{3}{2}}-3-\frac{6(1-\mu)}{\mu}-\frac{3(2s-5)}{\mu}-\frac{3(1-\mu)^2}{\mu^2}\right.$$
$$\left.-\frac{3(2s-5)\,(1-\mu)}{\mu^2}-\frac{(2s-5)\,(2s-4)}{\mu^2}\right]+\frac{6(2s-5)}{8\mu}\alpha^{s-\frac{5}{2}}\left[(2s-4)+(1+\mu)\right]+\frac{(2s-5)\,(2s-4)}{8\mu}\alpha^{s-2}\left[\frac{4(2s-3)}{(1-\mu)}+\frac{6(1+\mu)}{\mu}+\frac{2(2s-3)}{\mu}\right]+\frac{2(2s-5)\ldots(2s-2)}{8\mu(1-\mu)^2}\alpha^{s-\frac{3}{2}}$$

$$E_3^6 = \frac{1}{2\mu^3(1-\alpha)}\left[9-9\alpha^{s-\frac{5}{2}}+9(2s-5)-9(2s-5)\,\alpha^{s-2}+3(2s-5)\,(2s-4)\,(1-\alpha^{s-\frac{3}{2}})\right]-\frac{9\alpha^{s-\frac{5}{2}}}{4\mu^3}\left[(2s-5)\,(1+\mu)+(2s-5)\,(2s-4)+\frac{(2s-5)\,(2s-4)\,(2s-3)}{3}\right]$$
$$-\frac{3\,(2s-5)\ldots(2s-2)}{4\mu^2(1-\mu)^2}\alpha^{s-\frac{3}{2}}-\frac{(2s-5)\ldots\ldots(2s-1)}{2\mu(1+\mu)^4}\alpha^{s-3}$$

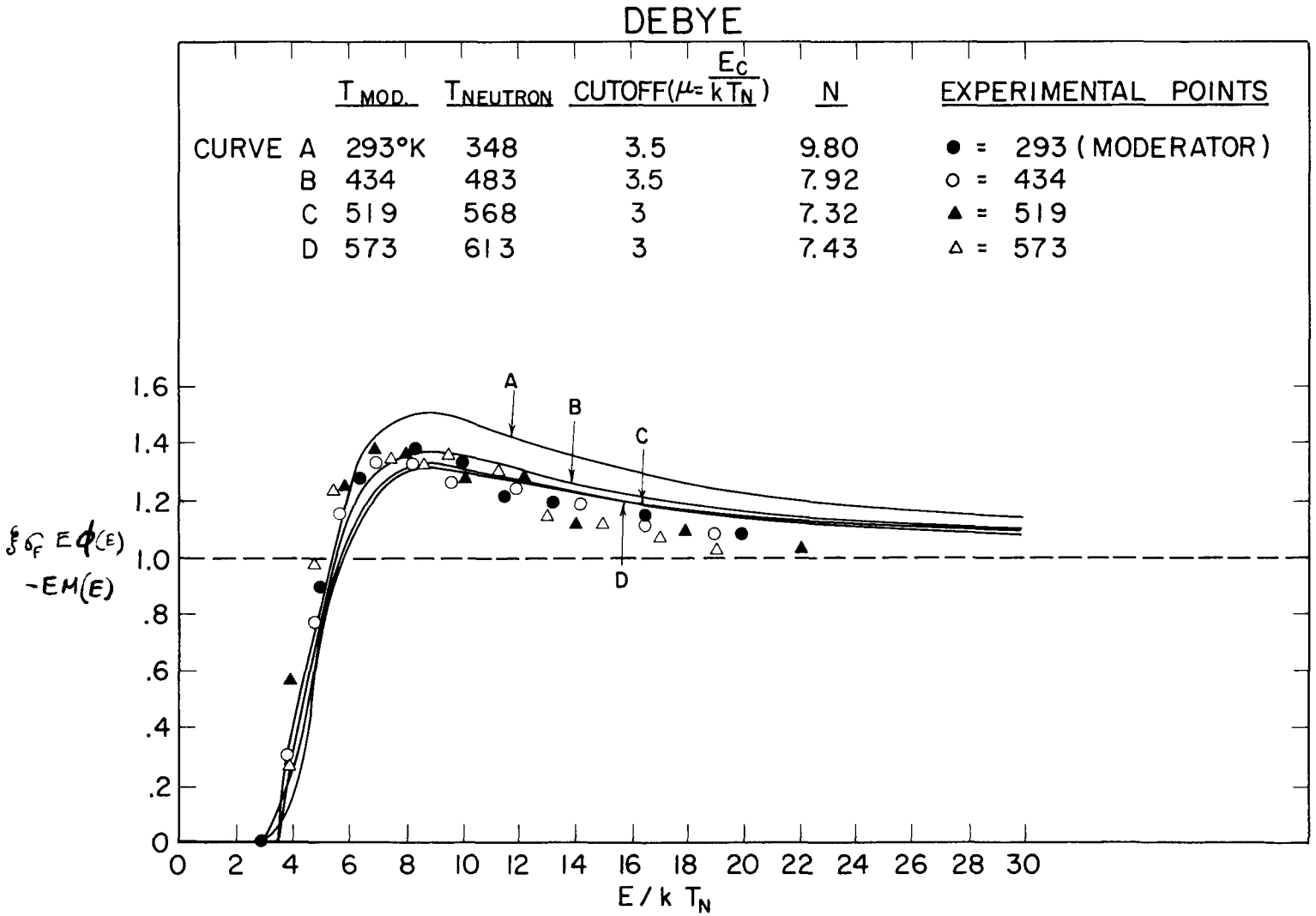
DEBYE
T MOD.
T NEUTRON
CUTOFF(μ = Ec/kTN)
N
EXPERIMENTAL POINTS
CURVE A 293°K 348 3.5 9.80
B 434 483 3.5 7.92
C 519 568 3 7.32
D 573 613 3 7.43
● = 293 (MODERATOR)
○ = 434
▲ = 519
△ = 573
A
B
C
D
∫σF Eφ(E) / -EM(E)
E / k TN
0
.2
.4
.6
.8
1.0
1.2
1.4
1.6
0 2 4 6 8 10 12 14 16 18 20 22 24 26 28 30

KRUMHANSL & BROOKS

	$T_{MOD.}$	$T_{NEUTRON}$	CUTOFF($\mu = \frac{E_c}{kT}$)	N	EXPERIMENTAL POINTS
CURVE A	293°K	348	3.5	8.45	● = 293 (MODERATOR)
B	434	483	3.5	7.59	o = 434
C	519	568	3	7.04	▲ = 519
D	573	613	3	7.22	△ = 573

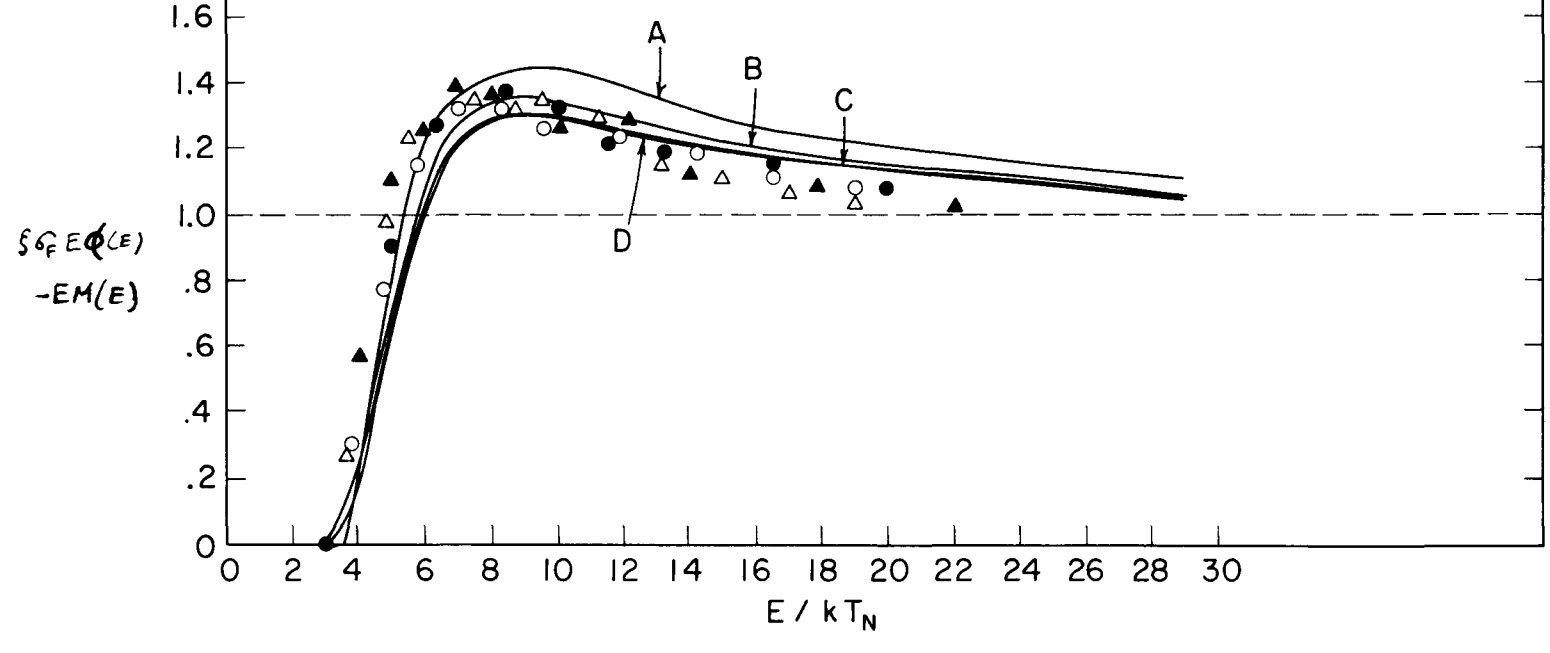

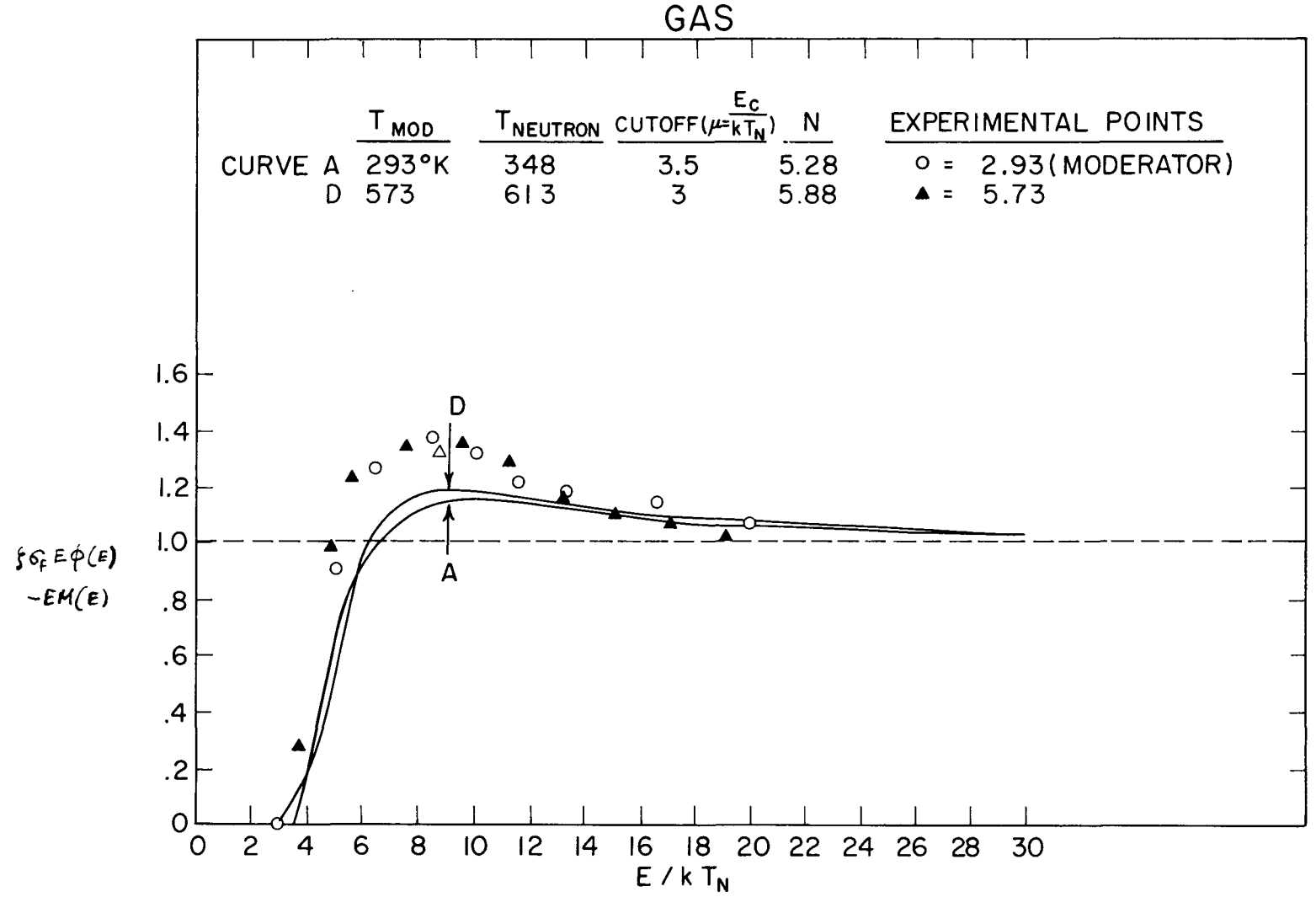
GAS
T MOD
T NEUTRON
CUTOFF(μ=E_C/kT_N)
N
EXPERIMENTAL POINTS
CURVE A 293°K 348 3.5 5.28
D 573 613 3 5.88
○ = 2.93(MODERATOR)
▲ = 5.73
D
A
1.6
1.4
1.2
1.0
.8
.6
.4
.2
0
0 2 4 6 8 10 12 14 16 18 20 22 24 26 28 30
E / k T_N
∫σ_F Eφ(E)
-EM(E)

E U R A T O M
CCR ISPRA

Reactor Physics
Department

Ispra, March 2, 1962

THERMAL NEUTRON SPECTRUM IN A MEDIUM WITH TWO DIFFERENT TEMPERATURES

Hiroshi Takahashi

EUR/C/-IS/502/62 e

Abstract

The energy dependent equation in the heavy gas model with the first order correction of μ is considered for the case of a non-absorbing homogeneously mixed medium, whose components have the absolute temperatures T_1 and T_2, the mass ratio μ_1, μ_2 (neutron mass to the mass of the moderator atom) and the macroscopic cross section Σ_1, Σ_2. In the heavy gas approximation, the distribution of the neutron spectrum is the maxwellian distribution with the effective temperature defined by :

$$T_{eff} = \frac{\mu_1\Sigma_1T_1 + \mu_2\Sigma_2T_2}{\mu_1\Sigma_1 + \mu_2\Sigma_2}$$

If the mass ratio μ approaches 1, the distribution deviates from the maxwellian distribution.

By means of the perturbation method, the simple expression for the deviated flux distribution is obtained. The more rigorous calculation is carried out by expanding the flux in terms of Laguerre polynomials of first order of energy. This expansion method was used for the study of time and space dependent problem (3). The generating functions for the matrix element of scattering kernel expanded by the Laguerre polynomials, whose variable $\bar{E}$ is normalized by a temperature other than the components temperature are calculated for the free gas and the crystalline material.

The results obtained from the above two methods show that when the moderator components have the some mass, the neutron spectra are shifted to lower energy than the Maxwellian distribution calculated by the heavy gas approximation.

1. Introduction

In the reactor analysis of a power reactor, the neutron spectrum is important to determinate a reactivity and a long term reactivity change, etc. The ORGEL type reactor which is planned in our laboratory is composed of a hot fuel assembly and a cold heavy water moderator. As preliminary study of the neutron spectrum in this reactor type, we studied the neutron spectrum in a homogeneous medium whose components have two different temperatures.

When neutrons are put into a non-absorbing infinite medium with temperature T, the neutron spectrum approaches the maxwellian distribution with temperature T. In the case of a non-absorbing homogeneous medium, whose components have two different temperatures T_1, T_2, the neutron spectrum approaches some distribution which is between the two maxwellian distributions with T_1 and T_2.

By measuring the neutron spectrum in the homogeneous medium, the effect of chemical binding of moderator atom on the neutron spectrum will be studied. The neutron spectrum which is deviated from the maxwellian distribution by putting an additional absorber has been measured for this kind of study. Using the homogeneous medium whose components have two different temperatures, this effect will be studied without to sacrifice the neutron intensity.

In this paper, a medium composed of free gases is studied by using a heavy gas approximation with a first order correction of the mass ratio μ. If a perturbation method is used, a simple expression for a neutron spectrum distribution can be obtained as a function of mass ratios, scattering cross sections and temperatures of components. The more accurate formalism is obtained in the cases of free gas and a crystalline material. The case of free gas with mass 1 is numerically calculated and is compared with the result obtained by the perturbation method.

2. Formalism

In the non-absorbing medium which is composed of two atoms component, the neutron balance equation is expressed by

$$[\Sigma_{s1}(E) + \Sigma_{s1}(E)]\ \phi(E) = \int_0^\infty (\Sigma_{s1}(E' \to E) + \Sigma_{s2}(E' \to E))\ \phi(E')dE' \tag{1}$$

where $\Sigma_s(E)$, $\Sigma_s(E' \to E)$ are the scattering cross section and the differential cross section respectively.

In the heavy gas approximation corrected in the first order of μ, the neutron balance equation is a medium whose components have two different temperatures T_1 and T_2, the mass ratios of a neutron to the composing atom μ_1 and μ_2 is expressed in the following equation

$$\sum_{i=1}^{2} \mu_i \Sigma_i \left[\left\{\left(ET_i \frac{d^2\phi}{dE^2} + E \frac{d\phi}{dE} + \phi\right)\right\}\right.$$

$$+\mu_i \left\{ \frac{4}{3} E^2 T_i^2 \frac{d^4\phi}{dE^4} + \frac{8}{3} (T_i E^2 + T_i^2 E) \frac{d^3\phi}{dE^3}\right.$$

$$+ \left(\frac{4}{3} E^2 + 6 E T_i + T_i^2\right) \frac{d^2\phi}{dE^2} \tag{2}$$

$$\left.\left. + \left(\frac{10}{3} E + T_i - \frac{T_i^2}{E} \right) \frac{d\phi}{dE} + \left(\frac{2}{3} + \frac{T_i^2}{E^2} \right) \phi \right\}\right] = 0$$

where ϕ is the neutron flux per unit energy interval.

The first terms proportional to μ represent the so-called heavy gas approximation, and the second terms proportional to μ^2 represent the correction for it. In order to solve this equation by a perturbation method, let us consider the terms proportional to μ^2 as perturbation, and write :

$$\phi(E) = \phi^{(o)}(E) + \phi^{(1)}(E) \tag{3}$$

where $\phi^{(o)}(E)$, $\phi^{(1)}(E)$ are an unperturbed solution and the perturbed term of the 1st order, respectively. From the usual perturbation theory, we get the following equations :

$$\sum_{i=1}^{2} \mu_i \Sigma_i \left\{ E T_i \frac{d^2\phi^{(o)}}{dE^2} + E \frac{d\phi^{(o)}}{dE} + \phi^{(o)} \right\} = 0 \tag{4}$$

$$\sum_{i=1}^{2} \mu_i \Sigma_i \left\{ E T_i \frac{d^2\phi^{(1)}}{dE^2} + E \frac{d\phi^{(1)}}{dE} + \phi^{(1)} \right\}$$

$$+\mu_i \left\{ \frac{4}{3} E^2 T_i^2 \frac{d^4\phi^{(o)}}{dE^4} + \frac{8}{3} (T_i E^2 + T_i^2 E) \frac{d^3\phi^{(o)}}{dE^3} \right.$$

$$+ \left(\frac{4}{3} E^2 + 6 E T_i + T_i^2 \right) \frac{d^2\phi^{(o)}}{dE^2}$$

$$\left. + \left(\frac{10}{3} E + T_i - \frac{T_i^2}{E} \right) \frac{d\phi^{(o)}}{dE} + \left(\frac{2}{3} + \frac{T_i^2}{E^2} \right) \phi^{(o)} \right\}] = 0 \tag{5}$$

The equation (3) is rewritten as follows :

$$E \left(\frac{\sum_{i=1}^{2} \mu_i \Sigma_i T_i}{\sum_{i=1}^{2} \mu_i \Sigma_i} \right) \frac{d^2\phi^{(o)}}{dE^2} + E \frac{d\phi^{(o)}}{dE} + \phi^{(o)} = 0$$

and the unperturbed solution $\phi^{(o)}$ is given by the following maxwellian distribution :

$$\phi^{(o)} = \frac{4}{\sqrt{\pi}} \frac{E}{T_{eff}^2} e^{-\frac{E}{T_{eff}}} \tag{6}$$

where

$$T_{eff} = \frac{\sum_{i=1}^{2} \mu_i \Sigma_i T_i}{\sum_{i=1}^{2} \mu_i \Sigma_i}$$

From now on this effective temperature T_{eff} is expressed by T throughout this paper.

In the heavy gas approximation, the neutron spectrum becomes the Maxwell distribution with T. And, if one of the moderator components has infinite mass, that is $\mu = 0$ and the energy change by scattering is zero, the effective temperature T becomes the temperature of another moderator component.

By substituting equation (6) to equation (5) and rearranging it, we get :

$$\left(T \frac{d^2\phi^{(1)}}{dE^2} + E \frac{d\phi^{(1)}}{dE} + \phi^{(1)} \right)$$

$$= - \frac{1}{\sum_{i=1}^{2} \Sigma_i \mu_i} \sum_{i=1}^{2} \Sigma_i \mu_i^2 \left\{ \frac{4}{3} (T_i - T) \frac{E^3}{T^3} - 2 (4 T_i - 3 T) \frac{E^2}{T^2} \right.$$

$$\left. + (9 T_i - 4 T) \frac{E}{T} - T_i \right\} \left(\frac{T_i}{T} - 1 \right) \frac{4}{\sqrt{\pi}} \frac{1}{T^2} e^{-\frac{E}{T}} \tag{7}$$

Now, in order to solve equation (7), let us expand $\phi^{(1)}$ and one term of the right hand side of equation (7) by the Laguerre Polynomial of 1 ~~st~~ order as follows :

$$\phi^{(1)}(E) = \sum_{m=0}^{\infty} n_m^{(1)} \; L_m^{(1)} \left(\frac{E}{T}\right) \frac{4}{\sqrt{\pi}} \; \frac{E}{T^2} \; e^{-\frac{E}{T}} \tag{8}$$

$$\frac{4}{3}(T_i - T)\frac{E^3}{T^3} - 2(4T_i - 3T)\frac{E^2}{T^2} + (9T_i - 4T)\frac{E}{T} - T_i$$

$$= \left[T_i \sum_{m=0}^{\infty} a_m L_m^{(1)}\left(\frac{E}{T}\right) + T \sum_{m=0}^{\infty} b_m L_m^{(1)}\left(\frac{E}{T}\right) \right] \left(\frac{E}{T}\right) \tag{9}$$

where a_m and b_m are obtained by using the generating function for the series of the Laguerre polynomials :

$$\frac{\exp -\left(\frac{xt}{1-t}\right)}{(1-t)^2} = \sum_{m=0}^{\infty} L_m^{(1)}(x)\, t^k \quad (t < 1) \tag{10}$$

Let us consider the following integration :

$$\int_0^{\infty} \frac{e^{-\frac{xt}{(1-t)}}}{(1-t)^2} \; e^{-x} \left(\frac{4}{3}x^3 - 8x^2 + 9x - 1\right) dx$$

$$= 8(1-t)^2 - 16(1-t) + 9 - \frac{1}{(1-t)}$$

$$= -t + 7t^2 - t^3 - t^4 - t^5 - \ldots\ldots \tag{11}$$

On the other hand, from equation (8) this expression is equal to :

$$\sum_{m=0}^{\infty} \sum_{k=0}^{\infty} a_m \int_0^{\infty} L_m^{(1)}(x)\, L_k^{(1)}(x)\, x\, e^{-x}\, dx \; t^k \tag{12}$$

$$= \sum_{m=0}^{\infty} a_m (m+1)\, t^m$$

We get :

$$\begin{aligned} a_o &= 0 \\ a_1 &= -\frac{1}{2} \\ a_2 &= \frac{7}{3} \\ a_3 &= -\frac{1}{4} \\ a_4 &= -\frac{1}{5} \\ &\cdots\cdots \end{aligned} \tag{13}$$

but the convergence of the summation of the "a_m" terms is very slow. Similarly, we get the b_m as follows :

$$\begin{aligned} b_o &= b_3 = b_4 = \cdots = 0 \\ b_1 &= 1/2 \\ b_2 &= -\frac{8}{3} \end{aligned} \tag{14}$$

By substituting equation (8) and (9) to (7) and using the orthogonality relation of the Laguerre polynomials, $\phi^{(1)}$ is obtained as follows :

$$\phi^{(1)}(E) = \frac{1}{\sum_{i=1}^{2} (\mu_i \Sigma_i)} \sum_{m=o}^{\infty} \sum_{i=1}^{2} (\mu_i^2 \Sigma_i) \left[T_i a_m + T b_m \right] \left(\frac{T_i}{T} - 1 \right)$$

$$\cdot \frac{1}{m} L_m \left(\frac{E}{T} \right) \frac{4}{\sqrt{\pi}} \frac{E}{T^2} e^{-\frac{E}{T}} \tag{15}$$

The convergence of the sum of the a_m terms in this equation is also very slow. Therefore the same technique which was used for obteining a_m and b_m is applied for obtaining their summation.

Now, we assume that the sum of the a_m terms is obtained as follows :

$$\sum_{m=o}^{\infty} \frac{a_m}{m} L_m (x) \, x = f(x) \tag{16}$$

By using equations (16) and (10) , we get :

$$\int_0^\infty \frac{e^{-xt/(1-t)}\; e^{-x}}{(1-t)^2} \cdot f(x)\, dx$$

$$= \sum_{m=o}^{\infty} a_m \frac{(m+1)}{m} t^m \qquad (17)$$

$$= -t + \frac{7}{2} t^2 - \frac{t^3}{3} - \frac{t^4}{4} - \frac{t^5}{5} \ldots .$$

$$= 4 - 8(1-t) + 4(1-t)^2 - \log(1-t)$$

From this equation, f (x) is easily obtained by an inverse Laplace transformation, that is :

$$f(x) = 4x - 4x^2 + \frac{2}{3} x^3 - x\psi(2) - x \log x \qquad (18)$$

where ψ (x) is the Euler's Psi function.

In a similar way, we get for the b_m terms :

$$g(x) = \sum_{m=o}^{\infty} b_m \frac{L_m(x)}{m} x = 2x^2 - \frac{2}{3} x^3 \qquad (19)$$

Thus, the neutron spectrum distribution is :

$$N(E) = \frac{4}{\sqrt{\pi}} \frac{E}{T^2} e^{-\frac{E}{T}} \left[1 + \frac{1}{2 \sum_{i=1}^{2} \Sigma_i \mu_i} \right.$$

$$\left. \sum_{i=1}^{2} \Sigma_i \mu_i^2 \left(\frac{T_i}{T} - 1 \right) \left\{ \left(\frac{T_i}{T}\right) \frac{f\left(\frac{E}{T}\right)}{\frac{E}{T}} + \frac{g\left(\frac{E}{T}\right)}{\frac{E}{T}} \right\} \right] \qquad (20)$$

Now, if we substitute the following ratio for values of two components into equation :

$$l = \frac{T_2}{T_1}, \qquad m = \frac{\mu_2}{\mu_1}, \qquad n = \frac{\nu_2}{\nu_1} \tag{21}$$

we get :

$$\phi(E) = \frac{4}{\sqrt{\pi}} \frac{E}{T^2} e^{-\frac{E}{T}} \left[1 + \mu_1 (l - 1) m n \right.$$

$$\left. \cdot \left\{ \frac{(ml - 1)}{(1 + lmn)^2} \frac{f(\frac{E}{T})}{\frac{E}{T}} + \frac{(m-1)}{(1+lmn)(1+mn)} \frac{g(\frac{E}{T})}{\frac{E}{T}} \right\} \right] \tag{22}$$

where

$$T = T_1 \left(\frac{1 + lmn}{1 + mn}\right) \tag{23}$$

In the case of $l = 1$, that is, the two components have the same temperature, and in the case of m or n equal to zero or infinite, the correction factor vanished and the neutron spectrum becomes maxwellian. In the case when m equals zero or infinite, the energy change due to neutron scattering by either component is negligible, and in the case when n equals zero or infinite, the neutron scattering by either component is negligible. Thus, the distribution of neutron spectrum becomes the maxwellian distribution of other components.

In the case of $m = 1$ that is, the masses of the two components are the same, the correction term proportional to $g(\frac{E}{T})$ vanishes, and if $lm = 1$ is satisfied the correction term proportional to $f(\frac{E}{T})$ vanishes. These correction terms proportional to $f(\frac{E}{T})$ and $g(\frac{E}{T})$ have maximum coefficients in the case of $n = \frac{1}{lm}$ and $n = \frac{1}{m\sqrt{l}}$, respectively, for fixed values of l and m.

So far, the neutron spectrum for the free gas has been calculated in the heavy gas model corrected in a first order of by a perturbation method. However, this is not a good solution for the light atom. A more accurate spectrum is obtained in this section by using the expansion of scattering kernel in terms of a orthogonal set of Laguerre polynomial of energy in the ~~set~~ order, which was used in the analysis of the space dependent problem in paper I (3). i.e. it is assumed that the fluxes ϕ in the equation (1) are expanded in the following way :

$$\phi(E) = \sum_{i=o}^{\infty} \frac{A_i}{\sqrt{(i+1)}} L_i\left(\frac{E}{T}\right) \frac{E}{T^2} e^{-\frac{E}{T}} \qquad (24)$$

substituting eq(24) into eq(1) and multiplying the resulting equation by $\frac{1}{\sqrt{(j+1)}} L_j\left(\frac{E}{T}\right)$ and integrating over E, we get

$$[S_{ij1} + S_{ij2}] A_i = 0 \qquad (25)$$

where

$$S_{ijk} = \frac{1}{\sqrt{(i+1)(j+1)}} \left[\int_0^\infty\int_0^\infty dE' \, dE \, \Sigma_{sk}(E' \to E) \, L_i^{(1)}\left(\frac{E'}{T}\right) L_j^{(1)}\left(\frac{E}{T}\right) \frac{E'}{T^2} e^{-\frac{E'}{T}} \right.$$

$$\left. - \int_0^\infty\int_0^\infty dE \, dE' \, \Sigma_{sk}(E' \to E) \, L_i^{(1)}\left(\frac{E}{T}\right) L_j^{(1)}\left(\frac{E'}{T}\right) \frac{E'}{T^2} e^{-\frac{E'}{T}} \right] \qquad (26)$$

In this case, although the temperature used in the expansion of flux eq(26) is different from the temperatures of components, since the generating function S can calculate in the same way as the case of space dependent problem in the paper I. The results are shown in the following. In the case of free gas, we get :

$$S_k = -4\Sigma_B \frac{m}{M_k} \frac{T_k}{T} \frac{\left[\left(1 - \frac{T}{T_k}\right) + \frac{T}{T_k} P\right] 1}{(1 - P1)^2 \left(1 + \frac{m}{M_k}\right)^4} \sqrt{\frac{1 + \frac{\frac{mT_K}{M_K T}}{1 + \frac{mT_K}{M_K T}} \left(\frac{P}{1-P} + \frac{1}{1-1}\right)}{\left[1 + 4\frac{T_K}{T}\frac{m}{M_K}\frac{\left(1 - \frac{T}{T_K}\right)}{\left(1 + \frac{m}{M_K}\right)^2} 1 - \frac{\left(1 - \frac{m}{M_K}\right)^2}{\left(1 + \frac{m}{M_K}\right)^2} P1\right]}}$$

The generating function S in the case of crystalline material is obtained by the method is mass expansion as follows

$$S_k = -2\Sigma_B \frac{(1-P)^{-1}(1-1)^{-1}}{(1-Pl)} \sum_{q=1}^{\infty} \left(-\frac{m}{M_k} K_k\right)^q \sum_{n=1}^{q} \frac{1}{\Gamma(q-n+1)\,\Gamma(n+1)}$$

$$\int_0^{\omega_m} \sinh\left(\left(\frac{P}{1-P} + 1 - \frac{T}{T_k}\right)\zeta\right) \sinh\left(\frac{1}{1-1}\zeta\right) G_n'(\zeta)\zeta^{q+1} K_{q+1}\left(\left(1 + \frac{P}{1-P} + \frac{1}{1-1}\right)\zeta\right) d\omega \tag{28}$$

and by the Phonon expansion method, we get :

$$S_k = -2\Sigma_B \frac{(1-P)^{-1}(1-1)^{-1}}{(1-Pl)} \sum_{q=1}^{\infty} \left(\frac{m}{M_k}\right)^q \frac{1}{\Gamma(q+1)} \int_0^{\omega_m} \sinh\left(\left(\frac{P}{1-P} + 1 - \frac{T}{T_k}\right)\zeta\right)$$

$$\sinh\left(\frac{1}{1-1}\zeta\right) G''_q(\zeta) \frac{K_{q+1}\left(\gamma\left(1 + \frac{P}{1-P} + \frac{1}{1-1}\right)\zeta\right)}{\gamma^{(q+1)}} d\omega \tag{29}$$

In these equations the same notation are used as in paper I. We can also get the generating function by using the two Phonon dividing models. The matrix elements $S_{ij}^{(i)}$ are obtained as the coefficients of $\sqrt{(i+1)(j+1)}\, P^i\, 1^j$ terms.

Let us consider the case of heavy gas, that is $\frac{m}{M} \to 0$, the generating function of equation (27) becomes

$$\sum_{k=1}^{2} S_k = -4 \sum_{k=1}^{2} \Sigma_{Bk} \frac{m}{M_k} \frac{T_k}{T} \frac{\left[\left(1 - \frac{T_k}{T_k}\right) + \frac{T}{T_k} P\right] 1}{(1 - Pl)^3} \tag{30}$$

If we choose the temperature T in such a way that

$$\sum_{k=1}^{2} \frac{\Sigma_{Bk}}{M_k} \left(\frac{T_k}{T} - 1\right) = 0 \tag{31}$$

we get

$$\sum_{k=1}^{2} S_k = -4 \sum_{k=1}^{2} \Sigma_{Bk} \frac{m}{M_k} \frac{Pl}{(1-Pl)^3} \tag{32}$$

which is the generating function in the case of heavy gas with

$$\sum_{i=1}^{2} \Sigma_{Bk} \frac{m}{M_k}$$

instead of

$$\Sigma_B \frac{m}{M}$$

and its matrix is diagonalized. Thus, the lowest eigenfunction becomes the Maxwellian distribution with the effective temperature

$$T = \frac{\sum_{k=1}^{2} (\mu_k \Sigma_k T_k)}{\sum_{k=1}^{2} (\mu_k \Sigma_k)} \qquad (33)$$

This is the result obtained in the last section.

3. Numerical results

In figures 1, 2 and 3, the neutron spectrum is calculated using eq.(22) for the cases where $l = 2.0$ and 3.0 and $\mu_1 = 1.0$, $m = 1$, $n = 1$ for both cases. Also the case of $l = \frac{1}{2}$, $\mu_1 = 1.0$, $m = 2.0$, $n = 1$ is shown. In all cases an neutron spectra with effective temperature T, which are calculated from the heavy gas approximation also are shown as Maxwellian distribution.

In the first two cases, the deviation from the maxwellian distribution is due to the term proportional to $f(\frac{E}{T})$ and the peak of the neutron spectrum is shifted to the lower energies. In the third case, the deviation is only due to the term proportional to $g(\frac{E}{T})$ and the peak of the neutron spectrum does not shift appreciably. Furthermore, the case of $\mu_1 = 1$, $l = 2.0$, $m = \frac{1}{3}$, $n = 1.0$ are added in figure 3 where both correction terms (f and g) are included. These deviations decrease as the mass of moderator atom is increased.

In table 1, the coefficients of proportional to f $(\frac{E}{T})/\frac{E}{\Phi}$ and g $(\frac{E}{T})/\frac{E}{T}$

$$C_1 = \frac{(l-1)\,mn\,(ml-1)}{(1+lmn)^2}$$

$$C_2 = \frac{(l-1)\,mn\,(m-1)}{(1+lmn)\,(1+mn)}$$

are tabulated for the several typical cases.

Table I

The value of C_1 and C_2

	$\frac{\sigma_2}{\sigma_1}$ / $\frac{T_2}{T_1}$ / $\frac{\mu_2}{\mu_1}$	1		2		3	
		2	3	2	3	2	3
C_1	1	$\frac{1}{9}$	$\frac{1}{4}$	$\frac{1}{8}$	$\frac{8}{25}$	$\frac{3}{25}$	$\frac{1}{3}$
	$\frac{1}{2}$	0	$\frac{2}{25}$	0	$\frac{4}{49}$	0	$\frac{2}{9}$
	$\frac{1}{3}$	$-\frac{1}{25}$	0	$-\frac{1}{32}$	0	$-\frac{3}{121}$	0
C_2	1	0	0	0	0	0	0
	$\frac{1}{2}$	$-\frac{1}{12}$	$-\frac{2}{15}$	$-\frac{1}{15}$	$-\frac{4}{35}$	$-\frac{3}{56}$	$-\frac{2}{21}$
	$\frac{1}{3}$	$-\frac{1}{10}$	$-\frac{1}{6}$	$-\frac{1}{14}$	$-\frac{8}{63}$	$-\frac{3}{55}$	$-\frac{1}{10}$

In order to compare the spectrum obtained by the expansion method with the ~~last~~ spectrum obtained by an approximate method, the neutron spectra in the medium of the free gas with mass 1 are calculated in the case of T_2/T_1 = 2 and 3. Their spectra are shown in figure 1,2 with the numerical results calculated by the perturbation method.

Their deviations from the Maxwellian distribution of the heavy gas approximation are smaller than the deviation which result from the perturbation method. In the medium which is composed of the same mass atoms, we find that the energies where the maximum of neutron spectrum is located are deviated to an energy lower than the one calculated by the heavy gas approximation.

REFERENCES

(1) H. Hurwitz, M. Nelkin ang G. Habetler
Nuclear Science and Engineering, 1, 280-312 (1956)

(2) N. Corngold
Annals of Physics, 6, 368-398 (1958)

(3) H. Takahashi
Space and Time dependent eigenvalue problem in Neutron Thermalization.

Acknowledgments

The author wishes to express his sincere gratitude to V. Raievski for suggesting this work and for the considerable attention and interest he has shown towards its progress. He also wants to thank H. Rief for discussing it. Thanks are also also due to B. Dorpema for programming a part of the mathematical expressions.

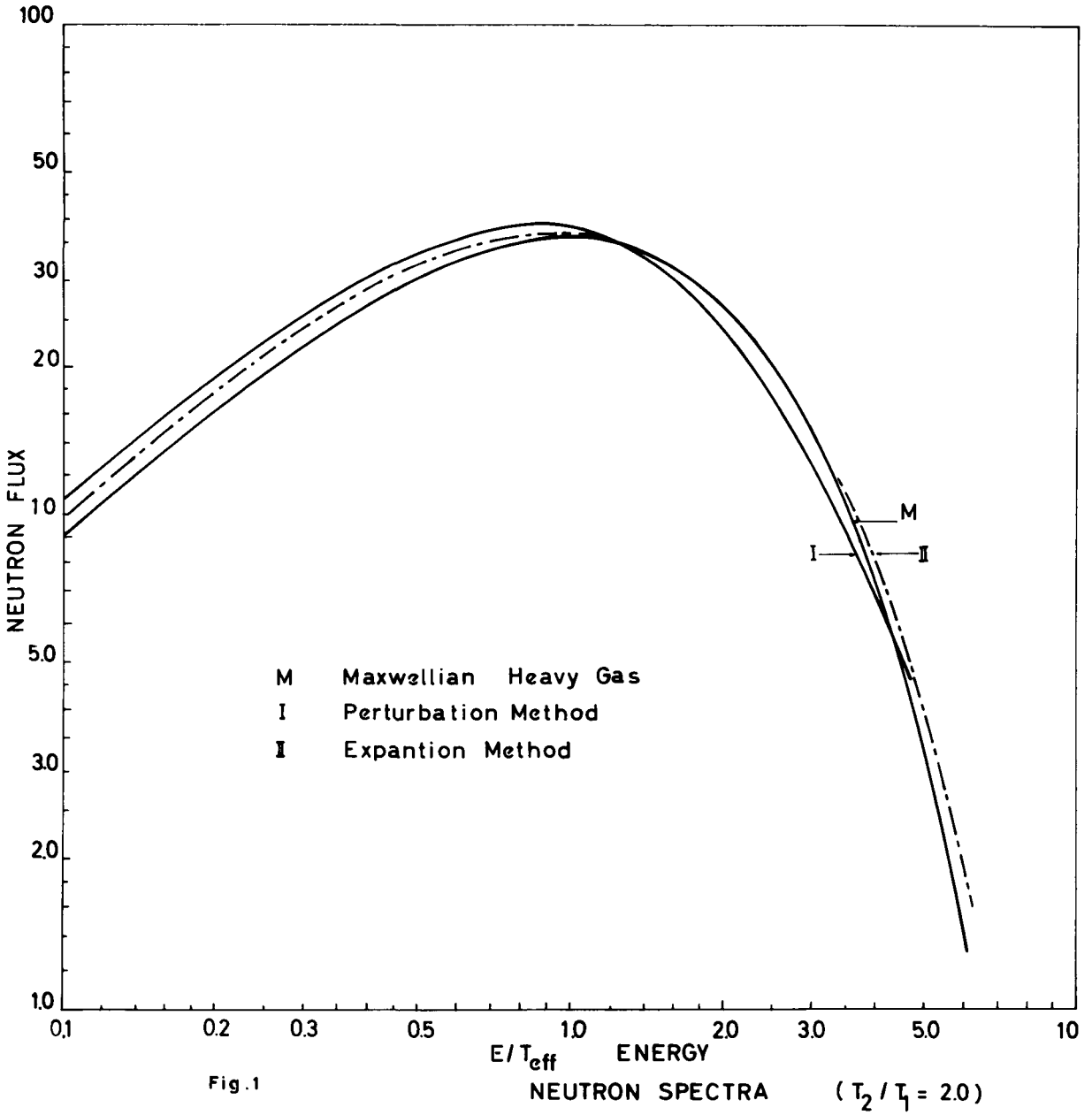

Fig.1 NEUTRON SPECTRA ($T_2 / T_1 = 2.0$)

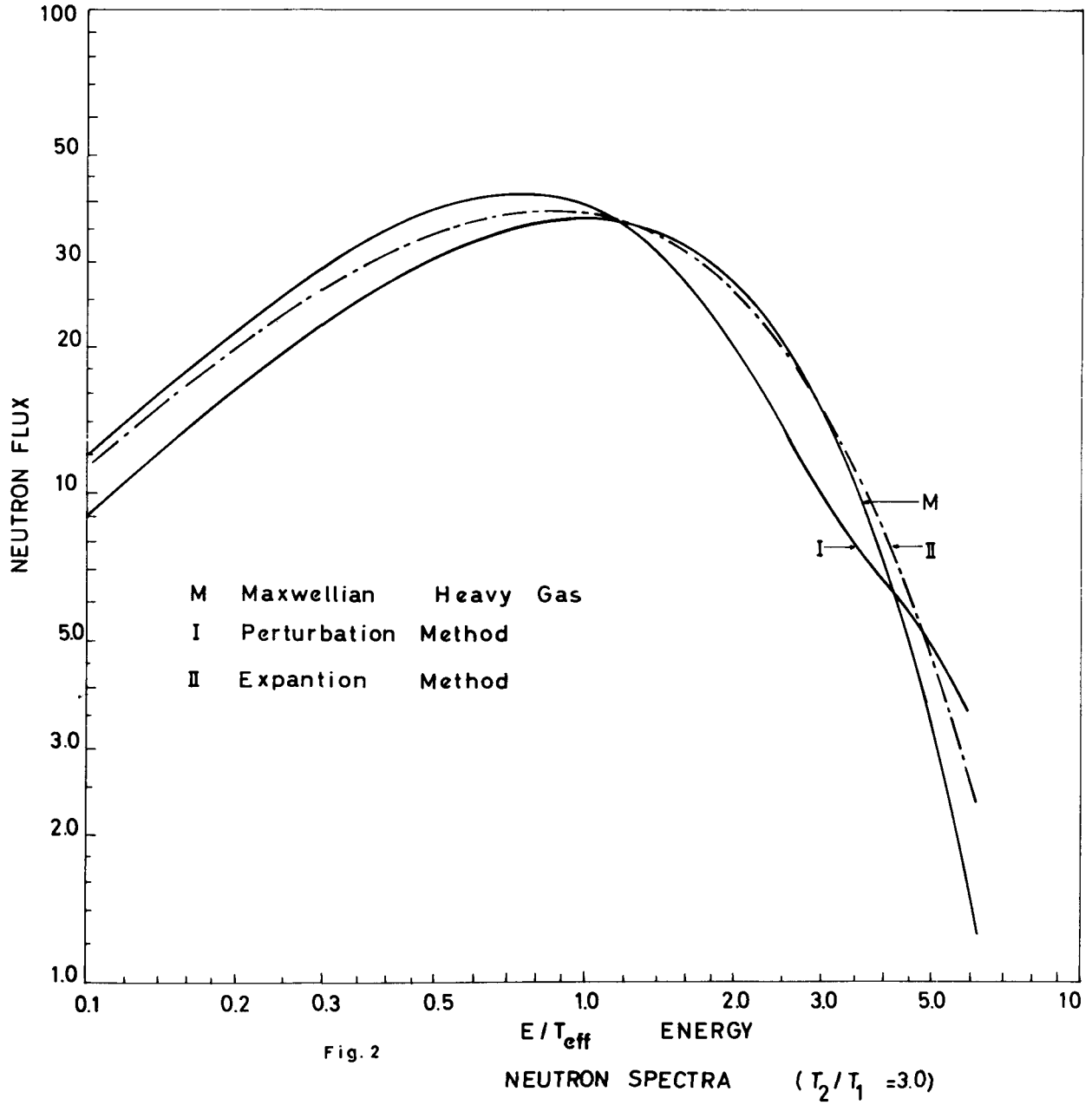

Fig. 2

NEUTRON SPECTRA (T_2 / T_1 =3.0)

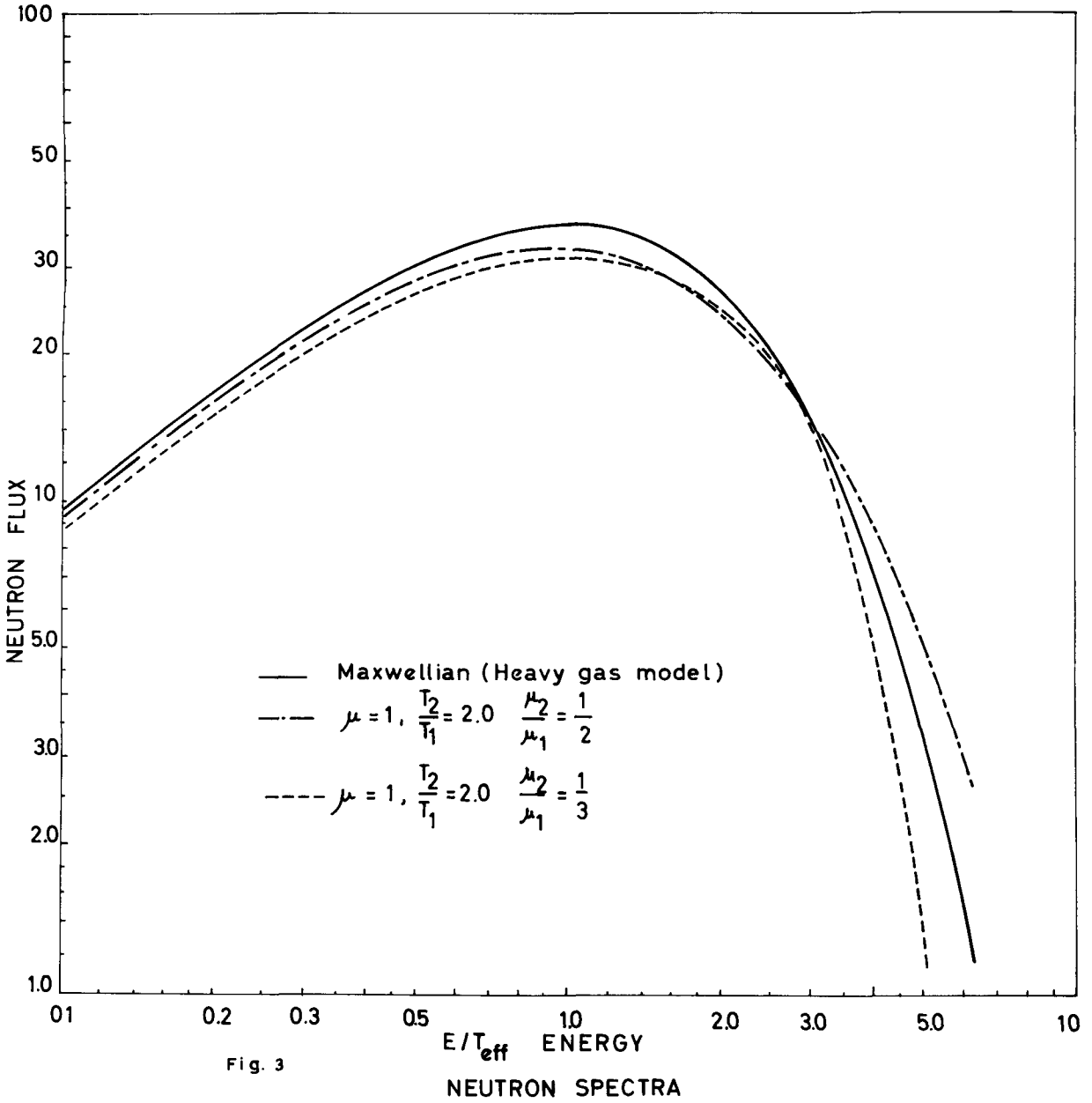

Fig. 3

NEUTRON SPECTRA

*SIMPLE EXPANSIONS FOR THERMAL NEUTRON FLUX AND IMPORTANCE IN A CYLINDRICAL CELL

by

E. U. Vaughan

Atomics International

March, 1962

*The research for this paper was carried out under AEC Contract AT(11-1)-GEN-8

SIMPLE EXPANSIONS FOR THERMAL NEUTRON FLUX and IMPORTANCE IN A CYLINDRICAL CELL

by

E. U. Vaughan

Atomics International

Corrections to subject paper:

On P.3, equation (6) should read:

$$\xi \Sigma_s E\left(\left[1-\frac{kT}{E}\right]\varphi + kT\frac{\partial \varphi}{\partial E}\right) = q(r) \quad \text{at} \quad E = E_o$$

On P.4, the paragraph immediately below the list of notations should read:

That the boundary condition (6) at $E = E_o$ is correct can be seen most readily from the neutron conservation equation in the case $D = 0$, obtained by integration of equation (2) with respect to energy:

$$\int_0^{E_o} dE\, \Sigma_a(E)\,\varphi(E) = \xi\Sigma_s\left[(E_o - kT)\,\varphi(E_o) + kT E_o \left.\frac{\partial \varphi}{\partial E}\right|_{E_o}\right].$$

On P.6, equation (8) should have a factor $(1-kT/E_o)$ multiplying $\varphi(r,E_o)$; equation (11) should have in the numerator an additional term

$$-\frac{kT}{E_o}\int_a^b r\,dr\,\psi(r,E_o)\,\varphi(r,E_o).$$

On P.7, equation (14) should read: $\frac{\partial \psi}{\partial E} - \frac{\psi}{E} = 0$ at $E = E_o$; equation (18) should have a factor $(1-kT/E_o)$ multiplying $\varphi(r,E_o)$.

Corrections to "Simple Expansions for Thermal Neutron Flux and Importance in A Cylindrical Cell"

On P.10, equation (29) should have in the square bracket of the denominator a factor $(1-1/\varepsilon_0)$ multiplying $H(k_n^2, \varepsilon_0)$.

On P.11, the denominator of equation (32), the numerator of equation (33), and the denominator of equation (34) should each have a factor $(1-1/\varepsilon_0)$ multiplying $H(k_0^2, \varepsilon_0)$.

On P.12, equation (36) should have a factor $(1-1/\varepsilon_0)$ multiplying $H(\mu_1, \varepsilon_0)$.

On P. 15, the equation at the top of the page and equation (45) should have factors $(1-1/\varepsilon_0)$ multiplying $H(k_n^2, \varepsilon_0)$. Two terms of (44) put factor $\left[1 - \frac{\nu(2-\nu)}{\varepsilon_0}\right]$ on right of (45).

On P.16, near the top of the page, the statement about the probability that one or the other of the power-series and asymptotic representations of $H(k_n^2, \varepsilon_0)$ converges is too optimistic, except for $H(k_0^2, \varepsilon_0)$.

The succeeding two paragraphs, extending on to P.17 and including equation (48), are largely superfluous, since the change in equation (36) makes $\nu = 0$ an exact eigenvalue for every value of ε_0.

On P.17, equation (48) should read $\nu_0 = 0$.
equation (50) should read $\mu_0 = -\Sigma_a / D$.

April, 1962

I INTRODUCTION

The investigation reported here deals with neutron thermalization in a lattice of parallel cylindrical fuel rods. A cell of the lattice is supposed to have cylindrical symmetry, and to consist of two regions, of which the inner region contains fuel (and possibly other materials) but no moderator, while the outer region contains a homogeneous moderator but no fuel. The most important approximation is the use of diffusion theory in the moderator region; this requires the dimensions of that region to be considerably greater than a moderator mean-free-path. The physical system thus described commonly occurs in reactors having metallic fuel, graphite or heavy-water moderator, and heavy-water or liquid-metal coolant. Hydrogenous moderators are excluded because they require either consistent P_1 or transport theory rather than diffusion theory.

Since diffusion theory cannot be applied in the fuel region, the fuel and moderator regions require separate treatment. A transport-theory calculation in the fuel and adjacent moderator provides an evaluation of the logarithmic derivative, at the fuel-moderator interface, of the asymptotic (diffusion-theoretical) neutron flux in the moderator. The absence of moderator from the fuel permits making this calculation independently for each neutron energy using one-group transport theory; the calculation is relatively easy because the neutron will not make many collisions in the fuel. The resulting energy-dependent values of

the logarithmic derivative impose an energy-dependent boundary condition on the neutron flux in the moderator. The effective inner boundary of the moderator region is taken at the fuel-moderator interface, rather than approximately a mean-free-path into the moderator, because it is desired that all sources of thermal neutrons be included in the effective moderator region, and such sources exist wherever there is moderator. Consequently, the region includes the moderator near the fuel in which diffusion theory is not satisfactory; this is only a small part of the moderator, however, and the error in its treatment - namely, use of the asymptotic flux instead of the correct flux - is expected to affect the thermal utilization but slightly.

The heavy-gas model of thermalization is employed because it is simple, common, and valuable for illustrative purposes; some of the results obtained will hold for more general models, however. The way to combine this model with diffusion theory has been indicated by Hurwitz, Nelkin and Habetler[1]. The source of the thermalizing neutrons is the slowing down density at some cutoff energy E_o above which thermalization effects are not important. If this energy is taken as 0.5 ev, near the cadmium cutoff, then for a reactor whose moderator temperature is not above 500°C, the relation

$$E_o > 7.5\ kT \qquad (1)$$

will hold. This relation probably holds in most cases, and will be used occasionally to test the validity of approximations.

The problem described above is expressed mathematically as a boundary-value problem, consisting of the partial differential equation

$$\xi\Sigma_s\left(1+E\frac{\partial}{\partial E}+kTE\frac{\partial^2}{\partial E^2}\right)\varphi(r,E)+D\nabla^2\varphi(r,E)=\Sigma_a(E)\varphi(r,E), \quad (2)$$

and the boundary conditions

$$\frac{\partial\varphi}{\partial r} = \alpha(E)\varphi \quad at \quad r=a, \quad (3)$$

$$\frac{\partial\varphi}{\partial r} = 0 \quad at \quad r=b, \quad (4)$$

$$\varphi(r,E) = 0 \quad at \quad E=0, \quad (5)$$

$$\xi\Sigma_s E\left(\varphi+kT\frac{\partial\varphi}{\partial E}\right)=q(r) \quad at \quad E=E_0, \quad (6)$$

where

$\varphi(r,E)$ = neutron flux as function of energy E and radial coordinate r,

ξ = mean logarithmic energy loss per collision of moderator,

Σ_s = macroscopic bound scattering cross-section of moderator,

kT = characteristic thermal energy,

D = diffusion constant of moderator,

$\Sigma_a(E)$ = macroscopic absorption cross section of moderator,

$\alpha(E)$ = logarithmic derivative of moderator neutron flux at fuel surface, determined in previous transport-theory calculations in and near fuel,

a = radius of fuel-moderator interface,

b = radius of outer cell boundary,

$q(r)$ = slowing down density at $E = E_0$.

That the boundary condition at $E = E_0$ is correct can be seen most readily by introducing on the left side of equation (2) a source term concentrated at energy E_0,

$$S(r, E) = q(r)\,\delta(E - E_0),$$

and integrating over a small energy range about $E = E_0$, assuming that $\varphi(r, E)$ vanishes for all $E > E_0$.

The solution of this problem would enable all the questions about thermal neutrons to be answered. It may be somewhat difficult to solve, however, unless further restrictions are introduced, such as requiring some of the functions $\Sigma_a(E)$, $\alpha(E)$, $q(r)$ to be constants. Such restrictions can be introduced as approximations, and the necessary corrections treated as perturbations of the resulting approximate solutions. Since the most important result of a thermal neutron calculation is the thermal multiplication factor $\overline{\eta f}$, the perturbation theory should be based on a variational expression for this factor. The following discussion will accordingly set up such a variational expression, and then consider various approximate solutions related to it. Since the problem

is not self-adjoint, the treatment of the adjoint function, or importance, will be conducted separately.

II VARIATIONAL FORMULATION of the PROBLEM

The thermal multiplication factor is brought into the problem by writing the slowing down density $q(r)$ in the form

$$q(r) = Q\, f(r) \,/\, V_m,$$

where

V_m = area of moderator transverse to fuel rods (i.e., volume per unit length)

$$= \pi (b^2 - a^2),$$

$$Q = 2\pi \int_a^b r\, dr\, q(r),$$

and consequently,

$$\int_a^b r\, dr\, f(r) = V_m / 2\pi = \tfrac{1}{2}(b^2 - a^2). \qquad (7)$$

When the system is just critical, the non-thermal neutron balance will demand that

$$Q = p\varepsilon \cdot 2\pi a \int_0^{E_0} dE\, \eta(E) \cdot D \frac{\partial \varphi}{\partial r}\Big|_{r=a},$$

where $\eta(E)$ is the fuel multiplication factor at energy E; while the criticality condition will be

$$1 = k_\infty = p\varepsilon \cdot \overline{\eta f}.$$

Then, equation (6) can be written in the form

$$\varphi(r, E_0) + kT \left.\frac{\partial \varphi}{\partial E}\right|_{E=E_0} = \lambda f(r) \int_0^{E_0} dE\, \eta(E) \alpha(E) \varphi(a, E), \tag{8}$$

$$\lambda = \frac{2aD}{\xi \Sigma_s E_0 \overline{\eta f} (b^2 - a^2)}, \tag{9}$$

in which equation (3) has been used to eliminate $(\partial\varphi/\partial r)_a$.

Equation (8), which replaces equation (6), is homogeneous in $\varphi(r, E)$, and since equations (2) through (5) are similarily homogeneous, there will be solutions only for certain values of the parameter λ. For one of these values, the corresponding solution will never change sign in the relevant range of r and E; this is the required solution, and the value of λ yields a value of $\overline{\eta f}$ by means of equation (9).

Instead of the usual importance function

$$F(r, E),$$

an adjoint function will be employed that is related to it through the equation

$$\psi(r, E) = E F(r, E). \tag{10}$$

In terms of this function, the eigenvalue λ can be expressed in the variational form

$$\lambda = \frac{\int_0^{E_0} dE \left[\frac{Da}{\xi \Sigma_s} \frac{\alpha(E)}{E} \psi(a, E) \varphi(a, E) + \int_a^b r\,dr \left\{\frac{\partial \psi}{\partial E}\left(\varphi + kT \frac{\partial \varphi}{\partial E}\right) + \frac{1}{E}\left(\frac{D}{\xi \Sigma_s} \frac{\partial \psi}{\partial r} \frac{\partial \varphi}{\partial r} + \left[\frac{\Sigma_a(E)}{\xi \Sigma_s} - 1\right] \psi \varphi\right)\right\}\right]}{\int_0^{E_0} dE\, \alpha(E) \eta(E) \varphi(a, E) \cdot \int_a^b r\,dr\, f(r)\, \psi(r, E_0)}. \tag{11}$$

The conditions that this expression be stationary with respect to variations of $\varphi(r,E)$ that satisfy equation (5), or variations of $\psi(r,E)$ such that

$$\psi(r,E) = 0 \quad \text{at} \quad E = 0, \tag{12}$$

are that $\varphi(r,E)$ satisfy equations (2), (3), (4) and (8), and that $\psi(r,E)$ satisfy the partial differential equation

$$\Sigma_t\left(1 - E\frac{\partial}{\partial E} + \tfrac{1}{2}E^2\frac{\partial^2}{\partial E^2}\right)\psi + D\nabla^2\psi = \Sigma_0(E)\psi \tag{13}$$

and the further boundary conditions

$$\frac{\partial\psi}{\partial E} = 0 \qquad \text{at } E = E_0, \tag{14}$$

$$\frac{\partial\psi}{\partial r} = 0 \qquad \text{at } r = b, \tag{15}$$

$$\frac{\partial\psi}{\partial r} = \alpha(E)\left[\psi - \lambda\frac{\xi\Sigma_s}{2a}E\eta(E)\int_a^b r\,dr\,f(r)\,\psi(r,E_0)\right] \qquad \text{at } r = a. \tag{16}$$

Equations (12) through (16) constitute the adjoint problem.

Equation (11) is homogeneous of order zero in $\varphi(r,E)$ and also in $\psi(r,E)$, and consequently independent of the normalization of these functions. If the special normalization condition

$$\lambda\int_0^{E_0} dE\ \eta(E)\alpha(E)\varphi(a,E) = 1 \tag{17}$$

is introduced, equation (8) simplifies to

$$\varphi(r,E_0) - \tfrac{1}{2}T\left.\frac{\partial\varphi}{\partial E}\right|_{E_0} = f(r). \tag{18}$$

Conversely, a function $\psi(r,E)$ that satisfies equations (2) through (5) and (18), together with a value of λ chosen to satisfy (17), will satisfy (8) and constitute a solution of the eigenvalue problem. The thermal multiplication factor determined by (9) and (17) is

$$\overline{\eta f} = \frac{2\,a\,D}{3\,\Sigma_s E_0 (b^2 - a^2)} \int_1^b \eta(E)\,\alpha(E)\,\phi(1,E)\,dE. \tag{19}$$

Similarly, the special normalization

$$\lambda \frac{3\Sigma_s}{D\,a} \int_a^b r\,dr\,f(r)\,\psi(r,E_1) = 1 \tag{20}$$

simplifies equation (16) to

$$\frac{\partial \psi}{\partial r} = \alpha(E)\left[\psi - E\,M(E)\right] \qquad \text{at} \quad r = a. \tag{21}$$

and the system (12) through (16) is solved by solving (12) through (15) and (21), and calculating λ from (20). The resulting thermal multiplication is

$$\overline{\eta f} = \frac{2}{E_1 (b^2 - a^2)} \int_1^b r\,dr\,f(r)\,\psi(r,E_1). \tag{22}$$

Thus, the above special normalizations lead to replacement of the eigenvalue problems by inhomogeneous systems, thus avoiding the search for eigenvalues. The associated expressions for λ, equations (17) and (20), naturally do not have the variational property of equation (11).

As an example of a perturbation, a change from $\alpha(E)$ to $\alpha(E) + \delta\alpha(E)$ may be considered. The change $\delta\lambda_\alpha$ in λ may be estimated

from equation (11), without recomputing $\varphi(r,E)$ and $\psi(r,E)$; the result is

$$\delta\lambda_a = \frac{Da}{\xi\Sigma_1} \frac{\int_0^{E_0} dE \cdot \delta\alpha(E) \cdot \psi(a,E)\varphi(a,E)/E}{\int_0^{E_0} dE\, \alpha(E)\eta(E)\varphi(a,E) \int_a^b r\,dr\, f(r)\psi(r,E_0)} \qquad (23)$$

$$-\lambda \frac{\int_0^{E_0} dE \cdot \delta\alpha(E) \cdot \eta(E)\varphi(a,E)}{\int_0^{E_0} dE\, \alpha(E)\eta(E)\varphi(a,E)} .$$

III SOLUTIONS In The CASE of CONSTANT FUEL BLACKNESS

Specification of the logarithmic derivative $\alpha(E)$ is equivalent to specification of the energy-dependent blackness of the fuel element, $\beta(E)$. The blackness varies between the limits zero and one, and must tend toward the upper limit over much of the thermal range of energy if the thermal utilization is not to fall too low. Thus the blackness, and with it $\alpha(E)$, is expected to vary over a limited range; it is then permissible to replace it by a suitable constant value in computing trial functions for the variational principle. Of course, the blackness will decrease at higher energies; the use of the constant-blackness approximation therefore imposes an upper limit on the value of the cutoff energy E_0.

If $\alpha(E)$ does not depend on energy, the flux can be expanded in terms of a well-known complete set of Bessel functions:

$$\varphi(r,E) = \sum_{n=0}^{\infty} A_n H(k_n^2, E/kT) R(k_n b, k_n r), \qquad (24)$$

$$R(y,x) = Y_1(y)\,J_0(x) - J_1(y)\,Y_0(x), \tag{25}$$

in which the sum is over all the values $k_n(\alpha)$ for which $R(k_n b, k_n r)$ satisfies the boundary condition of equation (3),

$$\frac{\partial}{\partial a} R(k_n b, k_n a) = \alpha R(k_n b, k_n a), \tag{26}$$

The advantage of a constant α is that the values of $k_n(\alpha)$ are not functions of the energy, and consequently that the operators on energy in the differential equation (2) do not operate on the functions R_n. Because of the orthogonality of these functions, the conditions (2) and (5) on $\varphi(r,E)$ are satisfied if the function $H(k_n^2, \varepsilon)$ satisfies the conditions

$$\varepsilon H''(k_n^2, \varepsilon) + \varepsilon H'(k_n^2, \varepsilon) + \left[1 - \frac{D k_n^2 + \Sigma_a(kT\varepsilon)}{\xi \Sigma_s}\right] H(k_n^2, \varepsilon) = 0, \tag{27}$$

$$H(k_n^2, 0) = 0, \tag{28}$$

where primes denote differentiation with respect to $\varepsilon = E/kT$. These equations are merely a case of the problem of thermalization in an infinite homogeneous moderator with heavy-gas slowing down model.

The remaining condition (18) on φ fixes the coefficients A_n:

$$A_n = \frac{\int_a^b r\,dr\, f(r)\, R(k_n b, k_n r)}{\left[H(k_n^2, \varepsilon_0) + H'(k_n^2, \varepsilon_0)\right] \cdot \int_a^b r\,dr\, [R(k_n b, k_n r)]^2} \tag{29}$$

$$\varepsilon_0 = E_0 / \pi T. \tag{30}$$

It is customary to take $f(r)=1$, in which case the theory of Bessel functions leads to analytic expressions for the integrals in (29). A still simpler procedure is to take f(r) proportional to the first eigenfunction,

$$f(r) = C\, R(k_0 b, k_0 r), \tag{31}$$

since all A_n except A_0 will then vanish because of the orthogonality of the R_n. There seems to be no reason to think (31) inferior physically to f(r) = 1. If equation (7) is used to evaluate the constant C, the resulting expression for φ is

$$\varphi(r,E) = \frac{b^2-a^2}{-a\alpha} \frac{k_0^2 H(k_0^2, E/kT)}{H(k_0^2,\varepsilon_0)+H'(k_0^2,\varepsilon_0)} \frac{R(k_0 b, k_0 r)}{R(k_0 b, k_0 a)}, \tag{32}$$

while the value of λ from equation (17) is

$$\lambda = \frac{2a}{b^2-a^2} \frac{H(k_0^2,\varepsilon_0)+H'(k_0^2,\varepsilon_0)}{\int_0^{E_0} dE\, \eta(E)\, H(k_0^2, E/kT)}, \tag{33}$$

from which and equation (9) follows

$$\overline{\eta T} = \frac{D k_0^2}{\xi \Sigma_s} \frac{\int_0^{\varepsilon_0} d\varepsilon\, \eta(kT\varepsilon)\, H(k_0^2,\varepsilon)}{\varepsilon_0 \left[H(k_0^2,\varepsilon_0)+H'(k_0^2,\varepsilon_0)\right]}. \tag{34}$$

This simple result is not enough unless $\alpha(E)$ is really a constant to a sufficient approximation. If the difference between the actual function and an approximating constant is to be treated as a perturbation, using equation (23), it will also be necessary

to evaluate $\psi(r,E)$. For this purpose an expansion of the type used for the flux will not succeed because of the difference between the flux problem and its adjoint. This difference does not arise mainly from the difference between the differential equations (2) and (13), since the function $\exp(-E/kT)\ \psi(r,E)$ satisfies equation (2), and could be used instead of ψ itself. The essential difference is that the source f(r) of the flux appears in the condition at $E = E_o$, equation (18), whereas the source $\alpha(E)\ \eta(E)$ of the importance appears in the condition at r = a, equation (21).

The appropriate expansion is

$$\psi(r,E) = e^{E/kT} \sum_{l=0}^{\infty} B_l H(\mu_l, E/kT) R(\sqrt{\mu_l}\, b, \sqrt{\mu_l}\, r), \qquad (35)$$

where the function $R(y,x)$ is still defined by equation (25), and the function $H(\mu,\varepsilon)$ by equations (27) and (28). But now the separation constants μ_l are not fixed by an equation like (26), but by the condition (14)at $E = E_o$ applied to the function $e^{\varepsilon} H(\mu_l,\varepsilon)$, which takes the form

$$H(\mu_l, \varepsilon_o) + H'(\mu_l, \varepsilon_o) = 0. \qquad (36)$$

The numbers μ_l thus do not depend on the value of α, but rather on the function $\Sigma_a(E)/\xi\Sigma_s$ and the values of kT, E_o, and $D/\xi\Sigma_s$. They are therefore entirely unrelated to the numbers k_n^2 determined by equation (26), and there is no indication that they are all positive, as the values of k_n^2 are, nor even that they all have the same sign. For negative values of μ_l, equation (25) may be

rewritten in terms of the hyperbolic Bessel functions I_0, I_1, K_0, and K_1, with arguments $\sqrt{-\mu_l}\,b$ and $\sqrt{-\mu_l}\,r$.

Since the operator

$$e^{\varepsilon}\left[\partial/\partial\varepsilon + \partial^2/\partial\varepsilon^2\right]$$

is self-adjoint, and the conditions at $\varepsilon = 0$ and $\varepsilon = \varepsilon_0$ are homogeneous, the functions $H(\mu_l, \varepsilon)$ must be orthogonal with respect to the weight function $\varepsilon^{-1} e^{\varepsilon}$ in the range $0 < \varepsilon < \varepsilon_0$. With the usual normalization, there holds

$$\int_0^{\varepsilon_0} d\varepsilon\, H(\mu_l, \varepsilon)\, H(\mu_m, \varepsilon)\, e^{\varepsilon}\varepsilon^{-1} = \delta_{lm}. \tag{37}$$

Moreover, the set $H(\mu_l, \varepsilon)$ is expected to be complete in the range $0 < \varepsilon < \varepsilon_0$, thus ensuring the validity of the expansion (35). The coefficients B_l are found from equation (21) to be

$$B_l = \frac{kT\alpha \int_0^{\varepsilon_0} d\varepsilon\, \eta(kT\varepsilon)\, H(\mu_l, \varepsilon)}{\alpha K(\sqrt{\mu_l}\,b, \sqrt{\mu_l}\,a) - \frac{\partial}{\partial a} K(\sqrt{\mu_l}\,b, \sqrt{\mu_l}\,a)}. \tag{38}$$

It may seem that, since the values of the μ_l do not depend on α, it would be possible to carry through the above solution for $\psi(r, E)$ even if $\alpha(E)$ were not constant. The procedure would fail, however, at the point where the coefficients B_l are evaluated, because a sum of the form

$$\sum_m B_m K(\sqrt{\mu_m}\,b, \sqrt{\mu_m}\,a) \int_0^{\varepsilon_0} d\varepsilon\, \alpha(kT\varepsilon)\, \varepsilon^{-1} e^{+\varepsilon} H(\mu_m, \varepsilon)\, H(\mu_l, \varepsilon)$$

appears in the equation for B_l, and does not reduce to the single term having $m = l$ unless $\alpha(E)$ is a constant.

IV THE CASE of CONSTANT MODERATOR ABSORPTION

If not only $\alpha(E)$ is independent of energy, but also $\Sigma_a(E)$ has this property, the situation is especially simple. Since $\Sigma_a(E)$ is small for the moderators being considered, the latter approximation is probably better-justified than the former. In this case, the equations (27) and (28) that define the spectral function $H(\mu, \varepsilon)$ take the form

$$\varepsilon H''(\mu,\varepsilon) + \varepsilon H'(\mu,\varepsilon) - (\nu-1) H(\mu,\varepsilon) = 0, \tag{39}$$

$$H(\mu,0) = 0, \tag{40}$$

where

$$\nu = (D\mu + \Sigma_a)/\xi\Sigma_s \tag{41}$$

is a constant. This is a confluent hypergeometric equation[2], and the required solution may be represented in terms of the confluent hypergeometric series

$$F(a|c|z) = 1 + \frac{a}{c} z + \frac{a(a+1)}{c(c+1)} \frac{z^2}{2!} + \cdots, \tag{42}$$

which satisfies the equation

$$z F''(z) + (c-z) F'(z) - a F(z) = 0,$$

in the alternative forms

$$H(\mu,\varepsilon) = \varepsilon F(2-\nu|2|-\varepsilon) \tag{43a}$$

$$= \varepsilon e^{-\varepsilon} F(\nu|2|\varepsilon). \tag{43b}$$

In the expansion of the flux, where $\mu = k_n^2$ is positive, ν will be positive, and equation (43b) shows that $H(\mu,\varepsilon)$ will be positive for all positive ε. Moreover, the series approaches unity,

and the solution approaches the Maxwellian $\varepsilon e^{-\varepsilon}$, as ν approaches zero. In order to evaluate the quantity

$$H(k_n^2, \varepsilon_0) + H'(k_n^2, \varepsilon_0)$$

that appears in equations (29) and (32) through (34), an asymptotic approximation may suffice because of the large value of ε_0 (> 7.5), provided the reactor is thermal. Thus the expression[2]

$$H(k_n^2, \varepsilon) \sim \frac{\nu}{\nu!}\varepsilon^{\nu-1}\left[1 + \frac{(1-\nu)\cdot(2-\nu)}{\varepsilon} + \frac{(1-\nu)(2-\nu)\cdot(2-\nu)(3-\nu)}{2!\,\varepsilon^2} + \cdots\right] \quad (44)$$

may be used. If a single term is enough, the result is

$$H(k_n^2, \varepsilon_0) + H'(k_n^2, \varepsilon_0) \sim \frac{\nu}{\nu!}\varepsilon_0^{\nu-1}. \quad (45)$$

In addition to the other approximations, it is usually possible to take $\eta(E)$ to be a constant. In this case, the quantity

$$N(\varepsilon_0) = \int_0^{\varepsilon_0} d\varepsilon\, \eta(kT\varepsilon)\, H(k_n^2, \varepsilon) \quad (46)$$

that appears in the expressions (33) and (34) for the eigenvalue, will satisfy the confluent hypergeometric equation

$$\varepsilon_0 N''(\varepsilon_0) + (\varepsilon_0 - 1) N'(\varepsilon_0) - \nu N(\varepsilon_0) = 0$$

and the initial conditions

$$N(0) = 0, \quad N''(0) = \eta.$$

Consequently, it can be represented by confluent hypergeometric functions as

$$N(\varepsilon_0) = \frac{1}{2}\eta\,\varepsilon_0^2\, F(2-\nu|3|-\varepsilon_0)$$

$$= \frac{1}{2}\eta\,\varepsilon_0^2\, e^{-\varepsilon_0} F(1+\nu|3|\varepsilon_0),$$

with the asymptotic form

$$N(\varepsilon_0) \sim \frac{M}{\nu!}\,\varepsilon_0^{\nu}\left[1 + \frac{(-\nu)\cdot(2-\nu)}{\varepsilon_0} + \frac{(-\nu)(1-\nu)\cdot(2-\nu)(3-\nu)}{2!\,\varepsilon_0^{2}} + \cdots\right], \qquad (47)$$

agreeing with term-by-term integration of equation (44), the constant of integration vanishing.

It is probable that, for the relevant values of k_n^2, one or the other of the power series (43b) and the asymptotic series (44) will converge rapidly to a close approximation of $H(k_n^2, \varepsilon)$, which would accordingly be well represented for all values of ε.

The expansion of the importance involves a new and unfamiliar set of energy eigenfunctions, for which the distribution of eigenvalues μ_l has not yet been determined. The discussion of these functions may be initiated by noting that, if ε_0 were infinite, $\nu = 0$ would be an eigenvalue, since equations (43b) and (42) show that the corresponding eigenfunction would be a Maxwellian, $\varepsilon e^{-\varepsilon}$, which satisfies equation (36) for $\varepsilon_0 \to \infty$. Of course, ε_0 is not infinite, but its value (> 7.5) is substantially larger than the values (≈ 1 or 2) for which the Maxwellian is large. It may accordingly be expected that there will be an eigenvalue ν_0 differing only slightly from zero, with an eigenfunction differing only slightly from a Maxwellian.

The asymptotic behavior indicated in equation (44) is quite different from the Maxwellian unless ν actually vanishes. As ν departs from zero, the Maxwellian will be only slightly modified, while the principal change will be the introduction of the asymptotic

behavior (44). The value of ν_0 may then be estimated by using the sum of (44) and the Maxwellian to represent $H(\mu, \varepsilon_0)$,

$$H(\mu, \varepsilon_0) \approx \varepsilon_0 e^{-\varepsilon_0} + \frac{\nu_0}{\nu_0!} \varepsilon_0^{\nu_0 - 1},$$

and substituting this expression in condition (36). The result is

$$\nu_0 \approx - \varepsilon_0 e^{-\varepsilon_0}, \tag{48}$$

which gives the value $\nu_0 \approx -0.0042$ when $\varepsilon_0 = 7.5$ --a value that is indeed very close to zero. Improving this estimate by using more terms of the asymptotic expression will not change its order of magnitude.

If $\eta(E)$ is nearly constant, the integral in the expression (38) for the expansion coefficients B_ℓ is approximately

$$\int_0^{\varepsilon_0} d\varepsilon\, \eta(kT\varepsilon) H(\mu_\ell, \varepsilon) \approx \eta \int_0^{\varepsilon_0} d\varepsilon\, H(\mu_\ell, \varepsilon)$$

$$\approx \eta \int_0^{\varepsilon_0} d\varepsilon\, H(\mu_\ell, \varepsilon) H(\mu_0, \varepsilon) e^{\varepsilon} \varepsilon^{-1}$$

$$\approx \eta \delta_{\ell 0}$$

by virtue of the orthogonality condition (37). The expansion (35) is thus reduced, to a good approximation, to the single term

$$\psi(r, E) \approx \frac{\alpha \eta E R(\sqrt{\mu_0}\, b, \sqrt{\mu_0}\, r)}{\alpha R(\sqrt{\mu_0}\, b, \sqrt{\mu_0}\, a) - \frac{\partial}{\partial a} R(\sqrt{\mu_0}\, b, \sqrt{\mu_0}\, a)}, \tag{49}$$

where from equations (41) and (48),

$$\mu_0 \approx -\frac{1}{D}\left[\int \Sigma_s \varepsilon_0 e^{-\varepsilon_0} + \Sigma_a\right]. \tag{50}$$

This shows that the importance, $F(r,E) = \psi(r,E)/E$, is insensitive to the energy, and has a radial dependence well represented by a hyperbolic Bessel function. In the usual case of a cell much smaller than the moderator diffusion length, the radial factor also will be nearly constant. The near-constancy of the importance explains the success of the usual non-variational thermalization calculations, which are often equivalent to the use of a constant importance.

If the higher members of the set of eigenfunctions $H(\mu_\ell, \varepsilon)$ are required, it is natural to attempt to repeat the argument made for the lowest member. Imposition of condition (36) at $\varepsilon_c \to \infty$ leads to integer eigenvalues $\mu_\ell = -\ell$, the corresponding eigenfunctions being products of the Maxwellian by Laguerre polynominals. These functions will approximate the correct functions only if ε_0 is effectively large--which must mean that it exceeds all values of ε where the functions show such structures as zeros and maxima. For $\varepsilon_0 = 7.5$, this condition already fails for $\ell = 1$, while for $\varepsilon_0 = 10$ it is satisfied for $\ell = 1$ but fails for $\ell = 2$. These results, as well as improved estimates of the functions when ε_0 is not large enough to justify the preceding treatment, may be established by the WKB approximation method. The significance of these higher eigenfunctions seems insufficient to justify more extended treatment, however, except to note that the successive eigenfunctions belong to successively larger negative values of μ_ℓ, and the corresponding radial functions are successively more rapidly attenuated with increasing radius.

REFERENCES

1. Hurwitz, Nelkin and Habetler, Nucl. Sci. and Eng. 1, 280 (1956).

2. Morse and Feshbach, "Methods of Theoretical Physics", McGraw-Hill, New York, 1953, Vol. I, pp. 604 ff.

G. I. Marchuk, V. G. Turchin, V. V. Smelov,
G. A. Il'yasova

METHODS OF CALCULATING SLOW-NEUTRON SPECTRA

INTRODUCTION

The question of formation of the slow-neutron spectrum is of appreciable interest in connection with the development of the reactor building technology. The most complete solution to this problem was obtained within the framework of the theoretical model of neutron scattering by monatomic gas nuclei. The main results of this theory were presented in a paper delivered to the first and second Geneva Conferences on Peaceful Use of Atomic Energy (E. Cohen [1], J. Chernick [2], A. McReynolds, M. Nelkin, M. Rosenbluth, and W. Whittemore [3], M. V. Kazarnovskiĭ, A. V. Stapanov, F. L. Shapiro [4], and others). As our knowledge concerning thermalization of neutrons became further developed, it became quite clear that a deeper phy-

sical analysis is necessary for the mechanism of neutron scattering in matter, with an account of the crystal effect and molecular bonds. The main efforts of the scientists have been aimed in recent years towards further improvement of the theoretical models for interaction between slow neutrons with matter, free of the serious limitations of the monatomic-gas moderator model. The work carried out in this direction has been presented in the previously cited Geneva Conference papers, and also in a large number of journal articles. The initial theory of slow-neutron scattering in crystalline matter was proposed by R. Weinstock [5]. Since then, many papers have been devoted to this question (A. I. Akhiezer and I. Ya. Pomeranchuk [6], J. M. Cassels [1], G. Placzek and P. Van Hove [8], Finkelstein [9], A. Zemach and R. Glauber [10] and others). At present the most general and most fruitful method of calculating the differential cross section for the interaction between slow neutrons and matter is apparently the Van Hove method [11], which was further developed in recent investigations.

Since the purpose of our paper is essentially a discussion of the mathematical problems arising in the analysis of various aspects of thermalization of neutrons in nuclear reactors, we shall not delve into the principal theoretical problems concerning the interaction between slow neutrons and matter, and will base ourselves on the

mathematical formalism developed in references [12] and [13], within the framework of the Van Hove formalism, for the calculation of the differential scattering cross sections of slow neutrons in matter.

Using the adopted theoretical model for the scattering of slow neutrons, the subsequent problem consists of developing effective mathematical algorithms for solving the integro-differential transport equation of the neutrons in the medium. This problem appears to be mathematically the most complicated and most interesting problem in computational mathematics. The complexity of the problem lies primarily in the fact that the integral operator in the neutron transport equation is a Fredholm-type operator in the region of thermal energies. Consequently, the integro-differential transport equation cannot be solved in this case step by step, starting with the higher neutron energies and dropping into the region of the lower energies, as was done for the neutron slowing-down interval. When determining the spectrum of the slow neutrons with account of thermal motion of the nuclei of the medium, the molecular bonds, and crystal effects it becomes necessary to find simultaneous solutions for all the energies compatible with the neutron transitions from all possible energy intervals to the given energy interval. These singularities of the problem have necessitated the development

of a new mathematical apparatus. A very convenient mathematical apparatus was found to be the method of spherical harmonics in the P_n approximation. The system of integro-differential equations for the Fourier coefficients of the series in spherical harmonics is written in the many-group approximation. The problem is then reduced by the finite-difference method to a system of linear equations, represented in the form of three-point Jacobian matrix systems, the solution of which is obtained with the aid of an iteration process by groups, combined with matrix factorization. This method is quite effective when applied to the calculation of the slow-neutron spectrum in regions of one-dimensional geometry. The basic ideas of the method were developed in the paper by G. I. Marchuk and V. V. Smelov at the second Geneva Conference [14], and also in references [15], [16], and [17].

A. D. Galanin [15] and P. P. Blagovolin [16] made an effort to solve the slow-neutron transport equation for the cell of a heterogeneous reactor in the diffusion approximation, using analytic methods. The calculation was based on the monatomic-gas moderator model. The calculations made by the above methods, however, are more qualitative than quantitative. Apparently only effective methods can lead to quantitative results of practical significance concerning the spectrum of slow neutrons.

Although we do not plan to discuss in detail theoretical problems involved in the scattering of low-energy neutrons, we note that there is great need at present in fundamental experimental data on inelastic scattering of neutrons in matter, data which can help estimate the degree to which calculations based on the continuously arising theoretical models are approximate. Of course, experiments on the spectrum of slow neutrons in various reactor systems are also of great interest. The information highlighted by these experiments is essential primarily for the design of reactor systems. We do not propose to discuss in this paper experimental work on thermalization of neutrons, since a special paper by V. I. Mostovoi and others [18] will deal with the subject, and note only the special importance of setting up such experiments, in which the shortcomings of the theory are particularly clearly pronounced.

1. DIFFERENTIAL SCATTERING CROSS SECTIONS OF SLOW NEUTRONS

1. The first to formulate the problem of scattering of slow neutrons on free atoms were H. Hurwitz and E. Cohen. [19]. The given theoretical model does not take into account the crystal effects and molecular bonds, which are of great importance in the calculation for neutrons in real media. However, the results obtained in the approximation of the monatomic gas moderator model make it possible to

examine the features governing the establishment of the neutron spectrum in the medium under the influence of thermal motion of the atoms of the matter and in many cases yield more or less reliable quantitative estimates. An exact expression for the cross section for scattering of slow neutrons on the nuclei of a monatomic moderator, obtained by V. V. Smelov and L. V. Maĭorov (see [20]), has the following form:

$$\sigma(x_0 \to x, \mu_0) = \frac{\sigma_{el}}{4\pi} \frac{(M+1)^2 \tau^2}{M\sqrt{\pi M}} \frac{x^2}{x_0} \frac{1}{\sqrt{x_0^2 + x^2 - 2xx_0\mu_0}} \times$$

$$\times \exp\left\{ -\frac{\varepsilon\tau^2}{\beta^2} x_0^2 - \frac{\varepsilon + M\beta^2}{4} \left[\frac{\sqrt{x_0^2 + x^2 - 2xx_0\mu_0}}{M\beta} \lambda + \frac{\tau^2}{\beta} \frac{x_0^2 - x^2}{\sqrt{x_0^2 + x^2 - 2xx_0\mu}} \right] \right\} \quad (1)$$

where

$$\beta = \frac{1}{\sqrt{2kT}}, \quad \tau = \sqrt{\frac{M\beta^2}{M\beta^2 + \varepsilon}}, \quad \lambda = 1 + M(1-\tau), \quad x = \beta v$$

X_0 -- neutron velocity prior to collision, x -- neutron velocity after collision, μ_0 -- cosine of the scattering angle in the laboratory system. In the derivation of formula (1) it was also assumed that the elastic-scattering cross section has the form

$$\sigma_{el}(x_R) = \sigma_{el}\, e^{-\varepsilon x_R^2}$$

where x_R -- velocity of the neutron relative to the moving nucleus and ε is a specified constant.

Of greatest interest from the point of view of practical applications are the first two moments of the cross section $\sigma_0(x_0 \to x, \mu_0)$ with respect to the cosine of the scattering angle.

These have the following form [1], [21], [22]:

$$\sigma_0(x_0 \to x) = \sigma_{el} \frac{(M+1)^2}{4M} \frac{\tau^3}{\lambda} \frac{x}{x_0^2} \left[e^{-\frac{\varepsilon\tau^2}{\beta^2} x_0^2} (\operatorname{erf} z_1 + \varepsilon \operatorname{erf} z_2) + \right.$$
$$\left. + e^{x_0^2 - \lambda x^2} (\operatorname{erf} z_3 - \zeta \operatorname{erf} z_4) \right] \quad (2)$$

$$\sigma_1(x_0 \to x) = \sigma_{el} \frac{(M+1)}{4M} \frac{\tau^3 \nu}{\lambda} \frac{x}{x_0^2} \left\{ e^{-\frac{\varepsilon\tau^2}{\beta^2} x_0^2} \left[\left(\frac{x}{x_0}\Theta - \frac{x_0}{x}\eta - \frac{\nu}{x x_0} \right) \cdot \right. \right.$$
$$\cdot (\operatorname{erf} z_1 + \zeta \operatorname{erf} z_2) + \frac{2}{\sqrt{\pi}} \frac{x + x_0}{x x_0} e^{-z_1^2} - \frac{2}{\sqrt{\pi}} \frac{|x - x'|}{x x'} e^{-z_2^2} \Big] +$$
$$\left. + e^{x_0^2 - \lambda x^2} \left(\frac{x_0}{x}\Theta - \frac{x}{x_0}\eta - \frac{\nu}{x x_0} \right) (\operatorname{erf} z_3 - \zeta \operatorname{erf} z_4) \right\} \quad (3)$$

where

$$\left. \begin{aligned} &\Theta = \frac{M+1}{2\tau\sqrt{M}}, \quad \eta = \tau\sqrt{M} - \Theta, \quad \nu = \frac{\tau\sqrt{M}}{\lambda} \\ &z_1 = x\Theta - x_0\eta, \quad z_2 = x\Theta + x_0\eta \\ &z_3 = x_0\Theta - x\eta, \quad z_4 = x_0\Theta + x\eta \\ &\zeta = \begin{cases} 1 & \text{for } x < x_0 \\ -1 & \text{for } x > x_0 \end{cases} \end{aligned} \right\} \quad (4)$$

1.2. The differential cross section for the scattering of slow neutrons with account of crystalline effet and chemical bonds will be considered in the form [3],[12], [22]

$$\sigma(x_0 \to x, \mu_0) = \sigma_{el} \frac{(M+1)^2}{4\pi^2 M^2} \frac{x^2}{x_0} e^{\frac{x_0^2 - x^2}{2}} \int_0^\infty e^{-\frac{\gamma(t)}{2\mu}(x_0^2 + x^2 - 2x_0 x \mu_0)} \cos\frac{x_0^2 - x}{2} t\, dt$$

where $\gamma(t)$ is a certain function having the meaning of dispersion in the Gaussian representation of the autocorrelation function. The first two moments of the slow-neutron scattering function are determined from the formulas

$$\sigma_0(x_0 \to x) = \frac{(M+1)^2}{2\pi M} \frac{x}{x_0^2} e^{\frac{x_0^2 - x^2}{2}} \int_0^\infty \frac{1}{\gamma(t)} \left[e^{-\frac{\gamma(t)}{2M}(x_0 - x)^2} - e^{\frac{\gamma(t)}{2M}(x_0 - x)^2} \right] \cos\frac{x_0^2 - x^2}{2} t\, dt \quad (6)$$

$$\sigma_1(x_0 \to x) = \frac{(M+1)^2}{2\pi M} \frac{x}{x_0^2} e^{\frac{x_0^2 - x^2}{2}} \int_0^\infty \frac{1}{\gamma(t)} \left[\left(1 - \frac{M}{x_0 x \gamma(t)}\right) e^{-\frac{\gamma(t)}{2\mu}(x_0 - x)^2} + \left(1 + \frac{M}{x_0 x \gamma(t)}\right) e^{-\frac{\gamma(t)}{2M}(x_0 + x)^2} \right] \cos\frac{x_0^2 - x^2}{2} t\, dt \quad (7)$$

The function $\gamma(t)$ is the dispersion of the autocorrelation function in the incoherent approximation [23]

$$G(r,t) = \left[2\pi\gamma(t)\right]^{-\frac{3}{2}} e^{-\frac{r^2}{2\gamma(t)}} \qquad (8)$$

This is the form that the autocorrelation function has for an ideal gas, a cubic crystal, and a liquid in the model of continuously diffusing nuclei.

In the case of the scattering of neutrons by a monatomic gas, the function $\gamma(t)$ has the same form as (8) with a dispersion

$$\gamma(t) = \frac{t(Tt - ih)}{M} \qquad (9)$$

where T is the temperature of the medium.

For a cubic crystal we have [8]

$$\gamma(t) = \frac{h^2}{M}\left[\omega - \int_{-\infty}^{\infty} \frac{e^{-\frac{\varepsilon}{2T}}\, g(|\varepsilon|)}{2\varepsilon \operatorname{sh}\frac{\varepsilon}{2T}}\, e^{-i\frac{\varepsilon}{h}t}\, d\varepsilon\right] \qquad (10)$$

where $\varepsilon = h\omega$, $g(\varepsilon)d\varepsilon = g(\omega)d\omega$, and $g(\omega)$ -- spectrum of normal oscillations of the crystal.

As follows from formulas (9) and (10), $\gamma(t)$ for a gas moderator increases as t^2 when $t \longrightarrow \infty$, while for a crystal it tends to a definite limit $\gamma_\infty = h^2\omega/M$.

For a liquid the situation is intermediate and the dispersion $\gamma(t)$ as $t \longrightarrow \infty$ can be connected with the self-diffusion coefficient D by the formula

$$\gamma(t) = 2Dt \qquad \text{for} \quad t \to \infty$$

The motion of an atom in a liquid consists of relatively rapid oscillations about an instantaneous equilibrium position and relatively slow random displacements of the instantaneous equilibrium position, leading to diffusion. Consequently when t is small the function $\gamma(t)$ should behave as in the case of the crystal, while for large t, when diffusion comes into play, it should increase in accord with (10).

References [24] and [35] derived interpolation formulas for $\gamma(t)$, in which these requirements are satisfied. For a liquid and a cubic crystal we have

$$\gamma(t) = \frac{T}{\varepsilon}\left(1+\delta\sqrt{t^2+1}\right)\left[1 - e^{-\frac{\varepsilon(t^2+1)}{2T(1+\delta\sqrt{t^2+1})}}\right] \qquad (11)$$

where we must put $\delta = 0$ for a crystal. Formula (11) can be used, in particular, to calculate the differential cross section for scattering on water.

In the case of graphite, in which the spectrum of the normal oscillations is broader, we can assume

$$\gamma(t) = \frac{1}{2}\,\frac{(t^2+1) + \frac{\beta}{2T}(t^2+1)^{3/2}}{1 + \frac{\beta}{2T}(t^2+1)^{1/2} + \frac{\alpha}{2T}(t^2+1)} \qquad (12)$$

This formula can also be used to calculate the differential cross section of scattering in water. We note that in the case of a graphite crystal we must put in this formula $\beta = 0$.

The parameters α and δ in (11) and (12) are chosen such as to obtain best agreement between the calculated values of the total scattering cross section with the experimental values over the entire energy interval below the end point.

For a temperature T = 300° K the following values were assumed in the calculations for the effective parameters:

For beryllium -- $\delta = 0$, $\varepsilon = 0.01276$.

For graphite -- $\beta = 0$, $\alpha = 0.01547$.

For water -- $\beta = 0.00884$, $\alpha = 0.05200$.

The total scattering cross sections calculated for the given parameters are in good agreement with experiment.

The method of computation and the program for calculating the differential cross sections for the scattering of slow neutrons, in accord with the scheme developed above, were devised by V. V. Smelov and G. A. Ilyasova. Appendix II lists tables of the differential cross sections for the scattering of neutrons on beryllium, graphite, and water. These tables can be used to

calculate the space-energy distribution of slow neutrons in the physical design of reactors.

2. CALCULATION OF THE SLOW-NEUTRON SPECTRUM

2.1. The spectrum of slow-neutrons is usually calculated with the aid of the many-group representation of the neutron transport equation. These problems, depending on their specific features, can be arbitrarily subdivided into those involving the calculation of the microstructure of neutron fields, with which one deals in the calculation of cells of heterogeneous reactors and in the problem involving the determination of the average neutron spectrum in the reactor. From this point of view the fundamental problem is that of the neutron spectrum within a cell of the heterogeneous reactor, since the physical indices of a nuclear reactor are very closely related with the coefficient of thermal utilization, with the aid of which one determines not only the critical parameters of the reactor, but also the conversion ratio of the nuclear fuel in the reactor during the reactor lifetime. The calculation of the spectrum of the slow neutrons entails many mathematical difficulties, which in general reduce to the need of solving as accurately as possible the transport equation, both in space and in energy. Problems involving the calculation of the averaged neutron spectrum in the

reaction, on the basis of information concerning the neutron spectrum in individual reactor cells, can as a rule be solved by using simpler methods, such as the P_1-approximation of the spherical-harmonics method. Even the latter case may involve the need for more accurate calculations if the gradients of the neutron fields, due to the physical or thermal inhomogeneities, turn out to be appreciable. By now there have been developed more or less satisfactory programs for solving one-dimensional problems, and we are at the threshold of solving the many-dimensional problems that must be solved if more justified recommendations are to be made for the design of nuclear-power installations.

2.2. We proceed now to formulate the main problems entailed in the calculation of the spectrum of slow neutrons. In order not to complicate the mathematical aspect of the matter, we start with the simplest P_1-approximation, and will discuss the necessary refinements as we proceed in the solution of the problem. We shall first discuss the many-group representation of the fundamental neutron diffusion equations. Although this appears to be a trivial problem, there is still no unified point of view concerning the methods used to realize the group representations. Some general principles in this direction have been advanced in [16] and [22].

The gist of these principles is that the initial neutron transport equations are replaced by a system of many-group equations in such a way that the chosen basic functionals of the problem retain in this transition their initial value. Let us consider by way of an example the system of basic slow-neutron diffusion equations in the P_1-approximation:

$$\left.\begin{aligned} \nabla\varphi_1 + \alpha\varphi_0 - \int_0^{x_{gr}} \alpha_0(x'\to x)\,\varphi_0(\vec{r},x')\,dx' &= q_{g0}(\vec{r},x) \\ \tfrac{1}{3}\nabla\varphi_0 + \alpha\vec{\varphi}_1 - \int_0^{x} \alpha_1(x'\to x)\,\vec{\varphi}_1(\vec{r},x')\,dx' &= \vec{q}_{g1}(\vec{r},x) \end{aligned}\right\} \qquad (13)$$

subject to the condition

$$2\vec{\varphi}_1\,\vec{n} - \varphi_0 = 0 \qquad \text{on} \qquad S, \qquad (14)$$

where $\vec{n}$ is the outward normal to the surface S. The remaining need no special explanation.

We set the problem (13), (14) in correspondence with the following many-group problems:

$$\left.\begin{aligned} \nabla\vec{\Phi}_1^{\,j} + \alpha_0^j\Phi_0^j - \sum_{l=1}^{m}\alpha^{l\to j}\Phi_0^l &= Q_0^j \\ \tfrac{1}{3}\nabla\Phi_0^j + \alpha_0^j\vec{\Phi}_1^{\,j} - \sum_{l=1}^{m}\alpha_1^{l\to j}\Phi_1^l &= \vec{Q}_1^{\,j} \end{aligned}\right\} \qquad (15)$$

subject to the condition

$$2\vec{\Phi}_1^j \vec{n} - \Phi_0^j = 0 \qquad \text{on } S, \tag{16}$$

where Φ_0^j, $\vec{\Phi}_1^j$, Q_0^j, and Q_1^j are the integral values over the groups (x_{j-1}, x_j) and the coefficients α_0^j, α_1^j, $\alpha_0^{l\to j}$, and $\alpha_1^{l\to j}$ are unknown quantities, which must be chosen to satisfy the condition that on going from the problem (13), (14) to the problem (15), (16) the chosen functional of the problem remains unchanged. In order to find these coefficients, we introduce formally the many-group problem which is adjoint to the problem (15), (16)

$$\left.\begin{aligned} -\nabla\vec{\Phi}_1^{*j} + \alpha_0^j \Phi_0^{*j} - \sum_{l=1}^{m} \alpha_0^{j\to l} \Phi_0^{*l} &= Q_0^{*j} \\ -\tfrac{1}{3}\nabla\Phi_0^{*j} + \alpha_1^j \vec{\Phi}_1^{*j} - \sum_{l=1}^{m} \alpha_1^{j\to l} \Phi_1^{*l} &= \vec{Q}^{*j} \end{aligned}\right\} \tag{17}$$

subject to the condition

$$2\vec{\Phi}_1^{*j}\vec{n} + \Phi_0^{*j} = 0 \qquad \text{on } S, \tag{18}$$

Integrating further the equations of the system (13), (14) within the limits (x_j, x_{j+1}), we arrive at the system

$$\left.\begin{aligned} \nabla\vec{\Phi}_1^{\,j} + \int_{x_j}^{x_{j+1}} \alpha\varphi_0\,dx - \sum_{\ell=1}^{m}\int_{x_\ell}^{x_{\ell+1}} dx'\varphi_0 \int_{x_j}^{x_{j+1}} \alpha_0(x'\to x)\,dx = Q_0^j \\ \tfrac{1}{3}\nabla\Phi_0^j + \int_{x_j}^{x_{j+1}} \alpha\vec{\varphi}_1\,dx - \sum_{\ell=0}^{m}\int_{x_\ell}^{x_{\ell+1}} dx'\vec{\varphi}_1 \int_{x_j}^{x_{j+1}} \alpha_1(x'\to x)\,dx = \vec{Q}_1^{\,j} \end{aligned}\right\} \quad (19)$$

subject to the condition (16).

We now multiply the equations of (19) by Φ^{*j}_0 and $3\Phi^{*j}_1$, add the products, and sum the resultant expressions over j. We then multiply the system (17) by Φ^j_0 and $3\vec{\Phi}^j_1$, add, and sum the resultant expressions also with respect to j. The final results are subtracted from each other and integrated over the volume of the domain G. As a result we can readily obtain the following functional equation

$$\int_G d\vec{r}\left\{\sum_{j=1}^{m}\left[\alpha_0^j\Phi_0^j - \int_{x_j}^{x_{j+1}}\alpha\varphi_0\,dx\right]\Phi_0^{*j} + 3\left(\alpha_1^j\vec{\Phi}_1^j - \int_{x_j}^{x_{j+1}}\alpha\vec{\varphi}_1\,dx\right)\vec{\Phi}_1^{*j} - \sum_{j=1}^{m}\Phi_0^{*j}\sum_{\ell=1}^{m}\alpha_0^{\ell\to j}\Phi_0^{\ell} -\right.$$

$$\left. -\int_{x_\ell}^{x_{\ell+1}} dx'\varphi_0\int_{x_j}^{x_{j+1}} dx\,\alpha_0(x'\to x) + \sum_{j=1}^{m}\vec{\Phi}_1^{*j}\sum_{\ell=1}^{m}\left[\alpha_1^{\ell\to j}\vec{\Phi}_1^{\ell} - \int_{x_\ell}^{x_{\ell+1}} dx'\vec{\varphi}_1\int_{x_j}^{x_{j+1}} dx\,\alpha_1(x'\to x)\right]\right\} = 0 \quad (20)$$

Eq. (20) will be satisfied if we put

$$\alpha_0^j = \frac{\int_{G_u} d\vec{r}\,\Phi_0^{*j}\int_{x_j}^{x_{j+1}}\alpha\varphi_0\,dx}{\int_{G_u} d\vec{r}\,\Phi_0^{*j}\Phi_0^j}\,, \quad \alpha_1^j = \frac{\int_{G_u} d\vec{r}\,\vec{\Phi}_1^{*j}\int_{x_j}\alpha\vec{\varphi}_1\,dx}{\int_{G_u} d\vec{r}\,\vec{\Phi}_1^{*j}\vec{\Phi}_1^{\,j}}\,, \quad (21)$$

$$\alpha_1^{l\to j} = \frac{\int_{G_n} d\vec{r}\,\Phi_0^{*j} \int_{x_l}^{x_{l+1}} dx' \varphi_0 \int_{x_j}^{x_{j+1}} dx\, \alpha_0(x'\to x)}{\int_{G_n} d\vec{r}\,\Phi_0^{*j}\Phi_0^{l}}, \quad \alpha_1^{l\to j} = \frac{\int_{G_n} d\vec{r}\,\vec{\Phi}_1^{*j} \int_{x_l}^{x_{l+1}} dx' \vec{\varphi}_1 \int_{x_j}^{x_{j+1}} dx\, \alpha_1(x'\to x)}{\int_{G_n} d\vec{r}\,\vec{\Phi}_1^{*j}\vec{\Phi}_1^{l}}, \quad (21)$$

where G_n -- partial domains, into which the entire domain G of the solution breaks up.

So far we have left the quantities Q^{*j}_0 and $\vec{Q}^{*j}_1$ arbitrary, and consequently the solution of the adjoint equations is likewise not fixed. The choice of the functions Q^{*j}_0 and Q^{*j}_1 is dictated by the physical meaning of the problem. Let us assume that the most important functional of the problem is the total number of the neutrons captured every second in the subdomain G_n, i.e.,

$$J = \sum_{j=1}^{m} \int_{G_n} d\vec{r}\,\alpha_c^j \Phi_0^j \qquad (22)$$

In this case we must put

$$Q_0^{*j} = \begin{cases} \Sigma_c & \text{, when } \vec{r} \text{ belongs to } G_n \\ 0 & \text{, when } \vec{r} \text{ does not belong to } G_n. \end{cases}$$

2.3. Formulas (21) can be used to determine the coefficients by successive approximation, using the approxi-

mate solutions $\varphi_0(\vec{r}, x)$ and $\vec{\varphi}_1(\vec{r}, x)$, obtained during the process of going over from the integral fluxes ϕ_0^j and $\vec{\phi}_1^j$ to $\varphi_0(\vec{r}, x_{j+1/2})$ and $\vec{\varphi}_1(\vec{r}, x_{j+1/2})$ and reconstituting these functions with the aid of the interpolation formulas. After the coefficients $\alpha_0^j, \alpha_1^j, \alpha_0^{\ell\to j}$ and $\alpha_1^{\ell\to j}$ are obtained, we arrive at the many-group problem (15), (16). This problem can be solved by finite differences. To obtain the corresponding difference system of equations, we rewrite theproblem (15), (16) in vector matrix form

$$\left.\begin{aligned} \nabla\vec{\Phi}_1 + \underline{\Sigma}_0\vec{\Phi}_0 &= \vec{Q}_0 \\ \tfrac{1}{3}\nabla\vec{\Phi}_0 + \underline{\Sigma}_1\vec{\Phi}_1 &= \vec{Q}_1 \end{aligned}\right\} \qquad (23)$$

subject to the condition

$$2\vec{\Phi}_1\vec{n} - \vec{\Phi}_0 = 0 \qquad \text{on } S, \qquad (24)$$

where $\vec{\phi}_0$, $\vec{\phi}_1$, $\vec{Q}_0$, and $\vec{Q}_1$ are vectors whose components are respectively ϕ_0^j, ϕ_1^j, q_0^j, and q_1^j, while $\underline{\Sigma}_1$ and $\underline{\Sigma}_0$ are the following matrices:

$$\underline{\Sigma}_0 = \| \delta_{j\ell}\alpha_0^j - \alpha_0^{\ell\to j} \| , \quad \underline{\Sigma}_1 = \| \delta_{j\ell}\alpha_1^j - \alpha_1^{\ell\to j} \|$$

where $\delta_{j\ell}$ -- Kronecker symbol.

In case of one-dimensional geometry, the system (23)

assumes the form

$$\left.\begin{aligned} \frac{1}{r^{\nu}}\frac{d}{dr}\left(r^{\nu}\vec{\Phi}_1\right) + \underline{\Sigma}_0\vec{\Phi}_0 &= Q_0 \\ \frac{1}{3}\frac{d\vec{\Phi}_0}{dr} + \underline{\Sigma}_1\vec{\Phi}_1 &= \vec{Q}_1 \end{aligned}\right\} \qquad (25)$$

where the parameter ν takes on the values 0, 1, and 2 respectively for plane, cylindrical, and spherical geometry.

By using the methods developed in [15] and [22], the system (25) can be reduced to the form

$$\vec{\Phi}_{k+1} - \underline{B}_k\vec{\Phi}_k + \underline{C}_k\vec{\Phi}_{k-1} = -\vec{f}_k \,, \qquad (26)$$

subject to the following condition at the center

$$\vec{\Phi}_0 = \vec{\Phi}_1 \qquad (27)$$

and the following condition on the outer boundary

$$\vec{\Phi}_{n-1} - \underline{\Gamma}\,\vec{\Phi}_n = -\vec{g} \qquad (28)$$

Here $\vec{\Phi}_k = \Phi_{0k}$, $\vec{f}_k$ and $\vec{g}$ are vectors, while $\underline{B}_k$, $\underline{C}_k$, and $\underline{\Gamma}$ are matrices.

The system (26) -- (28) is solved by matrix factorization

$$\underline{\beta}_{k+1} = \underline{C}_{k+1}\left(\underline{B}_k - \underline{\beta}_k\right)^{-1} \qquad (29)$$

$$\left.\begin{aligned} \vec{z}_{k+1} &= \underline{\beta}_{k+1}\left(\vec{z}_k + \vec{f}_k\right) \\ \vec{\Phi}_k &= \underline{C}_{k+1}^{-1}\left(\underline{\beta}_{k+1}\vec{\Phi}_{k+1} + \vec{z}_{k+1}\right) \end{aligned}\right\} \qquad (29)$$

subject to the conditions

$$\left.\begin{aligned} \underline{\beta}_1 &= \underline{C}_1 \\ \vec{z}_1 &= 0 \\ \vec{\Phi}_M &= \left[\left(\underline{B}_{M-1} - \underline{\beta}_{M-1}\right)^{-1} - \Gamma\right]^{-1}\left[\vec{q} - \left(\underline{B}_{M-1} - \underline{\beta}_{M-1}\right)^{-1}\left(\vec{z}_{M-1} + f_{M-1}\right)\right] \end{aligned}\right\} \qquad (30)$$

This method of solution is stable from the computational point of view and is readily set up for computers. However, if the number of groups is large this method entails operations on vectors and matrices of high order. It is preferable apparently to use in this case the iteration method.

The arguments presented above can be extended in natural fashion to include the calculation of the neutron spectrum in a cell of a heterogeneous reactor.

2.4. However, the calculation of the slow-neutron spectrum in the P_1-approximation, particularly for cells of a heterogeneous reactor, does not lead to results of sufficient accuracy. It is necessary in this case to solve the problem in a higher approximation than the P_1-

approximation. The corresponding mathematical apparatus can be the numerical methods of Vladimirov [26] and Carlson [27] or the method of spherical harmonics. To solve problems in one-dimensional geometry it is apparently most effective to use spherical harmonics, a method which we chose as the basis for programming the corresponding problems. The gist of the method consists of the following.

We consider a many-group system of transport equations for slow neutrons in a certain domain G:

$$\vec{\Omega}\nabla\Phi^j + \alpha^j\Phi^j - \sum_{l=1}^{m}\int d\vec{\Omega}'\,\alpha^{l\to j}(\vec{\Omega}'\to\Omega)\,\Phi^l(\vec{r},\vec{\Omega}') = S^j(\vec{r},\vec{\Omega}) \qquad (31)$$

subject to suitable boundary conditions.

The system of equations is written formally in the form

$$L^j\Phi^j = \sum_{l\neq j}\int d\vec{\Omega}'\,\alpha^{l\to j}\Phi^l + S^j, \qquad (32)$$

where

$$L^j\Phi^j \equiv \vec{\Omega}\nabla\Phi^j + \alpha^j\Phi^j - \int d\vec{\Omega}'\,\alpha^{j\to j}\Phi^j \qquad (33)$$

We seek the solution of (32) by using successive approximations in a fashion similar to that of Seidel

$$L^j \Phi_n^j = \sum_{\ell<j} \int d\vec{\Omega}' \alpha^{\ell\to j} \Phi_n^\ell + \sum_{\ell\geq j} \int d\vec{\Omega}' \alpha^{\ell\to j} \Phi_{n-1}^\ell + S^j , \qquad (34)$$

where n is the number of the iteration.

To improve the convergence of the successive approximation method, it is convenient to employ the ideas of H. Takahashi [28] concerning the advisability of normalization of iterations. It is proposed to normalize the iterations in the following manner.

We assume that in the n-th cycle of iteration we have found approximate values of the solution in the groups $\ell = 1, \ldots, (j-1)$. We calculate the function Φ^j by solving (34). We then examine the exact equation (32), integrated over all solid angles in the domain G, and sum the result over all the groups. If we assume, for example, that the domain G is a reactor cell, we arrive at the formula

$$\sum_j \int d\vec{r} \int d\vec{\Omega}\, \alpha_c^j \Phi^j = \sum_j \int d\vec{r} \int d\vec{\Omega}\, S^j \qquad (35)$$

where the left half of the equation describes the total number of slow neutrons captured every second in the reactor cell, while the right half describes the total number of generated external sources. We stipulate that (35) be satisfied in each cycle of iteration when calculating each value of Φ^j. Thus, after we obtain the value of the

flux ϕ^j with the aid of (34) in the n-th iteration, we must require that the balance equation (35) be satisfied. This is most conveniently done by renormalizing the sources s^j, i.e., by assuming that all the s^j are replaced by cs^j, where c is a constant calculated with the aid of the relation

$$C = \frac{\sum_{\ell \leq j} \int d\vec{r} \int d\vec{\Omega}\, \alpha_\ell^j \phi_n^j + \sum_{\ell > j} \int d\vec{r} \int d\vec{\Omega}\, \alpha_\ell^j \phi_{n-1}^j}{\sum_j \int d\vec{r} \int d\vec{\Omega}\, S^j} \qquad (36)$$

Of course, the values of s^j are constantly replaced by new ones on going from group to group.

2.5. Once the iteration process is formulated, the solution of the problem reduces to a successive solution of the single-velocity transport equations.

The solution of the single-velocity equations is carried out by the method of spherical harmonics on the basis of the finite-difference method. We illustrate this method using a Wigner-Seitz cylindrical cell as an example. In this case we shall have the following equation

$$\sin\theta\left[\cos\psi \frac{\partial \phi}{\partial r} - \frac{\sin\psi}{r} \frac{\partial \phi}{\partial \psi}\right] + \alpha(r)\phi = \int_0^{2\pi} d\psi' \int_0^{\pi} d\theta\, \alpha_s(r,\theta) \phi(\vec{r}, \theta'\psi') + q(\vec{r},\theta,\psi) \qquad (37)$$

where θ -- angle between the vectors $\vec{\Omega}$ and $\vec{\Omega}'$, subject to the condition that in the center of the region the neu-

tron flux is isotropic, while on the outer boundary of the cell R we have

$$\Phi(R,\theta,\psi)=\Phi(R,\pi-\theta,\pi-\psi) \tag{38}$$

We seek a solution of (37) with the aid of a series in spherical functions

$$\Phi(r,\theta,\psi)=\frac{1}{2\pi}\sum_{n=0}^{\infty}\frac{2n+1}{2}A_{n0}(r)P_n(\cos\theta)+ \tag{39}$$

$$+\frac{1}{2\pi}\sum_{n=1}^{\infty}\sum_{m=1}^{n}(2n+1)\frac{(n-m)!}{(n+m)!}A_{nm}(r)P_n^m(\cos\theta)\cos m\psi$$

In the P_3-approximation for the Fourier coefficients, we arrive at a system of six ordinary differential equations, which can be represented in matrix form by means of the system of two equations

$$\left.\begin{aligned}\underline{a}_0\frac{d\vec{J}}{dr}+\frac{1}{r}\underline{T}_0\vec{J}+\underline{\Sigma}_0\vec{\Phi}&=\vec{S}_0,\\ \underline{a}_1\frac{d\vec{\Phi}}{dr}+\frac{1}{r}\underline{T}_1\vec{\Phi}+\underline{\Sigma}_1\vec{J}&=\vec{S}_1,\end{aligned}\right\} \tag{40}$$

where

$$\vec{\Phi}(r)=\begin{vmatrix}A_{00}\\A_{20}\\A_{22}\end{vmatrix},\qquad \vec{J}=\begin{vmatrix}A_{11}\\A_{31}\\A_{33}\end{vmatrix}$$

$$\underline{a}_0 = \begin{Vmatrix} 1 & 0 & 0 \\ -1 & 1 & 0 \\ \frac{1}{2} & -\frac{1}{12} & \frac{1}{24} \end{Vmatrix}$$

$$\underline{a}_1 = \begin{Vmatrix} 1 & -1 & \frac{1}{2} \\ 0 & 1 & -\frac{1}{12} \\ 0 & 0 & \frac{1}{24} \end{Vmatrix}$$

$$\underline{T}_0 = \begin{Vmatrix} 1 & 0 & 0 \\ -1 & 1 & 0 \\ -\frac{1}{2} & \frac{1}{12} & \frac{1}{8} \end{Vmatrix}$$

$$\underline{T}_1 = \begin{Vmatrix} 0 & 0 & 1 \\ 0 & 0 & -\frac{1}{6} \\ 0 & 0 & -\frac{1}{12} \end{Vmatrix}$$

$$\underline{\Sigma}_0 = \begin{Vmatrix} \Sigma_c & 0 & 0 \\ 0 & 5\Sigma_2 & 0 \\ 0 & 0 & \frac{5}{12}\Sigma_2 \end{Vmatrix}$$

$$\underline{\Sigma}_1 = \begin{Vmatrix} 3\Sigma_{tr} & 0 & 0 \\ 0 & \frac{7}{6}\Sigma_3 & 0 \\ 0 & 0 & \frac{7}{360}\Sigma_3 \end{Vmatrix}$$

$$\vec{S}_0 = \begin{Vmatrix} Q_{00} \\ 5Q_{20} \\ \frac{5}{12}Q_{22} \end{Vmatrix}$$

$$\vec{S}_1 = \begin{Vmatrix} 3Q_{11} \\ \frac{7}{6}Q_{31} \\ \frac{7}{360}Q_{33} \end{Vmatrix}$$

with

$$\Sigma_c = \alpha - \alpha_0 \ , \ \Sigma_{tr} = \alpha - \alpha_1 \ , \ \Sigma_2 = \alpha - \alpha_2 \ , \ \Sigma_3 = \alpha - \alpha_3$$

Here α_n are the coefficients of expansion of the scattering indicatrix $\alpha(\tau, \theta)$ in Legendre polynomials $P_n(\cos \theta_0)$.

It is necessary to add to the system (40) the boundary conditions

$$\left.\begin{aligned} &\frac{d\vec{\Phi}}{dr} = 0 \ , \quad \text{for} \quad r=0 \\ &\frac{d\vec{\Phi}}{dr} - \frac{1}{R}\underline{q}\vec{\Phi} = 0 \ , \ \text{for} \ r=R \end{aligned}\right\} \qquad (41)$$

where

$$\underline{q} = \begin{Vmatrix} 0 & 0 & -\frac{5}{3} \\ 0 & 0 & \frac{1}{3} \\ 0 & 0 & 2 \end{Vmatrix}$$

Eliminating from the system (40) the vector function $\vec{I}$, we arrive at an equation for the vector flux $\vec{\Phi}$. This equation coincides formally with the corresponding equation for the scalar quantities in the P_1-approximation. Using the conventional methods we can arrive at a finite-difference system of matrix equations in the following form

$$\vec{\Phi}_{k+1} - \underline{B}_k \vec{\Phi}_k + \underline{C}_k \vec{\Phi}_{k-1} = -\vec{f}_k \ , \qquad (42)$$

subject to the condition that

$$\left.\begin{aligned} \vec{\Phi}_0 - \underline{\omega}\vec{\Phi}_1 &= \vec{\gamma} \\ \vec{\Phi}_{n-1} - \underline{\Gamma}\vec{\Phi}_n &= -\vec{g} \end{aligned}\right\} \qquad (43)$$

where $\underline{B}_k$, $\underline{C}_k$, $\underline{\omega}$, and $\underline{\Gamma}$ are certain functions while $\vec{f}_k$, γ, and $\vec{g}_n$ are vectors. It must be noted that in the vicinity of the center of the system the connection between the solution at the points k = 0 and k = 1 is obtained with the aid of the first condition in (41) in combination with the initial equation, which for this case is transformed with account of approximate equations of the form

$$\frac{1}{r}\frac{d\vec{\Phi}}{dr} \longrightarrow \frac{d^2\Phi}{dr^2}$$

These equations are valid by virtue of the analytic properties of the solutions in the spherical-harmonic method.

The problem (42), (43) coincides in its structure with the previously considered problem (26) -- (28), the only difference being that the condition regarding the center of the system has been modified somewhat, and it becomes necessary to deal with third-order matrices. The solution of the system (42), (43) is with the aid of matrix factorization, on the basis of formulas (29) and (30), where the initial conditions for β_1 and z_1 must be replaced by the conditions

$$\left.\begin{aligned} \underline{\beta} &= \underline{c}_1 \underline{\omega} \\ \vec{\underline{z}}_1 &= \underline{c}_1 \vec{\gamma} \end{aligned}\right\} \qquad (44)$$

2.6. From the point of view of numerical calculations, it remains to discuss the question of obtaining single-group effective constants for the homogenized reactor cell. Such constants are essential for further calculations of the critical parameters of the reactors.

We shall assume that many-group methods were used to calculate the slow-neutron spectrum in the reactor cell. The effective single-group constants are determined from the condition that the chosen functional of the problem remain unchanged as we go from the many-group problem to the single-group one. Since the most important characteristic in the calculation of the cell is the thermal utilization coefficient, it is advantageous to choose for the main functional of the problem the number of neutrons captured in the block.

We consider further a system of many-group equations, which we shall write for the sake of simplicity in the P_1-approximation:

$$\left.\begin{aligned} \nabla \vec{\Phi}_1^j + \alpha_0^j \Phi_0^j - \sum_\ell^{\ell\to j} \alpha_0^\ell \Phi_0^\ell &= Q_0^j \\ \tfrac{1}{3} \nabla \Phi_0^j + \alpha_1^j \vec{\Phi}_1^j - \sum_\ell^{\ell\to j} \alpha_1^\ell \vec{\Phi}_1^\ell &= \vec{Q}_1^j \end{aligned}\right\} \qquad (46)$$

subject to the condition

$$\vec{\Phi}_1^j \vec{n} = 0 \qquad \text{on } S, \tag{47}$$

We now introduce the effective single-group equation

$$\left.\begin{aligned} -\nabla \vec{\Phi}_1^* + \Sigma_{cr.} \Phi_0^* &= \bar{\alpha}_c^{bl.} \\ -\tfrac{1}{3} \nabla \Phi_0^* + \Sigma_{tr.} \vec{\Phi}_1^* &= 0 \end{aligned}\right\} \tag{48}$$

subject to the condition

$$\vec{\Phi}_1^* \vec{n} = 0 \qquad \text{on } S, \tag{49}$$

where

$$\bar{\alpha}_c^{bl.} = \begin{cases} \sum_j \int_{V_{bl}} \alpha_c^j \Phi^j \, dr \Big/ \sum_j \int_{V_{bl.}} \Phi^j \, d\vec{r} & \text{inside} \\ 0 & \text{outside} \end{cases}$$

We then arrive by the methods developed in item 2.2 to the following formulas for the effective homogenized constants

$$\Sigma_{cr.} = \frac{\int d\bar{r} \, \overline{\alpha_c^j \Phi_0^j} \, \Phi_0^*}{\int d\bar{r} \, \Phi_0 \Phi_0^*} , \tag{50}$$

$$\Sigma_{jT} = \frac{\int d\bar{r}\, \overline{\alpha_j \Phi_0^j}\, \Phi_0^*}{\int d\bar{r}\, \Phi_0 \Phi_0^*}, \quad \Sigma_{t_v T} = \frac{\int d\bar{r}\, \overline{\alpha_{t_v}^j \Phi_1^j}\, \Phi_1^*}{\int d\bar{r}\, \overline{\Phi}_1\, \overline{\Phi}_1^*} \qquad (50)$$

where the integration is over the entire volume of the cell.

3. RESULTS OF NUMERICAL CALCULATIONS

3.1. The methods developed in the present paper were used in calculations of slow-neutron spectra in homogeneous media as well as in heterogeneous ones. The simplest problems solved were those for the determination of the neutron spectrum in graphite, beryllium, and water. Calculations were also made for homogeneous mixtures of the foregoing substances with an absorber having a capture cross section that varies as 1/v. For the sake of convenience, we choose as the parameter the number of absorber capture barns at E = 0.026 ev per nucleus of graphite, beryllium, and hydrogen respectively. The graphite density was taken to be 1.67 g/cm^3, the beryllium density 1.85 g/cm^3, and the water density $1 g/cm^3$. The calculation was

carried out for T = 300° K.

All the calculations were made in the 15-group approximation, with the group numbered j = 0 introduced to specify the external sources. We shall henceforth eliminate the group j = 0 from consideration, starting the analysis each time with the group j = 1. The interval of the zero group is chosen to be $\Delta x_1 = 0.9$, while in all others $\Delta x_j = 0.3$. Thus, $x_{gr} = 5.1$. By way of the center points of the intervals we choose the centers of the intervals in all groups, with the exception of some of the last groups where we find the center points by considering the mathematic expectation of the quantity X within the limits of the group, with account of the neutron spectrum. Such an analysis provided a certain correction of negative sign to the coordinate of the center of the corresponding interval.

The physical constants at energy E = 0.026 ev were chosen in accord with Table I.

Table I

№	moderator	σ_s (barns)	σ_c (barns)
1	beryllium	6.0	0.010
2	graphite	4.8	0.003
3	water	43.8	0.660

The necessary constants for U-235 and U-238 were chosen in accord with the data of [30] and [31]. It was assumed that the cross sections for capture by beryllium, graphite, and water obey the 1/v law. Of course, this assumption was not made for the uranium isotopes.

The results of calculation of the slow-neutron spectra in infinite volumes of beryllium, graphite, and water are plotted in Figs. 1, 2, and 3. The function employed here is not the neutron flux $\varphi = nv$, but the quantity nv^2, in accord with [18]. The abscissas are plotted in the variable 1/x. A recalculation of the corresponding quantities to other variables entails no difficulty. The function nv^2 has been normalized in the figures in arbitrary fashion. Tables 1, 2, and 3 of Appendix I contain integral group neutron fluxes in beryllium, graphite, and water as functions of the absorber capture cross section, which obeys a 1/v law.

Fig. 4 shows the dependence of the neutron-gas temperature in different homogeneous media on the absorber capture cross section. The temperature of the neutron gas was arbitrarily calculated from the maximum of the function nv^2.

3.2. The greatest interest is attached to the calculations of heterogeneous cells. The reason for it is that in such calculations one uses information not only concerning the zero moment of the scattering kernel, as occurs in the calculations of the neutron spectrum in an infinite homogeneous medium, but also higher terms of the expansion of the scattering kernel in Legendre polynomials. It is usually assumed that the greatest contribution to the scattering of slow neutrons is made by the zero and first moments, and therefore the remaining terms of the expansion of the scattering kernel, starting with the second, can be neglected. Such an assumption is justified apparently at least for cases when the spatial inhomogeneities of the physical properties of the medium are commensurate with the mean free path, although it does call for a separate analysis.

The theory and methods of calculation of the neutron spectrum in a heterogeneous reactor lattice, with account of thermalization, were investigated by many researchers. Mention should be made in this connection of the work by A. D. Galanin [16], P. P. Blagovolin [17], H. Takahashi [28], L. de Sobrino [31], and also the authors of the present paper [15], [32]. The interest in such calculations has particularly increased in recent years, since progress has been made in the theory of the slowing down of neutrons,

in computation methods, and also in the experiments.

In the present article we made an attempt to investigate more or less systematically the neutron spectra in heterogeneous cells with account of the latest information on the mechanism governing the scattering of neutrons in substances and the latest accomplishments in computational mathematics.

For the sake of being definite, we considered a two-zone cylindrical Wigner-Seitz cell, consisting of a center block made of natural uranium, surrounded with a moderator. In all the calculations the diameter of the uranium block was taken to be d = 35 mm. The choice of the block thickness was determined essentially by the experiments made by V. I. Mostovoĭ [18], [32], which will be used later on to compare the theoretical results with the experimental ones. The moderators used were beryllium, graphite and water. The parameter in the calculations was the external radius of the Wigner-Seitz cell. As in the case of homogeneous media, the calculations were made at a temperature $T = 300^{\circ}$ K.

The calculation of the space-energy distribution of slow neutrons over the cell was made in the five-group representation of the velocity interval $0 < x \leq 5.1$ in the P_3-approximation of the spherical-harmonic method. The spectra of the integral group fluxes in uranium-beryllium

cells over the radius are listed in Table 4 of Appendix I. The analogous results for graphite and water are listed in Tables 5 and 6 of Appendix I. Figs. 5, 6, and 7 give the total fluxes of thermal neutrons, obtained as a result of summing the group fluxes at the corresponding points. Normalization of the curves is made in such a fashion that the total flux on the boundary of the Wigner-Seitz cell is equal to unity. An analysis of Figs. 5 -- 7 shows that the neutron flux in the block decreases with increasing amount of moderator in the cell. One can note simultaneously that the maximum gradients of the flux correspond to the case of minimum amount of moderator. At first glance it may appear strange that the derivative of the neutron flux does not vanish on the outer boundaries of small cells, a condition essential in diffusion theory. This apparent paradox is simply due to the fact that the absence of a neutron flux through the outer boundary of the cell in the P_n-approximation is not equivalent to the aforementioned condition. However, as the dimensions of the cell increase the diffusion condition is satisfied all the more accurately. The fact that the diffusion condition does not hold true on the outer boundary of the cell makes doubtful the possibility of using diffusion theory for approximate calculations of heterogeneous-reactor cells of analogous dimensions. The position is all the more

aggravated in the calculation of multi-zone cells, which are essentially inhomogeneous radially. Fig. 8 shows plots of the coefficient of thermal utilization for uranium-beryllium, uranium-graphite, and uranium-water cells. Fig. 9 shows the temperatures of the neutron gas for certain cells.

We proceed to an analysis of the results of the calculation from the point of view of comparing these results with the experimental data. We had at our disposal the paper by V. I. Mostovoĭ et al. [18], presented to the second Geneva Conference of 1958, and also the results of the latest researches of V. I. Mostovoĭ and his co-workers on neutron spectra in uranium-water lattices, reported to the Brookhaven Conference [33]. Calculations of the experiments by V. I. Mostovoĭ and his co-workers were undertaken by L. de Sobrinoand by M. Clark [31], and also by L. V. Maĭorov. The authors used as the theoretical basis the model of monatomic gas moderator with effective mass of the water molecules. We shall not go on to discussions of the results of these investigations, since we do not have enough information on the algorithms used in the calculations and other essential details, which frequently determine the success or failure of the results, but will attempt to make as careful a comparison of the results as possible based on the methods formulated in the present article.

The initial lattice considered was a triangular lattice of blocks made of natural uranium, placed in water [18], [33]. In the experiments the uranium block was clad in aluminum 2 mm thick. Thus, a three-zone cell was considered, consisting of the uranium block, with diameter d = 35 mm, an aluminum layer 2 mm thick, and a layer of water 6.6, 9.2, and 11.8 mm thick, corresponding to the lattice periods of 50, 55, and 60 mm. The mean temperature in the cells was taken to be 323° K in all the variants.

Figs. 10 -- 11 show plots of the neutron spectrum in the uranium block and water in a cell with pitch 35 mm. The solid lines denote the results of theoretical calculation of the neutron spectrum at the center of the uranium block and on the outer boundary of the cell. The points represent the data obtained in [33]. We note that [18] gives spectra averaged over the block and over the water, and therefore do not correspond fully to the calculation conditions.

Fig. 12 shows the calculated values of the curves for the spatial distribution of the thermal-neutron flux over the cells, corresponding to H = 50 mm, 55 mm, and 60 mm.

An analysis of the results shows that the theoretical spectra are in general in satisfactory agreement with experiment. One can conclude, in particular, that the

calculated and experimental values are in satisfactory agreement in the position of the maximum of the neutron spectrum both in the uranium block and in the water. If we assume that the point of the maximum of the spectrum characterizes the temperature of the neutron gas, we can state that the calculated and experimental temperatures of the neutron gas are in good agreement. Also in agreement are the differences of the neutron-gas temperatures in the block and in the water. Plots showing the dependence of the neutron-gas temperature on the lattice pitch are shown in Fig. 14. It follows from Fig. 14 that the difference in temperature in the indicated interval of variation of the lattice pitch remains almost constant, having a certain tendency towards decreasing when the lattice pitch increases. This difference is approximately 80°, as confirmed by experiment [18]. A slight difference in the theoretical and experimental results shown in Figs. 10 and 11 occurred in the region of transition energies, where the Fermi spectrum goes into a Maxwellian spectrum. Unfortunately, we have not as yet a sufficient variety of experiments for an all-out theoretical study of this problem on the basis of detailed calculations. It appears to us, however, that the probable cause of the discrepancies lies in the mathematical model which we choose as the basis. In fact, in all the calculations it was assumed

that the neutron sources are distributed in a sufficiently narrow group with number j = 0. Apparently in the future calculations the neutron sources must be shifted as far as possible towards the higher energies. Then the slowing down of the neutrons to energies at which the effect of thermalizations become noticeable will cause the neutron spectrum to be close to a Fermi spectrum, and in this case the comparison of the spectra in the region of the transition energies will become more justified. We note incidentally that a certain rise in the nv^2 curves in Figs. 9 -- 14 towards the larger energies (decreasing values of 1/x) is the consequence of precisely the factors noted above.

4. DIFFUSION OF SLOW NEUTRONS IN INHOMOGENEOUS MEDIUM

4.1. The numerical computation methods developed in the preceding sections of this paper make it possible to determine with sufficient accuracy the spectrum of the slow neutrons in the medium, provided the scattering kernel has been determined completely rigorously. However, in many cases there is no reliable basis for satisfactory calculation of the kernel, and the assumptions of the gas model turn out to be insufficiently justified. In such cases it is possible to use the method of calculating the spatial determination of the slow-neutron field, developed by I. P. Stakhanov and A. S. Stepanov. This method is valid

in those cases, when the neutron distribution function is nearly Maxwellian. In addition to a general approach to the solution of the problem, interest is attached also to the possibility of calculating the neutron distribution not with the aid of the scattering kernel, but on the basis of determination of certain effective constants from the fundamental experiments. This method consists of the following. For a rather extensive group of problems the average kinetic energy of the neutrons differs from 3/2 kT' (T' is the temperature of the medium). This is due, first of all, to the presence of absorption, and second, to the weak exchange of energy between the neutrons and the moderator. The question arises of generalizing the diffusion theory to include the case when there is no thermodynamic equilibrium between the diffusing components.

We shall start from the following premises: a) we investigate only thermal neutrons, i.e., the spectrum has no Fermi component; b) there are no sources in the investigated medium; c) the absorption is small. Following [29], we seek the solutions of the kinetic equation

$$\frac{\partial f}{\partial t} + v_i \frac{\partial f}{\partial x_i} + \gamma f = \int \left\{ \varphi(\vec{v}', \vec{v}) f(\vec{v}') - \varphi(\vec{v}, \vec{v}') f(\vec{v}') \right\} d\vec{v}' \quad (51)$$

in the form of an expansion in symmetrized Hermite polynomials

$$f(\vec{v}) = a^{\circ} f_{\circ} + a_i^{(1)} \frac{\partial f_{\circ}}{\partial v_i} + a_{ik}^{(2)} \frac{\partial^2 f_{\circ}}{\partial v_i \partial v_k} + \cdots \qquad (52)$$

where γ is the absorption coefficient, $\mathcal{G}(v', v)$ is a function determining the probability that the neutron with velocity v' prior to collision will have a velocity $\vec{v}$ after collision, and f_0 is defined by the relationship

$$f_{\circ} = n\left(\frac{m}{2\pi k T}\right)^{3/2} e^{-\frac{v^2}{2kT}} \qquad (53)$$

The expansion coefficients in (52) are functions of $\vec{r}$ and t, and are simply related with the moments of the distribution function:

$$a^{\circ} = 1 \;,\; a_i^{(1)} = -\frac{1}{n}\gamma_i \;,\; a_{ik}^{(2)} = -\frac{kT}{m}\delta_{ik} + \frac{1}{n}\gamma_{ik}$$

$$n = \int f d\vec{v} \;,\; \gamma_{i\ldots s} = \int v_i \cdots v_s f d\vec{v} \qquad (54)$$

Usually the distribution function differs little from iso-

tropic, and therefore $a_{ik}^{(2)}$ is close to zero when $i \neq k$. In order to make the third term of the expansions small, it is necessary to cause the trace of the tensor a_{ik} to vanish. This is accomplished by choosing the parameter $T(\vec{x}, i)$ -- the temperature of the neutron gas:

$$T = \frac{m}{3kn} J_{ii} \qquad (55)$$

with such a choice of the parameter T, we can confine ourselves in the expansion (52) to the first two terms (diffusion approximation):

$$f(\bar{v}) = f_0 \left(1 + \frac{m v_i}{nkT} J_i\right) \qquad (56)$$

Integrating (51) with account of (56) we obtain a system of equations for n, $\vec{I}$, and T:

$$\left.\begin{aligned} &\frac{\partial n}{\partial t} + \frac{\partial J_k}{\partial x_k} + \gamma n = 0 \\ &\frac{\partial nT}{\partial t} + \frac{5}{3}\frac{\partial}{\partial x_k} J_k T + \gamma n T = \frac{T' - T}{\tau} n \frac{T}{T'} \\ &J_i = -\frac{k}{m}\frac{1}{\lambda}\frac{\partial}{\partial x_i} nT \end{aligned}\right\} \qquad (57)$$

where τ -- relaxation time of the neutron temperature, λ -- kinetic coefficient determining the diffusion and the thermal diffusion of the neutrons. Since λ and τ are generally speaking dependent on T(x, t) and T', it is possible to solve (57) in general form only by numerical means. For the gas model of a heavy moderator ($\alpha = \sqrt{M/m} \gg 1$) we obtain the following relationships:

$$\left.\begin{aligned} \lambda &= \frac{8}{3\sqrt{\pi}} n' \sigma_0 \sqrt{\frac{2kT'}{m}} \left\{1 - \frac{1}{\alpha^2}\left[\frac{3}{4}\frac{T'}{T} - \frac{1}{2}\right]\right\} \\ \frac{1}{\tau} &= \frac{16}{3}\frac{1}{\sqrt{\pi}} \sigma_0 n' \left(\frac{T'}{T}\right)^4 \sqrt{\frac{2kT}{m}} \left\{\frac{1}{\alpha^2} - \frac{3}{2}\frac{1}{\alpha^4}\right\} \end{aligned}\right\} \qquad (58)$$

where σ_0 is the scattering cross section of the neutrons on the moderator atom, and n' is the density of the moderator atoms.

It must be noted that the theory developed here is applicable at distances of several free paths from the boundaries and the discontinuity points of the medium parameters. It was assumed in addition that the fourth term of the expansion (52) is small, meaning that the energy isotropy of the neutron distribution is small, i.e., the theory is not exact near the neutron sources when the neutrons have a temperature differing from the temperature

of the medium.

Using (57) and (58), we calculate the field T(x) in the stationary case (spherical source of neutrons of temperature T and of radius r in an infinite space), when there is no absorption. We obtain the following values:

$$|T' - T| = |T - T_0| \exp\left(-\frac{1}{L^2}\frac{r^2 - r_0^2}{2}\right), \quad L^2 = \frac{5}{3}\frac{\tau}{\lambda}\left(\frac{kT'}{m}\right), \qquad (59)$$

where L is the relaxation length (for water, 0.7 -- 0.8 cm). The corresponding experimental value obtained by E. Ya. Dol'nitsyn, turned out to be 1 ± 0.2 cm.

For a planar problem with a temperature gradient $T' = T_0(1 - \alpha x)$ in the case when $(1 - \alpha a) \ll 1$ (a -- characteristic scale of the medium), we have

$$T - T' \cong L^2\alpha^2\left(-e^{-\frac{x}{L^2\alpha}} + 1\right) T_0 \qquad (60)$$

At the point x = 0 the neutrons are in equilibrium with the medium and have a temperature $T = T_0$. As can be seen from (60), the value of $|T - T'|$ tends to $T_0\alpha^2 L_2$ with increasing x.

In the case where absorption exists ($\gamma \neq 0$) we can obtain from (57) the effective neutron temperature

$$T_{eff} = T'\left(1+\frac{2}{3}\gamma\tau\right) =$$

$$= T'\left[1+\frac{1}{4}\frac{\sigma_a(T')}{\sigma_0}\alpha^2\left(\frac{T_{eff}}{T'}\right)^4\left(1+\frac{3}{2}\frac{1}{\alpha^2}\right)\right] \cong$$

$$\cong T'\left[1+\frac{1}{4}\frac{M}{m}\frac{\sigma_a(T')}{\sigma_0}\right] \qquad (61)$$

The method developed makes it possible, in particular, to determine on the basis of an analysis of experimental data the two constants λ and τ in the system (57). The system of equations can then be employed to solve specific problems. Naturally, depending on the circumstances, the method developed here can be used to solve both non-stationary and stationary problems.

BIBLIOGRAPHY

1. E. Cohen, Collection, Experimental Reactors and Reactor Physics [Translation of First Geneva Conference Paper No. 611], GITTL, 1956.

2. J. Chernick, ibid. [Translation of Paper No. 603].

3. A. MacReynolds, M. Nelkin, M. Rosenbluth, W. Whittemore, Tranactions of the Second International Conference on the Peaceful Use of Atomic Energy (Geneva, 1958). Papers of foreign scientists, Moscow, Atomizdat, 1959.

4. M. V. Kazarnovskii, A. V. Stepanov, F. L. Shapiro. Collection: Yadernye reaktory i yadernaya energetika [Nuclear Reactors and Nuclear Power], Atomizdat, 1959.

5. R. Weinstock, Phys. Rev. 65, 1944.

6. A. I. Akhiezer, I. Ya. Pomeranchuk, Nekotorye voprosy teorii yadra [Certain Problems in Nuclear Theory], Gosizdat, 1950.

7. J. M. Cassels, Proc. Roy. Soc. A208, 527, 1951.

8. G. Placzek and L. van Hove, Nuovo cimento 1955.

9. Finkelstein, Phys. Rev. 101, No. 1, 1952.

10. L. van Hove, Phys. Rev. 95, 249, 1954.

11. V. F. Turchin, Collection, Neitronnaya fizika [Neutron Physics], Gosatomizdat, 1961.

12. V. F. Turchin, ibid.

13. G. I. Marchuk, V. V. Smelov, et al. Collection, Yadernye reaktory i yadernaya energetika, Atomizdat, 1959.

14. G. I. Marchuk, V. V. Smelov, Collection, Neitronnaya fizika, Gosatomizdat, 1961.

15. A. D. Galanin, ibid.

16. P. P. Blagovolin, ibid.

17. V. I. Mostovoĭ, V. S. Dikarev, M. B. Egiazarov, Yu. S. Saltykov, Collection Yadernye reaktory i yadernaya energetika, Atomizdat, 1959.

18. M. Nelkin and E. Cohen, Transactions of Second International Conference on Peaceful Use of Atomic Energy (Geneva 1958), Papers of foreign scientists, Moscow, Atomizdat, 1959.

19. G. I. Marchuk, Numerical Methods Designing Nuclear Reactors [Chislennye metody rascheta yadernykh reaktorov], Gosatomizdat, 1958.

21. V. V. Smelov, Atomnaya energiya [Atomic Energy] 3, No. 10 (1957).

22. G. I. Marchuk, Metody rascheta yadernykh reaktorov [Methods of Calculating Nuclear Reactors], Gosatomizdat, 1961.

23. M. Nelkin and D. Parks, Phys. Rev. 119, 1060, 1960.

24. V. F. Turchin, Paper delivered to Symposium on Scattering of Neutrons in Solids and Liquids, Vienna, 1960.

25. G. I. Marchuk and V. V. Orlov, Collection Neitronnaya fizika, Gosatomizdat, 1961.

26. V. Vladimirov, Collection, Vychislitel'naya matematika [Computational Mathematics] No. 3, 1958.

27. B. Carlson and J. Bell, Collection "Physics of Nuclear Reactors" [Translations of Second Geneva Conference Papers], Atomizdat, 1959.

28. H. Takahashi, Nuclear Science and Engineering, 5, 338 -- 346, 1959.

29. D. Hughes and R. Schwartz, Neutron Cross Sections New York, Mc-Graw Hill Book Company, 1959.

30. I. V. Gordeev, D. A. Kardashev, A. V. Malyshev, Spravochnik p yaderno-fizicheskim konstantam dlya rashetov reaktorov [Handbook for Nuclear-Physics Constants for Design of Reactors], Gosatomizdat, 1960.

31. L. de Sobrino, M. Clark, Nuclear Science and Engineering, 10, 337, 1961.

32. V. I. Mostovoĭ, V. S. Dikarev, M. B. Egiazarov, Yu. S. Saltykov, Measurement of Spectra of Neutrons in a Uranium-Water Lattice and Uranium-Mono isopropyl diphenyl, Paper delivered at Brookhaven Conference, 1962.

34. H. Grad, Communications in Pure and Applied Mathematics, 2, 231, 1949.

35. V. F. Turchin, V. V. Smelov, G. A. Ilyasova, Calculations of Differential Cross Sections for the Scattering of Slow Neutrons in the Approximation of Isotropic Atomic Bond. Conference on Slow-Neutron Physics, Dubna, December 1961.

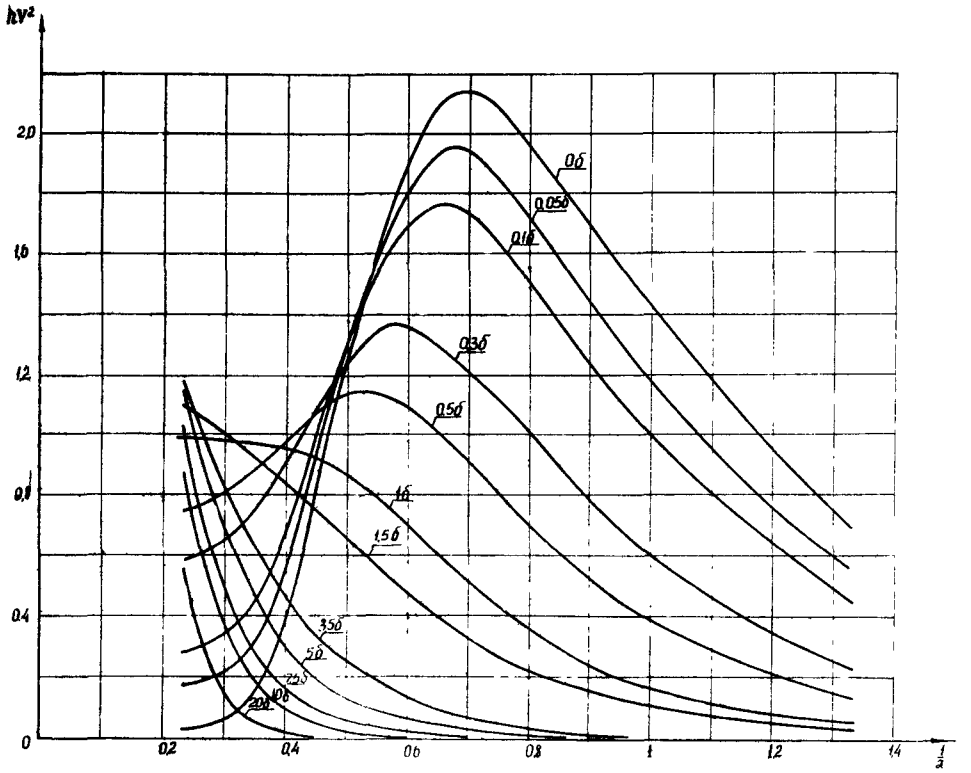

Figure 1. Neutron spectra in a homogeneous mixture of beryllium and (1/v) absorber in relation to absorption cross section in barns per nucleus of beryllium. Temperature of medium, 300°K.

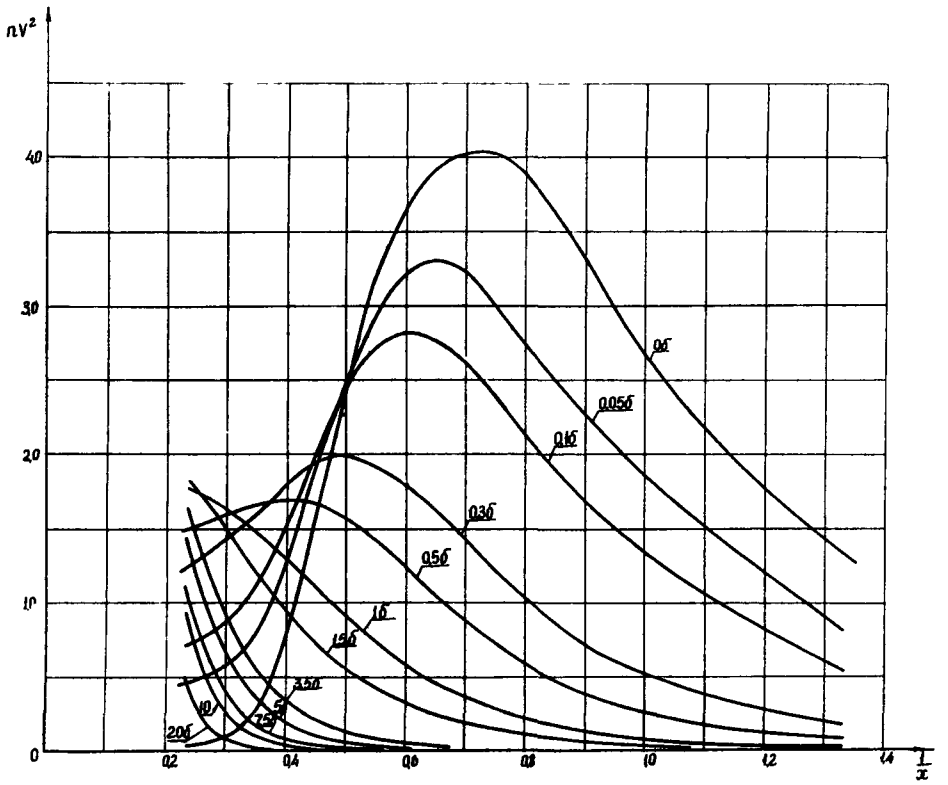

Figure 2. Neutron spectra in a homogeneous mixture of graphite and (1/v) absorber in relation to absorption cross section in barns per nucleus of graphite. Temperature of medium, 300°K.

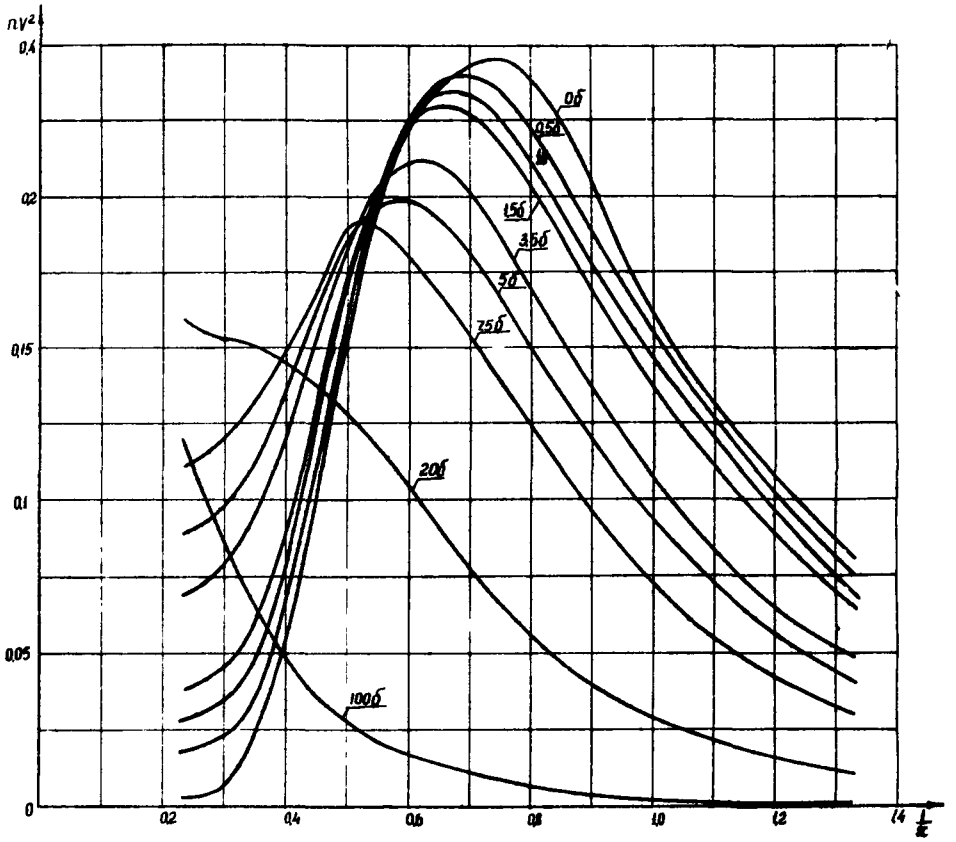

Figure 3. Neutron spectra in a homogeneous mixture of water and (1/v) absorber in relation to absorption cross section in barns per nucleus of hydrogen. Temperature of medium, 300°K.

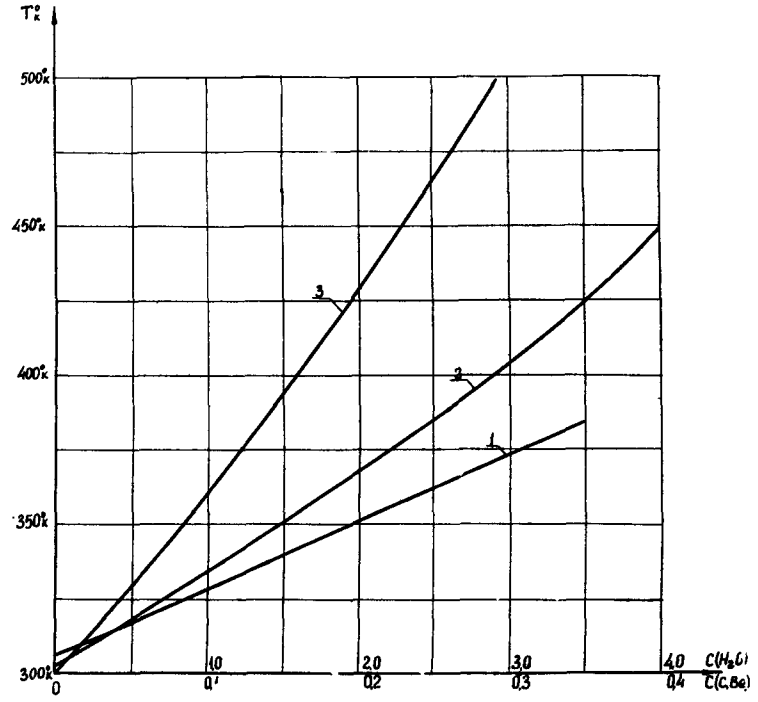

Figure 4. Calculated values of the temperature of neutron gas, T, in homogeneous moderating medium with absorber in relation to absorption cross section per nucleus of moderator. Temperature of medium, 300°K. 1, water; 2, beryllium; 3, graphite.

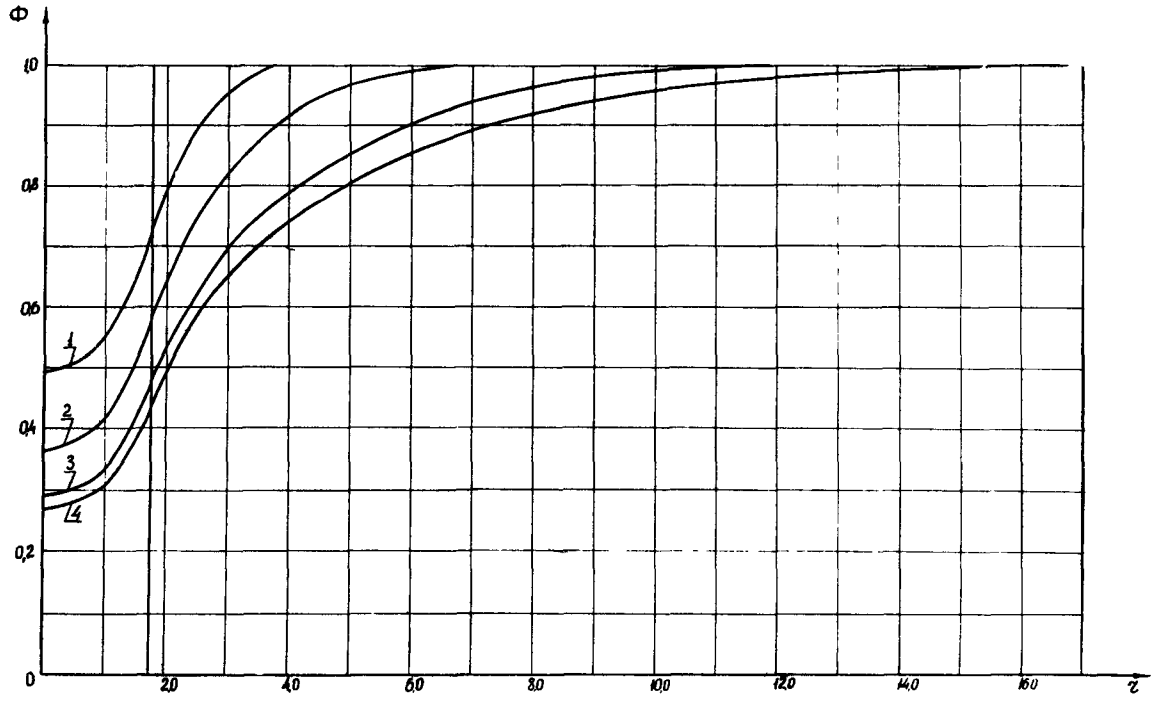

Figure 5. Distribution of flux of slow neutrons in uranium-beryllium cell with medium temperature of 300°K for different thicknesses of beryllium layers - a.

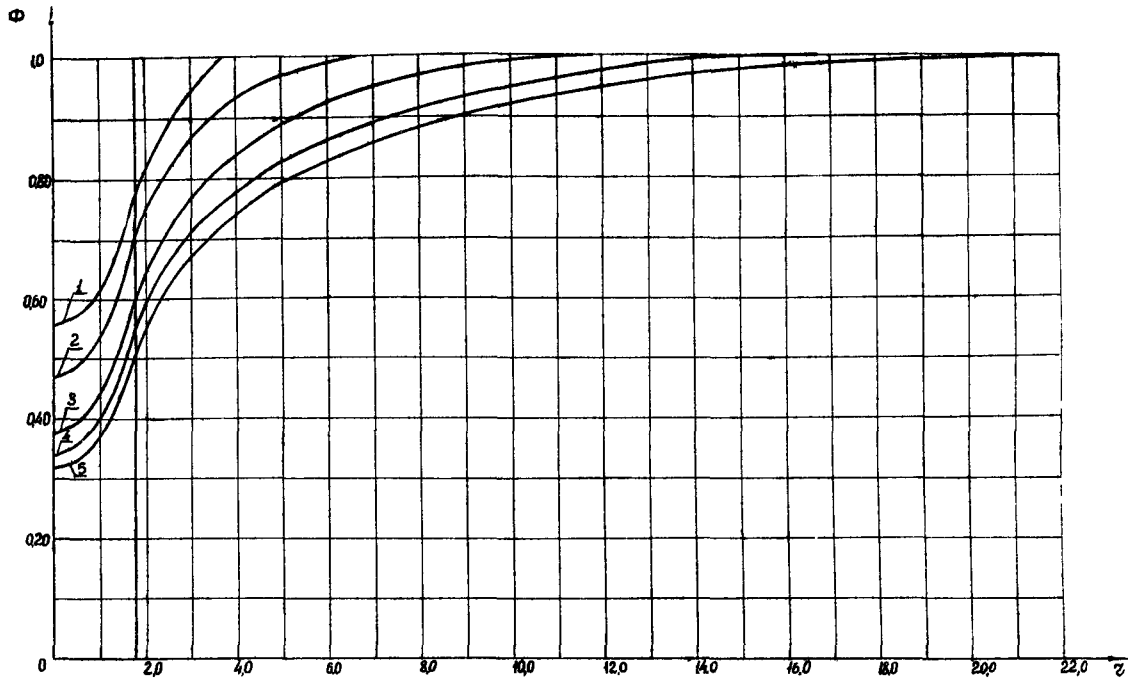

Figure 6. Distribution of flux of slow neutrons in uranium-graphite cell with medium temperature of 300°K for different thickness of graphite layers - a.

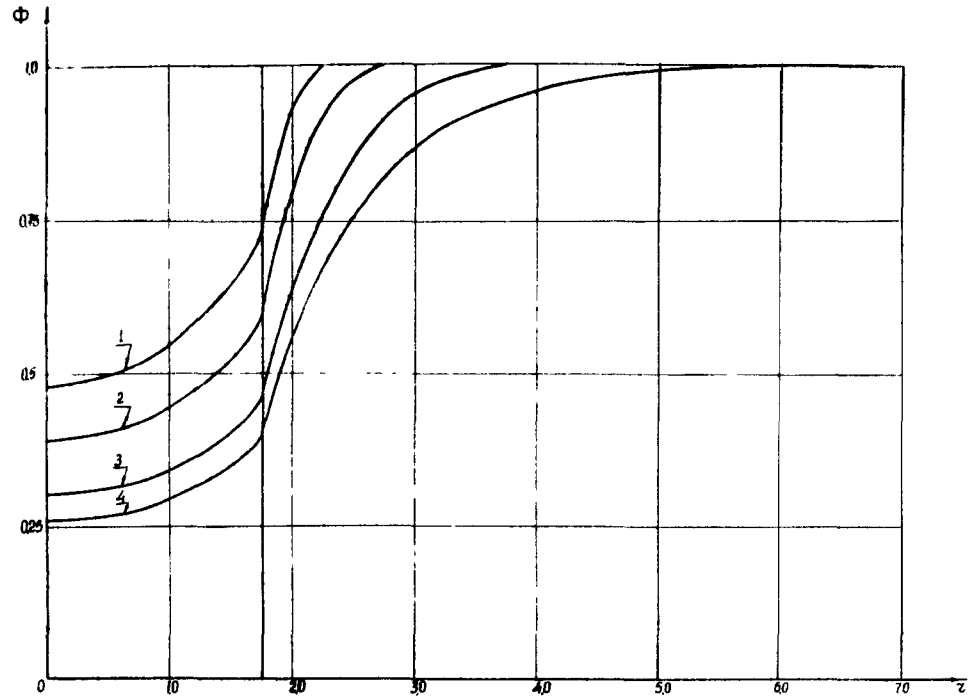

Figure 7. Distribution of flux of slow neutrons in uranium-water cell with medium temperature of 300°K for different thicknesses of water layers - a.

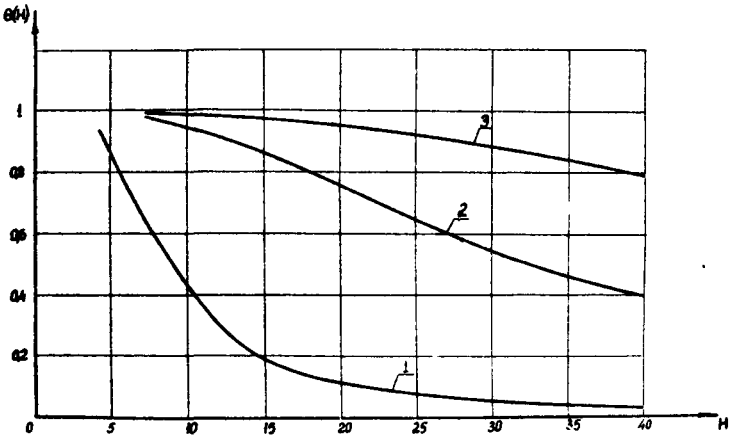

Figure 8. Relation of thermal utilization coefficient θ to lattice spacing for medium temperature of 300°K. 1, uranium-water lattice; 2, uranium-beryllium lattice; 3, uranium-graphite lattice.

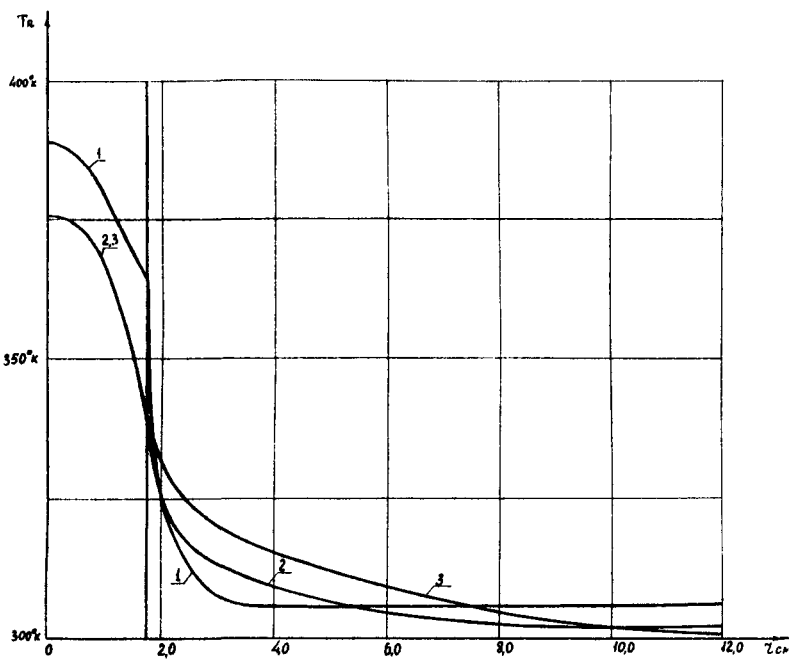

Figure 9. Calculated values of temperature of neutron gas T_n as a function of the distance from the center of uranium block to the location under consideration in an infinite homogeneous medium. 1, water; 2, beryllium; 3, graphite.

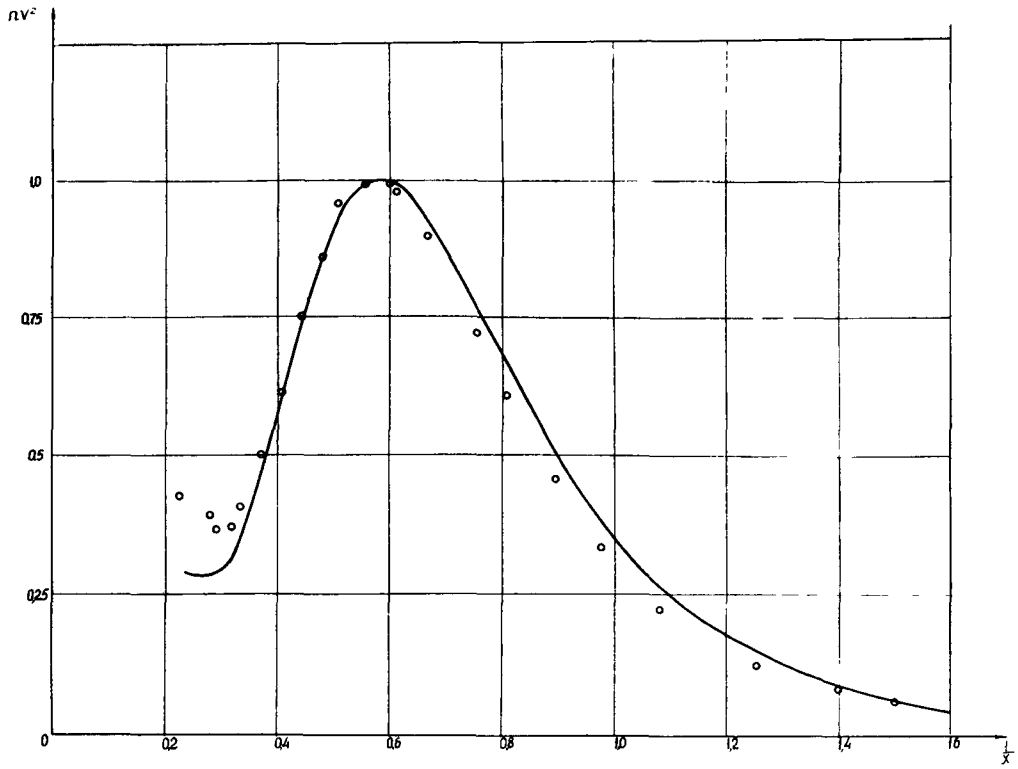

Figure 10. Neutron spectra in the center of a uranium block-water lattice with spacing H = 55 mm for temperature 323°K. Full line = calculated; points = experimental.

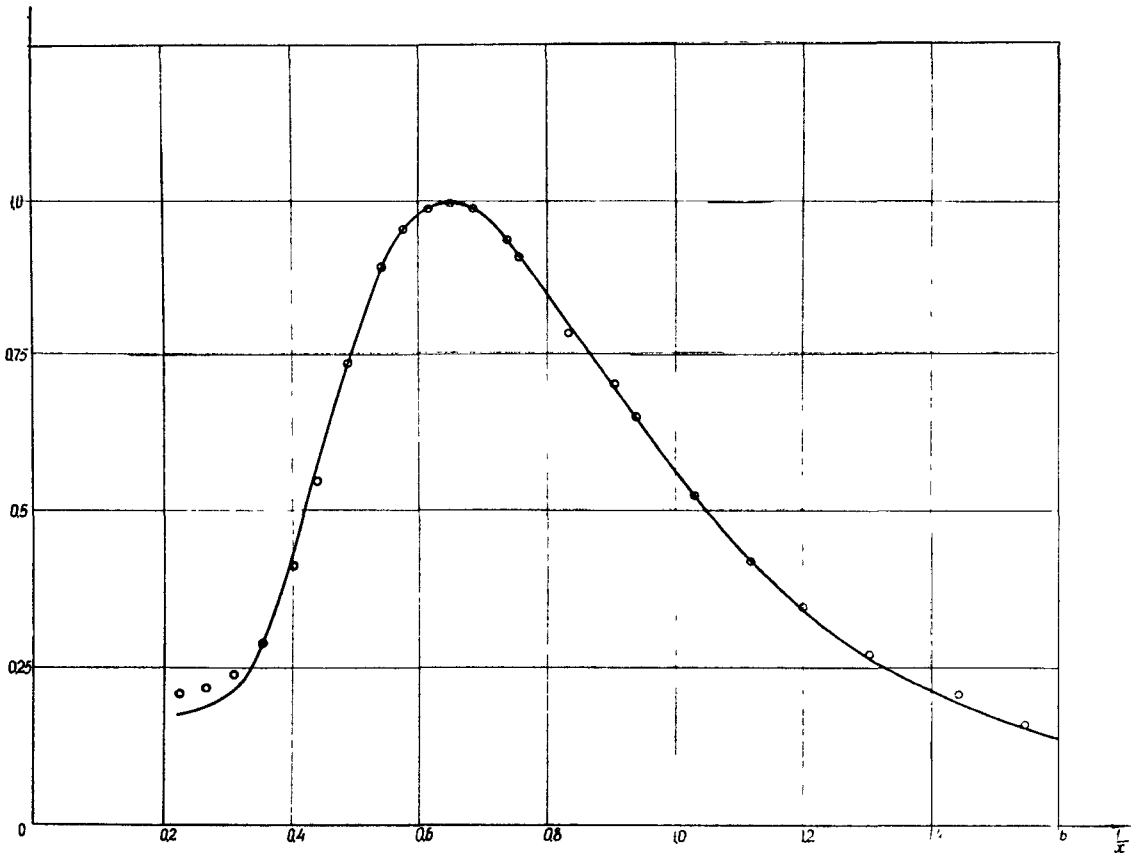

Figure 11. Spectra of neutrons in water at the boundary of a cell of uranium-water lattice with a spacing of H = 55 mm for temperature 323°K. Full line = calculated; points = experimental.

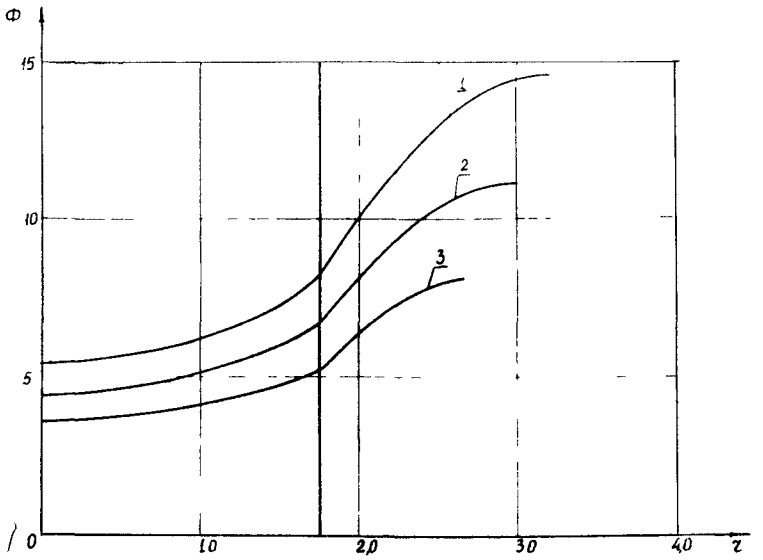

Figure 12. Distribution of slow neutron flux in uranium-water lattices corresponding to experiment of Mostovoi et al. [18] [33] for temperature of 323°K. 1, in a lattice with spacing of H = 60 mm; 2, in a lattice with spacing of H = 55 mm; 3, in a lattice with spacing of H = 50 mm.

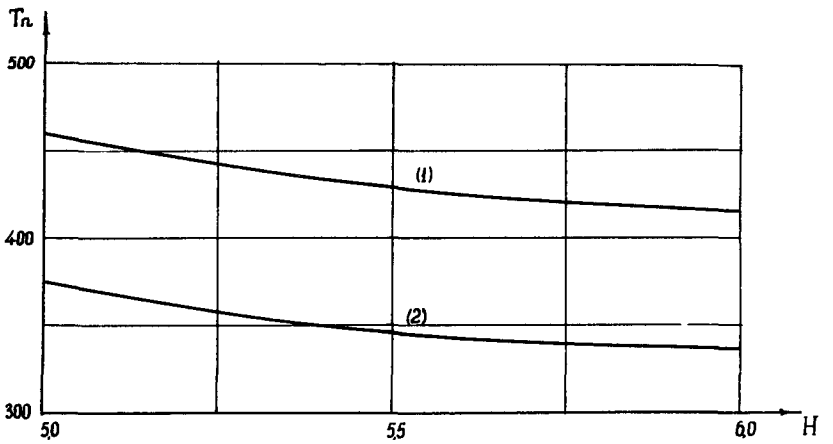

Figure 13. Calculated values of the temperature of neutron gas -T, in uranium-water lattices in relation to the lattice spacing H, for medium temperature of 323°K. 1, in the center of uranium block; 2, in water at the boundary of cell.

APPENDIX I

Table 1 Spectra of slow neutrons φ_j in an infinite homogeneous mixture of beryllium and an absorber which follows 1/v law. The φ_j corresponding to velocity groups 1 to 14 are given for various values of the parameter C. C is the capture cross section of absorber for energy E = 0.026 ev per one nucleus of beryllium.

№ группы \ C	0	0.05	0.I	0.3	0.5	I	I.5	3.5	5	7.5	I0	20
I	I.I4	I.0992	I.0902	I.0628	I.0367	0.9768	0.9223	0.7482	0.65I7	0.5322	0.4464	0.2625
2	I.47	I.328I	I.3034	I.2469	I.2026	I.095I	I.0028	0.7327	0.5975	0.4444	0.3448	0.I627
3	I.96	I.564I	I.5084	I.4077	I.34I2	I.I808	I.0509	0.7002	0.5403	0.3726	0.27I8	0.I085
4	3.23	I.990I	I.8444	I.6402	I.5297	I.2855	I.I026	0.6563	0.4747	0.3004	0.2047	0.0683
5	7.06	2.92I5	2.492I	2.0I05	I.8003	I.4I52	I.I555	0.5984	0.40I5	0.2306	0.I459	0.0403
6	I8.05	5.I232	3.8598	2.636I	2.I99I	I.5692	I.I997	0.5235	0.3220	0.I66I	0.0970	0.0220
7	44.74	9.9I48	6.6025	3.6549	2.7594	I.7269	I.2I28	0.4306	0.240I	0.II02	0.059I	0.0II0
8	95.33	I8.3550	II.I440	5.0457	3.4076	I.82I9	I.I560	0.3238	0.I62I	0.0657	0.0324	0.0050
9	I63.49	28.9930	I6.52I0	6.33I2	3.8426	I.7362	0.985I	0.2I33	0.0955	0.0342	0.0I55	0.0020
I0	2I5.23	36.0970	I9.6240	6.5343	3.5888	I.3665	0.6905	0.II55	0.0465	0.0I49	0.0063	0.0007
II	205.34	32.7830	I7.06I0	4.9530	2.46II	0.7903	0.3577	0.0477	0.0I77	0.0052	0.002I	0.0002
I2	I28.32	I9.34I0	9.5775	2.3990	I.0803	0.2987	0.I239	0.0I4I	0.0049	0.00I4	0.0005	0.0000
I3	4I.64	5.8632	2.75I4	0.6009	0.2505	0.0626	0.0247	0.0026	0.0009	0.0002	0.000I	0.0000
I4	3.3I	0.44II	0.I99I	0.0399	0.0I60	0.0038	0.00I5	0.0002	0.0000	0.0000	0.0000	0.0000

Table 2 Spectra of slow neutrons φ_j in an infinite homogeneous mixture of graphite and an absorber following 1/v law. See Table 1.

№ группы \ C	0	0.05	0.I	0.3	0.5	I.0	I.5	3.5	5	7.5	I0	20
I	3.I8	2.892I	2.856I	2.7296	2.6I28	2.35I5	2.I305	I.5I58	I.2256	0.9099	0.7I03	0.3534
2	4.55	3.5257	3.4364	3.2007	2.9832	2.5349	2.I829	I.3I73	0.9670	0.63II	0.4452	0.I7I0
3	6.78	4.205I	4.0254	3.6377	3.3009	2.6576	2.I876	I.I525	0.7855	0.4669	0.3070	0.0998
4	I2.85	5.3377	4.9359	4.2345	3.7025	2.7784	2.I622	0.97I3	0.6095	0.3275	0.2002	0.0550
5	30.99	7.5I43	6.4980	5.0773	4.2II9	2.8796	2.0895	0.7795	0.4467	0.2I58	0.I224	0.0286
6	82.2I	I2.0450	9.3506	6.2646	4.8242	2.9I86	I.9430	0.586I	0.3049	0.I32I	0.0696	0.0I39
7	205.3I	20.9560	I4.32I0	7.797I	5.4394	2.82I3	I.6954	0.4043	0.I903	0.074I	0.0365	0.0064
8	437.7I	35.3690	2I.4850	9.3035	5.7650	2.495I	I.3356	0.2484	0.I059	0.0372	0.0I7I	0.0025
9	75I.I5	5I.8780	28.5420	9.8675	5.3732	I.9099	0.9546	0.I325	0.05I8	0.0I67	0.0073	0.00I0
I0	990.22	60.6I00	30.5730	8.4939	4.0472	I.I79I	0.4982	0.0592	0.02I6	0.0065	0.0027	0.0003
II	946.9I	5I.7930	23.9800	5.3486	2.2365	0.5455	0.2I0I	0.02I5	0.0075	0.0022	0.0009	0.000I
I2	593.74	28.5730	I2.0490	2.I672	0.8I40	0.I753	0.0639	0.0060	0.002I	0.0006	0.0002	0.0000
I3	I93.32	8.0033	3.079I	0.4698	0.I657	0.0336	0.0II9	0.00II	0.0004	0.000I	0.0000	0.0000
I4	I5.39	0.5646	0.2052	0.0290	0.0I00	0.0020	0.0007	0.000I	0.0000	0.0000	0.0000	0.0000

Table 3 Spectra of slow neutrons φ_j in an infinite homogeneous mixture of water and an absorber which follows 1/v law. See Table 1.

№ группы \ C	0	0.5	I.0	I.5	3.5	5.0	7.5	20.0
I	0.I25	0.I370	0.I2I4	0.I202	0.II58	0.II29	0.I07I	0.0897
2	0.I5I	0.I464	0.I438	0.I4I8	0.I349	0.I303	0.I222	0.0976
3	0.I87	0.I736	0.I684	0.I647	0.I542	0.I477	0.I369	0.I048
4	0.274	0.2265	0.2I20	0.2036	0.I840	0.I739	0.I583	0.II45
5	0.5I6	0.3459	0.2994	0.2756	0.23II	0.2I24	0.I875	0.I249
6	I.I64	0.6269	0.4875	0.4203	0.3I06	0.272I	0.228I	0.I340
7	2.68I	I.2480	0.8839	0.7I3I	0.4536	0.3734	0.292I	0.I460
8	5.478	2.3465	I.5588	I.I948	0.6630	0.5II2	0.3702	0.I535
9	9.I95	3.7502	2.3894	I.7664	0.8790	0.6390	0.4298	0.I467
I0	II.982	4.732I	2.9293	2.I094	0.9640	0.6669	0.4202	0.II96
II	II.373	4.3852	2.6554	I.8734	0.799I	0.5302	0.3I57	0.0766
I2	7.098	2.6830	I.5946	I.I058	0.4445	0.2845	0.I6I3	0.0342
I3	2.3I2	0.8580	0.50I4	0.3423	0.I306	0.08I0	0.044I	0.0085
I4	0.I85	0.0676	0.0389	0.0262	0.0096	0.0058	0.003I	0.0006

Table 4 Neutron spectrum in uranium-beryllium cell in relation to the distance from center of uranium block. Temperature of medium is equal to 300°K. Thickness of beryllium layer = 2 cm. See Table 1.

№ группы \ τ	0	0.457	0.913	1.370	1.674	1.800	2.000	2.300	2.700	3.200	3.750
1	0.4818	0.4882	0.5081	0.5434	0.5774	0.5964	0.6238	0.6528	0.6770	0.6964	0.7042
2	0.5122	0.5203	0.5454	0.5907	0.6346	0.6590	0.6946	0.7333	0.7667	0.7910	0.8056
3	0.5232	0.5330	0.5635	0.6188	0.6732	0.7032	0.7465	0.7941	0.8357	0.8666	0.8850
4	0.5787	0.5896	0.6239	0.6861	0.7473	0.7810	0.8301	0.8851	0.9343	0.9716	0.9939
5	0.6798	0.6921	0.7303	0.7995	0.8674	0.9049	0.9605	1.0237	1.0815	1.1251	1.1527
6	0.8065	0.8214	0.8680	0.9523	1.0351	1.0810	1.1492	1.2273	1.2994	1.3556	1.3891
7	0.9506	0.9702	1.0317	1.1440	1.2553	1.3168	1.4075	1.5115	1.6078	1.6829	1.7275
8	1.1058	1.1314	1.2121	1.3608	1.5096	1.5920	1.7128	1.8516	1.9805	2.0813	2.1406
9	1.1413	1.1730	1.2737	1.4625	1.6551	1.7620	1.9164	2.0937	2.2582	2.3864	2.4608
10	0.9596	0.9925	1.0982	1.3011	1.5138	1.6332	1.8030	1.9977	2.1775	2.3165	2.3953
11	0.5799	0.6053	0.6885	0.8537	1.0343	1.1[illegible]	[illegible].2826	1.4481	1.6001	1.7162	1.7792
12	0.2203	0.2332	0.2766	0.3678	0.4740	0.5366	0.6220	0.7191	0.8078	0.8745	0.9090
13	0.0409	0.0444	0.0568	0.0855	0.1232	0.1460	0.1758	0.2091	0.2392	0.2616	0.2726
14	0.0010	0.0012	0.0019	0.0042	0.0087	0.0120	0.0151	0.0186	0.0218	0.0240	0.0251

Table 4a Neutron spectrum in uranium-beryllium cell in relation to the distance from center of uranium block. Temperature of medium is equal to 300°K. Thickness of beryllium layer = 5 cm. See Table 1.

№ группы \ τ	0	0.457	0.913	1.370	1.674	1.875	2.375	3.125	4.125	5.375	6.750
1	0.5848	0.5922	0.6154	0.6564	0.6958	0.7326	0.7930	0.8362	0.8600	0.8710	0.8744
2	0.6426	0.6523	0.6825	0.7366	0.7889	0.8374	0.9203	0.9845	1.0231	1.0424	1.0486
3	0.6854	0.6976	0.7357	0.8046	0.8720	0.9335	1.0397	1.1252	1.1797	1.2113	1.2180
4	0.8187	0.8334	0.8793	0.9624	1.0437	1.1178	1.2502	1.3630	1.4402	1.4838	1.4986
5	1.1099	1.1288	1.1876	1.2934	1.3968	1.4914	1.6674	1.8269	1.9443	2.0155	2.0406
6	1.6696	1.6986	1.7890	1.9520	2.1112	2.2570	2.5343	2.7964	3.0008	3.1314	3.1792
7	2.6710	2.7228	2.8848	3.1788	3.4683	3.7322	4.2356	4.7213	5.1118	5.3697	5.4653
8	4.2017	4.2932	4.5808	5.1076	5.6317	6.1082	7.0182	7.9066	8.6317	9.1176	9.2984
9	5.5933	5.7400	6.2043	7.0688	7.9450	8.7394	10.2352	11.6886	12.8733	13.6670	13.9618
10	5.7541	5.9416	6.5419	7.6860	8.8774	9.9634	11.9731	13.9057	15.4676	16.5102	16.8917
11	4.1070	4.2794	4.8404	5.9473	7.1476	8.2582	10.2795	12.2054	13.7512	14.7747	15.1435
12	1.7674	1.8676	2.2020	2.8989	3.7044	4.4638	5.8143	7.0941	8.1175	8.7916	9.0290
13	0.3409	0.3695	0.4696	0.6993	0.9979	1.[illegible]	1.7665	2.2193	2.5785	2.8132	2.8943
14	0.0070	0.0084	0.0139	0.0306	0.0626	0.0960	0.1417	0.1828	0.2143	0.2343	0.2411

Table 4b Neutron spectrum in uranium-beryllium cell in relation to the distance from center of uranium block. Temperature of medium is equal to 300°K. Thickness of beryllium layer = 10 cm. See Table 1.

№ группы \ τ	0	0.457	0.913	1.370	1.674	2.000	3.000	4.500	6.500	9.000	11.750
1	0.6476	0.6556	0.6806	0.7250	0.7674	0.8340	0.9212	0.9594	0.9725	0.9762	0.9769
2	0.7260	0.7367	0.7701	0.8297	0.8873	0.9764	1.1043	1.1687	1.1945	1.2028	1.2045
3	0.8033	0.8173	0.8610	0.9397	1.0166	1.1332	1.3075	1.4043	1.4483	1.4649	1.4685
4	1.0419	1.0602	1.1172	1.2202	1.3207	1.4728	1.7182	1.8736	1.9566	1.9935	2.0029
5	1.6526	1.6800	1.7651	1.9182	2.0671	2.2938	2.6932	2.9849	3.1684	3.2638	3.2907
6	3.0749	3.1268	3.2886	3.5798	3.8634	4.2952	5.0995	5.7487	6.2067	6.4702	6.5493
7	5.9788	6.1928	6.4443	7.0822	7.7093	8.6560	10.4502	11.9640	13.0929	13.7780	13.9913
8	10.7714	11.0004	11.7177	13.0288	14.3294	16.2847	20.0068	23.2001	25.6378	27.1546	27.6351
9	15.6183	16.0175	17.2802	19.6249	21.9936	24.7825	32.1357	37.7461	42.0376	44.7324	45.5907
10	16.9728	17.5136	19.2411	22.5229	25.9298	31.0278	40.2985	48.0269	53.8775	57.5393	58.7124
11	12.6072	13.1247	14.8068	18.1122	21.6826	27.0890	36.7000	44.5637	50.4143	54.0462	55.2043
12	5.5793	5.8892	6.1730	9.0638	11.5273	15.3012	21.8617	27.1599	31.0372	33.4097	34.1578
13	1.0828	1.1723	1.4840	2.1946	3.1123	4.5152	6.8491	8.6999	10.0255	10.8220	11.0705
14	0.0215	0.0258	0.0425	0.0931	0.1888	0.3376	0.6103	0.7018	0.8083	0.8706	0.8898

Table 4c Neutron spectrum in uranium-beryllium cell in relation to the distance from center of uranium block. Temperature of medium is equal to 300°K. Thickness of beryllium layer = 15 cm. See Table 1.

№ группы \ τ	0	0.457	0.913	1.370	1.674	2.125	3.625	5.875	8.875	12.625	16.750
1	0.6781	0.6864	0.7118	0.7568	0.7999	0.8946	0.9898	1.0184	1.0250	1.0261	1.0262
2	0.7720	0.7830	0.8175	0.8791	0.9385	1.0671	1.2146	1.2685	1.2838	1.2870	1.2875
3	0.8774	0.8923	0.9387	1.0223	1.1037	1.2762	1.4889	1.5794	1.6105	1.6188	1.6202
4	1.2049	1.2255	1.2897	1.4053	1.5180	1.7562	2.0862	2.2574	2.3316	2.3568	2.3618
5	2.0985	2.1324	2.2378	2.4269	2.6104	3.0012	3.6171	4.0066	4.2137	4.2987	4.3178
6	4.3062	4.3774	4.5988	4.9964	5.3830	6.2056	7.6092	8.6171	9.2269	9.5090	9.5782
7	8.9509	9.1160	9.6317	10.5648	11.4786	13.4065	16.7750	19.3295	20.9833	21.8043	22.0179
8	16.7078	17.0554	18.1442	20.1299	22.0945	26.2162	33.4604	39.0689	42.8280	44.7796	45.3040
9	24.6571	25.2750	27.2253	30.8374	34.4770	42.0482	55.0442	65.0359	71.8254	75.4569	76.4597
10	27.0440	27.8874	30.5802	35.6798	40.9575	51.9341	70.1935	83.9656	93.3214	98.4166	99.8555
11	20.2097	21.0232	23.6592	28.8217	34.3761	46.0447	64.9425	78.8641	88.2261	93.3588	94.8225
12	8.9858	9.4754	11.1036	14.4610	18.3036	26.4392	40.5614	48.6228	54.7682	58.1219	59.0830
13	1.7487	1.8910	2.3843	3.5009	4.9324	7.9269	12.4796	15.6844	17.7449	18.8530	19.1694
14	0.0348	0.0416	0.0683	0.1480	0.2970	0.6024	0.9991	1.2596	1.4203	1.5052	1.5293

Table 5 Neutron spectrum in uranium-graphite cell in relation to the distance from center of uranium block. Temperature of medium is equal to 300°K. Thickness of graphite layer = 2 cm. See Table 1.

№ группы \ τ	0	0.457	0.913	I.370	I.674	I.800	2.000	2.300	2.700	3.200	3.750
I	I.0694	I.0844	I.I308	I.2I36	I.2935	I.3308	I.3760	I.4308	I.4870	I.54I4	I.5882
2	I.05I2	I.0687	I.I235	I.2224	I.3I88	I.3637	I.4I69	I.4822	I.550I	I.6I64	I.6732
3	I.0028	I.0228	I.085I	I.I985	I.3I04	I.3624	I.4230	I.4975	I.5752	I.65II	I.7I62
4	I.0225	I.043I	I.I079	I.2260	I.3428	I.3972	I.4607	I.5393	I.62I8	I.7027	I.77I8
5	I.0822	I.I03I	I.I685	I.2873	I.4044	I.459I	I.5238	I.6042	I.689I	I.7727	I.8437
6	I.I042	I.I260	I.I944	I.3I9I	I.442I	I.5996	I.5679	I.6529	I.7426	I.8303	I.9055
7	I.0502	I.0734	I.I462	I.280I	I.4I35	I.4760	I.5495	I.6407	I.7369	I.83I0	I.9I03
8	0.93I2	0.9542	I.0270	I.I620	I.2979	I.36I8	I.4364	I.5288	I.626I	I.7207	I.7998
9	0.70I6	0.7225	0.7888	0.9I38	I.0423	I.I030	I.I726	I.2586	I.3486	I.4356	I.5074
I0	0.4282	0.4439	0.4940	0.59I6	0.6946	0.7437	0.7985	0.8662	0.9365	I.0038	I.0585
II	0.I945	0.2036	0.2334	0.293I	0.359I	0.39II	0.4254	0.4676	0.5III	0.5522	0.5850
I2	0.0602	0.0640	0.0767	0.I036	0.I354	0.I5I2	0.I67I	0.I866	0.2066	0.2252	0.2396
I3	0.0I02	0.0II2	0.0I45	0.0223	0.0327	0.038I	0.0429	0.0490	0.0550	0.0606	0.0648
I4	0.0003	0.0003	0.0006	0.00I3	0.0026	0.0035	0.004I	0.0048	0.0055	0.006I	0.0067

Table 5a Neutron spectrum in uranium-graphite cell in relation to the distance from center of uranium block. Temperature of medium is equal to 300°K. Thickness of graphite layer = 5 cm. See Table 1.

№ группы \ τ	0	0.457	0.913	I.370	I.674	I.875	2.375	3.I25	4.I25	5.375	6.750
I	I.5I26	I.53I4	I.5900	I.6939	I.7934	I.8627	I.9750	2.0772	2.I504	2.I948	2.2I76
2	I.6546	I.7685	I.756I	I.8936	2.0264	2.II77	2.2653	2.409I	2.5060	2.5709	2.6046
3	I.7540	I.7866	I.88I9	2.0569	2.228I	2.3446	2.5308	2.7067	2.8394	2.9247	2.969I
4	2.0350	2.07I6	2.I859	2.3926	2.5950	2.7329	2.9557	3.I696	3.3348	3.4434	3.5002
5	2.5502	2.5939	2.730I	2.9759	3.2I57	3.3800	3.6500	3.9I38	4.I2I9	4.26I5	4.3346
6	3.2857	3.3435	3.5239	3.8498	4.I685	4.3875	4.7492	5.I050	5.3883	5.5806	5.6809
7	4.2304	4.3I37	4.5748	5.0498	5.5I83	5.8402	6.3686	6.8888	7.3043	7.5868	7.7332
8	5.2933	5.4I08	5.7804	6.4587	7.I349	7.5999	8.3605	9.II08	9.7I23	I0.I2I0	I0.3308
9	5.7207	5.8736	6.3584	7.2630	8.I820	8.8I39	9.8337	I0.8395	II.6435	I2.I897	I2.4655
I0	4.9289	5.0927	5.6I72	6.6I98	7.6666	8.3872	9.5294	I0.6547	II.5534	I2.I6II	I2.46I0
II	3.0407	3.I709	3.5958	4.4368	5.3523	5.9838	6.9590	7.9I78	8.6837	9.I992	9.4464
I2	I.I730	I.24I0	I.4688	I.9458	2.5000	2.8643	3.4525	4.0I06	4.4560	4.7545	4.8937
I3	0.2I7I	0.2358	0.30I3	0.4530	0.652I	0.7922	0.9826	I.I690	I.3I75	I.4I66	I.46I5
I4	0.0050	0.0060	0.0099	0.022I	0.0459	0.0649	0.0846	0.I037	0.II88	0.I287	0.I33I

Table 5b Neutron spectrum in uranium-graphite cell in relation to the distance from center of uranium block. Temperature of medium is equal to 300°K. Thickness of graphite layer = 10 cm. See Table 1.

№ группы \ τ	0	0.457	0.913	1.370	1.674	2.000	3.000	4.500	6.500	9.000	11.750
1	1.7002	1.7210	1.7856	1.8999	2.0092	2.1280	2.3158	2.4382	2.5026	2.5320	2.5408
2	1.9188	1.9469	2.0341	2.1898	2.3403	2.5002	2.7589	2.9391	3.0423	3.0934	3.1094
3	2.1215	2.1584	2.2729	2.4798	2.6816	2.8928	3.2354	3.4812	3.6021	3.7058	3.7307
4	2.6523	2.6988	2.8441	3.1067	3.3633	3.6319	4.0784	4.4126	4.6256	4.7438	4.7830
5	3.7833	3.8468	4.0437	4.3984	4.7435	5.1084	5.7321	6.2205	6.5504	6.7437	6.8106
6	5.9436	6.0461	6.3641	6.9378	7.4973	8.0903	9.1179	9.9442	10.5251	10.8792	11.0042
7	9.7407	9.9282	10.5149	11.5793	12.6272	12.2804	15.6504	17.2068	18.3213	18.9185	19.2607
8	15.4096	15.7441	16.7947	18.7193	20.6330	22.6533	26.1498	29.0034	31.0649	32.6225	32.8187
9	20.3881	20.9215	22.6095	25.7525	28.9380	32.2833	37.9566	42.6609	46.0208	48.1282	48.8743
10	20.7924	21.4692	23.6361	27.7655	32.0653	36.5637	44.1361	50.2745	54.6881	57.4472	58.4138
11	14.8200	15.4433	17.4723	21.4768	25.8204	30.3333	37.7846	43.8043	48.1307	50.8244	51.7570
12	6.4114	6.7771	7.9976	10.5508	13.5044	16.5423	21.4038	25.3335	28.1580	29.9142	30.5174
13	1.2429	1.3483	1.7177	2.5687	3.6796	4.8077	6.5083	7.8793	8.8633	9.4740	9.6811
14	0.0257	0.0308	0.0511	0.1141	0.2357	0.3655	0.5252	0.6514	0.7403	0.7945	0.8125

Table 5c Neutron spectrum in uranium-graphite cell in relation to the distance from center of uranium block. Temperature of medium is equal to 300°K. Thickness of graphite layer = 15 cm. See Table 1.

№ группы \ τ	0	0.457	0.913	1.370	1.674	2.125	3.625	5.875	8.875	12.625	16.750
1	1.7846	1.8064	1.8730	1.9908	2.1034	2.2691	2.4977	2.6132	2.6626	2.6791	2.6838
2	2.0538	2.0834	2.1753	2.3389	2.4972	2.7234	3.0519	3.2338	3.3214	3.3582	3.3672
3	2.3412	2.3808	2.5057	2.7295	2.9482	3.2559	3.7079	3.9732	4.1117	4.1758	4.1928
4	3.1042	3.1579	3.3252	3.6268	3.9214	4.3361	4.9690	5.3695	5.6014	5.7197	5.7542
5	4.9011	4.9817	5.2324	5.6834	6.1217	6.7451	7.2682	8.4200	8.8550	9.0996	9.1745
6	8.8088	8.9577	9.4219	10.2565	11.0699	12.2311	14.1251	15.4884	16.4211	16.9795	17.1586
7	16.4130	16.7241	17.6958	19.4579	21.1888	23.6502	27.6757	30.6295	32.7120	33.9991	34.4194
8	28.5890	29.1997	31.1178	34.6254	38.1075	43.0510	51.1317	57.1026	61.3628	64.0301	64.9066
9	40.4530	41.4949	44.7900	50.9149	57.1073	65.8397	79.9351	90.2840	97.6356	102.2304	103.7715
10	43.2947	44.6839	49.1241	57.5738	66.3534	78.6344	98.1493	112.3531	122.3674	128.5692	130.5956
11	32.0579	33.3869	37.7093	46.2179	55.4249	68.1630	88.0408	102.4331	112.5039	118.7010	120.6991
12	14.2905	15.0949	17.7816	23.3674	29.8157	38.5755	51.9187	61.5607	68.2809	72.3808	73.7004
13	2.8042	3.0396	3.8620	5.7489	8.2018	11.4408	16.1491	19.5399	21.8867	23.3057	23.7572
14	0.0566	0.0679	0.1122	0.2484	0.5099	0.8577	1.2856	1.5839	1.7847	1.9034	1.9402

Table 5d Neutron spectrum in uranium-graphite cell in relation to the distance from center of uranium block. Temperature of medium is equal to 300°K. Thickness of graphite layer = 20 cm. See Table 1.

№ группы \ τ	0	0.457	0.913	1.370	1.674	2.250	4.250	7.250	11.250	16.250	21.750
1	1.8430	1.8650	1.9306	2.0522	2.1662	2.3773	2.6286	2.7303	2.7660	2.7767	2.7787
2	2.1621	2.1928	2.2877	2.4571	2.6202	2.9139	3.2881	3.4620	3.5340	3.5594	3.5647
3	2.5362	2.5788	2.7113	2.9498	3.1820	3.5916	4.1272	4.3980	4.5470	4.5759	4.5881
4	3.5426	3.6030	3.7907	4.1285	4.4577	5.0392	5.8408	6.2926	6.5357	6.6497	6.6798
5	6.0645	6.1626	6.4677	7.0152	7.5471	8.4961	9.8834	10.7547	11.2901	11.5753	11.6574
6	11.9285	12.1271	12.7453	13.8563	14.9367	16.8720	19.7929	21.7596	23.0745	23.8338	24.0638
7	23.8435	24.2885	25.6780	28.1935	30.6612	35.0604	41.7295	46.3364	49.5402	51.4651	52.0647
8	43.4207	44.3353	47.2017	52.4372	57.6250	66.8573	83.1514	90.5910	97.4677	101.6713	103.0004
9	63.1621	64.7644	69.8282	79.2196	88.7020	105.4419	130.4398	147.7023	159.8428	167.2795	169.6687
10	68.8658	71.0430	77.9951	91.1958	104.8894	128.8046	163.9419	187.9243	204.6194	214.7813	217.9919
11	51.7219	53.8357	60.7019	74.1856	88.7394	113.7969	150.0020	174.5070	191.3515	201.5059	204.6941
12	23.3149	24.6111	28.9290	37.8805	48.1791	65.5036	90.0236	106.5544	117.8064	124.5114	126.6020
13	4.5969	4.9802	6.3110	9.3503	13.2822	19.6511	28.2182	34.1264	38.0291	40.3243	41.0344
14	0.0919	0.1102	0.1820	0.4004	0.8171	1.4747	2.2476	2.7480	3.0719	3.2570	3.3133

Table 6 Neutron spectrum in uranium-water cell in relation to the distance from center of uranium block. Temperature of medium is equal to 300°K. Thickness of water layers = 0.5 cm. See Table 1.

№ группы \ τ	0	0.457	0.913	1.370	1.674	1.762	1.812	1.888	1.988	2.112	2.25
1	0.0763	0.0775	0.0812	0.0877	0.0941	0.0968	0.0994	0.1024	0.1053	0.1076	0.1092
2	0.0815	0.0830	0.0876	0.0959	0.1042	0.1077	0.1111	0.1152	0.1191	0.1224	0.1243
3	0.0853	0.0871	0.0928	0.1031	0.1134	0.1179	0.1222	0.1274	0.1324	0.1364	0.1388
4	0.0987	0.1009	0.1074	0.1196	0.1315	0.1368	0.1419	0.1482	0.1542	0.1592	0.1620
5	0.1224	0.1249	0.1326	0.1466	0.1603	0.1664	0.1727	0.1804	0.1879	0.1940	0.1974
6	0.1547	0.1578	0.1676	0.1828	0.2030	0.2108	0.2192	0.2296	0.2088	0.2485	0.2375
7	0.2033	0.2078	0.2218	0.2474	0.2730	0.2815	0.2978	0.3124	0.3302	0.3434	0.3504
8	0.2670	0.2734	0.2935	0.3307	0.3681	0.3856	0.3960	0.4324	0.4584	0.4795	0.4902
9	0.3087	0.3175	0.3448	0.3959	0.4481	0.4737	0.5058	0.5456	0.5854	0.6172	0.6324
10	0.2898	0.2995	0.3295	0.3950	0.4518	0.4883	0.5273	0.5783	0.6327	0.6737	0.6922
11	0.1974	0.2057	0.2326	0.2855	0.3428	0.3752	0.4215	0.4773	0.5314	0.5729	0.5903
12	0.0841	0.0887	0.1042	0.1364	0.1733	0.1963	0.2308	0.2713	0.3094	0.3380	0.3494
13	0.0162	0.0175	0.0221	0.0326	0.0460	0.0553	0.0693	0.0850	0.0992	0.1096	0.1135
14	0.0003	0.0004	0.0007	0.0014	0.0029	0.0041	0.0056	0.0071	0.0084	0.0094	0.0097

Table 6a Neutron spectrum in uranium-water cell in relation to the distance from center of uranium block. Temperature of medium is equal to 300°K. Thickness of water layers = 1 cm. See Table 1.

№ группы \ τ	0	0.457	0.9I3	I.370	I.674	I.775	I.875	2.025	2 225	2.475	2.75
I	0.0845	0.0854	0.0892	0.0955	0.I0I6	0.I048	0.I094	0.II38	0.II73	0.II94	0.I2[illegible]
2	0.0925	0.0939	0.0985	0.I068	0.II49	0.II94	0.I256	0.I3I9	0.I368	0.I400	0.I4I5
3	0.0996	0.I0I5	0.I074	0.II80	0.I284	0.I342	0.I423	0.I506	0.I57I	0.I6I5	0.I634
4	0.I204	0.I226	0.I297	0.I424	0.I55I	0.I623	0.I725	0.I832	0.I920	0.I978	0.2005
5	0.I6I3	0.I64I	0.I729	0.I888	0.2044	0.2I34	0.2270	0.2420	0.2548	0.2638	0.2678
6	0.2324	0.2365	0.249I	0.272I	0.2946	0.3079	0.3292	0.3536	0.3759	0.3920	0.399I
7	0.3573	0.364I	0.3854	0.4243	0.4624	0.4856	0.5248	0.57I0	0.6I46	0.6470	0.6609
8	0.5408	0.5523	0.5880	0.6534	0.7I80	0.7590	0.8320	0.9I94	I.0032	I.0662	I.0925
9	0.6985	0.7I60	0.7709	0.8728	0.9754	I.0442	I.I707	I.32I3	I.4657	I.5738	I.6I7I
I0	0.7032	0.7248	0.7936	0.9235	I.0576	I.I549	I.3387	I.5533	I.7560	I.9063	I.964I
II	0.4960	0.5I55	0.5787	0.7020	0.8342	0.9403	I.I447	I.3750	I.5874	I.742I	I.7994
I2	0.2I23	0.2236	0.26I2	0.3383	0.4263	0.5056	0.6577	0.82I4	0.9670	I.07[illegible]	I.I078
I3	0.040I	0.0434	0.0545	0.0796	0.III6	0.I44I	0.2035	0.2632	0.3I4I	0.3492	0.36I5
I4	0.0008	0.0009	0.00I6	0.0034	0.0066	0.0I06	0.0I65	0.02I6	0.0258	0.0287	0.0296

Table 6b Neutron spectrum in uranium-water cell in relation to the distance from center of uranium block. Temperature of medium is equal to 300°K. Thickness of water layers = 2 cm. See Table 1.

№ группы \ τ	0	0.457	0.9I3	I.370	I.674	I.800	2.000	2.300	2.700	3.200	3.75
I	0.0582	0.0597	0.0613	0.0655	0.0696	0.0728	0.0775	0.08I0	0 0830	0.0838	0.0842
2	0.0639	0.0649	0.0680	0.0734	0.0789	0.0832	0.0900	0.095I	0.0980	0.0994	0.0997
3	0.0695	0.0707	0.0748	0.08I8	0.0888	0.0946	0.I035	0.II05	0.II46	0.II68	0.II7[illegible]
4	0.0869	0.0884	0.0934	0.I023	0.III0	0.II82	0.I30I	0.I402	0.I468	0.I506	0.I5I[illegible]
5	0.I282	0.I354	0.I369	0.I489	0.I605	0.I704	0.I888	0.2062	0.2I97	0.2279	0.2308
6	0.2I68	0.2204	0.23I5	0.25I3	0.2706	0.2875	0.3227	0.3604	0.3927	0.4I40	0.42I6
7	0.3930	0.4000	0.42I9	0.46I3	0.4998	0.535I	0.6I3I	0.70II	0.7799	0.8339	0.8527
8	0.6708	0.6842	0.7256	0.8008	0.8747	0.9466	I.III2	I.3002	I.47I4	I.5894	I.6301
9	0.9283	0.9503	I.0I97	I.I472	I.2749	I.4072	I.7I08	2.0528	2.3596	2.5693	2.6402
I0	0.9642	0.9927	I.0833	I.2539	I.4289	I.6280	2.0764	2.5630	2.9890	3.275I	3.370I
II	0.687I	0.7I34	0.7986	0.9640	I.I404	I.3663	I.8580	2.3642	2.792I	3.0728	3.I647
I2	0.2938	0.3092	0.3603	0.4644	0.5824	0.7548	I.I098	I.4525	I.7304	I.9089	I.9666
I3	0.055I	0.0596	0.0746	0.I082	0.I508	0.22I4	0.3533	0.47I2	0.5633	0.62[illegible]	0.640[illegible]
I4	0.00I0	0.00I2	0.0020	0.0044	0.0087	0.0I69	0.0287	0.0382	0.0454	0.05[illegible]	0.05I6

Table 60 Thru

Table 17

Illegible

Table 6c Neutron spectrum in uranium-water cell in relation to the distance from center of uranium block. Temperature of medium is equal to 300°K Thickness of water layers = 5 cm. See Table 1.

№ группы \ r	0	0.457	0.9I3	I.370	I.674	I.875	2.375	3.I25	4.I25	5.375	6.75
I	0.0677	0.0685	0.07I2	0.0759	0.0805	0.0873	0.0949	0.0977	0.0973	0.0986	0.0986
2	0.0743	0.0755	0.0790	0.0852	0.09I4	0.II24	0.II2I	0.II63	0.II75	0.II75	0.II79
3	0.082I	0.0833	0.0879	0.096I	0.I039	0.II67	0.I3I9	0.I385	0.I404	0.I4I2	0.I4I2
4	0.I070	0.I089	0.II48	0.I257	0.I358	0.I525	0.I759	0.I883	0.I930	0.I945	0.I949
5	0.I759	0.I786	0.I875	0.203I	0.2I87	0.2440	0.2899	0.32I4	0.3366	0.34I6	0.3424
6	0.34I6	0.347I	0.3634	0.394I	0.4233	0.4743	0.5859	0.6747	0.6038	0.7353	0.738I
7	0.6898	0.70I5	0.7388	0.8058	0.8707	0.9906	I.2734	I.5084	I.63I8	I.6722	I.6792
8	I.2520	I.276I	I.35I6	I.4886	I.6224	I.8862	2.5I92	3.0468	3.32I9	3.4II4	3.4265
9	I.7886	I.8302	I.9605	2.I998	2.4387	2.9464	4.II95	5.0704	5.5575	5.7I43	5.7407
I0	I.8843	I.9387	2.III5	2.4348	2.765I	3.5483	5.2408	6.55I9	7.2075	7.4I57	7.450[illegible]
II	I.3493	I.3999	I.56I3	I.8738	2.2045	3.I040	4.88I7	6.I8I5	6.8I65	7.0I69	7.0503
I2	0.5766	0.6058	0.70I9	0.8956	I.II24	I.7983	3.0[illegible]4	3.8456	4.247I	4.3743	4.3953
I3	0.I078	0.II59	0.I440	0.2050	0.2809	0.5 [illegible]	0.976[illegible]	I.2509	I.3824	I.4244	I.43I4
I4	0.00I9	0.0023	0.0039	0.0082	0.0I56	0.0[illegible]	0.0786	0.I004	0.II09	0.II44	0.II48

Table 6d Neutron spectrum in uranium-water cell in relation to the distance from center of uranium block. Temperature of medium is equal to 300°K. Thickness of water layers = 10 cm. See Table 1.

№ группы \ r	0	0.457	0.9I3	I.370	I.674	2.000	3.000	4.500	6.500	9.000	II.[illegible]
I	0.0738	0.0748	0.0774	0.0823	0.0870	0.0996	0.I077	0.I088	0.I090	0.I090	0.I090
2	0.0823	0.0839	0.0875	0.0937	0.0999	0.II80	0.I300	0.I320	0.I325	0.I325	0.I32
3	0.0777	0.0948	0.0994	0.I082	0.II65	[illegible].I408	0.I590	0.I62[illegible]	[illegible].I63I	0.I63I	0.I
4	0.I274	0.I300	0.I362	0.I48I	0.I595	0.I93I	0.2252	0.2340	0.235I	0.235I	0.2[illegible]
5	0.2226	0.2226	0.2366	0.2558	0.2739	0.3298	0.4033	0.4277	0.43I8	0.43I8	0.4[illegible]
6	0.4499	0.4572	0.4784	0.5I72	0.5545	0.6736	0.8667	0.9382	0.949I	0.[illegible]0I	0.9[illegible]
7	0.9I95	0.935I	0.9837	I.07I2	I.I556	I.4409	I.9385	2.I259	2.I554	2.I[illegible]5	2.I575
8	I.6724	I.7039	I.8028	I.9809	2.I560	2.7866	3.896I	4.3098	4.3740	4.3[illegible]	4.3[illegible]2
9	2.392I	2.4464	2.6I57	2.9259	3.2334	4.4465	6.4736	7.2072	7.3I75	7.3[illegible]	7.[illegible]253
I0	2.525I	2.5950	2.8I76	3.23I3	3.65I8	5.5157	8.383I	9.376I	9.5226	9.53[illegible]	9.[illegible]
II	I.80I8	I.8660	2.07I6	2.4640	2.875I	4.9959	7.9233	8.89[illegible]5	9.0344	9.043[illegible]	.[illegible]
I2	0.7606	0.7968	0.9I64	I.I54I	I.4I56	2.9999	4.93II	5.5488	5.6389	5.64[illegible]	5.6451
I3	0.I382	0.I538	0.I828	0.2553	0.3438	0.9547	I.6035	I.8070	I.8370	I.83[illegible]	I.039I
I4	0.0026	0.003I	0.0047	0.0098	0.0I76	0.077I	0.I289	0.I450	0.I476	0.I4[illegible]6	0.I[illegible]

APPENDIX II

Tables for the scattering cross sections of slow neutrons.

The differential scattering cross sections are represented in the form of a power expansion in Legendre polynomials. The appendix lists the zero and first moments of the scattering kernel, which we shall denote respectively by $G_0(x' \rightarrow x)$ and $G_1(x' \rightarrow x)$. The functions $G_0(x' \rightarrow x)$ and $G_1(x' \rightarrow x)$ are normalized in the following fashion:

$$\lim_{x' \to \infty} \int_0^x G_0(x' \rightarrow x)\, dx = 1$$

$$\lim_{x' \to \infty} \int_0^x G_1(x' \rightarrow x)\, dx = \bar{\mu}_0$$

where $\bar{\mu}_0$ -- average cosine of the scattering angle.

The functions $G_0(x' \rightarrow x)$ and $G_1(x' \rightarrow x)$ are connected with the scattering cross sections $\sigma_0(x'_1 \rightarrow x)$ and $\sigma_1(x' \rightarrow x)$ by the relation

$$\sigma_0(x' \rightarrow x) = \sigma_s G_0(x' \rightarrow x)$$

$$\sigma_1(x' \rightarrow x) = \sigma_s G_1(x' \rightarrow x)$$

where σ_s -- scattering cross section at energy E = 0.026

ev.

Here x -- dimensionless velocity of the neutron

$$X = \sqrt{\frac{E}{kT}}$$

The functions $G_0(x_0 \rightarrow x)$ and $G_1(x_0 \rightarrow x)$ are best resolved into an elastic and inelastic component, i.e.,

$$G_0(x_0 \rightarrow x) = G_{0es}(x_0 \rightarrow x) + G_{0is}(x_0 \rightarrow x)$$

$$G_1(x_0 \rightarrow x) = G_{les}(x_0 \rightarrow x) + G_{lis}(x_0 \rightarrow x)$$

The attached tables show the values of the function $G_{0is}(x_0 \rightarrow x)$ and $G_{lis}(x_0 \rightarrow x)$. In addition, the values of the function $f_1(x, x_0)$ are also given

$$f_i(x, x_0) = \int_0^x G_i(x_0 \rightarrow x')\, dx' \qquad (i = 0, 1)$$

This function is needed to calculate the cross section for the escape of neutrons.

Table 7 Table of the function $g_{ois}(x_o \rightarrow x)$ for beryllium, T = 300°K.

x \ x_o	0.0338I	0.15000	0.26619	0.3338I	0.45000	0.56619	0.6[illegible]I	0.75000	0.86619	0.9338I	I.00000	I.I6619
0.0338I	0.00000	0.00001	0.00002	0.00002	0.00003	0.00004	0.00005	0.00006	0.00007	0.00008	0.00009	0.00009
0.15000	0.00096	0.00041	0.00057	0.00057	0.00074	0.00093	0.00109	0.00125	0.00146	0.00157	0.00174	0.00184
0.26619	0.00850	0.00262	0.00[illegible]	0.00339	0.00272	0.00318	0.00359	0.00418	0.00481	0.00515	0.00566	0.00598
0.3338I	0.00[illegible]2	.00578	0.00[illegible]	0.00449	0.00483	0.00549	0.00592	0.00627	0.00783	0.00836	0.00915	0.00966
.45000	0.06554	0.01663	0.[illegible]52	0.01081	0.01073	0.01151	0.01217	0.01363	0.01522	0.01615	0.01758	0.01855
.56619	0.15184	0.03691	0.[illegible]173	0.02097	0.02084	0.02162	0.02353	0.02582	0.02726	0.02953	0.03120	
0.[illegible]338I	0.22351	0.05360	0.03[illegible]	0.03056	0.02786	0.02757	0.02873	0.03087	0.03365	0.03537	0.03828	0.04049
0.75000	0.34434	0.08100	0.05[illegible]	0.04963	0.04401	0.04294	0.04355	0.04601	0.04967	0.05209	0.05631	0.05989
0.86619	0.[illegible]650	0.[illegible]357I	0.08[illegible]	[illegible].72417	0.06275	0.06015	0.06062	0.06341	0.06813	0.07146	0.07753	0.08315
0.93 8I	0.[illegible]70	0.[illegible]74	0.09[illegible]	[illegible].[illegible]850	0.07390	0.07045	0.07068	0.07377	0.07927	0.08323	0.09061	0.09789
.00000	0.86374	0.[illegible]23	[illegible].[illegible]387	0.10278	0.09776	0.08618	0.08635	0.09004	0.09711	0.10229	0.11280	0.12116
[illegible]	0.[illegible]96	[illegible].[illegible]77	0.[illegible]883	0.[illegible]823	0.10147	0.09642	0.09674	0.10143	0.11029	0.11704	0.12831	0.14661
[illegible]	[illegible].[illegible]963	0.[illegible]774	0.[illegible]79	0.[illegible]045	0.10353	0.09862	0.09919	0.10453	0.11454	0.12262	0.13791	0.15674
I.00000	.93351	0.[illegible]256	0.[illegible]1408	0.[illegible]462	0.09859	0.09500	0.09608	0.10248	0.[illegible]1414	0.[illegible]2314	0.14239	0.16550
[illegible]	0.[illegible]256	0.[illegible]1529	0.[illegible]1448	0.[illegible]2[illegible]	0.08524	0.08269	0.08426	0.09132	0.10366	0.11332	0.13451	0.16141
[illegible]	0.[illegible]2[illegible]	0.16020	0.09788	0.08502	0.07454	0.07285	0.07439	0.08149	0.09367	0.10330	0.12464	0.15244
[illegible]	0.[illegible]354	0.11386	0.07066	0.06103	0.05354	0.05339	0.05520	0.06174	0.07248	0.08121	0.10103	0.12806
I.76619	0.[illegible]749	.07261	0.04529	0.03925	0.03508	0.03520	0.03675	0.04184	0.05043	0.05751	0.07366	0.09692
[illegible].8338I	0.[illegible]556	.05366	0.03333	0.02899	0.02603	0.02633	0.02764	0.03181	0.03886	0.04464	0.05846	0.07838
[illegible].95000	0.[illegible]395	0.[illegible]2933	0.[illegible]342	0.[illegible]1608	0.[illegible]1455	0.01486	0.01572	0.01838	0.02293	0.02671	0.03592	0.04997
2.06619	0.06440	0.0[illegible]524	0.00859	0.00638	0.00761	0.00781	0.00830	0.00980	0.01239	0.01458	0.02006	0.02872
2.[illegible]38I	0.[illegible]334	0.01026	0.00646	0.00564	0.00512	0.00526	0.00560	0.00662	0.00840	0.00993	0.01377	0.01995
[illegible].25000	0.02163	0.00612	[illegible].00422	0.00281	0.00255	0.00262	0.00278	0.00329	0.00418	0.00494	0.00689	0.01010
2.36619	0.01058	0.00250	0.00157	0.00137	0.00124	0.00128	0.00135	0.00160	[illegible].00203	0.00240	0.00334	0.00489
2.[illegible]38I	0.00687	0.00163	0.00102	0.00089	0.00081	0.00083	0.00088	0.00104	0.00132	0.00156	0.00217	0.00317
[illegible].50000	0.00315	0.00075	0.00047	0.00041	0.00037	0.00038	0.00041	0.00048	0.00061	0.00072	0.00101	0.00148
.66619	0.00137	0.00033	0.00021	0.00018	0.00016	0.00017	0.00018	0.00021	0.00027	0.00032	0.00045	0.00067
[illegible].7338I	0.00083	0.00020	0.00012	0.00011	0.00010	0.00010	0.00011	0.00013	0.00017	0.00020	0.00028	0.00041
[illegible].85000	0.00034	0.00008	0.00005	0.00004	0.00004	0.00004	0.00005	0.00005	0.00007	0.00008	0.00012	0.00017
[illegible].96619	0.00013	0.00003	0.00002	0.00002	0.00002	0.00002	0.00002	0.00002	0.00003	0.00003	0.00005	0.00007
3.0338I	0.00000	0.00000	0.00000	0.00000	0.00000	0.00000	0.00000	0.00000	0.00000	0.00000	0.00000	0.00000

x \ x_o	I.2338I	I.35000	I.46619	I.5338I	I.65000	I.76619	I.8338I	I.95000	2.0619	2.I338I	2.25000	[illegible].36619
0.0338I	0.00009	0.00009	0.00008	0.00008	0.00006	0.00005	0.00004	0.00003	0.00002	0.00002	0.00001	0.00001
0.15000	0.00186	0.00181	0.00167	0.00154	0.00127	0.00098	0.00082	0.00058	0.00041	0.00033	0.00023	0.00017
0.26619	0.00605	0.00592	0.00548	0.00506	0.00421	0.00327	0.00274	0.00196	0.00137	0.00111	0.00078	0.00056
0.3338I	0.00978	0.00955	[illegible].00890	0.00824	0.00688	0.00537	0.00452	0.00323	0.00226	0.00183	0.00130	0.00093
0.45000	0.01880	0.01854	0.01727	0.01616	0.01360	0.01072	0.00907	0.00654	0.00459	0.00372	0.00263	0.00189
0.56619	0.03170	[illegible].03147	0.02966	0.02776	0.02383	0.01905	0.01624	0.01183	0.00833	0.00678	0.00478	0.00343
0.6338I	0.04123	0.04117	[illegible].03909	1.03652	[illegible].03186	0.02572	0.02205	0.01618	0.01145	0.00932	0.00657	0.00470
0.75000	[illegible].05[illegible]	[illegible].05[illegible]	[illegible].04977	[illegible].04707	[illegible].04128	0.03432	0.03580	0.02670	0.01909	0.01556	0.01097	0.00783
0.86619	0.06577	[illegible].06[illegible]	[illegible].06668	[illegible].06431	[illegible].05936	0.05358	0.05584	0.04252	0.03081	0.02520	0.01778	0.01269
0.9338I	[illegible].07753	0.[illegible]753	[illegible].[illegible]6	[illegible].[illegible]4[illegible]	0.09367	0.08043	0.07115	0.05496	0.04022	0.03302	0.02334	0.01663
I.05000	[illegible].[illegible]34	[illegible].13763	[illegible].14019	0.13958	0.13156	0.11631	0.10521	0.08345	0.06245	0.05170	0.03672	0.02614
I.16619	0.[illegible]568	0.[illegible]69[illegible]	0.[illegible]7[illegible]1	0.[illegible]8[illegible]	0.17660	0.16208	0.14939	0.12294	0.09471	0.07933	0.05701	0.04060
I.2338I	0.16000	[illegible].[illegible]66[illegible]	[illegible].[illegible]8[illegible]	0.20098	0.20487	0.19262	0.18008	0.15193	0.11917	0.10081	0.07312	0.05218
I.35000	0.[illegible]0[illegible]	[illegible].[illegible]07[illegible]	0.[illegible]3[illegible]	0.24956	0.25297	0.24903	0.23924	0.21072	0.17284	0.14884	0.11059	0.07966
I.46619	0.17545	0.[illegible]2[illegible]64	0.[illegible]4[illegible]5	0.26779	0.29301	0.30389	0.30113	0.27970	0.24051	0.21320	0.16363	0.12000
I.5338I	0.17167	0.20533	0.25069	0.27385	0.30916	0.33101	0.33451	0.32145	0.28564	0.25717	0.20274	0.15107
I.65000	0.14755	0.18778	0.23550	0.26587	0.31752	0.36103	0.37820	0.38781	0.36725	0.34233	0.28503	0.22010
I.76619	0.11440	0.15245	0.20143	0.23474	0.29773	0.36135	0.39350	0.43352	0.44141	0.42860	0.37989	0.31042
I.8338I	0.09385	0.12850	0.17514	0.20816	0.27367	0.34528	0.38659	0.44458	0.47341	0.47225	0.43721	0.37002
I.95000	0.06134	0.08768	0.12602	0.15495	0.21739	0.29467	0.34440	0.42900	0.49549	0.52063	0.52420	0.47877
2.06619	0.03589	0.05365	0.08084	0.10272	0.15358	0.22383	0.27359	0.36964	0.46959	0.51909	0.57403	0.57410
2.I338I	0.02517	0.03831	0.05941	0.07668	0.11869	0.18020	0.22628	0.32202	0.43064	0.49213	0.57544	0.61112
2.25000	0.01286	0.02005	0.03212	0.04259	0.06962	0.11252	0.14758	0.22842	0.33525	0.40539	0.52869	0.62302
2.36619	0.00624	0.00982	0.01603	0.02159	0.03657	0.06254	0.08496	0.14191	0.22811	0.29286	0.42381	0.56218
2.4338I	0.00403	0.00636	0.01042	0.01410	0.02419	0.04222	0.05858	0.10140	0.17105	0.22691	0.34992	0.48692
2.55000	0.00188	0.00296	0.00484	0.00656	0.01136	0.02024	0.02860	0.05214	0.09399	0.13088	0.22327	0.35528
2.66619	0.00085	0.00134	0.00220	0.00298	0.00516	0.00922	0.01311	0.02449	0.04623	0.06684	0.12332	0.21795
2.7338I	0.00053	0.00084	0.00137	0.00186	0.00322	0.00576	0.00818	0.01534	0.02934	0.04298	0.08231	0.15307
2.85000	0.00022	0.00036	0.00059	0.00080	0.00140	0.00251	0.00358	0.00671	0.01292	0.01913	0.03797	0.07522
2.96619	0.00009	0.00015	0.00024	0.00033	0.00059	0.00106	0.00152	0.00286	0.00552	0.00818	0.01642	0.03352
3.0338I	0.00005	0.00009	0.00014	0.00020	0.00035	0.00063	0.00090	0.00171	0.00332	0.00493	0.00991	0.02034
3.I5000	0.00002	0.00003	0.00006	0.00008	0.00014	0.00025	0.00036	0.00069	0.00135	0.00202	0.00408	0.00840
3.26619	0.00001	0.00001	0.00002	0.00003	0.00005	0.00009	0.00014	0.00027	0.00053	0.00079	0.00162	0.00338
3.3338I	0.00000	0.00000	0.00000	0.00000	0.00000	0.00000	0.00000	0.00015	0.00030	0.00045	0.00093	0.00195

Table 7 (continued)

X \ λ_0	2.4338I	2.55000	2.6661I9	2.7338I	2.85000	2.9661I9	3.0338I	3.I5000	3.2661I9	3.3338I	3.45000	3.5661I9
0.3338I	0.00077	0.00055	0.00039	0.0003I	0.00022	0.000I5	0.000I2	0.00008	0.00000	0.00000	0.00000	0.00000
0.45000	0.00I56	0.00II2	0.00079	0.00064	0.00044	0.00030	0.00024	0.000I6	0.00000	0.00000	0.00000	0.00000
0.5661I9	0.00283	0.00203	0.00I44	0.00II7	0.0008I	0.00056	0.00045	0.00030	0.00000	0.00000	0.00000	0.00000
0.6338I	0.00389	0.00280	0.00I98	0.00I6I	0.00II2	0.00077	0.00062	0.00042	0.00028	0.00022	0.000I5	0.00000
0.75000	0.00648	0.00467	0.00333	0.0027I	0.00I90	0.00I3I	0.00I06	0.00072	0.00049	0.00039	0.00026	0.00000
0.8661I9	0.0I048	0.00757	0.00542	0.00444	0.00312	0.002I7	0.00I75	0.00I20	0.00082	0.00065	0.00043	0.00000
0.9338I	0.0I373	0.00992	0.00713	0.00585	0.004I2	0.00287	0.00232	0.00I60	0.00I09	0.00087	0.00058	0.00038
I.05000	0.02I58	0.0I559	0.0II26	0.00927	0.00657	0.0046I	0.00373	0.00259	0.00I78	0.00I42	0.00096	0.00064
I.I6619	0.03345	0.02418	0.0I753	0.0I449	0.0I034	0.00730	0.00593	0.004I4	0.00286	0.00230	0.00156	0.00I05
I.2338I	0.04298	0.03I05	0.02255	0.0I868	0.0I339	0.00949	0.00774	0.0054I	0.00376	0.00302	0.00207	0.00I40
I.35000	0.06555	0.04735	0.03445	0.02863	0.02069	0.0I477	0.0I209	0.00850	0.00595	0.00481	0.0033I	0.00226
I.4661I9	0.09917	0.07154	0.052II	0.04337	0.03157	0.02273	0.0I868	0.0I325	0.00932	0.00757	0.00525	0.00361
I.5338I	0.I2541	0.09060	0.06594	0.05496	0.040I5	0.02907	0.02395	0.0I707	0.0I205	0.0098I	0.00685	0.00473
I.65000	0.I8512	0.13487	0.09814	0.08I90	0.060I2	0.04392	0.03639	0.026I3	0.0I863	0.0I522	0.0I07I	0.00746
I.7661I9	0.26638	0.I98I3	0.I4472	0.I2078	0.08896	0.06550	0.05461	0.03960	0.02845	0.02338	0.0I656	0.0II66
I.8338I	0.32435	0.24568	0.I806I	0.I5066	0.IIII8	0.08215	0.06872	0.05014	0.0361I9	0.02985	0.02I26	0.0I503
I.95000	0.43492	0.34696	0.26I3I	0.2I875	0.I6I54	0.I2000	0.I0086	0.07440	0.05428	0.04497	0.03238	0.02308
2.0661I9	0.54730	0.46658	0.36809	0.3I2I4	0.24215	0.I7288	0.I4596	0.I0872	0.08029	0.06693	0.04864	0.03504
2.I338I	0.60I95	0.53905	0.44II9	0.379I4	0.28497	0.2I239	0.I7972	0.I3460	0.I0008	0.08378	0.06124	0.04442
2.25000	0.65396	0.64736	0.57344	0.5II54	0.39849	0.30036	0.25420	0.I9I80	0.I4419	0.I2I65	0.0900I	0.06597
2.3661I9	0.6I902	0.70073	0.68943	0.6471I	0.53696	0.4I72I	0.35507	0.26858	0.20418	0.I7347	0.I3012	0.09650
2.4338I	0.580I3	0.692I8	0.73I45	0.7I236	0.62I78	0.49890	0.42786	0.3251б	0.24784	0.2II46	0.I5987	0.II95I
2.55000	0.446I6	0.60823	0.73I46	0.7676I	0.74882	0.64872	0.57408	0.445I2	0.34III	0.29264	0.22415	0.I7005
2.6661I9	0.29397	0.45609	0.63280	0.7I07I	0.80506	0.78I6A	0.72509	0.59448	0.46244	0.39794	0.30791	0.23700
2.7338I	0.2I422	0.358I2	0.53I79	0.64546	0.787I2	0.828I3	0.799QI	0.6857I	0.54785	0.47238	0.36698	0.28468
2.85000	0.II073	0.20689	0.35674	0.466I3	0.66446	0.8I683	0.85620	0.82603	0.70590	0.62357	0.489I7	0.38324
2.9661I9	0.05096	0.I0280	0.I9865	0.28I28	0.46849	0.68008	0.78603	0.8838б	0.8495I	0.78253	0.64022	0.50563
3.0338I	0.03II7	0.06487	0.I3I42	0.I9353	0.35020	0.56053	0.68768	0.85445	0.899I5	0.86I64	0.73333	0.58902
3.I5000	0.0I292	0.02745	0.05879	0.09063	0.I8436	0.34392	0.46624	0.69832	0.87507	0.920II	0.87993	0.748I7
3.2661I9	0.0052I	0.0III3	0.02419	0.03830	0.08334	0.I7486	0.25953	0.46289	0.70609	0.8б898	0.953855	0.895I9
3.3338I	0.00303	0.00650	0.0I4I7	0.02248	0.050I0	0.I0962	0.I6926	0.33I24	0.56418	0.70940	0.90I05	0.9465I
3.45000	0.00II5	0.00251	0.00552	0.00880	0.0I980	0.04519	0.07259	0.I5961	0.32I85	0.45402	0.7I3I7	0.9I362
3.5661I9	0.00042	0.00093	0.00208	0.00334	0.00758	0.0I744	0.02850	0.06633	0.I5005	0.233II	0.44656	0.7I472
3.6338I	0.00023	0.00051	0.00II5	0.00I86	0.00427	0.00989	0.0I620	0.03829	0.08960	0.I4455	0.30550	0.55427
3.75000	0.00008	0.000I8	0.0004I	0.00066	0.00I54	0.00363	0.00599	0.0I426	0.03440	0.05731	0.I3535	0.29450
3.8661I9	0.00003	0.000006	0.000I4	0.00023	0.00054	0.00I28	0.002I3	0.00516	0.0I254	0.02II4	0.05215	0.I2643
3.9338I	0.00000	0.00000	0.00000	0.000I2	0.00028	0.00068	0.00II5	0.00280	0.00688	0.0II64	0.02901	0.07220
4.05000	- " -	- " -	- " -	0.00004	0.00009	0.00023	0.00038	0.00095	0.00238	0.00406	0.0I023	0.02601
4.I6619	- " -	- " -	- " -	0.0000I	0.00003	0.00007	0.000I2	0.0003I	0.00079	0.00I36	0.00349	0.00858
4.2338I	- " -	- " -	- " -	0.00000	0.00000	0.00000	0.00000	0.000I6	0.0004I	0.00070	0.00I83	0.00477

X \ λ_0	3.6338I	3.75000	3.8661I9	3.9338I	4.05000	4.I6619	4.2338I	4.35000	4.4661I9	4.5338I	4.65000	4.7661I9
I.2338I	0.00III	0.00073	0.00049	0.00037	0.00023	0.000I5	0.000II	0.00000	0.00000	0.00000	0.00000	0.00000
I.35000	0.00I79	0.00I20	0.00080	0.00063	0.00040	0.00026	0.000I9	0.00000	0.00000	0.00000	0.00000	0.00000
I.4661I9	0.00295	0.00I95	0.00I29	0.00I04	0.00067	0.00042	0.00034	0.00000	0.00000	0.00000	0.00000	0.00000
I.5338I	0.00360	0.00258	0.00I72	0.00I35	0.0009I	0.00057	0.00046	0.00028	0.00018	0.000I3	0.00000	0.00000
I.65000	0.00582	0.00413	0.00279	0.0022I	0.00I49	0.00097	0.00074	0.00045	0.00022	0.00023	0.00000	0.00000
I.7661I9	0.00947	0.00654	0.00448	0.00357	0.00239	0.00I6I	0.00I25	0.00083	0.00051	0.0004I	0.00000	0.00000
I.8338I	0.0I224	0.00851	0.00586	0.00470	0.003I7	0.002I4	0.00I68	0.00II2	0.00071	0.00057	0.00034	0.00022
I.95000	0.0I839	0.0I328	0.00924	0.00745	0.00509	0.00342	0.00274	0.00I80	0.00I2C	0.00092	0.00060	0.00039
2.0661I9	0.02882	0.02048	0.0I439	0.0II67	0.00807	0.0055I	0.00438	0.00297	0.00I99	0.00155	0.00I02	0.00063
2.I338I	0.03967	0.02620	0.0I853	0.0I508	0.0I050	0.0072I	0.00576	0.00395	0.00260	0.00I98	0.00I34	0.00085
2.25000	0.05454	0.03956	0.02832	0.02320	0.0I632	0.0II37	0.00915	0.00630	0.00425	0.00334	0.00224	0.00I48
2.3661I9	0.07859	0.05900	0.04269	0.03520	0.02505	0.0I766	0.0I433	0.00990	0.0068I	0.00543	0.00367	0.00241
2.4338I	0.I0039	0.07391	0.05384	0.04458	0.03I98	0.02267	0.0I846	0.0I287	0.00893	0.007I4	0.00486	0.00323
2.55000	0.I4406	0.I0733	0.07921	0.06608	0.04796	0.03448	0.02427	0.0I697	0.0I392	0.0II28	0.00772	0.00527
2.6661I9	0.I9[illegible]9	0.I53II	0.II453	0.09626	0.07080	0.05I54	0.0426I	0.03048	0.02I55	0.0I75I	0.0I22I	0.00835
2.7938I	0.24456	0.I866I	0.I4068	0.II885	0.08816	0.06468	0.05372	0.03876	0.02760	0.02252	0.0I572	0.0I092
2.85000	0.33219	0.25750	0.I9738	0.I6803	0.I2650	0.09414	0.07890	0.05760	0.04I62	0.03428	0.02428	0.0I709
2.9661I9	0.44086	0.3473I	0.27050	0.23275	0.I7782	0.I3436	0.II35I	0.08419	0.06I77	0.05I29	0.03686	0.02619
3.0338I	0.5I500	0.40872	0.32I73	0.27830	0.2I468	0.I6372	0.I3918	0.I0414	0.07695	0.06428	0.04656	0.03338
3.I5000	0.66415	0.53075	0.42452	0.37I03	0.29I44	0.22588	0.I9375	0.I4735	0.II080	0.093I8	0.06878	0.05000
3.2661I9	0.82219	0.67737	0.54596	0.48203	0.38574	0.30460	0.26376	0.20409	0.I5592	0.I3258	0.09917	0.07340
3.3338I	0.90272	0.76801	0.62643	0.55488	0.44865	0.35798	0.3I225	0.24388	0.I8829	0.I6I00	0.I2I68	0.09089
3.45000	0.96I3I	0.91391	0.7[illegible]47	0.69665	0.56529	0.46332	0.40849	0.32524	0.25555	0.22083	0.I699I	0.I2898
3.5661I9	0.85249	0.97I95	0.92249	0.84738	0.70753	0.58298	0.52008	0.42243	0.33847	0.29522	0.23I46	0.I7905
3.6338I	0.7I470	0.92783	0.97368	0.92643	0.79225	0.65852	0.59060	0.48555	0.39345	0.3457I	0.27401	0.2I4I7
3.75000	0.43240	0.7I385	0.9336I	0.9833I	0.93I42	0.80III	0.72273	0.60309	0.49886	0.4437I	0.35848	0.28565
3.8661I9	0.20525	0.42229	0.7I087	0.86065	0.98750	0.93448	0.86097	0.72952	0.6I472	0.55346	0.45663	0.37I00
3.9338I	0.I2I39	0.27647	0.53500	0.70848	0.93858	0.984I6	0.93542	0.80923	0.68504	0.62III	0.5I864	0.42698
4.05000	0.04480	0.II302	0.26492	0.40507	0.7034I	0.93928	0.98996	0.93570	0.8I309	0.74069	0.63I26	0.53055
4.I6619	0.0I56I	0.04074	0.I0505	0.I7798	0.39360	0.69728	0.85740	0.989I7	0.93442	0.86546	0.74644	0.64056
4.2338I	0.00832	0.02I85	0.05756	0.I0060	0.24670	0.50989	0.69328	0.93722	0.98I57	0.93306	0.8I7II	0.70529
4.35000	0.00274	0.00730	0.0I95I	0.03482	0.09329	0.23534	0.37495	0.68578	0.93424	0.98496	0.92967	0.8I840
4.4661I9	0.00086	0.00235	0.00639	0.0II45	0.03I50	0.08639	0.I5259	0.36302	0.67764	0.84606	0.98037	0.925I9
4.5338I	0.00043	0.00II9	0.003c7	0.0059I	0.0I633	0.04554	0.08256	0.2I785	0.48I58	0.67265	0.92707	0.96869
4.65000	0.00013	0.00036	0.00I00	0.00I83	0.00517	0.0I458	0.02684	0.07632	0.207II	0.34408	0.6637I	0.9c139
4.7661I9	0.00004	0.000I0	0.00029	0.00054	0.00I57	0.0045I	0.00835	0.02423	0.07648	0.I2964	0.33224	0.65[illegible]4
4.8338I	0.00000	0.00000	0.000I4	0.00026	0.00077	0.00223	0.0041I7	0.0I2I6	0.03580	0.06726	0.I9079	0.[illegible]5200
4.95000	- " -	- " -	0.00004	0.00007	0.00022	0.00064	0.00I22	0.00363	0.0I084	0.02057	0.06203	0.I[illegible]62
5.0661I9	- " -	- " -	0.0000I	0.00002	0.00006	0.000I8	0.00034	0.00I04	0.003I6	0.00605	0.0I854	0.05717
5.I338I	- " -	- " -	0.00000	0.00000	0.00000	0.00000	0.000I6	0.00049	0.00I5I	0.00292	0.00901	0.02[illegible]0
							0.00004	0.000I3	0.0004I	0.00080	0.00254	0.00[illegible]1
							0.0000I	0.00003	0.000II	0.0002I	0.00068	0.00220

Table 7a Table of the function $f_o(x,x_o)$ for beryllium, T = 300°K.

x \ x_o	0.0338I	0.15000	0.2669I	0.3338I	0.45000	0.5669I	0.6681	0.75000
0.0	0.00000000	0.00000000	0.00000000	0.00000000	0.00000000	0.00000000	0.00000000	0.00000000
0.3	I.2351I979	I.22859749	I.21515622	0.00027784	0.00032778	0.00019186	0.00049990	0.00054004
0.6	I.2583418I	I.23437272	I.21905482	I.20754219	I.1838f991	I.1538f408	0.00436151	0.00487030
0.9	I.37625586	I.26229464	I.23655412	I.22272079	I.19728905	I.16687293	I.14709945	I.10965363
I.2	I.62975016	I.32165586	I.27294252	I.25379427	I.22400299	I.19226888	I.17250479	I.13625847
I.5	I.90246874	I.38551657	I.3I2I230I	I.28730150	I.25293703	I.22004538	I.20066241	I.16624326
I.8	2.04946249	I.42009912	I.33355905	I.30579764	I.2C926342	I.23616868	I.21728431	I.18475316
2.I	2.09015428	I.42971893	I.33959182	I.3II05479	I.27400606	I.24099519	I.22237458	I.19067184
2.4	2.09753087	I.43146478	I.34068942	I.3I20I35I	I.27487624	I.24188936	I.2233244I	I.19179562
2.7	2.09863826	I.43172688	I.34085429	I.3I2I5755	I.27500704	I.24202376	I.22346718	I.19196450
3.0	2.09876331	I.43175656	I.34087304	I.3I2I7400	I.27502208	I.24203936	I.22348384	I.19198443
3.3	2.09876331	I.43175656	- " -	- " -	- " -	- " -	- " -	- " -

x \ x_o	0.8669I9	0.9338I	I.05000	I.1669I9	I.2338I	I.35000	I.4669I9	I.5338I
0.0	0.00000000	0.00000000	0.00000000	0.00000000	0.00000000	0.00000000	0.00000000	0.00000000
0.3	0.00060II7	0.00064548	0.00071058	0.00075I27	0.00075988	0.00074304	0.00068608	0.00063358
0.6	0.00543371	0.00576696	0.00647776	0.00663002	0.00672285	0.00663503	0.00620249	0.00580491
0.9	I.06840218	0.0I6I1394	0.02343599	0.02491934	0.02548I04	0.02566595	0.02464818	0.02347034
I.2	I.09714674	I.0730227I3	I.03030673	0.98518989	0.06416029	0.06692048	0.06708389	0.06568961
I.5	I.I3054644	I.I0806577	I.07I69310	I.03376896	0.III17206	0.97048939	0.92674702	0.I3742070
I.8	I.I5222I03	I.I3269763	I.I0I98822	I.07I628I2	I.054685II	I.02567479	0.99579044	0.97700235
2.I	I.I5954879	I.I4I793.0	I.II332I28	I.0872I647	I.07367507	I.052545I8	I.03392422	I.02356936
2.4	I.I60975II	I.I1347880	I.II566486	I.09063276	I.0780084I	I.059229I4	I.04449380	I.03743625
2.7	I.I6II894I	I.I4373210	I.II60I767	I.09II4958	I.07866785	I.060c6647	I.046I9II2	I.0397342Q
3.0	I.I6I2I500	I.I4376256	I.II606058	I.09I2I3I6	I.07874946	I.06039592	I.04640435	I.04002395
3.3	- " -	- " -	- " -	I.09I2I9I3	I.07875720	I.06040842	I.04642535	I.04005283
3.6	- " -	- " -	- " -	- " -	- " -	- " -	- " -	- " -

x \ x_o	I.65000	I.7669I9	I.8338I	I.95000	2.0669I9	2.I338I	2.25000	2.3669I9
0.0	0.00000000	0.00000000	0.00000000	0.00000000	0.00000000	0.00000000	0.00000000	0.00000000
0.3	0.00052552	0.00040775	0.00034159	0.00024343	0.000I6977	0.000I3779	0.00009753	0.00007006
0.6	0.00489762	0.00387237	0.00328026	0.00237109	0.00166408	0.00135175	0.00095497	0.00068468
0.9	0.02053587	0.0I682301	0.0I454366	0.0I082399	0.00773085	0.00630225	0.00444669	0.00317873
I.2	0.06059560	0.05254046	0.04695077	0.0367754I	0.02730I7I	0.02255859	0.0I6039I6	0.0II43352
I.5	0.I3581920	0.I27I2041	0.II894986	0.I0084017	0.08032039	0.06857052	0.0505I426	0.0364027I
I.8	0.24053677	0.8965261Z	0.23004489	0.21546179	0.I8973386	0.17I76I39	0.I3707047	0.I0420654
2.I	I.0351Z582	0.98324256	0.96728050	0.93077156	0.88134682	0.32341575	0.29I23380	0.24672021
2.4	I.0734696	I.0I847336	I.0I289484	0.99988874	0.98694786	0.9681I429	0.92596829	0.8781872.0
2.7	I.0830760	I.0254582Z	I.02268299	I.0I733I56	I.0I358726	I.0I305532	0.9991738I	0.9842971Q
3.0	I.0318II25	I.0263611Z	I.0239680I	I.0I974259	I.0I82I472	I.0I686902	I.0I246399	I.0089[illegible]7
3.3	I.0I.86249	I.0264548Q	I.024I0280	I.0I999944	I.0I971567	I.0I76I520	I.0I 96864	I.0I297I59
3.6	- " -	- " -	- " -	I.0200207Q	I.0I875844	I.0I767996	I.0I4I0.92	I.0I32[illegible]7
3.9	-	- " -	- " -	- " -	I.0I875844	I.0I767996	- " -	I.0I327505

Table 7a (continued)

X \ X_0	2.4338I	2.55000	2.666I9	2.7338I	2.85000	2.966I9	3.0338I	3.I5000
0.0	0.00000000	0.00000000	0.00000000	0.00000000	0.00000000	0.00000000	0.00000000	0.00000000
0.3	.00 05787	0.00000 27	0.00002896	0.00002338	0.00001608	0.00001095	0.00000000	0.00000000
0.6	0.00056546	0.000 05	0.00028598	0.00023I85	0.00016024	0.00010992	0.00007920	0.00005351
0.9	. 00	0.00185129	0.00134780	0.00109800	0.00076594	0.00052964	0.00041722	0.00028 ?
I.2	0.00	0.00	0.00402943	0.00284726	0.00195180	0.00160308	0.00110825	
I.5	0.00	.00167596	0.00157876	0.00130172	0.00095182	0.00064569	0.00054603	0.00379703
I.8	0.00	.00 .014	0.00463575	0.00385810	0.00282699	0.00238276	0.00168546	0.00120006
2.I	.00	0.00 538	0.I2092621	0.10631415	0.00827705	0.05763545	0.0461543S	0.03516105
2.4	0.00	0.00 648	0.29760271	0.26000050	0.19990288	0.I5014944	0.I2661298	0.09433230
2.7	0.00	0.93461787	0.87007554	0.48007744	0.41865126	0.34335744	0.29923701	0.23031911
3.0	I.00713369	I.00061300	0.58761224	0.97466567	0.94049145	0.88266840	0.54548286	0.47I25I88
3.3	I.0I788822	I.0I0L0604	I.00841856	I.00609948	I.00I20059	0.98960725	0.97921610	0.94785243
3.6	I.0I23291I	I.0II55915	I. 10 0858	I.00942360	I.00864825	I.00642139	I.00537406	I.00226542
3.	I.0I236099	I.0I163047	I.0I067074	I.00 68606	I.00925427	I.00783617	I.00770067	I.00778687
4.0	- " -	- " -	- " -	I.00970I18	.00923I4	I.00792921	".00785735	I.00817281

X \ X_0	3.266I9	3.3338I	3.45000	3.566I9	3.6338I	3.75000	3.866I9	3.9338I
0.0	0.00000000	0.00000000	0.00000000	0.00000000	0.00000000	0.00000000	0.00000000	0.00000000
0.3	0.00000000	0.00000000	0.00000000	0.00000000	0.00000000	0.00000000	0.00000000	0.00000000
0.6	0.00000000	0.00000000	0.00000000	0.00000000	0.00000000	0.00000000	0.00000000	0.00000000
0.9	0.00015663	0.0001241I2	0.00008223	0.00000000	0.00000000	0.00000000	0.00000000	0.00000000
I.2	0.00072326	0.00057775	0.00038919	0.0001 0488	0.00016053	0.0001 0605	0.00006855	0.00000000
I.5	0.00260543	0.00210208	0.00144053	0.00052316	0.000 3274	0.00048891	0.00032409	0.00020109
I.8	0.00846351	0.00589684	0.00481941	0.00328287	0.00263940	0.00179194	0.00121344	0.00090590
2.I	0.0 540627	0.02095845	0.0I496I75	0.0I053313	0.00858003	0.00598565	0.00413324	0.00326234
2.4	0.06998585	0.05861700	0.04291079	0.03107206	0.02567203	0.0I836039	0.0I301I36	0.0I054581
2.7	0.I7465663	0.I4841896	0.II177856	0.08345470	0.07011068	0.05158910	0.03760178	0.03109392
3.0	0.36522283	0.33613738	0.26053419	0.20041143	0.I7I5210I	0.I3041591	0.09818658	0.08279779
3.3	0.89006530	0.5599 0418	0.5I758I39	0.42385226	0.37150715	0.29168988	0.22709605	0.I9563019
3.6	0.99249736	0.98337436	0.95470237	0.8 853345	0.64554948	0.55854102	0.45956894	0.40537170
3.9	I.00559607	I.00482386	I.00255306	0.99452480	0.98700076	0.96II5937	0.90761547	0.68540266
4.2	I.00 5215	I.00644896	I.00662539	I.00475785	I.00439083	I.00266319	0.99627643	0.99003414
4.5	I.00660527	I.00654254	I.00687036	I.00540159	I.00552124	I.00565264	I.00420714	I.00401471

X \ X_0	4.05000	4.I66I9	4.2338I	4.35000	4.466I9	4.5338I	4.65000	4.766I9
0.0	0.00000000	0.00000000	0.00000000	0.00000000	0.00000000	0.00000000	0.00000000	0.00000000
0.3	0.00000000	0.00000000	0.00000000	0.00000000	0.00000000	0.00000000	0.00000000	0.00000000
0.6	0.00000000	0.00000000	0.00000000	0.00000000	0.00000000	0.00000000	0.00000000	0.00000000
0.9	0.00000000	0.00000000	0.00000000	0.00000000	0.00000000	0.00000000	0.00000000	0.00000000
I.2	0.00000000	0.00000000	0.00000000	0.00000000	0.00000000	0.00000000	0.00000000	0.00000000
I.5	0.0001L818	0.00008220	0.00006301	0.00000000	0.00000000	0.00000000	0.00000000	0.00000000
I.8	0.00060110	0.00039339	0.00030481	0.00015757	0.00010048	0.00007605	0.00000000	0.00000000
2.I	0.00221569	0.00148682	0.00II7504	0.00073830	0.00048546	0.00017524	0.0001 3778	0.0001 2253
2.4	0.00735780	0.00507562	0.00406972	0.00273074	0.00183654	0.00144668	0.00091010	0.00059445
2.7	0.02231763	0.01585768	0.0I292921	0.00900566	0.00623212	0.00500555	0.00336700	0.00226148
3.0	0.06134886	0.04499738	0.03738473	0.02693213	0.01922559	0.0I572786	0.01098067	0.00763193
3.3	0.I5024327	0.II4I4147	0.09679652	0.07226434	0.05340961	0.04455763	0.03229559	0.02319698
3.6	0.32249632	0.25433094	0.22062245	0.17II5513	0.13137928	0.11202040	0.08437864	0.06288905
3.9	0.59499806	0.4938960I	0.43794982	0.35282294	0.28190798	0.24611342	0.19306203	0.14974049
4.2	0.96710634	0.91736540	0.7I934610	0.62745014	0.52527504	0.46875250	0.38265303	0.30944224
4.5	I.00272776	0.99843292	0.99295096	0.97233285	0.92571947	0.74834088	0.65639964	0.55443541
4.8	I.00490815	I.00454783	I.00410532	I.00268187	0.99934005	0.99464497	0.97675105	0.93339343
5.I	I.00500570	I.00483487	I.00464357	I.00426631	I.00403161	I.00349728	I.0324658I	0.99994728
5.4	- " -	- " -	I.00466324	I.00432743	I.00422166	I.00386537	I.0036II65	I.00353212
5.7	- " -	- " -	- " -	- " -	- " -	I.00387696	I.00364974	I.0036528

Table 8 Table of the function $g_{1is}(x_o - x)$ for beryllium, T = 300°K.

X \ X_o	0.0338I	0.15000	0.266I9	0.3338I	0.45000	0.566I9	0.6338I	0.75000	0.866I9	0.9338I	.05000	I.I66I9
0.0338I	0.00000	0.00000	0.00000	0.00000	0.00000	0.00000	0.00000	0.00000	0.00000	0.00000	0.00000	0.00000
0.15000	-0.000I4	-0.000I4	-0.000I4	-0.000I4	-0.000I4	-0.000I5	-0.000I5	-0.000I5	-0.000I5	-0.000I5	-0.000I5	-0.000I4
0.266I9	-0.00074	-0.00074	-0.00076	-0.00077	-0.00078	-0.00080	-0.00082	-0.00084	-0.00085	-0.00084	-0.00082	-0.00078
0.3338I	-0.00I4I	-0.00I42	-0.00I45	-0.00I47	-0.00I52	-0.00I56	-0.00I59	-0.00I63	-0.00I65	-0.00I65	-0.00I62	-0.00I54
0.45000	-0.00323	-0.00327	-0.00329	-0.00339	-0.00350	-0.00363	-0.00370	-0.00382	-0.00391	-0.00392	-0.00389	-0.00374
0.566I9	-0.00587	-0.00593	-0.0060I	-0.00617	-0.00642	-0.0067I	-0.00688	-0.00717	-0.00739	-0.00749	-0.00752	-0.00734
0.6338I	-0.00767	-0.00775	-0.00798	-0.00813	-0.00846	-0.00890	-0.009I6	-0.0096I	-0.00999	-0.0I0I5	-0.0I029	-0.0I0I4
0.75000	-0.0II0I	-0.0II16	-0.0II48	-0.0II75	-0.0I235	-0.0I308	-0.0I355	-0.0I440	-0.0I520	-0.0I560	-0.0I608	-0.0I6I7
0.866I9	-0.0I4I0	-0.0I432	-0.0I480	-0.0I520	-0.0I6II	-0.0I722	-0.0I800	-0.0I94I	-0.02085	-0.02I63	-0.02278	-0.0234I
0.9338I	-0.0I553	-0.0I579	-0.0I637	-0.0I686	-0.0I795	-0.0I936	-0.02029	-0.02210	-0.02400	-0.02511	-0.02675	-0.02791
I.05000	-0.0I698	-0.0I730	-0.0I804	-0.0I866	-0.02007	-0.02I93	-0.02322	-0.0257I	-0.02853	-0.03020	-0.03308	-0.03550
I.I66I9	-0.0I687	-0.0I723	-0.0I807	-0.0I879	-0.02044	-0.02267	-0.02423	-0.02738	-0.03I05	-0.03337	-0.03759	-0.04I6I
I.2338I	-0.0I609	-0.0I646	-0.0I732	-0.0I807	-0.0I979	-0.02213	-0.02381	-0.02723	-0.03I36	-0.0340I	-0.03883	-0.04395
I.35000	-0.0I375	-0.0I4I0	-0.0I494	-0.0I567	-0.0I737	-0.0I974	-0.02I46	-0.02509	-0.02963	-0.03270	-0.03863	-0.04507
I.466I9	-0.0I07I	-0.0II02	-0.0II72	-0.0I234	-0.0I386	-0.0I60I	-0.0I760	-0.02I04	-0.02551	-0.02864	-0.03499	-0.04246
I.5338I	-0.00885	-0.009I2	-0.00976	-0.0I032	-0.0II67	-0.0I356	-0.0I50I	-0.0I8I8	-0.02238	-0.02539	-0.03I62	-0.03924
I.65000	-0.00596	-0.00616	-0.00663	-0.00704	-0.00804	-0.00952	-0.0I064	-0.0I3I3	-0.0I658	-0.0I9I3	-0.02463	-0.03I76
I.766I9	-0.00373	-0.00386	-0.00417	-0.00445	-0.00513	-0.00613	-0.0069I	-0.00869	-0.0II25	-0.0I3I5	-0.0I745	-0.02334
I.8338I	-0.00277	-0.00287	-0.00311	-0.00331	-0.00383	-0.00460	-0.00520	-0.00660	-0.00862	-0.0I0I9	-0.0I37I	-0.0I868
I.95000	-0.00160	-0.00166	-0.00180	-0.00192	-0.00223	-0.00269	-0.00306	-0.00393	-0.00519	-0.00618	-0.00852	-0.0II96
2.066I9	-0.000?0	-0.00093	-0.00101	-0.00108	-0.00126	-0.00152	-0.00173	-0.00223	-0.00297	-0.00357	-0.00457	-0.00710
2.I338I	-0.00064	-0.00066	-0.00072	-0.00077	-0.00089	-0.00108	-0.00123	-0.00158	-0.00211	-0.00254	-0.00356	-0.00516
2.25000	-0.00034	-0.00035	-0.00038	-0.00041	-0.00048	-0.00058	-0.00066	-0.00086	-0.00115	-0.00138	-0.00195	-0.00283
2.366I9	-0.00018	-0.00018	-0.00020	-0.00021	-0.00025	-0.00030	-0.00035	-0.00045	-0.00060	-0.00073	-0.00104	-0.00151
2.4338I	-0.00012	-0.00012	-0.00013	-0.00014	-0.00017	-0.00020	-0.00023	-0.00030	-0.00041	-0.00049	-0.00070	-0.00103
2.55000	-0.00006	-0.00006	-0.00006	-0.00007	-0.00008	-0.00010	-0.00011	-0.00015	-0.00020	-0.00024	-0.00035	-0.00052
2.66I9	-0.00003	-0.00003	-0.00003	-0.00003	-0.00004	-0.00004	-0.00005	-0.00007	-0.00009	-0.00011	-0.00016	-0.00025
2.7338I	-0.00002	-0.00002	-0.00002	-0.00002	-0.00002	-0.00003	-0.00003	-0.00004	-0.00006	-0.00007	-0.00010	-0.00016
2.85000	-0.00001	-0.00001	-0.00001	-0.00001	-0.00001	-0.00001	-0.00001	-0.00002	-0.00003	-0.00003	-0.00005	-0.00007
2.966I9	0.00000	0.00000	0.00000	0.00000	0.00000	0.00000	0.00000	-0.00001	-0.00001	-0.00001	-0.00002	-0.00004

X \ X_o	I.2338I	I.35000	I.466I9	I.5338I	I.65000	I.766I9	I.8338I	I.95000	2.066I9	2.I338I	2.25000	2.366I9
0.0338I	0.00000	0.00000	0.00000	0.00000	0.00000	0.00000	0.00000	0.00000	0.00000	0.00000	0.00000	0.00000
0.15000	-0.00013	-0.00012	-0.00010	-0.00009	-0.00007	-0.00005	-0.00004	-0.00003	-0.00002	-0.00002	-0.00001	-0.00001
0.266I9	-0.00074	-0.00066	-0.00056	-0.00050	-0.00039	-0.00030	-0.00026	-0.00019	-0.00014	-0.00009	-0.00007	-0.00007
0.3338I	-0.00147	-0.00131	-0.00112	-0.00100	-0.00079	-0.00061	-0.00052	-0.00039	-0.00029	-0.00025	-0.00019	-0.00014
0.45000	-0.00359	-0.00325	-0.00281	-0.00253	-0.00201	-0.00157	-0.00134	-0.00100	-0.00076	-0.00065	-0.00049	-0.00038
0.5661S	-0.00711	-0.00654	-0.00574	-0.00520	-0.00415	-0.00332	-0.00284	-0.00214	-0.00162	-0.00138	-0.00106	-0.00081
0.6336I	-0.00890	-0.00819	-0.00716	-0.00745	-0.00614	-0.00494	-0.00415	-0.00315	-0.00239	-0.00203	-0.00156	-0.00120
0.75000	-0.0I597	-0.0I5I7	-0.0I377	-0.0I273	-0.0I069	-0.00899	-0.00793	-0.00670	-0.00534	-0.00472	-0.00363	-0.00280
0.866I9	-0.02348	-0.02267	-0.02I32	-0.02001	-0.0I724	-0.0I4I9	-0.0I238	-0.0I062	-0.00878	-0.00784	-0.00634	-0.00478
0.9338I	-0.02825	-0.02759	-0.02655	-0.02518	-0.02207	-0.0I840	-0.0I625	-0.0I372	-0.0II05	-0.00944	-0.00765	-0.00607
I.05000	-0.0364I	-0.03734	-0.03662	-0.03541	-0.03208	-0.02756	-0.02467	-0.0I976	-0.0I549	-0.0I337	-0.0I04I	-0.00813
I.I66I9	-0.04365	-0.04614	-0.04706	-0.04653	-0.04380	-0.03903	-0.03560	-0.02942	-0.02342	-0.02036	-0.0I599	-0.0I257
I.2338I	-0.04669	-0.04984	-0.05266	-0.05287	-0.05097	-0.04651	-0.04299	-0.03610	-0.02927	-0.02556	-0.02020	-0.0I597
I.35000	-0.04835	-0.05531	-0.06019	-0.06192	-0.06264	-0.05984	-0.05672	-0.0495I	-0.04I30	-0.03670	-0.02942	-0.02350
I.466I9	-0.04719	-0.05559	-0.06344	-0.06724	-0.07145	-0.07188	-0.07018	-0.06420	-0.0556I	-0.0502I	-0.04133	-0.03352
I.5338I	-0.04428	-0.05345	-0.06284	-0.06779	-0.07437	-0.07728	-0.07684	-0.0725I	-0.06453	-0.05898	-0.0494I	-0.04048
I.65000	-0.0367I	-0.04650	-0.05746	-0.06396	-0.0743I	-0.08193	-0.08427	-0.08437	-0.0792I	-0.07436	-0.06442	-0.05445
I.766I9	-0.02762	-0.03663	-0.04764	-0.05480	-0.06757	-0.07935	-0.08488	-0.09047	-0.09037	-0.08766	-0.07960	-0.0695I
I.8338I	-0.02240	-0.03047	-0.04082	-0.04782	-0.06098	-0.07935	-0.08148	-0.09050	-0.09394	-0.09306	-0.08732	-0.078I6
I.95000	-0.0I458	-0.02060	-0.02892	-0.03495	-0.04729	-0.07448	-0.07010	-0.08360	-0.09326	-0.09616	-0.09619	-0.0908I
2.066I9	-0.00882	-0.0I282	-0.0I869	-0.02321	-0.03I2	-0.06I50	-0.05429	-0.06958	-0.08363	-0.08995	-0.09682	-0.09736
2.I338I	-0.00638	-0.00945	-0.0I399	-0.0I759	-0.02576	-0.04583	-0.04459	-0.05948	-0.07458	-0.08266	-0.09283	-0.09719
2.25000	-0.00355	-0.00533	-0.008II	-0.0I038	-0.0I574	-0.03686	-0.02948	-0.04I9I	-0.05655	-0.06540	-0.07924	-0.08935
2.366I9	-0.00I9I	-0.00290	-0.00448	-0.00578	-0.00905	-0.02358	-0.0I795	-0.02692	-0.03868	-0.04658	-0.06078	-0.07374
2.4338I	-0.00I3I	-0.00200	-0.00311	-0.00404	-0.00640	-0.0I40I	-0.0I307	-0.02009	-0.02979	-0.03662	-0.04969	-0.06265
2.55000	-0.00066	-0.00I02	-0.00I6I	-0.002I2	-0.00341	-0.0I008	-0.00730	-0.0II59	-0.0I799	-0.0228I	-0.03285	-0.04421
2.666I9	-0.00032	-0.00050	-0.00080	-0.00I06	-0.00I74	-0.00552	-0.00387	-0.00638	-0.0I028	-0.0I339	-0.02030	-0.02882
2.7338I	-0.00020	-0.00032	-0.00052	-0.00069	-0.00II5	-0.00388	-0.00262	-0.00439	-0.00725	-0.00959	-0.0I499	-0.02205
2.85000	-0.00009	-0.000I4	-0.00024	-0.00032	-0.00054	-0.00I93	-0.00I27	-0.0022I	-0.00384	-0.00517	-0.00850	-0.0I329
2.966I9	-0.00004	-0.00006	-0.000I0	-0.000I4	-0.00024	-0.00093	-0.00059	-0.00I05	-0.00I96	-0.00260	-0.00452	-0.00753
3.0338I	-0.00002	-0.00004	-0.00006	-0.00008	-0.000I5	-0.00042	-0.00036	-0.00066	-0.00I3I	-0.00I69	-0.00301	-0.00522
3.I5000	-0.00001	-0.00001	-0.00003	-0.00003	-0.00006	-0.00026	-0.000I5	-0.00028	-0.00053	-0.00076	-0.00I42	-0.00260
3.266I9	0.00000	-0.00001	-0.00001	-0.00001	-0.00002	-0.000II	-0.00006	-0.000I2	-0.00022	-0.00032	-0.00062	-0.00II9
3.3338I	- " -	0.00000	0.00000	0.00000	0.00000	-0.00004	-0.00004	-0.00007	-0.000I3	-0.00019	-0.00038	-0.00073
3.45000	- " -	- " -	- " -	- " -	- " -	-0.00003	-0.00001	-0.00003	-0.00005	-0.00008	-0.00015	-0.00030
3.566I9	- " -	- " -	- " -	- " -	- " -	-0.0000I	0.00000	-0.0000I	-0.00002	-0.00003	-0.00006	-0.000I2
3.6338I	- " -	- " -	- " -	- " -	- " -	0.00000	- " -	0.00000	0.00000	0.00000	-0.00003	-0.00007
							- " -	0.00000	0.00000	0.00000	-0.0000I	-0.00002
							- " -	- " -	- " -	- " -	0.00000	-0.0000I
							- " -	- " -	- " -	- " -	- " -	0.00000

Table 8 (continued)

X \ X_0	2.4338I	2.55000	2.66619	2.[illegible]	2.85000	2.9[illegible]I9	3.0338I	3.I5000	3.266I9	3.3338I	3.45000	3.[illegible]66I[illegible]
0.0338I	0.00000	0.00000	0.00000	0.00000	0.00000	0.00000	0.00000	0.00000	0.00000	0.00000	0.00000	0.00000
0.I5000	-0.00001	-0.00001	-0.00001	0.00001	0.00000	0.00000	0.00000	0.00000	0.00000	0.00000	0.00000	0.00000
0.2[illegible]	-0.00006	-0.00004	-0.00003	-0.00003	-0.00002	-0.00001	-0.00001	-0.00001	-0.00001	0.00000	0.00000	0.00000
0.3338I	-0.00012	-0.00009	-0.00007	-0.00005	-0.00004	-0.00003	-0.00002	-0.00002	-0.00001	-0.00001	-0.00001	0.00000
0.45000	-0.00032	-0.00024	-0.0001	-0.00014	-0.00010	-0.00007	-0.00006	-0.00004	-0.00003	-0.00002	0.00002	-0.00001
0.[illegible]	-0.00055	-0.00051	-0.00038	-0.00031	-0.00023	-0.0006	0.00013	-0.00009	-0.00006	-0.00005	0.00004	-0.00002
0.6138I	-0.00102	-0.00076	-0.00056	-0.0004	-0.00034	-0.00024	0.00010	-0.00014	-0.00010	-0.00008	-0.00005	-0.00004
0.75000	-0.00188	0.00141	-0.00105	-0.00087	-0.0006[illegible]	-0.00046	-0.00038	-0.00027	-0.00019	-0.00015	-0.00010	-0.00009
0.[illegible]6[illegible]	-0.00321	-0.00246	-0.00183	-0.00154	-0.00112	-0.0008I	-0.00067	-0.00048	-0.00034	-0.00027	-0.00019	-0.00013
0.9338I	-0.00436	-0.00332	-0.00249	-0.00209	-0.00153	-0.00111	-0.00092	-0.00066	-0.00047	-0.00038	0.00026	-0.00018
0.95000	-0.00702	-0.00540	-0.00409	-0.00345	-0.00255	-0.00187	-0.00177	-0.00112	-0.00079	-0.00065	0.00045	-0.00031
1.[illegible]66[illegible]	-0.01042	-0.00850	-0.00650	-0.00[illegible]	-0.00412	-0.00300	-0.00253	-0.00184	-0.00132	-0.00108	-0.00076	-0.00053
1.2338I	-0.01392	-0.01090	-0.00840	-0.00716	-0.00538	-0.00398	-0.00333	-0.00243	-0.00175	-0.00144	-0.00102	-0.00071
1.35000	-0.02061	-0.01636	-0.01278	-0.01088	-0.00834	-0.00624	-0.00525	-0.00386	-0.00281	-0.00232	-0.00165	-0.00117
1.466I9	-0.02959	-0.02382	-0.01853	-0.01647	-0.01265	-0.00958	-0.00810	-0.00602	-0.00442	-0.00367	-0.00264	-0.00188
1.5338I	-0.03567	-0.02824	-0.02348	-0.02048	-0.01593	-0.01217	-0.01033	-0.00773	-0.00571	-0.00476	-0.00345	-0.00247
1.65000	-0.04857	-0.04049	-0.03316	-0.02927	-0.02321	-0.01802	-0.01542	-0.01168	-0.00873	-0.00733	-0.00537	-0.00385
1.766I9	-0.06157	-0.05400	-0.04527	-0.04053	-0.03265	-0.02604	-0.02252	-0.01730	-0.01311	-0.01106	-0.00822	-0.00601
1.8338I	-0.07737	-0.06768	-0.05833	-0.04816	-0.03955	-0.03186	-0.02774	-0.02153	-0.01645	-0.01398	-0.01044	-0.00770
1.95000	-0.08614	-0.07714	-0.06809	-0.06256	-0.05123	-0.04305	-0.03879	-0.03075	-0.02388	-0.02048	-0.01553	-0.01161
2.066I9	-0.09533	-0.08930	-0.08182	-0.07710	-0.06907	-0.06154	-0.05758	-0.04287	-0.03386	-0.02933	-0.02264	-0.01719
2.1338I	-0.09714	-0.09389	-0.08836	-0.08461	-0.07695	-0.06747	-0.06144	-0.05087	-0.04096	-0.03513	-0.02788	-0.02138
2.25000	-0.09486	-0.09525	-0.09440	-0.09314	-0.08918	-0.08271	-0.07733	-0.06666	-0.05534	-0.04902	-0.03906	-0.03057
2.366I9	-0.07965	-0.08720	-0.09118	-0.09323	-0.09490	-0.09376	-0.09114	-0.08306	-0.07187	-0.06489	-0.05315	-0.04254
2.4338I	-0.06955	-0.07880	-0.08537	-0.08749	-0.09365	-0.09663	-0.09636	-0.09172	-0.08182	-0.07490	-0.06259	-0.05085
2.55000	-0.05079	-0.06082	-0.06905	-0.07357	-0.08234	-0.09216	-0.09702	-0.10082	-0.09722	-0.09186	-0.08011	-0.06765
2.666I9	-0.03431	-0.04305	-0.05030	-0.05401	-0.06227	-0.07474	-0.08371	-0.09794	-0.10476	-0.10453	-0.09719	-0.08517
2.7338I	-0.02631	-0.03432	-0.04041	-0.04344	-0.04933	-0.06024	-0.06978	-0.08873	-0.10338	-0.10727	-0.10523	-0.[illegible]
2.85000	-0.01666	-0.02275	-0.02959	-0.02922	-0.03056	-0.03451	-0.04079	-0.06047	-0.08596	-0.09873	-0.10[illegible]	-0.[illegible]
2.966I9	-0.00987	-0.01460	-0.01900	-0.02046	-0.01980	-0.01649	-0.01615	-0.02528	-0.05033	-0.06534	-0.09873	-0.11408
3.0338I	-0.00702	-0.01096	-0.01517	-0.01690	-0.01668	-0.01152	-0.00786	-0.00801	-0.02552	-0.04412	-0.08077	-0.10775
3.I5000	-0.00365	-0.00622	-0.00969	-0.01173	-0.01350	-0.00984	-0.00937	+0.00755	+0.01026	+0.00148	-0.03304	-0.[illegible]
3.266I9	-0.00172	-0.00317	-0.00548	-0.00723	-0.01015	-0.01036	-0.00737	+0.00543	+0.02351	+0.02986	+0.01948	-0.[illegible]
3.3338I	-0.00107	-0.00204	-0.00372	-0.00510	-0.00793	-0.00971	-0.00867	+0.00053	+0.02032	+0.02855	+0.02089	+0.01411
3.45000	-0.00045	-0.00090	-0.00174	-0.00252	-0.00449	-0.00697	-0.00799	-0.00599	+0.00668	+0.02060	+0.04532	+0.[illegible]
3.566I9	-0.00018	-0.00037	-0.00075	-0.00112	-0.00218	-0.00394	-0.00522	-0.00683	-0.00760	+0.00065	+0.02976	+0.[illegible]
3.6338I	-0.00010	-0.00021	-0.00044	-0.00067	-0.00135	-0.00260	-0.00364	-0.00564	-0.00567	-0.00234	+0.01551	+0.05175
3.75000	-0.00004	-0.00008	-0.00017	-0.00027	-0.00056	-0.00115	-0.00171	-0.00317	-0.00491	-0.00524	-0.00040	+0.02055
3.866I9	-0.00001	-0.00003	-0.00006	-0.00010	-0.00022	-0.00047	-0.00072	-0.00146	-0.00275	-0.00368	-0.00438	+0.00127
3.9338I	0.00000	-0.00002	-0.00003	-0.00005	-0.00012	-0.00027	-0.00042	-0.00088	-0.00177	-0.00253	-0.00390	-0.00278
4.05000	- " -	-0.00001	-0.00001	-0.00002	-0.00004	-0.00010	-0.00016	-0.00035	-0.00075	-0.00114	-0.00218	-0.00334
4.I66I9	- " -	0.00000	0.00000	-0.00001	-0.00001	-0.00003	-0.00005	-0.00013	-0.00029	-0.00045	-0.00097	-0.00187
4.2338I	0.00000	0.00000	0.00000	0.00000	-0.00001	-0.00002	-0.00003	-0.00007	-0.00016	-0.00026	-0.00057	-0.00118
4.35000	- " -	- " -	- " -	- " -	0.00000	-0.00001	0.00001	-0.00002	-0.00005	-0.00009	-0.00021	-0.00048
4.466I9	- " -	- " -	- " -	- " -	- " -	0.00000	0.00000	-0.00001	-0.00001	-0.00003	-0.00007	-0.00017

X \ X_0	3.0338I	3.75000	3.866I9	3.9338I	4.0500[illegible]	4.I66I	4.2338[illegible]	[illegible]	4.466I9	4.[illegible]	[illegible]	[illegible].76619
0.6338I	-0.00003	-0.00002	-0.00001	0.00000	0.00000	0.00000	0.00000	[illegible]	0.00000	0.00000	0.00000	0.00000
0.75000	-0.00007	-0.00004	-0.00002	0.00000	0.00000	0.00000	0.00000	[illegible]	0.00000	0.00000	0.00000	0.00000
0.866I9	-0.00010	-0.00008	-0.00004	0.00000	0.00000	0.00000	0.00000	-0.00001	0.00001	[illegible]	0.00000	0.00000
0.9338I	-0.00015	-0.00011	-0.00007	-0.00004	-0.00001	0.00000	0.00000	[illegible]	0.00000	+0.00048	-0.00001	0.00000
I.05000	-0.00025	-0.00017	-0.00013	-0.00009	-0.00002	0.00000	0.00000	+0.00026	0.00000	0.00060	+0.00094	0.[illegible]
I.I66I9	0.00043	-0.00029	-0.00023	-0.00017	-0.00008	0.00000	0.00000	+0.00027	0.00000	+0.00069	+0.00111	+0.001[illegible]
I.2338I	-0.00058	-0.00040	-0.00027	-0.00024	-0.00013	0.00000	0.00000	+0.00027	0.00000	+0.00072	+0.00120	+0.[illegible]
I.35000	-0.00095	-0.00066	-0.00045	-0.00036	-0.00026	-0.00010	0.00000	+0.[illegible]	0.00000	+0.00074	+0.00129	+0.00209
I.466I9	-0.00153	-0.00107	-0.00074	-0.00059	-0.00041	-0.00026	-0.00013	+0.00012	0.00000	+0.00070	+0.00130	+0.00220
I.5338I	-0.00242	-0.00142	-0.00099	-0.00079	-0.00055	-0.00039	-0.00024	+0.00003	-0.00010	+0.00063	+0.00127	+0.00221
I.65000	-0.00360	-0.00227	-0.00159	-0.00129	-0.00089	-0.00060	-0.00051	-0.00020	-0.00017	-0.00013	+0.00112	+0.00212
I.766I9	-0.00498	-0.00357	-0.00253	-0.00206	-0.00144	-0.00098	-0.00079	-0.00051	-0.00032	-0.00023	-0.00019	+0.00188
I.8338I	-0.00641	-0.00463	-0.00330	-0.00269	-0.00189	-0.00130	-0.00104	-0.00069	-0.00044	-0.00033	-0.00026	+0.00167
I.95000	-0.00974	-0.00712	-0.00514	-0.00407	-0.00302	-0.00208	-0.00168	-0.00113	-0.00075	-0.00058	-0.00042	-0.00028
2.066I9	-0.01454	-0.01078	-0.00788	-0.00653	-0.00453	-0.00340	-0.00300	-0.00186	-0.00124	-0.00098	-0.00069	-0.00046
2.1338I	-0.01819	-0.01361	-0.01003	-0.00835	-0.00603	-0.00424	-0.00366	-0.00311	-0.00165	-0.00131	-0.00092	-0.00062
2.25000	-0.02627	-0.01999	-0.01496	-0.01257	-0.00919	-0.00663	-0.00532	-0.00414	-0.00368	-0.00214	-0.00149	-0.00101
2.366I9	-0.03703	-0.02872	-0.02189	-0.01854	-0.01378	-0.01010	-0.00836	-0.00589	-0.00470	-0.00441	-0.00239	-0.00164
2.4338I	-0.04462	-0.03505	-0.02703	-0.02304	-0.01730	-0.01279	-0.01065	-0.00769	-0.00564	-0.00508	-0.00313	-0.00216
2.55000	-0.05995	-0.04830	-0.03805	-0.03284	-0.02510	-0.01889	-0.01587	-0.01165	-0.00811	-0.00692	-0.00491	-0.00344
2.666I9	-0.07757	-0.06439	-0.05211	-0.04554	-0.03561	-0.02730	-0.02320	-0.01732	-0.01272	-0.01056	-0.00759	-0.00538
2.7338I	-0.08825	-0.07479	-0.06158	-0.05434	-0.04307	-0.03343	-0.02863	-0.02160	-0.01603	-0.01337	-0.00970	-0.00693
2.85000	-0.10519	-0.09332	-0.07960	-0.07157	-0.05830	-0.04641	-0.04021	-0.03100	-0.02342	-0.01980	-0.01458	-0.01057
2.966I9	-0.11583	-0.10994	-0.09839	-0.09038	-0.07621	-0.06236	-0.05491	-0.04331	-0.03347	-0.02857	-0.02143	-0.01584
3.0338I	-0.11569	-0.11671	-0.10833	-0.10129	-0.08733	-0.07290	-0.06481	-0.05190	-0.04144	-0.03496	-0.02655	-0.01985
3.15000	-0.09791	-0.11798	-0.12047	-0.11696	-0.10607	-0.09222	-0.08360	-0.06904	-0.05555	-0.04845	-0.03762	-0.02867
3.266I9	-0.05201	-0.09670	-0.11974	-0.12383	-0.12101	-0.11074	-0.10308	-0.08831	-0.07335	-0.06492	-0.05178	-0.04042
3.3338I	-0.01464	-0.07019	-0.10898	-0.12052	-0.12562	-0.11979	-0.11342	-0.09980	-0.08461	-0.07584	-0.06148	-0.04870
3.45000	+0.04892	-0.00273	-0.06537	-0.09366	-0.12113	-0.12834	-0.12677	-0.11792	-0.10450	-0.09571	-0.08019	-0.06540
3.566I9	+0.07959	+0.06784	+0.00930	-0.03262	-0.09096	-0.12124	-0.12857	-0.12999	-0.12219	-0.11504	-0.10040	-0.08464
3.6338I	+0.07515	+0.09294	+0.05721	+0.01633	-0.05695	-0.10581	-0.12102	-0.13174	-0.12962	-0.12458	-0.11185	-0.09657
3.75000	+0.04331	+0.09128	+0.11312	+0.09779	+0.02840	-0.05103	-0.08542	-0.12014	-0.13331	-0.13434	-0.12848	-0.11628
3.866I9	+0.01206	+0.05117	+0.10563	+0.12950	+0.11645	+0.04044	-0.01157	-0.08110	-0.11869	-0.12990	-0.13658	-0.13213
3.9338I	+0.00214	+0.02750	+0.08050	+0.11587	+0.14472	+0.09906	+0.04741	-0.04077	-0.09816	-0.11760	-0.13479	-0.13734
4.05000	-0.00322	+0.00345	+0.03124	+0.06246	+0.13076	+0.16417	+0.14520	+0.05929	-0.03374	-0.07308	-0.11527	-0.13514
4.I66I9	-0.00251	-0.00259	+0.00455	+0.01792	+0.06880	+0.14487	+0.17638	+0.16282	+0.07102	+0.01099	-0.06730	-0.11240
4.2338I	-0.00171	-0.00258	-0.00077	+0.00510	+0.03618	+0.10489	+0.15280	+0.19387	+0.13879	+0.07777	-0.02179	-0.08658
4.35000	-0.00074	-0.00145	-0.00216	-0.00175	+0.00591	+0.03874	+0.07756	+0.16599	+0.21185	+0.18992	+0.08924	-0.01376
4.466I9	-0.00028	-0.00063	-0.00123	-0.00164	-0.00131	+0.00657	+0.02158	+0.08232	+0.17847	+0.21985	+0.20561	+0.10050
4.5338I	-0.00016	-0.00036	-0.00077	-0.00112	-0.00161	+0.00058	+0.00688	+0.04201	+0.12514	+0.18539	+0.23888	+0.17545
4.65000	-0.00005	-0.00013	-0.00030	-0.00048	-0.00094	-0.00131	-0.00072	+0.00733	+0.04944	+0.08866	+0.19671	+0.25499
							-0.00103	-0.00041	+0.00766	+0.02348	+0.09195	+0.20729

Table 9 Table of the function $f_1(x,x_0)$ for beryllium, T = 300°K.

x \ x_0	0.0338I	0.15000	0.2661I	0.3338I	0.45000	0.5661I	0.6338I	0.75000
0.0	0.00000000	0.00000000	0.00000000	0.00000000	0.00000000	0.00000000	0.00000000	0.00000000
0.3	0.00002598	0.00I98035	0.006266I3	-0.00008280	-0.00008422	-0.0000867[illegible]	-0.00008872	-0.00009052
0.6	-0.00I0II25	0.00093218	0.00520563	0.0086I910	0.0I669719	0.0[illegible]6287	-0.00I28716	-0.00I33331
0.9	-0.00429352	-0.00239475	0.00177655	0.005I0818	0.0I300295	0.0[illegible]4423I	0.02862803	0.04026912
I.2	-0.00825692	-0.00745284	-0.0034979I	-0.00035028	0.00712670	0.0I60I558	0.02I82327	0.03271781
I.5	-0.0I332235	-0.0II62309	-0.00791004	-0.00497317	0.00200646	0.0I020552	0.0I55III6	0.02535000
I.8	-0.0I5I6609	-0.0I352646	-0.00995490	-0.007I4480	-0.00046527	0.00729577	0.0I226585	0.02I36054
2.I	-0.0I568513	-0.0I406434	-0.0I063791	-0.00776505	-0.00II8[illegible]	0.00642661	0.0II27972	0.02010112
2.4	-0.0I579044	-0.0I4I8I84	-0.0I066539	-0.00790152	-0.00I3[illegible]	0.00623398	0.0II06020	0.0I981755
2.7	-0.0I56I759	-0.0I420I76	-0.0I068708	-0.00792480	-0.00I372I7	0.00620055	0.0II02I83	0.0[illegible]76736
3.0	-0.0I58I998	-0.0I4[illegible]0425	-0.0I068980	-0.00792773	-0.00I37562	0.00619628	0.0II0I609	0.0I976081
3.3	- " -	- " -	- " -	- " -	- " -	- " -	- " -	- " -
3.6	- " -	- " -	- " -	- " -	- " -	- " -	- " -	- " -

x \ x_0	0.8661I9	0.9338I	I.05000	I.1661I9	I.2338I	I.35000	I.4661I9	I.5338I
0.0	0.00000000	0.00000000	0.00000000	0.00000000	0.00000000	0.00000000	0.00000000	0.00000000
0.3	-0.00000[illegible]	-0.00009093	-0.00008865	-0.00008375	-0.00007969	-0.00007073	-0.000[illegible]600I	-0.00005343
0.6	-0.00I36[illegible]	-0.00I37567	-0.00I3678I	-0.00I32I35	-0.00I27385	-0.00I[illegible]50I	-0.00I00607	-0.00060787
0.9	0.05285363	0.006I0488	-0.00626740	-0.00627306	-0.006I8493	-0.005[illegible]526I	-0.0052989I	-0.00[illegible]343
I.2	0.04446I82	0.05163579	0.0641I988	0.07686638	-0.0I70320I	-0.0I700936	-0.0I63I63I	-0.0[illegible]559073
I.5	0.03577I94	0.04205497	0.0528I76I	0.06365659	0.06986284	0.0[illegible]059572	0.0[illegible]5[illegible]95	-0.0[illegible]3856I7
I.8	0.03075860	0.03629255	0.04544374	0.05420736	0.05897662	0.06688945	0.07467044	0.07927955
2.I	0.02910II4	0.03432I24	0.04275I39	0.05046474	0.0544[illegible]I73	0.06053515	[illegible].06[illegible]5[illegible]I9	0.06870II8
2.4	0.02872I67	0.03386444	0.0421080[illegible]	0.04953446	0.05326667	0.05879535	0.0[illegible]32341I	0.06536978
2.7	0.02865344	0.03378I50	0.04I98900	0.04935838	0.05304280	0.058450FI	0.06269338	0.06466202
3.0	0.02864437	0.03377036	0.04I97265	0.04933357	0.0530I070	0.05839975	0.06261007	0.06455021
3.3	- " -	0.03376923	0.04I97083	0.04933097	0.05300730	0.0583[illegible]420	0.06260074	0.06453744
3.6	- " -	- " -	- " -	- " -	- " -	- " -	- " -	- " -
3.9	- " -	- " -	- " -	- " -	- " -	- " -	- " -	- " -

x \ x_0	I.65000	I.766I9	I.8338I	I.95000	2.066I9	2.I338I	2.25000	2.366I9
0.0	0.00000000	0.00000000	0.00000000	0.00000000	0.00000000	0.00000000	0.00000000	0.00000000
0.3	-0.000042II	-0.000032I[illegible]	-0.00002724	-0.00002036	-0.0000I536	-0.0000I3I0	-0.00000999	-0.00000756
0.6	-0.00073246	-0.000568I0	-0.00048424	-0.0003650I	-0.00027600	-0.00023578	-0.000I8046	-0.000I3730
0.9	-0.00[illegible]06I4	-0.00029795	-0.00285262	-0.00[illegible]90I2	-0.00I66950	-0.00I4[illegible]924	-0.00I09966	-0.00084563
I.2	-0.0I387I98	-0.0II75755	-0.0I046279	-0.00833959	-0.00650568	-0.0056II95	-0.004364I6	-0.00339879
I.5	-0.03242842	-0.02960I52	-0.02745550	-0.02329996	-0.0I908536	-0.0I68I987	-0.0I34I429	-0.0I065626
I.8	0.0876I909	0.0967I566	-0.052I[illegible]866	-0.04[illegible]3096	-0.04255546	-0.03855427	-0.03275490	-0.02702[illegible]3I
2.I	0.07347093	0.07[illegible]49078	0.08I77[illegible]8I	0.08[illegible]2823I	0.0959I438	-0.057026I7	-0.0609[illegible]528	-0.05[illegible]8I858
2.4	0.0684706I	0.07II0848	0.0726[illegible].52	0.07549400	0.07893558	0.08I3[illegible]032	0.086I8I06	0.09I[illegible]340
2.7	0.[illegible]733729	0.06829308	0.07024[illegible]75	[illegible].07174267	0.07319768	0.074III76	0.07596871	0.07832591
3.0	0.[illegible] I4934	[illegible].06897338	0.0698II[illegible]I	0.07095I9	0.07I9I749	0.07240700	0.0732I002	0.07408787
3.3	0.0671270[illegible]	0.06893355	[illegible].[illegible]5469	0.0703[illegible]255	0.07I7I905	0.07[illegible]3774	0.0727I795	0.07320742
3.6	- " -	0.06892992	[illegible].0[illegible]574976	[illegible].[illegible]708825[illegible]	0.07169974	0.07[illegible]0822	0.07266I78	0.07309654
3.9	- " -	- " -	- " -	- " -	- " -	- " -	0.07[illegible]65725	0.07[illegible]0[illegible]707
4.2	- " -	- " -	- " -	- " -	- " -	- " -	- " -	- " -

Table 9 (continued)

Y \ λ_0	2.4939I	[illegible]000	2.6661[illegible]	2.7338I	2.85000	2.9661[illegible]	3.0338[illegible]	3.[illegible]
0.0	0.00000000	0.00000000	0.00000000	0.00000000	0.00000000	0.00000000	0.00000000	0.00000000
0.3	-0.00000838	-0.00000471	-0.00000343	-0.00000284	-0.00000204	-0.00000145	-0.00000[illegible]	-0.00000083
0.6	-0.00011638	-0.00006651	-0.00006334	-0.00005257	-0.00003787	-0.00002707	-[illegible].00002[illegible]5	-0.00001557
0.9	-0.00072179	-0.00054[illegible]	-0.00040247	-0.00033557	-0.00024433	-0.00017612	-0.00011448	-0.00010271
1.2	-0.00293108	-0.00224796	-0.00169620	-0.00[illegible]	-0.00105569	-0.00077083	-0.00056[illegible]5	-0.00045942
1.5	-0.00910498	-0.00732274	-0.00566784	-0.00[illegible]05	-0.00366894	-0.00273744	-0.00[illegible]113	-0.00167794
1.8	-0.02[illegible]852	-0.01965879	-0.01582864	-0.01384492	-0.01082795	-0.00831968	-0.00711440	-0.00[illegible]053
2.1	-0.04959[illegible]	-0.04260945	-0.036[illegible]	-0.03[illegible]475	-0.02697750	-0.02[illegible]374	-0.01[illegible]	-0.014[illegible]
2.4	-0.07670361	-0.07039948	-0.06371[illegible]	-0.05986674	-0.05318838	-0.04642735	-0.04[illegible]	-0.[illegible]
2.7	0.07992382	0.08299207	0.08605007	-0.08[illegible]6825	-0.07[illegible]3	-0.07[illegible]10	-[illegible].07[illegible]446	-0.0647[illegible]570
3.0	0.07468492	0.07588131	0.07742065	0.07840239	0.07951463	0.07[illegible]50	-0.08296442	-0.0[illegible]886
3.3	0.07347051	0.07387452	0.07440[illegible]	[illegible].07482794	0.07547504	0.07[illegible]42I	0.07638780	0.07645[illegible]54
3.6	0.07330610	0.07355448	0.07[illegible]	[illegible].07357289	0.07403759	0.07[illegible]54	0.07416[illegible]7	0.07[illegible]608
3.9	0.07329150	0.07352368	[illegible].07373[illegible]	0.07387121	0.07383262	0.07[illegible]102	0.07357[illegible]5	0.07[illegible]114
4.2	- " -	0.07352160	0.07373[illegible]	[illegible].07386571	0.07381573	0.07367[illegible]	0.07351[illegible]1	0.07[illegible]091
4.5	- " -	- " -	- " -	- " -	0.[illegible]477	[illegible].07367091	[illegible].07350[illegible]5	0.07398168

X \ λ_0	3.2661[illegible]	3.3338I	3.4[illegible]00	3.5661[illegible]	[illegible].6338I	3.75[illegible]00	3.8661[illegible]	3.9338I
0.0	0.00000000	0.00000[illegible]	[illegible].00000000	0.00000000	[illegible].00000000	0.00000[illegible]00	0.00000000	[illegible].00000000
0.3	-0.00000058	0.00000000	[illegible].00000000	[illegible].00000000	[illegible].00000000	0.00000000	[illegible].00000000	[illegible].00000000
0.6	-0.00001081	-0.00000[illegible]4	-0.00000565	-0.[illegible]00[illegible]84	0.00000000	[illegible].00000000	.00000000	0.00000000
0.9	-0.00007201	-0.00005[illegible]I	-0.00003992	-[illegible].00002[illegible]78	-[illegible].00001915	-0.00001[illegible]75	-0.00000662	0.00000000
1.2	-0.00002655	-0.00018[illegible]00	-0.00018596	-0.00[illegible].[illegible]95	-0.[illegible]I[illegible]8	-[illegible].60000[illegible]5	-0.00004796	-0.00[illegible]34
1.5	-0.00121476	-[illegible].00100[illegible]3	-0.00071172	-0.00056[illegible]92	-[illegible].00040236	-0.00[illegible]5[illegible]16	-0.00019219	-0.00[illegible]4662
1.8	-0.00394678	-[illegible].00[illegible]5838	-0.0023095[illegible]	-[illegible].00176565	-0.00141346	-0.00099[illegible]54	-0.00065737	-0.[illegible]5614
2.1	-0.01132377	-[illegible].00[illegible]3828	-0.00724706	-[illegible].00534769	-[illegible].00445723	-0.00321[illegible]I	-0.00231422	-0.00[illegible]716
2.4	-0.02810581	-0.02455886	-0.01910[illegible]	-[illegible].01475000	-0.01[illegible]5[illegible]053	-0.00[illegible]2486	-0.00656[illegible]6	-0.00578[illegible]6
2.7	-0.05661714	-[illegible].05175660	-0.04[illegible]5[illegible]3	-0.03[illegible]5538	-0.03073563	-0.02[illegible]5120	-0.01863707	-0.01[illegible]13
3.0	-0.08064[illegible]0	-0.07964077	-0.[illegible]6[illegible]3	-0.[illegible]719III	-0.06[illegible]76741	-0.05[illegible]8[illegible]80	-0.04258[illegible]0	-0.0374756[illegible]
3.3	[illegible].07332[illegible]7	-0.08063[illegible]4	-0.0[illegible]46[illegible]61	-0.[illegible]2[illegible]42[illegible]6	-0.08879680	-0.06[illegible]5504I	-[illegible].07764920	-0.07[illegible]3423
3.6	0.07564[illegible]4	0.07567178	[illegible].07[illegible]4[illegible]58	0.[illegible]791[illegible]70	-0.[illegible]686I42	-0.08606373	-[illegible].06467[illegible]9	-0.0570[illegible]63
3.9	0.07431[illegible]5	0.07447[illegible]0	0.0748[illegible]546	0.[illegible]07569	0.07479[illegible]4	0.07224904	[illegible].06339[illegible]0	-0.07[illegible]842
4.2	0.07474[illegible]3	0.07[illegible]I[illegible]3	0.07[illegible]I[illegible]6	[illegible].07[illegible]4[illegible]4	0.07433858	0.07478364	[illegible].07[illegible]464465	0.07[illegible]3[illegible]4
4.5	0.[illegible]7[illegible]0[illegible]	0.07[illegible]0[illegible]54	[illegible].07[illegible]48I[illegible]	0.07406633	0.07407376	[illegible].07[illegible]3[illegible]35	0.[illegible]4.8820	0.07[illegible]68I5
4.8	0.07[illegible]9[illegible]	0.07[illegible]03[illegible]4	0.07[illegible]043I0	0.07405376	0.07405257	0.07[illegible]2[illegible]92	[illegible].07407546	0.07[illegible]683
5.I	- " -	- " -	- " -	- " -	- " -	.07[illegible]2[illegible]60	[illegible].07406830	0. 7408442

X \ X_0	4.05000	4.1661[illegible]	4.2338I	4.35000	4.4661[illegible]	4.5338I	4.65000	4.7661[illegible]
0.0	0.00000000	0.00000000	[illegible].00000000	0.00000000	0.00000000	0.00000000	0.00000000	0.00000000
0.3	0.00000000	0.00000000	0.00000000	0.00000000	0.00000000	0.00000000	0.00000000	0.00000000
0.6	0.00000000	0.00000000	0.00000000	0.00000000	0.00000000	0.00000000	0.00000000	0.00000000
0.9	0.00000000	[illegible].00000000	0.00000000	-0.00000136	0.00000000	0.00000[illegible]67	-0.00000090	0.00000000
1.2	-0.00000864	[illegible].00000000	0.00000000	0.00005II2	[illegible].00000000	0.00002II[illegible]	0.00001[illegible]95	[illegible].00014265
1.5	-0.00008803	-0.00003439	-0.00000367	0.00CII6[illegible]2	0.00000000	0.00002[illegible]53	0.00059639	0.00076II6
1.8	-0.00037I82	-0.00022826	-0.00015779	0.00[illegible]3[illegible]06	-[illegible].00[illegible]5700	.00044428	0.00083612	0.00[illegible]845I
2.I	-0.00130916	-0.00089764	-0.00071957	-0.00[illegible]2[illegible]44	-[illegible].00[illegible]5[illegible]59	0.00070065	0.00044867	
2.4	-0.00418473	-0.00297708	-0.00243049	-0.00[illegible]455	-[illegible].[illegible]I[illegible]813	-0.00050[illegible]60	0.00042636	0.00012506
2.7	-0.01193953	-0.00883566	-0.00736756	-0.00[illegible]2[illegible]56	-0.00[illegible]2[illegible]883	-0.00[illegible]2[illegible]054	0.00003910	
3.0	-0.02965227	-0.02300670	-0.01968988	-0.01479472	-[illegible].00[illegible]I7639	-[illegible].00[illegible]63[illegible]	-0.00565797	-0.00326629
3.3	-0.06II5674	-0.05060580	-0.04482804	-0.03568[illegible]5	-[illegible].02[illegible]4855	-0.02[illegible]64655	-0.01740237	-0.[illegible]I397
3.6	-0.09535486	0.08780039	-0.08189623	-0.07055561	-0.05931570	-0.05[illegible]I43[illegible]	-0.04158474	-0.03154[illegible]2
3.9	-0.08660976	0.I0005573	-0.I0[illegible]3475	-0.I0[illegible]II7[illegible]	-0.07778319	-0.05I43I80	-0.07941821	-0.06[illegible]64
4.2	0.07068672	0.05986196	-0.06632626	-0.08[illegible]360[illegible]	-[illegible].06543[illegible]4	-0.II005984	-0.II[illegible]908	-0.I05[illegible]046
4.5	0.07438II2	0.07431526	0.07376919	0.06987954	0.0[illegible]4[illegible]I[illegible]	-0.05993389	-0.0[illegible]4[illegible]64	-0.I0601532
4.8	0.07408780	0.07412226	0.07416I82	0.07432[illegible]0I	0.07[illegible]4[illegible]36	0.07348008	0.07[illegible]343	[illegible].05705986
5.I	0.07405703	0.07405144	0.07405361	0.07414649	0.07393503	0.07457851	0.07[illegible]5[illegible]42I	[illegible].07[illegible]0[illegible]06
5.4	- " -	0.07404741	0.07404643	0.07412777	0.07389I41	0.0745II97	0.07[illegible]55/5	. 50[illegible]7
5.7	- " -	- " -	- " -	- " -	- " -	- " -	0.07494478	[illegible].[illegible]67I0I

Table 10 Table of the function $g_{ois}(x_o \rightarrow x)$ for graphite, T = 300°K.

x \ x_o	0.0338I	0.I5000	0.2669I	0.3338I	0.45000	0.5669I	0.6338I	0.75000	0.8669I	0.9338I	I.05000	I.I669I
0.0338I	0.0000I	0.0000I	0.00002	0.00002	0.00003	0.00004	0.00004	0.00004	0.00004	0.00004	0.00004	0.00004
0.I5000	0.00099	0.00044	0.00050	0.00056	0.00066	0.00074	0.00078	0.00083	0.00085	0.00085	0.00084	0.00080
0.2669I	0.00878	0.00266	0.00245	0.00245	0.00256	0.00270	0.00282	0.00290	0.00292	0.00290	0.0028I	0.00267
0.3338I	0.02038	0.00564	0.00464	0.00480	0.00476	0.00485	0.00487	0.00493	0.00490	0.00483	0.00466	0.00440
0.45000	0.05784	0.0I487	0.0I083	0.0I065	0.0II6I	0.0II06	0.0I085	0.0I059	0.0I023	0.00999	0.00947	0.00883
0.5669I	0.II996	0.02954	0.02023	0.0I92I	0.0I957	0.02259	0.02I72	0.02037	0.0I923	0.0I842	0.0I7I9	0.0I583
0.6338I	0.I6545	0.04050	0.02732	0.0249I	0.02484	0.028I0	0.03I3I	0.02890	0.02685	0.02564	0.02361	0.02I55
0.75000	0.25I0I	0.06043	0.03965	0.03564	0.03420	0.03717	0.04078	0.05066	0.04593	0.04317	0.03919	0.03530
0.8669I	0.32I5	0.07939	0.05093	0.045I7	0.04217	0.04480	0.04837	0.05864	0.0760I	0.07III	0.06332	0.05605
0.9338I	0.37038	0.08815	0.0561O	0.04947	0.04569	0.04762	0.05I23	0.06II4	0.07888	0.09344	0.08265	0.07268
I.05000	0.4I2I5	0.09758	0.06I5I	0.05379	0.04889	0.050I7	0.05326	0.06266	0.0793I	0.0933I	0.I2845	0.II026
I.I669I	0.4I9I5	0.09889	0.06I87	0.05379	0.04830	0.04893	0.05I49	0.05977	0.07434	0.08689	0.II677	0.I6956
I.2338I	0.4078I	0.09609	0.05989	0.05I92	0.04636	0.04666	0.0489I	0.0564I	0.06967	0.08I02	0.I0955	0.I5584
I.35000	0.36686	0.08630	0.0535I	0.0462I	0.04093	0.04081	0.04253	0.04856	0.05935	0.06862	0.09I98	0.I299I
I.4669I	0.30855	0.07244	0.04476	0.03854	0.03389	0.03354	0.03478	0.03937	0.0477I	0.05489	0.07297	0.I02I4
I.5338I	0.27069	0.0635I	0.03917	0.03368	0.02956	0.02915	0.030I2	0.03396	0.04097	0.04700	0.06222	0.08673
I.65000	0.20559	0.048I8	0.02965	0.02545	0.02230	0.02I88	0.02254	0.02526	0.03023	0.03455	0.04542	0.0629I
I.766I9	0.I477I	0.03458	0.02I24	0.0I820	0.0I586	0.0I550	0.0I594	0.0I782	0.02I23	0.024I8	0.03I56	0.04347
I.8338I	0.II884	0.02782	0.0I707	0.0I462	0.0I27I	0.0I240	0.0I274	0.0I4I7	0.0I688	0.0I92I	0.02502	0.03430
I.95000	0.07850	0.0I836	0.0II25	0.00962	0.00835	0.008I2	0.00833	0.00922	0.0I093	0.0I24I	0.0I6II	0.02208
2.0669I	0.04929	0.0II53	0.00706	0.00603	0.00522	0.00507	0.00519	0.00574	0.00677	0.00767	0.00993	0.0I353
2.I338I	0.03679	0.00860	0.00526	0.00450	0.00389	0.00377	0.00386	0.00426	0.00502	0.00568	0.00734	0.00998
2.25000	0.02I46	0.0050I	0.00307	0.00262	0.00226	0.00219	0.00224	0.00246	0.00290	0.00327	0.00422	0.00573
2.3669I	0.0II97	0.00280	0.00I7I	0.00I46	0.00I26	0.00I22	0.00I24	0.00I36	0.00I60	0.00I8I	0.00233	0.00315
2.4338I	0.00834	0.00I95	0.00II9	0.00I02	0.00088	0.00085	0.00086	0.00095	0.00III	0.00I26	0.00I62	0.00218
2.55000	0.00434	0.00I0I	0.00062	0.00053	0.00046	0.00044	0.00045	0.00049	0.00058	0.00065	0.00084	0.00II3
2.6669I	0.002I7	0.0005I	0.0003I	0.00026	0.00023	0.00022	0.00022	0.00025	0.00029	0.00032	0.0004I	0.00056
2.7338I	0.00I42	0.00033	0.00020	0.000I7	0.000I5	0.000I4	0.000I5	0.000I6	0.000I9	0.0002I	0.00027	0.00037
2.85000	0.00067	0.000I6	0.000I0	0.00008	0.00007	0.00007	0.00007	0.00008	0.00009	0.000I0	0.000I3	0.000I7
2.9669I	0.00030	0.00007	0.00004	0.00004	0.00003	0.00003	0.00003	0.00003	0.00004	0.00004	0.00006	0.00008
3.0338I	0.000I9	0.00004	0.00003	0.00002	0.00002	0.00002	0.00002	0.00002	0.00002	0.00003	0.00000	0.00005
3.I5000	0.00008	0.00002	0.0000I	0.0000I	0.0000I	0.0000I	0.0000I	0.0000I	0.0000I	0.0000I	- " -	0.00002
3.2669I	0.00003	0.0000I	0.00000	0.00000	0.00000	0.00000	0.00000	0.00000	0.00000	0.00000	- " -	0.0000I
3.3338I	0.00000	0.00000	- " -	- " -	- " -	- " -	0.00000	0.00000	0.00000	0.00000	- " -	0.00000

x \ x_o	I.2338I	I.35000	I.4669I	I.5338I	I.65000	I.7669I	I.8338I	I.95000	2.0669I	2.I338I	2.25000	2.3669I
0.0338I	0.00004	0.00004	0.00003	0.00003	0.00003	0.00002	0.00002	0.00002	0.00002	0.0000I	0.0000I	0.0000I
0.I5000	0.00077	0.00072	0.00065	0.00061	0.00054	0.00047	0.00043	0.00037	0.0003I	0.00028	0.00023	0.00019
0.2669I	0.00257	0.00236	0.002I4	0.00200	0.00I76	0.00I53	0.00I40	0.00II9	0.00I00	0.00090	0.00075	0.00061
0.3338I	0.00422	0.00387	0.00349	0.00326	0.00287	0.00249	0.00228	0.00I93	0.00I63	0.00I46	0.00I2I	0.00099
0.45000	0.00842	0.00766	0.00687	0.0064I	0.00562	0.00485	0.00443	0.00376	0.003I5	0.00283	0.00233	0.00I9I
0.5669I	0.0I500	0.0I352	0.0I203	0.0III8	0.00976	0.00839	0.00765	0.00647	0.0054I	0.00485	0.00400	0.00326
0.6338I	0.02033	0.0I822	0.0I6I4	0.0I495	0.0I30I	0.0III6	0.0I0I6	0.00857	0.007I6	0.00642	0.00528	0.0043I
0.75000	0.03309	0.02935	0.02577	0.02378	0.02057	0.0I760	0.0I594	0.0I340	0.0III7	0.0I000	0.0082I	0.00669
0.8669I	0.052I7	0.0458I	0.03987	0.03663	0.03I43	0.02676	0.02425	0.02028	0.0I684	0.0I506	0.0I233	0.0I003
0.9338I	0.06730	0.05875	0.05089	0.04662	0.03985	0.03382	0.03062	0.02553	0.02II6	0.0I890	0.0I546	0.0I256
I.05000	0.I0275	0.0889I	0.07637	0.06967	0.0595I5	0.04984	0.04503	0.03743	0.03092	0.02757	0.02250	0.0I824
I.I669I	0.I5478	0.I3298	0.II32I	0.I0286	0.08675	0.07269	0.06538	0.05433	0.04462	0.0397I	0.03234	0.02616
I.2338I	0.I9617	0.I6608	0.I4I68	0.I2840	0.I0797	0.09017	0.08097	0.06705	0.05500	0.04890	0.03976	0.032I2
I.35000	0.I6II3	0.24620	0.20608	0.I8674	0.I5636	0.I2988	0.II627	0.09572	0.07849	0.06974	0.0564I	0.04550
I.4669I	0.I2695	0.I9033	0.30II4	0.27I02	0.22474	0.I8602	0.I6608	0.I3613	0.III02	0.09855	0.07960	0.06406
I.5338I	0.10754	0.I6II9	0.2533I	0.33509	0.27750	0.22874	0.20395	0.I6676	0.I3574	0.I2030	0.0973I	0.07802
I.65000	0.07776	0.II607	0.I8063	0.23864	0.39625	0.325I2	0.28908	0.23567	0.I9II2	0.I6889	0.I3626	0.I0916
I.766I9	0.05355	0.0795I	0.I2330	0.I622I	0.268I2	0.46020	0.40937	0.33I6I	0.26823	0.23655	0.I90I0	0.I5245
I.8338I	0.04220	0.06245	0.09660	0.I2692	0.20918	0.3592I	0.49833	0.40405	0.32600	0.28743	0.23062	0.I8465
I.95000	0.02707	0.03983	0.06I33	0.08039	0.I3410	0.2254I	0.3I300	0.56476	0.45385	0.40043	0.32065	0.25589
2.0669I	0.0I657	0.02436	0.03732	0.0488I	0.07992	0.I3602	0.I8840	0.33858	0.63I50	0.54836	0.44408	0.35392
2.I338I	0.0I22I	0.0I795	0.02746	0.03587	0.05856	0.09945	0.I3772	0.24768	0.45465	0.670I4	0.53592	0.42664
2.25000	0.00699	0.0I023	0.0I563	0.02044	0.03328	0.0563I	0.07785	0.I3972	0.25939	0.37755	0.73552	0.58606
2.3669I	0.00384	0.0056I	0.00855	0.0III5	0.0I8I4	0.03072	0.04240	0.07585	0.I4062	0.20445	0.39867	0.79897
2.4338I	0.00266	0.00388	0.00592	0.00770	0.0I252	0.02I2I	0.02925	0.05226	0.09678	0.I4068	0.27409	0.54440
2.55000	0.00I37	0.00200	0.00304	0.00396	0.00643	0.0I085	0.0I497	0.02682	0.04949	0.07I90	0.I4004	0.28I00
2.6669I	0.00068	0.00099	0.00I5I	0.00I96	0.00318	0.00536	0.00739	0.0I32I	0.02448	0.03552	0.06903	0.I3855
2.7338I	0.00045	0.00065	0.00098	0.00I28	0.00207	0.00350	0.00482	0.0086I	0.0I592	0.02318	0.04507	0.09034
2.85000	0.0002I	0.00030	0.00046	0.00060	0.00097	0.00I63	0.00225	0.0040I	0.00742	0.0I078	0.02I00	0.04223
2.9669I	0.00009	0.000I4	0.0002I	0.00027	0.00044	0.00073	0.00I0I	0.00I8I	0.00334	0.00485	0.00946	0.0I902
3.0338I	0.00006	0.00008	0.000I3	0.000I7	0.00027	0.00045	0.00062	0.00II2	0.00207	0.00300	0.00585	0.0II77
3.I5000	0.00002	0.00004	0.00005	0.00007	0.000II	0.000I9	0.00027	0.00048	0.00088	0.00I28	0.00250	0.00503
3.2669I	0.0000I	0.0000I	0.00002	0.00003	0.00005	0.00008	0.000II	0.00020	0.00036	0.00053	0.00I03	0.00207
3.3338I	0.00000	0.00000	0.00000	0.00000	0.00000	0.00000	0.00000	0.00000	0.0002I	0.0003I	0.00060	0.00I22

Table 10 (continued)

X \ X_0	2.4338I	2.55000	2.6661I	2.7338I	2.85000	2.9661I	3.0338I	3.15000	3.2661I	3.3338I	3.45000	3.5661I
0.0338I	0.0000I	0.0000I	0.0000I	0.00000	0.00000	0.00000	0.00000	0.00000	0.00000	0.00000	0.00000	0.00000
0.15000	0.0001I7	0.0001I3	0.0001II	0.00009	0.00007	0.00006	0.00005	0.00004	0.00003	0.00000	0.00000	0.00000
0.2661I9	0.00054	0.00044	0.00033	0.0003I	0.00024	0.00019	0.0001I7	0.0001I3	0.0001I0	0.00000	0.00000	0.00000
0.3338I	0.00088	0.00071	0.00057	0.00050	0.00039	0.0003I	0.00027	0.00021	0.00016	0.00000	0.00000	0.00000
0.45000	0.00169	0.00136	0.00109	0.00096	0.00076	0.00059	0.00052	0.00040	0.0003I	0.00000	0.00000	0.00000
0.5661I9	0.00289	0.00233	0.00186	0.00163	0.00129	0.0010I	0.00088	0.00068	0.00053	0.00000	0.00000	0.00000
0.6338I	0.00362	0.00307	0.00246	0.00215	0.00170	0.00134	0.00116	0.00090	0.00070	0.00060	0.00046	0.00035
0.75000	0.00592	0.00476	0.00380	0.00333	0.00263	0.00207	0.00179	0.00139	0.00108	0.00093	0.00071	0.00054
0.8661I9	0.00886	0.00713	0.00569	0.00497	0.00393	0.00308	0.00267	0.00208	0.00161	0.00138	0.00106	0.00081
0.9338I	0.0II09	0.00891	0.00711	0.00621	0.00491	0.00385	0.00334	0.00260	0.00201	0.00173	0.00133	0.00101
1.05000	0.0I609	0.0I29I	0.0I029	0.00899	0.00710	0.00557	0.00482	0.00375	0.00291	0.00250	0.00192	0.00146
1.1661I9	0.02305	0.0I846	0.0I47I	0.0I284	0.0I0I3	0.00795	0.00689	0.00536	0.00415	0.00357	0.00274	0.00209
1.2338I	0.02830	0.02265	0.0I803	0.0I574	0.0I242	0.00974	0.00843	0.00656	0.00508	0.00437	0.00336	0.00257
1.35000	0.04002	0.03199	0.02544	0.0222I	0.0I750	0.0I373	0.0II89	0.00925	0.00716	0.00616	0.00473	0.00362
1.4661I9	0.05632	0.04494	0.03570	0.03II4	0.02456	0.0I925	0.0I667	0.0I297	0.0I005	0.00864	0.00665	0.00509
1.5338I	0.06855	0.05469	0.04340	0.03786	0.02984	0.02339	0.02026	0.0I577	0.0I22I	0.0I05I	0.00808	0.00619
1.65000	0.09582	0.07634	0.06052	0.05278	0.04158	0.03261	0.02824	0.02198	0.0I704	0.0I466	0.0II28	0.00865
1.7661I9	0.13384	0.10622	0.08418	0.07336	0.05777	0.04531	0.03926	0.03057	0.02371	0.02040	0.0157I	0.0I200
1.8338I	0.16194	0.12856	0.10I8I	0.08877	0.06987	0.05480	0.04749	0.03699	0.02870	0.02472	0.0I904	0.0I46I
1.95000	0.22416	0.17847	0.14053	0.12279	0.09666	0.07582	0.06572	0.05126	0.03979	0.03429	0.02644	0.02032
2.0661I9	0.30967	0.24568	0.19493	0.16942	0.13339	0.10463	0.09072	0.07078	0.05506	0.04745	0.03665	0.02818
2.1338I	0.37320	0.29590	0.23446	0.20450	0.16061	0.12607	0.10930	0.08534	0.06640	0.05729	0.04428	0.03410
2.25000	0.51224	0.40603	0.32102	0.28012	0.22036	0.17108	0.15019	0.11735	0.09142	0.07854	0.06112	0.04715
2.3661I9	0.69210	0.55422	0.43826	0.38192	0.30149	0.23669	0.20551	0.16087	0.12547	0.10843	0.08416	0.06505
2.4338I	0.83559	0.66II9	0.52408	0.45673	0.36012	0.28386	0.24616	0.19285	0.15059	0.13022	0.10II9	0.07837
2.55000	0.42619	0.89365	0.7068I	0.61773	0.48784	0.38432	0.33480	0.26236	0.2053I	0.17764	0.13845	0.10745
2.6661I9	0.21063	0.44070	0.94899	0.82394	0.6560I	0.51802	0.45100	0.35545	0.27845	0.24149	0.18854	0.14675
2.7338I	0.13735	0.28820	0.61652	0.97938	0.7754I	0.6I422	0.5351I	0.42I60	0.33I48	0.28776	0.22516	0.17551
2.85000	0.06413	0.13478	0.29069	0.45920	1.0288I8	0.8I4I5	0.7I3I4	0.56369	0.44515	0.38740	0.30366	0.23759
2.9661I9	0.02899	0.06090	0.13165	0.20863	0.46696	1.07249	0.94021	0.74643	0.59099	0.51533	0.40709	0.3I940
3.0338I	0.01793	0.03783	0.08174	0.12961	0.29168	0.67048	1.0561I4	0.87315	0.69436	0.60636	0.48043	0.37793
3.15000	0.00767	0.01618	0.03515	0.05572	0.12581	0.29046	0.47645	1.13307	0.90588	0.79477	0.63178	0.50155
3.2661I9	0.00317	0.00670	0.01457	0.02318	0.05255	0.12165	0.20042	0.47918	1.16531	1.02648	0.82252	0.65594
3.3338I	0.00186	0.00395	0.00860	0.01369	0.03113	0.07219	0.11911	0.28612	0.69859	1.18195	0.95167	0.76313
3.45000	0.00073	0.00155	0.00338	0.00540	0.01229	0.02873	0.04753	0.11460	0.28206	0.47952	1.20696	0.97685
3.5661I9	0.00028	0.00059	0.00129	0.00206	0.00470	0.01102	0.01828	0.04447	0.10994	0.18795	0.47747	1.22761
3.6338I	0.00000	0.00033	0.00072	0.00116	0.00265	0.00622	0.01031	0.02521	0.06256	0.10719	0.27392	0.70868
3.75000	- " -	0.0001I2	0.00026	0.00042	0.00096	0.00226	0.00377	0.00924	0.02315	0.03984	0.10243	0.26787
3.8661I9	- " -	0.00004	0.00009	0.00015	0.00034	0.00080	0.00133	0.00328	0.00825	0.01425	0.03707	0.09762
3.9338I	- " -	0.00000	0.00000	0.00000	0.00000	0.00043	0.00072	0.00177	0.00446	0.00772	0.02013	0.05338
4.05000	- " -	- " -	- " -	- " -	- " -	0.0001I4	0.00024	0.00059	0.00151	0.00262	0.00688	0.01841
4.1661I9	- " -	- " -	- " -	- " -	- " -	0.00005	0.00008	0.00019	0.00049	0.00086	0.00227	0.00613
4.2338I	- " -	- " -	- " -	- " -	- " -	0.00000	0.00000	0.00000	0.00025	0.00044	0.0011I7	0.00318

X \ X_0	3.6338I	3.75000	3.8661I9	3.9338I	4.05000	4.1661I9	4.2338I	4.35000	4.4661I9	4.5338I	4.65000	4.7661I9
1.2338I	0.00219	0.00166	0.00125	0.00106	0.00079	0.00059	0.00049	0.00000	0.00000	0.00000	0.00000	0.00000
1.35000	0.00309	0.00234	0.00177	0.00150	0.00112	0.00084	0.00070	0.00000	0.00000	0.00000	0.00000	0.00000
1.4661I9	0.00434	0.00330	0.00249	0.00211	0.00158	0.00118	0.00099	0.00000	0.00000	0.00000	0.00000	0.00000
1.5338I	0.00529	0.00402	0.00304	0.00258	0.00193	0.00144	0.00121	0.00090	0.00066	0.00055	0.00040	0.00000
1.65[illegible]	0.00739	0.00562	0.00426	0.00361	0.00271	0.00203	0.00171	0.00127	0.00093	0.00078	0.00057	0.00000
1.7661I9	0.01031	0.00785	0.00595	0.00506	0.00380	0.00285	0.00240	0.00178	0.00132	0.00110	0.00081	0.00000
1.8338I	0.01251	0.00953	0.00723	0.00615	0.00463	0.00347	0.00292	0.00218	0.00161	0.00135	0.00099	0.00072
1.95000	0.01739	0.01328	0.01009	0.00858	0.00648	0.00486	0.00411	0.00306	0.00227	0.00190	0.00140	0.00102
2.0661I9	0.02415	0.01846	0.01406	0.01197	0.00905	0.00681	0.00575	0.00430	0.00319	0.00268	0.00198	0.00145
2.1338I	0.02921	0.02236	0.01704	0.01452	0.01098	0.00827	0.00700	0.00523	0.00389	0.00327	0.00241	0.00177
2.25000	0.04047	0.03101	0.02367	0.02020	0.01532	0.01156	0.00980	0.00734	0.00547	0.00460	0.00341	0.00251
2.3661I9	0.05591	0.04295	0.03283	0.02804	0.02132	0.01613	0.01369	0.01028	0.00769	0.00647	0.00480	0.00354
2.4338I	0.06736	0.05181	0.03968	0.03392	0.02582	0.01957	0.01662	0.01250	0.00936	0.00789	0.00586	0.00433
2.55000	0.09259	0.07139	0.05484	0.04692	0.03582	0.02722	0.02315	0.01747	0.01312	0.01108	0.00825	0.00612
2.6661I9	0.12663	0.09802	0.07551	0.06474	0.04953	0.03775	0.03218	0.02436	0.01834	0.01553	0.01160	0.00863
2.7338I	0.15162	0.11757	0.09076	0.07794	0.05977	0.04561	0.03891	0.02952	0.02228	0.01887	0.01414	0.01053
2.85000	0.20567	0.16001	0.12409	0.10682	0.08214	0.06294	0.05380	0.04094	0.03103	0.02634	0.01979	0.01481
2.9661I9	0.27719	0.21655	0.16857	0.14544	0.11242	0.08651	0.07411	0.05660	0.04306	0.03663	0.02765	0.02076
3.0338I	0.32850	0.25745	0.20086	0.17357	0.13461	0.10384	0.08908	0.06819	0.05199	0.04431	0.03352	0.02522
3.15000	0.43736	0.34278	0.26993	0.23384	0.18223	0.14140	0.12162	0.09359	0.07164	0.06120	0.04652	0.03517
3.2661I9	0.57404	0.45591	0.35929	0.31246	0.24481	0.19098	0.16493	0.12758	0.09822	0.08409	0.06421	0.04880
3.3338I	0.66940	0.53384	0.42227	0.36811	0.28950	0.22664	0.19611	0.15237	0.11759	0.10096	0.07728	0.05890
3.45000	0.86194	0.69159	0.55332	0.48340	0.38309	0.30189	0.26222	0.20493	0.15933	0.13728	0.10576	0.08099
3.5661I9	1.09000	0.88405	0.71227	0.62658	0.50064	0.39785	0.34714	0.27325	0.21397	0.18501	0.14455	0.11068
3.6338I	1.23772	1.01093	0.82011	0.72376	0.58257	0.46434	0.40638	0.32139	0.25279	0.21524	0.17074	0.13218
3.75000	0.47113	1.25196	1.02896	0.91475	0.74245	0.60006	0.52695	0.42071	0.33363	0.29065	0.22824	0.17811
3.8661I9	0.17287	0.46541	1.26250	1.13274	0.93142	0.75983	0.67395	0.54280	0.43481	0.38097	0.30173	0.23740
3.9338I	0.09484	0.25720	0.70414	1.26704	1.05230	0.86538	0.76947	0.62610	0.50376	0.44277	0.35277	0.27919
4.05000	0.03294	0.09009	0.24988	0.45415	1.27231	1.06386	0.95388	0.78467	0.64152	0.56669	0.45653	0.36481
4.1661I9	0.01100	0.03051	0.08542	0.15650	0.44580	1.27465	1.15466	0.96566	0.79880	0.71370	0.58103	0.46986
4.2338I	0.00572	0.01593	0.04506	0.08276	0.23771	0.68667	1.27477	1.07764	0.89983	0.80640	0.66424	0.54015
4.35000	0.00181	0.00509	0.01452	0.02694	0.07823	0.22975	0.43113	1.27305	1.08374	0.98072	0.81849	0.67753
4.4661I9	0.00055	0.00157	0.00452	0.00842	0.02485	0.07385	0.13988	0.42111	1.26914	1.15922	0.98811	0.82937
4.5338I	0.00027	0.00078	0.00225	0.00421	0.01250	0.03756	0.07136	0.21692	0.65984	1.26596	1.08957	0.92421
4.65000	0.00008	0.00023	0.00066	0.00125	0.00374	0.01135	0.02181	0.06719	0.20875	0.40440	1.25910	1.09109
4.7661I9	0.00002	0.00006	0.00019	0.00036	0.00108	0.00331	0.00640	0.02006	0.06318	0.12369	0.39343	1.25070
4.8338I	0.00000	0.00000	0.00000	0.00000	0.00051	0.00159	0.00308	0.00972	0.03101	0.06092	0.19588	0.62927
4.95000	0.00000	0.00000	0.00000	0.00000	0.00014	0.00044	0.00085	0.00273	0.00880	0.01751	0.05717	0.18784
5.0661I9	0.00000	0.00000	0.00000	0.00000	0.00004	0.00012	0.00023	0.00074	0.00241	0.00482	0.01602	0.05358
5.1338I	0.00000	0.00000	0.00000	0.00000	0.00000	0.00000	0.00000	0.00034	0.00111	0.00224	0.00750	0.02539

Table 11 Table of the function $f_o(x,x_o)$ for graphite, T = 300°K.

x \ x_o	0.0338I	0.I5000	0.266I9	0.3338I	0.45000	0.566I9	0.6338I	0.75000
0.0	0.00000000	0.00000000	0.00000000	0.00000000	0.00000000	0.00000000	0.00000000	0.00000000
0.3	I.I7429917	I.I7021825	I.I6230857	0.00028069	0.00030349	0.00032648	0.00034247	0.00035548
0.6	I.I9369598	I.I7513179	I.I6585220	I.I59II3I3	I.I4437036	I.I2681305	0.00400448	0.00387591
0.9	I.26863047	I.I9317930	I.I7763217	I.I6970477	I.I5451429	I.I3784422	I.I2643378	I.I0406328
I.2	I.38937806	I.22177620	I.I9566366	I.I8548160	I.I6886555	I.I5257943	I.I4209519	I.I2249431
I.5	I.49798929	I.24732682	I.2II5I866	I.I99I8I67	I.I8I0I072	I.I6470498	I.I5473972	I.I3695068
I.8	I.56026759	I.26I92556	I.22050613	I.20689837	I.I8776862	I.I7I34245	I.I6158418	I.I4463299
2.I	I.58474554	I.26765246	I.2240I675	I.20590160	I.I9037650	I.I7388069	I.I64I8830	I.I4752265
2.4	I.59I66928	I.26927062	I.22500629	I.2I074657	I.I9II0696	I.I7458786	I.I649II23	I.I483I88I
2.7	I.5931I2479	I.26961055	I.2252I390	I.2I092368	I.I9I25975	I.I7473532	I.I6506I69	I.I484840I
3.0	I.59335742	I.26966488	I.22524705	I.2I095I94	I.I9I28409	I.I7475878	I.I6508560	I.I485I022
3.3	I.59338617	I.26967I60	I.2252511S	I.2I095544	I.I9I287I0	I.I7476I68	I.I6508855	I.I485I346
3.6	I.59338617	I.26967I60	I.2252511S	I.2I095544	I.I9I287I0	I.I7476I68	I.I6508855	I.I485I346

x \ x_o	0.866I9	0.9338I	I.05000	I.I66I9	I.2338I	I.35000	I.466I9	I.5338I
0.0	0.00000000	0.00000000	0.00000000	0.00000000	0.00000000	0.00000000	0.00000000	0.00000000
0.3	0.00036030	0.00035867	0.00034946	0.00033275	0.00032033	0.00029548	0.00026795	0.00025102
0.6	0.00373425	0.00362860	0.00343231	0.00319595	0.00304383	0.00276581	0.00247705	0.00230966
0.9	I.07745137	0.0I744610	0.0I590173	0.0I436860	0.0I349684	0.0I201520	0.0I058093	0.00977866
I.2	I.I0079483	I.08664348	I.05943832	I.04589321	0.04570362	0.03984762	0.03443815	0.03152482
I.5	I.II849057	I.I07II831	I.0869I242	I.06471199	I.0504I208	I.04II4I91	0.98I28535	0.08970845
I.8	I.I2770474	I.II765723	I.I0078397	I.08394911	I.07420500	I.05667550	I.03675345	I.023II427
2.I	I.I3II3342	I.I2I55207	I.I0584492	I.09087957	I.0827I08I	I.06922066	I.0560904S	I.04847687
2.4	I.I3207I83	I.I2261297	I.I0721346	I.09273795	I.0849813I	I.07254763	I.06II7550	I.05512019
2.7	I.I3226561	I.I22831I4	I.I0749399	I.093II7I0	I.08544344	I.07322063	I.06219987	I.05645388
3.0	I.I3229629	I.I2286601	I.I0753827	I.093I7682	I.0855I613	I.07332629	I.06236032	I.05666252
3.3	I.I3230007	I.I2287026	I.I0753827	I.093I8416	I.08552506	I.07333927	I.06238002	I.05668814
3.6	I.I3230007	I.I2287026	- " -	I.093I8416	I.08552506	I.07333927	I.06238002	I.05668814

x \ x_o	I.65000	I.766I9	I.8338I	I.95000	2.066I9	2.I338I	2.25000	2.366I9
0.0	0.00000000	0.00000000	0.00000000	0.00000000	0.00000000	0.00000000	0.00000000	0.00000000
0.3	0.00022II4	0.00019225	0.000I7610	0.000I4993	0.000I2606	0.000II34I	0.0000938I	0.00007686
0.6	0.00202340	0.00I74493	0.00I59349	0.00I35071	0.00II3I92	0.00I0I66I	0.00083879	0.00068585
0.9	0.00846928	0.00725195	0.00658677	0.00554287	0.0046213I	0.00413929	0.00340175	0.00277286
I.2	0.02690614	0.02277359	0.02059074	0.0I7I8878	0.0I422470	0.0I269936	0.0I038659	0.00843104
I.5	0.07548008	0.063I0636	0.05668063	0.04688277	0.03852475	0.03428537	0.02785366	0.02251252
I.8	0.99292342	0.94662397	0.I4633441	0.II983673	0.09767096	0.08654128	0.06997255	0.05627251
2.I	I.03462900	I.0I794702	I.00560681	0.97443467	0.32227415	0.20858049	0.16895149	0.13527215
2.4	I.04545782	I.03630197	I.03099630	I.02002487	1.00646540	0.99517020	0.96435533	0.90636892
2.7	I.04762380	I.03996322	I.03604523	I.02905710	1.02717005	I.0I943933	I.0II62045	I.00074786
3.0	I.04796198	I.04053309	I.03683094	I.03046020	1.02765718	I.023II324	I.0I896468	I.0I549219
3.3	I.04800751	I.04060313	I.03692749	I.03063280	I.02608466	I.02367766	I.0I987095	I.0I73I692
	I.04800751	I.04060313	I.03692749	I.03063280	I.026II594	I.02372323	I.0I996017	I.0I749728
					I.026II594	I.02372323	I.0I995017	I.0I749728

Table 11 (continued)

X \ X_0	-.43381	2.55000	2.66619	2.77381	2.85000	2.96619	3.03381	3.15000
0.0	0.00000040	0.00000000	0.00000000	0.00000000	0.00000000	0.00000000	0.00000000	0.00000000
0.3	0.00006[illegible]1	0.00005500	0.00004406	0.00003858	0.00003056	0.00002405	0.00002085	0.00001624
0.6	0.00060757	0.00048990	0.00039201	0.00034315	0.00027160	0.00021357	0.00018517	0.00014421
0.9	0.00445293	0.00197438	0.00157772	0.00138007	0.00109099	0.00085727	0.00074304	0.00057859
1.2	0.00744373	0.00597713	0.00476764	0.00416709	0.00329060	0.00258316	0.00223811	0.00174203
1.5	0.01983183	0.01587590	0.01263710	0.01103528	0.00870592	0.00682986	0.00591595	0.00460326
1.8	0.04947406	0.03946305	0.03134861	0.02734119	0.02154989	0.01690303	0.01464150	0.01139625
2.1	0.11866739	0.09444632	0.07485822	0.06522973	0.05137608	0.04029873	0.03492156	0.02721134
2.4	0.27573674	0.21942704	0.17372125	0.15144800	0.11926634	0.09360729	0.08118080	0.06317515
2.7	0.58962401	0.46088802	0.89687746	0.34053497	0.26898900	0.21167253	0.18391703	0.14404866
3.0	1.01[illegible]695	1.00795030	0.99798361	0.98868113	0.96035211	0.89301179	0.40194509	0.31654348
3.3	1.01501701	1.01381820	1.01065621	1.00884130	1.00581285	0.99775013	0.98981029	0.96239148
3.6	1.01529257	1.01440261	1.01197088	1.01087546	1.01043766	1.00851562	1.00759780	1.00522046
3.9	1.01529257	1.01444923	1.01207333	1.01103953	1.01081413	1.00940202	1.00907307	1.00882695
4.2	- " -	1.01444923	1.01407333	1.01103953	1.01081413	1.00946049	1.00917106	1.00906944
					- " -	1.00946049	1.00917106	1.00906944

X \ X_0	3.26619	3.33381	3.45000	3.56619	3.63381	3.75000	3.86619	3.93381
.	.00000000	0.00000000	0.00000000	0.00000000	0.00000000	0.00000000	0.00000000	0.00000000
0.3	0.00001256	0.00000000	0.00000000	0.00000000	0.00000000	0.00000000	0.00000000	0.00000000
0.6	0.00011159	0.00000000	0.00000000	0.00000000	0.00000000	0.00000000	0.00000000	0.00000000
0.9	0.00044776	0.00028884	0.00022161	0.00016404	0.00011440	0.00000000	0.00000000	0.00000000
1.2	.00034876	0.00106321	0.00081608	0.00062301	0.00053114	0.00029314	0.00022079	0.00018684
1.5	0.00156438	0.00296884	0.00228094	0.00174936	0.00148739	0.00101894	0.00076873	0.00065097
1.8	0.00462930	0.00749869	0.00576788	0.00441669	0.00377250	0.00275772	0.00208565	0.00176863
2.1	0.01[illegible]459	0.01808477	0.01394317	0.01069176	0.00914604	0.00686095	0.00520514	0.00442244
2.4	0.04[illegible]438	0.04241949	0.03278743	0.02594023	0.02164586	0.01641739	0.01251744	0.01066231
2.7	0.11[illegible]54	0.09710732	0.07539120	0.05832833	0.05014693	0.03844308	0.02942836	0.02513961
3.0	0.[illegible]166	0.21568564	0.16856627	0.13126019	0.11333294	0.08624132	0.06758368	0.05799718
3.3	0.[illegible]590	0.45772457	0.36136598	0.28427876	0.24688927	0.18629219	0.15025410	0.12967790
3.6	0.95796166	0.99074295	0.96490007	0.89578676	0.50637044	0.40310263	0.31857717	0.27702169
3.9	1.00694979	1.00617490	1.00447217	0.99869404	0.99264976	0.96791817	0.90035588	0.55369747
4.2	1.00756387	1.00723974	1.00725703	1.00610760	1.00586240	1.00390643	0.99946934	0.99378550
4.5	1.00759718	1.00729819	1.00741909	1.00651760	1.00662734	1.00600362	1.00553641	1.00497559
4.8	- " -	- " -	- " -	- " -	1.00666250	1.00614397	1.00582821	1.00552550

X \ X_0	4.05000	4.16619	4.23381	4.35000	4.46619	4.53381	4.65000	4.76619
0.0	0.00000000	0.00000000	0.00000000	0.00000000	0.00000000	0.00000000	0.00000000	0.00000000
.3	0.00000000	0.00000000	0.00000000	0.00000000	0.00000000	0.00000000	0.00000000	0.00000000
	0.00000000	0.00000000	0.00000000	0.00000000	0.00000000	0.00000000	0.00000000	0.00000000
.9	00000000	0.00000000	0.00000000	0.00000000	0.00000000	0.00000000	0.00000000	0.00000000
.2	00000000	0.00000000	0.00000000	0.00000000	0.00000000	0.00000000	0.00000000	0.00000000
1.5	0.00034762	0.00025899	0.00021765	0.00000000	0.00000000	0.00000000	0.00000000	0.00000000
1.8	0.00118745	0.00088704	0.00074676	0.00039241	0.00028960	0.00024204	0.00017705	0.00000000
2.1	0.00319054	0.00239149	0.00201743	0.00133960	0.00099214	0.00083096	0.00061027	0.00031702
2.4	0.00792485	0.00596679	0.00504761	0.00361138	0.00268672	0.00225671	0.00166558	0.00109402
2.7	0.01898032	0.01437320	0.01220141	0.00901201	0.00674480	0.00568552	0.00422189	0.00299038
3.0	0.04428205	0.03377468	0.02879367	0.02164721	0.01632617	0.01382201	0.01034261	0.00757219
3.3	0.10019694	0.07719567	0.06617791	0.05044083	0.03839463	0.03268170	0.02468962	0.01842976
3.6	0.21712106	0.16948510	0.14641132	0.11323345	0.08726923	0.07481629	0.05719449	0.04336109
3.9	0.44228062	0.35151123	0.30669557	0.24134340	0.18905283	0.16358765	0.12699936	0.09790708
4.2	0.87104634	0.70580290	0.59422364	0.47861341	0.38313569	0.33551940	0.26568703	0.20896921
4.5	1.00335688	0.99981173	0.99516811	0.97432417	0.91207338	0.83008395	0.51251482	0.41343096
4.8	1.00496612	1.00473021	1.00455605	1.00303061	1.00015823	0.99583242	0.97763308	0.91852647
5.1	1.00505059	1.00493032	1.00494548	1.00426525	1.00411627	1.00364620	1.00291388	1.00047665
5.4	- " -	- " -	- " -	1.00430558	1.00425308	1.00392232	1.00384436	1.00364106
5.7	- " -	- " -	- " -	- " -	- " -	- " -	1.00387079	1.00373[illegible]

Table 12 Table of the function $g_{1is}(x_o - x)$ for graphite, T = 300°K.

X \ X_o	0.0338I	0.I5000	0.266I9	0.3338I	0.45000	0.566I9	0.6338I	0.75000	0.866I9	0.9338I	I.05000	I.166I9
0.0338I	0.00000	0.00000	0.00000	0.00000	0.00000	0.00000	-0.00000	-0.00000	-0.00000	-0.00000	-0.00000	-0.00000
0.I5000	-0.000I4	-0.000I5	-0.000I4	-0.000I4	-0.000I3	-0.000I2	-0.000II	-0.000I0	-0.00009	-0.00009	-0.00007	-0.00006
0.266I9	-0.00073	-0.00075	-0.0008I	-0.00079	-0.00074	-0.00068	-0.00066	-0.00059	-0.00053	-0.00050	-0.00043	-0.00037
0.3338I	-0.00I35	-0.00I40	-0.00I49	-0.00I58	-0.00I49	-0.00I38	-0.00I30	-0.00II9	-0.00I06	-0.00098	-0.00085	-0.00074
0.45000	-0.00285	-0.00294	-0.003I2	-0.00334	-0.00379	-0.00353	-0.00334	-0.00302	-0.00269	-0.00250	-0.00218	-0.00I87
0.566I9	-0.00468	-0.00479	-0.00510	-0.00547	-0.00625	-0.00736	-0.00700	-0.00632	-0.00563	-0.00522	-0.00455	-0.0039z
0.6338I	-0.00575	-0.00593	-0.00636	-0.00668	-0.00765	-0.00905	-0.0I0I2	-0.00914	-0.00816	-0.00758	-0.00660	-0.00568
0.75000	-0.00732	-0.00755	-0.00808	-0.00859	-0.00976	-0.0II53	-0.0I296	-0.0I6I8	-0.0I442	-0.0I333	-0.0II65	-0.0I003
0.866I9	-0.00833	-0.00859	-0.00922	-0.00974	-0.0II09	-0.0I3I3	-0.0I470	-0.0I84I	-0.02388	-0.02225	-0.0I938	-0.0I663
0.9338I	-0.00859	-0.00885	-0.00948	-0.0I005	-0.0II44	-0.0I350	-0.0I5I6	-0.0I888	-0.02469	-0.02910	-0.02543	-0.02I85
I.05000	-0.00844	-0.00870	-0.00932	-0.00988	-0.0II24	-0.0I328	-0.0I490	-0.0I863	-0.02427	-0.02871	-0.02926	-0.02326
I.I66I9	-0.00769	-0.00792	-0.00849	-0.00899	-0.0I024	-0.0I2I0	-0.0I357	-0.0I699	-0.02206	-0.02612	-0.03523	-0.05077
I.2338I	-0.00705	-0.00727	-0.00778	-0.00825	-0.00939	-0.0III0	-0.0I244	-0.0I559	-0.02024	-0.02395	-0.03277	-0.04640
I.35000	-0.00578	-0.00596	-0.00638	-0.00676	-0.00769	-0.00909	-0.0I0I9	-0.0I278	-0.0I659	-0.0I964	-0.02695	-0.03819
I.466I9	-0.00447	-0.00462	-0.00494	-0.00522	-0.00595	-0.00705	-0.00788	-0.00987	-0.0I28I	-0.0I5I7	-0.02082	-0.02955
I.5338I	-0.00375	-0.00387	-0.00415	-0.00439	-0.00500	-0.00590	-0.00661	-0.00828	-0.0I076	-0.0I273	-0.0I748	-0.02481
I.65000	-0.00266	-0.00274	-0.00295	-0.00312	-0.00355	-0.00420	-0.00470	-0.00589	-0.00764	-0.00905	-0.0I242	-0.0I763
I.766I9	-0.00180	-0.00186	-0.00199	-0.00211	-0.00240	-0.00284	-0.00319	-0.00399	-0.00518	-0.00613	-0.00841	-0.0II94
I.8338I	-0.00I4I	-0.00I45	-0.00I50	-0.00I65	-0.00I87	-0.00221	-0.00248	-0.003I0	-0.00405	-0.00479	-0.00657	-0.00942
I.95000	-0.00089	-0.00092	-0.00098	-0.00I04	-0.00II8	-0.00I40	-0.00I56	-0.00I96	-0.00255	-0.00302	-0.00415	-0.00590
2.066I9	-0.00054	-0.00055	-0.00059	-0.00063	-0.00071	-0.00084	-0.00095	-0.00II9	-0.00I54	-0.00I83	-0.00251	-0.00357
2.I338I	-0.00039	-0.00041	-0.00043	-0.00046	-0.00052	-0.00062	-0.00069	-0.00087	-0.00II3	-0.00I34	-0.00184	-0.00262
2.25000	-0.00022	-0.00023	-0.00025	-0.00026	-0.00030	-0.00035	-0.00039	-0.00049	-0.00064	-0.00076	-0.00105	-0.00I49
2.366I9	-0.000I2	-0.000I3	-0.000I4	-0.000I4	-0.00016	-0.00019	-0.00022	-0.00027	-0.00035	-0.00042	-0.00057	-0.00082
2.4338I	-0.00008	-0.00008	-0.00009	-0.000I0	-0.000II	-0.000I3	-0.000I5	-0.000I8	-0.00024	-0.00029	-0.00040	-0.00057
2.55000	-0.00004	-0.00005	-0.00005	-0.00005	-0.00006	-0.00007	-0.00008	-0.000I0	-0.000I3	-0.00015	-0.00021	-0.00030
2.666I9	-0.00002	-0.00002	-0.00002	-0.00003	-0.00003	-0.00003	-0.00004	-0.00005	-0.00006	-0.00007	-0.000I0	-0.00015
2.7338I	-0.00001	-0.00001	-0.00002	-0.00002	-0.00002	-0.00002	-0.00003	-0.00003	-0.00004	-0.00005	-0.00007	-0.000I0
2.85000	-0.00001	-0.00001	-0.00001	-0.00001	-0.00001	-0.00001	-0.00001	-0.00002	-0.00002	-0.00003	-0.00005	-0.00005
2.966I9	0.00000	0.00000	0.00000	0.00000	0.00000	0.00000	-0.00001	-0.00001	-0.00001	-0.00001	-0.00001	-0.00002
							0.00000	0.00000	0.00000	0.00000	0.00000	0.00000

X \ X_o	I.2338I	I.35000	I.466I9	I.5338I	I.65000	I.766I9	I.8338I	I.95000	2.066I9	2.I338I	2.25000	2.366I9
0.0338I	-0.00000	-0.00000	-0.00000	-0.00000	-0.00000	-0.00000	-0.00000	-0.00000	-0.00000	-0.00000	-0.00000	-0.00000
0.I5000	-0.00006	-0.00005	-0.00004	-0.00004	-0.00003	-0.00003	-0.00002	-0.00002	-0.00001	-0.00001	-0.00001	-0.00001
0.266I9	-0.00033	-0.00028	-0.00024	-0.0002I	-0.000I8	-0.000I4	-0.000I3	-0.000I0	-0.00008	-0.00007	-0.00006	-0.00005
0.3338I	-0.00067	-0.00057	-0.00047	-0.00043	-0.00035	-0.00029	-0.00026	-0.00021	-0.000I7	-0.000I5	-0.000I2	-0.000I0
0.45000	-0.00I70	-0.00I44	-0.00I20	-0.00I08	-0.00090	-0.00073	-0.00065	-0.00053	-0.00043	-0.00038	-0.00031	-0.00025
0.566I9	-0.00357	-0.0030I	-0.00252	-0.00226	-0.00I87	-0.00I53	-0.00I36	-0.00III	-0.00090	-0.00080	-0.00064	-0.00052
0.6338I	-0.00517	-0.00437	-0.00365	-0.00328	-0.0027I	-0.00223	-0.00I98	-0.00I6I	-0.00I3I	-0.00II6	-0.00093	-0.00075
0.75000	-0.00914	-0.00772	-0.00646	-0.00580	-0.00480	-0.00394	-0.00350	-0.00285	-0.0023I	-0.00204	-0.00165	-0.00I33
0.866I9	-0.0I515	-0.0I28I	-0.0I07I	-0.00962	-0.00795	-0.00653	-0.00582	-0.00473	-0.00383	-0.00339	-0.00274	-0.0022I
0.9338I	-0.0I989	-0.0I68I	-0.0I407	-0.0I263	-0.0I043	-0.00858	-0.00763	-0.0062I	-0.00504	-0.00445	-0.00360	-0.00290
I.05000	-0.03073	-0.02605	-0.02179	-0.0I957	-0.0I6I7	-0.0I328	-0.0II83	-0.00965	-0.00781	-0.0069I	-0.00559	-0.00451
I.I66I9	-0.04608	-0.039I0	-0.03276	-0.02942	-0.02432	-0.0I997	-0.0I777	-0.0I45I	-0.0II77	-0.0I04I	-0.00842	-0.00680
I.2338I	-0.05786	-0.04860	-0.04I00	-0.03686	-0.03048	-0.02503	-0.02227	-0.0I8I9	-0.0I479	-0.0I306	-0.0I057	-0.00854
I.35000	-0.07I5	-0.07074	-0.05903	-0.05348	-0.04II	-0.03628	-0.03229	-0.02635	-0.02I46	-0.0I90I	-0.0I537	-0.0I243
I.466I9	-0.03674	-0.0545I	-0.0840I	-0.07574	-0.0625I	-0.05I56	-0.04592	-0.03751	-0.03054	-0.02710	-0.02199	-0.0I777
I.5338I	-0.03087	-0.046I6	-0.07079	-0.09I75	-0.076II	-0.0627I	-0.05589	-0.04569	-0.03722	-0.03300	-0.02685	-0.02I72
I.65000	-0.02I95	-0.03275	-0.05025	-0.06545	-0.I0474	-0.08668	-0.07698	-0.06324	-0.05163	-0.04583	-0.03728	-0.03035
I.766I9	-0.0I487	-0.0222I	-0.034I8	-0.04448	-0.07I48	-0.II696	-0.I046I	-0.08588	-0.07038	-0.06257	-0.05I05	-0.04I66
I.8338I	-0.0II6I	-0.0I735	-0.02671	-0.03478	-0.05570	-0.09I79	-0.I2353	-0.I0I75	-0.08354	-0.07439	-0.0608I	-0.04965
I.95000	-0.00734	-0.0I096	-0.0I690	-0.02203	-0.03545	-0.05837	-0.07882	-0.I336I	-0.II023	-0.09846	-0.08095	-0.06640
2.066I9	-0.00445	-0.00666	-0.0I026	-0.0I339	-0.02I59	-0.03569	-0.04828	-0.08223	-0.I4I82	-0.I2723	-0.I0534	-0.08703
2.I338I	-0.00326	-0.00489	-0.00755	-0.00984	-0.0I589	-0.0263I	-0.03564	-0.06090	-0.I0548	-0.I4560	-0.I2095	-0.I0069
2.25000	-0.00I86	-0.00279	-0.00432	-0.00564	-0.00911	-0.0I5I2	-0.02053	-0.03527	-0.06I53	-0.0852I	-0.I5018	-0.I2619
2.366I9	-0.00I02	-0.00I53	-0.00237	-0.00310	-0.00504	-0.00839	-0.0II40	-0.0I968	-0.03458	-0.04825	-0.08584	-0.I52I3
2.4338I	-0.0007I	-0.00I06	-0.00I65	-0.00216	-0.00350	-0.00586	-0.00798	-0.0I379	-0.0243I	-0.03405	-0.06095	-0.I0941
2.55000	-0.00037	-0.00055	-0.00086	-0.00II2	-0.00I83	-0.00306	-0.00419	-0.00729	-0.0I29I	-0.0I816	-0.03295	-0.05993
2.666I9	-0.000I8	-0.00028	-0.00043	-0.00057	-0.00092	-0.00I55	-0.00212	-0.00370	-0.00663	-0.00935	-0.0I7I4	-0.03I65
2.7338I	-0.000I2	-0.000I8	-0.00028	-0.00037	-0.0006I	-0.00I03	-0.00I4I	-0.00246	-0.00442	-0.00627	-0.0II52	-0.02I44
2.85000	-0.00006	-0.00009	-0.000I4	-0.000I8	-0.00029	-0.00049	-0.00067	-0.00II9	-0.002I4	-0.00304	-0.00567	-0.0I067
2.966I9	-0.00003	-0.00004	-0.00006	-0.00008	-0.00013	-0.00023	-0.00031	-0.00055	-0.00I00	-0.00I43	-0.00268	-0.0051z
3.0338I	0.00000	-0.00002	-0.00004	-0.00005	-0.00008	-0.000I4	-0.00020	-0.00035	-0.00063	-0.0009I	-0.00I7I	-0.00327
3.I5000	- " -	-0.00001	-0.00002	-0.00002	-0.00004	-0.00006	-0.00009	-0.00015	-0.00028	-0.00040	-0.00076	-0.00I48
3.266I9	- " -	-0.00000	-0.00001	-0.00001	-0.00002	-0.00003	-0.00004	-0.00007	-0.00012	-0.00017	-0.00033	-0.00064
3.3338I	- " -	0.00000	0.00000	0.00000	0.00000	0.00000	0.00000	-0.00004	-0.00007	-0.000I0	-0.00020	-0.00039

Table 12 (continued)

τ_0 / χ	2.4338I	2.55000	2.6661[illegible]	2.7[illegible]	2.85000	[illegible]	[illegible]	[illegible]	[illegible]	[illegible]	[illegible]
[illegible]	-0.00090	-0.00090	-0.00000	-0.00000	[illegible]	[illegible]	[illegible]	[illegible]	[illegible]	[illegible]	
[illegible]	-0.00001	-0.00001	-0.00000	-0.00000	[illegible]	[illegible]	[illegible]	[illegible]	[illegible]	[illegible]	[illegible]
[illegible]	-0.00004	-0.00003	-0.00003	[illegible]	[illegible]	[illegible]	[illegible]	[illegible]	[illegible]	[illegible]	[illegible]
[illegible]	-0.00009	-0.00007	-0.00005	[illegible]	[illegible]	[illegible]	[illegible]	[illegible]	[illegible]	[illegible]	[illegible]
[illegible]	-0.00042	-0.00017	-0.00074	[illegible]	[illegible]	[illegible]	[illegible]	[illegible]	[illegible]	[illegible]	[illegible]
[illegible]	-0.00047	-0.00017	-0.00026	[illegible]	[illegible]	[illegible]	[illegible]	[illegible]	[illegible]	[illegible]	[illegible]
[illegible]	[illegible]	-0.00053	-0.00042	[illegible]	[illegible]	[illegible]	[illegible]	[illegible]	[illegible]	[illegible]	[illegible]
[illegible]	[illegible]	-0.00054	-0.00075	[illegible]	[illegible]	[illegible]	[illegible]	[illegible]	[illegible]	[illegible]	[illegible]
[illegible]	-0.00156	-0.00125	[illegible]	[illegible]	[illegible]	[illegible]	[illegible]	[illegible]	[illegible]	[illegible]	[illegible]
[illegible]	-0.00246	-0.00208	[illegible]	[illegible]	[illegible]	[illegible]	[illegible]	[illegible]	[illegible]	[illegible]	[illegible]
[illegible]	-0.00397	[illegible]	[illegible]	[illegible]	[illegible]	[illegible]	[illegible]	[illegible]	[illegible]	[illegible]	[illegible]
[illegible]	-0.00569	[illegible]	[illegible]	[illegible]	[illegible]	[illegible]	[illegible]	[illegible]	[illegible]	[illegible]	[illegible]
[illegible]	-0.00753	[illegible]	[illegible]	[illegible]	[illegible]	[illegible]	[illegible]	[illegible]	[illegible]	[illegible]	[illegible]
[illegible]	-0.01097	-0.00884	[illegible]	[illegible]	[illegible]	[illegible]	[illegible]	[illegible]	[illegible]	[illegible]	[illegible]
[illegible]	-0.01571	-0.01268	[illegible]	[illegible]	[illegible]	[illegible]	[illegible]	[illegible]	[illegible]	[illegible]	[illegible]
[illegible]	-0.02[illegible]	-0.01553	[illegible]	[illegible]	[illegible]	[illegible]	[illegible]	[illegible]	[illegible]	[illegible]	[illegible]
[illegible]	-0.02[illegible]	-0.02173	-0.01758	[illegible]	[illegible]	[illegible]	[illegible]	[illegible]	[illegible]	[illegible]	[illegible]
[illegible]	[illegible]	[illegible]	-0.02442	[illegible]	[illegible]	[illegible]	[illegible]	[illegible]	[illegible]	[illegible]	[illegible]
[illegible]	-0.0441	[illegible]	-0.02921	[illegible]	[illegible]	[illegible]	[illegible]	[illegible]	[illegible]	[illegible]	[illegible]
[illegible]	[illegible]	-0.04850	-0.03953	[illegible]	[illegible]	[illegible]	[illegible]	[illegible]	[illegible]	[illegible]	[illegible]
[illegible]	[illegible]	[illegible]	-0.05280	[illegible]	[illegible]	[illegible]	[illegible]	[illegible]	[illegible]	[illegible]	[illegible]
[illegible]	-0.09042	[illegible]	[illegible]	[illegible]	[illegible]	[illegible]	[illegible]	[illegible]	[illegible]	[illegible]	[illegible]
[illegible]	-0.11[illegible]	[illegible]	-0.07965	[illegible]	[illegible]	[illegible]	[illegible]	[illegible]	[illegible]	[illegible]	[illegible]
[illegible]	-0.13[illegible]	-0.11[illegible]	-0.10010	[illegible]	[illegible]	[illegible]	[illegible]	[illegible]	[illegible]	[illegible]	[illegible]
[illegible]	-0.15[illegible]	-0.13[illegible]	[illegible]	[illegible]	[illegible]	[illegible]	[illegible]	[illegible]	[illegible]	[illegible]	[illegible]
[illegible]	-0.08428	[illegible]	[illegible]	[illegible]	[illegible]	[illegible]	[illegible]	[illegible]	[illegible]	[illegible]	[illegible]
[illegible]	-0.04518	-0.08[illegible]	[illegible]	[illegible]	[illegible]	[illegible]	[illegible]	[illegible]	[illegible]	[illegible]	[illegible]
[illegible]	-0.03081	-0.05701	-0.10[illegible]	[illegible]	[illegible]	[illegible]	[illegible]	[illegible]	[illegible]	[illegible]	[illegible]
[illegible]	-0.01547	-0.02[illegible]	-0.05456	[illegible]	[illegible]	[illegible]	[illegible]	[illegible]	[illegible]	[illegible]	[illegible]
[illegible]	-0.00749	-0.01442	-0.02766	-0.04[illegible]	[illegible]	[illegible]	[illegible]	[illegible]	[illegible]	[illegible]	[illegible]
3.0338I	-0.00482	-0.00937	-0.01823	-0.02669	-0.04992	-0.08483	[illegible]	[illegible]	[illegible]	[illegible]	[illegible]
3.15000	-0.00219	-0.00433	-0.00860	-0.01[illegible]	-0.02456	-0.04668	-0.06409	[illegible]	[illegible]	[illegible]	[illegible]
3.26[illegible]	-0.00086	-0.00[illegible]	-0.00389	[illegible]	[illegible]	[illegible]	[illegible]	[illegible]	[illegible]	[illegible]	[illegible]
3.3338I	-0.00068	-0.00117	-0.00240	-0.00365	-0.00747	-0.01503	-0.02226	-0.04096	-0.06171	-0.06453	-0.09[illegible]
3.45000	-0.00024	-0.00049	-0.00101	-0.00155	-0.00327	-0.00680	-0.01034	-0.02055	-0.03730	-0.04791	-0.04119
3.566I9	-0.00010	-0.00020	-0.00041	-0.00064	-0.00136	-0.00292	-0.00453	-0.00946	-0.01[illegible]	-0.02696	-0.04114
3.6338I	-0.00005	-0.00011	-0.00024	-0.00037	-0.00080	-0.00174	-0.00272	-0.00583	-0.01210	-0.01793	-0.03135
3.75000	-0.00002	-0.00004	-0.00009	-0.00014	-0.00031	-0.00069	-0.00109	-0.00242	-0.00528	-0.00817	-0.01634
3.866I9	-0.00001	-0.00002	-0.00003	-0.00005	-0.00012	-0.00026	-0.00042	-0.00095	-0.00216	-0.00344	-0.00742
3.9338I	+0.00000	+0.00000	+0.00000	-0.00003	-0.00006	-0.00015	-0.00024	-0.00054	-0.00124	-0.00201	-0.00449
4.05000	- " -	- " -	-	-0.00001	-0.00002	-0.00005	-0.00008	-0.00020	-0.00046	-0.00076	-0.00178
4.I6619	- " -	- " -	- " -	-0.00000	-0.00001	-0.00002	-0.00003	-0.00007	-0.00017	-0.00028	-0.00067
4.2338I	- " -	- " -	- " -	+0.00000	+0.00000	+0.00000	+0.00000	-0.00004	-0.00009	-0.00015	-0.00036

τ_0 / χ	3.6338I	3.75000	3.866I9	3.9338I	4.05000	4.I6619	4.2338I	4.35000	4.466I9	4.5338I	4.65000	4.766I9
0.9338I	-0.00023	-0.00018	-0.00014	-0.00011	-0.00013	[illegible]	-0.00004	-0.00006	+0.00000	-0.00000	+0.[illegible]	[illegible]
I.05000	-0.00036	-0.00028	-0.00021	-0.00018	-0.00018	-0.00009	-0.00007	-0.00009	[illegible]	-0.00000	+0.00000	- " -
I.I66I9	-0.00055	-0.00042	-0.00032	-0.00029	-0.00026	-0.00015	-0.00053	-0.00013	+0.00000	-0.00000	+0.[illegible]	[illegible]
I.2338I	-0.00069	-0.00053	-0.00041	-0.00035	-0.00027	-0.00019	-0.00019	-0.00016	+0.00000	-0.00000	+0.00018	+0.30156
I.35000	-0.00102	-0.00079	-0.00061	-0.00050	-0.00029	-0.00029	-0.00028	-0.00023	-0.00001	-0.00000	+0.00019	-0.00907
I.466I9	-0.00145	-0.00116	-0.00090	-0.00075	-0.00058	-0.00047	-0.00041	-0.00033	-0.00006	-0.00000	-0.00051	+0.00390
I.5338I	-0.00185	-0.00144	-0.00112	-0.00099	-0.00073	-0.00058	-0.00050	-0.00026	-0.00012	-0.00003	-0.00058	+0.00076
I.65000	-0.00265	-0.00207	-0.00159	-0.00138	-0.00105	-0.00083	-0.00072	-0.00043	-0.00024	-0.00013	-0.00074	-0.00001
I.766I9	-0.00376	-0.00295	-0.00232	-0.00197	-0.00153	-0.00119	-0.00102	-0.00066	-0.00041	-0.00028	-0.00088	-0.00[illegible]
I.8338I	-0.00460	-0.00361	-0.00281	-0.00242	-0.00189	-0.00146	-0.00117	-0.00084	-0.00057	-0.00041	-0.00098	-0.00[illegible]
I.95000	-0.00645	-0.00508	-0.00396	-0.00343	-0.00267	-0.00201	-0.00171	-0.00126	-0.00088	-0.00120	-0.00118	-0.00[illegible]
2.066I9	-0.00895	-0.00708	-0.00555	-0.00481	-0.00373	-0.00286	-0.00244	-0.00183	-0.00169	-0.00156	-0.00144	-0.00149
2.I338I	-0.01080	-0.00855	-0.00674	-0.00584	-0.00454	-0.00350	-0.00304	-0.00202	[illegible]	-0.00182	-0.00163	-0.00164
2.25000	-0.01481	-0.01179	-0.00932	-0.00811	-0.00635	-0.00481	-0.00408	-0.00340	-0.00271	-0.00242	-0.00207	-0.00195
2.366I9	-0.02010	-0.01609	-0.01281	-0.01115	-0.00873	-0.00687	-0.00592	-0.00458	-0.00350	-0.00298	-0.00[illegible]	-0.00058
2.4338I	-0.02390	-0.01922	-0.01534	-0.01330	-0.01058	-0.00830	-0.00718	-0.00555	-0.00427	-0.00365	-0.00275	-0.00101
2.55000	-0.03187	-0.02585	-0.02077	-0.01822	-0.01448	-0.01164	-0.01020	-0.00817	-0.00666	-0.00598	-0.00404	-0.00199
2.666I9	-0.04191	-0.03428	-0.02780	-0.02451	-0.01962	-0.01557	-0.01356	-0.01103	-0.00836	-0.00722	-0.00560	-0.00435
2.7338I	-0.04876	-0.04015	-0.03277	-0.02899	-0.02333	-0.01864	-0.01629	-0.01284	-0.01006	-0.00870	-0.00676	-0.00524
2.85000	-0.06223	-0.05203	-0.04298	-0.03828	-0.03115	-0.02510	-0.02156	-0.01748	[illegible]	-0.01195	-0.00932	-0.00724
2.966I9	-0.07744	-0.06991	-0.05532	-0.04966	-0.04089	-0.03331	-0.02942	-0.02362	[illegible]	-0.01517	-0.01113	-0.00767
3.0338I	-0.08650	-0.07463	-0.06336	-0.05717	-0.04755	-0.03901	-0.03459	-0.02[illegible]	-0.02235	-0.01956	-0.01380	-0.00[illegible]
3.15000	-0.10118	-0.09022	-0.07851	-0.07173	-0.06057	-0.05035	-0.04493	-0.[illegible]365	-0.02978	-0.02621	-0.02088	-0.01[illegible]
3.266I9	-0.11101	-0.10394	-0.09391	-0.08717	-0.07544	-0.06405	-0.05767	-0.[illegible]726	-0.[illegible]3886	-0.03458	-0.02770	-0.02[illegible]
3.3338I	-0.11196	-0.10951	-0.10202	-0.09584	-0.08445	-0.07273	-0.[illegible]0667	-0.[illegible]5[illegible]	-0.[illegible]536	-0.04022	-0.03271	-0.02607
3.45000	-0.09863	-0.11030	-0.11079	-0.10781	-0.09818	-0.08847	-0.[illegible]1[illegible]	-0.[illegible]	-0.05[illegible]0	-0.05214	-0.04259	-0.03[illegible]
3.566I9	-0.05221	-0.09105	-0.10800	-0.11138	-0.10986	-0.10239	-0.[illegible]0[illegible]53	-[illegible].	-[illegible].07306	-0.06625	-0.05[illegible]	-0.04502
3.6338I	-0.00467	-0.06478	-0.09689	-0.10641	-0.11205	-0.10871	-0.[illegible]7[illegible]18	[illegible].[illegible]3	-0.[illegible]8266	-0.07511	-0.06342	-0.05228
3.75000	-0.03019	+0.01962	-0.05138	-0.07745	-0.10320	-0.11[illegible]	-0.11250	-[illegible]17	-0.09746	-0.09079	-0.07938	-0.06666
3.866I9	-0.02042	-0.02324	+0.04454	-0.00821	-0.06794	-0.09538	-0.10665	[illegible].[illegible]363	-0.[illegible]09[illegible]87	-0.10504	-0.09[illegible]38	-0.09[illegible]01
3.9338I	-0.01394	-0.02178	-0.00510	+0.05925	-0.02882	-0.07967	-0.09693	-.[illegible]11	-0.[illegible]1401	-0.11137	-0.[illegible]2[illegible]6	-0.[illegible]0[illegible]47
4.05000	-0.00634	0.01252	-0.01823	-0.01244	+0.08459	-0.01379	-0.05163	-0.[illegible]0[illegible]233	-0.[illegible]1114	-0.11506	-0.11401	0.10[illegible]
4.I6619	-0.00258	-0.00571	-0.01117	-0.01441	-0.00578	+0.11006	+0.04094	-0.[illegible]0[illegible]27	-0.[illegible]0726	0.10279	-0.11[illegible]6	-0.[illegible]2[illegible]
4.2338I	-0.00147	-0.00340	-0.00726	-0.01042	-0.01287	+0.02435	+0.12481	+0.[illegible]1[illegible]	-0.[illegible]0[illegible]867	-0.08402	-0.10908	-0.11[illegible]
4.35000	-0.00053	-0.00130	-0.00304	-0.00482	-0.00920	-0.00968	+0.00434	+0.[illegible]2[illegible]	+0.[illegible]2674	-0.02247	-0.07823	-0.10[illegible]
4.466I9	-0.00018	-0.00046	-0.00114	-0.00191	-0.00431	-0.00807	-0.00912	+0.01[illegible]	+0.[illegible]7151	+0.09113	-0.01[illegible]55	-0.07[illegible]
4.5338I	-0.00009	-0.00024	-0.00062	-0.00106	-0.00254	-0.00541	-0.00743	-0.00497	+0.05187	+0.18857	+0.05[illegible]7	-0.01[illegible]
4.65000	-0.00003	-0.00008	-0.00021	-0.00036	-0.00093	-0.00226	-0.00358	-0.00[illegible]42	-0.00[illegible]23	+0.01[illegible]6	+0.[illegible]2[illegible]	+0.06841
4.766I9	-0.00001	-0.00002	-0.00007	-0.00012	-0.00031	-0.00082	-0.00139	-.[illegible]0317	0.00543	-0.00165	+0.[illegible]2467	+0.[illegible]2[illegible]4
4.8338I	0.00000	-0.00001	-0.00003	-0.00006	-0.00016	-0.00043	-0.00076	-0.[illegible]0[illegible]66	-0.00390	-0.00496	+0.00174	+0.07[illegible]
4.95000	- " -	0.00000	-0.00001	-0.00002	-0.00005	-0.00014	-0.00024	-0.00066	-[illegible].00164	-0.00[illegible]60	-0.00415	+0.00[illegible]
5.066I9	- " -	- " -	0.00000	0.00000	-0.00001	-0.00004	-0.00007	-0.00021	-0.00058	-0.00100	-0.[illegible]0[illegible]28	-0.00[illegible]
5.I338I	- " -	- " -	- " -	- " -	0.00000	-0.00002	0.00004	-0.00011	-0.00010	-0.00053	-0.[illegible]0[illegible]34	-0.00[illegible]
[illegible]	- " -	- " -	- " -	- " -	- " -	-0.00001	-0.00001	-0.00003	-0.00009	-0.00017	-0.00006	-0.[illegible]0[illegible]
5.366I9	- " -	- " -	- " -	- " -	- " -	0.00000	-0.00000	-0.00001	-0.00002	-0.00005	-0.[illegible]0014	-0.00040

Table 13 Table of the function $f_1(x,x_o)$ for graphite, T = 300°K.

X \ X_o	0.0338I	0.15000	0.2[illegible]19	0.[illegible]38I	0.45000	0.56619	0.6338I	0.75000
0.0	0.00000000	0.00000000	0.00000000	0.00000000	0.00000000	0.00000000	0.00000000	0.00000000
0.3	-0.0000I768	0.00II3[illegible]	0.00369522	-0.00008433	-0.00007881	-0.00007781	-0.00007007	-0.00006311
0.6	-0.00089970	0.00022753	0.00273012	0.00476141	0.00918356	0.0[illegible]	-0.00I20748	-0.00I09176
0.9	-0.00304969	-0.00I98903	0.00035471	0.00224727	0.00632125	0.0[illegible]	0.0I569658	0.02285350
I.2	-0.00553137	-0.00454765	-0.00[illegible]8591	-0.00065653	0.00301573	0.00814715	0.0II31674	0.0I738I03
I.5	-0.00726164	-0.00633208	-0.00[illegible]29662	-0.00268091	0.00071216	0.00542460	0.00826415	0.0I355998
I.8	-0.00807945	-0.00717530	-0.00[illegible]0064	0.00063836	-0.00077794	0.00413773	0.00682066	0.0II74759
2.I	-0.00835959	-0.00746420	-0.00551004	-0.00196816	-0.00075098	0.00369679	0.00632645	0.0III2828
2.4	-0.00843238	-0.00753924	-0.00559042	-0.00205132	-0.00084791	0.00356232	0.00619795	0.0[illegible]6720
2.7	-0.00844710	-0.00755445	-0.00560669	-0.00206899	-0.00086753	0.00355911	0.00617192	0.0I093454
3.0	-0.00844945	-0.00755686	-0.00560928	-0.00207130	-0.00080767	0.00355540	0.00616775	0.0I092931
3.3	- " -	- " -	- " -	- " -	- " -	- " -	- " -	- " -
3.6	- " -	- " -	- " -	- " -	- " -	- " -	- " -	- " -

X \ X_o	0.8619	0.9338I	I.05000	I.I6619	I.2[illegible]I	I.35000	I.4619	I.53I8I
0.0	0.00000000	0.00000000	0.00000000	0.00000000	0.00000000	0.00000000	0.00000000	0.00000000
0.3	-0.00005042	-0.0000523I	-0.00004555	-0.00003915	-0.00003565	-0.[illegible]0I3	-0.00002526	-0.00002269
0.6	-0.00097237	-0.00090260	-0.00078634	-0.00067626	-0.00061592	-0.[illegible]027	-0.[illegible]3535	-0.[illegible]I4
0.9	0.03I3I380	-0.00516615	-0.00450094	-0.00387249	-0.00352927	-0.[illegible]3I	-0.[illegible]3[illegible]	-0.00223941
I.2	0.024I8223	0.02860513	0.03707648	0.04726342	-0.0I3I2507	-0.0[illegible]160	-0.[illegible]I72	-0.00835[illegible]70
I.5	0.0I92I437	0.02272657	0.0290I754	0.03584188	0.04016911	0.04882067	0.06055760	-0.0[illegible]66[illegible]I
I.8	0.0I686709	0.0I994841	0.02520420	0.03042800	0.03843125	0.04[illegible]5669	0.0[illegible]A15	0.04863006
2.I	0.0I606I55	0.0I899514	0.02389354	0.02856760	0.03III383	0.03529400	0.03937007	0.04I67944
2.4	0.0I5852I4	0.0I874709	0.02355250	0.02808235	0.03050884	0.[illegible]I79	0.03796723	0.03984873
2.7	0.0I580963	0.0I869672	0.02348312	0.02798346	0.03038536	0.[illegible]23	0.03767931	0.03947169
3.0	0.0I580281	0.0I868863	0.02347I97	0.02796751	0.03036940	0.[illegible]I3	0.03763262	0.[illegible]I0I0
3.3	- " -	- " -	- " -	- " -	- " -	0.[illegible]I5	0.03762634	0.03940[illegible]0
3.6	- " -	- " -	- " -	- " -	- " -	- " -	- " -	- " -

X \ X_o	I.65000	I.766I9	I.8338I	I.95000	2.06619	2.I938I	2.25000	2.36619
0.0	0.00000000	0.00000000	0.00000000	0.00000000	0.00000000	0.00000000	0.00000000	0.00000000
0.3	-0.0000I873	-0.0000I534	-0.0000I365	-0.0000III2	-0.0000090I	-0.00000797	-0.00000643	-0.00000517
0.6	-0.00032355	-0.00026500	-0.00023566	-0.000I9I95	-0.000I5566	-0.000I3757	-0.000III08	-0.00008942
0.9	-0.00I85I58	-0.00I52I03	-0.00I33I50	-0.00I08984	-0.00089220	-0.00076892	-0.0006370I	-0.0005I3I0
I.2	-0.00690375	-0.00567075	-0.00504480	-0.00411255	-0.00333445	-0.00294940	-0.00238385	-0.00192200
I.5	-0.02053488	-0.0I689I78	-0.0I503337	-0.0I2267I0	-0.00997333	-0.00883I74	-0.00714729	-0.00577198
I.8	0.05706397	0.06909479	-0.0386725I	-0.03166380	-0.02582370	-0.02290679	-0.0I860997	-0.0I5I0000
2.I	0.04589I9	0.05068797	0.05406906	0.06I94774	0.07406926	-0.052835I8	-0.04324856	-0.03534362
2.4	0.04293770	0.04780I7	0.0474II68	0.05052993	0.06I9I369	0.05703829	0.06A20493	0.07573630
2.7	0.04232458	0.0475452	0.0460II43	0.048I0060	0.0498934[illegible]	0.0509996I	0.05330619	0.05596070
3.0	0.0422[illegible]375	0.04458469	0.04577844	0.0476911I	0.0491[illegible]56I8	0.04995237	0.05I365I7	0.0523550I
3.3	0.0422[illegible]056	0.04456[illegible]20	0.04574754	0.0476362I	0.04905607	0.04980875	0.05I05352	0.05I83I57
3.6	- " -	- " -	- " -	0.04763037	0.04904529	0.049793I4	0.05I0635I	0.05I77250
3.9	- " -	- " -	- " -	- " -	- " -	- " -	- " -	0.05I76728

Table 13 (continued)

X \ X_0	2.5[illegible]	2.55000	2.6661[illegible]	2.7[illegible]81	2.85000	2.9661[illegible]9	3.0338[illegible]	3.15000
0.0	0.00000000	0.00000000	0.00000000	0.00000000	0.00000000	0.00000000	0.00000000	0.00000000
0.3	-0.00000457	-0.00[illegible]0365	-0.00300[illegible]52	-0.00000[illegible]56	-0.00000203	-0.00000[illegible]6I	0.00000000	0.00000000
0.6	-0.00007876	-0.00[illegible]0315	-0.00005 5I	-0.00004427	-0.00003524	-0.00002798	-0.00002296	-0.00001810
0.9	-0.00045203	-0.00[illegible]6278	-0.00029053	-0.00025485	-0.00020309	-0.0001[illegible]32	-0.0001[illegible]9I	-0.00011007
1.2	-0.00[illegible]395	-0.00[illegible]137	-0.00109162	-0.00095888	-0.00076566	-0.0006[illegible]I4	-0.00053[illegible]03	-0.00042023
1.5	-0.00[illegible]77I	-0.00[illegible]38	-0.00329725	-0.00290069	-0.00232264	-0.00185410	-0.00162229	-0.00128711
1.8	-0.00[illegible]5018	-0.01079250	-0.00871196	-0.00768364	-0.00617[illegible]I	-0.00495554	-0.00434985	-0.00345882
2.1	-0.03[illegible]887	-0.02559846	-0.02[illegible]564	-0.01[illegible]339	-0.0[illegible]493996	-0.01207239	-0.01064710	-0.00[illegible]548I
2.4	-0.06570[illegible]	-0.05441524	-0.04[illegible]760	-0.04015223	-0.03300060	-0.02702[illegible]33	-0.02400134	-0.01952489
2.7	0.05835911	0.06478409	0.07499124	-0.0[illegible]1677	-0.06463132	-0.05433652	-0.04895313	-0.04072538
3.0	0.05310423	0.05492674	0.05[illegible]705	[illegible]	0.06415128	0.07246950	-0.08432166	-0.07[illegible]2111
3.	0.05233129	0.05340816	0.0[illegible]	0.05[illegible]246	0.05567870	0.0572[illegible]618	0.05879667	[illegible]
.6	0.05224285	0.05[illegible]873	[illegible]	0.0[illegible]96800	0.05450662	0.05463[illegible]	0.05518595	0.05[illegible]83I
	0.05223493	0.05[illegible]28	0.0[illegible]3[illegible]	0.05[illegible]3[illegible]5	0.05[illegible]8859	0.05457595	0.05477853	0.05510961
..	- " -	- " -	- " -	0.05[illegible]02	0.05437[illegible]56	0.05455[illegible]39	0.05474[illegible]9[illegible]	0.05502[illegible]40
.[illegible]	- " -	- " -	- " -	- " -	- " -	- " -	- " -	0.05[illegible]744

X \ Y_0	3.2661[illegible]9	3.3338I	3.45000	3.5661[illegible]9	3.6338I	3.75000	3.8661[illegible]S	3.[illegible]I
0.0	0.00000[illegible]00	0.00000000	0.00000000	0.00000000	0.00000000	0.00000000	0.00000000	0.00[illegible]0000
0.3	0.00000000	0.00000000	0.00000[illegible]00	-0.00000004	-0.00000040	0.00000000	0.00000000	0.0000[illegible]
0.6	-0.0000I423	-0.0000I[illegible]36	-0.00000064	-0.00000789	-0.00000[illegible]84	-0.00000490	-0.00000380	0.00000000
0.[illegible]	-0.0000[illegible]659	-0.00007517	-0.00005876	-0.00004609	-0.00003[illegible]975	-0.00003[illegible]095	-0.0000[illegible]3I	-0.0000[illegible]6I I
I.2	-0.00033II3	-0.00028775	-0.0002[illegible]527	-0.00017596	-0.00015[illegible]80	-0.0001I[illegible]08	-0.0000[illegible]76	-0.0000[illegible]4I5
I.5	-0.[illegible]0I0I772	-0.00068587	-0.00069567	-0.0005[illegible]4II	-0.0004[illegible]027	-0.0003[illegible]405	-0.[illegible]0002[illegible]018	-0.0002[illegible]I5
I.8	-0.00[illegible]75572	-0.00[illegible]40594	-0.00[illegible]898I6	-0.00[illegible]49I00	-0.00[illegible]29[illegible]I7	-0.00[illegible]0[illegible]73	-0.[illegible]0007[illegible]08	[illegible]
2.I	-0.00684587	-0.00600[illegible]00	-0.00[illegible]770I4	-0.00[illegible]77I4I	-0.[illegible]0I2[illegible]I00	-0.00[illegible]257[illegible]03	-[illegible].00200[illegible]46	-0.00[illegible]7[illegible]4I2
2.4	-0.0I580765	-0.0I[illegible]94[illegible]I	-0.0I[illegible]206I4	-0.00[illegible]85I32	-0.007[illegible]4056	-0.006[illegible]I[illegible]3I	-0.00[illegible]87550	-0.[illegible]0[illegible]2[illegible]
2.7	-0.03[illegible]63987	-0.03000I56	-0.02[illegible]5I76I	-0.0I[illegible]900I[illegible]	-0.0[illegible]756436	-0.0I4I0[illegible]52	-[illegible].0II[illegible]4[illegible]4	-[illegible].00[illegible]4[illegible]7
3.0	-0.0634I450	-0.05[illegible]7243I	-0.04[illegible]3I22	-0.04[illegible]6822	-0.03[illegible]637859	0.0[illegible]387[illegible]64	-0.[illegible]4[illegible]3[illegible]36	-0.0[illegible]146[illegible]7[illegible]
3.3	0.06889785	-0.08[illegible]89297	-0.08[illegible]605[illegible]0	-0.07[illegible]04236	-0.06[illegible]327[illegible]4	-0.05[illegible]678[illegible]35	-0.[illegible]4[illegible]8[illegible]4	-0.04[illegible]06I[illegible]
3.6	0.05[illegible]20840	0.05[illegible]380I2	0.06[illegible]2976	0.06[illegible]60[illegible]3	-0.[illegible]093I[illegible]0[illegible]	-0.08[illegible]2[illegible]7	-[illegible].0[illegible]40 59[illegible]8	-0.07[illegible]40[illegible]3
3.9	0.055 I665	0.05550950	0.05592I0I	0.05691946	0.0578[illegible]265	0.05[illegible]4[illegible]74	[illegible].0[illegible]68	-0.0545[illegible]72
4.2	0.055I3715	0.0552I696	0.0552537I	0.05545867	0.05566I08	0.0559[illegible]45	[illegible].05[illegible]9I9	0.0572730[illegible]
4.5	0.055I2509	0.0551[illegible]658	0.05520337	0.05533454	0.05545306	0.0554[illegible]8[illegible]	0.0554[illegible]5	0.05560333
4.8	- " -	- " -	0.05520066	0.05532745	0.0554[illegible]0[illegible]	0.0554[illegible]5[illegible]6	[illegible].05540662	0.05545685
5.I	- " -	- " -	- " -	- " -	[illegible].05544006	[illegible].05[illegible]4[illegible]77	[illegible]05540243	[illegible]44521

X \ X_0	4.05000	4.I66I9	4.2338I	4.35000	4.466I9	4.533[illegible]	4.65000	4.766I9
0.0	0.00000000	0.00000000	0.00000000	0.00000000	0.00000000	0.00000000	0.00000000	0.00000000
0.3	0.00000000	0.00000000	0.00000000	0.00000000	0.00000000	0.00000000	0.00000000	0.00000000
0.6	0.00000000	0.00000000	0.00000000	0.00000000	0.00000000	0.00000000	0.00000000	0.00000000
0.9	-0.00000960	0.00000000	0.00000000	0.00000000	0.00000000	0.00000000	0.00000000	0.00000000
I.2	-0.00006663	-0.00002043	-0.00005739	-0.0000[illegible]855	0.00000000	0.00000000	0.00000000	0.0001II23
I.5	-0.00017599	-0.000II380	-0.000I4495	-0.000I0077	-0.0000041[illegible]6	0.00000000	-0.0000[illegible]130	-0.000[illegible]372
I.8	-0.0005048I	-0.00037I63	-0.0003674I	-0.00023508	-0.00007992	-0.00004I89	-0.00022090	-0.00091[illegible]05
2.I	-0.00I32868	-0.00099960	-0.000896I8	-0.0006[illegible]504	-0.00038509	-0.00036593	-0.00057956	-0.00[illegible]3[illegible]3[illegible]
2.4	-0.00328I50	-0.00250434	-0.002I872I	-0.00I62835	-0.00I20597	-0.00I08799	-0.00II786I	-0.00I74[illegible]02
2.7	-0.007[illegible]299I	-0.00604528	-0.00527485	-0.00409968	-0.003I4555	-0.002790[illegible]20	-0.00241243	-0.[illegible]246[illegible]47
3.0	-0.0I723394	-0.0I[illegible]72082	-0.0II95889	-0.00946873	-0.00738681	-0.00637318	-0.005I4667	-0.00450[illegible]74
3.3	-0.035558I7	-0.02902371	-0.02563822	-0.02[illegible]8032	-0.0I645830	-0.0I437888	-0.0II38862	-0.00935286
3.6	-0.06497496	-0.0554I284	-0.05003087	-0.04I66465	-0.03408663	-0.03020319	-0.02437766	-0.0I985250
3.9	-0.09373526	-0.08772935	-0.08276624	-0.[illegible]7[illegible]243I3	-0.063I2526	-0.05732056	-0.048III59	-0.0400I5I4
4.2	0.05853179	0.05627941	-0.09431748	-0.09826976	-0.09471650	-0.09050902	-0.08150549	-0.07I47169
4.5	0.05587333	0.05634577	0.05685I40	0.05724634	0.05253678	-0.09291339	0.I0I80516	30.I0I54927
4.8	0.0555II39	0.055526I3	0.05563832	0.0557II32	0.056I0547	0.05645440	0.056I5662	0.04878330
5.I	0.05549026	0.05546843	0.05553602	0.05545015	0.0555I282	0.0556I0I9	0.05555795	0.05540655
5.4	- " -	0.05546597	0.05553I42	0.05543666	0.05547396	0.05553953	0.05537227	0.05499020
5.7	- " -	- " -	- " -	- " -	- " -	- " -	0.05536370	0.05496426
							"	" -

Table 14 Table of the function $g_{ois}(x_o \to x)$ for water, T = 300°K.

x \ x_o	0.03381	0.15000	0.26619	0.33381	0.45000	0.56619	0.63381	0.75000	0.86619	0.93381	1.05000	1.16619
0.03381	∞	0.08512	0.01405	0.00717	0.00309	0.00171	0.00131	0.00092	0.00071	0.00063	0.00053	0.00046
0.15000	7.27609	∞	0.69999	0.24676	0.08077	0.03955	0.02923	0.01962	0.01478	0.01296	0.01080	0.00932
0.26619	6.39282	3.72723	∞	3.90596	0.51946	0.18445	0.12317	0.07354	0.05233	0.04478	0.03626	0.03075
0.33381	6.17674	2.48817	7.40420	∞	1.70255	0.42080	0.25178	0.13641	0.09103	0.07636	0.06023	0.05026
0.45000	5.95705	1.82144	2.20013	3.80791	∞	2.16653	0.93094	0.37273	0.21185	0.16795	0.12433	0.09982
0.56619	5.82750	1.57866	1.38272	1.66582	3.83474	∞	5.47571	1.13829	0.49062	0.35254	0.23603	0.17847
0.63381	5.80276	1.50894	1.19431	1.28924	2.13129	7.08260	∞	2.57746	0.84085	0.55389	0.33940	0.24467
0.75000	5.74948	1.42905	1.01150	0.98547	1.20391	2.07722	3.63638	∞	2.71500	1.37733	0.65699	0.41834
0.86619	5.67643	1.37458	0.91394	0.83964	0.87362	1.14308	1.51460	3.46634	∞	5.09826	1.49338	0.74535
0.93381	5.58017	1.33738	0.86769	0.78129	0.76833	0.91120	1.10683	1.95081	5.65585	∞	2.70264	1.12735
1.05000	5.31093	1.25852	0.79326	0.69573	0.64213	0.68874	0.76570	1.05058	1.87040	3.05124	∞	2.52121
1.16619	4.89493	1.14977	0.71235	0.61489	0.54597	0.55153	0.58457	0.70845	0.98863	1.34789	2.77595	∞
1.23381	4.58962	1.07451	0.66089	0.56677	0.49536	0.48898	0.50889	0.58997	0.76562	0.95006	1.64354	4.28434
1.35000	3.98606	0.92932	0.56528	0.48167	0.41284	0.39633	0.40381	0.44527	0.53400	0.61974	0.89756	1.50000
1.46619	3.32992	0.77396	0.46749	0.39513	0.33404	0.31465	0.31746	0.33950	0.38947	0.43589	0.56361	0.82250
1.53381	2.94685	0.68405	0.41198	0.34736	0.29197	0.27286	0.27251	0.28758	0.32562	0.35961	0.44994	0.61464
1.65000	2.31464	0.53640	0.32182	0.27046	0.22565	0.20876	0.20697	0.21499	0.23710	0.25756	0.31058	0.39847
1.76619	1.73777	0.40225	0.24070	0.20295	0.16842	0.15471	0.15261	0.15688	0.17063	0.18350	0.21621	0.26784
1.83381	1.44896	0.33519	0.20031	0.16777	0.13893	0.12728	0.12595	0.12887	0.13936	0.14926	0.17430	0.21318
1.95000	1.02992	0.23805	0.14198	0.11873	0.09796	0.08932	0.08766	0.08964	0.09625	0.10259	0.11853	0.14285
2.06619	0.70642	0.16317	0.09717	0.08115	0.06677	0.06065	0.05937	0.06010	0.06453	0.06851	0.07859	0.09393
2.13381	0.55829	0.12891	0.07671	0.06402	0.05260	0.04770	0.04663	0.04709	0.05043	0.05345	0.06110	0.07271
2.25000	0.36286	0.08374	0.04977	0.04150	0.03402	0.03077	0.03003	0.03021	0.03224	0.03408	0.03877	0.04588
2.36619	0.22831	0.05267	0.03127	0.02605	0.02132	0.01924	0.01874	0.01880	0.01987	0.02109	0.02390	0.02816
2.43381	0.17184	0.03963	0.02352	0.01959	0.01601	0.01443	0.01405	0.01407	0.01484	0.01573	0.01780	0.02093
2.55000	0.10294	0.02373	0.01407	0.01171	0.00956	0.00860	0.00836	0.00835	0.00879	0.00924	0.01048	0.01229
2.66619	0.05986	0.01379	0.00817	0.00680	0.00554	0.00497	0.00483	0.00482	0.00506	0.00531	0.00599	0.00700
2.73381	0.04308	0.00993	0.00588	0.00489	0.00398	0.00357	0.00347	0.00345	0.00362	0.00379	0.00427	0.00499
2.85000	0.02394	0.00552	0.00326	0.00271	0.00221	0.00197	0.00192	0.00190	0.00199	0.00209	0.00233	0.00272
2.96619	0.01251	0.00288	0.00171	0.00142	0.00116	0.00104	0.00101	0.00102	0.00106	0.00112	0.00124	0.00144
3.03381	0.00857	0.00197	0.00000	0.00000	0.00000	0.00000	0.00000	0.00000	0.00000	0.00000	0.00000	0.00000
3.15000	0.00437	0.00101	-"-	-"-	-"-	-"-	-"-	-"-	-"-	-"-	-"-	-"-
3.26619	0.00216	0.00050	-"-	-"-	-"-	-"-	-"-	-"-	-"-	-"-	-"-	-"-
3.33381	0.00000	0.00000	-"-	-"-	-"-	-"-	-"-	-"-	-"-	-"-	-"-	-"-
3.45000	-"-	-"-	-"-	-"-	-"-	-"-	-"-	-"-	-"-	-"-	-"-	-"-

x \ x_o	1.23381	1.35000	1.46619	1.53381	1.65000	1.76619	1.83381	1.95000	2.06619	2.13381	2.25000	2.36619
0.03381	0.00043	0.00039	0.00035	0.00033	0.00030	0.00028	0.00026	0.00024	0.00022	0.00021	0.00019	0.00018
0.15000	[illegible]	[illegible]	0.00695	0.00658	0.00599	0.00545	0.00518	0.00475	0.00436	0.00416	0.00383	0.00354
0.26619	0.02833	[illegible]	0.02217	0.02109	0.01916	0.01737	0.01648	0.01508	0.01383	0.01317	0.01213	0.01120
0.33381	0.04601	0.04031	0.03580	0.03367	0.03049	0.02774	0.02614	0.02388	0.02188	0.02082	0.01915	0.01768
0.45000	0.08995	0.07726	0.06769	0.06330	0.05689	0.05149	0.04841	0.04406	0.04025	0.03825	0.03511	0.03235
0.56619	0.15716	0.13129	[illegible]	0.10471	0.09316	0.08372	0.07849	0.07111	0.06472	0.06139	0.05622	0.05167
0.63381	0.21155	0.17302	[illegible]	0.13527	0.11946	0.10682	0.10047	0.09027	0.08195	0.07763	0.07096	0.06512
0.75000	0.34602	0.26916	[illegible]	0.20140	0.17508	0.15491	0.14503	0.13022	0.11704	0.11060	0.10073	0.09216
0.86619	0.5731	0.41213	0.32547	0.29114	0.24652	0.21512	0.20023	0.17853	0.16043	0.15123	0.13723	0.12434
0.93381	[illegible]	[illegible]	0.40410	0.35669	0.29710	0.24665	0.23791	0.21110	0.18897	0.17781	0.16094	0.14642
1.05000	1.74140	[illegible]	0.58991	0.50385	0.40443	0.34141	0.31367	0.27534	0.24474	0.22948	0.20669	0.18735
1.16619	[illegible]	1.5355	0.91168	0.72896	0.54952	0.44709	0.40628	0.35144	0.30977	0.28922	0.25903	0.23377
1.23381	∞	[illegible]	[illegible]	0.91482	0.66203	0.52378	0.47014	0.40209	0.35231	0.32795	0.29260	0.26336
1.35000	2.39516	∞	2.32552	1.50121	0.93566	[illegible]	0.60471	0.50534	0.43457	0.40201	0.35587	0.31858
1.46619	1.06314	[illegible]	∞	3.46243	1.46065	0.94371	0.79266	0.63167	0.53064	0.48701	0.42674	0.37941
1.53381	0.76616	1.29583	3.23612	∞	[illegible]	1.17184	0.94229	0.72268	0.59562	[illegible]	0.47186	0.41756
1.65000	[illegible]	0.69455	1.17416	1.85005	∞	2.02010	1.38542	0.93562	[illegible]	[illegible]	0.55755	0.48816
1.76619	[illegible]	0.42440	0.62551	0.63105	1.66607	∞	2.85703	1.32666	[illegible]	[illegible]	0.65793	0.56654
1.83381	0.24502	0.32482	0.46102	0.58637	1.00251	2.50634	∞	1.82694	[illegible]	0.90858	0.72746	0.61726
1.95000	[illegible]	[illegible]	0.28460	0.34837	0.52416	0.90177	[illegible]	∞	1.71205	1.23087	0.88448	0.71891
2.06619	[illegible]	[illegible]	0.17846	0.21420	[illegible]	[illegible]	[illegible]	[illegible]	∞	2.35362	1.17214	0.85799
2.13381	[illegible]	[illegible]	[illegible]	0.16182	0.22610	0.13475	0.43534	0.76133	[illegible]	∞	1.54991	0.98143
2.25000	[illegible]	[illegible]	[illegible]	0.05912	0.13618	0.19487	0.24556	0.38541	[illegible]	1.09188	∞	1.45432
2.36619	0.03152	[illegible]	0.05067	0.05966	0.08111	0.11415	0.14173	0.21310	[illegible]	[illegible]	0.98930	∞
2.43381	0.02339	[illegible]	[illegible]	0.04395	[illegible]	[illegible]	0.10281	0.15252	0.23759	0.31726	0.57880	1.53743
2.55000	0.01370	[illegible]	[illegible]	0.02550	[illegible]	0.04771	0.05860	0.06573	[illegible]	0.16954	0.28030	0.52085
2.66619	[illegible]	[illegible]	0.01232	0.01442	[illegible]	[illegible]	0.03277	[illegible]	[illegible]	0.09180	0.14648	[illegible]
2.73381	0.00555	[illegible]	0.00874	0.01022	[illegible]	[illegible]	0.02311	0.03345	[illegible]	0.06401	0.10105	[illegible]
2.85000	0.00302	[illegible]	0.00474	[illegible]	[illegible]	[illegible]	[illegible]	[illegible]	[illegible]	0.03406	0.05312	[illegible]
2.96619	[illegible]	[illegible]	[illegible]	[illegible]	[illegible]	[illegible]	0.00652	[illegible]	[illegible]	[illegible]	[illegible]	[illegible]
3.03381	[illegible]	[illegible]	[illegible]	0.00198	[illegible]	0.00363	0.00442	[illegible]	[illegible]	[illegible]	[illegible]	[illegible]
3.15000	[illegible]	[illegible]	0.00086	0.00100	0.00133	0.00183	0.00222	[illegible]	[illegible]	[illegible]	[illegible]	[illegible]
3.26619	[illegible]	[illegible]	0.00042	0.00049	0.00065	0.00089	[illegible]	[illegible]	[illegible]	0.00292	0.00451	[illegible]
3.33381	[illegible]	0.00000	[illegible]	0.00000	0.00000	0.00000	0.00071	[illegible]	0.00150	[illegible]	[illegible]	[illegible]
3.45000	-"-	-"-	-"-	-"-	-"-	-"-	[illegible]	[illegible]	0.00070	[illegible]	[illegible]	[illegible]

Table 14 (continued)

X / X_0	2.4338I	2.55000	2.6661I	2.7338I	2.85000	2.9661I	3.0338I	3.15000	3.2661I	3.3338I	3.45000	3.5661I
0.0338I	0.00017	0.00015	0.00015	0.00014	0.00013	0.00012	0.00012	0.00011	0.00010	0.00010	0.00009	0.00009
0.15000	0.00139	0.00115	0.00094	0.00085	0.00065	0.00041	0.00232	0.00217	0.00203	0.00195	0.00183	0.00172
0.2661I	0.01071	0.00994	0.00926	0.00891	0.00835	0.00761	0.00731	0.00683	0.00639	0.00615	0.00577	0.00542
0.3338I	0.01689	0.01567	0.01459	0.01402	0.01314	0.01199	0.01151	0.01075	0.01005	0.00967	0.00907	0.00853
0.45000	0.03089	0.02861	0.02660	0.02554	0.02391	0.02184	0.02056	0.01956	0.01828	0.01759	0.01650	0.01549
0.5661I	0.04927	0.04555	0.04222	0.04056	0.03785	0.03468	0.03327	0.03101	0.02897	0.02787	0.02612	0.02452
0.6338I	0.06205	0.05729	0.05311	0.05092	0.04753	0.04353	0.04174	0.03889	0.03632	0.03493	0.03272	0.03071
0.75000	0.08768	0.08076	0.07470	0.07153	0.06664	0.06219	0.05858	0.05454	0.05088	0.04891	0.04579	0.04294
0.8661I	0.11809	0.10847	0.10008	0.09571	0.08897	0.08311	0.08008	0.07480	0.06986	0.06720	0.06296	0.05915
0.9338I	0.13886	0.12657	0.11660	0.11141	0.10342	0.09649	0.09290	0.08682	0.07883	0.07572	0.07078	0.06631
1.05000	0.17735	0.16197	0.14851	0.14142	0.13035	0.12052	0.11529	0.10691	0.09949	0.09551	0.08921	0.08351
1.1661I	0.22086	0.20113	0.18397	0.17499	0.16102	0.14865	0.14209	0.13178	0.12234	0.11738	0.10955	0.10246
1.2338I	0.24848	0.22587	0.20631	0.19610	0.18024	0.16624	0.15883	0.14721	0.13661	0.13103	0.12220	0.11424
1.35000	0.29985	0.27163	0.24746	0.23492	0.21552	0.19847	0.18946	0.17538	0.16283	0.15614	0.14523	0.13575
1.4661I	0.35606	0.32137	0.29193	0.27673	0.25339	0.23294	0.22222	0.20545	0.19054	0.18261	0.17060	0.15841
1.5338I	0.39108	0.35200	0.31919	0.30231	0.27651	0.25398	0.24212	0.22372	0.20730	0.19863	0.18495	0.17216
1.65000	0.45523	0.40764	0.36827	0.34824	0.31783	0.29139	0.27761	0.25615	0.23715	0.22709	0.21132	0.19718
1.7661I	0.52531	0.46705	0.42001	0.39644	0.36084	0.33031	0.31442	0.28974	0.26802	0.25651	0.23836	0.22223
1.8338I	0.56924	0.50338	0.45142	0.42546	0.38664	0.35343	0.33625	0.30969	0.28619	0.27382	0.25456	0.23721
1.95000	0.65414	0.57042	0.50766	0.47714	0.43204	0.39404	0.37448	0.34436	0.31796	0.30411	0.28225	0.26262
2.0661I	0.76019	0.64630	0.56775	0.53110	0.47889	0.43546	0.41330	0.37952	0.35006	0.33459	0.31044	0.28859
2.1338I	0.84165	0.69778	0.60596	0.56472	0.50723	0.45995	0.43619	0.40002	0.36875	0.35238	0.32677	0.30407
2.25000	1.08171	0.81270	0.68116	0.62799	0.55747	0.50345	0.47650	0.43558	0.40084	0.38269	0.35465	0.32988
2.3661I	1.95455	1.02729	0.78335	0.70624	0.61390	0.54857	0.51792	0.47153	0.43301	0.41314	0.38239	0.35561
2.4338I	∞	1.31825	0.87613	0.76649	0.65274	0.57671	0.54210	0.49296	0.45246	0.43078	0.39849	0.36998
2.55000	0.84971	∞	1.24124	0.94809	0.73769	0.63285	0.58947	0.53170	0.48479	0.46143	0.42596	0.39522
2.6661I	0.35211	0.77392	∞	1.64621	0.90252	0.70979	0.64722	0.57343	0.51922	0.49287	0.45370	0.42012
2.7338I	0.23050	0.44232	1.23178	∞	1.13231	0.76126	0.69406	0.60242	0.54054	0.51206	0.47013	0.43477
2.85000	0.11615	0.20381	0.39992	0.67055	∞	1.07087	0.83615	0.66801	0.58360	0.54853	0.49962	0.46045
2.9661I	0.05891	0.10028	0.18039	0.26536	0.61420	∞	1.40537	0.79807	0.64330	0.59252	0.53635	0.49782
3.0338I	0.03949	0.06661	0.11730	0.16811	0.34200	1.00220	∞	0.98406	0.68950	0.62954	0.55505	0.50478
3.15000	0.01959	0.03279	0.05671	0.07962	0.14909	0.31055	0.53697	∞	0.93502	0.74360	0.60797	0.53619
3.2661I	0.00951	0.01581	0.02716	0.03779	0.06890	0.13241	0.21190	0.45460	∞	1.21603	0.71234	0.62678
3.3338I	0.00616	0.01024	0.01755	0.02436	0.04406	0.08300	0.12367	0.26770	0.82760	∞	0.86560	0.69146
3.45000	0.00287	0.00476	0.00814	0.01127	0.02023	0.03758	0.05494	0.11028	0.24428	0.43615	∞	0.66619
3.5661I	0.00130	0.00216	0.00368	0.00509	0.00911	0.01683	0.02442	0.04754	0.09135	0.15552	0.40363	∞
3.6338I	0.00081	0.00135	0.00230	0.00317	0.00566	0.01043	0.01510	0.02935	0.05633	0.09191	0.22712	0.69263
3.75000	0.00035	0.00059	0.00100	0.00138	0.00246	0.00452	0.00651	0.01257	0.02514	0.03825	0.08216	0.15415
3.8661I	0.00015	0.00025	0.00042	0.00058	0.00104	0.00190	0.00274	0.00528	0.01048	0.01587	0.03333	0.07176
3.9338I	0.00000	0.00000	0.00000	0.00035	0.00062	0.00114	0.00164	0.00315	0.00624	0.00943	0.01970	0.04241
4.05000	- " -	- " -	- " -	0.00014	0.00025	0.00046	0.00066	0.00127	0.00252	0.00381	0.00796	0.01715
4.1661I	- " -	- " -	- " -	0.00006	0.00010	0.00019	0.00026	0.00050	0.00099	0.00150	0.00314	0.00677
4.2338I	- " -	- " -	- " -	0.00000	0.00000	0.00000	0.00000	0.00000	0.00000	0.00000	0.00000	0.00000

X / X_0	3.6338I	3.75000	3.8661I	3.9338I	4.05000	4.1661I	4.2338I	4.35000	4.4661I	4.5338I	4.65000	4.7661I
0.0338I	0.00006	0.00003	0.00008	0.00007	0.00007	0.00007	0.00006	0.00006	0.00006	0.00006	0.00005	0.00005
0.15000	0.00166	0.00157	0.00148	0.00143	0.00135	0.00128	0.00124	0.00118	0.00112	0.00109	0.00104	0.00099
0.2661I	0.00523	0.00493	0.00465	0.00450	0.00426	0.00403	0.00391	0.00371	0.00353	0.00343	0.00326	0.00311
0.3338I	0.00823	0.00775	0.00732	0.00708	0.00669	0.00634	0.00615	0.00583	0.00554	0.00538	0.00512	0.00488
0.45000	0.01495	0.01408	0.01328	0.01285	0.01215	0.01150	0.01115	0.01058	0.01005	0.00976	0.00929	0.00886
0.5661I	0.02365	0.02226	0.02099	0.02030	0.01919	0.01816	0.01760	0.01670	0.01586	0.01540	0.01466	0.01397
0.6338I	0.02962	0.02787	0.02627	0.02541	0.02401	0.02272	0.02202	0.02088	0.01983	0.01925	0.01832	0.01746
0.75000	0.04140	0.03894	0.03669	0.03547	0.03350	0.03169	0.03070	0.02911	0.02763	0.02683	0.02553	0.02431
0.8661I	0.05578	0.05178	0.04876	0.04712	0.04448	0.04206	0.04074	0.03861	0.03664	0.03557	0.03382	0.03221
0.9338I	0.06389	0.06004	0.05651	0.05461	0.05154	0.04871	0.04718	0.04470	0.04241	0.04116	0.03914	0.03727
1.05000	0.08043	0.07553	0.07106	0.06863	0.06475	0.06116	0.05921	0.05609	0.05320	0.05162	0.04906	0.04671
1.1661I	0.09865	0.09257	0.08701	0.08403	0.07921	0.07477	0.07241	0.06857	0.06499	0.06306	0.05992	0.05700
1.2338I	0.10956	0.10311	0.09693	0.09359	0.08818	0.08317	0.08058	0.07629	0.07229	0.07012	0.06664	0.06334
1.35000	0.13056	0.12236	0.11487	0.11090	0.10446	0.09855	0.09540	0.09040	0.08555	0.08301	0.07875	0.07506
1.4661I	0.15231	0.14269	0.13417	0.12933	0.12174	0.11479	0.11099	0.10505	0.09937	0.09635	0.09179	0.08701
1.5338I	0.16554	0.15504	0.14547	0.14038	0.13210	0.12454	0.12056	0.11388	0.10781	0.10466	0.09908	0.09427
1.65000	0.18898	0.17685	0.16584	0.15995	0.15047	0.14170	0.13716	0.12954	0.12245	0.11882	0.11282	0.10704
1.7661I	0.21370	0.19916	0.18680	0.18014	0.16927	0.15960	0.15439	0.14578	0.13813	0.13420	0.12727	0.12076
1.8338I	0.22790	0.21346	0.19912	0.19194	0.18111	0.17000	0.16413	0.15519	0.14674	0.14216	0.13480	0.12804
1.95000	0.25245	0.23611	0.22141	0.21278	0.20005	0.18829	0.18215	0.17233	0.16356	0.15863	0.15036	0.14283
2.0661I	0.27732	0.25918	0.24288	0.23414	0.22010	0.20659	0.19956	0.18822	0.17795	0.17278	0.16374	0.15546
2.1338I	0.29199	0.27270	0.25548	0.24625	0.23160	0.21806	0.20954	0.19819	0.18711	0.18055	0.17227	0.16367
2.25000	0.31657	0.29592	0.27727	0.26697	0.25104	0.23669	0.22911	0.21456	0.20092	0.19682	0.18657	0.17727
2.3661I	0.34102	0.31852	0.29812	0.28752	0.27033	0.25450	0.24614	0.23110	0.21945	0.21234	0.20020	0.19016
2.4338I	0.35494	0.33151	0.31037	0.29895	0.28112	0.26526	0.25670	0.24105	0.22803	0.22353	0.20954	0.19904
2.55000	0.37898	0.35349	0.33091	0.31891	0.29970	0.28213	0.27317	0.25871	0.24558	0.23891	0.22627	0.21511
2.6661I	0.40262	0.37548	0.35120	0.33813	0.31778	0.29965	0.28963	0.27356	0.26008	0.25282	0.24146	0.23185
2.7338I	0.41637	0.38800	0.36293	0.34947	0.32803	0.30915	0.29921	0.28297	0.26784	0.26076	0.24922	0.23915
2.85000	0.44030	0.40960	0.38258	0.36836	0.34599	0.32549	0.31471	0.29767	0.28268	0.27452	0.26208	0.25136
2.9661I	0.46487	0.43279	0.40239	0.38708	0.36314	0.34190	0.33040	0.31218	0.29606	0.28728	0.27435	0.26305
3.0338I	0.48007	0.44738	0.41407	0.39814	0.37317	0.35103	0.33936	0.32055	0.30364	0.29443	0.28114	0.26964
3.15000	0.50929	0.46801	0.43442	0.41724	0.39077	0.36701	0.35436	0.33472	0.31713	0.30734	0.29320	0.28100
3.2661I	0.54532	0.49501	0.45628	0.43723	0.40699	0.38138	0.36999	0.34872	0.32991	0.31986	0.30438	0.29171
3.3338I	0.57398	0.51258	0.47005	0.44965	0.42038	0.39279	0.37906	0.35733	0.33746	0.32703	0.31084	0.29751
3.45000	0.66749	0.55474	0.49754	0.47314	0.43858	0.40960	0.39479	0.37181	0.35100	0.34006	0.32225	0.30651
3.5661I	1.06530	0.64174	0.53777	0.50151	0.46088	0.42794	0.41157	0.38651	0.36450	0.35298	0.33446	0.31747
3.6338I	∞	0.77000	0.57533	0.52778	0.47567	0.43999	0.42197	0.39544	0.37284	0.36066	0.34164	0.32445
3.75000	0.35885	∞	0.73820	0.60474	0.51143	0.46693	0.44154	0.41203	0.38870	0.37608	0.35630	0.33845
3.8661I	0.12128	0.33390	∞	0.94360	0.58337	0.45604	0.46672	0.43030	0.40253	0.38938	0.36876	0.35019
3.9338I	0.06916	0.17003	0.58656	∞	0.69600	0.52687	0.48750	0.44325	0.41271	0.39925	0.37804	0.35904
4.05000	0.02690	0.06206	0.15650	0.29865	∞	0.66556	0.55237	0.47347	0.43224	0.41827	0.39626	0.37632
4.1661I	0.01043	0.02354	0.05576	0.09528	0.27210	∞	0.84306	0.53439	0.46025	0.44541	0.40442	0.39422

Table 15 Table of the function $f_o(x,x_o)$ for water, T = 300°K.

x \ x_o	0.033EI	0.15000	0.2661 9	0.3338I	0.45000	0.5661 9	0.6338I	0.75000
0.0	0.00000000	0.00000000	0.00000000	0.00000000	0.00000000	0.00000000	0.00000000	0.00000000
0.3	6.98I968I9	3.82452I70	2.7805I034	0.38335934	0.05473730	0.02082538	0.0I428399	0.00885729
0.6	8.77725550	4.40754970	3.83624024	3.63I7802I	3.I7031451	2.25592473	0.62835673	0.I6503356
0.9	I0.50047510	4.83339872	4.I4682629	3.9406498I	3.58I66850	3.23252900	3.03932053	2.638I6I65
I.2	I2.08I52770	5.2I340472	4.30426643	4.I4976533	3.77[illegible]696	3.44627017	3.28240636	3.00009736
I.5	I3.27296430	5.49I4I350	4.55366888	4.29414748	3.90097876	3.5660838I	3.4051II85	3.I3692605
I.8	I3.97I96830	5.65345833	4.65096830	4.37606719	3.96943039	3.62954890	3.468I3408	3.20263I26
2.I	I4.28890540	5.72672872	4.69468860	4.4I264203	3.99963395	3.657II988	3.49526624	3.23033088
2.4	I4.40283620	5.75302539	4.7I032334	4.42568227	4.0I032921	3.66680028	3.5047I805	3.23985047
2.7	I4.43586910	5.76064I66	4.7I484076	4.42944256	4.0I339991	3.66956347	3.50740645	3.24253855
3.0	I4.44369430	5.76244452	4.7I590830	4.43032995	4.0I4I2239	3.6702I08I	3.50803486	3.24316544
3.3	I4.445I7I20	5.76278476	- " -	- " -	- " -	- " -	- " -	- " -
3.6	- " -	- " -	- " -	- " -				
3.9	- " -	- " -	- " -	- " -				

x \ x_o	0.8661 9	0.9338I	I.05000	I.I661 9	I.2338I	I.35000	I.4661 9	I.5338I
0.0	0.00000000	0.00000000	0.00000000	0.00000000	0.00000000	0.00000000	0.00000000	0.00000000
0.3	0.00639I60	0.00551329	0.00450711	0.00303491	0.00355075	0.003I4209	0.00282034	0.00266196
0.6	0.083I3496	0.06365670	0.04577379	0.03621420	0.03247480	0.02774323	0.02423403	0.02263430
0.9	I.89I90330	0.72690374	0.28628634	0.I7451426	0.I4402250	0.II239630	0.09325873	0.08502I37
I.2	2.70425768	2.52913670	2.20I7I030	I.64935657	0.7764I8I9	0.40040II5	0.28I5769I	0.24267549
I.5	2.87172586	2.72728831	2.50549725	2.28I8I075	2.I4570530	I.89029865	I.47934620	0.8I283877
I.8	2.94469420	2.80689252	2.60242236	2.40848740	2.29906839	2.I2639922	I.963I7518	I.86557030
2.I	2.97451844	2.8387I92I	2.63930061	2.45312729	2.34997372	2.I927471 4	2.0544I669	I.97874798
2.4	2.98467582	2.84947506	2.65I55386	2.46765II8	2.3662877I	2.2I324712	2.08III978	2.0I042092
2.7	2.98750600	2.85246I34	2.65493353	2.47I6I757	2.37071436	2.2I824024	2.088I6509	2.0I868557
3.0	2.98816196	2.85314904	2.65570285	2.47251542	2.37I7I300	2.2I997176	2.08973392	2.02051799
3.3	- " -	- " -	- " -	- " -	2.37I8997I	2.22020II9	2.09002506	2.02085725
3.6	- " -	- " -	- " -	- " -	2.37I8997I	2.22020II9	2.09002506	2.02085725
					- " -	- " -	- " -	- " -

x \ λ_o	I.65000	I.7661 9	I.8338I	I.95000	2.0661 9	2.I338I	2.25000	2.3661 9
0.0	0.00000000	0.00000000	0.00000000	0.00000000	0.00000000	0.00000000	0.00000000	0.00000000
0.3	0.00242II8	0.002I9793	0.00208546	0.0019095I	0.00I75266	0.00I66922	0.00I53806	0.00 42I09
0.6	0.02031033	0.0I835I59	0.0I725884	0.0I570006	0.0I433634	0.0I36I9I4	0.0I250052	0.0I I5I250
0.9	0.07415315	0.06583484	0.06I65479	0.[illegible]55462 8I	0.050I4032	0.04743749	0.04328I2I	0.03958850
I.2	0.I9863065	0.I7006804	0.I57I600I	0.I3905346	0.I2433323	0.II695297	0.I0583779	0.09625074
I.5	0.50040799	0.38481068	0.34302681	0.29258061	0.25588I32	0.23846769	0.2I32 I296	0.I9229249
I.8	I.66[illegible]4	I.37973324	0.84873363	0.58820592	0.47954461	0.437I4973	0.38I72259	0.3J9J8913
2.	I.8[illegible]7775	I.75230842	I.68I47587	I.54470594	I.30821I89	0.87687451	0.65803779	0.55818058
2.4	[illegible]	I.8[illegible]4IC	I.7C23I842	I [illegible]7739318	I.59440719	I.54I88490	I.43956484	I.2555545J
2.7	I.9I9[illegible]8	I.83I23486	I.78I43105	I.70549849	I.63751286	I.59858946	I.53746243	I.477I473I
3.0	I.92I[illegible]9	[illegible]46I008	I 78555838	I.7II46034	I.64638502	I.60994II0	I.55525996	I.5062II3I
	.922II593	[illegible]I3	I.7863I403	I.7I254573	I.64798939	I.6II98I84	I.5584I859	I.5II24[illegible]
.6	" -	- " -	I.7864[illegible]79	I.7I27II54	I.64823387	I.[illegible]2292[illegible]	I.558[illegible]703	I.5I20054
3.9	- " -	- " -	" -	- " -	- " -	- " -	- " -	I.5I2I0I80

Table 15 (continued)

λ_0 / X	2.[illegible]38I	2.55000	2.666I9	2.7338I	2.85000	2.96619	3.0338I	3.15000
0.0	0.00000000	0.00000000	0.00000000	0.00000000	0.00000000	0.00000000	0.00000000	0.00000000
0.3	0.00135[illegible]00	0.00126185	0.00117583	0.00113051	0.00106018	0.00096667	0.00092820	0.00086687
0.6	0.01[illegible]1[illegible]2	0.01017824	0.00945641	0.00908462	0.00849647	0.00776845	0.00745406	0.00695404
0.9	0.03769322	0.03475862	0.03218220	0.03084091	0.02875720	0.02664079	0.02541612	0.02353327
1.2	0.09131632	0.08366293	0.07703060	0.07356375	0.06817456	0.06313831	0.06037029	0.05582100
1.5	0.18167353	0.16548337	0.15154477	0.14428958	0.13304594	0.12286577	0.11738655	0.10859287
1.8	0.31873666	0.28808968	0.26224744	0.24895114	0.22853560	0.21040837	0.20077931	0.18553450
2.1	0.51674404	0.45995329	0.41486676	0.39228892	0.35826752	0.32868867	0.31317210	0.28888349
2.4	0.81728553	0.71214416	0.62147226	0.58193074	0.52603392	0.47985894	0.45621564	0.41959033
2.7	1.14389682	1.36069232	1.21586602	0.91233470	0.75402251	0.67145460	0.63352455	0.57934972
3.0	1.47861046	1.43315909	1.38987811	1.36037960	1.30013735	1.11377572	0.92300793	0.78518607
3.3	1.48530651	1.44440025	1.40948146	1.38816276	1.35432413	1.32243868	1.22967425	1.25190026
3.6	1.48631193	1.44[illegible]0925	1.41233609	1.39212084	1.36145218	1.33577117	1.31934809	1.22923471
3.9	1.48[illegible]1940	1.44628027	1.41269557	1.39261750	1.36233863	1.33740210	1.32170412	1.29749825
4.2	- " -	- " -	- " -	1.39267008	1.36243183	1.33757350	1.32195121	1.29797257
4.5	- " -	- " -	- " -	- " -	- " -	- " -	- " -	1.29801441

λ_0 / X	3.26619	3.33381	3.45000	3.56619	3.63381	3.75000	3.86619	3.93381
0.0	0.00000000	0.00000000	.[illegible]0000000	0.00000000	0.00000000	0.00000000	0.00000000	0.00000000
0.3	0.0006[illegible]112	.0007[illegible]0[illegible]	0.00073279	0.00068876	0.00066486	0.00062651	0.00059128	0.00057209
0.6	0.00650020	0.00[illegible]554[illegible]	0.00586482	0.00550837	0.00531518	0.00500548	0.00472136	0.00456665
0.9	0.0[illegible]196562	0.0[illegible]12[illegible]4	0[illegible]778[illegible]	0.0[illegible]855559	0.01789405	0.01683542	0.01586577	0.01533941
1.2	0.0[illegible]0[illegible]45	0.0[illegible]4[illegible]56	0.04670863	0.04375369	0.04216339	0.03962317	0.03729990	0.03604411
1.5	0.1[illegible]0[illegible]2	.0[illegible]0[illegible]29	.0[illegible]46500	0.09457195	0.08142772	0.07642130	0.07187435	0.06947099
1.8	0.17215870	0.16[illegible]11[illegible]6	0.15391690	0.14372946	0.13822816	0.12951740	0.12167457	0.11744304
2.1	[illegible].26767677	0.2[illegible]3[illegible]03	.2[illegible]3[illegible]88	0.22266213	0.21359053	0.20038503	0.18803045	0.18132034
2.4	.38[illegible]591	(.[illegible]/4[illegible]	0.34500718	.32154707	0.30894975	0.28910369	[illegible].27113341	0.26139669
2.7	0.53345[illegible]1	0.[illegible]0[illegible]3[illegible]	0.47282726	0.44[illegible]8564	0.42261012	0.39515669	0.37038583	0.35700881
3.0	0.70[illegible]6[illegible]10	[illegible].6[illegible]48340	0.62246367	0.[illegible]7[illegible]3575	0.55475397	0.51817024	0.48517290	0.46750256
3.3	[illegible].15[illegible]9925	0.[illegible]301[illegible]6[illegible]	0.80772083	0.74079778	0.70811069	0.65885447	0.61562573	0.59274885
3.6	1.26908765	1.[illegible]1[illegible]3[illegible]4	1.[illegible]381[illegible]68	1.[illegible]3[illegible]33	0.93592369	0.8[illegible]0632I	0.76595566	0.73510008
3.9	1.27826825	1.[illegible]653[illegible]646	1.[illegible]45[illegible]652	1.[illegible]27[illegible]911	1.21321109	1.18302433	1.11745514	0.94038602
4.2	1.27920676	[illegible].[illegible]66 [illegible]466	1.[illegible]48[illegible]605	1.[illegible]3[illegible]085	1.22343584	1.20748057	1.19392440	1.18247[illegible]
.5	1.27928926	1.[illegible]68[illegible]685	1.[illegible]4847260	1.[illegible]410740	1.22425689	1.20941009	1.19840998	1.18997180
.8	- " -	- " -	- " -	1.[illegible]34[illegible]755	1.22436000	1.20955044	1.19873171	1.19050082

λ_0 / X	4.05000	4.16619	4.[illegible]3381	4.[illegible]5000	4.46619	4.53381	4.65000	4.76619
0.0	0.00000000	0.00000000	0.00000000	0.00000000	0.00000000	0.00000000	0.00000000	0.00000000
.3	0.00054116	0.00051263	0.[illegible]0047[illegible]	0.00047179	0.00044835	0.00043549	0.00041463	0.00039525
.6	0.00431782	0.00408803	0.00396261	0.00375995	0.00357211	0.00346907	0.00330207	0.00314690
0.9	0.01449185	0.01371105	0.01328541	0.01[illegible]9839	0.01196270	0.01161448	0.01105056	0.01052710
1.2	0.03402050	0.03215893	0.03114597	0.0[illegible]95161	0.02800597	0.02718278	0.02584733	0.02460[illegible]
1.5	0.06544253	0.06180485	0.05982939	0.0[illegible]66550[illegible]	0.05371779	0.05212387	0.04954708	0.04714674
1.8	0.11061959	0.10440114	0.10102980	0.[illegible]5[illegible]7[illegible]	0.09053970	0.08787252	0.08345132	0.07934330
2.1	0.17070285	0.16088845	0.15564614	0.14716167	0.13927302	0.13513249	0.12839605	0.12192534
2.4	0.24601993	0.23172704	0.22416705	0.21[illegible]1111	[illegible].20020467	0.19411574	0.18431146	0.17505627
2.7	0.33589706	0.31642019	0.30611677	0.28915742	0.27380804	0.26566598	0.25206331	0.23913191
3.0	0.43962778	0.41407253	0.40054578	0.37844252	0.35848973	0.34793715	0.33049112	0.31441060
3.3	0.55685819	0.52420776	0.50690701	0.47884550	0.45356935	0.44010772	0.41826780	0.39830186
3.6	0.68877467	0.64726161	0.62543230	0.59040686	0.55886714	0.54211538	0.51501256	0.49035011
3.9	0.84526612	0.78694799	0.75836430	0.71[illegible]5699	0.67507379	0.65441490	0.62120030	0.[illegible]105564
4.2	1.15843186	1.10291798	0.94486262	0.85[illegible]0015	0.80545784	0.77904838	0.73798392	0.70109648
4.5	1.17763885	1.16716537	1.15831500	1.13[illegible]554	1.09188970	0.94963352	0.87246881	0.[illegible]18964
4.8	1.17891563	1.17035313	1.16385095	1.15350608	1.14640942	1.13930892	1.12379213	1.08447695
5.1	1.17899320	1.17054445	1.16417895	1.15435767				

Table 16 Table of the function $g_{1is}(x_o - x)$ for water, T = 300°K.

x_o \ x	0.0338I	0.15000	0.2661 9	0.3338I	0.45000	0.5661 9	0.6338I	0.75000	0.8661 9	0.9338I	I.05000	I.1661 9
0.0338I	∞	-0.0II89	-0.00II3	-0.00046	-0.000I4	-0.00006	-0.00004	-0.00002	-0.00002	-0.00001	-0.00001	-0.00001
0.15000	-I.0I654	∞	-0.I8762	-0.05780	-0.0I499	-0.00598	-0.00395	-0.00220	-0.00I38	-0.00109	-0.00077	-0.00057
0.2661 9	-0.5I353	-0.99905	∞	-0.99I57	-0.I3644	-0.04224	-0.02612	-0.0I353	-0.00813	-0.00634	-0.00438	-0.00319
0.3338I	-0.39367	-0.58282	-I.87772	∞	-0.44762	-0.I0658	-0.05990	-0.02917	-0.0I686	-0.0I294	-0.00879	-0.00634
0.45000	-0.27750	-0.33812	-0.57788	-I.00II4	∞	-0.5I0I7	-0.23312	-0.08887	-0.04596	-0.03407	-0.02251	-0.0I579
0.5661 9	-0.2I289	-0.23885	-0.3I669	-0.42I93	-0.90300	∞	-0.69259	-0.26221	-0.II233	-0.07784	-0.04743	-0.03220
0.6338I	-0.I8648	-0.20369	-0.25327	-0.30670	-0.53372	-0.89583	∞	-0.46637	-0.I8615	-0.I2224	-0.07017	-0.04608
0.75000	-0.I5097	-0.I6029	-0.I8506	-0.2I075	-0.28706	-0.47850	-0.65797	∞	-0.37798	-0.25586	-0.I3I75	-0.08012
0.8661 9	-0.I2278	-0.I2824	-0.I4205	-0.I5548	-0.I8954	-0.26I70	-0.33530	-0.48258	∞	0.03024	-0.22399	-0.I3I23
0.9338I	-0.I0859	-0.II268	-0.I2283	-0.I3245	-0.I5586	-0.20II8	-0.24427	-0.36240	0.03355	∞	-0.I9693	-0.I6576
I.05000	-0.08700	-0.08957	-0.09579	-0.I0I50	-0.II624	-0.I3839	-0.I5831	-0.2I068	-0.28053	-0.22233	∞	-0.07680
I.1661 9	-0.06832	-0.06998	-0.07396	-0.07752	-0.08635	-0.0995I	-0.II0I0	-0.I3568	-0.I7406	-0.I98I9	-0.08I33	∞
I.2338I	-0.05866	-0.05997	-0.06307	-0.0658I	-0.07252	-0.08254	-0.09021	-0.I0803	-0.I3379	-0.I5I95	-0.I5923	0.55933
I.35000	-0.04II	-0.04498	-0.04703	-0.04882	0.05310	-0.05922	-0.06413	-0.07435	-0.08819	-0.09797	-0.II453	-0.08801
I.4661 9	-0.03212	-0.03271	-0.03406	-0.03524	-0.03801	-0.04189	-0.04473	-0.05II7	-0.0591I	-0.06456	-0.07459	-0.07890
I.5338I	-0.02630	-0.02676	-0.02783	-0.02875	-0.03090	-0.03388	-0.03605	-0.04085	-0.04676	-0.05074	-0.05803	-0.06288
I.65000	-0.0I8I7	-0.0I848	-0.0I917	-0.0I976	-0.02II5	-0.02304	-0.02440	-0.02719	-0.03089	-0.03322	-0.0374I	-0.04074
I.7661 9	-0.0I2I5	-0.0I234	-0.0I278	-0.0I3I6	-0.0I404	-0.0I522	-0.0I606	-0.0I778	-0.0I986	-0.02133	-0.02377	-0.02576
I.8338I	-0.00947	-0.00962	-0.00995	-0.0I024	-0.0I090	-0.0II79	-0.0I242	-0.0I37I	-0.0I522	-0.0I630	-0.0I807	-0.0I950
2.00000	0.00632	0.00611	0.00632	0.00649	0.00689	0.00743	-0.00781	-0.00858	-0.00948	-0.0I004	-0.0II06	-0.0II84
2.06619	0.00372	0.00377	0.00389	0.00399	0.00423	0.00455	-0.00477	-0.0052I	-0.00573	-0.00605	-0.00658	-0.00699
2.13381	0.00177	0.00181	0.00190	0.00197	0.00314	0.00337	-0.00353	-0.00385	-0.00422	-0.00444	-0.00482	-0.00508
2.20000	0.00163	0.00166	0.00171	0.00175	0.00185	0.00197	-0.00206	-0.00224	-0.00244	-0.00256	-0.00276	-0.00287
2.26619	0.00094	0.00095	0.00098	0.00100	0.00105	0.00112	-0.00117	-0.00127	-0.00138	-0.00144	-0.00153	-0.00159
2.34381	0.00067	0.00068	0.00000	0.00072	0.00075	0.00080	-0.00083	-0.00090	-0.00097	-0.00102	-0.00108	-0.00111
2.55000	0.00037	0.00037	0.00000	0.00039	0.00041	0.00044	-0.00046	-0.00049	-0.00053	-0.00055	-0.00058	-0.00059
2.66619	0.00020	0.00020	- " -	0.00021	0.00022	0.00023	-0.00024	-0.00026	-0.00028	-0.00029	-0.00030	-0.00030
2.73381	0.00000	0.00000	- " -	0.00000	0.00000	0.00000	0.00000	-0.00018	-0.00019	-0.00019	-0.00020	-0.00020
								- " -	-0.00009	-0.00010	-0.00010	-0.00010

x_o \ x	1.0338I	I.95000	I.4661 9	I.5338I	I.65000	I.7661 9	I.8338I	I.95000	2.0661 9	2.1338I	2.25000	2.3661 9
0.0338I	-0.00001	0.00000	0.00000	0.00000	0.00000	0.00000	0.00000	0.00000	0.00000	0.00000	0.00000	0.00000
0.15000	-0.00048	-0.00027	-0.00019	-0.00026	-0.00021	-0.00017	-0.00015	-0.00012	-0.00010	-0.00008	-0.00008	-0.00006
0.2661 9	-0.00208	-0.00208	-0.00163	-0.00142	-0.00114	-0.00092	-0.00082	-0.00067	-0.00055	-0.00050	-0.00042	-0.00035
0.3338I	-0.00534	-0.00409	-0.00319	-0.00279	-0.00223	-0.00180	-0.00160	-0.00131	-0.00108	-0.00097	-0.00081	-0.00068
0.45000	-0.00819	-0.00594	-0.00470	-0.00403	-0.00323	-0.00429	-0.00380	-0.00310	-0.00255	-0.00229	-0.00190	-0.00160
0.5661 9	-0.01023	-0.01962	-0.01502	-0.01300	-0.01028	-0.00823	-0.00727	-0.00592	-0.00485	-0.00433	-0.00361	-0.00302
0.6338I	-0.03774	-0.02775	-0.02075	-0.01789	-0.01408	-0.01124	-0.00991	-0.00804	-0.00658	-0.00588	-0.00487	-0.00408
0.75000	-0.06356	-0.04654	-0.03349	-0.02864	-0.02214	-0.01756	-0.01543	-0.01246	-0.01015	-0.00904	-0.00747	-0.00622
0.8661 9	-0.10019	-0.07307	-0.04940	-0.04181	-0.03211	-0.02504	-0.02186	-0.01758	-0.01425	-0.01265	-0.01039	-0.00861
0.9338I	-0.12667	-0.09268	-0.05984	-0.05033	-0.03832	-0.02983	-0.02599	-0.02066	-0.01669	-0.01476	-0.01211	-0.00999
I.05000	-0.14933	-0.11011	-0.07807	-0.06498	-0.04872	-0.03753	-0.03252	-0.02569	-0.02050	-0.01810	-0.01472	-0.01198
I.1661 9	0.55554	-0.04010	-0.08745	-0.07487	-0.05623	-0.04307	-0.03716	-0.02914	-0.02306	-0.02021	-0.01621	-0.01318
I.2338I	∞	0.10004	-0.07139	-0.07089	-0.05679	-0.04399	-0.03800	-0.02970	-0.02341	-0.02043	-0.01626	-0.01304
I.35000	0.09707	∞	0.19784	0.00832	-0.0388I	-0.03696	-0.03304	-0.02638	-0.02076	-0.01800	-0.01409	-0.01103
I.4661 9	-0.06397	0.18671	∞	0.85018	0.06894	-0.00356	-0.01166	-0.01364	-0.01162	-0.01016	-0.00770	-0.00560
I.5338I	-0.05937	0.00718	0.79461	∞	0.32297	0.04869	0.01774	0.00147	-0.00175	-0.00187	-0.00124	-0.00030
I.65000	-0.04050	-0.02881	0.05541	0.27774	∞	0.38936	0.15705	0.05467	0.02846	0.02207	0.01644	0.01376
I.7661 9	-0.02613	-0.02263	-0.00236	0.03453	0.32109	∞	0.98507	0.20627	0.09097	0.06683	0.04635	0.03614
I.8338I	-0.01960	-0.01775	-0.00678	0.01164	0.11764	0.86436	∞	0.47048	0.16162	0.11128	0.07238	0.05454
2.00000	-0.01199	-0.01098	-0.00615	0.00071	0.03065	0.14021	0.36446	∞	0.50906	0.27202	0.14451	0.09941
2.06619	-0.00705	-0.00645	-0.00391	-0.00063	0.01190	0.04613	0.09340	0.37955	∞	I.02317	0.30710	0.17518
2.13381	-0.00510	-0.00467	-0.00283	-0.00056	0.00765	0.02810	0.05332	0.16825	0.84832	∞	0.55333	0.25020
2.20000	-0.00226	-0.00215	-0.00126	-0.00046	0.00401	0.01373	0.02443	0.06297	0.17938	0.38981	∞	0.57161
2.26619	-0.00156	-0.00145	-0.00075	-0.00004	0.00229	0.00728	0.01252	0.02947	0.06960	0.11990	0.38884	∞
2.34381	-0.00109	-0.00093	-0.00048	0.00000	0.00167	0.00512	0.00867	0.01983	0.04440	0.07188	0.18739	0.79274
2.55000	-0.00057	-0.00047	-0.00021	- " -	0.00087	0.00282	0.00467	0.01030	0.02189	0.03396	0.07502	0.18861
2.66619	-0.00029	-0.00024	-0.00009	- " -	0.00056	0.00154	0.00251	0.00540	0.01116	0.01693	0.03508	0.07591
2.73381	-0.00010	-0.00015	0.00000	- " -	0.00040	0.00108	0.00174	0.00369	0.00755	0.01137	0.02303	0.04806
2.85000	-0.00010	-0.00008	- " -	- " -	0.00022	0.00057	0.00091	0.00190	0.00384	0.00572	0.01137	0.02286
3.00000	-0.00005	-0.00003	- " -	- " -	0.00012	0.00029	0.00046	0.00096	0.00192	0.00284	0.00558	0.01102
3.06619	.00000	0.00000	- " -	- " -	0.00000	0.00000	0.00031	0.00064	0.00127	0.00188	0.00366	0.00719

Table 16 (continued)

Table 17 Table of the function $f_1(x,x_o)$ for water, T = 300°K.

x \ x_o	0.0338I	0.I5000	0.266I9	0.3338I	0.45000	0.5669I	0.6338I	0.75000
0.0	0.00000000	0.00000000	0.00000000	0.00000000	0.00000000	0.00000000	0.00000000	0.00000000
0.3	0.8421054	0.2252I424	0.[illegible]	-0.0663441I	-0.0I295866	-0.00428368	-0.00269254	-0.00I4I966
0.6	0.7552[illegible]	0.[illegible]	0.[illegible]	0.2062BI78	0.2735367I	0.4I39256I	-0.0638263[illegible]	-0.03729786
0.9	0.70[illegible]	0.0639078[illegible]	0.[illegible]	0.[illegible]	0.I754I625	0.2678388	0.3I99II07	0.40095233
I.2	0.[illegible]	0.0367442[illegible]	0.I03031I8	0.I087046[illegible]	0.I9738[illegible]	0.2243379[illegible]	0.2693073[illegible]	0.33I60856
I.5	0.[illegible]	0.0[illegible]	0.0[illegible]	0.0[illegible]	0.I2344793	0.2067[illegible]	0.2495I3I5	0.30843[illegible]
..	0.[illegible]	0.0[illegible]	0.[illegible]	.0[illegible]	0.II[illegible]	0.I9891002	0.24I9I785	0.29951758
2.I	.[illegible]	0.0I537I40	0.0807[illegible]	0.[illegible]	0.II47[illegible]	0.I9655773	0.[illegible]	0.29719744
2.4	0.[illegible]	0.0.4837[illegible]	0.0801E[illegible]	0.[illegible]	0.I[illegible]	0.[illegible]	0.23[illegible]	0.29[illegible]
2.7	0.[illegible]	0.0[illegible]	- " -	0.0[illegible]	0.[illegible]	0.[illegible]	0.[illegible]	0.2[illegible]
3.0	- " -	- " -	- " -	- " -	- " -	- " -	- " -	0.[illegible]
3.3	- " -	- " -	- " -	- " -	- " -	- " -	- " -	- " -

x \ x_o	0.866I9	0.9338I	I.05000	I.I66I9	[illegible]	I.[illegible]5000	I.46619	I.533[illegible]
0.0	0.00000000	0.00000000	0.00000000	0.00000000	.00000000	0.00000000	.[illegible]	0.00000000
0.3	-0.00086199	-0.00067444	-0.00046800	-0.0003[illegible]	-[illegible]	-0.000[illegible]	-[illegible]	-.[illegible]
0.6	-[illegible].0I772974	-0.0I277279	-0.00815I0I	-0.00565775	-0.[illegible]	-0.00[illegible]	-0.[illegible]	-.[illegible]
0.9	0.4331856I	-0.04596375	-0.05005028	-0.03I04748	-0.[illegible]	-0.0I747544	-[illegible]	-0.[illegible]
I.2	0.39333263	0.42494899	0.46795045	0.43370388	-0.[illegible]	-0.[illegible]	-.[illegible]	-.[illegible]
I.5	0.36550899	0.39386394	0.4333758I	0.46888376	0.[illegible]	0.[illegible]	.[illegible]	.[illegible]
I.8	0.3558394I	0.38342964	0.42I57326	0.4560679[illegible]	0.47I[illegible]	.[illegible]	.[illegible]	0.[illegible]
2.I	0.3528B3033	0.380[illegible]8I0	0.4I80[illegible]	0.45[illegible]8I76	0.[illegible]	0.[illegible]	.[illegible]	.[illegible]
2.4	0.35203869	0.37939655	0.4I7I4750	0.45I34315	0.466[illegible]9I	0.[illegible]	.[illegible]	[illegible]
2.7	0.35I8640I	0.3792I466	0.4I695492	0.45II4690	0.46603752	0.[illegible]	.[illegible]	- " -
3.0	0.35I83I32	0.37918090	0.4I69I988	0.45III2I9	0.46600446	0.[illegible]	- " -	- " -
3.3	- " -	- " -	0.4I69I44I	- " -	- " -	- " -	- " -	- " -

x \ x_o	I.65000	I.766I9	I.8338I	I.95000	[illegible] 066I9	2.I3[illegible]	2.25000	2.3[illegible]
0.0	0.00000000	0.00000000	0.00000000	0.00000000	0.00000000	0.00000000	0.00000000	.00000000
0.3	-0.000I2282	-0.00009937	-0.00008818	-0.00007227	-0.00005969	-0.00005359	-0.00004[illegible]	-[illegible]
0.6	-0.00187628	-0.00150765	-0.00I33349	-0.00I08730	-0.0008938I	-0.00080043	-[illegible]	-0.[illegible]
0.9	-0.00867800	-0.00687I88	-0.00603841	-0.00488537	-0.00398255	-0.00355028	-0.00[illegible]	-.[illegible]
I.2	-0.02305I53	-0.0I795019	-0.0I563559	-0.0I245847	-0.0I00[illegible]	-0.00887845	-0.00725644	-.[illegible]
5	-0.02709882	-0.02[illegible]	-0.02[illegible]	-0.0I958634	-0.0I57I615	-0.0I38[illegible]	-0.0III3I86	-[illegible]
I.8	0.00444326	0.[illegible]	0.08470690	0.005II264	-0.00447679	-0.00546799	-0.00[illegible]	-0.00417740
.I	0.5I9I0652	0.5249[illegible]	0.5[illegible]	0.5[illegible]	0.[illegible]	0.I[illegible]	0.045[illegible]	[illegible]
2.4	0.52047I33	0.5[illegible]	0.[illegible]	0.5[illegible]	0.53339694	0.5[illegible]	.5[illegible]	0.[illegible]
2.7	0.52078669	0.53064346	0.53302363	0.53563669	0.54095036	0.54079326	[illegible]	[illegible]
3.0	0.52085904	0.53[illegible]	0.5333[illegible]	0.536[illegible]	0.542[illegible]	0.54274I64	0.543I4I[illegible]	0.54[illegible]
3.3	- " -	- " -	0.53338070	[illegible].53638584	0.54246[illegible]	0.54305416	[illegible]	0.54[illegible]
3.6	- " -	- " -	- " -	- " -	- " -	0.54305758	.[illegible]	[illegible]

Table 17 (continued)

X \ Y_0	2.4338I	2.55000	2.666I9	2.7338I	2.85000	2.96619	3.0338I	3.15000
0.0	0.00000000	0.00000000	0.00000000	0.00000000	0.00000000	0.00000000	0.00000000	[illegible]
0.3	-0.00003433	-0.00002929	-0.00002519	-0.00002315	-0.00002014	0.00000000	-0.00001647	[illegible]
0.6	-0.00050724	-0.00043129	-0.00036963	-0.00033908	-0.00029408	-0.00025319	-0.00021306	[illegible]
0.9	-0.00220883	-0.00186564	-0.00158886	-0.00145252	-0.00126295	-0.00107127	-0.00090306	[illegible]
I.2	-0.00537049	-0.00448711	-0.00378130	0.00343591	-0.00293543	-0.00248123	-0.00206329	[illegible]
I.5	-0.00799292	-0.00653208	-0.00540237	-0.00484625	-0.00406605	-0.00341056	-0.00284261	[illegible]
I.8	-0.00357914	-0.00260833	-0.00184132	-0.00146048	-0.00084881	-0.00055228	-0.00030700	[illegible]
2.I	0.02360144	0.01892677	0.01GII798	0.01492361	0.01326266	0.01193884	0.01125553	[illegible]
2.4	0.I7346933	0.05065069	0.067I9988	0.05930410	0.04987863	0.04313739	0.03955506	[illegible]
2.7	0.5340674I	0.5I604638	0.45054672	0.42I63I084	0.I36I2590	0.I0856993	[illegible]	[illegible]
3.0	0.54638902	0.54426169	0.5437202J	0.53875065	0.52275819	[illegible]	[illegible]	[illegible]
3.3	0.548I4846	0.54777554	0.55093240	0.54995I73	0.54850503	[illegible]	[illegible]	[illegible]
3.6	0.54838609	0.5482J843	0.55185214	0.55I33552	0.55I35I52	[illegible]	[illegible]	[illegible]
3.9	0.54841252	0.54829165	0.55195699	0.55I45200	0.55I66877	[illegible]	[illegible]	[illegible]
4.2	- " -	- " -	- " -	- " -	0.55I6994I	[illegible]	[illegible]	[illegible]

X \ Y_0	3.2669I9	3.3338I	3.45000	3.5669I9	3.6338I	3.75000	[illegible]	[illegible]
0.0	0.00000000	0.00000000	0.00000000	0.00000000	[illegible]	[illegible]	[illegible]	[illegible]
0.3	0.00000000	0.00000000	0.00000000	0.00000000	[illegible]	[illegible]	[illegible]	[illegible]
0.6	-0.000I7355	-0.000I6229	-0.000I4518	-0.000I3048	[illegible]	[illegible]	[illegible]	[illegible]
0.9	-0.000I6940	-0.00007I824	-0.00064066	-0.00057454	[illegible]	[illegible]	[illegible]	[illegible]
I.2	-0.00I77075	-0.00I64783	-0.00I46226	-0.00I30625	[illegible]	[illegible]	[illegible]	[illegible]
I.5	-0.00229882	-0.002I2748	-0.00I86152	-0.00I64556	[illegible]	[illegible]	[illegible]	[illegible]
I.8	-0.00001938	0.00003126	0.000I0091	0.000I6122	[illegible]	[illegible]	[illegible]	[illegible]
2.I	0.00927022	0.00877714	0.00796896	0.00726759	[illegible]	[illegible]	[illegible]	[illegible]
2.4	0.03I47920	0.02952240	0.02651JI7	0.02393945	[illegible]	[illegible]	[illegible]	[illegible]
2.7	0.07427448	0.06919598	0.06164758	[illegible]	[illegible]	[illegible]	[illegible]	[illegible]
3.0	0.I4974349	0.I3744477	0.I2065010	0.I0726647	[illegible]	[illegible]	[illegible]	[illegible]
3.3	0.479I9307	0.29287346	0.22026799	[illegible]	[illegible]	[illegible]	[illegible]	[illegible]
3.6	0.55328386	0.54987176	0.53773952	[illegible]	[illegible]	[illegible]	[illegible]	[illegible]
3.9	0.55808176	0.55765995	0.55653285	[illegible]	[illegible]	[illegible]	[illegible]	[illegible]
4.2	0.55852505	0.55836367	0.55795243	[illegible]	[illegible]	[illegible]	[illegible]	[illegible]
4.5	0.55856093	0.55845034	0.55785234	[illegible]	[illegible]	[illegible]	[illegible]	[illegible]

X \ X_0	4.05000	4.I6619	4.2638I	4.35000	4.46619	4.5338I	4.65000	4.766I9
0.0	0.00000000	0.00000000	0.00000000	[illegible]	[illegible]	[illegible]	[illegible]	0.00000000
0.3	0.00000000	0.00000000	[illegible]	[illegible]	[illegible]	[illegible]	[illegible]	0.00000000
[illegible]	[illegible]	[illegible]	[illegible]	[illegible]	[illegible]	[illegible]	[illegible]	[illegible]
0.9	- 0.00038I63	- 0.00034500	-0.00033176	-0.00033469	-0.00028043	-0.00026739	-0.00024648	- 0.00022704
I.2	- 0.00085735	-0.00077459	-0.00074501	-0.00066159	-0.00059257	-0.00055852	-0.00055087	-0.00050319
I.5	-0.00103951	-0.00095997	-0.00090728	[illegible]	- 0.00077326	-0.00072836	-0.00067950	-0.00063494
I.8	0.00026169	0.00026257	0.00023523	[illegible]	0.00015545	0.00015349	0.00016650	0.00005508
2.I	0.00494538	0.00449851	0.00433096	[illegible]	[illegible]	[illegible]	0.00325378	0.00269298
2.4	0.0IIn145F5	0.0I462592	0.0I238540	[illegible]	[illegible]	[illegible]	.0I023444	0.00936241
2.7	0.03696117	0.03373295	0.03226988	[illegible]	0.I2726790	[illegible]	0.02304383	0.02230169
3.0	0.07 55139	0.06943223	0.06142712	0.05646605	0.05213440	0.05033127	0.04642610	0.04402975
3.3	0.I2037321	0.I0969554	0.I0440732	0.09588076	[illegible]	0.08496I2[illegible]	0.07769727	0.07491936
3.6	0.I4030613	0.I2769013	0.I2403985	[illegible]	0.I1637583	0.I1254635	0.I2268912	0.II5c0544
3.9	0.29I36416	0.25903973	0.24439905	0.22261569	[illegible]	0.I9509670	0.I8019270	0.I6883627
4.2	0.55340209	0.5I942II8	0.38I88324	0.32205398	0.29027451	0.27578363	0.25352I[illegible]	0.23559589
4.5	0.56688224	0.56932I69	0.56794578	0.56I30488	0.53I8I538	0.4065I833	0.35052409	0.32072496
4.8	0.56769580	0.57I46793	0.57I80235	0.57250791	0.57555498	0.57488439	0.56946728	0.5453I9I4
5.I	0.56774I90	0.57I58776	0.57201381	0.57306220	0.57717262	0.57789487	0.57877830	0.58377034
5.4	- " -	- " -	0.57202399	0.57310964	0.57724873	0.57803413	0.57918230	0.58498496
5.7	- " -	- " -	- " -	- " -	-			

The Proceedings of the

BROOKHAVEN CONFERENCE ON NEUTRON THERMALIZATION

have been published in four volumes.

Volume I, The Scattering Law

Volume II, Neutron Spectra in Lattices and Infinite Media

Volume III, Experimental Aspects
of Transient and Asymptotic Phenomena

Volume IV, Theoretical Aspects
of Transient and Asymptotic Phenomena

BNL 719 (C-32)
Volume III of IV, Experimental Aspects
of Transient and Asymptotic Phenomena

3245

PROCEEDINGS OF THE BROOKHAVEN CONFERENCE ON NEUTRON THERMALIZATION

Volume III, Experimental Aspects of Transient and Asymptotic Phenomena

April 30 to May 2, 1962

BROOKHAVEN NATIONAL LABORATORY
ASSOCIATED UNIVERSITIES, INC.
under contract with the
UNITED STATES ATOMIC ENERGY COMMISSION

BNL 719 (C-32)
(Physics - TID 4500, 18th Ed.)

PROCEEDINGS OF THE BROOKHAVEN CONFERENCE ON NEUTRON THERMALIZATION

Volume III, Experimental Aspects of Transient and Asymptotic Phenomena

April 30 to May 2, 1962

BROOKHAVEN NATIONAL LABORATORY
UPTON, NEW YORK

LEGAL NOTICE

PRINTED IN USA
PRICE $15 00 FOR THE FOUR VOLUMES

Available from the
Office of Technical Services
Department of Commerce
Washington 25, D C

November 1962 1100 copies

PREFACE

A conference on the subject of neutron thermalization was held at the Brookhaven National Laboratory from April 30 to May 2, 1962, precisely four years after the close of the last thermalization conference, the Gatlinburg conference of April 28-30, 1958. The subject of thermalization, which concerns the approach to thermal equilibrium and the manner of the equilibrium distribution of neutrons in matter, has elicited a great deal of interest in the meantime. While the seventeen papers contributed at Gatlinburg could be assembled into a single, convenient volume, presenting the seventy Brookhaven papers has required four weighty books.

The Brookhaven conference was conducted as a "reporter" conference. The technical papers which were submitted were sorted into six categories, viz., the experimental and theoretical aspects of the "scattering law," of spectra in infinite media, and of transient phenomena. A reporter was chosen for each of the six topics, and was asked to prepare a talk which would contain an appreciation of the technical papers. The reporter talk, followed by a general discussion constituted each session. Thus, the individual papers were not presented, though copies were available to all who attended, and are presented in these proceedings. (While the papers from our Soviet colleagues were received too late for discussion at the conference, translated versions will also be found in these volumes.)

The success of a technical conference is always due to the efforts of many people. We must first thank the reporters and authors for the fine quality of their contributions. Mr. Robert Brown of Brookhaven's Graphic Arts Division was responsible for the prompt publication of the proceedings and for having more than ten thousand copies of the technical papers ready in time for the conference. Mrs. Mariette Kuper and Mr. Edward Bergin and their staffs directed the mechanics of the conference with skill and aplomb, while several members of the Theoretical Reactor Physics Group made important contributions to its planning and execution. In particular, we should thank Drs. Paul Michael and Henry Honeck, and for his kind encouragement throughout, Mr. Jack Chernick, the Group's Director.

NOEL CORNGOLD

VOLUME III

PROGRAM AND TABLE OF CONTENTS

TRANSIENT EFFECTS IN SPACE, TIME, AND ENERGY

K. H. Beckurts

Kernforschungszentrum Karlsruhe, Germany

CONTENTS

ABSTRACT

A review of 16 papers (1 - 16) submitted to the Brookhaven conference and dealing with the experimental aspects of "asymptotics" or "transients" in space, time, and energy is given. Most of these papers deal with diffusion parameter measurements using pulsed or stationary methods; numerous new data have been reported and are critically compared. A number of new techniques for the investigation of space- and time-dependent thermalization phenomena are reviewed.

1. Introduction

About four years ago, the whole field of "transients" or "asymptotics" research appeared to be in a very good state; measurements by different authors using either pulsed or stationary methods were in reasonable agreement. Attempts to interpret the data theoretically were in general quite successful. There seemed to be not much incentive for further research work. However, with the arrival of more advanced experimental techniques and of more sophisticated analysis methods, the situation has almost completely changed. Today, there exists a considerable amount of discrepant data on almost any moderator. Reported data for thermalization times and diffusion cooling coefficients diverge by up to a factor of three and even for one of the most fundamental constants of neutron physics, the diffusion length of thermal neutrons in water, data differing to up to 6% have been found. Only in very few cases the data can be calculated theoretically with sufficient accuracy. The author hopes that discussions at this conference will contribute towards a better understanding of all these problems and clarify some discrepancies.

In order to give a formal classification of the problems which will be discussed in this paper, let us start from the space- time- and energy

dependent diffusion equation for the neutron flux $\phi(r,E,t)$ in a nonmultiplying scattering medium:

$$\frac{1}{v}\frac{\partial\phi}{\partial t} = -\Sigma_a\phi + D\Delta\phi + H\phi + S(r,E,t) \tag{1}$$

Here H is the thermalization operator

$$H\phi = \int\Sigma_s(E' \rightarrow E)\phi(E')dE' - \Sigma_s\phi \tag{2}$$

while S(r,E,t) represents the neutron sources.

At large distance from the source (in the stationary case) or at large times after the injection of a source neutron burst (in the time-dependent case) there may be asymptotic solutions of Eq. (1). In a pulsed medium, they can be written

$$\phi(r,E,t) = R(r)\phi_\alpha(E)e^{-\alpha t} \tag{3}$$

where α is the lowest eigenvalue of

$$[-\frac{\alpha}{v} + \Sigma_a + DB^2]\phi(E) = H\phi(E) \tag{4}$$

and $\phi_\alpha(E)$ the corresponding eigenfunction. B^2 is the geometrical buckling, i.e., the lowest eigenvalue of

$$\Delta R + B^2R = 0 \tag{5}$$

with adequate boundary conditions on the surface of the moderator. R is the corresponding spatial eigenfunction.

In an infinite source-free stationary moderator, the asymptotic solution of Eq. (1) is

$$\phi(r,E) = e^{-\kappa z}\phi_{\kappa}(E) \tag{6}$$

where κ is the lowest eigenvalue of

$$[\Sigma_a - D\kappa^2]\phi(E) = H\phi \tag{7}$$

and ϕ_{κ} the corresponding eigenfunction. Apparently, both asymptotic solutions are closely related and it is for this reason that we will discuss the experiments for the determination of κ and α and their evaluation together in section 2. Eleven papers dealing with related subjects have been submitted (1,2,3,4,6,9,10,11,14,15,16) and the main part of this paper deals with these "asymptotics."

Non-asymptotic solutions of Eq. (1) are important:

a) to describe the neutron flux and spectrum during the thermalization process in the time-dependent case. From the behavior of the energy transients, a "thermalization time" can be derived which is closely connected with other thermalization properties

of a moderator. Four papers dealing with related subjects have been submitted (5,7,8,16) and will be discussed in section 3.

b) to describe neutron flux and spectrum transients near medium discontinuities. There may be different moderators in contact or different temperature regions of the same moderator. Two papers have been submitted dealing with this question; they will be discussed in section 4.

Other non-asymptotic solutions of Eq. (1) may be important near sources and absorbers, these problems are however not dealt with in this paper. Our interest is in general not in spectra, but rather in basic integral constants describing asymptotic decay or transient phenomena.

2. The Measurement of Thermal Neutron Diffusion Parameters ("Asymptotics" in space and time)

2.1 Pulsed Source Measurements

The principle of the pulsed source method is simple. The asymptotic decay constants of moderator blocks with different bucklings are measured; the resulting α vs. B^2 curve is plotted and, using a least squares method, fitted by

$$\alpha = \alpha_0 + D_0 B^2 - C B^4 \tag{8}$$

In this way, the absorption probability $\alpha_o = v_o \Sigma_a(v_o)$, the thermal neutron diffusion coefficient D_o, and the diffusion cooling coefficient C are determined. The procedure appears quite straightforward; it involves however three very difficult problems:

a) The exact determination of the fundamental mode decay constant α.

b) The exact calculation of the buckling B^2.

c) The fitting of the α vs. B^2 curve by only three terms.

2.1.1 The determination of the asymptotic decay constant. Let us assume that the experimenter has an ideal neutron detection equipment, i.e., no deadtime effects exist which may affect α measurements considerably. Then, the following causes for errors in the α determination still are present: background neutrons from the source, backscattering of neutrons, presence of higher spatial modes, and presence of higher energy modes. In addition, there may be physical effects which prevent the establishment of the pure fundamental mode. An excellent example for this is the "trapping effect" report by E. G. Silver (9). Figure 1 shows the observed decay constant of a beryllium block at various temperatures as a function of the "waiting time," i.e., the time elapsed between the injection of the neutron burst into the beryllium block and the beginning of the data analyzing interval.

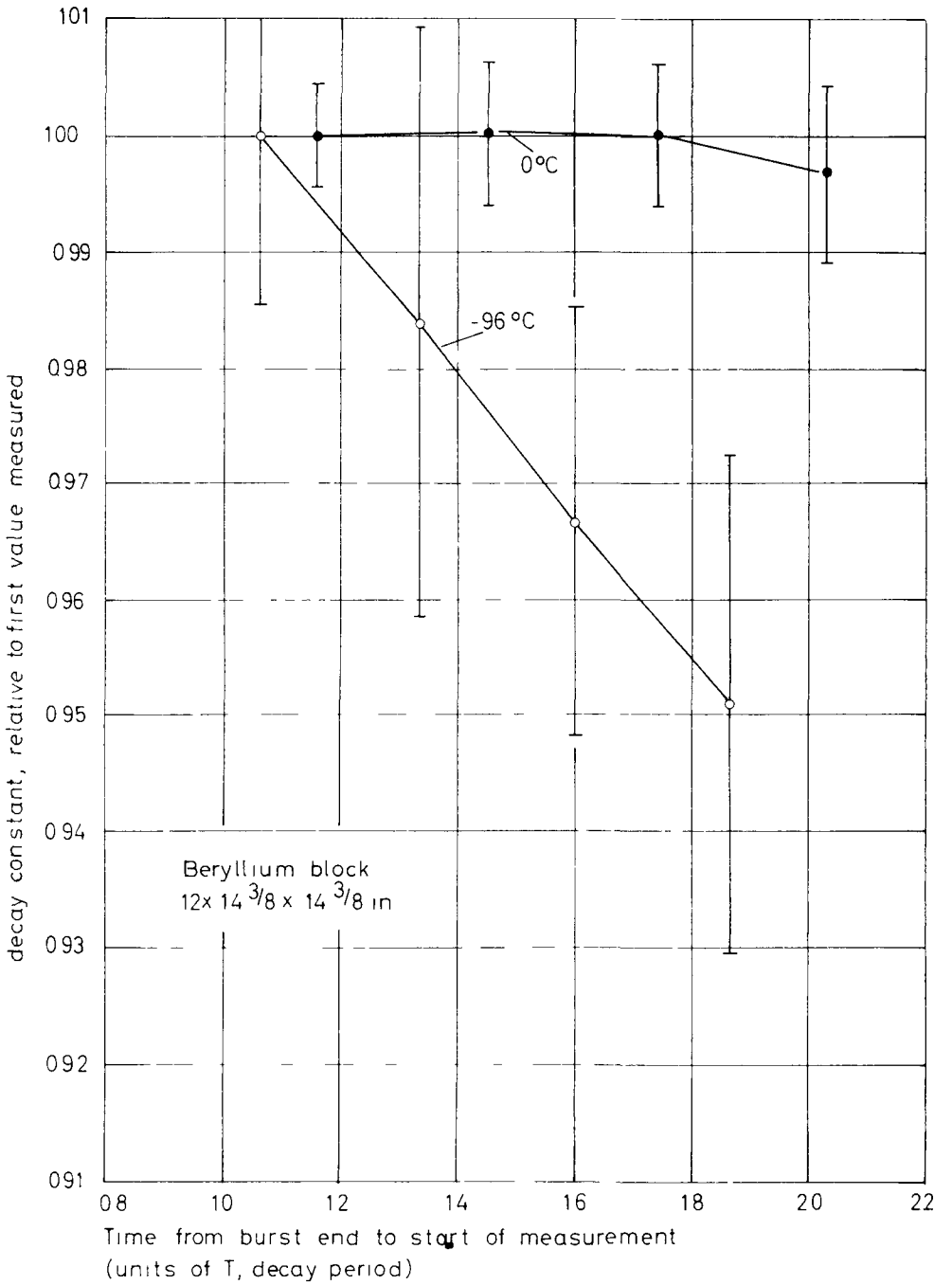

Fig. 1: Relative values of decay constant, α, as a function of time elapsed between end of neutron pulse and start of data analysis. Time is in units of $T = 1/\alpha$; α normalized to unity at about $T = 1$. The lines are drawn to connect points obtained from the same run and do not represent the rate of change in α. [from ref. (9)]

The size of the block was 12 × 14 3/8 × 14 3/8 in.; data were taken at 0° and at -96°C. While there is almost no dependency of the decay constant on the waiting time at 0°C, a strong dependency exists at -96°C. The explanation of this effect is probably the following one: at low temperatures, the cross section for energy gain scattering processes of very slow neutrons becomes extremely small. Therefore a neutron which once has been scattered into the very low energy region will remain there for very long times; returning into the "thermal" group it acts as a source with a slower decay time than that of the fundamental mode.

For graphite at room temperature, fortunately no such effect exists. In order to suppress higher spatial harmonics and especially higher energy modes, a certain minimum waiting time is required. This problem is investigated in two papers submitted to this conference (10,15). Both experimenters find that for large bucklings ($B^2 > 70 \times 10^{-4}$ cm^{-2}) the waiting time has to be about 2 millisec due to the appearance of higher energy modes. If measurements are started too early, larger values of α are observed though the decay curve might look like a good exponential. At smaller bucklings, the waiting time is dependent on the way in which the higher harmonics are suppressed; this was different in the Brookhaven (15) and

the Karlsruhe (10) experiments. Klose et al. (10) used two detectors to suppress the most pronounced harmonics and found that a waiting time of 3 fundamental mode decay periods was sufficient.

In water, especially at very large geometries, higher spatial modes are important and a considerable waiting time may be required. This problem has been dealt with carefully in a recent paper by Lopez and Beyster (17) who show that waiting times up to 50 $\times$ the fundamental mode decay period are required in large geometries. These authors also show that a Fourier analysis technique can be used to isolate the fundamental mode, thus eliminating the need for a long waiting iime. Fourier analysis techniques were also used by H. Meister (18) for the determination of the fundamental and higher modes' α on a subcritical D_2O-natural U pile.

Since long waiting times have to be used and the neutron decay has to be observed over a large interval, any background neutrons from the source can do great harm to a measurement. The background intensity of neutrons should be less than 10^{-5} the "normal" intensity; the Brookhaven group reports a modification (15) of their van de Graaff which leads to a remarkably low background ratio of $<10^{-6}$.

Finally, backscattering of neutrons from the walls of the laboratory

may lead to a time-dependent background which can influence α measurements. It should be possible to protect the moderator block against stray neutrons by appropriate shielding. This needs however careful investigations in each case; for instance a 0.5 mm cadmium lining may be insufficient due to large amounts of epicadmium neutrons entering the pile.

2.1.2 The determination of the buckling. In order to determine the geometrical buckling of the moderator blocks, most authors use the "classical" prescription, i.e., all linear dimensions are increased by twice the extrapolation length

$$d = 0.71\,\lambda_{tr} = 2.13\,\frac{D_o}{v} \tag{9}$$

This is certainly correct as long as a moderator is large so that errors in the extrapolation length do not affect B^2. However, if small assemblies with linear dimensions of only a few transport mean free paths are used, this procedure may be incorrect. Due to the energy dependency of the mean free paths, space-energy transients may arise near the surfaces which lead to a different "effective extrapolation length." The latter may also depend on the shape of the moderator.

In graphite, even the smallest assemblies investigated have linear dimensions exceeding 15 mean free paths. Also, the transport mean free

path of graphite is not very dependent on the neutron energy. Therefore Eq. (9) should be a reasonable approximation. This was checked experimentally by Klose et al. (10) who evaluated α vs. B^2 curves in a three- and four-parameter fit with d as an open parameter. It was found that the minimum fluctuation of the experimental points around the $\alpha(B^2)$ curve was obtained when the above equation (9) was used for the calculation of d.

The situation is quite different, however, for water. Gelbard (19) has computed extrapolation lengths for slabs as a function of buckling in various approximations. While he finds $d = 0.76\,\lambda_{tr}$ for zero buckling, the extrapolation length decreases steadily with increasing buckling. This is due to the strong energy dependency of the transport mean free path and the diffusion cooling effect. In a more recent paper (20), Gelbard has shown that a very different result applies for the extrapolation length in cylindrical systems. Lopez and Beyster (17) and Küchle (21) have investigated the influence of the change of extrapolation length reported in (19) on the evaluation of their measurements in water; both find a very small effect. It will certainly be worthwhile to continue theoretical studies on effective extrapolation lengths in small water geometries.

I. A. de Juren et al. (1) have submitted a paper to this conference

describing an attempt to measure extrapolation lengths directly by the investigation of space-dependent neutron fluxes in pulsed water geometries using a small Li^6I counter. Their preliminary results on a 16.4 cm diameter cylinder and a 11.28 cm cube indicate extrapolation lengths in the region 0.402 to 0.475 cm, i.e., much greater than one would anticipate. The continuation of this work deserves great interest. Evidence for a very strong effect of extrapolation lengths in small water geometries is contained in a recent paper by R. S. Hall et al. (22) who did pulsed measurements on a set of "square" and of "flat" systems, yielding quite different results.

Since the buckling of higher modes depends considerably less on the extrapolation lengths than the fundamental mode buckling, decay measurements on higher modes using the aforementioned Fourier analysis technique seem worthwhile. Meister (18) could determine the decay constant of the fundamental mode and the next three higher modes of his system with reasonably accuracy. This may be difficult to achieve with small water systems.

2.1.3 The evaluation of α vs. B^2 curves. Physically, there is no a priori reason for only three terms describing the α vs. B^2 curve, Eq. (8).

In fact, various theories show that higher order terms exist in order to describe the diffusion cooling effect and the transport theory corrections to elementary diffusion theory. The accuracy of the measured data however does not permit to determine more than three parameters in most cases. The problem arises how to extract these three parameters in the presence of higher order terms. A useful method, originally proposed by the Brookhaven group, is discussed in three papers submitted to this meeting (2,4,15):

The relation Eq. (8) between α and B^2 can be written

$$\alpha - \alpha_o = D_o B^2 - C B^4 + \ldots \tag{8a}$$

We can also use the inverse series

$$B^2 = \frac{\alpha - \alpha_o}{D_o} + \frac{C}{D_o}\left(\frac{\alpha - \alpha_o}{D_o}\right)^2 + \ldots \tag{8b}$$

D_o and C can now be determined using either fit (8a) or the fit (8b), each trunctuated after two terms. Due to the neglect of higher order terms, these two fits will yield different results for D_o and C. One can now plot D and C as a function of the buckling range. When the points of maximum B^2 are dropped successively, D_o and C from both evaluations approach

continuously. This is shown in Figure 2 for D_o in one of the Brookhaven measurements on graphite-bismuth systems (15). One gets a good indication in this way over which buckling range a three-parameter fit can be reasonably applied. Unfortunately, with a decreasing length of the B^2 interval the statistical accuracy of the diffusion parameters, in particular of C, decreases.

A somewhat different technique for the indication of the "reasonable" B^2_{max} was employed by the Karlsruhe group (10); we shall discuss it together with the results on graphite in section 2.3.4. In general, there is agreement among most authors that it is more useful to compare α vs. B^2 curves directly instead of comparing parameters derived by a least-squared fit of the α vs. B^2 curves.

2.2 Diffusion Length Measurements

A number of papers were submitted to this conference (2,6,11,14) dealing with diffusion length measurements, mainly in light water. While for solid moderators like graphite and beryllium the "Σ-pile" method seems to be generally accepted now, various methods are in use in order to measure the diffusion length in light water:

a) The "cadmium-difference" method (23). A thermal point source

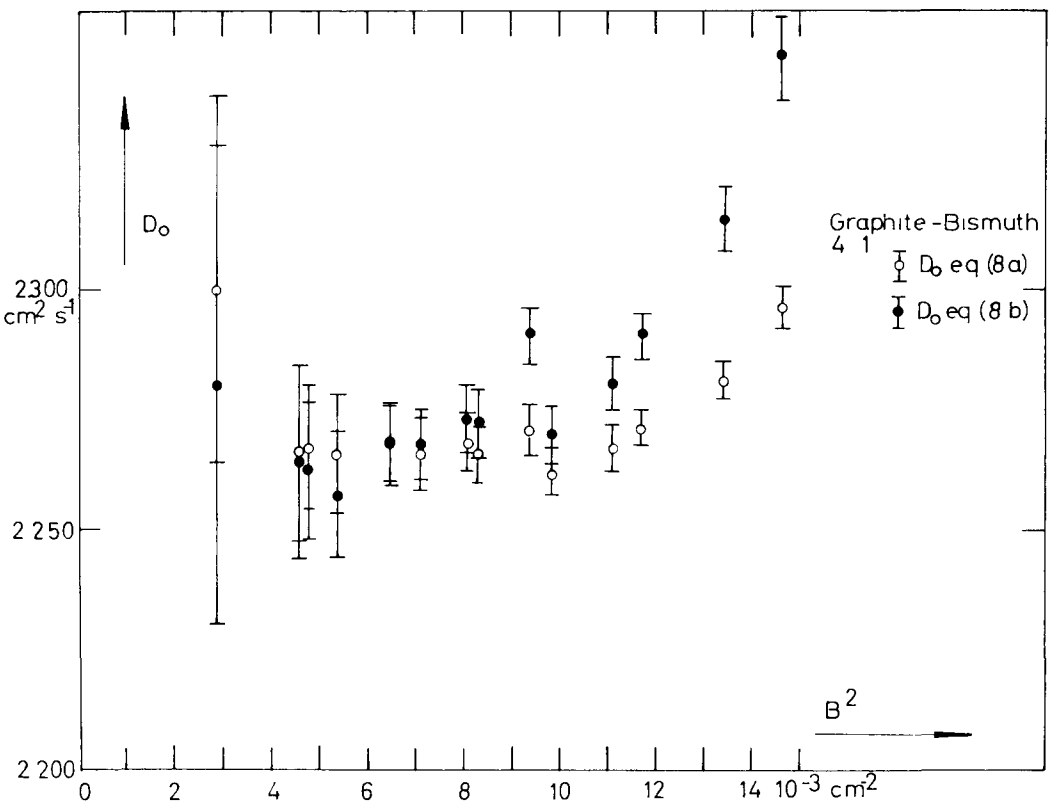

Fig. 2: Values of D_o as maximum B^2 points are successively dropped [from ref. [15]]

in an infinite medium is obtained by measuring the neutron flux around a Ra + Be source with and without a concentric Cd shell and taking the difference. The method does not yield extremely accurate results since the differences may be small.

b) The "Sb + Be source" method (11,24,25,26). A Sb + Be photoneutron source emits ~25 kev neutrons which become thermalized quite close to the source. The resulting thermal flux is therefore due to almost a "thermal point source." However, as Reier and de Juren have shown (24), at source distances <30 cm corrections for slowed-down neutrons, though small, have to be applied. These corrections should be checked using the Cd-difference method.

c) The "thermal column" method (2,6,27,28). Neutrons from a thermal column are fed into a water column of cylindrical or square cross section. The axial relaxation length is measured and converted into a diffusion length, using the well-known geometric corrections.

While the two latter methods are certainly superior to the first one, it is not clear which of them is the more reliable one. The results which are discussed in section 2.3.1 show discrepancies but no systematical dependency on the experimental methods.

The technique of poisoning a moderator in order to measure independently the diffusion coefficient and the absorption cross section has been used extensively on D_2O (14,29), on graphite (30), and on H_2O (11, 23,31). Several authors have discussed the importance of "Diffusion Hardening" in such experiments (23,32) and have corrected their data for this effect (14,23). That the poisoning technique can also be used to determine C and is therefore entirely equivalent or even superior to pulsed source measurements is demonstrated in a paper by Starr and Koppel (2) submitted to this conference. These authors have measured diffusion lengths in water and in aqueous boric acid solutions over a great range of boron concentrations with extreme precision. From Eqs. (1), (4), (7), and (8) the diffusion length in a poisoned system* can be derived to obey

$$\kappa^2 = \frac{1}{L^2} = \frac{v_o \Sigma_a}{D_o} \left[1 - \frac{v_o \Sigma_a}{D_o^2} C + \ldots \right. \tag{10}$$

Plotting κ^2 vs. Σ_a yields D_o and C like in a pulsed source experiment. While this has been well-known for many years, the experiment by Starr and Koppel is the first which yields data sufficiently accurate to determine the C term.

*We restrict ourselves to 1/v poisons.

2.3 A Discussion of Recent Experimental Results

2.3.1 The diffusion length of thermal neutrons in water. Table 1 shows some more recent results on diffusion lengths in H_2O. The conversion to 22°C was done using dL/dT = 0.006 cm/°C. While the first seven values were derived from direct (stationary) measurements, the last three were inferred from pulsed neutron measurements using the formula

$$L^2 = \frac{D_o}{\alpha_o}\left[\, 1 + \frac{\alpha_o C}{D_o^2}\,\right] \tag{11}$$

and the respective values of D_o, α_o, and C. The following comments apply to the different results: The value of Beckurts and Klüber, though one of the lowest, does not contradict other due to the large error limits given. The next three determinations are in a very reasonable agreement. However Rohr's measurement is not quite an independent one since the source neutron correction factors given by Reier and de Juren (24) were used. The result of Rockey and Skolnik's measurement seems very high; this might possibly be due to the neglect of source neutron corrections at source distances < 30 cm. There is also a very high value reported by Ballowe which is very difficult to explain. Miller's experiment cannot be compared since the water temperature was not stated in his publication.

Table 1: Diffusion Length Measurements in H_2O

Author	Year	Ref.	Method	Measured at	L (cm)	L at 22°C (cm)
Beckurts und Kluber	1958	23	Cd difference	15°	2,70 ± 0,03	2,742 ± 0,030
Starr and Koppel	1961	2	Thermal Col.	21°	2,754±0,008	2,760 ± 0,008
de Juren and Reier	1961	11	Sb - Be	23°	2,781±0,006	2,775 ± 0,006
Rohr	1962	26	Sb - Be	16°	2,742±0,011	2,778 ± 0,011
Rockey and Skolnik	1961	25	Sb - Be	26°	2,859±0,018	2,835 ± 0,018
Ballowe	1962	6	Thermal Col.	24°	2,870±0,008	2,858 ± 0,012
Miller	1961	28	Thermal Col.	?	2,81	
Küchle	1960	21	Pulsed source	22°	2,744±0,080	2,744 ± 0,080
Lopez and Beyster	1962	17	Pulsed source	26,7°	2,749±0,016	2,795 ± 0,016
Dio	1958	33	Pulsed source	22°	2,739±0,06	2,739 ± 0,060

2,767 ± 0,008

The author would tend to consider the Reier-de Juren and the Starr-Koppel experiments as the most reliable ones; the average is 2.767 ± 0.008 at 22°C. The weighted average of all six stationary measurements is 2.785 ± 0.012 at 22°C.

The pulsed measurements of Dio and of Küchle lead to lower values of the diffusion length; however the limits of error in both cases are large, so no genuine discrepancy exists. The pulsed source result of Lopez and Beyster is high and slightly discrepant to the above "best value." We shall discuss pulsed source results more extensively in the next session.

The temperature dependency of the diffusion length in H_2O is plotted in Figure 3. It is seen that the various results are in a good agreement.

2.3.2 D_o and C for H_2O from pulsed and from poisoning experiments.

(a) Poisoning experiments. Figure 4 shows κ^2/Σ_a as a function of Σ_a for aqueous boric acid solutions as measured by Starr and Koppel (2). At low boron concentrations, some results of Beckurts and Klüber (23) and of Reier and de Juren (11) are also plotted.* With the exception of Reier's

*The values of Miller (28) and of Ballowe (27) were not plotted here since no numerical results were available to the author; extracting numbers from diagrams seemed to be inaccurate.

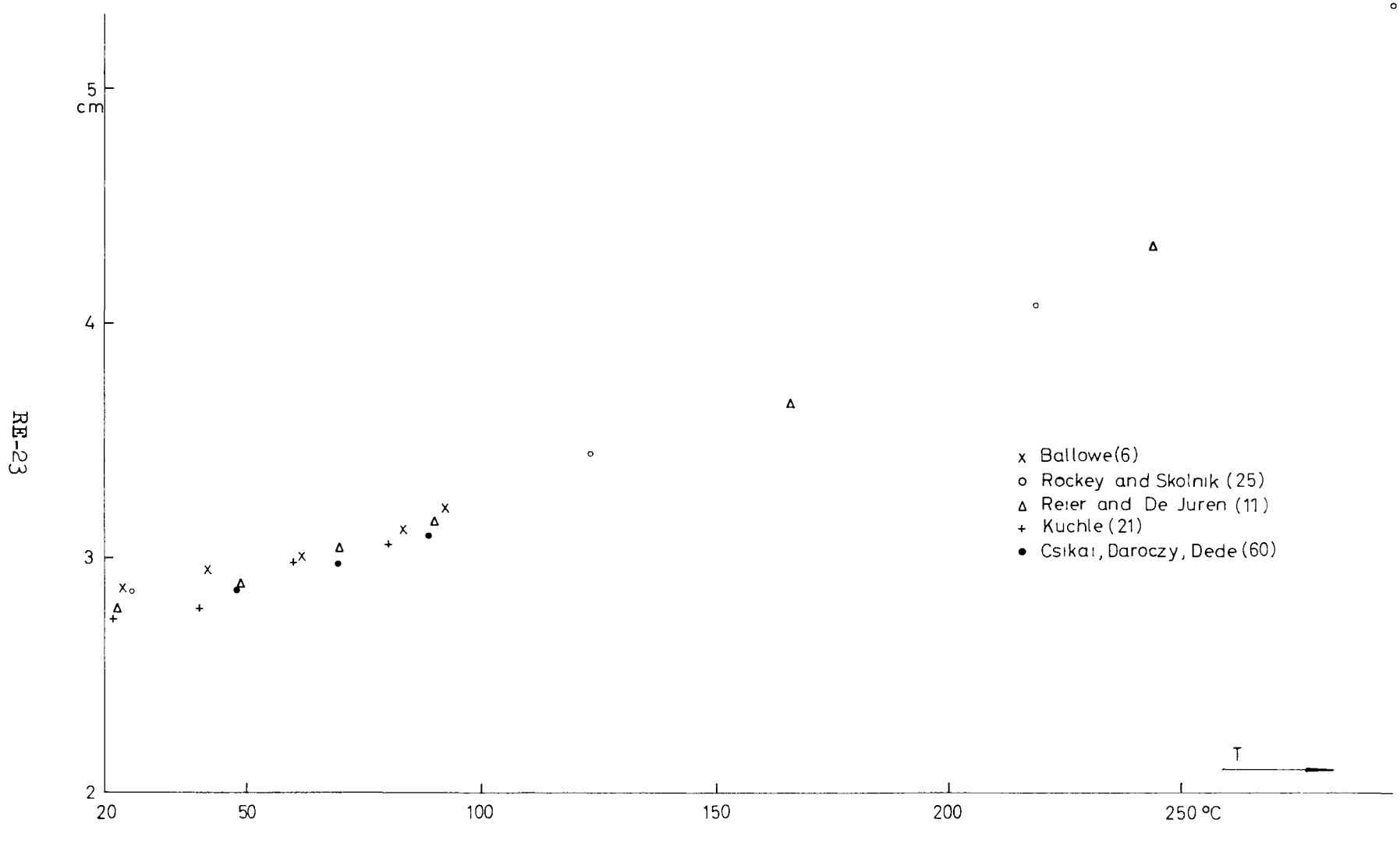

Fig. 3: Temperature dependence of the diffusion length in H_2O

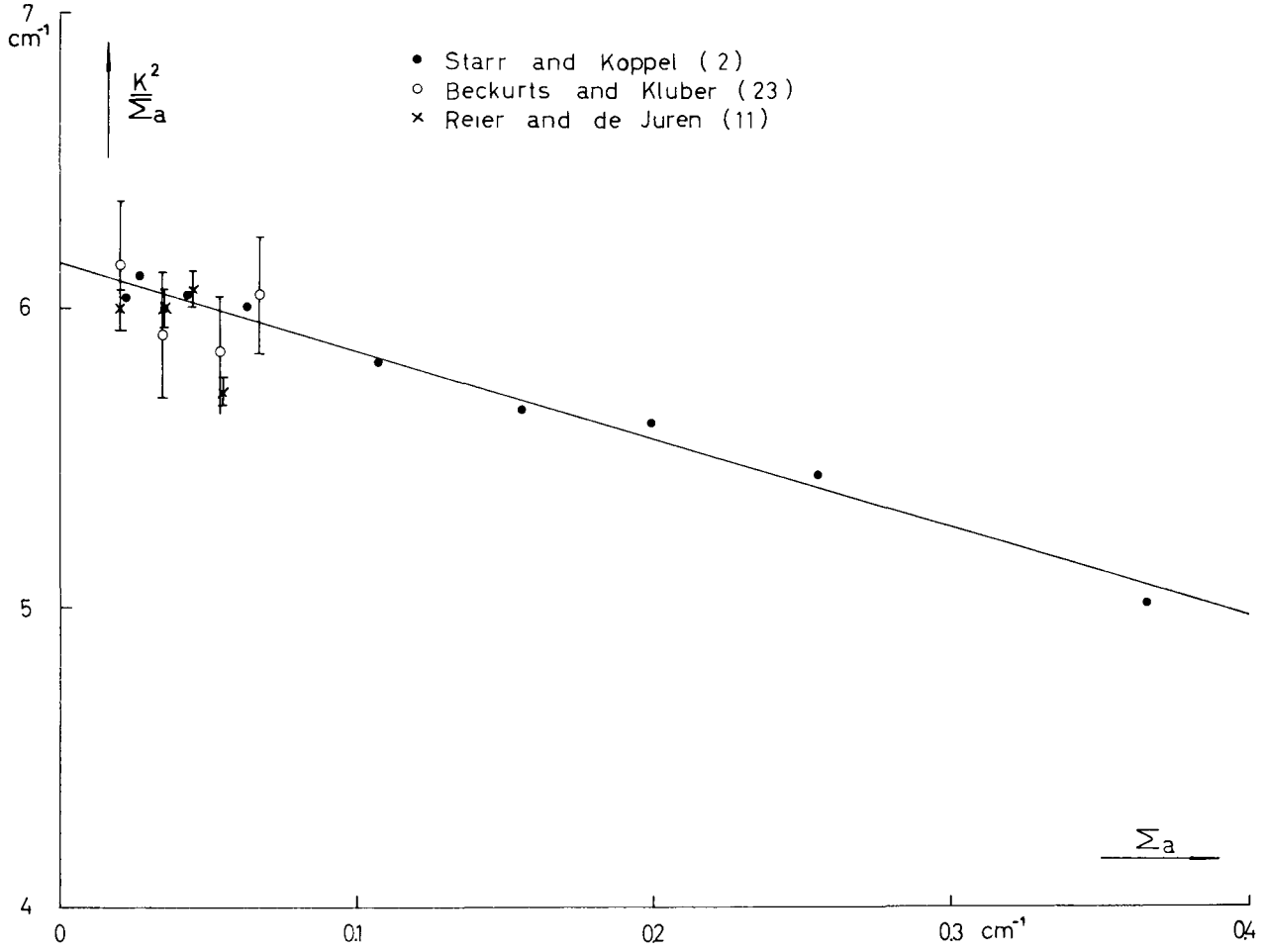

Fig. 4: K^2/Σ_a from poisoning experiments in H_2O (21° C)

point at the highest boron concentration, all measurements are in reasonable agreement.

Evaluating their data with the method outlined in section 2.1.3, Starr and Koppel (2) find for H_2O at 21°C

$D_o = 35{,}800 \pm 100$ cm^2/sec, $C = 2{,}900 \pm 350$ cm^4/sec, and

$\sigma_a = 326.9 \pm 1.6$ mb.

The experiment of Beckurts and Klüber is not sufficiently accurate to yield a value for C. Correcting for diffusion hardening using published values of C, the following diffusion parameters are derived:

$D_o = 35{,}500 \pm 1100$ cm^2/sec and $\sigma_a = 327 \pm 12$ mb.

Within the limits of error, these are in good agreement with the above results.

Reier and de Juren have derived a value of 37,618 cm^2/sec for D_o from their measurement. However, if one corrects their measurements for diffusion hardening a D_o of about 36,000 cm^2/sec can be derived. One can therefore state that all poisoning experiments on H_2O are in good agreement; due to their high accuracy the Starr and Koppel results should be considered as representative.

(b) Pulsed experiments. Figure 5 shows α vs. B^2 curves for H_2O as observed by Küchle* (21) and by Lopez and Beyster (17). It is seen that there is a systematic discrepancy between the two curves. Küchle's curve is similar to previous α vs. B^2 curves (33,34,35); therefore background, backscattering, or even higher spatial modes cannot be the reason for the discrepancies. Lopez and Beyster used their Fourier analysis technique only for the first few low B^2 points, i.e., in the region where the discrepancy exists they use the same technique as Küchle and previous experimenters. The reason for the discrepancy can only be that Lopez used near-cubical systems while Küchle and many others preferred rather flat cylindrical assemblies. Therefore, the discrepancy is similar to the afore-mentioned observation of Hall et al. (22). Until the problems of shape-dependency of the buckling on small water systems are cleared, the accuracy of pulsed measurements in water is subject to some doubts; more confidence should be put into the poisoning experiment.

A three-parameter analysis of the Lopez-Beyster data using the methods outlined in section 2.1.3 yields the following diffusion parameters at 26.7°C (4,17):

*Küchle's data were taken at 22°C and are corrected to 26.9°C here.

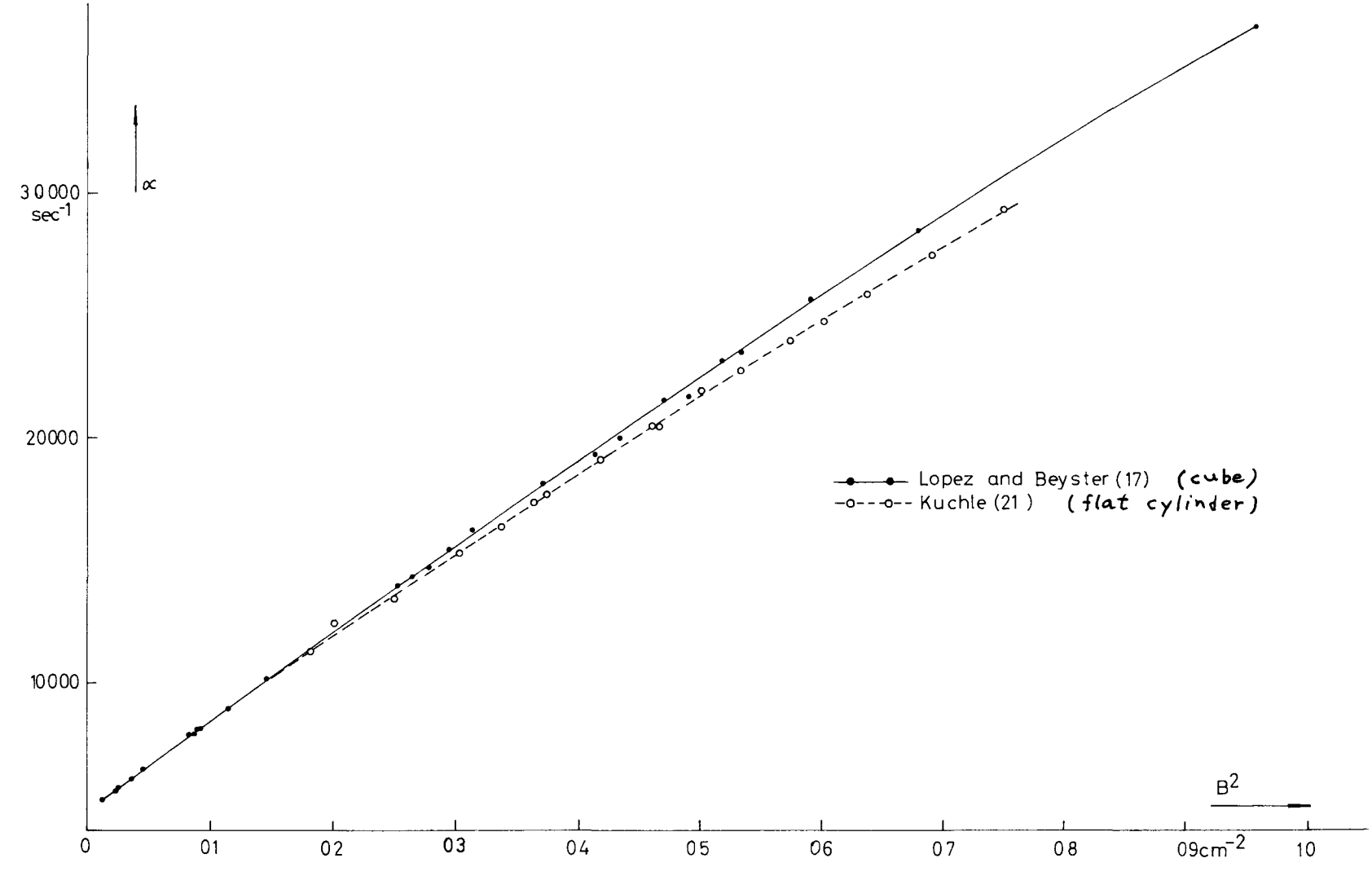

Fig. 5: α vs. B^2 for H_2O at 26,7°C

D_o = 37,426 ± 368 cm^2/sec, σ_a = 325.5 ± 1.6 mb, and

C = 4852 ± 763 cm^4/sec.

Küchle's data yield the following diffusion parameters at 22°C:

D_o = 35,400 ± 700 cm^2/sec, C = 4200 ± 800 cm^4/sec, and

σ_a = 326 ± 6 mb.

This evaluation was performed by a three-parameter analysis in the region B^2 = 0 to 0.7 cm^{-2}; Küchle (21) discussed the role of a B^6 term and showed that it is probably very small. While the absorption cross sections agree well, there are discrepancies in D_o and C:

	D_o cm^2/sec	C cm^4/sec
Starr and Koppel	35,800 ± 100	2900 ± 350
Lopez and Beyster*	36,700 ± 370	4852 ± 800
Küchle*	35,300 ± 700	4200 ± 800

Within the limits of error, Küchle's data agree with the Starr-Koppel data whereas the Lopez-Beyster data agree worse. Apparently, a very careful investigation of the "buckling" problem would be very helpful.

2.3.3 The diffusion parameters in D_2O. As a most valuable contribution to this conference, Brown and Henelly (14) have reported the diffusion

*D_o was corrected to 21°C using dD_o/dT = 130 cm^2/sec °C. No attempt to correct C was made since this would shift C only by a fraction of the error limits.

coefficient of D_2O in the temperature range 20^0 to 220^0C. This has been a long-standing "Priority I" - request of the European-American Nuclear Data Committee. The experiment to determine D was done by a poisoning technique (heterogeneous poisoning with copper) in the "pressurized sub-critical facility" at Savannah River (36). Unfortunately, not many details of the experiment are described in reference (14). Some more details about the hardening correction might be of interest. The resulting values for $D = D_0/v$, together with some other data, are plotted in Figure 6. Within their limits of error, the different results agree. The temperature dependency of D is well described by a simple calculation based on the "Radkowsky prescription" (41).

Ganguly and Waltner (40) have recently reported the first complete study of D_2O diffusion parameters by the pulsed source method. Their results for the diffusion coefficient were shown in Figure 6. For the diffusion cooling coefficient at room temperature, they obtained $C = 3.72 \pm 0.50 \times 10^5$ cm^4/sec in agreement with Sjöstrand's preliminary value $3.5 \pm 0.8 \times 10^5$ cm^4/sec (42).

2.3.4 The diffusion parameters of graphite. Pulsed measurements on graphite had been performed previously by Antonov (46), Beckurts (47),

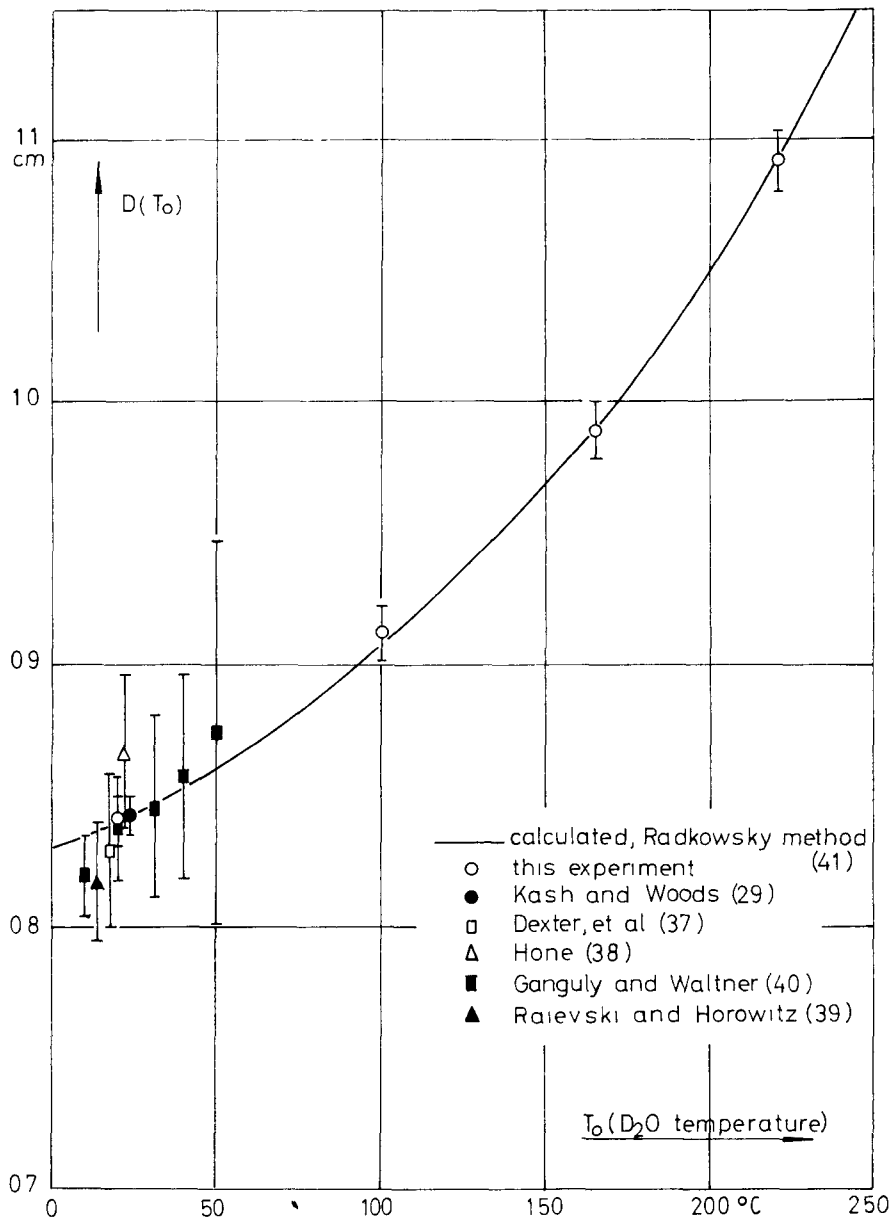

Fig. 6: Diffusion coefficient of D_2O as a function of temperature [from ref. (14)]

and by Starr and Price (45). These early investigations yielded values of C in the region 12 to 16×10^5 cm^4/sec (at 1.6 g/cm^3 density). Since later French (44) and German* investigations seemed to indicate a considerably stronger diffusion cooling, the question was carefully re-examined. Three papers dealing with this subject were submitted to this conference (10,15,16).

Figure 7 shows α vs. B^2 curves for graphite as obtained by Klose et al. (10) and by Starr and Price (15).** It is seen that both experimenters' data are in reasonably good agreement. Compared to previously published curves, the α values in the high B^2 region are much lower. Most previous authors measured too high α's at small block sizes due to contribution of higher energy modes (see section 2.1.1).

Starr and Price (15) made a three-parameter fit of their data using the method outlined in section 2.1.3. They derived the following diffusion parameters for a GBF graphite of 1.697 g/cm^3 density:

$$\lambda_o = 79.2 \pm 0.6 \text{ sec}^{-1}, \; D_o = 2.02 \pm 0.01 \times 10^5 \text{ cm}^4/\text{sec}, \text{ and}$$

$$C = 34 \pm 3 \times 10^5 \text{ cm}^4/\text{sec}.$$

Klose et al. (10) tried a three- and a four-parameter fit of their

*Quoted in reference (61).

**Referring to a density of 1.6 g/cm^3.

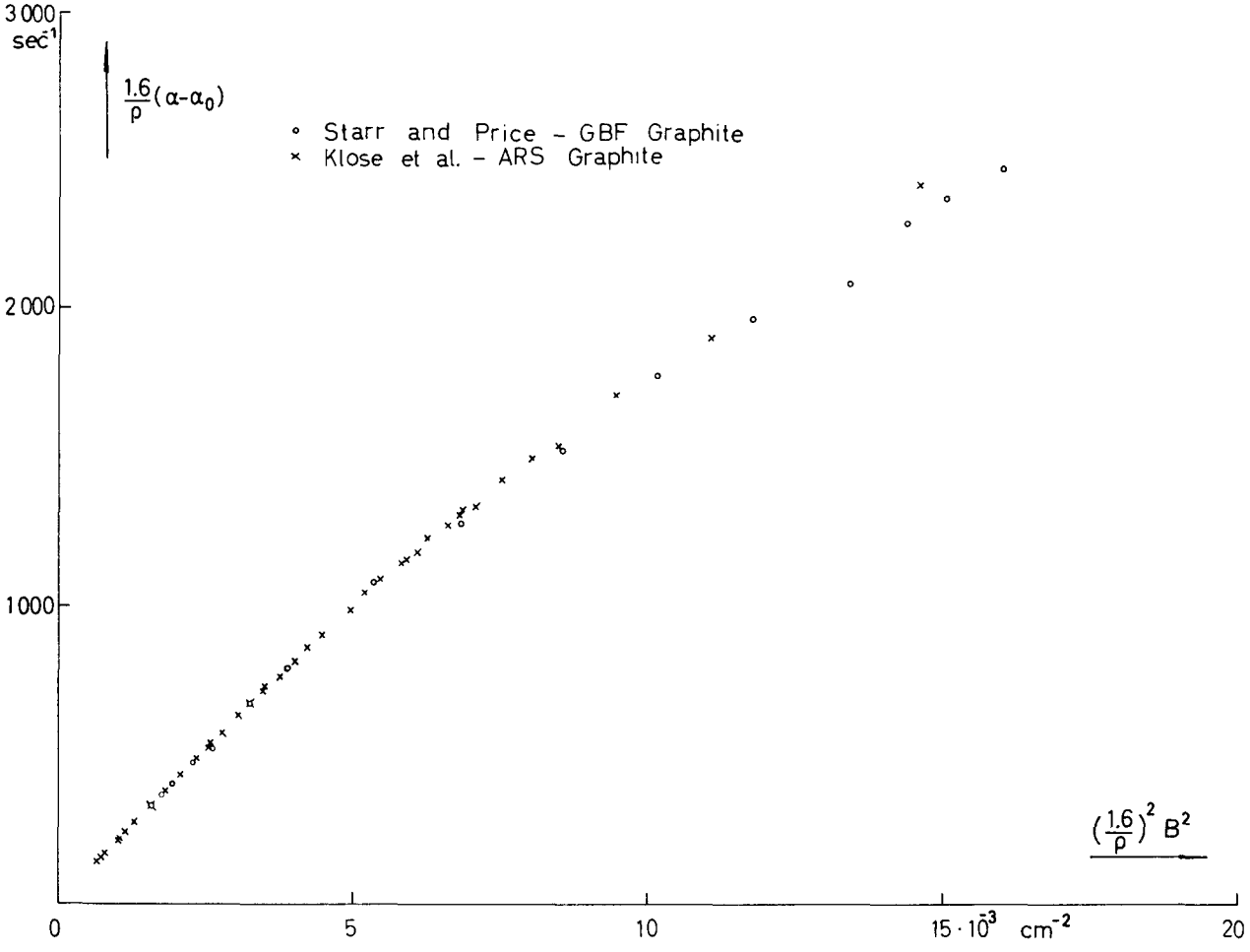

Fig. 7: α versus B^2 for graphite (values are corrected to the same density of 1.6 g/cm^3

data. Figures 8a and 8b show C and $\lambda_{tr} = (3D_o\sqrt{\pi})/2v_o$ as a function of the B^2 region used for the least square fitting. It is seen that in the three-parameter fit there is a considerable dependency of the diffusion parameters on the B^2_{max} used; it seems not reasonable to extend the three-parameter fit above $B^2 = 60 \times 10^{-4}$ cm^{-2}. Then, the following parameters are found (at 1.6 density):

$\lambda_o = 88.3 \pm 1.2$ sec^{-1}, $D_o = 2.13 \pm 0.02 \times 10^5$ cm^2/sec, and

$C = 26 \pm 5 \times 10^5$ cm^4/sec.

For a four-parameter fit, the dependency of the diffusion parameters from the B^2 region used for the fit is apparently less critical. The following parameters were found:

$\lambda_o = 88.6 \pm 1.6$ sec^{-1}, $D_o = 2.11 \pm 0.02 \times 10^5$ cm^2/sec,

$C = 16 \pm 5 \times 10^5$ cm^4/sec, and $F = -20 \pm 10 \times 10^7$ cm^6/sec.

The large size and the negative sign of the B^6 term are most surprising since previous theoretical estimations predicted a small positive value for F. However, Honeck (3) has done calculations based on the Parks (48) model of graphite which indicate clearly the existence of a B^6 term of the same sign and order of magnitude as observed here (see section 2.3.5). The physical explanation of this effect may be related to

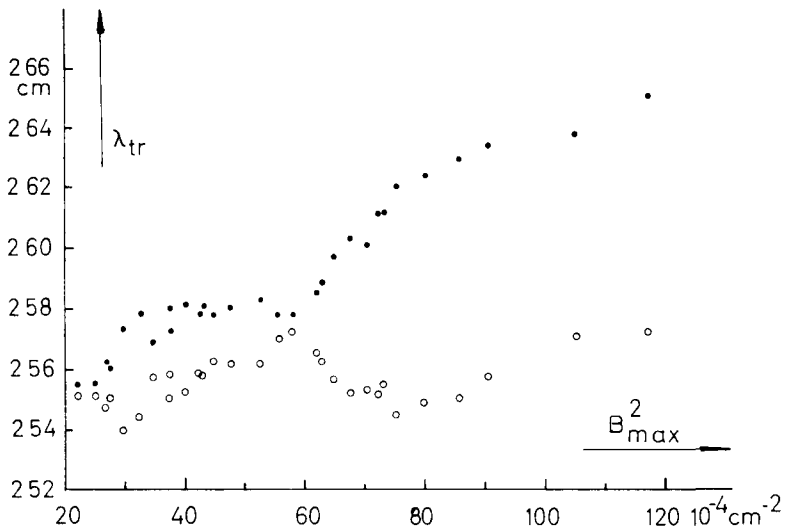

Fig. 8a

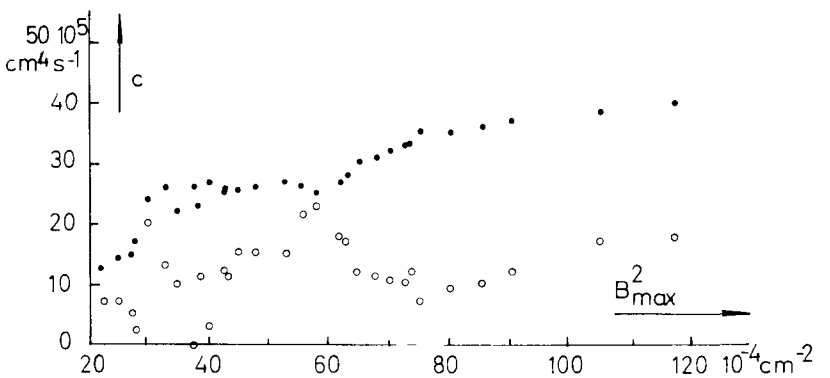

Fig. 8b: Values of C and λ_{tr} as B^2_{max} values are successively dropped [from ref. (10)]

• 3 parameter fit
o 4 parameter fit

the fact that the thermalization power of graphite decreases strongly with decreasing neutron "temperature."

The fact that different interpretations of data so similar as those reported in (10) and (15) lead to so discrepant results is astonishing. More and more accurate $\alpha(B^2)$ measurements on graphite have to be made in order to derive diffusion parameters independent of evaluation schemes. Variations in density and purity and anisotropy effects tend to complicate the evaluation of α measurements on graphite. However, there is agreement now that the diffusion cooling effect in graphite is considerably higher than was found in the early measurements.

Starr and de Villiers (16) have reported a direct observation of diffusion cooling in graphite. Combining a black and a 1/v neutron detector, they measured the average velocity of neutrons leaking from various graphite blocks. This decreases during the thermalization process and reaches an asymptotic value. The observed asymptotic value of $\bar{v}$ as a function of B^2 is shown in Figure 9. Using the formula

$$\bar{v} = \bar{v}_o\left(1 - \frac{C}{D_o} B^2\right) \tag{12}$$

a value of $C = 38 \pm 5 \times 10^5$ cm^4/sec was derived by Starr and de Villiers,

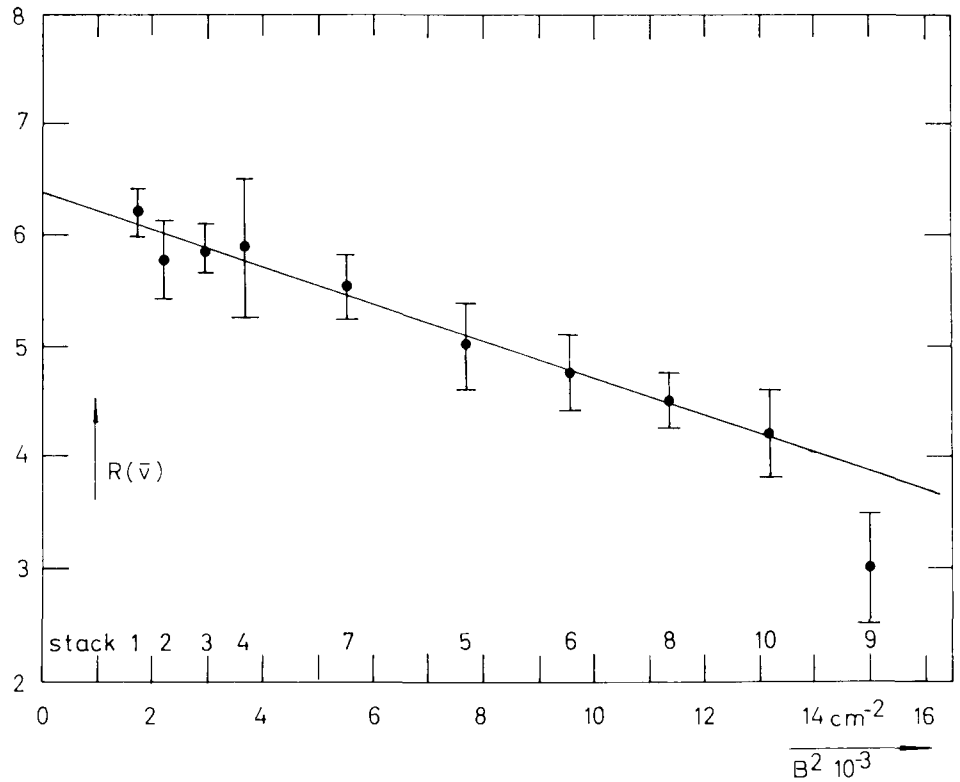

Fig.9: Average neutron velocity as a function of buckling [from ref. (16)]

in good agreement with the C value found by Starr and Price (15).

2.3.5 A direct comparison of experimental and theoretical diffusion data. H. Honeck (3) has made extensive calculations of diffusion parameters in graphite, D_2O, and H_2O. Since theoretical methods are dealt with elsewhere in this conference, only a very brief summary of his work will be given here.

Honeck starts directly from the eigenvalue Eq. (4) resp. (7) (in a transport theory formulation rather than the diffusion theory approximation chosen here). He solves the eigenvalue problem numerically for different bucklings resp. different amounts of poison. For H_2O, he uses the Nelkin (47) scattering kernel, for graphite a scattering law derived by Parks (48), and for D_2O a modified kernel which takes into account incoherent scattering effects (49). For H_2O, calculated and measured eigenvalues are compared in Figure 11.

Honeck has also made a power series expansion of his calculated eigenvalues in order to obtain values of D_o, C, and F. These are compared with some experimental data in Table 2.

For H_2O, the agreement between the calculated diffusion parameters and those observed by Starr and Koppel (2) is good. Note that for graphite

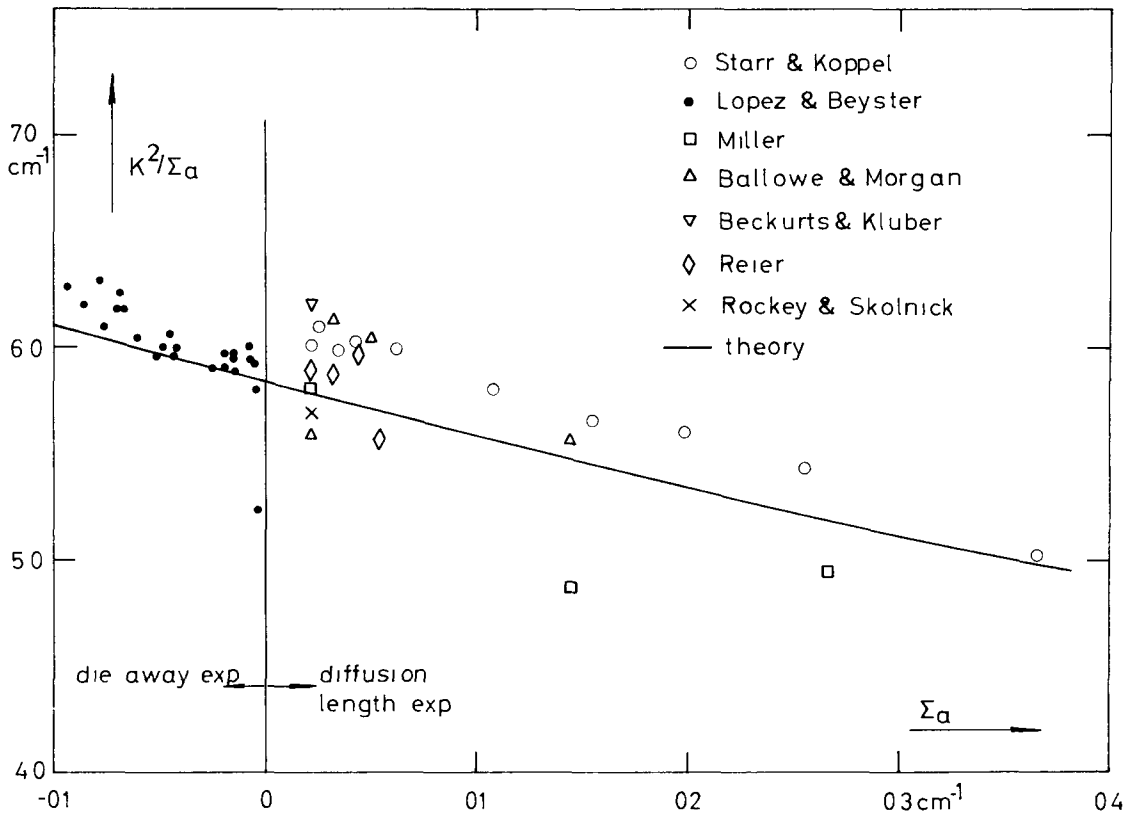

Fig. 11: Computed and measured diffusion parameters of water [from ref. (3)]

Table 2: A Comparison of Theoretical and Experimental Diffusion Parameters (from H.Honeck (3))

	D_o (cm^2/s)	C (cm^4/s)	F (cm^6/s)
H_2O: Theory (Nelkin Kernel)	$3{,}746 \times 10^4$	$2{,}878 \times 10^3$	-
Experiment (Starr and Koppel)	$3{,}585 \pm 0{,}010 \times 10^4$	$2{,}900 \pm 0{,}350 \times 10^3$	-
D_2O: Theory (Honeck Kernel)	$2{,}11 \times 10^5$	$3{,}65 \times 10^5$	-
Experiment (Ganguly and Waltner)	$2{,}08 \pm 0{,}05 \times 10^5$	$3{,}72 \pm 0{,}5 \times 10^5$	-
Graphite (density 1.6) Theory (Parks model)	2.178×10^5	2.457 ~~2.42~~ $\times 10^6$	-8,3 ~~-7.44~~ $\times 10^7$
Experiment Starr and Price (GBF-graphite)	$2.14 \pm 0.01 \times 10^5$	$4.00 \pm 0.30 \times 10^6$	-
Experiment Klose et al. (4-Parameter fit)	$2.11 \pm 0.02 \times 10^5$	$1.6 \pm 0{,}5 \times 10^6$	$-20 \pm 10 \times 10^7$

a negative F term is predicted. In general, the prediction of the Parks-Honeck calculations compare better with the four-parameter fit of Klose et al. (10) than with any other set of parameters. However the experimental F term is very inaccurate.

In heavy water, very good agreement with the experimental results of Ganguly and Waltner (40) is obtained when the fitting of the theoretical α vs. B^2 curve is restricted to the same region where the experiments were performed, i.e., $B^2 = 0$ to 0.1 cm^{-2}.

3. Investigations on the Time Dependency of Neutron Thermalization

Early investigations (50,51,43) defined the "thermalization time" by the rate of approach of the average neutron energy to equilibrium, putting

$$\overline{E} - \frac{3}{2}\kappa T = \text{const. } e^{-t/\tau} \qquad (14)$$

The average neutron energy was determined by transmission measurements through silver or boron absorbers. These early measurements can now be criticized for several reasons: In order to calculate the average neutron energy from the transmission, it must be assumed that the neutrons have a Maxwellian energy distribution which is certainly not true far from equilibrium. The transmission measurement is affected by changes in the

angular distribution of the neutrons and by time-of-flight effects. The most serious error in this procedure may be due to the fact that for many moderators τ as defined by Eq. (14) is not constant but increases with decreasing $\bar{E}$. Since the accuracy of a transmission measurement permits normally only one exponential to be fitted, the observed thermalization time will come out as some kind of an "average," depending on the length of the observation interval.

More advanced theoretical treatments (52,53) make use of the "energy mode" concept. In an infinite medium, the decay of a neutron burst can be described by

$$\phi(E,t) = \Sigma\, a_\nu \varphi_\nu(E) e^{-\lambda_\nu t} \tag{15}$$

Here $\nu = 0$ is the fundamental mode where $\varphi_o(E)$ is a Maxwellian and

$$\lambda_o = v_o \Sigma_a(v_o) \tag{16}$$

For the next mode, we have

$$\lambda_1 = \lambda_o + (1/\tau) \tag{17}$$

where τ now represents the "thermalization time." It is easy to show that the old definition of the thermalization time, Eq. (14), is identical to the new one in the limit $\bar{E} \to \frac{3}{2}\kappa T$, i.e., very close to equilibrium. Thermalization times measured far away from equilibrium are mostly too low since

the thermalization process in that region is influenced by still higher energy modes.

3.1 Thermalization Studies in Water

Möller and Sjöstrand (7) have submitted a paper wherein the decay of a short (0.2 μsec) nuetron burst in an essentially infinite water geometry is studied. Very small amounts of cadmium resp. gadolinium were dissolved in a large water vessel. After the injection of the neutron burst, capture γ-rays were detected using a fast scintillation counter. In this way, a space integration was performed which partially eliminates effects of neutron diffusion. Since the gadolinium and cadmium cross sections vary with energy in a quite different manner, information on the time-dependent neutron spectrum can be gained. From about 7 μsec after the injection of the burst, the cadmium as well as the gadolinium capture rate can be described as the sum of two exponentials, one "fast" with about 4 μsec, the other "slow" with about 200 μsec decay time. Apparently the slow decay is caused by the absorption of neutrons in water whilst the fast one represents the "first higher energy mode." The thermalization time for water would therefore be 4 μsec instead of 7 μsec which were found in a transmission measurement by von Dardel (50). Purohit (52)

has predicted 9 μsec for $1/\lambda_1$; it is however not clear whether the assumptions of this theory apply in water.* A quite different conclusion could be drawn from a paper submitted by Crouch and Holzer (8). These authors investigated the thermal neutron decay in a large water vessel, using a special network of sources to suppress the higher harmonic excitations. They observed an increase of the thermal neutron intensity during the first 35 μsec after the start – quite in contradiction with Sjöstrand and Möller who, for their gadolinium detector, pass over the maximum at 10 μsec. Holzer and Crouch discuss several explications of this phenomena and found it most probable that the thermalization time is much longer than was anticipated. Unfortunately, the paper (8) contains no information on further details, especially on the experimental procedure. It is therefore impossible to draw any further conclusions.

3.2 On the Thermalization Time of Graphite

Early measurements of the thermalization time were performed by a Russian group (51) and by the author (43). Transmission through silver was used to determine the average neutron energy; the data were analyzed with Eq. (14). A thermalization time of about 200 μsec was found by both

*Recently, Purohit (personal communication) has shown that the theoretical value is 4.7 μsec.

experimenters.* In graphite, the "thermalization time" as defined by Eq. (14) increases very strongly with decreasing $\bar{E}$ (59); therefore the results of these early measurements are probably too low for the reasons discussed above. It is however possible to re-evaluate these old measurements using the "energy mode" formalism; assume that no spatial harmonics are present. The counting rate of a boron counter will then be given by

$$z(t) \sim a_o e^{-\lambda_o t} + a_1 e^{-\lambda_1 t} + \ldots \tag{18a}$$

The counting rate of the same counter covered with an absorber is given by

$$z^*(t) \sim a_o^* e^{-\lambda_o t} + a_1^* e^{-\lambda_1 t} + \ldots \tag{18b}$$

a_1^*/a_o^* is different from a_1/a_o due to the energy dependency of the transmission through the absorber. Therefore both measurements can be combined to yield λ_o and λ_1 separately, even in the presence of higher (λ_2, λ_3) energy modes. In this way, a value of $1/\lambda_1 = 240 \pm 60$ μsec can be derived from the old measurement of the author on a 80 × 80 × 80 cm cube. More recently, Küchle and Schweikert (54) have obtained $1/\lambda_1 = 300 \pm 30$ μsec on a 60 × 60 × 60 cm^3 graphite stack using the same method. This is in agreement with values reported by Starr and de Villiers (16) which were obtained

*Beckurts (43) found 185 ± 45 μsec on a graphite stack of 80 × 80 × 80 cm^3. Correcting this value to infinite geometry would raise it to about 200 μsec.

by a similar technique (partly outlined in section 2.3.4). Unfortunately, it is not quite clear how a thermalization time can be extracted from the first energy mode decay constant λ_1 in a small moderator block. If we put just

$$1/\tau \approx \lambda_1 - D_0 B^2 \tag{19}$$

we arrive at thermalization times in the 500 μsec region, i.e., about twice as high as was previously accepted! Eq. (19) seems to be justified from the measurements of Starr and de Villiers (16) who observed $\lambda_1 - \lambda_0$ as a function of buckling and found it was not very dependent. A more accurate experimental investigation and a thorough theoretical analysis would be of greatest value here.

In the case of constant transport mean free path, the diffusion cooling coefficient C can be calculated from the thermalization time, using the well-known relation

$$C = \frac{D_0^2 \tau}{6} \tag{20}$$

With τ = 500 μsec, C $\approx 30 \times 10^5$ cm^4/sec is found which is in rough agreement with the results of section 2.3.4. Due to the large uncertainties of τ and C, Eq. (20) has no great meaning for the time being.

Let us note finally that in order to explain a thermalization time of 500 μsec, an effective mass 80 must be attributed to each carbon nucleus if the "Heavy Gas" model is used.

3.3 The Neutron Life History Experiment

The Harwell linac group (5) has submitted a paper describing the measurement of time-dependent neutron spectra in graphite. After the injection of a neutron burst into a $60 \times 60 \times 60$ cm^3 graphite stack, neutron spectra from the center of the cube are measured as a function of time, using a synchronized chopper and the time-of-flight method. The details of this experiment are described in the Harwell paper (5) and were discussed in the session on neutron spectra; we shall discuss here some of the more important results. Figure 12 shows the observed neutron spectrum at 300, 450, 600, 800, and 1000 μsec after the source burst. Though the 1000 μsec spectrum is already "cooler" than the equilibrium Maxwellian, it is not yet the asymptotic spectrum which will be reached about $\frac{1}{2}$ to 1 msec later. Unfortunately, due to intensity limitations the asymptotic spectrum could not be observed. From the spectra in Figure 12, it is possible to extract the time behavior of the average neutron energy which is plotted in Figure 13, together with theoretical curves based

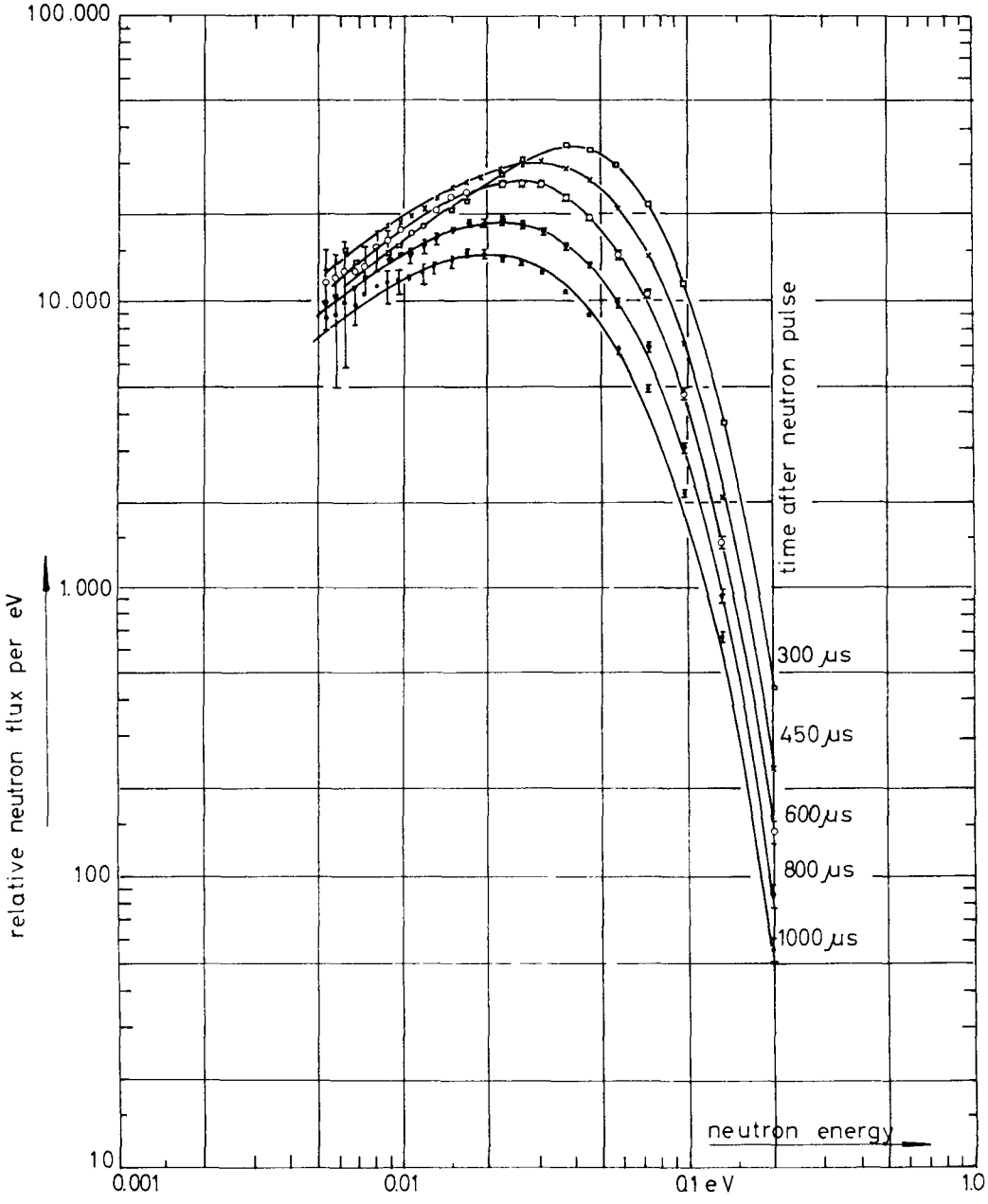

Fig. 12: Time dependent neutron spectra in graphite [from ref.(5)]

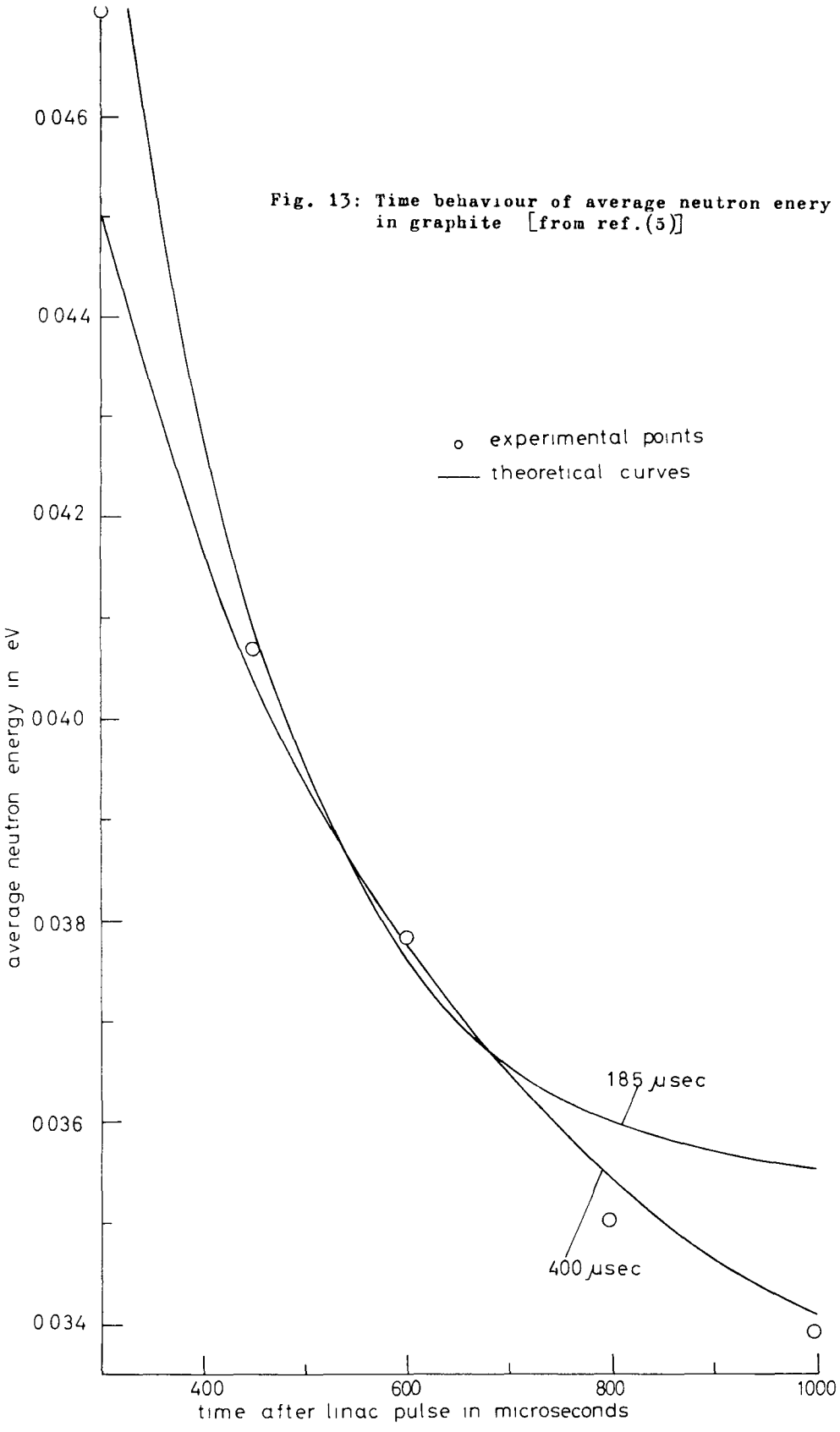

Fig. 13: Time behaviour of average neutron enery in graphite [from ref.(5)]

on 185 or 400 μsec thermalization time. It is seen that the 400 μsec curve describes the measured values well, thus indicating a 400 μsec thermalization time.

The time-dependent neutron spectrum in graphite was also calculated by a numerical solution of the transport equation. For the scattering kernel of graphite, the results of the Egelstaff scattering law experiment were used (56). Comparison between measured and calculated spectra shows good agreement at 300, 450, 600, and 800 μsec. At 1000 μsec, the agreement becomes worse but the experimental data are less accurate there. Surprisingly, a calculation based on a heavy gas model with an effective mass of only 33 also yields very satisfactory agreement!

It might be worthwhile to search for some intermediate ways to evaluate the neutron life history experiment. Instead of comparing measured and computed spectra, one should try to extract certain important parameters which have a well-defined physical meaning and compare them. For instance it should be tried to decompose the observed spectra into various energy modes.

In conclusion, it should be stressed that the measurement of time-dependent neutron spectra is probably the most powerful tool for studies

of the thermalization process. The completion of the first experiment of this kind marks an important progress; further work will contribute much more to the solution of the problems discussed in this section.

4. Studies of Space-Energy-Transients

On first view, the experiments to be discussed now have no direct connection with the thermalization experiments described in the previous sections. Suppose two different media are in contact and that there are (slowed down) thermal neutron sources existing throughout the media. Then, far away from the interface, and "asymptotic" spectrum characteristic for each region exists which in case of weak absorption can be approximated by the superposition of a 1/E spectrum and a moderator temperature Maxwellian. However, close to the interface transients appear in order to match the spectra from both sides. These transients are related to the thermalization properties of the respective moderator; their analysis may yield data which can be compared to pulsed neutron experiments, at least in some cases.

4.1 Neutron "Rethermalization" Studies in Graphite and Water

Bennett (13) has submitted a paper describing extensive studies of transients near temperature discontinuities in graphite and water. The

work is an extension of previous experiments (57). The experiment in principle consists in a measurement of reaction rates of Cu^{63} detectors (Lu^{176} was also used as a check) in various annular zones of the PCTR reactor consisting of graphite at different temperatures or of water and graphite. Figure 14 shows the measured radial Cu^{63}-traverses. While the outer graphite annulus was nearly at room temperature during all experiments, the temperature of the central zone was varied between 144° and 828°K. Lampblack was used as heat insulation at the temperature discontinuity.

The measured flux traverses were analyzed using a multithermal group model proposed by Selengut (58). The epithermal flux is regarded as being one group $\varphi_0(r)$ with a 1/E spectrum. The diffusion parameters for this group were determined by measurements with epicadmium gold detectors. An equilibrium group of neutrons with a Maxwellian energy distribution $M(E,T_i)$ is defined for each region with a different physical temperature T_i. Since two thermal groups exist in the experiments, the thermal flux is written

$$\phi(r,E) = \varphi_1(r)M(E,T_1) + \varphi_2(r)M(E,T_2) \qquad (21)$$

Neutron balance equations are established which connect $\varphi_0(r)$, $\varphi_1(r)$, and $\varphi_2(r)$ with the diffusion parameters. The most important parameters

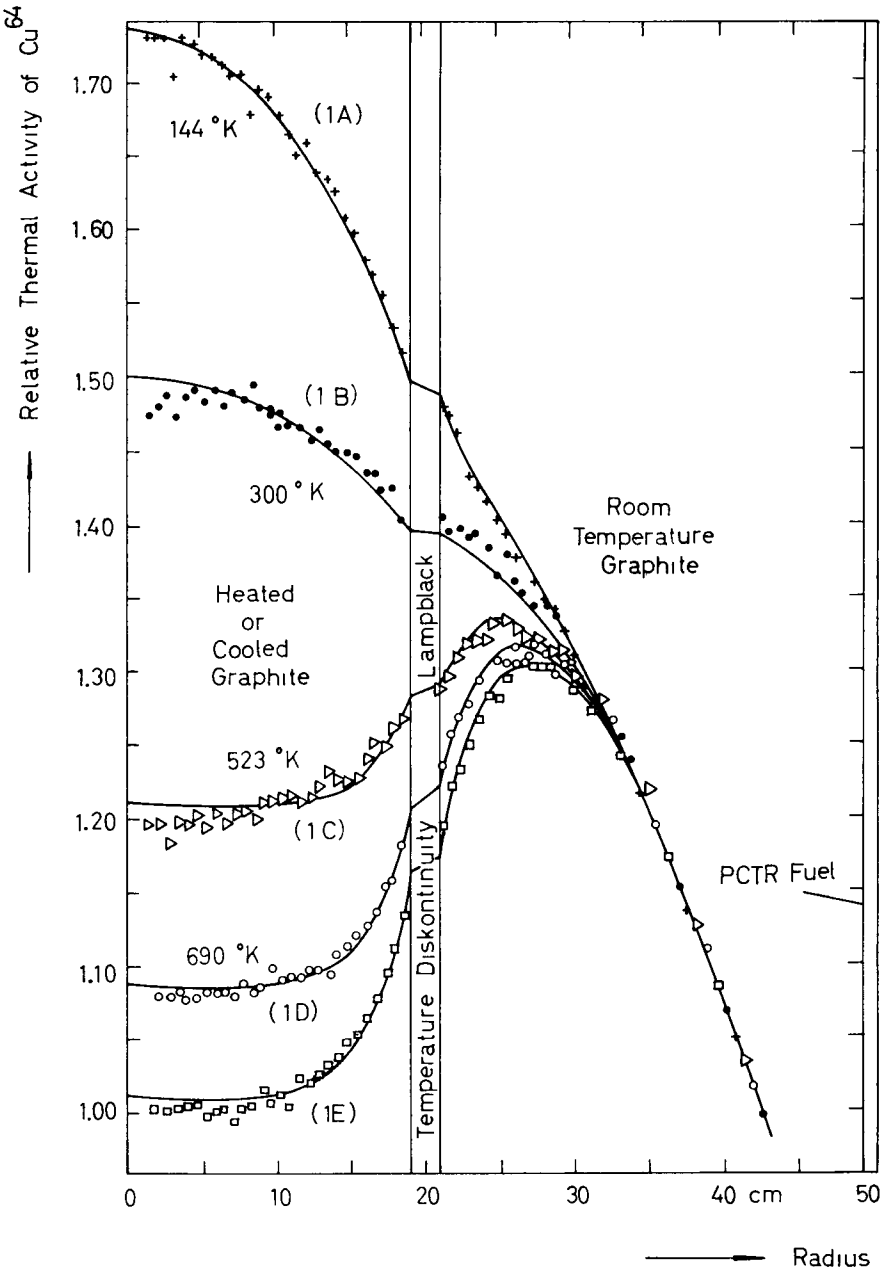

Fig. 14: Radial traverses of Cu^{64} activities in graphite regions [from ref. (13)]

are the cross sections $\Sigma_{1\to2}$ and $\Sigma_{2\to1}$ which describe the transfer of a neutron from thermal group 1 into group 2 and vice versa. They are called "rethermalization cross sections." In the analysis of the Cu^{64}-traverses (Figure 14) all diffusion parameters are known except the rethermalization cross sections; these are determined during the analysis by a trial-and-fit method. Figure 15a shows the observed rethermalization cross section for the $\sim 300^0$K neutrons from the outer annular zone at different temperatures of the central zone; Figure 15b shows the rethermalization cross sections for neutrons with different temperatures (from the inner zone) in the $\sim 300^0$K outer graphite zone. With increasing temperature, both cross sections approach the "free gas limit" value of the rethermalization cross section

$$\Sigma_{RTF} = \Sigma_{so} \frac{2}{A} \tag{22}$$

From this equation and Figure 15b, the following values of the "effective mass" of 300^0K graphite can be deduced:

$T_n = 828^0K : A_{eff} = 22 \pm 1$ $\quad$ $T_n = 523^0K : A_{eff} = 20 \pm 1$

$T_n = 300^0K : A_{eff} = 30$ (extrapolated) $\quad$ $T_n = 144^0K : A_{eff} = 46 \pm 2$

The effective masses appear very low compared to those which can be

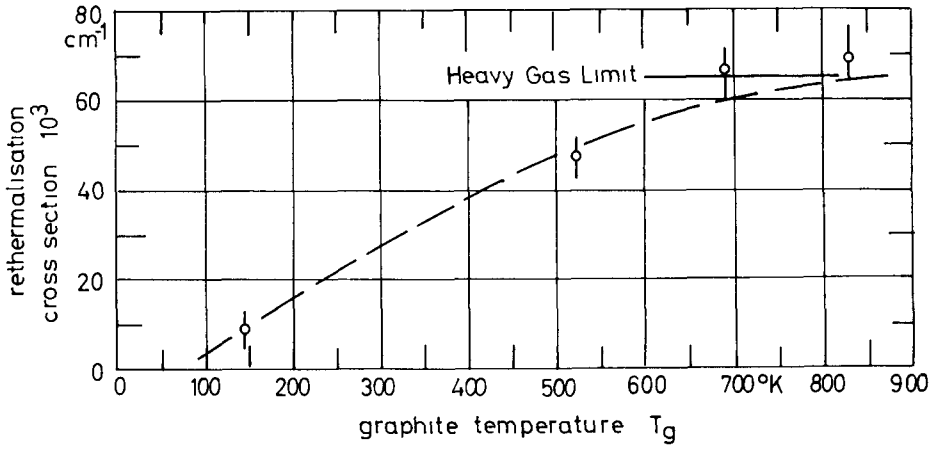

Fig. 15a

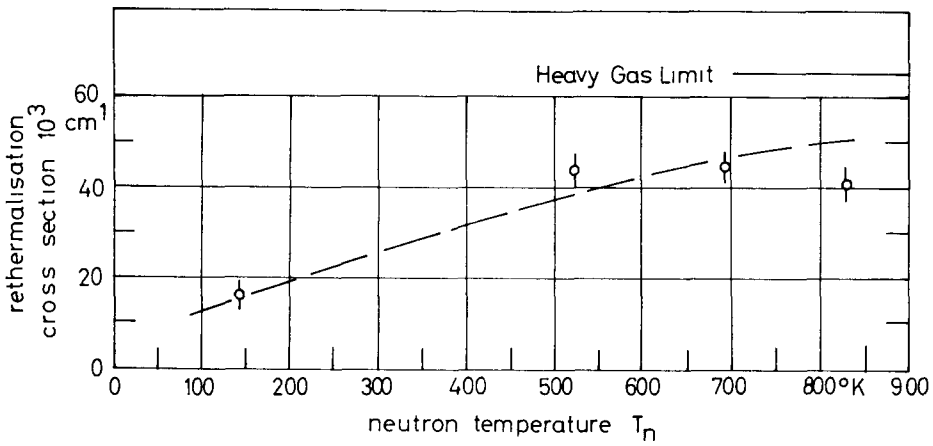

Fig. 15b

Fig. 15 : Rethermalisation cross sections of graphite
a: Neutron temperature 300°, graphite temperature varying
b: Graphite temperature 300°, neutron temperature varying

derived from the pulsed integral experiments; this may be due to the specific model which is used here to analyze the data. However, the way in which the effective mass of graphite changes with temperature is clearly seen; this might lead to a physical understanding of a possibly existing positive B^6 term in graphite.

Bennett tried to compare the measured rethermalization cross sections (or rather the related "relaxation lengths") with predictions based on the theoretical model of graphite given by Kothari and Khubchandani (59). It was found that this model slightly underestimates the rethermalization cross section. This is very surprising since the same theoretical model yields a thermalization time of 170 μsec which seems too low by a factor of two.

For water, the following values of the rethermalization cross section were found:

Water temperature: $293^0 \pm 5^0$K

Neutron temperature: 410^0K: $\Sigma_{RT} = 1.25 \pm 0.12$ cm^{-1}

$558^0 \pm 5^0$K: 1.27 ± 0.12 cm^{-1}

$720^0 \pm 5^0$K: 0.83 ± 0.08 cm^{-1}

The strong decrease of the rethermalization cross section at 720^0K is

difficult to explain. No attempt was made to compare these rethermalization cross sections with predictions of a theoretical model; the "effective mass" as deduced from the above cross sections using Eq. (22) is about 5. The rethermalization cross section for $\sim 400^{\circ}K$ neutrons as found in these experiments is much larger than the value reported by Springer (63).

4.2 Flux Transients Near Medium Discontinuities

Let us finally discuss very briefly a paper submitted by Feiner et al. (12) dealing with spatial transients near medium discontinuities. These authors introduced disturbances into a quasihomogeneous hydrogen-moderated critical assembly and investigated the resulting flux distortion near the perturbation by using foil activation techniques. For the perturbation they used either absorbers (cadmium, boron glass) or moderators (polyethylene slabs). It was found that within the limits of experimental error the spatial transients could be represented by single exponentials, i.e., by

$$A(x) = A_0 e^{-x/L} \tag{23}$$

where x is the distance from the lattice-perturbation interface. The peaking factor A_0 and the relaxation length L depend strongly on the kind of perturbation. A simple one-group diffusion model was employed to calculate the relaxation length. It was assumed that the spectrum of the

transient is a pure Maxwellian in the case of a moderating perturbation and a transmission-hardened Wigner-Wilkins spectrum for absorbing perturbations. Diffusion lengths calculated by averaging over these spectra are in agreement with the observed relaxation lengths. It was also possible to calculate the flux peaking factors by essentially this simple method with reasonable accuracy. These results are definitely of great importance for the design physics of hydrogen-moderated reactors.

5. Conclusions

This review shows that very relevant progress has been made in the field of "asymptotics" research, especially by the contributions to the present Brookhaven conference on neutron thermalization.

In water, most measurements now seem to be in a reasonable agreement. The main problem to be solved is the shape dependency of the buckling at small assemblies and the resulting uncertainty of D_o and C. It appears that using the Nelkin scattering kernel for H_2O all experimental results can be calculated theoretically with reasonable accuracy.

The situation is less favorable in graphite. Here, there exists still considerable uncertainty about the size of the diffusion cooling effect

and about the thermalization time. Before further experiments can be done in order to remove existing discrepancies, theory must be developed showing how these experiments can be evaluated. The experimental technique of the "life history experiment" appears most promising for further studies.

In heavy water, the few experimental data existing so far agree good among themselves and with theories. More experimental data should be taken, especially the "thermalization time" should be measured and the pulsed source experiments extended. The same may be true for other moderators like beryllium, and the multitude of "organic moderators" now becoming available.

The rethermalization experiments yield a great amount of data and appear to be well-consistent among themselves. This is probably sufficiently accurate for the design physics of reactors where these problems may arise. However, since the physics of these experiments is so closely related to the pulsed experiments, a theoretical treatment of these rethermalization experiments by the same models as used for the pulsed experiments might be of great value.

The author is indebted to M. Küchle and to W. Reichardt for valuable discussions on most of the subjects treated.

REFERENCES

1. J. A. de Juren, R. Stooksberry, and E. E. Carroll, "Measurements of Extrapolation Lengths in Pulsed Water Systems," paper at this conference.
2. E. Starr and J. Koppel, "Determination of Diffusion Hardening in Water," paper at this conference.
3. H. C. Honeck, "On the Calculation of Thermal Neutron Diffusion Parameters," paper at this conference.
4. J. Koppel and W. M. Lopez, "Comparison of Diffusion Parameters Obtained for Water by the Pulsed and the Poisoning Techniques," paper at this conference.
5. E. Barnard, N. A. Khan, M. J. Poole, J. H. Tait, R. C. F. McLatchie, "Thermalization of Neutrons in Graphite," paper at this conference.
6. W. C. Ballowe, "Measurement of the Diffusion Length of Thermal Neutrons in Light Water," paper at this conference.
7. E. Möller and N. G. Sjöstrand, "The Time Scale of Neutron Slowing Down in Water," paper at this conference.
8. F. Holzer and M. F. Crouch, "Large Delay Times Observed in Establishment of Single Mode Decay in Water Moderators," paper at this conference.
9. E. G. Silver, "Experimental Investigation of Persisting Changes in the Thermal Neutron Decay Constant in Finite Media of Ice and Beryllium as a Function of Temperature and Buckling," paper at this conference.
10. H. Klose, M. Küchle, W. Reichardt, "Pulsed Neutron Measurements on Graphite," paper at this conference.

11. M. Reier and J. A. de Juren, "Diffusion Length Measurements of Thermal Neutrons in Water," paper at this conference.
12. F. Feiner, S. Weinstein, W. B. Wright, "Flux Transients Near Medium Discontinuities," paper at this conference.
13. R. A. Bennett, "Neutron Rethermalization in Graphite and Water," paper at this conference.
14. H. D. Brown and E. J. Hennelly, "Neutron Thermalization Studies at Savannah River," paper at this conference.
15. E. Starr and G. A. Price, "Diffusion Parameters of Graphite," paper at this conference.
16. E. Starr and J. Q. L. de Villiers, "Determination of Diffusion Cooling in Graphite by Measurement of the Average Neutron Velocity," paper at this conference.
17. W. M. Lopez and J. R. Beyster, Nucl. Sci. and Eng. 12, 190 (1962).
18. H. Meister, to be published in Nucl. Sci. and Eng.
19. E. Gelbard, J. Davis, and J. Pearson, WAPD-T-1065 (1959).
20. E. Gelbard and J. A. Davis, Trans. Am. Nuclear Soc. 4, 290 (1961).
21. M. Küchle, Nukleonik 2, 131 (1960).
22. R. S. Hall, S. A. Scott, and J. Walker, Proc. Phys. Soc. 79, 257 (1962).
23. K. H. Beckurts and O. Klüber, Z. Naturforschung 13a, 822 (1958).
24. M. Reier and J. A. de Juren, J. Nucl. Eng. A14, 18 (1961).
25. K. S. Rockey and W. Skolnik, Nuclear Sci. and Eng. 8, 62 (1960).
26. G. Rohr, personal communication (1962).
27. W. C. Ballowe and W. R. Morgan, Trans. Am. Nuclear Soc. 4, 281 (1961).
28. J. Miller, Trans. Am. Nuclear Soc. 4, 282 (1961).

29. S. W. Kash and D. C. Woods, Phys. Rev. 90, 564 (1953).
30. J. M. Hendrie et al., Progr. Nuclear Energy I, 3 (1959).
31. M. Reier and J. A. de Juren, J. Nuclear Energy A14, 186 (1961).
32. H. Hurwitz and M. Nelkin, Nuclear Sci. and Eng. 3, 1 (1958).
33. W. H. Dio, Nukleonik 1, 13 (1958).
34. A. Bracci and C. Coceva, Nuovo Cimento 4, 59 (1956).
35. G. F. von Dardel and N. G. Sjöstrand, Phys. Rev. 96, 1245 (1954).
36. E. J. Hennelly, Nucleonics 19, 104 (1961).
37. A. H. Dexter et al., ANL-4746, 14 (1951).
38. D. W. Hone, J. Nuclear Energy A11, 34 (1959).
39. V. Raievski and J. Horowitz, Geneva 1955, P/360.
40. N. K. Ganguly and A. W. Waltner, Trans. Am. Nuclear Soc. 4, 282 (1961).
41. A. Radkowsky, ANL-4476, 93 (1950).
42. N. G. Sjöstrand, Arkiv för Fysik 15, 145 (1958).
43. K. H. Beckurts, Thesis, Göttingen 1956. See also Nuclear Sci. and Eng. 2, 516 (1957).
44. G. Lalande, Industries Atomiques 5/6, 71 (1961).
45. E. Starr and G. A. Price, Trans. Am. Nuclear Soc. 2, 125 (1959).
46. A. V. Antonov et al., Geneva 1955, P/661.
47. M. Nelkin, Phys. Rev. 119, 791 (1960).
48. D. Parks, Trans. Am. Nuclear Soc. 4, 135 (1961).
49. H. Honeck, to be published.
50. G. F. von Dardel, Trans. Roy. Inst. Technol., Stockholm 75 (1954).
51. A. V. Antonov, Proc. 1955 Geneva Conference, Vol. 5, p. 83.
52. S. N. Purohit, Nuclear Sci. and Eng. 9, 157 (1961).

53. M. Nelkin, Report GA 746 (1959).

54. M. Küchle and H. Schweickert, personal communication (1962).

55. M. Nelkin, J. Nuclear Energy 8, 48 (1958).

56. P. Egelstaff, AERE-R 3931, (1962).

57. R. A. Bennett and R. E. Heinemann, Nuclear Sci. and Eng. 8, 294 (1960).

58. D. S. Selengut, HW-56919 (1958).

59. L. S. Kothari and P. G. Khubchandani, Nuclear Sci. and Eng. 8, 400 (1960).

60. Csikai, Daroczy, and Dede, J. Nuclear Eng. A14 (1961).

61. K. H. Beckurts, Nuclear Instr. and Meth. 11, 144 (1961).

62. K. H. Beckurts, Z. Naturforschung 16a, 611 (1961).

63. T. Springer, Nukleonik 2, 144 (1960).

MEASUREMENT OF THE DIFFUSION LENGTH OF THERMAL NEUTRONS IN LIGHT WATER

By

W. C. Ballowe*

General Electric Company, Vallecitos Atomic Laboratory
Pleasanton, California

I. INTRODUCTION

Various experimental techniques have been used to measure the diffusion length of thermal neutrons in light water, but they all fall into three distinct groups based on the source of thermal neutrons:

(1) Thermal neutrons from a thermal column

(2) A point source of low energy neutrons such as the 25 kev neutrons from the Sb^{124}-Be source

(3) The pulsed neutron source.

The experiment described in this paper is of the first type. The results are compared to those of other experiments of all three classes. A theoretical comparison is made between the first and last types.

II. EXPERIMENT

The neutrons from the Nuclear Test Reactor are allowed to impinge on the face of the experimental apparatus called the "Water Gun" which is depicted schematically in Figure 1. Reference to the figure shows that the water gun consists of a right-circular cylinder of graphite 58.5 cm in diameter and 29.3 cm long. This graphite cylinder is an extension of the thermal column

---

* William C. Ballowe died on March 14, 1962, from injuries sustained in an automobile accident of the previous week. His paper entitled "Measurement of the Diffusion Length of Thermal Neutrons in Light Water" was not completed. The most significant information which was to be included is in this summary. We would appreciate inclusion of this information in the Proceedings as recognition of one of Mr. Ballowe's contributions to the field of reactor physics.

B. Kerr
J. Russell

and serves the purpose of matching the radial flux shape of the square thermal column to the smaller (in diameter) water column. A slot is provided in the graphite for insertion of a cadmium sheet for the background measurements.

The procedures employed are straightforward and consist of four runs per measurement. A run is a series of count rates at several positions over the travel range of the piston (approximately 25 cm) from the full "in" to the full "out" positions. The direction of travel is reversed and another series of counting rates versus position are obtained. The cadmium sheet is inserted and the count rate versus position is again determined in both directions. These latter runs serve to establish the background for the measurement. The water temperature is measured and recorded throughout each run and is held constant to within $\pm 0.5^{\circ}C$.

The power level of the NTR is 10 kw during a run and does not vary by more than 0.05%. The thermal neutron flux at the face of the thermal column is $10^5 \frac{nv}{sec\text{-}cm^2\text{-}watt}$.

III. RESULTS

The measured diffusion length, L_m, was corrected for radial leakage:

$$L = \frac{L_m}{\sqrt{1 - L_m^2 \left(\frac{2.405}{R + 71\lambda}\right)^2}} \qquad (1)$$

The results are shown in Figure 2. For purposes of comparison, the results of other investigators[1,2,3] are shown. The data of Wilson et al.[2] have been corrected by using $0.71\ \lambda$ for the extrapolation distance in the buckling correction, rather than 7.5 cm as was used in the original paper. This change was only for purposes of comparison of their data with ours since the geometries are very similar and we had used $0.71\ \lambda$ as the extrapolation distance.

Calculational models of diffusion length experiments were designed at the laboratory in order to investigate the difference in L's measured with

different methods. The results of pulsed neutron measurements have been consistently lower than the results from thermal column measurements.

In a thermal column, if the leakage is small compared to the absorption, then the flux at any given energy is attenuated as[4]:

$$\Phi(X,E) = \Phi(0,E)^{-X/L} \qquad (2)$$

where L is a parameter of the system and not dependent on a particular energy. The flux in such a column is "diffusion heated", that is, the spatial source of the higher energy neutrons is relatively greater than that prescribed by a pure Maxwellian. A multigroup treatment of the flux in a thermal column results in a system of simultaneous equations which can be solved for the eigenvalues $(1/L^2)$ [5]. The Nelkin model [6] for neutron scattering in light water was used as a basis for the calculations.

The results of the pulsed neutron source experiments are diffusion lengths for a pure Maxwellian flux in an infinite medium. These results are extrapolations from measurements in finite media with diffusion-cooled spectra. Calculations of $\bar{D}/\bar{\Sigma}_A$ for pure Maxwellian spectra in water were done for various temperatures. These values were also calculated from the Nelkin kernels.

The results of the calculations are compared with experimental values in Figure 2. Because of cross-section uncertainties, the absolute value of the calculated curves is considered to be good to about two per cent. The calculated curves were normalized to the experimental L by adjusting the oxygen scattering. The difference between the curves is independent of the normalization.

No attempt was made to analyze the point source method. These experiments are complicated by a neutron spectrum dependence on radius. The spectrum at small radius is colder than a Maxwellian, and hotter at large radius.

REFERENCES

(1) Rockey, K. S., and Skolnik, W., Nucl. Sci. Eng. 8, 62 (1960)

(2) Wilson, V. C., Bragdon, E. W., and Kanner, H., CP 2306 (1944)

(3) Reier, M., and de Juren, J. A., J. Nucl. Energy, 14, 18 (1961)

(4) Russell, J. L. and Kear, G. H., GEAP 3128 (1959)

(5) Kerr, B. A. GEAP 3599 (1960)

(6) Nelkin, M., Physics Rev. 119, 2 (1960)

(7) Beyster, J. R. et al., GA 2544 (1961)

(8) Ballowe, W. C., Morgan, W. R., and Mosgovoy, W. V., GEAP 4018 (1962)

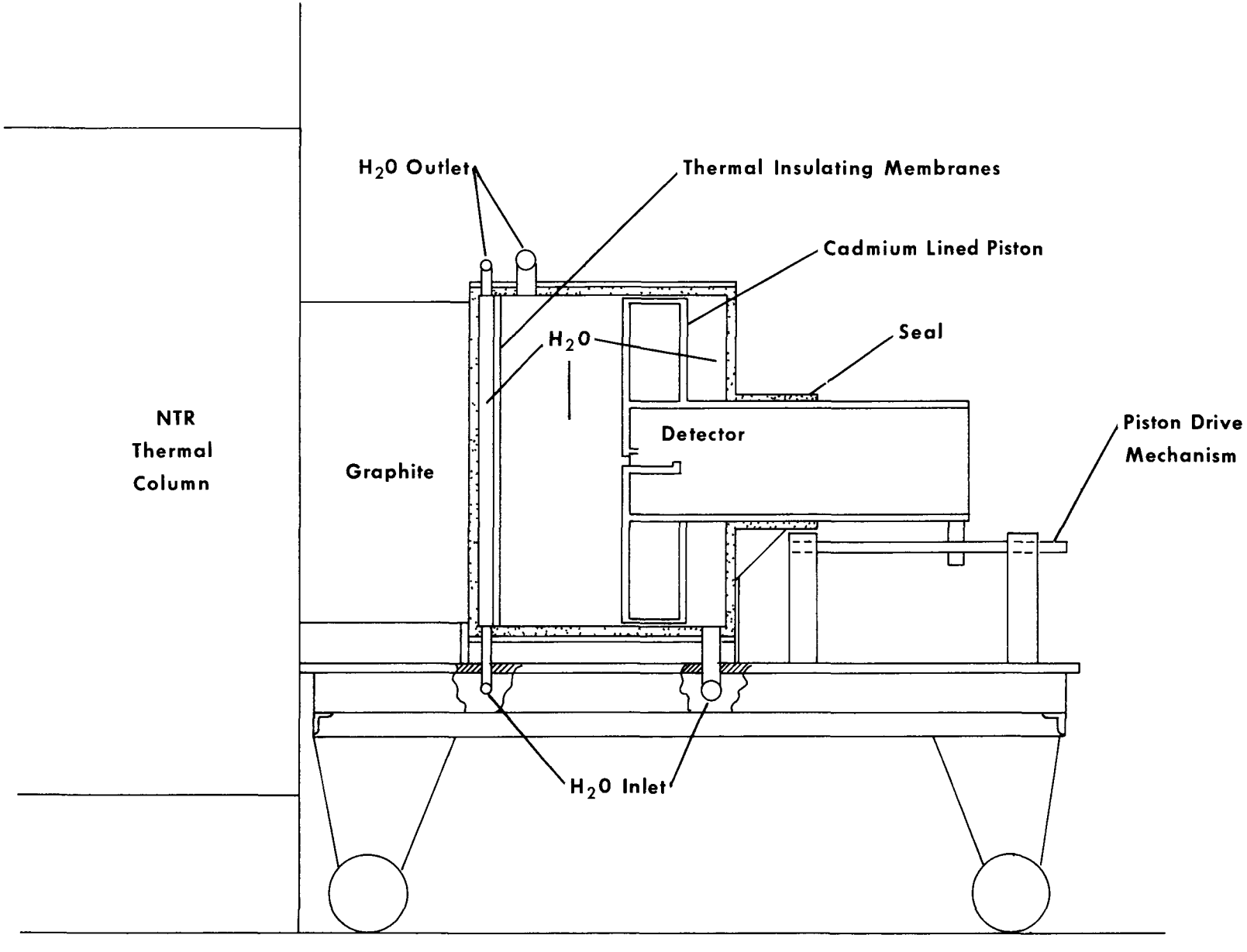

Figure 1. WATER GUN

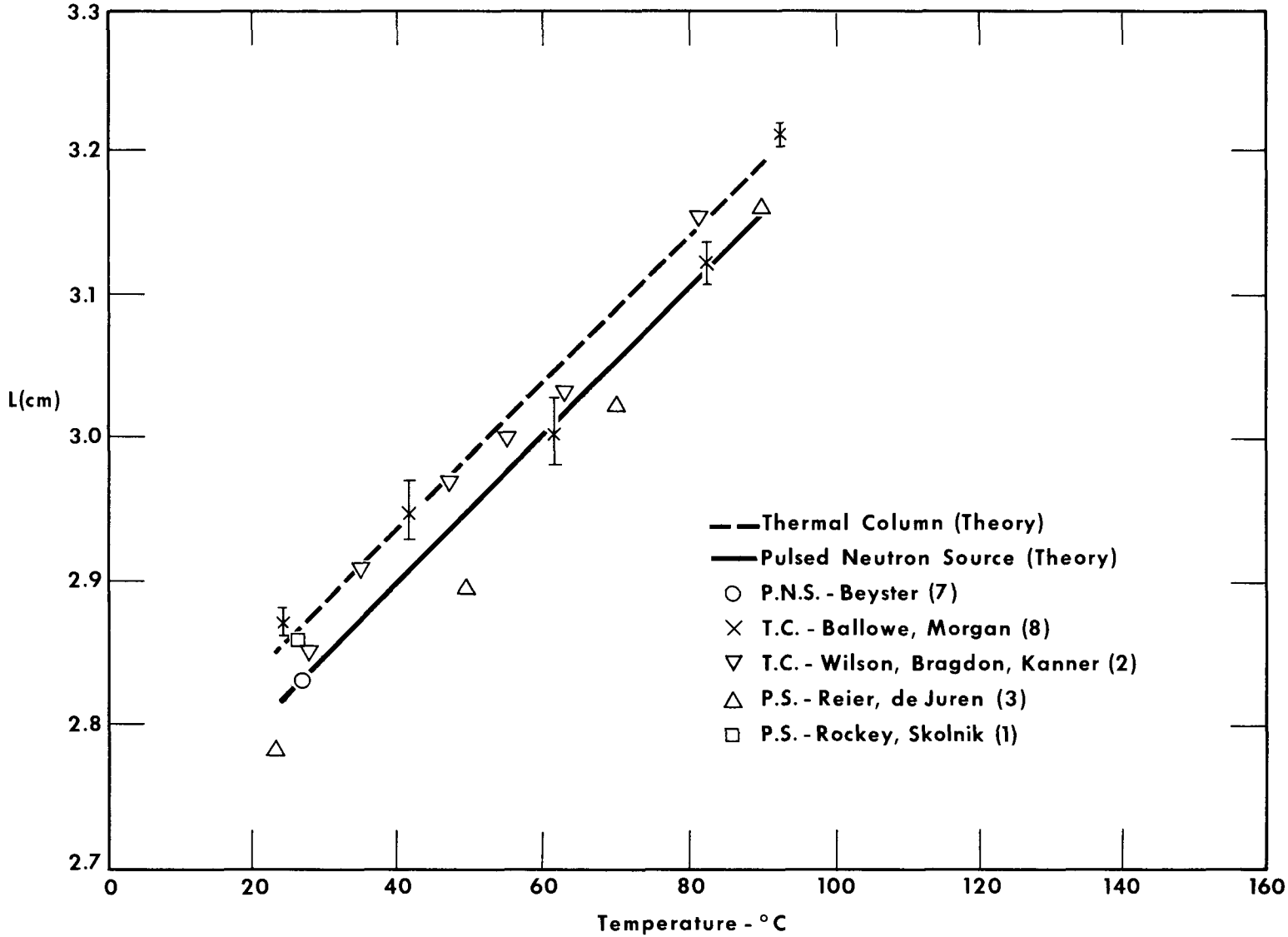

Figure 2. DIFFUSION LENGTH VERSUS TEMPERATURE

THERMALISATION OF NEUTRONS IN GRAPHITE

E. Barnard

N. A. Khan

M. J. Poole

J. H. Tait

R. C. F. McLatchie

Atomic Energy Research Establishment

Harwell, England

1. Introduction

With the growth of practical reactors there has been an increasing interest in the details of the neutron spectrum set up in a system containing absorbers and moderators. This stems very largely from the need to predict temperature coefficients throughout the life of the reactor, and is particularly pressing when problems of plutonium fuelled reactors are considered, because of the resonance at 0.3 eV in the fission cross section. The problem of predicting the neutron spectrum in a reactor can to some extent be considered in two parts. First we can try to calculate the spectrum in an infinite homogeneous medium, and only when this aspect is fully understood is there any sense in considering the effect of heterogeneities. The equation governing the steady state neutron spectrum in an infinite homogeneous medium is

$$\Sigma_t(E)\,\phi(E) = \int_0^\infty \Sigma(E' \to E)\,\phi(E')\,dE' + S(E) \qquad \cdots(1)$$

where $\Sigma_t(E)$ is the total neutron cross-section for the medium $\Sigma(E' \to E)$ is the inelastic scattering cross section for scattering from energy E' to energy E and S(E) the source density at energy E. (Normally S(E) is assumed to have the form $S\delta(E_0)$ where $\delta(E_0)$ is the Kronecker delta function).

Mathematical methods exist (') for solving this equation once $\Sigma_t(E)$ and $\Sigma(E' \to E)$ are known. In general $\Sigma_t(E)$ is available but until recently little has been known about $\Sigma(E' \to E)$. Various models have been developed which enable $\Sigma(E' \to E)$ to be calculated in a few cases, (e.g. Nelkin's model for water [2], Park's model for graphite [3] and more recently data is becoming available from the Chalk River Scattering Project [4]. In

principle this latter should give all the required information, but mainly due to intensity considerations, regions of $\Sigma'(E' \rightarrow E)$ involving large energy changes* are inaccessable to the experiment, and resort has once again to be made to theoretical models to fill in the gaps in the experiment. It is to test the validity of such models that neutron spectrum measurements are made.

Now, if in equation (I) we write $\Sigma'_t = \Sigma'_s + \Sigma'_a$, where $\Sigma'_s = \int_0^\infty \Sigma'(E \rightarrow E')dE'$ and apply the principle of detailed balance, we obtain

$$\phi(E)\Sigma'_a(E) = M(E)\int_0^\infty \Sigma'(E \rightarrow E') \left\{ \frac{\phi(E')}{M(E')} - \frac{\phi(E)}{M(E)} \right\} dE' + SS(E_o) \text{------ II}$$

where $\Sigma'_a(E)$ is the macroscopic absorption cross section while $M(E)$ and $M(E')$ are the intensities of a Maxwellian energy distribution at E and E' respectively.

Equation II shows immediately that for $\Sigma'_a = 0$ the distribution must become an equilibrium Maxwellian distribution and no information is given about the scattering kernel $\Sigma'(E \rightarrow E')$; as Σ'_a increases then the spectra become progressively more sensitive to the forms of $\Sigma'(E \rightarrow E')$ and progressively more distorted from the Maxwellian form. It is considerations of this nature that have lead to the wealth of experiments made in poisoned homogeneous media ([5 to 8]), and substantial agreement with theoretical calculations is shown in these papers. However poisoned moderator experiments suffer from the disadvantage that as the poison concentration is increased, so the neutron intensity available decreases, and there is thus a compati-

---

* The quantity measured in the Scattering Project is not simply $\Sigma'(E' \rightarrow E)$ but is $\Sigma'(E', E, \theta)$ where θ is the scattering angle and $\Sigma'(E' \rightarrow E) = 2\pi \int_0^\pi \Sigma'(E', E, \theta) \sin\theta \, d\theta$

tion between accuracy of the measurement and sensitivity to the quantity of interest. An alternative approach therefore is to distort the equilibrium Maxwellian obtained in a pure moderator, not by introducing poison but by using a pulsed neutron source and studying the variation of the spectrum with time after the pulse.*

Equation II is then replaced by

$$\Sigma_a \Phi(E) + \frac{1}{v}\frac{d\Phi(E)}{dt} = M(E)\int_0^\infty \Sigma(E\to E')\left\{\frac{\Phi(E')}{M(E')} - \frac{\Phi(E)}{M(E)}\right\}dE' \quad \text{---III}$$

Again the asymptotic solution for long times and low absorption is

$$\left.\frac{d\Phi(E)}{dt}\right|_{t\to\infty} \to 0 \qquad \Phi(E) \to M(E)$$

but now the principal distortion accurs at intermediate times after the pulse when the neutron intensity is relatively high. A further advantage of this type of experiment is seen when working with solid moderator (e.g. graphite) when it is in practice extremely difficult to obtain a completely homogeneous distribution of poison of known intensity. In the time dependent experiment only pure moderator is used and this difficulty vanishes.

Time dependent spectrum measurements reported in the literature are mostly confined to studies of the diffusion cooling effect by measuring the relaxation time of moderator assemblies of different sizes [9,10] and to studies of the mean temperature of neutrons in an assembly as a function of time after a neutron pulse by measuring the variation with time of the

---

* It can be formally demonstrated that the time dependent spectra and the 1/v poison spectra are related through the Laplace transformation, but this is of little practical value.

absorption coefficient of e.g. silver [11,12]. Beckurts [13] has used a time of flight method to measure the infinite time asymptotic spectrum in water in small geometry. However this experiment depends on distortion of the Maxwellian by leakage of neutrons and is thus less general than the work to be described. In the following paper experiments will be described which measure the spectrum of neutrons existing in a graphite block at times ranging from 300 μsec to 1000 μsec, after the introduction of a fast neutron pulse. Theoretical spectra, obtained by inserting the scattering kernel for graphite deduced by Egelstaff into equation III and solving numerically are also presented.

2. Experimental method

The experiment is best understood by reference to Figs. 1 and 2 which show the layout of the experiment and a schematic diagram of the electronics respectively. The Harwell 28 MeV linac provided a pulsed electron beam which was stopped in a mercury target to produce X-rays which then liberated neutrons by the γ-n and γ-f reactions from a natural uranium target placed at A. In this way, pulses of neutrons 1 μsec long and containing $\sim 10^{11}$ neutrons per pulse, were obtained. A proportion of these neutrons enter and are thermalized in the graphite block B of size 60 cm by 62.2 cm by 71.1 cm. This is positioned so that the neutron source lies in the centre of the face in order to minimise the effect of spatial harmonics on the flux at the centre of the block.

Fast neutrons entering the block will first of all be slowed down to near thermal energies by elastic collisions with individual carbon atoms. At this stage their spectrum will be approximately Maxwellian but with a mean energy above that of the atoms in the block. This "hot"

neutron population will then proceed to exchange energy with the graphite crystals and will gradually achieve - in the case of an infinite graphite block - true thermal equilibrium with the graphite lattice. The effect of leakage from the graphite will be to cause the magnitude of the neutron flux to decay with time after the pulse, and also by virtue of the "diffusion cooling" effect the thermalisation proceeds more rapidly and the asymptotic spectrum achieved at long times will have a lower mean energy than would an equilibrium spectrum. The relaxation time for the flux calculated from the block size, the diffusion coefficient and diffusion cooling coefficient of graphite is 775·5 μsec. in reasonable agreement with our measured value of (754 ±9) μsec

A beam of neutrons is extracted from the centre of this block by cutting a channel 5 cm by 6 cm from the centre to one face. In this beam is placed a slow neutron chopper C, flight tube D, and boron trifluoride proportional counters E. If now the chopper is rotated in synchronism with the pulses from the accelerator it serves two purposes; firstly it isolates a "bunch" of neutrons leaving the block at a definite moment after the fast neutron pulse from the accelerator and secondly it provides a neutron pulse for a time of flight experiment to measure the spectrum of neutrons present at this instant. How this is done in detail can be seen by reference to Fig 2. A pulse is generated, by a mirror and photcell system mounted on the chopper, coincident with the moment of opening. This pulse is then fed to an adjustable delay circuit where it is delayed by a time T_1 and the delayed pulse used to trigger the electron pulse from the accelerator. If now the period of rotation of the chopper is $2T_o$ (it transmits neutrons twice per revolution), then the accelerator pulse will

occur at time $(T_o - T_1)$ befpre the next time of opening of the chopper. The pulse is now fed through a second delay T_2 and used to initiate the first channel of a multichannel time spectrometer. Pulses from the BF_3 counters are analysed in time by this spectrometer, whose first channel will then open at a time $(T_1 + T_2 - T_o)$ also after the next chapper opening from the one initiating the sequence. Thus by suitably choosing T_1 and T_2 it is possible to select neutrons passing through the chopper ay any desired time after the fast neutron burst into the block, and then to measure any desired part of the neutron spectrum by time-of-flight, subject to the limitations that

(a) $T_1 < T_o$

(b) $T_1 + T_2 - T_o + n\Delta < T_o$ i.e. $T_1 + T_2 + n\Delta < 2T_o$

where Δ is the width of a timing channel and n the number of channels in use.

(c) The flight time of the slowest neutron measured from the block to the chopper must not be greater than $(T_o - T_1)$.

(d) $T_o \gg \tau$ where τ is the relaxation time of thermal neutrons in the block.

(e) The flight time to the counters of the slowest neutron transmitted by the chopper must be less than $(2T_o - T_1 - T_2)$

3. Details of Equipment

The graphite block was 60 cm by 62.2 cm by 71.1 cm in size and was completely surrounded by cadmium sheet to absorb stray neutrons. A channel 5 cm by 6 cm was cut to the centre of the block and a conventional multiplate "Fermi" chopper whose rotor was constructed of K-monel alloy, was located in front of this channel; the distance from the block centre

to the chopper centre being 57.9 cm. This chopper had five slits 0.45 cm high by 1.3 cm long and was normally rotated at a speed of 80 r.p.s. to give 160 neutron bursts per second. Thus the burst width was 136 μsec. Neutrons passing through the chopper travelled a 2.81 metre flight distance before impinging on the boron trifuoride counters used as a neutron detector. This detector consisted of a bank of ten counters each 2 in. in diameter, mounted in three rows behind one another, and filled to a pressure of 70 cm. mercury with 90% enriched boron trifuoride. The variation of sensitivity with neutron energy of these counters was determined by experimental comparison with the sensitivity of boron trifuoride counters "thin" enough to have a 1/v sensitivity law. This comparison was done on an independent chopper spectrometer using the LIDO reactor as the neutron source. The chopper flight path and counter were all completely surrounded by a cadmium shield and in addition a lead wall 10 cm thick was built to shield the counters as far as possible from the intense X-ray flash from the linac target. A cadmium shutter could be lowered into the beam immediately before the chopper in order to make background measurements.

As times taken for neutrons from the centre of the block to the chopper depended on their energy, the spectrum as measured did not represent the spectrum of neutrons in the block at one definite time, and to derive this it was necessary to make use of a whole family of spectra measured for different delay times ($T_o - T_1$). Thus the absolute intensities of different spectra must be related, and to do this neutron monitors were mounted at F and G. These each consisted of a small ionisation chamber containing U-235. Amplified fission pulses from these

were fed through a time "gate" which allowed them to pass during a definite interval after the accelerator pulse, to standard scaling units.

4. Determination of the Transmission function of the Chopper

Before spectra can be calculated from the data it is necessary to know the transmission function of the chopper and collimator assembly as a function of neutron velocity (energy). Stone and Slovacek [14] and Mostovoi [15] have calculated the transmission of a rotating slit in a parallel beam of neutrons. However in our case collimators were used to determine the area viewed in the graphite and the beam was considerably divergent.((Fig 3 shows the beam geometry). Thus the calculations given in the above references are not applicable. To calculate the cut-off function the effect of collimators and rotor was separated. If a neutron passes through the complete system, it does so because it would both

(a) be acceptable by the fixed slits in the absence of the rotating slits

(b) be accepted by the rotating slits in the absence of the fixed slits

Using this principle an IBM 7090 programme was written by M.S. Marlow of The Theoretical Physics Division, Harwell, and the results of these computations are shown in Fig.4, together with the cut-off function for the same rotor in a parallel neutron beam calculated according to the method of Stone and Slovacek. By making use of the fact that the transmission is always a function of $\frac{V}{\omega}$ (ω = angular velocity of rotor, V = velocity of neutrons). and by taking measurements with different values of ω it is possible to verify these calculations experimentally.

The results of such an experiment are also shown in Fig.4. The calculations do not take account of the exponential decay of the neutron density which is itself not negligible during the time the chopper is open. However it is easy to show that the effect of this on the overall cut-off function is less than 0.1% so that this has been neglected and a constant source assumed.

5. Calculation of Neutron Spectra from Experimental data

Experimental runs were taken for a range of $(T_0 - T_1)$ from 300 μsec to 2000 μsec. The counts obtained were corrected for counting losses due to the fact that the analyser could only accept one pulse per chopper burst, for neutron background (cadmium shutter closed), for variation of counter sensitivity with energy, and for attenuation by air and quartz windows in neutron beam. The finite resolution of the spectrometer was then allowed for using the formula given by Stone and Slovacek[7]

$$I(t) = O(t)\left[1 - \frac{1}{2O(t)}\frac{d^2O(t)}{dt^2}\int_{-\infty}^{+\infty}\lambda^2 R(\lambda)\,d\lambda + \left\{\frac{1}{4}\left(\int_{-\infty}^{+\infty}\lambda^2 R(\lambda)\,d\lambda\right)^2 - \frac{1}{4!}\int_{-\infty}^{+\infty}\lambda^4 R(\lambda)\,d\lambda\right\}\frac{d^4O(t)}{O(t)\,dt^4} + \cdots\right] \qquad \text{IV}$$

and the transmission function of the chopper put in using the curve shown in Fig.4 above. At this stage it is possible to plot the data as a series of decay curves of neutron intensity for each neutron energy (Fig.5). From these decay curves it is possible to read off the neutron intensity for each energy for neutrons leaving the source block at a fixed time and so to construct a series of neutron spectra for neutrons present in the block at different times after the accelerator pulse. Such spectra are shown in Fig. 6.

6. Discussion of the results

Before making detailed comparisons with computed spectra, it is useful to look at this data in the light of the elementary thermalisation theory suggested inter alia, by Beckurts[16]. By considering the energy balance per neutron in unit volume of the moderator at any given moment in the thermalisation process, we have

$$\text{Mean rate of energy loss to moderator} = \frac{3}{2}k\gamma(T-T_o)$$

$$\text{Mean rate of loss of energy by escape of neutrons} = \frac{\lambda_{tr}\bar{v}}{3} B^2(E_D - \frac{3}{2} kT)$$

where

T = effective temperature of neutron population

T_o = moderator temperature

E_D = mean energy of escaping neutrons

γ = "heat transfer coefficient" between neutrons and moderator

k = Boltzman's constant

λ_{tr} = transport mean free path for neutrons

$\bar{v}$ = mean velocity of neutron population

B^2 = the geometric buckling

Then

$$\frac{3}{2} k \frac{dT}{dt} = \frac{3}{2} k\gamma(T-T_o) - \frac{\lambda_{tr}}{3} \bar{v}B^2(E_D - \frac{3}{2} kT) \qquad V$$

and as in graphite, E_D is very nearly equal to $2kT$,

$$\frac{dT}{dt} = -(\gamma + \frac{\lambda_{tr}}{9} \bar{v} B^2)(T - \frac{\gamma}{\gamma + \frac{\lambda_{tr}\bar{v}B^2}{9}} T_o) \qquad VI$$

So that

$$(T - \frac{\gamma}{\gamma + \frac{1}{9} \lambda_{tr}\bar{v}B^2} T_o) = K \exp\{-(\gamma + \frac{1}{9} \lambda_{tr}\bar{v}B^2)t\} \qquad VII$$

where K is an arbitrary constant, from which it is immediately obvious that the asymptotic neutron temperature at infinite time is.

$$T_{as} = \frac{\gamma}{\gamma + \frac{1}{9}\lambda_{tr}\bar{v}B^2} T_o \qquad \text{VIII}$$

and the relaxationt time for neutron temperature is

$$\tau = \gamma + \frac{1}{9}\lambda_{tr}\bar{v}B^2 \qquad \text{IX}$$

It can also be easily shown that if the asymptotic time dependence of the total flux is given by

$$\phi = \phi_o \exp - \alpha t$$

with

$$\alpha = \Sigma_a \bar{v} + DB^2 - CB^4$$

Then C is the diffusion cooling coefficient, given by

$$C = \frac{(\frac{\lambda_{tr}\bar{v}}{3})^2}{6\gamma} \qquad \text{X}$$

Using these relations, values of C, T_{as}, $\frac{1}{\alpha}$ and τ have been calculated for $\frac{1}{\gamma}$ = 185 μsec and $\frac{1}{\gamma}$ = 400 μsec, and Fig. 7 shows corresponding graphs of $\bar{E}$ against time ($\bar{E}$ is the mean neutron energy in the distribution and is related to T by $\bar{E} = \frac{3}{2}$ kT). On fig. 7 are also plotted experimental values of $\bar{E}$ obtained by integrating the measured energy distribution and it will be immediately obvious that the data are in better agreement with the assumption of $\frac{1}{\gamma}$ = 400μsec than the presently accepted value of 185 μsec. This of course also implies that the diffusion cooling coefficients as published are also too small by about a factor two*. Unfortunately the shape of the $\bar{E}$ versus t curves becomes rather insensitive to $\frac{1}{\gamma}$ for values of $\frac{1}{\gamma}$ greater than 400 μsec;

---

*Beckurts (private communication) has also suggested that the published values for C are too small by a factor two.

so it is not possible to give from these experiments any reliable upper limit to $\frac{1}{\gamma}$; what is clear is that no value less than about 350 μsec will give acceptable fit to the data.

A further check on the most appropriate value for $\frac{1}{\gamma}$ is given from the measurement of the relaxation time α for the total flux and the value of 775.5 μsec computed from the assumption $\frac{1}{\gamma}$ = 400 μsec is in reasonable agreement with the measured value of (754 ± 9) μsec, whereas if $\frac{1}{\gamma}$ were 185 μsec then a relaxation time for this block of 708.7 μsec would be predicted. Table I summarises the parameters obtained.

Comparison of the spectra with detailed theoretical computations are given in the next section.

Table I

Assumed $\tau_\infty (= \frac{1}{\gamma})$ in μ sec.	τ (for $B^2 = 6.43.10^{-3}$ cm^{-2}) μ sec.	C $cm^4\ sec^{-1}$	E_{as} $(= \frac{3}{2} kT_{as})$ eV	Computed relaxation time $\frac{1}{\alpha}$, for overall decay of neutron flux μ-sec.	Observed relaxation time $\frac{1}{\alpha}$, for overall decay of neutron flux μ-sec.
185	170.4	$14.4.10^5$	0.0353	708.7	754. ±9.
400	339.7	$28.5.10^5$	0.0325	775.5	

7. Theory of time dependent spectra

Equations

In this section we describe calculations of the time dependent neutron spectra in a slab. We restrict ourselves to the diffusion

approximation and consider the equation

$$\frac{1}{v} \cdot \frac{\partial \phi(E,\underline{r},t)}{\partial t} = -[\Sigma_a(E)+\Sigma_s(E)-D(E)\nabla^2]\phi(E,\underline{r},t) + \int_o^{E_o} \Sigma_s(E').F(E'\rightarrow E).\phi(E',\underline{r},t).dE' + S(E,\underline{r},t). \quad XI$$

Here $\phi(E,\underline{r},t)$ is the flux of neutrons at the point $\underline{r}$ in the slab having energy E at time t;

$\Sigma_a(E)$ and $\Sigma_s(E)$ are the macroscopic absorption and scattering cross sections at energy E respectively; D(E) is the diffusion coefficient which is equal to $\frac{\lambda_t(E)}{3(1-b)}$, where $\lambda_t(E)$ is the total mean free path and b is the average of the cosine of the angle of scatter;

$F(E'\rightarrow E)dE$ is the probability that a neutron which undergoes a scattering collision at energy E' is scattered into the energy interval dE at E;

$S(E,\underline{r},t)$ is the number of neutrons of energy E coming directly from the sources at the position $\underline{r}$ and at time t, E_o is the energy .258 eV. (10KT)

In the derivation of (1) from the Boltzmann transport equation it is assumed that the distribution is almost isotropic. This is a valid assumption at most points in the slab because the dimensions of the latter (60 cm × 62 cm × 71 cm) are many neutron mean free paths.

A further assumption is made in the derivation of XI. A term $\frac{3D}{v^2}\frac{\partial^2\phi}{\partial t^2}$ is neglected in comparison with $\frac{1}{v} \cdot \frac{\partial \phi}{\partial t}$. We can test the validity of this assumption by an examination of the experimental results. At a time 100 μsecs. after the introduction of the source the magnitude of the term $\frac{3D}{v^2} \cdot \frac{\partial^2\phi}{\partial t^2}$ is 10% of the term $\frac{1}{v} \cdot \frac{\partial \phi}{\partial t}$ at the energy 0.135 e.v. at later times the ratio of the two terms becomes smaller.

We now expand $\phi(E,\underline{r},t)$ and $S(E,\underline{r},t)$ as follows

$$\phi(E,\underline{r},t) = \sum_{n=0}^{\infty} \phi_n(\underline{r})\phi_n(E,t), \quad XII$$

$$S(E,\underline{r},t) = \sum_{n=0}^{\infty} \phi_n(\underline{r}).S_n(E,t), \quad XIII$$

where $\phi_n(\underline{r})$ satisfies the equation

$$\nabla^2\phi_n(\underline{r}) = - B_n^2\ \phi_n(\underline{r}),$$

and $\phi_n(\underline{r}) = 0$ at the extrapolated boundary. Substituting (2) and (3) into equation (1) we find that $\phi_n(E,t)$ satisfies the equation

$$\frac{1}{v} \cdot \frac{\partial\phi_n(E,t)}{\partial t} = - [\Sigma_a(E)+\Sigma_s(E)+D(E).B_n^2].\phi_n(E,t)$$

$$+ \int_0^{E_o} \Sigma_s(E')F(E'\rightarrow E).\phi_n(E',t)dE' + S_n(E,t). \qquad \text{XIV}$$

In the experiment neutrons enter one face of the block and the spectrum is examined at its centre. This means that the second mode does not contribute to the measured spectrum as $\phi_2(\underline{r})$ is zero at this point. The third mode is quite negligible compared with the first for energies near to thermal, because the ratio of the fast non leakage probabilities during slowing down $\exp[-B_n^2-B_o^2\tau]$ is of the order of 10^{-7}. We therefore solve equation XIV for the first mode $\phi_o(\underline{r})$.

$S_o(E,t)$ is the source term for neutrons being scattered to energies below E_T = .285 e.v. We assume that this is given by Fermi age theory.

$S_o(E,t_s)$ is given by

$$\delta(t-t_s) \int_{E_T}^{E/\alpha} \frac{\Sigma_s.\exp[-B_o^2\tau(E').S(E_o)dE'}{\xi.\Sigma_s.E'.(1-\alpha)} \qquad \text{XV}$$

where ξ is the mean logarithmic energy loss in a collision with an atom of carbon;

$(1-\alpha)$ is the maximum fractional energy change in a collision; $S(E_o)$ is the source strength at energy E_o;

$\tau(E')$ is the Fermi age for the energy interval E_o to E';

$\exp[-B_o^2.\tau(E')]$ is the non escape probability factor;

t_s is the slowing down time of neutrons having a final energy in the

interval between E_T and E_T/α. Assuming that $\exp[-B_0^2\tau(E')]$ does not change in the energy interval E_T to E/α then,

$$S(E,t_s) = \delta(t-t_s).\ \frac{S(E_o).\exp[-B_0^2\tau].(1-\frac{\alpha E_T}{E})}{\xi.(1-\alpha).E_T.} \qquad \text{XVI}$$

Numerical solution of the equations.

The slowing-down scattering integral, the source term of the equation, is approximated by a (2n+1) point Simpson rule quadrature formula. Taking (2n+1) initial values of $\phi_o(E,t)$ we get a set of (2n+1) linear differential equations with constant coefficients in the (2n+1) unknowns $\phi_o(E_i,t)$, i=1, 2, ..., 2n+1. These equations may be written

$$\frac{\partial \underset{\sim}{\phi}_o}{\partial t} = \underset{\sim}{\phi}_o . A , \qquad \text{XVII}$$

where A is the (2n+1) x (2n+1) matrix with ith column A_i given by

$$A_i = \begin{bmatrix} \Sigma(E_1\to E_i)\phi_o(E_1)V(E_i).\frac{\Delta E}{3} \\ 4\Sigma(E_2\to E_i)\phi_o(E_2)V(E_i).\Delta E/3 \\ 2\Sigma(E_3\to E_i)\phi_o(E_3)V(E_i).\Delta E/3 \\ \cdots\quad\cdots\quad\cdots\quad\cdots \\ \left\{\left(4-2(i-2[\frac{i}{2}])\right)\Sigma(E_i\to E_i)\phi_o(E_i)\frac{\Delta E}{3} - \Sigma(E_i) - B^2\Delta(E_i)\right\}V(E_i) \\ \cdots\quad\cdots\quad\cdots\quad\cdots \\ \Sigma(E_{2n+1}\to E_i)\phi_o(E_{2n+1})V(E_i)\frac{\Delta E}{3} . \end{bmatrix}$$

Here $D(E_i) = \dfrac{1}{3\Sigma_s(E_i)(1-\frac{2}{3.A})}$.

The solution of (7) is $\underset{\sim}{\phi}_o(t) = Be^{At}$,

$$\text{i.e. } \underset{\sim}{\phi}_o(t+\Delta t) = e^{A.\Delta t}\,\underset{\sim}{\phi}_o(t), \qquad \text{XVIII}$$

where the exponential of the matrix $A\Delta t$ is given by

$$e^{A\Delta t} = I + A\,\Delta t + \frac{A^2\Delta t^2}{2!} + \frac{A^3\Delta t^3}{3!} + \cdots .$$

To calculate $e^{A\Delta t}$ we first use Gersgorin's theorem to estimate the absolutely largest eigenvalue, λ_M, of the matrix A. A maximum step length, h_M, is then found from

$$\lambda_M . h_M = \varepsilon,$$

where ε is a small constant and the smallest value of S is found for which

$$h = \frac{\Delta t}{2^s} \leq h_M, \quad s \geq 0.$$

The matrix e^{Ah} is calculated from

$$e^{Ah} = \left[\left(\left[\left(\frac{Ah}{4} + I\right)\frac{Ah}{3} + I\right]\frac{Ah}{2} + I\right)\frac{Ah}{1} + I\right]$$

Finally $e^{A\Delta t}$ is given by

$$e^{A\Delta t} = (e^{Ah})^{2^s}.$$

For p × p matrix A, approximately $2(3 + s)p^3 + p^2$ multiplications are required to evaluate $e^{A\Delta t}$, with p^2 multiplications for each step.

In the cases we have considered s has been found to be about 8(ε = .02, Δt = 50 μs) so that 20 steps require $22p^3 + 21p^2$ multiplications which take approximately .000034,$(22p^3 + 21p^2)$ seconds on an IBM 7090.

Data used in the calculations

Calculations were carried out using cross sections for the energy transfer in the thermal region obtained from the heavy gas model and also from the data obtained from the scattering law experiments at Chalk River. In these latter experiments the differential scattering cross section $\sigma(E \to E', \theta)$ for scattering from energy E to energy E' through an angle θ is measured. This data is augmented by theoretical

estimates to obtain a complete scattering law in the thermal region, a paper by J.D. Macdougall[17] describes a programme PIXSE which produces multigroup cross sections from the scattering law.

The programme PIXSE also gives the cross sections for scattering by a monatomic gas. In this case $\sigma(E \to E')$ is evaluated directly from the formulae

$$\sigma(E \to E') = \frac{\sigma_s \eta^2}{2E} \left[\exp(x^2 - x'^2)\{\mathrm{erf}(\eta x - \rho x') + \mathrm{erf}(\eta x + \rho x')\} + \mathrm{erf}(\eta x' - \rho x) - \mathrm{erf}(\eta x' + \rho x)\right] \text{ for } E < E'$$

$$\sigma(E \to E') = \frac{\sigma_s \cdot \eta^2}{2E} \left[\exp(x^2 - x'^2)\{\mathrm{erf}(\eta x - \rho x') - \mathrm{erf}(\eta x + \rho x')\} + \mathrm{erf}(\eta x' - \rho x) + \mathrm{erf}(\eta x' + \rho x)\right] \text{ for } E > E',$$

where σ_s is the free atom cross section, $x^2 = E/kT$, $x'^2 = E'/kT$, $\eta = (A+1)/2\sqrt{A}$, $\rho = (A-1)/2\sqrt{A}$, A is the mass of the scatterer in units of neutron mass, T is the temperature of the scatterer in °K and k is Boltzmann's constant.

8. Comparison with experimental data

Fig. 8 shows the results of this theory for times of 300 μsec to 1000 μsec, and these are further compared with the experimental data in Figs. 9 to 13. The theoretical and experimental spectra have been normalised to give the best fit on the intensity scale for the 300 μsecs spectrum, but apart from this no normalisation has been carried out. It will be seen that reasonable agreement is obtained with the exception of the 1000 μsecs spectrum where the accuracy of the experimental data is in any case not very good. For comparison a spectrum calculated from the heavy gas model (A = 12) is shown in the 300 μsec case, and the lack of agreement with experiment is obvious, the free gas calculation giving far too rapid progress of thermalisation. Figs. 9 to 13 also show heavy

gas calculations made with an "effective mass" of 33 and it is clear that these results are much closer to those obtained using the true scattering law. However significant differences are seen for "medium" times after the neutron pulse, and it is interesting that these differences are qualitatively similar to those obtained between heavy gas and crystal model calculations for poisoned systems (i.e. heavy gas gives too many low energy neutrons). The experimental data are as yet not sufficiently accurate to give a clear decision between the merits of the two calculations, but it can be seen that in the 450 μsec and 600 μsec spectra they do appear to lie closer to the calculations using the Egelstaff scattering law.

9. Acknowledgements

The numerical method outlined in section 7 was suggested by A.R. Curtis, S. Marlow gave considerable help in the coding of the FORTRAN programme for the theory and K. Diment assisted in setting up the experimental equipment and doing the actual runs. Thanks are also due to the operating crew of the linac for their efforts during this work.

10. References

1. A.M. Weinberg and E.P. Wigner, "The Physical Theory of Neutron Chain Reactors". University of Chicago Press.
2. M.S. Nelkin, Phys.Rev. 119, 741 (1960)
3. D.E. Parks, Nucl. Sci. Eng. 9, 430 (1961)
4. P.A. Egelstaff, AERE – R.3931 (1962)
5. M.J. Poole, J. Nucl. Eng. 5 325 (1957)
6. J.R. Beyster, J.L. Wood, W.M. Lopez and R.B. Walton Nucl. Sci. Eng. 9, 168 (1961)
7. R.S. Stone and R.E. Slovacek, Nucl. Sci. Eng. 6, 466 (1959)
8. D.E. Parks, J.R. Beyster and N.F. Wikner GA – 2437 September (1961)
9. G.F. von Dardel and N.G. Sjöstrand Phys.Rev. 96, 1245 (1945)
10. K.H. Beckurts Nucl. Sci. Eng. 2, 516 (1957)
11. A. Antonov et al, Geneva Conf. 5 87 (1956b)
12. G.F. von Dardel, Trans. Roy. Inst. Technol. Stockholm 75, 1 (1954)
13. K.H. Beckurts, Zeits of Naturforschung 16a, 611 (1961)
14. R.S. Stone and R.E. Slovacek, KAPL – 1499 (1956)
15. V.I. Mostovoi, M.I. Pevzner and A.P. Isitovich P/640 Geneva Conf 1955
16. K. Wirtz and K.H. Beckurts "Elementare Neutronenphysik" Springer-Verlag, Berlin(1958)
17. J.D. Macdougall "Application of scattering law data to the calculation of thermal neutron spectra" Current Conference Paper.

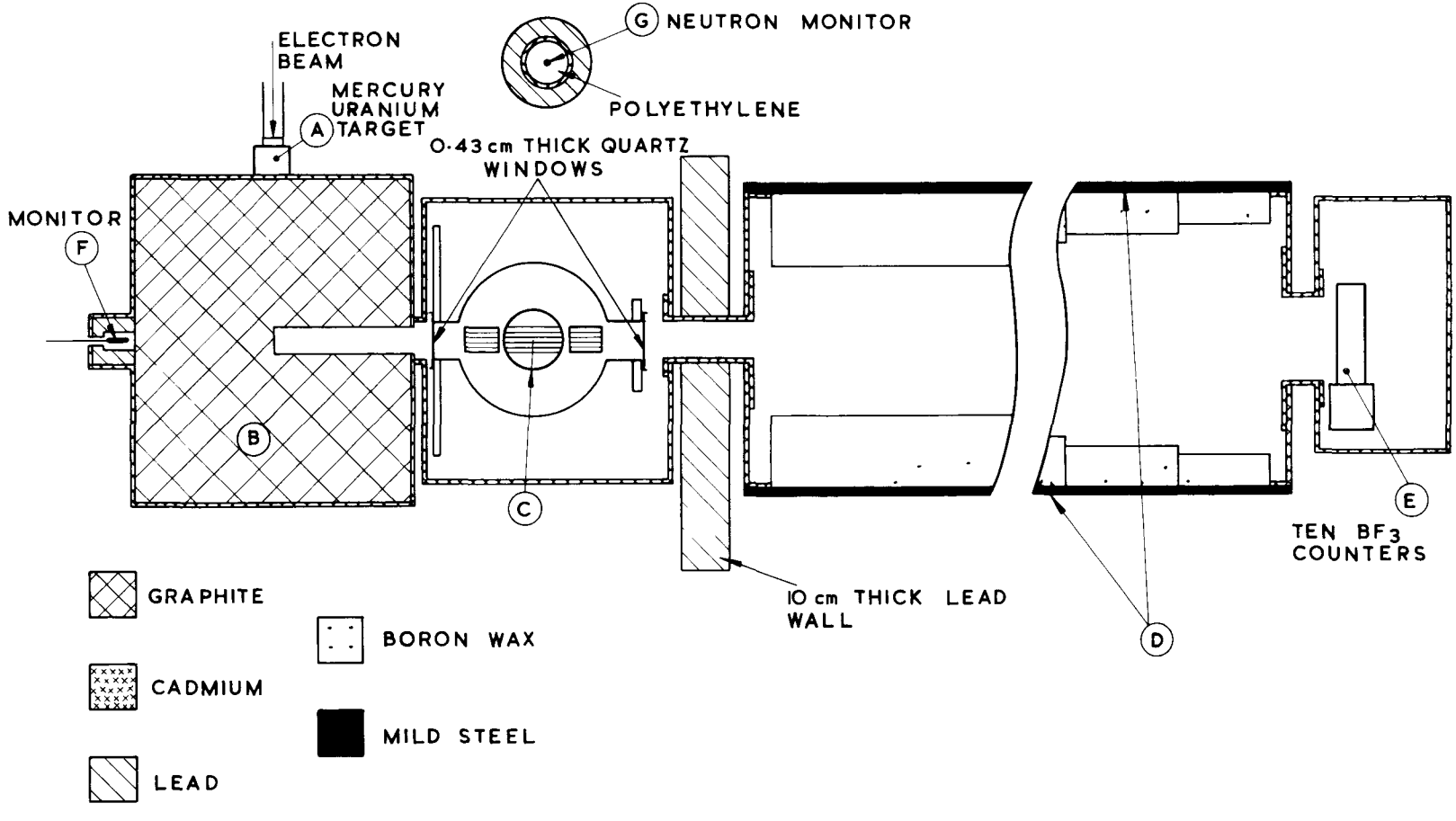

FIG 1 EXPERIMENTAL ARRANGEMENT.

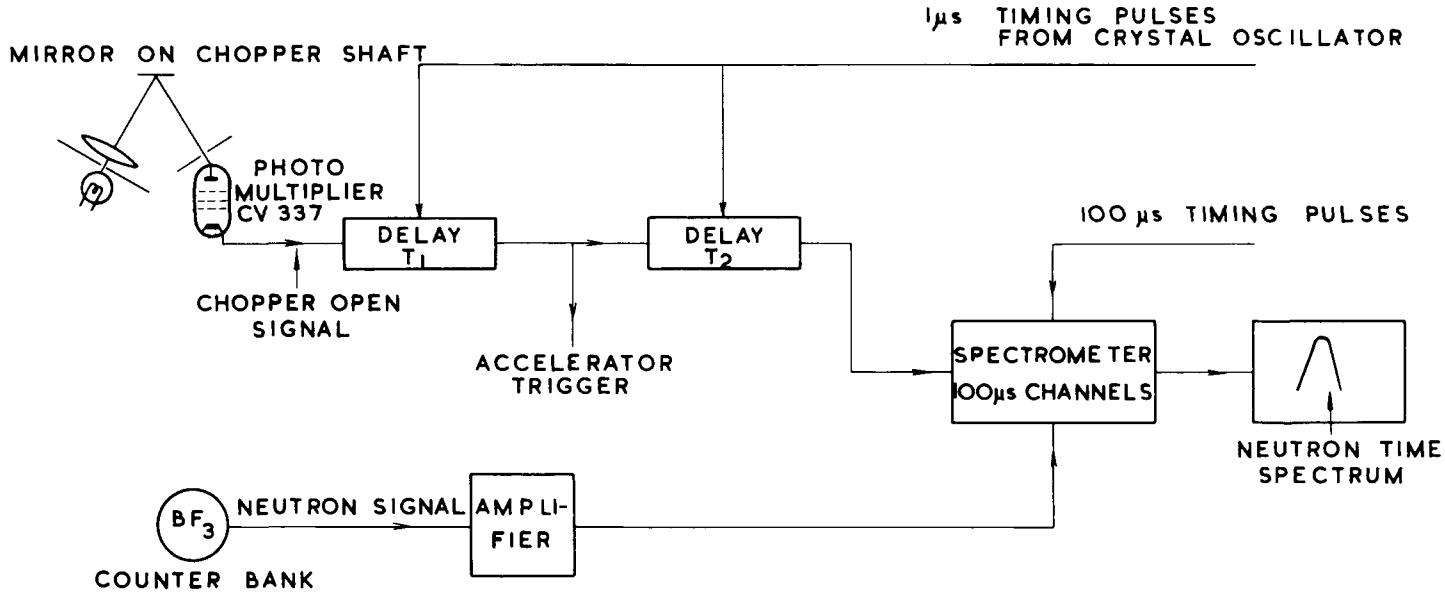

FIG. 2. BLOCK DIAGRAM FOR ELECTRONICS

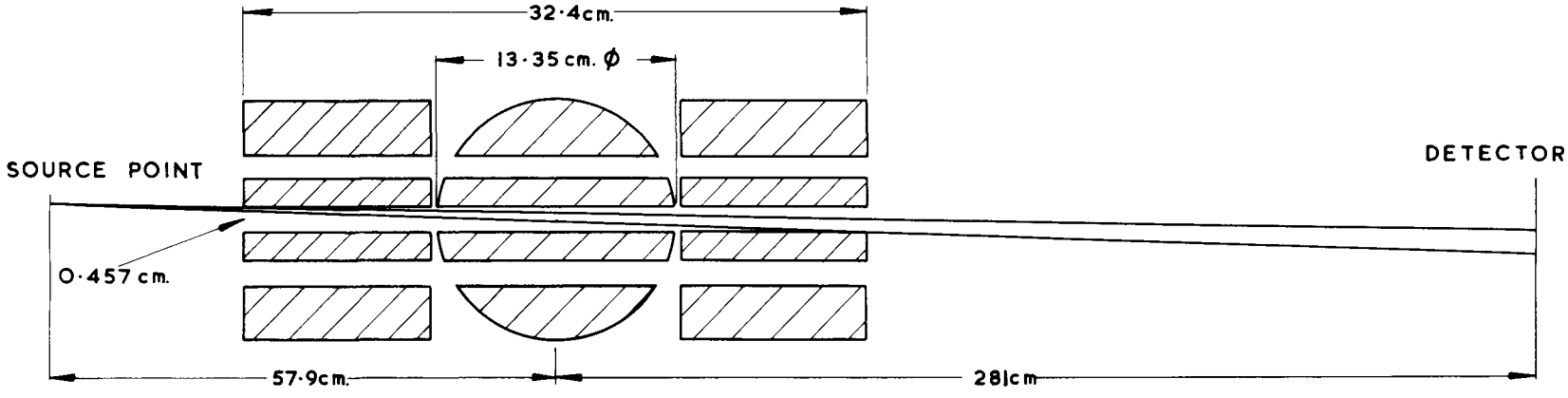

FIG. 3. NEUTRON BEAM GEOMETRY SHOWING REDUCTION IN EFFECTIVE WIDTH OF OBLIQUE BEAMS.

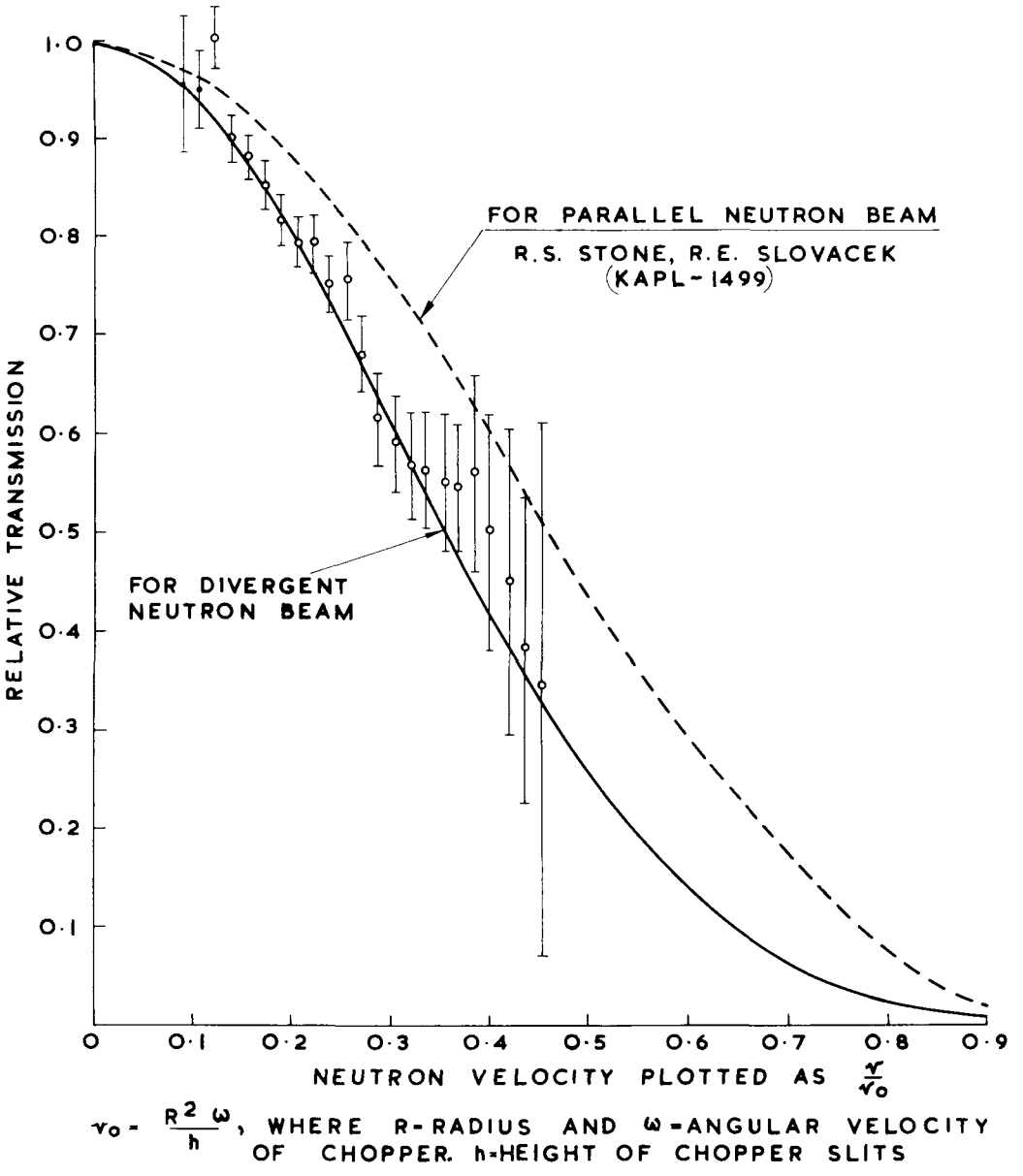

FIG. 4. CHOPPER CUT OFF FUNCTION

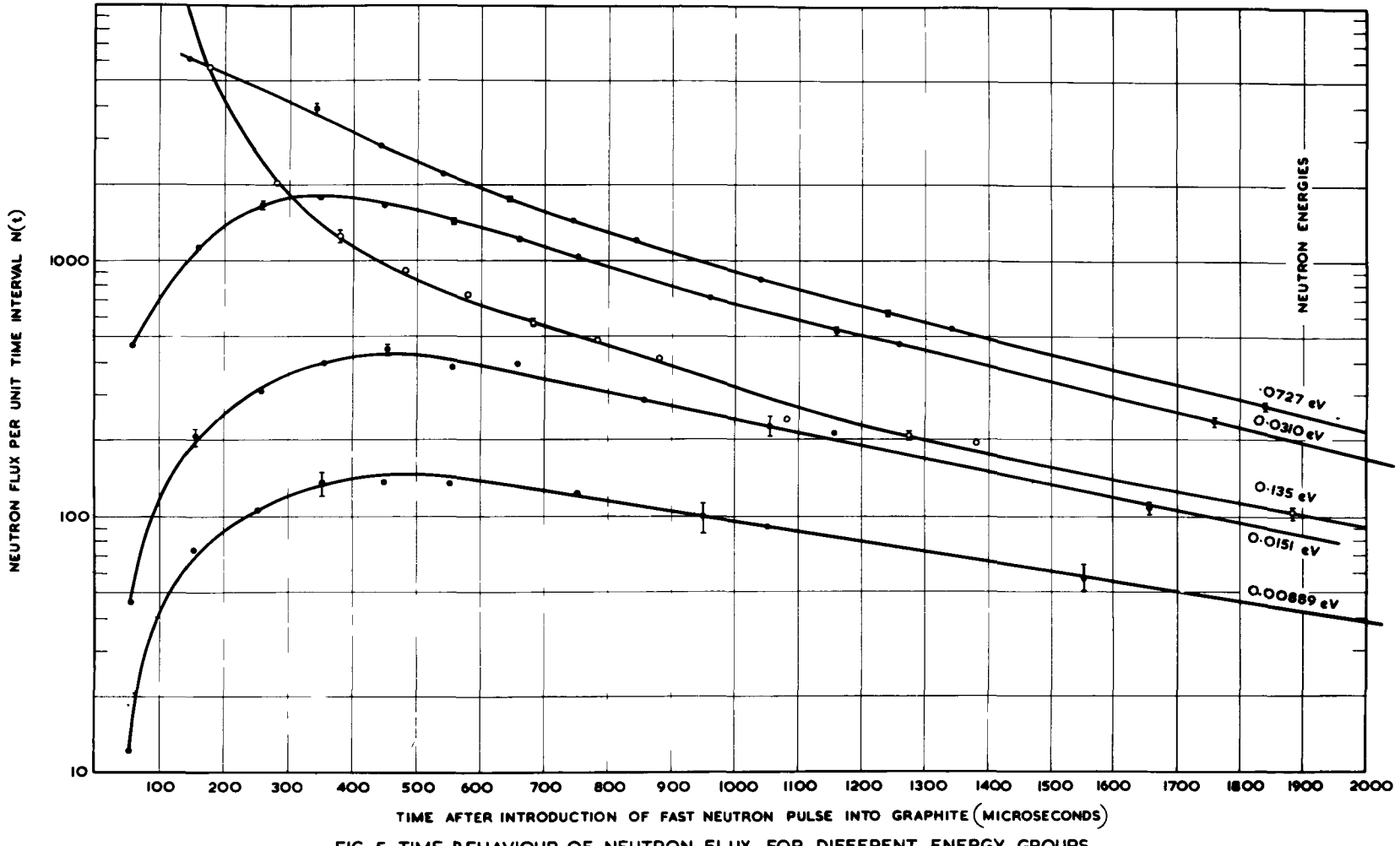

FIG 5. TIME BEHAVIOUR OF NEUTRON FLUX FOR DIFFERENT ENERGY GROUPS.

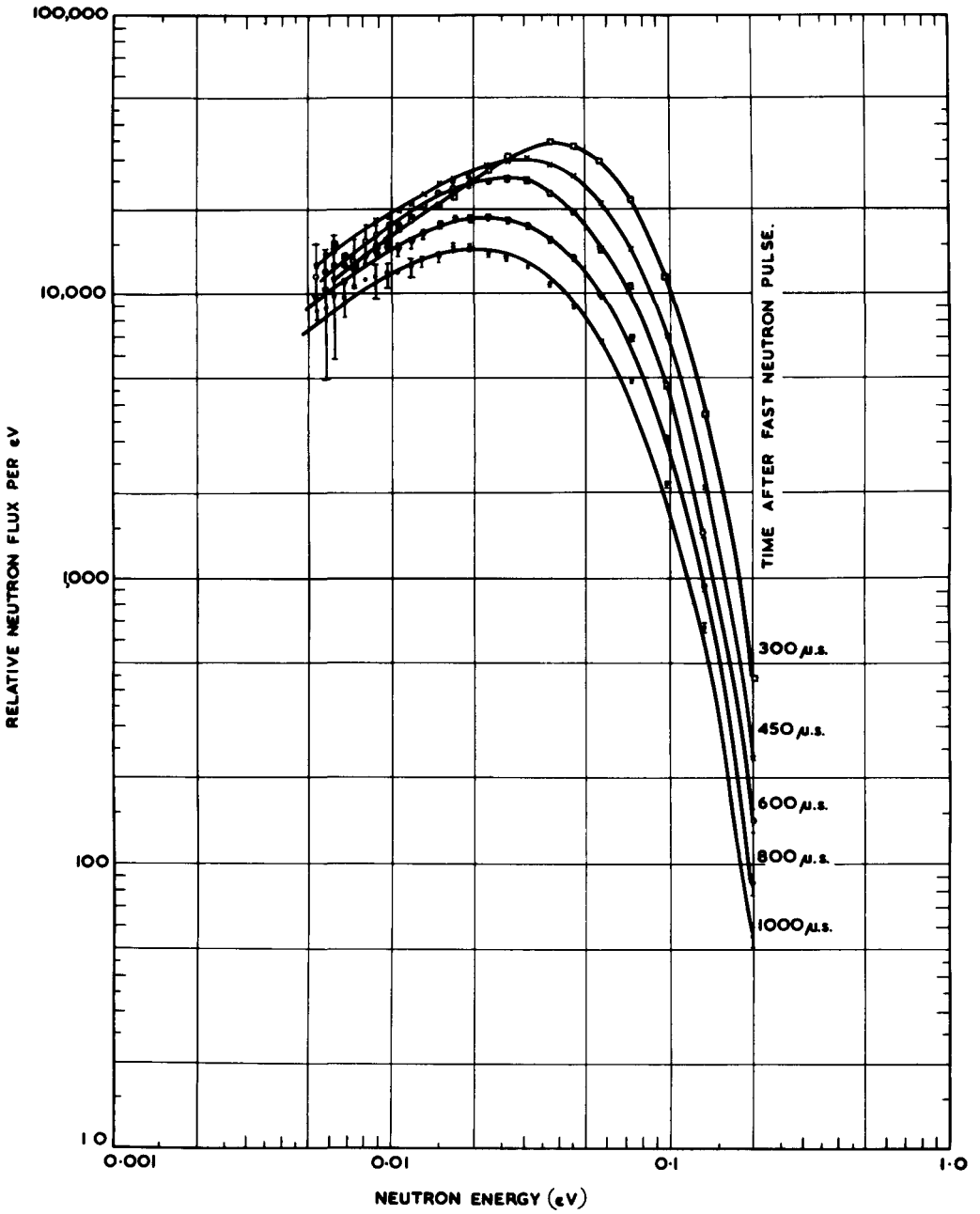

FIG. 6. TIME DEPENDENT NEUTRON SPECTRA

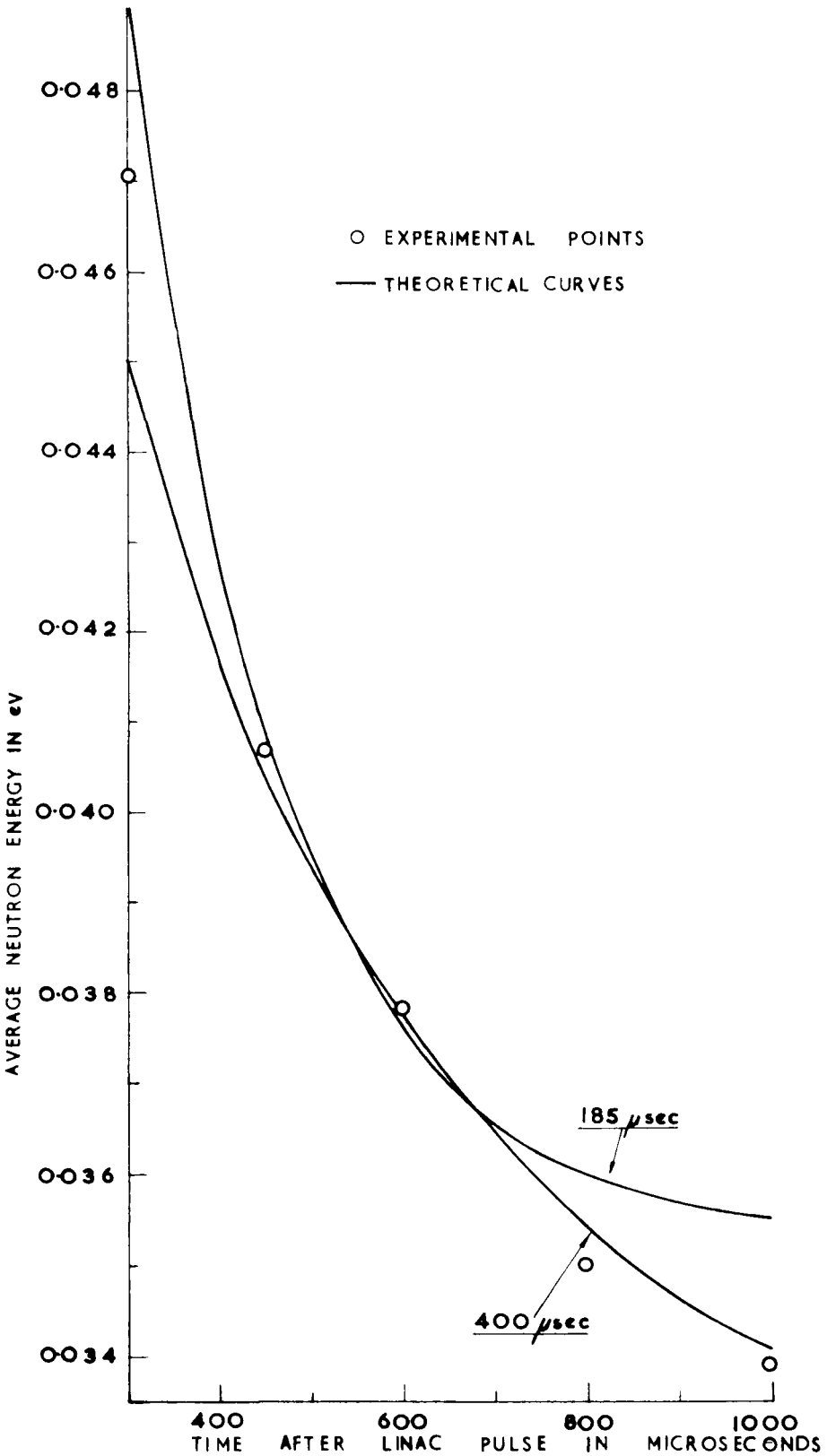

FIG 7. TIME BEHAVIOUR OF AVERAGE NEUTRON ENERGY

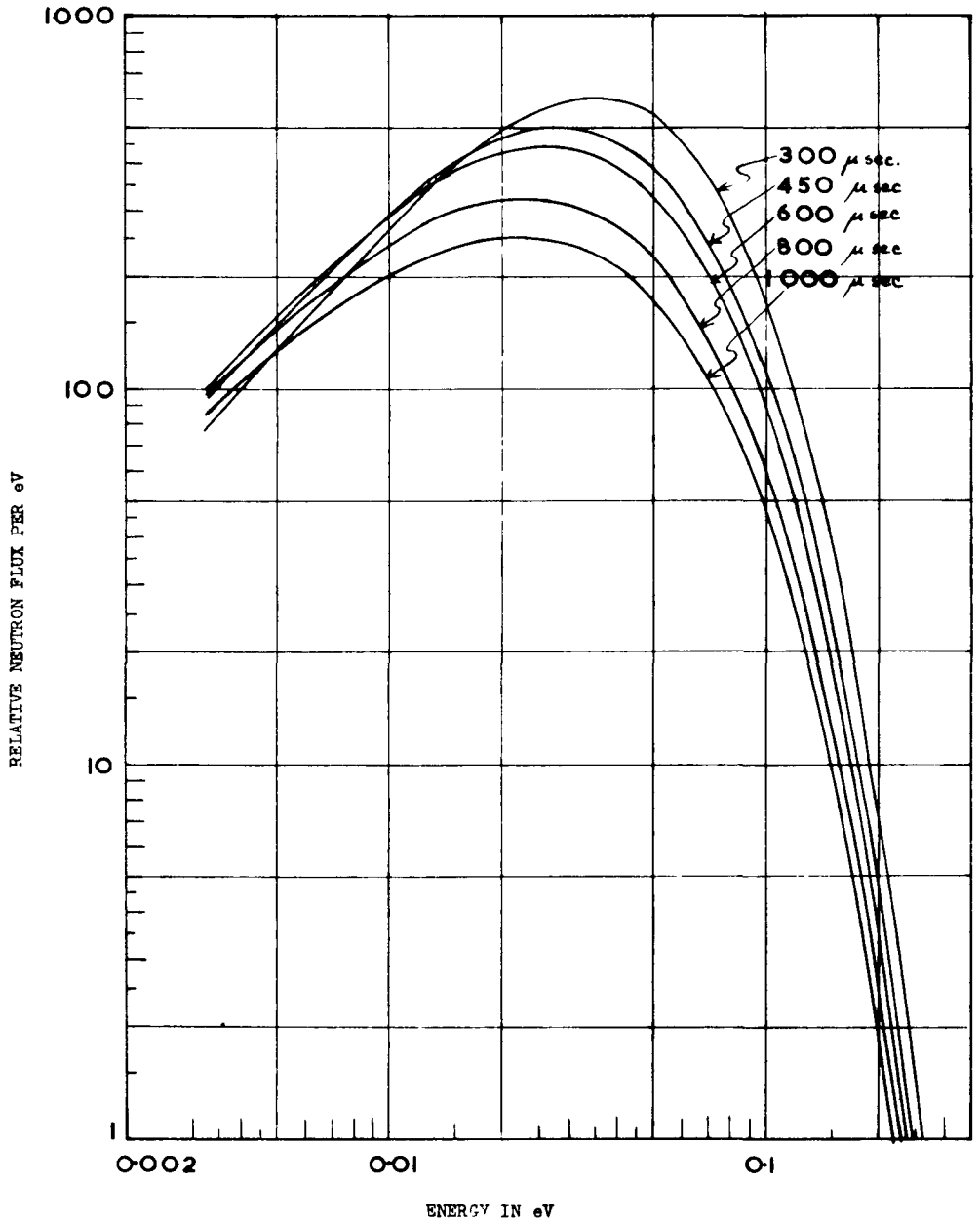

FIG.8 TIME DEPENDENT NEUTRON SPECTRUM AS CALCULATED USING CROSS SECTIONS OBTAINED FROM THE SCATTERING LAW FOR GRAPHITE

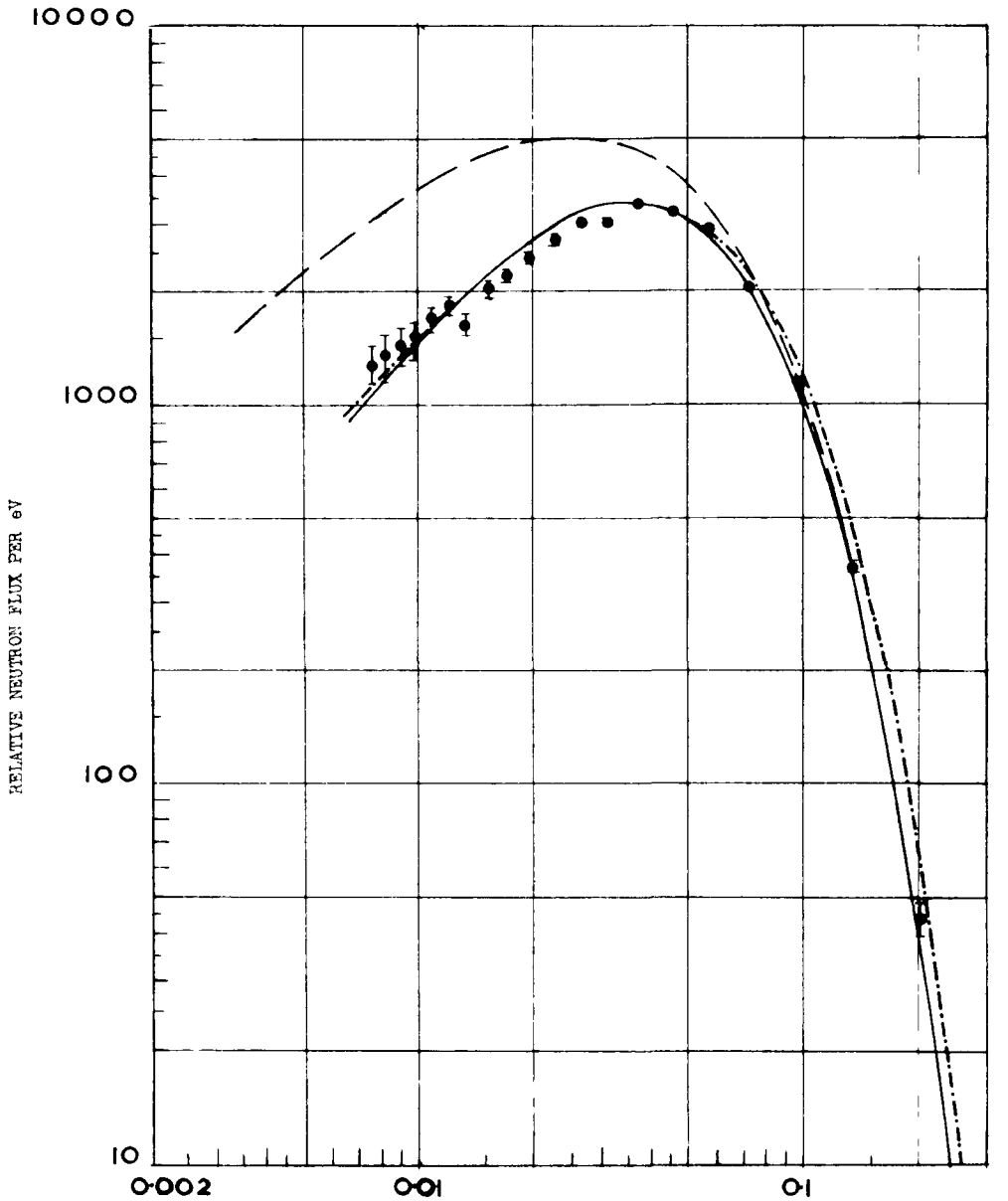

FIG.9 NEUTRON SPECTRUM IN GRAPHITE 300 μs AFTER THE LINAC PULSE
——— CALCULATED SPECTRUM (Egelstaff Scattering Law)
— — — CALCULATED SPECTRUM (Perfect Gas Model, Mass Number 12)
— · — · — CALCULATED SPECTRUM (Perfect Gas Model, Mass Number 33)
● EXPERIMENTAL POINTS

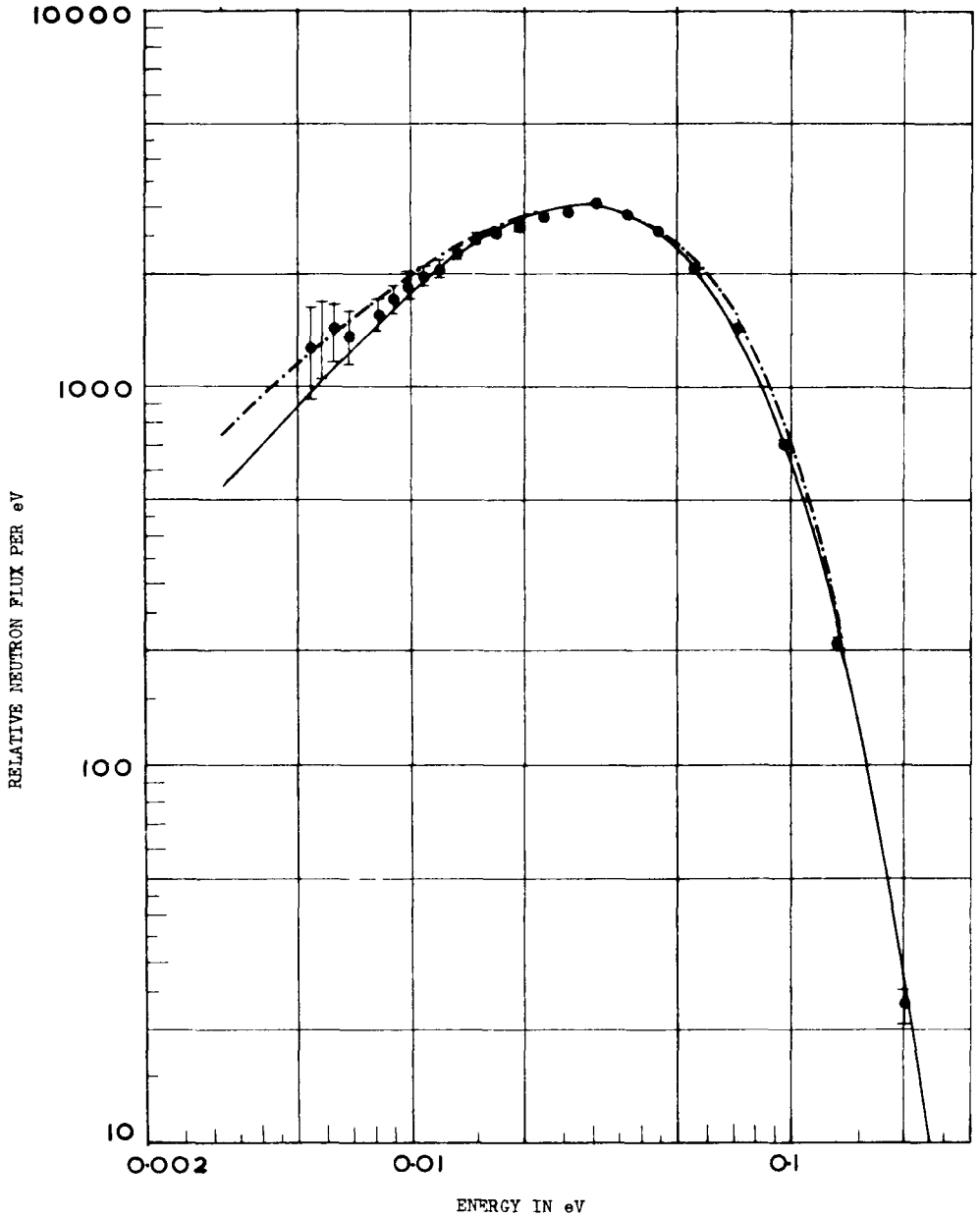

FIG.10 NEUTRON SPECTRUM IN GRAPHITE 450 μs AFTER THE LINAC PULSE
- - - - CALCULATED SPECTRUM (Egelstaff Scattering Law)
— — — CALCULATED SPECTRUM (Perfect Gas Model, Mass Number 33)
● EXPERIMENTAL POINTS

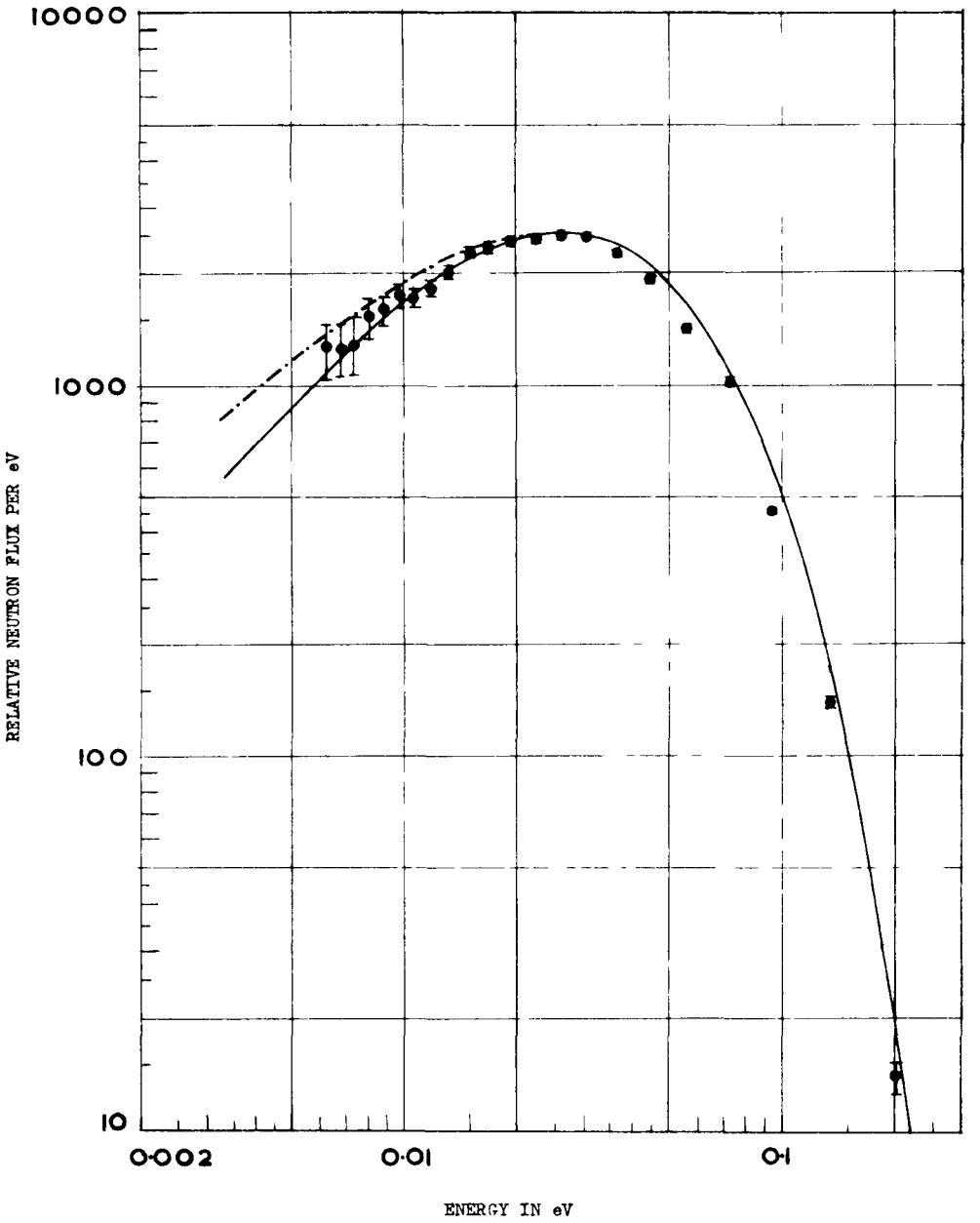

FIG.11. NEUTRON SPECTRUM IN GRAPHITE 600 μs AFTER THE LINAC PULSE
——— CALCULATED SPECTRUM (Egelstaff Scattering Law)
—·—·— CALCULATED SPECTRUM (Perfect Gas Model, Mass Number 33)
● EXPERIMENTAL POINTS

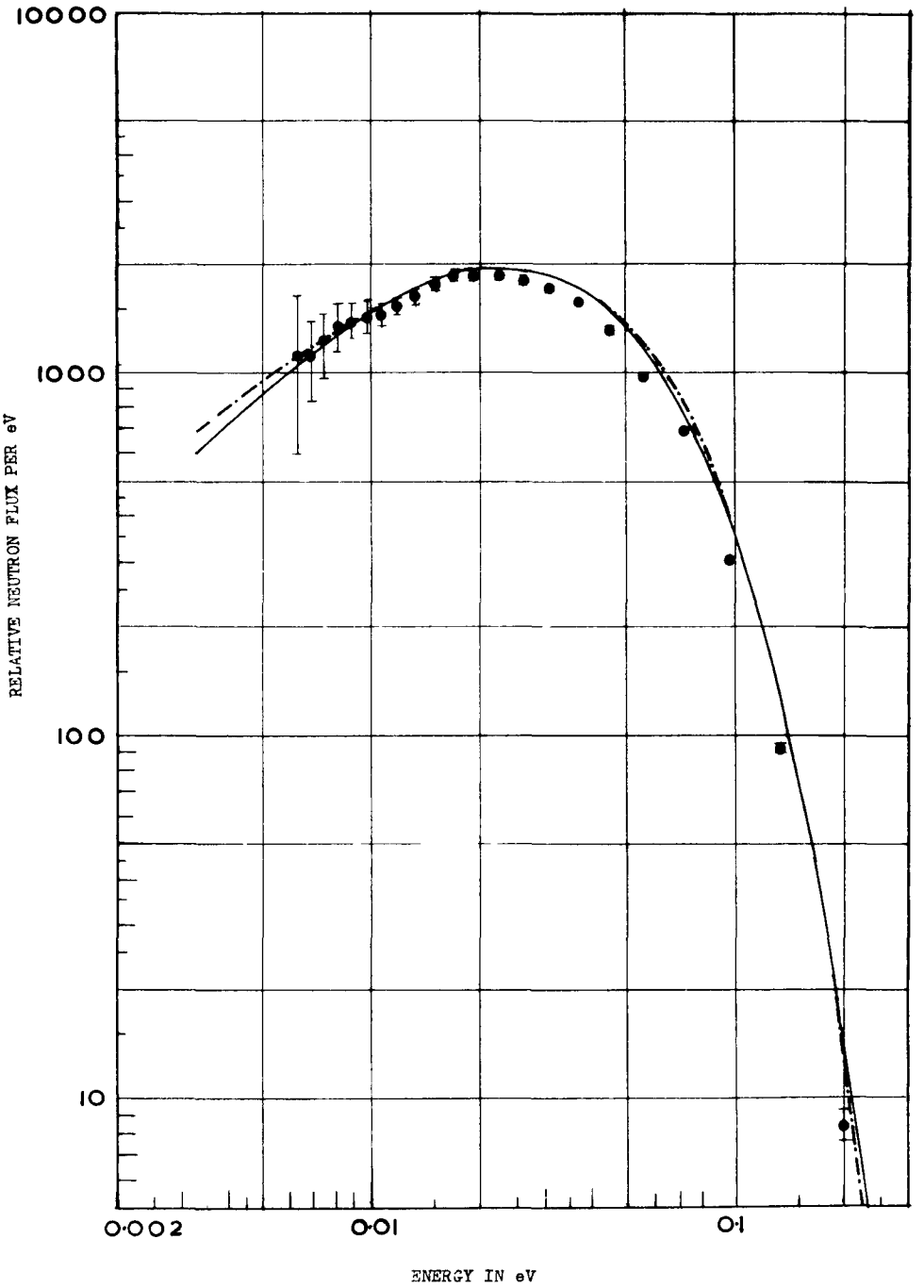

FIG.12. NEUTRON SPECTRUM IN GRAPHITE 800 μs AFTER THE LINAC PULSE
——— CALCULATED SPECTRUM (Egelstaff Scattering Law)
– – CALCULATED SPECTRUM (Perfect Gas Model, Mass Number 33)
● EXPERIMENTAL POINTS

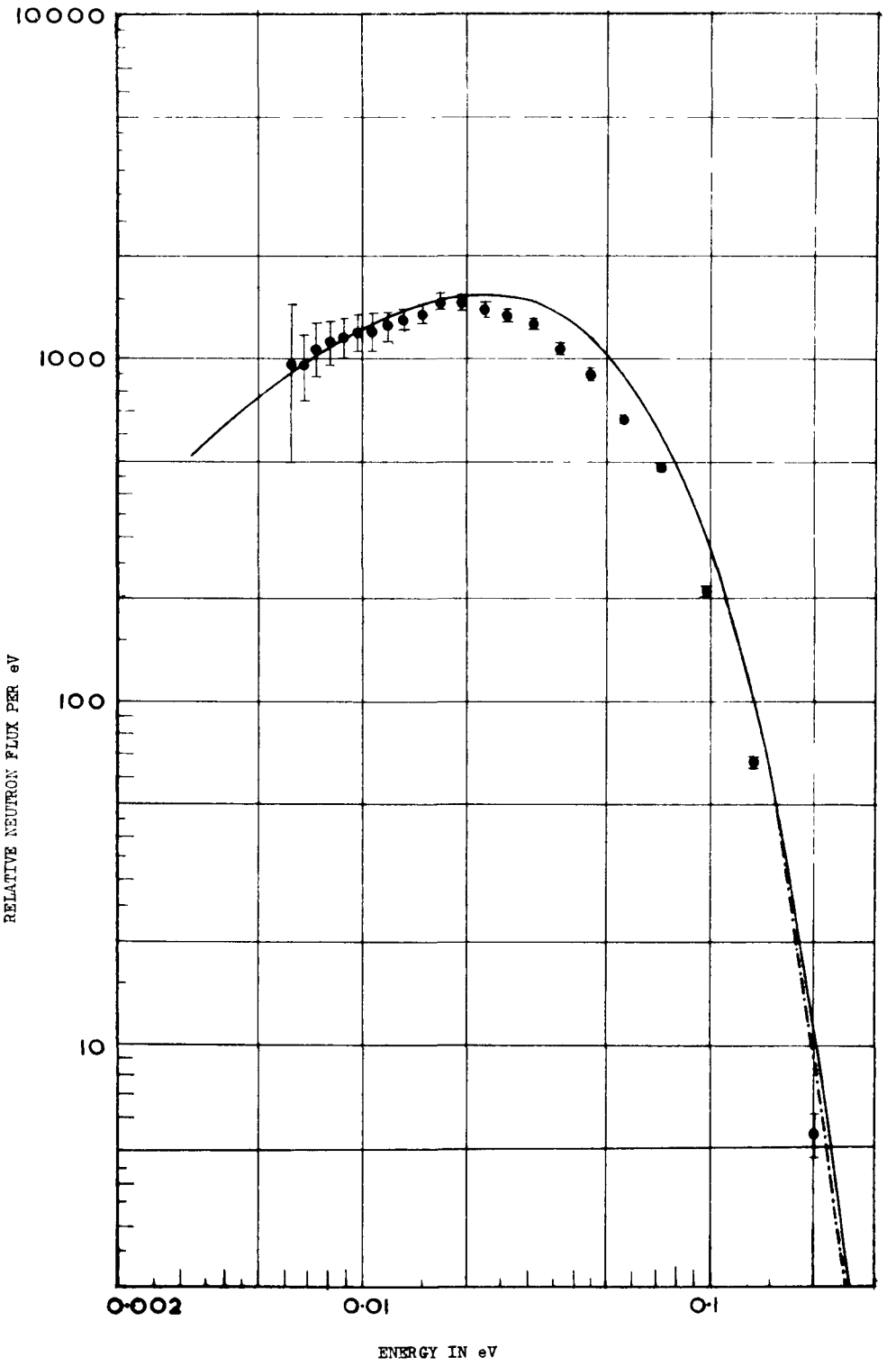

FIG.13. NEUTRON SPECTRUM IN GRAPHITE 1000 μs AFTER THE LINAC PULSE
——— CALCULATED SPECTRUM (Egelstaff Scattering Law)
—·—·— CALCULATED SPECTRUM (Perfect Gas Model, Mass Number 33)
● EXPERIMENTAL POINTS

NEUTRON RETHERMALIZATION IN GRAPHITE AND WATER

R. A. Bennett

Hanford Laboratories

General Electric Company

Richland, Washington

Work performed under Contract No. AT(45-1)-1350

between the Atomic Energy Commission and General Electric Company

ABSTRACT

Spatial distributions of radioactivities of Cu^{64} and Lu^{177} induced by thermal neutrons near temperature discontinuities in graphite and in graphite and water systems have been analyzed with a multithermal-group diffusion model of the space-energy distribution of the thermal neutrons. Rethermalization cross sections for graphite and water have been inferred from the Cu^{64} data. For graphite at a physical temperature of 300°K the cross sections vary from 0.009 to 0.069 cm^{-1} for neutron spectra with characteristic temperatures in the range from 144 to 828°K, respectively. For graphite at physical temperatures in the range from 144 to 828°K the cross sections vary from 0.016 to 0.044 cm^{-1} respectively for a neutron spectrum with a characteristic temperature of approximately 300°K. For water at a physical temperature of approximately 300°K the cross sections vary from 1.25 to 0.75 cm^{-1} for neutron spectra characterized by temperatures in the range from 410 to 720°K, respectively. Calculated traverses of the thermal activities of Lu^{177}, which were made with the multithermal-group model using those rethermalization cross sections, agree to within ± 10% with the observed traverses. Effective masses of graphite inferred from the cross sections agree to within ± 20% with those obtained from differential measurements of the energy distributions of neutrons from the graphite of a graphite-uranium lattice. Relaxation lengths also inferred from the cross sections agree to within 30% with those calculated from the results of a theoretical investigation of elastic and one phonon inelastic scattering of hot neutrons in 300°K graphite.

INTRODUCTION

Precise specification of the space-energy distribution of neutrons in reactor media is essential to good design and optimization of reactors. Specifically this information is required for calculations of neutron reaction rates and hence determinations of neutron economy. A fundamental difficulty encountered is the deviation of the energy distributions of neutrons from equilibrium Maxwellian distributions caused by preferential absorption in strongly absorbing media or by variations in scattering properties of the media. Near physical boundaries between dissimilar media spatial transients are then induced. Temperature gradients and discontinuities further complicate the problem in heterogeneous reactors that operate at high power levels. Ideally in studies of this problem one would measure these spatial variations of the energy distributions of neutrons. However, extreme difficulties are encountered in obtaining adequate spatial detail while maintaining sufficient neutron intensity, in say, chopper measurement techniques. An alternative is, of course, the measurement of spatial variations of neutron reaction rates in combination with subsequent comparisons with theoretical models of space-energy distributions of neutrons.

The latter approach has been used in this work. Traverses of the reaction rates of thermal neutrons with Cu^{63}, Lu^{176}, and Au^{197} have been measured near temperature discontinuities in graphite systems and in graphite and water systems. This work extends the work on neutron rethermalization reported earlier[1]. The

experiments were done in the core of the Physical Constants Testing Reactor[2] in cylindrical geometry rather than the slab geometry used in the earlier work. This change constitutes an improvement in the sense that the experimental geometry in this work was more consistent with the cylindrical shell array of fuel in the PCTR. The temperature range of the experiments extended from 144 to 828°K with temperature discontinuities up to 500°C. The analysis consisted of comparisons of calculated and observed traverses of the Cu^{64} and Lu^{177} data.

The calculations were made with the multithermal group model proposed by Selengut[3]. The variations in the energy distribution of neutrons near interfaces are accounted for in the multithermal group model by defining the total thermal spectrum as a weighted sum of equilibrium spectra. An equilibrium spectrum is defined for each region having different physical properties and each equilibrium spectrum is assumed to exist in all regions. After a mean number of collisions in a region neutrons that are in non-equilibrium spectra are assumed to transfer to the equilibrium spectrum of that region. Rethermalization cross sections defined in the model specify the probabilities for neutron transfer. Values of the cross sections for rethermalization have been inferred in the analyses of these experiments. A simplified version of this model was used in the earlier report. The overlapping thermal group model, which is quite similar, has been used in analyses of neutron flux peaking in water gaps[4].

The model, the experimental apparatus and techniques, the analysis procedures, and the results are presented in subsequent

sections. The model, as used in this work, allows for the dependence of the diffusion coefficient of graphite upon the neutron and physical temperatures and for the possibilities of unequal probabilities for neutron rethermalization to higher or lower energies, which were not accounted for in the earlier work. The cylindrical nature of the experimental geometry and PCTR fuel loading are illustrated in the discussion of the experimental apparatus. The discussion of the analysis includes a description of the bivariate statistical procedures used in inferring rethermalization cross sections from the Cu^{64} data. The results include values of the cross sections, effective masses, and relaxation lengths for rethermalization and comparisons of calculated and observed traverses of the activities of Cu^{64} and Lu^{177}. The values of the effective masses and relaxation lengths for graphite are compared with results obtained from the work of others[5,6].

MULTITHERMAL GROUP MODEL

The multithermal group model is used in the diffusion approximation. An equilibrium group of neutrons, with a Maxwellian energy distribution, $M(E, T_i)$, is defined for each region with a different physical temperature, T_i. To a first approximation, only two distinct physical temperatures exist in these experiments. The magnitude of each equilibrium group is given by a spatial weighting function, $\varphi_i(x)$, the integrated group flux for the i^{th} group. The total space-energy distribution of the thermal neutron flux is given by

1) $\Phi(E,r) = \varphi_1(r)\, M(E,T_1) + \varphi_2(r)\, M(E,T_2)$

The epithermal component of the spectrum is assumed to have the form

$$2) \quad \varphi_e(E,r) = \varphi_0(r)\Delta/E \text{ where } \begin{matrix} \Delta = 0 \text{ for } E<\mu kT_k \\ \Delta = 1 \text{ for } E\geq\mu kT_k \end{matrix}$$

and $\mu \sim 5.1$[7], and T_k is the physical temperature of the region of concern.

The neutron balance equations are derived by conserving neutrons and neutron energy through calculation of the zero and first energy moments of the Wilkins heavy gas equation[8] or with the variational principle[9]. For these experiments, which have five or seven regions and only two physical temperatures, the neutron balance equations for regions k at temperature T_i are;

$$\begin{aligned} &D_{01}\nabla^2\varphi_0 - \Sigma_{a01}\varphi_0 - \Sigma_{0\to1}\varphi_0 = -\nu\Sigma_{f11}\varphi_1 - \nu\Sigma_{f21}\varphi_2 \\ 3) \quad &D_{11}\nabla^2\varphi_1 - \Sigma_{a11}\varphi_1 + \Sigma_{2\to1}\varphi_2 = -\Sigma_{0\to1}\varphi_0 \\ &D_{21}\nabla^2\varphi_2 - \Sigma_{a21}\varphi_2 - \Sigma_{2\to1}\varphi_2 = 0 \end{aligned}$$

where the subscript for the region (k) is understood for all quantities. For regions k at temperature T_2 the balance equations are;

$$\begin{aligned} &D_{02}\nabla^2\varphi_0 - \Sigma_{a02}\varphi_0 - \Sigma_{0\to2}\varphi_0 = -\nu\Sigma_{f12}\varphi_1 - \nu\Sigma_{f22}\varphi_2 \\ 4) \quad &D_{12}\nabla^2\varphi_1 - \Sigma_{a12}\varphi_1 - \Sigma_{1\to2}\varphi_1 = 0 \\ &D_{22}\nabla^2\varphi_2 - \Sigma_{a22}\varphi_2 + \Sigma_{1\to2}\varphi_1 = -\Sigma_{1\to2}\varphi_0 \end{aligned}$$

where the subscript for the region (k) is understood for all quantities. The quantities D_{ijk}, Σ_{aijk}, and Σ_{fijk} are the group diffusion coefficients, absorption cross sections, and fission cross sections, respectively, for groups i in regions k that are at a physical temperature T_j. The quantity ν is the mean number of fast neutrons per fission. The quantities $\Sigma_{i\to j,k}$ are the cross

sections for rethermalization of neutrons from groups i to groups j in regions k. All quantities are flux averaged over the appropriate equilibrium spectrum. The quantities D_{ijk} of regions k at temperature T_j for the thermal neutrons are

5) $$D_{ijk} = \int_0^\infty D_k(E,T_j)\, M(E,T_i)dE / \int_0^\infty M(E,T_i)dE$$

where T_i is the characteristic temperature of the i^{th} thermal group. The thermal cross sections are similarly given by

6) $$\Sigma_{xijk} = \int_0^\infty \Sigma_{xjk}(E) M(E,T_i)dE / \int_0^\infty M(E,T_i)dE$$

where the subscript x refers to a, f, or s for absorption, fission, or scattering, respectively. The fast group constants (i = 0) D_{ojk}, Σ_{aojk}, and $\Sigma_{o\to j,k}$ were obtained from calculations made with a modified age theory[10] and were subsequently adjusted empirically as necessary to give the observed spatial variation of the epi-cadmium activity of Au^{198}.

The cross Sections $\Sigma_{2\to1,k}$ and $\Sigma_{1\to2,k}$ are those for rethermalization of neutrons from group two to one and from group one to two, respectively. In the limit of high neutron and moderator temperatures the rethermalization cross section is expected to be given by the heavy gas model as

7) $$\Sigma_{reth} = \xi\Sigma_s = \frac{2n}{M}\Sigma_s$$ where the quantities n and M are the masses of the neutron and moderator respectively and Σ_s is the macroscopic cross section for scattering. For lower temperatures Eqn. 7 defines an effective mass for the moderator of region k for transfer of neutrons from group i to group j as

8) $$M_{e\ i\to j,k} = \frac{2\Sigma_{sijk}}{\Sigma_{i\to j,k}} .$$

The quantities directly inferred from the foil counting data are the relaxation lengths for neutron rethermalization. These lengths are defined as

$$9) \quad L_{i\to j,k} = \left(\frac{D_{ijk}}{\Sigma_{i\to j,k}} \right)^{\frac{1}{2}}.$$

The solutions of the neutron balance equations $\varphi_0(r)$, $\varphi_1(r)$ and $\varphi_2(r)$ for the experimental conditions in these experiments are found by numerical methods using estimated values of the rethermalization cross sections. The fluxes are then used to calculate the traverses of the activities of Cu^{64} for comparison with the observed traverses. On the basis of this comparison better values of $\Sigma_{i\to j,k}$ are estimated and again the calculated activities are compared to the observed traverses.

EXPERIMENTAL APPARATUS AND PROCEDURES

The irradiations required to obtain traverses of the activities of Cu^{64}, Lu^{177} and Au^{198} near temperature discontinuities in graphite, and in graphite and water media were made with the Physical Constants Testing Reactor. Nine irradiations were made, five in the all graphite system and four in the graphite and water system. The essential geometrical features of each set of experiments were similar. A cross sectional view of the reactor and experimental media taken normal to the longitudinal axis of symmetry is shown in Figure 1 for the graphite and water system. Progressing radially outward from the central axis the respective regions are a column of water, and annuli of Zircaloy II, graphite, insulation, graphite, fuel, and graphite. In the all graphite experiments the

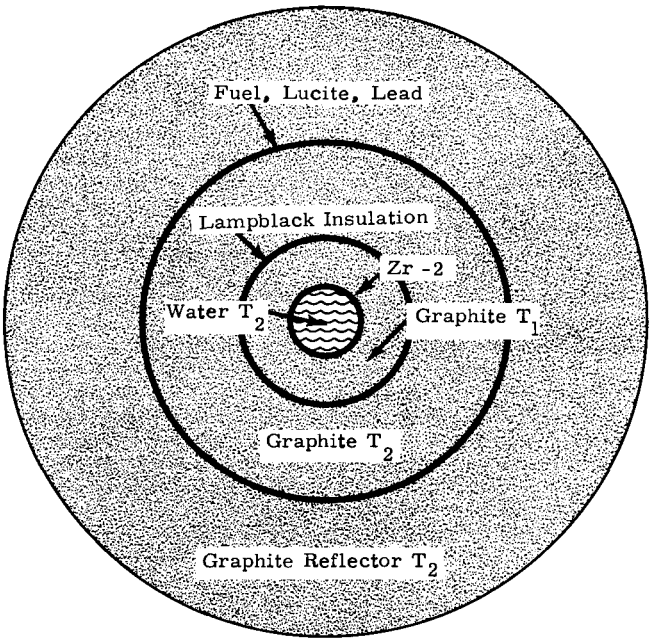

Outside Radii of Regions

Water	= 3.400 cm
Zircaloy-2	= 4.254 cm
Hot Graphite	= 19.050 cm
Insulation	= 20.955 cm
Room Temp. Graphite	= 49.530 cm
Fuel	= 50.750 cm
Reflector	= 110.750 cm

Figure 1 Caption:

Schematic equivalent of the cross section of the Physical Constants Testing Reactor and experimental regions. The ring of PCTR fuel rods and lucite is shown as a homogeneous annulus of fuel, lucite, and lead. The PCTR reflector, which is actually rectangular, is shown as an annulus of equivalent cross section. This geometry was assumed in the analysis of the experiments. The quantities T_1 and T_2 are the physical temperatures of the regions.

region occupied by the column of water and annulus of Zircaloy II was filled with a graphite cylinder.

The annulus of insulation was lampblack tamped between an inner and outer shell of aluminum, each 0.0625 of an inch thick. The layer of lampblack was 0.625 of an inch thick. The annulus of fuel, shown in Figure 1, simulates a ring of 32 standard PCTR fuel tubes. The metal is a Pb-U^{235} alloy in the form of a tube 1.170 inches inside diameter and 1.235 outside diameter. Each tube was filled with a lucite rod 0.75 of an inch in diameter in an attempt to localize neutron moderation and decrease the fast to slow flux ratio in the inner regions. The decrease in the flux ratio was approximately 40%.

The temperature discontinuities occurred in a 0.0625 of an inch air gap between the Zircalloy II and the inner graphite region or in the annulus of lampblack. The inner region of graphite was either heated with calrods or cooled with liquid nitrogen. The water was held near room temperature by adjustment of the flow rate. The lampblack insulated the outer regions from the hot or cold inner region of graphite. The water temperature was monitored with mercury thermometers at the inlet and outlet. The axial and radial distributions of temperature in the graphite regions inside and outside the lampblack insulation were monitored with iron-constantan thermocouples. Prior to irradiations the calrods were removed and the vacancies were filled with pre-heated graphite filler bars. In the cold experiments the residual liquid nitrogen was allowed to evaporate prior to irradiations.

The Cu, Au, and Lu neutron detectors, both bare and cadmium covered, were irradiated simultaneously in each experiment. The bare detectors were centered in a plane that was normal to the axis of symmetry at a position three inches from the midpoint of the axis. The cadmium covered detectors were centered in a mirror image plane. The six inch separation between the planes was sufficient to reduce to a negligible amount the flux perturbations at the bare detector positions caused by the cadmium. The latter fact was established experimentally by comparing spatial variations of the activities of Cu^{64} taken at room temperature with and without the cadmium present. Copper foils used in the water regions were strips 0.25 of an inch wide and 0.003 of an inch thick. They were positioned along a diameter of the column of water by peening the ends in the wall of 0.020 of an inch thick aluminum sleeve that fit inside the Zircaloy II tube. The copper used in the graphite was in the form of pins 0.0625 of an inch in diameter and 0.500 of an inch in length. These pins were positioned on 0.635 cm centers radially outward to a radius of 42.5 cm. The gold was in the form of disks 0.005 of an inch thick and 0.500 of an inch in diameter. The lutetium detectors were ceramic disks of Al_2O_3-Lu_2O_3 weighing approximately 450 mg and containing 10 mg of Lu_2O_3 [11]. The disks were 0.045 of an inch thick and 0.450 of an inch in diameter. The gold and lutetium disks were positioned radially outward to a radius of 42.5 cm with a spacing of approximately 2 cm. The cadmium covered detectors were spaced approximately 5 cm apart. The cadmium covers fit each type of detector snugly and the walls were 0.040 of an inch thick.

The activated detectors were γ-counted on a NaI(Tl) crystal photomultiplier system. Only the Cu^{64}, Lu^{177} and Au^{198} activities were counted The activities of Cu^{66} and Lu^{177} had decayed to a negligible amount prior to the start of the counting

ANALYSIS, RESULTS, AND DISCUSSION

The cross sections, effective masses, and relaxation lengths for neutron rethermalization were inferred in making comparisons of calculated and observed traverses of the thermal activities of Cu^{64}. The analyses included the reduction of bare and cadmium covered activity data to thermal activities, calculations and empirical determinations of the group constants for the neutron balance equations, and iterative adjustment of the rethermalization cross section to minimize the variance of the fit of the calculated curves to the observed traverses.

The thermal activities A_{th} were calculated from the bare A_B and the cadmium covered A_{ec} activities under the assumption that in every region the spectrum of epithermal neutrons was 1/E, as given by Eqn. 2. The effective cadmium cutoff energy was calculated to be 0.64 ev. Activities of bare foils due to epithermal-subcadmium neutrons, relative to their activities due to epicadmium neutrons, were estimated from the respective resonance integrals of Cu^{63}. The calculations were made with the expression

10) $$A_{th} = A_B - \alpha^{63} A_{ec}$$

where $\alpha^{63} = RI^{63}_{et}/RI^{63}_{ec}$ and RI^{63}_{et} is the total resonance integral of $Cu^{63}$and RI^{63}_{ec} is the epicadmium resonance integral of Cu^{63}.

The self shielding effects of the thick detectors were accounted for by using effective resonance integrals measured in previous work.[12]

The fast group constants were estimated initially with a modified age theory of slowing down[10]. Subsequently, the diffusion coefficients and absorption cross sections were empirically adjusted to yield a minimum variance of the fit between the calculated and observed traverses of the epithermal activity of Au^{198}. The slowing down cross sections were not adjusted in order to maintain the correct rate of thermalization. The epicadmium activity of Au^{198}, due primarily to the absorption resonance at 4.9 ev, was assumed to be an adequate measure of the source of thermal neutrons and was assumed to be proportional to the fast group flux, φ_0. The observed traverses and the calculated curves that fit the data best are shown in Figures 2 and 3 for the graphite experiment and for the graphite and water experiment, respectively. These spatial variations were not affected by heating or cooling the inner region of graphite within the temperature range of 144 to 523°K (below the melting point of cadmium). Therefore, the assumption was made that the data in Figures 2 and 3 would adequately describe the spatial variations in the experiments at higher temperatures, also.

The thermal group constants were, in general, calculated from microscopic cross section data[13], using Eqn. 5 and 6. The fuel absorption cross sections for the room temperature experiments were determined empirically by adjusting their values to minimize the variances of the fits of the calculated and observed traverses of the thermal activities of Cu^{64} observed in the room temperature

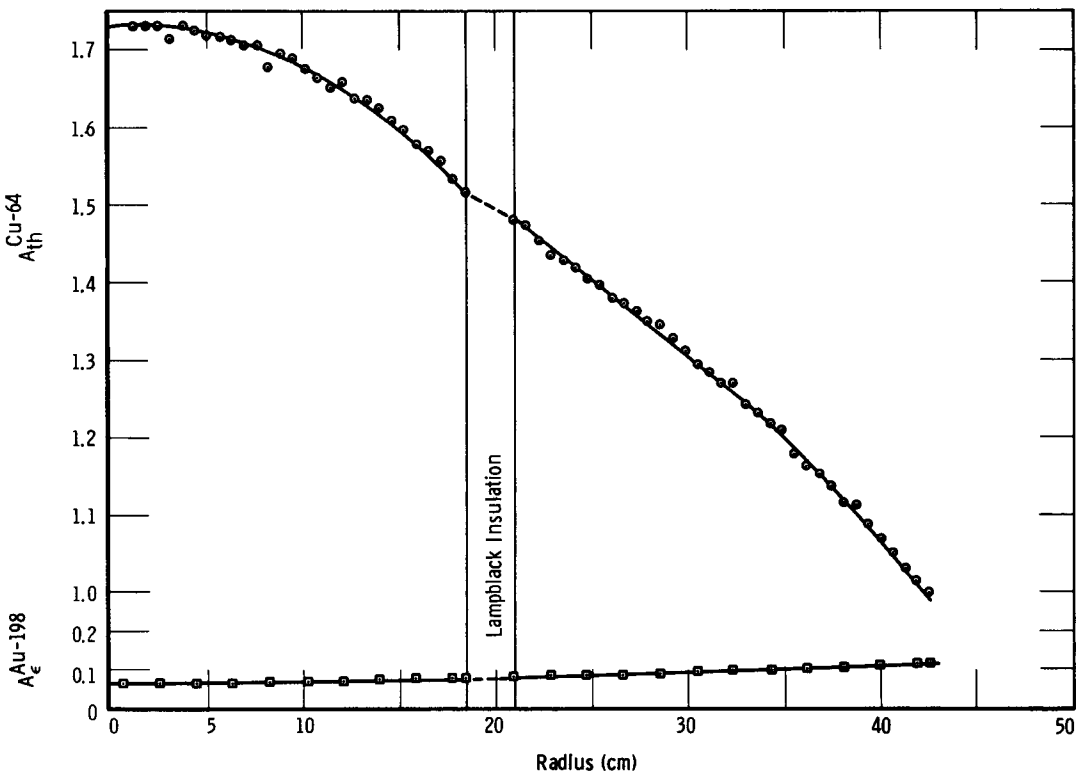

Figure 2 Caption

Graphite Experiment-Room Temperature. The comparison of calculated curves of the epicadmium activity of Au^{198} and thermal activity of Cu^{64} with the observed traverses. The group constants used to obtain these calculated curves were used as the basis for calculating the group constants for experiments 1A, 1C, 1D, and 1E.

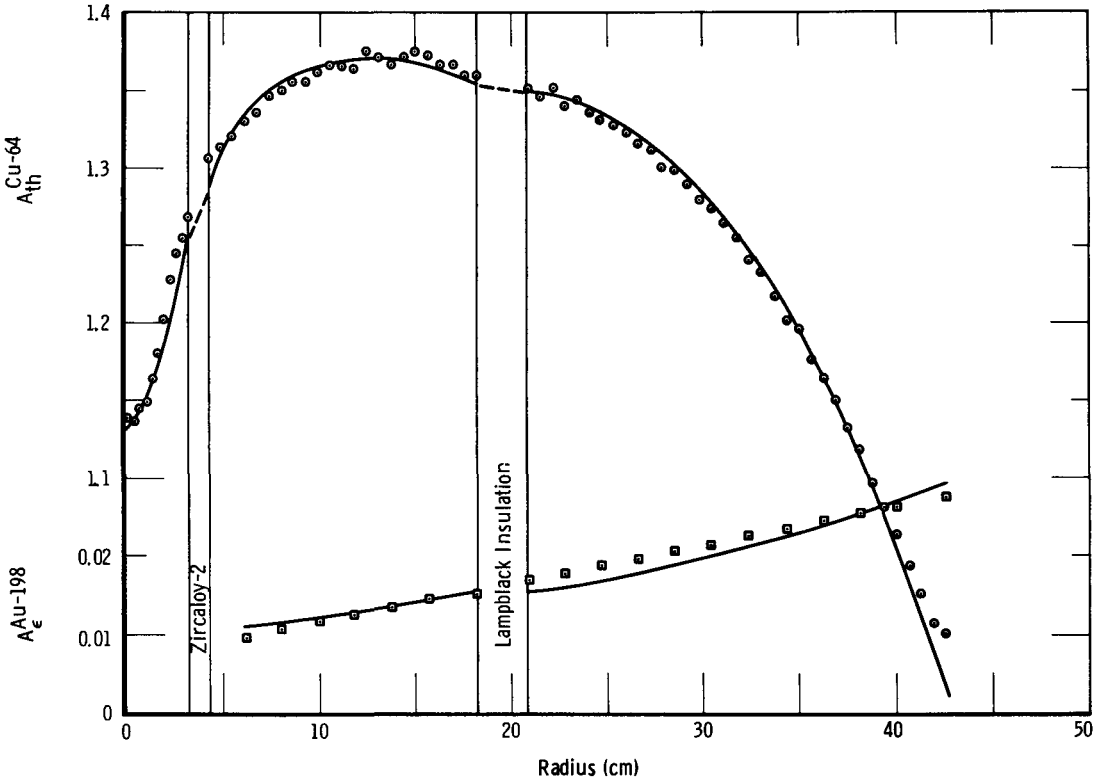

Figure 3 Caption

Graphite and Water Experiment-Room Temperature. The comparison of the calculated curves of the epicadmium activity of Au^{198} and the thermal activity of Cu^{64} with the observed traverses. The group constants used to obtain these calculated curves were used as the basis for calculating the group constants for experiments 2B, 2E, and 2D.

experiments. The calculated curves that best fit the traverses are also shown in Figures 2 and 3. Values of the fuel absorption cross sections for the equilibrium groups with different characteristic temperatures were calculated from the empirical values obtained from the room temperature experiments under the assumption that the absorption cross section of the U^{235} fuel of the PCTR varied as 1/v. In the manner described, the room temperature experiments were used as normalizing experiments. The changes in reaction rates observed in subsequent experiments were due primarily to rethermalization and were accounted for with the introduction of the cross sections for rethermalization.

Rethermalization Cross Section of Graphite

The iterative adjustment of the two rethermalization cross sections in each graphite experiment was a bivariate analysis performed with the IBM-7090 computer code "Fit-1".(14) Values for each cross section were estimated initially to be less than those predicted by the heavy gas model, given by Eqn. 7. One value was varied while the other was held fixed in repeated calculations of the variance of the fit of the traverses of the thermal activity of Cu^{64}. With the variance minimized with respect to one variable, the fitting was repeated for the other variable. This method ultimately yielded a crude map of the isovariance lines in the cross section field. A typical map is shown in Figure 4 for experiment 1A. The straight lines on the cross section field indicate lines of iteration, the values of cross sections that were held fixed. The points on the iteration lines indicate the values of

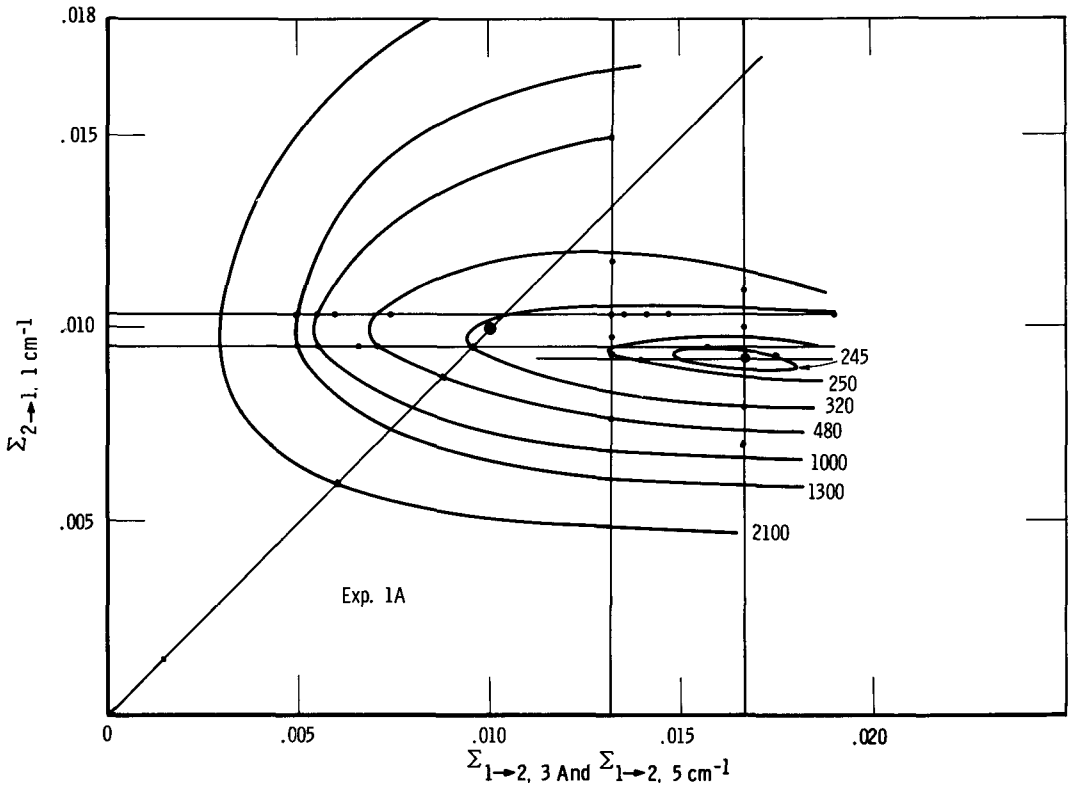

Figure 4 Caption

Isovariances of the rethermalization cross section field for the graphite Exp. 1A. The numerical values of the isovariances are proportional to the sum of the deviations of the experimental data from the calculated curve of thermal activity of Cu^{64}. The critical point at (0.0167, 0.0092) is the minimum of the field and its coordinates are the rethermalization cross sections for the experimental conditions, see Tables I and II, Exp. 1A. The point (0.0098, 0.0098) is a pseudo-critical point obtained under the assumption of equal probabilities of neutron rethermalization.

the cross section iterated upon. The isovariance curves are visual estimates based upon the field points indicated. The precise location of the critical point (minimum at 0.0167, 0.0092) of the field has been verified by least squares analysis under the assumption that the variance near the critical point is a quadradic function of the two cross sections for rethermalization. The point (0.010, 0.010) is the pseudo-critical point one would obtain under the assumption that the cross sections for rethermalization were equal.

This iteration procedure was repeated for each graphite experiment. The respective coordinates of the critical points, the pairs of cross sections for rethermalization in graphite, are listed in Tables I and II. The values for rethermalization of non-equilibrium neutrons in graphite at approximately 300°K are given in Table I; and values for the rethermalization of groups of thermal neutrons with characteristic temperatures near 300°K in graphite at various temperatures are given in Table II. The graphic presentation of these results in Figure 5 illustrates that the cross section for rethermalization of 300°K neutrons in graphite asymtotically approaches the heavy-gas value of 0.065 cm^{-1} at graphite temperatures near 800°K. The experimental results shown in Figure 6 illustrate a similar saturation behavior of the cross section of 300°K graphite for hot neutrons at a value significantly lower than 0.065 cm^{-1}. One would not expect the latter to saturate as the data indicate. A behavior similar to the curve in Figure 6, a visual estimate, is to be expected since the chemical binding energy becomes small relative to the neutron energy at high neutron temperatures.

RETHERMALIZATION PROPERTIES OF GRAPHITE

TABLE I

RETHERMALIZATION OF NEUTRONS WITH A MAXWELLIAN ENERGY DISTRIBUTION, $M(E,T_1)$, IN GRAPHITE HAVING A PHYSICAL TEMPERATURE, T_2

Experiment	Characteristic Temperature of Thermal Group	Physical Temperature of Graphite	Average[a,c] Diffusion Coefficient	Rethermalization[d,e] Cross Section	Relaxation Length	Effective Mass	Average Σ[b] Scattering Cross Section
	T_1	T_2	D_{123}	$\Sigma_{1\rightarrow 2,3}$	$L_{1\rightarrow 2,3}$	$M_{\epsilon 1\rightarrow 2,3}$	Σ_{s123}
	°K	°K	cm	cm^{-1}	cm	amu	cm^{-1}
1A	144 ± 5	283 ± 5	0.900	0.017 ± .001	7.3 ± 0.3	46 ± 2	~ 0.392
1C	523 ± 5	299 ± 5	0.794	0.044 ± .002	4.3 ± 0.2	20 ± 1	~ 0.445
1D	690 ± 5	308 ± 5	0.782	0.045 ± .002	4.2 ± 0.2	20 ± 1	~ 0.451
1E	828 ± 5	315 ± 5	0.776	0.041 ± .002	4.4 ± 0.2	22 ± 1	~ 0.455

a) Average diffusion coefficients are normalized to a value of $D(293°K, 293°K) = 0.832$ cm, $\sigma_{tr} = 4.95$ bn

b) Average scattering cross sections are assumed to be given by $\Sigma_{s123} = \frac{1}{3(1-\bar{\mu}_o)D_{123}}$; $\bar{\mu}_o = 0.056$

c) Graphite density = 1.614 gm/cm^3

d) Free gas values:
$\Sigma_{2\rightarrow 1,3} = 0.0665\ cm^{-1}$
$L_{2\rightarrow 1,3} = 3.53$ cm
$M_{\epsilon 2\rightarrow 1,3} = 12.011$ amu

e) The uncertainties are standard error limits based upon the variances of the calculated fits to the experimental Cu^{64} data, see Fig. 6. The estimated uncertainties due to spectrum uncertainties are ± 25%.

TABLE II

RETHERMALIZATION OF NEUTRONS WITH A MAXWELLIAN ENERGY DISTRIBUTION, $M(E,T_2)$ IN GRAPHITE HAVING A PHYSICAL TEMPERATURE, T_1

Experiment	Characteristic Temperature of Thermal Group	Physical Temperature of Graphite	Average[a,c] Diffusion Coefficient	Rethermalization[d,e] Cross Section	Relaxation[d,e] Length	Effective Mass	Average[b] Scattering Cross Section
	T_2	T_1	D_{211}	$\Sigma_{2\to1,1}$	$L_{2\to1,1}$	$M_{\epsilon\, 2\to1,1}$	Σ_{ss11}
	°K	°K	cm	cm^{-1}	cm	amu	cm^{-1}
1A	283 ± 5	144 ± 5	0.849	0.0092 ± .0005	9.6 ± 0.5	90 ± 4	0.416
1C	299 ± 5	523 ± 5	0.828	0.047 ± .002	4.2 ± 0.2	18 ± 1	0.426
1D	308 ± 5	690 ± 5	0.828	0.066 ± .003	3.5 ± 0.2	13 ± 1	0.426
1E	315 ± 5	828 ± 5	0.825	0.069 ± .004	3.5 ± 0.2	12 ± 1	0.428

a) Average diffusion coefficients are normalized to a value of $D(293°K, 293°K) = 0.832$ cm, $\sigma_{tr} = 4.95$ bn

b) Average scattering cross sections are assumed to be given by $\Sigma_{ss11} = \frac{1}{3(1-\bar{\mu}_0)\, D_{211}}$; $\bar{\mu}_0 = 0.056$

c) Graphite density = 1.614 gm/cm^3

d) Free gas values:
$\Sigma_{2\to1,1} = 0.0665\ cm^{-1}$
$L_{2\to1,1} = 3.53$ cm
$M_{\epsilon 2\to1,1} = 12.011$ amu

e) The uncertainties are standard error limits based upon the variances of the calculated fits to the experimental Cu^{64} data, see Fig. 6. The estimated uncertainties due to spectrum uncertainties are ± 25%.

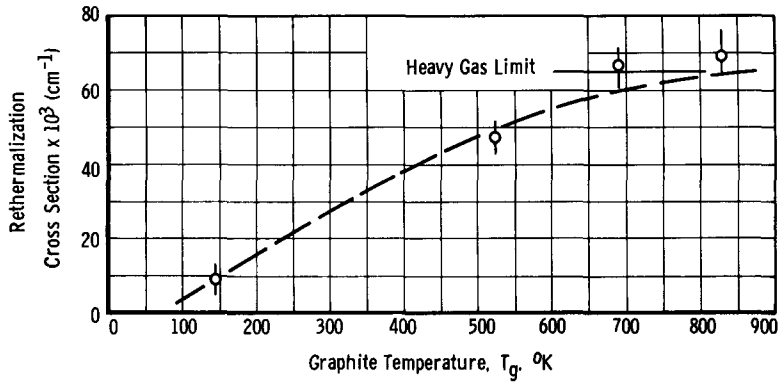

Figure 5 Caption

Rethermalization cross sections of graphite at physical temperatures T_1 for neutrons in Maxwellian energy distributions $M(E,T_2)$, where the values of T_2 in Table II have been assumed equal.

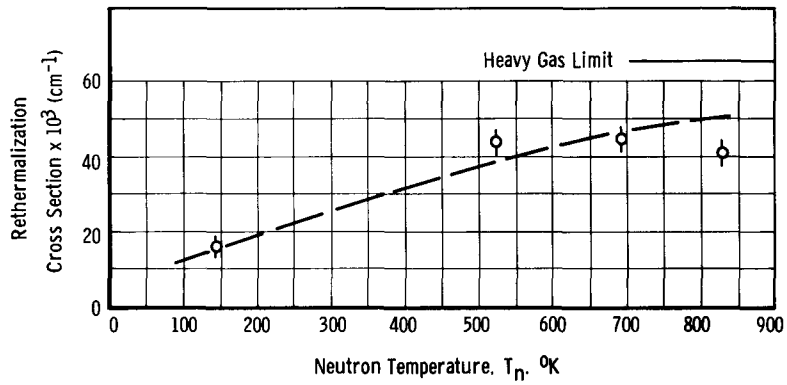

Figure 6 Caption

Rethermalization cross sections of graphite at a physical temperature T_2 (≈300°K) for neutrons in Maxwellian energy distributions $M(E,T_1)$. See Table I.

The calculated curves of the thermal activities of Cu^{64} that best fit the traverses observed in the graphite experiments are shown in Figure 7. The tendency of the experimental data near the axis of symmetry to fall below the curves that fit best is due to an increase in the flux perturbation caused by the relative increase in the concentration of detectors near the axis of symmetry. However, dropping the data points out to a radius of 5 cm. has a negligible influence upon the best values of the rethermalization cross sections.

Effective Masses of Graphite

Coates and Gaylher[5] have inferred effective masses of graphite from differential measurements of the neutron spectrum in the graphite of a graphite-natural uranium lattice. The measurements were made with a fast chopper in the energy range from 0.01 ev to 50 ev for lattice temperatures of 293, 433, 517, and 594°K. Values of the effective neutron temperatures, T_n, were found by determining the Maxwellian spectra that best fit the low energy regions of the observed spectra. Those effective neutron temperatures and the moderator temperatures, T_m, were then used to calculate effective masses with the approximate Coveyou[15] expression

$$11) \quad M_\epsilon = \frac{2\sigma_s}{\sigma_a(kT_n)} \left[(T_n - T_m)/T_n \right]$$

where σ_s is the microscopic scattering cross section of graphite of 4.8 barns. The quantity $\sigma_a(kT_n)$ is the effective microscopic absorption cross section of the lattice cell, and for $E = kT_n$, $T_n = 347°K$ $\sigma_a(kT_n) = 0.0512$ barns.

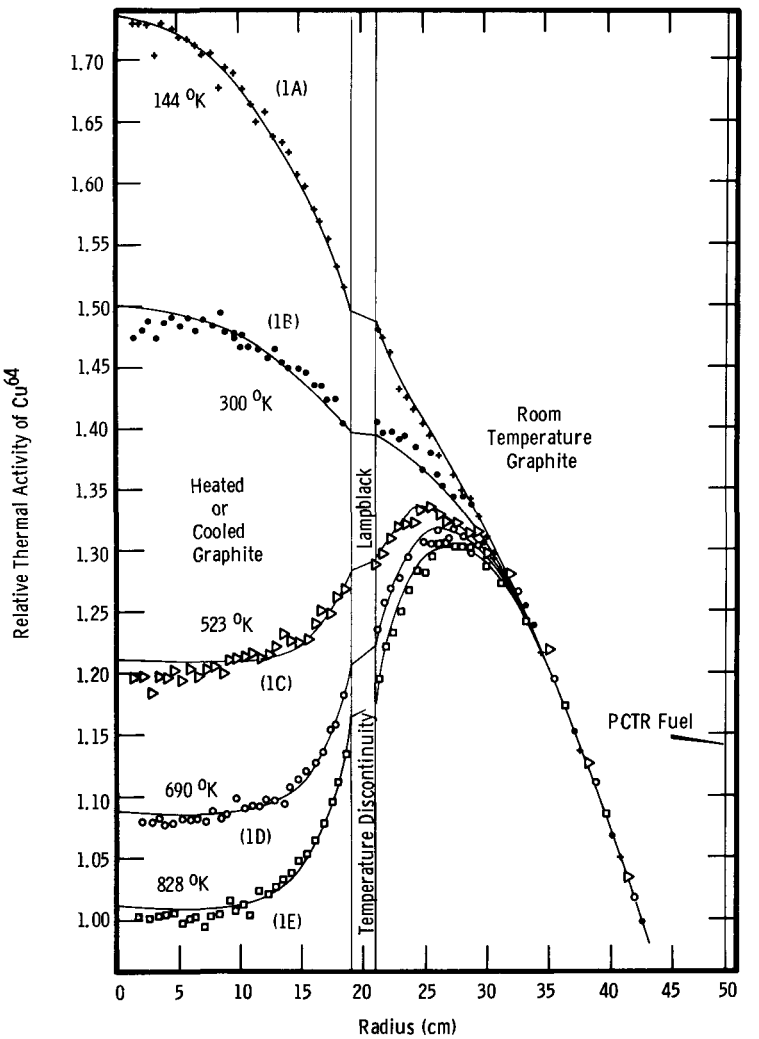

Figure 7 Caption

Graphite Experiments - Comparisons of calculated and observed traverses of the thermal activities of Cu^{64} near temperature discontinuities. The traverses are arbitrarily normalized at a radius of 42.5 cm. The calculated curves are normalized to the experimental data in a manner that minimizes the variance of the fit. The statistical uncertainties in the data points are standard deviations of approximately $\pm$ 1%. The physical temperatures of the graphite cylinder are indicated for each experiment and those of the graphite annulus are approximately 300°K and are given in detail in Table I.

It is somewhat difficult to compare their results with those given in Tables I and II. The primary difficulty is that their neutron temperatures are always only slightly higher than their graphite temperatures, whereas the temperatures given in Tables I and II are, in general, quite different. From the latter data estimates have been made of the values of $M_{i\rightarrow i,k}$ for neutrons in spectra that are in equilibrium with the graphite. The estimates are compared in Figure 8 to the values found from Eqn. 11. The shaded area is an area of uncertainty based upon the uncertainties of the measured values given in Tables I and II.

Relaxation Lengths in Graphite

The thermalization or rethermalization of non-equilibrium neutrons may be considered in at least two approximations; the continuous slowing down or Fermi age theory approximation and the multithermal group approximation presented in this paper. The mean square distance that neutrons travel in thermalizing to a temperature, T, is determined by an age τ (T) in the age theory. In the two group approximation the mean square distance that neutrons travel to reach an equilibrium temperature is determined by an L^2. If the two approximations describe the thermalization process reasonably well τ should be approximately equal to L^2 for the same mean temperature. The problem chosen to illustrate the methods of finding the mean temperatures for a given L and τ is that of the thermalization of near-equilibrium neutrons in graphite at physical temperature T_o = 300°K.

To illustrate the continuous slowing down approximation the results of a theoretical study[6] of the elastic and one phonon

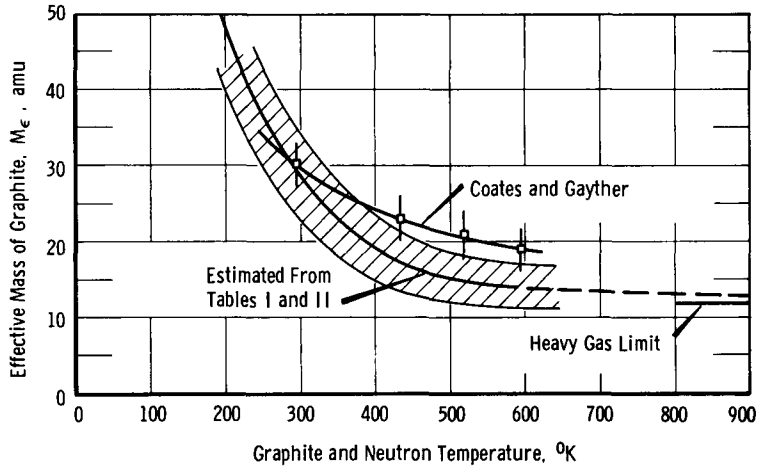

Figure 8 Caption

Effective mass of graphite for neutrons near equilibrium. For the Coates and Gayther data the characteristic neutron temperature is approximately 50°C greater than the moderator temperature. The neutron and moderator temperatures are assumed equal in determining the confidence zone shown.

inelastic scattering of neutrons in graphite are used. In the study, neutrons near equilibrium in graphite at a physical temperature T_0 are assumed to have attained a Maxwellian energy distribution $M(E,T_1)$, where $T_1 \neq T_0$. In thermalizing to the equilibrium temperature T_0 the neutrons are assumed to remain in a Maxwellian energy distribution with a characteristic temperature that changes with time. The time rate of change of the characteristic temperature T given in the paper may be approximated by

$$12) \quad \frac{dT}{dt} = -a(T-T_0).$$

Equation 12 is analagous to the Fermi age equation for the time rate of change of neutron energy during slowing down[16]. The Fermi age analogy leads to the expression

$$13) \quad \tau(T_1 \rightarrow T, T_0) = \frac{D}{a} \sqrt{\frac{8k}{\pi m}} \int_T^{T_1} \frac{T^{\frac{1}{2}}}{(T-T_0)} \, dT$$

for the age to thermalize from T_1 to T in graphite at T_0, where k is the Boltzmann Constant, D is the diffusion coefficient of graphite and m is the mass of a neutron.

For the thermal group problem, consider a plane source of $M(E,T_1)$ neutrons in an infinite region of graphite at a physical temperature T_0. The source neutrons thermalize exponentially with a relaxation length L; where L is given by Eqn. 9 for this case of a cross section for absorption that is small with respect to the cross section for rethermalization. The equilibrium group $M(E,T_0)$ builds up exponentially also, with the same relaxation length. The mean neutron temperature of the two groups is taken as the

spatially weighted sum of the respective characteristic temperatures and is given by

$$14) \quad \bar{T}(x) = T_1 e^{-x/L} + T_0(1-e^{-x/L}).$$

Equation 14 is used to calculate the mean temperature $\bar{T}(L)$ at x = L. The quantity $\bar{T}(L)$ is then used as the lower limit of the integration in Eqn. 13. Equation 13 is integrable and yields values of $\tau\{T_1 \rightarrow \bar{T}(L), T_0\}$ whose square roots are compared to L in Table III. It can be seen that $\sqrt{\tau}$ is greater than L by approximately $\sqrt{2}$ for all temperatures T_i. An increase in the quantity a by a factor of two would improve the agreement significantly.

Rethermalization Cross Sections of Water

The analyses of the graphite and water experiments and the determination of the rethermalization cross sections of water were similar to that described for the graphite experiments. The only significant difference was in the use of fixed values of the cross sections for rethermalization in the graphite regions, which were inferred from the results of the graphite experiments. This of course, introduces dependence of the values of the cross sections for water upon those found for the graphite. The values of the cross sections for rethermalization of hot neutrons in ambient water inferred in the analyses and corresponding values for the graphite region are given in Table IV. The calculated curves of the thermal activity of Cu^{64} that best fit the observed traverses are shown in Figure 9. The water portion of Figure 9 is enlarged in Figure 10 for clarity. The agreemen' between the calculated and observed traverses in the graphite regions is relatively poor. No systematic error has been found that would improve the fit.

TABLE III

RELAXATION LENGTHS OF GRAPHITE AT PHYSICAL TEMPERATURE OF ~ 300°K FOR NON-EQUILIBRIUM NEUTRONS IN MAXWELLIAN ENERGY DISTRIBUTIONS $M(E,T_1)$

INITIAL GROUP TEMPERATURE	SLOPE OF THEORETICAL CURVE	DIFFUSION COEFFICIENT OF GRAPHITE	TEMPERATURE REACHED IN ONE RELAXATION DISTANCE	AGE TO RELAX TO TEMPERATURE T	CALCULATED RELAXATION DISTANCE	MEASURED RELAXATION DISTANCE
T_1	a	D	$\bar{T}(L)$	$\tau\{T_1 \rightarrow \bar{T}(L), T_0\}$	$\sqrt{\tau}$	L
°K	10^{+3} sec^{-1}	cm	°K	cm^2	cm	cm
260	3.4	0.820	285.3	58.2	7.63	5.3
305	4.8	0.810	301.8	42.4	6.52	4.8
350	6.6	0.795	318.4	31.9	5.65	4.5
400	7.7	0.780	336.8	28.1	5.30	4.3
500	8.8	0.775	373.6	26.4	5.14	4.2
600	8.8	0.775	410.4	28.3	5.32	4.2

TABLE IV

RETHERMALIZATION OF T_2 NEUTRONS IN WATER WITH A PHYSICAL TEMPERATURE T_1

Experiment	Physical[a] Temperature of Water	Characteristic Temperature of Neutron Group	Diffusion[17] Coefficient of Water	Rethermalization Cross Section of Water	Relaxation Length of Water	Effective Mass of Water	Scattering[c] Cross Section of Water	Physical[d] Temperature of Outer Annulus of Graphite	Rethermalization[b] Cross Section for Graphite	
									Inner Annulus	Outer Annulus
	T_1	T_2	D_{221}	$\Sigma_{2\to1,1}$	$L_{2\to1,1}$	$M_{e2\to1,1}$	Σ_{S221}	T_2	$\Sigma_{1\to2,3}$	$\Sigma_{2\to1,5}$
	°K	°K	cm	cm^{-1}	cm	amu	cm^{-1}	°K	cm^{-1}	cm^{-1}
2B	292 ± 5	410 ± 5	0.1749	1.25 ± .12	0.37 ± 0.04	5.0 ± 0.5	3.10	305 ± 5	0.038	0.037
2E	293 ± 5	558 ± 5	0.2112	1.27 ± .12	0.41 ± 0.04	4.5 ± 0.5	2.88	310 ± 5	0.052	0.043
2D	295 ± 5	720 ± 5	0.2290	0.83 ± .08	0.53 ± 0.05	6.5 ± 0.6	2.70	325 ± 5	0.063	0.043

a) Water density assumed = 1.0 gm/cm^3

b) Rethermalization cross sections of graphite found from Fig. 5 and 6

c) Macroscopic scattering cross section of water assumed to be $\Sigma_{S221} = 3.38 \sqrt[4]{T_o/T_2}$ cm^{-1}

d) In the analysis of these water experiments the physical temperatures of the water and the outer annulus of graphite where averaged.

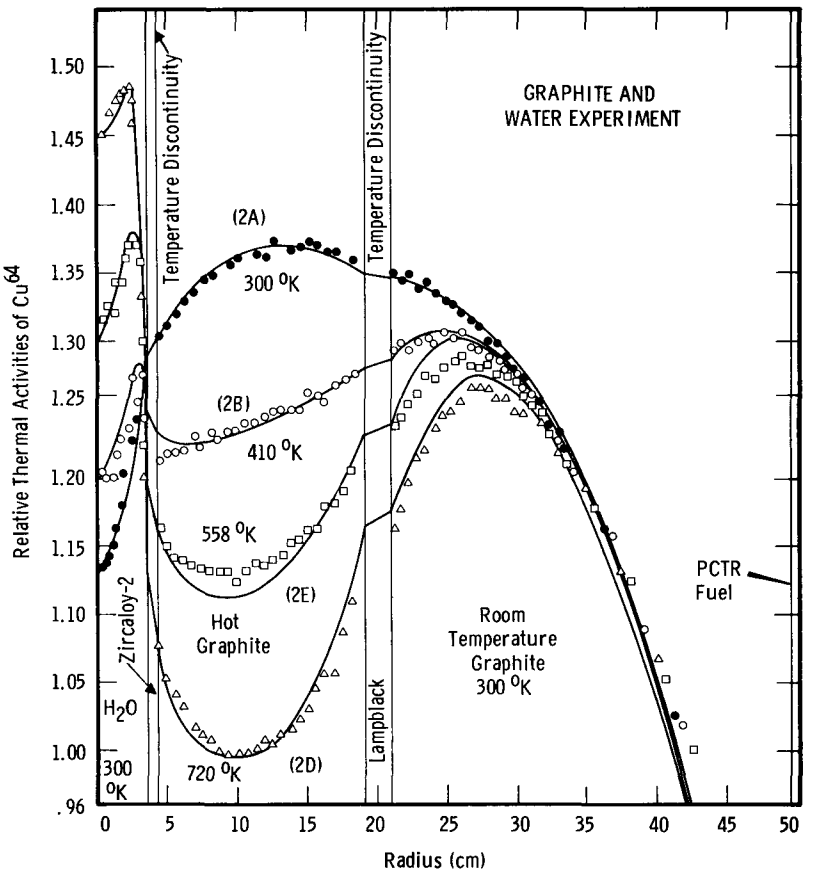

Figure 9 Caption

Graphite and Water Experiments. Comparisons of calculated and observed traverses of the thermal activities of Cu^{64} near temperature discontinuities. The calculated curves are normalized to the experimental data in a manner that minimizes the variance of the fit to the data in all regions. The statistical uncertainties in the data points are standard deviations of approximately $\pm$ 1%. The physical temperatures of the inner annulus of graphite are indicated while nominal values of 300°K are indicated for the water and outer annulus of graphite. Detailed temperatures for the latter are given for each experiment in Table IV.

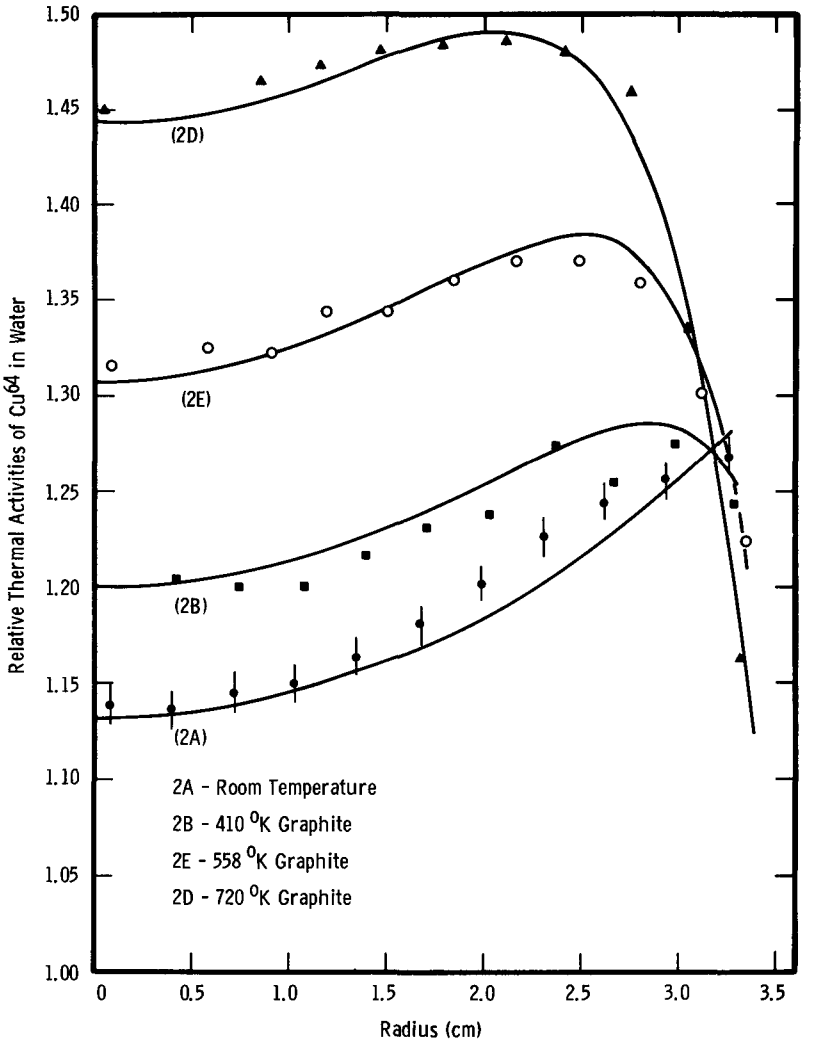

Figure 10 Caption

Graphite and Water Experiments. Enlargement of the water region of Figure 9. The graphite temperatures on the figure are also the characteristic temperatures of the rethermalizing neutrons.

Lutetium Traverses

The traverses of the bare and cadmium covered activities of Lu^{177} were obtained for testing the multithermal group diffusion model, the assumptions of Maxwellian energy distributions for the equilibrium spectra and a 1/E spectrum for the epithermal neutrons, and the values of the rethermalization cross sections inferred from the analyses of traverses of the activities of Cu^{64}. The experimental data were reduced to thermal activities in the manner described previously for Cu^{64}. Values of α for Lu^{177} were obtained from the work of Schmid.(18)

The equilibrium fluxes obtained in the Cu^{64} analyses and the thermal cross sections of Lu^{176} were used to compute the expected spatial distributions of the thermal activities of Lu^{177}. These calculated curves were normalized to the experimental traverses of the thermal activities in a manner that minimized the variance of the fit. Varying degrees of success were achieved, but the fits at higher temperatures tended to be poorer. These are illustrated for the graphite experiments in Figures 11 and 12. Additional comparisons have been made for the other experiments.(19)

The agreement between the calculated curves and experimental traverses at high temperature can be improved but it is done at the expense of destroying the agreement at the low temperatures. This has been done in the form of a first-order approximation. The Lu^{177} data were reduced to thermal activities using a Hurwitz epithermal spectrum(20) rather than the 1/E spectrum of Eqn. 2. This change of spectrum increased the epithermal correction to the bare activity. For the experiments illustrated in Figures

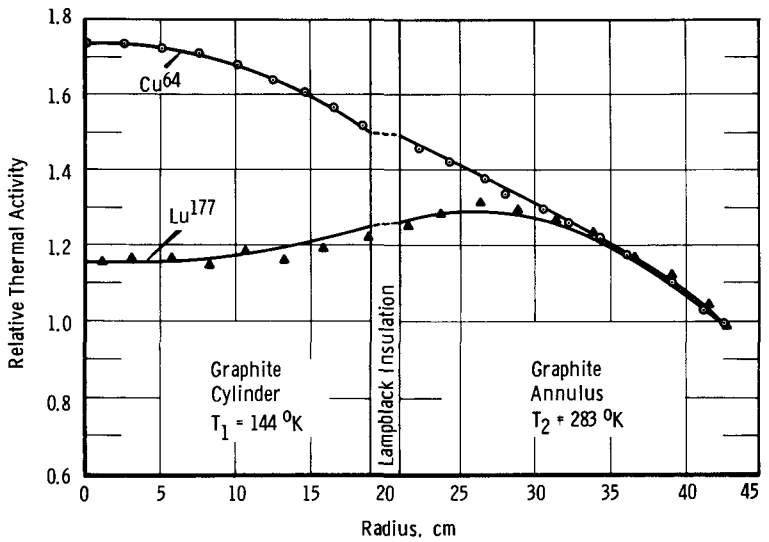

Figure 11 Caption

Comparison of calculated and observed traverses of the thermal activities of Cu^{64} and Lu^{177} near a temperature discontinuity in graphite. The experimental traverses are arbitrarily normalized to unity at a radius of 42.5 cm. The calculated curves are normalized to the experimental data in a manner that minimizes the variance of fit. The statistical uncertainties in the experimental data are standard deviations of approximately $\pm$ 1%.

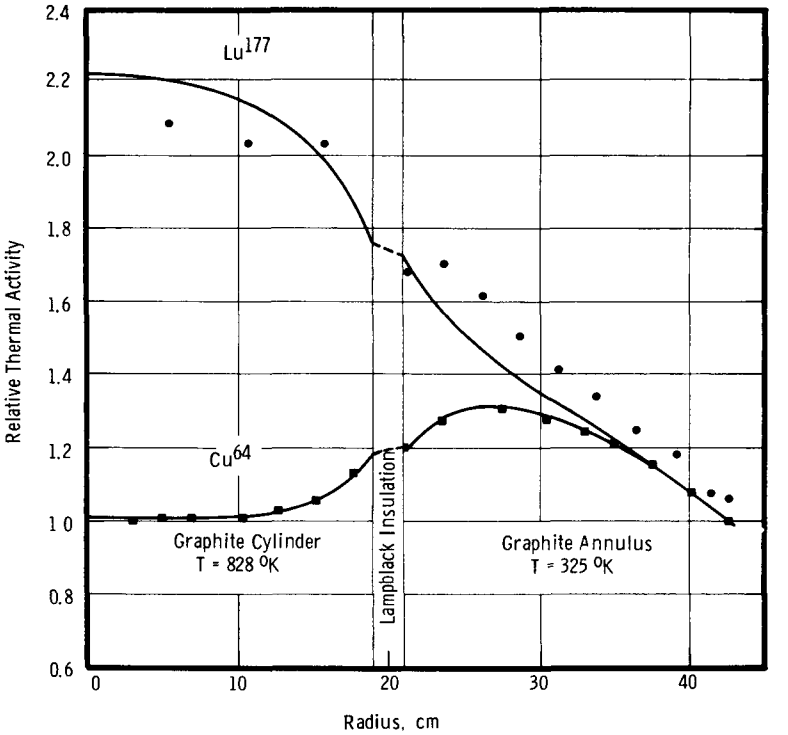

Figure 12 Caption

Comparison of calculated and observed traverses of the thermal activities of Cu^{64} and Lu^{177} near a temperature discontinuity in graphite. The experimental traverses are arbitrarily normalized to unity at a radius of 42.5 cm. The calculated curves are normalized to the experimental data in a manner that minimizes the variance of fit. The statistical uncertainties in the experimental data are standard deviations of approximately $\pm$ 1%.

11 and 12 the relative thermal activities of Lu^{177} in the inner graphite regions are increased. However, the overall goodness-of-fit for all experiments was not improved significantly. This analysis does indicate that perhaps some spectrum intermediate between Westcott and Hurwitz spectra could improve the goodness-of-fit with respect to the Lu^{177} data.

Model Comparisons

The significance of the transients interpreted by the use of the multithermal group model of the space energy distribution of neutrons has been illustrated by comparing its results to two extreme assumptions. In the first, two equilibrium thermal groups are assumed but transfer between groups is not allowed. This is equivalent to setting the rethermalization cross sections to zero. If the thermal activity of Cu^{64} is then calculated and normalized to the observed traverse by minimizing the variance of the fit the calculation over estimates the reaction rate in warm regions and under estimates in cold region. In the second, the rethermalization cross sections are assumed to be infinite, forcing the energy distribution of thermal neutrons to change abruptly at discontinuities in physical temperatures. Treating the thermal activity of Cu^{64} as before the error in the estimates are reversed from those found for the above extreme case. These results are compared in Figures 13 and 14 for a typical graphite experiment and a typical graphite and water experiment, respectively. Figure 14 is of particular interest in that the peak of the activity in the water is so poorly reproduced for the extreme approximations.

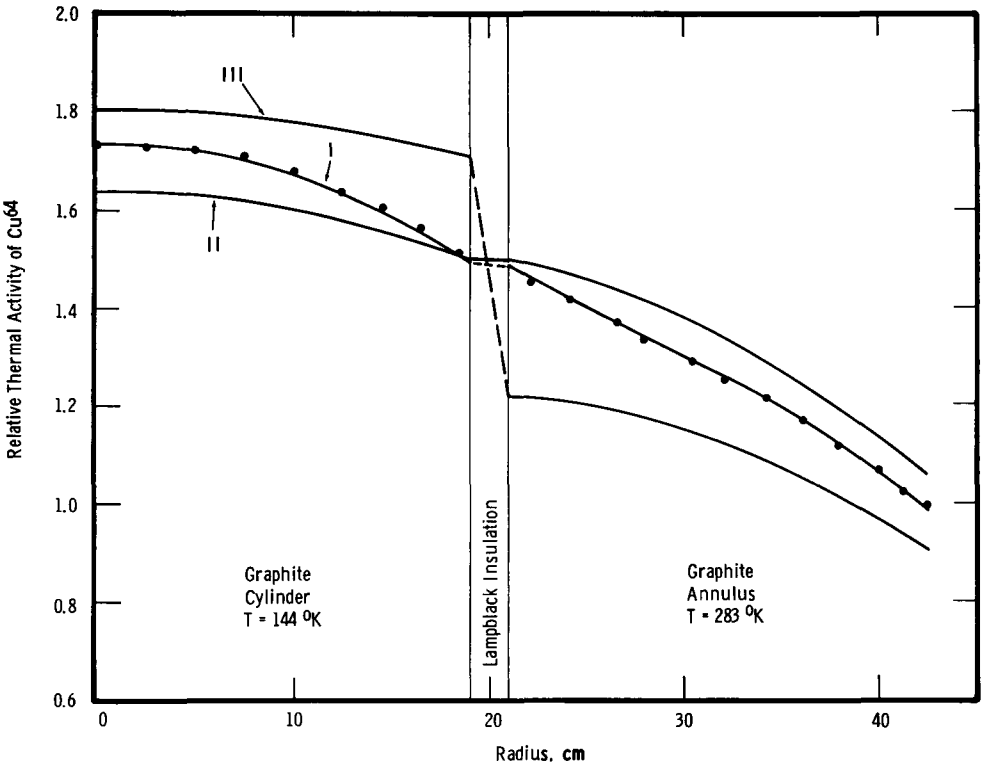

Figure 13 Caption

Comparisons of the observed traverse of the thermal activity of Cu^{64} near a temperature discontinuity in the all graphite system with the spatial variation predicted by the multithermal group model (I) and the two approximations (II) $\Sigma_{i\to j,k} = 0$ and (III) $\Sigma_{i\to j,k} = \infty$. The calculated curves are normalized to the experimental data in a manner that minimizes the variances of the fits.

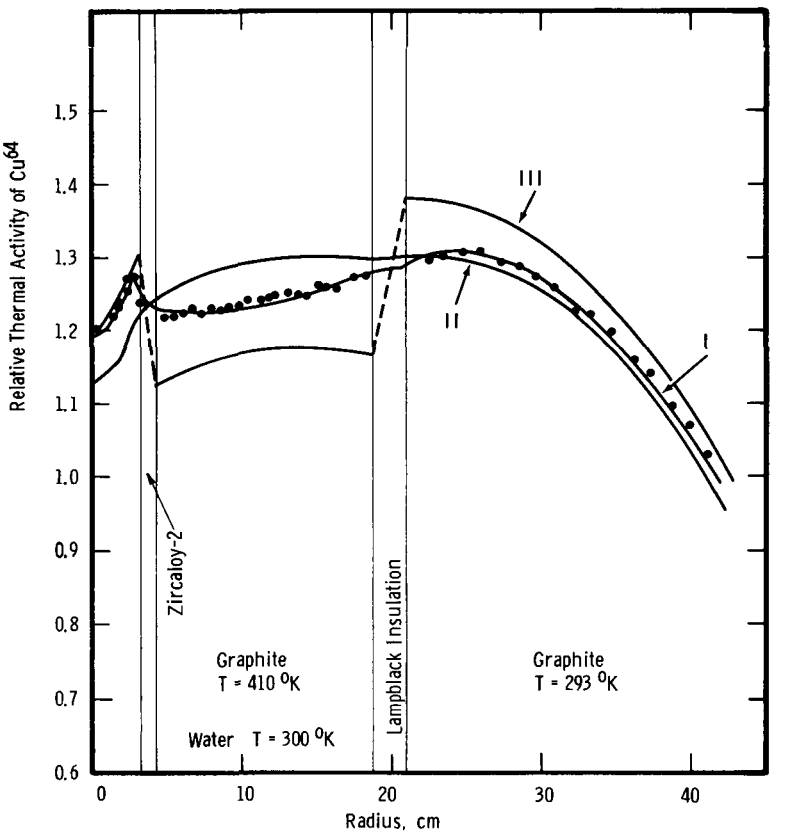

Figure 14 Caption

Comparisons of the observed traverses of the thermal activity of Cu^{64} near temperature discontinuities in the graphite and water system with the spatial variation predicted by the multithermal group model (I) and the two approximations (II) $\Sigma_{i\to j,k} = 0$ and (III) $\Sigma_{i\to j,k} = \infty$. The calculated curves are normalized to the experimental data in a manner that minimizes the variances of the fits.

Conclusions

The results of this work illustrate the rather strong dependence of the effective mass of graphite upon both neutron and moderator temperatures. The results agree approximately with those of Coates and Gayther and with the relaxation lengths calculated from a simplified theory of neutron thermalization in graphite. The cross section for rethermalization of 300°K neutrons in graphite asymptotically approaches the value for a heavy gas, at a physical temperature of about 800°K. One would expect the asymptotic behavior to occur above or at least near the Debye temperatures (1200 and/or 2000°K) where chemical binding energy is small relative to the neutron energy.

The values of the cross sections for rethermalization of hot neutrons in 300°K water indicate a surprising decrease with increasing temperature. This might be expected, however, in view of the rapid decline of the scattering cross section of water with increasing neutron energy. The indicated increase in the effective mass with temperature is unexpected and, in view of the rather large uncertainties in the rethermalization cross sections, may not be real.

The uncertainties in the results obtained from these experiments due to statistics are acceptable. However, those uncertainties attributed to the assumed energy distributions of neutrons are not. If a satisfactory model of the spectra in the epithermal-subcadmium region were available, the resolution of the neutron and moderator temperature dependence of the rethermalization properties could be improved significantly.

Acknowledgements

The author gratefully acknowledges R. E. Heineman for encouragement and constructive criticisms, J. R. Lilley for many helpful technical discussions and the computer programming, and the many others who prepared the experiments and data for processing.

REFERENCES

1. R.A. Bennett and R.E. Heineman, Nuclear Sci. and Eng. 8, 294-299 (1960).
2. D.J. Donahue, D.D. Lanning, R.A. Bennett, and R.E. Heineman, Nuclear Sci. and Eng. 4, 297 (1958).
3. D.S. Selengut, Nuclear Phys. Research Quart. Rept. April-June, 1958, HW-56919.
4. G.P. Calame, Nuclear Sci. and Eng. 8, 400-404 (1960).
5. M.S. Coates and D.B. Gayther, Time of flight measurements of neutron spectra in a graphite uranium lattice at different temperatures, AERE-R-3829 (September, 1961).
6. L.S. Kothari and P.G. Khubchandani, Nuclear Sci. and Eng. 7, 240-244, (1960).
7. G.R. Gavin, A determination of neutron temperature at the center of the thermal test reactor, KAPL-1142.
8. H. Hurwitz, Jr., M.S. Nelkin, and G.J. Habetler, Nuclear Sci. and Eng. 1, 280-312 (1956).
9. C.W. Lindenmeier, Nuclear Phys. Research Quart. Rept. October-December, 1960, HW-68389
10. D.S. Selengut, Criticality calculation on the 701 computer, XDC 55-3-18.
11. R.A. Bennett and W.P. Stinson, Nuclear Phys. Research Quart. Rept. July-September, 1959, HW-62727.
12. R.A. Bennett Nuclear Phys. Research Quart. Rept. October-December, 1959, HW-63576.
13. D.J. Hughes and R.B. Schwartz Neutron Cross Sections, BNL325, 2nd Edition (July 1, 1958).

14. J.R. Lilley, Correlation of Experimental Activity Traverses Using Few Group Diffusion Theory-Computer Code FIT-1, June 1961, HW-69871.

15. R.R. Coveyou, R.R. Bate, and R.K. Osborn, Journal Nuc. Eng. 2, 153, 1956.

16. B.S. Glasstone and M.C. Edlund. "The Elements of Nuclear Reactor Theory", D. Van Nostrand Company, Inc., 1952.

17. K.S. Rockey and W. Skolnic, Nuclear Sci. and Eng. 8, 62-65 (1960).

18. L.C. Schmid, Physic Research Quarterly Report, January-March 1961, HW-69475.

19. R.A. Bennett, Physic Research Quarterly Report, January-March 1961, HW-69475.

20. C.W. Lindenmeier Physic Research Quarterly Report, April-May 1961 HW-70716.

NEUTRON THERMALIZATION STUDIES AT SAVANNAH RIVER*

by

H. Dean Brown and E. J. Hennelly

E. I. du Pont de Nemours & Co.
Savannah River Laboratory
Aiken, South Carolina

SUMMARY

Recent experimental work on neutron thermalization at Savannah River has centered on the thermal neutron diffusion coefficient in D_2O as a function of temperature and on neutron spectra in D_2O lattices. The diffusion coefficient measurements were made by poisoning techniques in the Pressurized Subcritical Experiment (PSE) at temperatures up to 220°C. Excellent agreement was obtained with theoretical predictions. In addition an analysis of all the earlier room-temperature measurements in terms of more recent cross sections and spectral hardening corrections brought the old and new results into agreement, within experimental errors.

Spectrum measurements have dealt both with high temperature lattices and with flux hardening in heavy fuel assemblies. As an extreme example of the latter case, foil activation measurements have been made in lattices of 3-inch-diameter uranium metal rods containing 3 wt % U^{235} at a triangular pitch of 18 inches in D_2O. Similar measurements were made at temperatures up to 215°C for lattices of 2-inch-diameter uranium metal tubes in D_2O. Extensive use has been made of the THERMOS code for analysis.

*The information contained in this article was developed during the course of work under contract AT(07-2)-1 with the U. S. Atomic Energy Commission.

THE NEUTRON DIFFUSION COEFFICIENT IN D_2O BETWEEN 20°C AND 220°C

Measurements of the thermal neutron diffusion coefficient for D_2O have been made at temperatures from 20°C to 220°C and compared to theory and other measurements. The method was to measure the relaxation length of the neutrons in D_2O to which known amounts of neutron poison had been added. A heterogeneous absorber was selected because of design features of the Pressurized Subcritical Experiment (PSE)[1], the facility used for the experiments. Copper tubes with a nominal OD of 1.125 inches and a wall thickness of 0.050 inch were used at square lattice pitches ranging from 4.55 to 12.87 inches. Tube weights and measured intracell flux profiles were combined with a copper cross section of 3.79 ±0.04 barns[2] to give effective macroscopic absorption cross sections. The purity of the copper was established by chemical analyses and neutron absorption tests. Relaxation lengths were measured by gamma counting of activated manganese foils.

The measurements were corrected for the volume displacement and scattering of the copper as well as for the thermal expansion of components. Table I gives values of the diffusion coefficient at the experimental moderator purity and at the calculated extrapolation to 100% D_2O. The values $D'(T_o)$ are obtained by direct extrapolation of the data without correction for the fact that the effective neutron temperature[3], T_N, is greater than the moderator temperature, T_o, in the poisoned lattices. The values $D(T_o)$ are corrected for this effect. Table I also gives values of the diffusion coefficient as obtained by other experimenters using comparable techniques. These latter values have been corrected by use of the latest boron cross section of 762 ±3 barns to put them on the same basis as the current experiments. Figure 1 shows the measurements of $D(T_o)$ and the equivalent curve calculated by Radkowsky's method[4] plotted against temperature.

If the diffusion coefficient is in cm and the temperatures are in ^{o}K, the experimental data as well as the calculations by Radkowsky's method can be fitted very closely by the formula

$$D(T_N, T_o) = 0.8395 \left[0.69 + 0.31(T_N/293)^{1/2} \right] \frac{\rho(293)}{\rho(T_o)} \qquad (1)$$

where the ρ's are D_2O densities.

The agreement among the experimental measurements and with the calculations is remarkable in that the measurements were made by such diverse methods as boron poisoning[5,6], measurement of extrapolation distance[7], pulsed sources[8], and pile oscillators[9].

LATTICE SPECTRUM MEASUREMENTS WITH FLUX HARDENING IN HEAVY FUEL ASSEMBLIES[10]

Experimental Arrangement

Neutron spectrum measurements were made on D_2O lattices of uranium rods 3.0 inches in diameter and about 48 inches long. The uranium metal was enriched to 3.00 ±0.005 wt % U^{235}. All measurements were carried out in the Savannah River Subcritical Experiment (SE), a cylindircal tank 5 ft in diameter and 7 ft tall. The tank rests on a graphite pedestal, which forms a thermal column above the Standard Pile (SP)[11]. The uranium rods were suspended vertically in the SE tank in a triangular lattice at an 18-inch pitch. The moderator purity was 99.3 mol % D_2O throughout the experiments. The lattice cells contained only fuel rods and moderator; however, the rods were coated with a thin layer of lacquer to prevent chemical reaction with the moderator.

Experimental Measurement of Thermal Flux Distributions

The experimental value of the disadvantage factor was obtained from measurement of the activation ratios of manganese foils placed throughout a unit cell of the lattice.

Bare Mn foils, 1/2 inch in diameter and 0.010 inch thick, and cadmium-covered Mn foils, 1/4 inch in diameter and 0.010 inch

thick, were loaded into a diametral hole, 1/2 inch in diameter, in one of the uranium rods, hereinafter referred to as the "traverse rod". The Cd covers were 0.030 inch thick. Uranium metal spacers, 0.48 inch long, 1/2 inch in diameter, and made of 3.0 wt % U, occupied the space in the diametral hole not otherwise taken up by foils. Aluminum foils, 0.002 inch thick and 1/2 inch in diameter, were used to prevent contamination of the Mn foils by fission fragments escaping from adjacent U.

Bare and Cd-covered Mn foils were also attached to three Al strips, which were fastened to the traverse rod and projected into the moderator. Two of these strips were pointed at neighboring U rods and the third was pointed at the midpoint of the moderator between the two rods.

The activity of each foil was determined after the irradiation by counting the induced Mn^{56} activity with a scintillation detector. The activity of the foils was corrected for the radial flux shape in the SE by multiplying each foil activity at the radius, r, from the center of the tank by the quantity $\left[J_o(0.0308r)\right]^{-1}$.

The foil activation profiles in a unit cell are shown in Figure 2. There was very little azimuthal variation (±1%) in the Mn foil activations in the moderator of the unit cell.

Comparison of Experiment and Calculation

A comparison between the thermal flux in the unit cell as predicted by THERMOS[12] and P-3 calculations, and the subcadmium Mn foil activations is given in Figure 3. The curves are normalized so that the calculated values of the average fluxes in the fuel are equal to the average Mn foil activations in the fuel.

Figure 4 compares the subcadmium Mn foil activation in a unit cell as predicted by THERMOS and as measured. The data show that, because of spectral hardening, the Mn foil activation ratio,

$A_{Mn}(Mod)/A_{Mn}(fuel)$, cannot be equated directly to the corresponding flux ratio $\Phi(Mod)/\Phi(fuel)$. The agreement between the calculated and experimental Mn foil activation profiles within the fuel rod is good. However, in the moderator, the predicted foil activation is about 5% greater than that which was observed experimentally.

In a second experiment in the same lattice, Pu and Mn foils were irradiated in the traverse rod. The 1/4-inch-diameter Pu foils were made of an alloy of 5 wt % Pu^{239} in Al and were Ni-clad. Each foil was about 0.006 inch thick and contained about 1 mg Pu^{239}. The Mn foils were identical to those used in the first experiment. Both bare and Cd-covered foils were also mounted on thin Al spears projecting into the moderator from the U rod. Only bare foils were placed in the traverse rod, inasmuch as the Cd ratio of Mn in the fuel was already available from the previous experiment. Decay corrections on the Pu foils were obtained from a reference foil counted repeatedly during the counting period. Decay corrections for the Mn foils were made analytically using a decay constant of 4.48×10^{-3} min^{-1}.

The corrected foil activities as a function of radius in the cell are shown in Figure 5. The shapes of the curves shown for the Mn data agree very well with those obtained previously.

A test of the validity of the calculated spectrum is available from the activation data on the Pu foils. The Pu activation data within the metal rod are compared to those calculated by THERMOS in Figure 6. The calculated Pu foil activation data are normalized to the subcadmium activity at a radius of about 3.6 cm (0.2 cm from the outer radius of the rod). Cd-covered Pu foil data were not obtained within the rod but were estimated as shown by the dashed part of the "Pu Epicadmium" curve given in Figure 5. At the normalization point the Cd ratio of the Pu foils is ≥ 20, so that this normalization should be subject to little error.

The standard deviation shown on the experimental points in Figure 6 includes a ±50% uncertainty in the Cd-covered Pu activation estimates.

The data of Figure 6 show that the Pu foil activations calculated from THERMOS agree very well with the measured activations within the fuel rod. This is an encouraging indication that the neutron flux spectrum upon which the calculated activations are based is close to that which actually occurs in the rod.

THERMOS Calculations of Spectral Hardening

Figure 7 depicts the neutron flux as a function of energy, as predicted by THERMOS, for three different positions in the unit cell: at the cell boundary, at the first space region inside the rod (near the outer rod radius), and at the rod center. The dashed curve shows the relative absorption cross section of U^{235} as a function of energy.

The Maxwellian shape is hardened by absorptions in the rod and is distorted severely by the capture resonance in U^{235} at 0.3 ev. Since the low-energy fission resonance in Pu^{239} also occurs at 0.3 ev, this depression in the flux at 0.3 ev distorts neutron temperature measurements made with Pu foils. The activations are less than would be expected if the foil were exposed to a thermal Maxwellian flux with a 1/E tail.

The THERMOS calculations were made on the basis of a constant epithermal neutron source distribution. It is believed that the agreement between calculated and measured activations in the moderator will be improved by changing to the epithermal source distribution suggested by the epithermal foil activations.

Experiments of this type with 2-inch rather than 3-inch diameter rods are now under way. In these new experiments, foil activation profiles with a variety of different materials, e.g., Mn, Dy, U, Au, Cu, and Mo will be obtained in order to compare the results with calculation.

Temperature Dependent Studies

Foil activations were obtained in the PSE[1] on lattices of uranium metal tubes that are 1.957 inches in OD, and 1.387 inches in ID and are clad with 0.030-inch aluminum. The measurements were made at 7- and 12-inch lattice pitches with D_2O moderator temperatures between 20°C and 220°C. Detectors used were 0.25-inch diameter Pb-In foils and 0.25-inch diameter Mn foils. No measurements could be made inside the fuel tubes because the cladding had to be kept intact to prevent a rapid uranium water reaction at elevated temperatures. The foil activation measurements were compared with THERMOS and P-3 calculations as in the previous cases. The THERMOS calculation, normalized to the foil data adjacent to the fuel, gave values of the flux which were in good agreement with the measurements over the whole range of temperature. Epicadmium measurements showed that the epithermal flux was almost constant over the lattice cell. This may account for the much better agreement in these cases between the THERMOS calculation and the measurements when compared with the results for massive U rods at wide pitches.

THERMOS was also useful in obtaining the "thermal" η for comparison of traverses with buckling measurements as a function of temperature.

FUTURE EXPERIMENTAL PROGRAM

The Savannah River D_2O critical reactor, the PDP, is ideally suited for making cell traverses at very wide lattice pitches -- e.g. 24 inches -- and we plan extensive activation experiments using a wide variety of foils in support of theoretical studies. In addition the PSE is well suited for making rethermalization measurements in D_2O similar to those that have been made in graphite at Hanford[12]. These experiments are also being considered.

FUTURE THEORETICAL PROGRAM

In addition to the interpretation of experimental cell traverses by THERMOS, extensive comparisons between THERMOS and Monte Carlo calculations are planned. New kernels will be generated to adapt THERMOS for use with organic moderators.

REFERENCES

(1) E. J. Hennelly, "Pressurized Subcritical Facility", Nucleonics 19, (1961), p. 104.

(2) D. J. Donahue, et al., "The Absorption Cross Section of Copper for Thermal Neutrons", Nuclear Sci. and Eng. 7, (1960) p. 184.

(3) A. M. Weinberg and E. P. Wigner, "Physical Theory of Neutron Chain Reactors", University of Chicago Press, Chicago, (1958) p. 336.

(4) A. Radkowsky, "Temperature Dependence of Thermal Transport Mean Free Path From Experimental Data on Scattering Cross Section of Water", ANL-4476, (1950), p. 93.

(5) S. W. Kash and D. C. Woods, "Measurement of the Transport Mean Free Path of Thermal Neutrons in D_2O by a Boron Poisoning Method", Phys. Rev. 90, (1953) p. 564.

(6) A. H. Dexter, et al., "The Diffusion Constant of Neutrons in Heavy Water", ANL-4746, (1951) p. 14.

(7) D. W. Hone, "The Value of Transport Mean Free Path for D_2O", J. Nuclear Energy, Pt. A, Reactor Science 11, (1959), p. 34.

(8) N. K. Ganguly and A. W. Waltner, "Measurement of Neutron Diffusion Parameters of Heavy Water at Different Temperatures by Pulsed Source Method", Trans. Am. Nucl. Soc., Vol. 4, (1961), p. 282.

(9) V. Raievski and J. Horowitz, "Determination of the Mean Transfer Free Path of Thermal Neutrons by Measurement of the Complex Diffusion Length", Proc. 1st Intern. Conf. Peaceful Uses Atomic Energy, Geneva, 1955, P/360, 5, (1956) p. 42.

(10) F. E. Kinard, Nuclear Parameters of Massive Uranium Rods in D_2O, E. I. du Pont de Nemours and Co., Savannah River Laboratory, Aiken, S. C. AEC Research and Development Report DP-644, 42 pp, November 1961.

(11) R. C. Axtmann, et al., Initial Operation of the Standard Pile. E. I. du Pont de Nemours and Co., Savannah River Laboratory, Aiken, S. C. AEC Research and Development Report DP-32, 43 pp. (December 1953) (declassified April 1957).

(12) H. C. Honeck and I. Kaplan, "The Distribution of Thermal Neutrons in Space and Energy in Reactor Lattices. Part I Theory. Part II Comparison of Theory and Experiment". Nuclear Science and Engineering 8, 193-202, 203-9 (1960).

(13) R. A. Bennett and R. E. Heineman, "Neutron Rethermalization Cross Section-Measurements in Graphite", Nuclear Science and Engineering 8, 294, Oct. 1960.

TABLE I

DIFFUSION COEFFICIENTS FOR D_2O FROM POISON ADDITION TECHNIQUES

($D'(T_o)$ is uncorrected, $D(T_o)$ is corrected for spectral hardening)

D_2O Temp., T_o, °C	99.30 mol % D_2O	100 mol % D_2O		Reference
	$D'(T_o)$, cm	$D'(T_o)$, cm	$D(T_o)$, cm	
20	0.827 ±0.010	0.852 ±0.010	0.841 ±0.010	This experiment
100	0.897 ±0.011	0.922 ±0.011	0.912 ±0.011	This experiment
165	0.974 ±0.012	1.000 ±0.012	0.989 ±0.012	This experiment
220	1.073 ±0.013	1.102 ±0.013	1.091 ±0.013	This experiment
23	--	0.852 ±0.008	0.843 ±0.008	Kash and Woods[5]
18	--	0.84 ±0.03	0.83 ±0.03	Dexter, et al.[6]
18	--	0.96 ±0.02	0.83 ±0.02	Dexter, et al.[6]

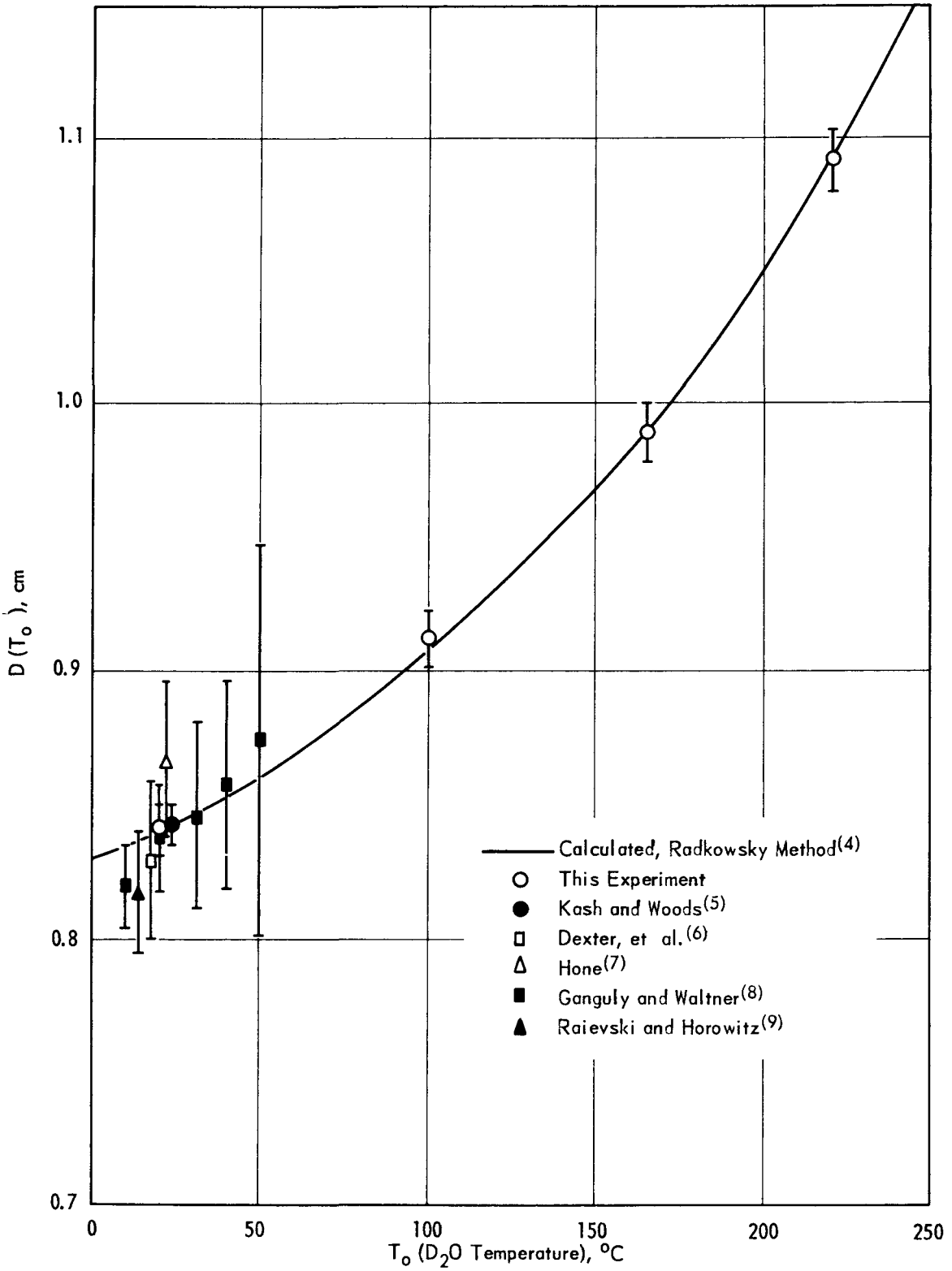

FIG. 1 DIFFUSION COEFFICIENT OF D_2O AS A FUNCTION OF TEMPERATURE

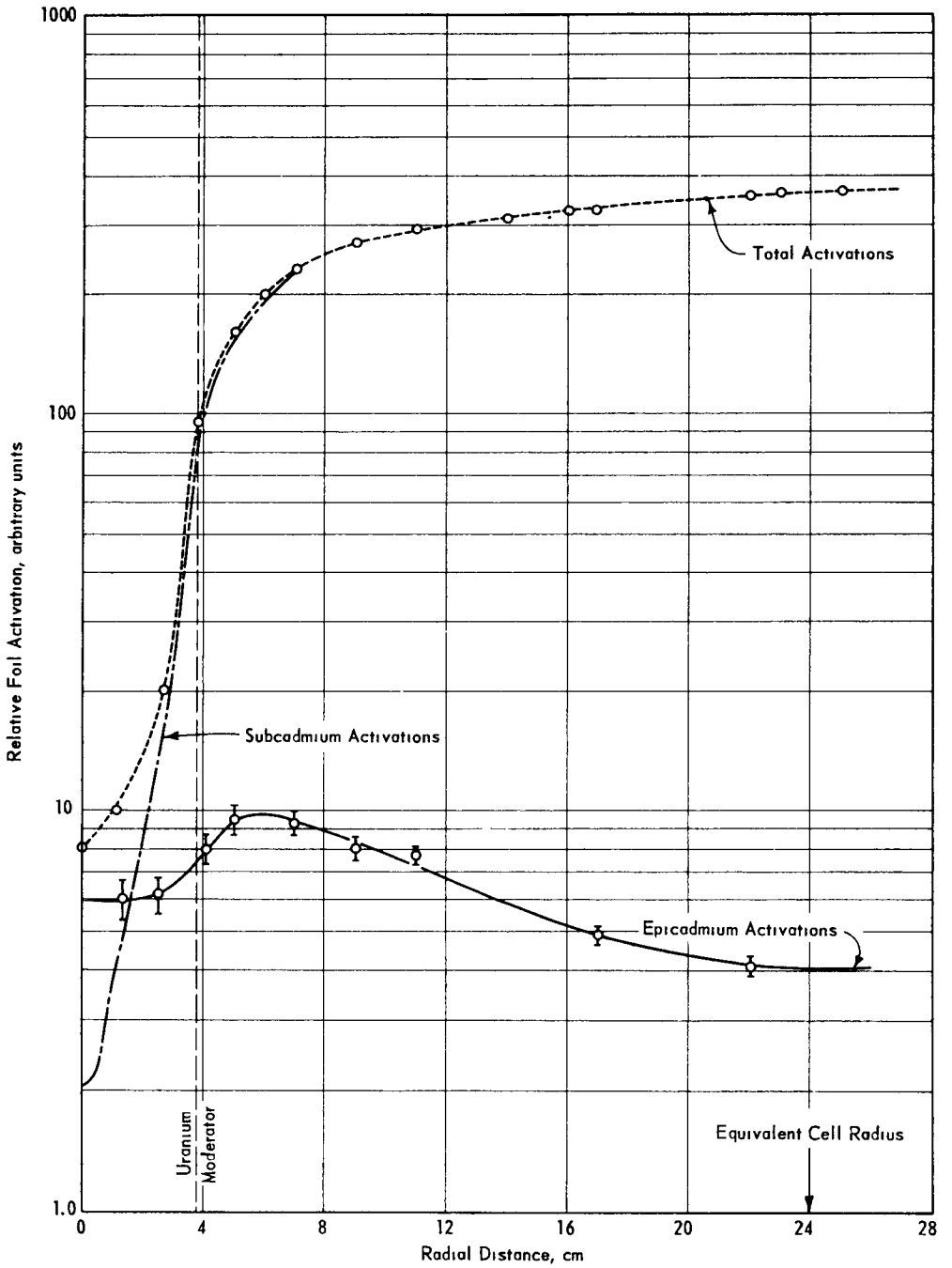

FIG 2 RELATIVE MANGANESE FOIL ACTIVATIONS IN A UNIT CELL

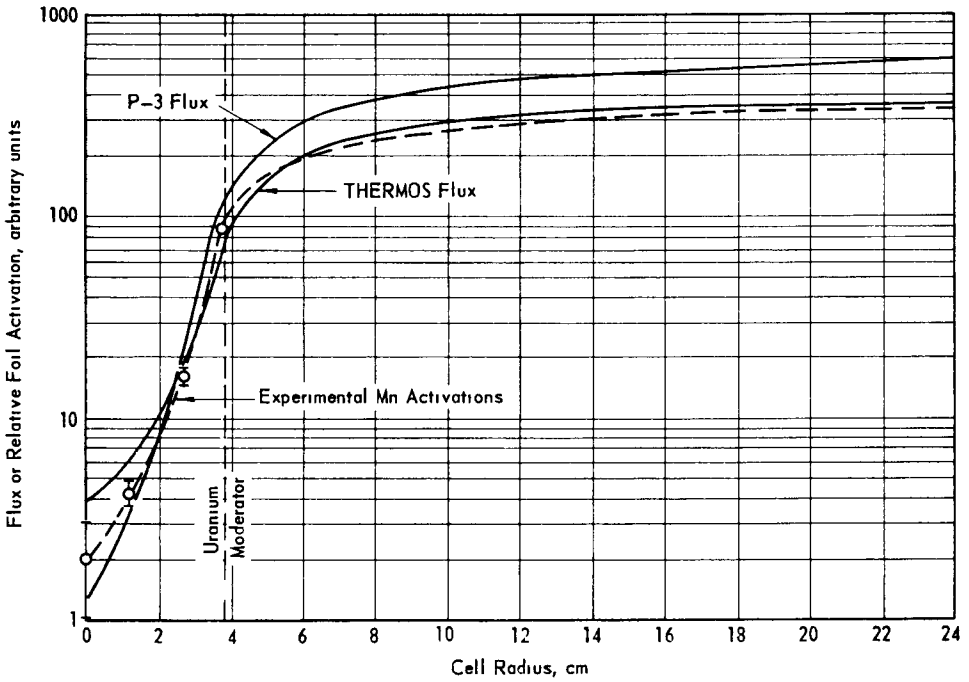

FIG. 3 COMPARISON BETWEEN RELATIVE Mn SUBCADMIUM FOIL ACTIVATIONS AND THERMAL NEUTRON FLUX IN A UNIT CELL AS CALCULATED BY THERMOS AND P–3 METHODS

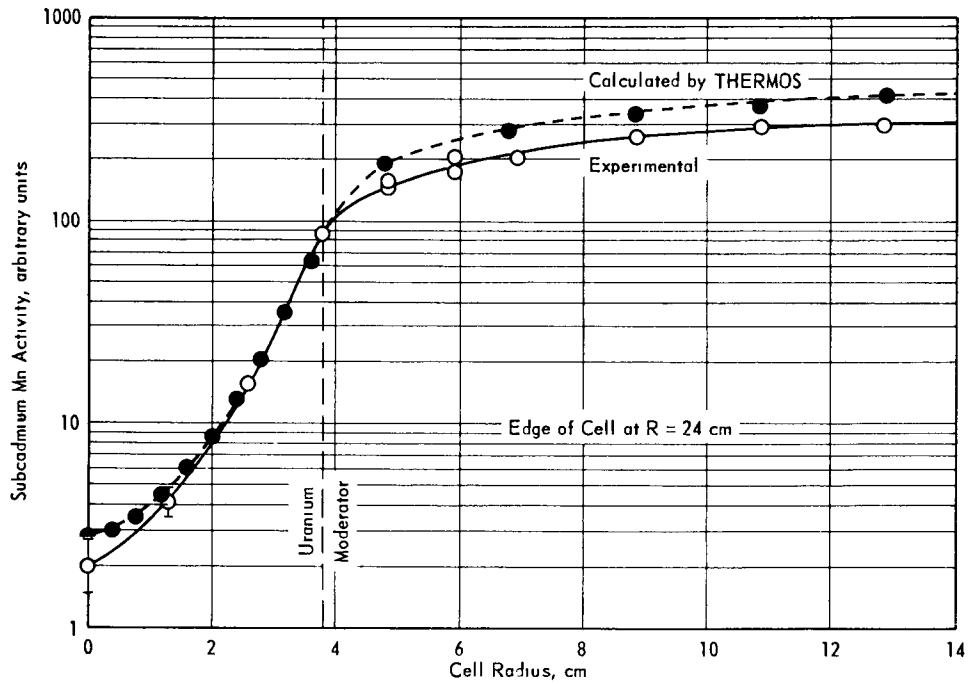

FIG. 4 COMPARISON BETWEEN EXPERIMENTAL AND CALCULATED Mn SUBCADMIUM FOIL ACTIVATIONS IN A UNIT CELL

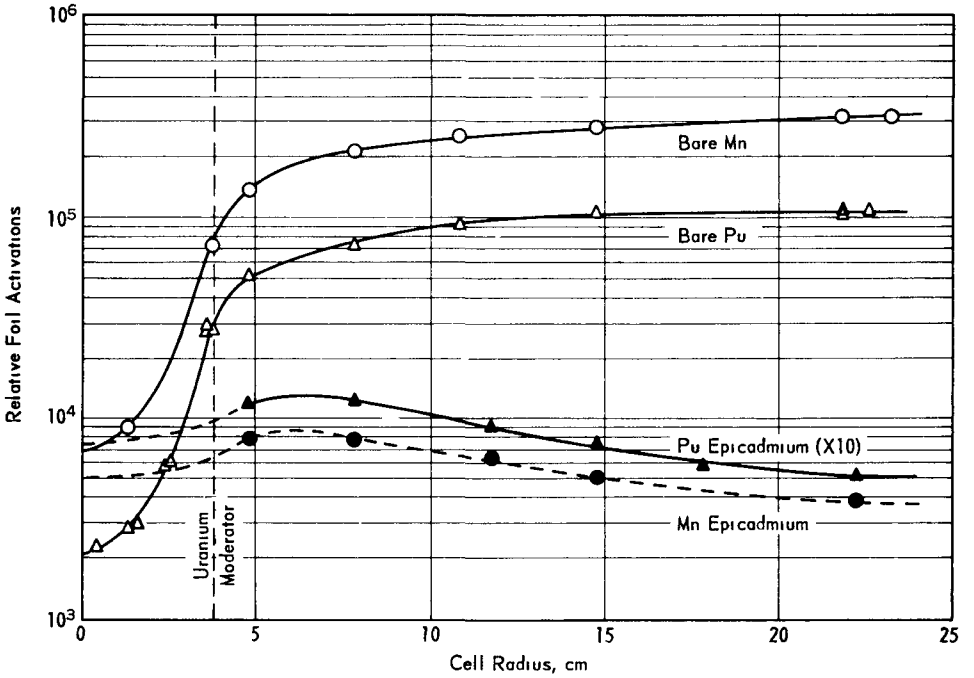

FIG. 5 RELATIVE ACTIVATIONS OF BARE AND CADMIUM-COVERED Mn AND Pu FOILS IN A UNIT CELL

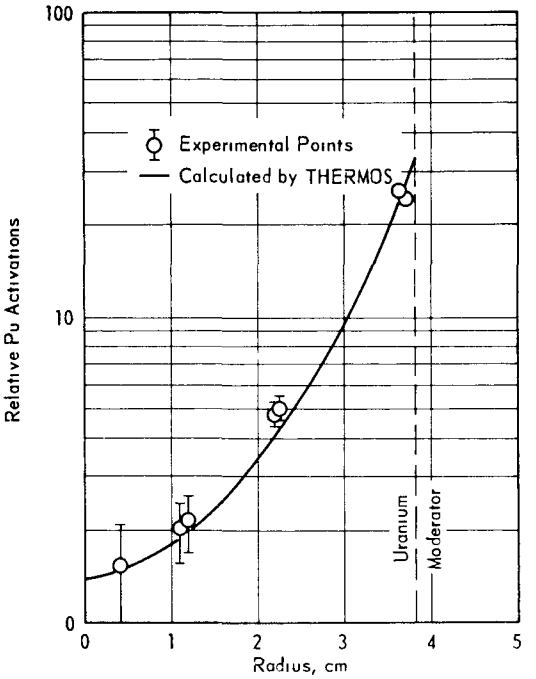

FIG. 6 COMPARISON BETWEEN MEASURED AND CALCULATED Pu FOIL ACTIVATIONS IN THE ROD

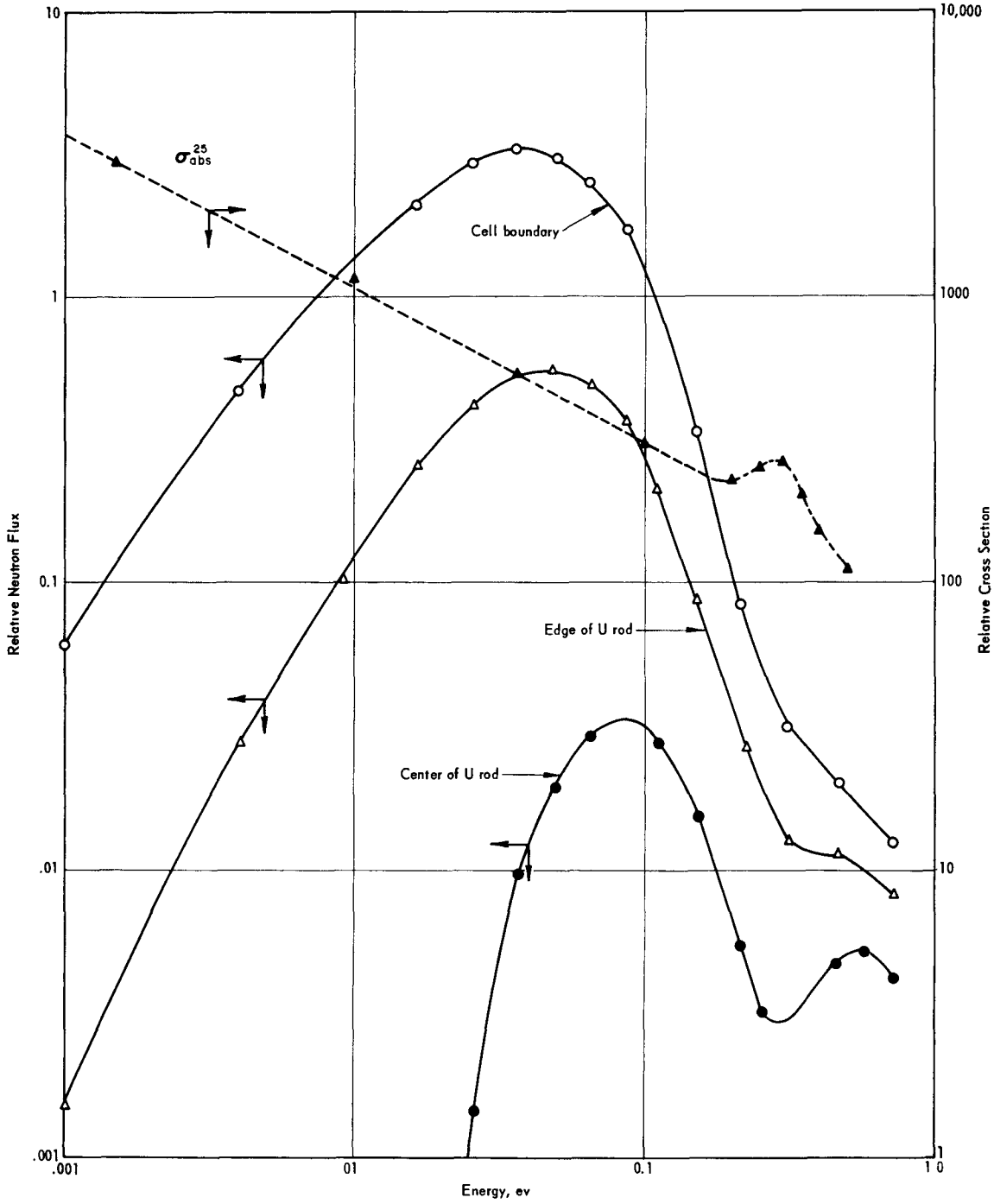

FIG. 7 PREDICTED NEUTRON FLUX AS A FUNCTION OF ENERGY FOR THREE POSITIONS IN A UNIT CELL

MEASUREMENTS OF EXTRAPOLATION LENGTHS IN PULSED WATER SYSTEMS

J. A. DeJuren, R. Stooksberry, and E. E. Carroll

AT-11-1-GEN-14

March 1962

BETTIS ATOMIC POWER LABORATORY PITTSBURGH, PA.

Operated for the U. S. Atomic Energy Commission
by Westinghouse Electric Corporation

MEASUREMENTS OF EXTRAPOLATION LENGTHS IN PULSED WATER SYSTEMS

J. A. DeJuren*, R. Stooksberry, and E. E. Carroll

Moderator parameters such as diffusion length and transport mean free path can be derived from both steady-state and pulsed-neutron decay measurements. In general, both parameters have lower values for a given medium when derived from decay measurements of the fundamental mode of thermal neutrons. The discrepancy is enhanced in hydrogenous media where the scattering cross section is not constant over the thermal spectrum. Following a neutron pulse the fundamental mode decays as $e^{-\alpha t}$ where $\alpha = v\Sigma_a + D_o B^2 - CB^4$.[1] In past interpretation of pulsed data, a value of the extrapolation length is usually assumed and D_o is obtained from a least squares fit of the α versus B^2 data. The transport mean free path, λ_{tr}, is obtained from $D_o = \frac{\lambda_{tr}\bar{v}}{3}$ where $\bar{v}$ is the mean thermal neutron velocity. Then a new extrapolation length d is computed from $d = 0.71\ \lambda_{tr}$ and iteration continues until values converge.

Recently both Nelkin[2] and Gelbard[3] have shown that in the case of water, $d = 0.76\ \lambda_{tr}$ for the zero buckling limit.

We have measured extrapolation lengths for cylinders of three different diameters and for one cube. A Li^6I crystal mounted on a lucite light pipe was used as a traverse detector. A black boron polyester crystal was also used with the 16.43 cm diameter cylinder to investigate the effect of neutron depression on the measurements. The cylinders were made of 1/32 in. Al and were filled with water to a height equal the diameter. The surfaces were shielded with cadmium and indium and the smaller sizes were also shielded with borax and paraffin to minimize room return background. A 100 kev accelerator was used as a source of pulsed 14 Mev neutrons. Decay curves were measured with the traverse detector inside the medium and a

---

* Now at Atomics International, Canoga Park, California.

2 in. diameter. Li^6I crystal mounted outside the cylinder at half water height.

A counting interval was selected in the region where the decays appeared to contain only the fundamental spatial mode. The neutron distribution parallel to the beam direction is more sensitive to the presence of modes and was measured first to determine the center. Then a more accurate measurement was made at right angles. Least square fits of the J_o function yielded the effective radii. Successive points near the edge were eliminated and several fits were obtained with the same data. Results are given for the 16.43 cm diameter cylinder and a 11.28 cm edge cube. The boron polyester would cause a neutron depression of 16% and the Li^6I, 3.5%, in an infinite water medium. In a finite cylinder the depression is greater at the center than at the edge of the medium. If no depression correction is made, the least square fit will yield a value which is too high. This effect probably causes the variation observed in the boron polyester case.

A small modal impurity will also cause incorrect results. It was not possible to increase the ratio of the fundamental to the nearest (third) harmonic by a large factor by delaying the counting interval because of source strength limitations. Our results, Table I, are consistent with an extrapolation length of 0.4 cm for all cases. Campbell and Stelson[4] obtained a value of $0.46 \pm .05$ cm for an 8 in. height by 8 in. diameter cylinder. Additional measurements utilizing higher intensity sources are required and are currently in progress. These measurements should determine the extent spatial modes may have influenced previous results. Thermal neutron time decays at each spatial point of the traverse are now being obtained. The analysis then involves a least square fit of the fundamental

modal function at successive times following the neutron pulse. Recent data indicate the presence of some modal contamination. It would only require 3/4 percent of a third harmonic contamination to increase the measured extrapolation length by 15%. However, indications are that this method should, after the accumulation of more data, give rise to an unambiguous value for the asymptotic extrapolation distance.

TABLE I

TRAVERSE MEASUREMENT RESULTS

	Case No.	Traverse Detector	Range of Fit (cm)	d (cm)
(1)	16.43 cm diam. cyl.	Li^6I	± 7 cm	.446 ± .023
			± 6.5	.467 ± .028
			± 6.0	.434 ± .037
			± 5.5	.456 ± .048
			± 5.0	.475 ± .066
(2)	16.43 cm diam. cyl.	Boron Polyester	± 7 cm	.518 ± .022
			6.5	.490 ± .027
			6.0	.471 ± .033
			5.5	.435 ± .048
(3)	11.28 cm cube	Li^6I	± 4.8	.402 ± .014
			± 4.6	.423 ± .016
			± 4.4	.436 ± .019
			± 4.2	.433 ± .023
			± 4.0	.425 ± .028

Note: The standard deviations listed for the extrapolation distance d, include only statistical errors due to counting.

REFERENCES

1. G. von Dardel and N. G. Sjöstrand, "Progress in Nuclear Energy," Vol. II, 183 (1958), Pergamon Press Ltd.

2. M. S. Nelkin, Nuc. Sci. & Eng., 7, 210 (1960).

3. E. M. Gelbard, WAPD-T-1315 (to be published). (1962).

4. E. C. Campbell and P. H. Stelson, ORNL-2204, 34 (1956).

FLUX TRANSIENTS NEAR MEDIUM DISCONTINUITIES

F. Feiner*, S. Weinstein* and W. B. Wright**

I. INTRODUCTION

In this paper, we discuss a series of measurements, performed in simple geometry, which provide extensive data on the variation of the neutron flux near the interface between material regions of considerably different nuclear properties. These measurements and concurrent progress in the theoretical treatment of the results have led to the development of a quite powerful calculational method.

The experiment is concerned with the behavior of the neutron flux near medium discontinuities. Prior to the initiation of this program, calculations were generally performed by assuming that infinite medium spectra for a given region and the group constants obtained from these spectra applied up to the boundary of the region. It is clear physically that such an abrupt change in spectrum is not realistic, but no simple prescription for describing the transition near the boundary existed. In order to formulate a theory or even a prescription to describe the phenomena encountered a significant amount of data needed to be obtained.

The Preliminary Pile Assembly (PPA), with its test lattice geometry, was considered to be well suited for a study of a number of lattices differing significantly in composition. The size of the test lattice region is just large enough that at its center spectra characteristic of a full size core of the lattice compositions are achieved. The reactivity effect of the lattice on the whole reactor, however, is small so that lattice changes can be made easily and safely.

With this geometry, it is then possible to perform activation experiments and use the results to guide and check the development of calculational techniques.

---

* Knolls Atomic Power Laboratory, operated by the General Electric Company for the Atomic Energy Commission.

** Now at General Atomic, San Diego, California.

We will proceed to describe the experimental set-up and techniques used in some detail, present the characteristics of the lattices studied, and then trace the development of the analytical models used to interpret the data.

II. EXPERIMENTAL ARRANGEMENT

As shown in Figure I, the PPA is a four-region assembly consisting of:

(I) the central test lattice region,

(II) the main part of the core,

(III) a booster region, and

(IV) a reflector.

The central region is approximately 8.4" in diameter; in hydrogen moderator lattices, this is sufficient to achieve the infinite medium spectrum of the lattice in question at the center provided a number of restrictions are kept in mind. (1) If the metal to moderator ratio is low, i.e. less than .5, the k_∞ of the test lattice region should be between .9 and 1.2 . (2) If the metal to moderator ratio is greater than 1, k_∞ may be as great as 1.4 but care must be taken that no slabs of material are inserted into the test lattice region which would allow significant neutron streaming in from the core region, II. When these conditions are satisfied, one can show both experimentally and analytically that the lattice infinite medium spectrum is achieved. Experimentally, one can see this by performing a radial flux traverse and noting that the buckling near the axis of the lattice region is very small, indicating very slight leakage into or out of the region. Calculationally, one can compare the flux ratios obtained from calculations for an infinite medium of this composition with that for simple one-dimensional radial calculations of the experiment. Results so obtained are shown in Table I for a number of lattices studied. The limitation on k_∞ of the lattices studied means that it is not possible to study directly all compositions of practical interest. However, since the neutron spectrum is determined by the ratio of absorptions to scattering, it is possible to produce the spectra of

interest by replacing some fuel with poison materials and thus lower the k_∞ to acceptable values without affecting the physics of the problem. The core region (II) of the PPA consists of slugs (Figure 2) held in a hexagonal matrix of steel tubes. Two inch diameter discs of enriched uranium- aluminum alloy, aluminum, and polyethylene are threaded on 3/16" diameter steel rods to form a repeating array of cells each 1.3" long. The atom densities of the elements in the core, both actual and effective, i.e. flux weighted, are presented in Table 2.

The booster region (III) is similarly constructed. The fuel density in this region is roughly twice as great as in the core and serves to flatten the radial flux shape.

The reflector region (IV) is composed of polyethylene cylinders inserted into the matrix tubes.

The control rods are located in the interstices between matrix tubes in the booster region (III). In this region, cadmium slivers may also be inserted as reactivity shims so that activations may be performed with the control rods essentially all out of the reactor.

We will now discuss the actual methods of performing the experiments. In Figure 3 are exhibited some of the component materials of the test lattice region. Hexagonal slabs of polyethylene, iron, fuel and aluminum form the building blocks from which the lattices are constructed. These are stacked into the test lattice region drawer in the fashion shown in Figure 4. A repeating array of small unit cells of the order of .1 to .2" thick is placed in the drawer in this fashion.

Medium discontinuities are introduced into the lattices by substituting moderator slabs and absorber plates for part of the lattice region. Pure polyethylene and polyethylene plus absorbers were used for the moderator gaps and hexagonal plates of cadmium and boron loaded glass for the absorber experiments. Activation profiles were measured by activating small foils of materials with different energy responses to neutrons. In Figure 5 are shown the hex plates which are especially equipped to have foils mounted in them as well as an example of a detector foil. The foils, made of fuel, manganese, indium and gold, are 7/16" in diameter and generally a few mils thick. They are mounted so as to minimize the perturbing effects which

they would impose on the lattice configuration. Measurements were also made with cadmium covers surrounding the foils in order to separate the sub and epi-cadmium contribution to the activity. Figure 6 is a schematic representation of the arrangement of the foils for a measurement.

III. CHARACTERISTICS OF LATTICES

The characteristics and salient parameters of the lattices studied are presented in Table 3. The metal to water ratios listed refer to the effective ratios had the moderator been in the form of water. The attempt was made to span a sizable range both in metal-water ratio and in spectrum hardness as characterized by

$$\beta\gamma = \frac{\Sigma_a(KT)}{\xi\Sigma_s} \quad .$$

In Figure 7, the unit cell construction of the lattices studied is shown schematically as well as the construction of the moderator gaps.

IV. EXPERIMENTAL RESULTS

Figure 8 is a schematic representation of the results obtained. By performing suitable normalized measurements with and without the perturbing absorber or moderator in place, two types of quantities are obtained from the data:

(1) The peaking or flux depression near or at the medium boundary, defined as the ratio of activity with perturbation present to that without, and

(2) The shape of the spatial transient, defined as the activity with perturbation minus activity without the perturbation.

These quantities may be obtained for a number of detectors with and without cadmium covers.

A striking feature of the initial results was that within the experimental uncertainty, the spatial transients could be represented by single exponentials, i.e. $A(x) = A_o e^{-x/L}$ where $A(x)$ is the position

dependent transient activity, A_o is an amplitude factor, x is the distance of the foil from the lattice-perturbation interface, and L is a characteristic length which we will call the relaxation length of the transient. Figure 9 is a graph of A(x) versus x for a representative case. Table 4 presents the relaxation length for the moderator gap measurements and Table 5 those for the absorber plates. It should be noted that for the 20 mil cadmium plate measurement in lattice L-7, a simple exponential was not obtained so that no relaxation length is listed. The measurements listed in Tables 4 and 5 were performed with 2 mil thick manganese foils.

In Tables 6 and 7 are listed the experimental peaking values, again as determined with manganese foils and fuel foils ($\Sigma_a t$ = .03 at .025 ev). It should be noted that the fuel values for (peaking - 1) are from 25-40% higher than the manganese values. This is a consequence of the relatively smaller epithermal contribution to the fuel activity as compared with manganese.

The errors quoted in the tables are arrived at by analyzing the individual components of error entering into the measurements such as counting statistics, foil weight and power level normalization uncertainties, as well as from reproducibility checks made in a fairly large number of instances.

In Figure 10 epi-cadmium traverse taken in lattice L-7 are plotted. Graphs are shown for a 1" moderator gap and the boron plate with $\Sigma_a t$ = 1 and indicate an epithermal source dip of 10 to 15%. For the case of a cadmium slab the dipping is less severe.

V. ANALYSIS

A. Spectrum-independent Model

Initial comparison of the experiments was made with the then existing programs; SOFOCATE[1] (Wigner-Wilkins spectrum) for thermal group constants, MUFT[2] for the fast group constants, and WANDA[3] - a one-dimensional few group diffusion code. In Tables 4 and 5, the

SOFOCATE diffusion lengths, $L = \sqrt{\frac{D}{\Sigma_a}}$, are listed for two values of the cut-off energy in the calculation. It is seen that L calculated with a 0.625 ev cut-off agrees reasonably well with the measured cadmium relaxation lengths. However, for the moderator gaps, a cut-off energy of about 0.3 ev is required to give agreement - a rather unsatisfactory state of affairs.

For the peaking values, MUFT-SOFOCATE group constants were obtained for the gap and lattice regions and four-group WANDA calculations performed. From the results, the manganese peakings listed in Table 6 were calculated.

It is clear that this procedure underestimates the peaking drastically.

B. Space-energy Separable Transient Model - $\gamma(E)$

(1) Relaxation Lengths

As mentioned before, a striking feature of the initial experimental results was that within the accuracy of the experiments, the spatial transients measured could be represented by single exponentials. That such a simple behavior should be found in a region of rapidly changing spectrum seemed quite surprising. The simplest form of diffusion theory of course predicts that there should only be one characteristic diffusion length,

$$L^2 = \frac{\int \phi(E)D(E)dE}{\int \phi(E)\Sigma_a(E)dE},$$

where D(E) is the energy dependent diffusion constant for the lattice composition and $\Sigma_a(E)$ the macroscopic absorption cross section. This picture, however, is clearly too simple since it was observed that the characteristic length, L, depended on whether the perturbation was a moderator or absorber.

In this attempt at analysis of the data, use was made of the two striking experimental observations:

(1) The transients are characterized by a single exponential.

(2) Their characteristic length depends on the nature of the perturbation.

Number (1) suggests that the analysis be made in terms of a spatially independent transient spectrum, $\phi_t(E)$. Number (2) suggests that $\phi_t(E)$ must be a function of the perturbation. Since the experiment emphasizes primarily the thermal region, we chose $\phi_t(E)$ to be a Maxwellian in the case of the moderator gaps and a transmission modified Wigner-Wilkins spectrum for the absorbers. Thus we write

$$L_t^2 = \int_0^\infty \frac{D(E)\phi_t(E)dE}{\Sigma_a(E)\phi_t(E)dE} \qquad (1)$$

$$\phi_t(E) = \phi_{max}(KT_{eff.})$$

$$KT_{eff} = (KT)\ (1 + \beta\gamma_{gap}) \quad \text{for the moderator slabs,}$$

and

$$\phi_t(E) = \frac{\phi_\infty(E)}{1 + \frac{2\bar{D}}{\bar{L}}\left(\frac{1 + T(E)}{1 - T(E)}\right)} \qquad (2)$$

for absorber plates

where $\phi_\infty(E)$ = Wigner-Wilkins spectrum for the lattice.

$\bar{D}$ and $\bar{L}$ are averages taken over this Wigner-Wilkins spectrum

$$T(E) = 2E_3\left[\xi(E)\right]$$

where

$$\xi(E) = \Sigma_a(E)t \quad \text{for the plate.}$$

The results obtained with this model are given in Tables 4 and 5 and indicated substantial agreement with the experiments. It should be noted that the value of L obtained from (1) is insensitive to the spectrum used to obtain $\frac{\bar{D}}{\bar{L}}$ in equation (2).

(2) Peaking Measurement

In order to apply this simple model to the peaking measurement, it must be extended to provide the relative amplitudes of $\phi_t(E)$ and $\phi_\infty(E)$. To do this, we present a derivation based on the following assumptions:

(a) There is an energy, E*, not too far above thermal such that for $E \geq E^*$ the flux, $\phi(E)$, is essentially unperturbed by the absorber plates and moderator gaps.

(b) The spectrum, $\phi(E,x)$ for $E < E^*$, in the gaps as well as in the lattice is a superposition of the infinite medium Wigner-Wilkins spectrum of the respective regions plus a spatially varying component separable in space and energy.

These assumptions plus the physically reasonable requirement of flux and current continuity at all energies permit the calculation of the peaking. The derivation proceeds as follows:

Consider an infinite medium A that has a well defined neutron spectrum $\phi_A(E)$ everywhere. Insertion of a region B of different cross sections into A will result in a position dependent spectrum in A near the A-B boundary. In the diffusion theory approximation, this spectrum will satisfy the equation

$$-D_A(E)\nabla^2\phi_A(E,r) + \Sigma^A_{total}(E)\phi_A(E,r) = S(E,r) + \int_0^{E^*} \phi_A(E',r)\Sigma_A(E'\rightarrow E)dE' \qquad (3)$$

where $S(E,r)$ is the source term:

$$\int_{E^*}^{\infty} \phi_A(E',r)\Sigma_A(E' \rightarrow E)dE'$$

and E^* is some cut-off energy. If $\frac{\Sigma_a(E)}{\Sigma_{tot}(E)} << 1$ for $E > E^*$ in both A and B, then the source will be independent of position and $S(E,r) = S(E)$.

Asymptotically in A the spectrum becomes stationary and will satisfy the equation

$$\Sigma^A_{total}(E)\phi_A(E) = S(E) + \int_0^{E^*} \phi_A(E')\Sigma_A(E' \rightarrow E)dE' \qquad (4)$$

Defining $\gamma(E,r) = \phi_A(E,r) - \phi_A(E)$ and subtracting (2) from (1):

$$-D_A(E)\nabla^2\gamma(E,r) + \Sigma^A_{total}(E)\gamma(E,r) = \int_0^{E^*} \gamma(E',r)\Sigma_A(E' \rightarrow E)dE' \qquad (5)$$

which is an equation for the transient introduced in A by the insertion of B. As pointed out before we observe experimentally in a large number of cases that the spatial transients were exponential, i.e.

$$\int \gamma(E,x)\sigma_{foil}(E)dE \sim e^{-kx}$$

A solution of equation (5) which would lead to this result is $\gamma(E,x) = \gamma(E)f(x)$.

Noting that $\Sigma_{total}(E) = \Sigma_a(E) + \int_0^{E^*} \Sigma(E \rightarrow E')dE'$ (since energies above E^* are not perturbed) the insertion of the separable solution into (5) yields:

$$- \frac{\nabla^2 f(x)}{f(x)} D_A(E)\gamma(E) + \Sigma_a(E)\gamma(E) = \int_0^{E^*} \Big[\gamma(E')\Sigma_A(E' \to E) - \gamma(E)\Sigma_A(E \to E')\Big] dE' \tag{6}$$

Letting $\frac{\nabla^2 f}{f} = \frac{1}{L_\gamma^2}$ and integrating equation (6) over energy:

$$- \frac{1}{L_\gamma^2} \int_0^{E^*} D_A(E)\gamma(E)dE + \int_0^{E^*} \Sigma_a^A(E)\gamma(E)dE = \int_0^{E^*}\int_0^{E^*} \gamma(E')\Sigma_A(E' \to E) - \gamma(E)\Sigma_A(E \to E')\ dEdE' \tag{7}$$

$$= 0$$

so that

$$L_\gamma^2 = \frac{\int_0^{E^*} D_A(E)\gamma(E)dE}{\int_0^{E^*} \Sigma_a^A(E)\gamma(E)dE} \tag{8}$$

To obtain $\gamma(E)$, we consider the spectrum equation in region B namely:

$$-D_B(E)\nabla^2\phi_B(E,r) + \Sigma_{total}(E)\phi_B(E,r) = S_B(E) + \int_0^{E^*} \phi_B(E;r)\Sigma_B(E' \to E)dE' \tag{9}$$

Again $S_B(E)$ is independent of position because of the choice of E*. There exists an asymptotic spectrum characteristic of the cross sections of B and the source $S_B(E)$ satisfying the equation

$$\Sigma^{B}_{tot}(E)\phi_B(E) = S_B(E) + \int_0^{E^*} \phi_B(E')\Sigma_B(E' \rightarrow E)dE' \qquad (10)$$

If the dimensions of B are small, an asymptotic spectrum never obtains but one can be defined, as in equation (10) and subtracted from equation (9) yielding:

$$\beta(E,r) = \phi_B(E,r) - \phi_B(E)$$

and

$$-D_B(E)\nabla^2\beta(E,r) + \Sigma^{B}_{total}(E)\beta(E,r) = \int_0^{E^*} \beta(E',r)\Sigma_B(E' \rightarrow E)dE'$$

We now assume that $\beta(E,x)$ is separable in energy and position for the case of a slab gap. Then writing the energy dependent flux explicitly for the lattice (A) and the gap (B) as:

$$\phi_A(E,x) = \phi_A(E) + \gamma(E)e^{-(x-a)/L_\gamma} \qquad (11)$$

and

$$\phi_B(E,x) = \phi_B(E) + \beta(E)\cosh\, x/L_\beta \qquad (12)$$

we equate flux and current at the gap boundary (x = a) so that:

$$\gamma(E) = \frac{\phi_B(E) - \phi_A(E)}{1 + \frac{D_A(E)}{D_B(E)}\,\frac{L_\beta}{L_\gamma}\coth\, a/L_\beta} \qquad (13)$$

and

$$\beta(E) = -\gamma(E)\,\frac{D_A(E)}{D_B(E)}\,\frac{L_\beta}{L_\gamma}\,\operatorname{csch}\, a/L_\beta \qquad (14)$$

where a is the half gap thickness and $\phi_A(E)$ and $\phi_B(E)$ are normalized at energies $E > E^*$ and L_β is defined analogously to L_γ.

For small gap thicknesses:

$$\lim_{a \to 0} \gamma(E) \to 0$$

$$\lim_{a \to 0} \beta(E) \to \phi_A - \phi_B; \qquad \phi_B(E,x) \to \phi_A(E)$$

For large gap thickness

$$\phi_B(E,x) = e^{-a/L_\beta}\, \gamma(E)\, \frac{D_A(E)}{D_B(E)}\, \frac{L_\beta}{L_\gamma}\, \operatorname{csch} x/L_\beta + \phi_B(E)$$

so that $\phi_B(E,\ a/L_\beta >> 1) \to \phi_B(E)$.

These relations indicate that the spectrum in the gap varies in hardness between the spectrum of the lattice and that of an infinite gap region, whereas the spectrum in the lattice is softened by the presence of the gap. In calculations of $\gamma(E)$, $\phi_A(E)$ and $\phi_B(E)$ were taken to be the Wigner-Wilkins spectra for the lattice and gap respectively, normalized in the 1/E region. At high $\beta\gamma$, a 2 ev cutoff is necessary in the Wigner-Wilkins calculation to insure 1/E behavior in the high energy tail.

Figure 11 compares the $\gamma(E)$ for a type B gap in L-7 with a Maxwellian spectrum at $T_{eff} = \left[1 + (\beta\gamma)_{gap}\right] T$ and the L-7 Wigner-Wilkins spectrum. The comparison shows that Maxwellian averages will be in good agreement with averages taken over $\gamma(E)$.

From equations (11) and (13), the experimental peaking measured by a foil of cross section $\sigma_{foil}(E)$ corresponds to:

$$\text{Peaking} = 1 + \frac{\int_0^\infty \gamma(E)\sigma_{foil}(E)dE}{\int_0^{E_{co}} \phi_{SOF}^{lattice}(E)\sigma_{foil}(E)dE + \phi(E_{c.o.})\int_{E_{co}}^\infty \sigma_{foil}(E)d\ \ell n\ E} \qquad (15)$$

Using the present terminology and applying transmission theory boundary conditions to the case of absorber plates leads to

$$\gamma(E) = \frac{-\phi_\infty}{1 + \frac{2D_A(E)}{L_\gamma}\left|\frac{1 + T(E)}{1 - T(E)}\right|}$$

quite similar to equation (2).

In Tables 4 through 7, the peakings and relaxation lengths calculated with the above model - called the $\gamma(E)$ model - are presented. It is clear that this simple space-dependent spectrum model produces significantly better agreement with experiment than the space independent (MUFT-SOFOCATE-WANDA) model and that moreover agreement within 10% in both the peaking and relaxation lengths is obtained for nearly all the cases studied. This good agreement is surprising in view of the crudity of the approximations of the model in particular that of the spatially independent epithermal source and the strict space-energy separability of the transient spectrum.

C. SWAKRAUM Variational Approach

The next development in the analysis of the experiments was the formulation of the SWAKRAUM variational approach by G. P. Calame and F. D. Federighi[4]. In the $\gamma(E)$ model, we set

$$\phi(E,x) = \phi_\infty(E) + \phi_t(E)e^{-x/L}$$

where $\phi_\infty(E)$ is the infinite medium Wigner-Wilkins lattice spectrum and $\phi_t(E)$ is a Maxwellian for the gap effective temperature. The SWAKRAUM approach generalizes this formulation to $\phi(E,x) = \sum_{i=1}^{N} \chi_i(x)\psi_i(E)$ $N \leq 4$ where the $\psi_i(E)$ (base spectra) may be arbitrarily chosen and the $\chi_i(x)$ are found from a variational principle.

In its simplest form, we perform P-1 calculations using a flat epithermal source, the mass one scattering kernel and the Radkowsky-Esch[5] prescription for D(E). The results of these calculations are also presented in Tables 4-7. It is seen that the values obtained are quite similar to those from the $\gamma(E)$ model.

D. Additional Effects

Having obtained agreement to within about 10% with experiment we may now turn to a number of less significant but still important and interesting effects. The SWAKRAUM program allows us to investigate them rather easily. We have chosen to investigate them for the case of a 1" polyethylene gap in lattice L-7 for two reasons: We have the most reliable data for this lattice and the lattice itself - being the hardest one studied - exhibits the most pronounced spectrum-dependent effects.

We have investigated the effect on the calculations of the following:

(1) Choice of trial spectra, $\psi_i(E)$

(2) Number of spectra used, - 2, 3, 4

(3) Transport approximation used

- P-1, DP-1, P-3

(4) Spatial distribution of the epi-thermal source

(5) Scattering kernel

(a) Radkowsky - water
(b) Radkowsky-Esch polyethylene
} mass 1

(c) Nelkin - water

(d) Goldman - polyethylene

The results are tabulated in Table 8 and reflected in Figures 12 and 13. Each of the effects is seen to be of a magnitude of a few percent and their relative importance will depend on the particular case studied.

Since SWAKRAUM is a thermal program, one may make the cleanest comparison with sub-cadmium activations. Figures 12 and 13 show such a comparison for the case of the boron plate absorber and a polyethylene gap in lattice L-7. It is seen that for these two quite different cases agreement to within a few percent is now achievable for the sub-cadmium energy region.

Table 1

PPA Lattice and Infinite Medium Epithermal to Thermal Flux Ratios (F.R.)

Lattice†	$(F.R.)^{*}_{PPA}$	$(F.R.)_{\text{infinite medium}}$
L-3	2.453	2.39
L-4	.725	0.68
L-5	1.286	1.26
L-7	4.27	4.32
HL-1	0.24	0.24

* $(F.R.)_{PPA}$ = Ratio of epithermal to thermal flux from a 4-group WANDA calculation

† See Table 3 for characteristics of the lattices

Table 2

PPA Regional Atom Densitites - atoms/barn-cm

Region	Elements	Actual Atom Densities	Effective (Flux-weighted) Atom Densities
Core II	H	.05160	.05160
	C	.02580	.02580
	U-235	$.782 \times 10^{-4}$	$.483 \times 10^{-4}$
	U-238	$.56 \times 10^{-5}$	$.35 \times 10^{-5}$
	Al	.00902	.00556
	Fe	.00537	.00494
Booster III	H	.03958	.03958
	C	.01979	.01979
	U-235	$.223 \times 10^{-3}$	$.183 \times 10^{-3}$
	U-238	$.163 \times 10^{-4}$	$.134 \times 10^{-4}$
	Al	.00422	.00395
	Fe	.00360	.0033
	Zr	.0111	.0078
Reflector IV	H	.0696	.0696
	C	.0348	.0348
	Fe	.00297	.00297

Table 3

Characteristics of the Lattices

Lattice	$k_{\infty}^{thermal}$	$\Sigma_a(KT)$ cm^{-1}	$\rho\gamma = \frac{\Sigma_a(KT)}{\xi\Sigma_s}$	$\left(\frac{\Sigma_a}{\Sigma_T}\right)^*$	$\frac{\Sigma_a(KT)}{\Sigma_s}$	Hydrogen to U^{235} atom ratio	Fractional metal volume	Equivalent metal-to-water ratio
L-3	1.03	0.146	0.43	0.119	0.213	147	0.71	3.4
L-4	1.13	0.062	0.096	0.039	0.078	632	0.73	2.3
L-5	1.11	0.074	0.19	0.069	0.133	316	0.57	1.1
L-7	1.02	0.30	0.78	0.167	0.295	79	0.74	2.7
HL-1	0.99	0.067	0.031	0.0116	0.031	2200	0	0.0006

* Maxwellian averages

Σ_a = macroscopic absorption cross section

Σ_T = macroscopic total cross section

Σ_s = macroscopic epithermal scattering cross section

ξ = logarithmic energy decrement

$= \frac{2}{A+2/3}$ for $A > 10$

= 1 for A = 1

Table 4

Relaxation Lengths from Moderator Gaps (Manganese Foils) - in cm

Lattice	Gap Type	Gap Thickness cm	Experimental Relaxation Length	SOFOCATE $L = \sqrt{\frac{D}{\Sigma_a}}$ .3 ev cut-off	.625 ev cut-off	$\gamma(E)$ Model	SWAKRAUM Flat Epithermal Source
L-3	CH_2O+U	0.828	1.71 ± .10	2.08	2.28	1.708	1.590
	CH_2O+U	1.722	1.75 ± .06	2.08	2.28	1.703	1.625
	CH_2O+U	2.616	1.78 ± .05	2.08	2.28	1.700	1.640
	CH_2O	.381	1.82 ± .16	2.08	2.28	1.689	1.620
	CH_2O	2.667	1.64 ± .04	2.08	2.28	1.685	1.575
L-4	CH_2+U	2.037	2.14 ± .08	2.53	2.68	2.360	2.125
L-5	CH_2+U	2.490	2.35 ± .06	2.89	3.15	2.563	2.330
L-7	CH_2	0.826	1.23 ± .05	1.23	1.42	0.998	0.96
	CH_2	1.638	1.10 ± .03	1.23	1.42	0.994	0.935
	CH_2	2.451	1.00 ± .01	1.23	1.42	0.992	0.925

Table 5

Relaxation Lengths 20 mil Cadmium Plates (Manganese Foils) in cm

Lattice	Experimental Relaxation Length	SOFOCATE $L=\sqrt{D/\Sigma_a}$ .3 ev cut-off	SOFOCATE $L=\sqrt{D/\Sigma_a}$ .625 ev cut-off	$\gamma(E)$ Model	SWAKRAUM*
L-3	2.29	2.08	2.28	2.26	2.14
L-4	2.75	2.53	2.68	2.68	2.41
L-5	2.99	2.89	3.15	3.18	2.78

*Flat epi-thermal source

Table 6

Moderator Gap Peaking

Lattice	Gap Type	Gap Thickness cm	Experimental Peaking Manganese	Experimental Peaking Fuel	MUFT-SOFOCATE WANDA (Mn)	γ(E) Model Mn	γ(E) Model Fuel	SWAKRAUM Flat Epi-Thermal Source
L-3	CH_2O+U	0.821	1.390±.012		1.260	1.340		1.389
	CH_2O+U	1.772	1.646±.020		1.482	1.590		1.672
	CH_2O+U	2.616	1.852±.025		1.627	1.749		1.820
	CH_2O	0.381	1.209±.012		1.227	1.286		1.305
	CH_2O	2.667	2.483±.025		2.085	2.758		2.881
L-4	CH_2+U	2.037	1.373±.014		1.292	1.371		1.382
L-5	CH_2+U	2.490	1.750±.022		1.601	1.796		1.819
L-7	CH_2	0.826	2.090±.025	2.37±.04	1.600	2.098	2.35	2.138
	CH_2	1.638	3.000±.030	3.64±.04	2.012	3.061	3.54	3.141
	CH_2	2.451	3.650±.040	4.18±.05	2.350	3.888	4.54	3.988
	CH_2+U	0.889	1.847±.018	2.07±.03	1.452	1.702	1.86	1.770
	CH_2+U	1.740	2.186±.022	2.66±.03	1.733	2.056	2.30	2.145
	CH_2+U	2.629	2.560±.030	3.02±.04	1.901	2.236	2.52	2.320
	CH_2+Fe	2.778	2.636±.030		1.850	2.780		
	CH_2+Dy	1.968	1.898±.025			1.884		2.038
	CH_2+Al	1.956	2.093±.025		1.597	2.076		2.135

Table 7

Absorber Plate Activity Depression

Lattice	Absorber Type	Absorber Thickness mil	Experimental Activity Depression	$\nu(E)^{\dagger}$ Model	SWAKRAUM† Blackness Flat Epi-thermal Source	SWAKRAUM† DP-1
L-3	Cd	3	0.517	0.522	0.504	0.460
	Cd	20	0.421	0.402		0.397
L-4	Cd	3	0.312	0.302	0.299	0.261
	Cd	20	0.230	0.209		0.202
L-5	Cd	3	0.396	0.396	0.389	0.345
	Cd	20	0.317	0.285		0.284
L-7	Cd	3	0.632		0.609	0.569
	Cd	3	0.420*		0.409*	0.350*
	Cd	20	0.615	0.507		0.503
	Boron	$\Sigma_a t=1$ at .025 ev	0.455*			0.425*
	Boron	$\Sigma_a t=2$ at .025 ev	0.365*			0.305*

*Sub-cadmium depression only

†The epicadmium contributions to the calculated values have been determined rather crudely. Since they amount to 30-50% of the total activity with absorber, the quoted calculated values are uncertain to 10-20%.

Table 8

Effect of Various Quantities on the Peaking (L-7)

Quantity	Relative to	Case	Effect
Experimental epithermal source	Flat source	1" moderator gap B plate absorber	-4.6% -7.8%(thermal)
Approximation			
DP-1	P-1	1" moderator gap .1" moderator gap	+1.0% +3.9%
P-3	P-1	1" moderator gap .1" moderator gap	0.7% 2.8%
No. of Spectra			
3 spectra	2 spectra	1" moderator gap	-0.4% (thermal peaking)
4 spectra	2 spectra	1" moderator gap	+0.2% (thermal peaking)
Kernel			
Radkowsky-water	Radkowsky-Esch[5] Polyethylene	1" moderator gap	-1.6%
Goldman-Federighi[7] polyethylene	"	1" moderator gap	-5.7%

References

1. H. Amster and R. Suarez, "The Calculation of Thermal Constants Averaged over a Wigner-Wilkins Spectrum: Description of the SOFOCATE Code" WAPD-TM-39 Jan. 1957.

2. H. Bohl, E. M. Gelbard, G. H. Ryan, "MUFT-4 Fast Neutron Spectrum Code for the IBM-704" WAPD-TM-72 July 1957.

3. O. J. Marlowe, C. P. Saalbach, L. M. Culpepper, D. S. McCarthy, "WANDA - A One Dimensional Few Group Diffusion Code for the IBM-704" WAPD-TM-28 Nov. 1956.

4. G. P. Calame, F. D. Federighi, Nuclear Science and Eng. 10, 190 (1961).

5. Reactor Technology Report #19 KAPL-2000-16 p.III.23

6. M. Nelkin, Phys. Rev., 119, 741 (1960).

7. D. T. Goldman, F. D. Federighi, Reactor Technology Report #19 KAPL-2000-16 p.11.2.

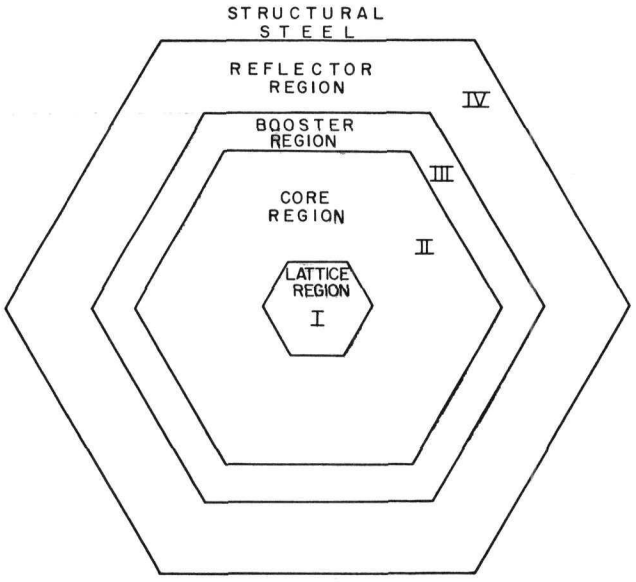

SCALE: $\frac{1}{8}$" = 1"

FIGURE I PPA REACTOR GEOMETRY

KS-46191
UNCLASSIFIED

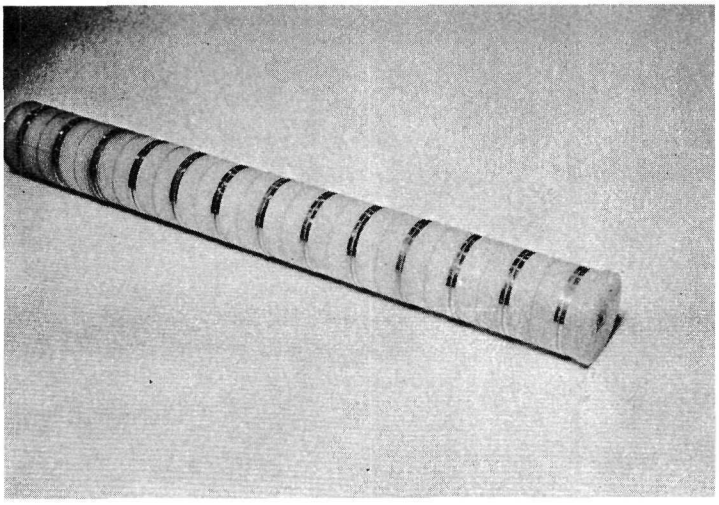

Fig. 2 PPA Core Slug

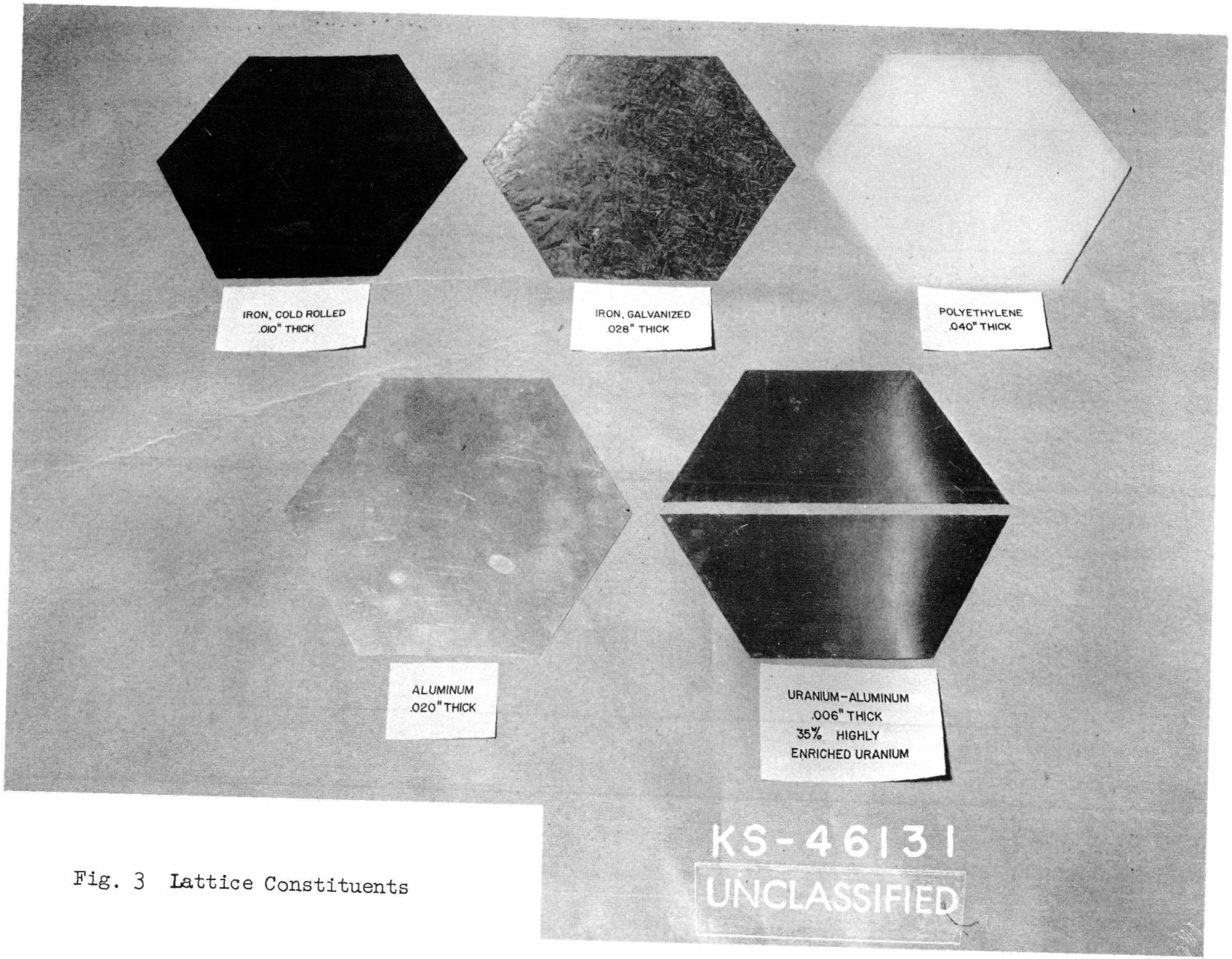

Fig. 3 Lattice Constituents

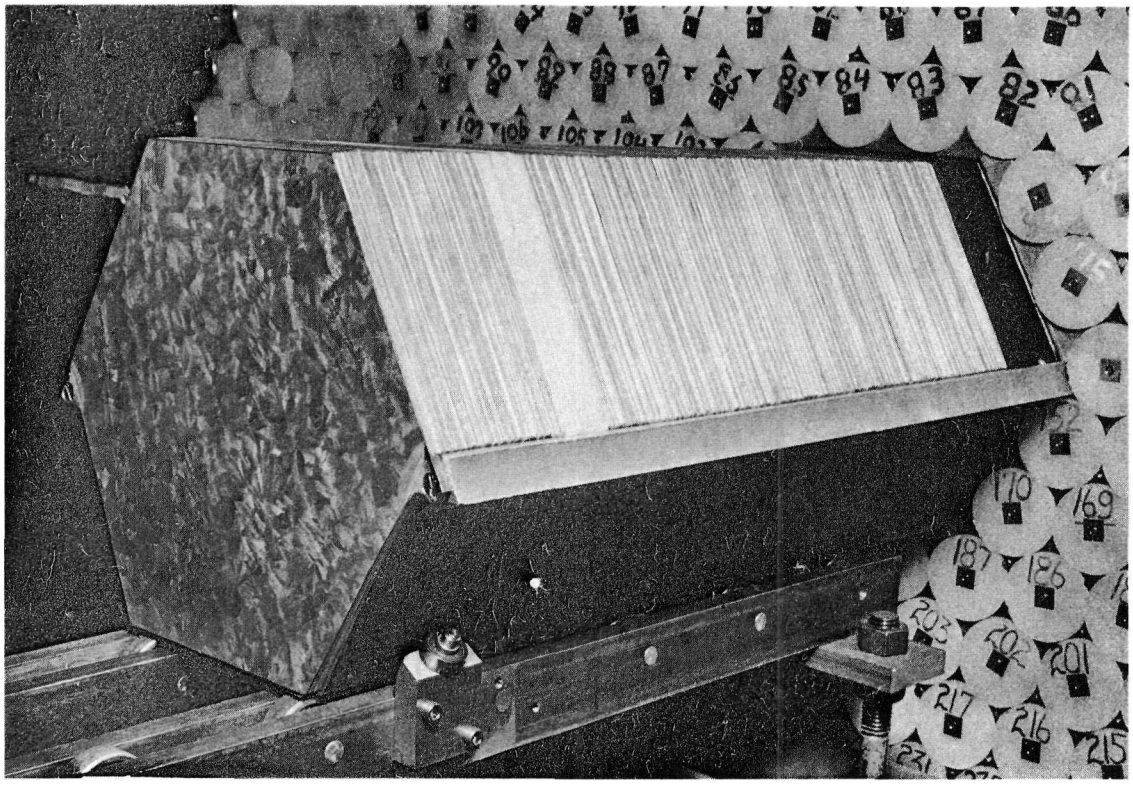

Fig. 4 PPA Test Lattice Drawer

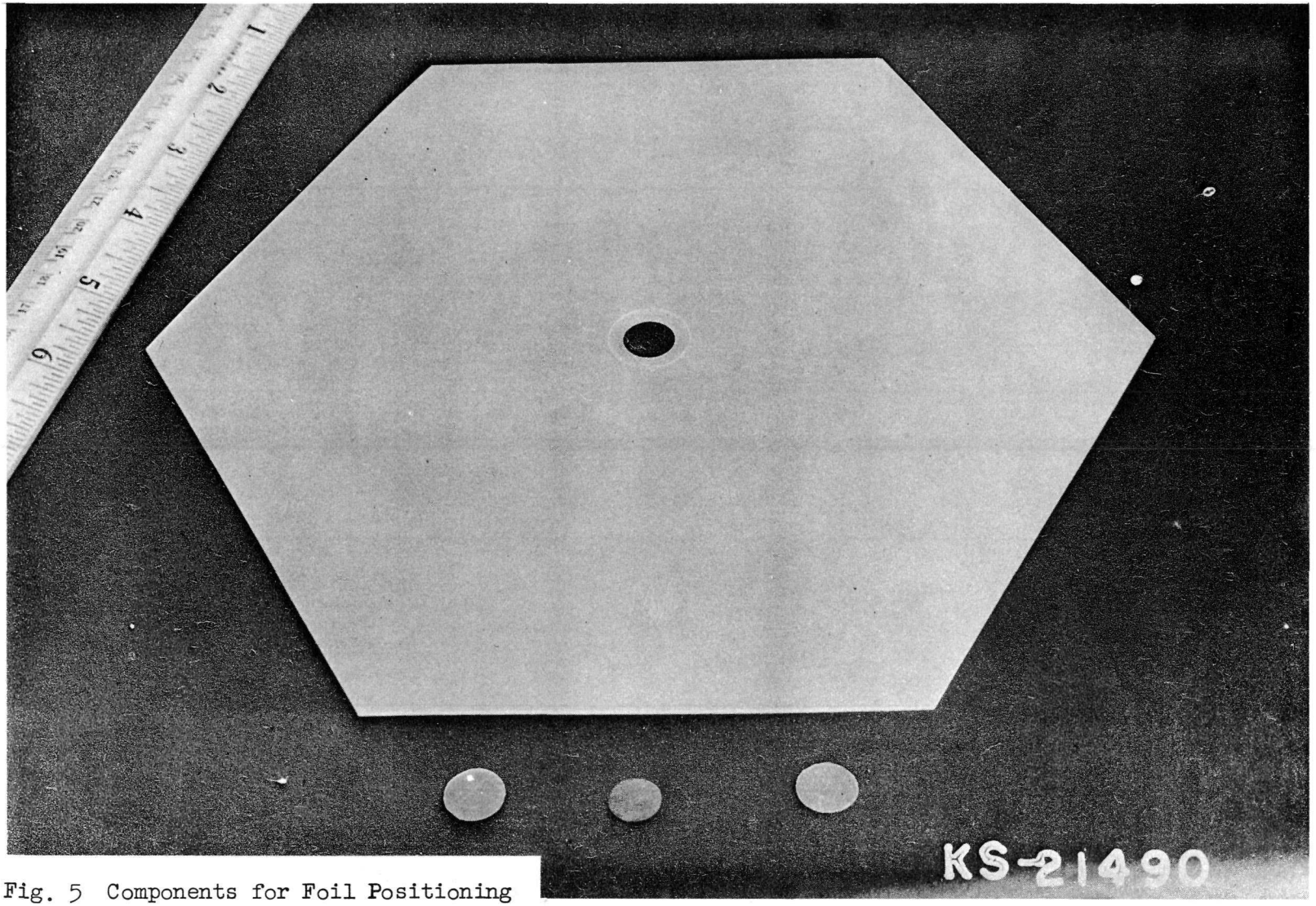

Fig. 5 Components for Foil Positioning

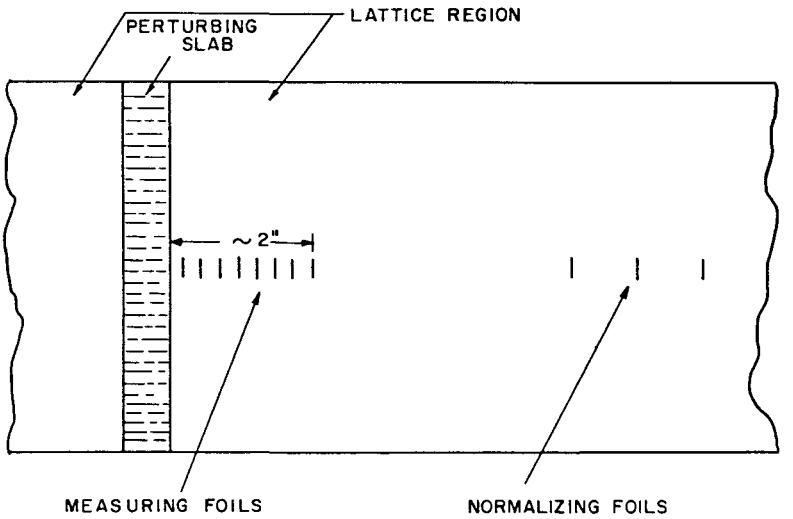

FIGURE 6 EXPERIMENTAL ARRANGEMENT

KS-46192
UNCLASSIFIED

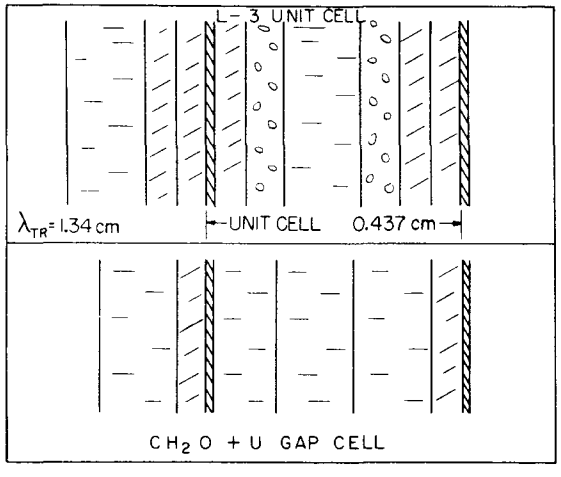

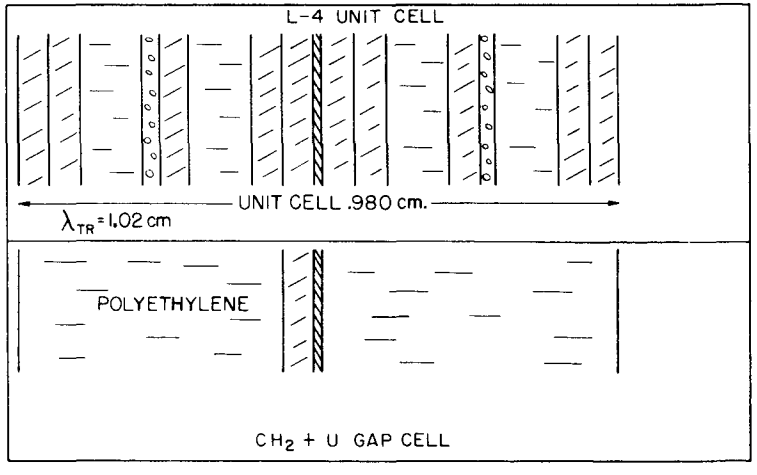

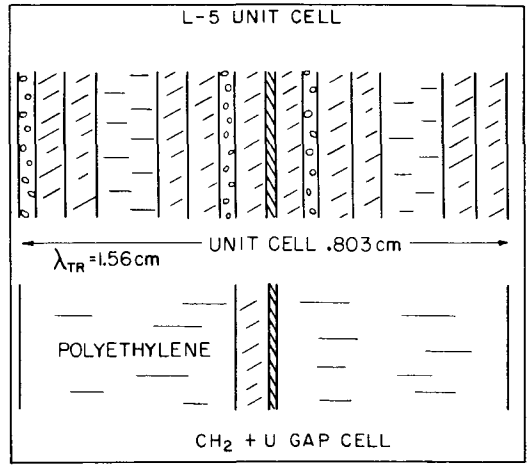

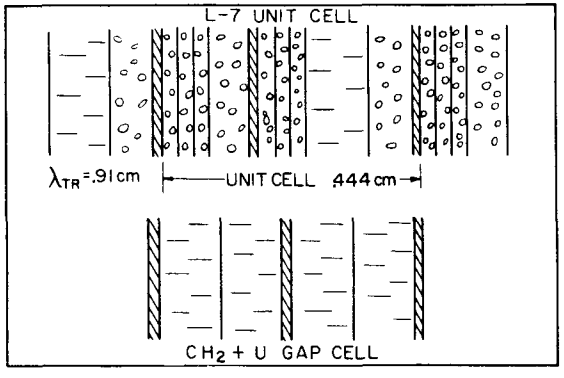

LEGEND:

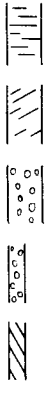

DENSITIES:
CH_2O: 1.20 gm/cc
CH_2: 0.907 gm/cc
Aℓ: 2.74 gm/cc
Fe: 7.79 gm/cc
U-Aℓ: 3.95 gm/cc (35 w/o HIGHLY ENRICHED URANIUM)

FIGURE 7 CELL AND FUEL GAP CONSTRUCTION

KS-46193
UNCLASSIFIED

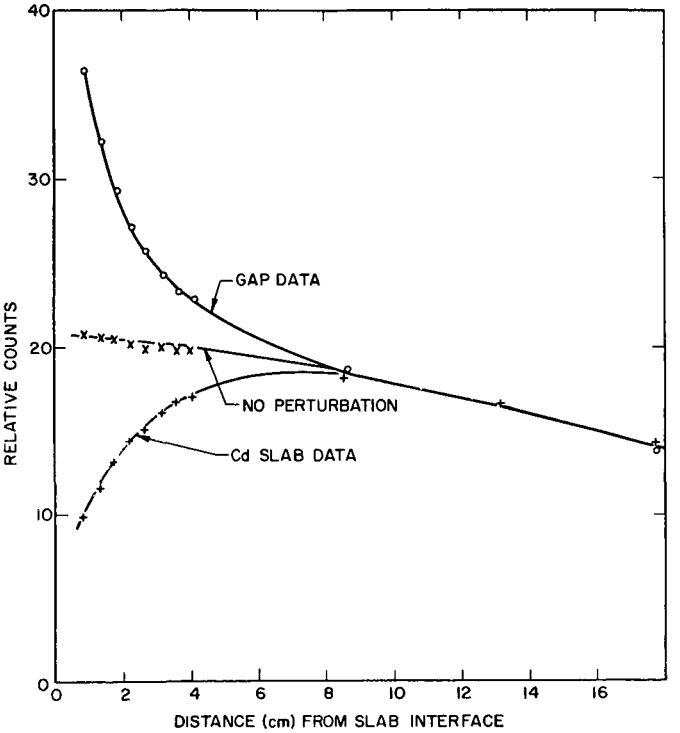

FIGURE 8 RAW TRANSIENT DATA

KS-46194
UNCLASSIFIED

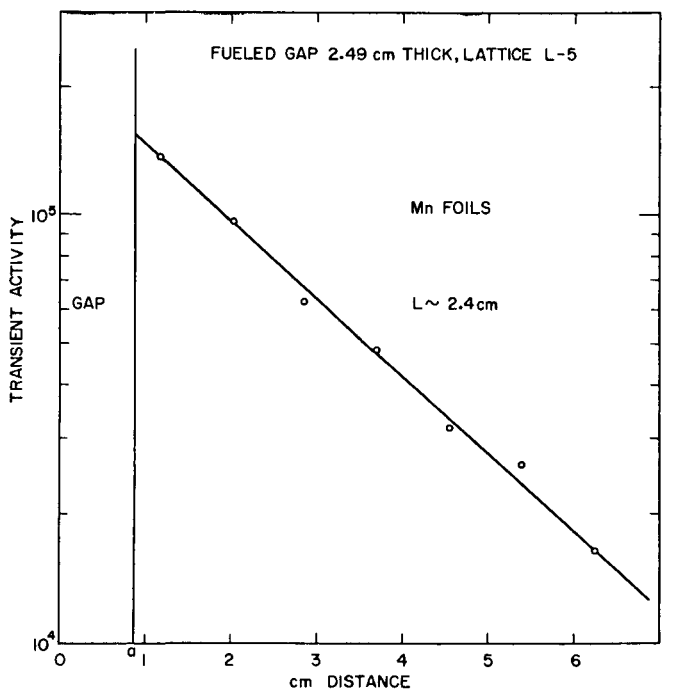

FIGURE 9 TRANSIENT ACTIVITY vs DISTANCE

KS-46195
UNCLASSIFIED

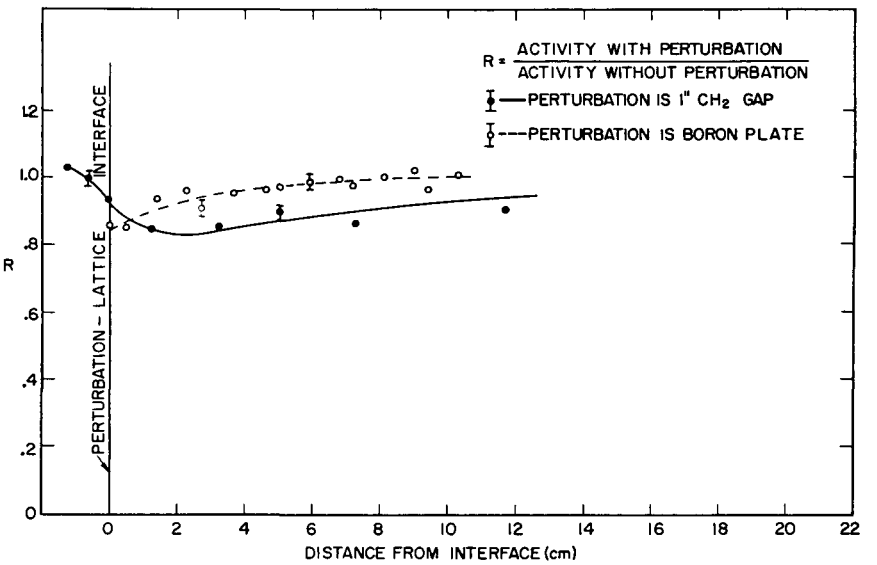

FIGURE 10 CADMIUM COVERED 0.1 MIL GOLD TRAVERSES IN LATTICE L-7 KS-46196 UNCLASSIFIED

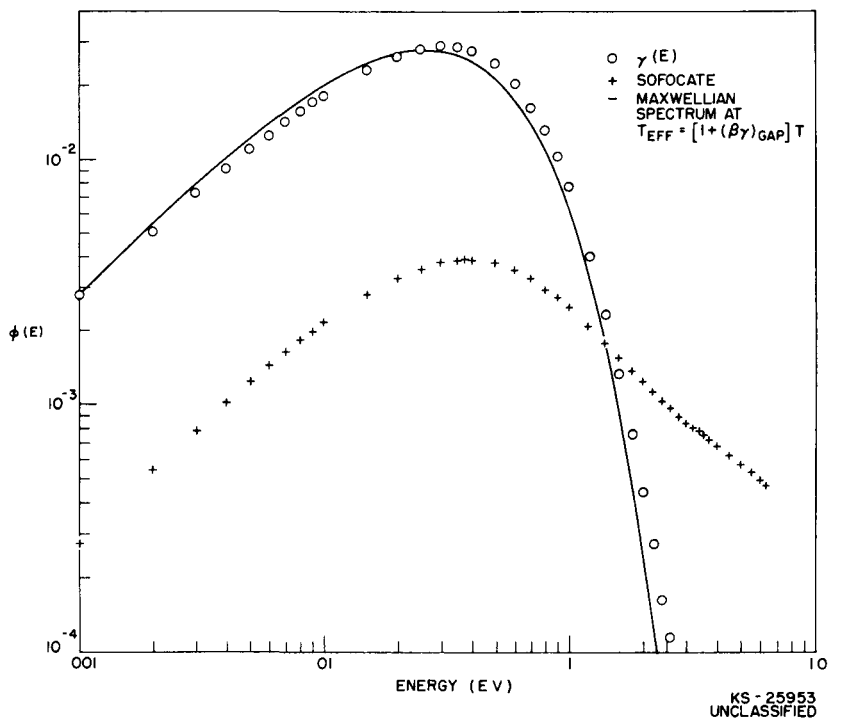

Fig. 11 Comparison of Spectra

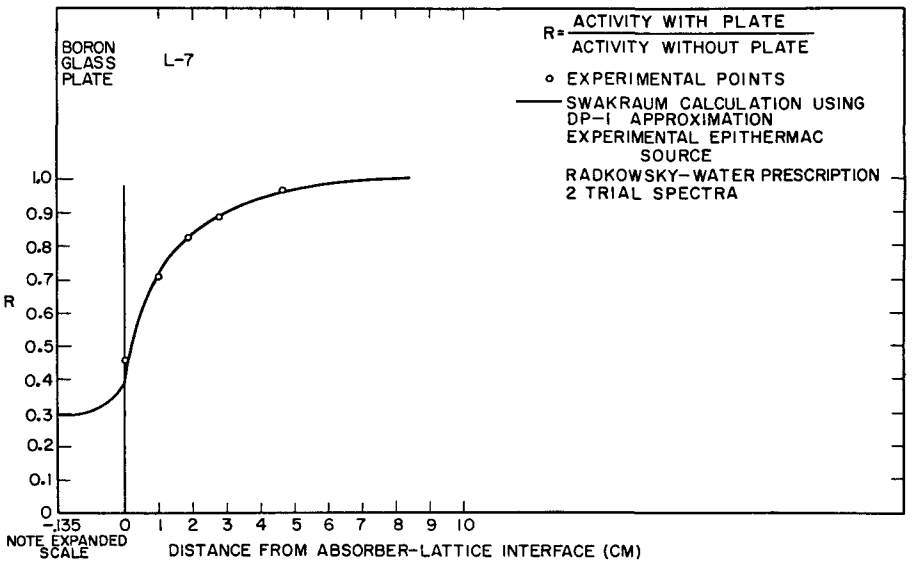

FIGURE 12 SUBCADMIUM MANGANESE ACTIVITY TO BORON GLASS PLATE IN LATTICE L-7

KS-46197
UNCLASSIFIED

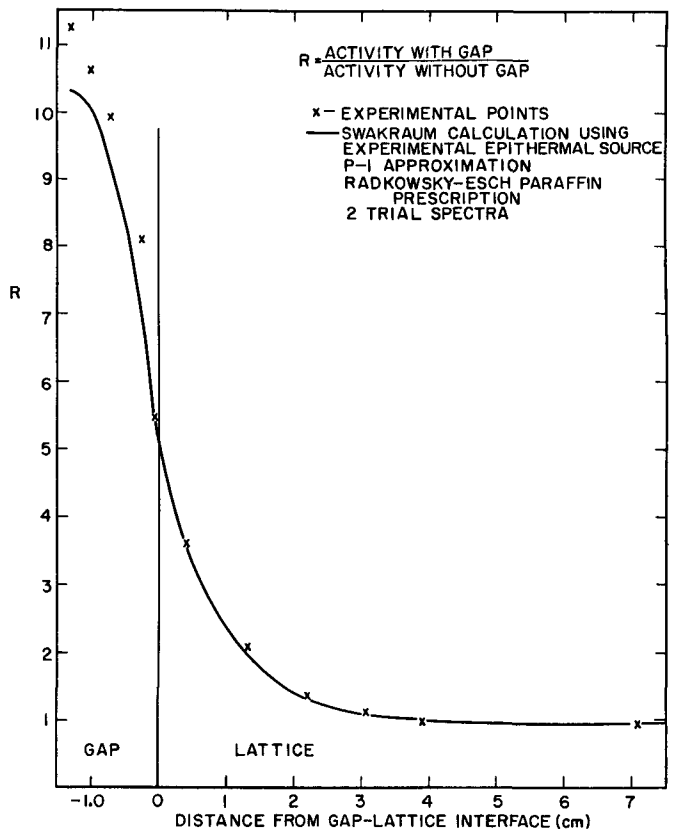

FIGURE 13 SUB-CADMIUM MANGANESE ACTIVITY CH_2 GAP IN L-7

KS-46198
UNCLASSIFIED

Large Delay Times Observed in Establishment of Single Mode Decay in Water Moderators

Fred Holzer and Marshall F. Crouch
Case Institute of Technology

We have performed a measurement of the thermal neutron mean lifetime in a large cylindrical moderator in order to determine the neutron proton capture cross section.[1,2,3] A network of sources was used to synthesize the fundamental mode of the neutron density distribution, so that higher modes would not be excited. Although better analyses can be made, it is noted that the Fermi age equation, which crudely describes conditions during the slowing down process, has the same eigenfunctions as the time dependent diffusion equation,[2,4] and therefore it was expected that a simple exponential decay would be observed after $\sim$ 10 microseconds, since the slowing down time in water to the cadmium edge is $\sim$ 2 microseconds.[5]

Somewhat surprisingly, the simple exponential decay did not commence until after about 35 microseconds (See Fig. 1) Thus the behavior was similar to that observed by von Dardel and Sjöstrand[6] and by Stooksberry and Crouch in large moderators[7] using a point source of fast neutrons.

There are several possible interpretations of the long delay preceding the exponential decay. Analysis in terms of age theory may be too crude for present purposes, though this analysis has proved to be surprisingly good even for hydrogen. Or the slight differences in boundary conditions for the age equation and the diffusion equation may affect the distributions. The mode synthesis procedure may not be sufficiently precise, giving some admixture of

higher modes, although several different assumptions regarding the point source distribution led to virtually the same mode synthesis network. Finally it is possible that the long observed delay indicates that the time required for the neutrons to reach thermal equilibrium with the moderating nuclei is somewhat longer than expected. This latter explanation is not completely unreasonable considering that measurements of slowing down time utilize detectors of epithermal neutrons, and models for calculating the details of the slowing down process are not very satisfactory in the region where the neutron energy is comparable to molecular binding energies.

[1]Fred Holzer and Marshall F. Crouch, Bull. Am. Phys. Soc. 4, 415 (1959).

[2]Fred Holzer and Marshall F. Crouch, Nuclear Sci. and Eng. 6, 545 (1959).

[3]Fred Holzer, Thesis, Case Institute of Technology, 1960 (unpublished).

[4]A.V. Antonov, A.I. Isakoff, I.D. Murin, B.A. Neupocoyev, I.M. Frank, F.L. Shapiro, and I.V. Shtranich, Proc. Intern. Conf. Peaceful Uses of Atomic Energy, Geneva, 1955 (United Nations, New York, 1956), Vol. 5, p. 3.

[5]N.G. Sjöstrand, private communication.

[6]G. von Dardel and N.G. Sjöstrand, Phys. Rev. 96, 1245 (1954).

[7]R.W. Stooksberry and M.F. Crouch, Phys. Rev. 114, 1561 (1959).

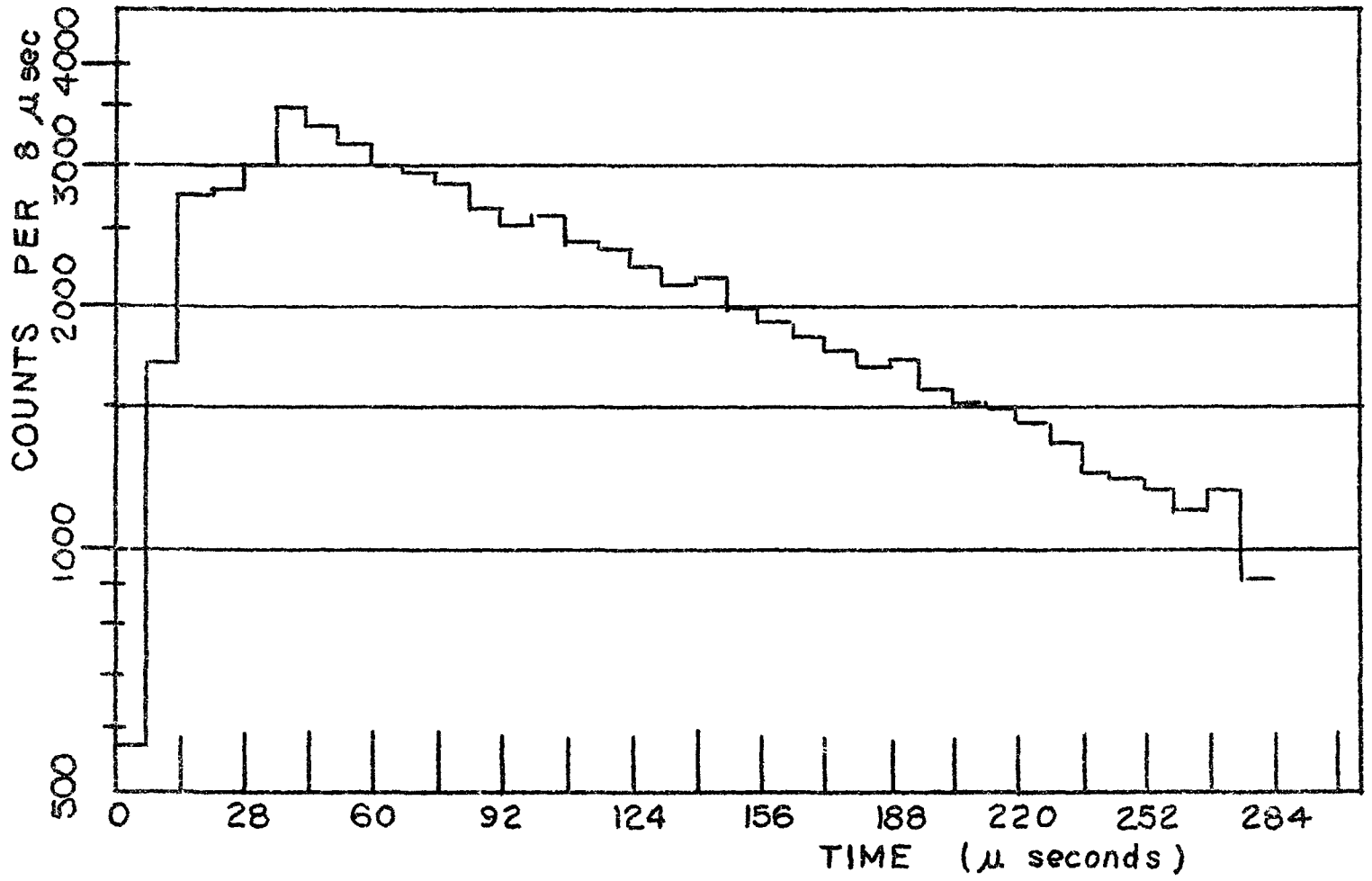
COUNTS PER 8 μ sec
500
1000
2000
3000
4000
0
28
60
92
124
156
188
220
252
284
TIME (μ seconds)

Figure 1

Pulsed Neutron Measurements on Graphite

by

H.Klose, M.Küchle and W.Reichardt

Institut für Neutronenphysik und Reaktortechnik

des Kernforschungszentrums Karlsruhe

Abstract

The α vs. B^2 curve for graphite has been carefully remeasured. Lifetimes were observed on 45 different blocks with B^2 ranging from $7 \cdot 10^{-4}$ - $240 \cdot 10^{-4}$ cm^{-2}. The results are compared with all previous measurements on graphite. The validity of the power serious expansion of $\alpha(B^2)$ is discussed.

1. Introduction

When a burst of fast neutrons is injected into a finite moderator the asymptotic thermal neutron flux dies away exponentially. According to simple one-group theory the decay constant α should be a linear function of B^2. A deviation from this linear dependence was found by v. Dardel and attributed to the so-called diffusion cooling effect. In a power series expansion

$$\alpha = \alpha_0 + DB^2 - CB^4$$

C should be a measure of the thermalization properties of the moderator; for this reason, pulsed neutron experiments could be a

---

Submitted to the Conference on Neutron Thermalization, Brookhaven National Laboratory, April 30 - May 2, 1962

tool for testing thermalization theories. A lot of work has been done along these lines, but the agreement between theory and experiments was not always satisfactory[1].

For graphite Antonov et al.[2] and Beckurts[3] have made measurements obtaining a value of about 15 . 10^5 cm^4/sec for the diffusion cooling coefficient C, which agrees well with a theoretical value of C = 14 . 10^5 cm^4/sec as calculated by Nelkin[4]. However recent measurements showed a C value about twice as high[5][6], and there also were discrepancies in other parameters. Therefore, careful remeasurement seemed necessary to investigate all possible sources of error.

45 piles were constructed out of blocks 20 x 20 cm square with different lengths, B^2 ranging from 7 . 10^{-4} to 240 . 10^{-4} cm^{-2}. The measurements were performed with the apparatus described by Beckurts[3]; the T (d,n) He^4 reaction was used.

2. Measurements and analysis of decay constants.

2.1 Waiting time for the asymptotic mode.

After a burst of fast neutrons has been injected into a moderator, one has to wait for thermalization and the decay of harmonic modes, before one may start measuring the asymptotic mode. By varying the waiting time it was found to be sufficient to wait for about 3 decay times of the asymptotic mode, provided source and detector had been arranged properly to suppress the most pronounced harmonic and $B^2 \leq 70 . 10^{-4}$. For larger bucklings thermalization time

exceeds decay time of the harmonics, and a waiting time of about 2 msec was necessary, nearly indipendent of buckling. When measurements were started too early, larger values of α were obtained, though the decay looked like a good exponential.

2.2 Background and backscattering.

When using long waiting times background and backscattering become serious problems, particularly for large bucklings. Therefore, this point was investigated in a 4o x 4o x 4o cm cube.

Measurements were made with the pile covered with cadmium only, with Cd and 2o cm $B_2 O_3$, and with Cd and 2o cm paraffine. The first two measurements agreed well enough, but the paraffine-covered pile yielded a higher value of α . This may be due to backscattering of epicadmium neutrons from paraffine.

Moreover, in one case with the pile covered by cadmium only and $B^2 = 6o \cdot 1o^{-4}$ cm^{-2}, a waiting time of 15 decay times was used and the α-value agreed well with the other ones.

2.3 Accuracy of α-measurements.

Usually, the asymptotic mode was observed over three or four decay times and some $1o^6$ counts were taken giving an accuracy of about o,2% for α. For piles with $B^2 \geq 1oo \cdot 1o^{-4}$ cm^{-2} the intensity was too low and only an accuracy of 1% or even worse could be achieved. Moreover, with $B^2 \geq 15o \cdot 1o^{-4}$cm^{-2} waiting time was restricted to 1 msec or less for background and intensity reasons, and one cannot very well rely on the α values in this region.

3. Analysis of α vs. B^2

3.1 Determination of B^2

The values of B^2 were calculated from geometry with an extrapolation length of $0{,}71\ \lambda_{tr} = 1{,}82$ cm.[+)] Corrections for density and temperature were applied, where necessary.

The anisotropy of neutron diffusion in the graphite blocks was investigated by measuring α in extremely flat geometries, where one direction of diffusion is preferred. It was found that $\frac{D_{\parallel}}{D_{\perp}} = 1{,}010 \pm 0{,}005$, where $D_{\parallel}$ and $D_{\perp}$ are the diffusion coefficients parallel and perpendicular to the central axis of a single block. This gives a negligible effect for nearly cubical assemblies.

3.2 Three and four-parameter analysis.

With a least squares fit of the decay constants α versus B^2 to

$$\alpha = (\Sigma_a v) + DB^2 - CB^4 \qquad \text{or}$$

$$\alpha = (\Sigma_a v) + DB^2 - CB^4 + FB^6$$

the parameters $(\Sigma_a v)$, D, C, and F were obtained. The result of a diffusion length measurement was included as a point with $\alpha = 0$ and $B^2 = -\frac{1}{L^2}$. The α values are weighted according to their relative

---

[+)] Other values for the extrapolation length were also tried, but when the α vs. B^2 dependence was fitted to a parabola, a minimum fluctuation of the experimental points around the curve was achieved with the value given here.

accuracy. Fig.1 shows the experimental points and a three-parameter fit.

The calculation was repeated; all points with B^2 larger than an arbitrarily fixed value B^2_{max} were successively omitted in order to investigate the dependence of diffusion parameters on the B^2 range used. The results are given in Fig.2 and 3. The case of the 3-parameter fit shows these features:

1) If the B^2 range is small and includes only a few points - the graph starts with 11 points - low values for λ_{tr} and C are obtained. This is due to the fact that the fluctuation of experimental points allows almost a straight line to fit them.

2) When B^2_{max} exeeds 6o . 10^{-4} cm^{-2} λ_{tr} and C grow continuously, indicating that a 3-parameter fit is no longer adequate.

For the 4-parameter fit no definite tendencies can be recognized, but the λ_{tr} and C values are somewhat lower in the whole B^2_{max} range. Thus we obtain the following results; referred to the density ρ = 1,6o g/cm^3 with $\lambda_{tr} = \frac{3\,D}{\bar{v}}$

3-parameter analysis

σ_a = 4,77 ± o,o7 mb λ_{tr} = 2,58 ± o,o2 cm

C = (26 ± 5) . 10^5 cm^4/sec

4-parameter analysis

σ_a = 4,8o ± o,o7 mb λ_{tr} = 2,56 ± o,o2 cm

C = (16 ± 5) . 10^5 cm^4/sec F = - (2o ± 1o) . 10^7 cm^6/sec

The most striking feature is the value for F. A B^6-term was predicted by theory due to (1) non-applicability of diffusion theory[4),7)] (2) more accurate description of the diffusion cooling effect,

but always it turned out that F should be positive, the order of magnitude being about $\frac{C^2}{D}$, whereas the measurement yielded

$$F = - 11 \frac{C^2}{D} .$$

4. Discussion of results.

4.1 Comparison with other measurements.

For comparison of our results with previous measurements, all data of pulsed neutron experiments on graphite available in literature and unpublished work of this institute were plotted in one diagram of α versus B^2. The absorption term, different for different graphites, was subtracted and all values were reduced to the same density. The result is given in Fig.4.

Satisfactory agreement exists for $B^2 < 6o \cdot 1o^{-4}$, but then deviations start to become appreciable, higher values of α often corresponding to lower waiting times used by the authors, as is to be expected from our statement in 2.1.

4.2 Validity of the power series expansion of α vs. B^2.

If a power series expansion

$$\alpha = \Sigma_a v + DB^2 - CB^4 + FB^6 + \ldots$$

is an appropriate description of the α vs. B^2 dependence and the diffusion cooling coefficient C is a constant to be checked with theory, there should be a range of B^2 values for which $FB^6 \ll CB^4$ and from which C could be determined with reasonable accuracy. This is not the case for graphite, where, for instance, $FB^6 = o,1\ CB^4$ when $B^2 \approx 1o^{-3}$ and no accurate value of C can be obtained from measurements with $B^2 \leq 1o^{-3}$, because then CB^4 would always be less than 1% of α.

Moreover, careful inspection of the 4-parameter curve will reveal that it does not fit the points very well for low B^2, because λ_{tr} is too small. The general impression is that a parabola does not describe the dependence of α on B^2 very well. Nevertheless, it is reasonable to make a power series expansion for the determination of σ_a and λ_{tr} although the physical meaning of the C-value remains doubtful.

4.3 Conclusions.

When experimental results of pulsed neutron measurements on moderators are compared, α-values should be compared instead of diffusion parameters which depend too much on the B^2-range and evaluation procedure used.

Besides when thermalization theories are tested, a direct comparison between calculated and measured α values is to be preferred.

Literature

1) K.H. Beckurts, Reactor Physics Research with Pulsed Neutron Sources. Nucl.Instr.Meth. 11, 144, (1961)

2) A.V. Antonov, A.J. Isakoff, J.D. Murin, B.A. Neupocoyev, J.M. Frank, F.L. Shapiro, J.V. Shtranich, Proc.Intern.Conf. Peaceful Uses Atomic Energy, Geneva 5, 3 (1955)

3) K.H. Beckurts, Nuclear Sci. and Eng. 2, 516 (1957) also Thesis, Göttingen, 1956

4) M. Nelkin, J. Nuclear Energy 8, 48 (1958)

5) Lalande, Industries atomiques, No.5-6, 71 (1961)

6) unpublished Karlsruhe work

7) M. Nelkin, Nuclear Sci.and Eng. 7, 21o (196o)

8) K.S. Singwi, J. Nuclear Energy 11, 19 (1959/6o)

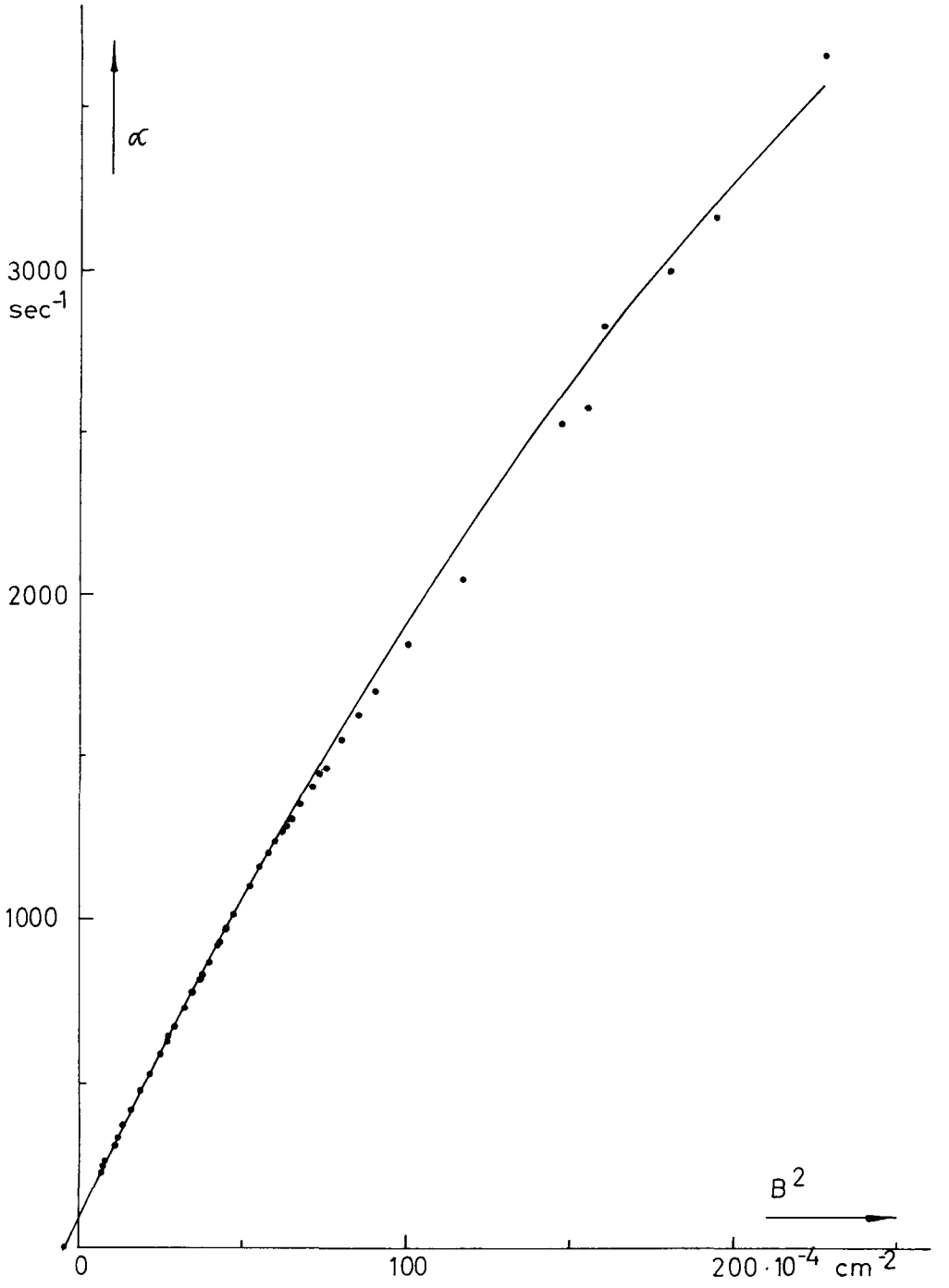

Fig.1 —— $\alpha = 87.8 + 2.072\ 10^5\ B^2 - 23.7\ 10^5\ B^4$

$\rho = 1.651\ g/cm^3$

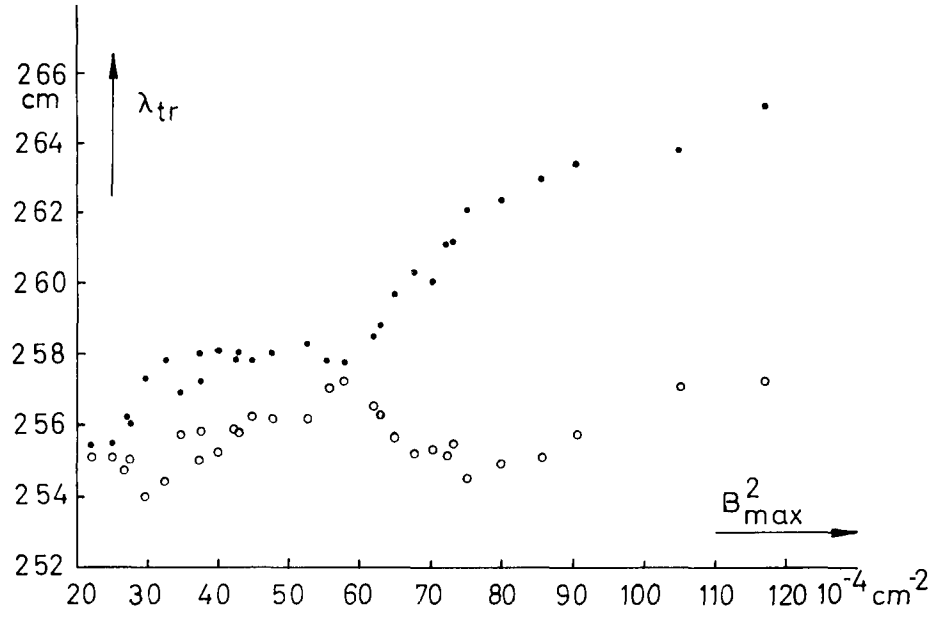

Fig 2

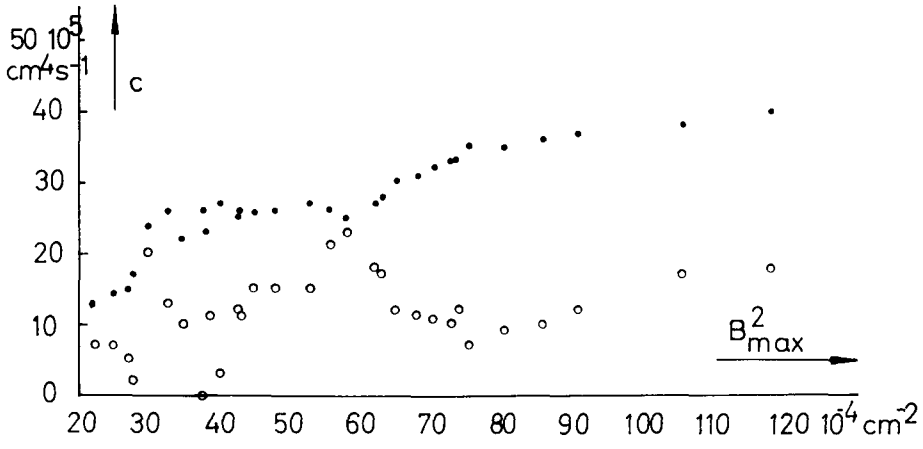

Fig 3

ϱ = 160 g/cm^3

• 3 parameter fit

o 4 parameter fit

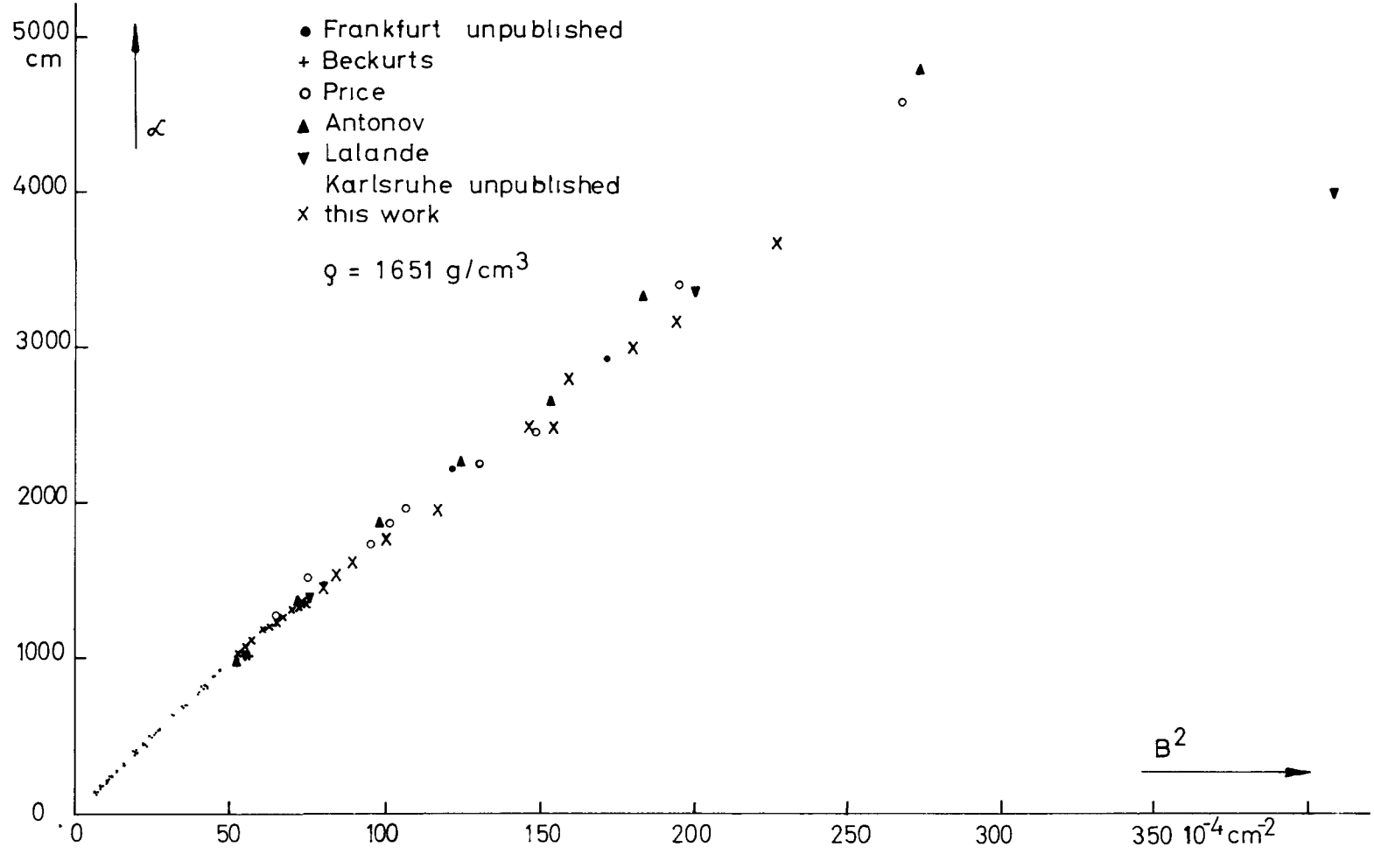
5000
cm
4000
3000
2000
1000
0
α
• Frankfurt unpublished
+ Beckurts
o Price
▲ Antonov
▼ Lalande
Karlsruhe unpublished
x this work
ϱ = 1651 g/cm³
0
50
100
150
200
250
300
350 10⁻⁴cm⁻²
B²

Fig. 4

GENERAL ATOMIC

DIVISION OF

GENERAL DYNAMICS

JOHN JAY HOPKINS LABORATORY FOR PURE AND APPLIED SCIENCE

P.O. BOX 608. SAN DIEGO 12. CALIFORNIA

COMPARISON OF DIFFUSION PARAMETERS OBTAINED FOR WATER BY THE PULSED AND THE POISONING TECHNIQUES

by

J. U. Koppel
W. M. Lopez

This is a preprint of a paper to be presented at the Conference on Neutron Thermalization, at Brookhaven National Laboratory, April 30, 1962.

Project 48.01
U. S. Atomic Energy Commission
Contract AT(04-3)-167, Project Agreement No. 2 April 2, 1962

COMPARISON OF DIFFUSION PARAMETERS OBTAINED FOR WATER BY THE PULSED AND THE POISONING TECHNIQUES

by J. U. Koppel and W. M. Lopez

Introduction

The measurement of neutron die-away times in pulsed assemblies of decreasing size and the measurement of diffusion lengths in media of increasing poison concentration are known[1] to be closely related experiments. This is most easily seen from the space-time-energy dependent Boltzmann equation in the diffusion theory approximation

$$-Dv\,\Delta n(v,r,t) + \frac{\partial n(v,r,t)}{\partial t} = -(\Sigma_s+\Sigma_a)\, n(v,r,t)\, v + \int n(v',r,t)\, v'\Sigma\,(v'\rightarrow v)dv' \qquad (1)$$

The (asymptotic) solution corresponding to the experiment mentioned in first place is of the kind

$$n(v,r,t) = e^{iB\cdot r-\alpha t}\, N(v) \qquad (2)$$

where B^2 is usually called the geometrical buckling of the assembly, α being the decay constant measured for different valued of B^2.

The (asymptotic) solution applying to the second experiment is

$$n(v,r) = e^{-\kappa r}\, N(v) \qquad (3)$$

where κ is the inverse of the diffusion length. Obviously eq. (3) is a special case of (2) with $\alpha = 0$ and $B = i\kappa$. Thus κ^2 is equivalent to a negative buckling.

Now, replacing (2) in (1) yields

$$(B^2Dv-\alpha+\Sigma_a v)\, N(v) = -\Sigma_s\, v\, N(v) + \int N(v')\, v'\Sigma\,(v'\rightarrow v)dv' \qquad (4)$$

which is an eigenvalue problem with either B^2 or α being the eigenvalue.

It is seen that the time dependent problem can be reduced to a stationary one just by introducing a fictitious 1/v poison with cross section $-\alpha/v$. Integrating eq. (4) over all energies and considering only 1/v absorbers, it is found

$$B^2 \overline{Dv} + \alpha_o - \alpha = 0 \qquad (5)$$

with

$$\alpha_o = \Sigma_a v \; ; \qquad \overline{Dv} = \frac{\int N(v) v D dv}{\int N(v) dv}$$

For $B^2 = 0$ (Pulsed infinite medium) the solution of eq. (4) is a Maxwellian and $\alpha = \alpha_o$. For $B^2 > 0$ the spectrum N(v) is shifted to lower energies (diffusion cooling) whereas for $B^2 < 0$ it is shifted to higher energies (diffusion hardening). Thus $\overline{Dv}$ is a continuous function of B^2 and can be expanded in the power series:

$$\overline{Dv}\,(B^2) = D_o - C B^2 + F B^4 - \ldots \qquad (6)$$

where C is known as the diffusion cooling constant. Substituting (6) into (5)

$$\alpha - \alpha_o = B^2 D_o - C B^4 + F B^6 - \ldots \qquad (7)$$

of course the relation between $\alpha - \alpha_o$ and B^2 can also be expressed by the inverse series

$$B^2 = \frac{\alpha-\alpha_o}{D_o} + C'\left(\frac{\alpha-\alpha_o}{D_o}\right)^2 + \ldots \qquad (8)$$

It is easily seen that:

$$C' = \frac{C}{D_o^2} \qquad (9)$$

The shape of the function relating α and B^2 is shown in Figure 1. It follows from the foregoing discussion that the portion of the curve

lying in the first quadrant can be measured by the pulsed technique. The intercept α_o corresponds to the decay in an assembly of infinite dimensions. The intercept κ_o^2 is the inverse of the diffusion length in the unpoisoned medium. If now a 1/v poison is uniformly added to the medium the curve of Figure 1 will be shifted in the direction of positive α without changing its shape. As the magnitude of the shift, $\Delta\alpha = v\Delta\Sigma_a$ (where $\Delta\Sigma_a$ is the increase in absorption) is known, the measurement of the diffusion length for increasing poison concentration yields points of the curve of Figure 1 lying in the third quadrant. Only the small segment between the intercepts cannot be measured by either one of the techniques mentioned above.

Interpretation of Experimental Data

The parameters of the function $\alpha = f(B^2)$ which are of physical interest are $\alpha_o = v_o\Sigma_a(v_o)$ (intercept at $B^2 = 0$), D_o (slope at $B^2 = 0$) and C (one-half times the second derivative at $B^2 = 0$). α_o and D_o can be obtained with good accuracy by both methods, and the values measured are in fair agreement with each other and with theory (2). Concerning C, however, there is a large discrepancy between different published values(*). We believe that this is largely due to different ways of analyzing data, and simply reflects the inherent difficulty of determining the curvature of an unknown function defined by a set of experimental points with finite standard deviation. The usual way to determine the two mentioned parameters is to fit the experimental points by a least squares technique to an expression like (7) or (8) truncated after two or three terms. As the higher order terms are obviously not zero, the result of the analysis will depend on the range

*For a complete list of references see (3) and (4)

covered by the experiment. It appears that for a given experimental error of the measured points there is an optimum range beyond which no further accuracy is gained in the determination of the three diffusion parameters. In fact, as more terms have to be retained in order to fit larger B^2 intervals, the uncertainty in the first three coefficients remains roughly constant. Thus a three parameter fit of the optimum interval seems to be as good as a fit to more parameters over a wider range of B^2. It is possible to get a feeling of the error involved in truncating the fit, by plotting the coefficients obtained for a decreasing number of points, thus dropping progressively those of maximum buckling. The plots obtained for the two ways of fitting, (7) and (8), should approach roughly the same limit, obviously with a continuously increasing uncertainty. On the other hand, in order to determine the number of terms of (7) or (8) to be retained for the best fit of given experimental data, a good criterion is to compute the empirical variance

$$X = \frac{\Sigma(y_i - y_{calc})^2}{n - m}$$

and to retain that number of terms which makes X minimum. y_i and y_{calc} are the measured and the calculated values of either α or κ^2, n is the number of points and m the number of parameters.

Comparison of Recent Measurements in Water

We are going to show briefly how the foregoing considerations apply to the results of two recent measurements of Σ_a, D_o and C for water (3, 4). The first is a pulsed experiment while the second uses the stationary method.(*)

*The stationary experiment was first suggested by P. Michael (private communication).

1) Since the publication of paper (3) more data has been obtained by its authors, extending the buckling range from 0.6 to 1.5cm^{-2}. The results for the complete range are shown in Figure 2 and Table I. Case 1 and 2 refer to different ways of computing the bucklings. In Case 1 the extrapolation distance was supposed constant and given by

$$d = 2.131 \frac{D_o}{\bar{v}}$$

with

$$\bar{v} = \frac{2}{\sqrt{\pi}} 2.2 \times 10^5 \text{cm/sec}$$

In Case 2, d was supposed to vary with B^2 according to the formula $d' = \frac{r}{r - d} d$, r being the radius of an equivalent sphere with the same buckling:

$$B^2 = \left(\frac{\pi}{r+d'}\right)^2 = \left(\frac{\pi}{a+2d'}\right)^2 + \left(\frac{\pi}{b+2d'}\right)^2 + \left(\frac{\pi}{c+2d'}\right)^2$$

The dropping points technique is illustrated by Table II and Figures 3,4. From Table III it is seen that the three parameters fit of the 0 - 0.6cm^{-2} interval is in fair agreement with the four parameters fit of the 0 - 1.6cm^{-2} interval (X is minimum for M = 4). It is also seen that the uncertainties of Σ_a, D_o, and C are practically the same for those two fits.

2) The experiment reported in (4) has already been analyzed the way we are suggesting in this note. The results are reproduced in Figures 5, 6, and 7, and Tables IV and V*. The error bars of the

---

*The figures of Table V are slightly different from those appearing in Ref. (4) because in the present analysis α_o was recalculated for each B^2 interval.

least squares fitted coefficients have been recalculated using the correct statistical expression (5). It is seen that while Σ_a and D_o are in good agreement** with the previous results, a large discrepancy seems to remain between the values found for C. That the uncertainty due to the extrapolation distance applying to the pulsed experiment may account at least for part of the discrepancy is seen from the following considerations. For the sake of simplicity let us take the case of spherical assemblies. Their buckling is given by

$$B^2 = \frac{\pi^2}{R^2}$$

where $R = r + d$ is the extrapolated radius. Suppose $R = R_o + \epsilon$ where ϵ is the error of d, then

$$B^2 = \frac{\pi^2}{R_o^2}\left[1 - 2\frac{\epsilon}{R_o} + 3\left(\frac{\epsilon}{R_o}\right)^2 - \cdots\right] \qquad (10)$$

Substituting this expression for B^2 into the expansion (7) it follows

$$\alpha - \alpha_o = D_o B_o^2\left[1 - \frac{2}{\pi}\epsilon B_o + \frac{3}{\pi^2}\epsilon^2 B_o^2 - \cdots\right] - CB_o^4 + \cdots$$

with $B_o = \pi/R_o$ (20)

Rearranging terms on the right side of (20)

$$\alpha - \alpha_o = D_o B_o^2 - \left(C + \frac{2}{\pi}\frac{\epsilon D_o}{B_o} - \frac{3}{\pi^2}\epsilon^2 D_o\right) B_o^4 + \cdots$$

For $\epsilon = 0.1$ cm and $B_o = 1$ cm^{-1} the term in ϵ introduces a correction of more

---

** The experiments reported in (2) and (4) were performed at 26.7° C. and 21° C. respectively.

than 50% of C. The term in ϵ^2 becomes significant only for much larger bucklings.

Another source of discrepancies is the weighting of the experimental points. The figures of tables II and III were obtained assuming a constant relative error in the measurement of $\alpha = f(B^2)$. The results listed in Table V were obtained assuming a constant relative error of κ^2. Figures 2 and 5 seem to justify both assumptions.

Conclusions

It appears that both the pulsed and the poisoning method are suitable experiments for measuring Σ_a and the infinite medium diffusion constant D_o However, in view of the unavoidably increasing uncertainty in the determination of higher order coefficients of the series (7) or (8) it seems to be preferable to compare the function $\alpha = f(B^2)$ obtained with different experiments (and theoretical calculations) point by point rather than by the coefficients of their least square fits.

TABLE I

Experimental Data From (3)

Size (cm)	α (sec^{-1})	B^2 (cm^{-2}) Case 1	Case 2
44.5 x 44.5 x 48.9	5336	0.01372	0.01370
28.6 x 31.1 x 60.2	5668	0.02400	0.02399
31.1 x 60.2 x 26.4	5722	0.02598	0.02594
31.1 x 60.2 x 19.1	6147	0.03769	0.03775
31.1 x 60.2 x 16.5	6437	0.04599	0.04599
15.2 x 29.7 x 16.5	7854	0.08341	0.08346
15.2 x 29.7 x 16.5	7904	0.08341	0.08346
76.2 x 76.2 x 10.2	7908	0.08795	0.08702
17.6 x 17.6 x 17.7	8132	0.08871	0.08847
15.2 x 29.7 x 14.6	8140	0.09232	0.09231
17.6 x 17.6 x 12.6	8989	0.1156	0.1153
17.6 x 17.6 x 12.6	9037	0.1156	0.1153
76.2 x 76.2 x 7.62	10205	0.1478	0.1471
10.2 x 10.2 x 10.2	13970	0.2538	0.2503
10.2 x 10.2 x 9.5	14330	0.2647	0.2621
10.2 x 10.2 x 8.9	14749	0.2779	0.2744
10.2 x 10.2 x 8.26	15430	0.2940	0.2903
10.2 x 10.2 x 7.62	16230	0.3139	0.3099
10.2 x 10.2 x 6.35	18116	0.3712	0.3660
10.2 x 10.2 x 5.72	19315	0.4136	0.4069
7.62 x 7.62 x 7.62	19843	0.4340	0.4288
7.62 x 7.62 x 7.62	20012	0.4340	0.4288
10.2 x 10.2 x 5.08	21547	0.4709	0.4626
7.62 x 7.62 x 6.35	21656	0.4913	0.4846
6.84 x 6.95 x 6.95	23100	0.5192	0.5117
7.62 x 7.62 x 5.72	23473	0.5338	0.5252
7.62 x 7.62 x 5.08	25168	0.5910	0.5807
5.93 x 6.00 x 5.95	28400	0.6798	0.6667
4.91 x 4.93 x 4.92	36800	0.9576	0.9308
4.49 x 4.49 x 4.47	42000	1.1292	1.0913
3.82 x 3.79 x 3.82	53000	1.4935	1.4251

TABLE IIa

Fit (7) With 3 Parameters (pulsed data)

	B^2max.	Σ_a	ϵ_σ	α_o	ϵ_α	D_o	ϵ_d	C	ϵ_c
	cm^{-2}	mb		sec^{-1}		cm^2/sec		cm^4/sec	
Case 1	1.4935	327.7	1.4	4806	20	36681	193	3179	234
	1.1292	326.8	1.4	4793	20	36925	221	3647	325
	.95757	326.5	1.5	4788	22	37033	265	3878	450
	.67977	326.1	1.6	4782	24	37165	347	4180	677
	.5910	325.3	1.6	4771	24	37426	368	4852	763
	.47090	325.3	1.7	4771	25	37424	418	4800	1024
Case 2	1.4251	327.2	1.5	4798	22	36863	215	2420	272
	1.0913	326.1	1.5	4783	22	37142	243	2971	367
	.93078	325.7	1.6	4777	23	37272	289	3255	501
	.66668	325.3	1.8	4771	26	37410	374	3576	741
	.58070	324.6	1.8	4761	26	37630	404	4153	852
	.46265	324.8	1.8	4764	27	37557	458	3869	1138

TABLE IIb

Fit (8) With 3 Parameters (pulsed data)

	B^2	Σ_a	ϵ_σ	α_o	ϵ_α	D_o	ϵ_d	C	ϵ_c
	cm^{-2}	mb		sec^{-1}		cm^2/sec		cm^4/sec	
Case 1	1.4935	326.5	1.4	4788	20	37078	193	4461	308
	1.1292	325.9	1.4	4779	20	37271	221	4933	433
	.95757	325.7	1.5	4777	22	37309	265	5028	587
	.67977	325.7	1.6	4777	24	37310	347	5030	839
	.59100	325.0	1.6	4766	24	37586	368	5890	976
	.47090	325.1	1.7	4768	25	37519	419	5578	1251
Case 2	1.4251	326.5	1.5	4789	22	37063	215	3052	334
	1.0913	325.6	1.5	4775	22	37348	243	3726	459
	.93078	325.3	1.6	4770	23	37443	289	3976	622
	.66668	325.1	1.8	4768	26	37493	374	4114	891
	.58070	324.5	1.8	4759	26	37718	404	4805	1049
	.46265	324.8	1.8	4763	27	37589	458	4258	1338

Temperature: 26.7°C

TABLE III

Fit (7) With a Variable Number of Parameters (pulsed data)

Case	$B^2_{max.}$ cm^{-2}	Parameters	$\alpha_o=\Sigma_a v$ sec^{-1}	ϵ_α	D_o cm^2/sec	ϵ_d	C cm^4/sec	ϵ_c	F cm^6/sec	ϵ_f	$10^{-4}X$ sec^{-2}
1	1.4935	3	4806	21	36681	193	3179	234	-	-	0.6142
	1.4935	4	4770	24	37476	367	5500	961	1354	550	0.5201
	1.4935	5	4774	29	37389	585	5066	2423	720	3287	0.5393
	0.5910	3	4771	24	37426	368	4852	763	-	-	
2	1.4251	3	4798	22	36863	215	2420	272	-		0.6908
	1.4251	4	4760	26	37715	407	4997	1103	1585	660	0.5903
	1.4251	5	4768	31	37487	641	3819	2760	-219	3923	0.6079
	0.5807	3	4761	26	37630	404	4153	852	-		

Temperature" 26.7°C.

TABLE IV

Experimental Data From (4)

L	κ^2	$\Delta\Sigma_a$	$\alpha=v\Delta\Sigma_a$
cm	cm^{-2}	cm^{-1}	sec^{-1}
2.754	0.1318	-	-
2.459	0.1653	0.005245	1153.9
2.166	0.2130	0.013870	3051.4
1.978	0.2556	0.020470	4503.4
1.639	0.3721	0.040397	8887.3
1.255	0.6348	0.087314	19209
1.063	0.8848	0.13427	29539
0.9429	1.1248	0.17895	39369
0.8469	1.3942	0.23462	51616
0.7308	1.8724	0.34655	76241

TABLE Va

Fit (7) With 3 Parameters (poisoning data)

$\kappa^2_{max.}$	Σ_a	ϵ_σ	α_o	ϵ_α	D_o	ϵ_d	C	ϵ_c
cm^{-2}	mb		sec^{-1}		cm^2/sec		cm^4/sec	
1.8724	317.5	2.1	4663	31	34833	170	4238	187
1.3942	324.9	1.4	4771	21	35609	129	3413	179
1.1248	326.1	1.6	4790	24	35751	148	3234	253
.8848	323.2	1.7	4747	25	35405	169	3754	367
.6348	324.3	2.0	4763	30	35541	229	3507	674

TABLE Vb

Fit (8) With 3 Parameters (poisoning data)

$\kappa^2_{max.}$	Σ_a	ϵ_σ	α_o	ϵ_α	D_o	ϵ_d	C	ϵ_c
cm^{-2}	mb		sec^{-1}		cm^2/sec		cm^4/sec	
1.8724	326.6	1.4	4796	21	35874	105	2662	101
1.3942	328.6	1.5	4826	22	36079	120	2481	150
1.1248	328.6	1.7	4825	25	36074	141	2499	223
.88481	325.8	1.7	4784	25	35754	156	2878	310
.63481	326.2	2.0	4791	29	35808	213	2797	596

Notes

1) Temperature: 21°C

2) The large errors appearing in the first line of Table Va show the need of retaining one more term of expansion (7) in order to fit these data

References

1. H. Hurwitz and M. S. Nelkin, Nucl. Sci. Eng. 3, p. 1 (1958).

2. H. Honeck, to be presented at this meeting.

3. W. M. Lopez and J. R. Beyster, Nucl. Sci. Eng. 12, p. 135 (1962).

4. E. Starr and J. U. Koppel, to be published in Nucl. Sci. Eng.

5. B. L. Van der Waerden, Mathematische Statistik, Springer (1957).

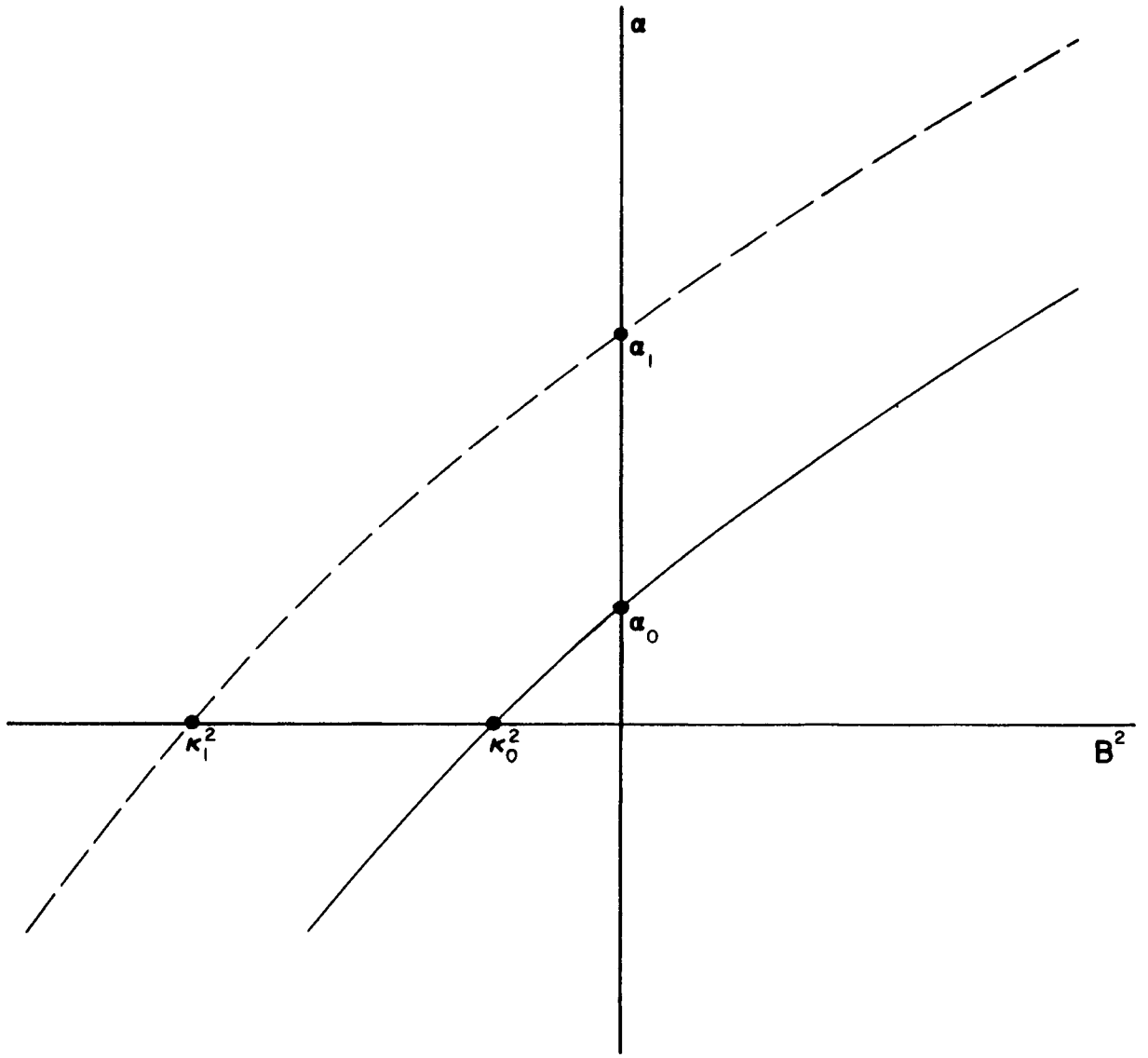

Fig. 1

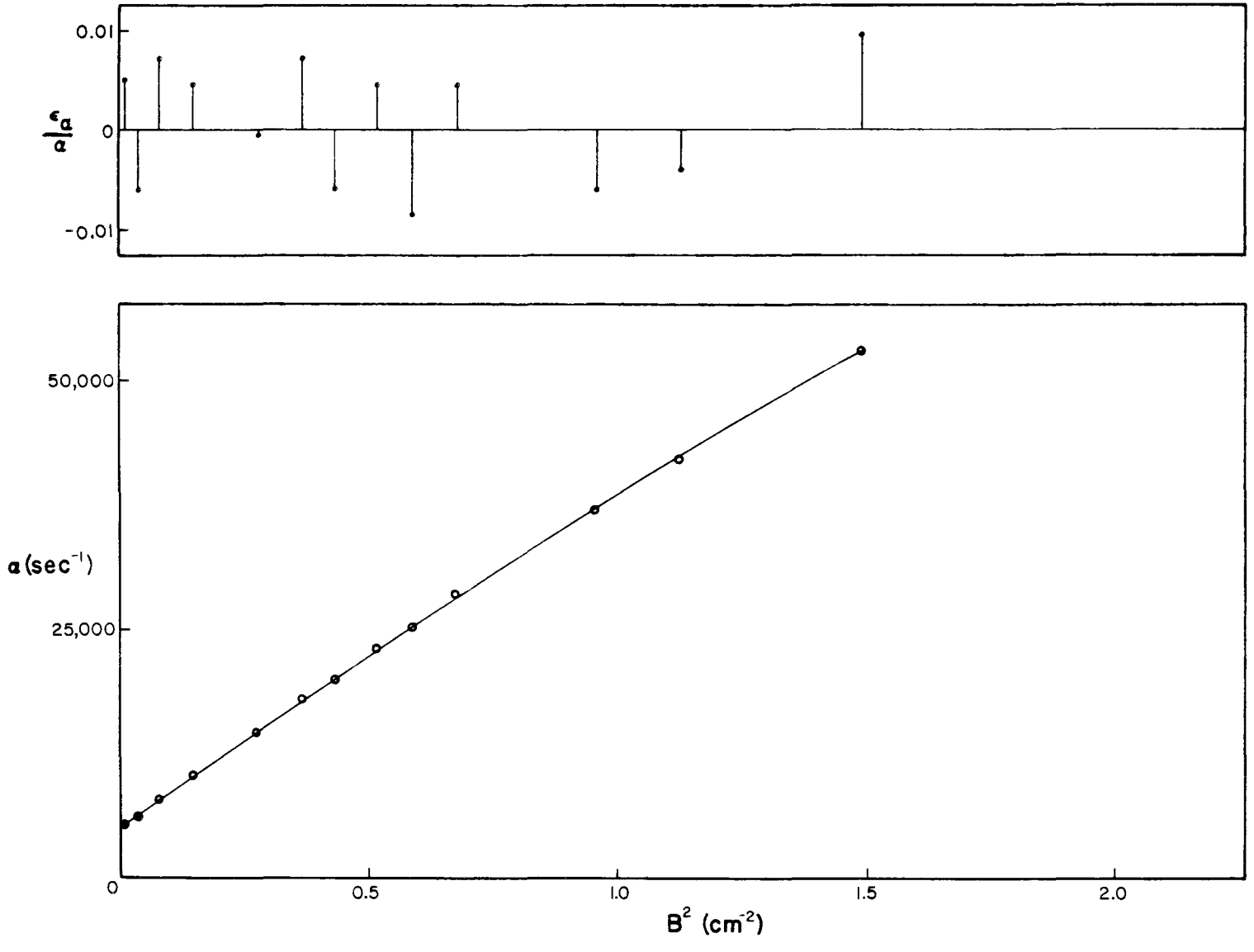
0.01
0
-0.01
$\frac{\epsilon}{\alpha}$
50,000
25,000
0
α (sec^{-1})
0.5
1.0
1.5
2.0
B^2 (cm^{-2})

Fig. 2

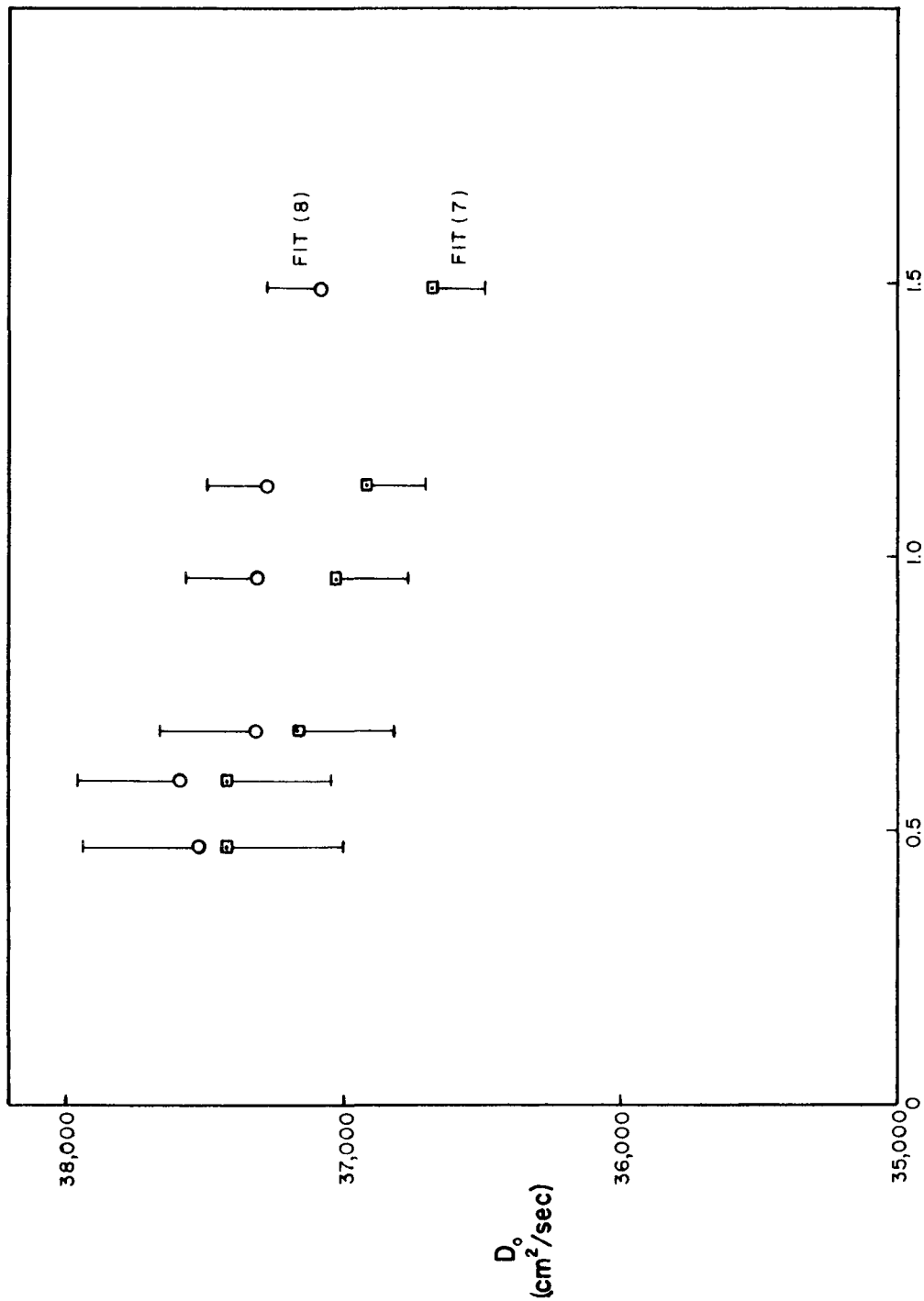
FIT (8)
FIT (7)
38,000
37,000
36,000
35,000
0
0.5
1.0
1.5
D_o (cm²/sec)
B^2_{max} (cm⁻¹)

Fig. 3

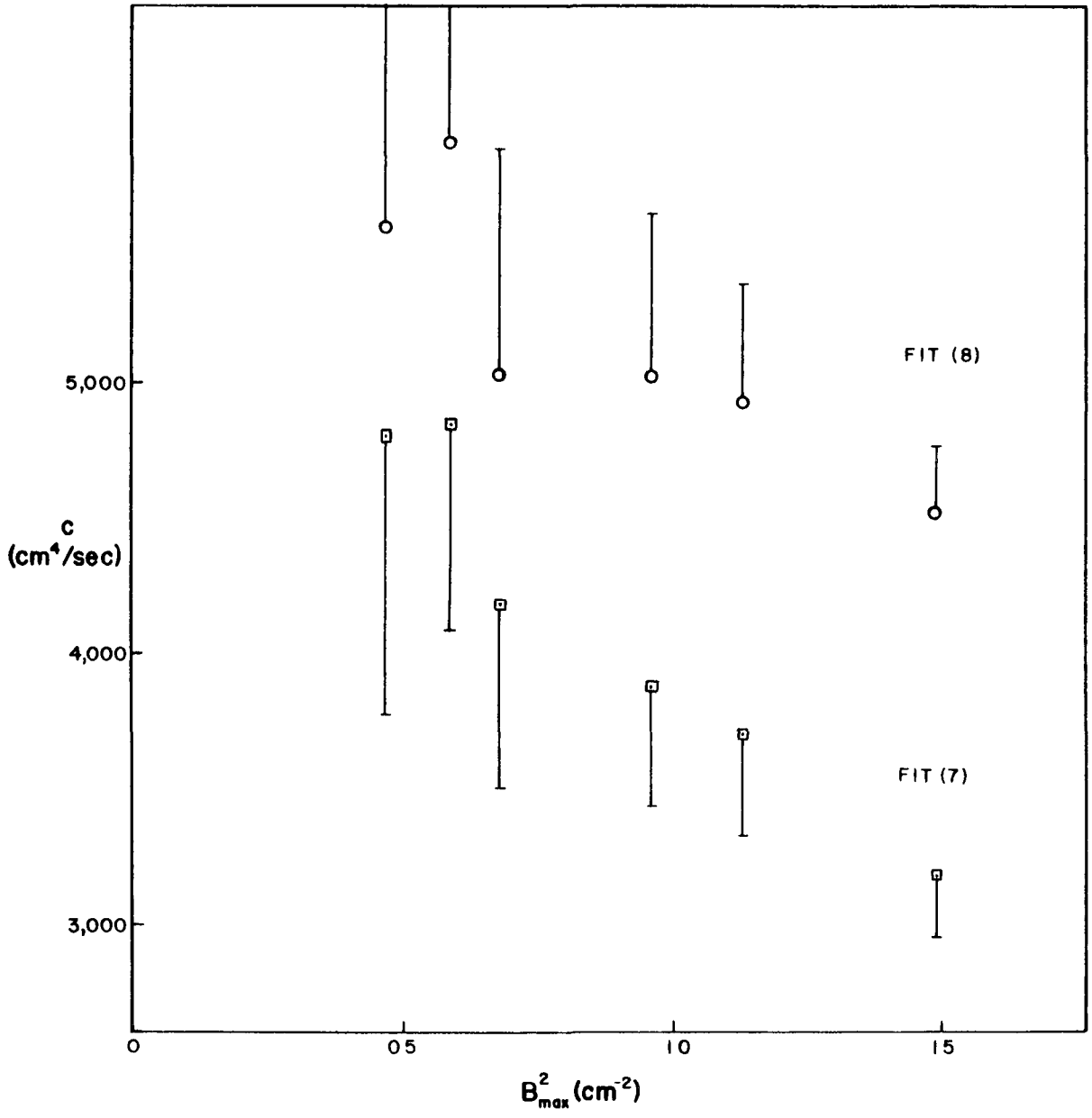

Fig. 4

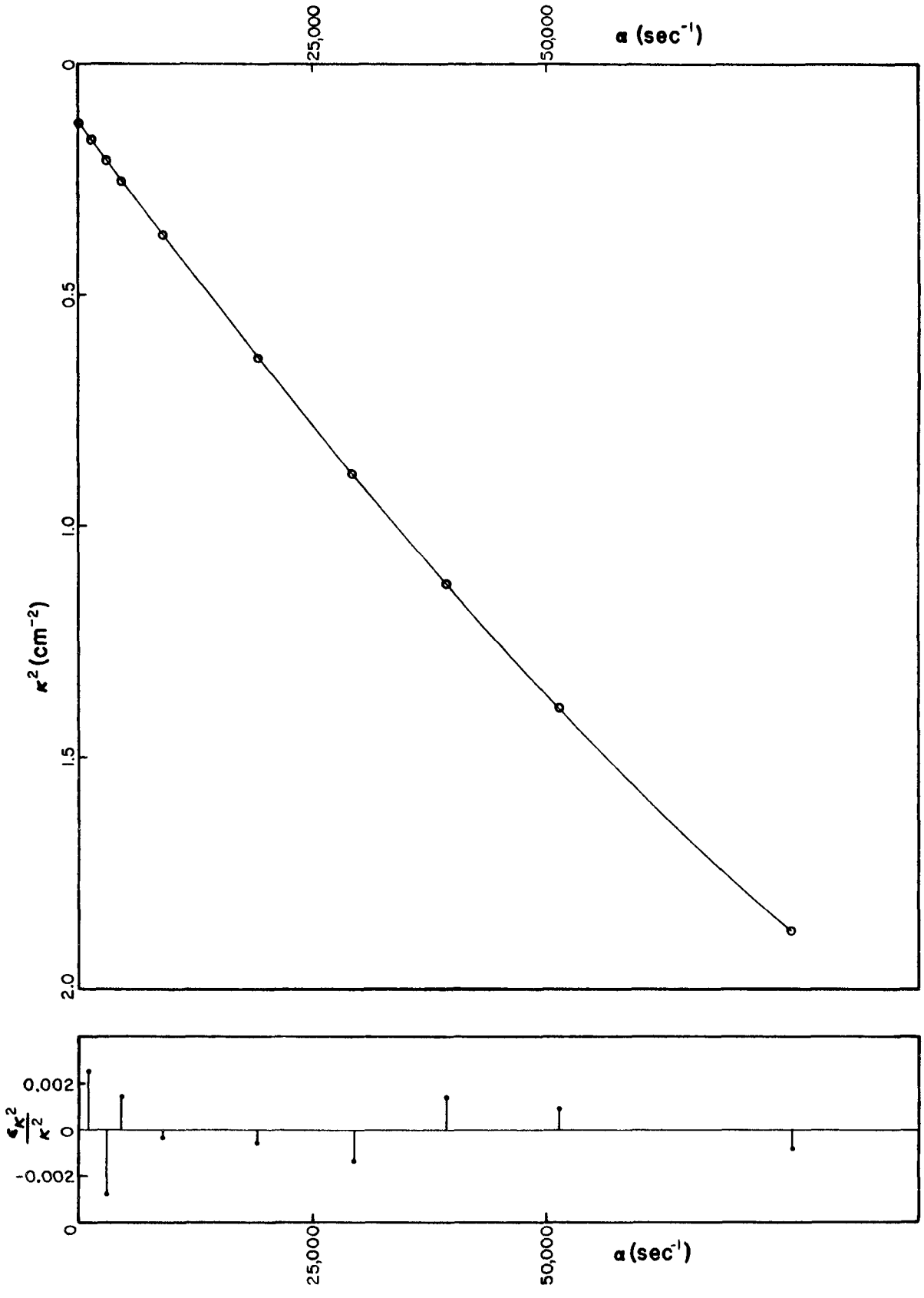
α (sec⁻¹)
25,000
50,000
0
0.5
1.0
1.5
2.0
κ² (cm⁻²)
0.002
0
-0.002
σκ²/κ²
25,000
50,000
α (sec⁻¹)

Fig. 5

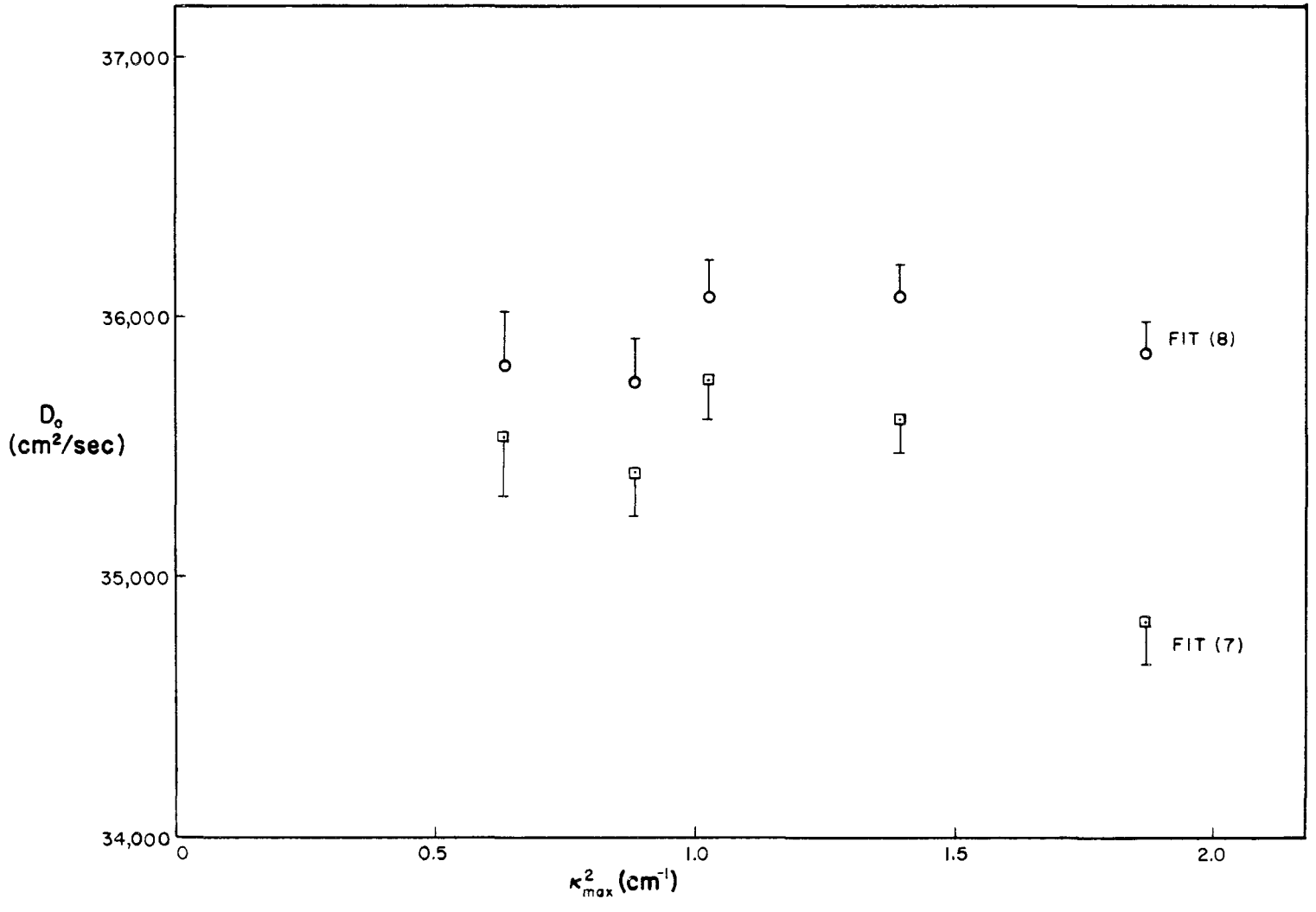
37,000
36,000
35,000
34,000
D_o
(cm²/sec)
0
0.5
1.0
1.5
2.0
κ^2_{max} (cm⁻¹)
FIT (8)
FIT (7)

Fig. 6

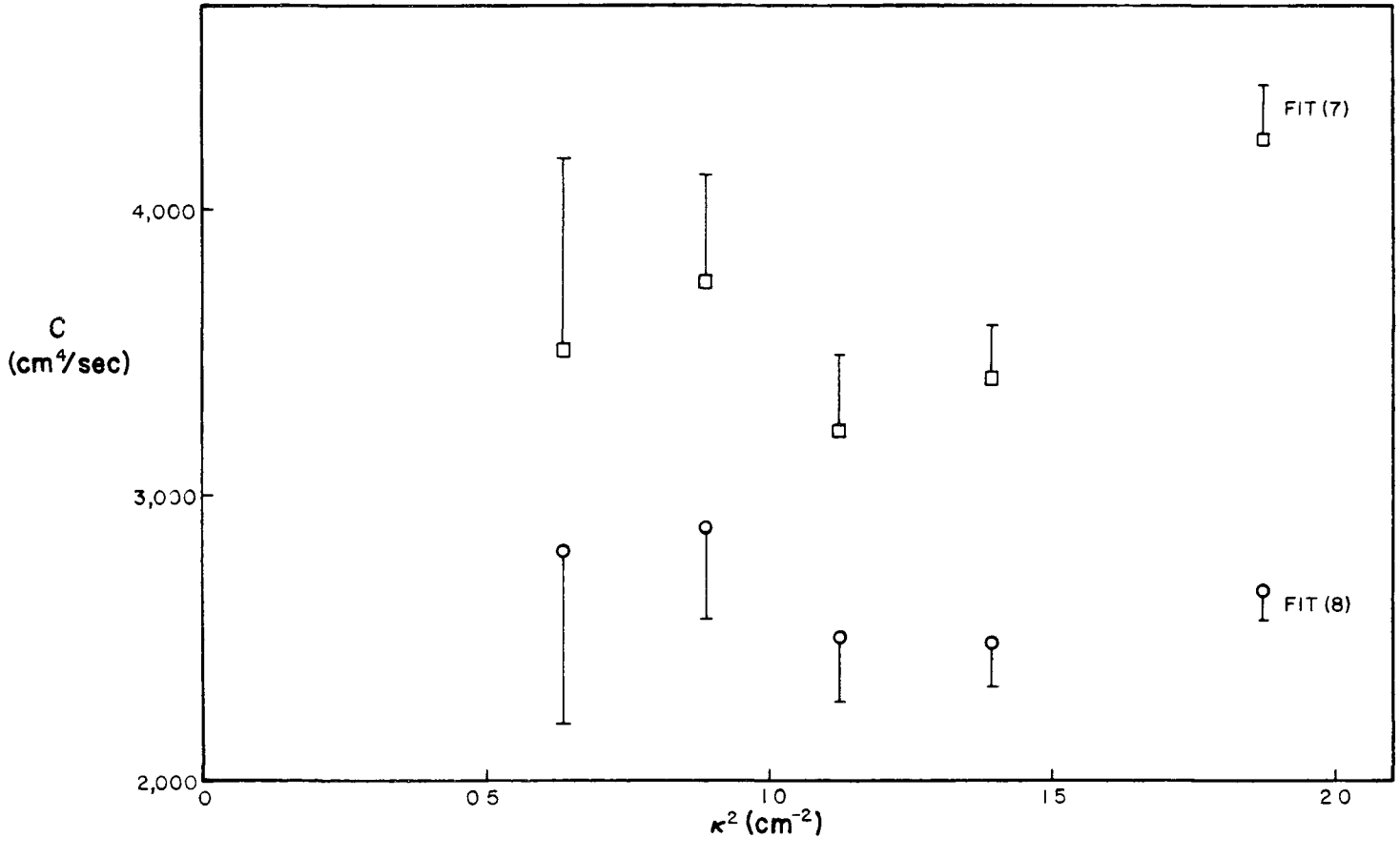

Fig. 7

The time scale of neutron slowing down in water

by

E. Möller, AB Atomenergi, Studsvik, Tystberga, Sweden

and

N.G. Sjöstrand, Chalmers University of Technology, Göteborg, Sweden

Abstract.

The time scale of neutron slowing down in water has been studied using the pulsed beam of the van de Graaff-accelerator at Studsvik for the production of neutron bursts in the moderator. The moderation process is followed by the measurement of the neutron capture rate in non-disturbing amounts of cadmium and gadolinium dissolved in the water, the time resolution being ten times better than in earlier studies. With both elements a thermalization time constant of about 4 μsec was found.

The time scale of neutron slowing down in water.

by E. Möller
AB Atomenergi, Studsvik, Tystberga, Sweden
and
N.G. Sjöstrand
Chalmers Univ. of Technology, Göteborg, Sweden

Introduction

The process of slowing down and thermalization of fast neutrons in hydrogenous materials is of very short duration since the neutron may loose all its energy in one collision with a proton. The elementary theory (1) predicts that on the average only 18 collisions are needed to make the neutron thermal, and this process can be estimated to take about 10 μsec in water. These figures, based as they are on assumptions which are valid only for heavier moderators, give a qualitative indication of the orders of magnitude involved. Important parameters, which characterize the time behaviour of the neutrons in the moderator, are the slowing down time to the cadmium limit, the thermalization time constant, which describes the time rate of energy exchange between the thermalizing flux and the moderator, and the life time of the thermal neutrons in the moderator.

Earlier experimental information about water

The slowing down time to the cadmium cut-off energy may be obtained from steady state measurements as pointed out by DeJuren (2). The reaction rate between a neutron flux and a 1/v-detector is independent of the energy of the neutrons. Hence the counting rates of a bare 1/v-detector and a cadmium-covered one in a constant flux are proportional to the time the neutron can spend in the energy region for which the detector is sensitive, that is to the whole neutron life time and the slowing down time respectively. From available data a value of 1.54 ± 0.13 μsec was found for the slowing down time to 0.35 eV.

A natural approach to the problem is to apply the pulsed neutron source technique with time analysis of detector pulses. The first extensive use of this method was made by von Dardel (3) using a time resolution of 2 μsec and boron counters. The measurements supported the assumption that the flux during the thermalization is very like a Maxwell distribution, the temperature of which decreases exponentially during the energy exchange with the moderator. The thermalization time constant was found to be about 7 μsec.

A direct measurement of the slowing down time, combining the two principles now mentioned, was performed by Crouch (4), who made a time analysis of the neutron capture in a boron counter without and with a cadmium shield, using a weak Po-Be source, the time for neutron emission being given by the accompanying 4.4 MeV γ-ray. The difference between the two measurements gives the rate of arrival into the region below the cadmium cut-off. The result was a mean slowing down time of 5.2 μsec to 0.35 eV.

Since the values of the slowing-down times presented are in disagreement, and as Monte Carlo calculations (5, 6) indicated a large error in the most direct measurement, we decided to make a more thorough investigation of the slowing down and thermalization process using the pulsed source method.

Principles of the present investigation

With the low intensity of the available neutron source, only an integral measurement, similar to the earlier ones, could be made. However, to yield improved information, the experiment ought to be improved in several respects. 1. The neutron pulse must be short, 0.5 μsec being the maximum tolerable. 2. The time analyzer must have an equally short channel width. 3. The detector must be fast. 4. Time-of-flight effects in detectors and outside moderating assemblies must be reduced or eliminated.

In connection with the choice of a suitable detector the limited value of the boron counter must be pointed out. Its 1/v sensitivity makes it a neutron density detector, and to get energy selective information by the use of it, the sensitivity has to be modified for example by a shield, the neutron absorbing properties of which are energy dependent. The time resolution which can be achieved with a boron counter is also rather bad. To study the moderation in water it would therefore be advantageous to use a method without the mentioned limitations.

In our investigation we have used the following method for the detection. A small amount of a neutron capturing element of known cross section is dissolved in water. Of the fast neutrons injected in the medium, some are captured in the solute during the slowing-down process. The capture γ-rays are detected by a fast scintillation counter. The counting rate depends on the time-varying energy spectrum and the capture cross section of the solute. Thus the added element serves as a spectrum indicator for the slowing-down process.

There are several advantages with this method of measurement. 1. The detector is fast, a time resolution of 10 mμsec being easily obtained. 2. The measurement is made within the medium. 3. The medium is practically undisturbed, since there is no tube for extraction of neutrons, and the amount of absorber added is very small. 4. Time-of-flight effects are completely absent. 5. The energy sensitivity can be chosen by the use of elements of suitable capture cross sections.

In the experiments to be described here, cadmium and gadolinium are chosen for the neutron detection. Having large cross sections with strong deviations from the 1/v-law in the thermal region (Fig. 1), they can be expected to give information about the state of affairs in the near-thermal region. It is also natural to get a connection with earlier work using cadmium. The two cross sections have quite different shapes, which should manifest itself in a large difference in the reaction rate curve for the two elements.

Experimental procedure

Fast neutrons are produced in bursts by the Li(p,n) reaction at the center of a tank of water, the volume being 1 m^3. The proton source is the 5.5 MV van de Graaff generator in Studsvik. The neutron absorber solution is contained in a 250 cm^3 plastic bottle which can be placed at a chosen position. The γ-rays are detected by a plastic scintillator, linked to a photomultiplier above the water tank by a lucite light guide. The whole γ-ray detection arrangement has practically no disturbing effect in the water, the neutron cross sections for lucite and water being very similar. Before the time analysis the detector pulses pass through a discriminator, which is used to suppress the γ-ray background from neutron capture in water. The time between successive neutron bursts is long enough to assure complete thermalization of each neutron burst before the next is injected. The time resolution is 0.30 μsec.

Preliminary results of the measurements

In Fig. 2 the first results of the measurements, the reaction rates between the changing flux and the cross sections of cadmium and gadolinium, are shown. The curves are corrected for overlap and dead-time in the analyzer, and the contribution from neutron capture in water is subtracted. The curves have been normalized at the end of the time period for ease of comparison. The plastic bottle was placed 10 cm from the neutron source.

It is immediately evident that the peak in the cadmium curve at 4 μsec must depend on the cadmium resonance, which has the energy of 0.18 eV. The mean energy of the flux seems to pass the resonance at this time. Gadolinium has a low cross section at this energy, which explaines the low reaction rate in the gadolinium curve at this time. Later, both curves approach an almost horizontal line. From about 7 μsec the cadmium curve can be described as a sum of two exponentials, with time constants of about 4 and 200 μsec respectively. (More precise values will be

measured within short.) For gadolinium the same seems to be true in the same region, the fast exponential being smaller in amplitude and of opposite sign.

The slow decay expresses the normal neutron absorption in water during the time when the neutrons are in thermal equilibrium with the slightly absorbing medium. In a separate measurement without any foreign element added to the water, this exponential decay law is found to be valid from the very beginning of the curve for the reaction between the flux and the protons. Hence no appreciable changes in the neutron density occur in the volume of interest during the fast exponential. Therefore, the fast decay reflects mainly the effect of moderation.

It is reasonable to assume that the neutron distribution is near Maxwellian with a higher temperature even some time before the thermalization is finished. It is then of interest to see how the effective cross sections of the chosen elements depend on the temperature. From the tables of Westcott (7) the relative deviation from the room temperature value of the effective cross section may be calculated, Fig. 3. (The deviation is of interest here since in the exponential division, the subtraction of the slow decay implies both correction for absorption and subtraction of the effective cross section at room temperature.) The figure shows that the deviation is a linear function of temperature. In our experiment, we measure in fact the effective cross section if we have no effects of neutron density changes. Therefore an exponential decay of the reaction rate means an exponentially decreasing temperature. Thus the fast decay constant is the thermalization time constant.

The neutron temperature concept being somewhat obscure, the thermalization time constant may be defined in other ways. A popular method in the theorists' treatment of the time-dependent flux during thermalization is the following:

$$\varphi(E,t) = \sum_{\nu} \varphi_{\nu}(E) \cdot e^{-\lambda_{\nu} t}$$

where $\frac{1}{\lambda_o}$ is the decay constant for the equilibrium distribution

(Maxwellian) and $\lambda_1 = \lambda_0 + \frac{1}{t_{th}} \sim \frac{1}{t_{th}}$ if λ_0 is small, t_{th} being named the thermalization time constant (8). Using this formalism, the reaction rate is

$$R(t) = \int \varphi(E,t) \cdot \Sigma(E)\, dE = \int \sum_{\nu} \varphi_{\nu}(E) \cdot \Sigma(E) \cdot e^{-\lambda_{\nu} t}\, dE = R_0 e^{-\lambda_0 t} +$$

$$+ R_1 e^{-\lambda_1 t} + \ldots\ldots$$

This means that the fast decay constant even in this respect should be considered as the thermalization time constant if the higher terms can be neglected. The preliminary numerical value obtained here agrees rather well with recent theoretical predictions by Purohit (9).

Further experimental and theoretical work is under way. Among other things it is important to study the space dependence of the time behaviour.

References:

1. S. Glasstone and M. Edlund, The Elements of Nuclear Reactor Theory
2. J.A. DeJuren, Nuclear Sci. and Eng. 2, 408 (1961)
3. G.F. von Dardel, Trans. Royal Inst. Techn. Stockholm 75 (1954)
4. M.F. Crouch, Nuclear Sci. and Eng. 2, 631-639 (1957)
5. T.J. Krieger and F.D. Federighi, Trans. Am. Nucl. Soc. 2, 102-103 (1959)
6. G.E. Haynam and M.F. Crouch, Nuclear Sci. and Eng. 2, 626-630 (1957)
7. C.H. Westcott, AECL - 1101 (1960)
8. S.N. Purohit, Nuclear Sci. and Eng. 9, 157-167 (1961)
9. S.N. Purohit, private communication.

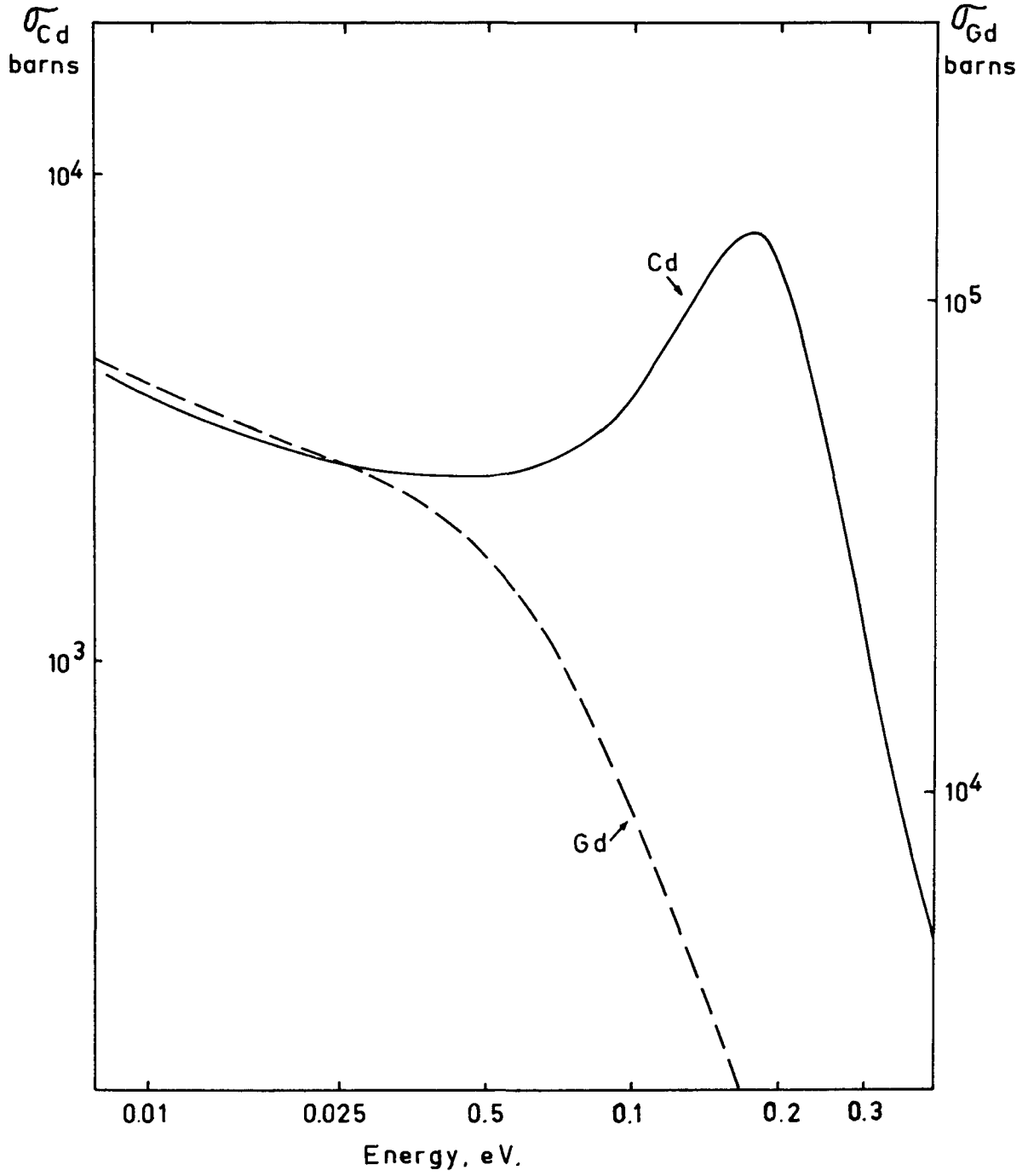

Fig.1. Thermal neutron cross sections of cadmium and gadolinium.

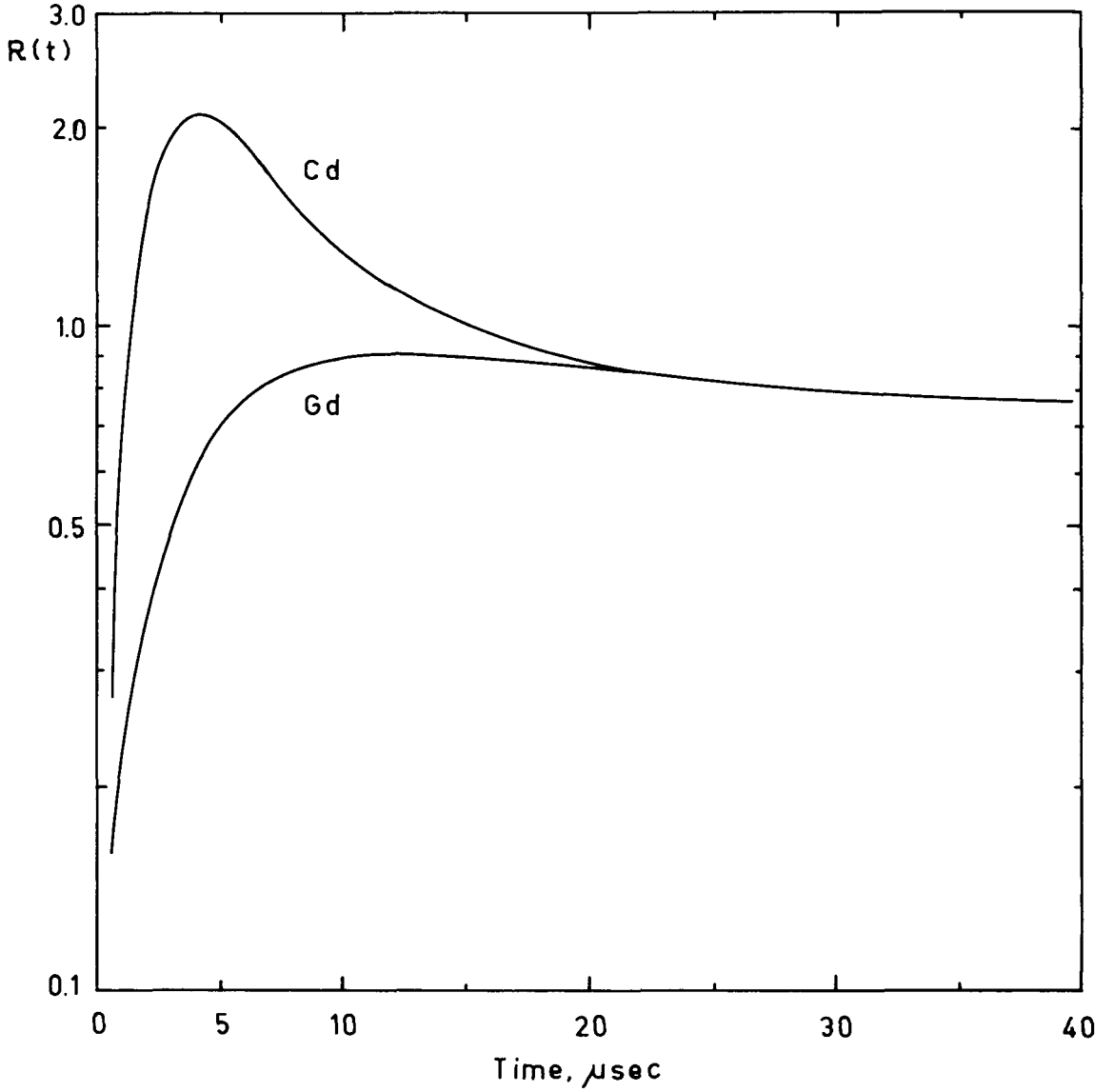

Fig. 2. Reaction rate between the slowing-down flux and cadmium and gadolinium respectively. Time resolution 0.30 μsec.

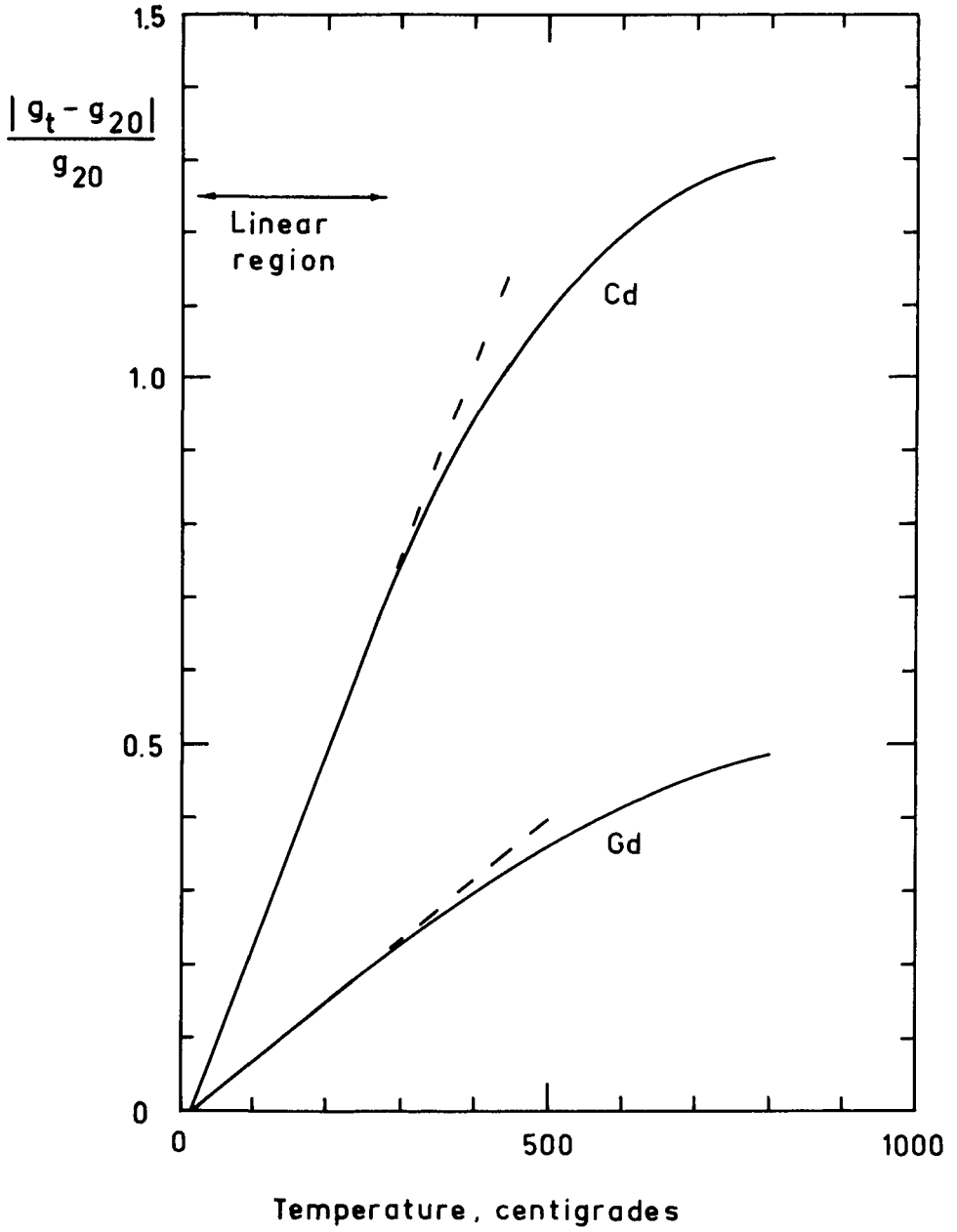

Fig.3. Relative deviation with temperature of the effective neutron cross sections of cadmium and gadolinium in a Maxwell flux.

DIFFUSION LENGTH MEASUREMENTS OF THERMAL NEUTRONS IN WATER*

M. Reier+ and J. A. DeJuren+
Bettis Atomic Power Laboratory

Steady state diffusion measurements of thermal neutrons have been made in water at 23°, 49°, 70°, 165.6°, and 244.4° centigrade and at 23° with various amounts of boron poison and one cadmium poison.

Because of the unavailability of an intense reactor source of thermal neutrons, an Sb^{124}-Be photoneutron source was used in all the measurements. The neutrons are emitted at an energy of about 24 kev and slow down into the thermal region. The diffusion equation, therefore, has a source term, q, which varies as $e^{-r/b}/r^2$ at large distances from the source. The relaxation length of the fast neutrons, b, was measured to be 1.58 $\pm$ 0.02 cm. The solution of the inhomogeneous diffusion equation, assuming spherical symmetry, varies as $e^{-r/L}/r$ multiplied by a slowly-varying correction term which involves exponential integrals. Fortunately, it is not necessary to know the absolute value of the source strength in order to evaluate the correction. It is sufficient to know the ratio of the thermal neutron density to the slowing down density. This is accom-

---

* This summarizes the work reported in J. Nucl. Energy 14, 18 (1961) and J. Nucl. Energy 14, 186 (1961).

+ Now at Atomics International, Canoga Park, California.

plished by effectively measuring the cadmium ratio as a function of radius and the ratio of the integrals $\frac{\int A_{Cd} r^2 dr}{\int A_{th} r^2 dr}$, where A_{Cd} and A_{th} are the activities of Cd-covered foils and bare minus Cd-covered foils, respectively. The correction for the source term should be made if possible as it reduces the measured L by 0.8% for pure water at 23°C evaluated for r between 15 and 25 cm. Usually ln (rA_{th}) vs. r appears to be a straight line within statistics in the region where L is evaluated. In spite of this, the correction for the source term is not negligible and cannot be accurately inferred from the change in L from the region where the curve is obviously bending. This correction becomes progressively greater at a given radius as L approaches b and breaks down for $L \leqslant b$. As L approaches b, data should be taken farther from the source.

Indium-tin foils were used except in some of the high temperature measurements where foils made of dysprosium oxide in an aluminum oxide matrix were employed. All foils were counted in continuous gas-flow proportional counters on both sides and the results averaged.

The data is shown in Table I. ρ/ρ_o is the specific gravity.

T°C	L(cm)	L ρ/ρ_o (cm)
23	2.781 ± 0.006	2.775 ± 0.006
49	2.895 ± 0.011	2.862 ± 0.011
70	3.024 ± 0.013	2.957 ± 0.013
90	3.162 ± 0.006	3.051 ± 0.006
166*	3.653 ± 0.017	3.302 ± 0.016
244*	4.328 ± 0.025	3.497 ± 0.020
$\Sigma_{aB} = 0.5\,\Sigma_{aH}$	2.270 ± 0.011	
$\Sigma_{aB} = 1.0\,\Sigma_{aH}$	1.951 ± 0.011	
$\Sigma_{aB} = 1.5\,\Sigma_{aH}$	1.806 ± 0.006	
$\Sigma_{aCd} = 1.5\,\Sigma_{aH}$	1.762 ± 0.004	

* Uncorrected for the source term.

The pure water measurements were compared with a theoretical model suggested by Radkowsky (ANL-4476). This model averages the flux-weighted diffusion constant and cross section over the Maxwellian spectrum to obtain L^2.

$$D = \frac{D_o}{v} \quad \frac{\lambda_{sc}}{3(1 - \overline{\cos\theta})},$$

where $\overline{\cos\theta} = 2/3A$. A is the effective mass of the target and is assumed to be a free proton whose mass increases from a value of one when σ_{sc} = 20b to a value determined by the energy dependence of the scattering cross section of neutrons in water as given by the Born approximation.

$$\sigma_{sc}(E) = K\mu^2,$$

where μ, the reduced mass of the neutrons, equals A/A+1. The calculated value is higher than the measured diffusion length by about one percent at 23°. This divergence increases to about six percent at 244°C. The Selengut-Goertzel approximation is implicit in the calculations and may cause the calculated value to be high by about one percent at 23°C.

A plot of $1/L^2$ vs. Σ_a/Σ_H for the poisoned cases shows a departure from linearity at $\Sigma_a/\Sigma_H = 2.5$, the highest poison used. Based on measurements by E. Starr (private communication) who used a thermal column on the Brookhaven reactor and consequently did not require a large source term correction, this departure may be spurious and the value reported here may be in error. A weighted average of $L^2\Sigma_a$ for $\Sigma_a/\Sigma_H = 1.0$, 1.5, and 2.0 gives a value of $D_o = vD = 37618 \pm 205$ cm^2/sec. The boron cross section was assumed to be $755 \pm 2b$. In addition, the ratio σ_{aB}/σ_{aH} was calculated in terms of the ratio of L^2 for the different amounts of poison assuming D_o is a constant and $\sigma_{aB} = 755 \pm 2b$. A value of $\sigma_{aH} = 0.328 \pm 0.006$ is obtained.

Experimental Investigation of Persisting Changes in the Thermal Neutron Decay Constant in Finite Media of Ice and Beryllium as a Function of Temperature and Buckling

E. G. Silver

Oak Ridge National Laboratory*
Oak Ridge, Tennessee

ABSTRACT

During investigations of the decay constant of the fundamental-mode neutrons in finite beryllium bodies, using the pulsed-neutron-source technique, it was observed that long-term changes in the decay "constant" occurred which were not expected on the basis of the approximate solutions of the transport equations usually applied to this experiment.

More extensive experiments in both beryllium and water (ice) as a function of temperature from + 25°C to - 100°C showed that in beryllium such changes, which continue over the time span accessible to observation (approximately 10 half-lives), are a strong function of temperature and buckling, increasing with buckling, and decreasing with increasing temperature. In ice, on the other hand, it appears that, within the limits of experimental accuracy, an asymptotic value of the decay constant is attained a few thermal-neutron half-lives after the neutron burst at all temperatures down to - 100°C.

These observations are in accord with the "trapping effect" postulated by G. de Saussure in another paper submitted to this Conference.

1. Introduction

For some time G. de Saussure and the author have been engaged in measurements of the diffusion parameters of beryllium metal by the pulsed-neutron source method at elevated temperatures up to 500°C, at

---

*Operated by Union Carbide Nuclear Company for the U. S. Atomic Energy Commission.

room temperature, and more recently at low temperatures in the range down to - 100°C.[1,2,3]

We had long observed that measurements of the decay constants in small assemblies (large buckling) at room temperature, and on all bodies at very low temperatures, yielded results which appeared to continue to exhibit small changes for long periods after the neutron pulse which, by their duration, could not be ascribed to either spatial modes or "primary" thermalization effects.

In a companion paper to this one, G. de Saussure describes a theoretical model which apparently accounts for the observed effects in beryllium. In this paper experimental evidence supporting this model will be presented.

Since there existed the possibility that instrumental or analytical difficulties might be the cause of a spurious effect, similar measurements to those performed in beryllium were also done in H_2O (ice). It was expected that, if the theoretical model were valid and if a spurious effect did not exist, the H_2O data would not exhibit changes in the decay constant, or that they would at least be at a very much reduced amplitude, since the ratio of incoherent to coherent scattering cross sections is much smaller in H_2O (ice) than in beryllium. Thus, in H_2O (ice) no significant trapping effect would be expected, and much less change in the decay constant should occur after thermalization has occurred.

2. The Experiment

The beryllium data were obtained with neutrons of about 14 Mev incident on the beryllium assembly. Following a waiting period after

the end of the burst, some of the moderated neutrons leaking from the assembly were detected in a Li^6-I crystal-photomultiplier detector, and the counts stored in an 18-channel time analyzer with variable channel width. Immediately following the closing of the gate in the 18th channel the next burst was delivered to the assembly.

The data from the 18 channels, or selected portions thereof, were then analyzed by means of the "Cornell Method"[4] fitting to the equation

$$C(t) = a_0 + a_1 \exp(-\lambda t)$$

where $C(t)$ is the detector count rate at time t, a_0 and a_1 are constants, and λ is the presumed asymptotically constant value of the fundamental mode decay constant.

That is to say, N_i, the number of counts in the ith channel (of width (Δt)) is given by

$$N_i = a_0(\Delta t) + a_1 \exp\left[-\lambda i(\Delta t)\right] \quad .$$

The variance of λ was calculated from the deviations of the observed N_i from the calculated values obtained by the best fit to the points analyzed.

It is, therefore, apparent that deviations in the decay from the shape assumed in the model will be reflected in an increased variance associated with the values of the parameters. The analysis does not weight the data points by the counting statistics and is, therefore, strictly applicable only if all the data points have enough counts so as to make counting statistics a negligible source of error. In the data presented here this condition holds fairly well. The statistical uncertainties in the decay constants are of the order of fractions of

a percent, so that the large standard deviations shown are almost entirely due to the variation of λ with time over the interval of analysis.

In order to determine the change in decay constant with time, successive portions of the 18-channel data series were separately analyzed utilizing four overlapping series of 15 channels each (1-15, 2-16, 3-17, and 4-18), or seven overlapping series of 12 channels each (1-12, ..., 7-18).

In order to facilitate comparisons between changes in decay curves observed in different materials and with different bucklings all curves of decay constant vs time are plotted in time units of the reciprocal decay period, $T = 1/\lambda$, using the "best" measured value of λ. Further, the decay constants are in all cases normalized to unity for the value obtained in the analysis commencing as close as possible to $t = T$ after the end of the neutron burst. All values of λ are, therefore, relative to this norm for each material and buckling. In several cases more than one run was made at a given condition, with varying waiting times to the beginning of data collection, in order to extend the time of observation. In such cases all the points from all the runs are normalized to the first point.

Figure 1 shows the results for a beryllium block of dimensions 8" x 8-5/8" x 8-5/8" whose buckling (fundamental mode buckling at room temperature is meant in all cases) is 0.054 cm^{-2}, both at 25°C and at - 98°C. Each point represents a value from an analysis extending over a time interval of about 4.7 T, i.e. the first point in each curve represents a value obtained in the interval from 1 T to 5.7 T, whereas

the last point is obtained from data covering the interval from about 1.9 T to 5.6 T. The relatively large errors, of the order of $\pm$ 2% to $\pm$ 4%, are due largely to the large variation in λ over the course of each measurement, as discussed above. It will be noted that lower temperature leads to larger variation. At 175°K the variation per unit time is about 3.6 times as big as at 300°K in this case. While the errors are large, as noted, there is no evidence, over the interval shown, of a diminution of the rate of decrease of λ with time.

Figure 2 shows the same information for a larger beryllium assembly of dimensions 12" x 14-3/8" x 14-3/8" whose buckling is 0.0236 cm^{-2}, both at 0°C and at - 96°C. There is no evidence of change in the decay constant within experimental limits of accuracy at 0°C. Accordingly the errors in this case appear much smaller, being of the order of $\pm$ 0.5% to $\pm$ 0.8%. At the low temperature in the same assembly the same linearly changing behavior is noted as in the two cases shown in the previous figure.

Since these data all terminate with analyses beginning at approximately 1.9 T (i.e. extending from 1.9 T to about 6.6 T), further experimental data were obtained with still longer waiting times to determine whether the rate of change of slope would continue unaltered for longer times. Such data are difficult to obtain with the equipment available since it makes extreme demands on background suppression and source intensity. By long counting times and careful minimizing of background, it was possible to extend the observation time to about 8 T.

A beryllium assembly of dimensions 11.5" x 11.5" x 9" (B^2 = 0.0359 cm^2) was pulsed, therefore, with extended waiting times at both 25°C and - 25°C. Figure 3 shows the result of 12-channel analyses from two runs at 25°C. After an initial decrease in λ which extends to the 12-channel segment of data 2.4 T to 5.7 T, there is no further evidence of change in λ as far as the data extend. The later values are all, within the probable errors, consistent with a constant value from 2.4 T on.

Figure 4 gives the data for the same beryllium assembly but at - 25°C. The difference is obvious. In this case there is no evidence of leveling out and the large probable errors associated with changing slope are observed. In this case, then, with data extending to 7.3 T (the last point represents an analysis from 4.2 T to 7.3 T) an almost constant rate of change of slope with time is observed.

As a check on possible instrumental sources of the observed change in λ as well as to test the predictions of the theoretical model, similar measurements extending to long waiting times were carried out on a right-cylindrical ice block with a buckling of 0.300 cm^{-2}. Figure 5 shows the results at - 5°C, and Figure 6 gives the results at - 90°C. In ice the familiar initial drop observed in all small bodies, ascribable to higher modes or slowing down, is seen; but thereafter the value of λ levels out even at the very low temperature and remains constant within the limits of accuracy of the experiment.

It should be observed that the H_2O data were obtained using 2.4-Mev neutrons from the D-D reaction, even though the yields from this reaction are much smaller than the yields from the D-T reaction.

This change was necessitated by the large neutron background observed in H_2O experiments with 14-Mev neutrons. This large background was due to photoneutrons from the heavy hydrogen component of the water; the gammas initiating these photoneutron reactions arise from the decay of 7.4 sec N^{16} which, in turn, was produced by the primary neutrons from the $O^{16}(n,p)N^{16}$ reaction. In view of the long half-life of the N^{16} this reaction sequence caused a flat neutron background. The use of 2.4-Mev D-D neutrons eliminated this source of background since the threshold for the (n,p) reaction is about 10.5 Mev. (The cross section at 14 Mev is 51.2 mb.)[5]

3. Conclusion

In all the curves, except in the largest Be assembly, the analyses commencing prior to about 2 T after the end of the neutron burst show a decrease in λ which is most likely associated with "primary" neutron thermalization or higher modes and which, therefore, is expected even if no long-term spectrum-change effects exist. Its absence in the case of the largest Be assembly may be ascribed to the fact that in this case T is large and, therefore, "primary" thermalization is essentially complete at 1.1 T when the data analysis begins. The decrease in λ in the same assembly at low temperatures is thus to be ascribed to the long-term effect. Table I summarizes the decay constants and initial rates of change of λ observed in all the cases presented here.

At times greater than 2T the value of λ became constant in the Be assembly at the high temperature, and in the H_2O block at both high and low temperatures, whereas in Be even at the relatively high

temperature of - 25°C no evidence of leveling out was observed over the time span accessible to observation.

To the limited extent that these data permit, it may thus be concluded that a long-term spectrum-change effect does exist in Be which is absent or much reduced in magnitude in H_2O, and thus these data support the model discussed by de Saussure.

TABLE I

Values of λ and Initial Rate of Change of λ in H_2O and Be Bodies

Material	Buckling cm^{-2}	Temp. ^{o}C	λ at t = 2T 10^3 sec^{-1}	% Change in λ per time T from $\sim T \rightarrow \sim 2T$	Figure No.
Be	0.054	+25	6.59 ± .11	2.4	1
		-98	5.99 ± .21	6.6	1
	0.0359	+25	4.53 ± .02	2.0	3
		-25	4.25 ± .06	3.8	4
	0.0236	0	2.90 ± .02	0	2
		-96	2.54 ± .04	5.7	2
H_2O	0.300	-5	12.58 ± .09	1.8	5
		-90	11.34 ± .08	1.9	6

REFERENCES

1. G. de Saussure and E. G. Silver, "Determination of the Neutron Diffusion Parameters in Room-Temperature Beryllium," ORNL-2641 (1959).

2. G. de Saussure and E. G. Silver, "Measurements of the Transport Mean Free Path of Thermal Neutrons in Beryllium as a Function of Temperature," Nuclear Sci. and Eng. 6, No. 2 (1960).

3. G. de Saussure and E. G. Silver, "Pulsed-Neutron Measurements in Beryllium," Neutron Phys. Ann. Prog. Rep., Sept. 1, 1961, ORNL-3193, pp. 215-222; G. de Saussure, "A Note on Measurements of Diffusion Parameters by the Pulsed-Neutron Source Technique," Neutron Phys. Ann. Prog. Rep., Sept. 1, 1961, ORNL-3193, pp. 223-228.

4. R. G. Cornell, "A New Estimation Procedure for Linear Combinations of Exponentials," ORNL-2120 (1956).

5. N. Tralli et al., "Neutron Cross Sections for Titanium, Potassium, Magnesium, Nitrogen, Aluminum, Silicon, Sodium, Oxygen, and Manganese," UNC-5002, p. 102 (January 31, 1962).

March 23, 1962

Fig. 1

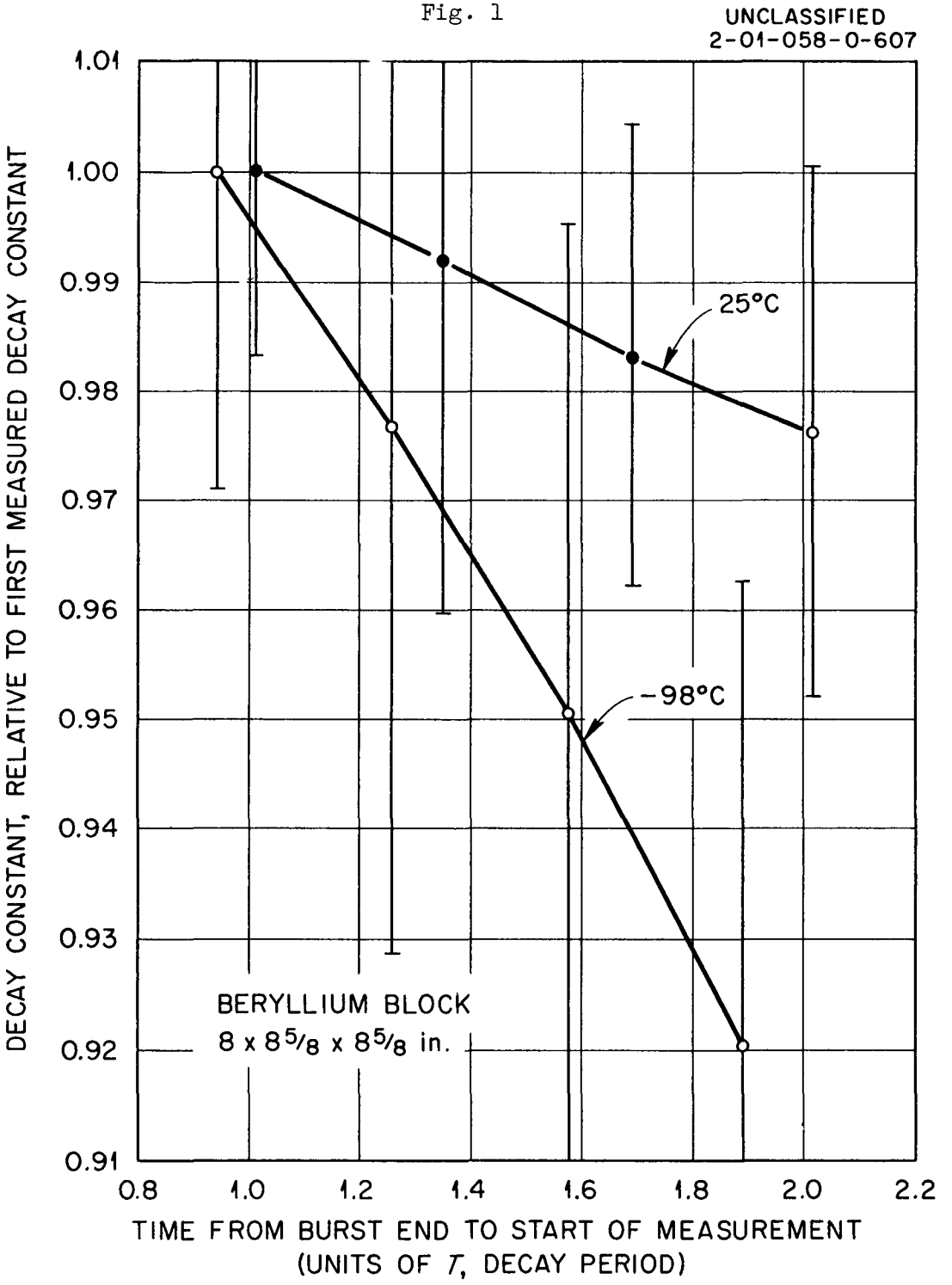

Relative Values of Decay Constant, λ, as a Function of Time Elapsed Between End of Neutron Pulse and Start of Data Analysis. Time is in units of $T = 1/\lambda$; λ normalized to unity at about $T = 1$. The lines are drawn to connect points obtained from the same run and do not represent the rate of change in λ.

Fig. 2

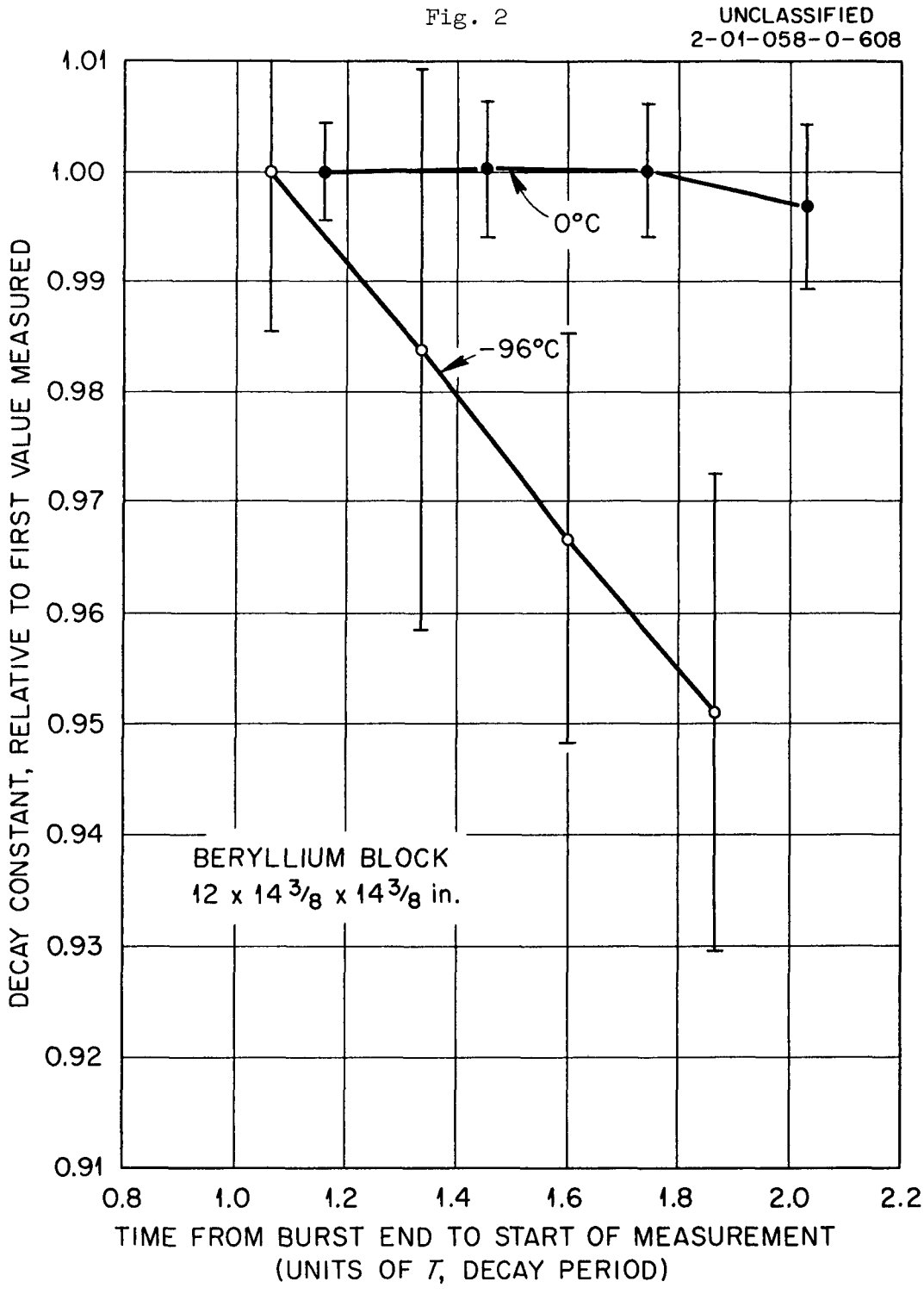

Relative Values of Decay Constant, λ, as a Function of Time Elapsed Between End of Neutron Pulse and Start of Data Analysis. Time is in units of $T = 1/\lambda$; λ normalized to unity at about $T = 1$. The lines are drawn to connect points obtained from the same run and do not represent the rate of change in λ.

Fig. 3

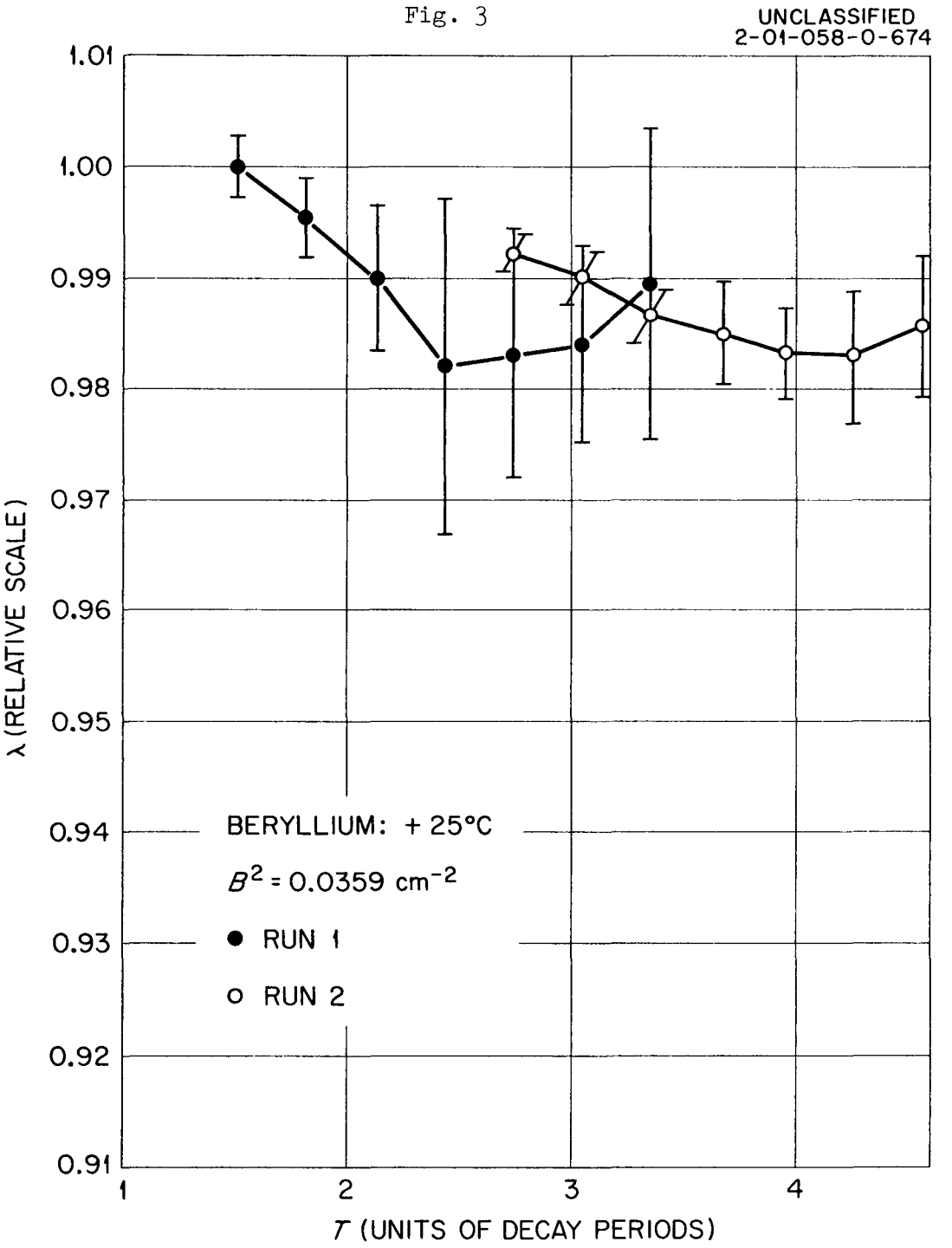

Relative Values of λ as Functions of Time Elapsed Between End of Neutron Pulse and Start of Data Analyzed. Time is in Units of $\mathcal{T} = 1/\lambda$; λ is Normalized to Unity at $\sim\mathcal{T} = 1$.

The lines are drawn to connect points obtained from the same run and do not represent the rate of change in λ.

Fig. 4

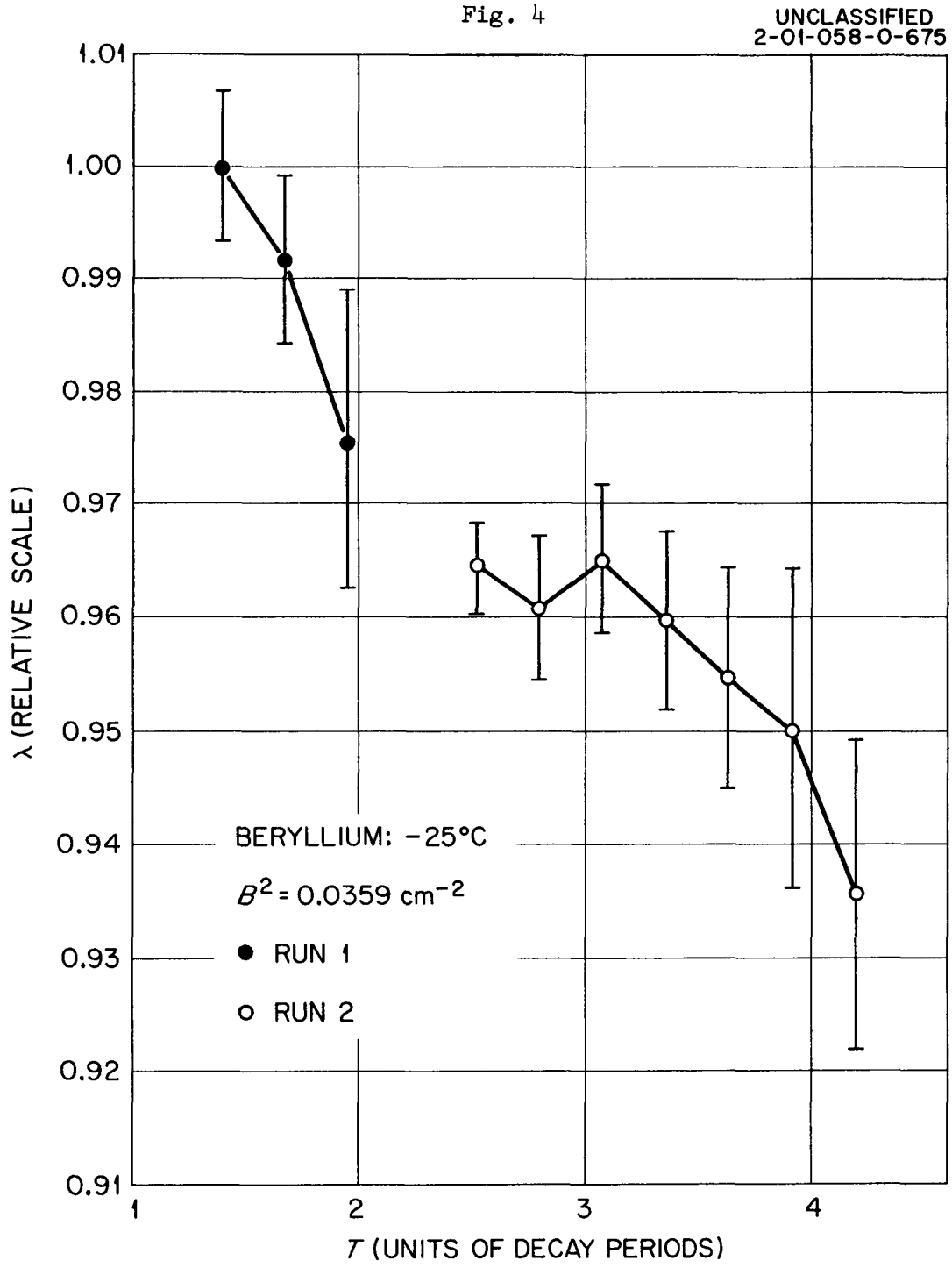

Relative Values of λ as Functions of Time Elapsed Between End of Neutron Pulse and Start of Data Analyzed. Time is in Units of $\mathcal{T} = 1/\lambda$; λ is Normalized to Unity at $\sim\mathcal{T} = 1$.

The lines are drawn to connect points obtained from the same run and do not represent the rate of change in λ.

Fig. 5

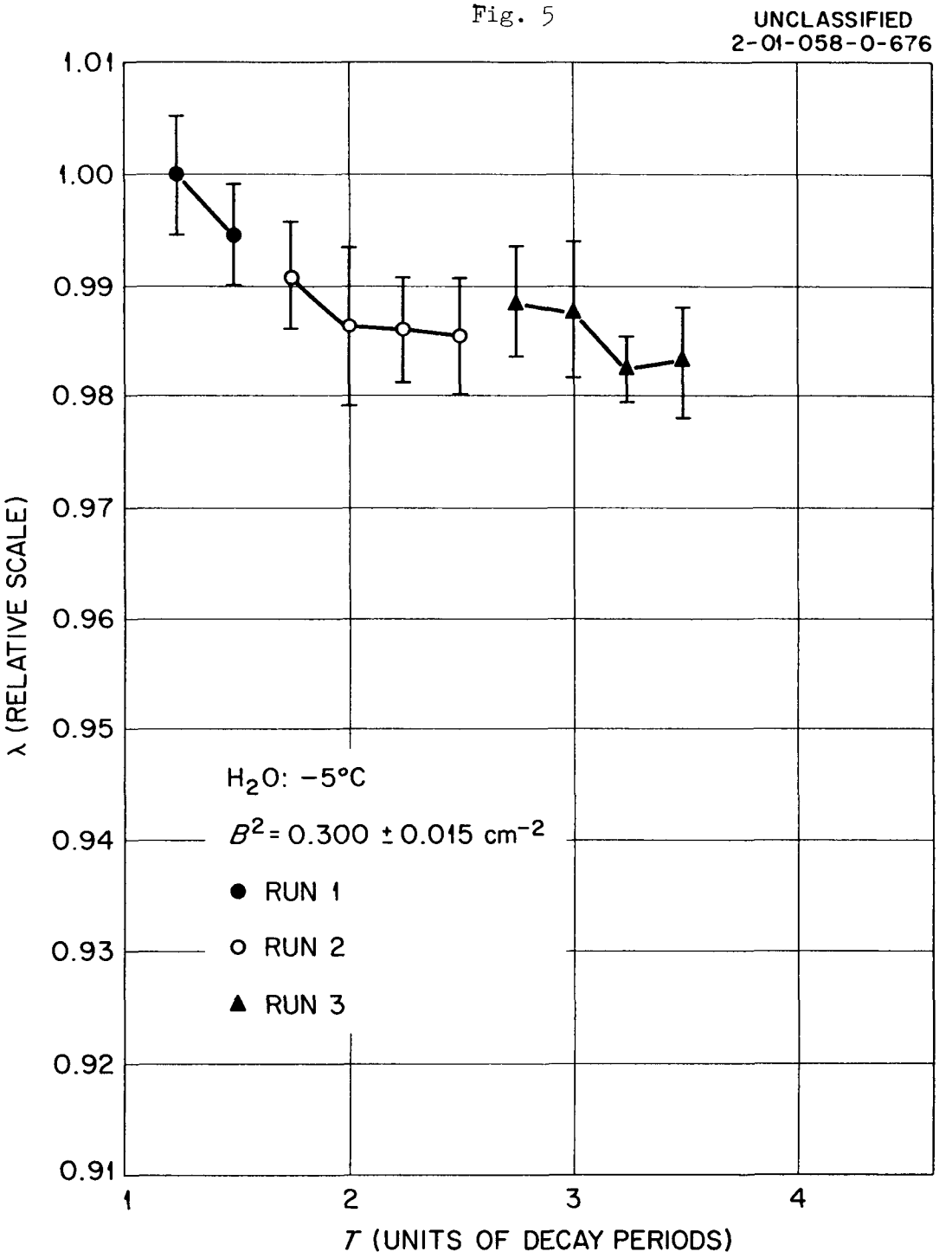

Relative Values of λ as Functions of Time Elapsed Between End of Neutron Pulse and Start of Data Analyzed. Time is in Units of $T = 1/\lambda$; λ is Normalized to Unity at $\sim T = 1$.

The lines are drawn to connect points obtained from the same run and do not represent the rate of change in λ.

Fig. 6

UNCLASSIFIED
2-01-058-0-677

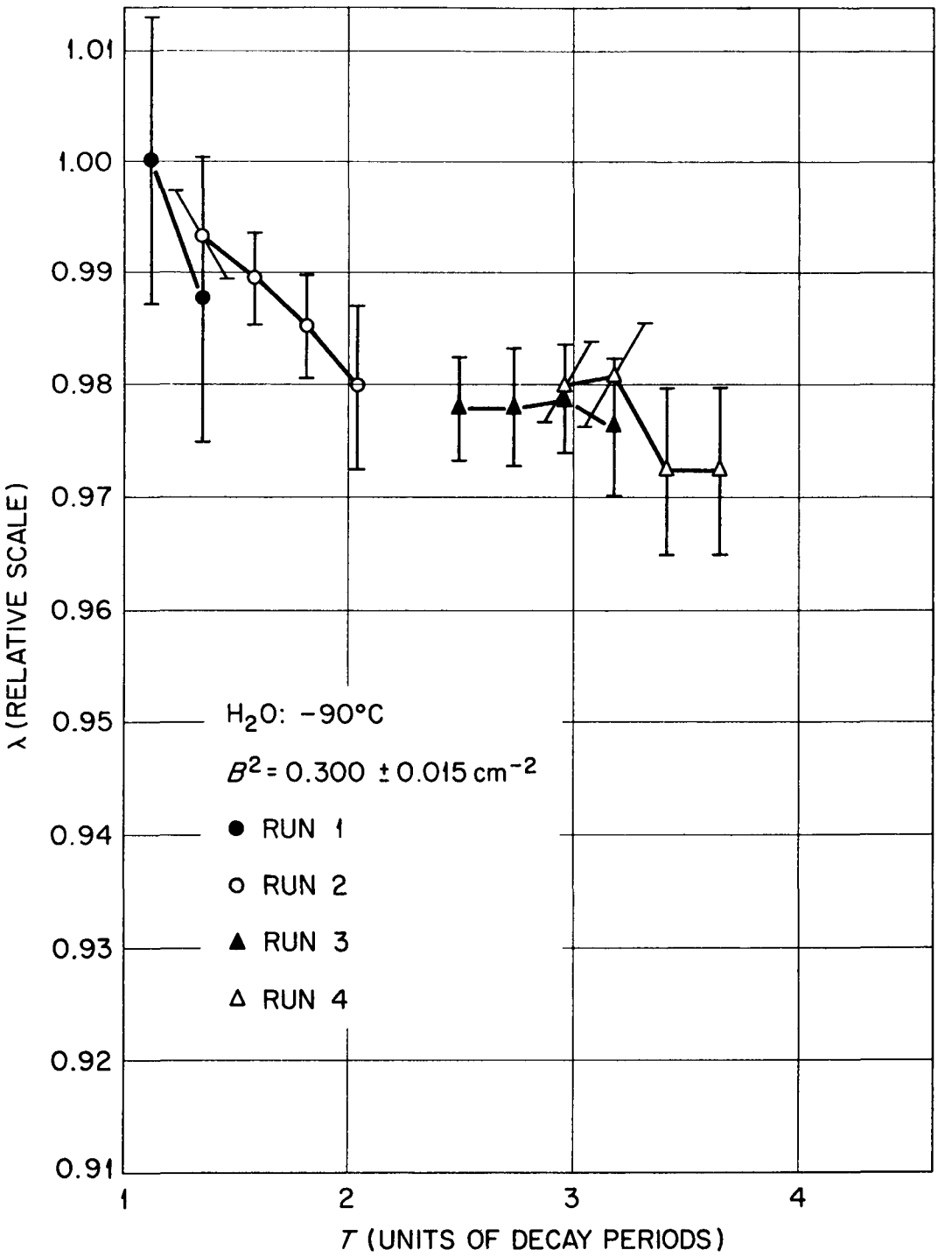

Relative Values of λ as Functions of Time Elapsed Between End of Neutron Pulse and Start of Data Analyzed. Time is in Units of $T = 1/\lambda$; λ is Normalized to Unity at $\sim T = 1$.

The lines are drawn to connect points obtained from the same run and do not represent the rate of change in λ.

DETERMINATION OF DIFFUSION COOLING IN GRAPHITE BY MEASUREMENT OF THE AVERAGE NEUTRON VELOCITY

E. Starr and J. W. L. de Villiers*

Brookhaven National Laboratory
Upton, New York

January 2, 1962

* On leave from South African Atomic Energy Board.

ABSTRACT

The diffusion cooling coefficient in graphite has been determined by measuring the change in the asymptotic average velocity with buckling, by pulsed neutron methods. The times necessary to establish equilibrium spectra in graphite and heavy water have been measured and are reported.

Theory

If a moderator has been injected with a burst of neutrons, the asymptotic decay constant is given by

$$\lambda = \lambda_o + \overline{Dv}\, B^2 \left[1 - C'B^2 + \ldots\ldots \right] \tag{1}$$

which if D is constant can be rewritten

$$\left[\frac{\lambda - \lambda_o}{B^2 D} \right] = \bar{v} = \bar{v}_o \left[1 - C'B^2 + \ldots\ldots \right] \tag{2}$$

Therefore a direct measurement of the average velocity as a function of buckling will yield the diffusion cooling coefficient.

The average of a given neutron velocity distribution can be measured by comparing the response of two detectors with sensitivities which differ in behavior as a function of velocity. The measurements described below were done using BF_3 detectors: one in which every neutron is counted, and a second which has a 1/v neutron response sensitivity.

The rate of absorption of neutrons in either detector is given as

$$\Sigma\phi = \int \Sigma(E)\, \phi(E)\, dE \tag{3}$$

where Σ is the absorption cross section.

The flux ϕ can be expanded in a set of time eigenfunctions of the form

$$\phi(E,t) = \sum_n A_n \phi_n\, e^{-\lambda_n t} \tag{4}$$

Equation (3) then becomes

$$\Sigma\phi = \sum_n A_n \langle \Sigma\phi_n \rangle\, e^{-\lambda_n t} \tag{5}$$

where

$$\langle \Sigma \phi_n \rangle = \int \phi_n \Sigma \, dE$$

The absorption cross section Σ depends on the nature of the detector. The ratio R of count rates of two different detectors will be given from equation (5) as

$$R = \frac{\sum_n A_n \langle \Sigma_1 \phi_n \rangle e^{-\lambda_n t}}{\sum_n A_n \langle \Sigma_2 \phi_n \rangle e^{-\lambda_n t}} \tag{6}$$

Rewriting the summation and factoring out the lowest eigenfunction ϕ_o leads to

$$R = \frac{\langle \Sigma_1 \phi_o \rangle}{\langle \Sigma_2 \phi_o \rangle} \left[\frac{1 + \frac{A_1}{A_o} \frac{\langle \Sigma_1 \phi_1 \rangle}{\langle \Sigma_1 \phi_o \rangle} e^{-(\lambda_1 - \lambda_o)t} + \cdots\cdots}{1 + \frac{A_1}{A_o} \frac{\langle \Sigma_2 \phi_1 \rangle}{\langle \Sigma_2 \phi_o \rangle} e^{-(\lambda_1 - \lambda_o)t} + \cdots\cdots} \right] \tag{7}$$

At sufficiently long times, the summation can be approximated by the expression involving the first order terms. If the denominator is small, it can be expanded in a power series:

$$R = \frac{\langle \Sigma_1 \phi_o \rangle}{\langle \Sigma_2 \phi_o \rangle} \left[1 + \frac{A_1}{A_o} \left(\frac{\langle \Sigma_1 \phi_1 \rangle}{\langle \Sigma_1 \phi_o \rangle} - \frac{\langle \Sigma_2 \phi_1 \rangle}{\langle \Sigma_2 \phi_o \rangle} \right) e^{-(\lambda_1 - \lambda_o)t} \right] \tag{8}$$

This equation relates the eigenfunctions ϕ and eigenvalues λ to R, to the ratio of the counting rates in the two detectors. At long times, R reduces to

$$R = \frac{\langle \Sigma_1 \phi_o \rangle}{\langle \Sigma_2 \phi_o \rangle} \qquad (9)$$

Equation (9) will then give the value of the ratio R after equilibrium is reached for a given size of moderator. Since Σ_1 is assumed to be constant for an energy range $0 \rightarrow E_1$ and Σ_2 varies as 1/v in this same interval, R is proportional to the density weighted average velocity $\bar{v}$. If the lowest eigenfunction ϕ_o is a maxwellian form, the error introduced by integrating from $0 \rightarrow \infty$ instead of to the finite limit E_1 is in our case about 1%.

During the transient period after the burst of neutrons, the ratio R will change. The approach to equilibrium will be governed by the decay constant $(\lambda_1 - \lambda_o)$.

Detectors

The detectors were two physically identical BF_3 proportional counters, filled to 70 cm pressure. The black detector contained 96% enriched Boron 10, and the grey detector contained 11% depleted Boron 10. The counters were placed in a sleeve of cadmium inside an annular cylinder of borated paraffin 3" in thickness. The leakage spectrum from a block of moderator was passed through a collimator of cadmium in the end of the sleeve, and into the detector parallel to its length.

Apparatus

The same pre-amplifier, amplifier and voltage supply were used for the two detectors, so as to eliminate any error associated with different electronics. Both detectors were operated at the same voltage plateau and discriminator settings. The neutron pulses were fed into a 100 channel time analyzer. To normalize runs with separate detectors, a monitor BF_3 detector

was used to record the total number of neutron counts. The burst of neutrons was obtained from a 1 MEV Van de Graaff generator by means of the Be^9 (d,n) Be^{10} reaction.

Procedure

The variations of detector sensitivities with energy were measured through use of neutrons from a crystal spectrometer. The variation of the ratio with energy is shown in figure 1. If R is assumed to be linear with velocity in the range 1.5×10^5 cm/sec to 4×10^5 cm/sec, the average value $\bar{R}$ for a maxwellian spectrum at 20°C differs by about 5% from the value of $\bar{R}$ obtained by using the general equation of the curve in figure 1, and averaging over the same maxwellian. Therefore the approximation of the linearity of ratio with velocity is justified for the range of this experiment.

The average velocity was determined for the sizes of graphite moderator listed in table 1. The graphite stacks were placed in an enclosure of cadmium covered boral to eliminate the effect of room return neutrons. The source was situated in the moderator. The collimator was aligned parallel to the graphite bars, so that the neutrons leaking out of a beam hole in one of the graphite bars entered the end of the detector in a direction parallel to the detector axis. The data were accumulated by the time analyzer, and the ratio was normalized by the ratio of total monitor counts obtained during the same time interval. The value of the ratio $\bar{R}$ for one of the stack sizes is shown in figure 2. Two different channel widths were used to record the data from each detector, to substantiate that the asymptotic value of $\bar{R}$ was reached, and to test the calibration of the time analyzer.

Results

The values of the asymptotic ratio as a function of buckling are tabulated in table 1 and plotted in figure 3. The value of the diffusion cooling coefficient for graphite was found to be $36 \pm 5 \times 10^5$ cm^4/sec.

The time necessary for $\bar{R}$ to reach the equilibrium value appears to be independent of buckling; and is approximately 2 milliseconds for graphite. Hence, this is the minimum waiting time in order to measure the fundamental decay constant in pulsed neutron experiments with graphite.

The time rate of change of $\bar{R}$ is shown in figure 4. It was obtained by subtracting the asymptotic value $\bar{R}$ from the curve of R as a function of time. Since the accuracy of the measurement is not extremely good, no attempt has been made to determine if the decay constant associated with $\frac{d\bar{R}}{dt}$ is buckling dependent. The decay constant given in figure 4 is an average for the five stacks shown. If the black triangles of stack 6 are typical of the decay constant, then the value of 1905 sec^{-1} should represent $(\lambda_1-\lambda_o)$ at a buckling of .00959. This may be compared with the values of λ_o and λ_1 obtained from the decay data of one of the detectors. We find the asymptotic decay constant λ_o is 1690 sec^{-1} while λ_1 is approximately 3500 sec^{-1}. The value of $(\lambda_1-\lambda_o)$ is then 1800 sec^{-1} which agrees very well with the value obtained from the measurement of time rate of change of $\bar{R}$.

The time for equilibrium has also been determined in a tank of heavy water, with the measurement showing that approximately 600 μsec is necessary for the higher modes to die away. From the value of the ratio obtained for this one tank, which had an equivalent buckling of .0076,

and with the value of $\bar{\nu}$ at $B^2 = 0$, an estimated value of the diffusion cooling coefficient of heavy water is 5×10^5 cm^4/sec.

Conclusion

The technique of using the average ratio of the two detectors is ideally suited to pulsed neutron measurements, if only to measure the time necessary to wait in order to determine the fundamental decay constant. The technique also yields information about thermalization beyond simply the equilibrium time. More information about the thermalization process can be obtained with improved systems of detectors.

Acknowledgement

The authors wish to thank Robert Schermer for his assistance in the use of the crystal spectrometer, and to Henry Honeck for his valuable discussions.

References

1. A. M. Weinberg and L. P. Wigner, "The Physical Theory of Neutron Chain Reactions", Univ. Chicago Press 1958.
2. M. S. Nelkin, "A Decay of a Thermalized Pulse," GA-816.
3. G. F. von Dardal and N. G. Sjöstrand, "Progress in Nuclear Energy," Series I, Vol. 2 (1958).
4. K. H. Beckurts, "Reactor Physics Research with Pulsed Neutron Sources".

Figure Captions

1. Ratio B^{10}/B^{11} Vs Velocity cm/sec - Neg. # 12-339-61.
2. Ratio Vs Time - Neg.# 12-198-61.
3. Average Neutron Velocity as a Function of Buckling - Neg. # 12-197-61.
4. Change of Average Velocity as a Function of Time - Neg. # 12-199-61.

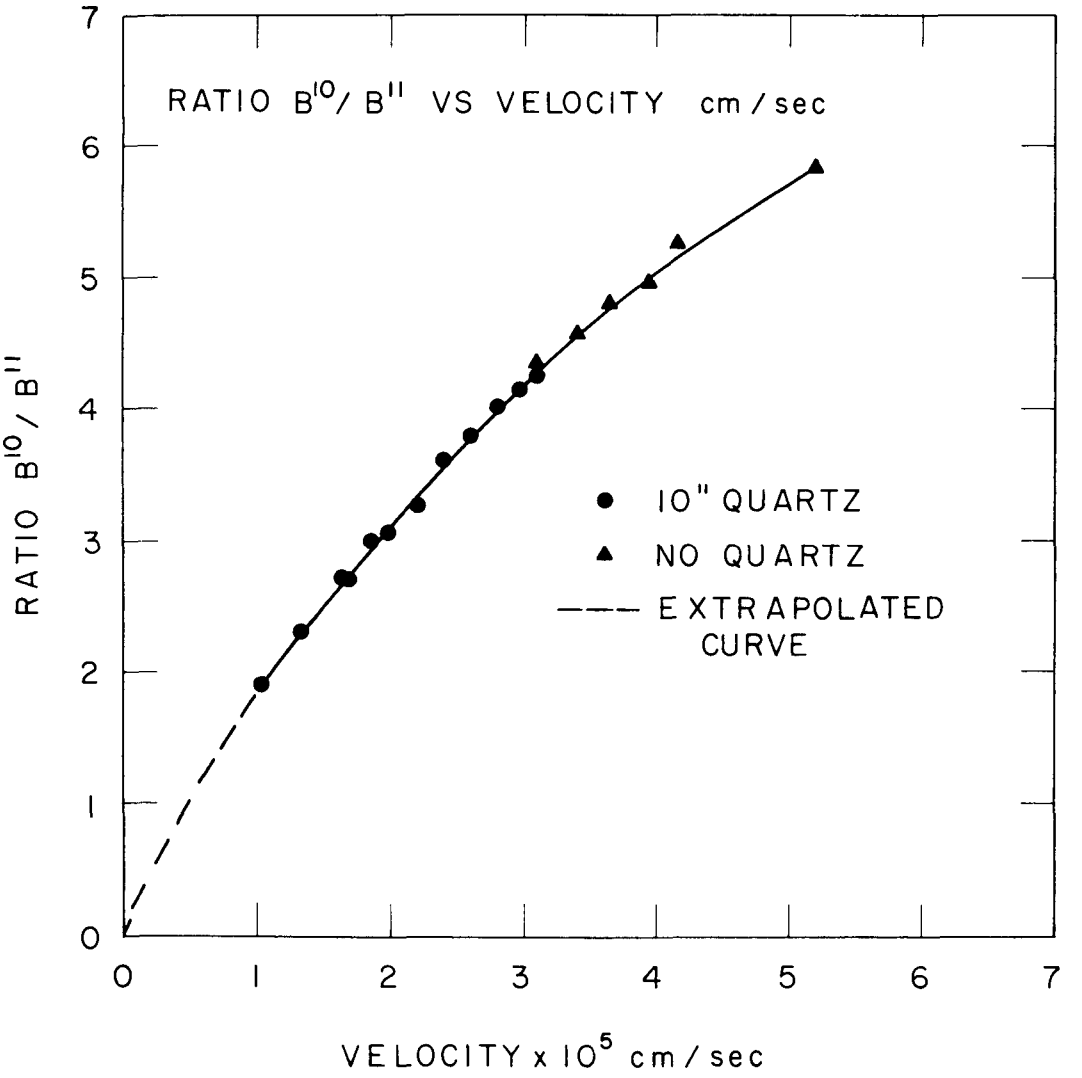
RATIO B^{10}/B^{11} VS VELOCITY cm/sec
RATIO B^{10}/B^{11}
VELOCITY x 10^5 cm/sec
10" QUARTZ
NO QUARTZ
EXTRAPOLATED CURVE
0
1
2
3
4
5
6
7

FIG. 1

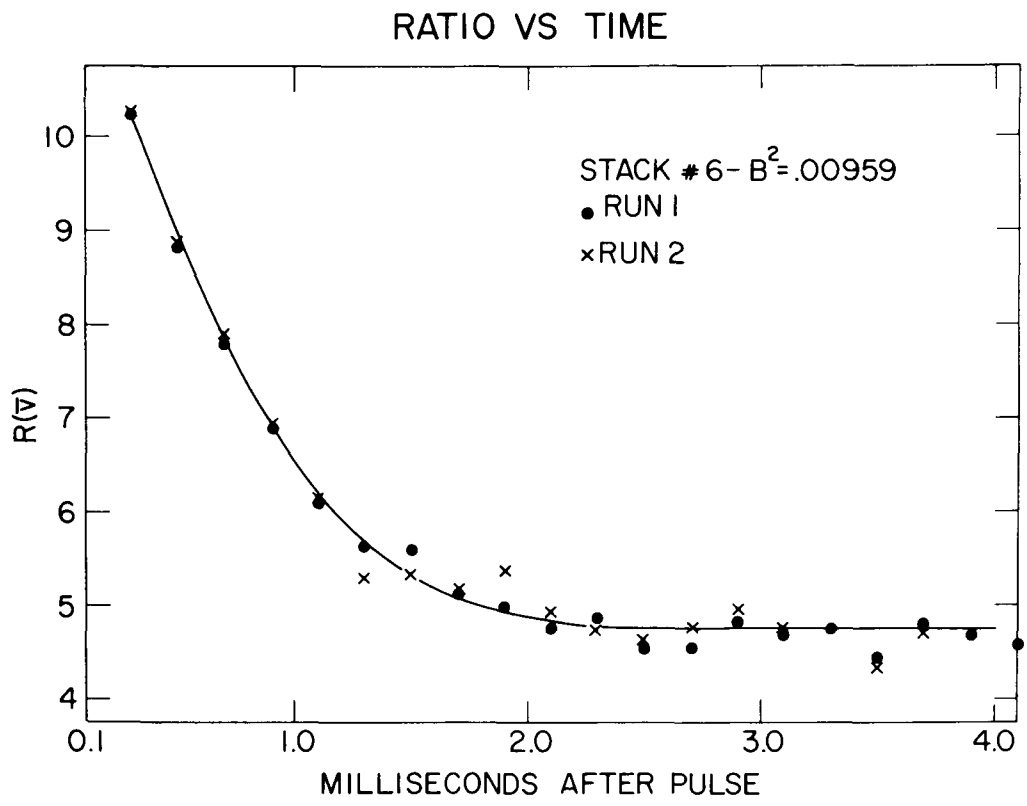
RATIO VS TIME
STACK # 6 - B² = .00959
• RUN 1
× RUN 2
R(V)
10
9
8
7
6
5
4
0.1
1.0
2.0
3.0
4.0
MILLISECONDS AFTER PULSE

FIG. 2

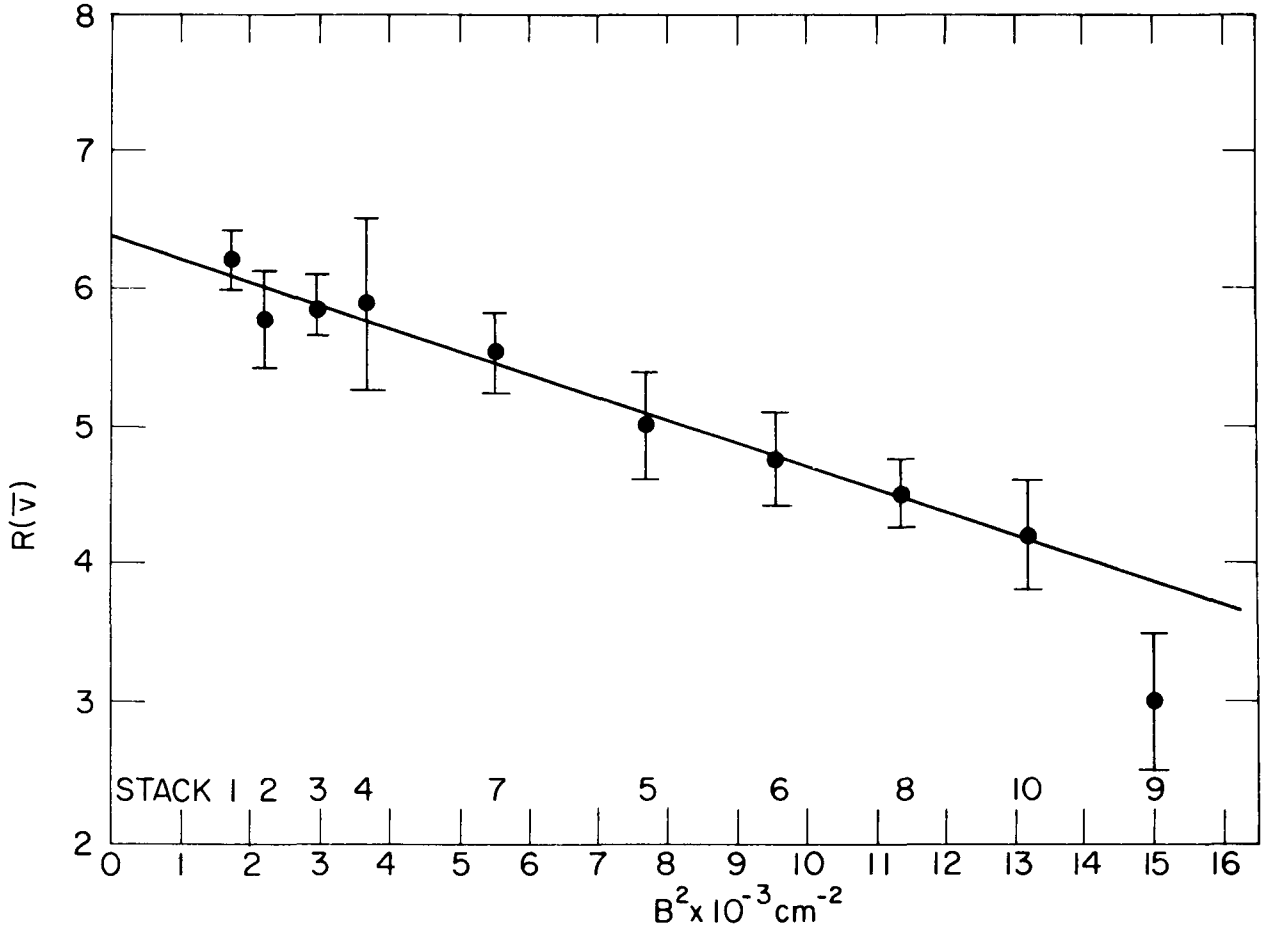

AVERAGE NEUTRON VELOCITY AS A FUNCTION OF BUCKLING

FIG. 3

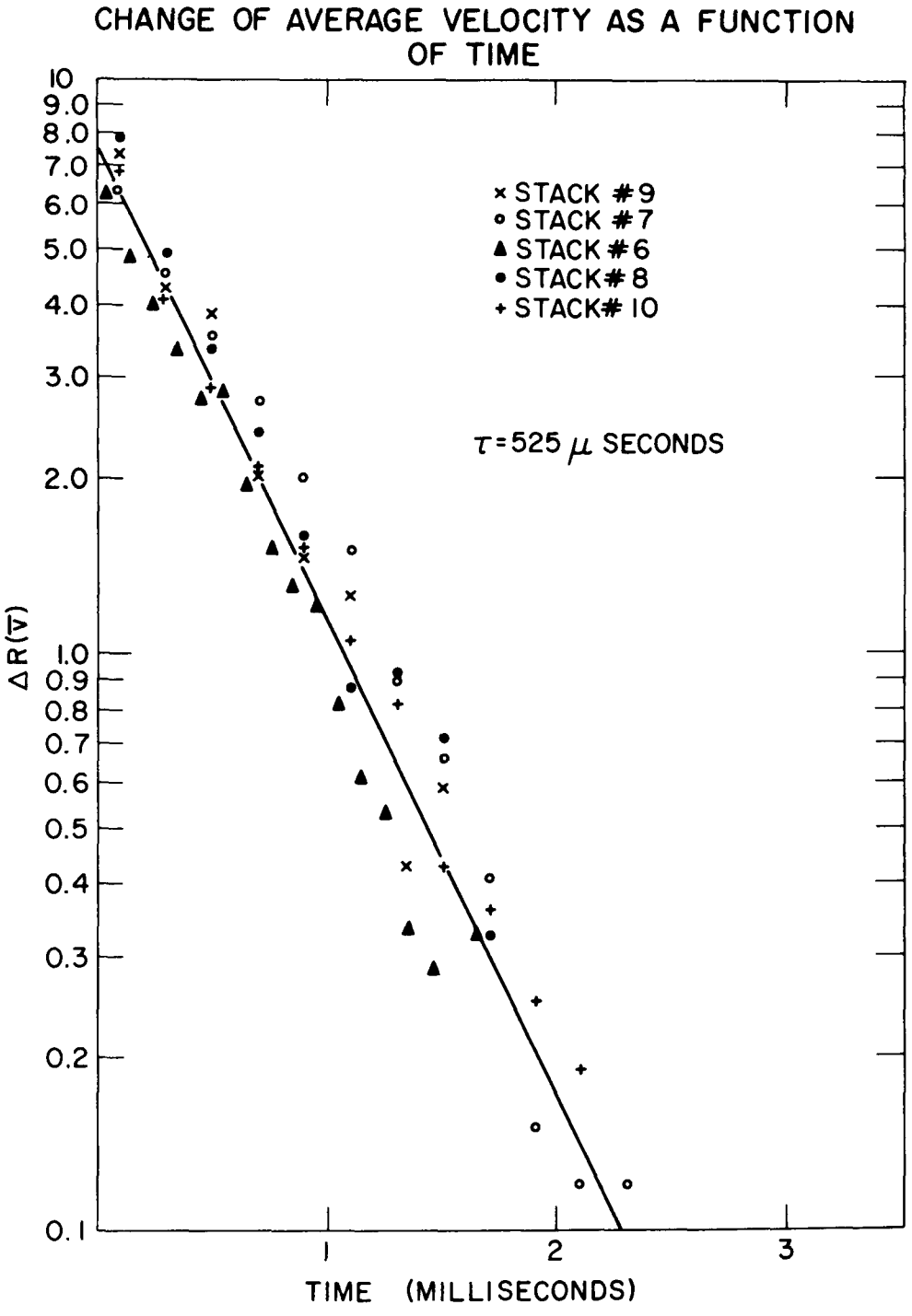
CHANGE OF AVERAGE VELOCITY AS A FUNCTION OF TIME
10
9.0
8.0
7.0
6.0
5.0
4.0
3.0
2.0
1.0
0.9
0.8
0.7
0.6
0.5
0.4
0.3
0.2
0.1
ΔR(v̄)
× STACK #9
○ STACK #7
▲ STACK #6
● STACK #8
+ STACK #10
τ = 525 μ SECONDS
1
2
3
TIME (MILLISECONDS)

FIG. 4

TABLE I

Tabulation of Measured Ratio

Stack No.	R ($\bar{\nu}$)	B^2 (cm^{-2})	Stack Size (cm)
1	6.20 ± .25	.001765	128 x 128 x 122
2	5.77 ± .35	.00220	109 x 108 x 122
3	5.85 ± .20	.00295	89 x 89 x 122
4	5.87 ± .65	.00366	69 x 89 x 122
5	5.00 ± .40	.00770	49 x 49 x 122
6	4.75 ± .35	.00959	49 x 49 x 59
7	5.54 ± .30	.00550	69 x 89 x 59
8	4.50 ± .25	.01139	49 x 39 x 59
9	3.00 ± .50	.01505	29 x 49 x 59
10	4.20 ± .40	.01320	39 x 39 x 59

DETERMINATION OF DIFFUSION HARDENING IN WATER

EUGENE STARR AND JUAN KOPPEL

BROOKHAVEN NATIONAL LABORATORY

UPTON, NEW YORK

SEPTEMBER 1961

ABSTRACT

Diffusion lengths have been measured in poisoned H_2O of increasing concentration of boric acid. Values of Σa, $\overline{Dv}$ and diffusion hardening coefficient are therefrom determined.

INTRODUCTION

The one dimensional transport problem of thermal neutrons in a source free infinite medium has the asymptotic solution

$$N(r,v) = n(v)\ e^{-\chi r} \tag{1}$$

where $1/\chi$ is usually called the diffusion length. $n(v)$ represents the spectrum of this asymptotic solution which holds at large distance from any source. For very weak absorption $n(v)$ is a maxwellian at room temperature but in general it deviates progressively from a maxwellian and becomes hardened as the absorption in the medium is increased. The reason for this is that usually the average energy of the neutrons absorbed in any volume element is lower than the average energy of the neutrons leaking into the same element to compensate for the absorption losses. As a matter of fact in the case of $1/v$ absorption the latter are proportional to the neutron density while the leakage is proportional to the flux.

Let us write down the neutron balance equation in the diffusion theory approximation:

$$-D\nabla^2 N(v)v + \Sigma a\ N(v)v = \int N(v')v'\ \Sigma_s(v' \rightarrow v)\ dv' - \Sigma_s\ N(v)v \tag{2}$$

Substituting (1) into (2) we have in abbreviated notation

$$(\Sigma a - D\chi^2)n(v)v = Ln(v) \tag{3}$$

This is a standard eigenvalue problem and we are interested in the lowest eigenvalue χ_o^2 and lowest eigenfunction $n_o(v)$. If the ratio $\Sigma a/D$ were energy independent the simple relation $\chi_o^2 = \Sigma a/D$ would hold and $n_o(v)$ would be the maxwellian spectrum $n_o(v) = v^2 \exp\left(-\frac{mv^2}{2kt}\right)$.

However $\Sigma a/D$ is usually energy dependent and taking the most common case we shall assume a 1/v absorption:

$$\Sigma a = \frac{\lambda_o}{v} \tag{4}$$

Now the expression for χ_o^2 is found by integrating eq. (3) over all energies. The integral over the right side being zero, it follows

$$\chi_o^2 = \frac{\lambda_o}{\overline{Dv}(\lambda_o)} \tag{5}$$

where $\overline{Dv}(\lambda_o)$ is the average value

$$\overline{Dv}(\lambda_o) = \frac{\int n(v) Dv dv}{\int n(v) dv} \tag{6}$$

Since $\overline{Dv}(\lambda_o)$ is a smooth function of λ_o we can make the expansion

$$\chi_o^2 = \frac{\lambda_o}{\overline{Dv}} \left[1 - H \frac{\lambda_o}{\overline{Dv}} + \ldots . \right] \tag{7}$$

where now

$$\overline{Dv} = \overline{Dv}(o) = \frac{\int Dv^3 \exp\left(-\frac{mv^2}{2kT}\right) dv}{\int v^2 \exp\left(-\frac{mv^2}{2kT}\right) dv} \tag{8}$$

because $n(v)$ goes over into a Maxwellian at room temperature T as λ_o goes to 0. H is the so called hardening coefficient, which we want to determine for H_2O from the present experiment by measuring the diffusion lengths of solution of H_3BO_3 of increasing concentrations.

We want to point out that this experiment is closely related to the well known pulsed neutron experiment where a burst of fast neutrons is produced in a finite medium and the asymptotic decay constant of the neutron population is measured for different sizes of the moderator assembly.

As a matter of fact, inverting the series (7) it is

$$\lambda_o = \overline{Dv}\,\kappa_o^2\,(1 + H\kappa_o^2 + \ldots) \qquad (9)$$

Let us compare this expression with the familiar formula of the inverse decay constant λ in the pulsed experiment:

$$\lambda - \lambda_o = B^2\,\overline{Dv}\,(1 - CB^2 + \ldots) \qquad (10)$$

where B^2 is the geometrical buckling of the stack. The similitude is not fortuitous as κ_o^2 is equivalent to a negative buckling whereas the term $\frac{dn}{ndt} = -\lambda$ which appears in the time dependent balance equation can be correlated to a negative poison. Thus C and H are identical.

EXPERIMENTAL TECHNIQUE

The diffusion length in poisoned demineralised water was measured in an existing cylindrical tank 5 1/2 feet in diameter and 5 feet high situated atop the Brookhaven Graphite Reactor. The available thermal flux from the graphite face of the reactor is approximately 10^7 neutrons/cm^2/sec.

The relative flux was measured by situating bare indium foils .150 inches in diameter and .010 inches thick weighing approximately 21 mg, along the direction perpendicular to the almost infinite plane source. Accurate spacing of the foils was accomplished with the use of a plexiglass holder, as shown in Figure 1, having dimensions .390 inches wide x .125 inches thick. The distance between adjacent foils was .375 inches for the slightly poisoned measurements and .250 inches for the heaviest poison measurements. All foils used for any given measurement were sorted into groups having a weight spread less than .3% of each other. Figure 2 shows the experimental arrangement for the diffusion length measurement.

The activated foils were counted in each of four gas flow proportional counters with each side of the foil counted twice. To insure that the spacing between foils did not result in any large perturbation, activations were made at twice the normal spacing for each poison measurement. To determine the epi-cadmium component to the measured activity, bare indium foils were used with a cadmium sheet placed between the source and the water tank.

With the addition of each poison, the tank was agitated for 1 hour and two poisoned water samples, one from the bottom of the tank and one from the top of the tank were chemically analyzed* for boric acid content.

THE ANALYSIS OF DATA

The presence of higher spacial modes to the radial flux was found to have no significant contribution to the foil positions nearest the source. Hence the fundamental flux in a cylindrical tank is then given as:

$$\phi(r, z) = J_o \left(\frac{2.405r}{R}\right) e^{-z\alpha}$$

where J_o is the zero order Bessel function

α is the inverse relaxation length

R is the extrapolated radius of the tank

Since the total length of the equally spaced foils was small compared to the overall axial dimension, no end effect correction is required. With the medium being radially finite, the diffusion length L is then related to the relaxation length $1/\alpha$ by the equation

$$\frac{1}{L^2} = \alpha^2 - \left(\frac{2.405}{R}\right)^2 \qquad (12)$$

In the reduction of the data, the activities of the foils were corrected for dead time, background and the known indium decay and finally

* Method involved boric acid titration with mannitol.

normalised to a given counter by a standard source intercalibration of detectors.

The relative foil activity was then least square fitted to an exponential, with all foils situated in a region whose epi-cadmium component exceeded .3% eliminated from the fit. Figures 3, 4, and 5 show the normalised activity plotted as a function of axial distance for all poison measurements. The value of relaxation length was then corrected for the leakage effect by the data obtained from the J_o fit of the radial activity shown in Figure 6. This correction was greatest for the pure water data and amounted to .6%. Consideration was given to the effect of the foil holder on the diffusion length for the heavy poison measurements, but calculation of the upper limit of such an effect showed it was extremely small. The tabulated values of the diffusion lengths in Table I were obtained by a weighted average of all the runs for a given poison.

TABLE I

Measured Diffusion Length at 21° C

L (cm)	Boric Acid (mg/ml)	Σ_{Boron} (cm^{-1})
2.7540 ± .0080	-	-
2.4594 ± .0025	.7160	.005245
2.1665 ± .0070	1.8935	.013870
1.9779 ± .0021	2.7945	.020470
1.6394 ± .0012	5.5150	.040397
1.2551 ± .0020	11.920	.087314
1.0631 ± .0021	18.330	.13427
.9429 ± .0019	24.430	.17895
.8469 ± .0032	32.030	.23462
.7308 ± .0015	47.310	.34655

DETERMINATION OF Σ_{ga}, $\overline{Dv}(o)$ and H:

The set of experimental points $(\mathscr{L}^2_i, \Sigma a_i)$ has been fitted by a least square method to the function

$$\frac{\mathscr{L}^2}{\Sigma a} = A_1 + A_2 \Sigma a \tag{13}$$

$$\frac{\Sigma a}{\mathscr{L}^2} = B_1 + B_2 \mathscr{L}^2 \tag{14}$$

where $\Sigma a = \Sigma_H + \Sigma_B$ is the total macroscopic absorption cross section of the poisoned medium. The value of the absorption cross section of hydrogen was found by varying the value of Σ_H in the expression $\sum_n \left\{ \frac{\mathscr{L}^2}{\Sigma a} - \frac{\mathscr{L}^2}{\Sigma a} \text{ (calculated)} \right\}^2$, until the variance from a least squares fit to A_1, A_2 was a minimum. Equal weights were attributed to all points, which corresponds to the assumption of constant absolute errors of the values of $\frac{\mathscr{L}^2}{\Sigma a}$. The scattering of the experimental points with respect to the fit as shown in Fig. 9 has justified this assumption. Other weighting procedures were tried but the influence on all the coefficients was very small. The values obtained for constant weights are shown by the first line of table II.

$\overline{Dv}$ and H are determined either by (7) or by (9). If terms of higher order than Σa^2 in (7) or $\mathscr{L}^4$ in (9) are at first neglected, these two equations become identical with (13) and (14), therefore yielding

$$\left.\begin{aligned} (\overline{Dv})_A &\cong \frac{v_o}{A_1} = 35852 \text{ cm}^2 \text{ sec}^{-1} \\ H_A &\cong \frac{A_2}{A_1^2} = .07648 \text{ cm}^2 \end{aligned}\right\} \tag{15}$$

and

$$\left.\begin{aligned} (\overline{Dv})_B &\cong B_1 v_o = 35,506 \text{ cm}^2 \text{ sec}^{-1} \\ H_B &\cong \frac{B_2}{B_1} = .11045 \text{ cm}^2 \end{aligned}\right\} \tag{16}$$

It is seen that both values of $\overline{Dv}$ are in excellent agreement with each other, whereas the values obtained for H are quite different. This shows that the higher order terms cannot be neglected (which is not too surprising with a roughly 20% spectral shift in the most heavily poisoned medium), hence neither (15) nor (16) are correct. However if one repeats fit (13) and (14) with a decreasing number of points, dropping progressively those of maximum shift, the values yielded by (15) and (16) should asymptotically approach the same limit. This is shown in Fig. 8 and table II. It is seen that in fact the difference $(H_B - H_A)$ decreases but obviously at the same time the uncertainty in both coefficients increases. As the trend of the change in H_A and H_B is of opposite sign, we may assume that H satisfies the inequality

$$H_{B_{max}} < H < H_{A_{min}}$$

where $H_{B_{max}}$ and $H_{A_{min}}$ are the endpoints of the error bars for the point of Fig. 8 yielding the minimum total uncertainty,

$$\mathcal{E}_H = H_{B_{max}} - H_{A_{min}}$$

From this technique of analyzing the experimental data, our final results for σ_{aH_2O}, $\overline{Dv}$ and H (or C) are:

$$\sigma_{aH_2O} = 326.9 \pm 1.6 \text{ mb}$$
$$\overline{Dv} = 35,850 \pm 100 \text{ cm}^2 \text{ sec}^{-1}$$
$$H = .081 \pm .010 \text{ cm}^2$$
$$\overline{DvH} = 2900 \pm 350 \text{ cm}^4 \text{ sec}^{-1}$$

From the foregoing discussion it follows that even for quite accurate experimental data, the error in determining the diffusion hardening constant might be extremely large because of the uncertainty involved

TABLE II

n	A_1	A_2	$\overline{(Dv)}_A = \frac{V_0}{A_1}$	$H_A = \frac{A_2}{A_1^2}$	B_1	B_2	$\overline{(Dv)}_B = B_1 v_0$	$H_B = \frac{B_2}{B_1}$	$(\overline{DvH})_A$	$(\overline{DvH})_B$
10	6.1364 $\pm 6.44 \times 10^{-3}$	2.8799 $\pm 5.37 \times 10^{-2}$	35852	.076480	.16139 $\pm 3.55 \times 10^{-4}$	.017825 $\pm 7.28 \times 10^{-4}$	35506	.110447	2742 ± 51	3922 ± 160
9	6.1201 $\pm 6.55 \times 10^{-3}$	2.6687 $\pm 3.75 \times 10^{-2}$	35947	.071250	.16271 $\pm 1.97 \times 10^{-4}$	.014748 $\pm 2.21 \times 10^{-4}$	35796	.090640	2561 ± 36	3245 ± 49
8	6.1228 $\pm 8.29 \times 10^{-3}$	2.7137 $\pm 7.86 \times 10^{-2}$	35931	.072387	.16284 $\pm 2.36 \times 10^{-4}$	.014355 $\pm 3.46 \times 10^{-4}$	35825	.088154	2601 ± 75	3158 ± 76
7	6.1335 $\pm 9.83 \times 10^{-3}$	2.9319 $\pm 8.82 \times 10^{-2}$	35869	.077935	.16262 $\pm 3.01 \times 10^{-4}$	.015106 $\pm 5.76 \times 10^{-4}$	35776	.092891	2795 ± 84	3323 ± 127
6	6.1263 $\pm 1.46 \times 10^{-2}$	2.7581 $\pm 2.44 \times 10^{-1}$	35911	.073488	.16301 $\pm 4.44 \times 10^{-4}$	.013520 $\pm 1.39 \times 10^{-3}$	35862	.082940	2639 ± 233	2974 ± 306

in the influence of higher order terms. This fact is most easily realized by comparing the extremely small uncertainties of A_2 or B_2 in obtaining the least square fit with the actual error bar quoted for H. It is also interesting to point out that H_A changes much less than H_B when points are dropped and that for the largest spectral shift H_A has a much smaller uncertainty than H_B. This means that the data of the present experiment are better fit by formula (13) than by (14).

COMPARISON WITH PREVIOUS EXPERIMENTAL DATA

The measurement of diffusion length in poisoned water has been obtained by other investigators[1,2]. The experimental data obtained by Beyster-Lopez[3] for the pulsed neutron method have been compared in Fig. 7 and shows good agreement with the extrapolated least square fit of our data. Furthermore, table III compares our result of σ_{aH_2O}, $\overline{Dv}$ and $H\overline{Dv}$ (or $C\overline{Dv}$) with other recently determined values. The theoretical calculation tabulated was obtained by Honeck[4] using the Nelkin water model.

TABLE III

	Present Results	Beyster-Lopez[a,c]	Beckurts[d]	Kuchle[5](c)	Reier[6](b)	Theoretical
σ_{aH_2O}(mb)	326.9±1.6	325.3±1.6	326.5±1.2	326±6	328±6	-
$\overline{Dv}$ (cm^2-sec^{-1})	35,850±100	37,503±366	35,300±1100	35,400±700	37,618±205	37,590
$\overline{Dv}C$ or $\overline{Dv}H$ (cm^4-sec^{-1})	2900±350	5116±776	3650±400	4200±800		3116
T (°C)	21	26.5	-	22	22	20.5

(a) Data analyzed using .32 cm for extrapolation distance

(b) Poisoned water data

(c) Pulsed data

(d) σ_a and $\overline{Dv}$ measured by poison water; $\overline{Dv}C$ by pulse measurement.

CONCLUSION

$\sigma_{a_{H_2O}}$, $\overline{Dv}$ and H have been obtained with good accuracy from the measurement of diffusion lengths in poisoned water. Since the same set of experimental data can be fitted very accurately by different expansions, large discrepancies with previously quoted values of H are not surprising. The dropping points technique shows that higher order terms should be retained in the analysis of data and that the usual 3 parameter fit yields values of H which are largely dependent upon the range of the variables covered by the measurement. However, in practice with a finite number of points and finite experimental errors, it has been found very difficult to reduce the uncertainty in H by fitting the data to an expression with more parameters. Therefore we feel it is preferable to compare different measurements point by point rather than by the coefficients of their least square fits.

ACKNOWLEDGEMENTS

The authors wish to express their appreciation to Alfred P. Tierney for his assistance in preparation and counting of foils, to Helen Connell for reduction of data, and to Dr. R. W. Stoenner for the boric acid analysis.

REFERENCES

1. M. Reier and J. De Juren, WAPD-MRJ-8 (1959).
2. K. H. Beckurts, Proceedings of Second Symposium on the Application of Pulsed Neutron Source Techniques, UCRL 5665.
3. W. M. Lopez and J. R. Boyster, GA 1584(Rev) (1961).
4. Henry Honeck, BNL Private Communication.
5. M. Kuchle, Nucleonik 2, 131 (1960).
6. M. Reier, WAPD-T-1140 (1960).
7. M. Nelkin, H. Hurwitz, Jr., Nucl. Sci. and Eng. 3 (Jan. 1958).

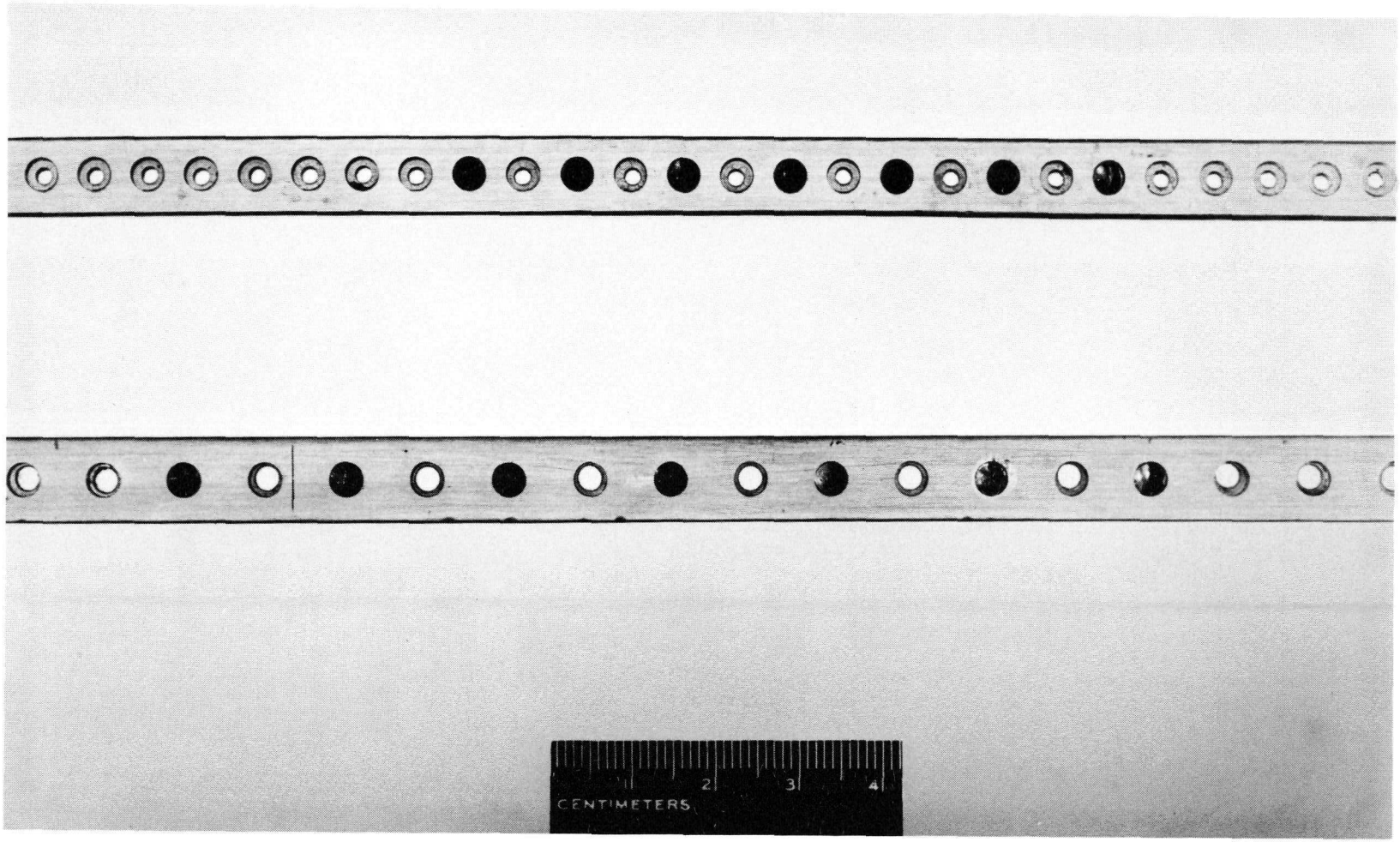

Figure 1

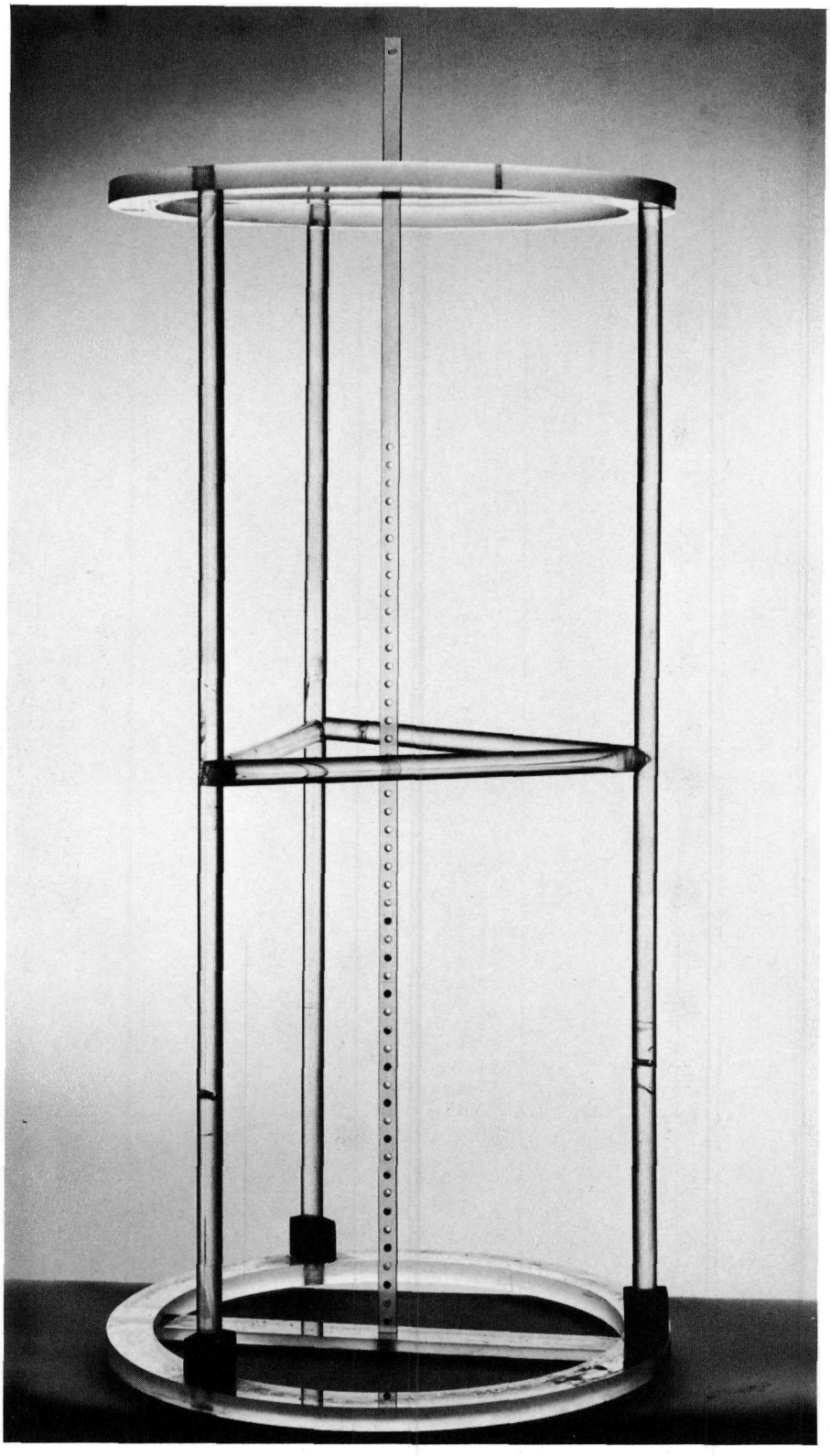

Figure 2

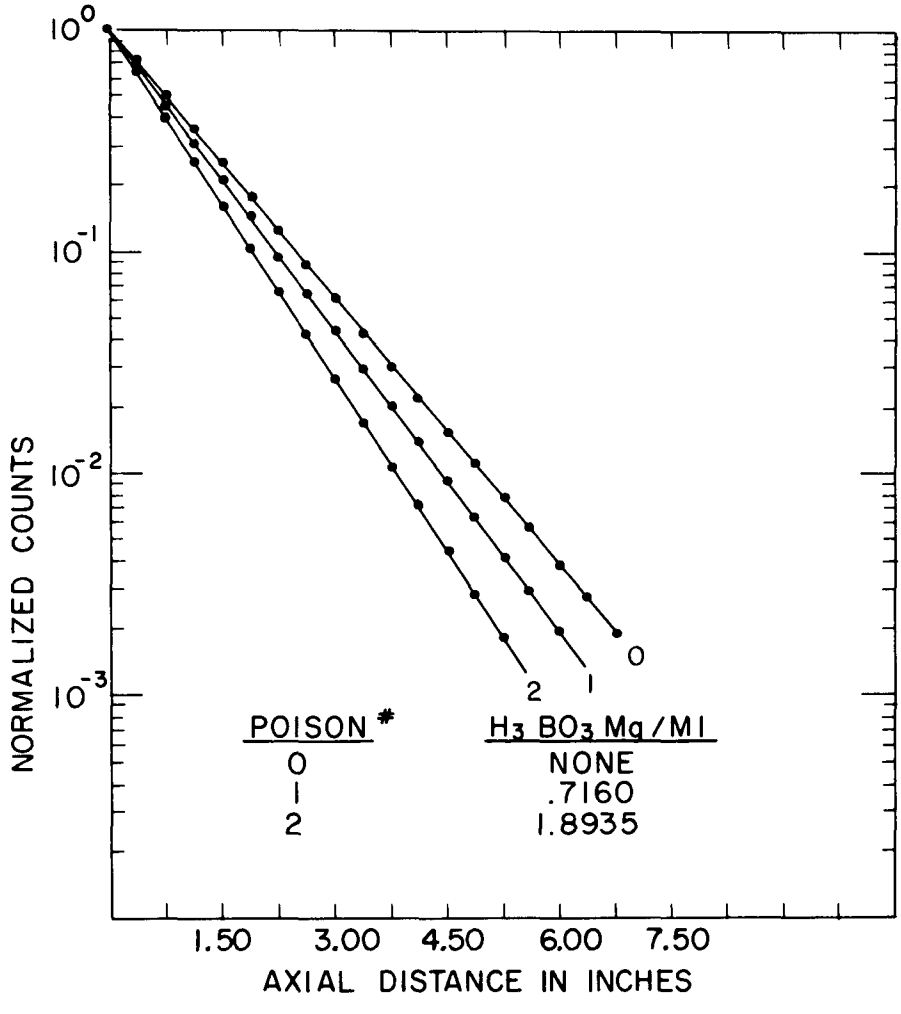
NORMALIZED COUNTS
10^0
10^{-1}
10^{-2}
10^{-3}
0
1
2
POISON #
H_3BO_3 Mg/Ml
0 NONE
1 .7160
2 1.8935
1.50
3.00
4.50
6.00
7.50
AXIAL DISTANCE IN INCHES

FIG. 3

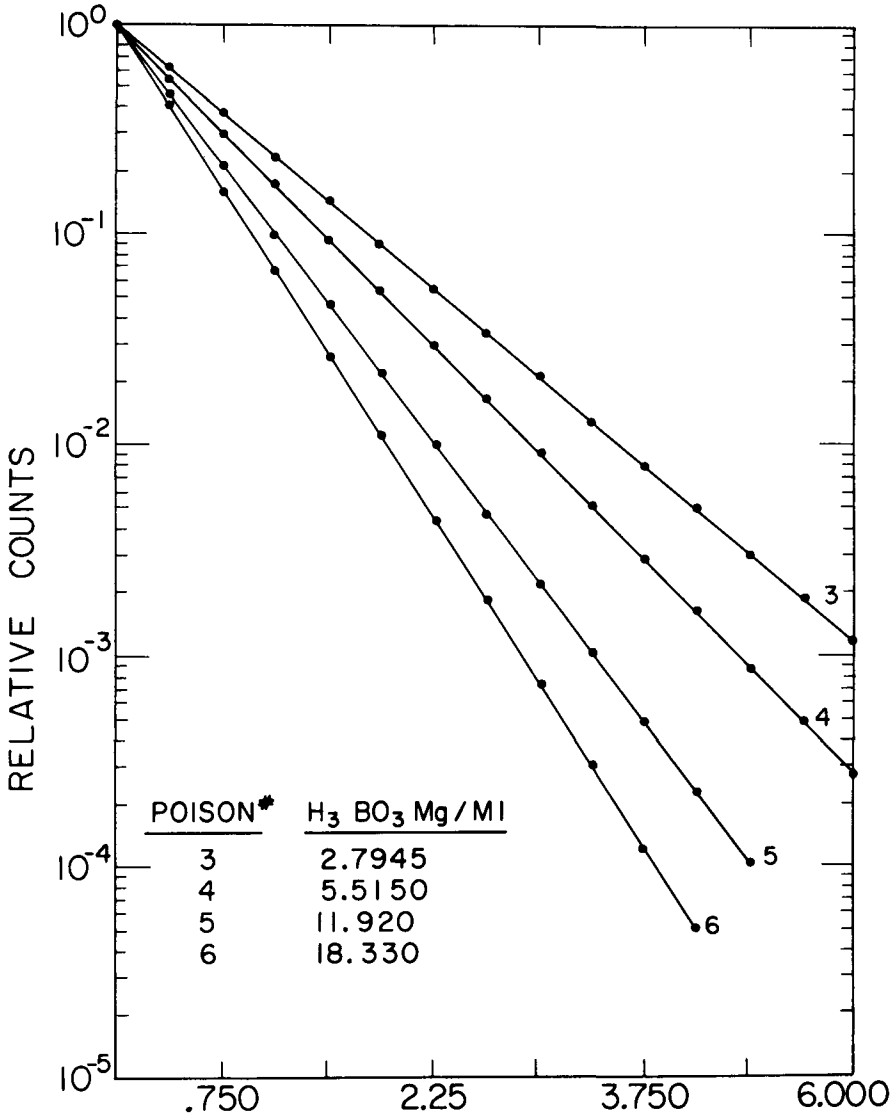
RELATIVE COUNTS
10^{0}
10^{-1}
10^{-2}
10^{-3}
10^{-4}
10^{-5}
.750
2.25
3.750
6.000
AXIAL DISTANCE IN INCHES
POISON* $H_3 BO_3$ Mg/Ml
3 2.7945
4 5.5150
5 11.920
6 18.330
3
4
5
6
FIG. 4

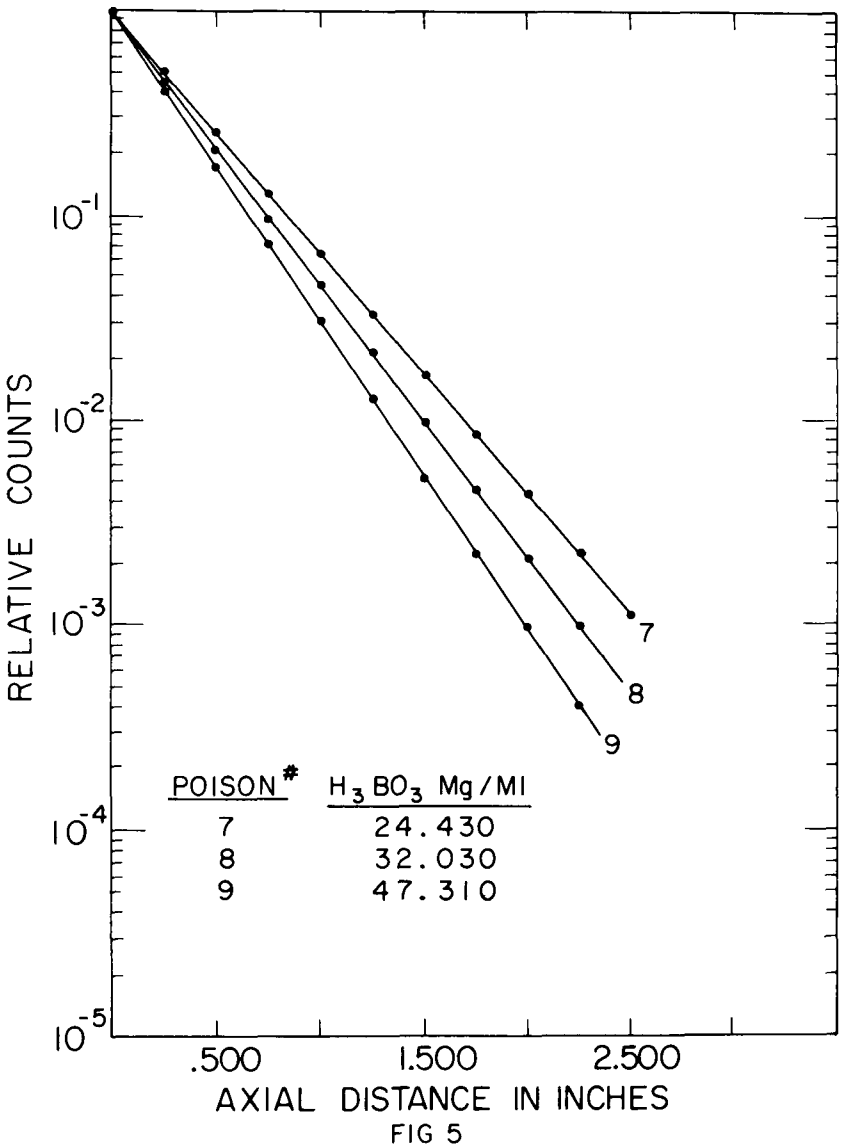
RELATIVE COUNTS
10^{-1}
10^{-2}
10^{-3}
10^{-4}
10^{-5}
.500
1.500
2.500
AXIAL DISTANCE IN INCHES
7
8
9
POISON # | H_3BO_3 Mg/Ml
7 | 24.430
8 | 32.030
9 | 47.310
FIG 5

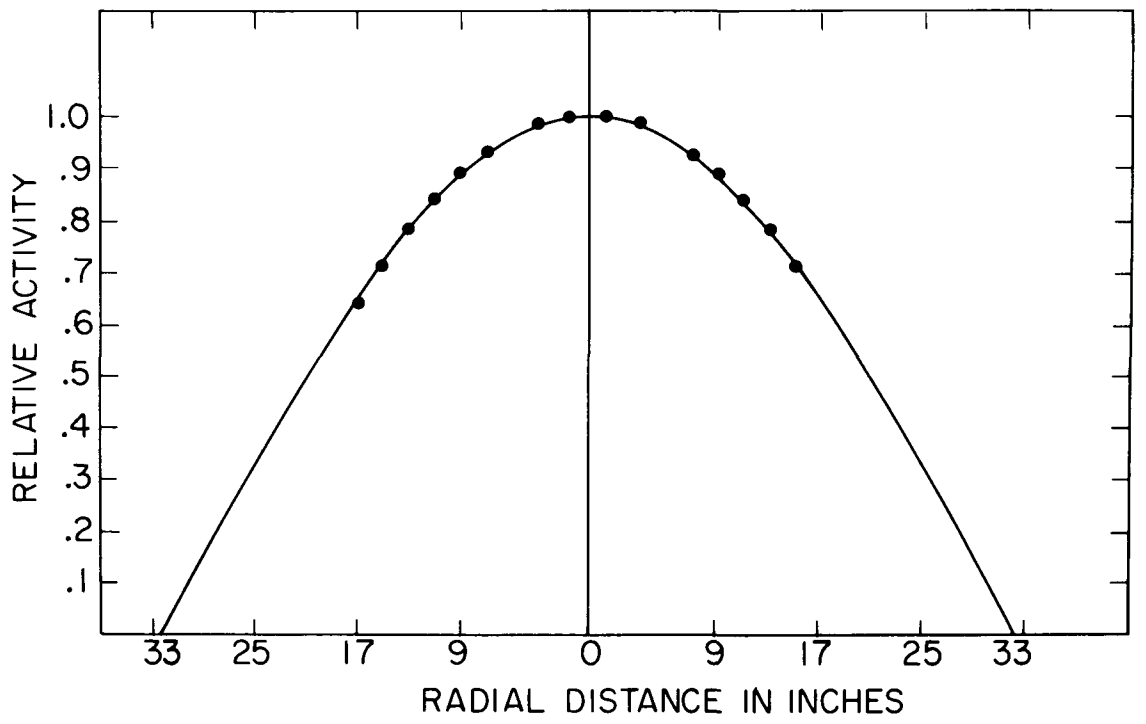
RELATIVE ACTIVITY
1.0
.9
.8
.7
.6
.5
.4
.3
.2
.1
33
25
17
9
0
9
17
25
33
RADIAL DISTANCE IN INCHES

FIG. 6

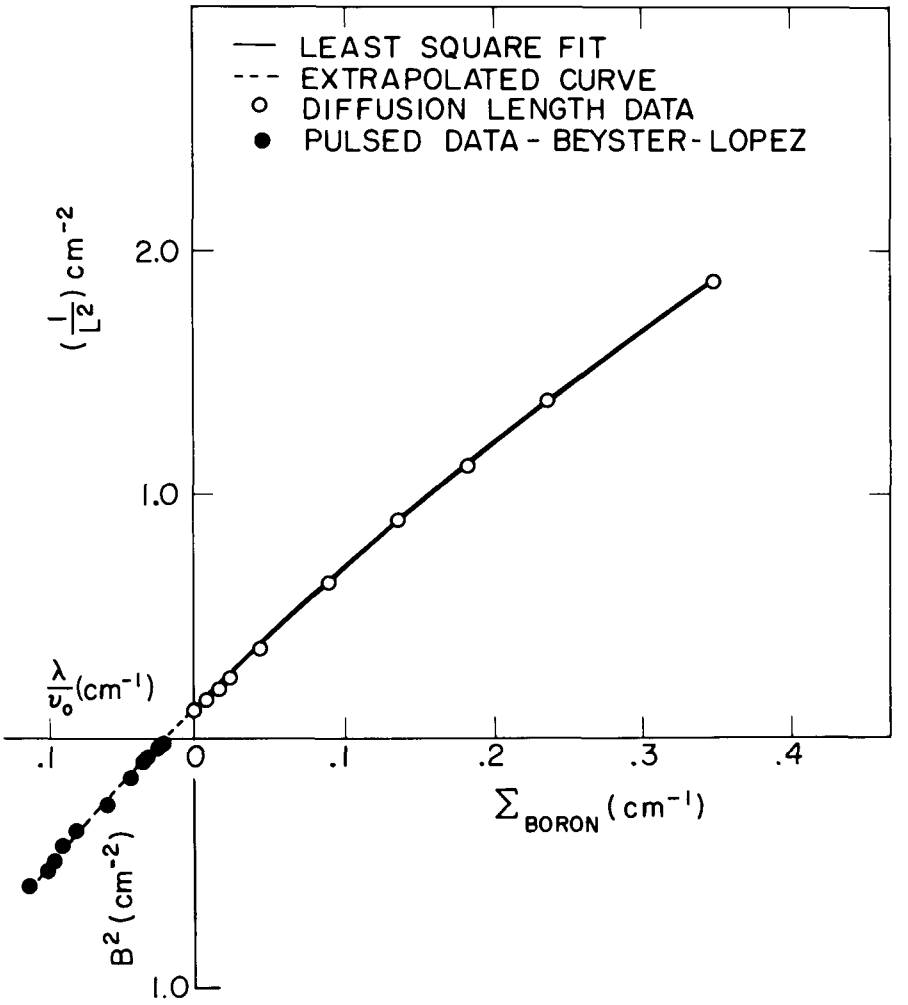

FIG. 7 (INVERSE DIFFUSION LENGTH)^2 vs MACROSCOPIC CROSS SECTION

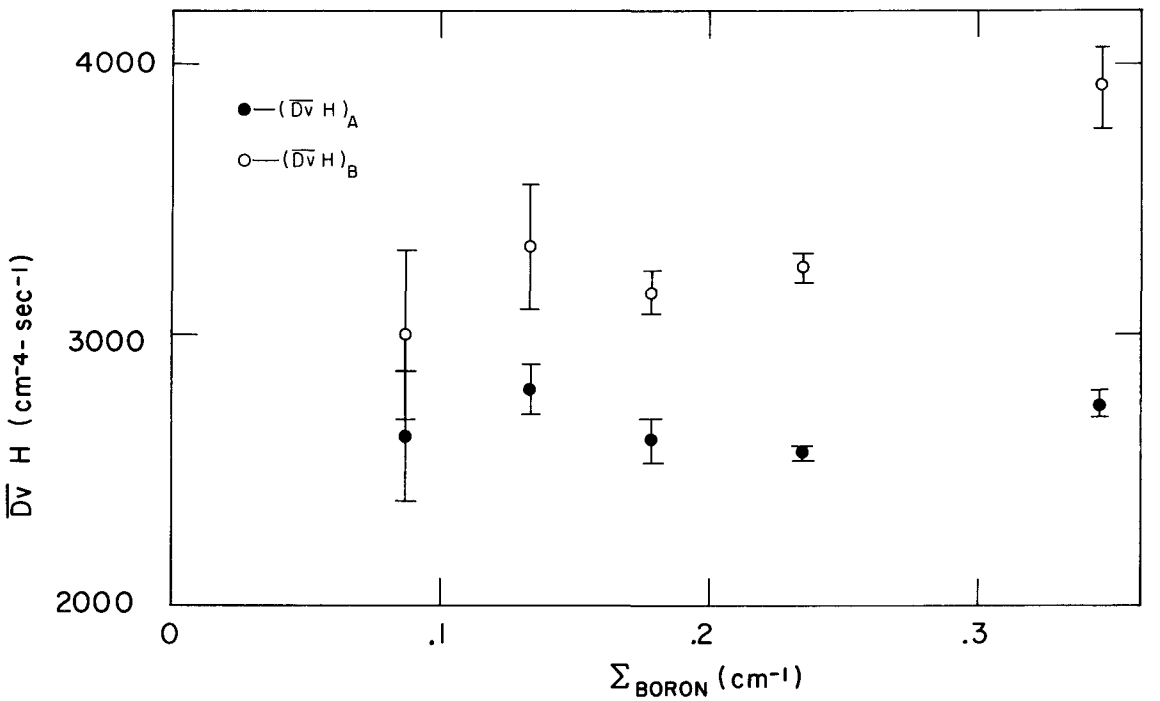

FIG. 8 VALUES OF $\overline{Dv}$ H AS MAXIMUM Σ_B POINTS ARE DROPPED.

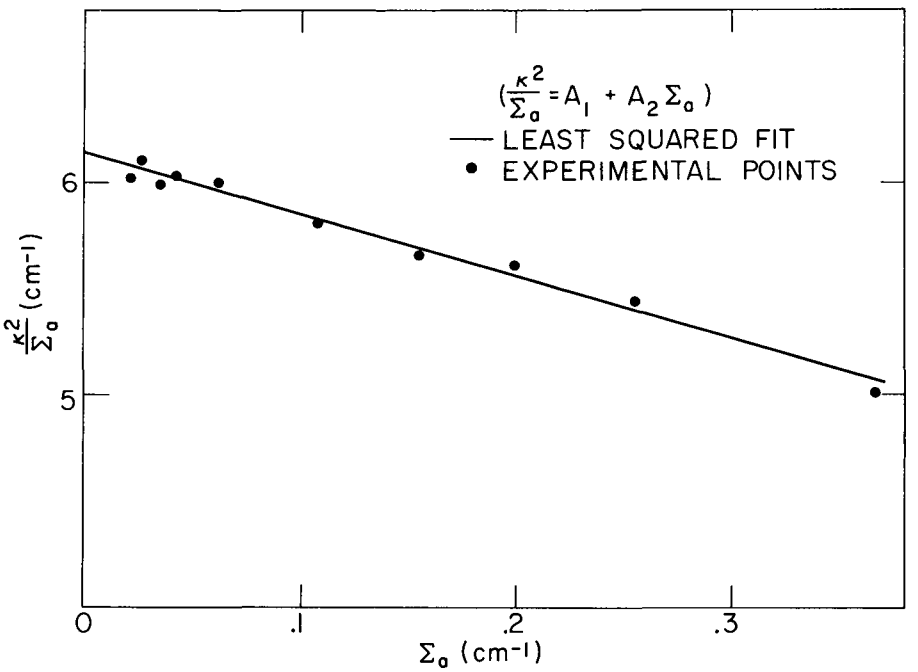
$(\frac{\kappa^2}{\Sigma_a} = A_1 + A_2 \Sigma_a)$
LEAST SQUARED FIT
EXPERIMENTAL POINTS
$\frac{\kappa^2}{\Sigma_a}$ (cm⁻¹)
6
5
0
.1
.2
.3
Σ_a (cm⁻¹)

FIG. 9

Measurement of the Diffusion Parameters of Graphite and Graphite-Bismuth by Pulsed Neutron Methods[1]

E. Starr and G. A. Price
Brookhaven National Laboratory
Upton, New York

March 1962

[1] This work was done under the auspices of the United States Atomic Energy Commission.

Abstract

The pulsed neutron method was used to determine the absorption cross section, the diffusion coefficient and the diffusion cooling constant of high purity graphite, bismuth, and graphite-bismuth systems with volume ratios of 4:1, 2:1, and 1:1 by measuring the decay rate of thermal neutrons as a function of moderator geometry. Values of decay data are reported for each of the systems investigated, together with the geometric size. The measurements of the diffusion length by exponential methods have been included in the data reductions which resulted in a more accurate value of the diffusion parameters.

Introduction

In connection with the investigation of the Liquid Metal Fuel Reactor systems, the diffusion length has been measured in graphite and various ratios of graphite-bismuth by exponential measurements[1]. The pulsed neutron technique was then used to measure the diffusion parameters of these same systems and the results were compared; and then they were combined to yield a more accurate set of diffusion parameters.

Theory

The transport equation for the angle dependent flux $\phi(\underline{r},E,\underline{\Omega},t)$ is:

$$\frac{1}{v}\frac{\partial\phi}{\partial t} = -\underline{\Omega}\cdot\nabla\phi - \Sigma\phi + S + \int dE' \int d\Omega'\ \Sigma_s(E' \to E,\ \Omega \to \Omega')\phi \qquad (1)$$

where Σ is the total macroscopic cross section, Σ_s is the macroscopic scattering kernel and S is the source term given by a δ-function at time t = 0.

We consider the solution of equation (1) in the form

$$\phi(\underline{r},E,\underline{\Omega},t) = \sum_{k,n} A_{kn}\phi_{kn}(E,\underline{\Omega})e^{-\alpha_{kn}t}\, e^{i\underline{\beta}_k\cdot\underline{r}} \qquad (2)$$

which substituted into equation (1) yields

$$\left[i(\underline{\beta}_k\cdot\underline{\Omega}) - \frac{\alpha_{kn}}{v} + \Sigma\right]\phi_{kn} = \int dE' \int d\Omega'\ \Sigma_s(E' \to E,\ \Omega \to \Omega')\phi_{kn} + S_{kn} \qquad (3)$$

Equation (3) defines the eigenfunction ϕ_{kn} and the eigenvalues α_{kn} as a function of the buckling $\underline{\beta}_k$. Generally, we are interested mainly in the lowest value $\alpha_{oo}(\equiv \lambda)$ as a function of $|\beta_o|$ $(\equiv B)$. If λ is expanded in terms of B, the familiar form of the fundamental decay constant as a function of buckling is obtained for a 1/v absorption cross section

$$\lambda = \lambda_o + D_o B^2 \left[1 - CB^2 + FB^4 \ldots\right] \tag{4}$$

where

$$D_o = \overline{Dv} = \frac{\int Dv^3 \exp\left(-\frac{mv^2}{2kT}\right) dv}{\int v^2 \exp\left(-\frac{mv^2}{2kT}\right) dv}$$

The flux for times which are not long compared to the fundamental decay constant will contain terms of both higher space and energy modes as given by equation (2)

$$A_\infty \phi_\infty e^{-\lambda_\infty t} e^{i\underline{B}_0 \cdot \underline{r}} + A_{01}\phi_{01} e^{-\alpha_{01} t} e^{i\underline{\beta}_0 \cdot \underline{r}} + A_{10}\phi_{10} e^{-\alpha_{10} t} e^{i\underline{\beta} \cdot \underline{r}} + \ldots$$

Proper choice of the point $\underline{r}$ at which the flux is measured will eliminate certain spacial harmonics. If we choose $\underline{r}$ as the center of the moderating medium, the spacial mode given by K = 1 is zero. Then for large values of buckling the decay constant associated with the next possible spacial harmonic

will be large and it is possible for the first energy mode $n = 1$ to dominate all the higher modes. Hence, the value of the flux will be given by the first two terms dependent only on λ_1 and λ_o.

Experimentally, a burst of fast neutrons is injected into a medium either multiplying [2] or non-multiplying, slowing down and thermalization of the fast neutrons occurs, and then after a sufficient time the neutron will be in equilibrium with the moderator material. At this time, the spacial flux and energy spectrum assume their fundamental value. The neutron density then decays exponentially. If we measure the time rate of change of the neutron density in this asymptotic state, the relaxation time can be determined as a function of the lowest eigenvalue B^2 for various geometric sizes. The inverse relaxation time λ vs. B^2 is fitted to the polynomial in equation (4) and the coefficients can be determined. The pulsed neutron technique then offers a method of measuring the absorption probability λ_o, the average diffusion coefficient $\overline{Dv}$, and diffusion cooling coefficient C. The accurate determination of C depends on the measurement of the decay constant for small sizes of moderator; great effort has been taken to eliminate effects due to spacial [3] and in the present work energy harmonics, both of which if treated incorrectly could lead to erroneous results.

Van de Graaff Generator

The neutron source was produced by the reaction of deuterons on beryllium, using a 1 Mev Van de Graaff generator. The accelerator has an extraction electrode ion chamber in which the ion bottle is normally biased to a cut-off condition with a positive potential on the extraction electrode. To pulse the system, a negative pulse of the duration desired is impressed on the extraction electrode, driving the positive potential to ground and allowing the positive ions to be accelerated. This system is in principle superior to magnetically deflecting the beam, but the extraction method has difficulty in that some ions will always leak out of the bottle and produce an inherent background. Since, in the pulsed neutron method it is not the total neutron intensity that is important but rather the number of decades that can be observed in the exponential decay, this background is quite undesirable.

The Van de Graaff generator pulsing system was designed so that a given frequency and pulse width could be mechanically selected at the high voltage terminal. This proved to be undesirable, because of the limitation in the choice of pulse width and pulse duration. The pulsing system shown in Figure 1 was therefore designed to satisfy the present operating requirements. The pulse is obtained from a standard pulse generator which operates from a 1 MC crystal oscillator. The

output of the pulse generator can be varied in frequency from 1 cycle per second to 1 megacycle per second. Pulse shaping provides a pulse width from 1 μsec to 1 millisecond duration. This pulse is fed into the low voltage end of the Van de Graaff and used to drive a standard neon bulb (NE-2H). The output is relayed to the high voltage terminal of the Van de Graaff by means of a light pipe and a photomultiplier. The pulse at this point is again shaped and amplified to drive the extraction electrode as previously described.

The background problem has been solved by placing two parallel plates, 24 in. long and 1/2 in. apart, inside the accelerating tube and electrostatically deflecting the beam in the off pulse condition. This is accomplished by maintaining one of the plates at approximately 500 volts and pulsing the other plate with a voltage synchronized with the signal driving the neon bulb in the Van de Graaff generator. This results in a potential on both plates of 500 volts when the deuterons were being accelerated toward the target, and a large deflecting potential, about 2000 volts/cm, when the beam is in a cut-off condition. The end result of this entire system is to improve the signal-to-noise ratio from approximately 500 to 1 to the present 10^6 to 1. Figure 2 shows a comparison of decay data measured with and without the deflecting voltage.

Time Analyzer

The neutron density as a function of time is recorded by a time analyzer. The time analyzer was designed with a channel selector to provide 10, 20, 40, or 100 total channels with any desired duration. The repetition rate is determined by the product of the channel width and the total number of channels selected. This means that the total time between pulses is a constant, with any error in time divided by the number of channels that have been selected.

The basic system operates by means of a Burroughs magnetic beam switching tube triggered by the pulse generator. The amplified neutron pulses enter the time analyzer through a synchronizer which has a second input of 1 megacycle pulses. This circuit essentially "quantizes" the neutron pulses with the 1 megacycle frequency so that any single neutron can be counted in only one channel. This permits the Burroughs tube, which selects the channel into which the data is recorded, to have a switching dead time of about 1 μsec without losing a neutron pulse or counting one pulse in two successive channels. The time analyzer can also be adjusted to permit a time delay between the start of the pulse generator and the opening of the first counting channel.

Counting

The counting system included an aluminum BF_3 proportional

counter 1/2 in. diameter and 12 in. long. The output pulses were fed into a model 205B Atomic preamplifier which had been modified to permit a faster input time constant. These pulses were amplified by a model 204C Atomic linear amplifier, and then sent to the time analyzer to be counted. At intervals during the series of measurements, the detector and the time analyzer were both checked by a chi-square test for randomness and reproducibility.

Procedure

The moderating assemblies that were investigated consisted of GBF[1] graphite and volume ratios of graphite to bismuth of 4:1, 2:1, 1:1 and finally an attempt was made to measure the diffusion parameters of an all bismuth array. The stacks were pulsed with the neutron source on the central axis parallel to the direction of the graphite extrusion. The cubes of moderating material were placed in a box situated on a table movable in the vertical direction as shown by the 1:1 graphite-bismuth array in figure 3. The base of the table was filled with paraffin, and a sheet of 40 mil cadmium covered boral[2] was placed between the stack and the table. After the stack was constructed, sheets of cadmium covered boral was placed around the remaining faces of the cube to prevent room return neutrons from affecting the decay data.

In order to establish that the reflection of neutrons from the concrete confines of the room produced no appreciable

effect, measurements were performed for different experimental arrangements with a given size stack. The first experiment was to measure the decay of the fast neutron source produced by reflection from the walls of the room by pulsing the box of cadmium covered boral without a moderating stack. The decay data is shown in figure 4. A graphite stack was then placed in the box and surrounded on all sides with approximately 6 inches of cadmium covered paraffin which served to reduce the time necessary for the leakage neutrons to return to the stack. Figure 5 shows the physical arrangement and the decay curves with and without the graphite stack. Finally an arrangement of nine stacks of graphite, all with the same dimensions, was constructed as shown in figure 6 with a sheet of cadmium placed between each adjacent array. The decay data was then measured in the central stack. Since each of the nine stacks has the same fundamental decay constant, any effect due to room return would only change the decay data for the stacks on the periphery. The decay measured for the nine stack array and the stack surrounded by paraffin was the same within the observed statistical error with approximately 2 milliseconds eliminated for higher harmonic content. The decay constant for the empty boral box and the paraffin pulsed without the central graphite region was also the same but decayed to background in approximately 1 millisecond. Therefore, the neutrons returned

from the wall in a time short compared to the predominance of the higher harmonics and their effects were eliminated in the reduction of data.

The anisotropic structure of pressed graphite should cause the diffusion coefficient to be different in the direction perpendicular to the extrusion axis as compared to the diffusion coefficient parallel to the axis. With the leakage rate given by:

$$\left(\frac{\pi^2}{(a + 2\epsilon)^2} + \frac{\pi^2}{(b + 2\epsilon)^2}\right) D_{\perp} + \frac{\pi^2}{(c + 2\epsilon)^2} D_{\parallel} \qquad (5)$$

where a, b, and c are the dimensions of the graphite stack, and ϵ is the extrapolation distance. The extrapolation distance is assumed to be independent of the stack dimensions and equal to $2.13\ D_{\circ}/\bar{v}$, where $\bar{v}$ is the mean neutron velocity at room temperature.

For all stacks investigated, the graphite blocks were placed with their extrusion axis parallel to each other. A method to measure the anisotropy is to determine the change in decay constant as the sides of the two axial directions are varied while maintaining a constant value of buckling. Large changes in the dimensions of the stack are needed to measure the small difference between $D_{\perp}$ and $D_{\parallel}$ since the anisotropy, in this method, is determined by the sum of the diffusion coefficients. This technique is not quite as accurate as the exponential method[4], which measures the difference of the two diffusion coefficients. The results obtained by pulsed

neutron methods showed no appreciable difference between the parallel and perpendicular diffusion coefficients, within the accuracy of the measurement.

The effect of spacial harmonics on the measured decay constant was determined for a combination of detector and source positions in both large and small size stacks.

For the large size stacks of graphite, the source was situated at the center of one interface and the decay data was measured with the detector at the center of the stack and then at the center of each of two outside faces. This decay data is shown in figure 7, and it can be seen that the harmonics are most pronounced when the detector and source are both outside the moderator. The relaxation time for the individual curves appear to be slightly different, but if the decay data is corrected for the effect of the detector perturbation and if the harmonics are properly corrected for, all curves yield the same decay constant.

The source was then placed 10 inches inside the moderator and the decay curves were obtained with the same detector locations as previously discussed. The movable table served to always maintain the source on the centerline as the size of the stack was being changed. Figure 8 shows the decay curves for the three conditions investigated. The location of the detector at the geometric center and the source inside the

stack yields the smallest content of higher spacial modes to the decay data. Therefore, in all pulsed measurements, the source was inserted in the moderating material as close to the center of the stack as was physically possible. The detector was placed in the center of the X-Y plane along the centerline of the Z axis such that the peak of the fundamental mode was in the center of the active length of the detector. With the detector located in this position all even harmonics are eliminated from the recorded data. To correct for the effect of the perturbing influence of the detector and source inside the stack, a dummy detector and source which were identical with the active detector and source were placed at a symmetrical location. The decay was then obtained with and without the dummy source and detector, and the data linearly extrapolated to the value of the decay constant without a perturbation. The experimental values of the difference in the decay constants was approximately 2.5% for the large stacks and about 4% for the small stacks.

The measurement of the effect of harmonics for the small size stacks was obtained with the arrangement shown in figure 6. The source is situated inside one of the adjacent stacks to reduce the perturbating effects. The detector is located inside the stack and is progressively moved from a position near the source to a position near the opposite boundry with decay data

recorded at each position. The effect of spacial harmonics should cause a definite change at the beginning of the decay curve as was evident for the large size stacks. The detector was then situated outside the stack and the decay data measured. In all measurements there was no change in either the observed harmonic content or the measured decay constant, therefore the effect cannot be due to spacial harmonics, but rather due to energy harmonics which must be taken into consideration. The measurement of the decay constant for the small size stacks is made more difficult when the background is high, since any finite region of the decay curve can be assumed to be a pure exponential. Figure 9 shows that the decay data with the electrostatic deflection will imply a different relaxation time than the data without deflection.

The decay measurements for the pure bismuth stacks were obtained by placing large cadmium covered paraffin blocks on all sides surrounding the array. With this technique the neutrons are slowed down in the paraffin, leading to a higher intensity of epi-cadmium neutrons in the bismuth, and thus allowing the diffusion of thermal neutrons in the bismuth to be investigated.

Analysis of Data

The decay data were first analyzed by graphic methods and then by analytical means. The data from each decay measurement

were plotted to determine the approximate number of points that contained significant harmonic content. These points were then eliminated from the decay data. The remaining points were then least square fitted to a linear function using an LGP-30. The program fitted the logarithmic of the difference of the counts in the two successive time channels. If the number of counts in a given channel is of the form:

$$N_n = Ae^{-\alpha t_n} + B \tag{6}$$

where B is the background and assumed to be constant. Then the difference between the n^{th} channel and the (n + 1) channel will not contain the background. Hence the logarithm of the difference is:

$$\ell n\ (N_n - N_{n+1}) = -\alpha t_{n+1} + \ell n \left[A(e^{-\alpha \Delta t} - 1)\right] \tag{7}$$

The result is a straight line independent of the background with a slope of α. The first points are then successively dropped in the least square fit until the value of the decay constant does not change. The decay constant for a given size moderator together with the associated values of buckling are tabulated in Tables I-V for the different graphite and graphite-

bismuth ratios. The value of any relaxation time is the average of several individual decay measurements.

Determination of the Diffusion Parameters

The absorption cross section Σ_a, the diffusion coefficient $\overline{Dv}$ and the diffusion cooling coefficient C were determined by least squares fitting the data points (λ, B^2) to the linear function (5)

$$\frac{(\lambda - \lambda_o)}{B^2} = A_1 + A_2 B^2 \qquad (8)$$

where A_1 and A_2 are coefficients determined by varying the value of λ_o until a minimum variance in the expression

$$\sum_n \left[\left(\frac{\lambda - \lambda_0}{B^2}\right) - \left(\frac{\lambda - \lambda_o}{B^2}\right) \text{(calculated)} \right]^2$$

is obtained for the values of A_1 and A_2. With the assumption of constant per cent probable error in the value of $\left(\frac{\lambda - \lambda_o}{B^2}\right)$, all points were assigned equal weights. The effect of analyzing the data by equation (8) is to accentuate the influence of the higher coefficients and this is clearly shown in Figure 10 where the points have a much larger spread than in a plot of λ vs B^2. Since the value of C in equation (4) is the coefficient of the quadratic term in the polynomial expansion about $B^2 = 0$, the determination of the diffusion

cooling contains an error if the polynomial is terminated at three terms because the influence of the higher order terms is then relegated to the coefficients of the truncated form. On the other hand an attempt to fit the data to higher order terms only results in extremely large errors for the coefficients.

The method used was to fit the data points to equation (8), and also to the inverted series.

$$\left[\frac{B^2}{\lambda - \lambda_o}\right] = F_1 + F_2 \ (\lambda - \lambda_o) \qquad (9)$$

The two equations (8) and (9) then represent a bound on the values of the coefficients. It was found that the values of the diffusion cooling coefficient obtained from fitted values of A_2 and F_2 were quite different. This showed that the higher order terms could not be neglected, and neither equation (8) nor (9) are individually correct. However, if the least squares fit to equations (8) and (9) are repeated successively dropping points of maximum B^2 in equation (8) and maximum $(\lambda - \lambda_o)$ in equation (9), the values would asymptotically approach the same limit. Hence the values of the diffusion parameters were found as B^2 (or $\lambda - \lambda_o$) approached zero as defined by equation (4). The values of the diffusion coefficients obtained in this way agree quite well with each other, except for the values obtained at maximum buckling as shown in Figure 11.

The difference between the values of diffusion cooling $(C_A - C_F)$ obtained from the coefficients A_2 and F_2 of equations (8) and (9) decrease as the points of maximum buckling are progressively dropped but at the same time the error associated with the least squares fit rapidly increases. As the diffusion cooling coefficients in each series approaches its asymptotic value, the difference $(C_A - C_F)$ approaches a minimum. The value of diffusion cooling coefficient reported is obtained when the maximum total error spread in the difference reaches a minimum value; and then the error associated with the diffusion parameters is not the statistical error obtained by fitting the data but a more realistic value determined by the bound of equations (8) and (9) given by:

$$\mathcal{E} = \left[C_{F_{max}} - C_{A_{min}} \right]$$

The resulting diffusion parameters of graphite and graphite-bismuth combinations are tabulated in Table VII.

Measurements of the diffusion lengths were made of the graphite and all the graphite-bismuth volume ratios by exponential methods using the same material as the pulsed experiment. The values were determined in the directions parallel and transverse to the extrusion axis and then averaged in the manner given in equation (5). The results are plotted

in Figure 12 as a function of the volume of bismuth divided by the total volume; and are tabulated in Table VI. In all cases the diffusion length determined only from the pulsed experiment agreed with the average diffusion length from the exponential measurement, within the statistical error. The least squares fit to equation (8) and (9) were done with and without the inclusion of the diffusion length as a point at a negative buckling. Since the pulsed neutron technique yields an accurate value of the average diffusion constant, and the exponential method yields an accurate value of the diffusion length, the combined data results in greater accuracy for the determination of the thermal absorption cross sections. The values of the mean lifetime given in Table VII are the results of this analysis with the diffusion length included. The value of the absorption cross section of graphite is found to be 3.83 ± .06 mb, corrected for nitrogen content and the value for bismuth is 33.8 ± .7 mb, where these values are obtained by combining the results measured with different volume ratios.

Conclusion

The value obtained for the diffusion cooling coefficient of graphite is 33 ± 3 x 10^5 cm^4/sec; this is quite different in magnitude from the results of other measurements (6,7) including those of the authors (8). The large difference between the values can be explained by the incorrect measurement of the

fundamental decay constant for small size stacks of moderator. The analysis of the decay data depends on correctly eliminating not only the spacial harmonics but also the energy harmonics.

A calculation of the decay constants for the higher spacial harmonics was made for a point thermal source located at the geometric center of the stack as a function of buckling. The results, even though it was a slight overestimation of the effect, agreed well with the harmonics obtained experimentally for the large size stacks. For the small size stacks, the calculation did not agree at all with the measured higher modes. The experimental results of the harmonic investigation showed that the effect is not due to spacial harmonics but rather to the energy harmonics which persists long after the spacial harmonics reach a fundamental value.

If the ratio of maximum neutron yield to background is small, it is obvious that the presence of energy harmonics will produce an incorrect decay constant. This effect would lead to a wrong determination in the value of the diffusion cooling coefficient. Recent measurements [9] in graphite show that the time required to wait for equilibrium after the end of the burst of neutrons is approximately 2 milliseconds, and is apparently independent of buckling. This means that if the signal-to-background ratio is small, the observer would erroneously measure the decay constant of the higher energy

modes instead of the fundamental decay. The existence of a linear portion of the curve on a semi-log plot is real, but the decay constant is too short and the inferred value of the diffusion cooling coefficient is incorrect.

Hence the combined requirements of the equilibrium time and the maximum signal-to-background ratio determine the smallest size moderator that can be measured. These recent measurements were made with a signal-to-noise ratio greater by approximately 10^3 than the authors earliest measurements. The decay constant associated with small bucklings agreed quite well with the earlier measurements, but the decay constants at large bucklings were considerably different, and clearly showed the effect of the higher energy modes. The relaxation time of the next highest energy mode has been estimated to be approximately 300 μsec as found by subtracting the fundamental decay from the decay data of some of the smallest size graphite stacks. If this value of τ_1 is used in an equation (10) relating the diffusion cooling coefficient to the higher energy modes, reasonable agreement is obtained with the value of diffusion cooling reported.

Furthermore, the method of analysis used is less dependent on the large buckling measurements, as the value of the diffusion cooling coefficient is obtained in the limit as $B^2 \rightarrow 0$. This method also reduces the dependence of coefficients on knowing

an accurate value of the extrapolation distance, since the value of the buckling becomes less dependent on the extrapolation distance as the data points are successively dropped. The value of the extrapolation distance used in the determination of the buckling was obtained from an iteration of the diffusion coefficient calculation utilizing all the data points. The value was then kept constant as the successive points were dropped.

The bismuth diffusion length, diffusion coefficient, and diffusion cooling coefficient were measured and are recorded in Tables VII and VIII. The bismuth diffusion length, as measured by the exponential method, is not consistent with the pulsed neutron data. Consequently, the bismuth diffusion coefficients were calculated entirely from pulsed neutron data. The bismuth errors are not tabulated because of the possibility of a systematic error in the measurements as may be inferred by the inconsistency of the pulsed and static neutron measurements. In all the other assemblies of graphite and graphite-bismuth mixtures the exponential and pulsed neutron measurements are entirely consistent.

The mixed stacks were composed of GBF graphite bars, approximately 3 7/8" x 3 7/8" x 24" each, and bismuth bars, approximately .985" x .985" x 24" each. The AA graphite, which is a selected lot of GBF graphite, had been machined into 1" x 1" x 24" bars. The AA graphite and bismuth are the same

material which was used in earlier slowing down and diffusion length measurements. (1)

Acknowledgements

The authors would like to thank W. Bornstein for his assistance in the reduction of data, John Graebner for his assistance in the measurements of the decay data, Dr. Henry Honeck for his valuable discussions, and Dr. James Phelps for his assistance in the diffusion length measurements.

References

1. J. M. Hendrie, J. P. Phelps, G. A. Price, E. V. Weinstock, Progress in Nuclear Energy, Series I, Vol. 3 (1959).
2. G. F. von Dardel and N. G. Sjöstrand, Progress in Nuclear Energy, Series I, Vol. 2 (1958).
   K. H. Beckurts, Reactor Physics Research with Pulsed Neutron Sources.
3. W. M. Lopez and J. R. Beyster, Measurements of Diffusion Parameters of Water by Pulsed Neutron Method, (GA-1584 Rev) 1961.
4. J. P. Phelps, E. V. Weinstock, Transactions of American Nuclear Society, Nov. 1959, Session 12, Paper 5.
5. E. Starr and J. Koppel, Determination of Diffusion Hardening In Water, BNL-5704 (1961).
6. Antonov et al, A Study of Neutron Diffusion in Beryllium, Graphite and Water by the Impulse Method, Vol. 5 Geneva Papers 1955.
7. K. H. Beckurts, Nuc. Sci. & Eng. 2, 516 (1957).
8. E. Starr and G. A. Price, Trans. Am. Nuc. Soc., Nov. 1959 Session 12, Paper 6.
9. E. Starr and J. W. L. de Villiers, Determination of Diffusion Cooling in Graphite by Measurement of the Average Neutron Velocity - to be published.

10. S. Purohit, Neutron Thermalization and Diffusion in Pulsed Media, ORNL-60-7-32 (1960).

11. M. Nelkin, A Decay of a Thermalized Neutron Pulse, GA-816.

Footnotes

1 Less than .04% impurities by chemical analysis.

2 36% by weight B_4C sandwiched between two sheets of aluminum.

Table of Results I
GBF Graphite
Stack Density = 1.697

Height (cm)	Width (cm)	Length (cm)	B^2 ($cm^{-2} \times 10^{-3}$)	λ (sec^{-1})
128.3	127.9	121.9	1.766	429.2
108.5	127.9	121.9	1.985	467.5
108.5	108.3	121.9	2.201	507.0
88.8	108.3	121.9	2.575	579.8
88.8	88.6	121.9	2.950	630.4
69.1	88.6	121.9	3.662	790.9
69.1	69.0	121.9	4.379	919.5
49.3	69.0	121.9	6.042	1225.7
49.3	49.2	121.9	7.709	1436.0
49.3	49.2	59.1	9.599	1691.5
49.3	39.4	59.1	11.414	1960.4
39.4	39.4	59.1	13.225	2162.3
29.5	49.3	59.1	15.083	2292.2
49.3	49.3	29.5	16.143	2502.1
29.5	39.4	59.1	16.904	2585.0
39.4	49.2	29.5	17.972	2693.0

Table of Results II
Volume Ratio 4:1 GBF Graphite to Bismuth
Stack Density = 3.303

Height (cm)	Width (cm)	Length (cm)	B^2 ($cm^{-2} \times 10^{-3}$)	λ (sec^{-1})
128.4	135.6	121.9	1.639	474.9
108.6	135.6	121.9	1.910	509.7
88.9	135.6	121.9	2.277	594.1
69.1	135.6	121.9	2.982	725.8
49.3	135.6	121.9	4.610	1104.0
69.1	61.6	121.9	4.775	1117.3
69.1	86.1	61.0	5.416	1257.1
49.4	61.6	121.9	6.393	1414.4
59.3	73.9	61.0	6.447	1439.9
69.1	61.5	61.0	6.501	1435.3
59.3	61.5	61.0	7.119	1568.2
49.4	61.5	61.0	8.124	1728.8
59.3	49.2	61.0	8.309	1767.2
49.4	49.2	61.0	9.313	1910.7
29.7	135.6	121.9	9.887	2117.7
39.5	49.2	61.0	11.072	2204.0
29.6	61.5	121.9	11.698	2298.8
29.6	61.5	61.0	13.438	2480.9

Table of Results III
Volume Ratio 2:1 GBF Graphite to Bismuth
Stack Density = 4.378

Height (cm)	Width (cm)	Length (cm)	B^2 ($cm^{-2} \times 10^{-3}$)	λ (sec^{-1})
128.5	147.6	121.9	1.607	512.0
128.5	103.9	121.9	2.033	616.5
108.7	103.9	121.9	2.236	658.0
108.7	88.6	121.9	2.536	722.9
88.8	88.6	121.9	2.901	796.6
88.8	73.9	121.9	3.372	901.3
69.2	73.9	121.9	4.065	1045.5
88.8	73.8	61.0	5.072	1275.3
69.0	73.8	61.0	5.769	1413.3
49.4	59.0	121.9	6.509	1607.3
49.3	59.1	61.0	8.210	1894.4
39.4	73.8	61.0	9.095	2041.1
39.4	59.1	61.0	9.933	2177.5
39.4	44.3	61.0	11.653	2399.1
49.3	29.5	61.0	14.382	2598.7

Table of Results IV
Volume Ratio 1:1 GBF Graphite to Bismuth
Stack Density = 5.715

Height (cm)	Width (cm)	Length (cm)	B^2 ($cm^{-2} \times 10^{-3}$)	λ (sec^{-1})
128.4	128.2	121.9	1.730	598.3
128.5	118.2	121.9	1.824	623.9
118.7	98.4	121.9	2.189	725.6
98.7	98.4	121.9	2.464	800.9
98.7	88.6	121.9	2.671	836.1
88.8	78.7	121.9	3.157	932.7
79.0	78.7	121.9	3.438	1019.3
69.1	78.7	121.9	3.839	1108.4
98.8	98.4	61.0	4.131	1183.7
59.2	78.7	121.9	4.444	1259.4
98.8	68.9	61.0	5.022	1400.1
79.0	78.8	61.0	5.106	1424.8
79.0	68.9	61.0	5.509	1516.6
59.2	78.8	61.0	6.110	1620.7
69.0	59.1	61.0	6.513	1737.3
59.2	59.1	61.0	7.113	1867.2
59.2	49.3	61.0	8.074	2035.5
59.2	39.4	61.0	9.743	2319.3
49.3	39.4	61.0	10.722	2449.1

Table of Results V
Bismuth
Stack Density = 9.761

Height (cm)	Width (cm)	Length (cm)	B^2 ($cm^{-2} \times 10^{-3}$)	λ (sec^{-1})
113.4	115.7	121.9	1.980	874.9
113.4	105.8	121.9	2.106	893.4
103.5	105.8	121.9	2.238	950.4
103.5	96.0	121.9	2.400	1040.6
94.0	96.0	121.9	2.568	1184.4
94.0	86.7	121.9	2.824	1229.4
83.9	76.3	121.9	3.324	1420.8
74.0	76.3	121.9	3.652	1532.5

Table of Results VI
A A Graphite
Stack Density = 1.674

Height (cm)	Width (cm)	Length (cm)	B^2 ($cm^{-2} \times 10^{-3}$)	λ (sec^{-1})
111.9	121.8	122.1	1.993	477.7
101.7	101.5	122.1	2.410	560.3
86.4	86.3	122.1	3.065	683.5
71.2	71.0	122.1	4.160	846.1
81.3	81.2	61.0	5.106	1025.0
71.1	71.0	61.0	5.904	1167.0
61.0	60.9	61.0	7.101	1349.0
55.9	55.8	61.0	7.949	1484.0
50.9	50.8	61.0	9.030	1654.0
45.8	45.7	61.0	10.484	1861.0
43.2	43.2	61.0	11.390	1932.0
40.6	40.6	61.0	12.461	1965.0
38.1	38.1	61.0	13.726	2069.0

Table of Results VII

Exponential Diffusion Length Measurement

Material	Transverse $L_{\perp}$	Parallel $L_{\parallel}$	Average $L_{Avg.}$
A A Graphite	53.8 ±0.3	56.0 ±0.3	54.5 ±0.5
GBF Graphite	50.0 ±0.2	52.3 ±0.2	50.7 ±0.3
Graphite-Bismuth 4:1	47.4 ±0.1	49.4 ±0.1	48.0 ±0.2
Graphite-Bismuth 2:1	44.2 ±0.1	47.1 ±0.1	45.2 ±0.2
Graphite-Bismuth 1:1	42.5 ±0.1	45.5 ±0.1	43.5 ±0.2
Bismuth	40.8	41.0	40.9

Table VIII

Tabulation of Diffusion Parameters at 22°C

Stack	Partial Graphite Density (gms/cc)	Partial Bismuth Density (gms/cc)	Stack Density (gms/cc)	λ_o^* (sec^{-1})	Dv ($cm^2/sec \times 10^5$)	C (cm^4 $sec \times 10^5$)	ϵ (cm)
A A Graphite	1.674		1.674	71.2 ±.8	2.09 ±.03	41 ±4	1.79
GBF Graphite	1.697		1.697	79.2 ±.6	2.02 ±.01	34 ±3	1.73
Graphite-Bismuth 4:1	1.355	1.948	3.303	100.0 ±.8	2.27 ±.01	33 ±3	1.96
Graphite-Bismuth 2:1	1.130	3.248	4.378	126.1 ±.8	2.486 ±.005	43 ±2	2.15
Graphite-Bismuth 1:1	0.846	4.869	5.715	145.4 ±1.2	2.719 ±.006	51 ±5	2.38
Bismuth **		9.761	9.761	180.7	3.06	215	2.72

* Values of $(1\ L^2)$ are used in the least squares fit, except for Bismuth stack.

** See text for comments on probable errors.

Figure Captions

1. Neg. No. 11-542-61
2. Neg. No. 11-539-61
3. View of the Graphite-Bismuth 1:1 Stack, Neg. No. 11-589-60.
4. Measurement of the Effect of Room Return to the Empty Closed Boral Box - Neg. No. 11-468-61.
5. Effect of Paraffin-Cadmium Reflector Around Graphite Stack Neg. No. 11-541-61.
6. Effect of Graphite-Cadmium Reflector Around Graphite Stack Neg. No. 11-540-61.
7. Spacial Harmonics for Various Positions with Source Outside Moderator - Neg. No. 11-472-61.
8. Spacial Harmonics for Various Positions with Source Inside Moderator - Neg. No. 11-470-61.
9. Effect of Energy Harmonics With and Without Beam Deflection System - Neg. No. 11-471-61.
10. $\left[\frac{\lambda - \lambda_o}{B^2}\right]$ vs B^2 for the Graphite-Bismuth 4:1 Stack - Neg. No. 11-671-61.
11. Values of $\overline{\overline{Dv}}$ as Maximum B^2 Points are Successively Dropped Neg. No. 11-672-61.
12. Exponential Measured Diffusion Length vs Volume Ratio - Neg. No. 11-469-61.
13. Decay Constant, λ vs Buckling, B^2 for the Graphite-Bismuth 4:1 Stack - Neg. No. 2-390-62.

PULSING SYSTEM FOR VAN DE GRAAFF GENERATOR

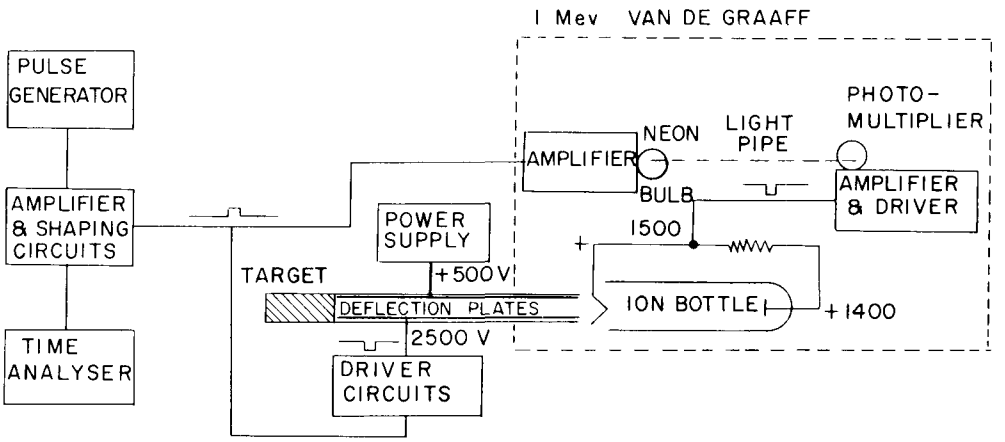

Figure 1

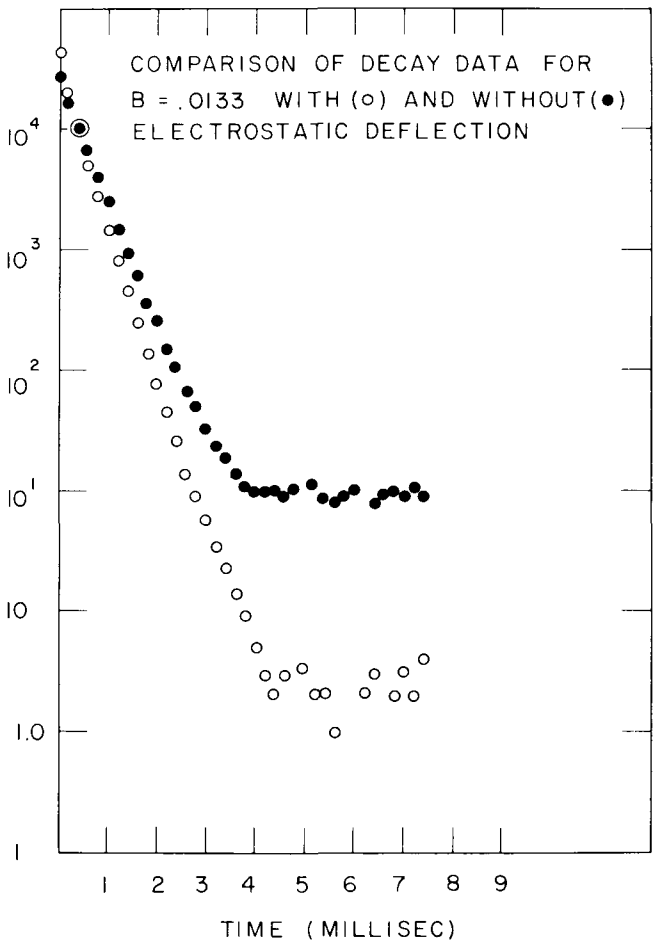

Figure 2

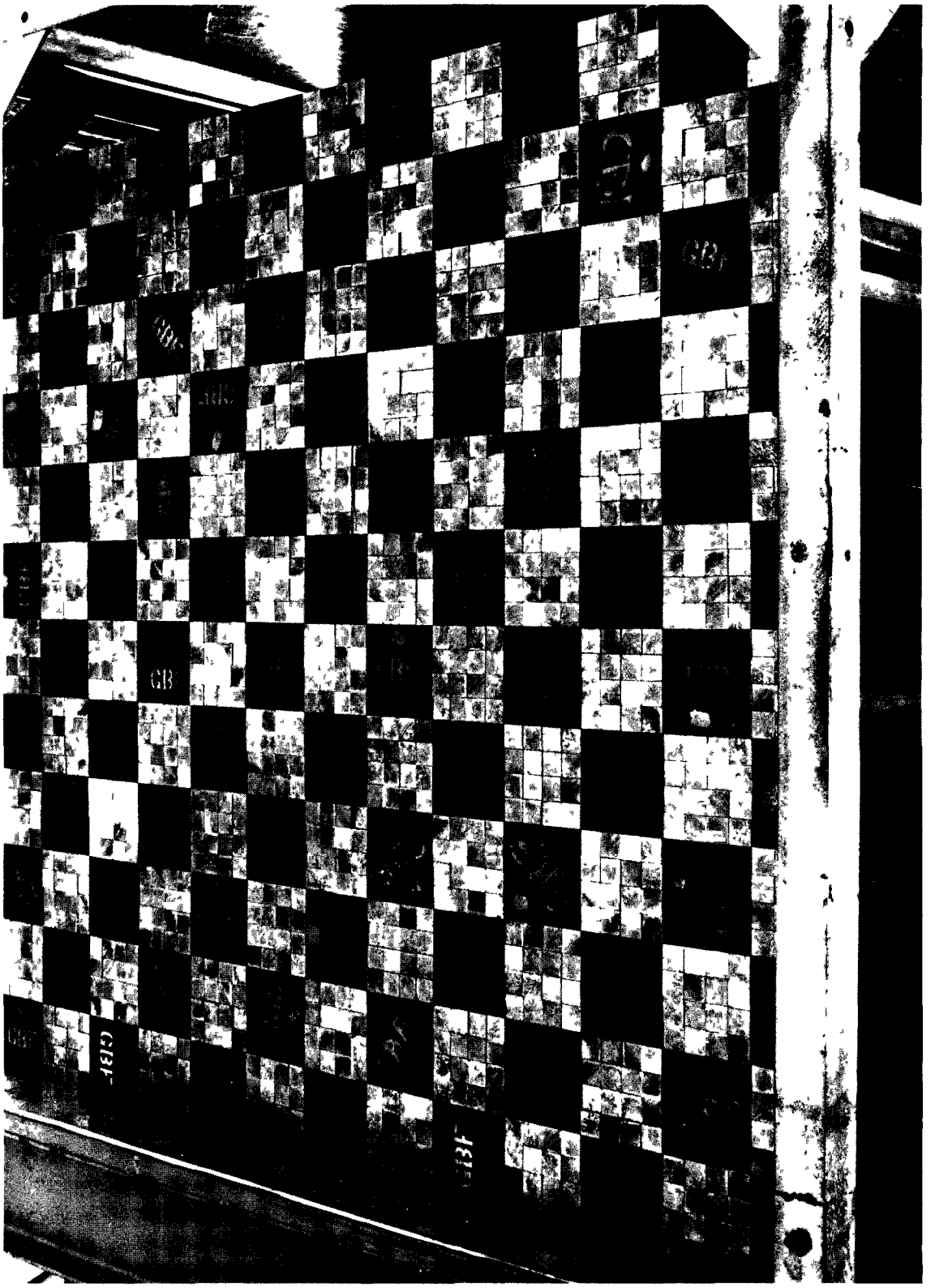

Figure 3

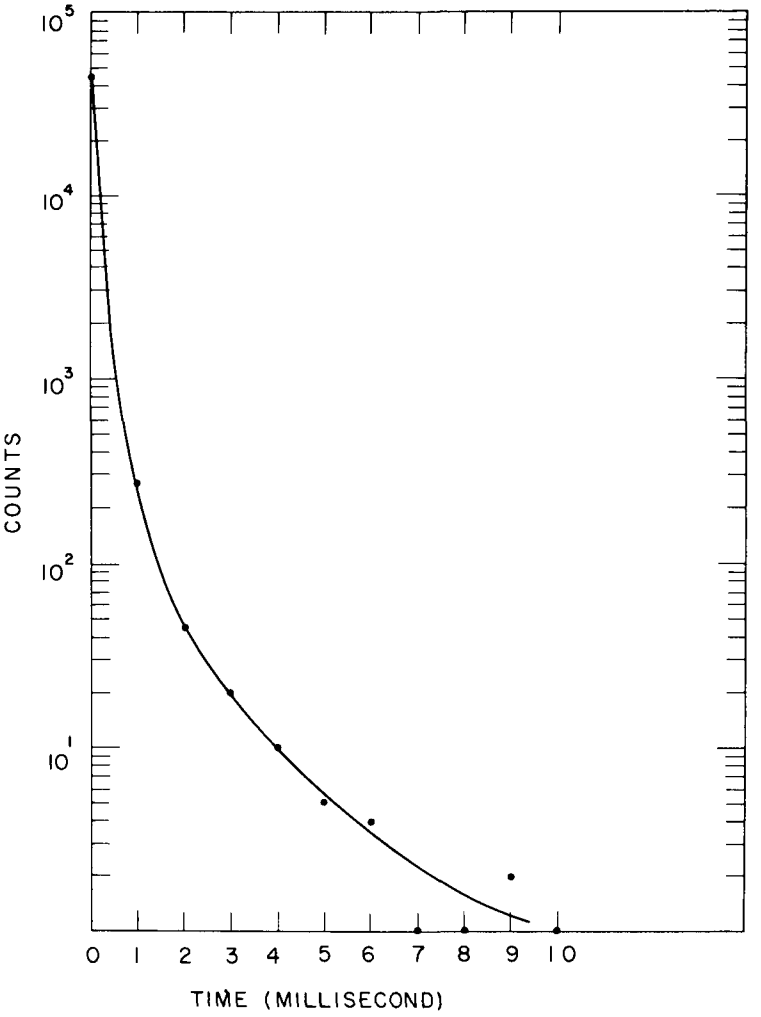

Figure 4

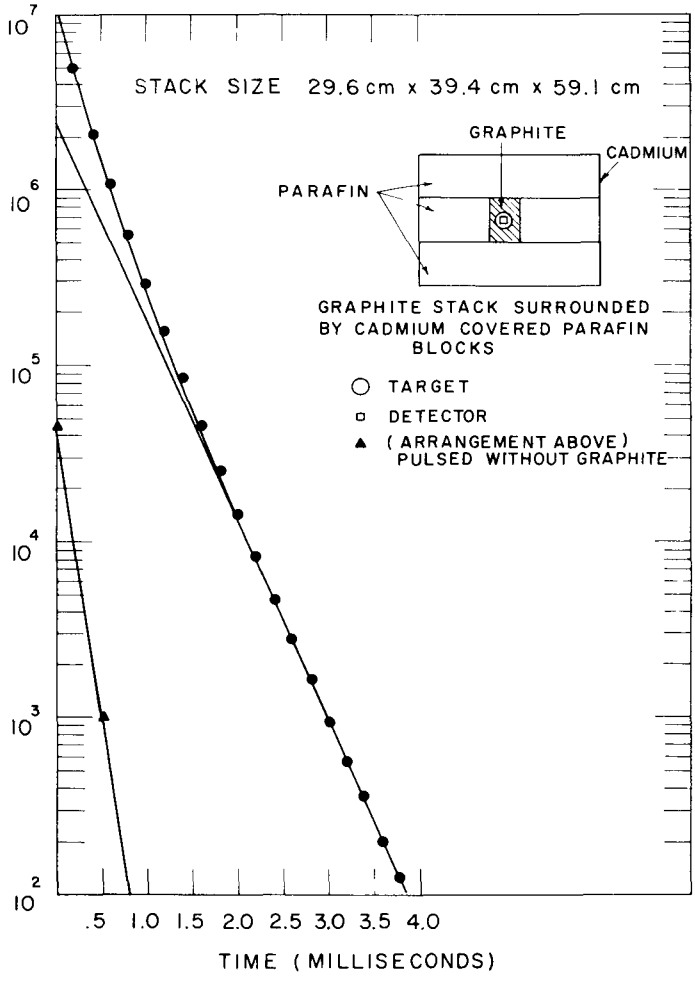
STACK SIZE 29.6 cm x 39.4 cm x 59.1 cm
GRAPHITE
CADMIUM
PARAFIN
GRAPHITE STACK SURROUNDED BY CADMIUM COVERED PARAFIN BLOCKS
TARGET
DETECTOR
(ARRANGEMENT ABOVE) PULSED WITHOUT GRAPHITE
10^7
10^6
10^5
10^4
10^3
10^2
.5 1.0 1.5 2.0 2.5 3.0 3.5 4.0
TIME (MILLISECONDS)

Figure 5

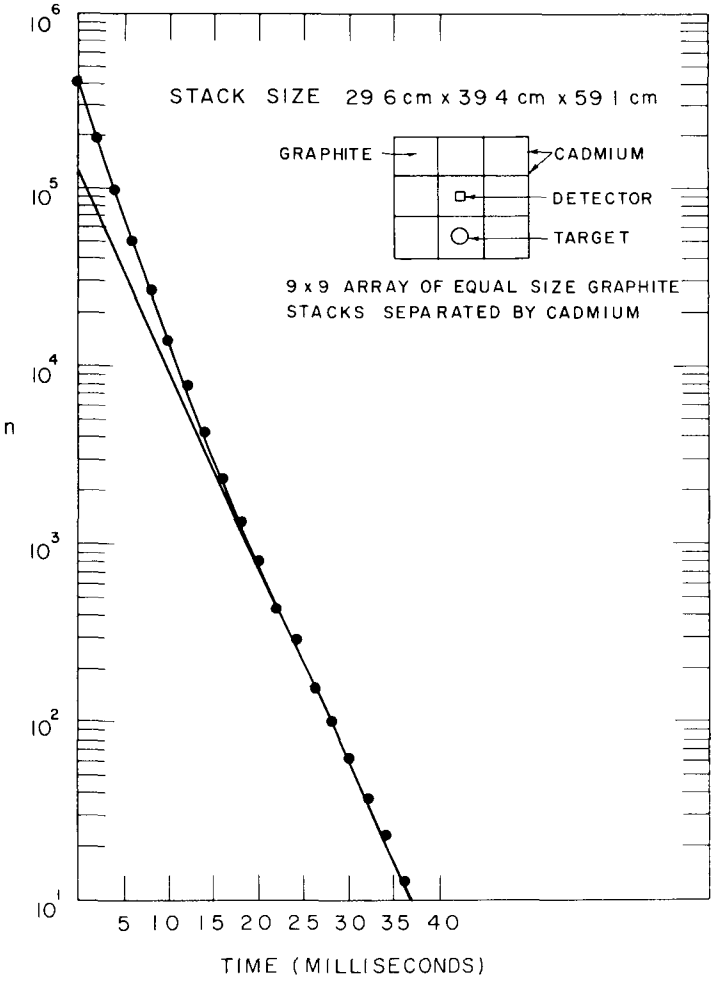
STACK SIZE 29 6 cm x 39 4 cm x 59 1 cm
GRAPHITE
CADMIUM
DETECTOR
TARGET
9 x 9 ARRAY OF EQUAL SIZE GRAPHITE STACKS SEPARATED BY CADMIUM
n
10^6
10^5
10^4
10^3
10^2
10^1
5 10 15 20 25 30 35 40
TIME (MILLISECONDS)

Figure 6

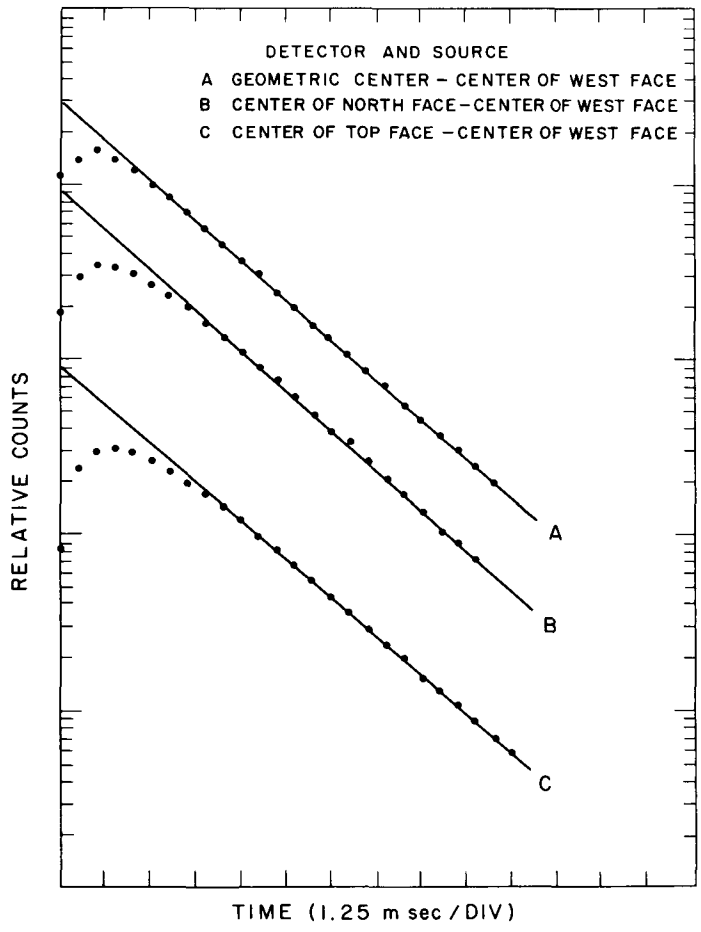
DETECTOR AND SOURCE
A GEOMETRIC CENTER - CENTER OF WEST FACE
B CENTER OF NORTH FACE - CENTER OF WEST FACE
C CENTER OF TOP FACE - CENTER OF WEST FACE
A
B
C
RELATIVE COUNTS
TIME (1.25 m sec / DIV)

Figure 7

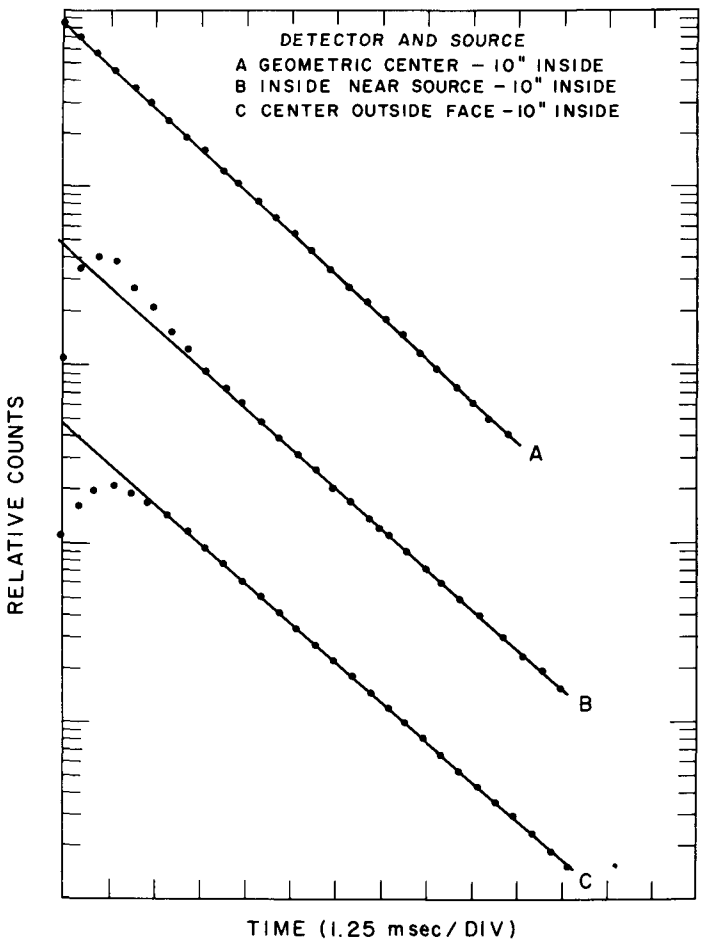
DETECTOR AND SOURCE
A GEOMETRIC CENTER – 10" INSIDE
B INSIDE NEAR SOURCE – 10" INSIDE
C CENTER OUTSIDE FACE – 10" INSIDE
A
B
C
RELATIVE COUNTS
TIME (1.25 msec / DIV)

Figure 8

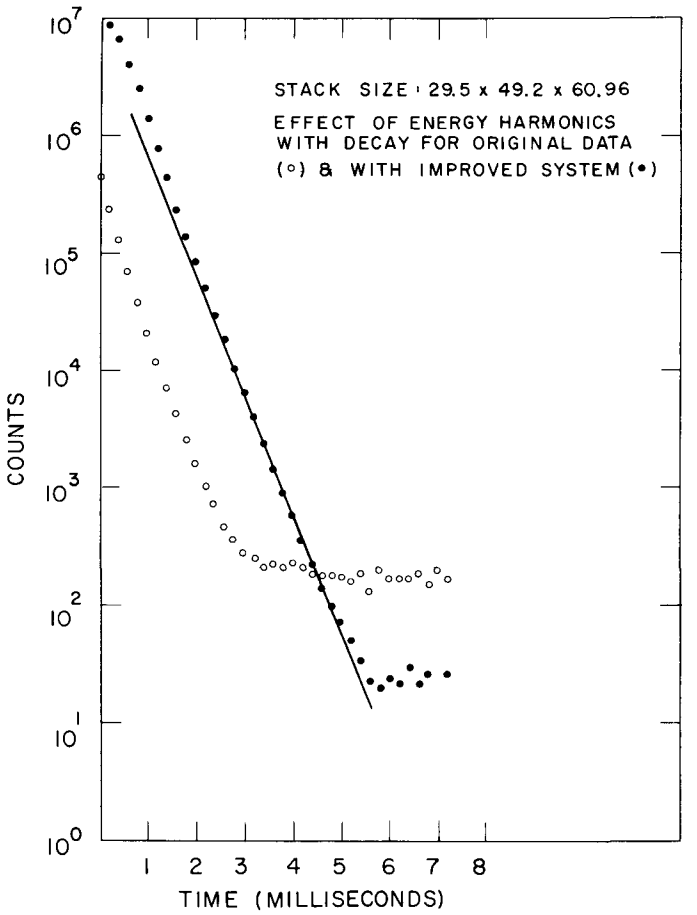
STACK SIZE : 29.5 x 49.2 x 60.96
EFFECT OF ENERGY HARMONICS
WITH DECAY FOR ORIGINAL DATA
(○) & WITH IMPROVED SYSTEM (•)
COUNTS
TIME (MILLISECONDS)

Figure 9

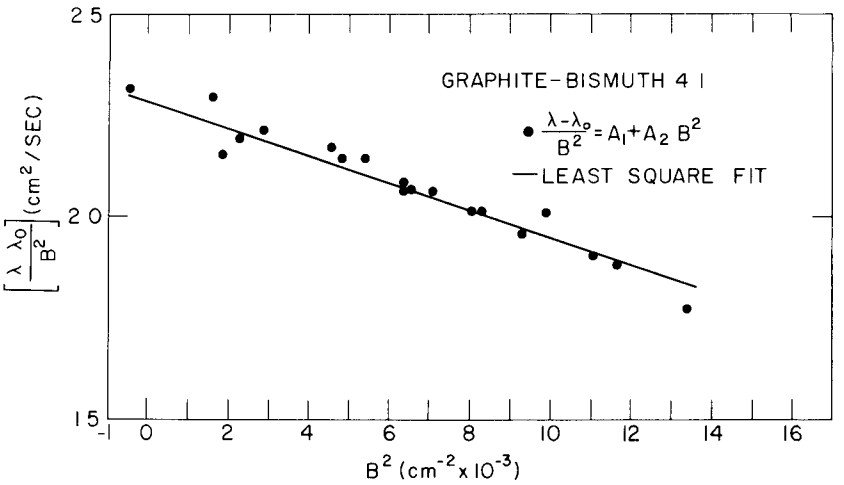

Figure 10

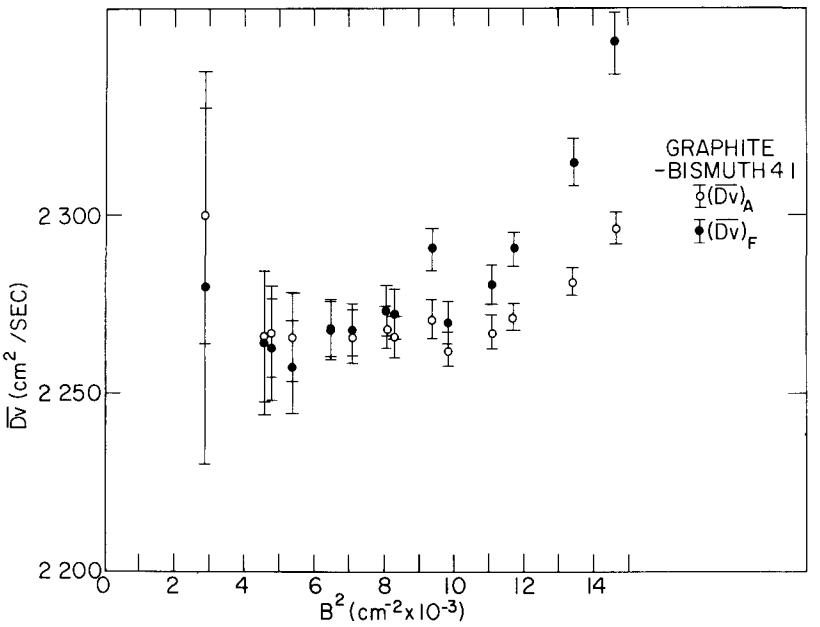

Figure 11

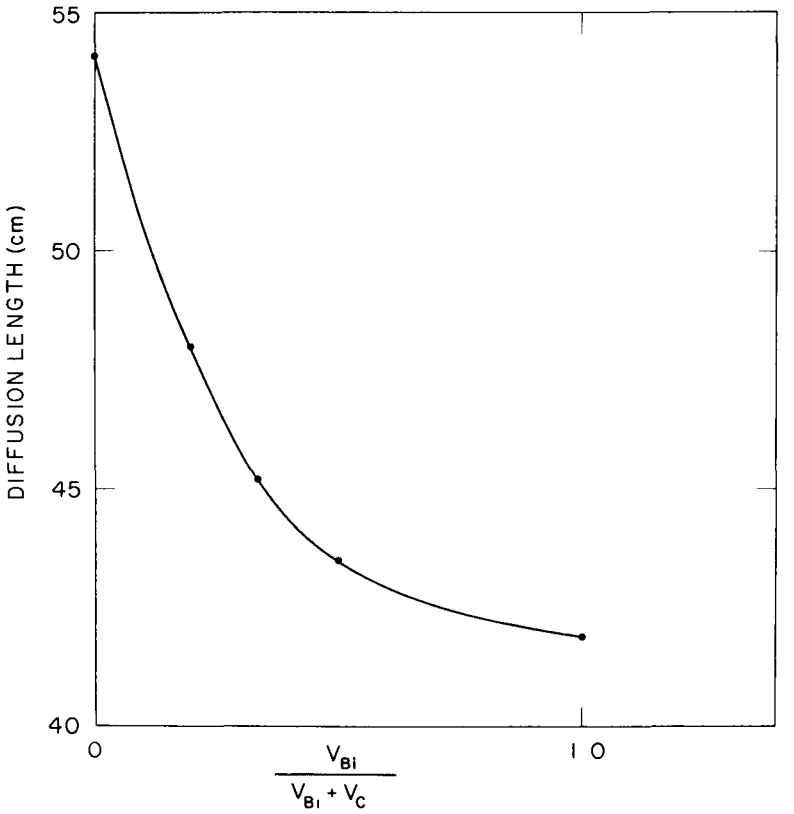

Figure 12

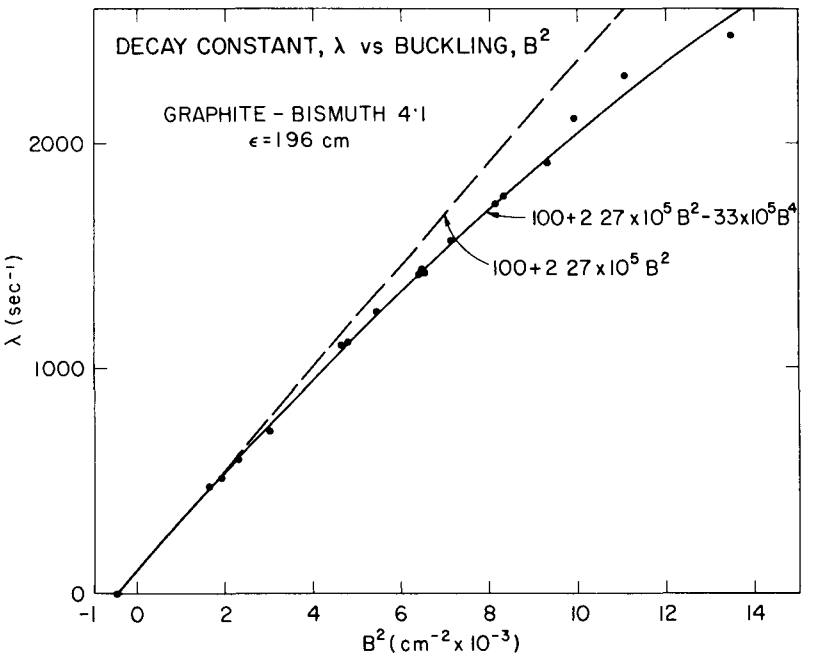

Figure 13

ABSTRACT

A review of 16 papers (1 - 16) submitted to the Brookhaven conference and dealing with the experimental aspects of "asymptotics" or "transients" in space, time, and energy is given. Most of these papers deal with diffusion parameter measurements using pulsed or stationary methods; numerous new data have been reported and are critically compared. A number of new techniques for the investigation of space- and time-dependent thermalization phenomena are reviewed.

1. Introduction

About four years ago, the whole field of "transients" or "asymptotics" research appeared to be in a very good state; measurements by different authors using either pulsed or stationary methods were in reasonable agreement. Attempts to interpret the data theoretically were in general quite successful. There seemed to be not much incentive for further research work. However, with the arrival of more advanced experimental techniques and of more sophisticated analysis methods, the situation has almost completely changed. Today, there exists a considerable amount of discrepant data on almost any moderator. Reported data for thermalization times and diffusion cooling coefficients diverge by up to a factor of three and even for one of the most fundamental constants of neutron physics, the diffusion length of thermal neutrons in water, data differing to up to 6% have been found. Only in very few cases the data can be calculated theoretically with sufficient accuracy. The author hopes that discussions at this conference will contribute towards a better understanding of all these problems and clarify some discrepancies.

In order to give a formal classification of the problems which will be discussed in this paper, let us start from the space- time- and energy

The Proceedings of the

BROOKHAVEN CONFERENCE ON NEUTRON THERMALIZATION

have been published in four volumes.

Volume I, The Scattering Law

Volume II, Neutron Spectra in Lattices and Infinite Media

Volume III, Experimental Aspects
of Transient and Asymptotic Phenomena

Volume IV, Theoretical Aspects
of Transient and Asymptotic Phenomena

BNL 719 (C-32)
Volume IV of IV, Theoretical Aspects
of Transient and Asymptotic Phenomena

3/25/2-19-63

PROCEEDINGS OF THE BROOKHAVEN CONFERENCE ON NEUTRON THERMALIZATION

Volume IV, Theoretical Aspects of Transient and Asymptotic Phenomena

April 30 to May 2, 1962

BROOKHAVEN NATIONAL LABORATORY
ASSOCIATED UNIVERSITIES, INC.
under contract with the
UNITED STATES ATOMIC ENERGY COMMISSION

BNL 719 (C-32)
(Physics - TID 4500, 18th Ed.)

PROCEEDINGS OF THE BROOKHAVEN CONFERENCE ON NEUTRON THERMALIZATION

Volume IV, Theoretical Aspects of Transient and Asymptotic Phenomena

April 30 to May 2, 1962

BROOKHAVEN NATIONAL LABORATORY
UPTON, NEW YORK

LEGAL NOTICE

PRINTED IN USA
PRICE $15 00 FOR THE FOUR VOLUMES

Available from the
Office of Technical Services
Department of Commerce
Washington 25, D C

December 1962 1100 copies

PREFACE

A conference on the subject of neutron thermalization was held at the Brookhaven National Laboratory from April 30 to May 2, 1962, precisely four years after the close of the last thermalization conference, the Gatlinburg conference of April 28-30, 1958. The subject of thermalization, which concerns the approach to thermal equilibrium and the manner of the equilibrium distribution of neutrons in matter, has elicited a great deal of interest in the meantime. While the seventeen papers contributed at Gatlinburg could be assembled into a single, convenient volume, presenting the seventy Brookhaven papers has required four weighty books.

The Brookhaven conference was conducted as a "reporter" conference. The technical papers which were submitted were sorted into six categories, viz., the experimental and theoretical aspects of the "scattering law," of spectra in infinite media, and of transient phenomena. A reporter was chosen for each of the six topics, and was asked to prepare a talk which would contain an appreciation of the technical papers. The reporter talk, followed by a general discussion constituted each session. Thus, the individual papers were not presented, though copies were available to all who attended, and are presented in these proceedings. (While the papers from our Soviet colleagues were received too late for discussion at the conference, translated versions will also be found in these volumes.)

The success of a technical conference is always due to the efforts of many people. We must first thank the reporters and authors for the fine quality of their contributions. Mr. Robert Brown of Brookhaven's Graphic Arts Division was responsible for the prompt publication of the proceedings and for having more than ten thousand copies of the technical papers ready in time for the conference. Mrs. Mariette Kuper and Mr. Edward Bergin and their staffs directed the mechanics of the conference with skill and aplomb, while several members of the Theoretical Reactor Physics Group made important contributions to its planning and execution. In particular, we should thank Drs. Paul Michael and Henry Honeck, and for his kind encouragement throughout, Mr. Jack Chernick, the Group's Director.

NOEL CORNGOLD

VOLUME IV

PROGRAM AND TABLE OF CONTENTS

THEORETICAL ASPECTS OF TRANSIENT AND ASYMPTOTIC PHENOMENA
Chairman: N.G. SJÖSTRAND, Chalmers University of Technology, Gothenburg, Sweden

GA-3122 C 10

NEUTRON THERMALIZATION a la MODE*

Mark Nelkin

John Jay Hopkins Laboratory for Pure and Applied Science
General Atomic, San Diego, California

*Project No. 48.01. This work was supported by the U. S. Atomic Energy Commission under Contract AT(04-3)-167.

I. Introduction

The theory of neutron thermalization has developed to a considerable extent toward its basic objective of the quantitative determination of the thermal neutron distribution function as determined from the transport equation. The two main channels of this development have been in the improved theoretical and experimental understanding of the "scattering law" for thermal neutrons in moderating materials, and in the improved ability to use this information in solving the transport equation. In this paper, the latter of these two subjects will be considered. The former is summarized in other papers for this conference.

The transport equation for thermal neutrons can be considered from three levels of approach. The first level is the study of the basic mathematical properties of the transport equation for cross sections obeying the general constraints which apply to thermal neutron scattering from moderators. The objective of this study is to reach a level of understanding comparable to that which we now have for the one-velocity transport equation. Considerations in this area include the nature of asymptotic solutions as defined by eigenvalue problems, the modification of the Milne problem due to velocity dependence of the mean free path, and new physical phenomena peculiar to the thermalization problem, such as the thermal diffusion of neutrons in the presence of a temperature gradient. Investi-

gations on this level are essential to our fundamental understanding of the problem, and also have application to the interpretation of pulsed neutron measurements and diffusion length measurements. Recent developments in this area have been very interesting. In the author's opinion, the study of the basic mathematical properties of the transport equation for thermal neutrons is a very important current area of research in neutron thermalization, and has considerable relevance also to an improved understanding of phenomena in kinetic theory and solid state physics which are described by linearized transport equations. It is in this area that most of the discussion in the present paper will be concentrated.

A second level of approach, which is advancing at an impressive rate, is the direct numerical solution of the transport equation using large digital computers. The comparison of theory and experiment, on which advance in our understanding is fundamentally based, depends in an essential manner on the intelligent use of large digital computers to analyze the actual experimental situation in terms of the best available input cross sections. It should be emphasized that the advance in the technology in this area has been extremely rapid and will probably continue to be so for some time. It is the author's opinion that the use of large digital computers will play an increasingly dominant role in our basic understanding of the complex phenomena with which we are concerned.

There is also an intermediate level of approach which is concerned with simplified models for the thermalization process, and semi-analytical solutions to the transport equation. This general approach is illustrated by the modified heavy gas model, by eigenfunction expansions of the solution to the transport equation, and by variational formulations of the space and energy dependent problem. This intermediate level has played an important role in developing a semi-quantitative understanding of many complex phenomena. For some time it even appeared that this would be the best way to a quantitative understanding. In the last few years, however, progress in this direction has been much less rapid than through direct numerical solutions with digital computers. There are several interesting papers for this conference on this level of approach. In order to maintain a somewhat coherent pattern to the presentation in this summary, it has been necessary to omit comment on these papers. Thus, this summary represents, to some extent, the approaches of greatest personal interest to the author.

In Section II we discuss the definition of the thermal diffusion length as an eigenvalue problem, and the numerical solution of this equation with comparison to experiment. This particular problem is a good illustration of the use of digital computers in combination with an examination of the mathematical nature of the transport equation to reach a rather satisfactory

degree of understanding. Section III is devoted to the considerably less well understood area of time-dependent problems. The emphasis is on the question of existence of an eigenvalue representing an asymptotic exponential decay.

II. The Diffusion Length

We define the thermal diffusion length κ^{-1} as the eigenvalue of the transport equation corresponding to a positive eigenfunction $e^{-\kappa x} f(E,\mu)$ describing the exponential relaxation of the thermal flux in an infinite source free medium with no spatial variation in the y and z directions. This definition was first given by Kuscer and Ribaric (1) who derived the integral equation defining the diffusion coefficient in the weak absorption limit, and gave a procedure for expansion of κ^2 in a power series in the absorption cross section. For the particular case of monatomic hydrogen moderation, the weak absorption limit corresponds to the calculation of the coefficient of self-diffusion for a gas of hard spheres. This very old problem in kinetic theory was first considered by Boltzmann and was first solved numerically by Pidduck (2) in 1916. For those with an interest in the history of the problem, the discussion given by Pekeris (3) is very interesting.

The eigenvalue problem we wish to solve is defined by

$$(\Sigma(E) - \kappa\mu)f(E,\mu) = \int_0^\infty \int_{-1}^{1} \Sigma(E',\mu' \rightarrow E,\mu)f(E',\mu')dE'd\mu' \qquad (1)$$

The essential features of the problem can be illustrated by considering the special case of isotropic scattering. Dividing through by $[\Sigma(E) - \kappa\mu]$ and integrating Eq. (1) over angles leads to an integral equation in the energy

$$\phi(E) = \frac{1}{2\kappa} \ln\left[\frac{\Sigma(E) + \kappa}{\Sigma(E) - \kappa}\right] \int_0^\infty \Sigma_o(E' \rightarrow E)\phi(E')dE' \qquad (2)$$

More generally, if the scattering kernel is expanded in a series of Legendre polynomials terminating with the L'th term, Eq. (2) is replaced by the set of (L+1) integral equations considered by Honeck (4) in a paper for this conference (for L = 3).

First let us consider the case of constant cross sections. Use of the detailed balance property of the energy transfer cross sections shows in this case that Eq. (1) is satisfied by a solution of the form $f(\mu)M(E)$, where $M(E)$ is a Maxwellian distribution at the moderator temperature, and $f(\mu)$ is the solution of the one velocity problem

$$(\Sigma - \kappa\mu)f(\mu) = \int_{-1}^{1} \Sigma(\mu' \rightarrow \mu)f(\mu')d\mu' \qquad (3)$$

which has been extensively studied. In particular, for isotropic scattering there is a single pair of eigenvalue $\pm\kappa$ satisfying

$$1 = \frac{\Sigma}{2\kappa} \ln\left(\frac{\Sigma + \kappa}{\Sigma - \kappa}\right) \qquad (4)$$

which determine the asymptotic solution far from a plane source. As the ratio of absorption to scattering increases, κ approaches Σ, and one must go farther from the source in order for the asymptotic exponential behavior to dominate. For any finite amount of scattering, however, the asymptotic solution is $e^{-\kappa x} f(\mu) M(E)$ with κ determined by Eq. (4).

Now consider the more general case. By the requirement that $f(E,\mu)$ be positive, we obtain the upper bound

$$|\kappa| \leq \underset{0 \leq E < \infty}{\text{minimum}} \{\Sigma(E)\} \tag{5}$$

For noncrystalline moderators or incoherently scattering moderators with an absorption cross section which goes to zero at large energy, this bound is determined by the free atom scattering cross section. For crystalline moderators at low temperature it is determined by the total cross section just below the Bragg cutoff.

The interest in the above formulation is not entirely academic as it applies quite well to the experimental situation in which the thermal diffusion length is measured by foil activation using the thermal column of a reactor as a source. Except for a small correction for transverse buckling, the formulation given is applicable to the analysis of experiments in which the diffusion length is measured as a function of 1/v poison concentration as has been done for water. (5) The previously mentioned paper by Honeck (4)

carried through this analysis in a way which to me illustrates very nicely the power of flexible use of a digital computer in advancing our understanding. The solving of four coupled integral equations in the energy was found to be well within the ability of the computer and allowed a direct comparison of theory and experiment without the ambiguities due to uncertain errors in the usual power series expansion.

There is one interesting unresolved point in this analysis. As the absorber concentration is increased, it is not clear whether κ approaches its bound in the limit of large absorber concentration or reaches it at some finite concentration. For a simple model discussed in Appendix A, the latter is the case. This would indicate that beyond a certain critical absorber concentration, the asymptotic behavior of the flux far from a plane thermal source is not exponential, and one has only the transient solutions to the transport equation. This point can be checked by extension of Honeck's calculations to larger absorber concentrations.

In demonstrating the upper bound Eq. (5) on the fundamental mode eigenvalue, we used the fact that the eigenfunction must be positive. If we merely require that the eigenfunction not be singular, then this upper bound also applies to the higher oscillatory eigenfunctions. It should be noted that many of the spatial eigenvalues which have been numerically calculated in diffusion theory (6) exceed this bound. The transients cor-

responding to these eigenvalues will play an important role only in a heavy moderator with weak absorption. In this case the approach of the spectrum to its asymptotic value and the decay of the asymptotic flux will be on a spatial scale long compared to a mean free path.

Two other problems which fall in the same category as the diffusion length problem are the Milne problem for velocity dependent mean free path (8), and the thermal diffusion of neutrons (9) in the presence of a temperature gradient. These problems, which help to elucidate the basic properties of the transport equation for thermal neutrons, are discussed rather thoroughly in other papers for this conference (8,9), and will not be discussed further in the present paper.

III. Time Dependent Problems

The basic physical process of interest in neutron thermalization is the approach to equilibrium of a neutron distribution. This is illustrated in its simplest form by considering an isotropic space independent velocity distribution in an infinite non-absorbing medium. Even for this problem, our understanding of the mathematical properties of the governing equation has, until recently, been very poor.

From the detailed balance condition on the energy transfer cross section, it follows that a Maxwellian distribution of neutron velocities at the moderator temperature is a time independent solution. It can also be

shown (10) that the entropy of the neutron distribution increases monotonically with time. If the kernel is sufficiently nonsingular (11), the entropy will approach its maximum value corresponding to an equilibrium Maxwellian, and the neutron distribution will therefore approach an equilibrium distribution.

Beyond this it has usually been assumed (12,13) that the approach to equilibrium can be described in terms of a complete set of discrete eigenfunctions. In an important recent paper (14), Corngold, Michael, and Wollman have given an explicit counterexample for the case of moderation by monatomic hydrogen. They showed that the discrete eigenvalue spectrum has a maximum decay constant

$$\lambda_{max} = \text{minimum } \{v\Sigma(E)\} \tag{6}$$

and that one must admit continuum eigenfunctions in the sense of Case (7) for a complete description of the approach to equilibrium. This approach has been developed more fully in a paper for this conference by Koppel (15).

The conclusions for monatomic hydrogen appear to be applicable to the general problem, since for any actual moderator the scattering probability $v\Sigma_s(E)$ will have a minimum value at zero velocity, and increase in an unbounded (though not necessarily monotonic) manner as the velocity increases. There are two nonphysical cases where the discrete eigenvalues are complete. The first is the case of a 1/v scattering cross section where

the bound still exists, but represents an actual upper limit on the decay rate at any energy. The second is the heavy monatomic gas in the limit of large mass ratio. If one considers this limit as one of a finite rate of slowing down, as is conventional, then the mean time between collisions goes to zero so that the bound on the decay constants goes to infinity.

For the practical calculation of time dependent problems, the eigenfunction expansion is still useful for heavy moderators at long times. For monatomic hydrogen, however, the distribution of eigenvalues is such that the expansion is of extremely limited utility. In looking toward the eventual objective of obtaining detailed solutions of the energy, space, and time dependent transport equation, it would be very helpful to have alternate procedures for treating the time dependence. The use of the time moments of the distribution as suggested by Koppel (16) is deserving of further investigation in this connection.

The concept of an upper bound on the decay constant has an interesting application to the problem of the decay constants measured in pulsed neutron experiments. Corngold and Michael (17) have pointed out that the measured decay constants in small beryllium and graphite assemblies exceed this bound. We note that the bound in these materials is quite low due to the small inelastic cross section below the Bragg cutoff, particularly at

low moderator temperatures. Their comment raises two interesting questions. First, what is the physical origin of the boundedness of the decay constant in the space dependent case? Second, if the experimenter could wait long enough, would he see a true decay constant? The answers to both these questions are quite subtle, and will be described in detail elsewhere (18), but a summary will be given below.

The essential conclusion is that the existence of a bound on the decay constant of a fundamental mode depends on the possibility of an infinite transit time of a neutron across the medium in question. For infinite medium problems, one always has a bound even for one velocity. This is illustrated by the work of Lehner and Wing (19) on the eigenvalues for a slab in one velocity. In this case, however, as opposed to the infinite medium with an exp(ikx) spatial dependence (7), a fundamental mode decay constant exists no matter how thin the slab. When one goes from a slab to a bounded finite medium, Jorgens (20) has shown that a fundamental mode decay constant exists under rather general conditions. In particular, for the case of a sphere in one velocity transport theory, the decay constant is not bounded. More generally, if the velocity domain is bounded away from zero, Jorgens has proved that an eigenvalue exists for a wide class of scattering kernels.

The problem is most easily understood by considering the integral

equation form of the transport equation (21) for a distribution which is decaying as $\exp(-\lambda t)$:

$$f(E,\vec{r},\vec{\Omega}) = \int_0^{R_o(\vec{r},\vec{\Omega})} dR \int dE' \int d\vec{\Omega}' \Sigma(E',\vec{\Omega}' \rightarrow E,\vec{\Omega}) \tag{7}$$

$$\times\ f(E',\vec{r} - R\vec{\Omega},\vec{\Omega}')\ \exp\{-R[\Sigma(E) - \frac{\lambda}{v}]\}$$

We see immediately that the integral on the right-hand side does not exist in an unbounded medium if $\Sigma(E) - \frac{\lambda}{v}$ is negative for any velocity. For a bounded medium, the integral exists except when $E = 0$. Since the cross section for scattering to zero energy vanishes only as some power of the energy, the right-hand side of Eq. (7) exists only if

$$\lambda \leq \lim_{E \rightarrow 0} v\Sigma(E) \tag{8}$$

even for a finite medium.

For any physical problem involving neutron moderation, the collision probability at zero energy will be the minimum value for all energies so that this bound is the same as Eq. (6). The origin of the bound in a finite medium is quite different, however, being explicitly associated with the behavior of the cross section in the limit of zero energy. This is most easily illustrated by considering the fictitious case of a cross section

crystalline moderators, the discussions given (17,24) indicate that the difficulty in interpretation is closely connected with a lack of space-energy separability. It therefore seems preferable to give up the concept of an equivalent buckling even for fairly large samples.

On the other hand, it seems to the author that the experiments are important ones to understand precisely because their understanding requires giving up simplifying concepts and forces a detailed analysis of the experimental situation. Insofar as a decay constant eigenvalue exists, its computation for a finite sample is well within our present capabilities for solving space and energy dependent problems using a digital computer. Our ability to calculate the time dependent problem in detail when there is no fundamental mode remains an interesting challenge for the future. Our physical understanding of time dependent problems is clearly still quite limited, and we can still profitably use semi-quantitative calculations (25) to help bring us to the point where detailed computer calculations can be performed with confidence.

APPENDIX A

Critical Absorption for the Existence of the Diffusion Length

As a simple calculational model, we will consider the case of constant isotropic scattering cross section, 1/v absorption cross section, and a separable scattering kernel (14) obeying detailed balance. Measuring energies in units of kT, we have

$$\Sigma(E) = \sigma(1 + \gamma E^{-\frac{1}{2}}) \tag{A1}$$

$$\Sigma_o(E' \rightarrow E) = \sigma M(E) \tag{A2}$$

where

$$M(E) = Ee^{-E} . \tag{A3}$$

Integrating (A2) over energy and measuring κ in units of σ, we reduce the eigenvalue problem to

$$\kappa = \int_0^\infty \ln \left(\frac{1 + \kappa + \gamma E^{-\frac{1}{2}}}{1 - \kappa + \gamma E^{-\frac{1}{2}}}\right) Ee^{-E} dE \tag{A4}$$

The right-hand side of (A4) is a monotonically increasing function of κ, and a monotonically decreasing function of γ varying from zero to $\ln(\frac{1+\kappa}{1+\kappa})$ as γ goes from infinity to zero. For κ equal to its upper bound of 1, the right-hand side becomes an unbounded function of γ so that there exists a value γ_c satisfying

$$1 = \int_0^\infty \ln\left(1 + \frac{2E^{\frac{1}{2}}}{\gamma_c}\right) E e^{-E} dE \ .$$

The value of γ_c will be of the order of one corresponding to roughly equal scattering and absorption at kT. For $\gamma > \gamma_c$, the right-hand side of (A4) will be less than κ for all κ between zero and one, so that no solution to the eigenvalue problem exists. It is not clear whether this feature will be found for more realistic thermalization models, but this can be easily checked numerically. Note that the important difference from the one velocity problem is that the upper bound for κ is 1 rather than $1 + \gamma$.

REFERENCES

1. I. Kuscer and M. Ribaric, Nuovo Cimento 7, 451 (1958).
2. F. B. Pidduck, Proc. London Math. Soc. 15, 89 (1916).
3. C. L. Pekeris, Proc. Nat. Acad. Sci. USA 41, 661 (1955).
4. Henry C. Honeck, "On the Calculation of Thermal Neutron Diffusion Parameters," this conference.
5. See references given by Honeck, op. cit.
6. Hiroshi Takahashi, "Space and Time Dependent Eigenvalue Problem in Neutron Thermalization," this conference.
7. K. M. Case, Annals of Physics 9, 1 (1960).
8. R. Kladnik, "Milne's Problem for Thermal Neutrons," this conference.
9. I. Kuscer, "Thermal Diffusion of Neutrons," this conference.
10. N. Van Kampen in Fundamental Problems in Statistical Mechanics, North Holland, Amsterdam (1961).
11. For example, the scattering from an isotropic harmonic oscillator in which the energy transfer is quantized does not give a proper approach to thermal equilibrium.
12. G. E. Uhlenbeck, "The Statistical Mechanics of Non-Equilibrium Phenomena," Higgins Lectures given at Princeton University, Fall, 1954.
13. M. S. Nelkin, Proceedings of Symposia in Applied Mathematics, Vol. II, p. 20, American Mathematical Society, 1961.
14. Noel Corngold, Paul Michael, and Warren Wollman, "The Time Decay Constants in Neutron Thermalization," this conference.
15. J. U. Koppel, "On the Solution of the Time Dependent Thermalization Problem," this conference.

16. J. U. Koppel, Nuclear Sci. and Eng. 12, 532 (1962).
17. N. Corngold and P. Michael, "On the Decay Constants in Pulsed Neutron Experiments," preprint.
18. Mark Nelkin, "Asymptotic Solution of the Transport Equation for Thermal Neutrons," manuscript in preparation.
19. J. Lehner and G. M. Wing, Comm. Pure Appl. Math. 8, 217 (1955); Duke Math. J. 23, 125 (1956). See also G. M. Wing, p. 140 of Ref. 13.
20. K. Jorgens, Comm. Pure Appl. Math. 11, 219 (1958).
21. B. Davison, Neutron Transport Theory, Oxford (1957).
22. M. M. R. Williams, "Space-Energy Separability in Pulsed Neutron Systems," this conference.
23. E. M. Gelbard and J. A. Davis, Nuclear Sci. and Eng., to be published.
24. G. de Saussure, "The Neutron Asymptotic Decay Constant in a Small Crystalline Moderator Assembly," this conference.
25. P. B. Daitch and D. B. Ebeoglu, "Transients in Pulsed Moderators," this conference.

BROOKHAVEN NATIONAL LABORATORY

CONFERENCE ON NEUTRON THERMALIZATION

APRIL 30 - MAY 2, 1962

THE PHASE INTEGRAL METHOD IN NEUTRON THERMALIZATION

NOEL CORNGOLD

BROOKHAVEN NATIONAL LABORATORY

UPTON, L. I., NEW YORK

Research performed under the auspices of the U.S. Atomic Energy Commission.

INTRODUCTION

The mathematical physicist faces two alternatives in the study of neutron thermalization. He may consider a scattering kernel which stems from a very simple physical model of the moderator, but which permits direct mathematical analysis of the Boltzmann equation, or he may use numerical schemes and large computing machines to solve the Boltzmann equation, incorporating into the equation as subtle a kernel as the capacity of his machine permits. Both types of study are necessary for the proper development of the subject. In this paper we take the first point of view and discuss phase integral (WKB) approximations to solutions of the Boltzmann equation, for those models for which the scattering operator may be taken to be a differential operator of second order. Of these, the heavy gas, or Wilkins' model (1) is best known. In addition, there are Wilkins' equations of higher order (2), and the equations for bound systems considered by Kazarnovskii, et.al. (3) and by Clark and deSobrino (4). The differential version of the proton gas model (5) does not stem from a differential representation of the scattering kernel, but yields a second order differential equation in energy, nevertheless. We shall discuss the proton gas in a later note.

GENERAL

We consider a homogeneous system, and in it, the Boltzmann equation in the diffusion approximation, viz.

$$\frac{1}{\sqrt{\epsilon}} \frac{\partial}{\partial t} \Phi - D(\epsilon) \nabla^2 \Phi + \Sigma_a(\epsilon) \Phi = S\Phi + Q \ . \qquad (1)$$

In (1), $\Phi \equiv \Phi(\underline{r},t,\epsilon)$ is the flux density of neutrons, a function of position, time, and energy. The energy is denoted by the dimensionless variable ϵ, where $\epsilon = E/k_B T = \left(\frac{v}{v_B}\right)^2$. k_B is Boltzmann's constant. Q is the appropriate source density, and S, the scattering operator, is defined through:

$$Sf(\epsilon) \equiv \int_0^\infty d\epsilon' \left[\Sigma_s(\epsilon' \to \epsilon) f(\epsilon') - \Sigma_s(\epsilon \to \epsilon') f(\epsilon) \right] \qquad (2)$$

Most of this paper will be devoted to the transient, or modal solutions of (1). These are the solutions to the source-free equation, which vanish exponentially as $\epsilon \to \infty$. It is generally assumed that they form a complete and denumerable set, and it is common practice to use them as a basis for the expansion of the flux in interpreting the results of a pulsed neutron experiment (6), or an experiment in space-dependent thermalization (7). To obtain them we write

$$\Phi \propto \exp\left[i\underline{B}\cdot\underline{r} + \lambda v_B t \right] \varphi(\epsilon) \qquad (3)$$

which gives, for $\varphi(\epsilon)$, the equation

$$\left[\frac{\lambda+\lambda_a f(\epsilon)}{\sqrt{\epsilon}} + D(\epsilon)B^2 \right]\varphi(\epsilon) = S\varphi(\epsilon) \qquad (4)$$

where $\Sigma_a(\epsilon) = \frac{1}{\sqrt{\epsilon}} \Sigma_a(v_B) f(\epsilon) = \frac{1}{\sqrt{\epsilon}} \lambda_a f(\epsilon)$. The solution of (4) which we seek should be free from singularities and should decrease exponentially at infinity. If we regard B^2 and the absorption as given and seek eigenvalues λ_j and corresponding eigenfunctions $\varphi_j(\epsilon;B^2)$ we obtain quantities suitable for the interpretation of pulsed neutron experiments. Thus, an initial burst of neutrons having the distribution $\exp\left[i\underline{B}_j\cdot\underline{r} \right] Q(\epsilon)$ at t=0 evolves in time according to

$$\Phi_j(\underline{r},t,\epsilon) = \exp\left[i\underline{B}_j\cdot\underline{r} \right] \sum_k a_k \varphi_k(\epsilon;B_j^2) \exp\left[\lambda_k(B_j^2) t \right] \qquad (5)$$

where the a_k may be determined through use of the ortho-normality condition,

$$\int_0^\infty \frac{d\epsilon}{\sqrt{\epsilon}} \varphi_k^+(\epsilon;B^2) \varphi_m(\epsilon;B^2) = \delta_{km} \qquad (6)$$

φ_k^+ is the solution to the equation adjoint to (4), and the "detailed-balance" property of the scattering operator ensures

that $\epsilon \exp[-\epsilon] \varphi_k^+(\epsilon)$ is proportional to $\omega_k(\epsilon)$ (3). The dependence of λ_o, the fundamental decay constant, upon B_o^2, the fundamental buckling, is the subject of considerable experimental effort (9).

If, on the other hand, we take $\lambda=0$ and ask for the modes $\Phi \propto \exp[\underline{\mu}_j \cdot \underline{r}] \Psi_j(\epsilon)$, we find functions suitable for the analysis of a steady-state diffusion-length experiment. Thus, if the neutron velocity distribution is prescribed to be $Q(\epsilon)$ on the plane $z=0$, the distribution of neutrons in space, $z \geq 0$ is given by:

$$\Phi(\underline{r},\epsilon) = \sum_j b_j \Psi_j(\epsilon) \exp[-K_j z]. \qquad (\underline{\mu}_j^2 \equiv K_j^2) \qquad (7)$$

In (7) the b_j may be determined through the use of

$$\int_0^\infty d\epsilon \, D(\epsilon) \, \Psi_k^+(\epsilon) \Psi_m(\epsilon) = \delta_{km} , \qquad (3)$$

where, once again $\epsilon \exp[-\epsilon] \Psi_k^+$ is proportional to $\Psi_m(\epsilon)$. The dominant decay constant, K_o, is the inverse of the thermal diffusion length.

Finally, the modal solutions may be used to represent steady-state slowing down spectra. If the source of neutrons leading to (5) is steady, rather than a burst, we find

$$\Phi_j(\underline{r},\epsilon) = \exp\left[iB_j\cdot r\right]\sum_k \frac{a_k}{\lambda_k(B_j^2)}\,\varphi_k(\epsilon;B_j^2) \qquad (9)$$

$$= \exp\left[iB_j\cdot r\right]\int_0^\infty d\epsilon'\; G(\epsilon,\epsilon';B_j^2)\,Q(\epsilon') \qquad (10)$$

where $G(\epsilon,\epsilon')$ is the Green's function corresponding to the operator $S-D(\epsilon)B^2$.

THE DIFFERENTIAL SCATTERING OPERATOR

As we mentioned in the INTRODUCTION we are considering models of the thermalization process in which the scattering operator may be represented by a differential operator of second order. In essence, we are generalizing the heavy-gas operator to include effects of chemical binding. The extent to which the generalization is valuable can be determined only after a great deal of calculation. In this paper we shall show that it is easy to extract a great deal of information from this model and shall illustrate with heavy gas results.

To begin, we state some properties of the scattering operator which are easily deduced (9). S^+, the adjoint operator is the integral operator whose kernel is the transpose of the

kernel of S. The symbol M represents the Maxwellian, $M=\epsilon \exp\left[-\epsilon\right]$. We have

$$\int_0^\infty d\epsilon \; Sf = 0 \qquad \text{(Neutron Conservation)} \qquad (11)$$

$$S^+ f = 0 \qquad \text{if f=constant} \qquad (12)$$

$$MS^+ f = SMf \qquad \text{(Detailed Balance).} \qquad (13)$$

The true scattering operator is to be replaced by a differential operator of second order. Thus,

$$S^+ = p(\epsilon) \frac{d^2}{d\epsilon^2} + q(\epsilon) \frac{d}{d\epsilon} + r(\epsilon). \qquad (14)$$

We see at once that condition (12) requires $r(\epsilon)=0$, while both (11) and (13) are satisfied if

$$M(\epsilon)q(\epsilon) = \frac{d}{d\epsilon} M(\epsilon)p(\epsilon). \qquad (15)$$

Thus, (14) contains but a single "free" function. To identify it, we recall that if S^+ operates upon the function ϵ, we obtain the first energy-transfer moment $A_1(\epsilon)$, where

$$A_n(\epsilon) \equiv \int_0^\infty d\epsilon' \; \Sigma_s(\epsilon \to \epsilon')(\epsilon'-\epsilon)^n. \qquad (16)$$

Thus, the identification is $q(\epsilon) <-> A_1(\epsilon)$, and $q(\epsilon)$ should be taken to be the "exact" energy transfer moment. If we now consider S^+ to act upon ϵ^2, we are led to the identification $p(\epsilon) <-> \frac{1}{2} A_2(\epsilon)$. However, we are not free to use the A_1 and A_2 which result from a precise calculation, since they will generally violate (15). We must, instead, fix $q(\epsilon)$ through $q <-> A_1$ and $p(\epsilon)$ through the integrated form of (15), namely

$$p(\epsilon) = M^{-1}(\epsilon) \int_{\epsilon}^{\infty} d\epsilon \; q(\epsilon) M(\epsilon) = \tfrac{1}{2} "A_2". \tag{17}$$

The fictitious A_2, which we denote by "A_2", has reasonable properties, which we shall note ahead. Most important is that it yields the same M_2 parameter,

$$M_2 = \int_0^{\infty} d\epsilon \; M(\epsilon) A_2(\epsilon) \tag{13}$$

as does the true kernel. One sees this through multiplication of (17) by $M(\epsilon)$ followed by a partial integration. Since M_2, which is a measure of the "width" of a particular scattering kernel, governs the behaviour of neutron distributions close to equilibrium (10) we can be optimistic about the utility of (14) in such situations. The higher moments of the synthetic kernel may be analyzed in a similar manner. They are determined

by $A_1(\epsilon)$ alone and so represent a rather special type of synthetic scattering kernel.

We can use (15) and (17) to see the behaviour of "A_2" for large and small ϵ. $q(\epsilon)$ will be proportional to ϵ, for ϵ large, whence "A_2" also turns out to be proportional to ϵ. This is not quite right, since a proper A_2 should be proportioned to ϵ^2, but it is a fair approximation for heavy, bound moderators. As ϵ decreases, "A_2" decreases. It approaches zero as $\epsilon^{\frac{1}{2}}$, remaining positive throughout. The correct second moment should pass through a minimum in the thermal region, then rise as $\epsilon^{-\frac{1}{2}}$. It would appear, then, that "A_2" is "weaker" - by a factor of ϵ - than it should be, in both high and low energy limits. For moderators other than hydrogen, though, the ranges of energy in which "A_2" fails significantly are not of great importance. They are, roughly, $E < \frac{m}{M} T$ and $E > \frac{M}{m} T$, where m is the neutron mass and M the mass of the moderator atom.

The differential equation for the neutron flux which stems from (14) is

$$\left[\frac{\lambda+\lambda_a f(\epsilon)}{\sqrt{\epsilon}} + D(\epsilon) B^2 \right] \varphi(\epsilon) = (p\varphi)'' - (q\varphi)' \qquad (19)$$

As it stands, (19) refers to a source-free medium. We can estimate its accuracy in the case of slowing down in an infinite

system having 1/v capture, by comparing its asymptotic solution (E>>T) with the exact solution (11,12). If we use

$$q(\epsilon) = A_1(\epsilon) = \frac{2\mu}{(1+\mu)^2}\Sigma_{sf}\epsilon\left[-1 + \frac{1}{\epsilon}(2-\mu)\frac{T_{eff}}{T} + O(\epsilon^{-2})\right], \quad (20)$$

where $\mu = m/M$, Σ_{sf} is the macroscopic free-atom scattering cross section, and T_{eff} the "effective temperature" (11,12) of the bound atom, we obtain the following limiting results:

$\mu \to 0$

$$\varphi(\epsilon) \sim \frac{1}{\epsilon}\left[1 - \left(\frac{\Delta}{2}\right)\frac{1}{\epsilon^{\frac{1}{2}}} + \left(\frac{\Delta^2}{8} + 2\frac{T_{eff}}{T}\right)\frac{1}{\epsilon} + O(\epsilon^{-3/2})\right] \quad (21)$$

which is the correct result, and

$\mu \to 1$

$$\varphi(\epsilon) \sim \frac{1}{\epsilon}\left[1 - 4\left(\frac{\Delta}{2}\right)\frac{1}{\epsilon^{\frac{1}{2}}} + \left(2\Delta^2 + \frac{T_{eff}}{T}\right)\frac{1}{\epsilon} + O(\epsilon^{-3/2})\right] \quad (22)$$

as against the exact result ,

$$\varphi(\epsilon) \sim \frac{1}{\epsilon}\left[1 - 3\left(\frac{\Delta}{2}\right)\frac{1}{\epsilon^{\frac{1}{2}}} + \left(\frac{3}{2}\Delta^2 + \frac{T_{eff}}{T}\right)\frac{1}{\epsilon} + O(\epsilon^{-3/2})\right]. \quad (23)$$

THE PHASE INTEGRAL METHOD

The WKB, or phase integral method is described in many places (13); we shall treat it superficially in this section. We begin by converting the equation adjoint to (4) to a Schrödinger

equation, through the transformation:

$$\varphi^{+}(\epsilon) = \exp\left[-\frac{1}{2}\int \frac{q}{p}\,d\epsilon\right] \Psi(\epsilon) \propto (Mp)^{-\frac{1}{2}} \Psi(\epsilon). \tag{24}$$

We obtain

$$\Psi'' + k^2(\epsilon)\Psi = 0\ , \tag{25}$$

where

$$-k^2(\epsilon) = \frac{1}{4}(q/p)^2 + \frac{1}{2}\frac{d}{d\epsilon}(q/p) + \frac{\alpha(\epsilon)}{p} \tag{26}$$

and

$$\alpha(\epsilon) = \frac{\lambda + \lambda_a f(\epsilon)}{\sqrt{\epsilon}} + D(\epsilon)B^2. \tag{27}$$

The neutron transport problem has now been replaced by the wave-mechanical analog, eq.(25), which describes the motion of a particle of energy W, moving in a potential $V(\epsilon)$. The function $k^2(\epsilon)$ is proportional to $W-V(\epsilon)$; we shall take W to be zero, so that we are discussing the motion of a particle of zero energy in a potential given by $V(\epsilon) \equiv -k^2(\epsilon)$.

We may conclude from our earlier discussion of the behaviour of q and p, that the potential becomes positively infinite, $V \sim \frac{21}{16}\epsilon^{-2}$, as $\epsilon \to 0$. As ϵ increases $V(\epsilon)$ decreases. There is a range of ϵ for which $V(\epsilon)$ is negative, after which $V(\epsilon)$ increases. For cross sections $f(\epsilon)$ such that $\alpha(\epsilon)/\epsilon$ is bounded as $\epsilon \to \infty$, we find $V(\epsilon)$ attaining a value of $\frac{1}{4}$ as $\epsilon \to \infty$.

Thus, $V(\epsilon)$ has quite a reasonable graph (see Figure 1). The shape of the bottom of the well is sensitive to the scattering model and to the value of λ and B^2. Solving the eigenvalue problem to obtain modal solutions is equivalent to varying the shape of the potential well until it "binds" a particle having zero energy.

It is known (13) that in order to apply the WKB method to a potential having a "centrifugal" component $\sim \epsilon^{-2}$, one must calculate with an effective potential $V_{eff} = V + \frac{1}{4}\epsilon^{-2}$. We shall denote the phase associated with the modified potential by w. Thus $w = \sqrt{|V_{eff}|}$. Motion in the modified potential will have two "turning-points" ϵ_1 and ϵ_2, at which $V_{eff}(\epsilon) = 0$. If we first consider the modal solutions, we find the following expressions for quantities of interest:

a) eigenvalues

$$\int_{\epsilon_1}^{\epsilon_2} d\epsilon\, w(\epsilon,\lambda,B^2) = (n + \tfrac{1}{2})\,\pi \tag{23}$$

b) eigenfunctions

$$\begin{aligned} \Psi_n(\epsilon) &= C_n\, w^{-\frac{1}{2}} \cos\Big[\int_{\epsilon_1}^{\epsilon} w(\epsilon)\,d\epsilon - \tfrac{1}{4}\pi\Big] && \epsilon_1<\epsilon<\epsilon_2 \\ &= \frac{(\pm)^n}{2}\, C_n\, w^{-\frac{1}{2}} \exp\Big[-\Big|\int_{\epsilon_1}^{\epsilon} w(\epsilon)\,d\epsilon\Big|\Big] && \begin{matrix}\epsilon<\epsilon_1 \\ \epsilon>\epsilon_2\end{matrix} \end{aligned} \tag{29}$$

c) normalization

Here, corresponding to the case of B^2 fixed, we have:

$$\int_0^\infty d\epsilon\ \epsilon^{-\frac{1}{2}}\ \varphi_n^+(\epsilon)\varphi_n(\epsilon) = 1 \qquad (30)$$

and its WKB counterpart

$$\frac{1}{2}\ C_n^2 \int_{\epsilon_1}^{\epsilon_2} d\epsilon\ \epsilon^{-\frac{1}{2}} \left[w(\epsilon)p(\epsilon)\right]^{-1} = 1 \qquad (31)$$

d) asymptotic behaviour, e.g. $\epsilon \to \infty$

To obtain the limiting behaviour of $\varphi^+(\epsilon)$ we note that the high energy behaviour of $w(\epsilon)$ is just such as to cancel the integrating factor in (24). The remaining portions of the phase integral readily lend themselves to numerical integration. For $B^2 = 0$ and 1/v absorption the ω_n^+ becomes constant at high energy. In most other cases it has a weak dependence on energy. A similar analysis may be made in the limit $\epsilon \to 0$.

At this point, some remarks about the accuracy of the WKB solutions may be in order. One customarily says that they are accurate for the higher modes only; in practice they often turn out to be good for all modes (14). We shall see in the next section that the heavy gas model is one such case. Since V_{eff} does not change drastically as we go from the heavy gas to other models, we may expect the accuracy found in that case to

be indicative of the accuracy to be expected in almost all models.

In the usual derivation of the normalization formula, eq.(31), the square of the cosine in (29) is replaced by its average value, 1/2. The replacement would appear to be justified only for those Ψ_n having many oscillations in $\epsilon_1<\epsilon<\epsilon_2$. However, W. Furry (14) has shown that (31) holds for all modes with an error roughly equal to the error in $\Psi_n(\epsilon)$ in the interior of the potential well. In the heavy gas case, the error turns out to be less than ten percent. In fact, we can summarize the accuracy of the WKB formulas in our case as one percent or less for eigenvalues, and ten percent or less for eigenfunctions.

e) the slowing down solutions

One would not expect the WKB solutions to be good approximations in this case, since we are dealing with "nodeless' wave functions. In fact, the solutions turn out to be pretty good when the absorption is moderate. The solution in this case is different from (29) only in the range $\epsilon>\epsilon_2$, where

$$\Psi(\epsilon) = C \cos \delta \; w^{-\frac{1}{2}} \exp\left[+\int_{\epsilon_2}^{\epsilon} w(\epsilon)\,d\epsilon\right] \qquad (32)$$

$$\delta = \int_{\epsilon_1}^{\epsilon_2} w(\epsilon)\,d\epsilon \; .$$

The slowing-down solutions may be characterized by the ratio of the source strength to the "amount of Maxwellian component" present. In the case of slowing down in a system having 1/v capture, the ratio may be taken to be

$$R = \lim_{\epsilon \to \infty} \epsilon\omega(\epsilon) \; / \; \lim_{\epsilon \to 0} \varphi^{+}(\epsilon) \qquad (33)$$

following E. R. Cohen (1). The ratio may be computed easily, using the functions (32). In the heavy gas case, we may compare with the exact values given by Cohen. We find an error that increases steadily with Δ, rising from zero to twenty percent as Δ increases from zero to two.

NUMERICAL RESULTS

We have done considerable calculation in the heavy-gas case (15). Here, $q(\epsilon) = 2\mu\Sigma_s(2-\epsilon)$ and $p(\epsilon) = 2\mu\Sigma_s\epsilon$. The quantity "$A_2$" is precisely the true second moment, $A_2(\epsilon)$. The moments q and p have the high energy behaviour discussed earlier, but have a different low energy behaviour because $q(\epsilon)$ lacks the typical 1/v behaviour there. The effective potential is:

$$V_{eff} = \frac{1}{4\epsilon^2} + \left(\frac{\lambda}{2\mu\Sigma_s} + \frac{\lambda_a}{2\mu\Sigma_s} f(\epsilon)\right) \frac{1}{\epsilon^{3/2}} + \left(\frac{DB^2}{2\mu\Sigma_s} - 1\right) \frac{1}{\epsilon} + \frac{1}{4} \qquad (34)$$

and we have calculated only for $f(\epsilon)=1$ (1/v capture).

a) Eigenvalues.

In Table I, we consider $B^2=0$, and list Δ_n, which is related to the λ_n through

$$\Delta_n = \frac{2}{\mu\Sigma_s} \quad (\lambda_a + \lambda_n). \tag{35}$$

The "exact" values were obtained through numerical integration of the differential equation.

It is a simple matter to estimate the dependence of Δ_n on n as $n \to \infty$. Under the change of variable $\epsilon = x^2$, $1 - \frac{DB^2}{2\mu\Sigma_s} = \nu$, $|\ \ _n| = \delta_n^3$, the eigenvalue equation (28) becomes

$$(n+\tfrac{1}{2})\pi = \int_{x_1}^{x_2} \frac{dx}{x} \quad \sqrt{4\nu x^2 + \delta^3 x - x^4 - 1} \quad . \tag{36}$$

For large δ we see that

$$\begin{aligned} x_1 &= \delta^{-3} + 0(\delta^{-9}) \\ x_2 &= \delta + 0(\delta^{-1}), \end{aligned} \tag{37}$$

and in this limit, the quartic approaches $(x-\delta^{-3})(\delta-x)(x^2+\delta x+\delta^2)$, a result independent of ν. We may also neglect the term δ^{-3} in the limit, to obtain

$$\int_{x_1}^{x_2} \frac{dx}{x} \sqrt{4\nu x^2 + \delta^3 x - x^4 - 1} \rightarrow \int_0^{\delta} \frac{dx}{x} \sqrt{x(\delta - x)(x^2 + \delta x + \delta^2)} \quad . \quad (38)$$

Thus, for large n

$$n\pi \approx \delta^2 \int_0^1 dx \sqrt{1 - x^3/x} = 1.820\ldots\delta^2 \qquad (39)$$

or,

$$|\Delta_n| \rightarrow 2.269\ n^{3/2} \ .$$

This asymptotic formula holds to within ten percent for n as low as 10.

In Table II we give the dependence of the lower eigenvalues Δ_0 and Δ_1 upon DB^2. Since the dependence of an eigenvalue upon DB^2 is small, and since we are discussing lower eigenvalues, we would expect the WKB predictions of the dependence to be poor. In fact, if we fit our WKB results to a power series in B^2, we find

$$\Delta_0 = -4.433\ \beta + 0.767\ \beta^2 - 0.036\ \beta^3 + \ldots \quad \text{(WKB)} \quad (40)$$

to be compared with the "exact" value,

$$\Delta_0 = -4.513\,\beta + 0.667\,\beta^2 + O(\beta^3) \quad . \tag{41}$$

Here, $\beta = DB^2/2\mu\Sigma_s$.

Exact results for Δ_1 are absent from the literature. The WKB result is:

$$\Delta_1 = -4.63 - 4.27\beta + 0.27\beta^2 + \ldots . \tag{42}$$

The space decay constants, κ_n, form a second interesting set of eigenvalues. They may be obtained by setting $\lambda=0$ and $B^2 = -\kappa^2$ in eq.(34). Just as the time decay constants are often studied as power series in B^2, so are the space decay constants developed in a series in λ_a, or Δ. The leading term, which is independent of Δ, is given correctly by the WKB calculation. In that limit, the eigenvalue integral is simple, and yields $D\kappa_n^2/2\mu\Sigma_s = n$. We find

$$\begin{aligned} \frac{D\kappa_0^2}{2\mu\Sigma_s} &= 0.225\Delta(1 - 0.049\Delta) + \ldots \\ \frac{D\kappa_1^2}{2\mu\Sigma_s} &= 1 + 0.196\Delta - 0.002\,\Delta^2 + \ldots \end{aligned} \tag{43}$$

which may be compared with the following results, which stem from the diagonalization of some rather large matrices (16)

$$\frac{D\varkappa_0^2}{2\mu\Sigma_s} = 0.2216\Delta(1 - 0.037\Delta) + 0(\Delta^3)$$

(exact) (44)

$$\frac{D\varkappa_1^2}{2\mu\Sigma_s} = 1 + 0.194\Delta - 0.004\Delta^2 + 0(\Delta^3).$$

Again, the reader should recall that the WKB approximation is at its worst for low eigenvalues.

b) Eigenfunctions.

Once the normalization constants, C_n are given, the WKB eigenfunctions (29) are specified at all points other than the turning points, ϵ_1 and ϵ_2. In the vicinity of these points once can use the exact solution, which is a combination of Bessel functions of order one-third, (13), or one can join the WKB solutions "by eye." The WKB solutions, so constructed were compared with the exact solutions for n=1 and 2 and $B^2=0$. The solutions were compared at six points each, and found to differ by less than twelve percent.

The behaviour of the eigenfunctions as $\epsilon \to \infty$ is, as we have noted above, of particular importance. The quantity $\omega_n^+(\infty)$ gives the "importance" of each mode when a pulse of neutrons of

high energy is inserted into the system. To compute $\varphi_n^+(\infty)$, we use (24) and (29). Thus

$$\varphi_n^+(\epsilon) = \exp\left[-\tfrac{1}{2}\int \frac{d\epsilon}{\epsilon}\,(2-\epsilon)\right] \Psi_n(\epsilon) \tag{45}$$

$$= \frac{(-)^n}{2}\, C_n\, \frac{e^{\frac{1}{2}\epsilon}}{\epsilon}\left[w(\epsilon)\right]^{-\frac{1}{2}} \exp\left[-\int_{\epsilon_2}^{\epsilon} w(\epsilon')\,d\epsilon'\right] \tag{46}$$

with

$$w(\epsilon) = \frac{1}{2\epsilon}\sqrt{\epsilon^2 - 4\epsilon\left(1 - DB^2/2\mu\Sigma_s\right) + \Delta\sqrt{\epsilon} + 1}\ . \tag{47}$$

To go properly to the limit $\epsilon \to \infty$, we write $w(\epsilon) = \frac{1}{2\epsilon}\sqrt{a+b}$, where $a = (\epsilon - 2\nu)^2$ and $b = \Delta\sqrt{\epsilon} - (4\nu^2 - 1)$. Then, w is split into two parts,

$$w(\epsilon) = \frac{1}{2\epsilon}\sqrt{a}\,\left(1 + \frac{b}{2a}\right) + \frac{1}{2\epsilon}\left(-\frac{b^2}{4a^{3/2}}\right)\frac{1}{\sqrt{1+\frac{b}{a}} + \left(1+\frac{b}{2a}\right)} \tag{48}$$

The first term in (43) is dominant as $\epsilon \to \infty$ and is integrable in terms of elementary functions. The second term must be integrated numerically; the integration is rapid, for the integrand behaves as ϵ^{-3} for large ϵ. We denote the latter integral by $-\frac{1}{8}J$, whence

$$\lim_{\epsilon\to\infty} \exp\left[-\int_{\epsilon_2}^{\epsilon} w(\epsilon')d\epsilon'\right] = \frac{e^{\frac{1}{2}\epsilon_2}}{\epsilon_2^{\nu}} \left(\frac{\sqrt{\epsilon_2} - \sqrt{2\nu}}{\sqrt{\epsilon_2} + \sqrt{2\nu}}\right)^{\frac{\Delta}{4\sqrt{2\nu}}} \left(\frac{\epsilon_2}{\epsilon_2 - 2\nu}\right)^{\frac{4\nu^2-1}{8\nu}}$$

$$\times\ e^{\frac{1}{8}J} \lim_{\epsilon\to\infty} \epsilon^{\nu}\ e^{-\frac{1}{2}\epsilon} \tag{49}$$

and

$$\lim_{\epsilon\to\infty} \varphi_n^{+}(\epsilon) = (-)^n \frac{C_n}{\sqrt{2}} \frac{e^{\frac{1}{2}\epsilon_2}}{\epsilon_2^{\nu}} \left(\frac{\sqrt{\epsilon_2} - \sqrt{2\nu}}{\sqrt{\epsilon_2} + \sqrt{2\nu}}\right)^{\frac{\Delta}{4\sqrt{2\nu}}} \left(\frac{\epsilon_2}{\epsilon_2 - 2\nu}\right)^{\frac{4\nu^2-1}{8\nu}} \frac{e^{\frac{1}{8}J}}{\epsilon^{1-\nu}} \tag{50}$$

The quantities $\varphi_n^{+}(\infty)$ are listed in Table I, for the case of no leakage, $\nu = 1$.

The value of $\varphi_n^{+}(\epsilon)$ at $\epsilon=0$ is another interesting quantity. It, too, may be calculated easily by splitting the phase integral. We find

$$\omega_n^{+}(0) = \frac{C_n}{4\sqrt{2}} \frac{1}{\sqrt{\epsilon_1}} \left(1 + \sqrt{1 + \Delta\sqrt{\epsilon_1}}\ \right)^2 \exp\left[2\left(1 - \sqrt{1 + \Delta\sqrt{\epsilon_1}}\right)\right]$$

$$\times\ e^{-L} \tag{51}$$

where

$$L = \tfrac{1}{2} \int_0^{\epsilon_1} d\epsilon\ \frac{\epsilon - 4\nu}{\sqrt{\epsilon^2 - 4\nu\epsilon + \Delta\sqrt{\epsilon} + 1}\ + \sqrt{\Delta\sqrt{\epsilon} + 1}} \tag{52}$$

may be calculated in a straightforward manner.

c) Slowing-down solutions.

The general form of the WKB slowing-down solution has been given earlier. One feature of the $\Delta > 0$ solutions is that the turning-points disappear when Δ exceeds $(4\nu^2-1)/\sqrt{2\nu}$. The only case we have considered in some detail is $\nu=1$ (infinite medium), where the critical Δ is $3/\sqrt{2\nu}$. In that case, the solutions are already rather poor (in error by twenty percent) when $\Delta = 2$, so that we have not examined Δ's above the critical Δ.

As noted earlier, we characterize the slowing down solutions by the ratio of $\epsilon\varphi(\epsilon)$ at high energy to $\varphi(\epsilon)/M(\epsilon)$ at low energy. The latter expression is given by eq.(51), while the former requires the use of eq.(49), along with a calculation of $\cos\delta$. If the ratio is expanded in a power series in Δ, we find that the leading WKB term is 0.2208Δ, while the exact value is $\frac{1}{8}\sqrt{\pi}\,\Delta = 0.2216\Delta$. The WKB terms of higher order are larger than they should be, so that for most values of Δ the WKB ratio is too high. When these values are compared with the correct ones quoted by Cohen (1), the error is found to increase with increasing Δ, over most of the range, achieving the value of + 20% at $\Delta = 2$.

ACKNOWLEDGEMENT

We acknowledge with gratitude the assistance given by Mrs. Joan Weisenbloom, Mr. Warren Wollman, and Mr. William Bornstein in the many numerical calculations which were needed for this paper.

REFERENCES

1. J. E. Wilkins, Jr., CP-2431 (1944);
E. R. Cohen, NUCLEAR SCI. & ENG. 2, 227 (1957);
H. Hurwitz, Jr., M. S. Nelkin, and G. J. Habetler, NUCLEAR SCI. & ENG. 1, 280 (1956).
2. J. E. Wilkins, Jr., ANNALS OF MATH. 49, 189 (1948);
N. Corngold, ANNALS OF PHYS. 6, 368 (1959).
3. M. V. Kazarnovskii, A. V. Stepanov, and F. L. Shapiro, Proc. 2nd Intern. Conf. on the Peaceful Uses of Atomic Energy, Vol. 16, p.279 Geneva (1958).
4. L. deSobrino and M. Clark, Jr., NUCLEAR SCI. & ENG. 10, 377 (1961).
5. E. P. Wigner and J. E. Wilkins, Jr., AECD-2275 (1948).
6. K. S. Singwi, ARKIV FÖR FYSIK 15, 147 (1960);
S. N. Purohit, NUCLEAR SCI. & ENG. 9, 157 (1960).

7. D. Kottwitz, NUCLEAR SCI. & ENG. 7, 345 (1960);
P. Michael, NUCLEAR SCI. & ENG. 8, 426 (1960).
8. H. Hurwitz, et. al., reference 1.
9. See, for example, K. H. Beckurts, NUCLEAR INST. & METHODS 11, 144 (1961);
M. S. Nelkin, NUCLEAR SCI. & ENG. 7, 210 (1960).
10. M. S. Nelkin, J. NUCLEAR ENERGY 8, 48 (1958).
11. N. Corngold, reference 2.
12. N. Corngold, ANNALS OF PHYS. 11, 338 (1960);
D. Parks, NUCLEAR SCI. & ENG. 9, 430 (1961).
13. P. M. Morse and H. Feshbach, "Methods of Theoretical Physics," McGraw-Hill (N. Y.) (1953);
W. Pauli, "Wellenmechanik," Edwards (1947).
14. W. Furry, PHYS. REV. 71, 360 (1947).
15. E. Garelis, NUCLEAR SCI. & ENG. (to be published), has also made some WKB calculations with the heavy gas model.
16. P. Michael, NUCLEAR SCI. & ENG. 8, 426 (1960).

TABLE I

EIGENFUNCTIONS AND EIGENVALUES FOR $\nu = 1$ ($B^2 = 0$)

	Turning Points		Δ_n				$\varphi_n^+(\infty)$		
n	ϵ_1	ϵ_2	WKB	exact	C_n	J	WKB	exact	L
0	0.268	3.73	0	0	0.841	0.258	1.00	1.06	-0.638
1	0.0346	5.76	- 4.64	- 4.69	0.891	0.932	-5.51	-5.83	-0.131
2	0.00916	7.53	-10.1	-10.1	0.969	1.60	2.90×10^{1}		-0.0407
3	0.00362	9.27	-16.4	-16.5	1.04	2.28	-1.56×10^{2}		-0.0172
4	0.00178	11.0	-23.5	-23.7	1.09	2.97	8.39×10^{2}		-0.00873
5	0.00100	12.7	-31.4		1.15	3.67	-4.68×10^{3}		-0.00504
6	0.000621	14.5	-40.0		1.19	4.36	2.61×10^{4}		-0.00315
7	0.000411	16.2	-49.3		1.23	5.07	-1.48×10^{5}		-0.00212
8	0.000286	17.9	-59.1		1.27	5.77	8.38×10^{5}		-0.00150
9	0.000207	19.6	-69.5		1.30	6.47	-4.78×10^{6}		-0.00110
10	0.000154	26.4	-80.4		1.34	7.18	2.76×10^{7}		-0.000774

TABLE II

EIGENFUNCTIONS AND EIGENVALUES FOR VARIOUS $\nu = 1 - \frac{DB^2}{2\mu\Sigma_s}$

		Turning Points				
n	ν	ϵ_1	ϵ_2	Δ	C_n	J
0	1.00	0.268	3.73	0	0.841	0.258
	0.90	0.234	3.55	-0.436	0.834	0.291
	0.80	0.204	3.37	-0.857	0.828	0.330
	0.70	0.178	3.19	-1.26	0.823	0.375
	0.60	0.155	3.02	-1.66	0.821	0.426
	0.50	0.135	2.85	-2.04	0.819	0.486
	0.40	0.118	2.69	-2.40	0.819	0.556
1	1.00	0.0346	5.76	-4.64	0.891	0.932
	0.90	0.0309	5.57	-5.06	0.893	0.984
	0.80	0.0277	5.38	-5.48	0.896	1.04
	0.70	0.0249	5.19	-5.89	0.899	1.10
	0.60	0.0225	5.02	-6.30	0.903	1.17
	0.50	0.0205	4.84	-6.71	0.907	1.24
	0.40	0.0187	4.67	-7.11	0.912	1.32

TABLE III

SLOWING-DOWN SPECTRA FOR $\nu = 1$ ($B^2 = 0$)

	Turning Points				
Δ	ϵ_1	ϵ_2	δ	J	L
0.25	0.309	3.59	1.39	0.219	-0.703
0.50	0.356	3.44	1.21	0.180	-0.776
0.75	0.413	3.28	1.04	0.142	-0.857
1.00	0.481	3.11	0.788	0.105	-0.949
2.00	1.00	2.19	0.168	0.0738	-1.535

FIGURE 1

EFFECTIVE POTENTIAL, HEAVY GAS MODEL

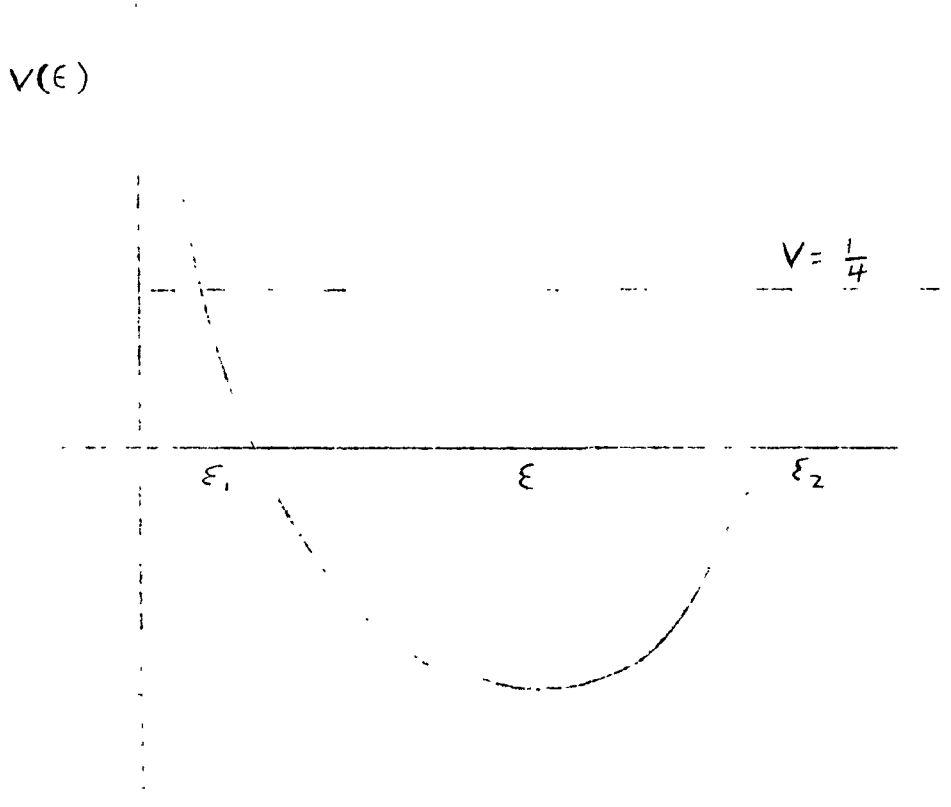

FIGURE 1

EFFECTIVE POTENTIAL, HEAVY GAS MODEL

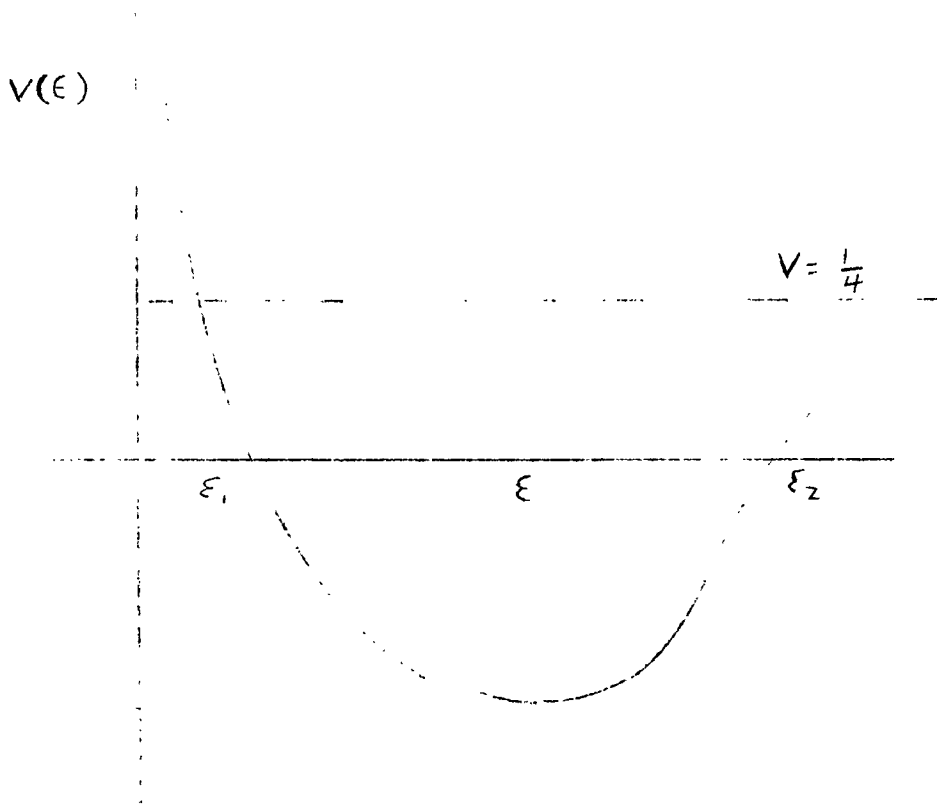

THE TIME DECAY CONSTANTS IN NEUTRON THERMALIZATION*

NOEL CORNGOLD, PAUL MICHAEL AND WARREN WOLLMAN+

BROOKHAVEN NATIONAL LABORATORY

FEBRUARY 1962

*Work performed under the auspices of the U. S. Atomic Energy Commission.

+Research Assistant, Summer 1961. Present Address: Department of Physics, U.C.L.A., Los Angeles, California.

ABSTRACT

We examine herein the decay constants, λ_k, which appear in the modal expansion of the neutron density in a study of the time-dependent thermalization of neutrons. A study of the proton gas moderator indicates the existence of an infinite number of discrete λ_k in the range $0 \leq \lambda < \frac{2}{\sqrt{\pi}} \Sigma_{sf} v_B$. The upper limit is a limit point for the eigenvalue sequence. Consideration of more general models indicates the existence of a discrete spectrum in the range $0 \leq \lambda \leq (v \Sigma_s)_{min}$ and $\lambda \geq (v \Sigma_s)_{max}$ and a continuous spectrum in $(v \Sigma_s)_{min} \leq \lambda \leq (v \Sigma_s)_{max}$.

This note contains some early results in a subject of considerable interest, namely, the character of the decay constants, λ_k, which appear in the modal expansion of the neutron density

$$N(x,t) = \sum_m c_m N_m(x) \exp\left[-\lambda_m \Sigma_{sf} v_B t\right] \tag{1}$$

in a study of the time-dependent thermalization of neutrons. Here x, defined through $x^2 = E/k_BT = (v/v_B)^2$ is a dimensionless velocity variable, Σ_{sf} is the macroscopic, free atom scattering cross section, and we neglect diffusive effects. The λ_m and N_m may be viewed as the eigenvalues and corresponding eigenfunctions, respectively, of the scattering operator which appears in the Boltzmann equation. It is generally assumed (and hoped!) (1) that scattering operators representing physically "reasonable" models of moderating materials will possess an infinite number of discrete eigenvalues, extending from zero to $+\infty$, with no limit point other than the point at infinity. To these eigenvalues, there correspond-so the assumption goes-eigenfunctions which form a complete set. In this note we show one model, the proton gas,

for which the assumption surely fails, and we shall indicate, in a rough way, how the assumption of a normal, point spectrum fails in almost all models.

In the case of the proton gas, the search for solutions of the form $N_m(x,t) \propto N_m(x) \exp\left[-\lambda_m \Sigma_{sf} v_B t\right]$ leads to an integral equation in velocity, which may be transformed-and this is the special feature of the proton gas model-into a differential equation, (2)

$$\frac{d}{dx}\left\{\frac{1}{P(x)}\frac{d}{dx}\left[(V(x)-\lambda_m)\,\nu_m(x)\right]\right\} + \left\{\frac{4}{\sqrt{\pi}} + \left[\frac{e^{-x^2}}{P^2(x)} - \frac{x^2}{P(x)}\right](V(x)-\lambda_m)\right\}\nu_m(x) = 0 \qquad (2)$$

In eqn.(2), $\nu_m(x) = \left[\frac{4}{\sqrt{\pi}} x^2 e^{-x^2}\right]^{-1/2} N_m(x)$, while $V(x)$ is proportional to the reaction rate for scattering, $V(x)\Sigma_{sf} = x\Sigma_s(x)$, and $\Sigma_s(x)$, the scattering cross section, is given by

$$\Sigma_s(x) = \left\{\left(1+\frac{1}{2x^2}\right)E_1(x) + \frac{1}{\sqrt{\pi}}\frac{e^{-x^2}}{x}\right\}\Sigma_{sf} \qquad (3)$$

Finally, the function $P(x)$ is $= \sqrt{\pi}\, x\, \mathrm{Erf}(x) + e^{-x^2}$.

A straightforward investigation of the differential equation for ψ_m, or for N_m shows that, 1) in the neighborhood of the origin, the two independent solutions $N^{(1,2)}$ are proportional to x^2 and to x respectively, while 2) in the neighborhood of infinity, the two independent solutions $N^{(3,4)}$ behave as $x^2 e^{-x^2}$ an x^{-2} respectively. The eigensolutions, N_m, will be taken to be those solutions of the differential equation, with properties

i) $N_m \to cx^2$ as $x \to 0$

ii) $N_m \to c' x^2 e^{-x^2}$ as $x \to \infty$

iii) N_m is finite for all $x \geq 0$.

The conditions above are precisely those obeyed by the solutions to the integral equation, which equation has a unique solution. They might also be deduced, on the basis of a more physical ~~agreement~~ argument, by demanding that the importance function -i.e. the adjoint function, $N_m^+ = N_m (x^2 e^{-x^2})^{-1}$ -belonging to each mode, be finite (indeed, constant) in the limits $x \to 0$, $x \to \infty$.

To simplify further discussion of the eigensolutions, we make the transformation

$$z_m(x) = [V(x) - \lambda_m] \exp\left[-\frac{\sqrt{\pi}}{2} \int dx \, \frac{E_f(x)}{P(x)}\right] \psi_m(x) \qquad (4)$$

which converts (2) into a Schrodinger equation,

$$\frac{d^2 z_m}{dx^2} + \mathcal{L}_m^2(x)\, z_m = 0 \tag{5}$$

where

$$\mathcal{L}_m^2 = \frac{2e^{-x^2}}{P(x)} - x^2 + \frac{4}{\sqrt{\pi}} \frac{P(x)}{V(x) - \lambda_m} - \frac{3\pi}{4} \frac{E\psi_0^2(x)}{P^2(x)} \tag{6}$$

and the boundary conditions on z are 1) $z(x) \sim ax$ as $x \to 0$ and 2) $z(x) \sim x^{3/2}\exp(-\frac{1}{4}x^2)$ as $x \to \infty$. The quantum mechanical analog of our eigenvalue problem is the following: we seek values of the parameter, λ, present in a potential $U(x,\lambda) \equiv -u^2(x,\lambda)$ for which there will be a bound state of zero energy having odd parity. (Note that U is an even function of x.)

In discussing the potential, we will want to distinguish those values of λ for which $V(x) - \lambda > 0$ throughout, from those for which $V(x) - \lambda$ can vanish for some x. Since V(x) is a positive, monotonic increasing function of x, having the minimum value $V_{min} = V(0) = \frac{2}{\sqrt{\pi}}$, we consider first $0 \le \lambda \le \frac{2}{\sqrt{\pi}}$, then $\lambda > \frac{2}{\sqrt{\pi}}$.

In the case $\lambda < \frac{2}{\sqrt{\pi}}$ the potential well, as sketched in figure 1, consists of a negative portion near the origin, which

joins with a well of harmonic oscillator type ($U \sim cx^2$) for large x. Suppose that for some fixed $\lambda < \frac{2}{\sqrt{\pi}}$, we find all of the energy levels (of odd parity) in our potential. It is clear that we will find a finite number of bound levels having energy < 0, and an infinite number having energy > 0. Next, let us increase λ, and observe the change in the energy levels. As λ increases, the potential becomes deeper, and the levels descend into the well. Those values of λ for which a level co-incides with the zero of energy are the eigenvalues of our thermalization problem. The number of levels which "pass through" E = 0 as λ is varied from zero to $\frac{2}{\sqrt{\pi}}$ is equal to the number of decay constants, λ_m which lie between zero and $\frac{2}{\sqrt{\pi}}$.

At this point, the reader will opine that there are "quite a few" λ_m less than $\frac{2}{\sqrt{\pi}}$. It is easy to see that there are in fact an infinite number lying in $0 \leq \lambda < \frac{2}{\sqrt{\pi}}$, that $\lambda = \frac{2}{\sqrt{\pi}} = V_{min}$ is a <u>limit point</u> for the infinite sequence of decay constants. The key to the argument lies in the spectrum of bound states for the $1/x^2$ potential, which is the limiting form of the negative portion of our potential. It is known (see, for example, (3)) that the spectrum of bound, orthonormal states extends to minus infinity for this potential,

whence an infinite number of levels "pass thru" E = 0, and our conjecture of a limit point is verified.

The modal solutions we have obtained, for $\lambda < \frac{2}{\sqrt{\pi}}$ are oscillatory functions. Their oscillations are limited, however, to a domain which we might roughly characterize as $0 \leq x \leq x_o$, where x_o, the "classical turning point," is the point at which U(x), the potential, is zero. (The turning point increases slowly, with λ, approaching a limiting value of 2.5 as $\lambda \to \frac{2}{\sqrt{\pi}}$.) It is clear, then, that the modal solutions do not form a complete set for the representation of admissible functions on the <u>full</u> domain $0 \leq x < \infty$. However, they are in practice quite useful for the representation of "sufficiently smooth" neutron distributions on $0 \leq x < \infty$. As an example, they

describe the evolution of the distribution after several collisions have intervened between time zero and time t, i.e. the quasi-asymptotic distributions considered by experimenters.

Consider, now, $\lambda > \frac{2}{\sqrt{\pi}}$. In this case, we deal with a potential well of quite another sort (figure 2). For large x the potential is again harmonic, and as x decreases, the potential decreases, becoming negatively infinite as $\frac{1}{x-x^*}$ when x approaches x^*, the point at which $V(x) = \lambda$. The potential below x^* has the unusual shape sketched in figure 2.

Our condition iii) above, that N(x) be finite, ensures, in connection with eqn.(4), that z(x) must approach zero as $x \to x^*$. Investigation of the differential equation shows that the regular solution about $x = x^*$ behaves as $x - x^*$, so that our eigensolutions would appear (but see ahead!) to be those solutions of the equation, regular at $x = x^*$, which join up with the exponentially decreasing solution in the neighborhood of infinity. Much of the argument goes as before; once more we are concerned with the number of bound states having energies less than zero, in a particular potential well.

In this case, the potential, which, for x near x^*, behaves like a one-dimensional Coulomb potential, has only a <u>finite</u> number of negative energy levels - i.e., it is bounded

from below. As λ increases beyond $\frac{2}{\sqrt{\pi}}$, x^* increases, but the separation between x^* and the turning point lying above x^* decreases. This "weakening" of the Coulomb potential forces the levels to ascend, rather than descend, and as $\lambda \to \infty$, a finite number of levels will pass through the zero energy level. As before, each λ for which a bound level coincides with zero energy, would appear to be a proper eigenvalue. The corresponding eigenfunctions are quite curious, they oscillate ever more rapidly in a narrowing range of x, located farther and farther from the origin.

We have said "would appear" to indicate that our argument is not finished. Indeed, we have neglected to impose condition i), which is equivalent to the vanishing of z_m at $x = 0$. This additional constraint, we believe, makes unlikely the existence of more than a few "discrete" modes, having $\lambda > \frac{2}{\sqrt{\pi}}$. Their existence has little bearing upon questions of completeness. We shall have to add an additional, infinite set of functions to the discrete eigenfunctions in order to get a set which appears complete. Such a set would be capable of representing delta function distributions of neutrons, for example.

We can find the additional functions, which have $\lambda > \frac{2}{\sqrt{\pi}}$, by removing condition iii), the condition of finiteness. If

the number density modes are permitted to have a singularity of delta-function type, new modes, characterized by a continuum of allowed values of λ, may be constructed. The nature of these modes, their orthogonality, etc. is best seen from a study of the integral form of the Boltzmann equation (see ahead). We will indicate, briefly, how they might be constructed from the differential equation we have been studying.

Let us choose for $\lambda > \frac{2}{\sqrt{\pi}}$, the solution of (5) which has proper behaviour at $x = 0$, and continue it to $x = x^*$. In the neighborhood of x^* the two solutions of the differential equation behave as $(x-x^*)$ and $b_1 + b_2 (x-x^*)\log(x-x^*) + \ldots$ respectively, so that our solution goes to some non-zero value as $x \to x^*$ from below. The solution for $x > x^*$ is defined as that solution-curve which originates at x^* and has the required exponential behaviour at infinity. The solution for $x > x^*$ may be normalized so that our overall solution is continuous in $0 \leq x < \infty$ though its derivatives are not.

The important feature of these solutions is that z need not vanish as $x \to x^*$. Eqn.(4) then allows us to deduce that (4)

$$N_\lambda(x) \sim P \frac{1}{V(x)-\lambda} + h(\lambda)\ \delta\big(V(x)-\lambda\big) \qquad (6a)$$

when x is close to x*. P signifies that, upon integration, the principal value of the singular function is to be taken. Since V(x) increases monotonically in the range $0 \leq x < \infty$, singular eigenfunctions, with index λ running from $\frac{2}{\sqrt{\pi}}$ to infinity, will contain delta functions $\delta(x-x^*)$ where x* runs from zero to infinity. It seems extremely likely that the set of functions consisting of the regular, discrete functions, and the singular eigenfunctions $_{\lambda}$ (6a) will be complete for the representation of all "physical" solutions to the time dependent Boltzmann equation.

The General Case

Results similar to those which we have obtained through the detailed consideration of the proton gas moderator seem to exist in the general case. We shall indicate, briefly, how they come about. The approach we use is quite similar to that introduced by Case (4).

We begin with the eigenvalue equation

$$(-\lambda_m + x\Sigma_s(x))\, N_m(x) = \int_0^\infty dx'\, x'\, \Sigma_s(x' \to x)\, N_m(x') \tag{7}$$

where λ_m, in accord with common usage, is equal to our earlier λ_m, multiplied by Σ_{sf}. We represent the kernel in (7) through

$$x'\, \Sigma_s(x' \to x) = \sum_{k=1}^{M} g_k(x')\, f_k(x) \tag{8}$$

whence

$$(-\lambda_m + x\Sigma_s(x))\, N_m(x) = \sum_{k=1}^{M} N_{mk}\, f_k(x) \tag{9}$$

in an obvious notation. If λ_m can never equal $x\Sigma_s(x)$, that is,

$\lambda_m < (x\,\Sigma_s)_{min}$, or $\lambda_m > (x\,\Sigma_s)_{max}$, eqn.(9) can be integrated to give the set of M equations,

$$N_{ml} = \sum_{k=1}^{M} N_{mk}\, a_{kl} \tag{10}$$

where

$$a_{kl} = \int_0^\infty \frac{f_k(x)\, g_l(x)}{-\lambda + x\,\Sigma_s(x)}\, dx \tag{11}$$

The vanishing of the determinant which appears in the solution of the homogeneous system (10) is, of course, the eigenvalue condition. Should we obtain an infinity of eigenvalues as $M \to \infty$, (with $0 \leq \lambda < (x\,\Sigma_s)_{min}$ and, possibly, $\lambda > (x\,\Sigma_s)_{max}$) we shall have duplicated the limit point behaviour noted earlier.

When we consider values of λ which can equal some $x\,\Sigma_s(x)$, the formal solution of (9) becomes, (4)

$$N_\lambda(x) = \sum_{k=1}^{M} N_{\lambda k}\, P\, \frac{f_k(x)}{-\lambda + x\,\Sigma_s(x)} + h(\lambda)\, \delta(\lambda - x\,\Sigma_s(x)) \tag{12}$$

where P denotes "principal value" and $h(\lambda)$ is a function to

be determined. Since the normalization of $N_\lambda(x)$ is arbitrary, we have, in fact, only M-1 components $N_{\lambda k}$ for given λ. Thus, when we multiply on the left by $g_j(x)$ and integrate we have M linear algebraic equations for the determination of M-1 components $N_{\lambda k}$, plus the unknown function $h(\lambda)$. The algebraic system is, then, generally solvable for <u>all</u> λ in the range $(x\,\Sigma_s)_{min} \leq \lambda \leq (x\,\Sigma_s)_{max}$. We have a continuum of allowed λ's, connected with orthogonal eigenfunctions having, in part, delta-function behaviour. There is the additional possibility that $h(\lambda)$ vanishes for some λ in the continuous range. In these cases, the set (12) reduces to the homogeneous set (10) and we have the case of discrete eigenvalues lying inside the continuous range. These are the $\lambda > \frac{2}{\sqrt{\pi}}$ modes mentioned earlier.

One might conjecture that the continuum solutions, when augmented by the discrete modes will form a set that is complete in the range $0 \leq x < \infty$. The conjecture is supported by the "trivial" completeness of the delta-functions, and the presence of "frequencies," λ, covering the entire range of possible reaction rates, and more. Of course, a proof of the completeness remains to be found.

In appendix B we give a proof for a simple model of the scattering kernel.

REFERENCES

1. M. S. Nelkin, Proceedings of Symposia in Applied Mathematics, American Mathematical Society, Vol XI, pp. 20-42 (1961).
2. E. P. Wigner and J. E. Wilkins Jr., AECD-2275 (1944).
3. K. M. Case, Phys. Rev. 80, pp. 797-806 (1950).
4. K. M. Case, Annals of Physics 9, pp. 1-23 (1960).

APPENDIX A

We shall discuss here some properties of a Boltzmann equation which possesses a very simple scattering kernel. The following may serve to illustrate some of the points made in the text.

Consider the scattering kernel

$$\Sigma_s(x' \to x) = \beta\, \Sigma_s(x')\, x\, \Gamma_s(x)\, M(x)$$

$$\frac{1}{\beta} = \int_0^\infty dx\, x\, \Gamma_s(x)\, M(x) \qquad \text{(A1)}$$

where $M(x)$ is $x^2 \exp(-x^2)$ and $\Sigma_s(x)$ is a typical "incoherent" scattering cross section. $x\Gamma_s(x)$ is to be monotonic increasing in $0 \leq x < \infty$, and proportional to x for large x. The kernel (A1) satisfies the requirement of detailed balance.

The equation corresponding to (9) in the text is:

$$\left[x\, \Gamma_s(x) - \lambda\right] N(x) = \beta\, x\, \Gamma_s(x) M(x) \int_0^\infty dx'\, x'\, \Gamma_s(x')\, N(x'). \qquad \text{(A2)}$$

It indicates directly that the x-dependence of $N(x)$ in the limits $x \to 0$ and $x \to \infty$ is the behaviour we required earlier. To discuss

the discrete spectrum, $(\lambda \neq x\,\Sigma_s(x))$, we multiply by $x\,\Sigma_s(x)\left[x\,\Sigma_s - \lambda\right]^{-1}$ and integrate. The eigenvalue condition appears as:

$$\frac{1}{\beta} = \int_0^\infty dx\; x\,\Sigma_s M \;=\; \int_0^\infty dx\; x\,\Sigma_s M \frac{x\,\Sigma_s}{x\,\Sigma_s - \lambda} \quad . \tag{A3}$$

Clearly (A3) has the solution $\lambda = 0$. It is also easy to see that $\lambda = 0$ is the only solution in the range $0 \leq \lambda < (x\,\Sigma_s)_{min}$. The corresponding eigenfunction is the Maxwellian, M(x).

The continuum eigenfunctions, N_λ, $(\lambda = x^*\Sigma_s(x^*) > (x\,\Sigma_s)_{min})$ satisfy the equation

$$N_\lambda(x) = \beta\; x\,\Sigma_s(x) M(x)\; P\frac{1}{x\Sigma_s(x) - \lambda} + h(\lambda)\;\delta(\lambda - x\,\Sigma_s(x)) \tag{A4}$$

where the normalization of $N_\lambda(x)$ has been chosen so that

$$\int_0^\infty dx'\; x'\;\Sigma_s(x')\; N_\lambda(x') = 1 \quad . \tag{A5}$$

If we multiply on the left by $x\,\Sigma_s$ and integrate,

$$1 = \beta\; P \int_0^\infty dx\, x\,\Sigma_s M \frac{x\,\Sigma_s}{x\,\Sigma_s - \lambda} + h(\lambda) \int x\;\Sigma_s\;\delta\big(\lambda - x\;\Sigma_s(x)\big)\,dx$$

we can solve for $h(\lambda)$. Indeed,

$$h(\lambda) = \frac{1-\beta \; P \int_0^\infty dx \; x \; \Sigma_s M \frac{x \Sigma_s}{x \Sigma_s - \lambda}}{\int_0^\infty dx \; x \; \Sigma_s \; \delta\left(\lambda - x \; \Sigma_s(x)\right)} \; . \qquad \text{(A6)}$$

The eigenfunction expansion of a solution $N(x,t)$ to our Boltzmann equation will be of the form

$$N(x,t) = C_0 \, M(x) + \int_{(x\Sigma_s)_{min}}^\infty d\lambda \; C(\lambda) \exp\left[-\lambda \, v_B t\right] N_\lambda(x) \; . \qquad \text{(A7)}$$

The single, discrete eigenfunction gives the steady state distribution of neutrons, while the continuum solutions, N_λ, are needed to represent the transient behaviour.

APPENDIX B

Completeness in the Simple Model

We wish to show, in this section, that all "reasonable" solutions to the special transport equation discussed in Appendix A may be given a representation in terms of the eigenfunctions considered there. By "reasonable" solution, we mean one generated by the requirement that $N(x,t)$ be equal to some prescribed $N(x,0)$ at $t=0$, and whose Laplace transform-with respect to time-exists. It will suffice to consider the case of the Green's function, $g(x,y;t)$, generated by $N(x,0) \sim \delta(x-y)$. We shall show that $g(x,y;t)$ has the modal representation,

$$g(x,y;t) \sim \sum_k N_k^+(y)\, N_k(x)\, e^{-\lambda_k t} + \int_{\lambda^*}^{\infty} d\lambda\, N_\lambda^+(y)\, N_\lambda(x) e^{-\lambda t} \qquad \text{(B1)}$$

where $\lambda^* = (v\Sigma_s)_{\min.}$. Having shown (B1) to be true, we infer that the solution stemming from arbitrary $N(x,0)$ has the usual modal representation in terms of the N_λ, with coeffi-

cients given by the inner products of $N(x,0)$ and N_λ^+, i.e.,

$$N(x,t) = \int_0^\infty dy\ g(x,y;t)\ N(y,0). \tag{B1a}$$

Consider

$$\frac{\partial N}{\partial \tau} + x\rho(x)\,N(x,\tau) = \int_0^\infty dx'\ x'\,\rho(x';x)\,N(x',\tau) \tag{B2}$$

where $\tau = v_B \Sigma_{sf} t$, and $\Sigma_s(x',x) = \Sigma_{sf}\rho(x',x)$. Σ_{sf} is the macroscopic, free atom scattering cross section. Our "simple model" has the scattering kernel

$$x'\rho(x';x) \quad \beta\, x'\rho(x')\, x\rho(x)\, M(x) = \beta\, v(x')\, v(x)\, M(x)$$

$$\beta^{-1} = \int_0^\infty dx\ v(x)\,M(x) \tag{B3}$$

where $v(x) = x\rho(x)$. We shall solve the initial-value problem, $N(x,0) = \delta(x-y)$, by means of the Laplace transform. If we define

$$\int_0^\infty d\tau\ e^{-\lambda\tau} N(x,\tau) \equiv \bar{N}(x,\lambda) \tag{B4}$$

calculations similar to those in Appendix A yield

$$\bar{N}(x,\lambda) = \beta \frac{\nu(x)M(x)}{\lambda+\nu(x)} \frac{\nu(y)}{\lambda+\nu(y)} \frac{1}{1-\beta\rho_T(\lambda)} + \frac{\delta(x-y)}{\lambda+\nu(x)} \qquad \text{(B5)}$$

with $b(\lambda) = \int_0^\infty d\xi \, \frac{v^2(\xi)M(\xi)}{\lambda+v(\xi)}$. The expression (B4) defines $\bar{N}(x,\lambda)$ for the $(\lambda) > 0$ where it is analytic; (B5) extends the definition throughout the λ-plane.

From its definition, we see that $b(\lambda)$, and hence $\bar{N}(\lambda)$ are discontinuous across the portion of the real λ-axis which extends from $-\nu(0)$ to $-\infty$. To invert (B5) we consider $\frac{1}{2\pi i}\int_\Gamma d\lambda \, e^{\lambda\tau} \bar{N}(x,\lambda)$, where the contour, Γ, is sketched in Figure 3. The sole points inside the contour which are singular points of $\bar{N}$, are those at which $1-\beta b(\lambda)=0$. This is the eigen-value equation for the discrete λ's, and a little consideration shows it is satisfied only at $\lambda=0$. The contribution to $N(x,\tau)$ from this pole is the normalized Maxwellian, $\frac{4}{\sqrt{\pi}} M(x)$.

The part of the integration extending from A to B yields $N(x,\tau)$, when A and B are made to approach $-\infty$ and $+\infty$,

respectively. In this limit, the portions BC and FA contribute nothing, because of the rapid decrease of $\exp(\lambda\tau)$. Thus, integration around Γ yields

$$N(x,\tau) = \frac{4}{\sqrt{\pi}} M(x) - \frac{1}{2\pi i} \int_{CDEF} d\lambda\, e^{\lambda\tau}\, \bar{N}(x,\lambda) \qquad \text{(B6)}$$

as C and F are made to approach infinity.

We now evaluate the integral over CDEF. To begin, we note that the integral over DE, that is, over a small semicircle, of radius ϵ, centered at $-v(0)$, vanishes as $\epsilon \to 0$. Next, we bring the lines CD and EF close to the real axis, so that (B6) becomes

$$N(x,\tau) = \frac{4}{\sqrt{\pi}} M(x) + \frac{1}{2\pi i} \int_{v(0)}^{\infty} ds\, e^{-s\tau} \left[\bar{N}(x,-s-i\varepsilon) - \bar{N}(-s+i\varepsilon) \right] \qquad \text{(B7)}$$

The quantity in square brackets is seen to be equal to:

$$2i\,\beta v(y)\, v(x) M(x)\, \delta m \left[\frac{1}{s+i\varepsilon - v(x)} \; \frac{1}{s+i\varepsilon - v(y)} \; \frac{1}{1-\beta \bar{\phi}_+(-s-i\varepsilon)} \right]$$

$$- \delta(x-y) \left[\frac{1}{s+i\varepsilon - v(x)} - \frac{1}{s-i\varepsilon - v(x)} \right] \qquad \text{(B8)}$$

and we shall rearrange it by making use of relation

$$\frac{1}{s-v(x)\pm i\varepsilon} = P\,\frac{1}{s-v(x)} \mp \pi i\,\delta(s-v(x)) \qquad \text{(B9)}$$

Then, the second term in (B8) becomes equal to $2\pi i\ \delta(x-y)\ \delta(s-v(x))$, which, in turn, is equal to $2\pi i|v'(x)|\ \delta(s-v(x))\ \delta(s-v(y))$.

To continue, we use (B9) to write

$$1-\beta\,\rho_r(s\mp i\varepsilon) = 1+\beta P\int_0^\infty d\tau\ \frac{v^2(\tau)M(\tau)}{s-v(\tau)} - \pi i\beta\left[\frac{v^2M}{|v'|}\right]_{x(s)}$$

$$= 1+\beta\,\rho_{r0}(s) - \pi i\,\beta\,\rho_{r1}(s) \qquad \text{(B10)}$$

The notation $\left[\ldots\right]_{x(s)}$ signifies that the function inside the square brackets is to be evaluated at the value of its argument, x, for which $v(x)=s$. This is the same value of x which appears in the term $2\pi i|v'(x)|$ ... mentioned in the last paragraph. The rest of the calculation is straightforward. We use (B9) in multiplying out (B8), to obtain

$$\frac{1}{2\pi i}\left[\bar{N}(x,-s-i\varepsilon)-\bar{N}(x,-s+i\varepsilon)\right]=$$

$$\beta^2 v(y)\,v(x)\,M(x)\,\frac{\rho_{r_1}(s)}{(1+\beta\rho_{r_0})^2+(\pi\beta\rho_{r_1})^2}\cdot \tag{B11}$$

$$\left[P\frac{1}{s-v(y)}-\frac{1+\beta\rho_{r_0}}{\beta\rho_{r_1}}\delta(s-v(y))\right]\left[P\frac{1}{s-v(x)}-\frac{1+\beta\rho_{r_0}}{\beta\rho_{r_1}}\delta(s-v(x))\right]$$

Thus,

$$g(x,y,\tau)=N_0^+(y)\,N_0(x)\,e^{-\lambda_0\tau}+\int_{v(0)}^{\infty}ds\;N_s^+(y)\,N_s(x)\,e^{-s\tau} \tag{B12}$$

where $N_0^+(y)=\frac{4}{\sqrt{\pi}}$, $N_0(x)=M(x)$, $\lambda_0=0$.

$$N_s^+=\beta\,\Lambda(s)\,\nu(y)\left[P\frac{1}{s-v(y)}-\frac{1+\beta\rho_{r_0}}{\beta\rho_{r_1}}\delta(s-v(y))\right]$$

$$N_s(x)=\Lambda(x)\;N_s^+(x) \qquad \text{and}$$

$$\Lambda(s)=\sqrt{\frac{\rho_{r_1}(s)}{(1+\beta\rho_{r_0}(s))^2+(\pi\beta\rho_{r_1}(s))^2}}$$

CAPTIONS

FIGURE 1. The effective potential, $U(x,\lambda)$, for a value of λ less than $\frac{2}{\sqrt{\pi}}$. x_o is the classical turning point for a particle of zero energy. The arrow indicates the manner in which the potential changes, as λ increases.

FIGURE 2. The effective potential, U, for a value of λ greater than $\frac{2}{\sqrt{\pi}}$. x^* is the point at which the reaction rate, $V(x)$, is equal to λ. The arrows indicate the manner in which the potential changes, as λ increases.

FIGURE 3. Integration contour, Appendix B.

$$\lambda < \frac{2}{\sqrt{\pi}}$$

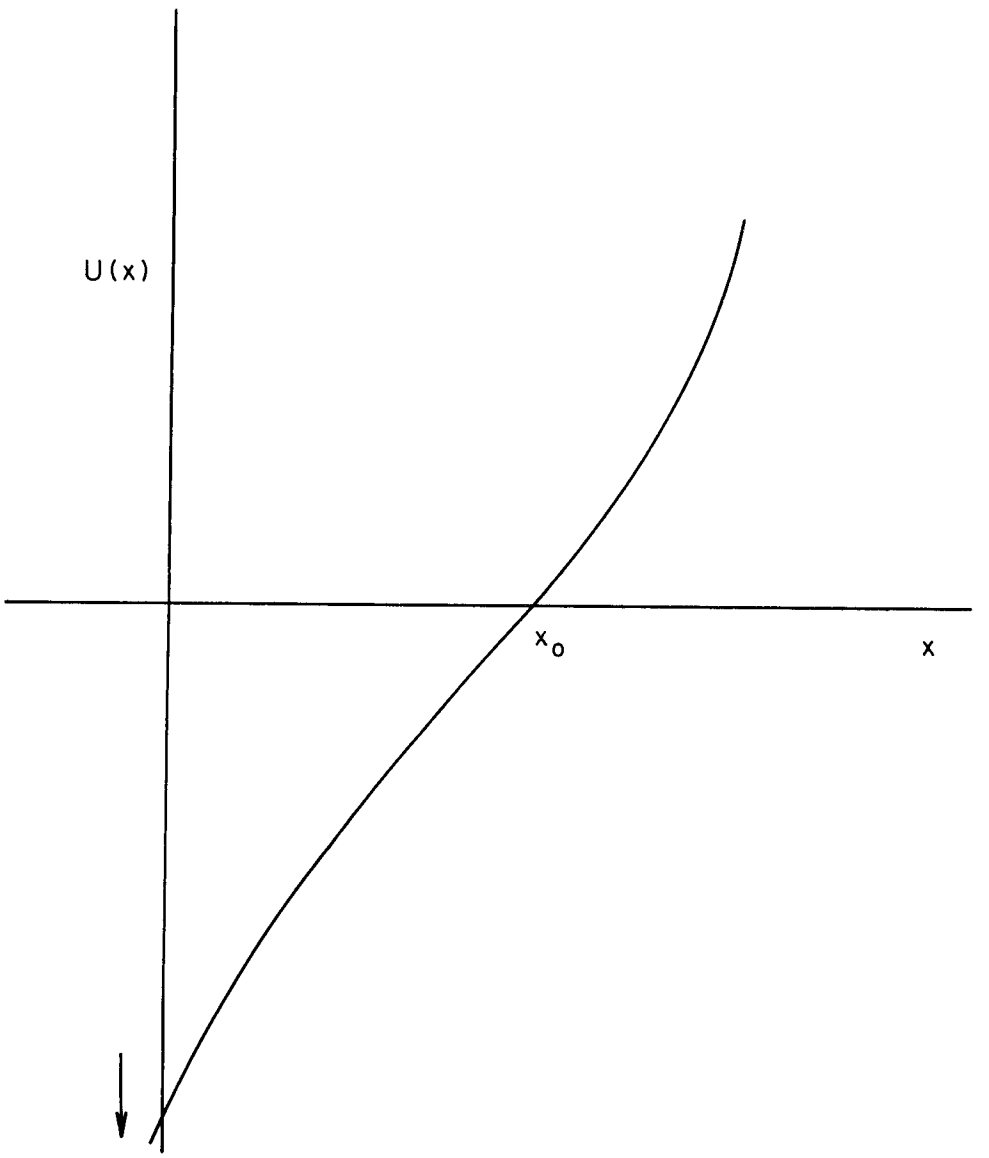

FIG. 1

$$\lambda > \frac{2}{\sqrt{\pi}}$$

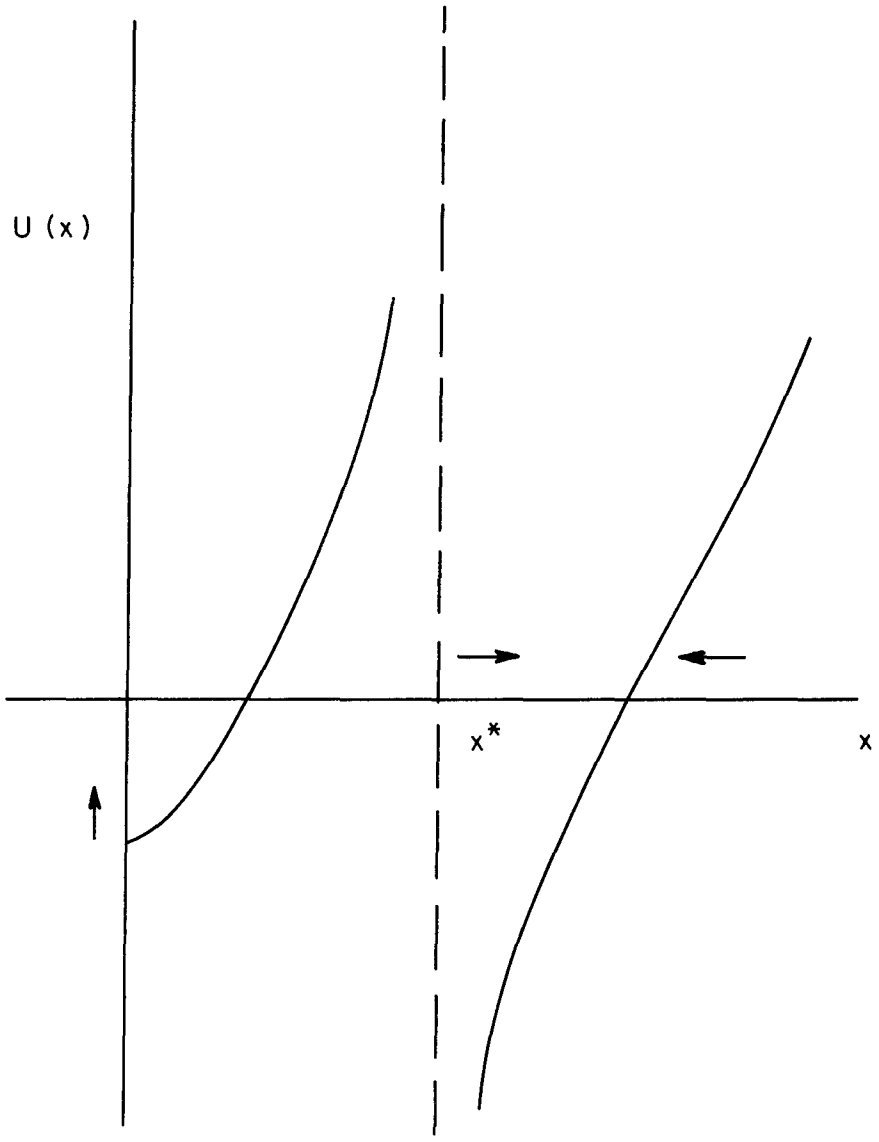

FIG. 2

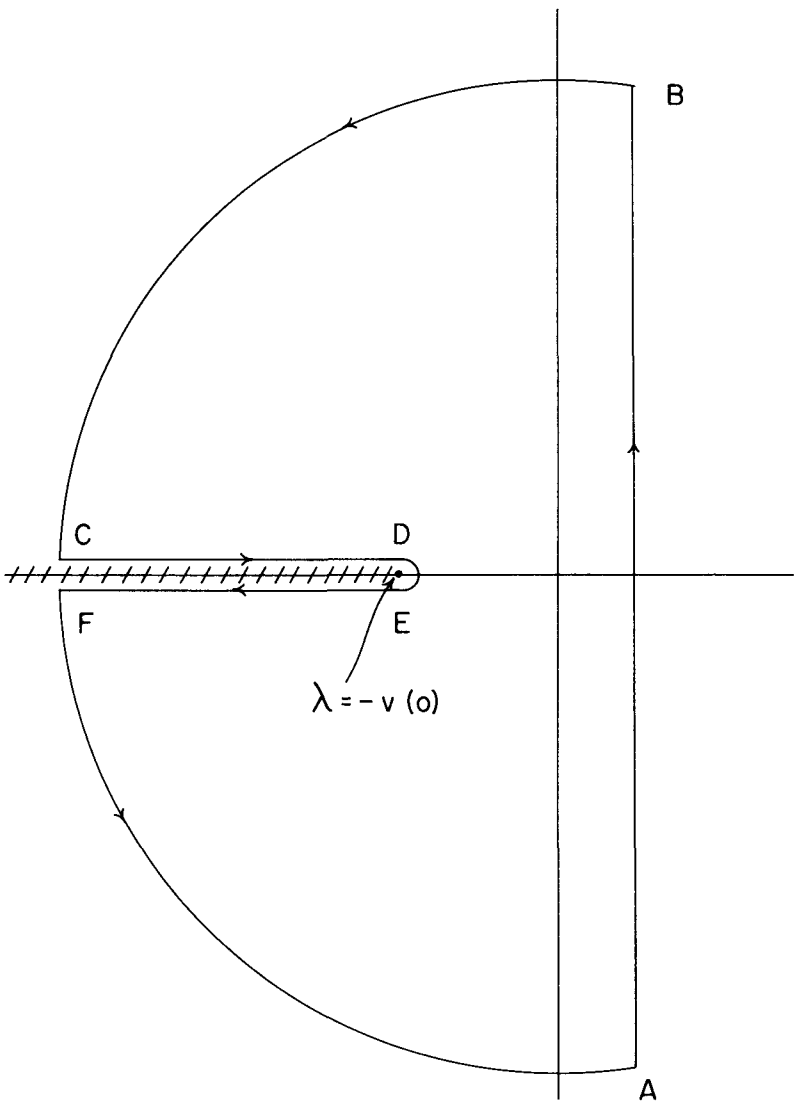

FIG. 3

found by the usual expansions which start with a Maxwellian as the leading term. In addition, the method also applies to the double P-L approximations which allows one rather directly to obviate most of the uncertainty due to vacuum boundary conditions and the assignment of an equivalent buckling when making comparison with experiment. In general, the few group time dependent P-L approximation is quite flexible and allows one to introduce into the study of a wide variety of problems a minimum amount of complexity.

GENERAL FORMULATION

The basic equations for this study are the time dependent P-L equations in slab geometry with isotropic energy transfer:

$$
\begin{aligned}
&\frac{1}{v_k}\frac{\partial F_0^k}{\partial t} = -\frac{\partial F_1^k}{\partial x} - \left(\Sigma_T^k - \Sigma_{s0}^k + \sum_{g=1}^{G\prime}\Sigma_k^g\right)F_0^k + \sum_{g=1}^{G\prime}\Sigma_g^k F_0^g \,, \\
&\frac{1}{v_k}\frac{\partial F_1^k}{\partial t} = -\frac{1}{3}\frac{\partial F_0^k}{\partial x} - \frac{2}{3}\frac{\partial F_2^k}{\partial x} - \left(\Sigma_T^k - \Sigma_{s1}^k\right)F_1^k \,, \qquad (1) \\
&\vdots \qquad\qquad\qquad\qquad\qquad\qquad\qquad\qquad\qquad\qquad k = 1, 2, \ldots, G \\
&\frac{1}{v_k}\frac{\partial F_L}{\partial t} = -\frac{L}{2L+1}\frac{\partial F_{L-1}^k}{\partial x} - \left(\Sigma_T^k - \Sigma_{sL}^k\right)F_L^k \,,
\end{aligned}
$$

where,

superscripts stand for the group of which there are G in all,

F_j^k is the j'th Legendre component of the directional flux in the k'th group,

v_k is the average speed in the k'th group,

Σ_T^k is the total cross section in the k'th group,

Σ_{sj}^k is the j'th Legendre component of the scattering cross section in the k'th group,

Σ_g^k is the isotropic energy transfer cross section from the g'th to the k'th group.

It should be noted that the time dependent P-1 approximation and diffusion theory are not the same; the time dependent diffusion equations are obtained from the P-1 equations by dropping the time derivative of the current.

A solution of the above equations is assumed of the form,

$$F_n^k(x,t) = f_n^k(x)\, e^{-\lambda t}, \qquad n = 1,2,\ldots,L\ , \qquad (2)$$

$$k = 1,2,\ldots,G.$$

The equations are then solved as in the static case except that the characteristic equation rather than determining the relaxation lengths in terms of the material parameters yields a relation between the relaxation lengths and the relaxation times. This relation between the relaxation lengths and the relaxation times must then be solved simultaneously with the boundary conditions to determine the eigenvalues, the λ's. This is usually a rather transparent equation which is however transcendental; it is solved by standard numerical techniques. If a buckling type of dependence is assumed for the $f_n^k(x)$ then the characteristic equation is simply a polynomial relationship between the λ's and the buckling and yields the eigenvalues for any given buckling.

If a buckling is assumed for the spatial dependence, there are L times G eigenvalues for each buckling. The same number of eigenvalues appear when boundary conditions other than the zero flux condition are assumed except that the equations also simultaneously yield the eigenvalues for the higher spatial modes - that is those corresponding to the harmonic bucklings. In diffusion theory there are only G eigenvalues for each spatial mode. Except for diffusion theory, the number of eigenvalues and eigenfunctions is just enough to allow a match to the initial values of the first L components of the directional flux in each energy group for each spatial harmonic. Diffusion theory has only enough flexibility to match the initial values of the scalar flux in each energy group for each spatial harmonic.

TIME TRANSIENTS

The consideration of time transients may be naturally split into consideration of two types: current transients and energy transients. By a current transient is meant those eigenfunctions besides the fundamental which are present due to the matching of the initial flux and current and higher P-L components since the fundamental mode by itself does not have enough freedom to match all the P-L components of the initial conditions in general. By an energy transient is meant those eigenfunctions besides the fundamental which are present due to fact that the energy distribution of the fundamental mode

does not by itself necessarily match the initial energy distribution.

It is simplest to examine the current transients in the one group P-1 approximation with a spatial dependence given by a buckling. The eigenvalues for this case are given by

$$\lambda_1 = \nu\left(\Sigma_a + \tfrac{1}{2}\Sigma_{TR} - \sqrt{(\tfrac{1}{2}\Sigma_{TR})^2 - \tfrac{1}{3}B^2}\right) ,$$

$$\lambda_2 = \nu\left(\Sigma_a + \tfrac{1}{2}\Sigma_{TR} + \sqrt{(\tfrac{1}{2}\Sigma_{TR})^2 - \tfrac{1}{3}B^2}\right) , \qquad (3)$$

where

$$\Sigma_a = \Sigma_T - \Sigma_{s0} ,$$

$$\Sigma_{TR} = \Sigma_{s0} - \Sigma_{s1} .$$

In the case of no absorption and no leakage ($B^2=0$) these eigenvalues reduce to

$$\lambda_1 = 0 , \qquad \lambda_2 = \nu\Sigma_{TR} . \qquad (4)$$

The eigenvalue zero corresponds to a mode which persists indefinitely; the corresponding eigenfunction has an arbitrary amplitude to match the initial flux but has no current component. The eigenvalue $\nu\Sigma_{TR}$ has an eigenfunction which has a zero value of the flux but an arbitrary current amplitude which may be used to match the initial current. The neutrons in this second mode do not leak out of the system nor are they absorbed since in this particular example $B^2=\Sigma_a=0$. However, there is no net number of neutrons in this second mode since integration over the directional flux of this mode yields no contribution from the scalar flux component since it has zero amplitude and no contribution from the

current component because of the orthogonality of unity and P_1 Legendre functions. This second mode then is simply an angular transient which is due to the mismatch of the angular distribution of the persisting mode with the initial angular distribution. The time for the angular distribution of the directional flux to rearrange itself into that of the persisting mode is on the order of $(\nu \Sigma_{TR})^{-1}$.

As the leakage and absorption terms increase from zero, the net number of neutrons in the current transient becomes non-zero. The net number of neutrons in the transient is just the number of neutrons that will actually leak from and be absorbed in that mode. For large enough leakage or absorption the net number of neutrons in the transient can be considerable, and the influence of the leakage is to make the properties of the transient more like that of the persisting mode.

If the leakage is increased to the point where leakage becomes more probable than a transport collision, that is if $\frac{B^2}{3} > \left(\frac{\Sigma_{TR}}{2}\right)^2$ then the character of the eigenfunctions in P-1 approximation changes. In particular, the eigenvalues as given by Eq. (3) become complex. The corresponding eigenfunctions describe damped travelling waves. The damping factor and phase velocity of these waves are given by

$$\delta = \nu \Sigma_a + \tfrac{1}{2} \nu \Sigma_{TR} \quad , \qquad (5)$$

$$V = (\nu/\sqrt{3}) \sqrt{1 - (\Sigma_{TR}/2B)^2} \quad .$$

If for a fixed odd order of P-L approximation and for a fixed number of groups the characteristic equation is written for a spatial dependence given by a buckling, one obtains the characteristic polynomial for the eigenvalues. The coefficients in the polynomial are functions of the cross sections and of the buckling. If the buckling is increased to the point where the cross sections become negligible in comparison with the buckling, it is easily seen that all the coefficients in the polynomial of degree $2L$ in λ become positive. The roots of such a polynomial are complex. Hence, regardless of the order of P-L approximation (odd L) or the number of groups employed, as long as the cross sections are finite, only a finite number of buckling modes have real eigenvalues and an infinite number have complex eigenvalues. It also follows then that for a system with a large enough fundamental buckling all of the eigenvalues are complex. Note that this does not apply to the diffusion approximation or the even L approximations.

This investigation then shows that travelling wave phenomena become important for systems where bucklings on the order of Σ_{TR} are important. For such systems, time dependent diffusion theory breaks down; the eigenvalues yielded by diffusion remain real and constantly increase with buckling. In addition the usual expansions of the eigenvalue in a power series in B^2 obviously are beyond their radius of convergence at this point since they do not yield complex eigenvalues.

It is simplest to consider energy transients in the two group diffusion approximation with a spatial dependence given by a buckling. The eigenvalues for this case are given by

$$\lambda_1 = \tfrac{1}{2}\left(\Lambda_1+\Lambda_2-\sqrt{(\Lambda_1-\Lambda_2)^2+\nu_1\Sigma_1^2\nu_2\Sigma_2^1}\right) ,$$
$$\lambda_2 = \tfrac{1}{2}\left(\Lambda_1+\Lambda_2+\sqrt{(\Lambda_1-\Lambda_2)^2+\nu_1\Sigma_1^2\nu_2\Sigma_2^1}\right) , \qquad (6)$$

where

$$\Lambda_1 = \nu_1\left(\Sigma_a^1+\Sigma_1^2+B^2/3\,\Sigma_{tr}^1\right) ,$$
$$\Lambda_2 = \nu_2\left(\Sigma_a^2+\Sigma_2^1+B^2/3\,\Sigma_{tr}^2\right) . \qquad (7)$$

In the case of no absorption and no leakage ($B^2=0$), the eigenvalues reduce to

$$\lambda_1 = 0 \quad , \qquad \lambda_2 = \nu_1\Sigma_1^2+\nu_2\Sigma_2^1 \quad . \qquad (8)$$

The eigenvalue zero corresponds to a mode which persists indefinitely; the corresponding eigenfunction has an arbitrary amplitude to match the persisting energy spectrum (and current). The eigenfunction corresponding to the eigenvalue $\nu_1\Sigma_1^2+\nu_2\Sigma_2^1$ when summed over energy has no net number of neutrons. The meaning of this eigenfunction then is simply a distortion of the fundamental mode spectrum which has a reciprocal relaxation time given by the total probability per unit time for collision with change of energy. It is essentially an eigenvalue of the scattering matrix.

As the leakage and absorption terms increase from zero the net number of neutrons in the energy transient becomes greater than zero. The net number of neutrons in the transient is just the number of neutrons that will actually leak

from and be absorbed in that mode.

The eigenvalues for the energy modes may be expanded in powers of B^2. However, in certain cases caution must be observed. In the particular case where for very small buckling the smaller eigenvalue grows more rapidly with increasing B^2 than the larger eigenvalue, there will arrive a point at which there is an "apparent crossing" of the eigenvalues. If the square root in Eq. (6) for the eigenvalues is expanded in terms of the difference of Λ_1 and Λ_2, it must be remembered that the absolute difference of this quantity is needed in the expansion and this term has to be rearranged if absolute value signs are not employed after the "apparent crossing" value of B^2. Also the expansion itself must be changed for values in the immediate vicinity of the apparent crossing where the coupling term is greater than the difference of the single group eigenvalues. It is certainly questionable whether the ordinary expansions of the eigenvalue in powers of B^2 are valid for the lowest eigenvalue when the eigenvalue of the energy transient approaches the lowest eigenvalue and for larger bucklings. Even if the expansion is that for the lowest eigenvalue in that range, it must certainly be necessary to take a great many terms to obtain any accuracy in order to reproduce the requisite sharp change in the behavior of the lowest eigenvalue with buckling.

It is apparent that there are large changes in the behavior of the eigenvalues for very leaky systems. Considering that these eigenvalues are then put back into the equations

to solve for the energy eigenfunctions it is apparent that large changes in the spectra may be expected for leaky systems. In a spectrum which is close to one dominated by a current transient or in a spectrum which is dominated by an energy transient, the approach of starting off with a Maxwellian as a first approximation is certainly questionable.

WATER EXAMPLE

Water has been chosen as an example to show up the current transients because of the large amount of important work that has been done on this medium. Also, the effects of various boundary conditions has been estimated because of the extreme importance of the boundary in small assemblies. The isotropic energy transfer cross sections were obtained from Nelkin[5] kernel. In the two group cases the groups were split at an energy corresponding to kT; this happens to give a fairly good fit to diffusion cooling experiments, but the main point is that the cross sections for water are consistently calculated in all cases. The results are given in the tables below.

The eigenvalues for a water assembly described by buckling are given in Table 1. In this table, the values are calculated on the basis of one group theory using the various approximations listed. The effects of the current transients

B^2	Diff Th	P-1		P-3			
0 cm^{-2}	.004296	.004296	.4750	.004296	.4750	.7996	.7996
.000987	.004329	.004330	.4750	.004330	.4750	.7996 ± i	.003521
.003948	.004430	.004431	.4749	.004431	.4751	.7996 ± i	.007022
.01579	.004832	.004838	.4745	.004838	.4751	.7993 ± i	.01403
.02467	.005134	.005143	.4742	.005142	.4752	.7991 ± i	.01755
.0987	.007648	.007703	.4716	.007691	.4755	.7977 ± i	.03521
.2014	.01114	.01130	.4680	.01125	.4760	.7957 ± i	.06343
.3948	.01770	.01824	.4611	.01804	.4766	.7920 ± i	.07134
2.467	.08809	.1148	.3645	.09944	.4625	.7583 ± i	.1925
9.870	.3395	.2397 ± i	.3222	.3602 ± i	.2457	.6791 ± i	.4333
39.48	1.345	.2397 ± i	.7626	.4818 ± i	.5062	.5576 ± i	1.083

TABLE 1

The tabular entries give the decay constants in (micro-seconds)$^{-1}$ for a one-group treatment of water using the bucklings and theories indicated.

become dominant at a buckling of about $B^2=3.5\ cm^{-2}$. This is beyond the range where pulsed work has been done on pure water assemblies; however, the range where current transients are important may be reached by some of the largest pulsed sources now available. In addition, it is clear that the bucklings or Fourier components important in some pulsed water lattic experiments do reach into the range in question. It should be noted that the time dependence of the angular transient is markedly different from that of the flux, hence any spectrum measurements even in a moderate size assembly must take this into account when time dependent experiments and theory are compared.

As is well known, the transport or non-diffusion corrections tend to be over-emphasized in P-1 theory and this shows up for small bucklings in the comparison of P-1 and P-3 calculations in Table 1. However, the dominance of the current transient in the range of interest for lattices is quite clear, and this physical phenomenon appears in all the odd order P-L approximations but does not appear at all in diffusion theory.

Since the transport and energy corrections to the eigenvalue for small bucklings are known to be of opposite sign, the eigenvalues for the same water systems were calculated on the basis of two energy groups. These results are given in Table 2. The values given show clearly that the lowest eigenvalue becomes imaginary at about the same

B^2	Diff Th		P-1			
0 cm^{-2}	.004296	.2238	.004296	.2238	.4974	.5348
.0009870	.004329	.2238	.004329	.2238	.4974	.5347
.003948	.004430	.2238	.004434	.2240	.4973	.5345
.01579	.004832	.2243	.004844	.2247	.4970	.5336
.02467	.005133	.2246	.005141	.2253	.4969	.5329
.09870	.007631	.2272	.006979	.2292	.4952	.5273
.2014	.01107	.2309	.01121	.2368	.4928	.5194
.3948	.01744	.2378	.01789	.2511	.4870	.5042
2.467	.07815	.3201	.09178	.3611 ± i	.1791	.4463
9.870	.2305	.6784	.3388 ± i	.4807	.2913 ± i	.1881
39.48	.6961	2.255	.3291 ± i	1.040	.3010 ± i	.5104

TABLE 2

The tabular entries give the decay constants in (micro-seconds)$^{-1}$ using two groups and the bucklings and theories indicated.

buckling as in one group theory. The basic physical phenomenon of traveling waves is not affected by multi-energy considerations although the magnitude of the eigenvalues is, of course, somewhat modified by the two group as opposed to the one group scheme.

One apparent difficulty of working with small assemblies is the lack of a satisfactory boundary condition in the lower order approximations which will accurately portray the leakage when it is the dominant effect. This is simply another way of stating that the low order approximations are usually unsatisfactory near boundaries. In order to investigate the magnitude of the breakdown of the low order approximations for small systems, the eigenvalues for water systems have been calculated on the basis of diffusion theory and P-1 theory using the double P-0 approximation with its natural vacuum boundary conditions. These results are given in Table 3. It is clear that the disagreement between the various theories is large.

The three values in Table 3 noted with an asterisk were not calculated due to the numerical code used to obtain the results - they could readily be obtained by modifying the code in a minor way. However, the authors were not able to satisfy the Marshak type boundary conditions in a simple direct way when the eigenvalue became imaginary.

Slab Thickness	Diff Th	P-1		double P-0	
cm.	.004296	.004296	.4750	.004296	.4750
99.4	.004325	.004328	.4750	.004318	.4749
49.4	.004411	.004412	.4745	.004383	.4746
24.4	.004757	.004837	.4727	.006480	.4733
19.4	.005017	.005141	.4712	.004848	.4722
9.4	.007201	.007236	.4574	.006558	.4619
6.4	.01027	.01063	.4323	.009015	.4439
4.4	.01611	.01805	.3470	.01384	.3929
1.4	.08383	.09980	*	*	*

TABLE 3

The tabular entries give the decay constants in (micro-seconds)$^{-1}$ using the theories indicated. The diffusion theory and P-1 calculations employed Marshak boundary conditions, the double P-0 calculations employed the natural vacuum boundary conditions of this theory. The slab thicknesses if increased by 0.6 cm would yield fundamental bucklings of the examples listed in Tables 2 and 3.

BERYLLIUM EXAMPLE

Beryllium has been chosen as an example to show up the energy transients because of their importance in this and other crystalline moderator cases. G. de Saussure has already pointed out the trapping effect in beryllium due to the large spike in the transport cross section at the Bragg cut-off. Some of the equations and cross sections used in the study of beryllium are the same as de Saussure's[3], and most of his results are essentially confirmed. However, the present work investigates the trapping from the point of view of a transient which leads to additional insight and suggests important further experimental approaches.

The two groups for Beryllium are divided on a physical basis as done by de Saussure. The trapped group consists of those neutrons with energy between .00685 ev and .00739 ev. The second group consists of all other neutrons. The inelastic scattering in the trapped group is taken as 0.4 b. and detailed balance is used. The transport cross section for the trapped group is taken as 18 b. and for the other group as 4.95 b. The absorption is given by $v\Sigma_a = 288/\text{sec}$.

The solid lines in Fig. 1 show the two lowest eigenvalues calculated on the basis of two group diffusion theory using Eq. 6. At low values of the buckling the second eigenvalue corresponds to a transient which distorts the asymptotic spectrum in order to fit the initial energy spectrum within the limits allowed by these two groups. As leakier

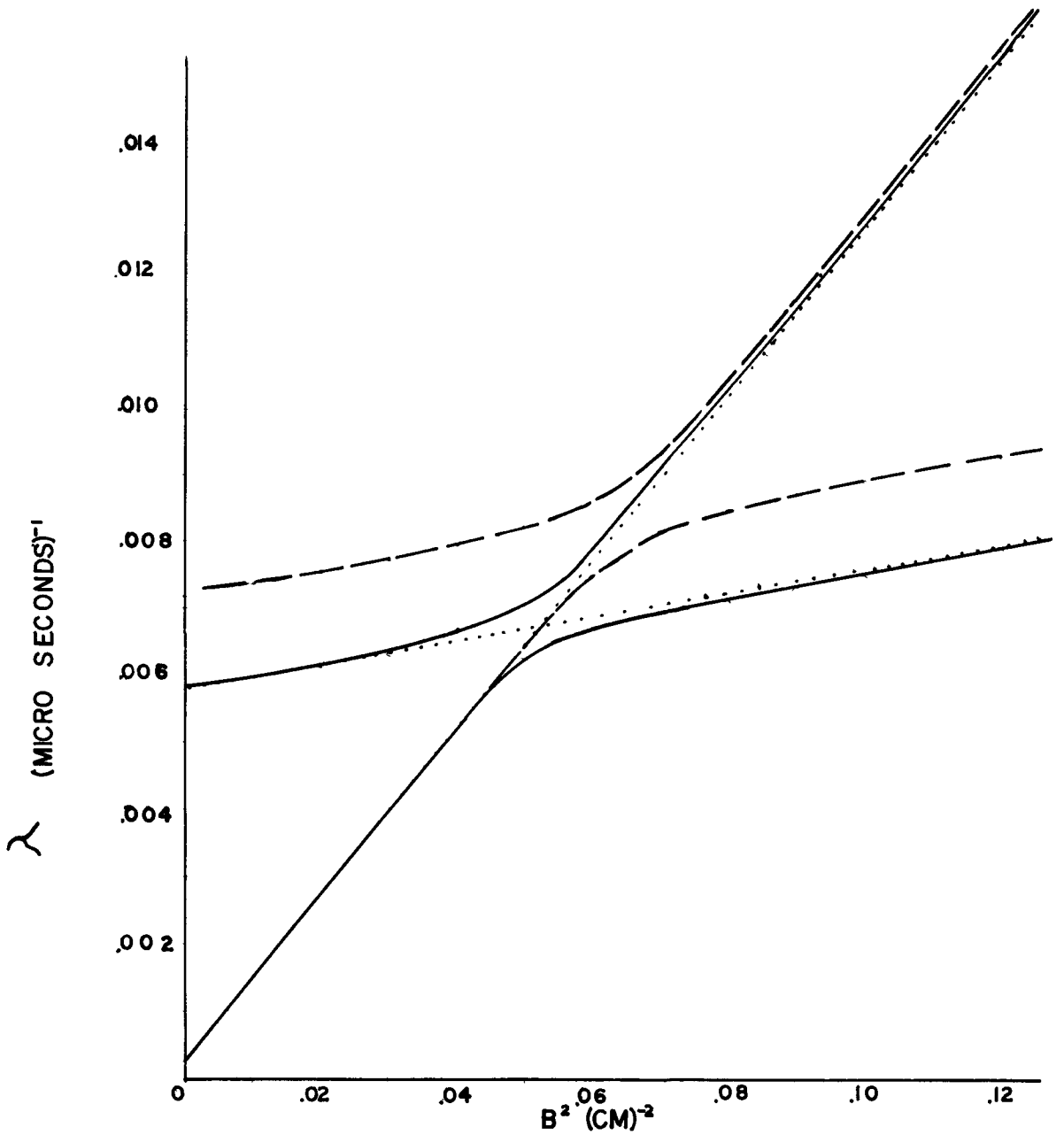

Figure 1. Eigenvalues for beryllium. The solid curves are based on the cross sections in the text; the dashed curves are based on an inelastic cross section increased by 25%. The dotted lines are due to de Saussure[3].

systems, that is systems of increased buckling, are considered, the number of neutrons in the mode which was a transient for small bucklings becomes such that it represents a positive number of neutrons in every group. For such leaky systems, the asymptotic spectrum is that of the trapped mode. This trapped mode for very leaky systems has a lifetime governed mainly by the lifetime of the trapped energy group.

The sharp bend in the curve of the lowest eigenvalue vs. B^2 comes when the eigenvalues of the separate energy groups are equal. The experimental values for beryllium lie close to the lowest eigenvalue up to the sharp bend; after the bend there is a great deal of scatter in the experimental measurements. The dashed curves in Fig. 1 represent the same calculation as the solid curves except that the inelastic cross sections are all increased by 25% (from 0.4 b to 0.5 b in the trapped group). It is thus seen from the curves that the decay constant for large bucklings is quite sensitive to the magnitude of the inelastic cross section.

The dotted lines in Fig. 1 are those given by de Saussure.[3] The more nearly horizontal of the two dotted lines is an upper limit to the lowest eigenvalue found by de Saussure by applying a variational principle due to Nelkin.[7] It is seen from Fig. 1 that the lowest eigenvalue is actually less than this upper limit. Of course, if the cross sections which are used in obtaining the upper limit

are changed the limit will change and so the dashed curves do not violate the principle of the upper limit. The second dotted line in Fig. 1 is given by de Saussure and is essentially the one group diffusion theory result. Clearly the lowest eigenvalue over its entire range may be understood from the point of view presented here.

Some eigenfunctions of the two group theory have also been constructed. They have been used to find the spectrum in the lowest geometrical mode as a function of time based on the condition that there are no neutrons in the trapped mode at t=0. These results, based on the higher two group cross sections, are listed in Table 4 where the amplitudes are given for the number density. Within the accuracy of the numbers presented it may be noted that there are no neutrons present at any time in the eigenfunction corresponding to the excited state for $B^2 = 0$; if the calculations were carried to more significant digits, there would be a few net neutrons in this mode in this case to correspond to the small number of neutrons which actually get absorbed. For the higher bucklings it is seen that in the range of $B^2 = .07$ to $B^2 = .1$ that 10% to 50% of the neutrons in the persistent mode are in the trapped group. It is thus suggested that a velocity selector such as a crystal spectrometer or a chopper might be used to obtain the decay constant of the persisting mode in this range of buckling. The contamination in the trapped group from the higher eigenfunction is

$$B^2=0cm^{-2} \quad N(E,t) = \begin{pmatrix} .005 \\ .995 \end{pmatrix} e^{-.000288\,t} + \begin{pmatrix} -.005 \\ .005 \end{pmatrix} e^{-.007197\,t}$$

$$B^2=.03 \quad N(E,t) = \begin{pmatrix} .009 \\ .983 \end{pmatrix} e^{-.004005\,t} + \begin{pmatrix} -.009 \\ .017 \end{pmatrix} e^{-.007767\,t}$$

$$B^2=.07 \quad N(E,t) = \begin{pmatrix} .030 \\ .225 \end{pmatrix} e^{-.008161\,t} + \begin{pmatrix} -.030 \\ .775 \end{pmatrix} e^{-.009326\,t}$$

$$B^2=0.1 \quad N(E,t) = \begin{pmatrix} .005 \\ .016 \end{pmatrix} e^{-.008902\,t} + \begin{pmatrix} -.005 \\ .984 \end{pmatrix} e^{-.01287\,t}$$

Table 4

This table gives the energy and time dependence for the number density of neutrons in a beryllium assembly of the buckling indicated calculated on the basis of two group theory. The upper entry in each mode refers to the number density of the trapped group, the lower entry to all other neutrons. The time is in micro-seconds. These distributions all satisfy the condition that there are no neutrons in the trapped group at t=0.

obviously considerable unless one waits a rather long time; however, the experiment may be feasible with the large pulsed sources available such as the Rensselaer Polytechnic Institute Linac facility. The difficulty of measuring the asymptotic lifetime has been pointed out by de Saussure; the point that is added here is that energy discrimination is an additional help. It may also be noted that if the set of cross sections based on a lower inelastic scattering cross section are used, the predictions for these experiments are more optimistic.

By working with B^2 on the order of 0.1 it may be possible to measure the lifetime of the second highest mode by utilizing a velocity selector and by working at shorter times. This will be investigated by breaking the energy range above that of the trapped neutrons into a few groups and looking at their population as a function of time. By focusing attention on a group of neutrons somewhat above the average energy transfer of a collision of a neutron in the trapped group, it may be possible to bias the counting strongly in favor of the second eigenvalue.

It should be pointed out that the above split into two energy groups does not reflect the usual diffusion cooling phenomenon. The diffusion cooling could be accounted for in an average fashion by the choice of the parameters for the non-trapped group. The use of additional groups which would bring in such effects as diffusion cooling would probably soften the bend in the eigenvalue vs. B^2 curve. Some calculations have been done using 3 groups: below the Bragg

cut-off, the trapped group, above the trapped group. These three group calculations show the sensitivity of the eigenvalue vs. B^2 curve to the scattering kernel at small B^2.

CONCLUSIONS

The role of transients in the interpretation of pulsed experiments has been investigated. These transients have been studied under two main classifications, namely, current and energy transients, and it has been shown that their role can be dominant in certain cases of interest. When there is a sharp change in the behavior of an eigenvalue with size of assembly being studied such as the eigenvalue becoming imaginary or the λ vs. B^2 curve bending sharply, the usual interpretation of the eigenvalue in terms of an expansion in B^2 becomes questionable. In these cases the decay with time of the assembly may depend strongly on the angle or energy of observation. In such cases, the authors would suggest that a different approach be attempted, namely, the measurement of angle and time dependent spectra. The angular dependence may be only the total number of neutrons being emitted in a few directions as a function of time and the time dependent spectra may be only the number of neutrons being emitted at a few energies as a function of time or the experiments may be more elaborate. These measured phenomena may be then directly confronted with theoretical predictions rather than working through say the diffusion cooling parameter. If carried far enough, such experiments offer very

sensitive tests of a scattering kernel and, in fact, actually allow one to infer elements of the scattering matrix from experiment.[7]

Although transients have been studied here as either current or energy transients and mainly as they arise in small systems, the various transients do affect each other somewhat, and they may arise due to other causes. In particular, a system which contains a high absorption cross section which is not (1/v) may also show a dominant transient behavior; such behavior is currently being studied in the theory of pulsed systems containing fissionable material and was not included in this study pertaining to moderators.

ACKNOWLEDGMENT

The authors thank Dr. G. P. Calame for help with the machine calculations. They also thank Dr. D. T. Goldman for a helpful discussion of beryllium cross sections.

REFERENCES

1) N. G. Sjostrand, Arkiv for Fysik, 15, 147 (1959).

2) Antonov et al, Proc. First Intern. Conf. Peaceful Uses of Atomic Energy. Geneva P/661 (1955).

3) G. de Saussure, ORNL-3193, 223-228 (1961) and Preprint of report for this conference.

4) H. C. Honeck and H. Takahashi, Angular dependence of thermal neutron spectra in lattices, Preprint of MSS. submitted to Nuc. Eng.&Sci. (1962).

5) M. Nelkin, Phys. Rev. 119, 791 (1960).

6) M. Nelkin, J. Nuclear Energy 8, 48 (1958).

7) P. B. Daitch, Neutron Physics: Proc. of Joint RPI-ANS Symposium of May 1961, Academic Press (1962) (in Press).

The Neutron Asymptotic Decay Constant in a Small Crystalline Moderator Assembly

G. de Saussure
Oak Ridge National Laboratory*
Oak Ridge, Tennessee

ABSTRACT

The effect of the narrow peak of the neutron transport cross section of crystalline materials at low energy is being investigated. It is shown that an upper bound can be found for the asymptotic decay constant in a small assembly. This upper bound is lower than the values usually measured by the pulsed-neutron source technique. This apparent discrepancy is discussed.

1. Introduction

The pulsed-neutron technique has been used extensively to measure diffusion parameters in a variety of moderators. A description of the technique and an excellent summary of the present status of experiments may be found in a recent review by K. H. Beckurts.[1] It may be seen from Beckurts' review that the values of the absorption cross section and of the diffusion constants obtained by the pulsed-neutron technique for the various moderators are quite consistent. However, some very puzzling discrepancies are observed between various measurements of the diffusion cooling constant, especially for crystalline moderators such as beryllium and graphite.

Beckurts proposes the following possible causes for these discrepancies: (1) the role of B^6 terms, (2) the effect of higher harmonics, and (3) the importance of the data-evaluation schemes. For the case of beryllium, at least, different laboratories measure different decay constants for the same value of the buckling.[2,3] Such discrepancies cannot be blamed on B^6 terms. It is also difficult

*Operated by Union Carbide Nuclear Company for the U.S. Atomic Energy Commission.

to see how the effect of space harmonics may not be properly accounted for since, for a small cube of a moderator with low absorption, the first spatial harmonic decays almost twice as rapidly as the fundamental mode.

The purpose of this note is to propose another possible cause for the observed discrepancies in the measurements of decay constants. It appears that under certain conditions the decay of the neutron population out of a moderating assembly may never be strictly exponential during the time available for measurement. In this case, the "asymptotic decay constant" is not directly measurable and the diffusion cooling constant is not a well defined concept.

2. Determination of an Upper Bound for the Asymptotic Decay Constant

An upper bound for the asymptotic value of the neutron decay constant in a finite moderating assembly, λ, can be obtained from Nelkin's variational principle.[4] For the case of $\frac{1}{v}$ absorption, the principle may be expressed as:

$$\lambda \leq v\,\Sigma a + \frac{J - I}{K} \tag{1}$$

$$J = \frac{1}{3} B^2 \int_0^\infty \lambda_{tr}(E) \left[\frac{\phi^2(E)}{M(E)}\right] dE \tag{2}$$

$$K = \int_0^\infty \frac{1}{v} \left[\frac{\phi^2(E)}{M(E)}\right] dE \tag{3}$$

$$I = \int_0^\infty dE \int_0^\infty dE'\ \Sigma(E \rightarrow E')\ \phi(E) \left[\frac{\phi(E')}{M(E')} - \frac{\phi(E)}{M(E)}\right] \tag{4}$$

where the symbols have the same meaning as in Nelkin's article.[4]

Using for a trial function the energy delta function $\phi(E)^2 = \phi(E_o)^2\,\delta(E - E_o)$, we obtain:

$$\lambda \leq v\,\Sigma a + v(E_o)\,\Sigma_{in}(E_o) + \frac{1}{3}\lambda_{tr}(E_o)\,v(E_o)\,B^2 \tag{5}$$

$$\Sigma_{in}(E_o) \equiv \int dE'\ \Sigma(E_o \rightarrow E') - \Sigma(E_o \rightarrow E_o). \tag{6}$$

The inequality (5) shows that the asymptotic decay constant is smaller or equal to the sum of the absorption, inelastic scattering, and leakage probabilities at any energy E_o. This rather obvious statement does not depend on the differential inelastic scattering law. In general, the upper bound (5) is not very useful; however, in the special case of a small crystalline moderating assembly, if the reference energy E_o is suitably chosen, it may not be trivial.

The transport cross section of beryllium, computed by Bhandari,[5] is shown in Fig. 1. At low energy this cross section exhibits a series of sharp peaks occurring whenever the neutron wavelength is just equal to the distance between parallel planes of a Miller's index. The largest of these peaks, at 6.85 mev (millielectronvolts) correspond to the Miller's index (1, 0, 1). At this energy the transport cross section is about 18 barns, whereas the inelastic scattering cross section at room temperature is about .4 barns.[5]

If we choose $E_o = 6.85$ mev as a reference energy to evaluate the upper bound (5), we obtain for beryllium:

$$\lambda[\text{msec}^{-1}] \leq 5.8 + 17.6\, B^2[\text{cm}^{-2}] = \lambda_1. \tag{7}$$

The numerical values of Eq. 7 were obtained using a beryllium density N = .12 atom/barn·cm and an absorption probability[1] $v\,\Sigma a = .29$ msec^{-1}. Fig. 2 shows the right-hand side of (7), as well as $\lambda_2 = v\,\Sigma a + DB^2$ where $D = 1.25 \times 10^5$ cm^2 sec^{-1} is the <u>infinite medium</u> diffusion constant,[1] and some experimental values $\lambda_3(B^2)$ obtained at various laboratories.[1,2,3] It may be seen from the figure that the discrepancies between values obtained at various laboratories are mostly in the buckling region where $\lambda_3 > \lambda_1$. In this region the asymptotic decay constant was not really obtained by the experimenters, since $\lambda \leq \lambda_1$.

The effects in graphite and BeO are analogous to that in beryllium. Fig. 3 shows the transport cross section of graphite.[6] It has a maximum value of about 17 barns at an energy of 1.89 mev. At this energy the inelastic scattering cross section at room temperature is 0.5 barns.[7] Using this energy as a reference energy, a density[8] $\rho = 1.6$ g/cm^3 and an absorption probability[8] $v\,\Sigma a = 71.2$ sec^{-1}, we obtain for the upper bound (5):

$$\lambda[\text{msec}^{-1}] \leq 2.48 + 14.77\, B^2[\text{cm}^{-2}] = \lambda_1. \tag{8}$$

Fig. 4 shows λ_1 vs B^2, $\lambda_2 = v\,\Sigma a + DB^2$ where[8] $D = 2.06 \times 10^5$ cm^2 sec^{-1} is the infinite medium diffusion constant and the parabola $\lambda_3 = v\,\Sigma a + DB^2 - CB^4$ where $C = 12.4 \times 10^5$ cm^4 sec^{-1} is the diffusion cooling constant obtained by E. Starr and G. A. Price by fitting their experimental data.[8] The parabola λ_3 is larger than the upper bound λ_1 for $B^2 > .014$ cm^{-2}. Beckurts[8] states that Starr and Price carried their measurements over the buckling range $.0016\ \text{cm}^{-2} \leq B^2 \leq .0275\ \text{cm}^{-2}$. Hence it seems that for their smallest assembly Starr and Price have not measured the true asymptotic decay constant.

3. Determination of a Lower Bound for the Diffusion Cooling Constant

A lower bound for the diffusion cooling constant C may be obtained from the upper bound λ_1 (5) for the asymptotic decay constant. If this asymptotic decay constant is expressed as a power series in B^2:

$$\lambda = v\,\Sigma a + DB^2 - CB^4 \tag{9}$$

and if (9) must satisfy the inequality (5) for all values of B^2, we obtain a lower bound for C:

$$C \geq \frac{\left[\frac{1}{3}\,\lambda_{tr}(E_o)\,v(E_o) - D\right]^2}{4v(E_o)\,\Sigma_{in}(E_o)}\,. \tag{10}$$

Using the reference energies determined previously, the lower bound on the right-hand side of (10) is 5.2×10^5 cm^4 sec^{-1} for beryllium and 45×10^5 cm^4 sec^{-1} for graphite. These values are much larger than all the diffusion cooling constants listed by Beckurts[1] for these two moderators. Of course, if more terms are included in the expansion (9) of λ in powers of B^2, the inequality (10) does not need to hold, yet it is usually assumed that the coefficient of B^6 in the expansion of λ is positive,[9] in such case (10) must still hold. The coefficient of the highest order of B^2 in the expansion of λ must be positive since the decay constant can never decrease with increasing buckling.

The existence of the upper bound (5) suggests, however, that the expansion of the asymptotic decay constant in powers of B^2 is not very desirable. It would probably be better to fit λ to the lower branch of a hyperbola which, for large values of B^2, would asymptotically approach the upper bound λ_1 (5).

4. Can the asymptotic decay constant in a small crystalline moderating assembly be measured?

An interesting problem that suggests itself is whether or not the asymptotic decay constant of the neutron population in a small assembly of crystalline moderator is a measurable quantity.

The "energy trap" corresponding to the peak in the transport cross section is very narrow: in beryllium, for instance, it is easy to compute that the transport cross section is larger than 15 barns only in the 0.54 mev wide energy interval 6.85 mev $\leq E \leq$ 7.39 mev. When fast neutrons are being pulsed in a small beryllium assembly, very few of them are slowed down in this low energy region. These few neutrons will eventually dominate the decay, but the study of their time behavior requires a very intense pulsed-neutron source and a detecting equipment almost free of background. The time after which the "trapped neutrons" will

dominate the decay is a sensitive function of the initial conditions and of the differential inelastic scattering cross section. A crude two-group computation (see Appendix) suggests that for beryllium this time is of the order of one millisecond or more. Many experimenters do not have the equipment necessary to measure accurately the decay constant after such a long time.

A more fundamental question is whether or not the neutron decay ever becomes exponential. The transport cross section within the trap 6.85 mev $\leq E \leq$ 7.39 mev is almost inversely proportional to the square of the energy so that a neutron of 7.39 mev has a leakage probability, $D(E)\, B^2$, about 20% larger than a neutron of 6.85 mev. On the average, a neutron of 7 mev that undergoes inelastic scattering increases its energy by about 2.5 mev.[5] Hence one may perhaps consider an inelastic scattering within the trap in a small assembly as equivalent to an absorption, since after the inelastic scattering the neutron is usually outside the trap where it has a large transport mean free path and will leak out of the small assembly before being scattered back into the trap. Most of the neutrons remaining in such a small assembly a long time after the pulse will be "trapped neutrons." These neutrons diffuse according to:

$$(11) \qquad -\lambda(E)\, n(E,\, t) = \frac{\partial n(E,\, t)}{\partial t} \qquad N(t) = \int n(E,\, t)\, dE = \int n_o(E)\, e^{-\lambda(E,\, t)}\, dE$$

$$(12) \qquad \lambda(E) \cong v\, \Sigma a + v(E_o)\left(\frac{E}{E_o}\right)^{1/2} \Sigma_{in}(E_o) + \frac{v(E_o)\, B^2}{3\Sigma_{tr}(E_o)}\left(\frac{E}{E_o}\right)^{5/2}$$

where the inelastic scattering cross section $\Sigma_{in}(E_o)$ is assumed to be constant over the trap region. The neutron density N(t) (11) has no <u>isolated</u> asymptotic decay constant; it is not separable in time and energy and never decays exponentially. If an experimenter fits a finite number of measured points $N_i(t_i) \pm \delta N_i$ to a sum of exponential, he will not determine unambiguously the asymptotic decay constant.

Of course it is not strictly correct to treat inelastic scattering within the trap as equivalent to absorption; nevertheless, before the asymptotic decay constant of a small assembly can be measured it must be proven that the flux is eventually separable in time and energy and decays according to:

$$N(t) = ae^{-\omega_1 t} + be^{-\omega_o t}, \text{ for } t \to \infty, \text{ with } \omega_1 - \omega_o \geq \epsilon \tag{13}$$

and a lower bound for ϵ must be found, for if ϵ is allowed to be arbitrarily small it is not possible to measure unambiguously ω_o.

5. Remarks on the Calculations of the Diffusion Cooling Constant

A few authors have computed the values of the diffusion cooling constants C of beryllium, BeO, and graphite. The results of most of these calculations give values for C much smaller than the lower bound defined in (10). This appears in direct contradiction to the argument presented to obtain (10). However, because of mathematical difficulties, the numerical calculations are always performed under certain simplifying assumptions.

First, the flux is usually assumed to be separable in time and energy, and the energy part is taken to be a Maxwellian,[4,10] or the product of a Maxwellian, and a power expansion in $(\frac{E}{kT})$ where kT is some reference energy;[9,11] in the latter case only a finite, usually small, number of coefficients of the expansion are considered. If the true asymptotic energy distribution of the neutrons has a very large peak in the narrow interval where the transport cross section has a maximum, this distribution cannot be represented by the usual power expansion without using a very large number of terms.

Second, C is often computed assuming a transport mean free path $\lambda_{tr}(E)$ constant[9] or proportional to E^{α}, where α is a constant.[4] Of course, such computations cannot display the effect of the narrow peak in the transport cross section.

Finally, the differential inelastic scattering cross section is usually obtained from a model that does not strictly apply to the case of a crystalline moderator--heavy gas model or incoherent approximation.

S. N. Purohit[12] has investigated the time-dependent energy spectrum of neutrons decaying in various assemblies of beryllium. His method consists of solving the appropriate differential equations on an analog computer. His results show that even in a very small beryllium assembly ($B^2 = .0718$ cm^{-2}) an equilibrium energy spectrum is established in about 0.5 milliseconds. This spectrum does not show any peak in the energy region 6.85 mev $< E <$ 7.39 mev. From the results of his investigation Purohit computes a value $C \cong 1.13 \times 10^5$ cm^4 sec^{-1} for beryllium. These results appear to contradict the arguments presented in this paper. However, although Purohit's model uses the correct transport mean free path, as computed by Bhandari,[5] it uses a heavy gas kernel. More important, the model is based on a multigroup formalism; in the low-energy region Purohit uses 2.5 mev wide groups. If the beryllium transport cross section (Fig. 1) is averaged linearly in the energy region 5 mev $< E <$ 7.5 mev, the value obtained is 6.3 barns. The strong peak of 18 barns at 6.85 mev is completely "smoothed out" by the averaging over the group. It should be interesting to repeat Purohit's computation with groups .05 mev wide in the energy region between 6 and 7 mev.

Recently, by a numerical iteration method and using the correct transport cross section, S. S. Jha[13] has investigated the equilibrium neutron energy spectrum in a few small assemblies of beryllium. This investigation showed that, indeed, in small assemblies the spectrum exhibits sharp peaks where the transport cross section has maxima. Jha has also computed the decay constant of a few assemblies, and these decay constants are consistent with the upper bound (7).

6. Conclusions

The arguments presented in this paper seem to indicate that the true asymptotic decay constant of a small crystalline moderating assembly has not been measured. The experimental values of the decay constants of small assemblies are larger than a theoretically determined upper bound; hence they must not refer to the asymptotic value. This asymptotic value may not be measurable.

Because the diffusion cooling constant must be determined from the measurements of the asymptotic decay constant in small assemblies, the difficulty in measuring these decay constants may explain the discrepancies between various experimental determinations of the diffusion cooling constant.

APPENDIX

Two-Group Computation of the Trap Effect in Beryllium

It is interesting to investigate the effect of the peak of the beryllium transport cross section at 6.85 mev on the decay constant of a small assembly in a two-group model. The model is extremely crude and the results should have only qualitative significance.

We shall divide the energy domain into two groups: the first group (group 0, index 0) comprises the neutrons of energy $6.85 \text{ mev} \leq E \leq 7.39 \text{ mev}$; the second group (group 1, index 1) comprises all the other neutrons. In group 0 the average transport cross section is $\sigma_{tr,o} = 18$ barns, the average inelastic scattering cross section is $\sigma_{in,o} = .4$ barns, and the average velocity is $v_o = 1.142 \times 10^5$ cm/sec. In group 1 the diffusion coefficient is $D_1 = 1.25 \times 10^5$ cm^2/sec. The absorption probability $v\,\Sigma a = 288 \text{ sec}^{-1}$ is the same for both groups. The density will be taken as $N = .12$ atom/barn·cm. Hence $D_o \equiv \frac{v_o}{3N\sigma_{tr,o}} = .176 \times 10^5$ cm^2/sec. The width of group 0 is very narrow compared to the average energy gain of a neutron undergoing inelastic scattering in that group so that the transfer probability from group 0 to group 1 will be assumed to be $\beta_o = vN\sigma_{in,o} = 5500 \text{ sec}^{-1}$. The transfer probability from group 1 to group 0 can be obtained from detailed balance as $\beta_1 = \gamma\beta_o$ where

$$\gamma = \frac{\int_{\Delta E_o} M(E)\,dE}{\int_{\Delta E_1} M(E)\,dE} \cong .005 \tag{A-1}$$

where M(E) is the Maxwellian density spectrum and the integration is carried over the energy width of the group.

The neutron densities n_i in the two groups obey the coupled differential equations:

$$(A\text{-}2) \qquad -(\alpha_1 + \beta_1)\, n_1 + \beta_o\, n_o = \frac{\partial n_1}{\partial t}\,,$$

$$(A\text{-}3) \qquad -(\alpha_o + \beta_o)\, n_o + \beta_1\, n_1 = \frac{\partial n_o}{\partial t}\,,$$

$$(A\text{-}4) \qquad \alpha_i \equiv v\,\Sigma a + D_i\, B^2,$$

which have the solution

$$(A\text{-}5) \qquad n_i(t) = a_i^+\, e^{\omega^+ t} + a_i^-\, e^{\omega^- t}$$

$$(A\text{-}6) \qquad \omega^{\pm} = -\left(\frac{\alpha_1 + \alpha_o}{2} + \frac{\beta_o + \beta_1}{2}\right) \pm \left[\left(\frac{\alpha_1 - \alpha_o}{2}\right)^2 + \left(\frac{\beta_o + \beta_1}{2}\right)^2 - 2\left(\frac{\alpha_1 - \alpha_o}{2}\right)\left(\frac{\beta_o - \beta_1}{2}\right)\right]^{\frac{1}{2}}.$$

The detailed balance condition (A-1) can be used to simplify (A-6): since $\beta_1 \ll \beta_o$

$$(A\text{-}7) \qquad \omega^{\pm} \cong -\left(\frac{\alpha_1 + \alpha_o}{2} + \frac{\beta_o}{2}\right) \pm \left[\left(\frac{\alpha_1 - \alpha_o}{2}\right)^2 + \left(\frac{\beta_o}{2}\right)^2 - 2\left(\frac{\alpha_1 - \alpha_o}{2}\right)\left(\frac{\beta_o}{2}\right)\right]^{\frac{1}{2}}$$

$$(A\text{-}8) \qquad \omega^+ \cong -(\alpha_o + \beta_o) \qquad \omega^- \cong -\alpha_1.$$

This result shows that for $B^2 < B_c^2 = \dfrac{v_o\, N\, \sigma_{in,o}}{D_1 - D_o} = .051\ \text{cm}^{-2}$ the decay constant of the "average neutron," α_1, is the asymptotic decay constant. For $B^2 > B_c^2$ the sum $\alpha_o + \beta_o$ of the absorption probability, leakage probability, and transfer probability of the "trapped neutron" will be the asymptotic decay constant.

For a beryllium assembly of buckling $B^2 = .0718\ \text{cm}^{-2}$, we obtain $\alpha_1 = 9263\ \text{sec}^{-1}$ and $\alpha_o + \beta_o = 7051\ \text{sec}^{-1}$. The "asymptotic" decay constant experimentally measured for this assembly is[2] $8500 \pm 300\ \text{sec}^{-1}$.

It is interesting to compute the time t_c at which the two modes on the right-hand side of (A-5) are equal. We have:

$$t_c = \frac{\ell_n\left\{\frac{a_o^+ + a_1^+}{a_o^- + a_1^-}\right\}}{\omega^- - \omega^+}. \tag{A-9}$$

The argument of the logarithm must be obtained from the initial conditions. If we assume that initially all the neutrons are in group 1, we obtain

$$\frac{a_o^+ + a_1^+}{a_o^- + a_1^-} = -\frac{\alpha_1 + \omega^-}{\alpha_1 + \omega^+}. \tag{A-10}$$

The small quantity $\alpha_1 + \omega^-$ must be evaluated using (A-6). For a beryllium assembly of buckling $B^2 = .0718\ cm^{-2}$ we find, using (A-10) $t_c \cong 1.5$ msec. For the same assembly, if we assume that initially the neutrons are in a Maxwellian distribution, we obtain $t_c \cong 1.3$ msec. During these 1.3 msec the neutron population in the assembly will have decayed by a factor of about 10^5.

Finally, it must be noted that the group constants, in this two-group model, should not really be taken as time constants. Indeed, because of the rapid variation of the transport cross section with energy, the flux averaged diffusion constant D_1 will decrease with time. This will result in a lower value for α_1 and hence a larger value for t_c.

REFERENCES

1. K. H. Beckurts, Nuclear Instruments and Methods **11**, 144-68 (1961).

2. G. de Saussure and E. G. Silver, "Determination of the Neutron Diffusion Parameters in Room-Temperature Beryllium," ORNL-2641 (1959).

3. W. M. Andrews, "Measurement of the Temperature Dependence of Neutron Diffusion Properties in Beryllium using a Pulsed-Neutron Technique," UCRL-6083 (1960).

4. M. Nelkin, J. Nuclear Energy 8, 48-58 (1958).

5. R. C. Bhandari, J. Nuclear Energy 6, 104-12 (1958).

6. K. S. Singwi and L. S. Kothari, "Transport Cross Section of Thermal Neutrons in Solid Moderators," A/Conf. 15/P/1638 (1958), Second UN International Conference on Peaceful Uses of Atomic Energy.

7. D. Hughes, "Pile Neutron Research," Addison-Wesley, 1953, p. 251.

8. E. Starr and G. A. Price, as quoted by K. H. Beckurts in reference 1.

9. K. S. Singwi, "On the Theory of the Diffusion Cooling of Neutrons in a Finite Moderator Assembly," Arkiv för Fysik, Bol 16 nr 36, 385-411 (1960).

10. K. S. Singwi, J. Nuclear Energy, 8, 59-62 (1958).

11. W. Häfele and L. Dresner, Nuclear Sci. and Eng. 7, 304-12 (1960). Also K. H. Beckurts, Z. Naturforsch 12a, 956-9 (1957).

12. S. N. Purohit, Nuclear Sci. and Eng. 9, 305-13 (1961) and ORNL-CF-60-7-32 (1960) and ORNL-CF-60-7-44 (1960).

13. S. S. Jha, J. Nuclear Energy Part A: Reactor Science, 12, 89-92 (1960).

ACKNOWLEDGMENT

The author wishes to acknowledge some helpful suggestions of Dr. A. F. Henry and many stimulating discussions with Dr. L. Dresner.

March 9, 1962

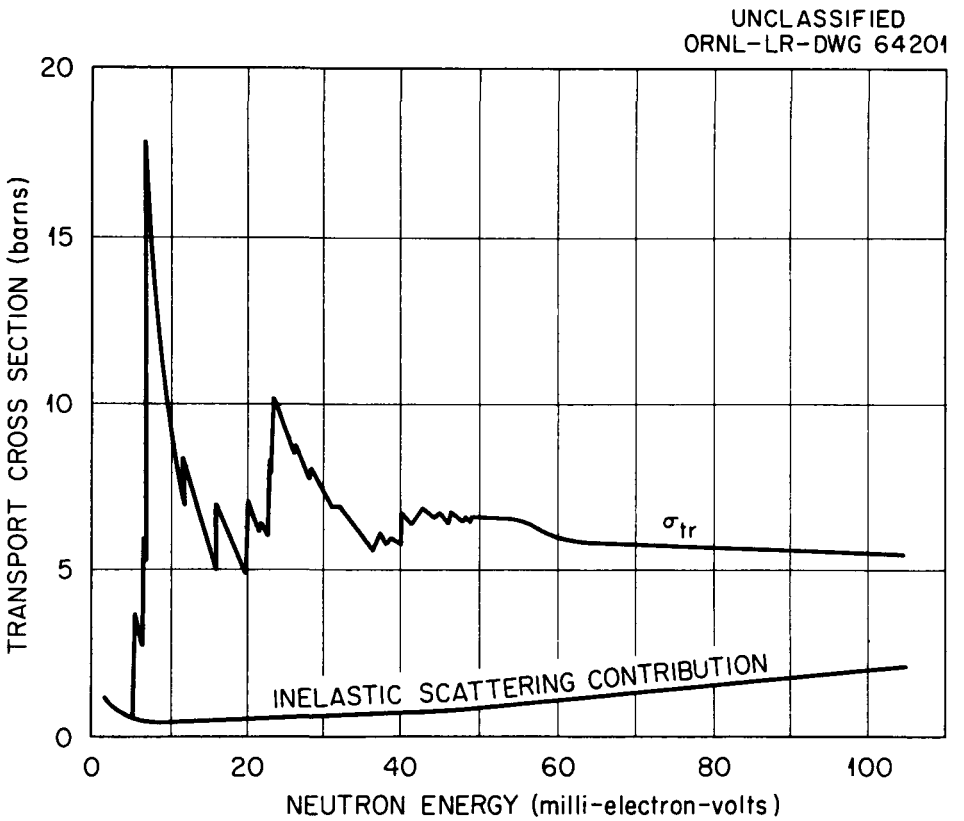

Fig. 1. Transport Cross Section of Beryllium (from Ref. 5).

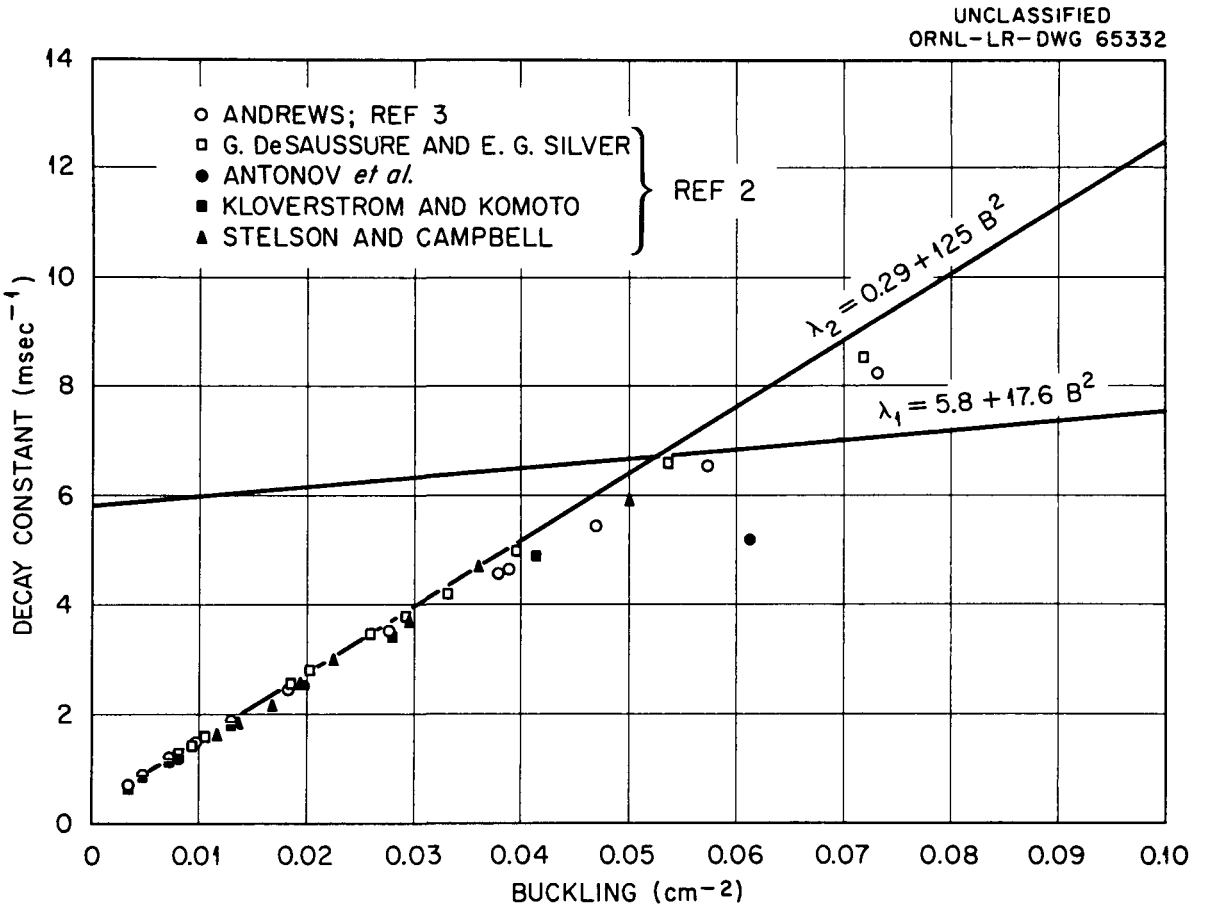

Fig. 2. Decay Constant vs Buckling for Beryllium.

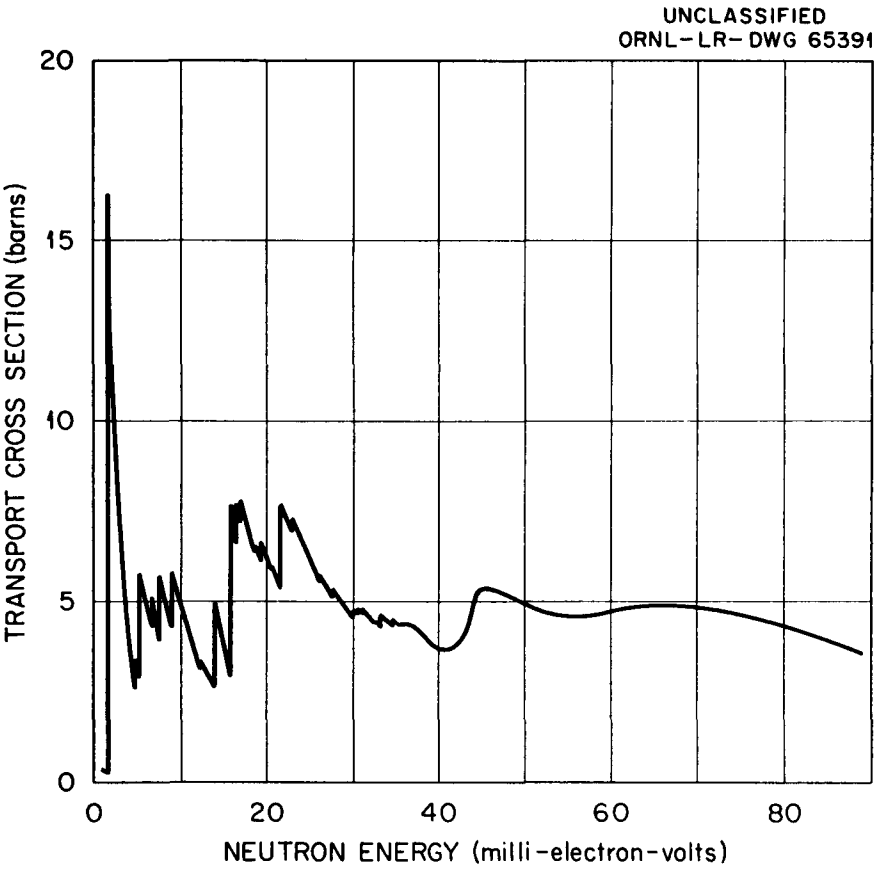

Fig. 3. Transport Cross Section of Graphite (from Ref. 6).

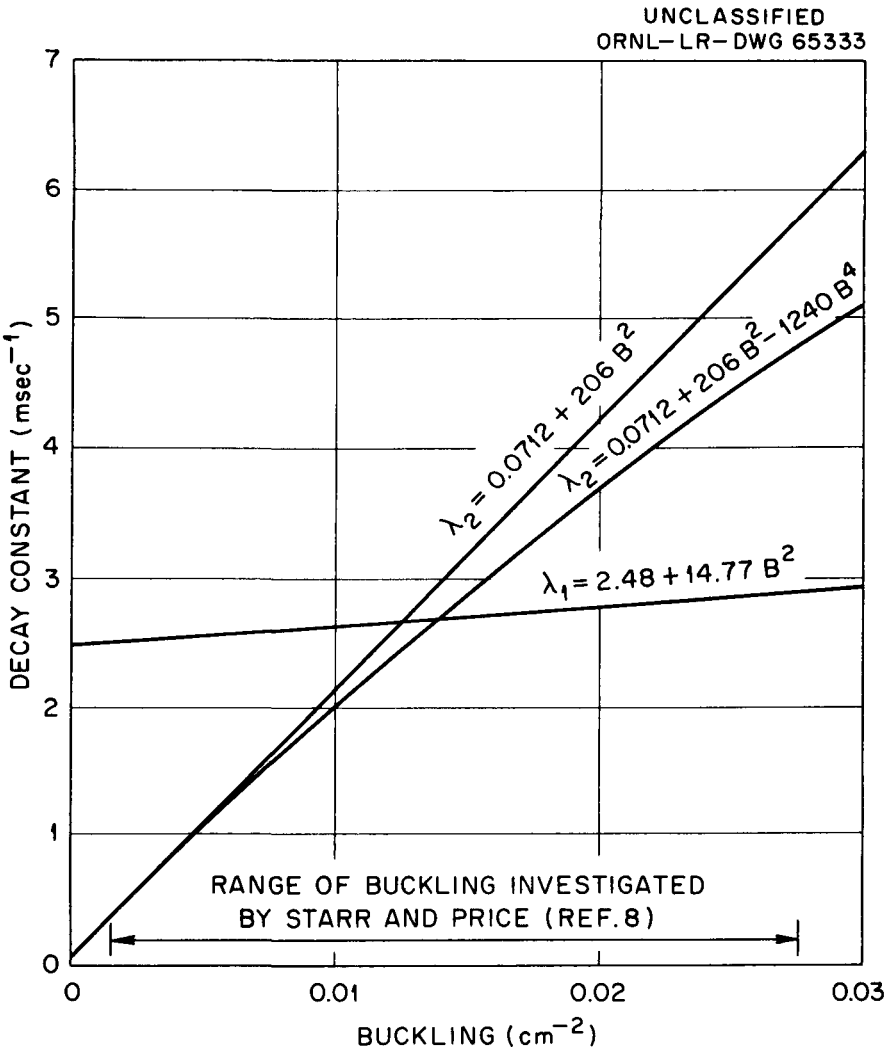

Fig. 4. Decay Constant vs. Buckling, for Graphite.

A COMPARISON OF THE PROPERTIES OF THE NELKIN AND RADKOWSKY THERMAL NEUTRON SCATTERING KERNELS FOR WATER[*]

E. M. Gelbard
J. A. Davis
E. Schmidt

Bettis Atomic Power Laboratory
Westinghouse Electric Corporation
Pittsburgh, Pennsylvania

March 1962

[*]Work performed under the auspices of the U. S. Atomic Energy Commission.

ABSTRACT

The authors have computed the coefficients ω_0, D_0, C and E in the expansion

$$\omega = \omega_0 + D_0 B^2 - CB^4 + EB^6 + \ldots$$

using the Radkowsky (Ref. 1) and Nelkin (Ref. 2) kernels. It has been found that both kernels give very similar pulse parameters. Extrapolation distances have been computed, using both kernels, for pulsed slabs of water. Again no significant differences were observed. Differences between the Nelkin and Radkowsky flux shapes in TRX lattices are quite small: they would be difficult to detect experimentally. In summary, it seems that thermal neutron flux shapes and decay rates are not very sensitive to details in the structure of the scattering kernel. Yet neither the Nelkin nor the Radkowsky kernels yield flux shapes and decay rates in good agreement with experiment.

I. INTRODUCTION

Our knowledge of the differential scattering cross section of water in the thermal energy band is still somewhat sketchy. At first glance it may seem that any uncertainty regarding the bound hydrogen kernel is a great handicap to the reactor physicist. This is not necessarily true. Often one is interested in the thermal neutron flux distribution in a narrowly limited range of geometries, temperatures, water densities fand fuel loadings. Within this limited range of conditions the flux may not be very sensitive to details of the scattering kernel.

How important, then, is the form of the scattering kernel? We attack this question, here, by comparing the results of computations based on the Nelkin and Radkowsky kernels. Both kernels incorporate chemical binding effects. The Nelkin and Radkowsky treatment of binding are very different; yet, in the cases studied, computations using both kernels give much the same results.

II. DIFFUSION LENGTHS

Diffusion lengths for the Nelkin and Radkowsky kernels have been computed via the SLOP-1 code (Ref. 1). At present results are available only for pure water at room temperature. One finds that the Radkowsky diffusion length

$$L\ (\text{Radkowsky}) = 2.81\ \text{cm}, \quad \text{while}$$

$$L\ (\text{Nelkin}) = 2.78\ \text{cm}.$$

It will be seen that the difference between the Nelkin and Radkowsky diffusion lengths is small.

Nelkin's approach leads to a differential scattering cross section containing spherical harmonics components of all orders. However, it is sometimes convenient to simplify the thermal scattering kernel through the use of

the Selengut-Goertzel approximation. When this is done it is assumed that the P_1 kernel is diagonal, while all higher P_ℓ components are ignored. Diagonal elements of the Selengut-Goertzel P_1 kernel are defined through the relations

$$K_{1SG}(E' \rightarrow E) \equiv \delta(E' \rightarrow E) \int_0^\infty K_1(E \rightarrow E')dE' \quad .$$

The introduction of the Selengut-Goertzel approximation has little effect on the Nelkin diffusion length. In fact, to three significant figures, one finds that

$$L \text{ (Nelkin S.G.)} = 2.78$$

as in the case of the full Nelkin kernel.

III. PULSED NEUTRON COMPUTATIONS

In the analysis of pulsed neutron experiments it is usually assumed that, after a sufficiently long time has elapsed, the flux decays exponentially:

$$\Phi(E,x,t) = \varphi(E,x)B^{-\omega t} \quad .$$

It is customary to expand the decay rate, ω, in powers of the bucklings

$$\omega = \omega_0 + D_0B^2 - CB^4 + EB^6 + \ldots . \qquad (1)$$

Again with the aid of SLOP-1 we have computed ω_0, D_0, C and E for the Radkowsky, Nelkin, and Nelkin S.G. kernels. As in Section II, results are available only for pure water at room temperature. Values of D_0, and C appear in Table I. The spread between D_0 and C values derived from the various kernels is small. As for the coefficient E, we find that

$$E \text{ (Radkowsky)} = 530 \text{ cm}^6/\text{sec, and}$$
$$E \text{ (Nelkin)} = 200 \text{ cm}^6/\text{sec} \quad .$$

Clearly the E values appropriate to Nelkin and Radkowsky kernels are considerably different, but it seems that the B^6 term as a whole is unimportant. Suppose that ω were given exactly by the four terms in Eq. (1). Suppose, further, that one were to fit ω, in the range $0 \leq B^2 \leq 1$, with a quadratic function of the buckling. Obviously the parameters ω_0, D_0 and C deduced from such a fit would be incorrect. If E = 600, this neglect of the B^6 term in a least square fitting process would lead to an error of 25% in C. If E = 190, the corresponding error in C would be 10%. In either case errors introduced through neglect of the B^6 term seem inconsequential at this time, in view of the uncertainties in the measured value of C.

In the Selengut-Goertzel approximation one finds that

E (Nelkin S.G.) = 160 cm^6/sec.

Apparently the Selengut-Goertzel approximation is accurate even at fairly high bucklings. Now, the use of the Selengut-Goertzel approximation introduces considerable distortion into the differential scattering cross section. If the agreement between the Nelkin E and the Selengut-Goertzel E is not accidental, then the decay rate, ω, must depend only on gross features of the angular distribution of scattered neutrons.

So far we have confined our attention to the behavior of neutrons in infinite homogeneous media. One might expect more complicated phenomena at interfaces, particularly at interfaces where the properties of the diffusing medium change sharply.

The behavior of the flux at an interface is involved in the computation of extrapolation distance at the surface of a pulsed moderator. We have computed multigroup extrapolation distances (in a P_3 approximation) for slabs at three bucklings. Results of these calculations are displayed in Table II. Again we find that details of the structure of the kernel are almost completely irrelevant.

This conclusion leads directly to an unresolved problem. The extrapolation distances in Table II lie in the range from .3 to .35 cm. Extrapolation distances have also been computed for cylinders and spheres with $0 < B^2 \leq 1$. These lie in the same range. On the other hand, direct measurements by Campbell et al in large rectangular boxes yield extrapolation distances near .46 cm (Ref. 3).* It is difficult to believe that the extrapolation distance at low bucklings depends so strongly on geometry. If it does not, then there is a large discrepancy between theory and experiment, a discrepancy which might indicate gross inadequacies in both the Nelkin and Radkowsky kernels.

IV. CELL CALCULATIONS

We turn now to a problem configuration of more direct interest to the reactor analyst. Multigroup thermal neutron fluxes have been computed for a cylindrical cell containing a fuel rod, zirconium cladding, and an annulus of water. The radius of the rod is .762 cm, the cladding is .08328 cm thick and the outer radius of the cell is .897162 cm. Number densities are listed in Table III.

This same problem has been treated by H. Honeck, whose work is discussed in Ref. 4. Honeck, however, has used a computer code which contains no provisions for anisotropic scattering. In contrast, the computations described here were carried out with the aid of a code, called EXCEL, which can handle any Selengut-Goertzel kernel. In view of the accuracy of the Selengut-Goertzel approximation in diffusion length and pulse calculations, one might expect it to be adequate in cell calculations also. Of course this is not necessarily

---

*DeJuren, Stooksberry and others at Bettis have recently measured extrapolation distances in pulsed water systems (private communication). Their results agree with Campbell's. Bettis work now in progress should determine whether existing measurements of extrapolation distances have been affected substantially by the presence of harmonics in the flux.

true. According to Nelkin's analysis (Ref. 5), the Selengut-Goertzel approximation is satisfactory in pulse problems because pulsed neutron spectra are almost Maxwellian. In inhomogeneous problems, however, the spectrum will have a 1/E tail. It seems worthwhile, then, to test the accuracy of the Selengut-Goertzel approximation in the presence of neutron sources. For this purpose we have made use, again, of the SLOP-1 code.

SLOP-1 can handle slab problems in double-P_1, and the code library contains P_0 through P_3 scattering matrices. Problems in other geometries are, generally,[*] treated in the P_1 approximation. In order to take full advantage of the capabilities of SLOP-1, we digress to consider a cell problem in slab geometry. The cell, again, consists of a fuel region and a water channel. Cladding has been ignored. Number densities in the fuel and water are identical with those in the cylinder. The thickness of the fuel plate in the slab is taken to be equal to the radius of the fuel rod in the cylinder, while the thickness of water region is the same in both the slab and cylinder problems.

In the slab case we have computed the double-P_1 flux cdistribution using, first, the full Nelkin kernel and, then, a Selengut-Goertzel approximation to it. At all points in the cell the computed absorption rates in a 1/v detector are practically unaffected by the Selengut-Goertzel approximation. Nelkin and Nelkin S.G. activations differ by less than 1%.

With some confidence in the accuracy of the Selengut-Goertzel approximation we turn from the slab cell to the cylindrical lattice. The computed 1/v activations in the cylinder are plotted in Fig. 1. Now, the lattice parameters for the cylindrical cell correspond with those in one of the TRX experiments. Experimental thermal activations are available for this particular lattice, and the experimental activations are also plotted in Fig. 1.

[*] In certain cases SLOP-1 can be used to solve the cylindrical and spherical P_3 equations, but the cylindrical cell discussed above can only be treated in P_1.

Again the differences between results obtained with the Radkowsky and Nelkin kernels are small although, in this case, these differences are not negligible. Again we note that the spread in computed results is not as large as the discrepancy between theory and experiment.

V. CONCLUSIONS

At this point we find ourselves in a disturbing position. An examination of computations using different kernels indicates that even a crude treatment of binding should be adequate for the analysis of pulse and TRX experiments. On the other hand the experimental results themselves suggest that a much more refined treatment of binding is necessary. In view of the insensitivity of our computed results to details of the kernel, drastic changes in the kernel would be required in order to bring theory and experiment into agreement. It seems most important, then, that measurements of extrapolation distance should be reexamined and that activation measurements in lattices be repeated and refined.

Table I

	D_o (cm^2/sec)	C (cm^4/sec)
Range of Experimental Results[*]	34800 to 38500	0 to 7500
"Best Value"[†]	35200	4400±1500
Radkowsky	38380	3614
Nelkin	37520	3283
Nelkin (S.G.)	37160	3113

[*] See Ref. 6.

[†] See Ref. 7.

Table II

Buckling (cm^{-2})	Radkowsky Extrap. Distance (cm)	Nelkin (S.G.) Extrap. Distance (cm)
0.3	0.338	0.330
0.5	0.331	0.324
1.0	0.316	0.312

Table III

	Element	Number Densities x 10^{-24}
Fuel	U^{235}	0.0006288
Rod	U^{238}	0.04719
Clad	Al	0.051164
Water	H	0.066749
	O	0.0333745

REFERENCES

1. H. Bohl, E. Gelbard, P. Buerger and G. Culpepper, "SLOP-1 - A Thermal Multigroup Program for the IBM-704," WAPD-TM-188 (1960).

2. M. Nelkin, "Scattering of Slow Neutrons by Water," Physical Review, 119, 2, pp. 741-746, (July 15, 1960).

3. E. C. Campbell and P. H. Stelson, ORNL-2204, pp. 34-36, (1956).

4. H. C. Honeck, "The Distribution of Thermal Neutrons in Space and Energy in Reactor Lattices, Part II: Comparison of Theory and Experiment," Nucl. Sci. and Eng., 8, 203-209 (1960).

5. M. Nelkin, "The Decay of a Thermalized Neutron Pulse," Nucl. Sci. and Eng. 7, 210 (1960).

6. Progress in Nuclear Energy, Series 1, p. 200.

7. N. G. Sjostrand, "On the Theory Underlying Diffusion Measurements with Pulsed Neutron Sources," Arkiv for Fysik, Vol. 15, No. 12, 147 (1959).

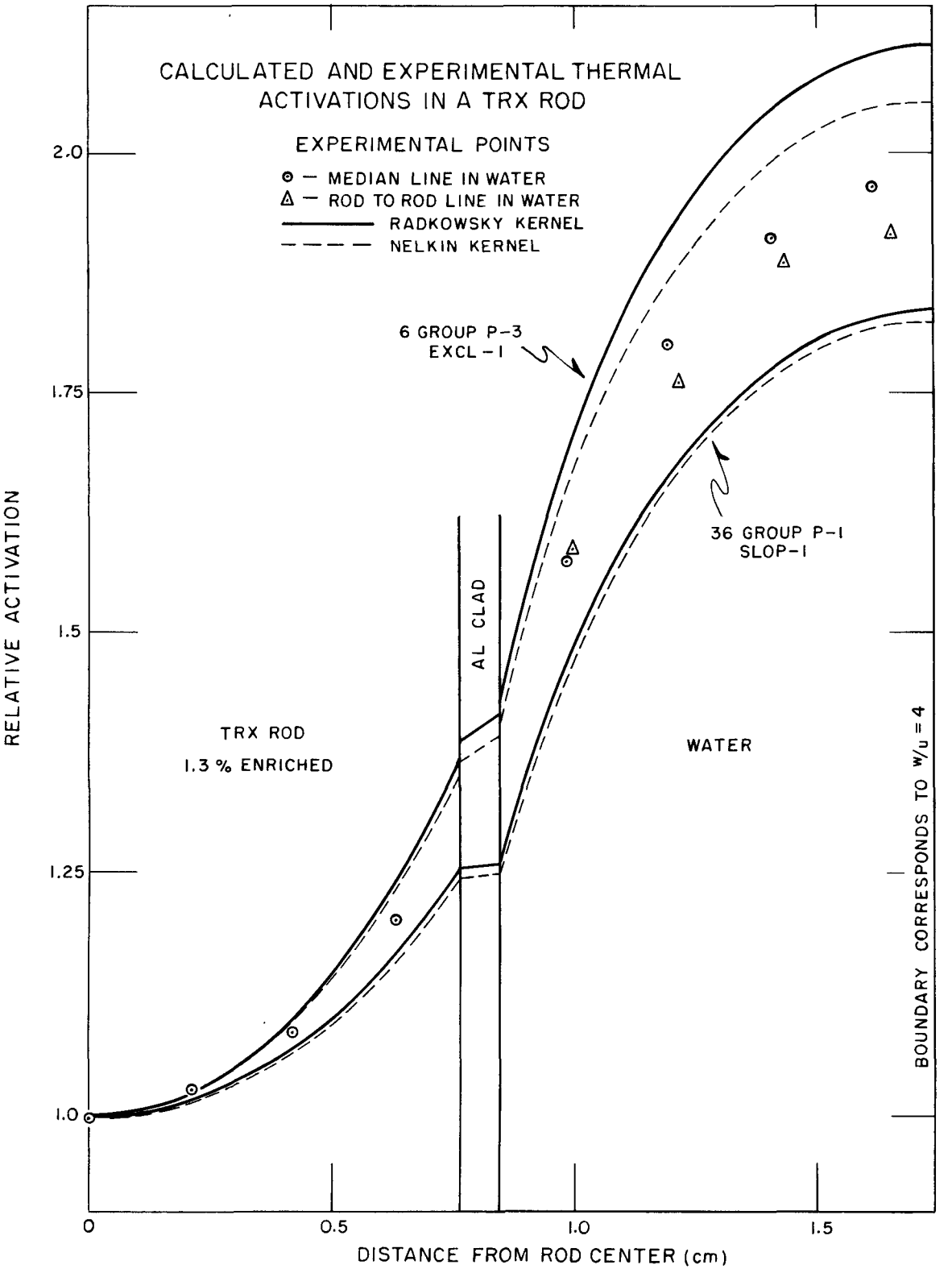
CALCULATED AND EXPERIMENTAL THERMAL ACTIVATIONS IN A TRX ROD
EXPERIMENTAL POINTS
⊙ — MEDIAN LINE IN WATER
Δ — ROD TO ROD LINE IN WATER
RADKOWSKY KERNEL
NELKIN KERNEL
6 GROUP P-3 EXCL-1
36 GROUP P-1 SLOP-1
AL CLAD
TRX ROD
1.3 % ENRICHED
WATER
BOUNDARY CORRESPONDS TO w/u = 4
RELATIVE ACTIVATION
DISTANCE FROM ROD CENTER (cm)
2.0
1.75
1.5
1.25
1.0
0
0.5
1.0
1.5

BROOKHAVEN NATIONAL LABORATORY

CONFERENCE ON NEUTRON THERMALIZATION

APRIL 30 - MAY 2, 1962

ON THE CALCULATION OF THERMAL NEUTRON DIFFUSION PARAMETERS

HENRY C. HONECK

BROOKHAVEN NATIONAL LABORATORY

UPTON, L. I., NEW YORK

MARCH 1962

Introduction

The pulsed neutron and diffusion length experiments both measure quantities related to the ability of neutrons to diffuse and thermalize in a moderator. The observed quantities are the asymptotic time and spatial decay constants, λ and κ. These decay constants and the neutron energy spectra associated with them are eigenvalues and eigenvectors of the transport equation. The problem is then: Given the scattering law for a moderator, solve the transport equation (an integral equation) and determine λ (or κ) and the neutron spectrum. Of course, the scattering law for a moderator is not accurately known. Indeed, the purpose of the experiment is to provide some integral properties of the scattering law so that theoretical scattering laws can be tested. The emphasis in this paper is on the accurate solution of the eigenvalue problem and on the computation of quantities observed in the experiment rather than derived from the experiment. The quality of theoretical scattering models can then be judged more accurately.

In the next section we will briefly review the theory of the two experiments and show how they are related. In the

third section a direct numerical method is developed for solving the eigenvalue problem. The decay constants and angular spectra are computed for light and heavy water and graphite. In the fourth section the series expansion method of Nelkin (1) is rederived and extended. The decay constants obtained from the expansion method are compared with those obtained in section 2.

Theory of the Experiments

The asymptotic flux in the pulsed neutron experiment can be written in the form

$$\Phi(z,E,\mu,t) = \Phi(E,\mu)e^{-\lambda t+iBz} \qquad (1)$$

where (z,E,μ,t) represent the position, energy, direction and time coordinates of the flux, and B^2 is the geometric buckling in the z direction. For simplicity, we have assumed here that the block is infinite in the x and y dimensions. When this flux is inserted in the transport equation, a homogeneous integral equation is obtained.

$$\left[-\frac{\lambda}{v}+\Sigma_a(E)+iB\mu\right]\Phi(E,\mu)= S\,\Phi(E,\mu) \qquad (2)$$

$$S\Phi(E,\mu) \equiv \int_{-1}^{1} d\mu' \int_{0}^{\infty} dE' \Sigma_s(E' \to E, \mu_o) \Phi(E',\mu') - \Sigma_s(E) \Phi(E,\mu) \tag{3}$$

Here v is the neutron speed, Σ_a and Σ_s are the absorption and scattering cross sections, $\Sigma_s(E' \to E, \mu_o)$ is the scattering kernel, and μ_o is the cosine of the angle between $\underline{\mu}$ and $\underline{\mu}'$. The eigenvalue, λ, is usually expressed in the form

$$\lambda = \lambda_o + D_o B^2 - CB^4 + FB^6 + \ldots . \tag{4}$$

where $\lambda_o = v\Sigma_a(E)$ = constant (we assume 1/v absorption throughout the paper). The coefficients D_o, C, F, etc. are to be determined.

The asymptotic flux in the diffusion length experiment can be written in the form

$$\Phi(z,E,\mu,t) = \Phi(E,\mu) e^{-\kappa z} \tag{5}$$

where κ is the inverse diffusion length. The eigenvalue equation is

$$\left[\Sigma_a(E) - \kappa\mu\right] \Phi(E,\mu) = S\Phi(E,\mu) \tag{6}$$

We will express the eigenvalue $\varkappa^2$ by the expansion

$$\varkappa^2 = \alpha_1 a - \alpha_2 a^2 + \alpha_3 a^3 .... \tag{7}$$

where α_1, α_2, α_3, etc. are to be determined, and $a \equiv \Sigma_a(kT) = \lambda_o / v_o$.

Equations (2) and (6) are of the form

$$\left[i\mu / k_1 - \frac{k_2}{v} \right] \Phi(E,\mu) = S\Phi(E,\mu) \tag{8}$$

where

$k_1 = B^2$, $k_2 = \lambda - \lambda_o$ pulsed experiment

$k_1 = -\varkappa^2$, $k_2 = -v_o a$ diffusion length experiment.

The power series expansion (7) is just the inverse of (4) with $\lambda = 0$. The coefficients are related by the expressions

$$\begin{aligned} \alpha_1 &= v_o / D_o \\ \alpha_2 &= v_o^2 C / D_o^3 \\ \alpha_3 &= v_o^3 (2C^2 - D_o F) / D_o^5 \end{aligned} \tag{9}$$

$$\begin{aligned} D_o &= v_o / \alpha_1 \\ C &= v_o \alpha_2 / \alpha_1^3 \\ F &= v_o (2\alpha_2^2 - \alpha_1 \alpha_3) / \alpha_1^5 . \end{aligned} \tag{10}$$

A schematic of these functions is shown in Figure 1. Here, λ_o is v_o times the absorption cross section of the pure moderator, and κ_o^2 is the square inverse diffusion length of the pure moderator. The regions accessible to the experimenter are shaded. The triangular area ($\kappa_o^2 \to \lambda_o \to 0 \to \kappa_o^2$) is not accessible to the experimenter.

Rewrite equation (6) in the form

$$\left[\Sigma_s(E) + \Sigma_a(E) - \kappa\mu\right] \Phi(E,\mu) = H(E,\mu) \tag{11}$$

$$H(E,\mu) \equiv \int_{-1}^{1} d\mu' \int_{0}^{\infty} dE' \Sigma_s(E' \to E, \mu_o) \Phi(E',\mu') \tag{12}$$

Then, since Φ and H must be everywhere real and positive

$$\kappa < \Sigma_s(E) + \Sigma_a(E) \tag{13}$$

Let κ^* = minimum value of $\Sigma_s(E)$. (14)

Then κ^{*2} is an upper bound on κ^2, and is shown as a vertical line in Figure 1. Corngold and Michael (2) have shown that $\lambda - \lambda_o$ is bounded by λ^*.

$$\lambda^* = \text{minimum value of } v\Sigma_s(E) \tag{15}$$

This bound on λ is shown as a horizontal line in Figure 1.

The two experiments are equivalent. The diffusion length experiment, however, is inherently more accurate since extrapolation length corrections to B^2 are unnecessary. We will then discuss only the diffusion length experiment and, when necessary, equations (10) will be used to compute the pulsed neutron parameters. We will also limit discussion to the case of 1/v absorbers.

Direct Calculation of $\varkappa$

The expansion of $\varkappa^2$ in powers of absorption is useful if only a few terms are required. In the case of large absorption, many terms are necessary and a direct calculation of $\varkappa^2$ is desirable. It is frequently difficult to extract the coefficients in the series expansion from the experimental data so that it is advantageous to compute directly the quantities observed in the experiment. We will therefore reduce equation (11) to a form in which it can be solved numerically and obtain $\varkappa^2$ for a given Σ_a.

Expand the flux and scattering kernel in Legendre polynomials.

$$\Phi(E,\mu) = \sum_{n=0}^{\infty} \frac{2n+1}{2} \Phi_n(E) P_n(\mu) \qquad (16)$$

$$\Sigma_s(E'\to E,\mu_o) = \sum_{n=0}^{\infty} \frac{2n+1}{2} \Sigma_{sn}(E'\to E) P_n(\mu_o) \quad (17)$$

Insert these expansions in (12) and use the addition theorem for Legendre polynomials. The result is

$$H(E,\mu) = \sum_{n=0}^{\infty} \frac{2n+1}{2} H_n(E) P_n(\mu) \quad (18)$$

$$H_n(E) = \int_0^{\infty} dE' \Sigma_{sn}(E'\to E) \Phi_n(E') \quad (19)$$

Divide eq. (11) by $\Sigma(E)-\varkappa\mu$, insert (16) and (18), multiply by $P_\ell(\mu)$ and integrate over μ. The result is

$$\Phi_\ell(E) = \sum_{n=0}^{\infty} \frac{2n+1}{2} H_n(E) \int_{-1}^{1} \frac{d\mu P_\ell(\mu) P_n(\mu)}{\Sigma(E) - \varkappa\mu} \quad (20)$$

Define

$$Q_{\ell n}(\varkappa,E) = \frac{2n+1}{2} \int_{-1}^{1} \frac{d\mu P_\ell(\mu) P_n(\mu)}{\Sigma(E) - \varkappa\mu} \quad (21)$$

The final set of integral equations to be solved is

$$\Phi_\ell(E) = \sum_{n=0}^{N} Q_{\ell n}(\varkappa,E) \int_0^{\infty} dE' \Sigma_{sn}(E'\to E) \Phi_n(E') \quad (22)$$

where N is the highest order of anisotropic scattering we wish to consider. If we include only isotropic scattering, N=0, and the set reduces to a single integral equation. We will consider terms to N=3.

The numerical solution of (22) would be straightforward except for the fact that the eigenvalue $\varkappa$ is implicit. We actually solve the equation

$$\omega\Phi_{\ell}(E) = \sum_{n=0}^{N} Q_{\ell n}(\varkappa,E) \int_{0}^{\infty} dE' \Sigma_{sn}(E'\rightarrow E)\Phi_{n}(E') \quad (23)$$

for ω given a value of $\varkappa$. We then vary $\varkappa$ until $\omega=1$. At any given $\varkappa$ eq.(23) is solved by power iteration until a converged value of ω is obtained. Details of the numerical method are given in the Appendix.

The computation of $Q_{\ell n}$ proceeds as follows. Let $C=C(E)=\varkappa/\Sigma(E)$.

$$Q_{\ell n}(\varkappa,E) = \frac{2n+1}{2\Sigma(E)} \int_{0}^{1} d\mu \frac{P_{\ell}(\mu)P_{n}(\mu)}{1-C^2\mu^2} \begin{cases} 1, & \text{if } \ell+n \text{ is even} \\ C\mu, & \text{if } \ell+n \text{ is odd} \end{cases} \quad (24)$$

Define

$$I_{m} = \int_{0}^{1} d\mu \frac{\mu^{m}}{1-C^2\mu^2} \quad (25)$$

from which the following recursion formula is obtained

$$C^2 I_m = I_{m-2} - \frac{1}{m-1} \tag{26}$$

and

$$I_o = \frac{1}{2C} \ln\left(\frac{1+C}{1-C}\right) \tag{27}$$

For small values of C a series expansion is used.

$$I_m = \sum_{k=0,2,4}^{\infty} \frac{C^k}{k+m+1} \tag{28}$$

The product $P_\ell(\mu) P_n(\mu)$ is expressed as a power series in μ, and $Q_{\ell n}(\varkappa, E)$ finally expressed as a sum of the I_m.

The $\Phi_\ell(E)$ from a typical calculation are shown in Figure 2. The scattering model used was the Nelkin (3) bound proton kernel with oxygen included. Details of the kernels used are given in the Appendix. Three anisotropic scattering terms were included. The absorption cross section was 5 barns/H atom and $\varkappa$ was computed to be $1.299 cm^{-1}$ corresponding to a diffusion length L=0.770cm. The scalar flux in Figure 2 resembles a Maxwellian at a temperature of 0.035ev. The higher angular components are peaked at a higher energy because of the increase in anisotropic scattering with energy. The irregular

behavior of Φ_2 and Φ_3 above 0.08ev is probably caused by the 0.06 ev oscillator in the Nelkin model.

The angular flux was reconstructed from eqs.(11) and (18) and is shown in Figure 3. The flux is nearly isotropic at low energies since $\Sigma(E) >> \varkappa$ and the Σ_{sn} are small for n>0. The flux is strongly peaked forward (μ=1) at high energies since $\Sigma(E)-\varkappa$ is minimum and the Σ_{sn} are large for n>0.

A series of these calculations were done for a range of equally spaced values of $a=\Sigma_a(kT)$. The values of $\varkappa^2/a$ were arranged in a table and divided differences computed. From this table the coefficients α_n were obtained and are given in Table I as a function of the number of anisotropic scattering terms included. The values of $\varkappa^2/a$ are plotted in Figure 4 along with many measured values (4-10). Pulsed neutron data are also included by using the relations $a=(\lambda_o-\lambda)/v_o$ and $\varkappa^2=-B^2$. The diffusion parameters for water predicted by the Nelkin kernel are in good agreement with measured values. The value of the diffusion coefficient is about 4% high while the cooling coefficient is within experimental uncertainty. Note that the coefficient α_3 is small and the curve in Figure 4 is nearly linear.

An incoherent scattering kernel for heavy water has been proposed by Honeck (11). The diffusion parameters predicted

by this model are given in Table I along with the experimental values measured by Ganguly and Waltner (12). In this case, the coefficient F is not negligible. Ganguly measured λ for values of B^2 in the range 0-0.1 cm^{-2} and fit these data to a quadratic. If we analyze our calculated results in the same way and in the same interval, we obtain $C = 3.65 \times 10^5 cm^4/sec.$ compared to Ganguly's value of $3.72 \pm 0.50 \times 10^5$. The correctly computed value of C from our data is 5.129×10^5. Both the computed values of D_o and C are in surprisingly good agreement with the experimental values.

An inelastic scattering kernel for graphite has been developed by Parks (13). An elastic isotropic scattering cross section selected to give the correct total cross section (14) was added to this kernel. The diffusion parameters computed are listed in Table I and plotted in Figure 5. Recent measurements by Starr and Price (15) are also included. The computed value of $C = 24.6 \times 10^5 cm^4/sec.$ lies between the older values of 12×10^5 (16) and the recent values of $40\text{-}47 \times 10^5$.

Power Series Expansion

Nelkin (1) has investigated (2) by expanding the flux in a Legendre series in μ and a power series in B^2. The same

technique will now be applied to eq.(6).

Expand the flux in Legendre polynomials in μ and a power series in a ($a=\Sigma_a(kT)$, $g(E)=\Sigma_a(E)/a$).

$$\Phi(E,\mu) = \sum_{n,k} \frac{2n+1}{2} \varkappa^n a^k \Phi_{nk}(E) P_n(\mu) \qquad (29)$$

Also expand $\varkappa^2$ in powers of a.

$$\varkappa^2 = \sum_{k=1} \alpha_k a^k (-1)^{k+1} \qquad (30)$$

Define

$$S_n\Phi_{nk} \equiv \int_0^\infty dE' \Sigma_{sn}(E' \to E) \Phi_{nk}(E') - \Sigma_{sn}(E) \Phi_{nk}(E) \qquad (31)$$

Insert these expansions in (6), multiply by $P_n(\mu)$, integrate over μ, and collect terms in powers of a. The result is

$$-\frac{n+1}{2n+1} \sum_{j=0}^{k-1} (-1)^{k-j+1} \alpha_{k-j} \Phi_{n+1,j} - \frac{n}{2n+1} \Phi_{n-1,k} +$$

$$+ g \Phi_{n,k-1} + \Sigma_s(1-b_n)\Phi_{nk} = S_n\Phi_{nk} \qquad (32)$$

where $b_n = \Sigma_{sn}/\Sigma_s$, and the argument E has been suppressed. Eq. (32) is a set of coupled integral equations which can be

solved recursively starting from Φ_{oo}. The procedure has been illustrated in (1). The solution is greatly simplified if we assume (as in (1)) that the anisotropic scattering is elastic. Then $S_n \Phi_{nk}=0$ for $n>0$. The equations for $n\neq 0$ are then algebraic and only the integral equations for $n=0$ need be solved. We will spare the reader the tedious algebra and simply list our results. The expressions are complicated so that we will define the following quantities (all functions of energy).

$$D_1 = 1/3\Sigma_s(1-b_1) \tag{33}$$

$$D_2 = 2/5\Sigma_s^2(1-b_1)(1-b_2) \tag{34}$$

$$D_3 = 2/35\Sigma_s^3(1-b_1)(1-b_2)(1-b_3) \tag{35}$$

$$A_1 = g-\alpha_1 D_1 \tag{36}$$

$$A_2 = 3D_1(gD_1 - \frac{2}{3}\alpha_1 D_2) \tag{37}$$

$$A_3 = 5D_2(gD_2 - \frac{3}{5}\alpha_1 D_3) \tag{38}$$

The α coefficients are given by

$$\bar{D}_1\alpha_1 = \int dE\, Mg \tag{39}$$

$$\bar{D}_1\alpha_2 = -\int dE\, \Phi_{01}A_1 \tag{40}$$

$$\bar{D}_1\alpha_{2t} = -\int dE\ M\ A_2 \tag{41}$$

$$\bar{D}_1\alpha_{3s} = \int dE\ \Phi_{02}A_1 + \int dE\ \Phi_{01}(\alpha_1A_2-\alpha_2D_1) - \alpha_{2s}\int dE\ M(A_2-2\alpha_1D_1D_2) \tag{42}$$

$$\bar{D}_1\alpha_{3t} = \int dE\ M\left[-\alpha_{2t}(A_2-2\alpha_1D_1D_2) - \frac{\alpha_1}{D_1}A_2^2 + \alpha_1^2A_3\right] \tag{43}$$

$$\bar{D}_1 = \int dE\ M D_1 \tag{44}$$

where M=M(E) is the Maxwellian distribution and subscripts t and s denote quantities independent and dependent on the shape of the hardened spectrum. The Φ_{01} and Φ_{02} are solutions of the equations

$$A_1M = S_o\,\Phi_{01} \tag{45}$$

$$(\alpha_1A_2 + \alpha_2D_1)M + A_1\Phi_{01} = S_o\Phi_{02} \tag{46}$$

The coefficients α_n computed from these equations are also given in Table I. In all cases they agree well with those computed directly from the integral equation, so that the approximation of elastic isotropic scattering is good for

these cases. It is apparent from eqs.(39-44) that the α_n depend on anisotropic scattering only up to order n. This result is also evident in Table I.

The transport and spectrum parts of the α_n coefficients are compared in Table II. The transport parts are generally small and the spectrum effects are dominant.

ACKNOWLEDGEMENTS

The author has benefited from many discussions with members of the Theoretical Reactor Physics Group at BNL. In particular, Drs. Paul Michael and Noel Corngold have made many useful suggestions. Mr. William Bornstein assisted in the calculations and preparations of illustrations.

REFERENCES

1. M. Nelkin, "The decay of a thermalized neutron pulse," NUCLEAR SCI. & ENG. 7, 210 (1960).
2. N. Corngold, P. Michael, W. Wollman, "The time decay constants in neutron thermalization," this Conference and submitted for publication in NUCLEAR SCI. & ENG. in February 1962.
3. M. Nelkin, "The scattering of slow neutrons by water," PHYS. REV 119, 791 (1960).

4. E. Starr and J. Koppel, "Determination of diffusion hardening in water," submitted for publication in NUCLEAR SCI. & ENG., October 1961.

5. W. Lopez and J. Beyster, "Measurement of neutron diffusion parameters in water by the pulsed neutron method," NUCLEAR SCI. & ENG. 12, 190 (1962).

6. J. Miller, "Thermal Neutron Diffusion length measurements in absorbing aqueous solutions," P24-6, Trans. Am. Nuclear Soc., Vol. 4, No. 2, 282 (1961).

7. W. Ballowe and W. Morgan, "Thermal neutron diffusion length measurements in light water," P24-5, Trans. Am. Nuclear Soc., Vol. 4, No. 2, 231 (1961).

8. K. Beckurts and O. Kluber, "Bestimmung der Diffusionsparameter thermischer Neutronen in Wasser nach einer Vergiftungsmethode," ZEITS. NATURF., 132, 822 (1958).

9. M. Reier, "The diffusion length of thermal neutrons in poisoned water," WAPD-T-1140 (1960).

10. K. Rockey and W. Skolnik, "Measurements on the diffusion length of thermal neutrons in water from 25 to 296°C.," NUCLEAR SCI. & ENG. 8, 62 (1960).

11. H. Honeck, "An incoherent scattering model for heavy water," Submitted to Trans. Am. Nuclear Soc.1962.

12. N. Ganguly and A. Waltner, "Measurements of neutron diffusion parameters of heavy water at different temperatures by pulsed source methods," P24-7, Trans. Am. Nuclear Soc., Vol. 4, No. 2, 282 (1961).

13. D. Parks, "Neutron spectra in poisoned graphite," Trans. Am. Nuclear Soc. Vol. 4, No. 1, 135 (1961).

14. D. Hughes and B. Schwartz, "Neutron cross sections," BNL-325 second edition (1958).

15. E. Starr and G. Price, "Measurement of diffusion parameter of graphite and graphite-bismuth by pulsed neutron methods," this Conference.

16. K. Beckurts, "Reactor physics research with pulsed neutron sources," NUCLEAR INSTRUMENTS AND METHODS 11, 144 (1961).

Appendix

The energy integrals were evaluated by first changing the energy variable to the dimensionless velocity variable $v = \sqrt{E/kT}$, evaluating all functions at 30 equally spaced intervals ($\Delta v = 0.1$), and using trapezoidal rule integration. The high energy cutoff is then 9kT (0.23ev). The scattering kernels were computed from

$$\Sigma_{sn}(v_i \rightarrow v_j) = 4\pi(.0253) v_i v_j \sum_{k=1}^{15} W_k P_n(\mu_k) \frac{d\Sigma(E_i \rightarrow E_j, \mu_k)}{d\epsilon \, d\Omega}$$

where the μ_k and W_k are Gauss quadrature angles and weights. The term i=j was treated separately by further dividing the interval Δv_i about v_i into four subintervals and computing an average $\Sigma_{sn}(v_i \rightarrow v_i)$.

The heavy water scattering kernel used here is identical to that for light water with the parameters given in Table III. This incoherent approximation for heavy water is justified by the fact that the interference scattering is small above $\frac{1}{5}$ kT.

A free gas kernel with mass 16 and $\sigma_s = 3.76$ barns is added to the water kernels to approximate the scattering from oxygen.

TABLE I

DIFFUSION PARAMETER OF H_2O, D_2O, AND GRAPHITE

Material	Method		α_1 cm^{-1}	α_2 cm^{-2}	α_3 cm^{-3}	D_o $cm^2/sec.$	C $cm^4/sec.$	F $cm^6/sec.$
H_2O	D^1	N=0	7.796	3.259	1.146	2.822×10^4	1.513×10^3	0.940×10^2
	D	N=1	5.862	2.751	1.403	3.753×10^4	3.004×10^3	2.190×10^2
	D	N=2	5.862	2.865	1.370	3.753×10^4	3.130×10^3	2.670×10^2
	D	N=3	5.862	2.865	1.353	3.753×10^4	3.130×10^3	2.700×10^2
	S	N=3	5.872	2.649	1.418	3.746×10^4	2.878×10^4	1.800×10^2
	Exp. Starr (4)		6.137 ±.017	3.047 ±.365	-	3.585×10^4 ±.010x10^4	2.900×10^4 ±.350x10^4	-
D_2O	D	N=0	1.202	2.907	9.95	1.831×10^5	3.687×10^5	4.34×10^5
	D	N=1	1.062	2.764	10.50	2.072×10^5	5.079×10^5	6.72×10^5
	D	N=2	1.062	2.792	10.40	2.072×10^5	5.129×10^5	7.39×10^5
	S	N=2	1.063	2.652	11.06	2.069×10^5	4.852×10^5	3.73×10^5

TABLE I (Continued)

Material	Method	α_1 cm^{-1}	α_2 cm^{-2}	α_3 cm^{-3}	D_o $cm^2/sec.$	C $cm^4/sec.$	F $cm^6/sec.$
D_2O	Exp. Ganguly[2] (12)	-	-	-	$2.08 \times 10^5 \pm .05 \times 10^5$	$3.72 \times 10^5 \pm .50 \times 10^5$	-
	D N=2 Quad. fit to $B^2=0.1$	-	-	-	2.11×10^5	3.65×10^5	-
Graphite	D,S N=0	0.988	9.301	498.0	2.226×10^5	2.120×10^6	-7.44×10^7
	S N=1	1.010	11.507	655.0	2.178×10^5	2.457×10^6	-8.31×10^7
	Exp.[3] Starr (15)						
	AA Graphite	-	-	-	$2.19 \times 10^5 \pm .03 \times 10^5$	$4.70 \times 10^6 \pm .40 \times 10^6$	-
	GBF Graphite	-	-	-	$2.14 \times 10^5 \pm .01 \times 10^5$	$4.06 \times 10^6 \pm .30 \times 10^6$	-

[1] D denotes direct calculation of κ^2, S denotes series expansion method.

[2] A quadratic fit to the data in the range $0<B^2<0.1$ was used.

[3] Data corrected to a density $\rho = 1.60$.

TABLE II

COMPARISON OF THE TRANSPORT AND SPECTRUM COEFFICIENTS

Material	N	α_{2s}	α_{2t}	α_{2t}/α_{2s}	α_{3s}	α_{3t}	α_{3t}/α_{3s}
H_2O	3	+2.810	-0.161	+0.057	1.618	-0.201	-0.124
D_2O	2	+2.960	-0.307	+0.104	12.08	-1.01	-0.084
Graphite	0	+9.894	-0.593	+0.060	497.6	0.14	0.0003

TABLE III

SCATTERING KERNEL CONSTANTS FOR WATER

Parameter	H_2O	D_2O	Units
ω_r	0.06	0.05	ev
ω_{v1}	0.205	0.15	ev
ω_{v2}	0.480	0.35	ev
λ_r	0.431	0.243	-
λ_{v1}	0.172	0.069	-
λ_{v2}	0.342	0.138	-
λ_t	0.055	0.050	-
σ_b	81.6	7.58	barns

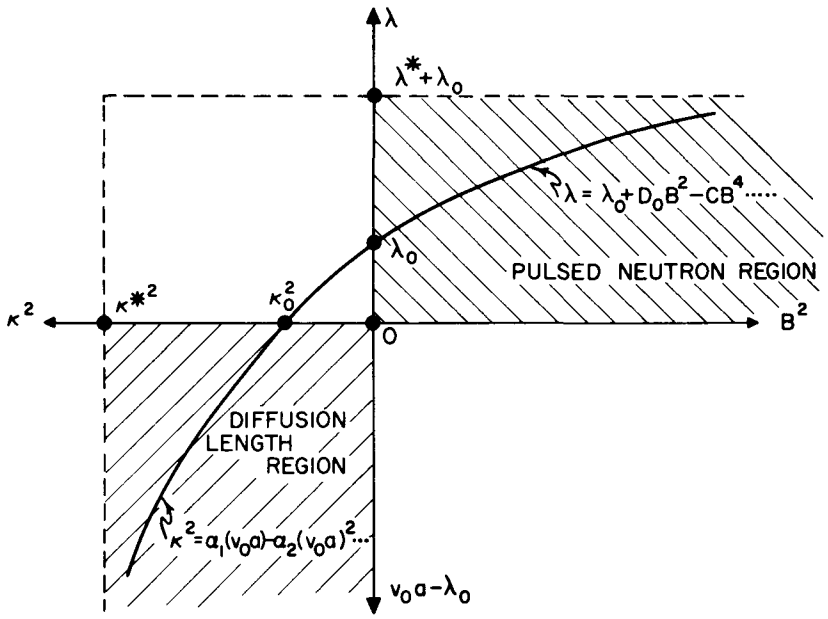

Figure 1. Schematic of the functions $\lambda(B^2)$ and $\kappa^2(v_0a)$.

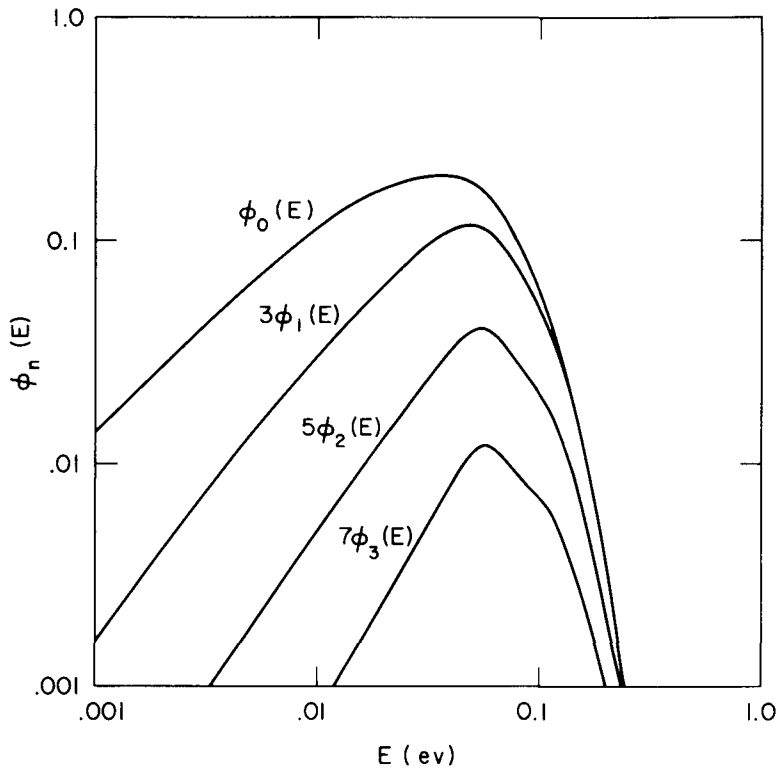

Figure 2. Angular components of the flux in a diffusion length experiment in water with 5b/H atom of boron poison.

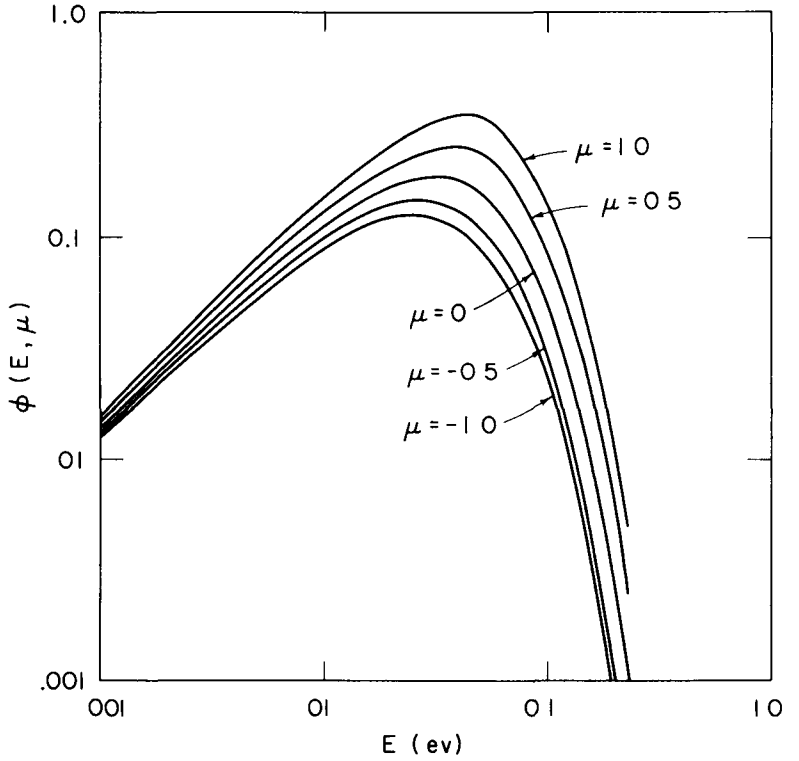

Figure 3. Angular flux in a diffusion length experiment in water with 5b/H atom of boron poison.

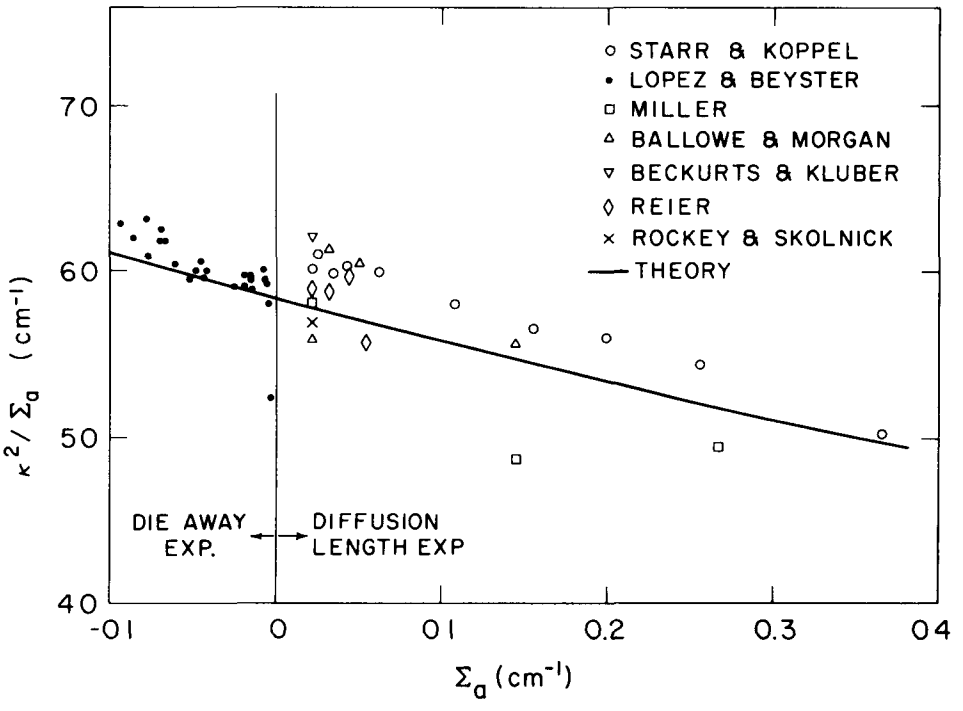

Figure 4. Computed and measured diffusion parameters of water.

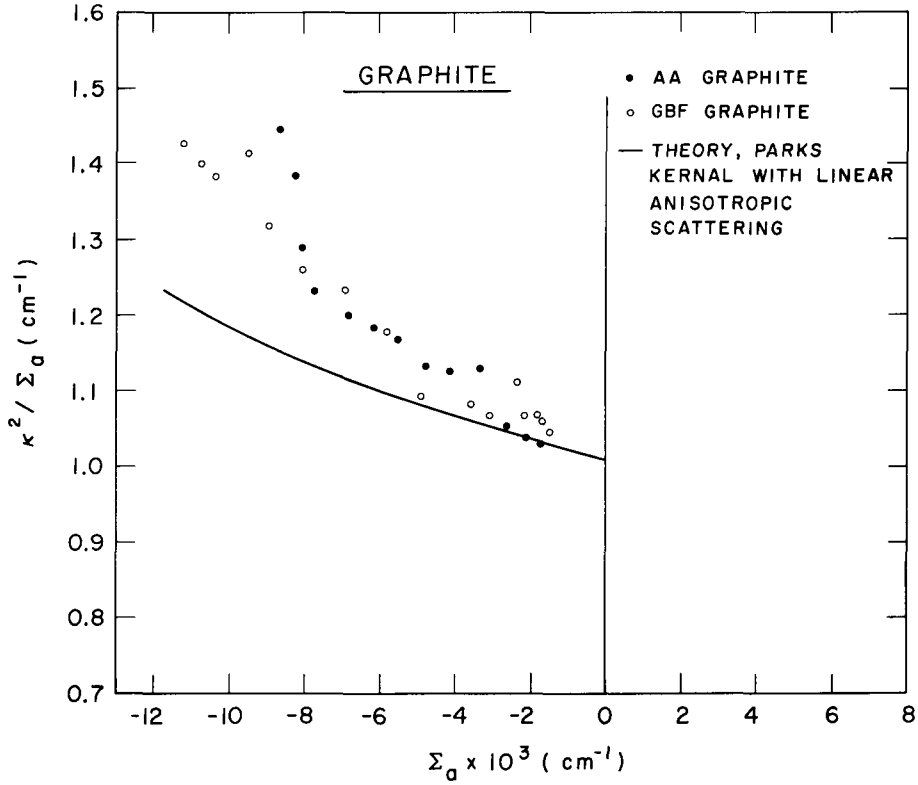

Figure 5. Computed and measured diffusion parameters of graphite.

MILNE'S PROBLEM FOR THERMAL NEUTRONS

R. Kladnik

Nuclear Institute "J. Stefan", Ljubljana, Yugoslavia*

---

* Currently with the International Institute of Nuclear Science & Engineering, Argonne National Laboratory, Argonne, Illinois

INTRODUCTION

In Milne's problem, we calculate the stationary distribution of neutrons in a semi-infinite spectrum-regenerating medium. Neutrons are supplied to the medium from infinity only and they are of maxwellian velocity spectrum at a temperature of the medium. The other half of the space is filled up with vacuum that swollows all neutrons crossing the boundary. There are no neutrons entering the medium at the boundary.

We will confine our problem to the case of a source-free nonmultiplying medium with anisotropic scattering-law and our main interest will be the determination of the linear extrapolation distance and of the velocity-angular distribution of neutrons streaming into vacuum. For this purpose, a variational method has been developed by Kuščer and the author, the details of which have already been published[1,2]. Here, a short review of this method will be given and the numerical methods with results will be discussed in more detail. The differential neutron flux $\Phi(x,v,\mu)$ satisfies under the above assumptions the following integro-differential equation,

$$\mu \frac{\partial \Phi(x,v,\mu)}{\partial x} + \ell^{-1}(v)\Phi(x,v,\mu) = \int_0^\infty dv' \int_{-1}^{1} d\mu' \ell_s^{-1}(v') f(v',\mu' \to v,\mu)\Phi(x,v',\mu') \; ; \qquad (1)$$

or, if we write $\Phi(x,v,\mu) = v^3 \exp(-v^2)\Psi(x,v,\mu)$ and use the detailed balance condition,

$$v'^3 \exp(-v'^2)\ell_s^{-1}(v') f(v',\mu' \to v,\mu) = v^3 \exp(-v^2)\ell_s^{-1}(v) f(v,\mu \to v',\mu') \, ,$$

equation (1) becomes

$$\mu \frac{\partial \Psi(x,v,\mu)}{\partial x} + \ell^{-1}(v)\Psi(x,v,\mu) = \ell_s^{-1}(v) \int_0^\infty dv' \int_{-1}^{1} d\mu' f(v,\mu \to v',\mu')\Psi(x,v',\mu') . \qquad (2)$$

The quantities used, are: x is a spatial coordinate (x = o at the boundary), μ a cosine of an angle between the neutron velocity and the symmetry - x axis, v neutron speed measured in units of the most probable velocity of the maxwellian spectrum (= $\sqrt{2kT/m}$, T = temperature of the medium), $\ell_s(v)$ and $\ell(v)$ are the scattering and the total mean free paths for neutrons moving with a speed v, respectively, and $f(v,\mu \to v',\mu')$ is the scattering function of an isotropic medium:

$$f(v,\mu\to v',\mu') = \sum_{n=0}^{\infty} \frac{2n+1}{2} f_n(v\to v') P_n(\mu) P_n(\mu') . \tag{3}$$

THE ASYMPTOTIC SOLUTION

The solution of the Milne's problem asymptotically approaches to the solution of the corresponding infinite-medium problem if we go away from the boundary into the medium. Any solution in an infinite medium that does not slow down neutrons indefinitely (spectrum-regenerating medium) can be built up of plane waves of the form, say

$$\Psi(x,v,\mu) \to g(v,\mu)\exp(-x/L), \tag{4}$$

where L is some parameter and $g(v,\mu)$ is a function which satisfies the homogeneous integral equation (put (4) into (2)),

$$g(v,\mu) = \frac{\ell(v)/\ell_s(v)}{1-\mu\ell(v)/L} \int_0^{\infty} dv' \int_{-1}^{1} d\mu' f(v,\mu\to v',\mu') g(v',\mu') . \tag{5}$$

$\underline{L}$ is to be determined from this equation as some sort of an eigenvalue of the homogeneous integral equation (3). To assure that $\underline{g}(\underline{v},\mu)$ will not be trivial $\underline{L}$ must obey the condition

$$|Re(L)| > (\ell(v))_{max} . \tag{5a}$$

Not much is known about the number and nature of the eigenvalues $\underline{L}$ of the equation (5). What we can see immediately, is that if $\underline{g}(\underline{v},\mu)$ corresponds to $\underline{L}$ then $\underline{g}(\underline{v},-\mu)$ is associated with $-\underline{L}$. This statement can be verified from equation (5) if the reciprocity behavior of the scattering function,

$$f(v,-\mu \rightarrow v',\mu') = f(v,\mu \rightarrow v',-\mu') ,$$

is taken into account. So, to each pair $\pm \underline{L}$ there corresponds a solution

$$\psi \rightarrow C_1(L)g(v,\mu)exp(-x/L) + C_2(L)g(v,-\mu)exp(x/L) \tag{6}$$

with $\underline{C}_1(\underline{L})$ and $\underline{C}_2(\underline{L})$ being arbitrary constants. The asymptotic solution for the flux would then be a linear combination of solutions like (6),

$$\Phi_{as}(x,v,\mu) = v^3 exp(-v^2)\sum_L \left\{C_1(L)g(v,\mu)exp(-x/L) + C_2(L)exp(x/L)\right\}, \tag{6a}$$

where the summation goes over the number of pairs of "eigenvalues" $\pm \underline{L}$ of the equation (5).

It is believed, though not yet proved, that in a nonmultiplying medium there exist only one pair of eigenvalues $\pm \underline{L}$ which satisfy the condition (5a), and that these are real. For our purpose, then the asymptotic flux would have the form:

$$\Phi_{as}(x,v,\mu) = v^3 exp(-v^2)\left[C_1 g(v,\mu)exp(-x/L) + C_2 g(v,-\mu)exp(x/L)\right], \tag{6b}$$

or, if we define new integration constants $\underline{x}_o$ and $\underline{C}$ as

$$C_1 = -0.5LC\,exp(-x_o/L) \quad and \quad C_2 = 0.5LC exp(x_o/L),$$

$$\Phi_{as}(x,v,\mu) = Cv^3\exp(-v^2)\left[g_1(v,\mu)L\sinh\frac{x+x_o}{L} - g_2(v,\mu)\cosh\frac{x+x_o}{L}\right] \tag{6c}$$

with

$$2g_1(v,\mu) = g(v,\mu) + g(v,-\mu)$$
$$2L^{-1}g_2(v,\mu) = g(v,\mu) - g(v,-\mu)\,. \tag{7}$$

$g_1(v,\mu)$ is, with respect to μ, an even part of $g(v,\mu)$ and $g_2(v,\mu)$ the odd one. The newly chosen integration constant x_o has a descriptive meaning: it gives a distance beyond the origin at which the integrated asymptotic flux $\Phi_{0,as}(x)$ would go to zero, i.e. $\Phi_{0,as}(-x_o) = 0$, where

$$\Phi_{0,as}(x) = 2\pi\int_0^\infty dv\int_{-1}^{1} d\mu\,\Phi_{as}(x,v,\mu) = 4\pi C\int_0^\infty dv\cdot v^3\exp(-v^2)\int_0^1 d\mu\, g_1(v,\mu)\cdot L\sinh\frac{x+x_o}{L}\,.$$

x_o is often referred to as being the extrapolated end point. Another way of describing the boundary condition instead of using x_o would be the introduction of the linear extrapolation distance Q, defined by

$$Q = \Phi_{0,as}(0)/\Phi'_{0,as}(0) = L\tanh\frac{x_o}{L}\,. \tag{8}$$

Having $g_1(v,\mu)$ and $g_2(v,\mu)$ we can also determine the diffusion coefficient D. This quantity is defined as the ratio between the net current and the gradient of the integrated flux,

$$J_{as}(x) = -D\frac{\partial}{\partial x}\Phi_{0,as}(x)\,.$$

If asymptotic solution (6c) is used, we get

$$D = \frac{\int_0^\infty dv\cdot v^3\exp(-v^2)\int_0^1 d\mu\,\mu\, g_2(v,\mu)}{\int_0^\infty dv\cdot v^3\exp(-v^2)\int_0^1 d\mu\, g_1(v,\mu)}\,. \tag{9}$$

Functions $\underline{g}_1(\underline{v},\mu)$ and $\underline{g}_2(\underline{v},\mu)$ are solutions of the system of two homogeneous integral equations which are readily obtained by combining equations (5) and (7),

$$g_1(v,\mu) = \mu \frac{l(v)}{L^2} g_2(v,\mu) + \frac{l(v)}{l_s(v)} \int_0^\infty dv' \int_{-1}^{1} d\mu' f(v,\mu \to v',\mu') g_1(v',\mu') , \tag{10}$$

$$g_2(v,\mu) = \mu l(v) g_1(v,\mu) + \frac{l(v)}{l_s(v)} \int_0^\infty dv' \int_{-1}^{1} d\mu' f(v,\mu \to v',\mu') g_2(v',\mu') . \tag{11}$$

We could evaluate $\underline{g}_1$ and $\underline{g}_2$ either from this system or directly by solving equation (5) for $\underline{L}$ and $\underline{g}(\underline{v},\mu)$. Usually, $\underline{f}(\underline{v},\mu \to \underline{v}',\mu')$ is approximated by a series (3) in which only a finite number of $\underline{N}$-terms is taken into account:

$$f(v,\mu \to v',\mu') = \sum_{n=0}^{N} \frac{2n+1}{2} f_n(v \to v') P_n(\mu) P_n(\mu') .$$

If this expression is used for $\underline{f}(\underline{v},\mu \to \underline{v}',\mu')$ in the equation (5), $\underline{g}(\underline{v},\mu)$ can be written in a more explicit form:

$$g(v,\mu) = \frac{l(v)/l_s(v)}{1-\mu l(v)/L} \int_0^\infty \sum_{n=0}^{N} \frac{2n+1}{2} P_n(\mu) G_n(v) , \tag{12}$$

where the functions $\underline{G}_n(\underline{v})$ represent solutions of a system of homogeneous integral equations,

$$\frac{l_s(v)}{l(v)} G_n(v) = \sum_{m=0}^{N} \int_0^\infty dv' f_n(v \to v') F_{nm}(v',L) G_m(v') , \quad n = 0, 1, 2, .., N \tag{13}$$

with

$$\frac{2}{2m+1} F_{nm}(v',L) = \int_{-1}^{1} \frac{P_n(\mu) P_m(\mu) d\mu}{1-\mu l(v')/L} = \sum_{K=0}^{\infty} \left[\frac{l(v')}{L}\right]^K \int_{-1}^{1} \mu^K P_n(\mu) P_m(\mu) d\mu . \tag{14}$$

In many practical cases $\underline{N} = 1$ will do good. System (13) then reduces to two homogeneous integral equations for $\underline{G}_0(\underline{v})$ and $\underline{G}_1(\underline{v})$ with $\underline{L}$ as an eigenvalue. One would probably have to transform these two equations into a system of linear algebraic equations by replacing the integration with a suitable summation procedure. Although the upper limits of the integrals are infinitely large, the effective range of the integration variable $\underline{v}'$ is, due to the shape of the kernel $\underline{f}_n(\underline{v} \rightarrow \underline{v}')$, reduced to a relatively narrow interval around the value of $\underline{v}$. Functions $\underline{G}_n(\underline{v})$ need not be determined for large values of $\underline{v}$, say greater than 4, as they appear in integrals together with a maxwellian factor $\underline{v}^3 e^{-\underline{v}^2}$ that cuts down the high-velocity portion of the $\underline{G}_n(\underline{v})$. The determinant of the above mentioned system of homogeneous algebraic equations must be zero. This condition gives us trancendental equation for $\underline{L}$. Only the largest root of this equation is needed. Much numerical work on high-speed digital computers has yet to be done until the optimized numerical method will be found. Once $\underline{L}$ is obtained and introduced into $\underline{F}_{nm}$, the problem reduces to an ordinary problem of finding the eigen-vector corresponding to an eigen-value $\lambda = 1$.

So far we have obtained numerical solutions for a nonabsorbing monatomic gaseous medium only. If $\underline{\ell}(\underline{v}) \rightarrow \underline{\ell}_s(\underline{v})$ then the diffusion length $\underline{L} \rightarrow \infty$ and from equations (10) and (11) we get that

$$g_1(v,\mu) \rightarrow 1 ,$$
$$g_2(v,\mu) \rightarrow \mu U(v), \tag{15}$$

where $\underline{U}(\underline{v})$ is a solution of the inhomogeneous integral equation,

$$U(v) = \ell_s(v) + \int_0^\infty f_1(v \rightarrow v') U(v') dv' . \tag{16}$$

The diffusion coefficient $\underline{D}$ (equation 9) for a nonabsorbing medium then is

$$D = \frac{2}{3}\int_0^\infty dv \cdot v^3 \exp(-v^2)\,\mathcal{U}(v) = \frac{1}{3}\bar{\lambda}_{tr} \tag{17}$$

whereas the asymptotic flux (6c) simplifies into

$$\phi_{as}(x,v,\mu) \to C v^3 \exp(-v^2)\left[x + x_0 - \mu\,\mathcal{U}(v)\right], \tag{18}$$

and $\underline{Q}$ becomes identical with $\underline{x}_0$.

INTEGRALS OF THE TRANSPORT EQUATION.

In the vicinity of the boundary the asymptotic solution is not valid anymore. However, it can be used to obtain integral conditions that must be satisfied by the exact solution throughout the whole medium. If we multiply equation (1) by $\underline{g}_i(\underline{v},\mu)\,d\underline{v}d\mu$ and integrate over $\underline{v}$ and μ we find that either of the two functions

$$K_i(x) = 2\pi\int_0^\infty dv \int_{-1}^{1} d\mu\,\Phi(x,v,\mu)\,\mu\,g_i(v,\mu), \quad i = 1,2 \tag{19}$$

is a solution of the following second-order differential equation,

$$\frac{d^2}{dx^2}K_i(x) - \frac{1}{L^2}K_i(x) = 0, \quad i = 1,2$$

The particular solutions of these two equations giving the correct description of $\underline{K}_1(\underline{x})$ and $\underline{K}_2(\underline{x})$ in the asymptotic region, are

$$K_1(x) = -2\pi C \alpha_{12} \cosh\frac{x+x_0}{L}, \tag{20}$$

$$K_2(x) = 2\pi C \alpha_{12} L \sinh\frac{x+x_0}{L}. \tag{21}$$

Here, the notation

$$\alpha_{ik} = 2\int_0^\infty dv\, v^3 \exp(-v^2)\int_0^1 d\mu\, \mu\, g_i(v,\mu)\, g_k(v,\mu) \tag{22}$$

has been used.

For nonabsorbing media, $\underline{K}_1(\underline{x})$ reduces to the net current-integral which, according to equation (20) for $\underline{L} \to \infty$, must be constant throughout the medium, whereas $\underline{K}_2(\underline{x})$, becomes equivalent to the so-called Chandrasekhar's $\underline{K}$-integral[4], being a linear function in $\underline{x}$.

Equations (20) and (21) together with the definition (19) give us two useful conditions to be obeyed by the flux of neutrons evaporating from the medium into the vacuum (at $\underline{x}$=o). As in our case $\Phi(o,\underline{v}, +\mu) = 0$, these conditions take the form

$$\int_0^\infty dv \int_0^1 d\mu\, \Phi(o,v,-\mu)\, \mu\, g_1(v,\mu) = C\alpha_{12}\cosh\frac{\underline{x}_o}{\underline{L}}\,, \tag{23}$$

$$\int_0^\infty dv \int_0^1 d\mu\, \Phi(o,v,-\mu)\, \mu\, g_2(v,\mu) = C\alpha_{12}\underline{L}\sinh\frac{\underline{x}_o}{\underline{L}}\,. \tag{24}$$

A rough estimate for $\underline{Q}$ can be obtained from equations (23) and (24) if we write $\Phi(o,\underline{v}, -\mu)$ in the form

$$\Phi(o,v,-\mu) = \Phi_{as}(o,v,-\mu) - Cv^3\exp(-v^2)\cosh\frac{\underline{x}_o}{\underline{L}}\, h(o,v,-\mu),$$

where the second term on the right side expresses the influence of the boundary on the flux of neutrons. In the vicinity of the boundary, the actual flux of neutrons moving towards the boundary is smaller than in the asymptotic region, hence, $\underline{h}(o,\underline{v}, -\mu)$ will be a positive quantity for all values of μ and $\underline{v}$ within the domain of our interest. If equation (23) is divided by $C\alpha_{12}\cdot\cosh(\underline{x}_o/\underline{L})$

and equation (24) by $\underline{C}\,\alpha_{11}\cdot\cosh(\underline{x}_o / \underline{L})$ and the expression (8) is used for $\underline{Q}$, we get

$$Q = \frac{\alpha_{12}}{\alpha_{11}} + \frac{2}{\alpha_{11}} \int_0^\infty dv \cdot v^3 \exp(-v^2) \int_0^1 d\mu\, h(0,v,-\mu)\, \mu\, g_1(v,\mu) \tag{25}$$

and

$$Q = \frac{\alpha_{22}}{\alpha_{12}} - \frac{2}{\alpha_{12}} \int_0^\infty dv \cdot v^3 \exp(-v^2) \int_0^1 d\mu\, h(0,v,-\mu)\, \mu\, g_2(v,\mu) . \tag{26}$$

Integral equations (10) and (11) indicate $\underline{g}_1(\underline{v},\mu)$ and $\underline{g}_2(\underline{v},\mu)$ will be positive quantities for $\mu > 0$. (One starts with weakly absorbing medium where $\underline{g}_1 \rightarrow 1$, $\underline{g}_2 \rightarrow \mu\,\underline{U}(\underline{v})$ and by iteration obtains that both functions remain positive). The integrals in the above equations are then positive and

$$Q_{max} = \frac{\alpha_{22}}{\alpha_{12}} , \tag{25a}$$

$$Q_{min} = \frac{\alpha_{12}}{\alpha_{11}} . \tag{26a}$$

Neglecting the absorption of the medium, $\underline{Q}_{min}$ becomes equal to $2\underline{D}$ (17), whereas $Q_{max} \rightarrow (1/2D) \int_0^\infty dv\, v^3 \exp(-v^2)\, U^2(v)$, or furthermore, in case of one-speed approximation with isotropic scattering, $\underline{Q}_{min} \rightarrow (2/3)\,\underline{\ell}_s$ and $\underline{Q}_{max} \rightarrow (3/4)\,\underline{\ell}_s$.

To describe the flux near the boundary it will be more convenient if we use, instead of $\Phi(\underline{x},\underline{v},\mu)$, a function $\mathcal{Q}(\underline{x},\underline{v},\mu)$ defined by

$$\Phi(x,v,\mu) = C\,v^3 \exp(-v^2)\cosh\frac{x_0}{L}\left[g_1(v,\mu)L\sinh\frac{x}{L} - g_2(v,\mu)\cosh\frac{x}{L} + \mathcal{Q}(x,v,\mu)\right] \tag{27}$$

According to the above definition,

$$\mathcal{Q}(0,v,\mu) = g_2(v,\mu),\quad \mu>0 \tag{28}$$

$$\mathcal{Q}_{as}(x,v,\mu) = Q\left[g_1(v,\mu)\cosh\frac{x}{L} - L^{-1}g_2(v,\mu)\sinh\frac{x}{L}\right]. \tag{29}$$

$\mathcal{Q}_{\underline{as}}$ is equal to the linear extrapolation distance in case the medium does not absorb neutrons. It can be seen that the integro-differential equation for $\mathcal{Q}(x,v,\mu)$ is the same as for $\Psi(x,v,\mu)$, namely,

$$\mu\frac{\partial\mathcal{Q}(x,v,\mu)}{\partial x} + \ell^{-1}(v)\mathcal{Q}(x,v,\mu) = \ell_s^{-1}(v)\int_0^\infty dv'\int_{-1}^{1} d\mu' f(v,\mu\to v',\mu')\mathcal{Q}(x,v',\mu'). \tag{30}$$

For our purpose, the integral form of this equation is needed. Taking into account the boundary condition (28), equation (30) can be integrated and we get

$$\mathcal{Q}(x,v,\mu) = \varepsilon(\mu)g_2(v,\mu)\exp\left[-\frac{x}{\mu\ell(v)}\right] + \mathcal{J}\{\mathcal{Q}(x,v,\mu)\} \tag{31}$$

with

$$\mathcal{J}\{\mathcal{Q}(x,v,\mu)\} = \int_{\eta(\mu)}^{x}\frac{dx'}{\mu\ell_s(v)}\left\{\int_0^\infty dv'\int_{-1}^{1} d\mu' f(v,\mu\to v',\mu')\mathcal{Q}(x',v',\mu')\right\}\exp\left[-\left|\frac{x-x'}{\mu\ell(v)}\right|\right], \tag{32}$$

where $\varepsilon(\mu)=0$ for $\mu<0$ and $\varepsilon(\mu)=1$ if $\mu>0$; $\eta(\mu)$ is equal to 0 or ∞ when $\mu>0$ or <0 , respectively. Integral equation (31) gives us some information about the range of the asymptotic region. To see, at what depth the asymptotic region is achieved, we take in Equs. (31), (32) $\underline{x}$ to be large. Then, the exponential factor $\exp\left[-\left|\frac{x-x'}{\mu\ell(v)}\right|\right]$ is different from zero only if $\underline{x}'$ is close to $\underline{x}$. This is especially true when μ or $\underline{v}$ are small (small $\underline{\ell(v)}$!). In this case, $\mathcal{Q}(\underline{x}',\underline{v}',\mu')$ can be replaced by $\mathcal{Q}_{as}(\underline{x}',\underline{v}',\mu')$ (29) and the left side

of Eqn. (31), indeed, gives $q_{as}(x,v,\mu)$, providing $x \gg \mu \ell(v)$. The asymptotic region is then closer to the boundary for neutrons of slower speeds and for direction of movement more parallel to the boundary ($\mu \to 0$).

We will solve Equ. (31) for $q(x,v,\mu)$ approximately using the variational method. The functional $I\{q\}$ approaching a stationary form if q is close to the exact solution of the integral equation (31), can be written as

$$I\{q\} = \int_0^\infty dx \int_0^\infty dv \int_{-1}^{1} d\mu\, q^\dagger(x,v,\mu)\left[2\varepsilon(\mu) q_2(v,\mu) \exp\left\{-\frac{x}{\mu \ell(v)}\right\} + J\{q\} - q(x,v,\mu)\right] \tag{33}$$

with

$$q^\dagger(x,v,\mu) = v^3 \exp(-v^2)\, \ell_s^{-1}(v) \int_0^\infty dv' \int_{-1}^{1} d\mu'\, f(v,-\mu \to v',\mu')\, q(x,v',\mu') \,. \tag{34}$$

As yet, we do not know much about the minimum- or maximum- behavior of the stationary value I_{st} of the functional $I\{q\}$ if the scattering is anisotrofic. It is known, however, that I_{st} is the maximum value of $I\{q\}$ in case of an isotropic scattering.

The stationary functional I_{st} has a relatively simple form

$$I_{st} = \int_0^\infty dx \int_0^\infty dv \int_0^1 q^\dagger(x,v,\mu)\, q_2(v,\mu) \exp\left[-\frac{x}{\mu \ell(v)}\right] d\mu \tag{35}$$

whenever the trial function for $q(x,v,\mu)$ is chosen to be a linear combination of suitable functions $q_i(x,v,\mu)$, i.e.,

$$q(x,v,\mu) = \sum_{i=1}^{M} A_i\, q_i(x,v,\mu) \,. \tag{36}$$

A_i are the variational parameters, to be determined from

$$\frac{\partial}{\partial A_i} I\{q\} = 0 \,, \quad i = 1,2,\cdots,M \,. \tag{37}$$

It is well known that even a crude trial function gives a fairly good result for I_{st}. The benefit of the variational method is that it expresses Q in terms of I_{st}. We get from Equs. (24) and (27)

$$\alpha_{12} Q = \int_0^\infty dv\, v^3 \exp(-v^2) \int_0^1 d\mu \left[q_2(v,\mu) + q(0,v,-\mu)\right] \mu\, q_2(v,\mu)$$

and, furthermore, if we replace $\psi(0,\nu,\mu)$ with the right side of the Equ.(31) and use the expression (35) for $\underline{I}_{st}$,

$$Q = \frac{1}{\alpha_{12}}\left(\frac{\alpha_{22}}{2} + I_{st}\right). \tag{38}$$

The surprisingly good, yet still simple trial function is $\psi(x,\nu,\mu) \approx \psi_{as}(x,\nu,\mu)$ with $\underline{Q}$ replaced by a variable parameter $\underline{A}_1$. From Equs. (37) and (35) we get the optimized value for $\underline{A}_1$ being equal to α_{12}/α_{11} and for $\underline{I}_{st} \approx \alpha_{12}^2/2\alpha_{11}$, so that

$$Q' = \frac{1}{2}\left(\frac{\alpha_{22}}{\alpha_{12}} + \frac{\alpha_{12}}{\alpha_{11}}\right), \tag{39}$$

being equal to the arithmetic mean of the maximum and minimum value for $\underline{Q}$. In the one-speed case with isotropic scattering and no absorption this value corresponds to $17/24 = .70833\,\underline{\ell}_s$, which is rather close to the exact value $.7104\,\underline{\ell}_s$.

To improve the trial function we will have to add terms describing the effect of the boundary on the flux distribution. According to our discussion, following the integral equation (31), these terms should have factors of the form, like, $\exp\left[-\underline{x}/\mu\underline{\ell}(\nu)\right]$. However, such functions do not enable us to evaluate parameters $\underline{A}_i$ and $\underline{I}_{st}$ analytically. For this reason we write our imporved trial function as

$$\psi(x,\nu,\mu) = A_1\frac{\psi_{as}(x,\nu,\mu)}{Q} - \left[A_2 g_1(\nu,\mu) + A_3 g_2(\nu,\mu)\right]\exp(-x/\ell_o), \tag{40}$$

where $\underline{\ell}_o$ is some suitably chosen fixed length, e.g. $\underline{\ell}_o = \ell(\infty)$. Once the parameters $\underline{A}_i$ have been optimized, this trial function can furthermore be improved by one iteration of the integral equation (31). The iterated solution is

$$\begin{aligned}\psi(x,\nu,\mu) = {} & A_1\left[g_1(\nu,\mu)\cosh\tfrac{x}{L} - L^{-1}g_2(\nu,\mu)\sinh\tfrac{x}{L}\right] \\ & - \left\{A_2\left[g_1(\nu,\mu) - \mu\frac{\ell(\nu)}{L^2}g_2(\nu,\mu)\right] + A_3\left[g_2(\nu,\mu) - \mu\ell(\nu)g_1(\nu,\mu)\right]\right\}\frac{\exp(-x/\ell_o)}{1-\mu\ell(\nu)/\ell_o} \\ & + \varepsilon(\mu)\left\{g_2(\nu,\mu) - A_1 g_1(\nu,\mu) + \frac{A_2\left[g_1(\nu,\mu) - \mu\frac{\ell(\nu)}{L^2}g_2(\nu,\mu)\right] + A_3\left[g_2(\nu,\mu) - \mu\ell(\nu)g_1(\nu,\mu)\right]}{1-\mu\ell(\nu)/\ell_o}\right\}\exp\left[-\frac{x}{\mu\ell(\nu)}\right].\end{aligned} \tag{41}$$

It is not expected that this approximation will give a good description of the flux near the boundary. However, fortunately enough, the results are very good for $\underline{x} = o$:

$$\chi(0,\nu,\mu) = \varepsilon(\mu) g_2(\nu,\mu) + [1-\varepsilon(\mu)]\left\{A_1 g_1(\nu,\mu) - \frac{A_2\left[g_1(\nu,\mu) - \mu\frac{\ell(\nu)}{L^2} g_2(\nu,\mu)\right] + A_3\left[g_2(\nu,\mu) - \mu\ell(\nu) g_1(\nu,\mu)\right]}{1-\mu\ell(\nu)/\ell_o}\right\}. \quad (42)$$

As it should be, $\chi(0,\underline{\nu},\mu) = g_2$ for $\mu > 0$. It can also be shown that $\chi(0,\nu,\mu)$ given by (42) exactly satisfies conditions (23) and (24) which could be, for our purpose, rewritten in a form:

$$2\int_0^\infty d\nu\, \nu^3 \exp(-\nu^2)\int_0^1 d\mu\, \chi(0,\nu,-\mu)\mu g_1(\nu,\mu) = \alpha_{12}\,, \quad (23a)$$

$$2\int_0^\infty d\nu\, \nu^3 \exp(-\nu^2)\int_0^1 d\mu\, \chi(0,\nu,-\mu)\mu g_2(\nu,\mu) = 2\alpha_{12}Q - \alpha_{22}\,, \quad (24a)$$

providing parameters $\underline{A_i}$ are determined through Eq$\mathfrak{u}$. (37) and $\underline{Q}$ is given by Eq$\mathfrak{u}$. (38).

The following formula for the flux $\Phi(0,\underline{\nu},-\mu)$ should then give a fairly good description of the angular and velocity distributions for neutrons streaming into the vacuum:

$$\Phi(0,\nu,-\mu) = C\nu^3 \exp(-\nu^2)\cosh\frac{x_o}{L}\left\{g_2(\nu,\mu) + A_1 g_1(\nu,\mu) - \frac{A_2\left[g_1(\nu,\mu) - \frac{\mu\ell(\nu)}{L^2} g_2(\nu,\mu)\right] + A_3\left[g_2(\nu,\mu) - \mu\ell(\nu) g_1\right]}{1-\mu\ell(\nu)/\ell_o}\right\}. \quad (43)$$

$\mu > 0$

NUMERICAL RESULTS FOR NON-ABSORBING MONATOMIC GASEOUS MEDIA

To get numerical results we have used gaseous models for the scattering function, having supposed that the scattering cross-section is independent of the relative speed between the neutron and the scattered nucleus. Integral equation for the function $\underline{\mathcal{U}(\nu)}$ (16) has been solved numerically on the Argonne's IBM 704 digital computer. The results for the atomic masses

A = 1, 2, 3, 4, 6, and 20 are given by the Fig. 1. It can be deduced from the shape of the integral equation (16) that $U(v)$ goes to zero with a constant derivative as $v \to 0$ and approaches asymptotically to the value $3A/(3A-2)$ for large values of v. Also, $U(v)$ is close to ℓ_s (∞) for all v if the moderator is very heavy. The approach to the asymptotic value is relatively slow, especially in the case of A = 1 moderator.

Function $U(v)$ was then used for the evaluation of the following integrals,

$$\bar{\lambda}_{tr} = 2\int_0^\infty dv \cdot v^3 \exp(-v^2) U(v), \qquad \text{Equ. (17)}$$

$$\bar{\lambda}^2_{tr} = 2\int_0^\infty dv \cdot v^3 \exp(-v^2) U^2(v),$$

$$Q_{min} = \frac{2}{3}\bar{\lambda}_{tr},$$

$$Q_{max} = \frac{3\bar{\lambda}^2_{tr}}{4\bar{\lambda}_{tr}}, \qquad \text{Equ. (26a)}$$

$$A_1, A_2, A_3, \qquad \text{Equ. (25a)}$$

$$Q = \frac{3\bar{\lambda}^2_{tr}}{8\bar{\lambda}_{tr}} + \frac{3}{\bar{\lambda}_{tr}} I_{st}. \qquad \text{Equ. (37)}$$

$$\text{Equ. (38)}$$

The results of the numerical integration are given in Table I. The improved variational result for Q (38) is only slightly larger than the first estimate Q' (39). Fig. 2 represents the dependence of the linear extrapolation distance Q and the transport mean free path $\bar{\lambda}_{tr}$ on the atomic mass A of the gaseous monatomic moderator. A rough comparison between the measured extrapolating end point in D_2O [5] and the calculated values for Q (Fig. 2) indicates that gaseous monatomic moderator with $A \approx 3.5 - 3.7$ would be a good representation for D_2O, in agreement with the estimate made by H. D. Brown[6]. In Fig. 3, a flux of neutrons leaving the medium in a perpendicular direction $\mu = -1$, is given for atomic masses A = 1, 2, and 20 (arbitrarily normalized to the same value 0.5 at $v = 1$). A shift in the temperature of the flux-

distribution has been estimated to be about 17% for $\underline{A} = 1$, few per cents for $\underline{A} = 2$, whereas a moderator with $A > 20$ emits neutrons of practically maxwellian velocity distribution.

DISCUSSION

The above results indicate that the velocity distribution of neutrons evaporating from the boundary of a non-absorbing medium is not appreciably influenced by the boundary. However, we expect the effect of the boundary upon the neutron spectrum be much more important if absorption is present in the medium. The linear extrapolation distance $\underline{Q}$ very slowly approaches the one-speed value $.7104\,\lambda_s(\infty)$ as the moderator is getting heavier. For practical cases, $\underline{Q}$ may be in the range $0.75 - 0.8\,\lambda_s(\infty)$.

The above variational method can be successfully applied also to problems like determination of the angular- and velocity- distribution of neutrons transmitted through or reflected from a thin layer of an absorbing medium.

ACKNOWLEDGEMENTS

The author would like to express his appreciation towards Dr. I. Kuščer for introducing him to this problem and for his continued interest and guidance, and also to Dr. R. G. Taecker, director of the International Institute of Nuclear Science and Engineering, Argonne National Laboratory, for making available the facilities needed for completing this work.

REFERENCES

1. R. Kladnik, I. Kuščer, Nuclear Sci. and Eng. 11, No. 2, 1961.
2. R. Kladnik, I. Kuščer, Nuclear Sci. and Eng., to be published.
3. B. Davison, "Neutron Transport Theory", Oxford University Press, London and New York, 1958, p. 251.

4. S. Chandrasekhar, "Radiative Transfer", Oxford University Press, London and New York, 1950.

5. P. Auger et al., Canad. J. Res. A25, 143 (1947).

6. H. D. Brown, D. S. St. John, DP-33, Feb. 1954.

TABLE I

A	$\overline{\lambda}_{tr}$	$\overline{\lambda^2_{tr}}$	Q_{min}	Q'	Q	Q_{max}	A_1	A_2	A_3
1	1.273	1.725	0.849	0.931	0.936	1.016	0.970	0.171	0.0147
2	1.133	1.325	0.755	0.816	0.818	0.876	0.842	0.131	0.0123
3	1.086	1.203	0.724	0.777	0.779	0.830	0.800	0.117	0.0095
4	1.064	1.148	0.709	0.759	0.761	0.809	0.780	0.111	0.0076
6	1.044	1.098	0.696	0.742	0.744	0.788	0.762	0.105	0.0053
20	1.028	1.059	0.685	0.729	0.730	0.772	0.747	0.100	0.0014
∞	1.000	1.000	0.667	0.708	0.710	0.750	0.726	0.096	0.0000

Figure 1 — Function $U(v)$ for monatomic gaseous media.

Figure 2 — Linear extrapolation distance a and average transport mean free path λ_{tr} versus atomic mass number A.

Figure 3 — Velocity distribution of the flux of thermal neutrons streaming out of the moderator in perpendicular direction ($\mu = -1$). (Flux has been arbitrarily normalized to 0.5 at $v = 1$).

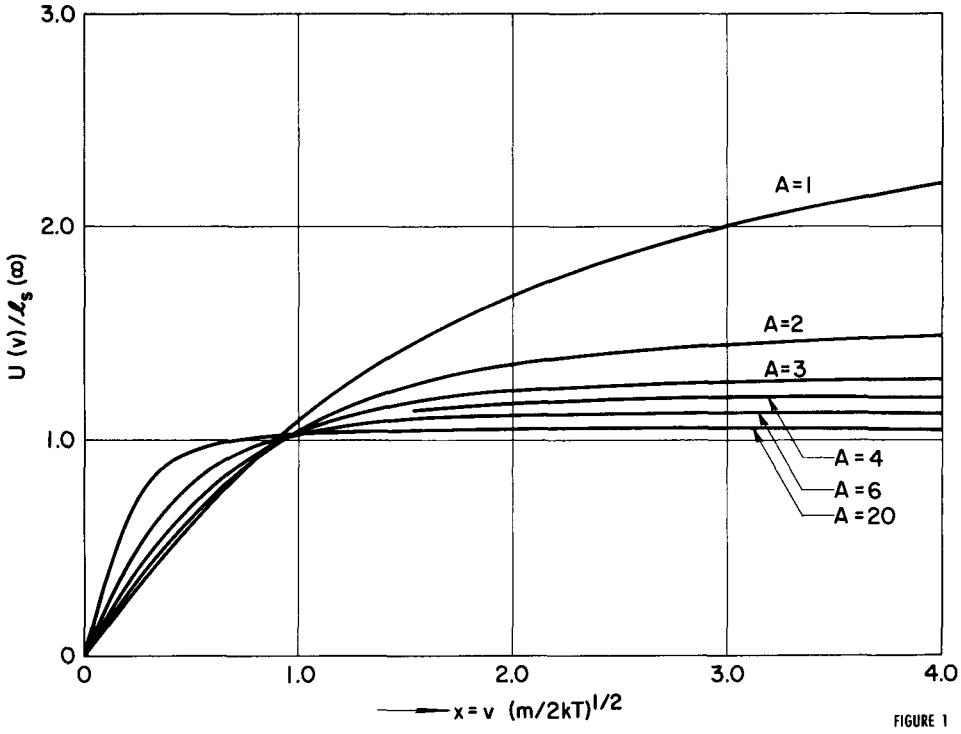

FIGURE 1

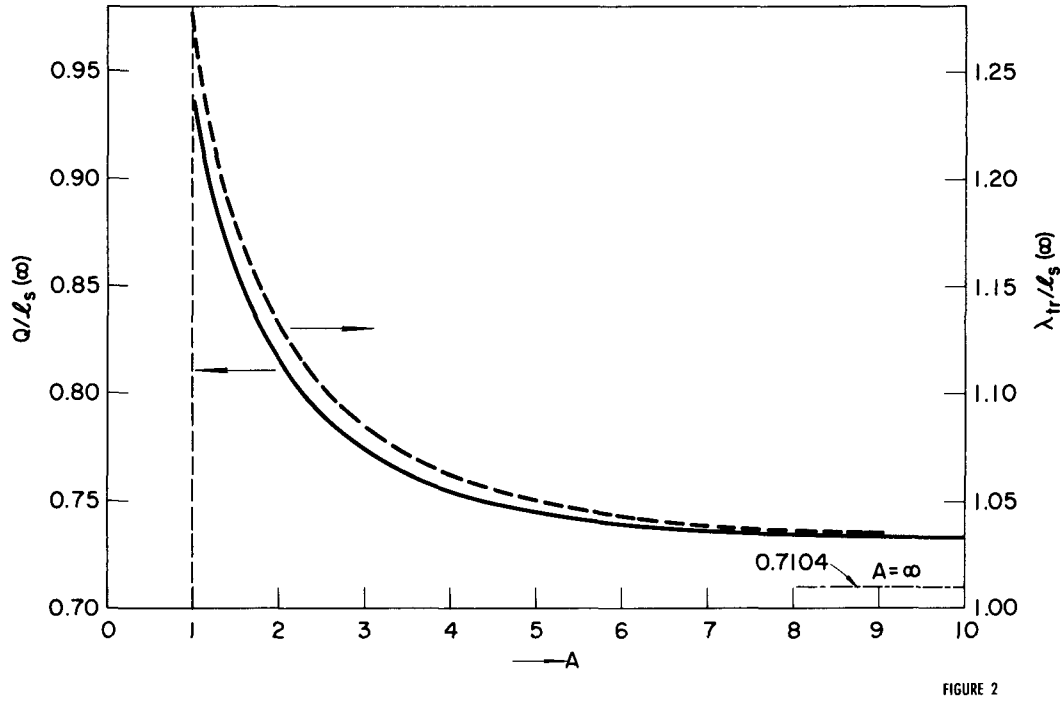

FIGURE 2

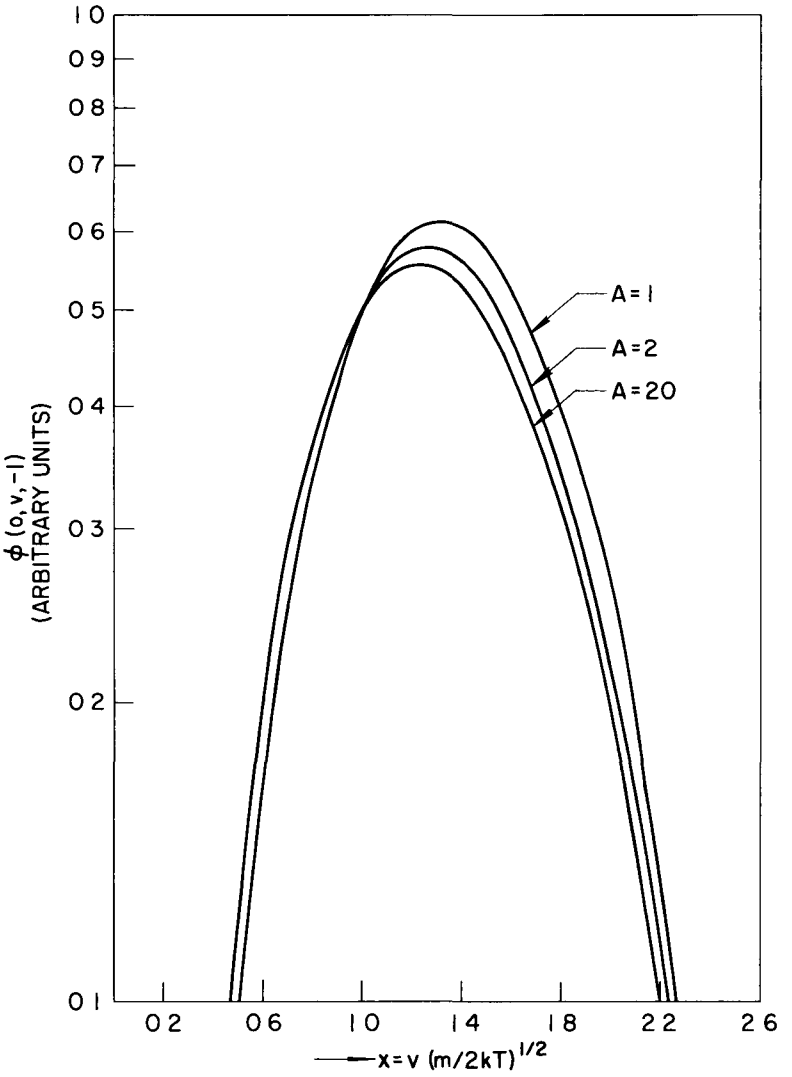
1 0
0 9
0 8
0 7
0 6
0 5
0 4
0 3
0 2
0 1
φ (o, v, -1)
(ARBITRARY UNITS)
A = 1
A = 2
A = 20
0 2
0 6
1 0
1 4
1 8
2 2
2 6
x = v (m/2kT)^1/2

FIGURE 3

ON THE SOLUTION OF THE TIME DEPENDENT NEUTRON THERMALIZATION PROBLEM*

by

Juan U. Koppel

John Jay Hopkins Laboratory for Pure and Applied Science
General Atomic Division of General Dynamics Corporation
San Diego, California

I. INTRODUCTION

For a long time it has been assumed that the time dependent neutron thermalization problem can be solved by separating time and energy variables in the Boltzmann equation and then expressing the time dependent spectrum as a sum of discrete energy modes or eigenfunctions, each decaying in time with a particular decay constant (or eigenvalue). Thus, in order to satisfy arbitrary initial conditions, implicitly it was assumed that this set of functions is complete. However, as it will become apparent in the following, this assumption is generally not true. In fact it will be seen that the sequence of discrete eigenvalues λ cannot exceed the limiting value $\lambda_\infty = (\Sigma v)_{min}$, but that for $\lambda > \lambda_\infty$ it is possible to construct a continuum of singular solutions of a special kind, all orthogonal to the set of discrete energy modes, thus proving the incompleteness of the latter.

The physical interpretation of the existence of a limiting value λ_∞ is simply the fact that no persistent neutron spectrum can possibly decay with a smaller time constant $(1/\lambda)$ than the maximum average time between collisions, which is $\frac{1}{(\Sigma v)_{min}}$.

*Work done under contract AT(04-3)-167, Project Agreement No. 2.

Only for the physically unrealistic assumption of $\frac{1}{(\Sigma v)_{min}} = 0$ the set of discrete eigenfunctions would be complete. This is the case of the heavy gas model.

The approach used in Section II for treating the time dependent neutron thermalization was first suggested by Van Kampen[1] in connection with a problem of plasma oscillations, and developed later on by Case[2] and Mika[2] in connection with a space dependent one velocity transport problem. Unfortunately in the present case the formulation becomes considerably more involved and most of the results are only given in the first order approximation of the scattering kernel. However, it is believed that they can be extended to any higher order, matter which will be considered in a subsequent paper.

In Section III a few numerical calculations are performed for the free hydrogen gas kernel. Finally, another approach to the problem is briefly outlined in the Appendix.

II: APPROXIMATE SOLUTION OF THE TIME AND ENERGY DEPENDENT BOLTZMANN EQUATION

We shall only consider the case of zero absorption. (1/v absorption can always be reduced to this case.) Hence the Boltzmann equation reads:

$$\frac{\partial n(x, t)}{\partial t} = -n(x, t)x\,\Sigma_s(x) + \int_0^\infty n(x', t)x'\Sigma(x' \to x)dx' + Q(x, t) \qquad (1)$$

where $n(x, t)$ is the neutron density' $x = v/v_o$ is the ratio of neutron velocity to the most probable velocity of a maxwellian spectrum at room temperature' t is the time and $\Sigma_s(x)$, $\Sigma(x' \to x)$ have their usual meanings. The time unit is $\frac{1}{\Sigma_{so} v_o}$ and the cross section unit is Σ_{so}, the free atom scattering cross section (at some given energy).

We want to express the solution of the homogeneous part of eq. (1) as a sum of functions of the kind:

$$n(x, t) = n(x)e^{-\lambda t} \qquad (2)$$

Thus n(x) must be a solution of

$$n(x)\left[x\,\Sigma_s(x)-\lambda\right] = \int_0^\infty n(x')\,x'\Sigma(x'\to x)\,dx' \tag{3}$$

It follows from the principle of detailed balance that the kernel of this equation can be symmetrized making

$$n(x) = N(x)\sqrt{M(x)}$$

$$x\,\Sigma\,(x'\to x) = S(x|x')\sqrt{\frac{M(x)}{M(x')}}$$

with $M(x) = x^2\,e^{-x^2}$

Then denoting $x\,\Sigma_s(x) = V(x)$, we have

$$N(x)\left[V(x)-\lambda\right] = \int_0^\infty N(x')\,S\,(x|x')\,dx' \tag{4}$$

Now let us expand $S(x'|x)$ in a double series of functions which are orthogonal in the interval $(0,\infty)$, and truncate this expansion after K+1 terms:

$$S(x|x') = \sum_0^K \sum_0^K S_{ij}\,\mu_i(x)\,\mu_j(x') \tag{5}$$

$$= \sum_{j=0}^K f_j(x)\,\mu_j(x') \text{ with } f_j(x) = \sum_{i=0}^K S_{ij}\,\mu_i(x) \tag{6}$$

Furthermore, let the μ_i be the odd Hermite polynomials times $e^{-x^2/2}$

Then
$$\sqrt{\frac{M(x')}{M(x)}} = \frac{\mu_o(x')}{\mu_o(x)} \tag{7}$$

and
$$V(x) = \int_0^\infty x\,\Sigma(x\to x')dx' = \int_0^\infty \frac{\mu_o(x')}{\mu_o(x)}\,S(x|x')\,dx' \tag{8}$$

or
$$V(x) = \frac{f_o(x)}{\mu_o(x)} \tag{9}$$

Now expand $N(x)$ in a series of μ_i

$$N(x) = \sum_{o}^{\infty} \phi_k \mu_k (x) \tag{10}$$

$$\phi_k = \int_{o}^{\infty} N(x) \mu_k(x) \, dx \tag{11}$$

Then

$$\int_{o}^{\infty} N(x') S(x|x') \, dx' = \sum_{o}^{K} f_j(x) \phi_j \tag{12}$$

or

$$N(x) = \frac{1}{V(x)-\lambda} \sum^{K} f_j(x) \phi_j \tag{13}$$

Now let us suppose that*

$$0 < V(0) < V(x) \text{ for all } x \tag{14}$$

This means that Σ_s goes like $\frac{1}{x}$ for $x \to 0$ and certainly holds for a gas model. Then the nature of eq. (4) is quite different for $\lambda < V(0)$ or $\lambda > V(0)$. In the first case eq. (4) is a homogeneous Fredholm equation of the second kind and has solutions only for particular values of λ. When $\lambda > V(0)$ eq. (4) becomes singular.

First let $\lambda < V(0) = V_o$

Because of the orthogonality of the μ_i

$$\phi_k = \sum_{j=o}^{K} \phi_j \int_{o}^{\infty} \frac{f_j(x) \mu_k(x)}{V(x)-\lambda} \, dx = \sum_{j=o}^{K} K_{kj}^{\lambda} \phi_j \qquad k = 0,1.....K \tag{15}$$

with

$$K_{kj}^{\lambda} = \sum_{i}^{K} L_{ki}^{\lambda} S_{ij} \tag{16}$$

and

$$L_{ki}^{\lambda} = \int_{o}^{\infty} \frac{\mu_i \mu_k}{V-\lambda} \, dx \tag{17}$$

*In order to have the same behavior for the approximate $V(x)$ given by (9) we shall consider only odd values of K

For the non trivial solution of (15)

$$\det\left(K^{\lambda}_{kj} - \delta_{kj}\right) = 0 \tag{18}$$

It is simple to show that there are at most K+1 values of λ satisfying (18) (See Appendix)

The lowest one is obviously $\lambda_o = 0$ corresponding to $N(x) = \mu_o(x)$

In fact:

$$K^{o}_{ko} = \int_o^\infty \mu_k(x)\, \mu_o(x)\, dx = \delta_{ko} \tag{19}$$

Thus $\lambda = o$ is a solution of (18)

In the absence of degeneration the K+1 eigenfunctions will be orthogonal to each other. To prove it write eq. (4) for two different eigenvalues, λ_m and λ_n.

$$N_n(x)\left[V(x)-\lambda_n\right] = \int_o^\infty N_n(x')\, S\,(x|x')\, dx' \tag{20}$$

$$N_m(x)\left[V(x)-\lambda_m\right] = \int_o^\infty N_m(x')\, S\,(x|x')\, dx \tag{21}$$

Multiply (20) by $N_m(x)$ and (21) by $N_n(x)$, then integrate over x and subtract:

$$(\lambda_n - \lambda_m) \int_o^\infty N_n(x)\, N_m(x)\, dx = 0 \tag{22}$$

Having assumed $\lambda_n \neq \lambda_m$ it follows that $N_n(x)$ and $N_m(x)$ are orthogonal to each other. An important consequence is the equation

$$\lambda_n\, \phi_o = 0 \tag{23}$$

which means that only $N_o(x)$ has a $\mu_o(x)$ component. Therefore, in order to find the eigenvalues $\lambda_n \neq 0$ we need only K of the K+1 eq. (15), for instance k = 0, 1 .... K-1. The determinant of these K eq. must vanish for $\lambda = \lambda_n \neq 0$ and the normalization of the corresponding eigenfunctions is arbitrary, for instance $\phi_1 = 1$. Once ϕ_1, ϕ_2 .... ϕ_x are known, the eigenfunction $N_n(x)$ are given directly by eq. (13).

Now let $\lambda \geq V(0) = V_o$ and assume $V(x)$ is non-decreasing in the interval $(0, \infty)$. Then in general there are no regular solutions of eq. (4). However, there is a continuum of singular solutions[1-3] (not strictly functions but distributions in the sense of Schwartz), which together with the discrete spectrum for $\lambda < V_o$ can be shown to be a complete set, at least in the first approximation K=1. These singular solutions are

$$N(x, \lambda) = P \frac{1}{V-\lambda} \sum_{j=o}^{K} f_j(x) \phi_j(\lambda) + \omega(\lambda) \delta(x-x_\lambda) \tag{24}$$

where $f_j(x)$ and $\phi_j(\lambda)$ have the same meanings as above and

$$V(x_\lambda)-\lambda = 0 \tag{25}$$

$P \frac{1}{V-\lambda}$ indicates that when integrated, the Canchy principal value is meant. As $V(x)$ is a constant for $K = 0$ from now on $K \geq 1$

Multiplying eq. (24) by $V(x)-\lambda$, and using the same method as above, it is easy to prove that these singular solutions are orthogonal to each other and to the discrete eigenfunction. Thus eq. (23) holds for the singular solutions too. In order to find the function $\phi_k(\lambda)$ and $\omega(\lambda)$ multiply eq. (24) by $\mu_k(x)$ and integrate; it follows:

$$\phi_k(\lambda) = \sum_{j=1}^{K} \phi_j(\lambda) K_{kj}(\lambda) + \omega(\lambda) \mu_k(x_\lambda) \quad k = 0,1, \ldots K \tag{26}$$

with

$$K_{kj}(\lambda) = \int_o^\infty \frac{\mu_k(x) f_j(x)}{V(x)-\lambda} dx \tag{27}$$

The $K_{kj}(\lambda)$ are Canchy principal values. The system of K+1 equation (26) is homogeneous. In order to have non-trivial solutions its determinant (with $\mu_k(x_\lambda) = \eta_k$)

$$\Delta = \begin{vmatrix} K_{01} & K_{02} \cdots\cdots K_{0K} & \eta_0 \\ K_{11}-1 & K_{12} \cdots\cdots K_{1K} & \eta_1 \\ K_{21} & K_{22}-1 \cdots\cdots K_{2K} & \eta_2 \\ \cdots\cdots & \cdots\cdots\cdots\cdots & \cdots \\ K_{K1} & K_{K2} \cdots\cdots K_{KK} & \eta_K \end{vmatrix} \qquad (28)$$

should be zero. In fact, it follows from eq. (25) that

$$\sum_{k=o}^{K} (K_{kj} - \delta_{kj})\, S_{ok} = \lambda\, K_{oj} \qquad j = 0, 1, \ldots K \qquad (29)$$

and

$$\sum_{j=o}^{K} S_{oj}\, \eta_j = \lambda \eta_o \qquad (30)$$

Thus

$$\Delta = 0 \qquad (31)$$

and the system eq. (26) has a non-trivial solution which can be normalized arbitrarily.

If the ϕ_j (λ) for $j > K$ are required, they can be found with the recursion relations

$$\sum_{n=o}^{i+K} \phi_n \sum_{l=o}^{K} S_{ol} \int_o^{\infty} \mu_n\, \mu_l\, \frac{\mu_i}{\mu_o}\, dx = \sum_{j=o}^{K} S_{ij}\, \phi_j + \lambda\, \phi_i \qquad (32)$$

or else, using eq. (26), but now with $k > K$. The relation eq. (32) obvicusly also holds for $\lambda = \lambda_n < V_o$. For i=o it yields the known result:

$$\lambda\, \phi_o = 0$$

Completeness for K = 1

This case is particularly simple because ϕ_o and ϕ_1 are known a priori.

We have $V(x) = \frac{f_o(x)}{\mu_o(x)} = S_{oo} + S_{o1} \frac{\mu_1(x)}{\mu_o(x)} = b\,(x^2 + a)$ (33)

b and a being constants.

For $\lambda \neq 0$ eq. (18) and (31) reduce to

$$K_{o1}^{\lambda} = \int_o^{\infty} \frac{\mu_o(x)\, f_1(x)}{V(x) - \lambda}\, dx = 0 \tag{34}$$

$$K_{o1}(\lambda) + \omega(\lambda)\, \eta_o = 0 \tag{35}$$

Eq. (34) defines the only non zero eigenvalue of the discrete spectrum, whereas eq. (35) gives $\omega(\lambda)$ for the singular solution.

In order to prove completeness of the set, it is sufficient to show that an arbitrary function F(x), orthogonal to the discrete spectrum, can be written as a linear combination of the singular solutions.

For simplicity let us change to the variable $y = x^2$ and adopt the notation

$$h_i(y) = \mu_i(\sqrt{y})$$

$$g_i(y) = f_i(\sqrt{y})$$

Now $$V(y) - \lambda = b(y+a) - \lambda = b(y-\alpha) \tag{36}$$

with $$\alpha = \frac{\lambda}{b} - a \tag{37}$$

The 2 discrete eigenfunctions are

$$N_o(y) = h_o(y) \tag{38}$$

$$N_1(y) = \frac{g_1(y)}{b(y+\alpha_1)} \tag{39}$$

with

$$\alpha_1 = a - \frac{\lambda_1}{b} \tag{40}$$

Eq. (24) and (35) can be written

$$N(y, \alpha) = P \frac{g_1(y)}{b(y-\alpha)} + 2\sqrt{\alpha}\, \omega(\alpha)\, \delta(y-\alpha) \tag{41}$$

$$\omega(\alpha) = \frac{-1}{b\, h_o(\alpha)} \oint_o^\infty \frac{h_o(y)\, g_1(y)}{y - \alpha} \frac{dy}{2\sqrt{y}} \tag{42}$$

If the set of functions (strictly, distributions) eq. (38), (40) and (41) is complete, it should be possible to express an arbitrary function F(y), obeying the conditions

$$\int_o^\infty F(y)\, N_n(y)\, \frac{dy}{\sqrt{y}} = 0 \qquad n = 0, 1. \tag{43}$$

by the integral

$$F(y) = \int_o^\infty A(\alpha)\, N(y, \alpha)\, d\alpha \tag{44}$$

or

$$F(y) = Q(y)\, A(y) + \frac{T(y)}{\pi i} \oint_o^\infty \frac{A(\alpha)\, d\alpha}{\alpha - y} \tag{45}$$

with

$$Q(y) = 2\sqrt{y}\, \omega(y) \tag{45a}$$

$$T(y) = -\frac{\pi i}{b}\, g_1(y)$$

The singular integral eq. (45) is of the dominant type[4] and its solution reduces to the Hilbert problem of finding a function X(z), sectionally holomorphic in the finite plane cut along the positive real axis, with lowest degree at infinity and satisfying the equation

$$G(y) = \frac{X^+(y)}{X^-(y)} = \frac{X(y + 0i)}{X(y - 0i)} \tag{46}$$

where

$$G(y) = \frac{2\sqrt{y}\,\omega(y) + \pi i g_1(y)/b}{2\sqrt{y}\,\omega(y) - \pi i g_1(y)/b} \tag{46a}$$

This last equation is equivalent to

$$G(y) = \frac{\Theta^-(y)}{\Theta^+(y)} \tag{47}$$

with

$$\Theta(z) = \frac{1}{2\pi i\ b} \int_0^\infty \frac{h_o(y) g_1(y)}{y - z} \frac{dy}{2\sqrt{y}} \tag{48}$$

where z is not on the positive real axis. Comparing (48) and (34) it is seen that

$$\Theta(z) = 0 \quad \text{at} \quad z = -\alpha_1$$

this being the only zero of $\Theta(z)$ in the finite plane. Thus it is found that

$$X(z) = (z + \alpha_1)\ \frac{1}{\Theta(z)} \tag{49}$$

is the solution of the Hilbert problem considered. The function $\Omega(z)$ defined as

$$\Omega(z) = \frac{1}{2\pi i} \int_0^\infty \frac{A(y)\,dy}{y - z} \tag{50}$$

will then be given by

$$\Omega(z) = \frac{X(z)}{2\pi i} \int_0^\infty \frac{F(y)}{X^+(y)\left[Q(y) + T(y)\right]} \frac{dy}{y - z} \tag{51}$$

or

$$\Omega(z) = \frac{1}{4\pi^2} \frac{z + \alpha_1}{\Theta(z)} \int_0^\infty \frac{F(y)\, h_o(y)}{(y + \alpha_1)(y - z)} \frac{dy}{2\sqrt{y}} \tag{51a}$$

As X(z) is of second degree at infinity, F(y) must obey the conditions

$$\int_0^\infty \frac{F(y) h_o(y) y^n}{y + \alpha_1} \frac{dy}{2\sqrt{y}} = 0 \qquad n = 0,\ 1 \tag{52}$$

in order to make $\Omega(z)$ vanish at infinity as required by eq. (50). Finally $A(y)$ can be obtained from

$$A(y) = \Omega^{+}(y) - \Omega^{-}(y)$$

It is easily verified that condition (52) and (43) are equivalent. Hence no further conditions are imposed on $F(y)$ and the completeness has been proved.

Normalization integral - From the orthogonality properties already shown it follows that

$$\int_{o}^{\infty} F(y)N(y,\alpha) \frac{dy}{2\sqrt{y}} = A(\alpha)R(\alpha) \tag{53}$$

where $F(y)$ and $A(\alpha)$ are related by eq. (44) and where $R(\alpha)$ depends on the normalization chosen for $N(y,\alpha)$. For $\phi(\alpha) = 1$ and using the Bertrand-Poincare formula it is found ($K = 1$):

$$R(\alpha) = \omega^2(\alpha)2\sqrt{\alpha} + \frac{\pi^2}{b^2} g_1^{\,2}(\alpha) \frac{1}{2\sqrt{\alpha}} \tag{54}$$

For the two discrete eigenfunction given by (38) and (39), the normalization integrals are

$$R_0 = \int_{o}^{\infty} h_o^{\,2}(y) \frac{dy}{2\sqrt{y}} = 1 \tag{55}$$

$$R_1 = \frac{1}{b^2} \int_{o}^{\infty} \frac{g_1^{\,2}(y)}{(y+\alpha_1)^2} \frac{dy}{2\sqrt{y}} \tag{56}$$

Green function - As an application of the previous results let us find the Green function corresponding to eq. (1). With the variables defined above we have

$$\frac{\partial N_G(y,y_o,t)}{\partial t} = -N_G(y,y_o,t)V(y) + \int_{o}^{\infty} N_G(y,y_o,t)S(y'|y) \frac{dy'}{2\sqrt{y'}} + \delta(t)\delta(y-y_o) \tag{57}$$

Integrating over t from -0 to +0, if $N_G(y,y_o,-0) = 0$

$$N_G(y,y_o,+0) = \delta(y-y_o) \tag{58}$$

Because of the completeness of the $N(y,\alpha)$ we can make the expansion (K = 1)

$$N_G(y,y_o,t) = \sum_{n=o}^{1} A_n N_n(y)\, e^{-\lambda_n t} + \int_o^{\infty} A(\alpha) N(y,\alpha) e^{-\lambda(\alpha)t}\, d\alpha \tag{59}$$

A_n and $A(\alpha)$ can then be determined from the boundary condition (58). Making

$$F(y) = \delta(y-y_o) - \sum_{n=o}^{1} A_n N_n(y) \tag{60}$$

it is seen that

$$A(\alpha) = \frac{N(y_o,\alpha)}{R(\alpha)} \tag{61}$$

and

$$A_n = \frac{N_n(y_o)}{R_n} \tag{62}$$

Finally

$$N_G(y,y_o,t) = \sum_{n=o}^{1} \frac{N_n(y_o)N_n(y)}{R_n}\, e^{-\lambda_n t} + \int_o^{\infty} \frac{N(y_o,\alpha)N(y,\alpha)e^{-\lambda(\alpha)t}}{R(\alpha)}\, d\alpha \tag{63}$$

Another case occurs when the source term is of the form

$$\delta(t)\, h_n(y) \qquad n \neq o \tag{64}$$

Then the boundary condition

$$N_{Hn}(y,+0) = h_n(y) \tag{65}$$

applies and from

$$A(\alpha)\, R\,(\alpha) = \int_o^{\infty} N(y,\alpha)\, h_n\,(y)\, \frac{dy}{2\sqrt{y}} = \phi_n(\alpha) \tag{66}$$

$$A_1\, R_1 = \int_o^{\infty} N_1\,(y)\, h_n(y)\, \frac{dy}{2\sqrt{y}} = \phi_{n,1} \qquad ; \quad A_o = 0 \tag{67}$$

it follows

$$N_{Hn}(y,t) = \frac{\phi_{n,1}}{R_1}\, N_1(y) e^{-\lambda_1 t} + \int_o^{\infty} \frac{\phi_n(\alpha)}{R(\alpha)}\, N(y,\alpha)\, e^{-\lambda(\alpha)t} d\alpha \tag{68}$$

III Numerical calculations for the monoatomic hydrogen gas kernel.

For a monoatomic gas kernel the matrix elements can be computed analytically (5). The kernel for monoatomic hydrogen is particularly simple

$$S(x|x') = 2\, e^{-(1/2)(x'^2-x^2)}\ \mathrm{erf}\,(x) \qquad x<x' \tag{69}$$

$$= 2\, e^{-(1/2)(x^2-x'^2)}\ \mathrm{erf}\,(x') \qquad x>x'$$

With

$$\mu_i(x) = \left[2^{2i}(2i+1)!\ \sqrt{\pi}\right]^{-1/2} e^{-x^2/2} H_{2i+1} \tag{70}$$

$$H_p(x) = (-1)^p\ e^{x^2}\ \frac{d^p}{dx^p}\ e^{-x^2} \tag{71}$$

the matrix elements are

$$S_{ij} = (-1)^{i-j+1}\ \frac{2^{5/2}}{\pi}\ \left[\frac{(2i+1)!\ (2j+1)!}{4(i-j)^2-1}\right]^{-1/2}\ \Gamma(i+j+3/2) \tag{72}$$

It is interesting to compare the values obtained for V(0) with the exact and the approximate kernels (see Fig. 1). The exact function is

$$V(x) = \left(x + \frac{1}{2x}\right)\ \mathrm{erf}\,(x) + \frac{e^{-x^2}}{\sqrt{\pi}} \tag{73}$$

and its minimum value is $V(0) = \frac{2}{\sqrt{\pi}}$ (74)

With the approximate kernel it is found

For K = 1 $$V_1(x) = S_{oo} + S_{o1}\ \frac{2x^2-3}{\sqrt{6}} = \sqrt{\frac{2}{\pi}}\left(\frac{3}{2} + \frac{x^2}{3}\right) \tag{75}$$

$$V_1(0) = 1.5\sqrt{\frac{2}{\pi}} = 1.06\ V(0) \tag{76}$$

For K = 2

$$V_2(x) = \sqrt{\frac{2}{\pi}}\left(\frac{x^4}{60} + \frac{5}{12}\ x^2 + \frac{23}{16}\right) \tag{77}$$

$$V_2(0) = \frac{23}{16}\sqrt{\frac{2}{\pi}} = 1.016\ V(0) \tag{78}$$

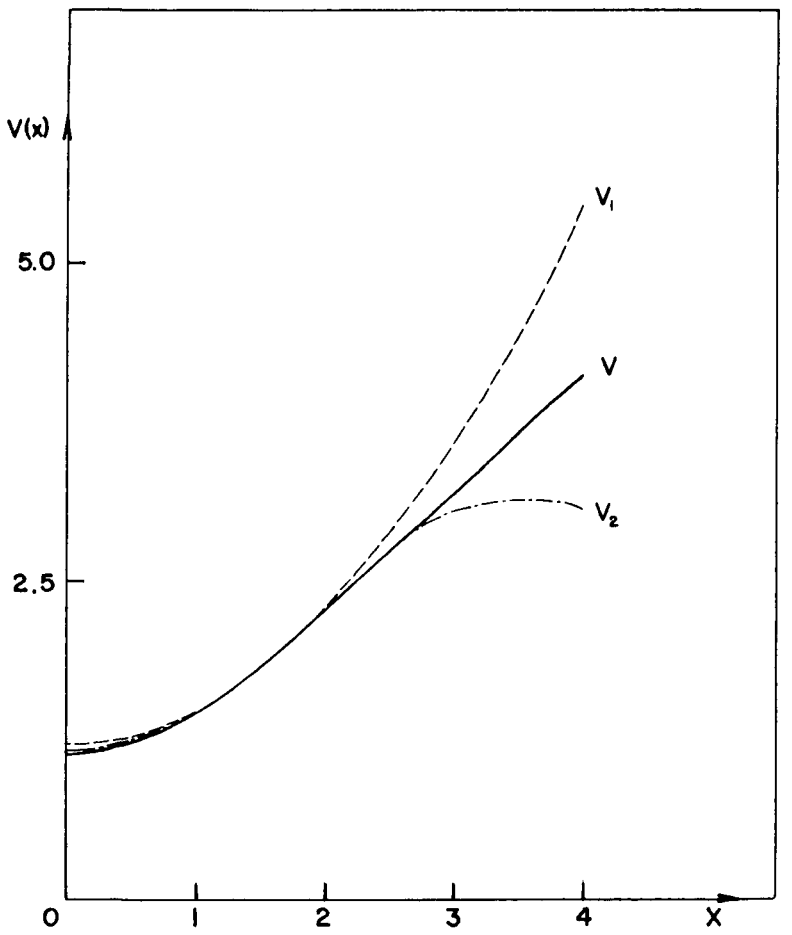

Figure 1

The magnitude V(0) is important because it is equal to the value of λ which separates the discrete spectrum from the continuum.

Next we are going to calculate α_1 and $\omega(\alpha)$ for the case K = 1. Eq. (34) reduces to

$$10B_2(\alpha_1) - 11B_1(\alpha_1) = 0 \tag{79}$$

where

$$B_n(\alpha_1) = \int_0^\infty \frac{e^{-x^2} x^{2n}}{x^2 + \alpha_1} \, dx \tag{80}$$

The B_n are related by the recursion relation

$$B_n(\alpha_1) = (-\alpha_1) B_{n-1}(\alpha_1) + \frac{1}{2} \Gamma (n - \tfrac{1}{2}) \tag{81}$$

and

$$B_o(\alpha_1) = \frac{\pi}{2} e^{\alpha_1} \operatorname{erfc} (\sqrt{\alpha_1}) \frac{1}{\sqrt{\alpha_1}} \tag{82}$$

Thus α_1 is the root of the transcendental equation

$$\sqrt{\pi} \sqrt{\alpha_1} e^{\alpha 1} \operatorname{erfc} \sqrt{\alpha_1} = \frac{0.6 + \alpha_1}{1.1 + \alpha_1} \tag{83}$$

It is found $\alpha_1 = 1.23$ or

$$\lambda_1 = (4.50 - 1.23) \frac{1}{3} \sqrt{\frac{2}{\pi}} = 0.77 \sqrt{\frac{2}{\pi}} \tag{84}$$

Now, in order to calculate $\omega(\alpha)$, again it is preferable to use the variable $y = x^2$. From eq. (42) it follows

$$\omega(\alpha) = - \frac{e^{\alpha/2}}{b \sqrt{\alpha}} \int_0^\infty \frac{g_1(y)dy}{y-\alpha} \tag{85}$$

For K = 1

$$\sqrt{\frac{\pi}{2}}\, g_1(y) = \frac{\pi^{-1/4}}{2\sqrt{6}} \quad (10y - 11)\sqrt{y}\, e^{-y/2} \tag{86}$$

$$b = \frac{1}{3}\sqrt{\frac{2}{\pi}} \tag{87}$$

Consequently

$$\omega(\alpha) = -\frac{e^{\alpha/2}}{\sqrt{\alpha}} \sqrt{\frac{3}{2}}\, \pi^{-1/4} \quad \left[10\, B_2(-\alpha) - 11\, B_1(-\alpha)\right] \tag{88}$$

where now the $B_n(-\alpha)$ are principal values:

$$B_n(-\alpha) = \frac{1}{2} \oint_0^\infty \frac{e^{-y}\, y^{n-1}\, \sqrt{y}\, dy}{y - \alpha} \tag{89}$$

Again we have the recursion relation

$$B_n(-\alpha) = \alpha\, B_{n-1}(-\alpha) + \frac{1}{2}\, \Gamma\left(n - \frac{1}{2}\right) \tag{90}$$

Let us calculate $B_1(-\alpha)$

$$2B_1(-\alpha) = \oint_0^\infty \frac{e^{-y}\sqrt{y}\, dy}{y - \alpha} = \int_0^\infty \frac{e^{-y} dy}{\sqrt{y} + \sqrt{\alpha}} + \sqrt{\alpha} \oint_0^\infty \frac{e^{-y} dy}{y - \alpha} = I_1 + \sqrt{\alpha}\, I_2$$

For I_2 we have

$$I_2 = e^{-\alpha} \oint_{-\alpha}^\infty \frac{e^{-t} dt}{t} = e^{-\alpha} \left[\int_\alpha^\infty \frac{e^{-t} dt}{t} - 2 \int_0^\alpha \frac{\mathrm{sh}\, t\, dt}{t}\right]$$

or

$$I_2 = e^{-\alpha} \left[E_1(\alpha) - 2\, \mathrm{Shi}(\alpha)\right]$$

The two integrals in the bracket are tabulated functions.

I_1 has to be evaluated numerically.

Conclusions

It has been shown that in general the time and energy dependent Boltzmann equation can be solved by separation of the variables only if a continuum of singular eigenvectors is introduced. Besides this continuum there also is a discrete spectrum of regular eigenfunctions. When the scattering kernel is approximated by K+1 terms of a double expansion in

orthogonal functions the number of regular eigenfunctions is at most K+1. The value $\lambda = (\Sigma_s v)$ min separates the discrete spectrum from the continuum. The completeness of the whole set of eigenvectors has been proved for K=1.

Concerning the accuracy of the present method, it should be emphasized that only the expansion of the scattering kernel is truncated after a finite number of terms. The solution corresponding to any truncated kernel is exact.

APPENDIX A

Proof that eq. (18) has at most K + 1 roots λ_i

Let us assume the symmetrized scattering kernel $S(x|x')$ is positive definite and consider the eigenvalue problem

$$\psi(x) = \frac{\gamma}{V(x)-\lambda} \int S(x|x')\,\psi(x')\,dx' \qquad \text{(A-1)}$$

where now λ is just a parameter, γ being the eigenvalue. Again, if $S(x|x')$ is approximated by (5), eq. (A-1) is equivalent to the system:

$$\tau_j = \gamma \sum_{l=o}^{K} K_{jl}^{\lambda}\,\tau_l \qquad j = 0,1,\ldots K \qquad \text{(A-2)}$$

$$\text{with } \tau_j = \int \psi(x)\,\mu_j(x)dx$$

It is known that there are at most K+1 values γ_i which satisfy eq. (A-2) and that for λ=0, the lowest one must be

$$\left[\gamma_o\right]_{\lambda=o} = 1 \qquad \text{(A-3)}$$

yielding

$$\left[\psi_o\right]_{\lambda=o} = \mu o$$

It follows that if we can show that the γ_i decrease monotonically for increasing values of λ, for each γ_i there can be only one λ_i such that γ_i= 1 and the thesis would be proved.

Now

$$\gamma_i = \frac{\int \psi_i^2(x)\,\left[V(x) - \lambda\right]\,dx}{\iint \psi_i(x)\psi_i(x')S(x|x')\,dxdx'} \qquad (A-4)$$

and from the variational principle

$$\left[\delta\gamma_i\right]_{\lambda=\text{ const}} = 0 \qquad (A-5)$$

it follows that

$$\delta\gamma_i = - \frac{\int \psi_i^2 \, V(x)dx}{\iint \psi_i(x)\, \psi_i(x')S(x|x')\, dxdx'} \delta\lambda \qquad (A-6)$$

Hence the thesis is proved if $S(x|x')$ is a positive definite kernel.

APPENDIX B

Laplace transform method

Taking the Laplace transform of

$$\frac{\partial N(x,t)}{\partial t} = - N(x,t)V(x) + \int N(x',t)S(x|x')dx + \delta(t)Q(x) \qquad (B\text{-}1)$$

it is found

$$\bar{N}(x,p)\left[p + V(x)\right] = \int \bar{N}(x',p)S(x|x')dx' + Q(x) \qquad (B\text{-}2)$$

Using the same expansions as above, this eq. is equivalent to the system

$$\phi_k(p) = \sum_{j=o}^{K} \phi_j(P) \int \frac{f_j(x)\ \mu_k(x)}{V(x) + p}\, dx + \int \frac{Q(x)\ \mu_k(x)}{V(x) + p}\, dx \qquad (B\text{-}3)$$

or

$$\sum_{j=o}^{K} \phi_j(p) \left[K_{kj}(-p)-\delta_{kj}\right] + Q_k(p) = 0 \quad k = 0,1,\ldots K \qquad (B\text{-}4)$$

This system can be solved yielding $\bar{N}(x,p)$. Then

$$N(x,t) = \frac{1}{2\pi i} \int_{a-i\infty}^{a+i\infty} e^{pt}\, \bar{N}(x,p)dp \qquad (B\text{-}5)$$

where a is to the right of all singularities of $\bar{N}(x,p)$. These singularities are obviously poles at $p= -\lambda_i$ and a cut from $p = -V_o$ to $p = -\infty$. Therefore the pass of integration can be deformed as shown in Fig. 2 (for K=1)

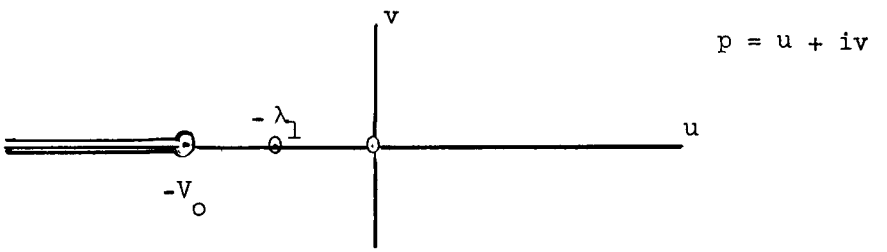

Fig. 2

The integration around the poles yields the terms

$$A_n N_n(x)\, e^{-\lambda_n t}$$

which correspond to the discrete eigenfunctions, $A_n N_n(x)$ being the residue of $\bar{N}(x,p)$ at $p = -\lambda_n$

The integration along the cut yields the contribution of the continuum of singular eigenfunctions.

ACKNOWLEDGEMENTS

The author wishes to express his appreciation for valuable discussions with M. Nelkin.

REFERENCES

1. N. G. Van Kampen, Physica 21, 949 (1955).
2. K. M. Case, Ann. Phys. (N.Y.) 9, 1 (1960).
3. J. R. Mika, Nucl. Sci. Eng. 11, 415 (1961).
4. N.I. Muskhelishvili, "Singular Integral Equation" Noordhoff, Groningen (1953).
5. B. Bailly du Bois, J. Horowitz, C. Maurette, Rapport SPM525 (Saclay 12/11/1958).

THERMAL DIFFUSION OF NEUTRONS

I. Kuščer

Institute of Physics, University of Ljubljana,
Ljubljana, Yugoslavia

ABSTRACT

The influence of temperature differences upon stationary neutron distributions in extended nonabsorbing media is studied for two cases. In the case with a plane temperature discontinuity in an otherwise uniform medium some information is obtained by aid of an integral of the transport equation. A more general treatment by a simple P_1 approximation is possible if the temperature is a slowly varying function of the coordinates. The general aspects of this case are known from the theory of thermal diffusion, and the results of this theory are easily taken over and adapted to the specific assumptions of neutron transport theory. Expressions are given, by which the thermal diffusion factor, along with the coefficient for ordinary diffusion of thermal neutrons, can be calculated for any given scattering law.

1. INTRODUCTION

The influence of temperature differences upon stationary distributions of thermal neutrons in nonabsorbing media has been subject of several recent papers (1-3). Kottwitz (1) considered an infinite heavy monatomic gaseous medium with a single plane temperature discontinuity. Using a modified age equation of Hurwitz et. al. (4) he derived among others the interesting result that the neutron flux ψ is constant throughout the medium, so that the neutron number density ($n = \psi/\bar{v}$, with $\bar{v} = \sqrt{8kT/\pi m}$) is greater on the colder side by a factor of $\sqrt{T_2/T_1}$ (where $T_2 > T_1$).

Kottwitz compares this effect to the thermal transpiration effect, associated with gas flow through a narrow hole (5). When carrying this comparison further, one should note that neutrons in a heavy medium only slowly accomodate to the temperature change after passing through the discontinuity, and hence have much chance to be reflected before accomodation - similarly as a gas molecule is likely to be reflected when hitting a wall with a very small hole. Consequently we may expect that the case with neutrons in a medium with very light atoms should be comparable to the case of a gas flow through a large hole, where the pressure becomes equal on both sides, so that the ratio of the number densities is $n_2/n_1 = T_1/T_2$, and therefore $\psi_2/\psi_1 = \sqrt{T_1/T_2}$. The general case should lie between both extremes:

$$p_2/p_1 = (T_2/T_1)^{\alpha}\ ,\quad n_2/n_1 = (T_1/T_2)^{1-\alpha},\quad \psi_2/\psi_1 = (T_1/T_2)^{\frac{1}{2}-\alpha}\ ,$$

with $0 < \alpha \leq \frac{1}{2}$.

Another promising comparison can be made if the thermal neutrons and the medium are considered as a mixture of two substances, in which a difference in concentration is produced by the temperature difference. This phenomenon is known as thermal diffusion. The theory of this effect in gases (6 - 9) can be directly applied to the neutron case, if the temperature discontinuity is smeared out over an interval of at least several neutron mean free paths, so that the second approximation of Enskog and Chapman, or, to say it otherwise, the P_1 or diffusion approximation, is applicable. For a gaseous medium under uniform pressure the relative neutron concentration, that is the ratio of the number densities of the neutrons and the atoms, is found (8) to be proportional to T^{α} , where α is the thermal diffusion factor. Hence the neutron number density is proportional to $T^{-(1-\alpha)}$, and

$$\psi \propto T^{-(\frac{1}{2}-\alpha)} , \qquad (1)$$

Chapman (6,7,9) derived a general formula for the first approximation to α . The case of neutrons in a nonabsorbing monatomic gas with the usual scattering properties (4) corresponds to a binary gaseous mixture with classical smooth hard spherical molecules, where one component is present in a very small concentration and the molecules of this component are much smaller in size than of the other. For this case Chapman's approximation reduces to

$$\alpha \approx \frac{5\,M\,(M+1)}{13\,M^2 + 16\,M + 30}\,, \qquad (2)$$

where M is the ratio of the atomic masses of the medium and the neutrons. With increasing M the approximate value of α increases from $\alpha \approx 10/59 = 0{,}1695$ for M = 1* to $\alpha \approx 5/13 = 0{,}385$ for $M = \infty$. Whereas the first value can be expected to be nearly correct, the second is known to be too low –

– as in this case the exact value of the thermal diffusion factor is (6): $\alpha = \frac{1}{2}$. This value applies to the case of Kottwitz, where, in agreement with equation (1), the neutron flux is constant.

It seems worth while to extend both mentioned problems, that of Kottwitz and that with slowly varying temperature, to media with more general scattering properties, and to base the derivations as far as possible upon transport theory. Before beginning with this task it seems useful to recall some general facts about the scattering characteristics of the medium and the properties of a function which occurs in the theory of diffusion of thermal neutrons.

---

*One might expect that in case of equal masses (M = 1) the factor α should vanish. However, this does not occur because of the different mean free paths of the gas atoms and the neutrons.

2. THE SCATTERING PROPERTIES OF THE MEDIUM

The scattering properties of the medium, which is supposed to be nonabsorbing, are characterized by the mean free path $\ell(u)$ and the scattering funtion $f(u \to u', \cos \Theta)$. It is convenient to use here the dimensionless "reduced velocity" u $\beta v = \sqrt{m/2kT} \cdot v$, where T is the temperature of the medium at the place considered. The scattering function expresses the probability per unit interval du' and per unit solid angle that a neutron of initial reduced velocity u acquires the reduced velocity u' and is deviated through an angle Θ, when scattered. An important general property of the scattering function is expressed by the detailed balance relation

$$\ell^{-1}(u)u^3 e^{-u^2} f(u \to u', \cos \Theta) = \ell^{-1}(u')u'^3 e^{-u'^2} f(u' \to u, \cos \Theta).$$

Often we need the Legendre development of the scattering function

$$f(u \to u', \cos \Theta) = \frac{1}{4\pi} \sum_{n=0}^{\infty} (2n + 1)\, f_n(u \to u')\, P_n(\cos \Theta),$$

and of its azimuthal integral,

$$f(u, \mu \to u', \mu') = \int_0^{2\pi} f(u \to u', \cos \Theta)\, d\varphi = \frac{1}{2} \sum_{n=0}^{\infty} (2n+1) f_n(u \to u') P_n(\mu) P_n(\mu').$$

It may happen that for two media the functions $\ell(u)$ differ only by a constant factor and that the scattering function is the same. Such is the case if both media consist of the same monatomic gas at different temperatures and pressures. We shall say in such cases that

both media have the same scattering characteristics.

Let us briefly remember a few facts about ordinary diffusion of thermal neutrons. If the medium is uniform, a stationary neutron distribution with a linear gradient can be expressed by the following solution of the transport equation:

$$\phi(z,v,\mu) = \beta^4 v^3 e^{-\beta^2 v^2}\left[C_1 + C_2\left\{ z - \mu\, U(\beta v)\right\}\right] . \qquad (3)$$

Herein ϕ is the neutron flux per unit velocity interval and per unit solid angle, C_1, C_2 are arbitrary constants, and U(u) is the solution of (10, 11)

$$U(u) = \ell(u) + \int_0^\infty f_1(u \rightarrow u')U(u')du'. \qquad (4)$$

In this case the net current,

$$J = 2\pi \int_0^\infty\int_{-1}^{1} \phi(z,v,\mu)\, \mu\, dv\, d\mu,$$

and the gradient of the neutron flux ψ,

$$\psi = 2\pi \int_0^\infty\int_{-1}^{1} \phi(z,v,\mu)\, dv\, d\mu,$$

or of the number density $n = \psi/\bar{v}$, are related through

$$J = -\frac{1}{3}\bar{U}\cdot\frac{d\psi}{dz} = -D\frac{dn}{dz}, \qquad (5)$$

where

$$\bar{U} = 2\int_0^\infty U(u)u^3 e^{-u^2} du, \qquad (6)$$

and

$$D = \frac{1}{3}\bar{U}\bar{v}. \qquad (7)$$

We observe that $\bar{U}$ plays the role of an average transport mean free path.

For the monatomic gas model the behaviour of the function U(u) is ~~roughly~~ approximately known (11), although numerical data exist only for the case M = 1 (10). U(u) is an odd monotonous function, a qualitative picture of which could be given by $U(u) \approx U(\infty) \cdot \ell(u)/\ell(\infty)$ or by $U(u) \approx \frac{2}{\pi} U(\infty) \operatorname{arctg}(u/a)$, with $U(\infty) = \ell(\infty)\left[1 - 2/(3M)\right]^{-1}$, and with a roughly proportional to $M^{-\frac{1}{2}}$.

As M increases U(u) approaches a step function: $U(u) = \ell = \text{const.}$ for $M = \infty$ and $u > 0$. The average $\bar{u}$ has the value 1,273 $\ell(\infty)$ for M = 1 (6, 10, 11), and for large M is given by $\bar{u} \approx \left[1 + 1/(6M)\right]\ell(\infty)$ (11).

3. Integrals of the transport equation

The subsequent considerations will be restricted to the plane case where the composition and temperature of the medium, as well as the neutron flux depend upon one coordinate only, z say. For a nonabsorbing medium with no sources and for a stationary axially symmetric flux distribution the transport equation reads as follows:

$$\mu \frac{\partial \phi(z,v,\mu)}{\partial z} + \ell^{-1}(z,\beta v)\,\phi(z,v,\mu) = \int_0^{\infty}\int_{-1}^{1} \beta \ell^{-1}(z,\beta v')\,\phi(z,v',\mu')\,f(z;\beta v',\mu' \to \beta v,\mu)\,dv'd\mu'. \quad (8)$$

Multiplying both sides of (8) by $dvd\mu$, and integrating, we verify that the net current J is constant.

According to the problem under investigation we shall assume that J = 0.

If neither ℓ nor f depend upon z, the so called K-integral (12),

$$K(z) = 2\pi \int_0^{\infty} \int_{-1}^{1} \phi(z,v,\mu) U(z,v) \mu^2 \, dv \, d\mu, \tag{9}$$

satisfies the equation

$$\frac{d\,K(z)}{dz} = -J, \tag{10}$$

which is deduced from (8). This means that in our case K is constant within every region of uniform composition and temperature.

4. THE CASE WITH A TEMPERATURE DISCONTINUITY

Following Kottwitz we consider two adjacent halfspaces, each filled with a macroscopically uniform nonabsorbing medium, one ($-\infty < z < 0$) of temperature T_1, and the other ($0 < z < \infty$) of temperature $T_2 > T_1$. The functions ℓ, f, U may be different for both media and will be distinguished by the subscripts 1 and 2. Each medium has its own K-integral (K_1 = const. for $z < 0$ and K_2 = const. for $z > 0$).

At great distances from the discontinuity the neutron distribution is Maxwellian,

$$\phi(-\infty, v, \mu) = (2\pi)^{-1} \psi(-\infty) \cdot \beta_1^4 v^3 \exp(-\beta_1^2 v^2),$$

$$\phi(\infty, v, \mu) = (2\pi)^{-1} \psi(\infty) \cdot \beta_2^4 v^3 \exp(-\beta_2^2 v^2).$$

We are primarily interested in the determination of the ratio of the fluxes $\psi(\infty)$ and $\psi(-\infty)$, and to find out how this ratio depends upon the ratio of the temperatures and upon the scattering properties of both media.

If the constants K_1 and K_2 are expressed by $\phi(z,v,\mu)$ at $z = -\infty$, $z = 0$, and $z = \infty$, the following equations are obtained:

$$\frac{1}{3}\bar{U}_1 \psi(-\infty) = 2\pi \int_0^\infty \int_{-1}^1 \phi(0,v,\mu)\, U_1(\beta_1 v)\, \mu^2 dv\, d\mu,$$

$$\frac{1}{3}\bar{U}_2 \psi(\infty) = 2\pi \int_0^\infty \int_{-1}^1 \phi(0,v,\mu)\, U_2(\beta_2 v)\, \mu^2 dv\, d\mu.$$

The right-hand sides of these equations are proportional to the averages of $U_1(\beta_1 v)$ and $U_2(\beta_2 v)$ over the unknown distribution $\phi(0,v,\mu)$. Denoting these averages by $\langle U_1 \rangle_0$ and $\langle U_2 \rangle_0$, we may write

$$\frac{\psi(\infty)}{\psi(-\infty)} = \frac{\bar{U}_1}{\langle U_1 \rangle_0} \cdot \frac{\langle U_2 \rangle_0}{\bar{U}_2}. \qquad (11)$$

If both media contain only infinitely heavy atoms, U_1 and U_2 are constants and therefore $\psi(\infty) = \psi(-\infty)$, in agreement with Kottwitz.

For finite atomic masses a general conclusion ~~is~~ can be obtained if $U(u)$ increases with increasing u (as in the case of the monatomic gas). We see then that the average of $U_1(\beta_1 v)$ over the "proper" Maxwellian distribution at T_1 must be smaller than the average over the "hotter" distribution $\phi(0,v,\mu)$. Similarly $\bar{U}_2 > \langle U_2 \rangle_0$. Hence

$$\frac{\psi(\infty)}{\psi(-\infty)} < 1,$$

i.e., the flux is smaller on the warmer side.

In order to obtain an estimate for the ration $\psi(\infty)/\psi(-\infty)$ we may, according to Kottwitz (1), approximate $\phi(0,v,u)$ either by a Maxwellian distribution at some medium temperature $\bar{T}$, or by a mixture of two Maxwellian distributions at T_1 and T_2. If both media have equal scattering characteristics and if the temperatures are not too diferent, a 1 : 1 mixture seems adequate, and we obtain

$$\frac{\psi(\infty)}{\psi(-\infty)} \approx \frac{\bar{U} + \langle U_2 \rangle_1}{\bar{U} + \langle U_1 \rangle_2},$$

where $\bar{U}$ stands for $\bar{U}_1 = \bar{U}_2$, and $\langle U_1 \rangle_2$ and $\langle U_2 \rangle_1$ are the averages of $U(\beta_1 v)$ and $U(\beta_2 v)$ over the "wrong" Maxwellian distributions at T_2 and T_1, respectively, e.g.,

$$\langle U_2 \rangle_1 = 2 \int_0^\infty U(u) \cdot (\beta_1/\beta_2)^4 u^3 \exp\left[-(\beta_1/\beta_2)^2 u^2\right] du.$$

For a small temperature difference this can be approximated by

$$\langle U_2 \rangle_1 \approx \bar{U}\left[1 - 2\,(\Delta T/T)\,(\bar{\bar{U}}/\bar{U} - 1)\right],$$

where

$$\bar{\bar{U}} = \int_0^\infty U(u) u^5 e^{-u^2} du.$$

With a similar expression for $\langle U_{12} \rangle$ we obtain finally

$$\frac{\psi(\infty)}{\psi(-\infty)} \approx 1 - 2 \frac{\Delta T}{T} \left(\frac{\bar{\bar{U}}}{\bar{U}} - 1 \right)$$

This is in accord with (1) if we put

$$\alpha = \frac{5}{2} - 2\bar{\bar{U}}/\bar{U}. \qquad (12)$$

For a monatomic gas with $M = \infty$ obviously $\bar{U} = \bar{\bar{U}}$, and therefore again $\alpha = \frac{1}{2}$.

5. MEDIUM WITH SLOWLY VARYING TEMPERATURE

And simpler and much more general treatment than in the previous case is possible, if the temperature of the medium only slowly varies with z, i.e., if $\bar{l}\ \mathrm{dln}\ T/dz \ll 1$, where $\bar{l}$ is some average mean free path. In such cases a P_1 approximation can be used, if boundary regions are excluded. The velocity distribution is almost Maxwellian. This must be true also if the composition of the medium is not uniform, since in any case with uniform temperature the Maxwellian distribution ($\phi \propto v^3 e^{-\beta^2 v^2}$) represents a solution of the transport equation.

We try to solve equation (8), where $\beta = \beta(z)$, by an approximation of the form

$$\phi(z,v,\mu) = (2\pi)^{-1}\left[\psi_0(z,v) + \mu\psi_1(z,v)\right]\beta^4(z)v^3\exp\left[-\beta^2(z)v^2\right]. \quad (13)$$

A system of two equations follows for the coefficients ψ_0 and ψ_1:

$$\frac{1}{3}\left[\frac{\partial\psi_1(z,v)}{\partial z} + \gamma(4 - 2\beta^2v^2)\psi_1(z,v)\right] + \bar{l}^{-1}(z,\beta v)\psi_0(z,v)$$
$$= \int_0^\infty \bar{l}^{-1}(z,\beta v)\beta f_0(z,\beta v\to\beta v')\psi_0(z,v')dv', \quad (14)$$

$$\left[\frac{\partial\psi_0(z,v)}{\partial z} + \gamma(4 - 2\beta^2v^2)\psi_0(z,v)\right] + \bar{l}^{-1}(z,\beta v)\psi_1(z,v)$$
$$= \int_0^\infty \bar{l}^{-1}(z,\beta v)\beta f_1(z,\beta v\to\beta v')\psi_1(z,v')\,dv', \quad (15)$$

where the abbreviation $\gamma = \gamma(z) = \mathrm{dln}\,\beta/dz = -\frac{1}{2}\,\mathrm{dln}\,T/dz$ has been introduced.

A restriction for ψ_1 is immediately apparent, if the net current is written down, which, according to our assumption, vanishes:

$$J = \frac{2}{3}\int_0^\infty \psi_1(z,v)\beta^4 v^3 \exp(-\beta^2 v^2)dv = 0. \qquad (16)$$

We know that the homogeneous equation obtained from (14) by omitting the first term has a non-trivial solution $\psi_0(z,v) = \psi(z)$, corresponding to a strictly Maxwellian distribution. Hence equation (14) is soluble only if the first term satisfies a certain orthogonality condition. It turns out that this condition has the form $dJ/dz = 0$, with the expression in (16) substituted for J, and therefore is satisfied automatically if ψ_1 obeys eq. (16).

Since ψ_1 is small compared to ψ_0, the first term in (14) is small of the second order ($\sim O(l^2\gamma^2\psi)$), and up to this order the solution of (14) must be equal to the solution of the homogeneous equation: $\psi_0(z,v) = \psi(z)$. When this is introduced into equation (15), its solution can be expressed in the following form:

$$\psi_1(z,v) = -\left[\frac{d\psi(z)}{dz} + 4\gamma\psi(z)\right] U(z,\beta v) + 2\gamma\psi(z)\, V(z,\beta v). \qquad (17)$$

As indicated the function U, a solution of (4), now may depend also upon z. V is the solution of a similar equation:

$$V(z,u) = u^2 l(z,u) + \int_0^\infty f_1(z,u\to u')V(z,u')\,du'. \qquad (18)$$

After substituting the right-hand side of (17) into (16) we obtain a differential equation for $\psi(z)$, which

is conveniently written in the form (6)

$$\frac{d\,\ell n\psi(z)}{dz} = -\left[\frac{1}{2} - \alpha(z)\right]\frac{d\ell n\, T(z)}{dz}, \qquad (19)$$

where $\alpha(z) = \frac{5}{2} - \bar{V}(z)/\bar{U}(z)$, and

$$\bar{V}(z) = 2\int_0^\infty V(z,u)\, u^3 e^{-u^2} du.$$

Multiplying both sides of equation (18) by $\ell^{-1}(z,u)\,U(z,u)u^3 e^{-u^2} du$, and integrating, we verify that $\bar{V}(z) = 2\,\bar{\bar{U}}(z)$, so that the thermal diffusion factor can be expressed by the averages of U alone, namely by equation (12).

Let us ~~also~~ recall the special case when the whole medium has uniform scattering characteristics, so that α = const. Then the solution of (19) has the simple form mentioned by equation (1).

Our initial restriction to the plane case with no net current has helped to simplify the above deductions somewhat. However, generalizations to three dimensional problems[5] and to cases with non-vanishing net current immediately suggest themselves. A general diffusion equation, which accounts for combined ordinary and thermal diffusion, should have the form (cf. the above equations (5) and (19))

$$\underline{J} = -\frac{1}{3}\bar{U}\left[\operatorname{grad}\psi + \left(\frac{1}{2} - \alpha\right)(\psi/T)\operatorname{grad} T\right]. \qquad (20)$$

Such equations are well known from phenomenological theories of these transport phenomena (13).

6. THE DUFOUR EFFECT

An alternative deduction of the formula (12) for the thermal diffusion factor can be achieved, if we cosider the Dufour effect, that is the heat flow associated with diffusion (13). Though with neutrons the effect in unobservably small even for the highest available fluxes, it deserves some interest because of its relationship to thermal diffusion.

The effect is described by the equation

$$\underline{I} = - C \operatorname{grad} \psi \ , \tag{21}$$

where $\underline{I}$ is the flow of kinetic energy, transported by neutrons in a medium of uniform temperature, and C may be called the Dufour coefficient. In order to find an expression for this coefficient, we consider an extended medium of uniform composition and uniform temperature, in which a stationary neutron distribution of the type described by equation (3) is set up. The net flow of kinetic energy of the neutrons is

$$I = 2\pi \int_0^\infty \int_{-1}^{1} \tfrac{1}{2} m v^2 \phi(z,v,\mu)\, \mu \, dv \, du$$

$$= - \tfrac{4}{3} \pi \bar{\bar{U}} k T C_2 = - \tfrac{2}{3} \bar{\bar{U}} k T \frac{d\psi}{dz} \ .$$

We see that

$$C = \tfrac{2}{3} \bar{\bar{U}} \, k \, T. \tag{22}$$

On the other hand the coefficients for diffusion, thermal diffusion and the Dufour effect can be expressed

by the quantities L_{11}, L_{ul} and L_{lu}, used by de Groot (13). Comparing his equations (13, pp. 113-119) with the above equations (20) and (21), and taking into account some modifications valid for the neutron gas in a medium at rest, we verify that

$$\frac{1}{3}\bar{U} = L_{11}(kT/m^2)\psi^{-1},$$

$$\frac{1}{3}\bar{U}\left(\frac{1}{2} - \alpha\right)\psi = L_{lu}/m - L_{11} \cdot 2kT/m^2 \quad ,$$

$$C = L_{ul}(kT/m)\psi^{-1}.$$

Observing that, according to the reciprocity principle of Onsager (13), $L_{lu} = L_{ul}$, we find $\frac{1}{2} - \alpha = 3\,C/(kT\,\bar{U}) - 2$. Then, in view of eq. (22), again equation (12) ensues.

REFERENCES

1. D.A. Kottwitz, Nuclear Sci. and Eng. 7, 345 (1960).
2. R.A. Bennett and Heinemann R.E., Nuclear Sci and Eng. 8, 294 (1960).
3. D.S. Selengut, Nuclear Sci. and Eng. 9, 94 (1961)
4. H, Hurwitz, Jr., M.S. Nelkin, and G.J. Habetler, Nuclear Sci. and Eng. 1, 280 (1956).
5. E.H. Kennard, "Kinetic Theory of Gases," McGraw-Hill Publ. Co., New York and London, 1938.
6. S. Chapman and T.G. Cowling, "The Mathematical Theory of Non-Uniform Gases." Cambridge Univ. Press, 1939.
7. S. Chapman, Proc. Roy Soc. A 177, 38 (1940).
8. R.C. Jones and W.H. Furry, Rev. Mod. Phys. 18, 151 (1946).
9. L. Waldmann, Encyclopaedia of Physics, ed by H. Flügge, Vol. XII, Springer, Berlin etc.,1958.
10. C.L. Pekeris, Proc. Nat. Acad. Sci. US 41, 661(1955).
11. I. Kuščer and M. Ribarič, Nuovo Cimento 7, 451 (1958).
12. R. Kladnik and I. Kuščer, Nuclear Sci. and Eng. 11, 116 (1961).
13. S.R. de Groot, "Thermodynamics of Irreversible Processes." North-Holland Publ.Co., Amsterdam, 1951.

CONFERENCE ON NEUTRON THERMALIZATION

BROOKHAVEN NATIONAL LABORATORY

UPTON, L.I., N.Y. - APRIL 30 - MAY 2, 1962

THE MODIFIED HEAVY GAS MODEL AND TWO THERMAL GROUP RETHERMALIZATION THEORY

C. W. Lindenmeier

Hanford Laboratories Operation
General Electric Company
Richland, Washington

The heavy gas model and associated Wilkins equation are particularly attractive for deriving neutron spectra since the usual integral expression involving the scattering kernel is replaced by a simple differential operator. The resulting model, however, does not give an adequate description for materials and energies where binding effects are important.

As reported by Triplett[1], Horowitz has proposed modifying the heavy gas thermalization model by allowing the slowing-down power to be a function of energy. This type of modification has two virtues. It preserves detailed balancing, and it generates a Maxwellian distribution in the limit of no neutron losses. The functional form of such a modification should be obtainable either from experiments or from the theoretical scattering kernel (when known) of the material in question. However, since the modified gas model only approximates the actual scattering behavior of the material, only certain features of the scattering kernel can be retained. As we will discuss, analysis of rethermalization experiments indicates that the cross section weighted average energy loss per collision is the important quantity in a slowing-down process. We, therefore, choose to modify the heavy gas model so that the cross section

weighted average energy loss per collision from an arbitrary Maxwellian spectrum is correctly reproduced. This allows a unique determination of the required variation in slowing down power from either the scattering kernel or from re-thermalization experiments.

To investigate the accuracy of the modified gas model, we have calculated the modification to the Wilkins equation using the kernel code KRYOS-II[2] and have compared the spectrum calculated directly from the kernel by the code SPECTRUM[2] with the spectrum obtained from the modified Wilkins equation. The solution to the modified Wilkins equation is obtained by iterating. In deriving a spectrum, we are free to choose the ratio of absorption to slowing down power for the system. In order to compare theory with experiment, as well as the direct spectrum calculation with the modified gas calculation, we have used a parameter characteristic of the system whose spectrum was measured by Coates and Gayther[4]. The two theoretical spectra and the experimental results agree with one another to within a few percent.

The importance of the cross section weighted average energy loss per collision is particularly evident in rethermalization phenomena. As noted by Selengut[5] rethermalization can be treated with two thermal groups, having Maxwellians as trial spectra. However, to obtain meaningful results one must not only require neutron balance but energy balance as well. A recent paper by Selengut[6] discusses energy balance in a two-group analysis, and derives the following two-group equations:

$$\begin{aligned} -D_1 \nabla^2 \phi_1 + (\Sigma_{a1} + \Sigma_{1\to 2})\,\phi_1 &= \Sigma_{12}\,\phi_2 + S_1 \\ -D_2 \nabla^2 \phi_2 + (\Sigma_{a2} + \Sigma_{2\to 1})\,\phi_2 &= \Sigma_{21}\,\phi_1 + S_1 \end{aligned} \qquad (1)$$

where

$$\Sigma_{2\to1} = \frac{\Delta E_2}{E_{D2}-E_{D1}}\ \Sigma_{s2} - \frac{E_{D2}-E_{a2}}{E_{D2}-E_{D1}}\ \Sigma_{a2}$$

$$\Sigma_{1\to2} = \frac{-\Delta E_1}{E_{D2}-E_{D1}}\ \Sigma_{s1} - \frac{E_{a1}-E_{D1}}{E_{D2}-E_{D1}}\ \Sigma_{a1} \qquad (2)$$

$$S_1 = \frac{E_{D2}-E_s}{E_{D2}-E_{D1}}\ S \qquad S_2 = \frac{E_s-E_{D1}}{E_{D2}-E_{D1}}\ S$$

$$\Sigma_{an} = \int \Sigma_a(E)\ \chi_n(E)\ dE \qquad S = \int S(E)\ dE$$

$$D_n = \int D(E)\ \chi_n(E)\ dE \qquad E_{Dn} = \int E\ D(E)\ \chi_n(E)\ dE/D_n \qquad (3)$$

$$\Sigma_{sn} = \int \Sigma_s(E)\ \chi_n(E)\ dE \qquad E_s = \int S(E)\ E\ dE/S$$

$$\Delta E_n = \int dE \int dE'\ (E-E')\ \Sigma_s(E\to E')\ \chi_n(E)/\Sigma_{sn}$$

The $\chi_n(E)$ represent trial spectra, $S(E)$, $D(E)$, $\Sigma_a(E)$, and $\Sigma_s(E)$ are, respectively, source, diffusion coefficient, absorption cross section, and scattering cross section. $\Sigma_s(E\to E')$ is the scattering kernel.

Bennett[7] has analyzed his rethermalization experiments by fitting the parameters $\Sigma_{1\to2}$ and $\Sigma_{2\to1}$ in equation (1) to reproduce the experimentally obtained activity traverses. He refers to these transfer cross sections as rethermalization cross sections. More details may be found in Bennett's paper. In graphite, since the absorption cross sections are small, the quantities of interest are the ΔEn's, and in a sense they are the quantities that rethermalization experiments measure. It should be noted that E_n is the average energy loss in a collision by an average neutron in group n. Note that we can also write

$$\Delta E_n = \int dE\ \overline{\Delta E}(E)\ \Sigma_s(E)\ \chi_n(E)/\Sigma_{sn}, \tag{4}$$

where

$$\overline{\Delta E}(E)\ \Sigma_s(E) = \int dE'\ (E-E')\ \Sigma_s(E \rightarrow E') \tag{5}$$

is the cross section weighted average energy loss by a neutron of energy E in a collision with a moderator nucleus. The quantity (5) has been calculated from the KRYOS code using parameters appropriate for 293 K graphite. Since the KRYOS kernel is normalized to the high energy free atom cross section, it is convenient to define

$$G(E) = \frac{\overline{\Delta E}(E)\ \Sigma_s(E)}{\Sigma_s} \tag{6}$$

where Σ_s is the free atom cross section. The results of the KRYOS calculation are plotted in the form (6) in Figure 1. The corresponding heavy gas expression

$$\overline{\Delta E}(E) = \xi(E-2T) \tag{7}$$

is shown for comparison. For large energies

$$G(E) = .1418E-.01116 \tag{8}$$

If one compares this result with the high energy limit from the gas kernel (see for instance, von Dardel[7]), one finds the coefficient of the E term should be

$$\frac{2A}{(A+1)^2} = .1419 \tag{9}$$

for A = 12.01. Thus, the KRYOS kernel gives the correct high energy behavior.

One can then use expressions (2), (4), and (5) to obtain the rethermalization cross sections for an arbitrary Maxwellian neutron distribution impinging on a region composed of 293 K graphite. (We have approximated, $E_{Dn} \simeq E_n$.) These results are shown in Figure 2. Included is the heavy gas value and the results obtained experimentally by Bennett. The crystalline binding effects taken account of by KRYOS are strongly in evidence.

Since graphite displays crystalline binding effects so strongly, it should provide a good test case for Horowitz' modification to the heavy gas model. The modified heavy gas approximation consists of the replacement

$$-\Sigma_s(E)\,\phi + \int dE'\,\Sigma_s\,(E' \rightarrow E)\,\phi\,(E') = \frac{d}{dE}\left[2\,\frac{\Sigma_o}{M}\,f(E)\left[E\,\phi - T\,\phi + ET\,\frac{\partial \phi}{\partial E}\right]\right] \quad (10)$$

(In the usual heavy gas approximation $f(E) = 1$.) As mentioned, this modification has two very desirable properties. First detailed balance is maintained, in the sense that since

$$\int_0^{\infty} \left[-\Sigma_s\,\phi + \int dE'\,\Sigma_s(E' \rightarrow E)\,\phi(E')\right] dE = 0 \quad (11)$$

the right hand side of (10) should also integrate to zero. For any reasonable flux the term in the brackets goes to zero for $E = 0$ or $E \rightarrow \infty$, and the right hand side of (10) has the desired property. Second, in the absence of losses, the solution to the Wilkins equation (the right hand side of (10) = 0) is still a Maxwellian.

Let us calculate ΔE_n on the basis of the modified gas model. We have

$$\Delta E_n = - \int dE\, E \left[- \Sigma_s \phi + \int dE' \, \Sigma_s(E' \rightarrow E)\, \chi_n(E') \right] / \Sigma_{sn} \tag{12}$$

$$= - \int dE\, E \frac{d}{dE} \left[2 \frac{\Sigma_o}{M} f(E) \left[E \chi_n - T \chi_n + ET \frac{\partial \chi_n}{\partial E} \right] \right] / \Sigma_{sn}$$

Integrating by parts, we find

$$\Delta E_n = + \int dE\, 2 \frac{\Sigma_o}{M} f(E) \left[E \chi_n - T \chi_n + ET \frac{\partial \chi_n}{\partial E} \right] / \Sigma_{sn}. \tag{13}$$

We cannot say anything about ΔE_n unless we make some assumption about χ_n. If we choose a Maxwellian of temperature, T_n, then ΔE_n is determined. Writing $T_n^{-1} = S$, we obtain from (13) in this case

$$\Delta E_n(S) = - 2 \frac{\Sigma_o}{M} \frac{S^2(ST-1)}{\Sigma_{sn}(S)} \int_o^{\infty} f(E)\, E^2\, e^{-SE}\, dE \tag{14}$$

Thus, if $\Delta E_n(S)$ is known, by taking the appropriate inverse Laplace transform, one can find $f(E)$. $\Delta E_n(S)$ <u>can</u> be determined experimentally or calculated from the scattering kernel. To calculate $\Delta E_n(S)$ from the scattering kernel, we substitute a Maxwellian for $\phi(E)$ in expression (4), obtaining

$$\Delta E_n(S) = \frac{S^2}{\Sigma_{sn}(S)} \int_o^{\infty} dE\, \overline{\Delta E}(E)\, \Sigma_s(E)\, E\, e^{-SE}\, dE \tag{15}$$

where again $S = T_n^{-1}$. By equating (14) and (15), we can obtain a relation between the scattering kernel as expressed by $\overline{\Delta E}(E)\, \Sigma_s(E)$ and the modification to the Wilkins equation $f(E)$. It is apparent that $f(E)$ and $\overline{\Delta E}(E)\, \Sigma_s(E)$ contain the same information although in somewhat different form.

Equating equations (13) and (15), we find

$$- \int_0^{\infty} dE\ G(E)\ E\ e^{-SE}\ dE = (ST-1) \int_0^{\infty} g(E)\ E^2\ e^{-SE}\ dE \qquad (16)$$

where

$$g(E) = \frac{2}{M} f(E) \qquad (17)$$

and we have used the definition of G(E), expression (6). The right hand side of (16) can be written as

$$R.S. = \int_0^{\infty} g(E)\ E^2\ (-1-T\ \frac{d}{dE})\ e^{-SE}\ dE \qquad (18)$$

and integrating by parts

$$R.S. = \int_0^{\infty} \left[- E^2\ g(E) + T\ \frac{d}{dE}(g(E)\ E^2) \right] e^{-SE}\ dE \qquad (19)$$

Since (19) holds for all S, we must have

$$-E\ G(E) = - E^2\ g(E) + T\ \frac{d}{dE}(g(E)\ E^2) \qquad (20)$$

Imposing the boundary condition that g(E) remains finite as $E \rightarrow \infty$, we can solve (20) to obtain

$$g(E) = E^{-2}\ e^{E/T} \int_E^{\infty} \frac{X}{T}\ e^{-X/T}\ G(X)\ dX \qquad (21)$$

Equation (21) enables one to find the required modification to the heavy gas equation from the cross section weighted average energy loss per collision. For a heavy gas

$$G(E) = \frac{2}{M} (2T-E) \qquad (22)$$

and we find on doing the integration

$$g(E) = \frac{2}{M}$$

and, hence,

$$f(E) = 1$$

as it should.

We have used G(E) obtained from the KRYOS code to evaluate g(E) from (21). For low energies, errors in the integration of (21) lead to errors in g(E). However, since T is the equilibrium temperature of the moderator,

$$0 = \int_0^\infty M(E,T)\, G(E)\, dE = \int_0^\infty \frac{X}{T}\, e^{-X/T}\, G(X)\, dX \qquad (23)$$

and one can rewrite (21) as

$$g(E) = -E^{-2}\, e^{E/T} \int_0^E \frac{X}{T}\, e^{-X/T}\, G(X)\, dX \qquad (24)$$

At low energies G(E) varies as $E^{-1/2}$, which enables one to start the integration of (24). In practice, it is satisfactory to use (24) for low energies and (21) for high energies. The results are shown in Figure 3.

With the modification (21), the Wilkins equation becomes

$$\Sigma_a\, \phi = \Sigma_o \frac{d}{dE} \left[g(E) \left[E\, \phi - T\, \phi + ET \frac{d\phi}{dE} \right] \right] \qquad (25)$$

If Σ_a varies as v^{-1}, we may express

$$\Sigma_a = \frac{\Sigma_a(T)}{\sqrt{E}} \sqrt{T}$$

Defining

$$\alpha = \frac{\Sigma_a(T)}{\Sigma_o} \qquad (26)$$

We can solve (25) by iteration if α is small. We follow the method used for the unmodified Wilkins equation by Hurwitz, Nelkin, and Habetler[3]. The result is

$$\phi = \frac{E}{T^2} e^{-E/T} \left[1 + \alpha Q(E) \right] \tag{27}$$

where

$$Q(E) = T \int_0^E \frac{\Gamma(3/2) - \Gamma(3/2, y/T)}{g(y)\, y^2\, e^{-y/T}} dy \tag{28}$$

$\Gamma(x)$ is the gamma function and $\Gamma(a,x)$ is the incomplete gamma function.

The function

$$H'(E) = \frac{E^2}{T^2} e^{-E/T} Q(E)$$

Corresponds to the Hurwitz function H(E) obtained by Hurwitz, et al[3]. The two functions have been plotted in Figure 4 to show their differences. Note that the modified Hurwitz function is nearly twice as large as the unmodified Hurwitz function in the thermal and epithermal regions. Coates and Gayther[4] give as parameters for their system

$$\begin{aligned} \Sigma_a(kT) &= 4.52 \times 10^{-3} \text{ cm}^{-1} \\ \Sigma_s &= .3862 \text{ cm}^{-1} \end{aligned} \tag{29}$$

These values have been used to calculate a spectrum directly with the code SPECTRUM and a spectrum from expression (27). Since the parameters (29) give a Δ of the order of .3, the correction factor

$$\left[1 - 0.799\, \Delta \right]^{-1}$$

discussed by Hurwitz, et al.,[3] has been applied to the original α to give an α of

$$\alpha = 1.52 \times 10^{-2} \tag{30}$$

Figure 5 shows a comparison of the modified gas results with the results from SPECTRUM. Figure 6 compares the modified gas results, the experimental results, and an attempted fit with a Maxwellian and the unmodified Hurwitz function. Note that the results from the modified Wilkins equation, the results from SPECTRUM, and the results from experiment all agree to within a few percent, while the unmodified gas fit exhibits discrepancies of 10-20% with the experimental results.

At least in the case of graphite at room temperature the modified Wilkins equation gives a successful description of actual measured spectra. With this encouragement we plan to look at graphite over a range of temperatures and at other moderators, including water. The modification we have described should also be applicable to the space dependent Wilkins equation.

Finally, note that by means of rethermalization type experiments, one can in a sense measure the modification f(E) experimentally. One essentially examines the energy transfer characteristics of the moderator in question using a Maxwellian spectrum as a probe. If a number of different temperature spectra are used, one finds $\Delta E_n(S)$ in equation (14). Taking the inverse Laplace transform will then determine f(E).

References

(1) Triplett, J.R., "French and British Methods in Reactor Theory," HW-71649, November, 1961.

(2) Perkel, D.H., "A Family of Thermalization Codes," GAMD-754 (Rev.).

(3) Hurwitz, H., Jr., M.S. Nelkin, and G.J. Habetler, "Neutron Thermalization," Nuc. Sci. and Eng. 1, 280-312 (1956).

(4) Coates, M.S. and D.B. Gayther, "Time of Flight Measurements of Neutron Spectra in a Graphite Uranium Lattice at Different Temperatures," AERE-R-3829.

(5) Selengut, D.S., "Variational Analysis of Multidimensional Systems," Nuclear Physics Research Quarterly Report, October-December, 1958, HW-59126.

(6) Selengut, D.S., "Variational Methods in Neutron Thermalization," September 29, 1961. To be published.

(7) Bennett, R.A., "Neutron Thermalization in Graphite and Water," 1962 Brookhaven Conference on Thermalization.

(8) von Dardel, G.F., "A Study of the Interaction of Neutrons with Moderating Materials," Phys. Rev. 94, 1272 (1954).

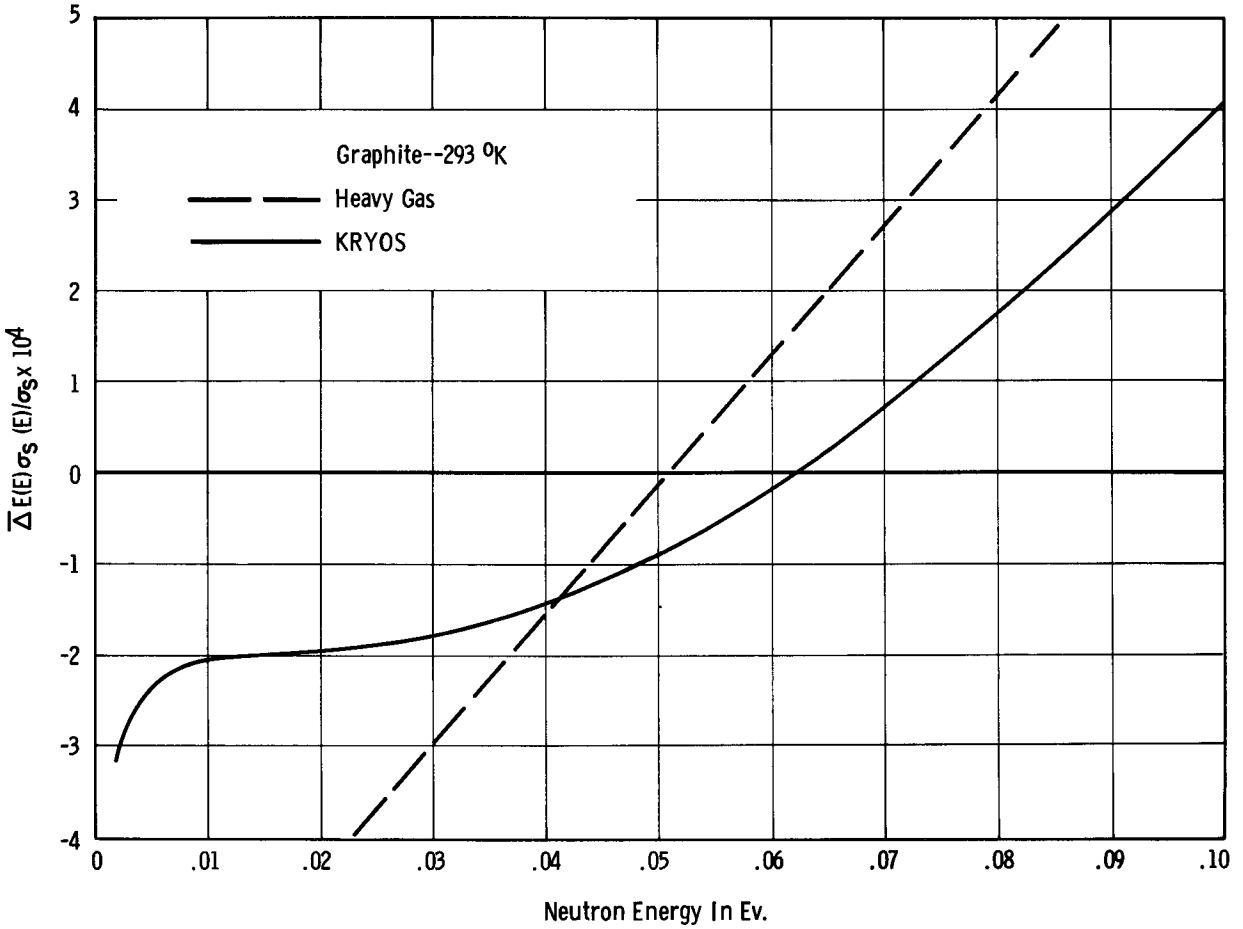

FIGURE 1

Cross Section Weighted Average Energy Loss per Collision in 293 K Graphite. Heavy Gas Model Compared with KYROS II.

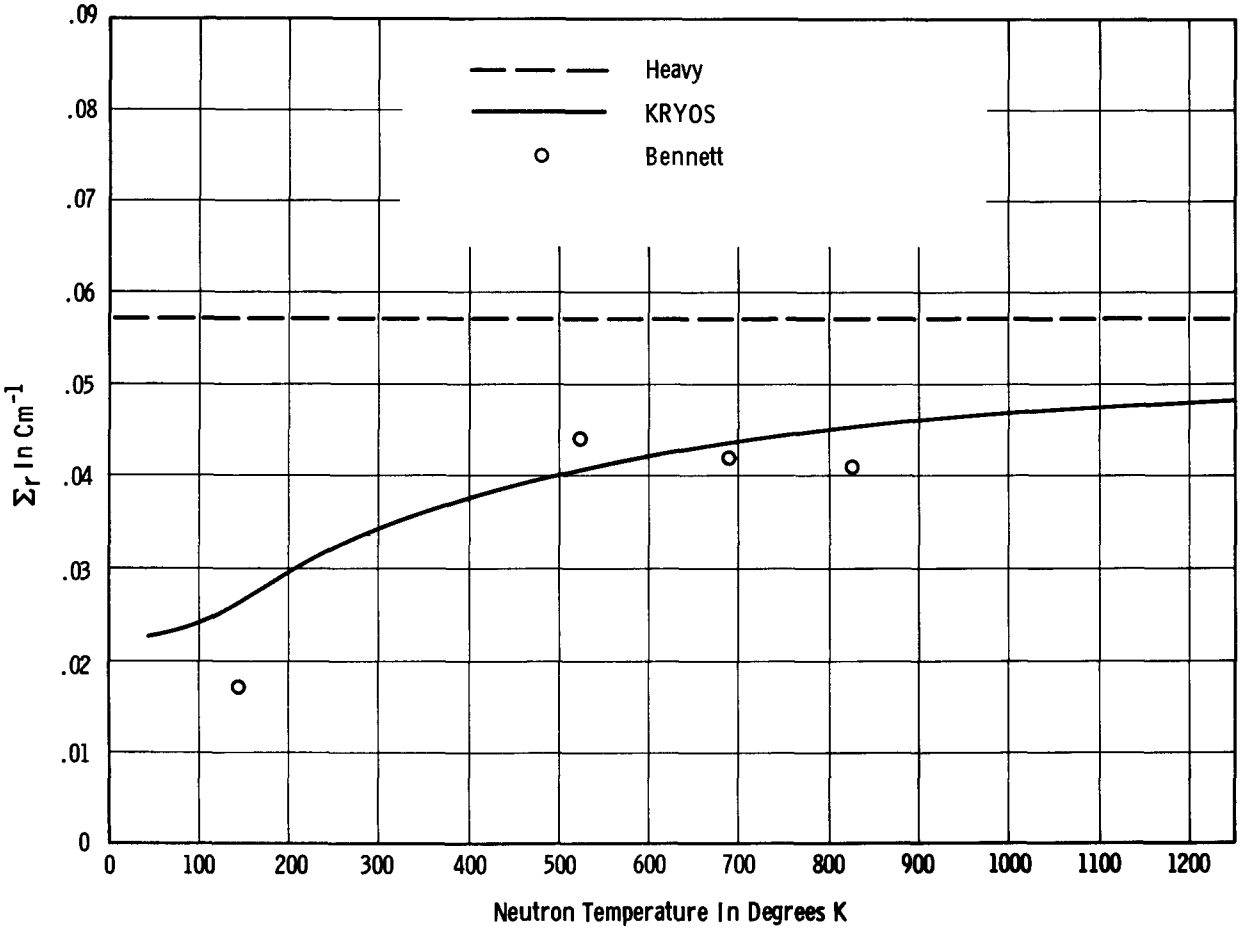

FIGURE 2

Rethermalization Cross Sections. KRYOS II and
the Heavy Gas Model Compared with Bennett's Experiment.

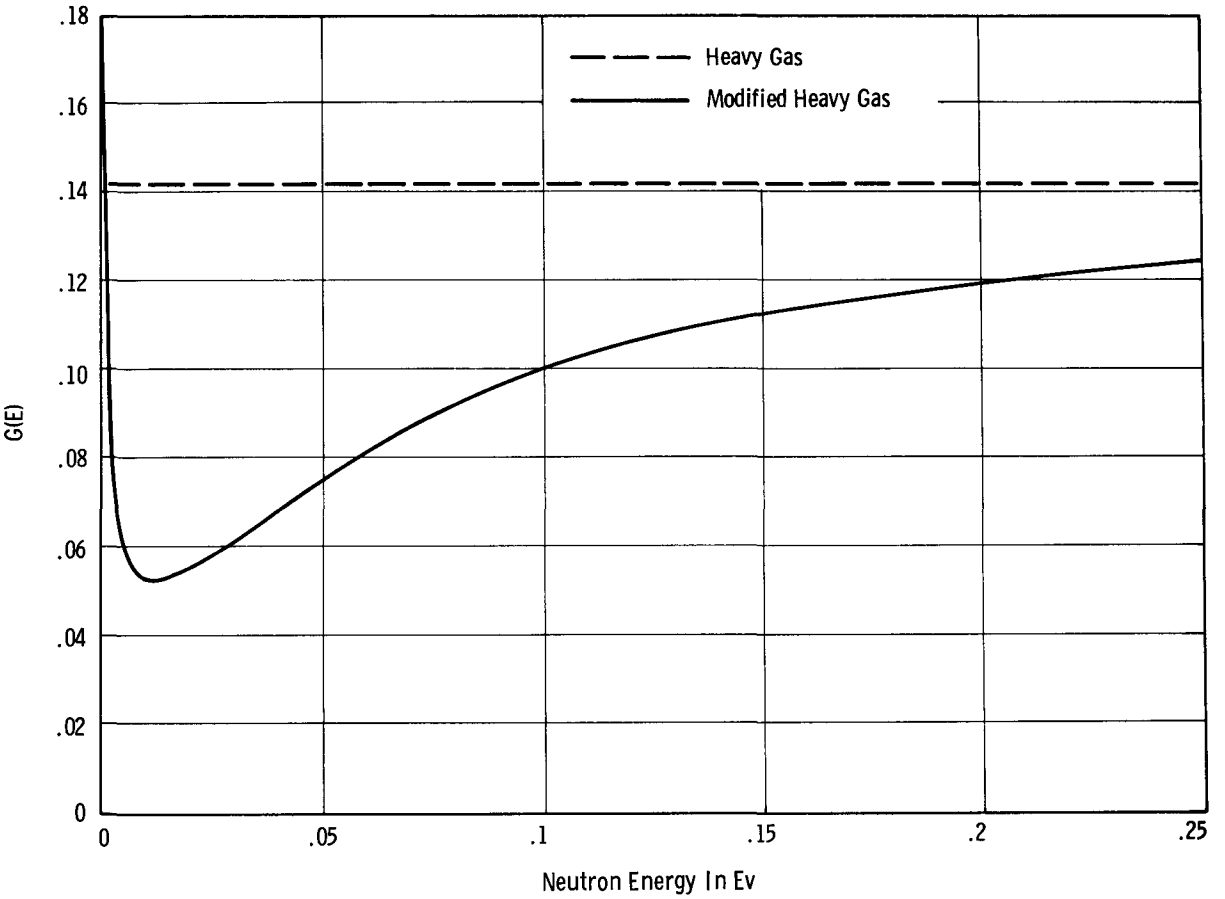

FIGURE 3

Heavy Gas Modification to G(E), the Cross Section Normalized Slowing Down Power

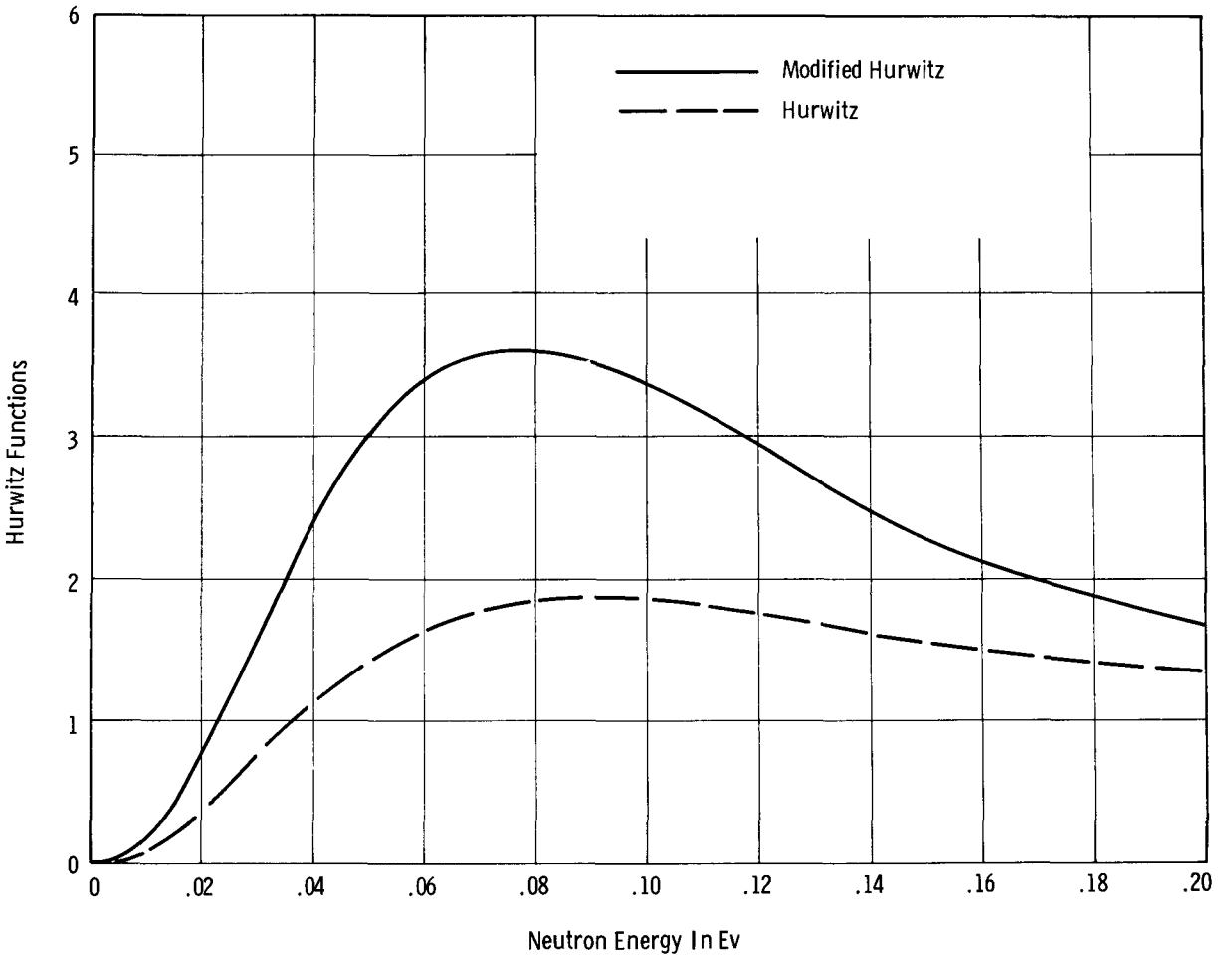

FIGURE 4

Comparison of Hurwitz Functions

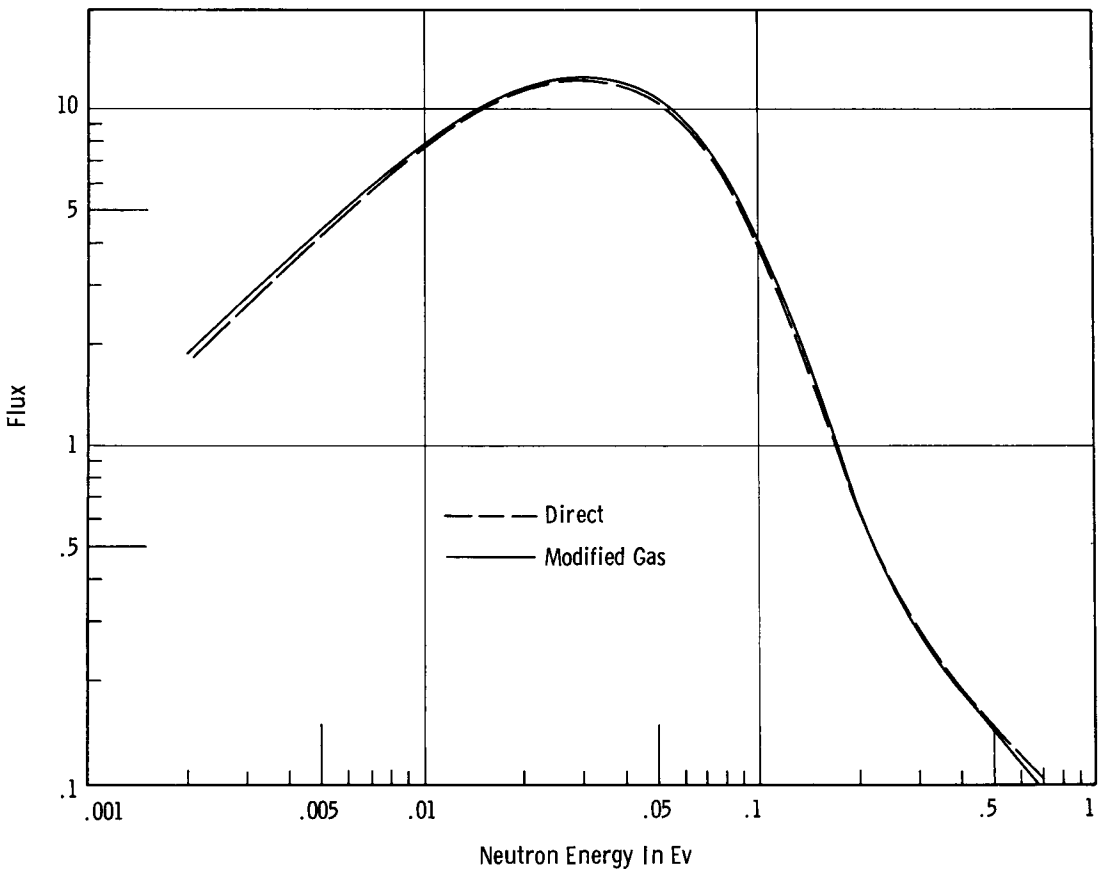

FIGURE 5

Comparison of Spectra Calculated Directly
and with the Modified Gas Model

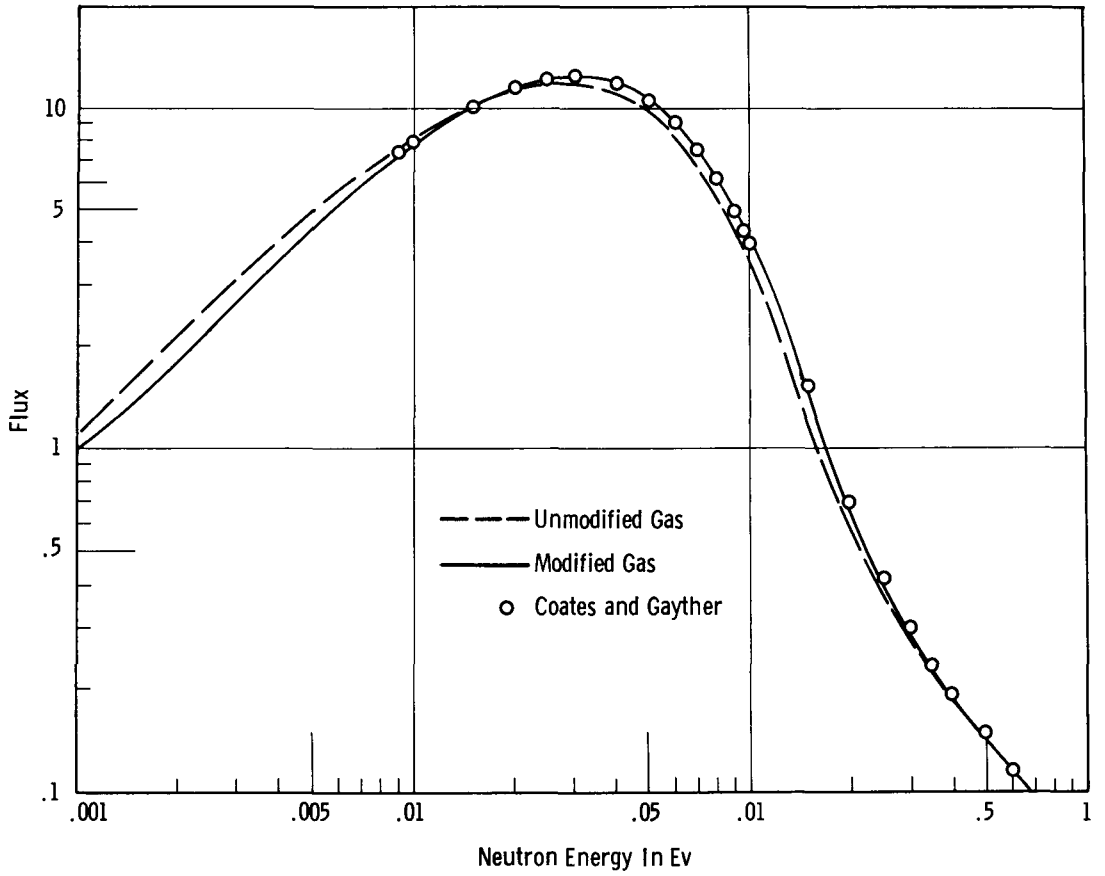

FIGURE 6

Comparison of Spectra Calculated from the Modified Gas Model and the Unmodified Gas Model with Experiment

SPACE-DEPENDENT NEUTRON THERMALIZATION

J. A. BEWICK, R. K. OSBORN, and P. F. ZWEIFEL

Department of Nuclear Engineering, University of Michigan,

Ann Arbor, Michigan

ABSTRACT

The thermal neutron spectrum is calculated using the P1 transport equations and the heavy gas cross section for scattering by moderator atoms. A consistent expansion of the gas cross section and the diffusion coefficient to first order in μ, the inverse moderator mass, leads to a spectrum which is nearly identical to that calculated by Hurwitz, et al (1) in which the diffusion coefficient is assumed to be constant and several terms of first order in u in the energy moments of the gas cross section are ignored.

INTRODUCTION

Hurwitz, et al (1) have shown that the gas cross section for neutron thermalization can be expanded in powers of the inverse moderator mass (u=1/M). This expansion may be substituted into the Pl equations which reduce to a fourth order differential equation in space-energy derivatives. The space derivatives may be replaced by the eigenvalue of the Helmholtz equation ($\nabla^2\varphi+B^2\varphi=0$). Retaining all first order quantities in u in the transport cross section as well as in the moments expansion of the scattering cross section in the Pl equations introduces energy dependent terms which modify the equations for the spectrum found by Hurwitz. However, even for highly absorbing, fast reactors, the resulting spectrum differs from the Hurwitz result by only 1%.

THEORY

The consistent, one dimensional, Pl transport equations are

$$\frac{\partial\varphi_1}{\partial x} + \sigma_t\varphi_0 = S + \int_{E'}\varphi_0(E')\,\sigma_0(E',E)\,dE' \qquad (1)$$

$$\frac{1}{3}\frac{\partial\varphi_0}{\partial x} + \sigma_t\varphi_1 = \int_{E'}\varphi_1(E')\,\sigma_1(E',E)\,dE' \qquad (2)$$

where

$$\sigma_\ell(E', E) = 2\pi \int_{-1}^{1} \sigma(E' \to E, x)\, P_\ell(x)\, dx \qquad (3)$$

and $x = \cos(\theta' \cdot \theta)$ = cosine of angle of scattering. Using the principle of detailed balance, the transport equations may be rewritten as

$$\frac{\partial \psi_1}{\partial x} + \sigma_t \psi_0 = \frac{S}{M} + \int_{E'} \psi_0(E')\, \sigma_0(E, E')\, dE' \qquad (4)$$

$$\frac{1}{3} \frac{\partial \psi_0}{\partial x} + \sigma_t \psi_1 = \int_{E'} \psi_1(E')\, \sigma_1(E, E')\, dE' \qquad (5)$$

where $\psi(E) = \varphi(E)/M(E)$ and $M(E)$ equals the Maxwellian flux.

Expand $\psi(E)$ in a Taylor series about E on the right hand side of (4) and (5), keeping terms up to the second derivative. Thus,

$$\int_{E'} \psi_\ell(E')\, \sigma_\ell(E, E')\, dE' = \sum_{n=0}^{2} \frac{\langle \Delta E^n \rangle_\ell}{n!} \frac{\partial^n \psi_\ell}{\partial E^n} \qquad (6)$$

where

$$\langle \Delta E^n \rangle_\ell = \int_{E'} (E' - E)^n\, \sigma_\ell(E, E')\, dE'$$

are the energy moments of the scattering cross section.

Following the technique described in the Hurwitz paper (Appendix A), the scattering cross section is expanded in a power series in u, the inverse of the moderator mass. This result is substituted into Eq. (6) for the energy moments (see Appendix B, ref. 1). The moments are

$$\langle \Delta E^{\circ} \rangle_{\circ} = \sigma_{\circ}\left[1 + \frac{\mu\theta}{2E}\right] = \sigma_{s} \tag{7a}$$

$$\langle \Delta E^{1} \rangle_{\circ} = \mu\sigma_{\circ}\left[-2E + 4\theta\right] \tag{7b}$$

$$\langle \Delta E^{2} \rangle_{\circ} = \frac{2\mu}{3}\theta \tag{7c}$$

$$\langle \Delta E^{1} \rangle_{1} = \frac{2}{3}\mu\sigma_{\circ}(E - 2\theta) \tag{7d}$$

$$\langle \Delta E^{2} \rangle_{1} = -\frac{4\mu}{3}\sigma_{\circ} E\theta \tag{7e}$$

Hurwitz, et al, drop the last two energy moments ((7d) and (7e)) and assume that the diffusion coefficient is zero order in u, that is

$$D = (3\sigma_{\circ})^{-1} + \Theta(u) \tag{8a}$$

and

$$\langle \Delta E^{1} \rangle_{1} \approx \langle \Delta E^{2} \rangle_{1} \approx 0 \tag{8b}$$

so that (5) becomes

$$\psi_{1}(E) = -\frac{1}{3\sigma_{\circ}}\frac{\partial \Phi_{\circ}}{\partial x}\left[1 + \Theta(u)\right] \tag{8c}$$

If D is expanded to first order in u, energy dependent terms are introduced which make the diffusion coefficient

$$D(E) = \frac{1}{3\sigma_{tr}} = 1/3\sigma_{tr_0}\left\{1 + \frac{\mu\sigma_0}{2\sigma_{tr_0}}\cdot\frac{\theta}{E} + \frac{\sigma_{a_0}}{\sigma_{tr_0}}\left(\sqrt{\frac{\theta}{E}} - 1\right)\right\} \qquad (9a)$$

where $\theta = KT$ and $\sigma_{tr_0} = \sigma_{a_0} + \sigma_0\left(1 - \frac{2\mu}{3}\right)$

Substituting (9a) into the transport equation results in an expression comparable to (8c), that is

$$\psi_1(E) = \Lambda^{-1} D(E) \frac{\partial \psi_0}{\partial x} \qquad (9b)$$

where the operator Λ is of the form

$$\Lambda = -1 + \frac{2\mu\sigma_0}{3\sigma_{tr}}\left(-E + 2\theta\right)\frac{\partial}{\partial E} - \frac{2\mu\sigma_0}{3\sigma_{tr}}\frac{\partial^2}{\partial E^2} \qquad (9c)$$

As a result of keeping all first order terms in u in the diffusion coefficient and in the energy moments of the scattering cross section, energy derivatives of the diffusion coefficient have been introduced. After $\psi_1(E)$ is substituted into Eq. (4), a fourth order differential equation in space-energy derivatives is determined. This may be reduced to a second order differential equation in energy by assuming that the spatial dependence obeys the Helmholtz equation which is of the form $\nabla^2\psi + B^2\psi = 0$. If ψ is the eigenfunction satisfying the Laplacian, B^2 (the eigenvalue), may replace the operator ∇^2. Let $\epsilon = E/\theta$. The second order differential equation for $\psi_0(E)$ is, then,

$$\epsilon\psi_0'' + \left[2 - \epsilon + F_1(\epsilon)\right]\psi_0' - \left[\frac{\sigma_a}{2\mu\sigma_0}F_2(\epsilon) - F_3(\epsilon)\right]\psi_0 = 0 \qquad (10)$$

where

$$\psi_0' = \frac{d\psi}{d\epsilon} \; ; \quad \psi_0'' = \frac{d^2\psi_0}{d\epsilon^2}$$

and

$$F_1(\epsilon) = \frac{2D_0^2B^2}{1+D_0^2B^2}\left(\frac{\mu\sigma_0}{2\sigma_{tr_0}}\cdot\frac{1}{\epsilon} + \frac{\sigma_{a_0}}{2\sigma_{tr_0}}\sqrt{\frac{1}{\epsilon}}\right)$$

$$\frac{\sigma_a}{2\mu\sigma_0}F_2(\epsilon) = \frac{3D_0^2B^2}{2\sigma_{tr_0}}\left(1+\frac{\sigma_{a_0}}{\sigma_{tr_0}}\right) + \left[\frac{\sigma_{a_0}}{2\mu\sigma_0} - \frac{3D_0^2B^2\sigma_a}{2\mu\sigma_0}\right]\sqrt{\frac{1}{\epsilon}} \qquad \left(\frac{3\sigma_{tr_0}D_0^2B^2}{2\mu\sigma_0}\right)$$

$$-\frac{3}{4}D_0^2B^2\cdot\frac{1}{\epsilon}$$

$$F_3(\epsilon) = \frac{D_0^2B^2}{1+D_0^2B^2}\left\{-\frac{\mu\sigma_0}{2\sigma_{tr_0}}\frac{1}{\epsilon} + \frac{\sigma_{a_0}}{2\sigma_{tr_0}}\left(-\sqrt{\frac{1}{\epsilon}} + \frac{1}{2}\epsilon^{-3/2}\right)\right\}$$

If terms of order uB^2 are neglected,

$$F_1(\epsilon) \approx F_3(\epsilon) \approx 0$$

$$\frac{\sigma_a}{2\mu\sigma_0}F_2(\epsilon) \approx \frac{3D_0^2B^2}{2\mu\sigma_0}\left(1+\frac{\sigma_a}{\sigma_{tr_0}}\right) + \frac{\sigma_{a_0}}{2\mu\sigma_0}\left(1-3D_0^2B^2\right)\sqrt{\frac{1}{\epsilon}} - \frac{3}{4}D_0^2B^2\cdot\frac{1}{\epsilon} \qquad (\sigma_{tr_0})$$

Consequently, Eq. (10) reduces to

$$\epsilon\psi_0'' + (2-\epsilon)\psi_0' - \frac{\sigma_a}{2\mu\sigma_0}F_2(\epsilon)\psi_0 = 0 \qquad (11)$$

Equation (11) may be converted to an integral equation whose solution in the sense of a first iteration is

$$\varphi(\epsilon) = M(\epsilon)\psi(\epsilon) = M(\epsilon)e^{-3D_o^2B^2/4}\chi(\epsilon), \quad (13)$$

where

$$\chi(\epsilon) = 1 + \int_0^{\epsilon} \frac{d\epsilon'}{\epsilon'^2} e^{\epsilon'} \int_0^{\epsilon'} d\epsilon'' \epsilon'' e^{-\epsilon''} \left(\frac{\epsilon'}{\epsilon''}\right)^{3D_o^2B^2/2}$$

$$(x)\left[\left\{\frac{\sigma_{a,o}/\sqrt{\epsilon''} + 3\sigma_{t+o} D_o^2 B^2}{2\mu\sigma_o}\right\} + \frac{3\sigma_{a,o} D_o^2 B^2}{2\mu\sigma_o}\left(1 - \frac{1}{\sqrt{\epsilon''}}\right) - \frac{3D_o^2B^2}{4}\right]. \quad (14)$$

This solution is to be compared with the corresponding one presented by Hurtwitz et al (reference 1, Equation (14)) which may be obtained from our equations (13) and (14) by setting $D_o^2B^2$ equal to zero wherever it appears as an exponential and by retaining only the term in curly brackets in the integrand of (14). The integrals in (14) were evaluated on a computer for both the Hurwitz and the cases.

CONCLUSION

The above procedure was discussed at the Mexico City meeting of the American Physical Society (2). The difference in the spectrum resulting from a consistent expansion of all quantities

in μ is less than 1% at all points for a wide range of reactors. This analysis was applied to reactors which varied from the large, thermal, graphite reactors ($B^2 = 60 \times 10^{-6}$ cm.$^{-2}$, $\Sigma_a = .00413$ cm.$^{-1}$) to small, fast reactors with high leakage and absorption ($B^2 = .019$ cm.$^{-2}$, $\Sigma_a = 4.7$ cm.$^{-1}$). Consequently, for most reactors, the Hurwitz approximations give very good results.

ACKNOWLEDGEMENTS

One of the authors (JAB) would like to thank Messrs. J. Olhoeft and J. Erickson for computational assistance.

REFERENCES

1. H. Hurwitz, Jr., M.S. Nelkin, and G. J. Habetler, Nuclear Science and Eng. 1, 280-312 (1956)
2. P. F. Zweifel, R. K. Osborn, and G. Gyorey, Bull. of the Amer. Phys. Soc. II, Vol. 6, 375 (1961)

E U R A T O M
C.C.R.- Ispra

Reactor Physics
Department

Ispra, March 5, 1962

SPACE AND TIME DEPENDENT EIGENVALUE PROBLEM IN NEUTRON THERMALIZATION

Hiroshi Takahashi

Abstract

The matrix elements of the neutron scattering kernel for a free gas and a crystalline material expanded in terms of Laguerre polynomials of energy, weighted by a Maxwellian distribution, are obtained by a generating function for the Laguerre polynomial. The eigenvalue problems in a spatial and time dependent neutron thermalization are solved by using the obtained matrix element. For the spatial problem first order Laguerre polynomials are used. Half order Laguerre polynomials are used for the time dependent problem, because they diagonalize respectively the spatial and the time dependent term.

The convergence of eigenvalues and eigenfunctions in the time dependent problem using half order Laguerre polynomials is rather slow compared with the spatial problem's convergence. The diffusion cooling coefficients for a Debye crystalline and a graphite are calculated from the eigen values and eigen functions in the time dependent problem.

The results obtained for beryllium and graphite are respectively 3.36 and 2.4 times larger than those obtained by the Nelkin theory.

1. Introduction

The time dependent problem using a pulsed neutron, and the space dependent problem have been considered by many authors (1~15) for the study of neutron thermalization. Experimental data (13, 14, 15) have been accumulated and theories also have been developed by using the variational method (3, 4) and the expansion method of flux in terms of orthogonal polynomials (5, 12). In the variational method, if simple trial functions are used, simple analytical formulations are obtained. From these formulations we can get the physical meaning of the phenomena avoiding a tedious numerical calculation. Sometimes, however, the numerical results obtained from variational approach are not very accurate. When an accurate numerical value is needed, it is better to adopt the expansion mentod. Although this method has been used for the neutron thermalization problem, only the low order expansion 5) 9) has been considered except the case of heavy gas model (6~ 7, 10~ 12) and of free gas with mass 1 (8). In the heavy gas model, the matrix of the scattering kernel is diagonalized in terms of first order Laguerre polynomials.

In this paper, the matrix elements of the scattering kernel for free gas and crystalline material expanded in terms of the Laguerre polynomial, which is weighed by the Maxwellian distribution, are obtained by using the generating function of Laguerre polynomials. In the case of space dependent problem with energy independent diffusion coefficient, first order Laguerre polynomials, diagonalizing the diffusion term, are used to expand the flux, and half order Laguerre polynomials are used for the time dependent problem, where the term differentiated by time with a $1/\sqrt{E}$ energy dependence is diagonalized. In Laguerre lopynomials, the generating function of the scattering kernel in the space dependent problem is simply related to the one of the time dependent problem. The generating function for the crystalline material is calculated by the Plazeck's mass expansion method, the phonon expansion method (17, 18) and two frequency dividing methods (21) which have been used for a calculation of total cross section and differential cross section of neutron scattering.

The time and space dependent eigenvalues and eigenfunctions for free gas, Debye crystalline and graphite are calculated. A convergence of spatial eigenvalues obtained by increasing the dimension of matrix is very good. However, the convergence of time dependent eigenvalues is rather slow. The diffusion

cooling coefficient obtained from the decay constant of pulsed neutrons in a small assembly has been calculated from the thermalization power M_2. The Nelkin's formulation for the diffusion cooling corresponds to the formulation in which only the first two terms of the Laguerre expansion are kept. The Nelkin's formulation gives a comparatively good numerical value in the case of free gas model. However, in the case of crystalline material, like beryllium and graphite, the accurate results are : in beryllium a 3.36 times larger value than the Nelkin's results, in graphite a 2.4 times larger value than the results from Nelkin's formula.

2. General formulation

The Boltzmann equation for the time and spatial dependent angular flux $f(\vec{r}, E, \vec{\Omega}, t)$ is (16) :

$$\frac{1}{v}\frac{\partial f(\vec{r},E,\vec{\Omega},t)}{\partial t} = -\vec{\Omega}\cdot \mathrm{grad}\, f(\vec{r},E,\vec{\Omega},t) + \iint dE'd\Omega' f(\vec{r},E',\vec{\Omega}',t)\,\Sigma_s(\vec{r},E'\to E,\vec{\Omega}'\cdot\vec{\Omega}) - \Sigma(\vec{r},E,\vec{\Omega})\,f(\vec{r},E,\vec{\Omega},t) + S(\vec{r},E,\vec{\Omega}) \qquad (1)$$

Since we are interested in the eigenvalue problem, we shall take the source term $S(\vec{r}, E, \vec{\Omega})$ to be zero. In the diffusion approximation equation (1) takes the form :

$$\frac{1}{v}\frac{\partial \phi(\vec{r},E,t)}{\partial t} - D(E)\nabla^2\phi(\vec{r},E,t) + \Sigma_a\phi(\vec{r},E,t) - \int_0^\infty \phi(\vec{r},E',t)\Sigma_s(E'\to E)dE' + \Sigma_s(E)\phi(\vec{r},E,t) = 0 \qquad (2)$$

where

$$\phi(\vec{r},E,t) = \int d\Omega\, f(\vec{r},E,\Omega,t)$$

By making a Laplace transformation for the time variation, and for the spatial variation, expanding the flux in terms of the eigenfunction of the equation :

$$\nabla^2 \chi_\ell(r) + B_\ell^2 \chi_\ell(r) = 0$$

where B^2 is the buckling corresponding to the 1th harmonic, the time variation and the spatial variation can be separated from the equation (2), and the problem reduces to a following time and space independent equation, in which the time constant λ or B^2 appears as an eigenvalue.

$$-\frac{\lambda}{v}\phi(E) + D(E)\,B^2\phi(E) + \Sigma_a(E)\phi(E) + \Sigma_s(E)\phi(E) - \int_0^\infty \phi(E')\,\Sigma_s(E'\to E)\,dE' = 0 \qquad (3)$$

In order to simplify matters, we shall consider the spatial eigenvalue problem and time eigenvalue problem separately. Since the moderator material generally shows the 1/v absorption cross section, it is suitable to include the absorption cross section terms in the time eigenvalue problem, and to treat the spatial eigenvalue problem in the non absorbing medium.

a) Space dependent problem

Let us first consider the spatial eigenvalue problem in the case of energy independent diffusion coefficient :

$$D B^2\phi(E) + \Sigma_s(E)\phi(E) - \int_0^\infty \phi(E')\,\Sigma_s(E'\to E)\,dE' = 0 \qquad (4)$$

We assume that $\phi(E)$ can be expressed as :

$$\phi(E) = \sum_{i=0}^{\infty} \frac{1}{\sqrt{i+1}}\, L_i^{(1)}\left(\frac{E}{T}\right) \frac{E}{T^2}\, e^{-\frac{E}{T}}\, a_i \qquad (5)$$

where $L_i^{(1)}(x)$ is the generalized Laguerre polynomial of order unity and degree of i and the Laguerre polynomial of order α, $L_i^{(\alpha)}(x)$ has the following generating function :

$$\frac{e^{-x\frac{p}{1-p}}}{(1-p)^{\alpha+1}} = \sum_{i=0}^{\infty} p^i L_i^{(\alpha)}(x) \qquad (*) \tag{6}$$

The polynomial has the following orthonormality :

$$\int_0^\infty L_i^{(\alpha)}(x) L_j^{(\alpha)}(x)\, x e^{-x} dx = \delta_{ij} \frac{\Gamma(i+1+\alpha)}{\Gamma(i+1)} \tag{7}$$

Substituting (5) into (4) and multiplying the resulting equation by $\frac{1}{\sqrt{(j+1)}} L_j^{(1)}\left(\frac{E}{T}\right)$ and integrating over E, we get

$$D B^2 \delta_{ij} a_i - S_{ij} a_i = 0 \tag{8}$$

where

$$S_{ij} = \frac{1}{\sqrt{(i+1)(j+1)}} \left[\int_0^\infty \int_0^\infty dE' dE\, \Sigma_s(E' \to E)\, L_i^{(1)}\left(\frac{E'}{T}\right) L_j^{(1)}\left(\frac{E}{T}\right) \frac{E'}{T^2} e^{-\frac{E'}{T}} \right.$$

$$\left. - \int_0^\infty \int_0^\infty dE' dE\, \Sigma_s(E' \to E)\, L_i^{(1)}\left(\frac{E'}{T}\right) L_j^{(1)}\left(\frac{E'}{T}\right) \frac{E'}{T^2} e^{-\frac{E'}{T}} \right] \tag{9}$$

It is well known that the heavy gas model has been frequently used in the neutron thermalization problem because the matrix (S_{ij}) is diagonalized simultaneously with energy independent spatial term DB^2 by this Laguerre polynomial.

Next, we shall consider the evaluation of the matrix (S_{ij}).

(*) In this paper, the Laguerre polynomial with the orthonormality eq (7) has been used instead of the Laguerre polynominal defined in the text book (Method of Theoretical Physics, Morse & Freshback). The reason is that this Laguerre polynomial is more convenient than the others for numerical calculation using the calculating machine.

In the incoherent approximation, the formula for the differential cross section in the neutron scattering by the crystalline material can be written in the form :

$$\frac{d^2\sigma}{d\Omega\, d\omega} = \frac{k}{k'}\frac{\Sigma_B}{8\pi^2}\int_{-\infty}^{\infty} \exp\left[-\kappa^2(M(0)-M(t))\right]\exp\left(i(\omega-\omega')t\right)dt \qquad (10)$$

$\omega = E/\hbar$, where E is the energy of the scattered neutron, Ω is the solid angle, k' and k are the wave vectors of the incoming and scattered neutron and $\vec{\kappa} = k' - k$, Σ_B is the bounded cross section, and M (t) is related to the frequency spectrum f (ω) as follows :

$$M(t) = \frac{\hbar}{2M}\int_0^{\omega_m}\left[\coth(\beta\omega)\cos(\omega t) + i\sin\omega t\right]\frac{f(\omega)}{\omega}\,d\omega \qquad (11)$$

$$= \frac{\hbar}{2M}\,\gamma(t)$$

where M is the mass of atom, m the neutron mass, and $\beta = \frac{\hbar}{2\ T}$.

In the calculation of matrix element (S_{ij}), we use the generating function of (6) for the Laguerre polynomial. Let us consider the first terms $S_{ij}^{(1)}$ in the matrix S_{ij} of eq (9), which are obtained as the coefficient of $\sqrt{(i+1)(j+1)}\ P^i \ell^j$ in the following generating function :

$$S^{(1)} = \iiint_0^{\infty} \frac{d^2\sigma}{d\Omega\, d\omega}\,(1-P)^{-2}(1-\ell)^{-2}\exp\left(-\frac{E'}{T}\left(\frac{P}{1-P}\right)\right)$$

$$\cdot\exp\left(-\frac{E}{T}\left(\frac{\ell}{1-\ell}\right)\right)\frac{E'}{T^2}\,e^{-\frac{E'}{T}}\,dE'\,d\Omega\,d\omega \qquad (12)$$

Substituting eq (10) to eq (12), we get :

$$S^{(1)} = \iiint_{-\infty}^{\infty} \frac{\hbar}{mk'}\frac{\Sigma_B}{8\pi^2}\exp\left[-\kappa^2(M(0)-M(t))\right]\exp\left(i(\omega-\omega')t\right)$$

$$\cdot(1-P)^{-2}(1-\ell)^{-2}\exp\left(-\frac{E'}{T}\left(\frac{P}{1-P}+1\right)\right)\exp\left(-\frac{E}{T}\left(\frac{\ell}{1-\ell}\right)\right)\frac{E'}{T^2}\,dt\,dE'\,d\vec{\kappa}^3 \qquad (13)$$

By substituting the following relation into eq (13) :

$$\hbar\omega = \hbar\omega' - 2\sqrt{\hbar\omega}\,\frac{\hbar\kappa}{\sqrt{2m}} + \frac{\hbar^2\kappa^2}{2m} \tag{14}$$

we get :

$$S^{(1)} = \frac{\Sigma_B}{8\pi^2}(1-P)^{-2}(1-\ell)^{-2}\int_{-\infty}^{\infty}\iiint \frac{\hbar}{m}\exp(-\hbar\omega'(I+J))\frac{E'}{E}$$

$$\exp\left(-\frac{\hbar\kappa^2}{2m}(it-\hbar J-\frac{2m}{\hbar}(M(0)-M(t))\right)\exp\left(-2\sqrt{\hbar\omega}\frac{\kappa}{\sqrt{2m}}(it-\hbar J)\cos\theta\right)d\vec{\kappa}^3dE'dt$$

$$= \frac{\Sigma_B}{8}\frac{\hbar^2}{T^2}(1-P)^{-2}(1-\ell)^{-2}\int_{-\infty}^{\infty}\frac{dt}{\left[(t-i\hbar I)(t+i\hbar J)+(I+J)2m(M(0)-M(t))\right]^{3/2}} \tag{15}$$

where $I = \left(\frac{P}{1-P}+1\right)\frac{1}{T}$ and $J = \left(\frac{\ell}{1-\ell}\right)\frac{1}{T}$ (16)

The generating function for the second term of eq (9) $S^{(2)}$ is obtained by the same way with $S^{(1)}$ as follows :

$$S^{(2)} = \iiint \frac{d^2\sigma}{d\Omega\,d\omega}(1-P)^{-2}(1-\ell)^{-2}\exp\left(-\frac{E'}{T}\left(1+\frac{P}{1-P}+\frac{\ell}{1-\ell}\right)\right)dE'\,d\Omega\,d\omega$$

$$= \frac{\Sigma_B}{8}\frac{\hbar^2}{T^2}(1-P)^{-2}(1-\ell)^{-2}\int_{-\infty}^{\infty}\frac{dt}{\left[t(t-i\hbar(I+J))+(I+J)2m(M(0)-M(t))\right]^{3/2}} \tag{17}$$

The generating function for matrix S is :

$$S = S^{(1)} - S^{(2)} \tag{18}$$

Free gas case

The effects of crystalline material are included in the term of $\lceil M(0) - M(t) \rceil$. If we take the upper limit ω_m(Debye frequency) of frequency function $f(\omega)$ to be zero, that is, the atomic force between the composed atom becomes zero, this expression becomes the one of the free gas model. In this case, the function $\lceil M(0) - M(t) \rceil$ is expressed in the following form :

$$M(0) - M(t) = -\frac{\hbar}{2M}\left(it - \frac{T}{\hbar}t^2\right) \tag{19}$$

Substituting eq (18) into eq (15),

$$S^{(1)} = \Sigma_B \frac{\left(1 + \frac{m}{M}\left(1 + \frac{P}{1-P} + \frac{\ell}{1-\ell}\right)\right)^{1/2}}{\left[(1-P\ell)^2\left(1+\frac{m}{M}\right)^2 + 4P\ell(1-P\ell)\frac{m}{M}\right]} \tag{20}$$

Similarly, we get :

$$S^{(2)} = \Sigma_B \frac{\left(1 + \frac{m}{M}\left(1 + \frac{P}{1-P} + \frac{\ell}{1-\ell}\right)\right)^{1/2}}{(1-P\ell)^2\left(1+\frac{m}{M}\right)^2} \tag{21}$$

and

$$S = -\frac{4\Sigma_B \frac{m}{M}}{\left(1+\frac{m}{M}\right)^{7/2}} \frac{P\ell}{(1-P\ell)^2} \frac{\left[1 + \frac{\frac{m}{M}}{1+\frac{m}{M}}\left(\frac{P}{1-P} + \frac{\ell}{1-\ell}\right)\right]^{1/2}}{\left[1 - \frac{\left(1-\frac{m}{M}\right)^2}{\left(1+\frac{m}{M}\right)^2} P\ell\right]} \tag{22}$$

In the case of heavy gas model, by putting $\frac{m}{M} \to 0$, we get :

$$S_{Heavy} = -4\Sigma_{free} \frac{m}{M} \frac{P\ell}{(1-P\ell)^3} \tag{23}$$

We can easily find out from eq (23) that the matrix in the heavy gas model is diagonalized.

Crystalline material

For the case of the crystalline material, the Plazeck's mass expansion method, the phonon expansion method, and the two frequency dividing methods

which have been used for the calculation of total cross section and differential cross section, are applied to the calculation of the integrations in eq (15) and (17).

In the mass expansion method, the integrant in eq (15) is expanded by the power series of $(\frac{m}{M})$ as follows :

$$S^{(1)} = \frac{\Sigma_B}{8}\frac{k^2}{T^2}(1-P)^{-2}(1-l)^{-2}$$

$$\cdot \sum_{q=0}^{\infty}(-1)^q \frac{\Gamma(\frac{3}{2}+q)}{\Gamma(\frac{3}{2})\Gamma(q+1)}\left(\frac{m}{M}\right)^q \int_{-\infty}^{\infty} \frac{[(I+J)k\,\Gamma(t)]^q}{[(t-ikI)(t+ikJ)]^{3/2+q}}\,dt \quad (24)$$

where

$$\Gamma(t)^q = [\gamma(0)-\gamma(t)]^q$$

$$= \gamma(0)^q \sum_{n=0}^{q} \frac{\Gamma(q+1)}{\Gamma(q-n+1)\Gamma(n+1)} \int_{-\omega_m}^{\omega_m} G_n(\omega)\, e^{-i\omega t}\,d\omega \quad (25)$$

where $G_0(\omega) = \delta(\omega)$

$$G_n(\omega) = \frac{(-1)^n}{\gamma(0)^n}\int_{-\omega_m}^{\omega_m}\cdots\int_{-\omega_m}^{\omega_m} \frac{f(\omega-\omega_1)}{(\omega-\omega_1)}\,\frac{\coth\beta(\omega-\omega_1)-1}{2}$$

$$\cdot\frac{f(\omega_1-\omega_2)}{(\omega_1-\omega_2)}\,\frac{\coth\beta(\omega_1-\omega_2)-1}{2}\,\cdots\,\frac{f(\omega_n)}{\omega_n}\,\frac{\coth\beta\omega_n-1}{2}\,d\omega_1\cdots d\omega_n \quad (26)$$

and using the formulation

$$\int_{-\infty}^{\infty}\frac{e^{-i\omega t}}{[(t-ikI)(t+ikJ)]^{3/2+q}}\,dt$$

$$= 2\,e^{\frac{I-J}{2}k\omega}\left(\frac{|\omega|}{(I+J)k}\right)^{q+1}\frac{\Gamma(\frac{1}{2})}{\Gamma(q+\frac{3}{2})}\,K_{q+1}\left(\frac{I+J}{2}k|\omega|\right) \quad (27)$$

where $K_q(x)$ is the modified Hankel function.

We get :

$$S^{(1)} = \frac{\sum_B}{2}\frac{k^2}{T^2}(1-P)^{-2}(1-\ell)^{-2}\left\{\sum_{q=0}^{\infty}\left(-\frac{mk}{M}\gamma(0)(I+J)\right)^q \cdot \sum_{n=0}^{q}\frac{1}{\Gamma(q-n+1)\Gamma(n+1)}\int_{-\omega_m}^{\omega_m} G_n(\omega)\left(\frac{|\omega|}{(I+J)k}\right)^{q+1} K_{q+1}\left(\frac{I+J}{2}k|\omega|\right) e^{\frac{I-J}{2}k\omega}\, d\omega\right\} \quad (28)$$

Similarly :

$$S^{(2)} = \frac{\sum_B}{2}\frac{k^2}{T^2}(1-P)^{-2}(1-\ell)^{-2}\left\{\sum_{q=0}^{\infty}\left(-\frac{mk}{M}\gamma(0)(I+J)\right)^q \cdot \sum_{n=0}^{q}\frac{1}{\Gamma(q-n+1)\Gamma(n+1)}\int_{-\omega_m}^{\omega_m} G_n(\omega)\left(\frac{|\omega|}{(I+J)k}\right)^{q+1} K_{q+1}\left(\frac{I+J}{2}k|\omega|\right) e^{\frac{I+J}{2}k\omega}\, d\omega\right\} \quad (29)$$

From eq (28) and eq (29) :

$$S = -2\frac{\sum_B}{(1-P\ell)(1-P)(1-\ell)}\left\{\sum_{q=1}^{\infty}\left(-\frac{m}{M}Z\right)^q \cdot \sum_{n=1}^{q}\frac{1}{\Gamma(q-n+1)\Gamma(n+1)} \cdot \int_0^{\omega_m} \sinh\left(\frac{P}{1-P}\zeta\right)\sinh\left(\frac{\ell}{1-\ell}\zeta\right) G_n'(\zeta)\,\zeta^{q+1} K_{q+1}\left(\left(1+\frac{P}{1-P}+\frac{\ell}{1-\ell}\right)\zeta\right) d\zeta\right\} \quad (30)$$

where

$$G_n'(\zeta) = \left(\frac{-1}{2}\right)^n \int_0^{\omega_m}\cdots\int_0^{\omega_m}\prod_{i=1}^{n-1}\left[\frac{f(\omega_{i-1}-\omega_i)}{(\zeta_{i-1}-\zeta_i)}\frac{1}{2\sinh(\zeta_{i-1}-\zeta_i)} + \frac{f(\omega_{i-1}+\omega_i)}{(\zeta_{i-1}+\zeta_i)}\frac{1}{2\sinh(\zeta_{i-1}+\zeta_i)}\right]\frac{f(\omega_n)}{\zeta_n\sinh\zeta_n}\, d\omega_1\cdots d\omega_n \quad (31)$$

$$z = \frac{\gamma(0)}{\beta}, \qquad \zeta_n = \beta\omega_n \quad \text{and} \quad \zeta_0 = \zeta ,$$

In phonon expansion method, the integrant in eq (17) is expanded by :

$$\sum_{q=0}^{\infty} \frac{\Gamma(\frac{3}{2}+q)}{\Gamma(\frac{3}{2})\Gamma(q+1)} \left(\frac{m}{M}\right)^q \int_{-\infty}^{\infty} \frac{[(I+J)\kappa\gamma(t)]^q}{[(t-i\kappa I)(t+i\kappa J)+\frac{m}{M}\kappa\gamma(0)(I+J)]^{3/2+q}} dt \qquad (32)$$

By similar calculation as the mass expansion method, we get :

$$S = \frac{-2\Sigma_B}{(1-P\ell)(1-P)(1-\ell)} \sum_{q=0}^{\infty} \left(\frac{m}{M}\right)^q \frac{1}{\Gamma(q+1)}$$
$$\cdot \int_0^{\omega_m} \sinh\left(\frac{P}{1-P}\zeta\right) \sinh\left(\frac{\ell}{1-\ell}\zeta\right) G_q'(\zeta) \frac{\zeta^{q+1} K_{q+1}\left(\gamma_1 \frac{1-P\ell}{(1-P)(1-\ell)}\zeta\right)}{\gamma_1^{q+1}} d\omega \qquad (33)$$

where

$$\gamma_1 = \sqrt{1 + 4\frac{m}{M}\frac{\gamma(0)}{\kappa T}\frac{(1-P)(1-\ell)}{(1-P\ell)}}$$

In the case that mass M approaches to one, the convergence of series in the eqs (32) and (33) becomes slow. In order to calculate the differential cross section, the author developed the two frequency dividing model (22) in which the frequency function is divided in two parts in such a way that the high energy approximation is applicable to the low energy frequency and the phonon or mass expansion method is applicable to the other part with high frequency. By using this model, we can improve the convergence of the series in the phonon or mass expansions. This means that the function $\lceil M(0) - M(t) \rceil$ is divided into the following two integrals by the cut frequency ω_c

$$[M(0)-M(t)] = \frac{\kappa}{2M}\left\{\int_0^{\omega_c} \coth\beta\omega \frac{f(\omega)}{\omega} d\omega - \int_0^{\omega_c} [\coth\beta\omega\cos\omega t + i\sin\omega t] \frac{f(\omega)}{\omega} d\omega \right.$$
$$\left. + \int_{\omega_c}^{\omega_m} \coth\beta\omega \frac{f(\omega)}{\omega} d\omega - \int_{\omega_c}^{\omega_m} [\coth\beta\omega\cos\omega t + i\sin\omega t] \frac{f(\omega)}{\omega} d\omega \right\} \qquad (34)$$

The integration in the low energy frequency part from 0 to ω_c is expanded by power series of t. However, if the ω_c is not small enough compared with the temperature, the neglect of higher term of t^n spoils the energy balance. If we assume that the low energy frequency part is located in the very small energy compared with the temperature T, the integration of M(0) - M(t) over the low energy region is expressed by :

$$-\frac{\hbar}{2M_e}\left(it-\frac{Tt^2}{\hbar}\right) \tag{35}$$

where M_e is the effective mass for the low frequency part, and is defined as:

$$M_e = M\left(1-\int_{\omega_c}^{\omega_m} f(\omega)\,d\omega\right) \tag{36}$$

By this approximation and applying the mass expansion method to the high frequency part, the generating function S is expressed by :

$$S = \frac{\sum_B}{2}\frac{T^2}{\hbar^2}(1-P)^{-2}(1-\ell)^{-2}\sum_{q=0}^{\infty}\frac{\left(-\frac{m}{M}\hbar\gamma(0)(I+J)\right)^q}{\left[1+\frac{m_e}{M}(I+J)T\right]^{3/2+q}}$$
$$\sum_{n=0}^{q}\frac{1}{\Gamma(q-n+1)\Gamma(n+1)}\int_{-\omega_m}^{''\omega_m}G_n''(\omega)\left\{\left(\frac{|\omega|}{(I'+J')\hbar}\right)^{q+1}K_{q+1}\left(\frac{I'+J'}{2}\hbar|\omega|\right)e^{\frac{I'-J'}{2}\hbar\omega}\right.$$
$$\left.-\left(\frac{|\omega|}{(I''+J'')\hbar}\right)^{q+1}K_{q+1}\left(\frac{I''+J''}{2}\hbar|\omega|\right)e^{\frac{I''+J''}{2}\hbar\omega}\right\}d\omega \tag{37}$$

where the signs ($''$) on the integration sign and $G_n(\omega)$ means that the integration in the expression is done only over the high energy frequency part, where

$$\begin{matrix} I' \\ -J' \end{matrix} = \frac{-\left[(J-I)-\frac{m_e}{M}(I+J)\right]\mp\sqrt{\left((J-I)-\frac{m_e}{M}(I+J)\right)^2+4\left(1+\frac{m_e}{M}T(I+J)\right)IJ}}{2\left[1+\frac{m_e}{M}T(I+J)\right]}$$
$$\begin{matrix} I'' \\ -J'' \end{matrix} = \frac{\left[(I+J)\left(1+\frac{m_e}{M}\right)\right]\pm\sqrt{(I+J)^2\left(1+\frac{m_e}{M}\right)^2+4\left(1+\frac{m_e}{M}T(I+J)\right)IJ}}{2\left[1+\frac{m_e}{M}T(I+J)\right]} \tag{38}$$

b) Time dependent problem

The method for the space dependent problem in the last section can easily be extended to the case of time dependent problem. The time dependent equation, in the medium with the 1/v absorption is expressed by :

$$-\frac{\lambda}{v}\phi(E)+\frac{\Gamma}{v}\phi(E)-\int_0^\infty \phi(E')\,\Sigma_s(E'\to E)\,dE' + \Sigma_s(E)\,\phi(E)=0 \qquad (39)$$

This equation is easily solved by expanding the terms $-\frac{\lambda}{v}\phi(E)$ and $\frac{\Gamma}{v}\phi(E)$ in terms of the Laguerre polynomial of first order energy (from now on, we will include the absorption term $\frac{\Gamma}{v}$ into decay term $\frac{\lambda}{v}$). But, in the following eigenvalue problem

$$A\psi = \lambda B \psi$$

since the large number of calculation codes have been developed for the case that matrix B is diagonalized, it is more convenient to use the other orthogonal set diagonalizing the term which is proportional to 1/v.

We assume that $\phi(E)$ can be expressed as :

$$\phi(E)=\sum_{i=0}^{\infty}\sqrt{\frac{\Gamma(i+1)}{\Gamma(i+\frac{3}{2})}}\,L_i^{(1/2)}\left(\frac{E}{T}\right)\frac{E}{T^2}e^{-E/T}a_i \qquad (40)$$

Substituting eq. (40) into eq (39) and multiplying the resulting equation by

$$\sqrt{\frac{\Gamma(j+1)}{\Gamma(j+\frac{3}{2})}}\,L_j^{(1/2)}\left(\frac{E}{T}\right)$$

and integrating over E, we get :

$$\left[\lambda\,\delta_{ij}-v_0\,S_{ij}^{T}\right]a_i=0 \qquad (41)$$

where $v_o = \sqrt{2mT}$

$$S_{ij}^{T} = \sqrt{\frac{\Gamma(i+1)\,\Gamma(j+1)}{\Gamma(i+\frac{3}{2})\,\Gamma(j+\frac{3}{2})}} \left[\int_0^\infty \int_0^\infty dE'dE\, \Sigma_s(E'\to E)\, L_i^{(1/2)}\left(\frac{E'}{T}\right) L_j^{(1/2)}\left(\frac{E}{T}\right) \frac{E'}{T^2} e^{-\frac{E'}{T}} \right.$$

$$\left. - \int_0^\infty \int_0^\infty dE'dE\, \Sigma_s(E'\to E) L_i^{(1/2)}\left(\frac{E'}{T}\right) L_j^{(1/2)}\left(\frac{E'}{T}\right) \frac{E'}{T^2} e^{-\frac{E'}{T}} \right] \qquad (42)$$

Since the Laguerre polynomial of half order $L_i^{(1/2)}(x)$ has the generating function of eq (6), the matrix elements S_{ij}^{T} in eq (42) are obtained as the coefficient of

$$\sqrt{\frac{\Gamma(i+\frac{3}{2})\,\Gamma(j+\frac{3}{2})}{\Gamma(i+1)\,\Gamma(j+1)}}\, p^i \ell^j$$

in the following generating function S^T

$$S^T = \sqrt{(1-p)(1-\ell)}\, S \qquad (43)$$

where S is the generating function of the space dependent problem in eq (18).

Furthermore, if the diffusion coefficient or the absorption cross section is proportional to E^α, the generating function S^α of the matrix for scattering kernel, where the flux is expanded in terms of Laguerre polynomial diagonalizing the diffusion term or the absorption term, is composed from the S in eq (18) as follows :

$$S^\alpha = \left[(1-p)(1-\ell)\right]^{-\alpha} S \qquad (44)$$

3. Numerical results

Since much more works have been studied for the time dependent problem than for the space dependent problem, we will consider mainly the time dependent problem as the application of the above described theory.

The decay constant λ of pulsed neutrons in a small assembly is expressed by : (1~3)

$$\lambda = (\Sigma_a v) + D_0 B^2 - C B^4 \tag{45}$$

where B is the buckling of the assembly, D_0 is the diffusion coefficient, Dv averaged over the Maxwellian distribution, and C is the diffusion cooling coefficient.

In the case of an energy independent diffusion coefficient, Nelkin (3) found :

$$C = \frac{\sqrt{\pi}}{4} \frac{D_0^2}{v_0 M_2} = \frac{D_0^2}{6 \lambda_{M_2}} \tag{46}$$

where M_2 is the thermalization power and is defined as :

$$M_2 = \frac{1}{T^4} \int_0^\infty dE' \int_0^\infty dE \, \Sigma(E' \to E)(E'-E)^2 E' e^{-\frac{E'}{T}} \tag{47}$$

and it is related to the matrix element S_{11} and S_{11}^T as follows :

$$M_2 = 4 S_{11} = \frac{3\sqrt{\pi} S_{11}^T}{2} \tag{48}$$

This diffusion cooling coefficient (12) is expressed more exactly by :

$$C = \sum_{m=1}^{\infty} \frac{\left[\int_0^\infty \phi_m^T(E) \phi_0^T(E) \frac{1}{E} e^{+\frac{E}{T}} dE \right]^2 D^2}{\lambda_m} = \frac{D_0^2}{6 \bar{\lambda}_1} \tag{49}$$

where λ_m, ϕ_m^T, the mth eigenvalue and eigenfunction of time dependent equation (39). Since the term of m = 1 contributes mainly in many cases and the value of $\int_0^\infty \phi_1^T(E)\phi_0^T(E)\frac{1}{E}e^{-\frac{E}{T}}dE$ is nearly $\left(\frac{2}{\sqrt{6\pi}}\right)$,

$$C = \frac{D_0^2}{6\lambda_1} \tag{50}$$

In table I, the time dependent eigenvalues for the free gas case are shown as unit of

$\frac{M}{m}\frac{1}{\Sigma_f v_0}$ where the 20 x 20 matrices which remain the terms until the $L_{20}^{(1/2)}(x)$ are solved.

Table I shows that the ratios of $\lambda_{n+1}/\lambda_n (n > 1)$ in the case of mass 1 are smaller than the ratio in the case of heavy mass. This makes it difficult to distinguish the λ_1 from the higher eigenvalues in case of free gas with mass 1. In the case of comparatively heavy gas like the one of mass 10, their eigenvalues approach those of the heavy gas model, but the high eigenvalues are different from those of the heavy gas. This means that, in this case, the heavy gas model is not applicable to the analysis in the high energy region.

Figure 1 shows the eigenfunctions of mass 1, 2, ∞, which are calculated from 10 x 10 dimensioned matrix.

The eigenvalues for mass 1, calculated from the several dimensioned matrices are shown in table II in order to see their convergence, and their eigenfunctions are shown in figure 2. The convergence appears comparatively slow, and the higher eigenfunctions show different shapes in the various matrix dimensions.

Next, the space dependent eigenvalues and eigenfunctions are shown in table III, and figure 4. Similarly to the time dependent case, the ratio of spatial eigenvalues B_{n+1}^2 / B_n^2 decreases when the mass approaches to 1. The convergence of spatial eigenvalues in the case of mass 1 is shown in table IV. The convergence is faster than in the time dependent case. We can easily understand this fact, if we consider that the first order Laguerre polynomials are the spatial eigenfunctions in the heavy gas model.

Heavy crystalline model

Next, we are going to consider the effect of the chemical binding on neutron thermalization by taking the heavy crystalline model, where the mass M is so heavy that the first power of 1/M is taken in the expansion for eq. (30). The time and spatial eigenvalues in the heavy crystalline model with the Debye frequency are shown with the thermalization power M_2 in table V.

The eigenvalues of graphite crystals in room temperature are calculated with the frequency which was Yoshimori and Kitame calculated for the study of specific heat. In the case that graphite is assumed to be the heavy crystalline model the eigenvalues are shown in table IV, and their eigenfunction in figure 4 .

In the case of simple energy independent diffusion coefficient, the formulation for the diffusion cooling coefficient is described in eq (49). However, we should carefully compare the results obtained with experimental values by including the effect of energy dependent diffusion coefficient and the correction of the B^6 term. Thus we just have to compare the obtained results with the values calculated from the other theories, i.e. the values of $\overline{\lambda}_1$ in eq (49), λ_1 in eq (50) are compared with λ_{M_1} in eq (46).

If we assume that Beryllium is the heavy crystalline material at the Debye temperature (θ = 1000°K), we get the value of $\lambda_1 M/\Sigma_B m = 0.38$, $\overline{\lambda}_1 M/\Sigma_B m = 0.5020$. The latter value is smaller than the value calculated from eq (46) $\lambda_{M_2} M/\Sigma_B m = 1.685$ by a factor 3.36, and approaches the old experimental value measured by Komoto and Kloverstom (1958) rather than the recent data measured by de Saussure and Silver (1958).

In the graphite which is assumed a heavy crystalline with the frequency function of the Yoshimori-Kitano model, $\lambda_1 M/\Sigma_B m = 0.333$ and $\overline{\lambda}_1 M/\Sigma_B m = 0.399$ are obtained, and the value is smaller than the $\lambda_{M_2} M/\Sigma_B m = 0.957$ by a factor 2.4. According to the Krumhansl and Brooks (21) model whose frequency function is the Debye frequency with θ_z = 900°K, θ_{xy} = 2500°K, the value of $\lambda_{M_2} M/\Sigma_B m$ is 0.843. These results show that high matrix elements are very important in the calculation of diffusion cooling coefficients.

Singwi calculated the effect of this non maxwellian distribution for the diffusion cooling coefficient by taking the first three terms of the Laguerre expansion of the flux. However, by using the heavy gas model instead of heavy crystalline model, he estimated this value to be nearly 20 %. This is underestimated. If we take the 3 x 3 matrix which corresponds to the Singwi's correction, the values of $\lambda M / \Sigma_B m$ Beryllium and graphite are 1.172, 0.649 respectively, where λ is the time dependent first eigenvalue calculated from the 3 x 3 matrix.

Acknowledgment

The author wishes to acknowledge the valuable discussions he has had with V. Raievski and H. Rief. He also wishes to express his appreciation to E. Caglioti for programming a part of the mathematical expressions. The author is indebted to J. Chernick and N. Corngold for studying the neutron thermalization problem during his stay in Brookhaven National Laboratory.

References

1. v. Dardel G., Trans. Roy. Inst. Technol. Stockholm, 75 (1954)
2. v. Dardel G & Sjöstrand G., Phys. Rev. 96, 1245 (1954)
3. Nelkin M., J. Nucl. Energy, 8, 48 (1958)
4. Corngold N., Private communication
5. Singwi K., Arkiv för Fysik, Band 16, 385 (1960)
6. Schofield P., AERE-R 3400
7. Haefel W. & Dresner L., Nuclear Sci. & Eng., 7 (1959)
8. Bailly du Bois, B. Horowitz, J. Maurette C., Rapport S.P.M. n° 525, Saclay (1958)
9. Purohit S., Nuclear Sci. & Eng., 9, 157 (1961)
10. Kottwitz D., Nuclear Sci. & Eng., 7, 345-54 (1958)
11. Michael P., Nuclear Sci. & Eng., 8, 426-431 (1960)
12. Takahashi H., unpublished Brookhaven National Laboratory Memorandum (Aug. 14, 1961)
13. Komoto T. & Kloverstrom, Trans. Am. Nucl. Soc. 1, 1 (1958)
14. De Saussure,G. & Silver E.G., ORNL-2609, 59 (1958)
15. Beckurts K., Nuclear Instrument & Method, 11, 144-168 (1961)
16. Weinberg A.M. & Wigner E., The Physical Theory of Neutron Chain Reactor, The University of Chicago Press (1958)
17. Zemach A. & Glauber R., Phys. Rev. 101, 118 (1956)
18. Sjölander A., Archiv för Fysik, Band 14, 315 (1958)
19. Yoshimori A. & Kitano Y., J. Phys. Soc. Japan 11, 352 (1956)

20. Komatsu K., J. Phys. Soc. Japan, 10, 346 (1955)

21. Krumhansl J. & Brooks H., J. Chem. Phys., 21, 1663 (1953)

22. Takahashi H., unpublished Brookhaven National Laboratory Memorandum (Aug. 25, 1960)

mass	(1)	0	1	2	3	4	5	6	7	8	9
1	1.064	0	0.9242	1.131	1.300	1.531	1.806	2.110	2.436	2.777	3.132
2	1.638	0	1.318	1.699	2.107	2.635	3.235	3.881	4.560	5.265	5.992
3	1.954	0	1.541	2.130	2.761	3.563	4.467	5.438	6.457	7.517	8.611
4	2.153	0	1.685	2.478	3.306	4.356	5.539	6.812	8.154	9.554	11.01
5	2.289	0	1.786	2.764	3.769	5.043	6.480	8.034	9.680	11.40	13.20
10	2.608	0	2.03	3.643	5.318	7.414	9.826	12.49	15.38	18.47	21.75
	3.009	0	2.352	5.207	8.889	13.54	19.19	25.85	33.57	42.40	52.45

mass	10	11	12	13	14	15	16	17	18	19
1	3.499	3.879	4.271	4.679	5.103	5.549	6.023	6.536	7.110	7.800
2	6.741	7.512	8.309	9.133	9.992	10.89	11.85	12.88	14.04	15.42
3	9.739	10.90	12.10	13.34	14.64	16.00	17.44	18.99	20.73	22.82
4	12.51	14.05	15.66	17.32	19.05	20.86	22.79	24.87	27.28	30.00
5	15.06	16.99	18.99	21.06	23.22	25.50	27.91	30.52	33.43	36.94
10	25.21	28.87	32.70	36.73	40.97	45.45	50.23	55.42	61.28	68.38
	63.83	76.69	91.20	107.6	126.0	146.9	170.8	199.0	277.8	277.9

Table I – The time dependent eigenvalues for the free gas.

Unit is $\frac{1}{\sum_f \nu_o} \frac{M}{m}$. The values in column (1) are the matrix element S^T_{11}.

Dimension of matrix	1	2	3	4	5	6	7	8
17 x 17	0.9244	1.141	1.339	1.606	1.918	2.262	2.629	3.014
14 x 14	0.9246	1.158	1.396	1.711	2.075	2.474	2.900	3.350
11 x 11	0.9252	1.186	1.486	1.872	2.315	2.800	3.326	3.899
8 x 8	0.9273	1.243	1.647	2.156	2.744	3.417	4.231	-

Dimension of matrix	9	10	11	12	13	14	15	16
17 x 17	3.416	3.835	4.273	4.734	5.224	5.754	6.345	7.056
14 x 14	3.827	4.335	4.885	5.499	6.237	-	-	-
11 x 11	4.541	-	-	-	-	-	-	-

Table II - The convergence of time dependent eigenvalues in the case of mass 1.

(The values of $\frac{\lambda}{\nu_0} \frac{1}{\Sigma_f}$ are shown .)

mass \ i	0	1	2	3	4	5	6	7	8	9
1	0	0.3284	0.6201	0.9022	1.179	1.453	1.725	1.994	2.263	2.532
2	0	0.5259	1.077	1.621	2.159	2.693	3.223	3.751	1.277	4.802
3	0	0.6370	1.406	2.199	2.993	3.783	4.571	5.356	6.136	6.917
4	0	0.7068	1.646	2.661	3.698	4.740	5.781	6.821	7.859	8.894
5	0	0.7543	1.827	3.033	4.293	5.576	6.864	8.156	9.445	10.74
10	0	0.8646	2.301	4.116	6.182	8.413	10.75	13.17	15.63	18.12
	0	1	3	6	10	15	21	28	36	45

mass \ i	10	11	12	13	14	15	16	17	18	19
1	2.796	3.062	3.327	3.592	3.855	4.119	4.382	4.649	5.069	11.14
2	5.324	5.847	6.368	6.888	7.407	7.925	8.441	8.965	9.483	16.70
3	7.696	8.474	9.250	10.03	10.80	11.57	12.35	13.12	13.90	21.41
4	9.930	10.96	12.00	13.03	14.05	15.09	16.12	17.16	18.21	25.71
5	12.02	13.31	14.60	15.89	17.18	18.47	19.77	21.08	22.42	29.80
10	20.63	23.16	25.70	28.25	30.81	33.39	36.03	38.83	41.77	48.35
	55	66	78	81	95	110	126	143	161	180

Table III – The space dependent eigenvalues for the free gas

(where the products of spatial eigenvalue times $\frac{M}{m}\frac{1}{4\Sigma_f}(i+1)$ are shown in this table)

Dimension of matrix	8	9	10	11	12	13	14	15	16
17 x 17	2.263	2.530	2.796	3.062	3.327	3.593	3.859	4.191	8.785
14 x 14	2.263	2.530	2.797	3.064	3.349	6.624	-	-	-
11 x 11	2.263	2.532	4.672	-	-	-	-	-	-

Table IV - The convergence of the space dependent eigenvalues in the free gas of mass 1.

The eigenvalues lower than 8th correspond to the results obtained from 20 x 20 matrix.
This table shows the products of the spatial eigenvalue times $\frac{M}{m}\frac{1}{4\Sigma_t}(i+1)$

Debye temp / Temp	S_{11}^T	$\frac{S_{11}^i}{S_{11} \text{ at } =0}$	0	1	2	3	4	5	6	7
0	3.009	1	0	-	-	-	-	-	-	-
1	2.839	0.9434	0	1.906	4.636	9.446	16.33	25.75	38.70	57.80
2	2.412	0.8017	0	1.025	3.271	7.542	14.03	23.13	35.81	54.62
3	1.901	0.6317	0	0.5093	2.089	5.645	11.51	20.02	32.13	50.32
4	1.425	0.4734	0	0.2708	1.205	4.072	9.157	16.91	28.23	45.52
5	1.037	0.3445	0	0.1571	0.6931	2.810	7.164	14.12	24.53	40.77
6	0.7447	0.2475	0	0.09754	0.4187	1.865	5.544	11.69	21.18	36.27
7	0.5349	0.1778	0	0.06466	0.2744	1.251	4.267	9.684	18.29	32.25
8	0.3876	0.1288	0	0.04452	0.1892	0.8632	3.239	8.026	15.81	28.68
9	0.2849	0.0947	0	0.03172	0.1357	0.6177	2.439	6.658	13.70	25.55
spectrum -graphite	0.9939	0.3303	0	0.3332	0.1072	2.949	6.548	12.57	21.78	36.44

Table V - The time dependent eigenvalues of the heavy Debye crystalline model and the graphite.

(where the values of $\frac{M \lambda_i}{\Sigma_\beta m V_o}$ are shown)

Debye temp / Temp	S_{11} \ i	0	1	2	3	4	5	6	7
0	1	0	1	3	6	10	15	21	28
1	0.9434	0	0.9382	2.739	5.358	8.825	13.25	18.79	25.69
2	0.8017	0	0.7492	1.996	3.906	6.782	10.79	16.10	23.07
3	0.6317	0	0.4985	1.270	2.717	5.162	8.775	13.77	20.65
4	0.4734	0	0.3003	0.7739	1.873	3.941	7.122	11.70	18.30
Spectrum of graphite	0.3303	0	0.2653	0.7496	1.582	3.049	5.416	9.020	14.55

Table VI - The spatial eigenvalues of the heavy Debye crystalline model and the graphite.

(where the product of spatial eigenvalue times $\frac{M}{m}\frac{1}{4\Sigma_s}$ (i + 1) are shown)

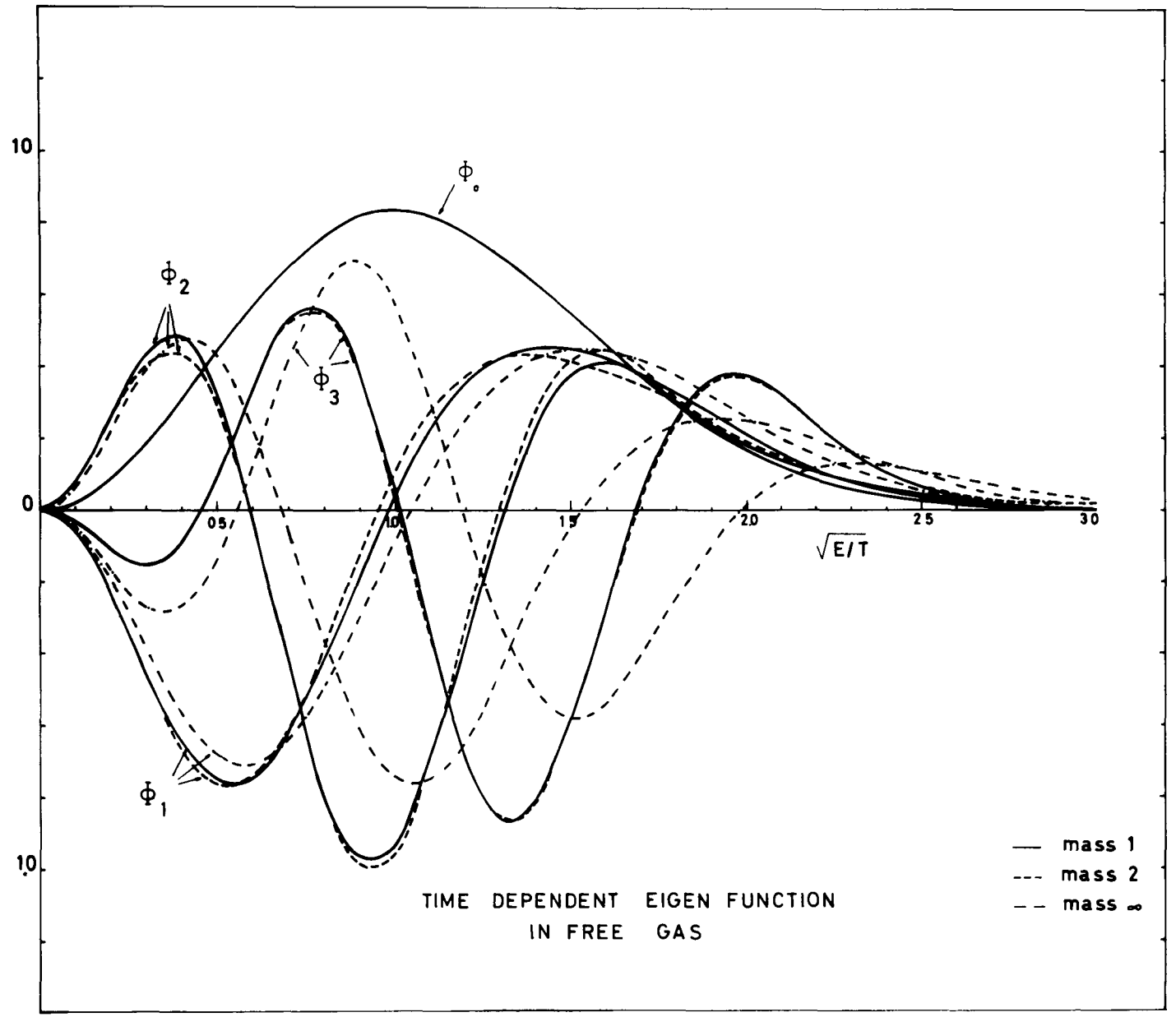
10
0
1.0
Φ_0
Φ_2
Φ_3
Φ_1
0.5
1.0
1.5
2.0
2.5
3.0
$\sqrt{E/T}$
mass 1
mass 2
mass ∞
TIME DEPENDENT EIGEN FUNCTION
IN FREE GAS

Fig 1

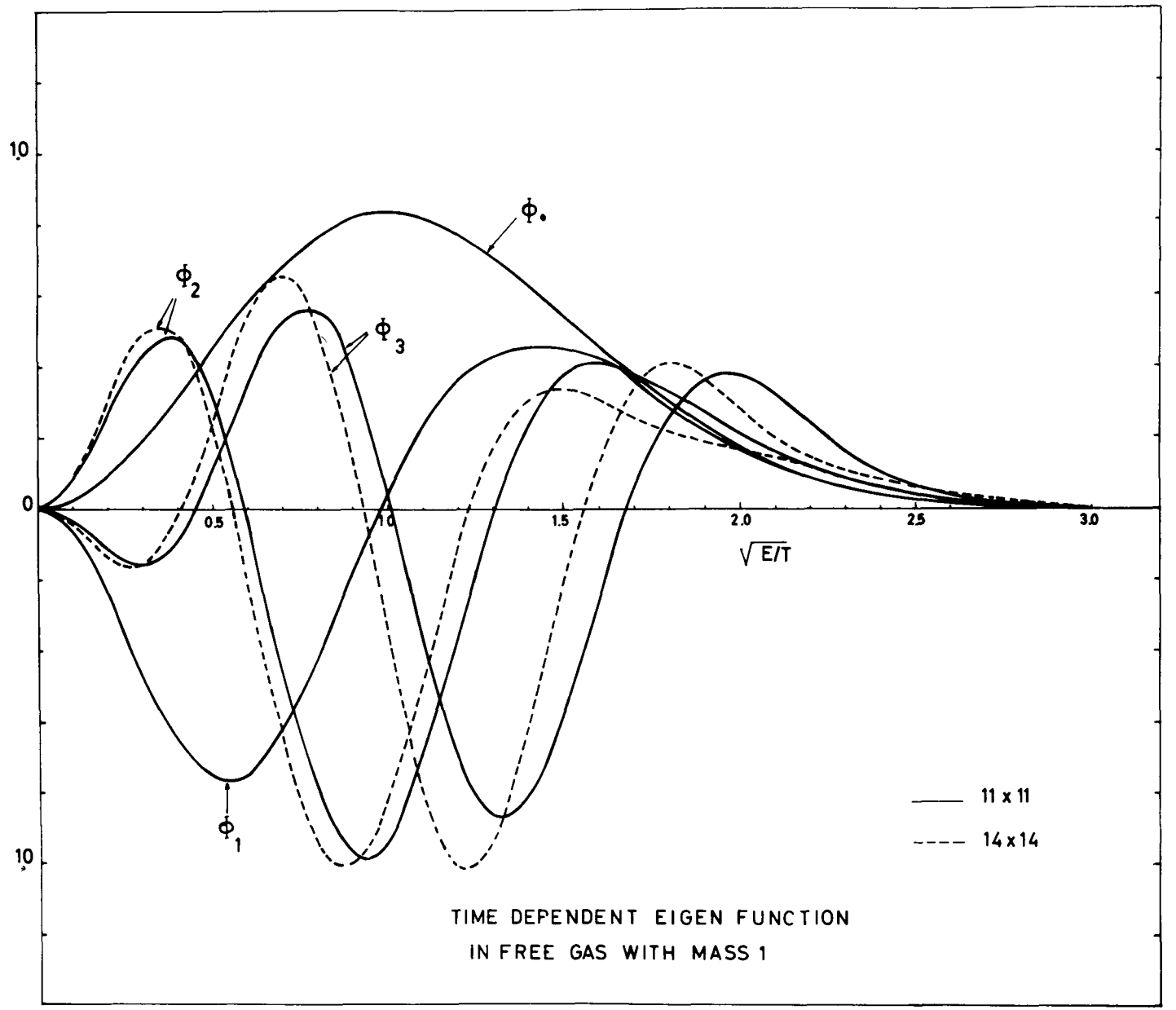
10
0
10
Φ_0
Φ_2
Φ_3
Φ_1
0.5
1.0
1.5
2.0
2.5
3.0
$\sqrt{E/T}$
11 x 11
14 x 14
TIME DEPENDENT EIGEN FUNCTION
IN FREE GAS WITH MASS 1

Fig 2

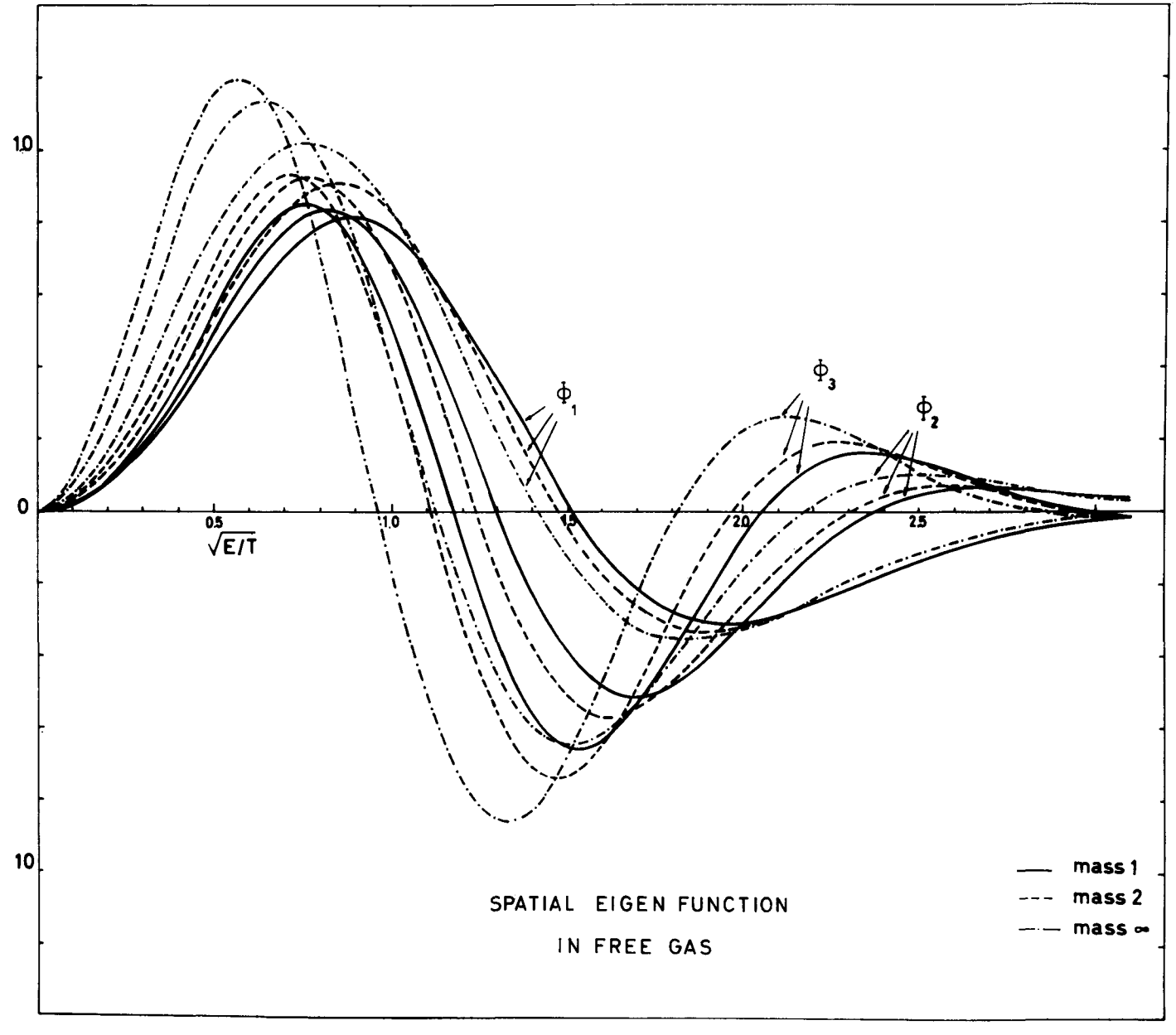
1.0
0
10
0.5
1.0
1.5
2.0
2.5
√E/T
Φ1
Φ2
Φ3
SPATIAL EIGEN FUNCTION
IN FREE GAS
mass 1
mass 2
mass ∞

Fig. 3

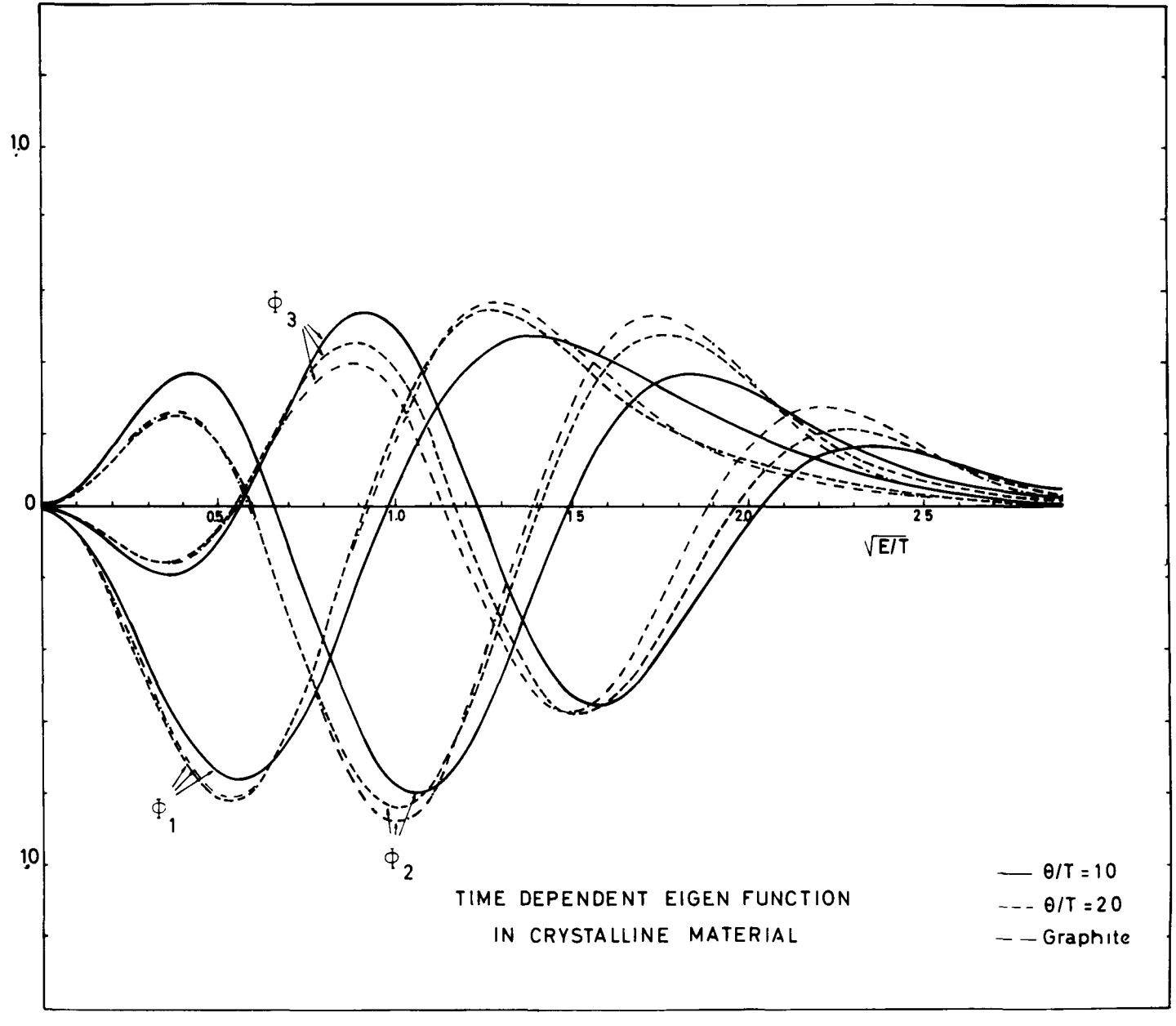
1.0
0
1.0
0.5
1.0
1.5
2.0
2.5
√E/T
Φ3
Φ1
Φ2
TIME DEPENDENT EIGEN FUNCTION
IN CRYSTALLINE MATERIAL
θ/T = 10
θ/T = 20
Graphite

Fig 4

A PAPER PRESENTED TO THE BROOKHAVEN CONFERENCE

ON NEUTRON THERMALIZATION

APRIL - MAY 1962

Space - Energy Separability in Pulsed Neutron Systems

by

M.M.R. Williams*

ABSTRACT

The time, energy and space dependent Boltzmann equation has been studied in order to obtain information on the diffusion cooling coefficient and other pulsed neutron parameters. In order to interpret experiments correctly it is essential to know what is meant by buckling in an energy dependent system. It is shown by an exact spatial analysis of the energy spectrum that this can be identified with the square of the infinite medium Fourier transform variable only if the extrapolation distance Zo is itself a function of buckling. The value of $Zo(B^2)$ has been calculated, together with the average energy of the spectrum across the system.

* Work done at Nuclear Engineering Department, Queen Mary College, London University.

Present address: Central Electricity Generating Board,
Friars House,
Blackfriars Road,
London.

CONTENTS

1. Introduction

The decay constant of the fundamental mode is frequently given in the form:

$$\lambda = \overline{\Sigma a_o V_o} + \overline{D_o} B^2 - C B^4 + F B^6 + O(B^8) \quad \ldots \quad \ldots \quad \ldots \quad (1)$$

where B^2 is the so-called "buckling" of the system. Nelkin[1] has shown how, by solving the infinite medium Fourier transformed Boltzmann equation, the coefficients $\overline{\Sigma a_o V_o}$, $\overline{D_o}$, C etc. can be obtained in terms of averages over the neutron energy spectrum. These equations are solved in this paper in terms of the eigen-functions of the scattering operator S_Q. The quantity B^2 has been left ill-defined in Nelkin's paper. The usual definition of B^2 depends upon the flux going to zero at the extrapolated boundary, however in systems in which the scattering mean free path is a function of energy this is not a unique condition. We shall see that it is possible to obtain a consistent value of B^2 and that this adds certain limitations in the interpretation of pulsed neutron experiments.

2. The Energy Dependent Boltzmann Equation

The exact solution of the Boltzmann equation contains terms corresponding to all the space and energy modes. In what follows we are concerned only with the asymptotic value of this solution such that the energy spectrum has become constant with time (assuming such a condition is possible). This allows the flux to be written:

$$\Phi(\underline{r}, E, t) = \varphi(\underline{r}, E) e^{-\lambda t} \quad \ldots \quad \ldots \quad \ldots \quad (2)$$

For simplicity we shall consider isotropic scattering in the laboratory system of coordinates and the geometry will be that of an infinite slab. The Boltzmann equation then takes the form:

$$\left[-\frac{\lambda}{v} + \Sigma o(E) + \Sigma s(E) + \mu\frac{\partial}{\partial x} \right] \varphi(E,x\mu) = \frac{1}{2}\int_0^\infty dE^1 \int_{-1}^{1} d\mu^1 \; \Sigma(E^1 \to E)\; \varphi\,(E^1,\; x,\; \mu^1) \quad \ldots (3)$$

Assuming a solution of the form $\varphi(E,x) = \varphi(E,B)e^{iBx}$ and solving this by the perturbation method Nelkin[1] arrives at the following set of equations:

$$\sum_{j=o}^{n} F_{2j}\,(E,\lambda)\; \varphi_{2(n-j)_1 o}(E) = \underset{\sim}{So}\; \varphi_{2n_1 o}(E) \quad \ldots \quad \ldots \quad \ldots \quad \ldots \quad (4)$$

where $\varphi(E,B) = \sum_{n=o}^{\infty} (iB)^{2n}\; \varphi_{2n_1 o}\,(E)$

and

$$Do = \frac{1}{Voo} \int_0^\infty \frac{1s(E)}{3}\, M(E)\, dE$$

$$Voo = \int_0^\infty \frac{1}{v}\, M(E)\, dE$$

$$C = C_D + C_t$$

$$C_D = \frac{1}{Voo} \int_0^\infty \left(\frac{1s(E)}{3} - \frac{Do}{v} \right) \varphi_{2\,1o}(E)dE \quad \ldots \quad \ldots \quad \ldots \quad \ldots \quad (5)$$

$$C_t = \frac{1}{Voo} \int_0^\infty \frac{1s^2(E)}{3} \left(\frac{41s}{15} - \frac{Do}{v} \right) M(E)\, dE$$

The values of the coefficients of B^{2n} in equation (1) are obtained by integrating equation (4) over all energy. The notation is that used in Nelkin's paper.

3. Application to a Finite Medium

Before discussing the solution of equation (4) it is necessary to see how this theory can be applied to a finite medium. At the moment it

is still the solution of the infinite medium problem. In spite of this, the solution can be used to construct physically useful solutions in the following way, which has many points in common with the method of images used in elementary electrostatic theory. Instead of dealing with a body of finite size, we consider an infinite medium for which $\varphi(B)$ gives an exact (mathematical) solution. The negative values of $\varphi(B)$ have no physical meaning but if the regions in which $\varphi(B)$ is negative occur only in that part of the medium external to the body we are considering, the negative values can be treated as convenient mathematical fictions introduced to obtain a solution of the physical problem. In general the value of $\varphi(B)$ obtained will not give an exact solution because it is not possible to fulfill the exact boundary conditions at the surface, viz: $\varphi(B, \mu) = 0$ for $0 < \mu < 1$. The mathematical picture is shown below:

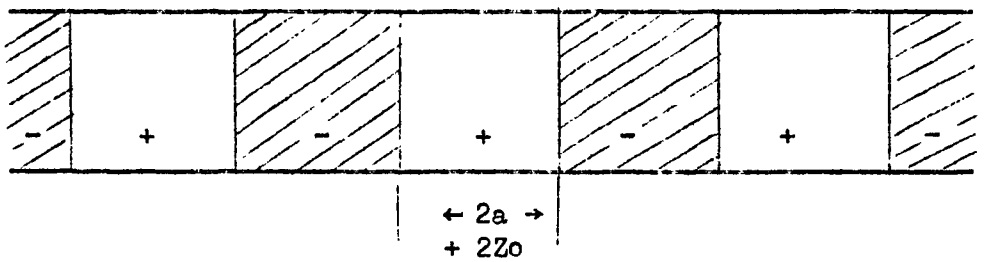

An infinite set of + ve and - ve systems of width '2a + 2Zo' exists (mathematically), the periodicity of the solution is B. It is possible, therefore, to associate this with a finite medium buckling if the periodicity is adjusted so that the solution goes through zero at the extrapolated boundary distant Zo from the surface.

For the present analysis, then, we assume that the square of the infinite medium Fourier transform variable, B^2, can be associated with a finite medium buckling. The validity of this approach and a method of

specifying the correct extrapolation distance Zo is investigated later in this report where the space dependence of the energy spectrum is considered.

4. Solution of the Perturbation Equations

The operation $\underset{\sim}{S}_o\varphi$ characterizes the thermal spectrum. In the one velocity case $\underset{\sim}{S}_o\varphi$ is identically zero. If therefore the flux $\varphi(E)$ is expanded in the eigenfns.of $\underset{\sim}{S}_o$ the deviations from one-velocity theory will be immediately obvious. The operator $\underset{\sim}{S}_o$ is usually extremely complicated, however we will assume that the discrete set of eigenfunctions $X_i(E)$ of it can be found, together with the corresponding eigenvalues. Thus we can write

$$\underset{\sim}{S}_o X_i(E) + K_i X_i(E) = 0 \quad \ldots \quad \ldots \quad \ldots \quad (6)$$

where K_i are the eigenvalues corresponding to the eigenfunctions X_i. It is further assumed that the eigenvalue spectrum is non-degenerate.

Associated with equation (6) is the adjoint equation

$$\underset{\sim}{S}_o^* X_i^*(E) + K_i X_i^*(E) = 0 \quad \ldots \quad \ldots \quad \ldots \quad (7)$$

where $\underset{\sim}{S}_o^*$ and X_i^* are defined through:

$$(X_i^*, \underset{\sim}{S}_o X_i) = (X_i, \underset{\sim}{S}_o^* X_i^*) \quad \ldots \quad \ldots \quad (8)$$

and $$(X_i, X_j^*) = \delta_{ij}$$

Because of detailed balance, the lowest eigenvalue K_o is always zero corresponding to $X_o = Ee^{-E}$ and $X_o^* = 1$. With these facts in mind equation (4) for n=o, 1 can be solved. We make the following expansions:

$$\varphi_{2,1,o}(E) = \sum_{i=0}^{\infty} C_{2,1,i} X_i(E) \quad \ldots \quad \ldots \quad \ldots \quad \ldots \quad (9)$$

We also know that for $\frac{1}{v}$ absorption $\varphi_{0,0}(E) = Ee^{-E} = M(E)$.

Inserting equation (9) into the equation obtained from (4), multiplying by the adjoint $X_k^*(E)$ and integrating gives:

$$C_{2\,k} = \frac{1}{K_k}\left(\frac{1}{3}\,l_{ok} - D_o\,V_{ok}\right), \quad k > o \qquad \ldots \qquad \ldots \qquad (10)$$

Using equations (9) and (10) in (5) gives:

$$C_D = \frac{1}{V_{oo}} \sum_{k=1}^{\infty} \frac{1}{K_k}\left(\frac{1}{3}\,l_{ok} - D_o\,V_{ok}\right)^2 \qquad \ldots \qquad \ldots \qquad (11)$$

where the definition $x_{ik} = \int_o^\infty x(E)\, X_i(E)\, X_k^*(E)\, dE$ is used.

5. The Heavy Gas Approximation

In the particular case of the heavy gas approximation, the eigenfunctions of $\underset{\sim}{S_o}$ are known. The heavy gas operators $\underset{\sim}{S_o}$ and $\underset{\sim}{S_o^*}$ are:

$$\underset{\sim}{S_o} = \frac{2\Sigma_s}{M}\left(E\,\frac{\partial^2}{\partial E^2} + E\,\frac{\partial}{\partial E} + 1\right)$$

$$\underset{\sim}{S_o}^* = \frac{2\Sigma_s}{M}\left(E\,\frac{\partial^2}{\partial E^2} + (2 - E)\,\frac{\partial}{\partial E}\right)$$

and the eigenfunctions and eigenvalues are:

$$X_i(E) = \frac{M(E)\, L_i^{(1)}(E)}{\sqrt{i!\,(i+1)!}}, \qquad X_i^*(E) = \frac{L_i^{(1)}(E)}{\sqrt{i!\,(i+1)!}}$$

$$K_i = \frac{2i\,\Sigma_s}{M} \qquad i = o, 1, \ldots\ldots$$

The diffusion cooling coefficient then becomes

$$C_D = \frac{2V_o\,l_s}{9\sqrt{\pi}\,\xi} \sum_{k=1}^{\infty} \frac{1}{K}\,(l_{ok} - 3\,D_o\,V_{ok})^2$$

For constant cross section

$$C_D = \frac{2\,V_o\,l_s\,D_o^2}{\sqrt{\pi}\,\xi} \sum_{k=1}^{\infty} \frac{V_{ok}^2}{k}$$

We also find the flux to order B^2:

$$\varphi(E,B) = M(E)\left\{1 - B^2 \sum_{i=1}^{\infty} \frac{l_s\, L_i^{(1)}(E)}{\xi i\sqrt{i!\,(i+1)!}}\left(\frac{l_{oi}}{3} - D_o\,V_{oi}\right) + O(B^4)\right\}$$

6. Chemical Binding

If the heavy gas approximation for $\underset{\sim}{So}\ \varphi$ is not a good one, there are two methods of approach. The first is to find a form of $\underset{\sim}{So}$ which includes chemical binding, the difficulties associated with this are well known.[2] The second approach, which is the most practical, utilizes the eigenfunctions of the heavy gas operator but admits that $\underset{\sim}{So}\ Xi \neq -K_i\ Xi$ because the Laguerre polynomials are not eigenfunctions of $\underset{\sim}{So}$.

In this case it is not possible to solve for the $C_{2,k}$ directly, but they can be obtained from the set of equations:

$$\frac{1}{3} 1ok - Do\ Vok = \sum_{i=1}^{\infty} C_{2,i}\ \gamma ik\ , \qquad k > o.$$
$$k = 1, 2, \ldots\ldots$$

where γik is defined as[3]:

$$\gamma ik = B_i\ B_k \int_o^\infty \int_o^\infty dE\ dE^1 M(E)\ \Sigma(E \to E^1) \left[L_i^{(1)}(E)\ L_k^{(1)}(E) - L_i^{(1)}(E^1) L_k^{(1)}(E) \right]$$

$$B_i = [i!\ (i+1)\ !\ ]^{-\frac{1}{2}}$$

Retaining terms i, k = o, 1 we find

$$C_D = \frac{2Vo\ \gamma_{22}\ 1oo^2}{9\sqrt{\pi}(\gamma_{11}\ \gamma_{12} - \gamma_{12}^2)} \left(\frac{1o_1}{1oo} - \frac{1}{2\sqrt{2}} \right)^2 \left\{ 1 + \frac{\gamma_{11}}{\gamma_{22}} \frac{\left(\frac{1o^2}{1oo} - \frac{\sqrt{3}}{8} \right)^2}{\left(\frac{1o_1}{1oo} - \frac{1}{2\sqrt{2}} \right)^2} - \frac{2\gamma_{12}}{\gamma_{22}} \frac{\left(\frac{1o^2}{1oo} - \frac{\sqrt{3}}{8} \right)}{\left(\frac{1o_1}{1oo} - \frac{1}{2\sqrt{2}} \right)} \right\}$$

For $\gamma_{12} = o$ this reduces to an expression obtained by K.S. Singwi[4].

If the $\gamma_{11} >> \gamma ik$ $(k \neq i)$, then C_D can still be represented as an infinite series:

$$C_D = \frac{2voloo^2}{9\sqrt{\pi}} \sum_{k=1}^{\infty} \frac{1}{\gamma kk} \left(\frac{1ok}{1oo} - \frac{Vok}{Voo} \right)^2$$

If the eigenfunctions can be found by any other method then equation (11) is still valid.

7. Average Energy

The average energies inside and outside are frequently of interest, they are defined by

$$\bar{E}_{\varphi} = \frac{\int_0^{\infty} E\ \varphi(E,B)\ dE}{\int_0^{\infty} \varphi\ (E,B)\ dE} \quad , \quad \bar{E}_{out} = \frac{\int_0^{\infty} E\ 1(E)\ \varphi\ (E,B)\ dE}{\int_0^{\infty} 1(E)\ \varphi\ (E)\ dE}$$

They are given by

$$\bar{E}_{\varphi} = 2\left\{1 - \frac{B^2\ \gamma_{22}\ l_{00}}{3\sqrt{2}(\gamma_{11}\ \gamma_{22}-\gamma_{12}^2)}\left(\frac{1}{2\sqrt{2}} - \frac{l_{01}}{l_{00}}\right)\left[1 - \frac{\gamma_{12}}{\gamma_{22}}\frac{\left(\frac{\sqrt{3}}{8} - \frac{l_{02}}{l_{00}}\right)}{\left(\frac{1}{2\sqrt{2}} - \frac{l_{01}}{l_{00}}\right)}\right] + O(B^4)\right\}$$

which for $\gamma_{12} = o$ reduces to

$$\bar{E}_{\varphi} = 2\left\{1 - \frac{B^2 l_{00}}{3\sqrt{2}\ \gamma_{11}}\left(\frac{1}{2\sqrt{2}} - \frac{l_{01}}{l_{00}}\right) + O\ (B^4)\right\}$$

Also

$$\bar{E}_{out} = 2 - \frac{\sqrt{2}\ l_{01}}{l_{00}} - \frac{\sqrt{2}\ B^2}{3\ \gamma_{11}\ l_{00}}\left(\frac{l_{00}}{2\sqrt{2}} - l_{01}\right)\left(l_{11} - \frac{l_{01}^2}{l_{00}}\right) + O(B^4)$$

For $B^2 = 0$ $\quad \bar{E}_{\varphi} = 2$ $\quad$ and $\bar{E}_{out} = 2 - \frac{\sqrt{2}\ l_{01}}{l_{00}}$

This is interesting because it shows that the leakage spectrum differs in average energy from the interior spectrum except for the case of constant m.f.p. in which case $l_{01} \equiv 0$ by the orthogonality of the Laguerre polynomials. Using the values of the cross section obtained by Singwi [5] we find for Beryllium $l_{01} = 0.155$, $l_{00} = 1.51$, $l_{11} = 1.65$. Therefore $\bar{E}_{out} = 1.855$. This differs by about 7% from the infinite medium value inside the assembly. Using a 1/v scattering law for water we find $l_{01}/l_{00} = -0.354$, therefore $\bar{E}_{out} = 2.5$ which is 25% greater than the infinite medium value.

The great difference between the values for Be and H_2O serve to illustrate how sensitive the leakage spectrum is to the variation of m.f.p.

with energy. We shall see further evidence of this in the section on space dependence where the extrapolation distance is calculated.

8. Terms of $O(B^6)$

For small systems terms of order B^6 may become important. In order to find their magnitude we retain higher orders in the set of equation (4), namely the $\varphi_{4,o}$ equation. After solving these equations by the expansion method illustrated above we find for the heavy gas case the coefficient for the B^6 term in the decay constant:

$$F = \frac{l_s^2}{3} C_D - \frac{D_o^3 l_s^2}{\xi^2} \left\{ \frac{1}{V_{oo}} \sum_{i=1}^{\infty} \frac{V_{oi}}{i} \sum_{j=1}^{\infty} \frac{V_{oj} V_{ij}}{j} - \sum_{i=1}^{\infty} \frac{V_{oi}^2}{i^2} - \frac{2}{V_{oo}^2} \left(\sum_{i=1}^{\infty} \frac{V_{oi}^2}{i} \right)^2 \right\}$$

A similar calculation based on the diffusion equation gives for F ($= F^1$ say)

$$F^1 = - \frac{D_o^3 l_s^2}{\xi^2} \left\{ \frac{1}{V_{oo}} \sum_{i=1}^{\infty} \frac{V_{oi}}{i} \sum_{j=1}^{\infty} \frac{V_{oi} V_{ij}}{j} - \sum_{i=1}^{\infty} \frac{V_{oi}^2}{i^2} - \frac{2}{V_{oo}^2} \left(\sum_{i=1}^{\infty} \frac{V_{oi}^2}{i} \right)^2 \right\}$$

$$\therefore \quad F - F^1 = \frac{l_s^2 C_D}{3} \qquad \ldots \quad \ldots \quad \ldots \quad \ldots \quad \ldots \qquad (12)$$

K.S. Singwi [4] has obtained the value F^1 in the first approximation $i, j = 1$. However, because of equation (12) his values are erroneous, the correction term $\frac{l_s^2 C_D}{3}$ which is due to the coupling of transport and energy effects is by no means negligible.

In order to investigate the effect of B^6 terms on the decay constant the diffusion cooling coefficient is rewritten

$$C^1 = C_D \left[1 - \frac{F}{C} B^2 \right]$$

Using $i, j = 1$ in the above we find

$$\frac{F}{C_D} = \frac{l_s^2}{8\xi} \left(1 + \frac{8\xi}{3} \right)$$

or in the more general case

$$\frac{F}{C_D} = \frac{l_s}{8\gamma_{11}} \left(1 + \frac{8 l_s \gamma_{11}}{3} \right)$$

For Be the largest assembly used by Andrews[6] was $B^2 = 0.075$ cu^{-2}, assume $\gamma_{11} = 0.08$, $l_s = 1.51$ we find $(F/C_D)B^2 = 0.234$, this is a correction of 23% somewhat greater than that predicted by Singwi of 16%.

An important conclusion of the above analysis is that diffusion theory can be used to order B^4 in the decay constant and to order B^2 in the flux. Transport corrections to the decay constant are additive and can be small up to B^4. Beyond this transport and energy effects are closely interlinked, however, the neglect of transport effects can be tolerated, c.f. the difference between 23% and 16% of an already small correction.

The weakest part of the above analysis lies in the association of the square of the infinite medium Fourier transform variable with the buckling B^2. In the next section we show how this can be made rigorous provided that the extrapolation distance is suitably defined.

9. The Space Dependent Energy Spectrum

The existence of a unique buckling depends on the validity of the first fundamental theorem of reactor theory viz. space and energy are separable:

$$\Phi(E, \underline{r}) = \Phi(\underline{r})\, f(E) \quad \ldots \quad \ldots \quad \ldots \quad \ldots \quad (13)$$

This is exactly true in a homogeneous infinite medium. It requires however, some justification in finite systems. What is done is to seek an "asymptotic" region inside the medium far from boundaries, in which the first fundamental theorem is valid. Experiments[7] have been performed to test this assumption. Those by Inönu at Oak Ridge are particularly interesting. Inönu measures the thermal and epithermal fluxes and shows that only if data

within 3 - $3\frac{1}{2}$" of the boundary of a large critical aqueous U^{235} solution are included is the extrapolation distance independent of energy i.e. equation (13) applies. (This case is an extreme example, in non-multiplying media the effect will be less).

On physical grounds the exact solution can be written

$$\Phi(E, \underline{r}) = \varphi(\underline{r})\, f\,(E) + \rho_{\text{transient}}(\underline{r}\ E) \quad \ldots \quad \ldots \quad \ldots \qquad (14)$$

The asymptotic part establishes a unique extrapolation distance for a given buckling. The distance 'd' is the width of the zone in which the term ρ_{trans} is important. In the theory which follows, analytical expressions for $Zo(B^2)$, the term ρ_{trans} and the distance 'd' are formulated. As far as possible these expressions have been compared with experimental or theoretical results obtained by other workers (of which there are few). In general the agreement is good although in such comparisons which are of the limit of experimental observation only the general trend can be observed. In particular the results show an increase of $Zo(B^2)$ with buckling for Be and a decrease for H_2O. This is a result of the great differences in the energy dependence of the m.f. paths for these elements.

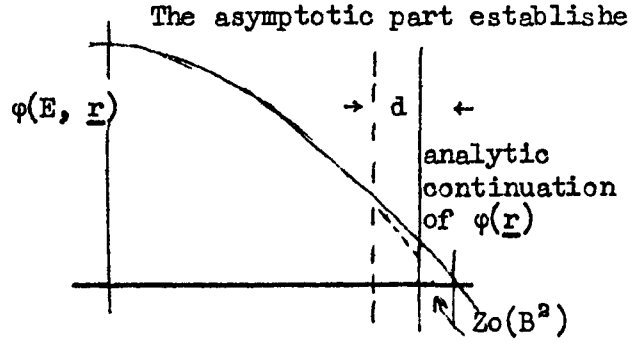

10. The Energy and Space Dependent Diffusion Equation

The analysis which is developed can be treated quite generally in the P_N approximation. However, the important physics of the problem can be illustrated very well by diffusion theory.

The diffusion equation can be written for an infinite slab:

$$\frac{1}{v}\frac{\partial \Phi(E, x, t)}{vt} + \left[\Sigma a(E) - \frac{1(E)}{3}\frac{\partial^2}{\partial x^2}\right]\Phi(E,x,t) = \underset{\sim}{So}\ \Phi(E,x,t) \quad \ldots \quad \ldots \qquad (15)$$

The boundary condition of zero return current is

$$\Phi(E,a,t) + \frac{2}{3} l(E) \left.\frac{\partial \Phi(E,x,t)}{\partial x}\right|_{x=a} = 0 \qquad \ldots \quad \ldots \qquad (16)$$

This equation is solved by means of the expansion

$$\varphi(E,x) = \sum_{i=o}^{\infty} \frac{Xi(x)\, M(E)\, Li^{(1)}(E)}{\sqrt{i!\,(i+1)!}} \qquad \ldots \quad \ldots \qquad (17)$$

Where we have assumed

$$\Phi(E,x,b) = \varphi(E,x)\, e^{-\lambda t}$$

Using these expansions in equations (15) and (16) multiplying by $\frac{L_k^{(1)}}{\sqrt{i!\,(i+1)!}}$ and integrating we find

$$\sum_{i=} \left\{ -\lambda\, Vik - \frac{lik}{3} \frac{\partial^2}{\partial x^2} + \gamma ik \right\} Xi\,(x) = 0 \qquad \ldots \quad \ldots \qquad (18)$$

$k = 0, 1, \ldots$

$$\sum_{i=o}^{\infty} \left\{ \delta ik\, Xi(a) + \frac{2}{3} lik \left.\frac{\partial Xi(x)}{\partial x}\right|_{x=a} \right\} = 0 \qquad \ldots \quad \ldots \qquad (19)$$

where we have assumed $\frac{1}{v}$ absorption and included $\Sigma_{ao}\, V_o$ in λ.

We consider only the i, k = 0, 1 terms:

$$\left.\begin{aligned} &-\lambda\, Voo\, Xo - \frac{loo}{3} \frac{\partial^2 Xo}{\partial x^2} - \lambda\, Vo_1\, X_1 - \frac{lo_1}{3} \frac{\partial^2 X_1}{\partial x^2} = 0 \\ &-\lambda\, Vo_1\, Xo - \frac{lo_1}{3} \frac{\partial^2 Xo}{\partial x^2} - \lambda\, V_{11}\, X_1 - \frac{l_{11}}{3} \frac{\partial^2 X_1}{\partial x^2} + \gamma_{11}\, X_1 = 0 \end{aligned}\right\}$$

$$Xo(a) + \frac{2}{3} loo \left.\frac{\partial Xo(x)}{\partial x}\right|_{x=a} + \frac{2}{3} lo_1 \left.\frac{\partial X_1(x)}{\partial x}\right|_{x=a} = 0$$

$$\frac{2}{3} l o_1 \left.\frac{\partial Xo(x)}{\partial x}\right|_{x=a} + X_1\,(a) + \frac{2}{3} l_{11} \left.\frac{\partial X_1\,(x)}{\partial x}\right|_{x=a} = 0$$

The equation for Xo can be written:

$$a \frac{\partial^4 Xo}{\partial x^4} + b \frac{\partial^2 Xo}{\partial x^2} + c\, Xo = 0 \qquad \ldots \quad \ldots \quad \ldots \quad \ldots \qquad (20)$$

where $a = \dfrac{l_{11}\, l_{00} - l_{01}^2}{9}$

$$b = \frac{1}{3}\left(\lambda V_{00}\, l_{11} + \lambda V_{11}\, l_{00} - \gamma_{11}\, l_{00} - 2\, l_{01}\, \lambda V_{01}\right)$$

$$c = \lambda^2 V_{11} V_{00} - \gamma_{11}\, \lambda V_{00} - \lambda^2 V_{01}^2$$

We seek a solution of the form $X_0(x) = \sum_i A_i e^{-\alpha_i x}$, the equation for α_i then becomes:

$$a\, \alpha_i^4 + b\, \alpha_i^2 + c = 0$$

We can show that the roots of this are $\pm i\,\alpha$, $\pm \alpha_3$ where α and α_3 are real.

Because of the symmetry condition $X_0(x) = X_0(-x)$ and the complete solution to (20) becomes:

$$X_0(x) = A_1 \cos \alpha x + A_2 \cosh \alpha_3 x$$

similarly

$$X_1(x) = \beta A_1 \cos \alpha x - \gamma A_2 \cosh \alpha_3 x$$

where $\beta = \dfrac{\alpha^2 l_{00} - \lambda V_{00}}{\lambda V_{01} - \dfrac{\alpha^2 l_{01}}{3}}$, $\gamma = \dfrac{\lambda V_{00} + \dfrac{\alpha_3^2 l_{00}}{3}}{\lambda V_{01} + \dfrac{\alpha_3^2 l_{01}}{3}}$

The substitution of these two equations into the boundary conditions leads to a determinantal equation, the usefulness of which will become evident after discussion of the parameters α and α_3. By considering the total flux:

$$\varphi(E,x) = M(E)\left[\cos \alpha x \left(1 + \frac{\beta}{\sqrt{2}} L_1^{(1)}(E)\right) + \frac{A_2}{A_1} \cosh \alpha_3 x \left(1 - \frac{\gamma}{\sqrt{2}} L_1^{(1)}(E)\right)\right]$$

and recalling equation (14) we can associate $M(E)\left(1 + \beta/\sqrt{2}\, L_1^{(1)}(E)\right)$ with $\varphi(\underline{r})\, f(E)$ and $\frac{A_2}{A_1} \cosh \alpha_3 x\, M(E)\left(1 - \gamma/\sqrt{2}\, L_1^{(1)}(E)\right)$ with $\rho_{trans}(E,x)$.

Consider further the equation for the decay constant. We find that the equation involving α and λ is

$$\lambda^2(Vo_1^2 - Voo\ V_{11}) + \lambda\left[\frac{a^2}{3}\ (Voo\ l_{11} + V_{11}\ loo - 2\ lo_1\ Vo_1) + \gamma_{11}\ Voo\right] -$$

$$- \frac{\gamma_{11}\ loo\ a^2}{3} - \frac{a^4}{9}(l_{11}\ loo - lo_1^2) = 0$$

which on rearrangement gives:

$$\lambda = \frac{2Vo\ loo}{3\sqrt{\pi}}\ a^2 - \frac{2\ loo^2\ Vo\ a^4}{9\sqrt{\pi}\ \gamma_{11}}\left(\frac{lo_1}{loo} - \frac{1}{2\sqrt{2}}\right)^2 + 0\ (a^6)$$

This is identical with the Fourier transform expression, so that taken with the expression for the total flux it implies that a^2 is equivalent to the buckling of the system provided it is calculated according to the determinantal equation discussed earlier, i.e. the buckling is the inverse wavelength of the asymptotic solution.

11. The Extrapolation Distance

The conventional definition of buckling ($a^2 = B^2$) is for the infinite slab of width '2a':

$$B^2 = \left(\frac{\pi}{2(a+Zo)}\right)^2 = \left(\frac{\pi}{2H}\right)^2$$

This definition can only be retained if Zo is a function of B^2. The value of $Zo(B^2)$ is obtained from:

$$\begin{vmatrix} 1 - \frac{2B}{3}(loo + \beta lo_1)\tan Ba\ , & 1 + \frac{2\alpha_s}{3}(loo - \gamma lo_1)\tanh \alpha_s a \\ \beta - \frac{2B}{3}(lo_1 + \beta l_{11})\tan Ba\ , & \frac{2\alpha_s}{3}(lo_1 - \gamma l_{11})\tanh \alpha_s a - \gamma \end{vmatrix} = 0$$

It will be shown later that $\alpha_s a \gtrsim 3$, hence $\tanh \alpha_s a = 1$.

Also $\tan Ba = \tan \frac{\pi a}{2H} = \tan \frac{\pi(H - Zo)}{2H}$

$$= \tan\left(\frac{\pi}{2} - \frac{\pi\ Zo}{2H}\right) = \tan\left(\frac{\pi}{2} - B\ Zo\right) = \cot B\ Zo$$

Thus we have an equation for $Zo(B^2)$. By expanding the determinant in powers of B^2 we find:

$$Zo = \frac{2}{3}\frac{A}{C}\left\{1 + \left(\frac{B}{A} - \frac{D}{C}\right) B^2 - \frac{4}{27} B^2 \left(\frac{A}{C}\right)^2 + O(B^4)\right\} \quad \ldots \quad \ldots \qquad (21)$$

where $\frac{A}{C} = l_{00}\left(1 + \frac{l_{01}^2/l_{00}^2}{1 + 2\, a_{s,o}^{-1}\, \gamma_{11}}\right)$, $a_{s_1 o} = \sqrt{\frac{3\,\gamma_{11}\, l_{00}}{l_{11}\, l_{00} - l_{01}^2}}$

In order to interpret these results we must assess what effect diffusion theory has on the extrapolation distance. A one velocity P_1 and P_3 calculation has been performed and it is found that:

$$(Zo)P_1 = \frac{2}{3} l_{00}\left(1 - \frac{4}{27} B^2 l_{00}^2 + O(B^4)\right)$$

$$(Zo)P_3 = 0.7051\, l_{00}\,(1 - 0.0148\, B^2 l_{00}^2 + O(B^4))$$

This shows that the P_1 effect overestimates by a considerable amount the variation of Zo with buckling. The P_3 calculation shows that in the one velocity case the variation of Zo with buckling can be neglected in the regions of interest. This implies that any variation of Zo with B^2 observed experimentally is due almost entirely to energy effects. In order to account for this at least to order B^2 we have subtracted the one-velocity P_1 effect from the value of Zo given above in equation (21), giving:

$$Zo = \frac{2}{3} l_{00}\left\{1 + \frac{1}{1 + 2\, a_{s_1}^{-1} o\, \gamma_{11}}\left[\frac{l_{01}^2}{l_{00}^2} + S\, l_{00}^2\, B^2\right] + O(B^4)\right\} \ldots . \qquad (22)$$

S = fn of l_{ik}, γ_{11}.

A P_3 L_1 calculation should be made to test the validity of this but up to order B^2 it should be quite accurate.

An interesting result of this analysis, which is independent of the P_1 subtraction, occurs where $B^2 \to 0$ i.e. we have an infinite half space, then:

$$Zo = \frac{2}{3} lo_0 \left(1 + \frac{l_{o_1}^2 / l_{oo}^2}{1+2\ \gamma_{11}\ \alpha_{s_1}^{-1}{}_0} \right) \quad \ldots \quad \ldots \quad (23)$$

This implies that the multivelocity effect increases the extrapolation distance no matter what the variation of mean free path with energy, for the half space. An approximate calculation for water, assuming it to be a $^1/v$ scatterer, and using diffusion cooling experimental results for γ_{11}, yields an increase of 6.5% for the extrapolation distance over the one velocity value. For Be the increase is only 0.75%. If the cross section is constant then $Zo = {}^2/3\ lo_0$ always.

Numerical results for $Zo(B^2)$ are presented in figures III and IV. They show how sensitive $Zo(B^2)$ is to the sign of lo_1. Gelbard and Davis[8] have performed a P_3 calculation using the Radkowsky kernel and their results for Zo are in close agreement with these, thus showing the validity of subtracting the P_1 one velocity effect.

Tables 5.2, 5.3 and 5.4 give some numerical results for water, with different effective masses for the water molecule, and for beryllium. The experimental results for Be are obtained from Andrew's[6] report by calculation from his values of cube size and buckling. The experimental results for water are obtained by assuming $Zo = 0.71\ \bar{l}$, where $\bar{l}$ is the averaged value of $l(E)$, assuming $l(E) \propto v$, over a maxwellian the average energy of which has been obtained from diffusion cooling experiments and is a function of buckling. Although agreement is not good it is encouraging that the results follow the theoretical trend, i.e. an increase of Zo for Be and decrease for water, with buckling.

12. The Relaxation Length

A relaxation length α_s^{-1} may be defined which is a measure of the width of the transient zone near the boundary. α_s^{-1} is given by:

$$\alpha_s = \sqrt{\frac{3\,\gamma_{11}\,l_{00}}{l_{11}\,l_{00} - l_{01}^2}}\left\{1 - \frac{B^2\,l_{00}}{6\,\gamma_{11}}\left[\left(\frac{l_{01}}{l_{00}} - \frac{1}{2\sqrt{2}}\right)^2 + 3/4\right] + O(B^4)\right\} \quad ..(24)$$

$\alpha_s(B^2 = 0) = \alpha_{s,0}$

We find $\frac{A_2}{A_1}\cosh \alpha_s x \propto$ constant $e^{-\alpha_s(a-x)}$

Thus for distances $> \alpha_s^{-1}$ this term decays rapidly. α_s^{-1} is seen to increase with buckling, this is to be expected since the energy spectrum deviates more from $\equiv$ bm for small systems. Calculations indicate that $\alpha_s^{-1} = 2.6$ cm. and 0.52 cm. for Be and H_2O respectively for the case $B^2 \to 0$. The results suggest that deviation from the asymptotic solution begins to become large at points of the order of α_s^{-1} cm. from the boundary. Tables 5.1 and 5.2 show the variation of α_s^{-1} with buckling. α_s^{-1} is very sensitive to the value of γ_{11} and the effect of chemical binding on space-energy separability can be studied through this parameter. Since γ_{11} appears in the denominator, the smaller it is then the less accurate is space-energy separability i.e. the smaller is the asymptotic region. For low temperatures where γ_{11} becomes very small, this is particularly important and it may well be that no unique buckling exists in the usual sense.

A further reason why at low temperatures pulsed neutron decay constants must be viewed with doubt, at least for crystals, is because of the large amount of elastic scattering at low energies. If this region becomes important then there is a possibility that no unique decay constant will exist, each energy group decaying independently.

13. Average Energy

Having obtained $\varphi(E,x)$ we are in a position to calculate $\bar{E}\varphi(x,B^2)$, this is a convenient measure of the way in which the neutron energy spectrum changes with position and leads to a criterion for judging how accurately space and energy can be made separable.

$$\bar{E}\varphi(x,B^2) = \frac{\int_0^\infty E\ \varphi(E,x)\ dE}{\int_0^\infty \varphi(E,x)\ dE}$$

This leads to:

$$\bar{E}\ \varphi(x,B^2) = 2\left[1 - \frac{1}{\sqrt{2}}\ \frac{\beta \cos Bx - \gamma\ {}^{A_2}/_{A_1} \cosh \alpha_3 x}{\cos Bx + {}^{A_2}/_{A_1} \cosh \alpha_3 x}\right] \quad \ldots \quad \ldots \quad (25)$$

The two extreme values $\bar{E}\ \varphi(o, B^2)$ and $\bar{E}\ \varphi(a, 0)$ are of interest:

$$\bar{E}\ \varphi(\bullet, B^2) = 2\left(1 - {}^{\beta}/_{\sqrt{2}}\right) + 0\left(e^{-\alpha_3 a}\right) \quad \ldots \quad \ldots \quad (26)$$

Apart from the very small correction term this is exactly the same as the result obtained assuming space and energy to be rigorously separable.

We find:

$$\bar{E}\varphi\ (a,o) = 2\left[1 - \frac{1\bullet_1}{\sqrt{2}\ 1\bullet o\ (1+2\ \gamma_{11}\ \alpha_{3,o}^{-1})}\right] \quad \ldots \quad (27)$$

It is also possible to obtain $\bar{E}\varphi(x)$ for a semi-infinite plane $x \leq \bullet$, in this case:

$$\bar{E}\varphi(x) = 2\left[1 - \frac{1o_1/\sqrt{2}}{3/2\left(1+2\ \gamma_{11}\ \alpha_{3,o}^{-1}\right)\left(\frac{2}{3}\ 1o\bullet - x\right)e^{-x/\alpha_{3_1 o}^{-1}} + \frac{1\bullet_1{}^2}{1\bullet\bullet}\left(e^{-x/\alpha_{3_1 o}^{-1}} - 1\right)}\right] \quad \ldots \quad (28)$$

For $x \simeq \bullet$ this reduces to $\bar{E}\varphi(a,\bullet)$.

Equation (27) is an extremely interesting result because apart from the factor $(1 + 2\ \gamma_{11}\ \alpha_{3,o}^{-1})$ it is exactly the expression obtained for $\bar{E}_{out}^{(3)}$ in the space-energy separable case c.f. section 7. The reason for this is apparent through the boundary conditions (16).

$$\bar{E}\varphi(a) = \frac{\int E\ \varphi(E,a)\ dE}{\int \varphi\ (E,a)\ dE} = \frac{\int_0^\infty E\ 1(E)\ \left.\frac{\partial\varphi(E,x)}{\partial x}\right|_{x=a} dE}{\int_0^\infty 1(E)\ \left.\frac{\partial\varphi(E,x)}{\partial x}\right|_{x=a} dE}$$

which is the definition of $\bar{E}_{out}$.

This shows clearly how the space dependent energy spectrum can account concisely for the average energy properties of the spectrum in a single definition. Previous authors[3][4] have had to redefine the average energy for leakage spectrum calculation. $\bar{E}\varphi(x)$ is shown for Be and water in figs. I and V. We notice that $\bar{E}\varphi(x)$ depends sensitively on lo_1. For Be lo_1 is positive but for a 1/v scatter it is negative consequently $\bar{E}\varphi(a)$ is less than $\bar{E}\varphi(o)$ for the former and greater than it for the latter. Furthermore $\bar{E}\varphi(x)$ is constant up to a distance of the order a_s^{-1} from the surface. This illustrates that in this region space and energy are accurately separable.

A physical explanation of these results can be given in the light of certain experiments. In the experiments of Fermi and Anderson[9][10] it was established that neutrons emitted from a cavity a graphite measuring 10 x 10 x 125 cms. have a temperature of 300°K. The temperature of neutrons emitted from the surface of the graphite was found to be 200°K. According to Zinn[11] the temperature of neutrons emitted from a paraffin surface was 390°K whereas their temperature inside the medium was 300°K. This is in agreement with the above theory.

An inevitable conclusion of these results is that the energy of neutrons emitted from a medium is not the same as their energy within the medium and depends on the conditions under which escape takes place.

It is suggested that the essential factor determining the spectrum of neutrons emitted from a surface is the energy dependence of the m.f.p. The spectrum of neutrons escaping from a surface will be enriched in faster neutrons if, with an increase in energy, l(E) is increased, and vice versa. For a precise calculation of the neutron spectrum it is necessary to take into account the changes in neutron density and spectrum in the vicinity of the boundary of

the medium, which are caused by escape, and also the transfer of neutrons from a group with one energy to a group with another as a consequence of the energy exchange in the medium.

Equation (27) shows that these arguments are correct and contains explicitly the energy dependence of the mean free path in the quantity lo_1 and also the energy sharing effect in the quantity $1 + 2\,\gamma_{11}\,\alpha_{3,0}^{-1}$.

In particular, if the mean free path is constant $lo_1 \equiv o$ and the emergent spectrum is the same as the medium spectrum. On the other hand if $l(v) \propto v$ then $lo_1 < o$ and the emergent spectrum is enhanced in high energy neutrons. Similarly if $l(v)$ has the form usually found for crystals where the mean free path increases rapidly for small velocities, the reverse happens, $lo_1 > o$ and the emergent spectrum is softened.

The mean leakage energy does not depend so sensitively on the γ_{11} term, thus showing that it is the mean free path rather than the differential scattering cross section which determines the characteristics of the leakage spectrum.

14. Variation of Buckling with Position

A convenient way of finding how well a single buckling characterizes a medium is to plot $-\nabla^2 \varphi(x,E)/\varphi(x,E)$ against position. This has been done for water and beryllium in figs. III and VI. The energy averaged value, corresponding to $E = 2$, is the least varying value but the relative variation is much greater than that of the average energy.

15. Conclusions

(a) The concept of buckling in energy dependent systems is shown to be valid as long as the asymptotic region is well established. This may not be possible for some substances at low temperatures.

(b) The leakage spectrum is determined mainly by the variation of mean free path with energy and is less sensitive to the differential scattering cross section.

(c) For calculation of neutron spectra in pulsed systems to order B^4 or greater, transport effects must not be neglected.

(d) The spatial calculations have only been performed in diffusion theory, it would be useful to extend the theory to higher orders, both in the P_N and $L_n(1)$ approximations, analytically. Work is proceeding along these lines but at present this is incomplete.

References

(1) M. Nelkin. Nucl. Sci. & Eng. 7, 210, 1960.

(2) N. Corngold. Ann. Phys. 11, 338, 1960.

(3) M. Kazarnovsky. P.I.C.G. 16, 279, 1958.

(4) K.S. Singwi. Ark. Fys. 16, 385, 1960.

(5) K.S. Singwi and L. Kothari. J. Nucl. E. 8, 59, 1958.

(6) Andrews. UCRL 6083.

(7) E. Inönu. ORNL 3016.

(8) Gelbard & Davis. Trans Am. Nuc. Soc. 4, No.2, 291, 1961

(9) E. Fermi. Phys. Rev. 72, 193, 1947

(10) Anderson et al. Phys. Rev. 70, 815, 1946

(11) Zinn. Phys. Rev. 71, 752, 1947.

TABLE 5.1

Relaxation Length for Water

M_2=3.55		M_2=1.044		M_2=7.8	
B^2	α_3^{-1}	B^2	α_3^{-1}	B^2	α_3^{-1}
0	0.5157	0	0.9512	0	0.3480
0.0472	0.5187	0.0477	0.9928	0.0471	0.3489
0.1430	0.5253	0.1480	1.0146	0.1418	0.3509
0.2406	0.5319	0.2544	1.0600	2.374	0.3529
0.3401	0.5387	0.3665	1.1081	0.3339	0.3549
0.4414	0.5456	0.4838	1.1594	0.4312	0.3569
0.5446	0.5526	0.6058	1.2144	0.5293	0.3590

The values of M_2= 1.044, 3.55 and 7.8 correspond to effective masses of the water molecule of 18, 5.3 and 2.4 respectively.

TABLE 5.2

Beryllium Extrapolation Distance (Theory)

B^2	Zo/1oo	α_3^{-1}
0	0.7153	2.607
0.0053	0.7166	2.641
0.0106	0.7178	2.678
0.0159	0.7190	2.717
0.0213	0.7202	2.757
0.0267	0.7214	2.799
0.0321	0.7225	2.842
0.0375	0.7236	2.887
0.0429	0.7247	2.934
0.0484	0.7258	2.984
0.0538	0.7268	3.036
0.0593	0.7278	3.090
0.0648	0.7287	3.147
0.0703	0.7296	3.207
0.0759	0.7305	3.270
0.0814	0.7314	3.337
0.0870	0.7322	3.408

TABLE 5.3

Beryllium Extrapolation Distance.

Experiment

B^2	Zo/1oo
.003369	0.7125
.004810	0.7137
.007419	0.7150
.01290	0.7186
.01823	0.7271
.02772	0.7315
.04693	0.7500
.05792	0.7616
.07313	0.7795

TABLE 5.4

Extrapolation Distance

Water as 1/V Scatterer

M_2=3.55		M_2=1.044		M_2=7.8	
B^2	Zo/1oo	B^2	Zo/1oo	B^2	Zo/1oo
0	0.756	0	0.769	0	0.748
0.0472	0.752	0.0477	0.755	0.0471	0.746
0.1430	0.744	0.1480	0.729	0.1418	0.742
0.2406	0.736	0.2544	0.705	0.2374	0.738
0.3401	0.728	0.3665	0.684	0.3339	0.734
0.4414	0.721	0.4838	0.667	0.4312	0.731
0.5446	0.714	0.6058	0.652	0.5293	0.727

FIGURE 1

VARIATION OF AVERAGE ENERGY WITH POSITION

Water as 1/V scatterer

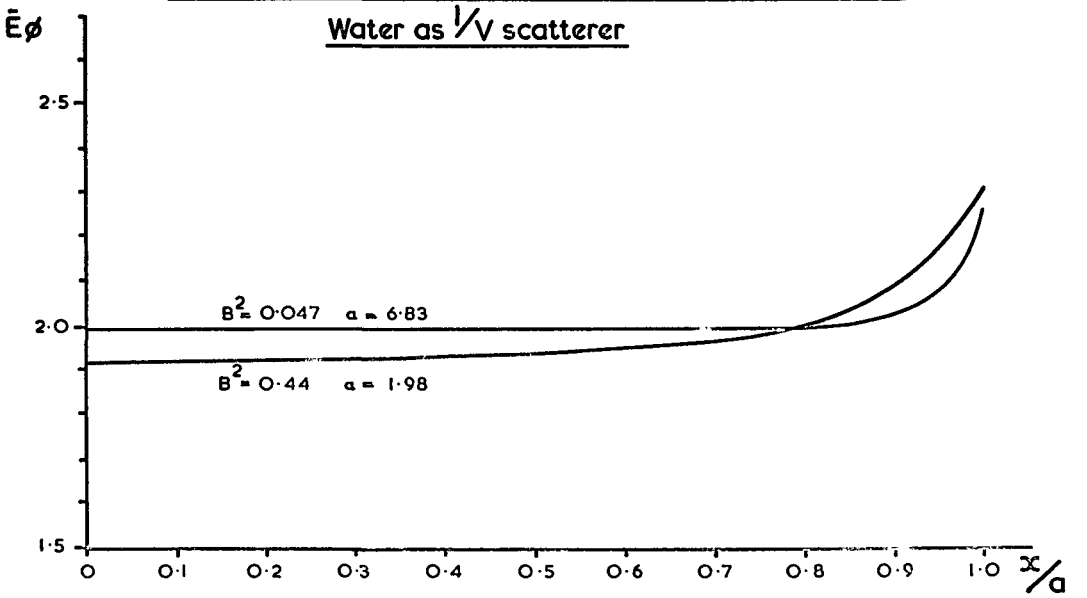

FIGURE 2

VARIATION OF EXTRAPOLATION DISTANCE WITH BUCKLING

Water as 1/V scatterer

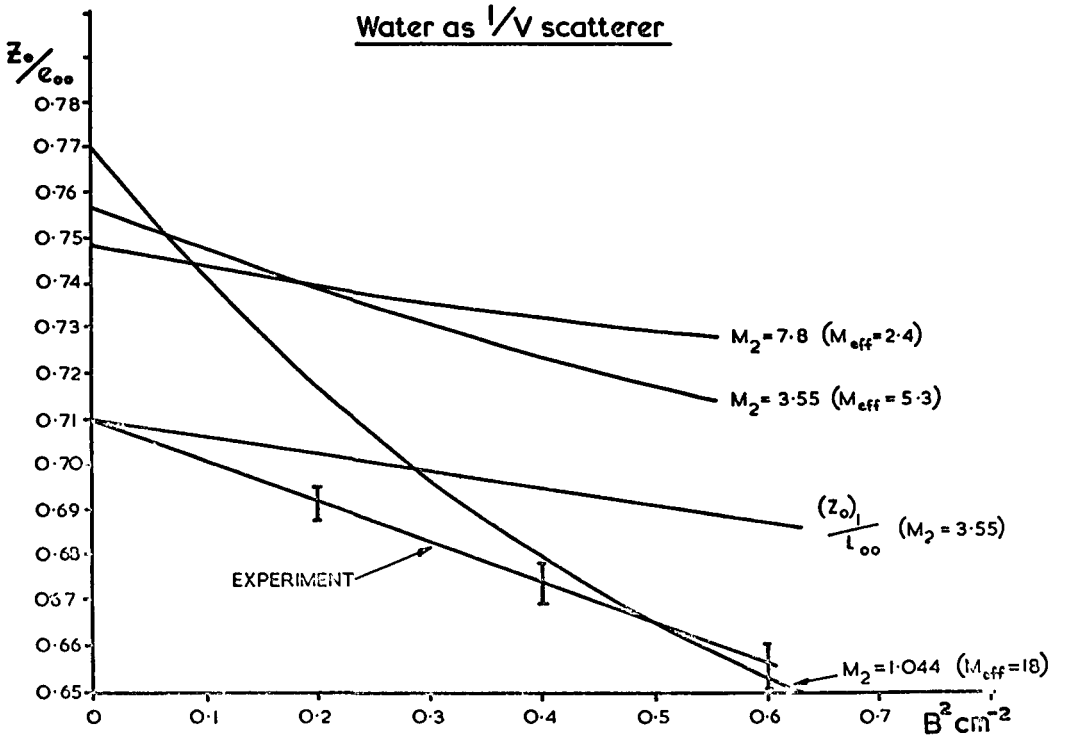

FIGURE 3

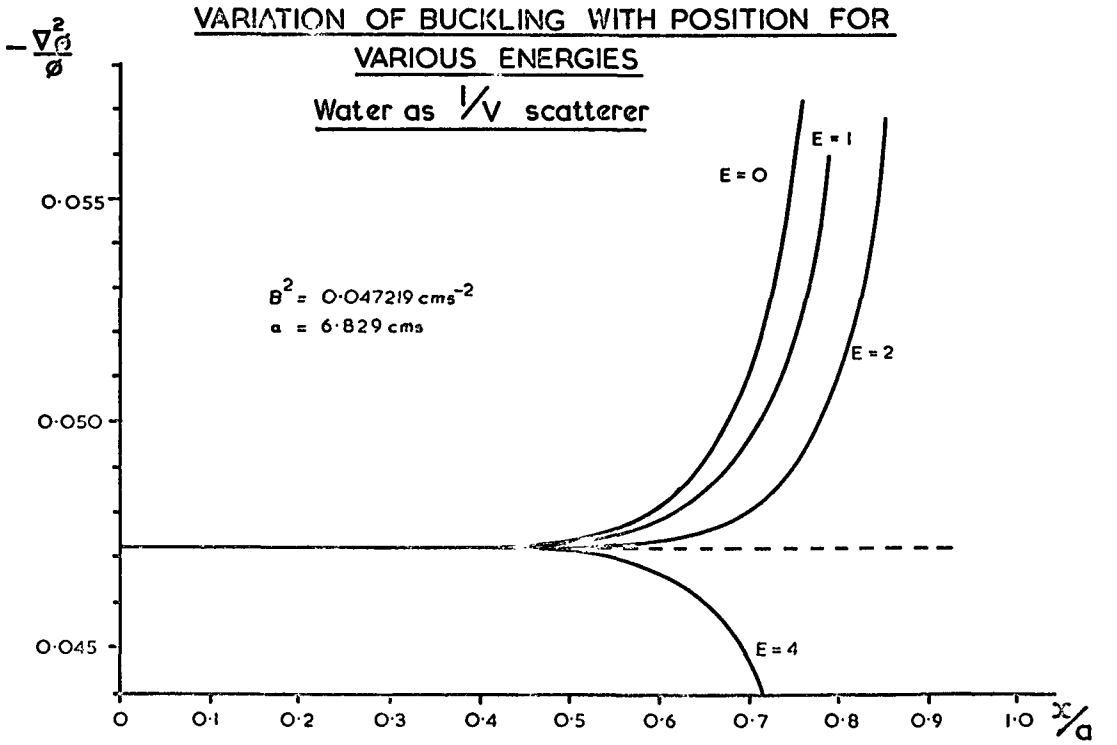
VARIATION OF BUCKLING WITH POSITION FOR VARIOUS ENERGIES
Water as 1/V scatterer
$-\frac{\nabla^2\phi}{\phi}$
$B^2 = 0.047219\ cms^{-2}$
a = 6.829 cms
E = 0
E = 1
E = 2
E = 4
0.055
0.050
0.045
0 0.1 0.2 0.3 0.4 0.5 0.6 0.7 0.8 0.9 1.0
x/a

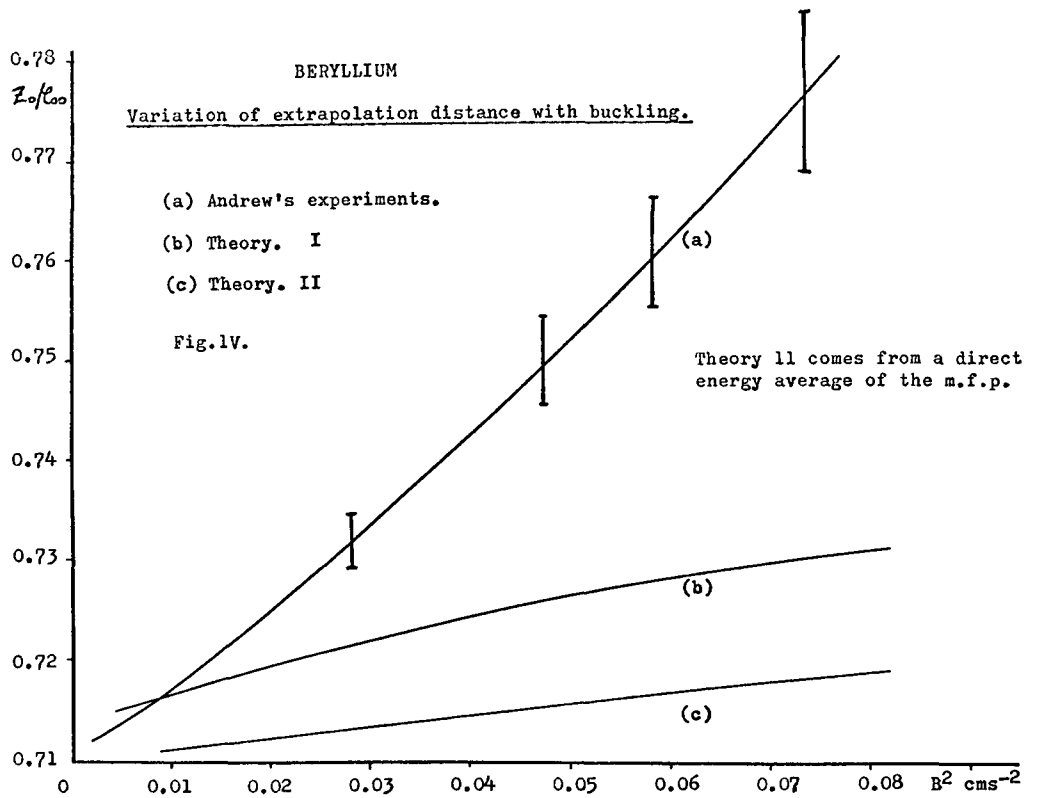
BERYLLIUM
Variation of extrapolation distance with buckling.
(a) Andrew's experiments.
(b) Theory. I
(c) Theory. II
Fig.1V.
Theory 11 comes from a direct energy average of the m.f.p.
z_0/ℓ_∞
0.78
0.77
0.76
0.75
0.74
0.73
0.72
0.71
0 0.01 0.02 0.03 0.04 0.05 0.06 0.07 0.08 $B^2\ cms^{-2}$
(a)
(b)
(c)

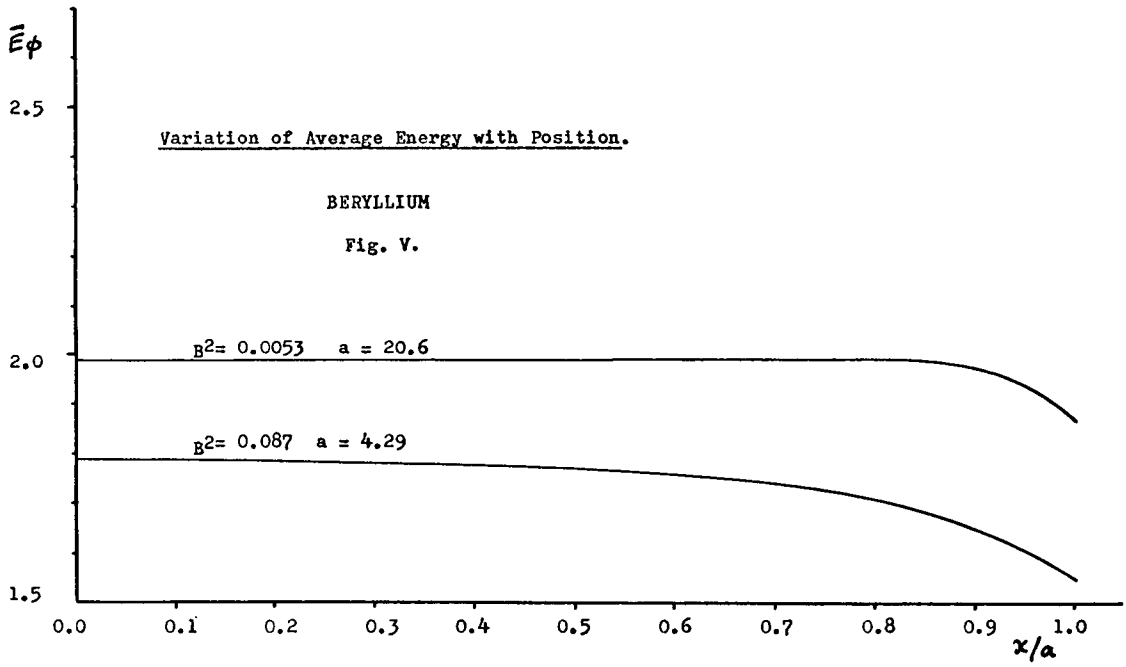

Variation of Average Energy with Position.

BERYLLIUM

Fig. V.

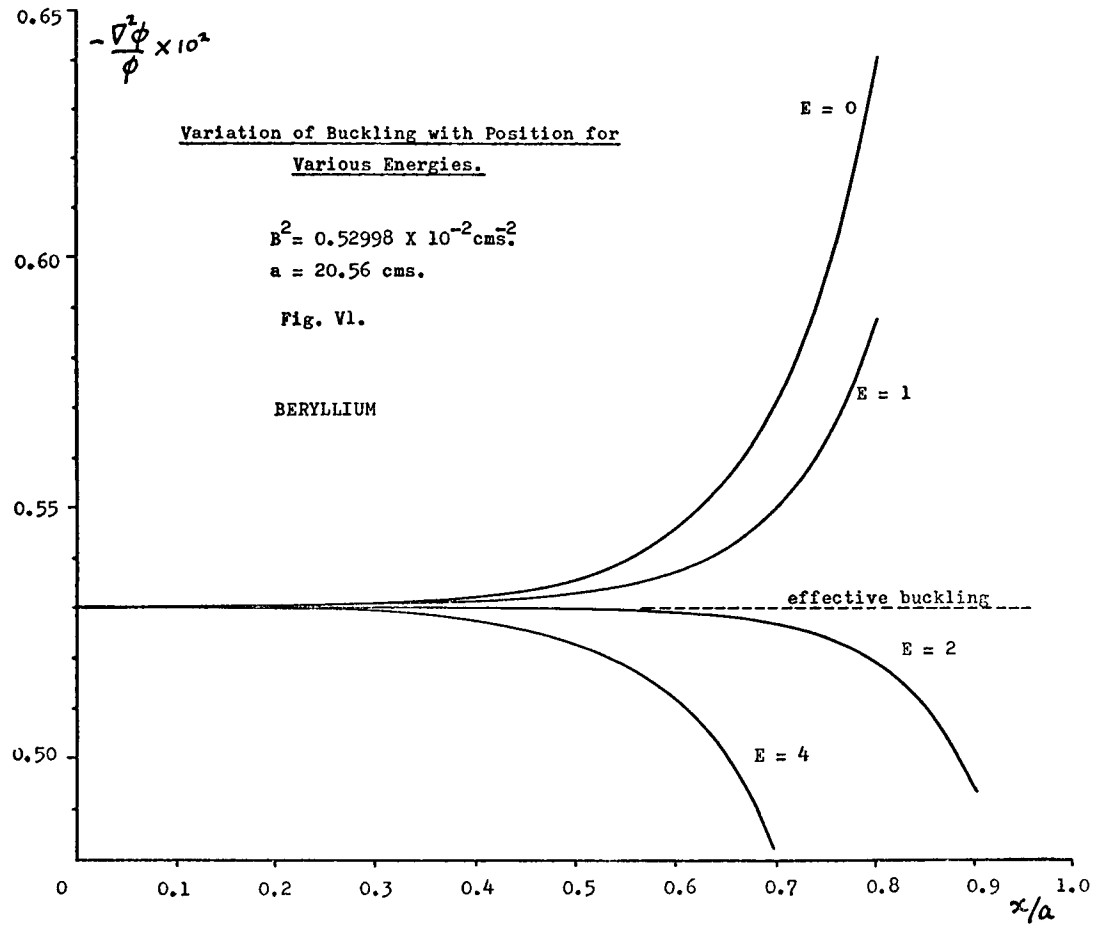

Variation of Buckling with Position for Various Energies.

B^2= 0.52998 X 10^{-2} cms^{-2}

a = 20.56 cms.

Fig. Vl.

BERYLLIUM

Transport Theory of Neutrons in Heavy Gas in Plane Geometry
I. The infinite medium and constant total cross-section

Roman S. Żelazny
Department of Physics, Case Institute of Technology, Cleveland, Ohio

Permanent address: Institute of Nuclear Research of Polish Academy of Sciences and Institute of Theoretical Physics of Warsaw University
Warsaw, Poland

Abstract

The purpose of the paper is to present a general method of solution of neutron transport equation in heavy gas in plane geometry in the case of infinite medium and constant total cross-section. This solution is based on the eigenfunction expansion method introduced originally in one-velocity transport theory by Case. The complete set of eigenfunctions has been derived and the calculation of the Green function for Boltzmann equation in infinite medium has been discussed. For total cross-section slowly varying with energy the perturbational procedure has been suggested.

I. Introduction

The knowledge of transport phenomena in the process of migration of neutrons in heavy gas moderator has became recently more and more important both from the theoretical and practical point of view. There exists quite a large number of works devoted to homogeneous problems, but the number of papers devoted to space-energetical considerations is very limited. The main tool used by the authors is the P_1 approximation [1,2] or some its extensions as for example the $P_N L_j$ method of Weiss [3].

The purpose of this paper, which is the first of planned series of works, is to apply to thermalization problems the Case method of eigenfunction expansion. As it turned out the problem of the solu-

tion of the Boltzmann equation for infinite medium in 1/M approximation with arbitrary external source distribution has been reduced to the solution of the forth order differential equation with respect to energy. The only restriction made is the constant total cross-section approximation, which may be used as the basis of phenomenological perturbational procedure in the case of slowly varying total cross-section

II. Basic equations for heavy gas moderator

The general form of the stationary Boltzmann equation for space-energetical distribution function of neutrons in plane geometry is

$$\mu \frac{\partial \psi(x,\mu,E)}{\partial x} + \sigma_{tot}(E)\psi(x,\mu,E) = \int_{-1}^{1}\int_{0}^{\infty} \sigma(E'\to E, \mu'\to\mu)\psi(x,\mu',E')\,d\mu'\,dE' + S(x,\mu,E) \qquad (1)$$

where

$$\sigma_{tot}(E) = \sigma_a(E) + \sigma_s(E). \qquad (2)$$

$\sigma_a(E)$ and $\sigma_s(E)$ denote the absorption and scattering cross-sections, respectively, and $\sigma(E'\to E, \mu'\to\mu)$ denotes the transfer cross-section. The expression for transfer and scattering cross-sections for a heavy gas moderator are [1] :

$$\sigma(E'\to E, \mu'\to\mu) = \frac{\sigma_0}{8\pi^2}\left(\frac{E}{E'}\right)^{1/2} \int_{-\infty}^{+\infty} dt \int_0^{2\pi} d\varphi \exp it(E-E') \exp\left\{\frac{1}{M}\left[E'+E - 2\mu_0(EE')^{1/2}\right]\left[it - Tt^2\right]\right\}, \qquad (3)$$

where T is the temperature of the moderator and

$$\mu_0 = \mu\mu' + (1-\mu^2)^{1/2}(1-\mu'^2)^{1/2}\cos\varphi,$$

$$\sigma_s(E) = \int_0^{\infty}\int_{-1}^{1} \sigma(E\to E', \mu\to\mu')\,d\mu'\,dE'. \qquad (4)$$

Following the well established ideas let us expand these cross-section

up to the linear terms with respect to $\gamma = \frac{1}{M}$, where M is the mass number of the diffusing medium. We get

$$\sigma(E' \to E, \mu' \to \mu) = \frac{\sigma_0}{2}\left(\frac{E}{E'}\right)^{1/2} \{\delta(E-E') + \gamma[E'+E-2\mu\mu'(EE')^{1/2}] \times$$
$$\times [\delta_E(E-E') + T\delta_{EE}(E-E')], \qquad (5)$$

$$\sigma_s(E) = \sigma_0\left[1-\gamma\left(2-\frac{T}{2E}\right)\right] \qquad (6')$$

(Index E standing by δ functions denotes differentiation with respect to E).

Inserting both cross-sections into Eq. (1) we get the Boltzmann equation in 1/M approximation (B. Eq. for heavy gas moderator):

$$\mu\frac{\partial\psi}{\partial x} + \sigma_{tot}(\varepsilon)\psi = \frac{\sigma_0}{2}\int_{-1}^{1}(\hat{\alpha}_\varepsilon + \mu\mu'\hat{\beta}_\varepsilon)\psi(x,\mu',\varepsilon)d\mu' + S(x,\mu,\varepsilon), \qquad (7)$$

where we have introduced operators defined as

$$\hat{\alpha}_\varepsilon = 2\varepsilon\frac{\partial^2}{\partial\varepsilon^2} + 2\gamma\varepsilon\frac{\partial}{\partial\varepsilon} + \frac{1}{2\varepsilon} + 1$$

$$\hat{\beta}_\varepsilon = -2\varepsilon\frac{\partial^2}{\partial\varepsilon^2} - 2\gamma\varepsilon\frac{\partial}{\partial\varepsilon}$$

and have performed the change of energy variable

$$\varepsilon = \frac{E}{\delta T}\,. \qquad (8)$$

Since our transport equation (1) has became now a differential equation with respect to energy variable we must add proper boundary conditions. It is reasonable to formulate generally that we shall be interested in such solutions of Eq. (7) which

i) for $\varepsilon \to 0$ $\quad \psi(x,\mu,\varepsilon) \to 0$,

ii) for $\varepsilon \to \infty$ $\quad \psi(x,\mu,\varepsilon) \to 0$

Sufficiently quickly to assure the existence of at least few first moments with respect to energy.

iii) $\psi(x,\mu,\varepsilon) < \infty$ for any ε in the interval $(0,\infty)$ (with possible exception for $x \longrightarrow \infty$).

III. Eigenfunctions of the Boltzmann equation with constant total cross-section

Let us limit our considerations to the case of constant total cross-section. The Eq. (7) wil then be rewritten in a slightly diffwrent form, corresponding to the change of a x variaole

$$\bar{x} = x\,\sigma_{tot} \tag{9}$$

It is

$$\mu\frac{\partial\psi}{\partial x} + \psi = \frac{c}{2}\int_{-1}^{1}(\hat{\alpha}_\varepsilon + \mu\mu'\hat{\beta}_\varepsilon)\,\psi(x,\mu',\varepsilon)\,d\mu', \tag{10}$$

where for convenience sake we have omitted the bar over the x variaole and have introduced the constant c

$$c = \frac{\sigma_0}{\sigma_{tot}}. \tag{11}$$

We have omitted also, temporarily, the source term on the right hand side.

Now let us seek, according to the general ideas of eigenfunction expansion method, the eigenfunctions of the homogeneous Eq. (10) in the form

$$\psi(x,\mu,\varepsilon) = e^{-x/\nu}\,\phi(\nu,\mu,\varepsilon) \tag{12}$$

The function $\phi(\nu,\mu,\varepsilon)$ must satisfy then the following equation

$$\left(1-\frac{\mu}{\nu}\right)\phi(\nu,\mu,\varepsilon) = \frac{c}{2}\int_{-1}^{1}(\hat{\alpha}_\varepsilon + \mu\mu'\hat{\beta}_\varepsilon)\,\phi(\nu,\mu',\varepsilon)\,d\mu' \tag{13}$$

Since $\hat{\alpha}_\varepsilon$ and $\hat{\beta}_\varepsilon$ do not depend on μ' we can introduce the

following functions

$$a(\nu,\varepsilon) \equiv \int_{-1}^{1} \phi(\nu,\mu',\varepsilon)\,d\mu', \tag{14}$$

$$b(\nu,\varepsilon) \equiv \int_{-1}^{1} \mu' \phi(\nu,\mu',\varepsilon)\,d\mu' \tag{15}$$

and Eq. (13) can be rewritten in the form

$$\left(1-\frac{\mu}{\nu}\right)\phi(\nu,\mu,\varepsilon) = \frac{c}{2}\left[\hat{\alpha}_\varepsilon\, a(\nu,\varepsilon) + \mu\hat{\beta}_\varepsilon\, b(\nu,\varepsilon)\right]. \tag{16}$$

The formal solution of this equation is

$$\phi(\nu,\mu,\varepsilon) = \frac{c}{2}\,\frac{\hat{\alpha}_\varepsilon a(\nu,\varepsilon) + \mu\hat{\beta}_\varepsilon b(\nu,\varepsilon)}{\nu-\mu}\,\nu + \lambda(\nu,\varepsilon)\,\delta(\nu-\mu) \tag{17}$$

provided conditions (14) and (15) will be satisfied. This requirement gives us

$$\frac{c}{2}\int_{-1}^{1}\frac{\hat{\alpha}_\varepsilon a(\nu,\varepsilon) + \mu'\hat{\beta}_\varepsilon b(\nu,\varepsilon)}{\nu-\mu'}\,\nu\,d\mu' + \lambda(\nu,\varepsilon)\int_{-1}^{1}\delta(\nu-\mu')\,d\mu' = a(\nu,\varepsilon), \tag{18}$$

$$\frac{c}{2}\int_{-1}^{1}\frac{\hat{\alpha}_\varepsilon a(\nu,\varepsilon) + \mu'\hat{\beta}_\varepsilon b(\nu,\varepsilon)}{\nu-\mu'}\,\nu\mu'\,d\mu' + \lambda(\nu,\varepsilon)\int_{-1}^{1}\mu'\delta(\nu-\mu')\,d\mu' = b(\nu,\varepsilon). \tag{19}$$

Let us introduce the following functions of complex argument

$$f(\nu) \equiv \int_{-1}^{1}\frac{d\mu}{\nu-\mu}, \tag{20}$$

$$\chi(\nu) \equiv \int_{-1}^{1}\delta(\nu-\mu)\,d\mu, \tag{21}$$

which have the following properties:

i) $f(\nu)$ is a sectionally holomorphic function of the complex argument ν with the cut along the interval $(-1, 1)$ of

the real axis. The Plemelj formulae for function f( ) are as follows

$$f^{\pm}(\nu) = \mp \pi i + \int_{-1}^{1} \frac{d\mu}{\nu - \mu} \equiv \mp \pi i + Pf(\nu) \quad \text{for } \nu \in (-1,1), \tag{22}$$

where index + and - denote the upper and lower limit, respectively.

ii)

$$\chi(\nu) = \begin{cases} 1 & \text{for } \nu \in (-1,1) \\ 0 & \text{otherwise} \end{cases} \tag{23}$$

With the help of these functions conditions (18) and (19) can be rewritten in the form:

$$\frac{c}{2}\nu f(\nu)\hat{\alpha}_\varepsilon a(\nu,\varepsilon) + \frac{c}{2}[\nu f(\nu) - 2]\nu\hat{\beta}_\varepsilon b(\nu,\varepsilon) + \lambda(\nu,\varepsilon)\chi(\nu) = a(\nu,\varepsilon),$$

$$\frac{c\nu}{2}[\nu f(\nu) - 2]\hat{\alpha}_\varepsilon a(\nu,\varepsilon) + \frac{c\nu^2}{2}[\nu f(\nu) - 2]\hat{\beta}_\varepsilon b(\nu,\varepsilon) + \nu\lambda(\nu,\varepsilon)\chi(\nu) = b(\nu,\varepsilon). \tag{24}$$

This is a system or two equations for three unknown functions. It means that we can express two of them in terms of the third one, which must be determine in the following course of any concrete neutron thermalization problem.

As the unknown function let us choose $a(\nu,\varepsilon)$. It is evident that function $a(\nu,\varepsilon)$ must behave with respect to ε in a completely analogous way as function $\psi(x,\mu,\varepsilon)$ itself. The boundary conditions (B.C.) will be then the same as the ones formulated in the paragraph II for $\psi(x,\mu,\varepsilon)$.

Multiplication of the first equation in formulas (24) by ν and subtraction from the second one gives us the following relation

$$b(\nu,\varepsilon) = \nu a(\nu,\varepsilon) - c\nu\hat{\alpha}_\varepsilon a(\nu,\varepsilon), \tag{25}$$

whien is valid for every γ and ε . It is sufficient now to discuss only the content of the first equation from the pair (24) with the help of (25).

Let us distinct the following cases:

A. $\gamma \in (-1,1)$

In this interval

$$\lambda(\nu,\varepsilon) = a(\nu,\varepsilon) - \frac{c}{2}\gamma P f(\nu)\hat{\alpha}_\varepsilon a(\nu,\varepsilon) - \frac{c}{2}[\gamma P f(\nu) - 2]\gamma\hat{\beta}_\varepsilon b(\nu,\varepsilon) =$$

$$= a(\nu,\varepsilon) - \frac{c}{2}\gamma P f(\nu)\hat{\alpha}_\varepsilon a(\nu,\varepsilon) - \frac{c}{2}[\nu P f(\nu) - 2]\gamma\hat{\beta}_\varepsilon[\nu a(\nu,\varepsilon)$$

$$- c\gamma\hat{\alpha}_\varepsilon a(\nu,\varepsilon)] = P\hat{\Lambda}_\varepsilon(\nu,\varepsilon)\, a(\nu,\varepsilon) \qquad (26)$$

and the function $\phi(\nu,\mu,\varepsilon)$ can be written in the form

$$\phi(\nu,\mu,\varepsilon) = \frac{c}{2}\,\frac{\hat{\alpha}_\varepsilon a(\nu,\varepsilon) + \mu\hat{\beta}_\varepsilon[\nu a(\nu,\varepsilon) - c\gamma\hat{\alpha}_\varepsilon a(\nu,\varepsilon)]}{\gamma-\mu}\gamma + P\hat{\Lambda}_\varepsilon(\nu,\varepsilon)\, a(\nu,\varepsilon)\,\delta(\nu-\mu) \qquad (27)$$

B. $\nu \notin (-1,1)$

In this domain we have the condition

$$\hat{\Lambda}_\varepsilon(\nu,\varepsilon)\, a(\nu,\varepsilon) = 0, \qquad (28)$$

which is a forth order differential eqiation with respect to $a(\nu,\varepsilon)$, ν plays a role of eigenvalue. It is plausible to assume that boundary conditions (B.C) formulated for $\psi(x,\mu,\varepsilon)$ in preceding paragraph and applied also to $a(\nu,\varepsilon)$, according to the remark made above, pick up the proper eigenvalues of ν . The character of differential equation (24) and applied boumdary conditions seems to favour only the discrete set of eigenvalues. The symmetry property of the operator

$$\hat{\Lambda}_\varepsilon(\nu,\varepsilon) = \hat{\Lambda}_\varepsilon(-\nu,\varepsilon) \qquad (29)$$

allow us to assume that the discrete eigenvalues are *

$$\pm \nu_j \qquad (j = 1, \ldots, N) \tag{30}$$

---

* Thorough examination of the conditions (28) with the calculation of discrete eigenvalues (30) will be made in the next paper.

The corresponding discrete eigenfunction will then have the form

$$\phi(\pm\nu_j, \mu, \varepsilon) = \frac{c}{2} \frac{\hat{\alpha}_\varepsilon a(\pm\nu_j, \varepsilon) \pm \mu \hat{\beta}_\varepsilon [\nu_j a(\pm\nu_j, \varepsilon) - c\nu_j \hat{\alpha}_\varepsilon a(\pm\nu_j, \varepsilon)]}{\nu_j \mp \mu} \nu_j \tag{31}$$

It is worthwhile to indicate that since the condition (28) is homogeneous with every function $a(\pm\nu_j, \varepsilon)$ is connected an arbitrary constant factor which must be determine in a concrete problem.
This ends our task of finding the whole set of eigenvalues ν and corresponding eigenfunctions.

IV. The completeness theorem

The next goal is to proove that the derived system of eigenfunctions form a complete set system. In another words we should proove that any function of μ and ε (satisfying proper conditions: the boundary conditions (B.C.) with respect to energy and of the Hölder class with respect to μ) can be expanded into this set of functions:

$$\sum_{j=1}^{N} \{\phi(\nu_j, \mu, \varepsilon) + \phi(-\nu_j, \mu, \varepsilon)\} + \int_{-1}^{1} \phi(\nu, \mu, \varepsilon)\, d\nu = f(\mu, \varepsilon). \tag{32}$$

Using the explicit form of our eigenfunctions (27) and (31) we can rewrite Eq. (32) in the form

$$P\hat{\lambda}_\varepsilon(\mu, \varepsilon)\, a(\mu, \varepsilon) + \frac{c}{2} \int_{-1}^{1} \frac{\hat{\alpha}_\varepsilon a(\nu, \varepsilon) + \mu \hat{\gamma}_\varepsilon a(\nu, \varepsilon)}{\nu - \mu} \nu\, d\nu = g(\mu, \varepsilon), \tag{33}$$

where

$$\hat{\delta}_\varepsilon(\nu,\varepsilon) \equiv \nu\hat{\beta}_\varepsilon[1-\sigma\hat{\alpha}_\varepsilon] \tag{34}$$

and

$$g(\mu,\varepsilon) \equiv f(\mu,\varepsilon) - \sum_{j=1}^{N}\{\phi(\nu_j,\mu,\varepsilon)+\phi(-\nu_j,\mu,\varepsilon)\}. \tag{35}$$

It is convenient to tranform Eq. (33) to the following form

$$P\hat{\Lambda}_\varepsilon(\mu,\varepsilon)a(\mu,\varepsilon) + \frac{c}{2}\mu[\hat{\alpha}_\varepsilon+\mu\hat{\delta}_\varepsilon]\int_{-1}^{1}\frac{a(\nu,\varepsilon)}{\nu-\mu}d\nu = g(\mu,\varepsilon) - \hat{\alpha}_\varepsilon\int_{-1}^{1}a(\nu,\varepsilon)d\nu$$

$$-\mu\int_{-1}^{1}(\nu-\mu)[\hat{\beta}_\varepsilon - 2\hat{\beta}_\varepsilon\hat{\alpha}_\varepsilon]a(\nu,\varepsilon)d\nu \equiv h(\mu,\varepsilon) \tag{36}$$

Eq. (36) has a dominant form of singular integral equation. The only difference from clkassical situtation consists in the fact that coefficients of our singular integral equation are differential forms with respect to additional parameter in our problem, viz. energy. It causes that in addition to usual requirements concerning ν and μ dependence of involved functions (they must be functions of Hölder class, see for example [4] or [5]) we must demand that all functions of energy satisfy the boundary conditions (B.C) from paragraph II.

To solve the Eq. (36) let us introduce the following functions

$$A(z,\varepsilon) \equiv \frac{1}{2\pi i}\int_{-1}^{1}\frac{a(\nu,\varepsilon)}{\nu-z}d\nu \tag{37}$$

$$H(z,\varepsilon) \equiv \frac{1}{2\pi i}\int_{-1}^{1}\frac{h(\nu,\varepsilon)}{\nu-z}d\nu \tag{38}$$

For functions $a(\mu,\varepsilon)$ and $h(\nu,\varepsilon)$ of Hölder class the above introduced functions are sectionally holomorphic functions in a complex z plane with a cut along the interval (- 1, 1) of the real axis.

The Plemelj formulae for these functions are:

$$A^+(\mu,\varepsilon) - A^-(\mu,\varepsilon) = q(\mu,\varepsilon),$$
$$\pi i\,[A^+(\mu,\varepsilon) + A^-(\mu,\varepsilon)] = \int_{-1}^{1} \frac{q(\nu,\varepsilon)}{\nu-\mu}\,d\nu, \tag{39}$$

$$H^+(\mu,\varepsilon) - H^-(\mu,\varepsilon) = h(\mu,\varepsilon),$$
$$\pi i\,[H^+(\mu,\varepsilon) + H^-(\mu,\varepsilon)] = \int_{-1}^{1} \frac{h(\nu,\varepsilon)}{\nu-\mu}\,d\nu, \tag{40}$$

where index + and - denotes the upper and lower limit for $\mu \in (-1,1)$, respectively.

Let us remind also that the similar Plemelj formulae for introduced earlier sectionally holomorphic operator are:

$$\Lambda^+(\mu,\varepsilon) - \Lambda^-(\mu,\varepsilon) = \pi i c\,[\mu\hat{\alpha}_\varepsilon + \mu^2\hat{\gamma}_\varepsilon]$$
$$\Lambda^+(\mu,\varepsilon) + \Lambda^-(\mu,\varepsilon) = 2P - \hat{L}_\varepsilon \tag{41}$$

With the help of formulae (39), (40) and (41) Eq. (36) has been reduced to the following Riemann-Hilbert problem:

$$\hat{\Lambda}_\varepsilon^+ A^+ - H^+ = \hat{\Lambda}_\varepsilon^- A^- - H^- \tag{42}$$

for $\mu \in (-1, 1)$.

The function $K(z,\varepsilon)$ defined as

$$K(z,\varepsilon) \equiv \hat{\Lambda}_\varepsilon A - H, \tag{43}$$

which vanish at $z = \infty$ must be, as a holomorphic function in an entire complex plane, equal identically to zero (Liouville theorem).

Hence we get the following differential equation for the function $A(z,\varepsilon)$

$$\hat{\Lambda}_{\varepsilon}(z,\varepsilon)\,A(z,\varepsilon) = H(z,\varepsilon) \qquad (44)$$

to which we must add the boundary conditions (B.C.).
We shall not solve this equation in this paper limiting ourselves to the general discussion. Let us noticethat the homogeneous part of Eq. (44) is identical formally with Eq. (28). It means that there are such values of z

$$z = \pm \gamma_j \qquad (j = 1, \ldots, N) \qquad (45)$$

for which the compatibility conditions for Eq. (44) must be

$$H(\pm \gamma_j, \varepsilon) = 0 \qquad (46)$$

These conditions determine all arbitrary constants, which enters the function $b(\mu,\varepsilon)$ through the discrete part of the expansion (formula (26)) Having determined the function A(z, ε) from Eq. (44) we can calculate the function $q(\nu,\varepsilon)$ from the first formula of (39). This is not the end of our considerations since our $q(\nu,\varepsilon)$ depend on some unknown functions of energy. Applying to $q(\nu,\varepsilon)$ appropriate operations we can very easily derive the proper equations for these functions. These equations with our boundary conditions (B.C) should determine them uniquely. This ends the scheme of a proof of the completeness theorem.
Let us conclude this paragraph by the statement that the general solution of Boltzmann Eq. (10) has the form:

$$\psi(x,\mu,\varepsilon) = \sum_{j=1}^{N}{}' \xi \phi(\gamma_j,\mu,\varepsilon) e^{-x/\gamma_j} + \phi(-\gamma_j,\mu,\varepsilon) e^{x/\gamma_j} \xi + \int_{-1}^{1}{}' \phi(\nu,\mu,\varepsilon) e^{-x/\nu}\, d\nu \qquad (47)$$

V. The possible applications

A. The Green function

The Green function for infinite mediam is the solution of the following equation

$$\mu \frac{\partial \psi_g}{\partial x} + \psi_g = \frac{c}{2} \int_{-1}^{1} (\tilde{\alpha}_\varepsilon + \mu\mu' \tilde{\beta}_\varepsilon) \psi_g \, d\mu' + \delta(x-x_0)\,\delta(\mu-\mu_0)\,\delta(\varepsilon-\varepsilon_0) \quad (48)$$

which satisfy the same boundary conditions (B.C.) with respect to energy as formulated in par. II and which additionally vanish at + and - infinity of the x variable.

From formula (47) we infer that $\psi_g(x-x_0, \mu, \mu_0, \varepsilon, \varepsilon_0)$ must has the form

$$\psi_g = \begin{cases} \sum_{j=1}^{N} \phi(\nu_j, \mu, \varepsilon)\, e^{-(x-x_0)/\nu_j} + \int_0^1 \phi(\nu, \mu, \varepsilon)\, e^{-(x-x_0)/\nu}\, d\nu, & x - x_0 > 0 \\ -\sum \phi(-\nu_j, \mu, \varepsilon)\, e^{(x-x_0)/\nu_j} - \int_{-1}^{0} \phi(\nu, \mu, \varepsilon)\, e^{-(x-x_0)/\nu}\, d\nu, & x - x_0 < 0 \end{cases} \quad (49)$$

Now integrating both sides of Eq. (48) with respect to x in the interval $(-\infty, -\eta)$ and in the interval $(-\infty, +\eta)$, respectively, taking the limit $\eta \to 0$ and subtracting the results, we get the following relation

$$\mu \left[\psi_g(0^+) - \psi_g(0^-) \right] = \delta(\mu-\mu_0)\,\delta(\varepsilon-\varepsilon_0), \quad (50)$$

where only the x argument of ψ_g has been written explicitly.

Inserting expression (49) into relation (50) we get the following equation for unknown coefficients of the expansion (49):

$$\sum_{j=1}^{N} \left\{ \phi(\nu_j, \mu, \varepsilon) + \phi(-\nu_j, \mu, \varepsilon) \right\} + \int_{-1}^{1} \phi(\nu, \mu, \varepsilon)\, d\nu = \frac{1}{\mu}\,\delta(\mu-\mu_0)\,\delta(\varepsilon-\varepsilon_0). \quad (51)$$

Eq. (51) is completely identical with Eq. (32) of Completeness Theorem

The only difference is that now the non-homogeneity termm is specified as a given function. The prescription for the solution given in the preceding paragraph may be used to explicit calculations of the Green function. It is worthwhile to mention that the Cauchy integral applied to δ function gives also a sectionally holomorphic function.
The explicit knowledge of the Green function enable us to write down the solution of Boltzmann equation with any prescribed sourceđ

$$\psi(x,\mu,\varepsilon) = \int \psi_g(x-x_0,\mu,\mu_0,\varepsilon,\varepsilon_0)\, S(x_0,\mu_0,\varepsilon_0)\, dx_0\, d\mu_0\, d\varepsilon_0 \qquad (52)$$

B. The case of slowly varying total cross-section
In the case of slowly varying total cross-section $\sigma_{tot}(\varepsilon)$ the Boltzmann Eq. (7) can be written in the form

$$\mu\frac{\partial\psi}{\partial x} + \bar{\sigma}_{tot}\psi = \frac{\sigma_0}{2}\int_{-1}^{1}(\alpha_\varepsilon + \mu\mu'\beta_\varepsilon)\psi\, d\mu' + S + [\bar{\sigma}_{tot} - \sigma_{tot}(\varepsilon)]\psi \qquad (53)$$

aor using the proper units for x variable

$$\mu\frac{\partial\psi}{\partial x} + \psi = \frac{\bar{\varepsilon}}{2}\int_{-1}^{1}(\alpha_\varepsilon + \mu\mu'\beta_\varepsilon)\psi\, d\mu' + \frac{S}{\bar{\sigma}_{tot}} + \frac{\bar{\sigma}_{tot} - \sigma_{tot}(\varepsilon)}{\bar{\sigma}_{tot}}\psi \qquad (54)$$

Assuming that the variation of $\sigma_{tot}(\varepsilon)$ is small we may treat the term

$$\frac{\bar{\sigma}_{tot} - \sigma_{tot}(\varepsilon)}{\bar{\sigma}_{tot}}\psi$$

as a small pertutbation. The knowledge of the Green function from the point A of this paragraph simplify the calculations of distribution function ψ .
It should be, hawever, stressed that such an appraach is purely phenomenological one, sbnce one part of the rigorous total cross-section ds known. It is the scattering cross-section given by formula (6).and it can be scarcely treated as a slowly varying one. Nevertheless in

many applications such an approach will be sufficiently accurate., unless the existence of free surfaces will not disturb seriously the neutron distribution function.

VI. Conclusions

The presented paper is treated as the introduction to a series of papers devoted to the study of transport phenomena in diffusion of neutron in a heavy gas moderator by means of eigenfunction expansion method. For simplification sake it has been assumed the total cross-section being independent of energy. In thse circumstances it has been shown that the application of eigenfunction expansion is possible . It has been prooved that there exists a complete set of eigenfunctions and the general solution of Boltzmann equation can be expanded into this complete set. It is to be noticed that the discrete eigenvalues should be determined from the solution of the forth order differential eqiation with respect to energy with appropriate boundary conditions, which resemble to great extent the problems of quantum mechanics. To this problem will be devoted the next paper of the series.
The subsequent paper wil touch the Milne problem and the related topics It is important that in the case of the so called "partial range" completeness theorem (the terminology of K.M. Case) the possibilities of the theory of singular integral equations become very limited by the operatorial character (with respect to energy) of their coefficient.

Acknowledgement

The author is very grateful to Dr. A. Kuszell for many valuable discussions in the very preparatory period of the work.
The author is also very indepted to Case Institute of Technology for the hospitality extended to him. Special thanks are due to Dr. O.K. Mawardi and Dr. F. Reines.

This work has been done in connection with the Case Plasma Research Program.

References

1. H.Hurwitz,Jr., M.S. Nelkin, G.J. Habetler, Nucl. Sc. and Eng.,1, 280 (1956)
2. D. Kottwitz, ORNL - 2739
3. Z. Weiss, Nukleonika, 6, 691 (1961) and 6, 703 (1961)
4. K. M. Case, Ann. of Phys.,9,1 (1960)
5. R. Żelazny, A. Kuszell, J. Mika, Ann. of Phys., 16,68 (1961)

L. V. Maĭorov

ASYMPTOTIC DISTRIBUTION OF THERMAL NEUTRONS FAR FROM A PLANAR SOURCE

The distribution of thermal neutrons far from a planar source, in homogeneous and inhomogeneous media, is analyzed with account of thermalization and fission.

I.

In subcritical homogeneous media, located sufficiently far from a planar source, the steady-state thermal-neutron energy spectrum is independent of the distance to the source. For a medium in which there is no neutron multiplication, this was demonstrated by Hurwitz and Nelkin [1]. In this case the asymptotic spectrum of the thermal neutron satisfies the following equation [1]:

$$\left(\sigma_a(E) - D(E)\frac{1}{L^2}\right)\Phi_L(E) = \frac{d\,q(E)}{dE} \qquad (1)$$

where

$$\frac{\partial q}{\partial E} = \int_0^\infty \sigma(E' \to E)\,\phi_L(E')\,dE - \phi_L(E)\int_0^\infty \sigma(E \to E')\,dE' \qquad (2)$$

Here L^2, which are the eigenvalues of the equation, satisfy the relation

$$L^2 = \left[\int_0^\infty D(E)\,\phi_L(E)\,dE\right]\left[\int_0^\infty \sigma_a(E)\,\phi_L(E)\,dE\right]^{-1} \qquad (3)$$

In operator form, Eq. (1) can be rewritten as

$$D^{-1}(E)\,A\,\phi_L(E) = L^{-2}\phi_L(E)$$

where

$$A\,\phi_L(E) = \sigma_a(E)\,\phi_L(E) - \frac{dq}{dE}$$

An investigation of the spectrum of the operator A/D(E) shows that for any moderator model there exists a smallest eigenvalue of the Eq. (1). It is single, isolated, and corresponds to a single positive eigenfunction. All the points of the spectrum lie on the real axis. If σ_a and $\int_0^\infty \sigma(\mathcal{E} \to E')dE'$ are independent of the energy, the

operator has a discrete spectrum. If on the other hand, as occurs in real cases, these quantities depend on the energy there exists a region where the operator A/D(E) has a continuous spectrum; this region is contained in the segment $[\beta_1, \beta_2]$, where

$$\beta_1 = \min_{0<E<\infty} \left\{ (\sigma_a + \sigma) D^{-1} \right\}$$

$$\beta_2 = \max_{0<E<\infty} \left\{ (\sigma_a + \sigma) D^{-1} \right\}$$

or, in real cases,

$$\left[\beta_1, \infty \right]$$

Consequently in a homogeneous non-multiplying medium the flux of the neutrons emitted by a plane source has the form

$$\phi(E,z) = \sum_i e^{-\frac{|z|}{L_i}} B_i \phi_{L_i}(E) + \int_{\beta_1}^{\infty} \left(dF_{1/L}(E) \right) e^{-\frac{|z|}{L}}$$

Here

$$L_0 > L_i > \frac{1}{\beta_1}$$

$F_{1/L^2}(E)$ depends on the spectrum of the source neutrons and on the moderator model.

These results can be readily obtained by using the theory of the spectrum of self-adjoint operators, particularly the Weyl theorem concerning perturbations of the spectrum of a self-adjoint operator by a self-adjoint completely continuous operator [2]. The corresponding proofs are given in [3].

In subcritical multiplying media, located sufficiently far from the planar source, the neutron flux has a form

$$\Phi(E,z) = \Phi_{L_0}(E) e^{-\frac{|z|}{L_0}} + o\left(e^{-\frac{|z|}{L_0}}\right) \qquad (*)$$

where $\Phi_{L_0}(E)$ satisfies the following equation [3]:

$$\sigma_a(E)\Phi_{L_0}(E) - \frac{D(E)}{L_0^2}\Phi_{L_0}(E) = \frac{dq}{dE} + \frac{dq_s}{dE} \qquad (6)$$

Here

$$\frac{d q_f}{dE} = \nu \int_0^\infty \sigma_f (E' \to E) \phi_{L_0}(E') dE'$$

is the density of the fission-neutron sources.

If we fix all the parameters of the medium and increase ν, starting with zero, the smallest eigenvalue $1/L_0^2$ of Eq. (6) decreases to zero at a certain value $\nu = \nu_{cr}$. When $\nu = \nu_{cr}$ there can exist in the medium a stationary neutron distribution, with an energy spectrum satisfying the equation

$$\sigma_a(E) \phi_0(E) = \frac{dq}{dE} + \frac{dq_f}{dE}$$

$\phi_0(E)$ describes the stationary distribution of the neutrons in a medium with a homogeneous spatial distribution of the sources. As ν increases, the eigenfunction of Eq. (6), $\phi_{L_0}(E)$, which describes the energy spectrum of the thermal neutrons far away from the sources, tends to $\phi_0(E)$. In [3] an investigation was made of the spectrum of the operator

$$\left\{ \phi(E)\sigma_a(E) - \frac{dq}{dE} - \frac{dq_f}{dE} \right\} \mathcal{D}^{-1}(E)$$

and it was shown that when $\nu < \nu_{cr}$ there exists a unique positive eigenfunction that determines the asymptotic behavior of $\Phi(E, z)$ given by Eq. (*).

II.

The dependence of the asymptotic spectrum of the thermal neutrons on the degree of criticality of the medium can be illustrated by using the approximation of a heavy monatomic gas.

In this case [1]:

$$q(E) = \xi\sigma_s\left[(E-T)\Phi(E) + ET\frac{d\Phi}{dE}\right]. \qquad (8)$$

In order to obtain an analytic solution, we assume that $\sigma_a = a + b/E$; $(T = 1)$, and

$$\frac{dq_f}{dE} = \nu\delta(E-E_0)\int_0^\infty \sigma_f(E')\Phi(E')\,dE'$$

E_0 -- energy of the neutrons produced by fission.

Then Eq. (6) can be reduced to the following form

$$E\frac{\partial^2\varphi}{\partial E^2}+(1+\beta-E)\frac{\partial\varphi}{\partial E}+\left(1-\frac{\beta+1}{2}-\frac{a}{\xi\sigma_s}\right)\varphi+\frac{\varphi}{3L^2\xi\sigma_s}+$$

$$+\frac{\nu}{\xi\sigma_s^2}P(E)\delta(E-E_0)\int_0^\infty\sigma_f(E')\Phi(E')\,dE'=0 \qquad (10)$$

where

$$\varphi=E^{-\frac{\beta+1}{2}}e^{E}\Phi(E) \qquad (11)$$

$$\beta=\sqrt{1+\frac{4b}{\xi\sigma_s}} \qquad (12)$$

When $\nu=0$, the eigenfunctions of Eq. (10) have the form

$$\varphi_{L_\eta}(E)=L_n^{(\beta)}(E)$$

(generalized Laguerre polynomials) and

$$\Phi_{L_\eta}(E)=E^{\frac{\beta+1}{2}}e^{-E}L_\eta^{(\beta)}(E)$$

$$\frac{1}{L_\eta^2}=\left[\eta+\frac{a}{\xi\sigma_s^2}+\frac{\beta-1}{2}\right]3\xi\sigma_s^2$$

Therefore the flux of thermal neutrons in a medium with planar source has the form

$$\Phi(E,z) = e^{-E} E^{\frac{\beta+1}{2}} \sum_{n=0}^{\infty} A_n L_n^{(\beta)}(E) e^{-\frac{|z|}{L_n}} \qquad (14)$$

If $\nu > 0$ and the medium remains subcritical, the eigenfunctions of Eq. (10) can be written in the form

$$\Phi_L(E) = E^{\frac{\beta+1}{2}} e^{-E} M(\alpha, \gamma, E) \qquad E < E_0$$

$$\Phi_L(E) = E^{\frac{1-\beta}{2}} e^{-E} M(\alpha-\gamma+1, 2-\gamma, E) \qquad E > E_0$$

where $M(\alpha, \gamma, E)$ are confluent hypergeometric functions. Here

$$\alpha = \frac{\beta-1}{2} + \frac{a}{\xi\sigma_s^2} - \frac{1}{3L^2} \cdot \frac{1}{\xi\sigma_s} \qquad (16)$$

Since $E_0 \gg 1$ (the neutrons produced by fission have a very high energy), we have for $E > E_0$

$$\Phi(E) \sim E^{\left(1 - \frac{a}{\xi\sigma_s} + \frac{1}{3L^2\xi\sigma_s^2}\right)} e^{-E} \qquad (17)$$

At high energies, smaller than the energy E_0 of the fission neutrons, we have

$$\Phi(E) \sim E^{-\left[1+\frac{1}{3L_0^2\xi\sigma_s^2}-\frac{\alpha}{\xi\sigma_s}\right]} \qquad (18)$$

If $1/L_0^2 = 0$ we get a = 0, i.e., the medium is critical and $\nu = \nu_{cr}$, and then $\phi(E) = E^{-1}$, i.e., it agrees with the Fermi spectrum.

The eigenvalue L_0^{-2} is determined from the balance equation

$$L_0^{-2}\int_0^\infty D(E)\Phi(E)dE + \nu\int_0^\infty \Phi(E)\sigma_f(E)dE = \int_0^\infty \sigma_a(E)\Phi(E)dE \qquad (19)$$

When $\nu = 0$, (19) coincides with (3).

Thus, the asymptotic spectrum of the thermal neutrons in a media where there is no fission has the following form far away from the source.

$$\Phi(E,z) \sim E^{\frac{\beta+1}{2}} e^{-E} e^{-\frac{|z|}{L_0}} \qquad (20)$$

In a critical infinite medium without external source we have

$$\Phi(E) = E^{\frac{\beta+1}{2}} e^{-E} M(\alpha,\gamma,E) \qquad (21)$$

Note. In real medium $\sigma_a = E^{-1/2}$ at thermal energies. The analytic solution given above can be used for an approximate calculation of the neutron spectrum in a medium with absorption $E^{-1/2}$, using the approximate method A. Nikiforov and V. Uvarov [5]. The gist of the method is to replace the absorption cross section $\sigma_a \sim E^{-1/2}$ by the approximate expression a + b/E. The parameters a and b are determined from relationships that are similar to the following:

$$\int_0^\infty \left(\alpha + \frac{\beta}{E} - \frac{\gamma}{\sqrt{E}}\right) E^{\frac{\beta+1}{2}} e^{-E}\, dE = 0$$

$$\int_0^\infty \left(\alpha + \frac{\beta}{E} - \frac{\gamma}{\sqrt{E}}\right) E^{\frac{\beta+3}{2}} e^{-E}\, dE = 0$$

III.

In a heterogeneous subcritical medium comprised of a series of homogeneous layers whose boundaries are perpendicular to the plane of the sources, the neutron flux

has the following form far away from the source [3]:

$$\Phi(E,z,\vec{r}) = e^{-\frac{|z|}{L_0}} \phi(E,\vec{r}) \qquad (22)$$

where ϕ $(E, \vec{r})$ satisfies the equation

$$-\nabla D(E,\vec{r})\nabla\Phi(E,\vec{r}) + \Sigma_a(E,\vec{r})\Phi(E,\vec{r}) = = \frac{dq}{dE} + \frac{dq_f}{dE} + \frac{D\phi}{L^2} \qquad (23)$$

In the region of small energies, $\frac{dq_f}{dE} = 0$

The asymptotic spectrum of the thermal neutrons depends on the criticality of the medium ν . At large energies, ϕ $(E, \vec{r})$ decreases exponentially if $\nu = 0$. If $\nu = \nu_{cr}$, then the energy spectrum of the neutrons is close to the Fermi spectrum at high energies. The eigenvalues and eigenfunctions of (23) can be determined by numerical means.

If $\nu = 0$ then we can assume that at sufficiently high energies ϕ $(E, \vec{r}) = 0$. In this case Eq. (23) reduces to the following:

$$-\nabla D\nabla\Phi + (\Sigma_a + \Sigma)\phi - \frac{D}{L^2}\phi = = \int_0^{E_c} \Sigma(E' \to E)\Phi(E',\vec{r})dE' \qquad (24)$$

If $\nu = \nu_{cr}$ and $L^{-2} = 0$, then Eq. (23) becomes inhomogeneous

$$-\nabla D \nabla \phi + (\sigma_a + \sigma)\phi - \int_0^{E_c} \sigma(E' \to E)\phi(E', \vec{r})\,dE' = \frac{dq_0}{dE} \qquad (25)$$

Here

$$\frac{dq_0}{dE} = \int_{E_c}^{\infty} \tilde{\phi}(E', \vec{r})\,\sigma(E' \to E)\,dE'$$

$\tilde{\phi}(E', \vec{r})$ can be calculated by the usual methods without account of thermalization.

Eq. (24) can be solved by Kellog's iteration method

$$-\nabla D \nabla \phi^{(n+1)} + (\sigma_a + \sigma)\phi^{(n+1)} - \int_0^{E_c} \sigma(E' \to E)\phi^{(n+1)}(E', \vec{r})\,dE' =$$

$$= D\bar{\phi}^{(n)}(E, r)$$

$$\bar{\phi}^{(n)}(E) = \left\| \phi^{(n)}(E, r) \right\|^{-1} \phi^{(n)}(E, r)$$

By way of the zeroth approximation it is useful to use the solution of Eq. (25). In this case the iteration converges very rapidly. The solutions of Eqs. (24) and (25)

as expected, differ from each other.

To solve Eq. (24) and (25), a program was developed for the "Strella" computer (L. V. Maĭorov, V. L. Ponomareva, V. N. Toroptseva, 1959). To calculate one point in the space grid of a 15-group system of equations one requires approximately 15 seconds.

By way of illustration we given the results of the calculation of the flux of thermal neutrons in a multi-zone cylindrical sleeve inserted in the thermal column of a reactor. The properties of the medium are constant in each zone [1].

The neutron sources are situated in the plane $z = 0$ (the thermal column was assumed in the calculation to have a cylindrical form).

The calculation was carried out for $\nu = 0$ and $\nu = \nu_{cr}$.

The composition of the zone was as follows: first zone -- natural uranium, second and fourth zones -- aluminum, third zone -- empty, and fifth -- graphite.

In reference [1] an experiment is described for the measurement of the ratio P_5^9 -- the ratio of fissions per second on Pu^{239} nuclei to the number of fissions on U^{235} in such a system

$$P_5^9 = \frac{\int_0^{R_1} r\,dr \int_0^{\infty} \sigma_f^9(E)\,\Phi(E,r)\,dE}{\int_0^{R_1} r\,dr \int_0^{\infty} \sigma_f^5(E)\,\Phi(E,r)\,dE}$$

This quantity was measured at different graphite temperatures T in the thermal column. In the figure, curve 1 shows the dependence $P_5^9(T)$ for a medium in which it is assumed that $\nu \simeq 0$ (corresponding to reality); curve 2 is experimental. Curve 3 was calculated under the condition $\nu = \nu_{cr}$. It is seen from Fig. 2 that the degree of criticality of the medium greatly influences the spectrum of the thermal neutrons. The solution of the problem for $\nu = \nu_{cr}$ was used as the zeroth approximation of the iteration process (26).

The author is grateful to E. S. Kuznetsov for interest in the work and to M. V. Maslennikov for a discussion of reference [3].

BIBLIOGRAPHY

1. H. Hurwitz and M. S. Nelkin, Nuclear Science and Engineering 3, 1 -- 10 (1958).

2. F. Riezs and B. Szekefalve-Nagy, Lessons on Functional Analysis (Russian translation), Moscow, IL, 1953.

3. L. V. Maĭorov, On the Distribution of Thermal

Neutrons in a Medium with Planar Source. Zh. vichisl. matem. i mat. fiziki (Journal of Computational Mathematics and Mathematical Physics, 3 (in press).

4. W. P. Stinson, L. C. Schmid, R. E. Heineman, Nuclear Science and Engineering 7, 435 -- 441 (1960).

5. A. Nikiforov and V. Uvarov, Zh. vichisl. matem. i mat. fizika, v. 1, pp. 177 -- 179 (1961).

FIGURE CAPTION

Figure 1. Ratio of Pu^{239} to U^{235} fission as a function of graphite temperature in thermal column. Curves 1 and 3 are theoretical, and correspond to $\nu = 0$ and $\nu = \nu_{crit.}$, respectively. Curve 2 is experimental.

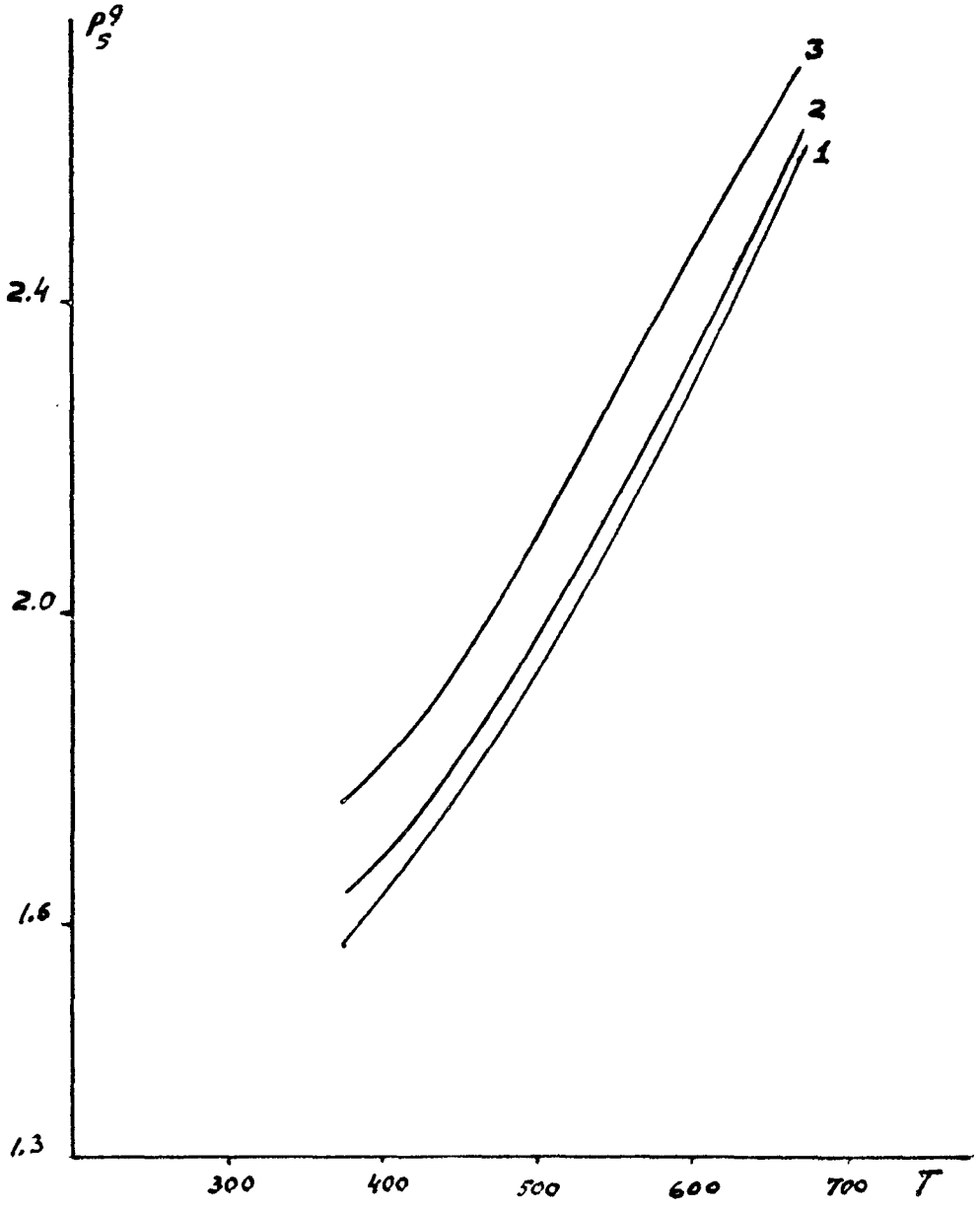
ρ_s^g
3
2
1
2.4
2.0
1.6
1.3
300
400
500
600
700
T

The Proceedings of the

BROOKHAVEN CONFERENCE ON NEUTRON THERMALIZATION

have been published in four volumes.

Volume I, The Scattering Law

Volume II, Neutron Spectra in Lattices and Infinite Media

Volume III, Experimental Aspects
of Transient and Asymptotic Phenomena

Volume IV, Theoretical Aspects
of Transient and Asymptotic Phenomena